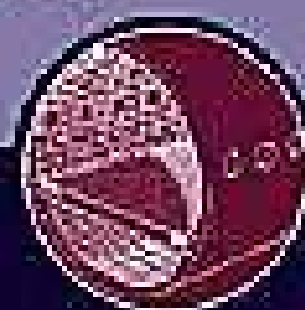




McGraw-Hill

THEORIES —AND— APPLICATIONS —OF— PLATE ANALYSIS

CLASSICAL, NUMERICAL AND
ENGINEERING METHODS



RUDOLPH SZILARD

Theories and Applications of Plate Analysis

Theories and Applications of Plate Analysis

Classical, Numerical and Engineering Methods

Rudolph Szilard, Dr.-Ing., P.E.

Professor Emeritus of Structural Mechanics

University of Hawaii, United States

Retired Chairman, Department of Structural Mechanics

University of Dortmund, Germany



JOHN WILEY & SONS, INC.

This book is printed on acid-free paper.∞

Copyright © 2004 by John Wiley & Sons, Inc. All rights reserved.

Published by John Wiley & Sons, Inc., Hoboken, New Jersey.

Published simultaneously in Canada.

No part of this publication may be reproduced, stored in a retrieval system, or transmitted in any form or by any means, electronic, mechanical, photocopying, recording, scanning, or otherwise, except as permitted under Section 107 or 108 of the 1976 United States Copyright Act, without either the prior written permission of the Publisher, or authorization through payment of the appropriate per-copy fee to the Copyright Clearance Center, Inc., 222 Rosewood Drive, Danvers, MA 01923, 978-750-8400, fax 978-750-4470, or on the web at www.copyright.com. Requests to the Publisher for permission should be addressed to the Permissions Department, John Wiley & Sons, Inc., 111 River Street, Hoboken, NJ 07030, (201) 748-6011, fax (201) 748-6008, e-mail: permreq@wiley.com.

Limit of Liability/Disclaimer of Warranty: While the publisher and author have used their best efforts in preparing this book, they make no representations or warranties with respect to the accuracy or completeness of the contents of this book and specifically disclaim any implied warranties of merchantability or fitness for a particular purpose. No warranty may be created or extended by sales representatives or written sales materials. The advice and strategies contained herein may not be suitable for your situation. You should consult with a professional where appropriate. Neither the publisher nor author shall be liable for any loss of profit or any other commercial damages, including but not limited to special, incidental, consequential, or other damages.

For general information on our other products and services please contact our Customer Care Department within the U.S. at (800)-762-2974, outside the U.S. at (317)-572-3993 or fax (317)-572-4002.

Wiley also publishes its books in a variety of electronic formats. Some content that appears in print, however, may not be available in electronic format. For more information about Wiley products, visit our web site at www.wiley.com.

Library of Congress Cataloging-in-Publication Data

Szilard, Rudolph, 1921-

Theories and applications of plate analysis : classical, numerical and engineering methods / by Rudolph Szilard.

p. cm.

Includes bibliographical references and index.

ISBN 0-471-42989-9 (cloth)

1. Plates (Engineering) I. Title.

TA660.P6S94 2003

624.1'7765—dc21

2003043256

Printed in the United States of America.

10 9 8 7 6 5 4 3 2 1

To the memory of my father,
Dipl.-Ing. Rudolph Seybold-Szilard, senior,
who encouraged and inspired my career in structural mechanics

Contents

Preface	xvii
Symbols	xxi
I Introduction	1
II Historical Background	10
PART I Plate Theories and Analytical Solutions of Static, Linear-Elastic Plate Problems	21
1 Elastic Plate Theories and Their Governing Differential Equations	23
1.1 Classical Small-Deflection Theory of Thin Plates ^{*1}	23
1.2 Plate Equation in Cartesian Coordinate System [*]	26
1.3 Boundary Conditions of Kirchhoff's Plate Theory [*]	35
1.4 Differential Equation of Circular Plates [*]	42
1.5 Refined Theories for Moderately Thick Plates	45
1.6 Three-Dimensional Elasticity Equations for Thick Plates	53
1.7 Membranes	57

¹Asterisks (*) indicate sections recommended for classroom use.

1.8	Summary*	60
	Problems*	61
2	Exact and Series Solutions of Governing Differential Equations	62
2.1	Rigorous Solution of Plate Equation	62
2.2	Solutions by Double Trigonometric Series (Navier's Approach)*	69
2.3	Solutions by Single Trigonometric Series (Lévy's Method)*	75
2.4	Further Examples of Series Solutions	83
2.5	Extensions of Navier's and Lévy's Methods	92
2.6	Method of Images	97
2.7	Plate Strips	99
2.8	Rigorous Solution of Circular Plates Subjected to Rotationally Symmetric Loading*	110
2.9	Solutions of Membrane Problems	116
2.10	Series Solutions of Moderately Thick Plates	120
2.11	Summary*	126
	Problems*	127
3	Further Plate Problems and Their Classical Solutions	129
3.1	Plates on Elastic Foundation*	129
3.2	Plates with Variable Flexural Rigidity	139
3.3	Simultaneous Bending and Stretching	147
3.4	Plates of Various Geometrical Forms	150
3.5	Various Types of Circular Plates	156
3.6	Circular Plate Loaded by an Eccentric Concentrated Force	161
3.7	Plates with Edge Moments	165

3.8	Solutions Obtained by Means of Superposition	168
3.9	Continuous Plates	173
3.10	Summary	179
	Problems	180
4	Energy and Variational Methods for Solution of Lateral Deflections	181
4.1	Introduction and Basic Concepts*	181
4.2	Ritz's Method*	187
4.3	Galerkin's Method and Its Variant by Vlasov*	196
4.4	Further Variational and Energy Procedures	212
4.5	Techniques to Improve Energy Solutions	226
4.6	Application of Energy Methods to Moderately Thick Plates	231
4.7	Summary*	234
	Problems*	235
PART II	Numerical Methods for Solution of Static, Linear-Elastic Plate Problems	237
5	Finite Difference Methods	247
5.1	Ordinary Finite Difference Methods*	247
5.2	Improved Finite Difference Methods	276
5.3	Finite Difference Analysis of Moderately Thick Plates	303
5.4	Advances in Finite Difference Methods	312
5.5	Summary and Conclusions*	314
	Problems*	315
6	Gridwork and Framework Methods	317
6.1	Basic Concepts*	317

6.2	Equivalent Cross-Sectional Properties	320
6.3	Gridwork Cells and Their Stiffness Matrices*	328
6.4	Computational Procedures for Gridworks	336
6.4.1	Procedures Using Commercially Available Programs*	337
6.4.2	Guidance for Gridwork Programming	343
6.5	Summary and Conclusions*	361
	Problems*	362
7	Finite Element Method	364
7.1	Introduction and Brief History of the Method*	364
7.2	Engineering Approach to the Method*	370
7.3	Mathematical Formulation of Finite Element Method*	380
7.3.1	Consideration of Total System*	380
7.3.2	Formulation of Element Stiffness Matrices*	383
7.4	Requirements for Shape Functions*	389
7.5	Various Shape Functions and Corresponding Element Families	392
7.5.1	Polynomials and Their Element Families	393
7.5.2	Hermitian Elements	399
7.5.3	Other Element Families	403
7.6	Simple Plate Elements*	406
7.6.1	Rectangular Element with Four Corner Nodes*	406
7.6.2	Triangular Element with Three Corner Nodes*	411
7.7	Higher-Order Plate Elements	418
7.7.1	Rectangular Element with 16 DOF	418
7.7.2	Discrete Kirchhoff Triangular Element	423
7.8	Computation of Loads and Stress Resultants*	434
7.9	Moderately Thick Plate Elements	446
7.10	Thick-Plate Elements	453

7.11	Numerical Integration	458
7.12	Modeling Finite Element Analysis*	463
7.13	Programming Finite Element Analysis*	465
7.14	Commercial Finite Element Codes*	469
7.15	Summary and Conclusions*	472
	Problems*	474
8	Classical Finite Strip Method	475
8.1	Introduction and Basic Concepts	475
8.2	Displacement Functions for Classical FSM	477
8.3	Formulation of the Method	481
8.4	Outline of Computational Procedures	489
8.5	Summary and Conclusions	494
	Problems	495
9	Boundary Element Method	496
9.1	Introduction	496
9.2	Basic Concepts of Boundary Element Method	497
PART III	Advanced Topics	505
10	Linear Considerations	507
10.1	Orthotropic Plates	507
10.2	Laminated and Sandwich Plates	530
10.2.1	Classical Laminated Plate Theory	531
10.2.2	Sandwich Plates	534
10.2.3	Moderately Thick Laminated Plates	539
10.3	Analysis of Skew Plates	546
10.4	Thermal Bending of Plates	561

10.5	Influence Surfaces	571
10.6	Continuous Plates Supported by Rows of Columns	578
10.7	Additional Topics Related to FEM	590
10.7.1	Various Convergence Tests	590
10.7.2	Elements with Curved Sides	594
10.8	Extensions of Classical Finite Strip Method	597
10.8.1	Spline Finite Strip Method	598
10.8.2	Computed Shape Functions	605
10.8.3	Finite Strip Formulation of Moderately Thick Plates	606
10.9	Summary and Conclusions	611
	Problems*	612
11	Nonlinear Aspects	614
11.1	Large-Deflection Analysis	614
11.2	Numerical Methods for Geometrically Nonlinear Analysis	624
11.2.1	Various Finite Element Procedures	637
11.3	Material Nonlinearity	645
11.3.1	Nonlinear Stress-Strain Relationships	645
11.3.2	Computational Procedures	648
11.4	Combined Geometrical and Material Nonlinearities	656
11.5	Reinforced-Concrete Slabs	662
11.6	Summary and Conclusions	672
	Problems	672
PART IV	Engineering Solution Procedures	673
12	Practical Design Methods	675
12.1	Need for Engineering Solution Procedures*	675
12.2	Elastic Web Analogy for Continuous Plate Systems*	676
12.3	Simplified Slope-Deflection Method*	689

12.4	Moment Distribution Applied to Continuous Plates*	700
12.5	Practical Analysis of RC Floor Slabs	710
12.6	Equivalent Frame Method Applied to Flat Slabs*	718
12.7	Other Practical Design Methods	727
12.7.1	Approximate Analysis of Bridge Decks	727
12.7.2	Simplified Treatments of Skew Plates	730
12.7.3	Degree-of-Fixity Procedure	733
12.8	Summary and Conclusions*	739
	Problems*	740
13	Yield-Line Method	742
13.1	Introduction to Yield-Line Method*	742
13.2	Work Method*	751
13.3	Equilibrium Method*	758
13.4	Further Applications of Yield-Line Analysis*	763
13.5	Yield Lines due to Concentrated Loads*	770
13.6	Summary and Conclusions*	781
	Problems*	782
PART V	Dynamic Analysis of Elastic Plates	785
14	Classical and Energy Methods in Dynamic Analysis	787
14.1	Introduction to Structural Dynamics*	787
14.2	Differential Equations of Lateral Motion*	802
14.3	Free Flexural Vibration of Plates*	804
14.4	Free Transverse Vibration of Membranes	810
14.5	Energy Methods for Determination of Natural Frequencies*	815
14.6	Natural Frequencies Obtained from Static Deflections*	824

14.7	Forced Transverse Vibration of Rectangular Plates*	830
14.8	Free Vibration of Moderately Thick Plates	839
14.9	Summary and Conclusions*	842
	Problems*	843
15	Numerical Methods in Plate Dynamics	845
15.1	Solution of Differential Equation of Motion by Finite Differences*	845
15.2	Application of Finite Element Method to Plate Dynamics*	856
15.2.1	Matrix Equations of Free Vibrations*	856
15.2.2	Mass Matrix*	860
15.2.3	Forced Vibrations*	870
15.3	Damping of Discrete Systems	883
15.4	Slab Bridges under Moving Loads	889
15.5	Large-Amplitude Free-Vibration Analysis	895
15.6	Summary and Conclusions*	899
	Problems*	902
PART VI	Buckling of Plates	903
16	Fundamentals of Stability Analysis	905
16.1	Basic Concepts*	905
16.2	Equilibrium Method*	911
16.3	Energy Methods in Stability Analysis*	919
16.4	Finite Differences Solution of Plate Buckling*	928
16.5	Finite Element and Gridwork Approach to Stability Analysis*	938
16.6	Dynamic Buckling	946
16.7	Buckling of Stiffened Plates	953
16.8	Thermal Buckling	961

16.9	Buckling of Moderately Thick Plates	963
16.10	Postbuckling Behavior	966
16.11	Inelastic Buckling and Failure of Plates	978
16.12	Summary and Conclusions*	982
	Problems*	983
Appendix A.1	Fourier Series	985
Appendix A.2	Conversion from One Poisson Ratio to Another	999
Appendix A.3	Units	1001
Appendix A.4	About the CD	1003
	A.4.1 Plate Formulas	1003
	A.4.2 WinPlatePrimer Program System	1004
Index		1015

Preface

This monograph represents a completely reworked and considerably extended version of my previous book on plates.¹ It is based on the courses taught and the pertinent research conducted at various universities in the United States and Germany, combined with my many years of experience as a practicing structural engineer. Like its predecessor, this new version intends, at the same time, to be a text and reference book. Such dual aims, however, put any author in a difficult position since the requirements of text and reference books are different. The global success of the first version indicates, however, that such an approach is justified. In spite of the number of books on plates, there is no single book at the present time that is devoted to the various plate theories and methods of analysis covering static, dynamic, instability and large-deflection problems for very thin, thin, moderately thick and thick plates. The author hopes that this *comprehensive* monograph will serve as a text and reference book on these highly diverse subjects. Thus, the main objectives of this book are as follows:

1. To serve as an introductory text to the classical methods in various plate theories.
2. To acquaint readers with the contemporary analytical and numerical methods of plate analysis and to inspire further research in these fields.
3. To serve as a reference book for practicing engineers not only by giving them diverse engineering methods for quick estimates of various plate problems but also by providing them with a user-friendly computer program system stored on a CD-ROM for computation of a relatively large spectrum of practical plate problems. In addition, the accompanying CD-ROM contains a collection of readily usable plate formulas for solutions of numerous plate problems that often occur in the engineering practice.

Requirements of a Textbook. A textbook must clearly formulate the fundamentals and present a sufficient number of illustrative examples. Thus throughout the text the mathematical modeling of physical phenomena is emphasized. Although

¹ Szilard, R., *Theory and Analysis of Plates: Classical and Numerical Methods*, Prentice-Hall, Upper Saddle River, New Jersey, 1974.

the occasionally complicated mathematical theories of plates cannot be simplified, they can certainly be presented in a clear and understandable manner. In addition, a large number of carefully composed figures should make the text graphically more descriptive. Rather than attempt the solutions of specific problems, the author has introduced *generally applicable* analytical, numerical and engineering methods for solution of static, dynamic and stability problems of plates. Since experience is the best teacher, numerous worked examples illustrate the applications of these methods. All the numerical examples are computed by using the *modernized metric system* as defined by the International System of Units (Système international d'unités).

Although higher mathematics is essential to the analytical solution of most plate problems, the mathematical prerequisites of the book are relatively modest. Merely the familiarity with differential-integral calculus and matrix algebra is assumed, and all further required mathematical tools are systematically developed within the text. The sections dealing with the *methods of higher analysis* are treated as integral parts of the text. The same procedure has been followed with such other prerequisites as the *theory of elasticity*, *structural dynamics*, *limit design* and so forth. This approach has resulted in a self-contained text on plates that can be used without consulting related works.

Working knowledge of the fundamentals of the classical methods is considered mandatory in spite of its serious limitations. As in most fields of *mathematical physics*, exact analytical solutions can be obtained only for the simplest cases. For numerous plate problems of great practical importance, the classical methods either fail to yield a solution or yield a solution too complicated for practical application. Here, the approximate and numerical methods offer the only reasonable approach. The "exact" solutions, however, perform an important function because they provide the benchmark against which all other solution techniques are tested.

With the present widespread availability of powerful desktop computers, there has been a real revolution in the numerical analysis of plate problems. From the various computer-oriented solution techniques, the finite difference, the gridwork, finite element and finite strip methods have been treated extensively. The reader will also find a short introduction to the recently emerging boundary element method. The actual coding of the computerized solutions of plate problems is considered to be outside the scope of this book. The numerical solutions of plate problems, however, are formulated so that either standard computer programs can be used or they can be easily programmed by utilizing readily available subroutines of numerical analysis procedures. In order to facilitate the numerical solution of certain problems, numerous finite difference stencils and finite element stiffness and mass matrices are given in *explicit* forms. Furthermore, plate programs of practical interest are also stored on the CD-ROM that accompanies this book. These include, in addition to the FORTRAN source codes, the executable forms of these computer codes for static and dynamic analysis of plates.

Of the analytical approaches, the energy methods are treated more extensively than others because the author believes that their relative simplicity, efficiency and almost universal use warrant this emphasis.

Sections marked with asterisks (*) in the table of contents are recommended for classroom use in a one-semester course on plates for graduate students of civil, mechanical, aeronautical, architectural, mining and ocean engineering and for students of engineering mechanics and naval architecture. The material presented, however, is sufficient for a two-semester course; preferably one semester of directed reading

would be offered following the first semester of formal classroom presentation. Exercises to be worked out by the students are included at the end of most chapters. They are listed in order of ascending difficulty.

Use of the Book by Practicing Engineers. Although the requirements of practicing engineers are different from those discussed above, there are also numerous overlapping areas. Practicing engineers must deal with “real-life” plate problems. Consequently, they require a much *broader coverage* than that usually given in “Analysis of Plates and Shells” textbooks. The present book, however, intends to satisfy this important need by covering a large spectrum of plate problems and their solution procedures. Plate analysis has undergone considerable changes during the past decades. These changes were introduced by (a) proliferation of powerful—yet relatively inexpensive—personal computers and (b) the development of computer-oriented numerical analysis techniques such as gridwork and finite element methods, to name the most important ones. Consequently, nowadays the practicing engineer will apply a suitable computer code to analyze plate structures for their static or dynamic behaviors and determine their stability performance under the given loads. However, to be able to use such contemporary analysis methods properly, he or she must have basic knowledge of pertinent plate theories along with the underlying principles of these numerical solution techniques. All these fundamental requirements for a successful computer-based plate analysis are amply covered in this book. Furthermore, it is of basic importance that the engineer properly *idealizes* the plate structures which are in essence two-dimensional continua replaced by equivalent discrete systems in the numerical approach. This idealization process includes definition of plate geometry along with the existing support conditions and the applied loads. It also incorporates the discretization process, which greatly influences the obtainable accuracy. Although proper idealization of a real structure is best learned under the personal guidance of an experienced structural engineer, numerous related guidelines are also given throughout in this book. To start a numerical analysis, *ab ovo* the plate thickness is required as input. For this purpose, this work contains various *engineering methods*. Using these, the required plate thickness can be determined merely by simple “longhand” computations. After obtaining a usable estimate for plate behavior under the applied load, the engineer can use a computer to compute more exact numerical results. For this purpose, interactive, easy to use computer programs covering the most important aspects of plate analysis are stored on the companion CD-ROM attached to the back cover of the book. This CD-ROM contains a finite element program system, WinPlatePrimer, which not only solves important static and dynamic plate problems but also teaches its users how to write such programs by using readily available subroutines. Consequently, next to the executable files the corresponding FORTRAN source codes are also listed. The finite elements used in these programs have excellent convergence characteristics. Thus, good results can be obtained even with relatively crude subdivisions of the continuum. To validate the computer results, the practicing engineer needs, again, readily usable *simple* engineering approaches that can provide valuable independent checks. It is also important that he or she knows the *effectiveness and economy* not only of these approximate solution techniques but also of *all methods* presented here. These important aspects are also constantly emphasized. As mentioned earlier, explicitly given structural matrices and finite difference stencils allow the practicing engineer to develop his or her own computer programs to solve some special problems not covered in commercially available program systems. In general, strong emphasis is placed on practical applications, as demonstrated by an

unusually large number of worked problems many of them taken directly from the engineering practice. In addition, considering the needs of practicing engineers, the book is organized so that particular topics may be studied by reading some chapters before previous ones are completely mastered. Finally, it should be mentioned that the practicing engineer has often to deal with such plate problems for which solutions are already available in the pertinent technical literature. For this reason, a collection of the 170 most important plate formulas is given on the companion CD-ROM attached to the back cover of the book. These formulas, along with the closed-form solutions of certain plate problems presented in this book, can also be used to test commercially available computer codes for their effectiveness and accuracy.

Guide to the Reference System of the Book. The mathematical expressions are numbered consecutively, in parentheses, throughout each section carrying the pertinent section number before the second period. Equation (2.7.4), for example, refers to Equation 4 in Section 2.7.

The author realizes that a complete volume could be written on each of the chapters treated. Liberal inclusion of bibliographical references extends the comprehensiveness of this book. The numbering system used for references is similar to that of equations. The numbers in brackets refer to bibliographical references, again with the pertinent section number as prefix. Numbers in brackets without a prefix indicate general reference books on plates and are listed after the Introduction. References pertinent to the history of development of various plate theories carry the prefix II. References with prefixes "A" refer to the Appendixes.

Finally, the author is particularly indebted to Dr. L. Dunai, Professor, Technical University of Budapest, Hungary, and his co-workers (N. Kovács, Z. Kósa and S. Ádányi) for developing the WinPlatePrimer program system. My thanks are also due to my wife, Ute, for her continuous encouragement and support in writing this book and for editing the manuscript and checking the page proofs.

Symbols

The following symbols represent the most commonly used notations in this book. Occasionally, the same symbols have been used to denote more than one quantity; they are, however, properly identified when first introduced.

a, b	Plate dimensions in X and Y directions, respectively
a_i, b_i	Coefficients
a_{ij}, b_{ij}	Elements of matrices A and B , respectively
a, b, c	Column matrices or vectors, respectively
$\{a\}, \{a\}^T$ or $[a]^T$	Column and row matrices, respectively
A	Area, constant
A, B, C, ...	Matrices
$[A], [B], \dots$	Matrices
B	Effective torsional rigidity of orthotropic plate, constant
c_1, c_2, \dots	Constants or numerical factors
$\bar{d}_i, d_{e,i}$	Elements of the displacement vectors $\bar{\mathbf{d}}, \mathbf{d}_e$, respectively
$\bar{\mathbf{d}}, \mathbf{d}_e$	Displacement vector (global/element)
D	Flexural rigidity of plate [$D = Eh^3/12(1 - \nu^2)$]
D_x, D_y	Plate flexural rigidities associated with X and Y directions, respectively
D_t	Torsional rigidity of plate
D , $[D]$	Dynamical matrix of vibrating structural system, and representing pertinent differentiations
E	Young's modulus of elasticity
E , $[E]$	Elasticity matrix
f	Frequency of a vibrating structural system (Hz)
$f_i(\cdot)$	Function
g	Acceleration of gravity ($\approx 9.81 \text{ m/s}^2$)
G, G_{xy}	Shear moduli
h	Thickness of plate
i, j, k, l	Indices and/or positive integers (1, 2, 3, ...)
I	Moment of inertia
I_{tx}, I_{ty}	Geometrical torsional rigidities of beams

k	Modulus of elastic foundation, numerical factor
$\bar{k}_{ij}, k_{e,ij}$	Elements of stiffness matrix (global/element)
$\bar{\mathbf{K}}, \mathbf{K}_e$	Stiffness matrix (global/element)
l_x, l_y, l	Span lengths
$L(\cdot), \mathcal{L}(\cdot)$	Differential operators
m, n	Positive integers (1, 2, 3, ...)
\bar{m}_{ij}	Elements of consistent mass matrix $\bar{\mathbf{M}}$ in global reference system
m_T	Thermal equivalent bending moment
m_u, m'_u	Ultimate bending moments per unit length
m_x, m_y	Bending moments per unit length in X, Y, Z Cartesian coordinate system
m_{xy}	Twisting moment per unit length in X, Y, Z Cartesian coordinate system
m_r, m_φ	Radial and tangential bending moments per unit length in r, φ, Z cylindrical coordinate system
$m_{r\varphi}$	Twisting moment per unit length in r, φ, Z cylindrical coordinate system
\mathfrak{M}	Moment-sum, $=(m_x + m_y)/(1 + \nu)$
$\bar{\mathbf{M}}, \mathbf{M}_e$	Mass matrix (global/element)
M_x, M_y, M_t	Concentrated and/or external moments
n	Normal to boundary, index
n_{cr}	Critical (buckling) load
n_T	Thermal force per unit length acting in X, Y plane
n_x, n_y	Normal forces per unit length acting in X, Y plane
n_{xy}	Shear forces per unit length acting in X, Y plane
p_u	Ultimate load
$\mathbf{N}, [\mathbf{N}]$	Matrix of shape functions
p_x, p_y, p_z	Load components per unit area in X, Y, Z Cartesian coordinate system
P_X, P_Y, P_Z	Concentrated forces in X, Y, Z Cartesian coordinate system
q_r, q_φ	Transverse shear forces per unit length in r, φ, Z cylindrical coordinate system
q_x, q_y	Transverse shearing forces in X, Y, Z Cartesian coordinate system
r, φ, z	Cylindrical coordinates
r_0, r_1	Radii
R, φ, Z	Cylindrical coordinate system
$\mathbf{R}, [\mathbf{R}]$	Rotational matrix
t	Time or tangent to boundary
T	Temperature or kinetic energy
$\mathbf{T}, [\mathbf{T}]$	Transformation matrix
u, v, w	Displacement components in X, Y, Z directions
U	Strain energy
v_x, v_y	Lateral edge forces per unit length associated with X and Y directions, respectively
V	Volume or potential of external forces
w_H, w_P	Homogeneous and particular solutions of plate equation, respectively
W_e, W_i	Work of external and internal forces, respectively
x, y, z	Cartesian coordinates

X, Y, Z	Coordinate axes of Cartesian coordinate system
α, β, ϑ	Angles
α_m, β_m	Constants
α_T	Coefficient of thermal expansion
γ, γ_{xy}	Shear strain, shear strain in X, Y plane
$\delta, \delta_{i,j}$	Displacement, flexibility coefficients
$\delta(\cdot)$	Variational symbol
$\varepsilon_T, \varepsilon_x, \varepsilon_y$	Thermal strain, normal strains in X and Y directions, respectively
$\varepsilon_i(x, y)$	Error function
η, ξ	Oblique coordinates
λ	Finite difference mesh width ($\Delta x = \Delta y = \lambda$)
λ_i	Lagrangian multiplier
$\vartheta, \theta, \phi, \phi$	Angles
$\lambda_1, \lambda_2, \dots$	Eigenvalues
λ_{cr}	Critical load factor
$\kappa_x, \kappa_y, \kappa_{xy}, \chi$	Curvatures of deflected middle surface
$\nu, \nu_x, \nu_y, \nu_{xy}$	Poisson ratios
Π	Total potential energy
ρ	Dimensionless quantity (r/r_0)
σ_x, σ_y	Normal stresses in X and Y direction, respectively
σ_u	Ultimate stress
τ, τ_{xy}	Shear stresses
$\varphi, \varphi_i(\cdot), \varphi_i(\cdot)$	Angle, functions
$\Phi(x, y)$	Stress function
χ	Warping of deflected middle surface
ω	Circular (angular frequency of free vibration (rad/s))

$$\nabla^2(\cdot) = \frac{\partial^2(\cdot)}{\partial x^2} + \frac{\partial^2(\cdot)}{\partial y^2}; \quad \nabla_r = \frac{\partial^2(\cdot)}{\partial r^2} + \frac{1}{r^2} \cdot \frac{\partial^2(\cdot)}{\partial \phi^2} + \frac{1}{r} \cdot \frac{\partial(\cdot)}{\partial r}$$

$$\nabla^4(\cdot) = \frac{\partial^4(\cdot)}{\partial x^4} + 2 \frac{\partial^4(\cdot)}{\partial x^2 \partial y^2} + \frac{\partial^4(\cdot)}{\partial y^4}$$

The various boundary conditions are shown in the following manner:

	Section	Plan view
Free edge		
Simple support		
Clamped edge		
Point support		
Elastic support		



Introduction

Plates are straight, plane, two-dimensional structural components of which one dimension, referred to as thickness h , is much smaller than the other dimensions. Geometrically they are bound either by straight or curved lines. Like their counterparts, the beams, they not only serve as structural components but can also form complete structures such as slab bridges, for example. Statically plates have free, simply supported and fixed boundary conditions, including elastic supports and elastic restraints, or, in some cases, even point supports (Fig. I.1). The static and dynamic loads carried by plates are predominantly perpendicular to the plate surface. These external loads are carried by internal bending and torsional moments and by transverse shear forces.

Since the load-carrying action of plates resembles to a certain extent that of beams, plates can be approximated by gridworks of beams. Such an approximation, however, arbitrarily breaks the continuity of the structure and usually leads to incorrect results unless the actual two-dimensional behavior of plates is correctly accounted for.

The two-dimensional structural action of plates results in lighter structures and, therefore, offers economical advantages. Furthermore, numerous structural configurations require partial or even complete enclosure that can easily be accomplished by plates, without the use of additional covering, resulting in further savings in material and labor costs. Consequently, plates and plate-type structures have gained special importance and notably increased applications in recent years. A large number of structural components in engineering structures can be classified as plates. Typical examples in civil engineering structures are floor and foundation slabs, lock-gates, thin retaining walls, bridge decks and slab bridges. Plates are also indispensable in shipbuilding and aerospace industries. The wings and a large part of the fuselage of an aircraft, for example, consist of a slightly curved plate skin with an array of stiffened ribs. The hull of a ship, its deck and its superstructure are further examples of stiffened plate structures. Plates are also frequently parts of machineries and other mechanical devices. Figure I.2 schematically illustrates some of these industrial applications.

This book deals with the various plate analysis techniques which, of course, cannot be learned without a well-founded knowledge in the underlying plate theories. The main objective to any structural analysis is to ensure that the structure under investigation shall have an adequate safety factor against failure within reasonable

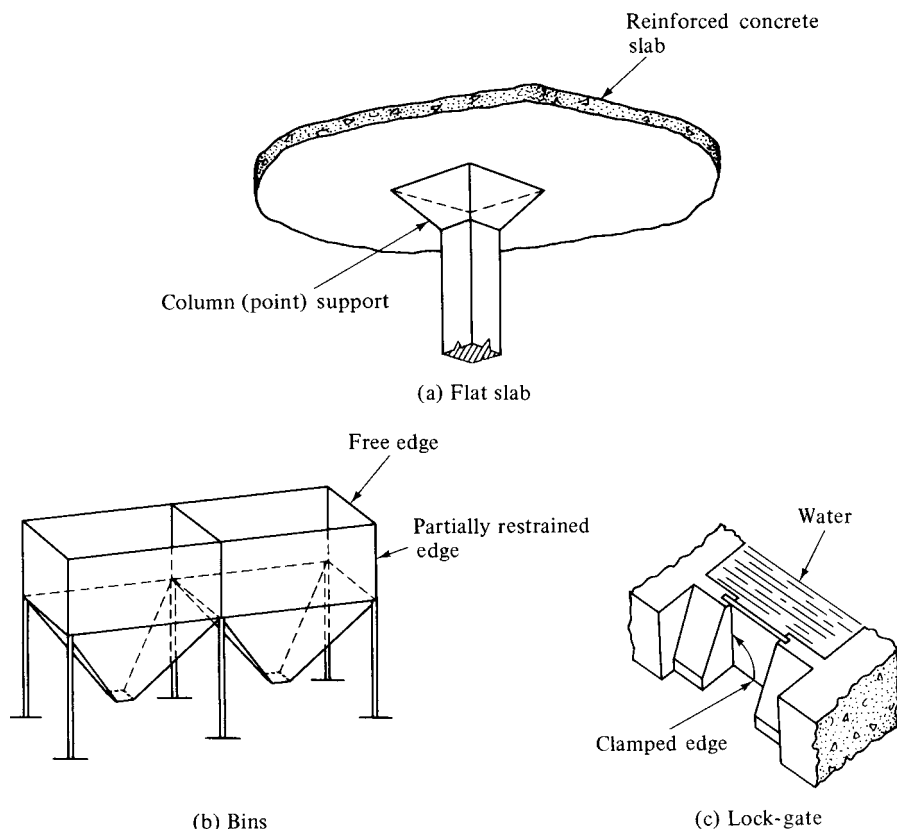


Figure I.1 Various boundary conditions for plates.

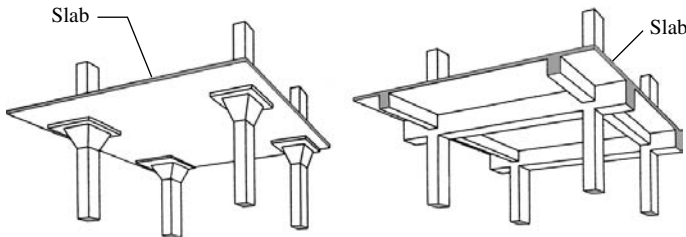
economical bounds. Furthermore, the structure shall be serviceable when subjected to design loads. A part of serviceability can be achieved, for example, by imposing suitable limitations on deflections.

The majority of plate structures is analyzed by applying the governing equations of the *theory of elasticity*. Consequently, a large part of this book presents various elastic plate theories and subsequently treats suitable analytical and numerical solution techniques to determine deflections and stresses.

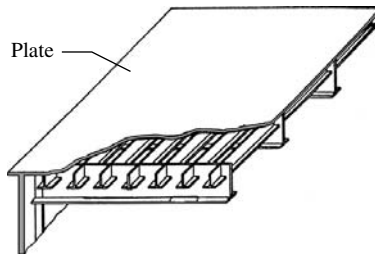
As already mentioned in the Preface, “exact” solutions of the various governing differential equations of plate theories can only be obtained for special boundary and load conditions, respectively. In most cases, however, the various energy methods can yield quite usable *analytical solutions* for most practical plate problems. Nowadays, with widespread use of computers, a number of numerical solution techniques have gained not only considerable importance but, as in the case of the finite element method, also an almost exclusive dominance. All numerical methods treated in this book are based on some discretization of the plate continuum. The *finite difference* and the *boundary element* methods apply mathematical discretization techniques for solution of complex plate problems, whereas the *gridwork*, *finite element* and *finite strip* methods use physical discretizations based on engineering considerations. Since

the results obtained by the different computer-oriented numerical approaches always require independent checks, *engineering* methods, capable of giving rough approximations by means of relatively simple “longhand” computations, are regaining their well-deserved importance. In addition, engineering methods can also be used for preliminary design purposes to determine the first approximate dimensions of plates. In addition to static plate problems, all the above-mentioned solution techniques also treat pertinent dynamic and elastic stability problems.

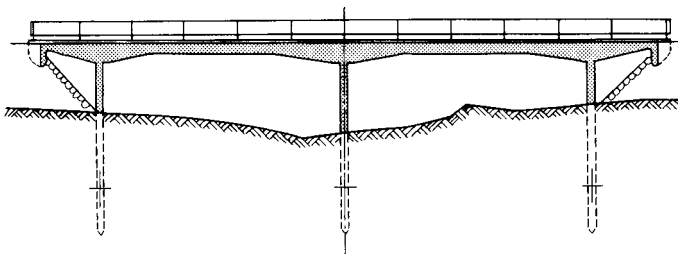
However, these methods, based on elastic theories, have certain limitations. The most important of these is that they do not give accurate indication of the factor of safety against failure. Partly due to this limitation, there is a tendency to replace the elastic analysis by *ultimate load* techniques. On the other hand, since this method cannot always deal with all the problems of serviceability, the author recommends that, if required, an elastic analysis should be augmented by a failure assessment using the ultimate load approach.



(a1) Reinforced concrete slabs in buildings



(a2) Steel bridge deck



Slab bridge

(a) Use of plates in construction industry

Figure I.2 Use of plates in various fields of engineering.

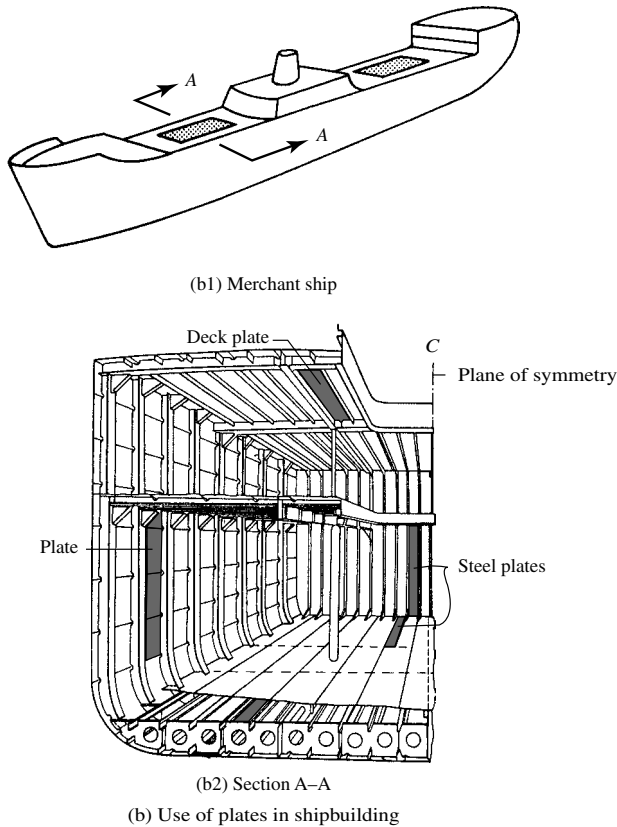
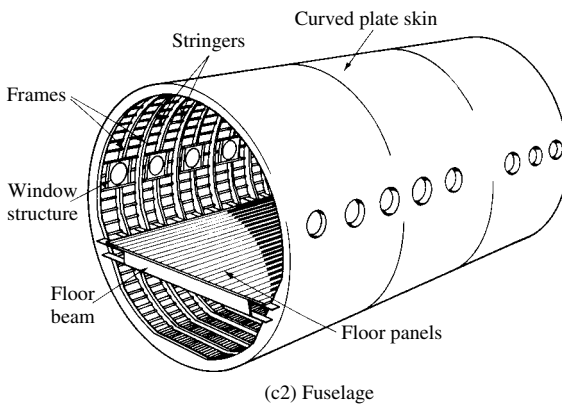
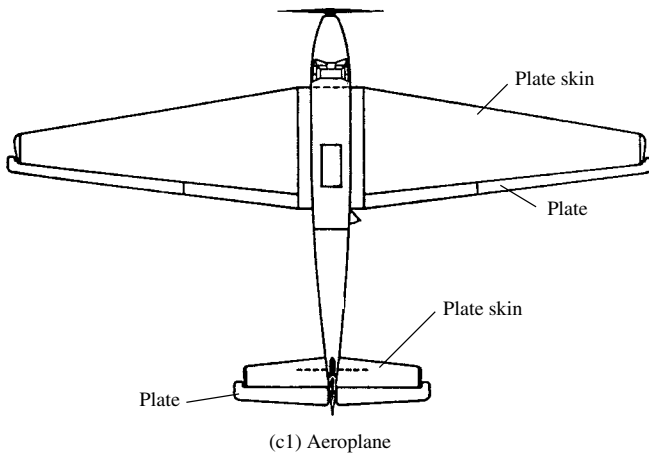


Figure I.2 (continued)

In all structural analyses the engineer is forced, due to the complexity of any real structure, to replace the structure by a simplified analysis model equipped only with those important parameters that mostly influence its static or dynamic response to loads. In plate analysis such idealizations concern

1. the geometry of the plate and its supports,
2. the behavior of the material used, and
3. the type of loads and their way of application.

A rigorous elastic analysis would require, for instance, that the plate should be considered as a three-dimensional continuum. Needless to say, such an approach is highly impractical since it would create almost insurmountable mathematical difficulties. Even if a solution could be found, the resulting costs would be, in most cases, prohibitively high. Consequently, in order to rationalize the plate analyses, we distinguish among four different plate categories with inherently different structural behavior and, hence, different governing differential equations. The four plate-types might be categorized, to some extent, using their ratio of thickness to governing length (h/L).



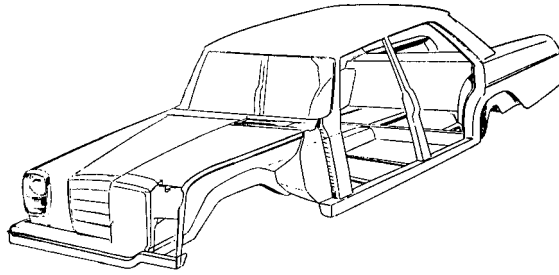
(c) Use of plates in aerospace structures

Figure I.2 (continued)

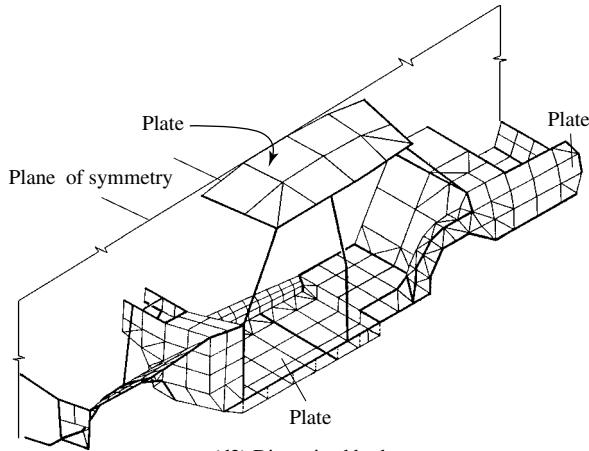
Although, the boundaries between these individual plate types are somewhat fuzzy, we can attempt to subdivide plates into the following major categories:

1. *Stiff plates* ($h/L = \frac{1}{50} - \frac{1}{10}$) are thin plates with flexural rigidity, carrying loads two dimensionally, mostly by internal (bending and torsional) moments and by transverse shear, generally in a manner similar to beams (Fig. I.3a). In engineering practice, *plate* is understood to mean stiff plate unless otherwise specified.
2. *Membranes* ($h/L < \frac{1}{50}$) are very thin plates without flexural rigidity, carrying loads by axial and central shear forces[†] (Fig. I.3b). This load-carrying action can be approximated by a network of stressed cables since, because of their extreme thinness, their moment resistance is of negligible order.

[†] Transverse shear force acts perpendicularly to the plane of the plate, whereas central shear force acts in the plane of the plate (see Figs. I.3a and b).



(d1) Car body



(d) Use of plates in automobile industry

Figure I.2 (continued)

3. *Moderately thick plates* ($h/L = \frac{1}{10} - \frac{1}{5}$) are in many respects similar to stiff plates, with the notable exception that the effects of transverse shear forces on the normal stress components are also taken into account.
4. *Thick plates* ($h/L > \frac{1}{5}$) have an internal stress condition that resembles that of three-dimensional continua (Fig. I.3d).

There is, however, a considerable “gray” area between stiff plates and membranes; namely, if we do not limit the deflections of stiff plates, we obtain so-called *flexible* plates, which carry the external loads by the combined action of internal moments, transverse and central shear forces and axial forces (Fig. I.3c). Consequently, elastic plate theories distinguish sharply between plates having small and large deflections. Plates having large deflections are avoided, for the most part, in general engineering practice since they might create certain problems in their analysis as well as in their use. The safety-driven and weight-conscious aerospace and submarine-building industries are forced, however, to disregard these disadvantages since such plates possess considerably increased load-carrying capacities. Consequently, large-deflection

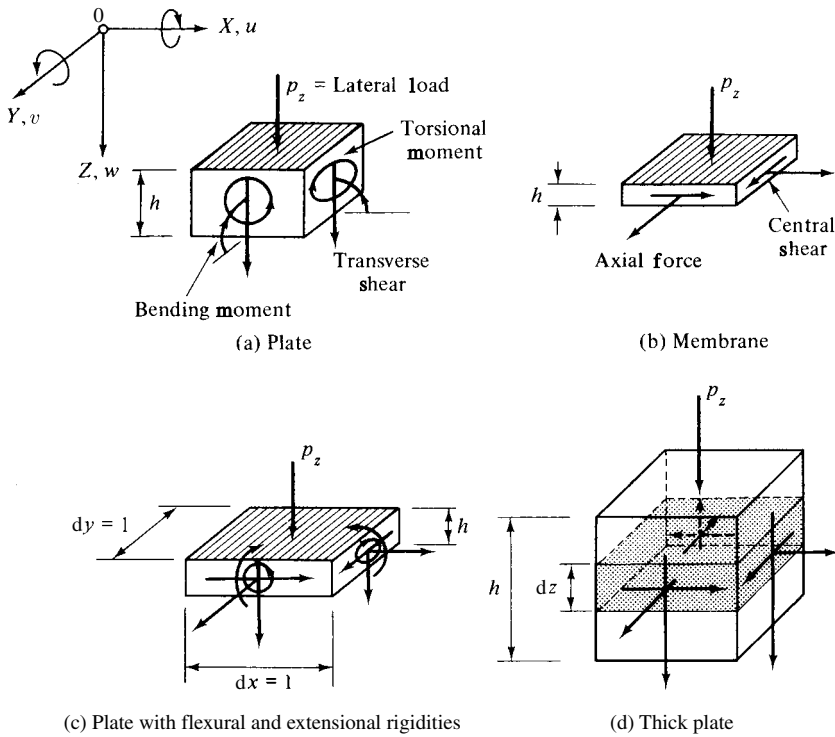


Figure 1.3 Internal forces in various types of plate elements.

plate theory, including pertinent solution techniques, is also treated in this book. Furthermore, since plates can have isotropic or orthotropic mechanical properties and can be composed of layered materials, these variations of plate theories are also presented.

Plate theories can also be grouped according to their stress-strain relationships. Linear-elastic plate theories are based on the assumption of a linear relationship between stress and strain according to the well-known Hooke's law, whereas non-linear elasticity, plasticity and viscoelasticity consider more complex stress-strain relationships. All these theories, with the exception of viscoelasticity, which treats dynamic conditions only, may be further subdivided into statics and dynamics of plates, depending on whether the external loads are of static or dynamic nature, as is done in the more elementary beam theories.

In treating all these various plate theories and the analytical or numerical solutions of the pertinent plate problems, emphasis is placed on the clear presentation of the fundamentals rather than on achieving exhaustive coverage of an inherently large body of subject matter. To encourage further study and research, several books are listed in the bibliographical references following this Introduction. In addition, there are also numerous published papers, each of which presents an in-depth study of a special field of plate analysis. Those that belong to the topics treated in this book are referred to and listed in the pertinent sections.

References to Introduction

- [I.1] ABRAMS, L. A., *Structural Design of Missiles and Spacecrafts*, McGraw-Hill Book Company, New York, 1962.
- [I.2] KOELLE, H. H., *Handbook of Astronautical Engineering*, McGraw-Hill Book Company, New York, 1961.
- [I.3] KUHN, P., *Stresses in Aircraft and Shell Structures*, McGraw-Hill Book Company, New York, 1956.
- [I.4] SECHLER, E. E., and DUNN, L. G., *Airplane Structural Analysis*, Dover Publications, New York, 1963.

General Reference Books on Plates

- [1] GIRKMAN, K., *Flächentragwerke*, 5th ed., Springer-Verlag, Vienna, 1959.
- [2] TIMOSHENKO, S., and WOINOWSKY-KRIEGER, S., *Theory of Plates and Shells*, 2nd ed., McGraw-Hill Book Company, New York, 1959.
- [3] NÁDAI, Á., *Die elastischen Platten*, Springer-Verlag, Berlin, 1925 and 1968.
- [4] GEIGER, H., and SCHEEL, K., *Handbuch der Physik*, Vol. 6, Springer-Verlag, Berlin, 1927.
- [5] BEYER, K., *Die Statik im Stahlbetonbau*, 2nd ed., Springer-Verlag, Berlin, 1956.
- [6] L'HERMITE, R., *Resistance des Matériaux*, Dunod, Paris, 1954.
- [7] VOLMIR, A. S., *Gibkie plastinki i obolochki (Flexible Plates and Shells)*, Gos. Izdvo Tekhniko-Teoret Lyt-ry, Moscow, 1956.[†]
- [8] SAWCZUK, A., and JAEGER, T., *Grenzfähigkeits-Theorie der Platten*, Springer-Verlag, Berlin, 1963.
- [9] YOUNG, W. C., *ROARK's Formulas for Stress and Strain*, 6th ed., McGraw-Hill Book Company, New York, 1989.
- [10] LAERMANN, K. H., *Experimentelle Plattenuntersuchungen*, W. Ernst und Sohn, Berlin, 1971.
- [11] WAH, T. (Ed.), *A Guide for the Analysis of Ship Structures*, U.S. Department of Commerce, OTS, P.B. 181168, Washington, D.C., 1960.
- [12] GALERKIN, B. G., *Thin Elastic Plates* (in Russian), Gostrojisdats, Leningrad-Moscow, 1933.
- [13] PAFKOVITCH, P. F., *Stroitel'naia mekhanika koroblia (Theory of Structure of Ships)*, Vol. 2, chapter on bending and buckling of plates), Gos. Izd. Sudostroitel. Promushl, Moscow, 1941.
- [14] PONOMAREV, S. D., et al., *Raschety na prochnost' v mashinostroenii (Stress Analysis in Machine Design)*, Mashgiz, Moscow, 1958.
- [15] HAMPE, E., *Statik Rotationssymmetrischer Flächentragwerke*, Vol. 1, VEB Verlag für Bauwesen, Berlin, 1963.
- [16] JAEGER, L. G., *Elementary Theory of Elastic Plates*, The Macmillan Company, New York, 1964.
- [17] HENKY, H., *Neues Verfahren in der Festigkeitslehre*, Oldenbourg, Munich, 1951.
- [18] MÁRKUS, G., *Körszimetrikus Szerkezetek Elmélete és Számítása (The Theory and Analysis of Rotational Symmetric Structures)*, Müszaki Könyvkiadó, Budapest, 1964.[‡]
- [19] MANSFIELD, E. H., *The Bending and Stretching of Plates*, 2nd ed., Cambridge University Press, Cambridge, 1989.
- [20] BITTNER, E., *Platten und Behälter*, Springer-Verlag, Vienna, 1965.
- [21] RABICH, R., "Statik der Platten, Scheiben, Schalen," in *Ingenieurtaschenbuch Bauwesen*, Vol. 1, Pfalz-Verlag, Basel, 1964, pp. 888–964.
- [22] JONES, L. L., and WOOD, R. H., *Yield Line Analysis of Slabs*, American Elsevier Publishing Company, New York, 1967.
- [23] STIGLAT, K., and WIPPEL, H., *Platten*, 3rd ed., Ernst & Sohn, Berlin, 1983.

[†] Available also in German translation, VEB Verlag für Bauwesen, Berlin, 1962.

[‡] Available also in German translation, Werner-Verlag, Düsseldorf, 1967.

- [24] MARGUERRE, K., and WOERNLE, H.-T., *Elastic Plates*, Ginn/Blaisdell, Waltham, Massachusetts, 1969.
- [25] DURGAR'YAN, S. M. (Ed.), Vsesoiuznaia konferentsiia po teorii plastin i obolochek (Theory of Shells and Plates), Proceeding of the 4th All-Union Conference on Shells and Plates at Erevan, Oct. 24–31, 1962, translated from Russian, National Aeronautics and Space Administration, NASA TT-F-341 Washington, D.C., 1966.
- [26] ANDERMANN, F., *Plaques rectangulaires chargées dans leur plan, analyse statique*, Dunod, Paris, 1969.
- [27] ULITSII, I. I., et al., *Zhelezobetonnye konstruksii (Reinforced Concrete Structures)*, Gos. Izd.-vo Techn. Lit-ry, Kiev, 1958.
- [28] LEISSA, A. W., *Vibration of Plates*, National Aeronautics and Space Administration, NASA-SP-160. Washington, D.C., 1969.
- [29] STIGLAT, K., and WIPPEL, H., "Massive Platten," in *Beton-Kalender 1973*, Vol. 1, W. Ernst & Sohn, Berlin, 1973, pp. 199–289.
- [30] Moscow Inzhenerno-stroitel'nyi Institut, Kafedra Stroitel'noi Mekhaniki, *Raschet plastin i obolochek (Design of Plates and Shells)*, Pod Obshchei Red. V. G. Rekach, Moscow, 1963.
- [31] KALMANOK, A. S., *Raschet plastinok; sprayochnoe posobie (Design of Plates; Reference Book)*, Gos. izd-vo lit-ry po stroitel'stvu, arkhitekture i stroit. materialam, Moscow, 1959.
- [32] VAINBERG, D. V., *Plastiny, diski, balki-stenki (Plates, Disks, Deep Beams; Strength, Stability and Vibration)*, Gos. izd-vo lit-ry po stroitel'stvu i arkhitekture, Kiev, 1959.
- [33] BULSON, P. S., *The Stability of Flat Plates*, American Elsevier Publication Company, New York, 1969.
- [34] DUNDOVÁ, V., et al., *Biegungstheorie der Sandwich-Platten*, Springer-Verlag, Vienna, 1970.
- [35] CUSENS, A. R., and PAMA, R. P., *Bridge Deck Analysis*, John Wiley & Sons, New York, 1975.
- [36] PANC, V., *Theories of Elastic Plates*, Noorhoff International Publishing, Leyden, The Netherlands, 1975.
- [37] FLORIN, G., *Slabs and Plates*, Trans. Tech. S. A., Aedermannsdorf, Switzerland, 1979.
- [38] HAMBLY, E. C., *Bridge Deck Behaviour*, Chapman & Hall, London, 1976.
- [39] AALAMI, B., and WILLIAMS, D. G., *Thin Plate Design for Transverse Loading*, John Wiley & Sons, New York, 1975.
- [40] CHANG, F.-V., *Elastic Thin Plates* (in Chinese), Science Press, Beijing, 1978.
- [41] CHIA, CH.-Y., *Nonlinear Analysis of Plates*, McGraw-Hill International Book, New York, 1980.
- [42] COURBON, J., *Plaques Minces Élastique*, Edition Eyrolles, Paris, 1980.
- [43] UGURAL, A. C., *Stresses in Plates and Shells*, McGraw-Hill Book Company, New York, 1981.
- [44] LOWE, P. G., *Basic Principles of Plate Theory*, Surrey University Press, London, 1982.
- [45] MÁRKUS, G., *Kreis- und Kreisringplatten unter periodischer Belastung*, Werner-Verlag, Düsseldorf, 1986.
- [46] HUSSEIN, R. M., *Composite Panels/Plates: Analysis and Design*, Technomic Publishing Company, Lancaster, Pennsylvania, 1986.
- [47] WHITNEY, J. M., *Structural Analysis of Laminated Anisotropic Plates*, Technomic Publishing Company, Lancaster, Pennsylvania, 1987.
- [48] REISMANN, H., *Elastic Plates: Theory and Application*, John Wiley & Sons, New York, 1988.
- [49] NEGRUTIU, R., *Elastic Analysis of Slab Structures*, M. Nijhoff, The Netherlands, 1988.
- [50] DING, D., *Calculations of Thin Slabs Following Elastic and Plastic Theories (in Chinese)*, Southeast University Press, Nanjing, 1991.
- [51] JAWAD, M. H., *Theory and Design of Plate and Shell Structures*, Chapman & Hall, London, 1994.
- [52] ALTENBACH, H., et al., *Ebene Flächentragwerke*, Springer-Verlag, Berlin, 1998.
- [53] UGURAL, A., *Stresses in Plates and Shells*, McGraw-Hill Book Company, New York, 1999.
- [54] REDDY, J. N., *Theory and Analysis of Elastic Plates*, Taylor and Francis, London, 1999.
- [55] DURBAN, D. (Ed.), *Advances in Mechanics of Plates and Shells*, Kluwer Academic Publishers, Dordrecht, The Netherlands, 2001.

//

Historical Background

Although the ancient Egyptians, Greeks and Romans already employed finely cut stone slabs in their monumental buildings in addition to the most widely used tombstones, there is a fundamental difference between these ancient applications of slabs and those of plates in modern engineering structures. That is, the ancient builders established the slab dimensions and load-carrying capacity by “rule of thumb” handed down from generation to generation, whereas nowadays engineers determine plate dimensions by applying various proven scientific methods.

The history of the evolution of scientific plate theories and pertinent solution techniques is quite fascinating. While the development of structural mechanics as a whole commenced with the investigation of static problems [II.1], the first analytical and experimental studies on plates were devoted almost exclusively to free vibrations.

The first mathematical approach to the membrane theory of very thin plates was formulated by L. Euler (1707–1783) in 1766. Euler solved the problems of free vibrations of rectangular, triangular and circular elastic membranes by using the analogy of two systems of stretched strings perpendicular to each other [II.2]. His student, Jacques Bernoulli (1759–1789), extended Euler’s analogy to plates by replacing the net of strings with a gridwork of beams [II.3] having only bending rigidity. Since the torsional resistance of the beams was not included in the so-obtained differential equation of plates, he found only general *resemblance* between his theory and experiments but no close agreement.

A real impetus to the research of plate vibrations, however, was given by the German physicist E. F. F. Chladni (1756–1827). In his book on acoustics [II.4], he described diverse experiments with vibrating plates. Chladni discovered various modes of free vibrations. In his experiments he used evenly distributed powder that formed regular patterns after introducing vibrations (Fig. II.1). The powder accumulated along the nodal lines, where no displacement occurred. In addition, he was able to determine the frequencies corresponding to these vibration patterns. Invited by the French Academy of Science in 1809, he demonstrated his experiments in Paris. Chladni’s presentation was also attended by Emperor Napoleon, who was duly impressed by his demonstration. Following Napoleon’s suggestion, the French Academy invited applications for a price essay dealing with the mathematical

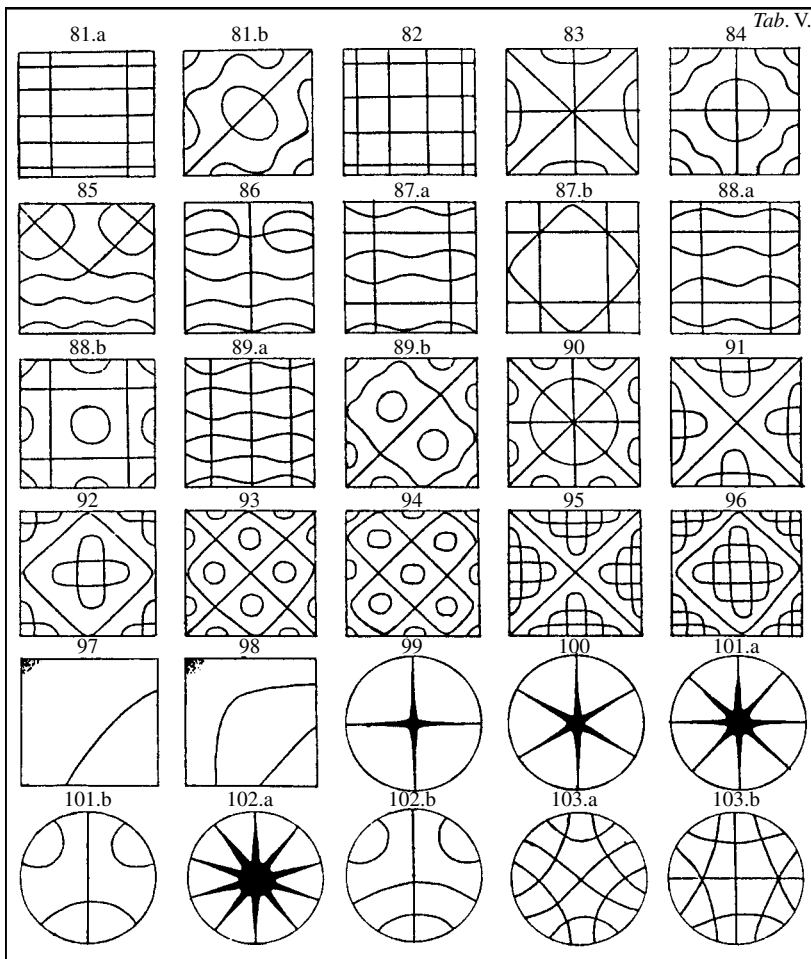


Figure II.1 Free vibration patterns of plates.

theory of plate vibrations substantiated by experimental verification of the theoretical results.[†] Since, at first, no papers were submitted, the delivery date had to be extended twice. Finally, in October 1811, on the closing day of the competition, the Academy received only one paper, entitled “Reserches sur la théorie des surfaces élastiques,” written by the mathematician Mlle. Germain (S. Germain, “L’état des sciences et des Lettres,” Paris, 1833).

Sophie Germain (1776–1831), whose portrait is engraved on a commemorating medallion shown in Fig. II.2, was indeed a colorful personality of her time. Since the development of the first differential equation of plate theory is closely connected with her, it appears to be justified to treat Germain’s person here in more detail.

[†] “Donnez la théorie des surfaces élastiques et la comparez à l’expérience.”



Figure II.2 Medallion showing Mlle. Germain's portrait.

Already as a young girl, Mlle. Germain began to study mathematics in all earnest to escape the psychological horrors created by the excesses of the French Revolution. She even corresponded with the greatest mathematicians of her time, including Lagrange, Gauss and Legendre, using the pseudonym La Blanc. Presumably, she used this pseudonym since female mathematicians were not taken seriously in her time. In 1806, when the French army occupied Braunschweig in Germany, where Gauss lived at the time, she personally intervened by General Pernetty on behalf of the city and Professor Gauss to eliminate the imposed fines.

In her first work on the theory of plate vibration, she used (following Euler's previous work on elastic curves) a strain energy approach. But in evaluating the strain energy using the virtual work technique, she made a mistake and obtained an erroneous differential equation for the free vibration of plate in the following form:

$$\frac{\partial^2 z}{\partial t^2} + \lambda^2 \left(\frac{\partial^6 z}{\partial x^4 \partial y^2} + \frac{\partial^6 z}{\partial x^2 \partial y^4} \right) = 0, \quad (\text{II.1})$$

where $z(x, y, t)$ represents the middle surface of the plate in motion expressed in an X, Y, Z Cartesian coordinate system, t is the time and λ^2 denotes a constant containing physical properties of the vibrating plate. This constant was, however, not clearly defined in her paper. Lagrange, who was one of the judges, noticed this mathematical error and corrected it. The so-obtained differential equation now correctly describing the free vibrations of plates reads

$$\frac{\partial^2 z}{\partial t^2} + k^2 \left(\frac{\partial^4 z}{\partial x^4} + 2 \frac{\partial^4 z}{\partial x^2 \partial y^2} + \frac{\partial^4 z}{\partial y^4} \right) = 0. \quad (\text{II.2})$$

Since the judges were not entirely satisfied with Germain's work, they proposed the subject again. In October 1813, Mlle. Germain entered the now-corrected equation (II.2) but left out the precise definition of the constant k^2 . Thus, she was again unsuccessful. Finally, at her third approach, she won the prize in 1816. But

the judges criticized anew her definition of the constant k^2 since she had thought that it contains the fourth power of the plate thickness instead of the correct value of h^3 . Although her original works are very hard to read and contain some dubious mathematical and physical reasonings, she must, nevertheless, be admired for her courage, devotion and persistence. The claim of priority for writing the first valid differential equation describing free plate vibrations belongs—without any doubt—to her!

Next, the mathematician L. D. Poisson (1781–1840) made an attempt to determine the correct value of the constant k^2 in the differential equation of plate vibration (II.2). By assuming, however, that the plate particles are located in the middle plane, he erroneously concluded that this constant is proportional to the square of the plate thickness and not to the cube. Later, in 1828, Poisson extended the use of Navier's equation[†] to lateral vibration of circular plates. The boundary conditions of the problem formulated by Poisson, however, are applicable only to thick plates.

Finally, the famous engineer and scientist L. Navier (1785–1836) can be credited with developing the first correct differential equation of plates subjected to distributed, static lateral loads $p_z(x, y)$. The task, which Navier set himself, was nothing less than the introduction of rigorous mathematical methods into structural analysis. In his brilliant lectures, which he held in Paris at the prestigious École Polytechnique on structural mechanics, Navier integrated for the first time the isolated discoveries of his predecessors and the results of his own investigations into a *unified system*. Consequently, the publication of his textbook *Leçons* [II.5] on this subject was an important milestone in the development of modern structural analysis.

Navier applied Bernoulli's hypotheses,[‡] which were already successfully used for treating bending of beams, adding to them the two-dimensional actions of strains and stresses, respectively. In his paper on this subject (published in 1823), he correctly defined the governing differential equation of plates subjected to static, lateral loads p_z as

$$D \left(\frac{\partial^4 w}{\partial x^4} + 2 \frac{\partial^4 w}{\partial x^2 \partial y^2} + \frac{\partial^4 w}{\partial y^4} \right) = p_z(x, y). \quad (\text{II.3})$$

In this equation D denotes the flexural rigidity of the plate, which is now proportional to the cube of the plate thickness, whereas $w(x, y)$ represents the deflected middle surface.

For the solution of certain boundary value problems of rectangular plates, Navier introduced a method that transforms the plate differential equation into algebraic equations. His approach is based on the use of double trigonometric series introduced by Fourier during the same decade. This so-called *forced* solution of the plate differential equation (II.3) yields mathematically correct results to various problems with relative ease provided that the boundary conditions of plates are simply supported. He also developed a valid differential equation for lateral buckling of plates subjected to uniformly distributed compressive forces along the boundary. He failed, however, to obtain a solution to this more difficult problem. Navier's further theoretical works established connections between *elasticity* and *hydrodynamics*, based on a “molecular hypothesis,” to which he was as firmly attached as Poisson [II.6].

[†] See below.

[‡] That is, normals to the midplane remain normal to the deflected middle plane.

The high-quality engineering education given at the École Polytechnique set the standards for other European countries during the nineteenth century. The German polytechniques, established soon after the Napoleonic wars, followed the very same plan as the French. The engineering training began with two years of courses in mathematics, mechanics and physics and concluded with pertinent design courses in the third and fourth years, respectively. Such a thorough training produced a succession of brilliant scientists in both countries engaged in developing the science of engineering in general and that of strength of materials in particular.

In Germany, publication of Kirchhoff's book entitled *Lectures on Mathematical Physics, Mechanics* (in German) [II.7] created a similar impact on engineering science as that of Navier's *Leçons* in France. Gustav R. Kirchhoff (1824–1887), whose picture is shown in Fig. II.3, developed the first *complete* theory of plate bending. In his earlier paper on this subject, published in 1850, he summarized, first, the previous works done by French scientists in this field, but he failed to mention Navier's above-discussed achievements. Based on Bernoulli's hypotheses for beams, Kirchhoff derived the same differential equation for plate bending (II.3) as Navier, however, using a different energy approach. His very important contribution to plate theory was the introduction of supplementary boundary forces. These "equivalent shear forces"[†] replace, in fact, the torsional moments at the plate boundaries. Consequently, all boundary conditions could now be stated in functions of displacements and their derivatives with respect to x or y . Furthermore, Kirchhoff is considered to be the founder of the extended plate theory, which takes into account the combined bending and stretching. In analyzing large deflection of plates, he found that nonlinear terms could no longer be neglected. His other significant contributions are the development of a frequency equation of plates and the introduction of *virtual displacement*



Figure II.3 Gustav R. Kirchhoff (1824–1887).

[†] *Kirchhoff'sche Ersatzkräfte* (Kirchhoff's supplementary forces).

methods for solution of various plate problems. Kirchhoff's book [II.7] was translated into French by Clebsch [II.8]. His translation contains numerous valuable comments by Saint-Venant, the most important being the extension of the differential equation of plate bending, which considers, in a mathematically correct manner, the combined action of bending and stretching.

Another famous textbook that deals with the abstract mathematical theory of plate bending is Love's principal work, *A Treatise on the Mathematical Theory of Elasticity* [II.9]. In addition to an extensive summary of the achievements made by his already mentioned predecessors, Love considerably extends the rigorous plate theory by applying solutions of two-dimensional problems of elasticity to plates.

Around the turn of the century, shipbuilders changed their construction methods by replacing wood with structural steel. This change in the structural material was extremely fruitful for the development of various plate theories. Russian scientists made a significant contribution to naval architecture by being the first to replace ancient shipbuilding traditions by mathematical theories of elasticity. Especially Krylov (1863–1945) [II.10] and his student Boobnov [II.11–II.13] contributed extensively to the theory of plates with flexural and extensional rigidities. Because of the existing language barrier, the Western world was slow to recognize these achievements and make use of them. It is to Timoshenko's credit that the attention of the Western scientists was gradually directed toward Russian research in the field of theory of elasticity. Among Timoshenko's numerous important contributions [2] are the solution of circular plates considering large deflections [II.14] and the formulation of elastic stability problems [II.15].

Föppl, in his book on engineering mechanics [II.16] first published in 1907, had already treated the nonlinear theory of plates. The final form of the differential equation of the large-deflection theory, however, was developed by the Hungarian scientist von Kármán [II.17], who in his later works also investigated the problem of effective width [II.18] and the postbuckling behavior of plates [II.19].

The book of another Hungarian engineer-scientist, Nádai [3], was among the first devoted exclusively to the theory of plates. In addition to analytical solutions of various important plate problems of the engineering practice, he also used the finite difference technique to obtain numerical results where the analytical methods failed. Westergaard [II.20] and Schleicher [II.21] investigated problems related to plates on elastic foundation. Prescott, in his book *Applied Elasticity* [II.22], introduced a more accurate theory for plate bending by considering the strains in the middle surface. The Polish scientist Huber investigated orthotropic plates [II.23] and solved circular plates subjected to nonsymmetrical distributed loads and edge moments.

The development of the modern aircraft industry provided another strong impetus toward more rigorous analytical investigations of various plate problems. Plates subjected to, for example, in-plane forces, postbuckling behavior and vibration problems (flutter) and stiffened plates were analyzed by many scientists. Of the numerous researchers whose activities fall between the two world wars, only Wagner, Levy, Bleich and Federhofer are mentioned here.

The most important assumption of Kirchhoff's plate theory is that normals to the middle surface remain normal to the deflected midplane and straight. Since this theory neglects the deformation caused by transverse shear, it would lead to considerable errors if applied to moderately thick plates. For such plates, Kirchhoff's classical theory underestimates deflections and overestimates frequencies and buckling loads. Reissner and Mindlin arrived at somewhat different theories for moderately thick

plates to eliminate the above-mentioned deficiency of the classical plate theory. The theory developed by Reissner [II.24] includes the effects of shear deformation and normal pressure by assuming uniform shear stress distribution through the thickness of the plate. Applying his theory, three instead of two boundary conditions must be satisfied on the edge. Of these three displacement boundary conditions, one involves deflection and the other two represent normal and tangential rotations, respectively. Mindlin [II.25] also improved the classical plate theory for plate vibrations by considering, in addition to the effect of shear deformation, that of the rotary inertia. In Mindlin's derivation displacements are treated as primary variables. It was necessary, however, to introduce a correction factor to account for the prediction of uniform shear stress distribution.

In addition to the analysis of moderately thick plates, Reissner's and Mindlin's plate theories received a great deal of attention in recent years for the formulation of reliable and efficient finite elements for thin plates. Since in both theories displacements and rotations are independent and slope continuity is not required, developments of finite elements are greatly facilitated. Direct application of these higher-order theories to thin-plate finite elements, however, often induced so-called shear locking behavior, which first had to be overcome before such elements could be used. To alleviate this undesirable effect, selective or reduced integration techniques were suggested, as discussed in the pertinent section of this book.

In the former Soviet Union the works of Volmir [7] and Panov are devoted mostly to solutions of nonlinear static plate problems, whereas Oniashvili investigated free and forced vibrations. Korenev's recent book [II.26] treats exclusively thermal stresses created by various types of thermal loadings on isotropic elastic plates.

A basically new approach to the static analysis of plates based on estimating the possible locations of fracture lines has been developed by Ingerslev. Johansen's so-called yield line analysis can be considered as the first important deviation from the classic theory of elasticity in the solution of transversely loaded plates. Hodge [II.27] and Reckling [II.28] extended the mathematical theory of plasticity to plates.

Plate-bending analysis is a classical field for the application of the *finite difference method*. This straightforward numerical approach yields very usable results for a large variety of specialized plate problems where analytical methods fail. The finite difference method is based on mathematical discretization of the plate continuum. In most cases, it merely requires an advanced scientific calculator to solve the resulting simultaneous equations. As mentioned previously, Nádai utilized this technique in 1925 for the solution of practical plate problems using "longhand" calculation! In the early 1940s, Southwell revived the finite difference method in England. Stüssi and Collatz further improved this important numerical technique, which is still regarded—despite the existence of the more powerful finite element—a practical tool for plate analysis.

The invention of electronic computers in the late 1940s exerted the most dramatic influence on the numerical analysis of plate structures. Although, in 1941, Hrennikoff had already developed an equivalent gridwork system for the static analysis of complex plate problems, his fundamental work [II.29] related to a physical discretization process of continua could not be fully utilized due to the lack of high-speed computers, since the resulting large number of coupled equations could not be solved by conventional means.

As already shown, structural plates have a multitude of applications in the building, aerospace, shipbuilding and automobile industries. Unfortunately, however, exact and approximate analytical solutions are limited to constant plate thickness and relatively

simple boundary and load conditions. What was most desired by these industries was a generally applicable, highly versatile and computerized procedure that could deal with all their complex “real-life” plate problems in a basically uniform fashion. In 1956 Turner, Clough, Martin and Topp [II.30]—using solely their creative engineering intuition and reasoning—introduced the *finite element method*, which became the most important tool for engineers and scientists to solve highly complex problems of elastic and nonelastic continua in an economical way. It is of interest to note that the finite element method was already invented in 1943 by the mathematician Courant, who in his paper on variational methods [II.31] discussed all the theoretical foundations of this extremely powerful numerical technique based, again, on physical discretization of the continuum. However, his work went, undetected for a decade mainly because of lack of proper communication between engineers and mathematicians. Numerous original contributions in this field are due to Argyris and Zienkiewicz. The majority of recently published scientific papers on plates is concerned with extension and refinement of the finite element method as related to various theoretical and practical problems in this field. Literally hundreds of papers are published every year dealing with all aspects of this very important numerical solution technique. Thus, it is impossible to mention here all additional contributors.

The *finite strip method*, introduced by Cheung [II.32], is a semianalytical procedure for plate structures with regular geometry, for example, rectangular or sectorial plates with various boundary conditions at the opposite edges. This method applies a series of beam eigenfunctions to express the variation of displacements in the longitudinal direction, whereas a finite element–type piecewise discretization is used in the transverse direction. A major advantage of this approach is a considerably smaller number of degrees of freedom. Consequently, the required storage and computer time are significantly reduced.

The formulation of elastic plate-bending problems via boundary *integral equation* furnishes a recent alternative to the finite element approach in form of the *boundary element method*, pioneered by Brebbia. If the external forces act only at the boundaries of a large undisturbed plate domain, the method may offer computational advantages by drastically reducing the number of unknowns in the resulting simultaneous equations, since merely the boundaries of the plate are discretized. In addition, the boundary element method yields higher accuracy than the finite element method, but only at some distance from the boundaries. Unfortunately, the resulting system matrix is unsymmetrical. Furthermore, since the mathematical requirements of the boundary element method are quite high, it is not as straightforward in its formulations and applications as the finite element method. In the numerical solution of specific types of plate problems, however, a combination of these two element methods may be advantageous.

References and Bibliography to Historical Background

- [II.1] TODHUNTER, I., and PEARSON, K., *A History of the Theory of Elasticity*, Vols. 1 and 2, Dover Publications, New York, 1960.
- [II.2] EULER, L., “De motu vibratorio tympanorum,” *Novi Commentari Acad. Petropolit.*, 10 (1766), 243–260.
- [II.3] BERNOULLI, J., “Essai théorique sur les vibrations de plaques élastiques rectangulaires et libres,” *Nova Acta Acad. Petropolit.*, 5 (1789), 197–219.
- [II.4] CHLADNI, E. F. F., *Die Akustik*, Breitkopf & Härtel, Leipzig, 1802.

- [II.5] NAVIER, L. M. H., *Résumé des Leçons de Mécanique*, first lecture notes published at the École Polytechnique, Paris, 1819.
- [II.6] DUGAS, R., *A History of Mechanics*, Dover Publications, New York, 1988.
- [II.7] KIRCHHOFF, G., *Vorlesungen über mathematische Physik*, Vol. 1, B. G. Teubner, Leipzig, 1876.
- [II.8] CLEBSCH, A., *Théorie de l'élasticité des corps solides, avec des notes entendues de Saint-Venant*, Dunod, Paris, 1883, pp. 687–706.
- [II.9] LOVE, A. E. H., *A Treatise on the Mathematical Theory of Elasticity*, 4th ed., Cambridge University Press, Cambridge, 1926.
- [II.10] KRYLOV, A., "On Stresses Experienced by a Ship in a Sea Way," *Trans. Inst. Naval Architects* (London), 40 (1898), 197–209.
- [II.11] BOOBNOV, I. G., "On the Stresses in Ships' Bottom Plating Due to Water Pressure," *Trans. Inst. Naval Architects* (London), 44 (1902), 15–47.
- [II.12] BOOBNOV, I. G., *Stoitel'nai mekhanika korablia (Theory of Structures of Ships)*, Vols. 1 and 2, St. Petersburg, 1912, 1914.
- [II.13] BOOBNOV, I. G., *Trudy po teorii plastin (Contributing Works to Plate Theory)*, Gos. Izd.-vo Techn.-Teoret. Lit.-ry, Moscow, 1953.
- [II.14] TIMOSHENKO, S. P., "On Large Deflections of Circular Plates" (in Russian), *Mem. Inst. Ways Commun.*, 89 (1915).
- [II.15] TIMOSHENKO, S. P., "Sur la stabilité des systèmes élastiques," *Ann. des ponts et chaussées*, 13, 496–566; 16, 73–132, 372–412 (1913).
- [II.16] FÖPPL, A., *Vorlesungen über technische Mechanik*, Vols. 3 and 5, 8th and 3rd eds., B. G. Teubner, Leipzig, 1923.
- [II.17] VON KÁRMÁN, TH., "Festigkeitsprobleme im Maschinenbau," *Encycl. der math. Wiss.*, 4 (1910), 348–351.
- [II.18] VON KÁRMÁN, TH., "Die mittragende Breite," in *Beiträge zur technischen Mechanik und technischen Physik*, August Föppl zum 70. Geburtstag am 24. Jannuar gewidmet, Springer-Verlag, Berlin, 1924, p. 114.
- [II.19] VON KÁRMÁN, TH., SECHLER, E. E., and DONNEL, L. H., "The Strength of Thin Plates in Compression," *Trans. ASME*, 54 (1932), 53–57.
- [II.20] WESTERGAARD, H. M., "On the Analysis of Plates on Elastic Supports ..." (in Danish), *Ingeniøren*, 32, No. 42 (1923), 513.
- [II.21] SCHLEICHER, F., *Kreisplatten auf elastischer Unterlage*, Springer-Verlag, Berlin, 1926.
- [II.22] PRESCOTT, J., *Applied Elasticity*, Longmans, Green and Company, London, 1924.
- [II.23] HUBER, M. T., *Teoria sprężystości, Théorie de l'élasticité*, Nakl. Polskiej Akademii Umiejętności, Krakow, 1948–1950, pp. 166–190.
- [II.24] REISSNER, E., "The Effect of Transverse Shear Deformation on the Bending of Elastic Plates," *J. Appl. Mech.*, 12 (1954), A69–A77.
- [II.25] MINDLIN, R. D., "Influence of Rotatory Inertia and Shear on Flexural Motions of Isotropic Elastic Plates," *J. Appl. Mech.*, 18 (1951), 31–38.
- [II.26] KORENEV, B. G., *Problems in the Theory of Thermal Conductivity and Thermoelasticity and Their Solutions with Bessel Functions*, (in Russian), Main Publisher of Mathematical Physics, Moscow, 1980.
- [II.27] HODGE, PH. G., *Limit Analysis of Rotational Symmetric Plates and Shells*, Prentice-Hall, Englewood Cliffs, New Jersey, 1963.
- [II.28] RECKLING, K.-A., *Plastizitätstheorie und ihre Anwendung auf Festigkeitsprobleme*, Springer-Verlag, Berlin, 1967.
- [II.29] HRENNIKOFF, A., "Solution of Problems of Elasticity by Framework Method," *J. Appl. Mech.*, 8 (1941), A169–A175.
- [II.30] TURNER, M. J. et al., "Stiffness and Deflection Analysis of Complex Structures," *J. Aeronaut. Sci.*, 23 (1956), 805–823.
- [II.31] COURANT, R., "Variational Methods for the Solution of Problems of Equilibrium and Vibration," *Bull. Am. Math. Soc.*, 49 (1943), 1–23.
- [II.32] CHEUNG, Y. K., *Finite Strip Method in Structural Analysis*, Pergamon Press, Oxford, 1976.

- [II.33] PANNEL, J. P. M., *An Illustrated History of Civil Engineering*, Frederick Ungar Publishing Company, New York, 1965.
- [II.34] STAUB, H., *A History of Civil Engineering*, MIT Press, Cambridge, Massachusetts, 1964.
- [II.35] BURSTALL, A. F., *A History of Mechanical Engineering*, MIT Press, Cambridge, Massachusetts, 1965.
- [II.36] TRUESDELL, C., *Essays in the History of Mechanics*, Springer-Verlag, Berlin, 1968.
- [II.37] TIMOSHENKO, S., *History of Strength of Materials*, McGraw-Hill Book Company, New York, 1953.
- [II.38] BENVENUTO, E., *An Introduction to the History of Structural Mechanics*, Springer-Verlag, Berlin, 1990.

Part I

Plate Theories and Analytical Solutions of Static, Linear-Elastic Plate Problems

1

Elastic Plate Theories and Their Governing Differential Equations

1.1 Classical Small-Deflection Theory of Thin Plates

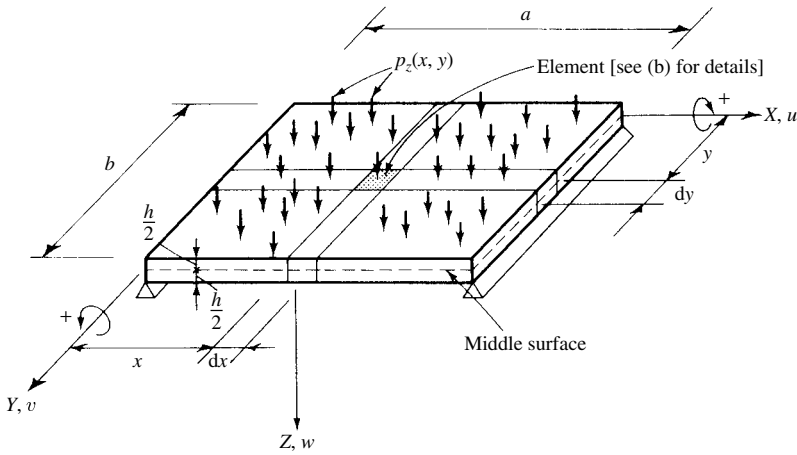
A mathematically exact stress analysis of a thin plate—subjected to loads acting normal to its surface—requires solution of the differential equations of three-dimensional elasticity [1.1.1]. In most cases, however, such an approach would encounter insurmountable mathematical difficulties. Yet, for the vast majority of technical applications Kirchhoff's classical theory of thin plates[†] yields sufficiently accurate results without the need of carrying out a full three-dimensional stress analysis. Consequently, classical plate theory occupies a unique position on this subject. It is formulated in terms of transverse deflections $w(x, y)$ for which the governing differential equation is of fourth order, requiring only two boundary conditions to be satisfied at each edge. The simplifications used in the derivation of the plate equation are based on the following assumptions:

1. The material is homogeneous, isotropic and linear elastic; that is, it follows Hooke's law.
2. The plate is initially flat.
3. The middle surface[‡] of the plate remains unstrained during bending.
4. The *constant* thickness of the plate, h , is small compared to its other dimensions; that is, the smallest lateral dimension of the plate is at least 10 times larger than its thickness.

[†] As already mentioned under Historical Background, other contributors to classical plate theory include Bernoulli, Navier, Saint-Venant and Lagrange.

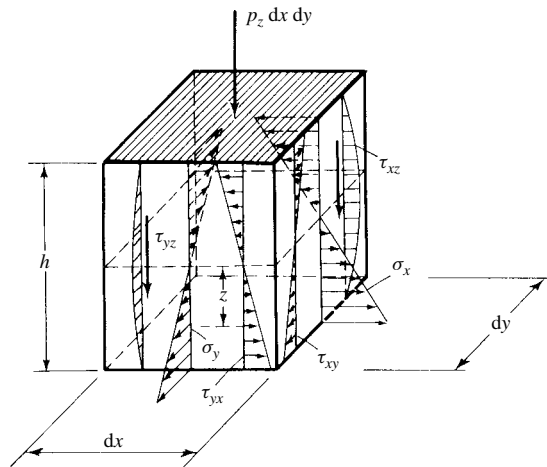
[‡] Equivalent to the neutral axis in elementary beam theory.

5. The transverse deflections $w(x, y)$ are small compared to the plate thickness. A maximum deflection of one-tenth of the thickness is considered the limit of the small-deflection theory.
6. Slopes of the deflected middle surface are small compared to unity.
7. Sections taken normal to the middle surface before deformation remain plane and normal to the deflected middle surface. Consequently, shear deformations are neglected. This assumption represents an extension of Bernoulli's hypothesis for beams to plates.
8. The normal stress σ_z in the direction transverse to the plate surface can be neglected.



(a)

Laterally loaded rectangular plate



(b)

Stress components on plate element

Figure 1.1.1 Laterally loaded rectangular plate.

With the help of these assumptions, the originally three-dimensional stress problems of elasticity are reduced to two-dimensional problems of plates. Many of these assumptions are familiar to the reader since they have their equivalent counterparts in elementary beam theory. In addition to more exact three-dimensional stress analysis, extensive small- and large-scale tests have proved the validity of these simplifying assumptions. Unless otherwise stated, Kirchhoff's classical plate theory is employed throughout this book.

For rectangular plates the use of a rectangular Cartesian coordinate system is most convenient (Fig. 1.1.1). The external and internal forces, stresses and deflection components u , v and w are considered positive when they point toward the positive direction of the coordinate axes X , Y and Z . In general engineering practice, positive moments produce tension in the fibers located at the bottom part of the pertinent section. This sign convention is also maintained for plates.

Considering an elemental parallelepiped cut out of the plate, as shown in Fig. 1.1.2, we assign positive internal forces and moments to the near faces of the plate element.

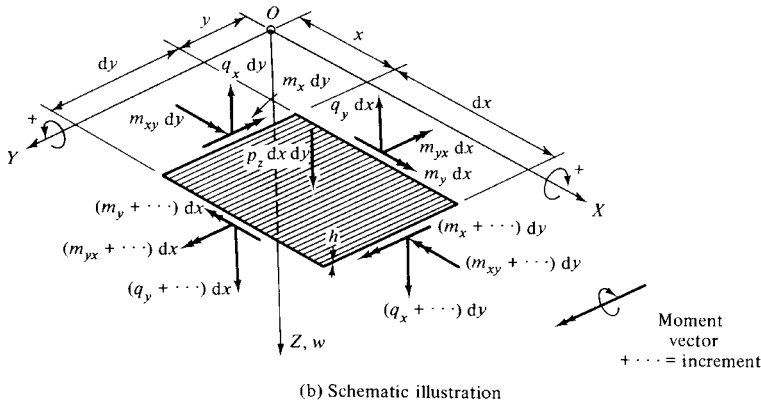
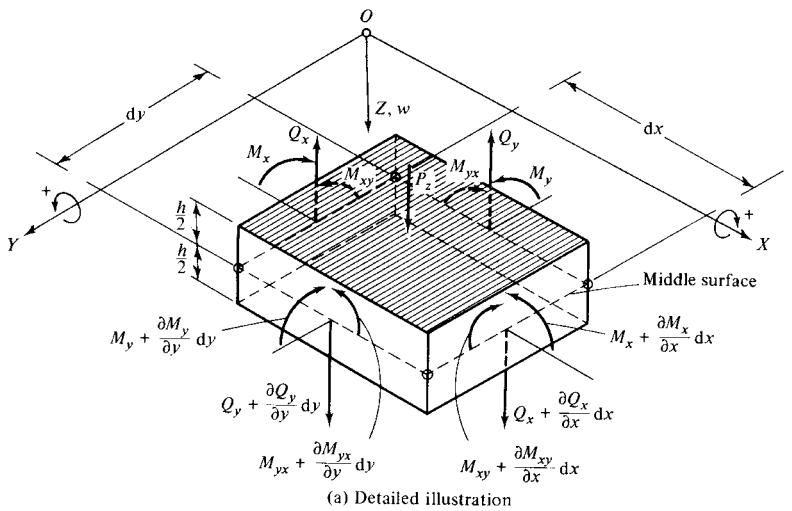


Figure 1.1.2 External and internal forces on the element of the middle surface.

To satisfy the equilibrium of the element, negative internal forces and moments must act on its far sides. The first subscript of the internal forces refers to the direction of the surface normal pertinent to the section on which the force acts. The subscripts of the internal bending and of the twisting moments refer to the stresses of which they are produced. Thus, the bending moment M_X , for instance, is caused by σ_X normal stresses and rotates around the Y axis. These notations are standard in the theory of elasticity but contradict those used in contemporary numerical methods, where M_X refers to a moment rotating around the X axis, as explained in the sections dealing with the *finite element* and *gridwork* methods. Finally, we should point out that the second subscript of the shear stresses (Fig. 1.1.1b) indicates the direction in which their vectors point.

Reference and Bibliography

[1.1.1] FLÜGGE, W. (Ed.), *Handbook of Engineering Mechanics*, McGraw-Hill Book Company, New York, 1962.

1.2 Plate Equation in Cartesian Coordinate System

In deriving the governing differential equation for thin plates, we employ, for pedagogical reasons, a similar method as used in elementary beam theory. Other possibilities, such as utilizing a variational approach or even simplifications of the differential equations of three-dimensional elasticity, are not considered here.

a. Equilibrium of Plate Element. Assuming that the plate is subjected to lateral forces only, from the six fundamental equilibrium equations, the following three can be used:

$$\sum M_x \doteq 0, \quad M_y \doteq 0 \quad \text{and} \quad \sum P_z \doteq 0. \quad (1.2.1)$$

The behavior of the plate is in many respects analogous to that of a two-dimensional gridwork of beams. Thus the external load P_z is carried by Q_x and Q_y transverse shear forces and by M_x and M_y bending moments. The significant deviation from the two-dimensional gridwork action of beams is the presence of the twisting moments M_{xy} and M_{yx} (Fig. 1.1.2a). In the theory of plates it is customary to deal with internal forces and moments per unit length of the middle surface (Fig. 1.1.2b). To distinguish these internal forces from the above-mentioned resultants, the notations $q_x, q_y, m_x, m_y, m_{xy}$ and m_{yx} are introduced.

The procedure involved in setting up the differential equation of equilibrium is as follows:

1. Select a convenient coordinate system and draw a sketch of a plate element (Fig. 1.1.2b).
2. Show all external and internal forces acting on the element.
3. Assign positive internal forces with increments ($q_x + \dots, q_y + \dots$, etc.) to the near sides.
4. Assign negative internal forces to the far sides.

5. Express the increments by a truncated Taylor's series[†] in the form

$$q_x + dq_x = q_x + \frac{\partial q_x}{\partial x} dx, \quad m_y + dm_y = m_y + \frac{\partial m_y}{\partial y} dy \quad \text{etc.} \quad (1.2.2)$$

6. Express the equilibrium of the internal and external forces acting on the element.

Let us express, for instance, that the sum of the moments of all forces around the Y axis is zero (Fig. 1.1.2b). This gives

$$\begin{aligned} \left(m_x + \frac{\partial m_x}{\partial x} dx \right) dy - m_x dy + \left(m_{yx} + \frac{\partial m_{yx}}{\partial y} dy \right) dx - m_{yx} dx \\ - \left(q_x + \frac{\partial q_x}{\partial x} dx \right) dy \frac{dx}{2} - q_x dy \frac{dx}{2} = 0. \end{aligned} \quad (1.2.3)$$

After simplification, we neglect the term containing $\frac{1}{2}(\partial q_x / \partial x)(dx)^2 dy$ since it is a small quantity of higher-order. Thus Eq. (1.2.3) becomes

$$\frac{\partial m_x}{\partial x} dx dy + \frac{\partial m_{yx}}{\partial y} dy dx - q_x dx dy = 0, \quad (1.2.4)$$

and, after division by $dx dy$, we obtain

$$\frac{\partial m_x}{\partial x} + \frac{\partial m_{yx}}{\partial y} = q_x. \quad (1.2.5)$$

In a similar manner the sum of the moments around the X axis gives

$$\frac{\partial m_y}{\partial y} + \frac{\partial m_{xy}}{\partial x} = q_y. \quad (1.2.6)$$

The summation of all forces in the Z direction yields the third equilibrium equation:

$$\frac{\partial q_x}{\partial x} dx dy + \frac{\partial q_y}{\partial y} dx dy + p_z dx dy = 0, \quad (1.2.7)$$

which, after division by $dx dy$, becomes

$$\frac{\partial q_x}{\partial x} + \frac{\partial q_y}{\partial y} = -p_z. \quad (1.2.8)$$

Substituting Eqs. (1.2.5) and (1.2.6) into (1.2.8) and observing that $m_{xy} = m_{yx}$, we obtain

$$\frac{\partial^2 m_x}{\partial x^2} + 2 \frac{\partial^2 m_{xy}}{\partial x \partial y} + \frac{\partial^2 m_y}{\partial y^2} = -p_z(x, y). \quad (1.2.9)$$

[†] $f(a + h) = f(a) + (h/1!)f'(a) + (h^2/2!)f''(a) + \dots + (h^n/n!)f^{(n)}(a) + \dots$

The bending and twisting moments in Eq. (1.2.9) depend on the strains, and the strains are functions of the displacement components (u, v, w). Thus, in the next steps, relations between the internal moments and displacement components are sought.

b. Relation between Stress, Strain and Displacements. The assumption that the material is elastic permits the use of the two-dimensional Hooke's law,

$$\sigma_x = E\varepsilon_x + \nu\sigma_y \quad (1.2.10a)$$

and

$$\sigma_y = E\varepsilon_y + \nu\sigma_x, \quad (1.2.10b)$$

which relates stress and strain in a plate element. Substituting (1.2.10b) into (1.2.10a), we obtain

$$\sigma_x = \frac{E}{1 - \nu^2}(\varepsilon_x + \nu\varepsilon_y). \quad (1.2.11)$$

In a similar manner

$$\sigma_y = \frac{E}{1 - \nu^2}(\varepsilon_y + \nu\varepsilon_x) \quad (1.2.12)$$

can be derived.

The torsional moments m_{xy} and m_{yx} produce in-plane shear stresses τ_{xy} and τ_{yx} (Fig. 1.2.1), which are again related to the shear strain γ by the pertinent Hookean relationship, giving

$$\tau_{xy} = G\gamma_{xy} = \frac{E}{2(1 + \nu)}\gamma_{xy} = \tau_{yx}. \quad (1.2.13)$$

Next, we consider the geometry of the deflected plate to express the strains in terms of the displacement coefficients. Taking a section at a constant y , as shown in

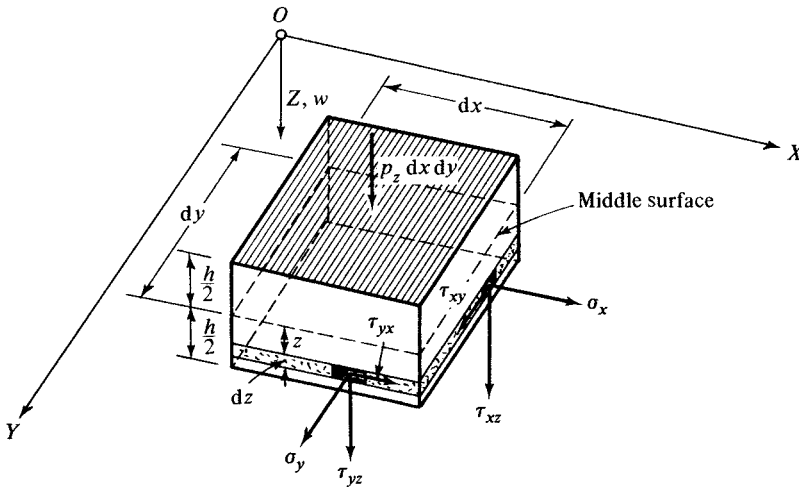


Figure 1.2.1 Stresses on a plate element.

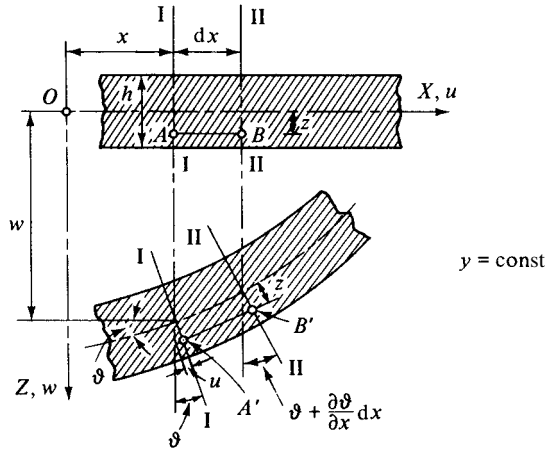


Figure 1.2.2 Section before and after deflection.

Fig. 1.2.2, we compare the section before and after deflection. Using assumptions 6 and 7, introduced earlier in sec. 1.1 we express the angle of rotation of lines I–I and II–II by

$$\vartheta = -\frac{\partial w}{\partial x} \quad \text{and} \quad \vartheta + \dots = \vartheta + \frac{\partial \vartheta}{\partial x} dx, \quad (1.2.14)$$

respectively. After the deformation the length \overline{AB} of a fiber, located at z distance from the middle surface, becomes $\overline{A'B'}$ (Fig. 1.2.2). Using the definition of strain, we can write

$$\varepsilon_x = \frac{\Delta dx}{dx} = \frac{\overline{A'B'} - \overline{AB}}{\overline{AB}} = \frac{[dx + z(\partial \vartheta / \partial x) dx] - dx}{dx} = z \frac{\partial \vartheta}{\partial x}. \quad (1.2.15)$$

Substituting into this expression the first of the equations (1.2.14), we obtain

$$\varepsilon_x = -z \frac{\partial^2 w}{\partial x^2}. \quad (1.2.16)$$

A similar reasoning yields ε_y , the strain due to normal stresses in the Y direction; thus

$$\varepsilon_y = -z \frac{\partial^2 w}{\partial y^2}. \quad (1.2.17)$$

Let us now determine the angular distortion $\gamma_{xy} = \gamma' + \gamma''$ by comparing an $ABCD$ rectangular parallelogram (Fig. 1.2.3), located at a constant distance z from the middle surface, by its deformed shape $A'B'C'D'$ on the deflected plate surface. From the two small triangles in Fig. 1.2.3, it is evident that

$$\gamma' = \frac{\partial v}{\partial x} \quad \text{and} \quad \gamma'' = \frac{\partial u}{\partial y}; \quad (1.2.18)$$

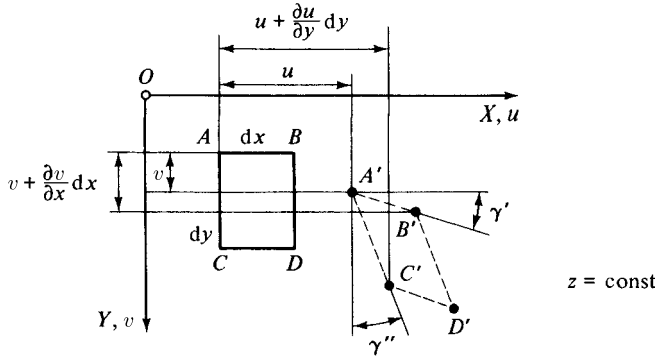


Figure 1.2.3 Angular distortion.

but from Fig. 1.2.2

$$u = z\vartheta = -z \frac{\partial w}{\partial x}; \quad (1.2.19)$$

similarly,

$$v = -z \frac{\partial w}{\partial y},$$

consequently,

$$\gamma_{xy} = \gamma' + \gamma'' = -2z \frac{\partial^2 w}{\partial x \partial y}. \quad (1.2.20)$$

The curvature changes of the deflected middle surface are defined by

$$\kappa_x = -\frac{\partial^2 w}{\partial x^2}, \quad \kappa_y = -\frac{\partial^2 w}{\partial y^2} \quad \text{and} \quad \chi = -\frac{\partial^2 w}{\partial x \partial y}, \quad (1.2.21)$$

where χ represents the *warping* of the plate.

c. Internal Forces Expressed in Terms of w . The stress components σ_x and σ_y (Fig. 1.2.1) produce bending moments in the plate element in a manner similar to that in elementary beam theory. Thus, by integration of the normal stress components, the bending moments, acting on the plate element, are obtained:

$$m_x = \int_{-(h/2)}^{+(h/2)} \sigma_x z \, dz \quad \text{and} \quad m_y = \int_{-(h/2)}^{+(h/2)} \sigma_y z \, dz. \quad (1.2.22)$$

Similarly, the twisting moments produced by the shear stresses $\tau = \tau_{xy} = \tau_{yx}$ can be calculated from

$$m_{xy} = \int_{-(h/2)}^{+(h/2)} \tau_{xy} z \, dz \quad \text{and} \quad m_{yx} = \int_{-(h/2)}^{+(h/2)} \tau_{yx} z \, dz; \quad (1.2.23)$$

but $\tau_{xy} = \tau_{yx} = \tau$, and therefore $m_{xy} = m_{yx}$.

If we substitute Eqs. (1.2.16) and (1.2.17) into (1.2.11) and (1.2.12), the normal stresses σ_x and σ_y are expressed in terms of the lateral deflection w . Thus, we can write

$$\sigma_x = -\frac{Ez}{1-\nu^2} \left(\frac{\partial^2 w}{\partial x^2} + \nu \frac{\partial^2 w}{\partial y^2} \right) \quad (1.2.24)$$

and

$$\sigma_y = -\frac{Ez}{1-\nu^2} \left(\frac{\partial^2 w}{\partial y^2} + \nu \frac{\partial^2 w}{\partial x^2} \right). \quad (1.2.25)$$

Integration of Eqs. (1.2.22), after substitution of the above expressions for σ_x and σ_y , gives

$$\begin{aligned} m_x &= -\frac{Eh^3}{12(1-\nu^2)} \left(\frac{\partial^2 w}{\partial x^2} + \nu \frac{\partial^2 w}{\partial y^2} \right) \\ &= -D \left(\frac{\partial^2 w}{\partial x^2} + \nu \frac{\partial^2 w}{\partial y^2} \right) = D(\kappa_x + \nu\kappa_y) \end{aligned} \quad (1.2.26)$$

and

$$m_y = -D \left(\frac{\partial^2 w}{\partial y^2} + \nu \frac{\partial^2 w}{\partial x^2} \right) = D(\kappa_y + \nu\kappa_x), \quad (1.2.27)$$

where

$$D = \frac{Eh^3}{12(1-\nu^2)} \quad (1.2.28)$$

represents the bending or *flexural rigidity* of the plate. In a similar manner, the expression of twisting moment in terms of the lateral deflections is obtained:

$$\begin{aligned} m_{xy} = m_{yx} &= \int_{-(h/2)}^{+(h/2)} \tau z \, dz = -2G \int_{-(h/2)}^{+(h/2)} \frac{\partial^2 w}{\partial x \partial y} z^2 \, dz \\ &= -(1-\nu)D \frac{\partial^2 w}{\partial x \partial y} = D(1-\nu)\chi. \end{aligned} \quad (1.2.29)$$

The substitution of Eqs. (1.2.26), (1.2.27) and (1.2.29) into Eq. (1.2.9) yields the *governing differential equation* of the plate subjected to distributed lateral loads,

$$\frac{\partial^4 w}{\partial x^4} + 2 \frac{\partial^4 w}{\partial x^2 \partial y^2} + \frac{\partial^4 w}{\partial y^4} = \frac{p_z(x, y)}{D}, \quad (1.2.30)$$

or using the two-dimensional Laplacian operator

$$\nabla^2(\bullet) = \frac{\partial^2(\bullet)}{\partial x^2} + \frac{\partial^2(\bullet)}{\partial y^2} \quad (1.2.31)$$

we can write Eq. (1.2.30) in a more condensed form,

$$D \nabla^2 \nabla^2 w(x, y) = p_z(x, y). \quad (1.2.32)$$

This equation is a fourth-order, nonhomogeneous, partial differential equation of the elliptic-type with constant coefficients, often called a *nonhomogeneous biharmonic equation*. Equation (1.2.30) is *linear* since the derivatives of $w(x, y)$ do not have exponents higher than 1.

We would like to also express the transverse shear forces in terms of the lateral deflections. The substitution of Eqs. (1.2.26), (1.2.27) and (1.2.29) into Eqs. (1.2.5) and (1.2.6) gives

$$q_x = \frac{\partial m_x}{\partial x} + \frac{\partial m_{yx}}{\partial y} = -D \frac{\partial}{\partial x} \left(\frac{\partial^2 w}{\partial x^2} + \frac{\partial^2 w}{\partial y^2} \right) = -D \frac{\partial}{\partial x} \nabla^2 w \quad (1.2.33a)$$

and

$$q_y = \frac{\partial m_y}{\partial y} + \frac{\partial m_{xy}}{\partial x} = -D \frac{\partial}{\partial y} \left(\frac{\partial^2 w}{\partial x^2} + \frac{\partial^2 w}{\partial y^2} \right) = -D \frac{\partial}{\partial y} \nabla^2 w. \quad (1.2.33b)$$

The plate problem is considered solved if a suitable expression for the deflected plate surface $w(x, y)$ is found that simultaneously satisfies the differential equation of equilibrium (1.2.30) and the boundary conditions. Consequently, it can be stated that the solution of plate problems is a specific case of a boundary value problem of mathematical physics.

In the X, Y coordinate system, the matrix of internal moments at a given point can be written as

$$\mathbf{M} = \begin{bmatrix} m_x & m_{xy} \\ m_{yx} & m_y \end{bmatrix}, \quad (1.2.34)$$

where $m_{xy} = m_{yx}$. If we desire to obtain these moments on any other transverse plane (Fig. 1.2.4), we should employ a coordinate transformation from the X, Y to the X', Y' coordinate system. Thus

$$\mathbf{M}' = \begin{bmatrix} m'_x & m'_{xy} \\ m'_{yx} & m'_y \end{bmatrix} = \mathbf{R} \mathbf{M} \mathbf{R}^T, \quad (1.2.35)$$

where \mathbf{R} represents the rotational matrix

$$\mathbf{R} = \begin{bmatrix} \cos \phi & \sin \phi \\ -\sin \phi & \cos \phi \end{bmatrix} = \begin{bmatrix} C & S \\ -S & C \end{bmatrix}. \quad (1.2.36)$$

Thus, we obtain

$$\mathbf{M}' = \begin{bmatrix} m_x C^2 + m_y S^2 + 2m_{xy} SC & m_{xy}(C^2 - S^2) + (m_y - m_x)SC \\ \text{symmetric} & m_x S^2 + m_y C^2 - 2m_{xy} SC \end{bmatrix}. \quad (1.2.37)$$

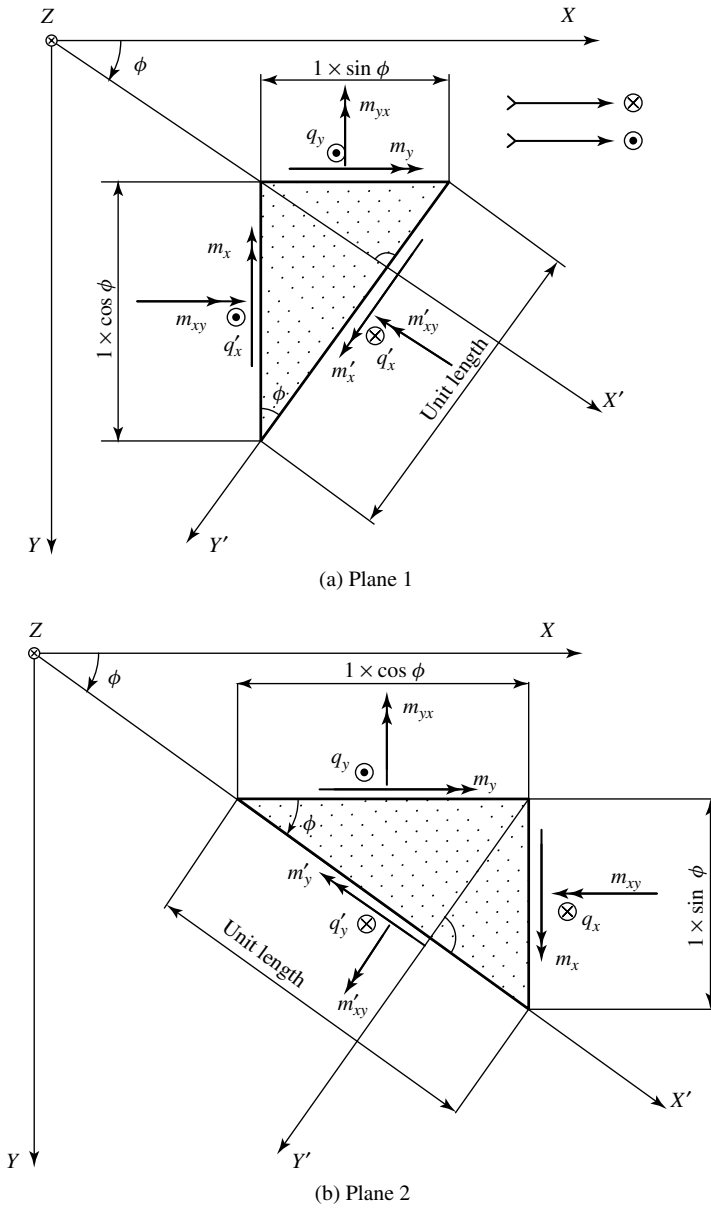


Figure 1.2.4 Internal forces on arbitrary transverse planes.

Another approach would be to consider the equilibrium of a small triangular element cut out from the plate at the point in question (Fig. 1.2.4). In this way, we obtain from Fig. 1.2.4a, for instance, the transverse shear force

$$q'_x = q_x \cos \phi + q_y \sin \phi. \quad (1.2.38)$$

The *principal stresses* can be calculated from

$$m_{1,2} = \frac{1}{2}(m_x + m_y) \pm \frac{1}{2}\sqrt{(m_x - m_y)^2 + 4m_{xy}^2}, \quad (1.2.39)$$

where $m_1 > m_2$. The *principal directions* for \mathbf{M} are

$$\tan 2\phi = \frac{2m_{xy}}{m_x - m_y}. \quad (1.2.40)$$

Since this equation can give the angle for either m_1 or m_2 , the use of the following expression is recommended:

$$\tan \phi_1 = \frac{2m_{xy}}{(m_x - m_y) + \sqrt{(m_x - m_y)^2 + 4m_{xy}^2}}, \quad (1.2.41)$$

where ϕ_1 uniquely represents the angle pertinent to m_1 .

Finally, it should be mentioned that occasionally[†] it might be advantageous to introduce the so-called *moment-sum* in the form.

$$\mathfrak{M} = \frac{1}{1 + \nu}(m_x + m_y) = -D \nabla^2 w. \quad (1.2.42)$$

The right-hand side of this equation is obtained from (1.2.26) and (1.2.27). The introduction of this moment-sum permits us to split the governing fourth-order differential equation of the plate into two second-order differential equations. Thus, we obtain

$$\nabla^2 \mathfrak{M} = -p_z \quad (1.2.43a)$$

and

$$\nabla^2 w = -\frac{\mathfrak{M}}{D}. \quad (1.2.43b)$$

Provided that the boundary conditions for \mathfrak{M} are known, we may solve the first differential equation. Then utilizing \mathfrak{M} , the lateral deflection $w(x, y)$ can be determined from Eq. (1.2.43b). It is interesting to note that Eqs. (1.2.43a) and (1.2.43b) have a form similar to that of the differential equation of the membrane.

Summary. It has been shown that in setting up the differential equation of an elastic plate the following basic steps are required:

1. The expression of equilibrium of external and internal forces acting on a plate element.
2. Linking strains and stresses by Hooke's law.
3. The use of certain geometrical relationships, obtainable from the shape of the deflected surface, which enables us to express strains in terms of displacement components.

[†] A simply supported boundary condition is one of these special cases.

4. The expression of internal forces in terms of stresses and strains and finally in terms of displacement components.

Plate problems, like all two- and three-dimensional stress problems of elasticity, are *internally statically* indeterminate; that is, the three equations of equilibrium [(1.2.5), (1.2.6) and (1.2.8)] contain five unknowns: three moments and two shear forces. To be able to obtain a solution, additional equations of elasticity have been utilized. In this way the governing differential equation of laterally loaded plates [Eq. (1.2.30)], which contains only one unknown (w), is derived.

References and Bibliography

- [1.2.1] KIRCHHOFF, G., *Vorlesungen über mathematische Physik*, Vol. 1, B. G. Teubner, Leipzig, 1876.
- [1.2.2] NÁDAI, Á., *Die elastischen Platten*, Springer-Verlag, Berlin, 1925.
- [1.2.3] TIMOSHENKO, S., and WOINOWSKY-KRIEGER, S., *Theory of Plates and Shells*, 2nd ed., McGraw-Hill Book Company, New York, 1959.
- [1.2.4] GIRKMANN, K., *Flächentragwerke*, 6th ed., Springer-Verlag, Vienna, 1963.
- [1.2.5] GOULD, P. L., *Analysis of Plates and Shells*, Springer-Verlag, Berlin, 1987.

1.3 Boundary Conditions of Kirchhoff's Plate Theory

An exact solution of the governing plate equation (1.2.30) must simultaneously satisfy the differential equation and the boundary conditions of any given plate problem. Since Eq. (1.2.30) is a fourth-order differential equation, two boundary conditions, either for the displacements or for the internal forces, are required at each boundary. In the bending theory of plates, three internal force components are to be considered: bending moment, torsional moment and transverse shear. Similarly, the displacement components to be used in formulating the boundary conditions are lateral deflections and slope. Boundary conditions of plates in bending can be generally classified as one of the following.

a. Geometrical Boundary Conditions. Certain geometrical conditions provided by the magnitude of displacements (translation and rotation) can be used to formulate the boundary conditions in mathematical form. At fixed edges (Fig. 1.3.1a), for instance, the deflection and the slope of the deflected plate surface are zero. Thus we can write

$$(w)_x = 0, \quad \left(\frac{\partial w}{\partial x} \right)_x = 0 \quad \text{at } x = 0, a,$$

(1.3.1)

and

$$(w)_y = 0, \quad \left(\frac{\partial w}{\partial y} \right)_y = 0 \quad \text{at } y = 0, b.$$

Such boundary conditions are called *geometrical*.

b. Statical Boundary Conditions (Free-Edges). For *statical* boundary conditions the edge forces provide the required mathematical expressions. At an unloaded free

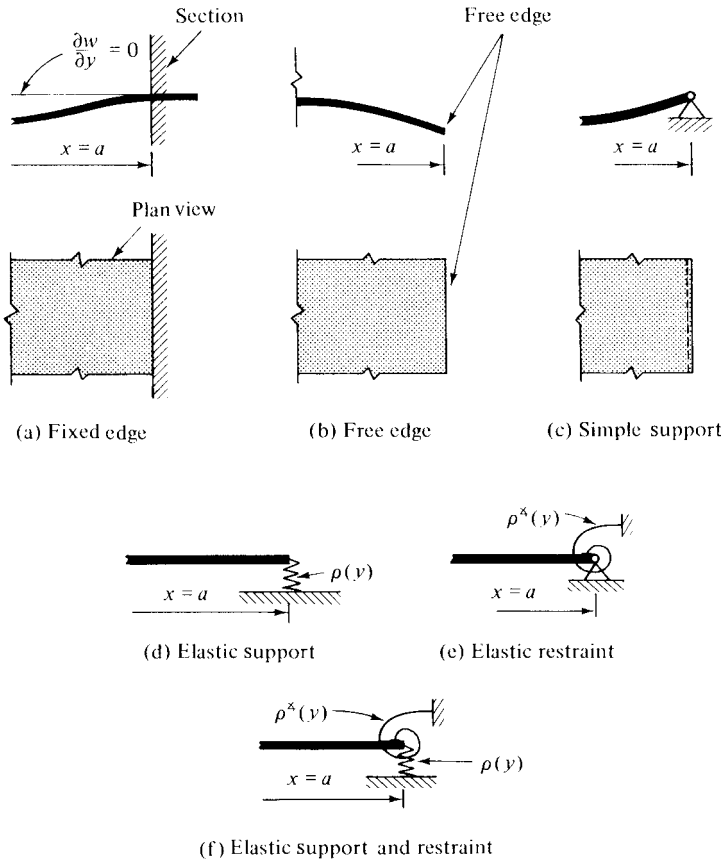


Figure 1.3.1 Various boundary conditions.

plate edge (Fig. 1.3.1b), for instance, we can state that the edge moment and the transverse shear force (v) are zero, giving

$$(m_x)_x = (v_x)_x = 0 \quad \text{at } x = 0, a,$$

or

$$(m_y)_y = (v_y)_y = 0 \quad \text{at } y = 0, b. \quad (1.3.2)$$

The shearing force at the edge of the plate consists of two terms, that is, transverse shear and the effect of the torsional moment. Considering plate edges having normals in the X and Y directions, respectively, the vertical edge forces per unit length can be written as

$$\begin{aligned} v_x &= q_x + \frac{\partial m_{xy}}{\partial y} = -D \left[\frac{\partial^3 w}{\partial x^3} + (2 - \nu) \frac{\partial^3 w}{\partial x \partial y^2} \right] & \text{at } x = 0, a, \\ v_y &= q_y + \frac{\partial m_{yx}}{\partial x} = -D \left[\frac{\partial^3 w}{\partial y^3} + (2 - \nu) \frac{\partial^3 w}{\partial x^2 \partial y} \right] & \text{at } y = 0, b, \end{aligned} \quad (1.3.3)$$

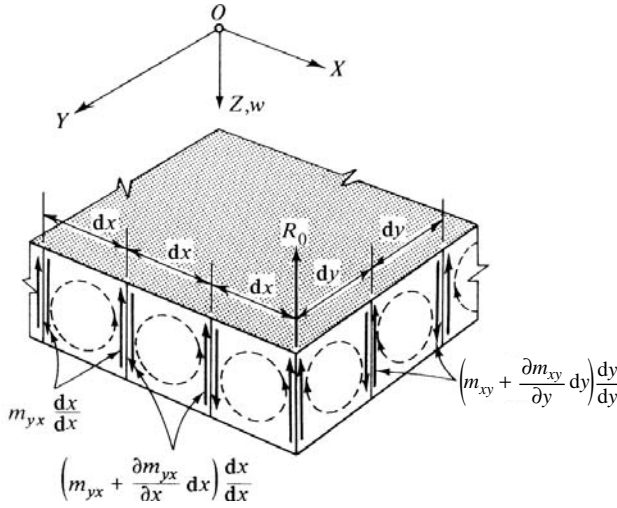


Figure 1.3.2 Edge effect of torsional moments.

where q_x and q_y are the lateral shear forces [Eq. (1.2.33)]. The second terms, $\partial m_{xy}/\partial y$ and $\partial m_{yx}/\partial x$, in Eq. (1.3.3) represent additional shearing forces at the edges, produced by the torsional moments $m_{xy} = m_{yx}$. Replacing the torsional moments by statically equivalent couples $m_{xy} dy/dy$ and $m_{yx} dx/dx$, respectively (Fig. 1.3.2), these forces cancel out at the adjoining elements, except for their incremental parts:

$$\frac{\partial m_{xy}}{\partial y} dy \quad \text{and} \quad \frac{\partial m_{yx}}{\partial x} dx.$$

Dividing these expressions by dy and dx , respectively, the additional shearing forces per unit length are obtained:

$$q_x^* = \frac{\partial m_{xy}}{\partial y} \quad \text{and} \quad q_y^* = \frac{\partial m_{yx}}{\partial x}. \quad (1.3.4)$$

These forces are called *Kirchhoff's supplementary forces* (*kirchhoffsche Ersatzkräfte*). Replacing the torsional moments by these *equivalent* shear forces, Kirchhoff reduced the number of internal forces to be considered from three to two. Thus from Eqs. (1.2.26), (1.2.27), (1.3.2) and (1.3.3) the boundary conditions at the free-edges are

$$\left(\frac{\partial^2 w}{\partial x^2} + \nu \frac{\partial^2 w}{\partial y^2} \right)_x = 0, \quad \left[\frac{\partial^3 w}{\partial x^3} + (2 - \nu) \frac{\partial^3 w}{\partial x \partial y^2} \right]_x = 0 \quad \text{at } x = 0, a \quad (1.3.5)$$

and

$$\left(\frac{\partial^2 w}{\partial y^2} + \nu \frac{\partial^2 w}{\partial x^2} \right)_y = 0, \quad \left[\frac{\partial^3 w}{\partial y^3} + (2 - \nu) \frac{\partial^3 w}{\partial x^2 \partial y} \right]_y = 0 \quad \text{at } y = 0, b. \quad (1.3.6)$$

c. *Mixed Boundary Conditions.* A simply supported edge (Fig. 1.3.1c) represents *mixed* boundary conditions. Since the deflection and the bending moment along the boundary are zero, formulation of this type of boundary condition involves statements concerning displacements and forces. Thus,

$$\begin{aligned} (w)_x = 0, \quad (m_x)_x &= \left(\frac{\partial^2 w}{\partial x^2} + \nu \frac{\partial^2 w}{\partial y^2} \right)_x = 0 \quad \text{at } x = 0, a, \\ (w)_y = 0, \quad (m_y)_y &= \left(\frac{\partial^2 w}{\partial y^2} + \nu \frac{\partial^2 w}{\partial x^2} \right)_y = 0. \quad \text{at } y = 0, b. \end{aligned} \quad (1.3.7)$$

At the corners of rectangular plates the above-discussed action of torsional moments add up instead of canceling (because $m_{xy} = m_{yx}$), producing an additional corner force

$$R_0 = 2m_{xy} = -2D(1 - \nu) \frac{\partial^2 w}{\partial x \partial y}. \quad (1.3.8)$$

If no anchorage is provided, these forces can lift up the corners, as illustrated in Fig. 1.3.3a. Since this condition is generally undesirable, it should be avoided by holding down the edges of simply supported plates. For reinforced-concrete slabs, when lifting up the corners is prevented, special corner reinforcing is required to eliminate local failures (Fig. 1.3.3b).

When two adjacent edges are fixed, the additional corner force is zero ($R_0 = 0$), since along these edges no torsional moment exists. The case at the intersection of two free-edges is similar.

If the solution of a given plate problem $w(x, y)$ was obtained by one of the approximate analytical or numerical methods, determination of the corner forces may require special considerations, as discussed in Sec. 13.3.

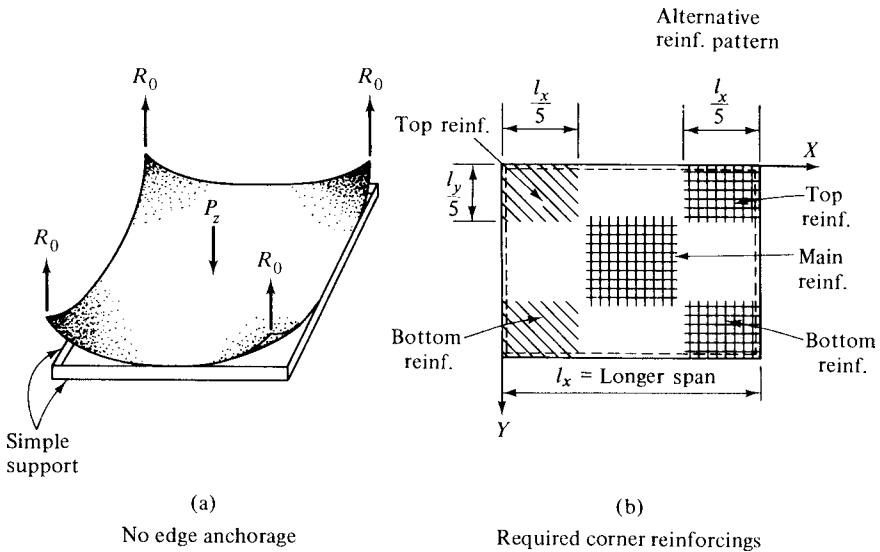


Figure 1.3.3 Up-lift of corners.

d. Elastic Support and Restraint. A special case of the *mixed* boundary condition occurs when the plate is resting on yielding support (Fig. 1.3.1d), such as provided by an edge beam without torsional rigidity. Assuming that the support is elastic and that its translational stiffness or spring constant is ρ (Fig. 1.3.4), the boundary conditions, for an edge having normals in the X direction, for instance, are

$$(w)_{x=a} = - \left[\frac{v_x}{\rho(y)} \right]_{x=a} = \frac{D}{\rho(y)} \left[\frac{\partial^3 w}{\partial x^3} + (2 - \nu) \frac{\partial^3 w}{\partial x \partial y^2} \right]_{x=a}, \quad (1.3.9)$$

$$(m_x)_{x=a} = \left[\frac{\partial^2 w}{\partial x^2} + \nu \frac{\partial^2 w}{\partial y^2} \right]_{x=a} = 0.$$

For continuous beam support, the first equation of (1.3.9) becomes

$$\left[EI_b \frac{\partial^4 w}{\partial y^4} \right]_{x=a} = D \left[\frac{\partial^3 w}{\partial x^3} + (2 - \nu) \frac{\partial^3 w}{\partial x \partial y^2} \right]_{x=a}, \quad (1.3.9a)$$

where I_b represents the moment of inertia of the edge beam.

If the edge beam has torsional rigidity ρ^Δ , it also provides partial restraint (fixity), as shown in Fig. 1.3.1f. Since the edge beam and the plate are built monolithically, they must have the same displacements. Consequently, the geometrical boundary conditions of elastic support and restraint along the edge at $x = a$ are

$$(w)_{x=a} = \frac{D}{\rho(y)} \left[\frac{\partial^3 w}{\partial x^3} + (2 - \nu) \frac{\partial^3 w}{\partial x \partial y^2} \right]_{x=a}, \quad (1.3.10)$$

$$\left(\frac{\partial w}{\partial x} \right)_{x=a} = - \frac{D}{\rho^\Delta(y)} \left[\frac{\partial^2 w}{\partial x^2} + \nu \frac{\partial^2 w}{\partial y^2} \right]_{x=a}$$

Similar expressions can be written for an edge at $y = b$.

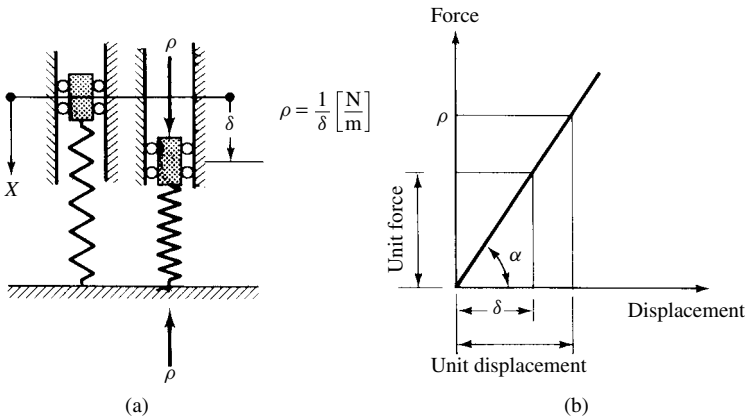


Figure 1.3.4 Force-displacement relationship of a linear spring.

Table 1.3.1 Summary of Boundary Conditions

Type of Support at $x = a$	Mathematical Expressions
Simple support (Fig. 1.3.1c)	$(w)_{x=a} = 0; (m_x)_{x=a} = \left(\frac{\partial^2 w}{\partial x^2} + \nu \frac{\partial^2 w}{\partial y^2} \right)_{x=a} = 0$
Fixed edge (Fig. 1.3.1a)	$(w)_{x=a} = 0; \left(\frac{\partial w}{\partial x} \right)_{x=a} = 0$
Free-edge (Fig. 1.3.1b)	$(m_x)_{x=a} = \left(\frac{\partial^2 w}{\partial x^2} + \nu \frac{\partial^2 w}{\partial y^2} \right)_{x=a} = 0$ $(v_x)_{x=a} = \left[\frac{\partial^3 w}{\partial x^3} + (2 - \nu) \frac{\partial^3 w}{\partial x \partial y^2} \right]_{x=a} = 0$
Partially fixed edge (Fig. 1.3.1e)	$(w)_{x=a} = 0$ $\left(\frac{\partial w}{\partial x} \right)_{x=a} = -(\rho^*)^{-1} D \left(\frac{\partial^2 w}{\partial x^2} + \nu \frac{\partial^2 w}{\partial y^2} \right)_{x=a}$
Elastic support (Fig. 1.3.1d)	$(m_x)_{x=a} = \left(\frac{\partial^2 w}{\partial x^2} + \nu \frac{\partial^2 w}{\partial y^2} \right)_{x=a} = 0$ $(w)_{x=a} = \rho^{-1} D \left[\frac{\partial^2 w}{\partial x^2} + (2 - \nu) \frac{\partial^3 w}{\partial x \partial y^2} \right]_{x=a}$
Elastic support and restraint (Fig. 1.3.1f)	$(w)_{x=a} = \rho^{-1} D \left[\frac{\partial^3 w}{\partial x^3} + (2 - \nu) \frac{\partial^3 w}{\partial x \partial y^2} \right]_{x=a}$ $\left(\frac{\partial w}{\partial x} \right)_{x=a} = -(\rho^*)^{-1} D \left(\frac{\partial^2 w}{\partial x^2} + \nu \frac{\partial^2 w}{\partial y^2} \right)_{x=a}$

Note: ρ = translational stiffness of support; ρ^* = rotational stiffness of support.

The analytical formulation of the various boundary conditions, illustrated in Fig. 1.3.1, is given in Table 1.3.1.

e. Curved Boundaries. In the case of curved boundaries (Fig. 1.3.5), the three most important boundary conditions are given below:

1. Simply supported edge:

$$w = 0 \quad \text{and} \quad m_n = -D \left[\nabla_r^2 w - (1 - \nu) \left(\frac{\partial^2 w}{\partial t^2} + \frac{1}{r_t} \frac{\partial w}{\partial n} \right) \right] = 0, \quad (1.3.11)$$

where[†]

$$\nabla_r^2 w = \frac{\partial^2 w}{\partial n^2} + \frac{\partial^2 w}{\partial t^2} + \frac{1}{r_t} \frac{\partial w}{\partial n} \quad (1.3.12)$$

and r_t represents the radius of curvature of the curved edge at a given boundary point (Fig. 1.3.5).

[†] See Sec. 1.4.

2. Fixed edge:

$$w = 0 \quad \text{and} \quad \frac{\partial w}{\partial n} = 0. \quad (1.3.13)$$

3. Free edge:

$$m_n = -D \left[\nabla_r^2 w - (1 - \nu) \left(\frac{\partial^2 w}{\partial t^2} + \frac{1}{r_t} \frac{\partial w}{\partial n} \right) \right] = 0 \quad (1.3.14)$$

and

$$v_n = -D \left[\frac{\partial \nabla_r^2 w}{\partial n} + (1 - \nu) \left(\frac{\partial^2}{\partial t^2} \frac{\partial w}{\partial n} - \frac{\partial}{\partial t} \left(\frac{1}{r_t} \frac{\partial w}{\partial t} \right) \right) \right] = 0. \quad (1.3.15)$$

Summary. In this chapter the fundamentals of the classical thin-plate theory are presented, which is based on Bernoulli-Kirchhoff hypotheses. These hypotheses are analogous to those used in elementary beam theory. In this way, the originally three-dimensional problem of elasticity was reduced to a problem involving only two dimensions. The governing differential equation of small-deflection, elastic thin-plate theory [Eq. (1.2.30)] is a differential equation of fourth order, linking the displacement of the midsurface $w(x, y)$ to the transverse load $p_z(x, y)$.

Bending problems of plates can be considered as solved if the function of lateral displacements $w(x, y)$ simultaneously satisfies the governing differential equation (1.2.30) and the boundary conditions, which require the specification of *any two* of the following quantities:

$$w, \quad \frac{\partial w}{\partial n}, \quad m_n \quad \text{and} \quad v_n,$$

where n represents the direction of the normal vector of the boundary (Fig. 1.2.5). Any two of these boundary conditions are sufficient to guarantee unique solutions of the plate equation.

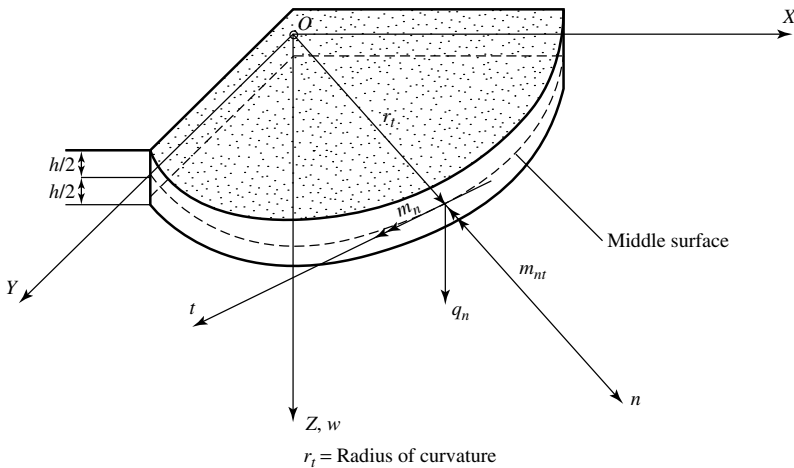


Figure 1.3.5 Curved boundary.

Reference and Bibliography

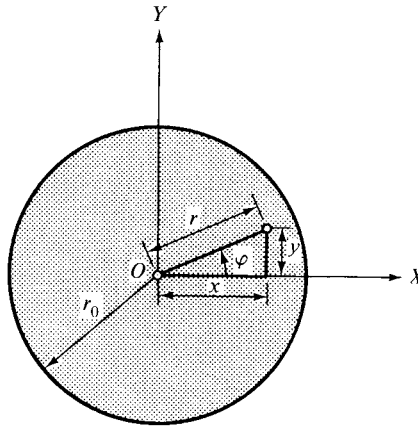
[1.3.1] L'HERMITE, R., *Résistance des matériaux*, Dumond, Paris, 1954.

1.4 Differential Equation of Circular Plates

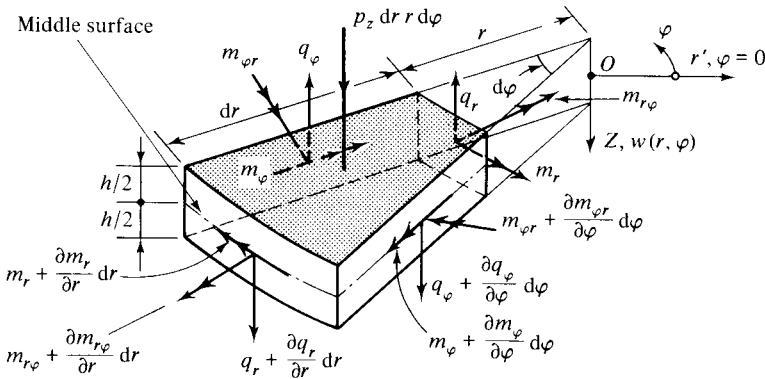
When circular plates are analyzed, it is convenient to express the governing differential equation (1.2.30) in a polar coordinate system, shown in Fig. 1.4.1a. This can be readily accomplished by a coordinate transformation. An alternative approach, based on the equilibrium condition of an infinitesimally small plate element (Fig. 1.4.1b), is analogous to the derivation given in Sec. 1.2.

If the coordinate transformation technique is used, the following geometrical relationships between the Cartesian and polar coordinates are applicable (Fig. 1.4.1a):

$$x = r \cos \varphi, \quad y = r \sin \varphi \quad (1.4.1a)$$



(a) Relationship between Cartesian and polar coordinates



(b) Plate element

Figure 1.4.1 Circular plate.

and

$$r = \sqrt{x^2 + y^2}, \quad \varphi = \tan^{-1} \left(\frac{y}{x} \right). \quad (1.4.1b)$$

Since x is a function of r and φ , the derivative of $w(r, \varphi)$ with respect to x can be transformed into derivatives with respect to r and φ . Thus, we can write

$$\frac{\partial w}{\partial x} = \frac{\partial w}{\partial r} \frac{\partial r}{\partial x} + \frac{\partial w}{\partial \varphi} \frac{\partial \varphi}{\partial x}. \quad (1.4.2)$$

Using Eq. (1.4.1), we obtain

$$\frac{\partial r}{\partial x} = \frac{x}{r} = \cos \varphi \quad \text{and} \quad \frac{\partial \varphi}{\partial x} = -\frac{y}{x^2 + y^2} = -\frac{1}{r} \sin \varphi; \quad (1.4.3)$$

therefore,

$$\frac{\partial w}{\partial x} = \cos \varphi \frac{\partial w}{\partial r} - \frac{1}{r} \sin \varphi \frac{\partial w}{\partial \varphi} = \left[\cos \varphi \frac{\partial(\bullet)}{\partial r} - \sin \varphi \frac{1}{r} \frac{\partial(\bullet)}{\partial \varphi} \right] w, \quad (1.4.4)$$

from which

$$\frac{\partial^2 w}{\partial x^2} = \frac{\partial}{\partial x} \left(\frac{\partial w}{\partial x} \right) = \left(\cos \varphi \frac{\partial}{\partial r} - \frac{1}{r} \sin \varphi \frac{\partial}{\partial \varphi} \right) \left(\cos \varphi \frac{\partial w}{\partial r} - \frac{1}{r} \sin \varphi \frac{\partial w}{\partial \varphi} \right). \quad (1.4.5)$$

Equation (1.4.5) can be reduced to

$$\begin{aligned} \frac{\partial^2 w}{\partial x^2} &= \cos^2 \varphi \frac{\partial^2 w}{\partial r^2} + \frac{1}{r^2} \sin^2 \varphi \frac{\partial^2 w}{\partial \varphi^2} + \frac{1}{r} \sin^2 \varphi \frac{\partial w}{\partial r} \\ &\quad - \frac{1}{r} \sin 2\varphi \frac{\partial^2 w}{\partial r \partial \varphi} + \frac{1}{r^2} \sin 2\varphi \frac{\partial w}{\partial \varphi}. \end{aligned} \quad (1.4.6)$$

In a similar manner we obtain

$$\frac{\partial w}{\partial y} = \sin \varphi \frac{\partial w}{\partial r} + \frac{1}{r} \cos \varphi \frac{\partial w}{\partial \varphi} \quad (1.4.7)$$

and

$$\begin{aligned} \frac{\partial^2 w}{\partial y^2} &= \sin^2 \varphi \frac{\partial^2 w}{\partial r^2} + \frac{1}{r^2} \cos^2 \varphi \frac{\partial^2 w}{\partial \varphi^2} + \frac{1}{r} \cos^2 \varphi \frac{\partial w}{\partial r} \\ &\quad + \frac{1}{r} \sin 2\varphi \frac{\partial^2 w}{\partial r \partial \varphi} - \frac{1}{r^2} \sin 2\varphi \frac{\partial w}{\partial \varphi}. \end{aligned} \quad (1.4.8)$$

Furthermore, Eqs. (1.4.4) and (1.4.7) give

$$\begin{aligned} \frac{\partial^2 w}{\partial x \partial y} &= \frac{1}{2} \sin 2\varphi \frac{\partial^2 w}{\partial r^2} - \frac{1}{r^2} \cos 2\varphi \frac{\partial w}{\partial \varphi} - \frac{1}{2r^2} \sin 2\varphi \frac{\partial^2 w}{\partial \varphi^2} \\ &\quad - \frac{1}{2r} \sin 2\varphi \frac{\partial w}{\partial r} + \frac{1}{r} \cos 2\varphi \frac{\partial^2 w}{\partial r \partial \varphi}. \end{aligned} \quad (1.4.9)$$

Therefore, the Laplacian operator ∇^2 (1.2.31), in terms of polar coordinates, becomes

$$\nabla_r^2 = \frac{\partial^2}{\partial r^2} + \frac{1}{r^2} \frac{\partial^2}{\partial \varphi^2} + \frac{1}{r} \frac{\partial}{\partial r}. \quad (1.4.10)$$

When the Laplacian operator ∇^2 is replaced by ∇_r^2 in Eq. (1.2.32), the plate equation in polar coordinates is obtained:

$$\boxed{\nabla_r^2 \nabla_r^2 w = \frac{p_s(r, \varphi)}{D}}. \quad (1.4.11)$$

The expressions for internal moments and shear forces, derived in Sec. 1.2, can also be transformed into polar coordinates; thus, we can write

$$m_r = -D \left[\frac{\partial^2 w}{\partial r^2} + \nu \left(\frac{1}{r^2} \frac{\partial^2 w}{\partial \varphi^2} + \frac{1}{r} \frac{\partial w}{\partial r} \right) \right], \quad (1.4.12)$$

$$m_\varphi = -D \left(\frac{1}{r} \frac{\partial w}{\partial r} + \frac{1}{r^2} \frac{\partial^2 w}{\partial \varphi^2} + \nu \frac{\partial^2 w}{\partial r^2} \right), \quad (1.4.13)$$

$$\begin{aligned} m_{r\varphi} = m_{\varphi r} &= -(1 - \nu) D \frac{\partial}{\partial r} \left(\frac{1}{r} \frac{\partial w}{\partial \varphi} \right) \\ &= -(1 - \nu) D \left[\frac{1}{r} \frac{\partial^2 w}{\partial r \partial \varphi} - \frac{1}{r^2} \frac{\partial w}{\partial \varphi} \right] \end{aligned} \quad (1.4.14)$$

and

$$q_r = -D \frac{\partial}{\partial r} \nabla_r^2 w \quad \text{and} \quad q_\varphi = -D \frac{1}{r} \frac{\partial}{\partial \varphi} \nabla_r^2 w. \quad (1.4.15)$$

Similarly, transformation of Eq. (1.3.3) into polar coordinates gives the lateral edge forces:

$$v_r = q_r + \frac{1}{r} \frac{\partial m_{r\varphi}}{\partial \varphi} \quad \text{and} \quad v_\varphi = q_\varphi + \frac{\partial m_{\varphi r}}{\partial r}. \quad (1.4.16)$$

These expressions for an edge with outward normal in the r or φ direction become

$$\begin{aligned} v_r &= -D \left[\frac{\partial}{\partial r} \nabla_r^2 w + \frac{1 - \nu}{r} \frac{\partial}{\partial \varphi} \left(\frac{1}{r} \frac{\partial^2 w}{\partial r \partial \varphi} - \frac{1}{r^2} \frac{\partial w}{\partial \varphi} \right) \right], \\ v_\varphi &= -D \left[\frac{1}{r} \frac{\partial}{\partial \varphi} \nabla_r^2 w + (1 - \nu) \frac{\partial}{\partial r} \left(\frac{1}{r} \frac{\partial^2 w}{\partial r \partial \varphi} - \frac{1}{r^2} \frac{\partial w}{\partial \varphi} \right) \right]. \end{aligned} \quad (1.4.17)$$

Summary. The governing differential equation of circular plates, expressed in polar coordinates, was derived by transformation of the Laplacian operator ∇^2 from Cartesian to polar coordinates. In the same way, expressions for moments and shear forces could be found in terms of r and φ . Exact solutions of Eq. (1.4.11) for nonsymmetric loading and boundary conditions are extremely tedious or, in many cases, impossible

to obtain. With symmetric boundary conditions, however, solutions for nonsymmetric loading can often be achieved by separating the loading into symmetric and antisymmetric parts, as discussed in pertinent sections.

1.5 Refined Theories for Moderately Thick Plates

Although classical plate theory yields sufficiently accurate results for *thin* plates, its accuracy decreases with growing thickness of the plate. Exact three-dimensional elasticity analysis of some plate problems indicates that its error is on the order of plate thickness square. Such an inherent limitation of classical plate theory for moderately thick plates[†] necessitated the development of more *refined* theories in order to obtain reliable results for the behavior of these structures.

Experiments have shown that Kirchhoff's classical plate theory underestimates deflections and overestimates natural frequencies and buckling loads for moderately thick plates. These discrepancies are due to the neglect of the effect of transverse shear strains, since (following elementary beam theory) it is assumed that normals to the middle plane remain straight and normal to the deflected midplane.

Nowadays many plate theories exist that account for the effects of transverse shear strains. The earliest attempt is due to M. Lévy who in his pioneering work [1.5.1] began to search for solutions using the equations of three-dimensional elasticity. More recently, primarily two approaches are used to take into account the transverse shear deformations. In the first one, which is attributed to Reissner [1.5.2], stresses are treated as primary variables. In the second approach, attributed to Mindlin [1.5.3], displacements are treated as unknowns. Both approaches provide for further development. Consequently, more sophisticated so-called higher-order theories have also been introduced in the last decades.

a. Reissner Theory. The above-discussed principal limitations of classical plate theory are partially eliminated by Reissner by introducing the influence of transverse shear and that of transverse direct stress σ_z [1.5.2]. Reissner made two assumptions. First, he assumed a linear variation of the displacement field through the plate thickness. Second, Reissner assumed that, as the plate bends, plane sections remain plane but lines originally perpendicular to the middle surface will not remain perpendicular to it after deformation (Fig. 1.5.1). Rotations of the normals to the middle surface are expressed by

$$\omega_x = -\frac{\partial w}{\partial x} + \frac{6}{5Gh}q_x, \quad \omega_y = -\frac{\partial w}{\partial y} + \frac{6}{5Gh}q_y. \quad (1.5.1)$$

This departure from the Bernoulli-Kirchhoff hypothesis makes it possible to partially account for the effect of transverse shear deformations.

Reissner formulated his plate equations by applying Castigliano's theorem of least work using stresses as variables. This stress-based theory yielded the following three simultaneous differential equations:

$$D \nabla^2 \nabla^2 w = p_z - \frac{h^2}{10} \frac{2-\nu}{1-\nu} \nabla^2 p_z, \quad (1.5.2)$$

[†] Moderately thick plates have an approximate thickness-to-span ratio $h/L \approx \frac{1}{10} - \frac{1}{5}$.

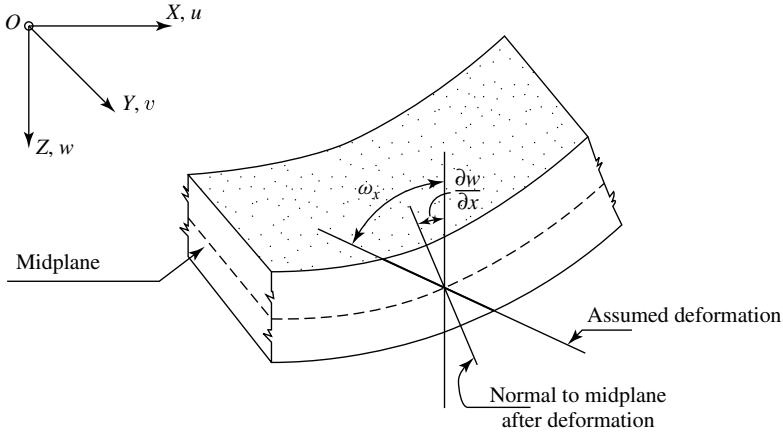


Figure 1.5.1 Reissner's cross-sectional assumption.

$$q_x = -D \frac{\partial \nabla^2 w}{\partial x} + \frac{h^2}{10} \nabla^2 q_x - \frac{h^2}{10} \frac{1}{1-\nu} \frac{\partial p_z}{\partial x}, \quad (1.5.3)$$

$$q_y = -D \frac{\partial \nabla^2 w}{\partial y} + \frac{h^2}{10} \nabla^2 q_y - \frac{h^2}{10} \frac{1}{1-\nu} \frac{\partial p_z}{\partial y}. \quad (1.5.4)$$

The bending and twisting moments are expressed by

$$m_x = -D \left(\frac{\partial^2 w}{\partial x^2} + \nu \frac{\partial^2 w}{\partial y^2} \right) + \frac{h^2}{5} \frac{\partial q_x}{\partial x} - \frac{h^2}{10} \frac{\nu}{1-\nu} p_z, \quad (1.5.5)$$

$$m_y = -D \left(\nu \frac{\partial^2 w}{\partial x^2} + \frac{\partial^2 w}{\partial y^2} \right) + \frac{h^2}{5} \frac{\partial q_y}{\partial y} - \frac{h^2}{10} \frac{\nu}{1-\nu} p_z, \quad (1.5.6)$$

$$m_{xy} = -D(1-\nu) \frac{\partial^2 w}{\partial x \partial y} + \frac{h^2}{10} \left(\frac{\partial q_y}{\partial x} + \frac{\partial q_x}{\partial y} \right). \quad (1.5.7)$$

The governing differential equations represent an integration problem of sixth order. Consequently, three mutually independent boundary conditions must be satisfied at the edges. These are

$$\text{For fixed edge (Fig. 1.3.1a): } (w)_{x=a} = 0, \quad (\omega_x)_{x=a} = 0, \quad (w_y)_{x=a} = 0; \quad (1.5.8)$$

$$\text{For free-edge (Fig. 1.3.1b): } (q_x)_{x=a} = 0, \quad (m_x)_{x=a} = 0, \quad (m_{xy})_{x=a} = 0; \quad (1.5.9)$$

For simply supported edge (Fig. 1.3.1c):

$$(w)_{x=a} = 0, \quad (m_x)_{x=a} = 0, \quad (m_{xy})_{x=a} = 0. \quad (1.5.10)$$

Although, over the years, Reissner refined his theory (Refs. [1.5.4–1.5.7]) and even formulated the governing differential equations in terms of transverse displacement $w(x, y)$ as a single variable, solutions of these differential equations remain extremely demanding. For this reason *simplified* stress-based theories have been introduced. Speare and Kemp [1.5.8], for instance, used the very same assumptions as Reissner but accepted a somewhat lower accuracy. The so-derived differential equation for the bending of moderately thick plate is

$$\nabla^2 w + \frac{h^2(2-\nu)}{10(1-\nu)} \nabla^3 w = \frac{p_z}{D}, \quad (1.5.11)$$

where

$$\nabla^3 w = \left(\frac{\partial^2 w}{\partial x^2} + \frac{\partial^2 w}{\partial y^2} \right)^3. \quad (1.5.12)$$

The pertinent bending and twisting moments are

$$m_x = -D \left(\frac{\partial^2 w}{\partial x^2} + \nu \frac{\partial^2 w}{\partial y^2} \right) - \frac{h^2 D}{10(1-\nu)} \left[(2-\nu) \frac{\partial^4 w}{\partial x^4} + 2 \frac{\partial^4 w}{\partial x^2 \partial y^2} + \nu \frac{\partial^4 w}{\partial y^4} \right], \quad (1.5.13)$$

$$m_y = -D \left(\frac{\partial^2 w}{\partial y^2} + \nu \frac{\partial^2 w}{\partial x^2} \right) - \frac{h^2 D}{10(1-\nu)} \left[(2-\nu) \frac{\partial^4 w}{\partial y^4} + 2 \frac{\partial^4 w}{\partial x^2 \partial y^2} + \nu \frac{\partial^4 w}{\partial x^4} \right], \quad (1.5.14)$$

$$m_{xy} = (1-\nu) D \frac{\partial^2 w}{\partial x \partial y} + \frac{h^2 D}{5} \left(\frac{\partial^4 w}{\partial x^3 \partial y} + \frac{\partial^4 w}{\partial x \partial y^3} \right), \quad (1.5.15)$$

and the transverse shear forces are expressed by

$$q_x = -D \left(\frac{\partial^3 w}{\partial x^3} + \frac{\partial^3 w}{\partial x \partial y^2} \right) - \frac{h^2(2-\nu)}{10(1-\nu)} D \left(\frac{\partial^5 w}{\partial x^5} + 2 \frac{\partial^5 w}{\partial x^3 \partial y^2} + \frac{\partial^5 w}{\partial x \partial y^4} \right), \quad (1.5.16)$$

$$q_y = -D \left(\frac{\partial^3 w}{\partial y^3} + \frac{\partial^3 w}{\partial x^2 \partial y} \right) - \frac{h^2(2-\nu)}{10(1-\nu)} D \left(\frac{\partial^5 w}{\partial y^5} + 2 \frac{\partial^5 w}{\partial x^2 \partial y^3} + \frac{\partial^5 w}{\partial x^4 \partial y} \right). \quad (1.5.17)$$

The boundary conditions remain the same as given by Reissner in Eqs. (1.5.8)–(1.5.10).

An alternative approach for a simplified Reissner theory is presented in Ref. [1.5.9]. Both theories are attractive from a computational point of view.

b. Mindlin Theory. The most widely used displacement-based theory for moderately thick plates was developed by Mindlin [1.5.3]. It is based on a so-called first-order deformation theory using the following kinematic assumptions for the in-plane displacements:

$$u = z\psi_x(x, y), \quad v = z\psi_y(x, y), \quad (1.5.18)$$

where $\psi_x(x, y)$ and $\psi_y(x, y)$ represent rotations at the midplane. Since the transverse displacements $w(x, y)$ are independent of z , no thickness stretch is permitted. The cross-sectional assumption of Mindlin's theory is identical to that of Reissner's assumption, shown in Fig. 1.5.1. Thus, in this case $\omega_x = \psi_x$ and $\omega_y = \psi_y$.

Equation (1.5.18) yields constant values for the transverse shear strains and corresponding stress distributions. Since the real stress distribution in moderately thick plates is parabolic, this assumption is incorrect. Furthermore, it fails to satisfy the zero-stress condition on the top and bottom surfaces of the plate. Consequently, it was necessary to introduce a correction factor κ^2 , which was evaluated by comparison with the exact elastic solutions. Following Timoshenko's earlier approach—used for moderately deep beams—the value $\kappa^2 = \frac{5}{6}$ was selected.

Mindlin notes that the values of the shear correction factor κ^2 are linear functions of Poisson's ratio ν . He provides two estimates based on comparison of his theory with the more exact solution of three-dimensional elasticity. The first estimate gives $0.75 \leq \kappa^2 \leq 0.91$ for $0 \leq \nu \leq 0.5$. The second estimate is based on shear wave velocity $\kappa^2 = \pi^2/12 = 0.822$. If $\nu = 0.3$, then $\kappa^2 \approx 0.86$, which compares favorably with the generally used assumption of $\kappa^2 = \frac{5}{6} = 0.8333$.

A more exact expression for the shear correction factor is $\kappa^2 = 20(1 + \nu)/(24 + 25\nu + \nu^2)$, which even considers the parabolic variation of shear forces [1.5.24]. This expression gives, for $\nu = 0.3$, $\kappa^2 = 0.823$, which is, for all practical purposes, the same as Mindlin's second estimate.

Applying the minimum of the potential energy theorem, Mindlin derived the following differential equations of equilibrium:

$$\kappa^2 Gh(\nabla^2 w + \phi) + p_z(x, y) = 0, \quad (1.5.19)$$

$$\frac{D}{2} \left[(1 - \nu) \nabla^2 \psi_x + (1 + \nu) \frac{\partial \phi}{\partial x} \right] - \kappa^2 Gh \left(\psi_x + \frac{\partial w}{\partial x} \right) = 0, \quad (1.5.20)$$

$$\frac{D}{2} \left[(1 - \nu) \nabla^2 \psi_y + (1 + \nu) \frac{\partial \phi}{\partial y} \right] - \kappa^2 Gh \left(\psi_y + \frac{\partial w}{\partial y} \right) = 0, \quad (1.5.21)$$

where D represents the plate bending rigidity given in Eq. (1.2.28) and E , G and ν are Young's modulus of elasticity, shear modulus and Poisson's ratio, respectively. The shear correction factor is κ^2 and

$$\phi = \frac{\partial \psi_x}{\partial x} + \frac{\partial \psi_y}{\partial y}. \quad (1.5.22)$$

The stress resultants in Mindlin's plate theory are

$$m_x = D \left(\frac{\partial \psi_x}{\partial x} + \nu \frac{\partial \psi_y}{\partial y} \right), \quad (1.5.23)$$

$$m_y = D \left(\frac{\partial \psi_y}{\partial y} + \nu \frac{\partial \psi_x}{\partial x} \right), \quad (1.5.24)$$

$$m_{xy} = m_{yx} = \frac{1 - \nu}{2} D \left(\frac{\partial \psi_y}{\partial x} + \frac{\partial \psi_x}{\partial y} \right), \quad (1.5.25)$$

$$q_x = \kappa^2 Gh \left(\psi_x + \frac{\partial w}{\partial x} \right), \quad (1.5.26)$$

$$q_y = \kappa^2 Gh \left(\psi_y + \frac{\partial w}{\partial y} \right). \quad (1.5.27)$$

In the case of rectangular plates, the boundary conditions (Fig. 1.3.1) are

$$\text{For fixed edge:} \quad (w_x)_{x=a} = (\psi_x)_{x=a} = (\psi_y)_{x=a} = 0; \quad (1.5.28)$$

$$\text{For simple support:} \quad (w)_{x=a} = (\psi_x)_{x=a} = (m_x)_{x=a} = 0; \quad (1.5.29)$$

$$\text{For free-edge:} \quad (m_x)_{x=a} = (m_{xy})_{x=a} = (q_x)_{x=a} = 0. \quad (1.5.30)$$

c. Higher-Order Shear Theories. While all “first-order” theories assume that the in-plane displacements u and v vary linearly, this kinematic approximation of reality can be avoided by introducing cubic—or even higher-order—variations for these displacement components. A higher-level theory is based upon the assumed displacement forms

$$\begin{aligned} u &= z\psi_x(x, y) + z^3\phi_x(x, y), \\ v &= z\psi_y(x, y) + z^3\phi_y(x, y). \end{aligned} \quad (1.5.31)$$

Here ψ_x and ψ_y represent rotations of the midplane of the plate, whereas the comparable quantities of the Reissner and Mindlin theories are, in some respect, *average* rotations. The quantities ϕ_x and ϕ_y are the so-called warping functions. The pertinent kinematic assumptions are

$$\begin{aligned} \phi_x &= -\frac{4}{3h^2} \left(\psi_x + \frac{\partial w}{\partial x} \right), \\ \phi_y &= -\frac{4}{3h^2} \left(\psi_y + \frac{\partial w}{\partial y} \right), \\ u &= z \left[\psi_x - \frac{4}{3} \frac{z^2}{h^2} \left(\psi_x + \frac{\partial w}{\partial x} \right) \right], \\ v &= z \left[\psi_y - \frac{4}{3} \frac{z^2}{h^2} \left(\psi_y + \frac{\partial w}{\partial y} \right) \right]. \end{aligned} \quad (1.5.32)$$

These kinematic assumptions satisfy the requirements for shear-free conditions on the top and bottom surfaces of the moderately thick plates and represent a parabolic distribution of shear stresses across the plate thickness. Furthermore, the cross sections at the midplane are allowed to warp, as shown in Fig. 1.5.2.

Using the kinematic assumptions given in Eqs. (1.5.31) and (1.5.32), Levinson [1.5.10] derived an improved approximation to the theory of moderately thick plates. Applying similar equilibrium considerations as used in the derivation of classical plate theory, the following differential equations have been obtained:

$$\frac{2}{3} Gh (\nabla^2 w + \phi) + p_z(x, y) = 0, \quad (1.5.33)$$

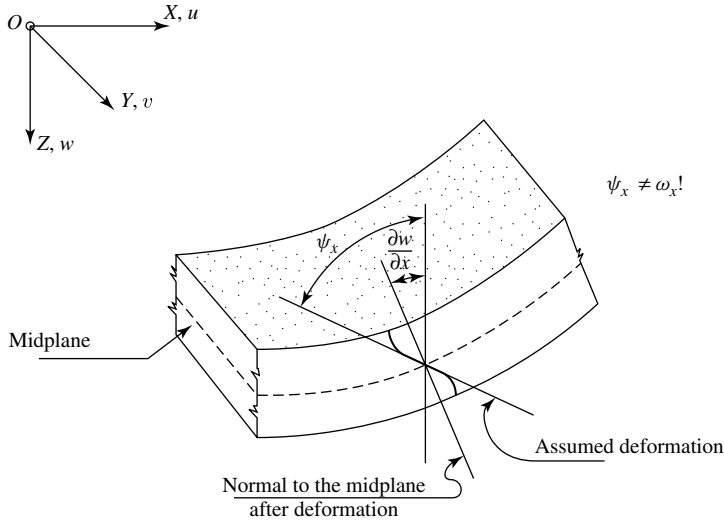


Figure 1.5.2 Levinson's cross-sectional assumption.

$$\frac{2D}{5} \left[(1 - \nu) \nabla^2 \psi_x + (1 + \nu) \frac{\partial \phi}{\partial x} - \frac{1}{2} \frac{\partial}{\partial x} (\nabla^2 w) \right] - \frac{2}{3} Gh \left(\psi_x + \frac{\partial w}{\partial x} \right) = 0, \quad (1.5.34)$$

$$\frac{2D}{5} \left[(1 - \nu) \nabla^2 \psi_y + (1 + \nu) \frac{\partial \phi}{\partial y} - \frac{1}{2} \frac{\partial}{\partial y} (\nabla^2 w) \right] - \frac{2}{3} Gh \left(\psi_y + \frac{\partial w}{\partial y} \right) = 0. \quad (1.5.35)$$

The three unknowns in these differential equations are, again, the deflection w and the rotations at the midplane ψ_x and ψ_y . The pertinent internal forces are expressed by

$$m_x = \frac{D}{5} \left[4 \left(\frac{\partial \psi_x}{\partial x} + \nu \frac{\partial \psi_y}{\partial y} \right) - \left(\frac{\partial^2 w}{\partial x^2} + \nu \frac{\partial^2 w}{\partial y^2} \right) \right], \quad (1.5.36)$$

$$m_y = \frac{D}{5} \left[4 \left(\frac{\partial \psi_y}{\partial y} + \nu \frac{\partial \psi_x}{\partial x} \right) - \left(\frac{\partial^2 w}{\partial y^2} + \nu \frac{\partial^2 w}{\partial x^2} \right) \right], \quad (1.5.37)$$

$$m_{xy} = \frac{D(1 - \nu)}{5} \left[2 \left(\frac{\partial \psi_y}{\partial x} + \frac{\partial \psi_x}{\partial y} \right) - \frac{\partial^2 w}{\partial x \partial y} \right] \quad (1.5.38)$$

and

$$q_x = \frac{2}{3} Gh \left(\psi_x + \frac{\partial w}{\partial x} \right), \quad (1.5.39)$$

$$q_y = \frac{2}{3} Gh \left(\psi_y + \frac{\partial w}{\partial y} \right). \quad (1.5.40)$$

The geometrical boundary conditions of the Mindlin and Levinson theories are *formally* the same. But the Levinson theory allows only the specification of the rotations at the midplane.

Another higher-order theory developed by Lo and co-workers [1.5.11] employs the following displacement forms:

$$\begin{aligned} u &= u^0 + z\psi_x + z^2\zeta_x + z^3\phi_x, \\ v &= v^0 + z\psi_y + z^2\zeta_y + z^3\phi_y, \\ w &= w^0 + z\psi_z + z^2\zeta_z, \end{aligned} \quad (1.5.41)$$

where u^0, v^0, ψ_x, ψ_y and w^0 are dependent on the in-plane coordinates x and y and w^0, ψ_x, ψ_y are weighted averages.

Subramanian introduced fourth- and fifth-order power series expressions for the displacement components [1.5.12]. As already mentioned, Reissner even used a twelfth-order theory for moderately thick plates [1.5.6]. Needless to say, the complexity of the solutions, if they can be obtained at all, are also increased with the order of polynomial expressions for displacements.

d. Governing Differential Equations for Circular Plates. The equilibrium equations for axisymmetric bending of circular Reissner-Mindlin plates of uniform thickness h are given in terms of displacement components in Refs. [46] and [1.5.23] as follows:

$$D \left(\frac{d^2\psi}{dr^2} + \frac{1}{r} \frac{d\psi}{dr} - \frac{\psi}{r^2} \right) - \kappa^2 Gh \left(\frac{dw}{dr} + \psi \right) = 0, \quad (1.5.42)$$

$$\kappa^2 Gh \left(\frac{d^2w}{dr^2} + \frac{1}{r} \frac{dw}{dr} + \frac{d\psi}{dr} + \frac{\psi}{r} \right) + p_z = 0. \quad (1.5.43)$$

The corresponding equations of the stress resultants are

$$m_r = D \left(\frac{d\psi}{dr} + \nu \frac{\psi}{r} \right), \quad m_\varphi = D \left(\nu \frac{d\psi}{dr} + \frac{\psi}{r} \right), \quad q_r = \kappa^2 Gh \left(\frac{dw}{dr} + \psi \right). \quad (1.5.44)$$

Summary. In the past decades a great deal of research work has been conducted on the effect of shear deformation in moderately thick plates. Since this effort is by no means completed, further important developments can be expected on this subject. In addition to the above-discussed refined plate theories, the reader will find additional pertinent information in Refs. [1.5.13–1.5.22]. Due to their inherent complexities, direct use of these refined theories is cumbersome, and their computation becomes increasingly demanding, since with each additional power in the kinematic assumptions additional dependent unknowns are introduced into the governing differential equations. Thus, it is recommended that simplified theories—such as those given in Refs. [1.5.8] and [1.5.9]—be employed whenever possible. However, if the thickness-to-span ratio h/L of the plate approaches $\frac{1}{5}$, the use of Levinson's theory (or its simplified version [1.5.22]) appears to be more advantageous.

References and Bibliography

- [1.5.1] LÉVY, M., "Mémoire sur la théorie des plaques élastiques," *J. Math. Pures Appl.*, 30 (1877), 219–306.
- [1.5.2] REISSNER, E., "On the Theory of Bending of Elastic Plates," *J. Math. Phys.*, 23 (1944), 184–191.
- [1.5.3] MINDLIN, R. D., "Influence of Rotatory Inertia on Flexural Motions of Isotropic, Elastic Plates," *J. Appl. Mech.*, 18 (1951), 31–38.
- [1.5.4] REISSNER, E., "The Effect of Transverse Deformation on the Bending of Elastic Plates," *J. Appl. Mech.*, 67 (1945), A67–A77.
- [1.5.5] REISSNER, E., "On Transverse Bending of Plates, Including the Effect of Transverse Shear Deformation," *Int. J. Solids Struct.*, 11 (1975), 569–573.
- [1.5.6] REISSNER, E., "A Twelfth Order Theory of Transverse Bending of Transversely Isotropic Plates," *ZAMM*, 63 (1983), 285–289.
- [1.5.7] REISSNER, E., "Reflections on the Theory of Elastic Plates," *Appl. Mech. Rev.*, 38 (1985), 1453–1464.
- [1.5.8] SPEARE, P. R. S., and KEMP, K. O., "A Simplified Reissner Theory for Plate Bending," *Int. J. Solids Struct.*, 13 (1977), 1073–1079.
- [1.5.9] BALUCH, M. H., and VOYIADIS, G. Z., "Higher Order Plate Equations Based on Reissner's Formulation of the Plate Problem," *Arab J. Sci. Eng.*, 5 (1980), 75–80.
- [1.5.10] LEVINSON, M., "An Accurate Simple Theory of the Statics and Dynamics of Elastic Plates," *Mech. Res. Commun.*, 7 (1980), 343–350.
- [1.5.11] LO, K. H., CHRISTENSEN, R. M., and WU, E. M., "A High-Order Theory of Plate Deformation; Part 1: Homogeneous Plates," *J. Appl. Mech.*, 44 (1977), 663–668.
- [1.5.12] SUBRAMANIAN, P., "A Higher Order Theory for Bending of Isotropic Plates," *Computers & Structures*, 49 (1993), 199–204.
- [1.5.13] HENKY, H., "Über die Berücksichtigung der Schubverzerrungen in ebenen Platten," *Ing. Arch.*, 16 (1947), 72–76.
- [1.5.14] GREEN, A. E., "On Reissner's Theory of Bending of Elastic Plates," *Q. Appl. Math.*, 7 (1949), 223–228.
- [1.5.15] SCHÄFER, M., "Über eine Verfeinerung der klassischen Theorie dünner schwach gebogener Platten," *ZAMM*, 32 (1952), 161–171.
- [1.5.16] KROMM, A., "Verallgemeinerte Theorie der Plattenstatik," *Ing. Arch.*, 21 (1953), 266–286.
- [1.5.17] GOL'DENVEIZER, A. L., "On the Reissner's Theory of Bending of Plates," *Akad. Nauk. SSSR*, 5 (1958), 69–77.
- [1.5.18] PANC, V., *Theory of Elastic Plates*, Noordhoff, Leyden, The Netherlands, 1975.
- [1.5.19] REHFELD, L. W., and VASILETTY, R. R., "A Simple, Refined Theory for Bending and Stretching of Homogeneous Plates," *AIAA J.*, 22 (1984), 90–95.
- [1.5.20] KRISHNA MURTY, A. V., and VELLAICHAMY, S., "A Higher-Order Theory of Homogeneous Plate Flexure," *AIAA J.*, 26 (1988), 719–725.
- [1.5.21] RYCHTER, Z., "A Sixth-Order Plate Theory—Derivation and Error Estimates," *J. Appl. Mech.*, 54 (1987), 275–279.
- [1.5.22] SALERNO, V. L., and GOLDBERG, M. A., "Effect of Shear Deformation on Bending of Plates," *J. Appl. Mech.*, 27 (1960), 54–58.
- [1.5.23] HAN, J.-B., and LIEW, K. M., "Analysis of Moderately Thick Circular Plates Using Differential Quadrature Method," *J. Eng. Mech., ASCE*, 123 (1997), 1247–1252.
- [1.5.24] NÄNNI, J., "Das Eulerische Knickproblem unter Berücksichtigung der Querkräfte," *Z. Angew. Phys.*, 51 (1971), 156–186.
- [1.5.25] WANG, C. M., et al., *Shear Deformable Beams and Plates: Relationships with Classical Solutions*, Elsevier, Amsterdam, 2002.

1.6 Three-Dimensional Elasticity Equations for Thick Plates

When the thickness of the plate becomes significant compared to its smallest span dimension,[†] the governing equations of three-dimensional elasticity (as given in Refs. [1.6.1–1.6.4]) must be applied to determine the *true* three-dimensional distribution of stresses in the plate. To describe the three-dimensional state of stresses in a rectangular Cartesian coordinate system, we take an infinitesimal element in the form of a parallelepiped (dx, dy, dz) with faces parallel to the coordinate planes, as shown in Fig. 1.6.1. The X, Y and Z components of the normal stresses are designated by σ_x, σ_y and σ_z , respectively. Again, the subscripts refer to the normal of the surface upon which the stress vector acts. The shearing stresses—as in the previous sections—carry two subscripts. The first subscript refers to the direction of the normal of the surface, and the second subscript indicates the direction of the stress vector τ . Since stresses are functions of their location in the body, their intensity is changed when we move their reference plane by dx, dy and dz . The resulting increments are expressed, again, by the first two terms of a Taylor series (Fig. 1.6.1).

Following the sign convention used throughout this book, we consider all stresses positive if they act in the direction of the positive coordinate axes. Consequently, on the near surfaces of the element (viewed from the tips of the positive coordinate axes), all stresses are positive. On the far sides of the element, all stresses acting in the negative coordinate direction are positive. This sign convention follows the customary rule in engineering practice; that is, tension is positive and compression is negative.

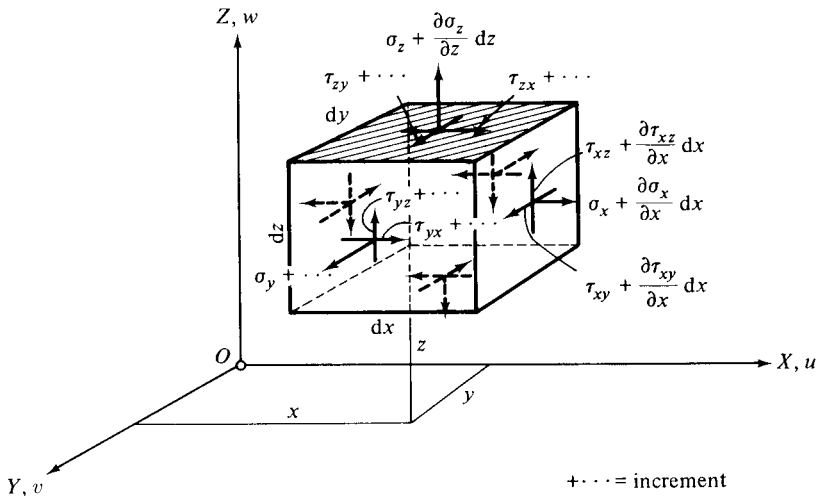


Figure 1.6.1 Three-dimensional element.

[†] That is, the thickness-to-span ratio is considerably greater than $\frac{1}{5}$.

The three-dimensional state of stress at any point of the elastic body is defined by nine components of the stress *tensor*[†] with the pertinent matrix

$$[\sigma] = \begin{bmatrix} \sigma_x & \tau_{xy} & \tau_{xz} \\ \tau_{yx} & \sigma_y & \tau_{yz} \\ \tau_{zx} & \tau_{zy} & \sigma_z \end{bmatrix}, \quad (1.6.1)$$

which is *symmetric* with respect to the principal diagonal. Because of this symmetry,

$$\tau_{xy} = \tau_{yx}, \quad \tau_{xz} = \tau_{zx} \quad \text{and} \quad \tau_{yz} = \tau_{zy}. \quad (1.6.2)$$

Equation (1.6.2) is called the *reciprocity law of shearing stresses* and can easily be verified by taking the moments of stresses about the coordinate axes.

In general, the solution of a three-dimensional elasticity problem consists of finding the stresses in the elastic body subjected to surface forces p_x, p_y, p_z and body forces X, Y, Z . If the displacements are small, we have 15 linear field equations for 15 unknowns:

1. three equilibrium equations,
2. six kinematic relationships, and
3. six stress-strain equations.

In addition to these field equations, a set of boundary conditions are also required to obtain a unique solution to a three-dimensional elasticity problem. We are, in general, faced with three types of boundary conditions for thick plates:

- (a) *Statical*: The surface forces (p_x, p_y, p_z) are prescribed.
- (b) *Kinematic*: The displacements (u, v, w) are prescribed.
- (c) *Mixed*: Some boundary forces and some displacements are prescribed.

The original 15 equations used in a stress-based analysis can be reduced to three differential equations in terms of the displacement components u, v and w . These so-called Lamé equations of equilibrium are

$$\begin{aligned} (\lambda + G) \frac{\partial e}{\partial x} + G \nabla_3^2 u + X &= 0, \\ (\lambda + G) \frac{\partial e}{\partial y} + G \nabla_3^2 v + Y &= 0, \\ (\lambda + G) \frac{\partial e}{\partial z} + G \nabla_3^2 w + Z &= 0, \end{aligned} \quad (1.6.3)$$

where

$$\lambda = \frac{\nu E}{(1 + \nu)(1 - \nu)} \quad (1.6.4)$$

[†] A tensor is a quantity having physical significance that satisfies a certain transformation law. This transformation law in the theory of elasticity is the *rotation of axes*. Tensors of second order are represented by matrices.

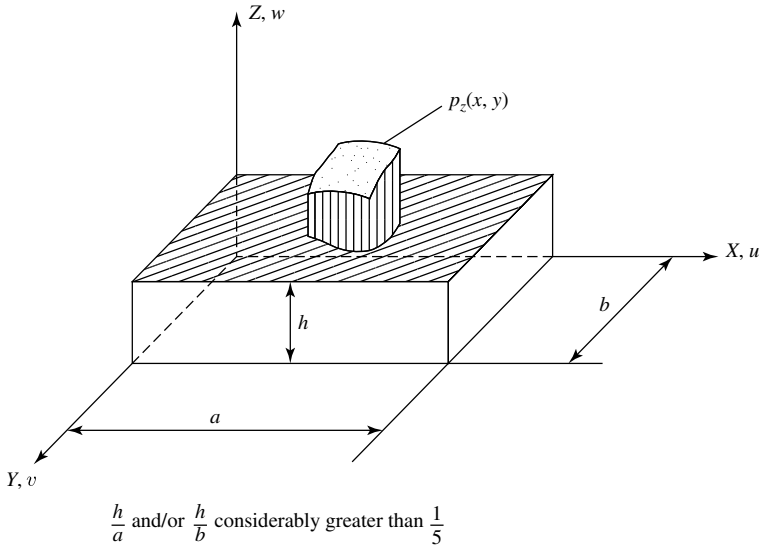


Figure 1.6.2 Thick plate in rectangular cartesian coordinate system.

represents the Lamé coefficient, G is the modulus of elasticity in shear and

$$\nabla_3^2(\bullet) = \frac{\partial^2(\bullet)}{\partial x^2} + \frac{\partial^2(\bullet)}{\partial y^2} + \frac{\partial^2(\bullet)}{\partial z^2} \quad (1.6.5)$$

is the three-dimensional Laplacian operator. In addition, e in Eq. (1.6.3) denotes the volume dilatation in the form

$$e = \varepsilon_x + \varepsilon_y + \varepsilon_z. \quad (1.6.6)$$

In practice, we usually eliminate the body forces and apply the weight of the plate as surface force $p_z(x, y)$ acting on the lower and upper faces of the plate. A similar approach is taken with the external load acting in the transverse direction. Furthermore, we can write Eq. (1.6.3) in terms of derivatives of the displacement components in more explicit form. Thus we obtain

$$(\lambda + 2G) \frac{\partial^2 u}{\partial x^2} + G \frac{\partial^2 u}{\partial y^2} + G \frac{\partial^2 u}{\partial z^2} + (\lambda + G) \frac{\partial^2 v}{\partial x \partial y} + (\lambda + G) \frac{\partial^2 w}{\partial x \partial z} = 0, \quad (1.6.7)$$

$$(\lambda + G) \frac{\partial^2 u}{\partial x \partial y} + G \frac{\partial^2 v}{\partial x^2} + (\lambda + 2G) \frac{\partial^2 v}{\partial y^2} + G \frac{\partial^2 v}{\partial z^2} + (\lambda + G) \frac{\partial^2 w}{\partial y \partial z} = 0, \quad (1.6.8)$$

$$(\lambda + G) \frac{\partial^2 u}{\partial x \partial z} + (\lambda + G) \frac{\partial^2 v}{\partial y \partial z} + G \frac{\partial^2 w}{\partial x^2} + G \frac{\partial^2 w}{\partial y^2} + (\lambda + 2G) \frac{\partial^2 w}{\partial z^2} = 0. \quad (1.6.9)$$

The three most important boundary conditions of thick plates (Fig. 1.6.2) are as follows:

1. For clamped edges:

$$\begin{aligned} \text{At } x = 0, a : \quad & u = 0, \quad v = 0, \quad w = 0, \\ \text{At } y = 0, b : \quad & u = 0, \quad v = 0, \quad w = 0, \\ \text{At } z = 0, h : \quad & \tau_{xz} = 0, \quad \tau_{yz} = 0, \quad \sigma_z = \pm p_z/2; \end{aligned} \quad (1.6.10)$$

2. For simply supported edges:

$$\begin{aligned} \text{At } x = 0, a : \quad & \sigma_x = 0, \quad \tau_{xy} = 0, \quad w = 0, \\ \text{At } y = 0, b : \quad & \sigma_y = 0, \quad \tau_{xy} = 0, \quad w = 0, \\ \text{At } z = 0, h : \quad & \tau_{xz} = 0, \quad \tau_{yz} = 0, \quad \sigma_z = \pm p_z/2; \end{aligned} \quad (1.6.11)$$

3. For free-edges:

$$\begin{aligned} \text{At } x = 0, a : \quad & \sigma_x = 0, \quad \tau_{xy} = 0, \quad \tau_{xz} = 0, \\ \text{At } y = 0, b : \quad & \sigma_y = 0, \quad \tau_{yx} = 0, \quad \tau_{yz} = 0, \\ \text{At } z = 0, h : \quad & \sigma_z = \pm p_z/2, \quad \tau_{zy} = 0, \quad \tau_{zx} = 0. \end{aligned} \quad (1.6.12)$$

From the displacement components the strains are obtained from

$$\varepsilon_x = \frac{\partial u}{\partial x}, \quad \varepsilon_y = \frac{\partial v}{\partial y}, \quad \varepsilon_z = \frac{\partial w}{\partial z} \quad (1.6.13)$$

and

$$\gamma_{xy} = \frac{\partial u}{\partial y} + \frac{\partial v}{\partial x}, \quad \gamma_{yz} = \frac{\partial v}{\partial z} + \frac{\partial w}{\partial y}, \quad \gamma_{zx} = \frac{\partial w}{\partial x} + \frac{\partial u}{\partial z}. \quad (1.6.14)$$

Finally, from the relationship between strains and stresses,

$$\begin{aligned} \varepsilon_x &= \frac{1}{E}(\sigma_x - \nu\sigma_y - \nu\sigma_z), \\ \varepsilon_y &= \frac{1}{E}(\sigma_y - \nu\sigma_z - \nu\sigma_x), \\ \varepsilon_z &= \frac{1}{E}(\sigma_z - \nu\sigma_x - \nu\sigma_y) \end{aligned} \quad (1.6.15)$$

and

$$\gamma_{xy} = \frac{\tau_{xy}}{G}, \quad \gamma_{yz} = \frac{\tau_{yz}}{G}, \quad \gamma_{zx} = \frac{\tau_{zx}}{G}, \quad (1.6.16)$$

the sought stresses can be computed. Solving Eq. (1.6.15), for instance, we obtain

$$\sigma_x = \frac{E}{(1+\nu)(1-2\nu)}[(1-\nu)\varepsilon_x + \nu(\varepsilon_y + \varepsilon_z)]. \quad (1.6.17)$$

Similar expressions can be written for σ_y and σ_z , respectively.

Summary. The three-dimensional elasticity solutions of thick plates have the ability to express precisely the high-order variation displacement and stress through the thickness of the plate. Although such a three-dimensional approach is rigorous, finding solutions is generally extremely difficult. The few analytical solutions available are usually restricted to problems with simple plate geometry, loading conditions and boundary conditions. Srinivas et al. [1.6.5], for instance, expressed the displacements in the form of double trigonometric series to obtain a three-dimensional solution for rectangular thick plates on simple supports. In a further work [1.6.6], the displacement components are expressed in terms of hyperbolic functions to obtain a better convergence of the solution. Practical alternatives to the analytical solutions are the various numerical methods. The *finite difference* technique, for example, transforms the partial differential equations of three-dimensional elasticity into a system of algebraic equations as demonstrated in Ref. [1.6.8]. The three-dimensional *gridwork* and *finite element* methods (as discussed later in this book) currently offer the most versatile solution techniques for almost all thick-plate problems.

References and Bibliography

- [1.6.1] SAADA, A. S., *Elasticity: Theory and Applications*, Pergamon Press, New York, 1974.
- [1.6.2] MUSKHELISHVILI, N. I., *Some Basic Problems of the Mathematical Theory of Elasticity*, P. Noordhoff, Groningen, 1963.
- [1.6.3] FORD, H., *Advanced Mechanics of Materials*, 2nd ed., Ellis Horwood, Chichester, England, 1977.
- [1.6.4] FLÜGGE, W. (Ed.), *Handbook of Engineering Mechanics*, McGraw-Hill Book Company, New York, 1962.
- [1.6.5] SRINIVAS, S., et al., "Flexure of Simply Supported Thick Homogeneous and Laminated Rectangular Plates," *ZAMM*, 49 (1969), 449.
- [1.6.6] SRINIVAS, S., and RAO, A. K., "Flexure of Thick Rectangular Plates," *J. Appl. Mech.*, 49 (1973), 298.
- [1.6.7] SUNDARA RAYA IYENGAR, K. T., et al., "On the Analysis of Thick Rectangular Plates," *Ing. Arch.*, 43 (1974), 317.
- [1.6.8] NG, S. F., and BENCHARIF, N., "A Finite Difference Computer Program for the Modelling of Thick Plates," *Comp. Struct.*, 33 (1983), 1011–1016.
- [1.6.9] MAU, S. T., et al., "Finite Element Solutions for Laminated Thick Plates," *J. Compos. Mater.*, 6 (1972), 304–311.

1.7 Membranes

Membranes are very thin plates with no flexural resistance. The structural behavior of stretched membranes resembles that of a network of stretched strings. Consequently, the lateral load-carrying capacity of the membranes is exclusively due to the in-plane tensile forces that are assumed to be uniform along any section at the boundary (Fig. 1.7.1). Membranes are extensively used in machine design for pumps, compressors, pressure regulators (Fig. 1.7.2), and so on.

Governing Differential Equations. In derivation of the differential equation of equilibrium, it is assumed that the *lateral deflections are small*,[†] and thus the tensile force per unit length acting on the middle surface ($\sigma_x h = \sigma_y h = \sigma h$) remains

[†] Most practical applications of nonstretched membranes require the use of large-deflection theory (Sec. 11.1.).

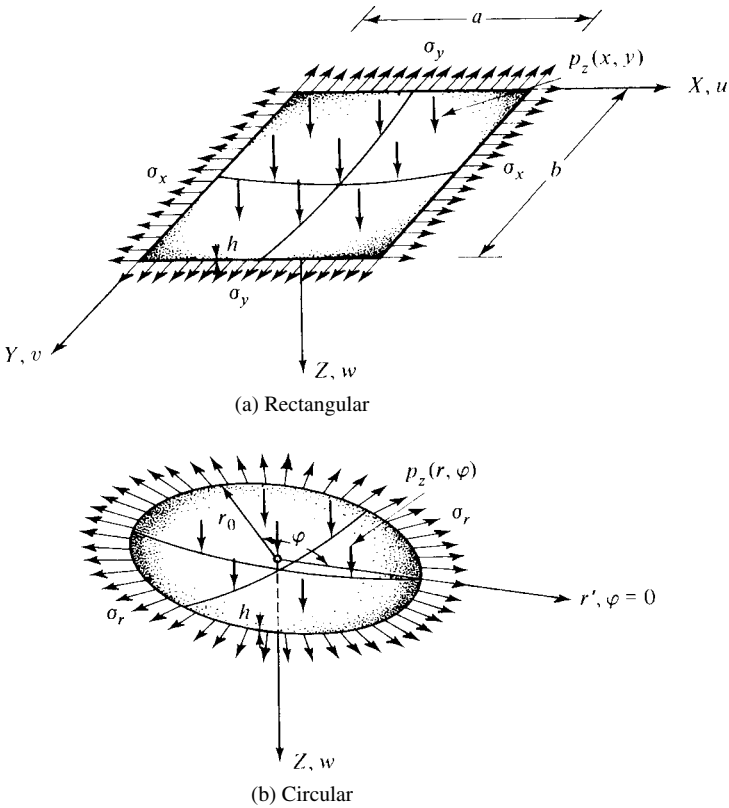


Figure 1.7.1 Stretched membranes.

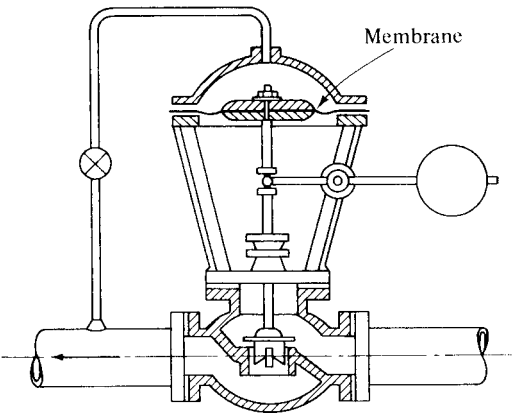


Figure 1.7.2 Pressure regulator.

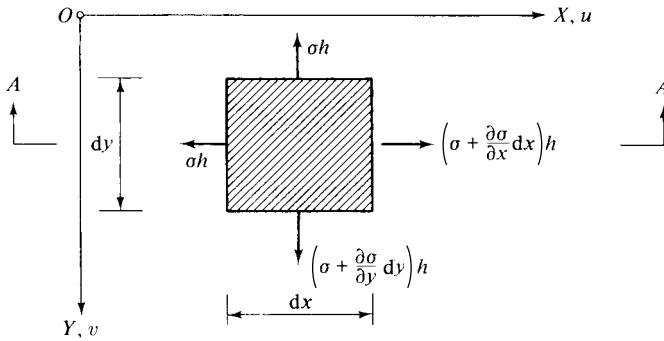
constant. This limitation of membrane theory requires that $(w_{\max}/h)^2$ be negligible in comparison with unity. Because of the assumed symmetric stretching forces, the in-plane shear stresses are zero. Consequently, expressing the vertical equilibrium of all forces acting on a $dx \, dy$ element (Fig. 1.7.3), the summation of the forces in the Z direction yields

$$\begin{aligned} & \left(\sigma + \frac{\partial \sigma}{\partial x} dx \right) \left(\frac{\partial w}{\partial x} + \frac{\partial^2 w}{\partial x^2} dx \right) dy h - \sigma \frac{\partial w}{\partial x} dy h \\ & + \left(\sigma + \frac{\partial \sigma}{\partial y} dy \right) \left(\frac{\partial w}{\partial y} + \frac{\partial^2 w}{\partial y^2} dy \right) dx h - \sigma \frac{\partial w}{\partial y} dx h + p_z(x, y) dx dy = 0, \end{aligned} \quad (1.7.1)$$

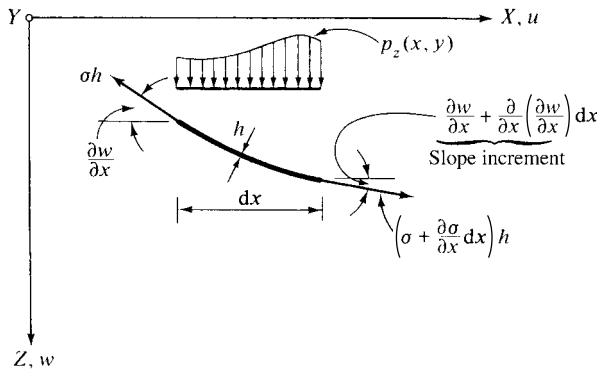
which, after neglecting small quantities of higher order, reduces to

$$\frac{\partial^2 w}{\partial x^2} + \frac{\partial^2 w}{\partial y^2} = -\frac{p_z(x, y)}{\sigma h}. \quad (1.7.2)$$

This differential equation is of Poisson's type and was first derived for membranes by Euler [1.7.1].



(a) Plan view



(b) Section A-A

Figure 1.7.3 Membrane element.

Using the two-dimensional Laplacian operator, Eq. (1.7.2) can be written as

$$\nabla^2 w = -\frac{p_z(x, y)}{\sigma h}. \quad (1.7.3)$$

Applying the coordinate transformation discussed in Sec. 1.4, the governing differential equation of circular membranes, expressed in polar coordinates, can be derived:

$$\frac{\partial^2 w(r, \varphi)}{\partial r^2} + \frac{1}{r^2} \frac{\partial^2 w(r, \varphi)}{\partial \varphi^2} + \frac{1}{r} \frac{\partial w(r, \varphi)}{\partial r} = -\frac{p_z(r, \varphi)}{\sigma h}, \quad (1.7.4)$$

or, using the Laplacian operator (1.4.10),

$$\nabla_r^2 w(r, \varphi) = -\frac{p_z(r, \varphi)}{\sigma h}. \quad (1.7.5)$$

Since in most cases the lateral load is rotationally symmetric, Eq. (1.7.4) becomes

$$\frac{d^2 w(r)}{dr^2} + \frac{1}{r} \frac{dw(r)}{dr} = -\frac{p_z}{\sigma h}. \quad (1.7.6)$$

Summary. Membranes are very thin plates with thickness-to-span ratios less than 1/50. Since they do not have flexural rigidity, they carry the transverse load by in-plane tension. Consequently, their edge support must be immovable. The membrane theory discussed above is based on small deflections of the middle surface. Membranes, however, may have deflections that are many times larger than their thickness. This is an important subject for engineering practice and is treated in Sec. 11.1.

References and Bibliography

- [1.7.1] EULER, L., "De motu vibratorio tympanorum," *Comment. Acad. Petropolit.*, 10 (1766), 243–260.
- [1.7.2] L'HERMITE, R., *Résistance des Matériaux*, Dumond, Paris, 1954.
- [1.7.3] DIMITROV, N., and HERBERG, W., *Festigkeitslehre*, Vol. 2, Walter de Gruyter, Berlin, 1972.
- [1.7.4] SZABÓ, I., *Höhere Technische Mechanik*, 3rd ed., Springer-Verlag, Berlin 1960.
- [1.7.5] TIMOSHENKO, S., *Strength of Materials*, Vol. 2, 3rd ed., D. Van Nostrand Company, Princeton, New Jersey, 1956.

1.8 Summary

In this chapter, the governing differential equations of equilibrium of the four most significant plate types[†] are derived using the classical methods of the theory of elasticity. Since the theory of elasticity is a part of mathematical physics, the methods used in these derivations are mathematical in nature, linked with pertinent physical and geometrical concepts. The so-obtained differential equations are limited to lateral loads, small deflections and linear-elastic material behavior.

[†] These are thin, moderately thick, thick and very thin plates (membranes).

In establishing suitable *mathematical models* capable of describing the actual physical phenomena of load carrying by plates, it was necessary to use certain simplifying assumptions. Although these assumptions, which concern the material properties and physical behaviors[†] inherent to the different plate types, are quite numerous, the errors arising from them are negligible, as the corresponding test results prove. Using these mathematical models, the bending of plates has been expressed in mathematically correct forms by the governing differential equations for thin, moderately thick and thick plates. In addition, the fundamentally different load-carrying behavior of very thin plates (i.e., membranes) has been treated.

Although nowadays—due to the widespread use of computers—the interest in numerical methods is quite dominant, the fundamental concepts of these plate theories remain the basis upon which all numerical methods are built. Other important plate theories covering, for example, large deflections, orthotropic and laminated plates and vibration and stability problems are treated in subsequent chapters.

Problems[‡]

- 1.2.1 Derive the differential equation of a plate bent into a cylindrical surface.
- 1.2.2 Derive the governing differential equation of a plate without any torsional rigidity.
- 1.2.3 Derive the governing differential equation of a square gridwork ($I_x = I_y$) using the beam equations. Compare your result with the solution of Problem 1.2.2.
- 1.3.1 Derive the boundary conditions for a rectangular plate supported by edge beams assuming that a uniformly distributed line load acts on two opposite edges.
- 1.3.2 Rework Problem 1.3.1 considering the torsional rigidity of the beams.
- 1.4.1 Discuss the boundary conditions of rectangular and circular membranes.
- 1.4.2 Verify the validity of Eq. (1.7.6) by using the equilibrium of the membrane element.

[†] Stress distributions, for instance.

[‡] The first two numbers refer to the corresponding section.

2

Exact and Series Solutions of Governing Differential Equations

2.1 Rigorous Solution of Plate Equation[†]

Mathematically, the differential equation of plates (1.2.30) is classified as a linear partial differential equation of the fourth order having constant coefficients [2.1.1, 2.1.2]. Its homogeneous form,

$$\nabla^2 \nabla^2 w = 0, \quad (2.1.1)$$

is called the *biharmonic equation*.

In general, there are four types of mathematically “exact” solutions available for plate problems:

1. closed-form solution,
2. solution of the homogeneous biharmonic equation upon which a *particular solution* of the governing differential equation of plate (1.2.30) is superimposed,
3. double trigonometric series solution, and
4. single series solution.

Since the boundaries of these categories are not rigid, some overlap is possible.

The rigorous solution of Eq. (1.2.30) must satisfy the boundary conditions characterizing each problem and the governing differential equation of the plate. Consequently, the rigorous solution of plate problems is essentially a *boundary value* problem of mathematical physics. Since the fulfillment of the boundary conditions

[†] In a Cartesian coordinate system.

usually presents considerable mathematical difficulties, in general, rigorous solutions of plate problems are rare. In the few cases that lend themselves to exact analysis, the linearity of Eq. (1.2.30) can be used to permit the linear combination of solutions in the form of superposition. Thus, the most general form of the rigorous solution of the governing differential equation can be written as

$$w(x, y) = w_H(x, y) + w_P(x, y), \quad (2.1.2)$$

where w_H represents the solution of the homogeneous equation (2.1.1) and w_P is a particular solution of the nonhomogeneous differential equation of the plate (1.2.30). There are a few cases, however, when the solution can be obtained directly, without employing the above-mentioned superposition principle (Fig. 2.1.1).

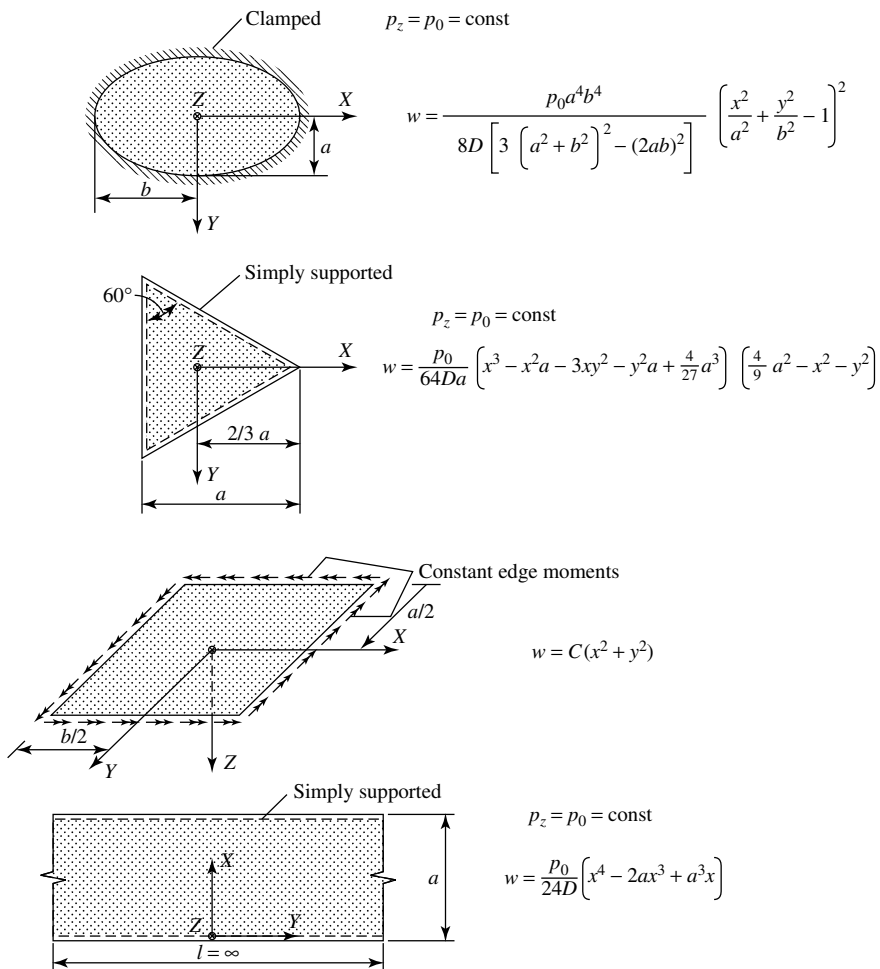


Figure 2.1.1 Closed-form, exact solutions of plate equation (1.2.30).

Certain boundary conditions permit the use of special solutions, such as the Navier solution, described in Sec. 2.2. In the Navier solution $w_H = 0$; thus

$$w(x, y) = w_P(x, y). \quad (2.1.3)$$

Furthermore, if the boundary conditions for the edge moments are known, we may use a two-step solution involving Eq. (1.2.43).

a. Solution of Homogeneous Equation. The physical interpretations of the solution of the biharmonic equation ($\nabla^4 w = 0$) is to obtain the deflection of the plate $w_H(x, y)$ when only edge forces are acting. Consequently, the solution of the homogeneous equation fulfills the prescribed boundary conditions and maintains the equilibrium with the external boundary forces. The fundamental difficulty of the rigorous solution is the proper choice of functions $w_H(x, y)$ for a given problem.

The biharmonic equation (2.1.1) permits the use of the solutions of the Laplace equation $\nabla^2 w = 0$, which are

$$x, \quad xy, \quad \cos \alpha x, \quad \cosh \alpha y, \quad x^2 - y^2 \quad \text{and} \quad x^3 - 3xy^2, \quad (2.1.4)$$

where α represents an arbitrary constant. In Eq. (2.1.4) we may interchange x and y and replace \cos by \sin and \cosh by \sinh , respectively. If $w_1(x, y)$ and $w_2(x, y)$ are solutions of the Laplace equation, then

$$w_1 + xw_2, \quad w_1 + yw_2 \quad \text{and} \quad w_1 + (x^2 + y^2)w_2 \quad (2.1.5)$$

are solutions of the homogeneous biharmonic equation $\nabla^2 \nabla^2 w = 0$.

Furthermore, the following expressions are solutions of the biharmonic equation:

$$\begin{aligned} w_H = & x^2, \quad x^3, \quad x^2y, \quad x^3y, \quad \cos \alpha x \cosh \alpha y, \quad x \cos \alpha x \cosh \alpha y, \\ & x \cos \alpha y \cosh \alpha x, \quad x^4 - y^4, \quad e^{\pm \alpha x} \cos \alpha y, \quad \ln(x^2 + y^2), \\ & (x + y) \ln(x^2 + y^2), \quad (x^2 + y^2) \ln(x^2 + y^2) \quad \text{etc.} \end{aligned} \quad (2.1.6)$$

Again, it is possible to interchange x and y and replace \cos by \sin and \cosh by \sinh , respectively.

Additional solutions are obtained using "biharmonic" polynomials [2.1.13], such as

$$\begin{aligned} w_H = & x^4 - 3x^2y^2, \quad x^4y - x^2y^3, \quad x^5 - 5x^3y^2, \quad x^5y - \frac{5}{3}x^3y^3, \\ & x^6 - 10x^4y^2 + 5x^2y^4, \quad x^6y - \frac{10}{3}x^4y^3 + x^2y^5, \\ & x^7 - 14x^5y^2 + \frac{35}{3}x^3y^4, \quad x^7y - \frac{14}{3}x^5y^3 + \frac{7}{3}x^3y^5, \\ & x^8 - 21x^6y^2 + 35x^4y^4 - 7x^2y^6, \quad x^8y - 7x^6y^3 + 7x^4y^5 - x^2y^7, \\ & x^9 - 27x^7y^2 + 63x^5y^4 - 21x^3y^6, \quad x^9y - 9x^7y^3 + \frac{63}{5}x^5y^5 - 3x^3y^7, \\ & \text{etc.} \end{aligned} \quad (2.1.7)$$

In Eq. (2.1.7) we may, again, interchange x and y .

All these expressions can be multiplied by arbitrary constants and, if required, added. Worch [2.1.14] gives an extensive listing of functions that can be used for solution of the biharmonic equation.

Since the homogeneous plate equation $\nabla^4 w_H = 0$ has the very same form as the differential equation describing two-dimensional stress problems $\nabla^4 \Phi = 0$, it is evident that an analogy exists between w_H and Φ [2.1.18]. Neou introduced a unique direct approach to determine the so-called Airy stress function $\Phi(x, y)$ in polynomial form [2.1.19]. Based on the above-mentioned analogy, Szilard extended Neou's method to rectangular plates [2.1.20] and directly obtained the homogeneous part of the solution, w_H , also in polynomial forms.

A special method for finding solutions of the biharmonic equation is based on *separation of variables* and is discussed in detail in Sec. 2.3.

b. Particular Solution. Although the solution w_H of the homogeneous biharmonic equation effectively describes the equilibrium conditions of the plate subjected to edge forces, the expression of the deflection $w(x, y)$ is not complete without also considering the equilibrium of the lateral forces p_z . For this purpose, a particular solution w_P of the nonhomogeneous differential equation (1.2.30) must also be determined. We require from the particular solution that it satisfy the differential equation of the plate (1.2.30), but the fulfillment of the boundary conditions is not mandatory. In the case of an infinite series solution, however, a more rapid convergence can be obtained if the particular solution at least fulfills the boundary conditions of two opposite edges of the plate.

For rectangular plates with fixed, or partially fixed, boundary conditions at certain or all edges, the expression of deflections of the simply supported plate can be used as a particular solution. This can be obtained with relative ease using Navier's method, described in Sec. 2.2. Upon this particular solution, the effects of the edge moments are superimposed. In certain cases, however, it is more expedient to choose the particular solutions as function of x or y only, which can be achieved by using the expressions of the corresponding beam deflections, as shown in Sec. 2.3.

Finally, the possibility of expressing the true *singularity*[†] of the problem, in the case of a concentrated lateral load, must be mentioned briefly. If such a force acts at the center of a rectangular plate (Fig. 2.1.2), for instance, the particular solution can be given by

$$w_P(x, y) = \frac{P_z}{16\pi D} (x^2 + y^2) \ln \frac{x^2 + y^2}{a^2}. \quad (2.1.8)$$

These types of solutions coupled with *Maxwell's law of reciprocity* are used for obtaining influence surfaces for plates, as described in Sec. 10.5.

Summary. Closed-form solutions of plate problems are rare. The general solution of the governing differential equation of the plate (1.2.30) is usually obtained as the sum of the solution of the homogeneous equation (2.1.1) and a particular solution. While obtaining a particular solution is relatively easy, finding suitable functions for the biharmonic equation presents considerable difficulties. Consequently, rigorous solutions of plate problems are usually limited to a number of cases, which are

[†] Theoretically, at the point of application of concentrated forces the internal forces (m , q) are infinitely large.

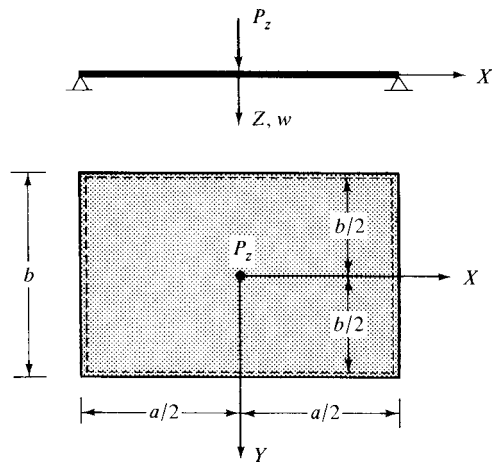


Figure 2.1.2 Rectangular plate under concentrated load.

discussed in Secs 2.2 and 2.3. For certain combinations of boundary and loading conditions, the rigorous solution has not yet been found.

ILLUSTRATIVE EXAMPLE

One of the rare cases of plate problems for which a closed-form solution can readily be obtained is the circular plate with clamped edges under a uniform load (Fig. 2.1.3).

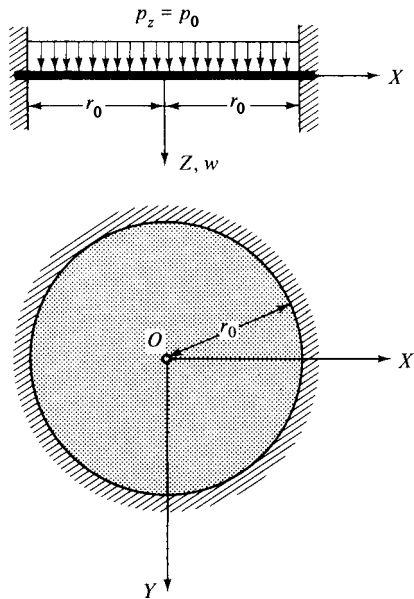


Figure 2.1.3 Clamped circular plate.

We assume that the deflection is in the form

$$w(x, y) = c \left(\frac{x^2}{r_0^2} + \frac{y^2}{r_0^2} - 1 \right)^2, \quad (2.1.9)$$

where r_0 represents the radius of the circular plate and c is an unknown constant.

The boundary conditions of the plate around the edge are

$$w = 0 \quad \text{and} \quad \frac{\partial w}{\partial x} = \frac{\partial w}{\partial y} = 0. \quad (2.1.10)$$

By introducing the notation

$$\mathfrak{W} = \left(\frac{x^2}{r_0^2} + \frac{y^2}{r_0^2} - 1 \right), \quad (2.1.11)$$

the deflection surface of the plate becomes

$$w = c\mathfrak{W}^2. \quad (2.1.12)$$

Since at the edge $r^2 = r_0^2 = x^2 + y^2$, Eq. (2.1.9) gives zero deflection along the circular edge.

Taking the first derivatives of Eq. (2.1.12), we can write

$$\frac{\partial w}{\partial x} = 2c\mathfrak{W} \frac{\partial \mathfrak{W}}{\partial x} \quad \text{and} \quad \frac{\partial w}{\partial y} = 2c\mathfrak{W} \frac{\partial \mathfrak{W}}{\partial y}. \quad (2.1.13)$$

These expressions vanish at $r_0^2 = x^2 + y^2$. Thus, we conclude that the assumed expression for the deflection (2.1.9) satisfies the prescribed boundary conditions of the plate (2.1.10).

Next, we substitute Eq. (2.1.12) into the governing differential equation of the plate (1.2.30). The calculation of the derivatives gives

$$\frac{\partial^4 w}{\partial x^4} = 24 \frac{c}{r_0^4}, \quad \frac{\partial^4 w}{\partial x^2 \partial y^2} = 8 \frac{c}{r_0^4}, \quad \frac{\partial^4 w}{\partial y^4} = 24 \frac{c}{r_0^4}. \quad (2.1.14)$$

Substituting these values into the governing differential equation of the plate,

$$\frac{\partial^4 w}{\partial x^4} + 2 \frac{\partial^4 w}{\partial x^2 \partial y^2} + \frac{\partial^4 w}{\partial y^4} = \frac{p_0}{D}, \quad (2.1.15)$$

we obtain

$$\frac{c}{r_0^4} (24 + 16 + 24) = \frac{p_0}{D}. \quad (2.1.16)$$

Hence

$$c = \frac{p_0 r_0^4}{64D}, \quad (2.1.17)$$

which substituted into Eq. (2.1.9) gives the sought-for expression of the deflected middle surface of the plate.

In a similar manner, the deflection of a uniformly loaded elliptical plate, clamped at the edge, is readily obtained. In most cases, however, the rigorous solution of the plate problems is extremely cumbersome or even impossible. Illustrative examples of series-type solutions are given in Secs. 2.2–2.4.

References and Bibliography

- [2.1.1] GROSSBERG, L., *Differentialgleichungen der mathematischen Physik*, Springer-Verlag, Berlin, 1952.
- [2.1.2] WEBSTER, A. G., *Partial Differential Equations of Mathematical Physics*, Dover Publications, New York, 1955.
- [2.1.3] KORN, G., and KORN, T., *Mathematical Handbook for Scientists and Engineers*, McGraw-Hill Book Company, New York, 1961.
- [2.1.4] STEPANOV, V. V., *Kurs differentsial'nykh Uravnenii (Textbook of Differential Equations)*, 7th ed., Gos Izd.-vo Tekhniko Teoret. Lit-ry, Moscow, 1958.
- [2.1.5] MADELUNG, E., *Die mathematischen Hilfsmittel des Physikers*, Springer-Verlag, Berlin, 1964.
- [2.1.6] BRONSTEIN, I. N., and SEMENDJAJEW, K. A., *Taschenbuch der Mathematik* (German translation of the original Russian text), B. G. Teubner Verlagsgesellschaft, m.b.H., Leipzig, 1958.[†]
- [2.1.7] MURRAY, D. A., *Introductory Course in Differential Equations*, Longmans, Green & Company, London, 1957.
- [2.1.8] SOMMERFELD, A., *Partial Differential Equations in Physics*, Academic Press, New York, 1949.
- [2.1.9] EGERVÁRY, T., *A mechanika differencialegyenleteiről (On the Differential Equations of Mechanics)*, Tankönyvkiadó, Budapest, 1948.
- [2.1.10] WEBSTER, A. G., and PLIMTON, S. T., *Partial Differential Equations of Mathematical Physics*, Dover Publications, New York, 1955.
- [2.1.11] HADAMARD, T., "Mémoire sur le problème d'analyse relatif à l'équilibre des plaques élastiques encastrées," *Mem. Acad. Sci. (Savants Étrangers, Sér. 2)*, 33, No. 4 (1908) 1–128.
- [2.1.12] BERGMAN, S., "Solutions of Linear Partial Differential Equations of Fourth Order," *Duke Math. J.*, 11 (Nov. 1944), 617–649.
- [2.1.13] ZWEILING, K., *Biharmonische Polynome*, Springer-Verlag, Berlin, 1952.
- [2.1.14] WORCH, G., "Elastische Scheiben," in *Beton-Kalender*, Vol. 2, W. Ernst und Sohn, Berlin, 1956, pp. 31–120.
- [2.1.15] TYCHONOW, A. N., and SAMARSKI, A. A., *Differentialgleichungen der mathematischen Physik* (German translation of the original Russian text), VEB Deutscher Verlag der Wissenschaften, Berlin, 1959.
- [2.1.16] PETROWSKI, I. G., *Vorlesungen über Partielle Differentialgleichungen* (German translation of the original Russian text), B. G. Teubner, Leipzig, 1955.[‡]
- [2.1.17] DINNIK, A. N., *Prilozhenie funktsii besselia k zadacham teorii uprugosti (Application of Bessel-functions to Problems in the Theory of Elasticity)*, Izbrannye Trudy t-II; gl-III, Izdvo Akademii Nauk Ukr. SSR, Kiev, 1955.

[†] Available also in English translation: *A Guide-Book to Mathematics*, The Macmillan Company, New York, 1964.

[‡] Available also in English translation: *Lectures on Partial Differential Equations*, Dover Publications, New York, 1990.

- [2.1.18] SCHAEFER, R., "Die vollständige Analogie ScheibePlatte," *Abhandlungen Braunschweig Wiss. Gesellschaft*, Heft 5 (1956).
- [2.1.19] NEOU, C. Y., "A Direct Method for Determining Airy Polynomial Stress Function," *J. Appl. Mech.*, 24 (1957), 387–390.
- [2.1.20] SZILARD, R., "Auswahl von biharmonischen Polynomen zur Lösung der Plattengleichung," *Die Bautechnik*, 54 (1977), 187–190.

2.2 Solutions by Double Trigonometric Series (Navier's Approach)

In 1820, Navier presented a paper to the French Academy of Sciences on the solution of bending of simply supported rectangular plates by double trigonometric series. Navier's solution is sometimes called the *forced* solution of the differential equations since it "forcibly" transforms the differential equation into an algebraic equation, thus considerably facilitating the required mathematical operations.

The boundary conditions of rectangular plates, for which the Navier solution is applicable, are[†]

$$\begin{aligned} (w)_{x=0, x=a} &= 0, & (m_x)_{x=0, x=a} &= 0, \\ (w)_{y=0, y=b} &= 0, & (m_y)_{y=0, y=b} &= 0, \end{aligned} \quad (2.2.1)$$

representing simply supported edge conditions at all edges.

The solution of the governing differential equation of the plate (1.2.30) subjected to a transverse loading is obtained by Navier's method as follows:

1. The deflections are expressed by a double sine series,

$$w(x, y) = \sum_{m=1}^{\infty} \sum_{n=1}^{\infty} W_{mn} \sin \frac{m\pi x}{a} \sin \frac{n\pi y}{b}, \quad (2.2.2)$$

which satisfies all the above-stated boundary conditions. In Eq. (2.2.2) the coefficients of expansion W_{mn} are unknown.

2. The lateral load p_z is also expanded into a double sine series:

$$p_z(x, y) = \sum_{m=1}^{\infty} \sum_{n=1}^{\infty} P_{mn} \sin \frac{m\pi x}{a} \sin \frac{n\pi y}{b}, \quad (2.2.3)$$

for $m, n = 1, 2, 3, \dots$

The coefficients P_{mn} of the double Fourier expansion of the load are determined from Eq. (A.1.34), as discussed in Appendix A.1.

3. Substituting Eqs. (2.2.2) and (2.2.3) into the governing differential equation (1.2.30), an algebraic equation is obtained from which the unknown W_{mn} can be readily calculated.

[†] For a coordinate system, see Fig. 1.1.1.

Thus, for specific m and n values, Eq. (1.2.30) becomes

$$W_{mn} \left[\frac{m^4 \pi^4}{a^4} + \frac{2m^2 n^2 \pi^4}{a^2 b^2} + \frac{n^4 \pi^4}{b^4} \right] \sin \frac{m\pi x}{a} \sin \frac{n\pi y}{b} = \frac{1}{D} P_{mn} \sin \frac{m\pi x}{a} \sin \frac{n\pi y}{b}; \quad (2.2.4)$$

hence

$$W_{mn} = \frac{P_{mn}}{D\pi^4[(m^2/a^2) + (n^2/b^2)]^2}. \quad (2.2.4a)$$

Summing the individual terms, an analytical solution for the deflection of the plate is obtained. Thus, we can write

$$w(x, y) = \frac{1}{D\pi^4} \sum_{m=1}^{\infty} \sum_{n=1}^{\infty} \frac{P_{mn}}{[(m^2/a^2) + (n^2/b^2)]^2} \sin \frac{m\pi x}{a} \sin \frac{n\pi y}{b}. \quad (2.2.5)$$

Substituting $w(x, y)$ into the expressions of internal moments and shears given in Eqs. (1.2.26), (1.2.27), (1.2.29) and (1.2.33), the internal forces, and thus the state of stress, at any point of the plate can be determined. For the moments in the plate, for instance, we obtain

$$\begin{aligned} m_x &= \pi^2 D \sum_{m=1}^{\infty} \sum_{n=1}^{\infty} \left[\left(\frac{m}{a} \right)^2 + \nu \left(\frac{n}{b} \right)^2 \right] W_{mn} \sin \frac{m\pi x}{a} \sin \frac{n\pi y}{b}, \\ m_y &= \pi^2 D \sum_{m=1}^{\infty} \sum_{n=1}^{\infty} \left[\left(\frac{n}{b} \right)^2 + \nu \left(\frac{m}{a} \right)^2 \right] W_{mn} \sin \frac{m\pi x}{a} \sin \frac{n\pi y}{b}, \\ m_{xy} &= -\pi^2 D(1 - \nu) \sum_{m=1}^{\infty} \sum_{n=1}^{\infty} \frac{mn}{ab} W_{mn} \cos \frac{m\pi x}{a} \cos \frac{n\pi y}{b} \end{aligned} \quad (2.2.6)$$

and for the transverse shear forces,

$$\begin{aligned} q_x &= \frac{\pi^3 D}{a} \sum_{m=1}^{\infty} \sum_{n=1}^{\infty} \left\{ m \left[\left(\frac{m}{a} \right)^2 + \nu \left(\frac{n}{b} \right)^2 + (1 - \nu) \left(\frac{n}{b} \right)^2 \right] \right\} \\ &\quad \times W_{mn} \cos \frac{m\pi x}{a} \sin \frac{n\pi y}{b}, \\ q_y &= \frac{\pi^3 D}{b} \sum_{m=1}^{\infty} \sum_{n=1}^{\infty} \left\{ n \left[\left(\frac{n}{b} \right)^2 + \nu \left(\frac{m}{a} \right)^2 + (1 - \nu) \left(\frac{m}{a} \right)^2 \right] \right\} \\ &\quad \times W_{mn} \sin \frac{m\pi x}{a} \cos \frac{n\pi y}{b}. \end{aligned} \quad (2.2.7)$$

Similarly, using Eq. (1.3.3), the vertical edge forces at the boundaries of the plate can be calculated.

By the skillful application of the superposition theorem, one can extend the use of Navier's solution to rectangular plates that have other than simply supported boundary

conditions.[†] The approach in such a case is similar to the solution of pertinent beam problems. That is, on the solution of the simply supported plate w_p , the effect of the boundary forces or moments are superimposed, giving

$$w(x, y) = w_p + \sum w_H. \quad (2.2.8)$$

The infinite series solution for the deflections, w , generally converges quickly; thus, satisfactory accuracy can be obtained by considering only a few terms. The convergence of the series solution is, however, slow in the vicinity of concentrated forces, as discussed in Appendix A.1. Since the internal forces are obtained from second and third derivatives of the deflections $w(x, y)$, some loss of accuracy in this process is inevitable. Although the convergence of the infinite series expressions of the internal forces (2.2.6) is less rapid, especially in the vicinity of edges, the results are acceptable, since the accuracy of the solution can be improved by considering more terms.

Summary. For simply supported rectangular plates, Navier's solution offers considerable mathematical advantages, since the solution of the governing fourth-order partial differential equation (1.2.30) is reduced to solution of an algebraic equation. The technique of application of Navier's method is summarized as follows:

1. Expand the lateral load into double Fourier (sine) series using the technique given in Appendix A.1.
2. Express the deflections also in double sine series.
3. Find the deflections using Eq. (2.2.5).
4. The substitution of the deflections, w , into the expressions for internal moments, shears and edge forces gives the required quantities.
5. Carry out all operations for a specific (m, n) th component; the final results are obtained by adding the terms.

The convergence of the series is usually fast in the case of distributed loads. The convergence, however, becomes slow for concentrated and discontinuous loads.

ILLUSTRATIVE EXAMPLE I

Find the deflections of a simply supported rectangular plate ($a \times 2a$) subjected to a uniformly distributed load (Fig. 2.2.1). Determine the maximum bending moments and calculate the edge reactions.

In the first step the uniformly distributed lateral load is expanded into a double Fourier series, applying the technique shown in Appendix A.1. Using Eq. (A.1.34), we can write

$$p_z = \frac{16p_0}{\pi^2} \sum_{m=1}^{\infty} \sum_{n=1}^{\infty} \frac{1}{mn} \sin \frac{m\pi x}{a} \sin \frac{n\pi y}{2a}, \quad (2.2.9)$$

[†] See Sec. 2.5.

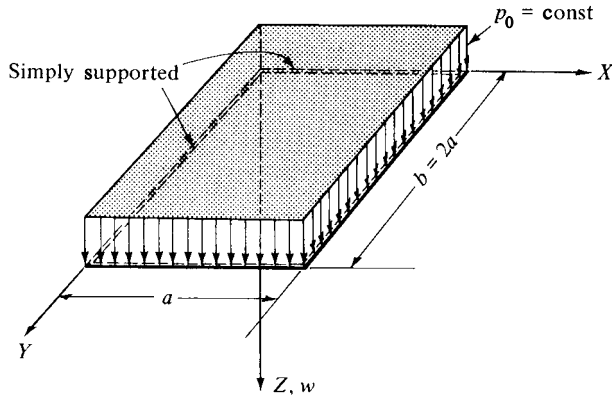


Figure 2.2.1 Simply supported rectangular plate.

where $16p_0/\pi^2 mn = P_{mn}$ and m, n are positive odd integers ($m, n = 1, 3, 5, \dots$).

Using also a double sine series expression for the deflections [Eq. (2.2.2)], the unknown constant W_{mn} , pertinent to a specific set of m, n values, is obtained from Eq. (2.2.4a); thus

$$W_{mn} = \frac{P_{mn}}{D\pi^4\{(m^2/a^2) + [n^2/(2a)^2]\}^2} = \frac{16p_0a^4}{D\pi^6 mn[m^2 + (n^2/4)]^2}; \quad (2.2.10)$$

hence

$$w(x, y) = \frac{16p_0a^4}{D\pi^6} \sum_{m=1}^{\infty} \sum_{n=1}^{\infty} \frac{\sin(m\pi x/a) \sin(n\pi y/2a)}{mn[m^2 + (n^2/4)]^2},$$

for $m, n = 1, 3, 5, \dots$ (2.2.11)

The maximum deflection occurs at $x = a/2$ and $y = a$, which is

$$\begin{aligned} w_{\max} &= \frac{16p_0a^4}{D\pi^6} (0.640 - 0.032 - 0.004 + 0.004 + \dots) \\ &\approx \frac{0.0101 p_0 a^4}{D}. \end{aligned} \quad (2.2.12)$$

Since this series converges very rapidly, the consideration of two terms gives an accuracy sufficient for all practical purposes.

Substituting $b = 2a$, $x = a/2$ and $y = a$ into Eq. (2.2.6), the maximum moments are obtained:

$$(m_x)_{\max} = \frac{16p_0a^2}{\pi^4} \sum_m \sum_n \frac{[m^2 + \nu(n^2/4)] \sin(m\pi/2) \sin(n\pi/2)}{mn[m^2 + (n^2/4)]^2} \quad (2.2.13a)$$

and

$$(m_y)_{\max} = \frac{16p_0a^2}{\pi^4} \sum_m \sum_n \frac{[(n^2/4) + vm^2] \sin(m\pi/2) \sin(n\pi/2)}{mn[m^2 + (n^2/4)]^2}$$

for $m, n = 1, 3, 5, \dots$ (2.2.13b)

Although these series converge somewhat more slowly than those of the deflections [Eq. (2.2.12)], the consideration of four terms gives sufficient accuracy. The convergence of the series expressions of the moments at the edges is slower; consequently more than four terms should be considered.

The vertical edge forces at the boundaries of the plate are calculated from Eq. (1.3.3). Substituting the m th and n th terms of the deflections [Eq. (2.2.11)] into Eq. (1.3.3), we obtain

$$(v_x)_{m,n} = \frac{16p_0a}{\pi^3} \left(\left\{ \frac{m^3}{mn[m^2 + (n^2/4)]^2} \right\} + (2 - \nu) \frac{m(n/2)^2}{mn[m^2 + (n^2/4)]^2} \right) \\ \times \cos \frac{m\pi x}{a} \sin \frac{n\pi y}{2a}. \quad (2.2.14)$$

Thus, the reactive edge force at $x = 0$ is

$$(\bar{v}_x)_{x=0} = -\frac{16p_0a}{\pi^3} \sum_m \sum_n \frac{m^2 + (2 - \nu)(n^2/4)}{n[m^2 + (n^2/4)]^2} \sin \frac{n\pi y}{2a}$$

for $m, n = 1, 3, 5, \dots$ (2.2.15)

Similarly, the reactive edge force at $y = 0$ is calculated from

$$(\bar{v}_y)_{y=0} = -\frac{16p_0a}{\pi^3} \sum_m \sum_n \frac{(n^2/4) + (2 - \nu)m^2}{2m[m^2 + (n^2/4)]^2} \sin \frac{m\pi x}{a}$$

for $m, n = 1, 3, 5, \dots$ (2.2.16)

ILLUSTRATIVE EXAMPLE II[†]

Let us determine the deflections, internal moments and edge forces of a simply supported rectangular plate under a hydrostatic pressure, shown in Fig. 2.2.2.

The coefficient P_{mn} of the double Fourier expansion of the load is obtained from Eq. (A.1.34):

$$P_{mn} = \frac{4}{ab} \int_0^a \int_0^b p_z(x, y) \sin \frac{m\pi x}{a} \sin \frac{n\pi y}{b} dx dy. \quad (2.2.17)$$

[†] Details in computation have been omitted since the reader should find no difficulty in working out the results.

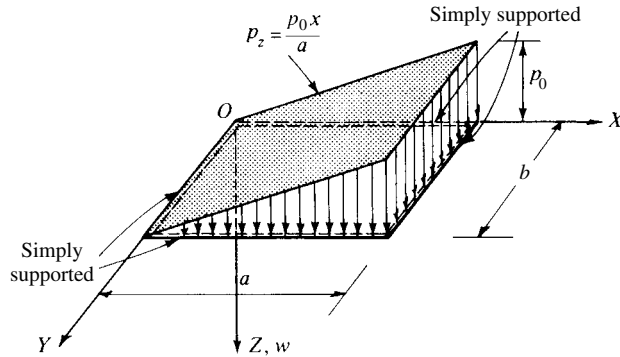


Figure 2.2.2 Hydrostatically loaded rectangular plate.

Since

$$p_z(x, y) = \frac{p_0 x}{a},$$

Eq. (2.2.17) can be written as

$$P_{mn} = \frac{4p_0}{a^2 b} \int_0^a x \sin \frac{m\pi x}{a} dx \int_0^b \sin \frac{n\pi y}{b} dy. \quad (2.2.18)$$

The evaluation of these integrals yields

$$P_{mn} = \frac{4p_0}{a^2 b} \left(-\frac{a^2}{m\pi} \cos m\pi \right) \left(\frac{2b}{n\pi} \right) = -\frac{8p_0 \cos m\pi}{mn\pi^2} \quad (2.2.19)$$

for all integers m and n .

By substituting Eq. (2.2.19) into Eq. (2.2.5), the following double Fourier series expression of the deflected plate surface is obtained:

$$w(x, y) = \frac{8p_0}{\pi^6 D} \sum_{m=1,2,3,\dots}^m \sum_{n=1,2,3,\dots}^m \frac{(-1)^{m+1} \sin(m\pi x/a) \sin(n\pi y/b)}{mn[(m^2/a^2) + (n^2/b^2)]^2}. \quad (2.2.20)$$

Let us compare this result with the more rigorous solution given on p. 125 of Ref. [2]. If $a = b$, the deflection at the center of the plate becomes

$$\begin{aligned} (w)_{x=y=a/2} &= \frac{8p_0}{\pi^6 D} \sum_{m=1,2,3,\dots}^{\infty} \sum_{n=1,2,3,\dots}^{\infty} \frac{(-1)^{[(m+n)/2]-1}}{mn[(m^2/a^2) + (n^2/b^2)]^2} \\ &= 0.00203 \frac{p_0 a^4}{D}, \end{aligned} \quad (2.2.21)$$

which checks with the more rigorous solution mentioned above.

The internal moment m_x is obtained by substituting Eq. (2.2.20) into Eq. (1.2.26). Similarly, the edge force v_x is computed from Eq. (1.3.3). Since the

derivatives of $w(x, y)$ are used in these expressions, first the differentiation is carried out for a specific set of m and n values, and then the summation is applied after the results are obtained. Thus, Eq. (1.2.26) gives

$$\begin{aligned} m_x &= -D \left(\frac{\partial^2 w}{\partial x^2} + \nu \frac{\partial^2 w}{\partial y^2} \right) \\ &= \frac{8p_0}{\pi^6} \sum_{m=1,3,5,\dots}^{\infty} \sum_{n=1,3,5,\dots}^{\infty} \frac{(-1)^{m+1} [(m\pi/a)^2 + \nu(n\pi/b)^2]}{mn[(m^2/a^2) + (n^2/b^2)]^2} \\ &\quad \times \sin \frac{m\pi x}{a} \sin \frac{n\pi y}{b}. \end{aligned} \quad (2.2.22)$$

Considering only four terms ($m, n = 1, 3$) in the summation and using $\nu = 0.3$, the moment m_x at $x = y = a/2$ becomes

$$m_x = 0.0235a^2 p_0, \quad (2.2.23)$$

which checks closely with the “exact” value ($0.0239a^2 p_0$). Since the load is not symmetrical, $m_x \neq m_y$.

The edge reaction [Eq. (1.3.3)] at $x = 0$ and $y = b/2$ for $\nu = 0.3$ is

$$\bar{v}_x = D \left[\frac{\partial^3 w}{\partial x^3} + (2 - \nu) \frac{\partial^3 w}{\partial x \partial y^2} \right] = -0.12685 p_0 a. \quad (2.2.24)$$

Again, a comparison with the more exact solution ($-0.126 p_0 a$) indicates only a very small discrepancy.

The reader will find further examples of Navier's method in Sec. 2.4.

2.3 Solutions by Single Trigonometric Series (Lévy's Method)

The solution of plate problems by a single trigonometric series may be considered as a specific application of the rigorous solutions that were treated in general terms in Sec. 2.1.

This powerful method, introduced by Lévy [2.3.1], obtains the solution of Eq. (1.2.30) in two distinctly separated steps in accordance with Eq. (2.1.2); thus

$$w(x, y) = w_H + w_P,$$

where w_H represents the solution of the homogeneous plate equation (2.1.1) and w_P is a particular solution of Eq. (1.2.30).

To obtain a particular solution by Lévy's method, it is required that two opposite edges of the plate be simply supported and it is assumed that the plate is infinitely long in the other direction. In our further discussion we assume that the edges at $x = 0$ and $x = a$ are simply supported and that the origin of the coordinate system is

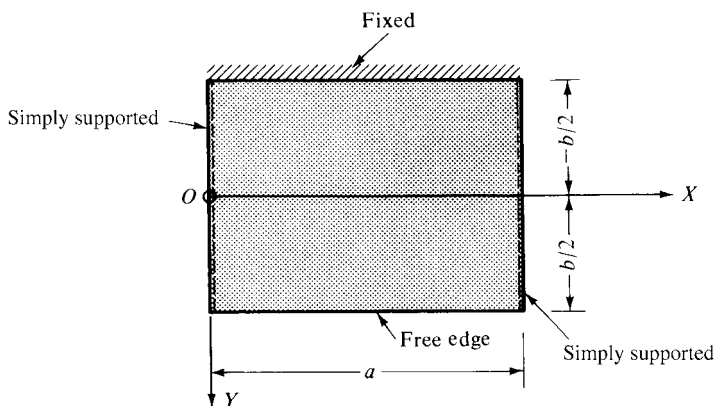


Figure 2.3.1 Location of coordinate system for Lévy's method.

moved to $x = 0$ and $y = b/2$ (Fig. 2.3.1). Furthermore, it is required that the lateral loading have the same distribution in all sections, parallel to the X axis.

From the assumption that $b \rightarrow \infty$, it follows that the differential equation of the plate degenerates into

$$\frac{d^4 w(x)}{dx^4} = \frac{p_z(x)}{D}. \quad (2.3.1)$$

Since $w(x)$ is a function of one variable only, Eq. (2.3.1) resembles the differential equation of the beam:

$$\frac{d^4 w^*(x)}{dx^4} = \frac{p_z(x)}{EI}. \quad (2.3.2)$$

Comparing Eqs. (2.3.1) and (2.3.2), the simple relationship

$$w = w^*(1 - \nu^2) \quad (2.3.3)$$

is evident.

Equation (2.3.1) can be solved by utilizing Navier's method; thus, we seek the solution in the form

$$w_P(x) = \sum_{m=1}^{\infty} W_m \sin \frac{m\pi x}{a}. \quad (2.3.4)$$

Expressing the load by a similar type of Fourier expression (see Sec. 2.2), we obtain

$$p_z(x) = \sum_{m=1}^{\infty} P_m \sin \frac{m\pi x}{a}. \quad (2.3.5)$$

Substituting Eqs. (2.3.4) and (2.3.5) into (2.3.1), the differential equation is transformed into an algebraic equation from which W_m , pertinent to a specific m value, can easily be obtained.

In the second step the solution of the homogeneous biharmonic equation

$$\nabla^2 \nabla^2 w_H(x, y) = 0 \quad (2.3.6)$$

is found in the form

$$w_H = X(x) \cdot Y(y), \quad (2.3.7)$$

the substitution of which into Eq. (2.3.6) yields

$$X^{\text{IV}}Y + 2X''Y'' + XY^{\text{IV}} = 0. \quad (2.3.8)$$

Let us express w_H by a single trigonometric series; thus, we can write

$$w_H(x, y) = \sum_{m=1}^{\infty} Y_m(y) \sin \frac{m\pi x}{a}. \quad (2.3.9)$$

This expression satisfies the assumed simply supported boundary conditions in the X direction, since at $x = 0$ and $x = a$,

$$w_H = 0 \quad \text{and} \quad \frac{\partial^2 w_H}{\partial x^2} = 0. \quad (2.3.10)$$

Substitution of Eq. (2.3.9) into Eq. (2.3.6) gives

$$\sum_{m=1}^{\infty} \left[\frac{m^4 \pi^4}{a^4} Y_m(y) - 2 \frac{m^2 \pi^2}{a^2} Y_m''(y) + Y_m^{\text{IV}}(y) \right] \sin \frac{m\pi x}{a} = 0, \quad (2.3.11)$$

or, for a specific m value,

$$\frac{m^4 \pi^4}{a^4} Y_m(y) - 2 \frac{m^2 \pi^2}{a^2} Y_m''(y) + Y_m^{\text{IV}}(y) = 0. \quad (2.3.12)$$

Equation (2.3.12) is a linear, homogeneous, differential equation of the fourth order with constant coefficients; consequently, its solution may be sought in $e^{\pm m\pi y/a}$ form.[†] Nádaí [3] has introduced the solution of Eq. (2.3.12) in the form of hyperbolic functions:

$$\begin{aligned} Y_m(y) = & A_m \cosh \frac{m\pi y}{a} + B_m \frac{m\pi y}{a} \sinh \frac{m\pi y}{a} + C_m \sinh \frac{m\pi y}{a} \\ & + D_m \frac{m\pi y}{a} \cosh \frac{m\pi y}{a}. \end{aligned} \quad (2.3.13)$$

[†] See Sec. 2.1.

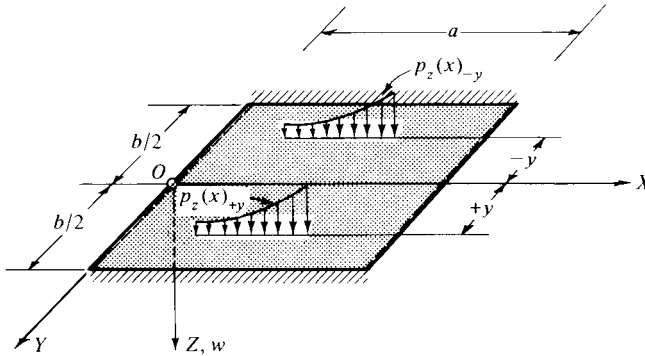


Figure 2.3.2 Use of symmetry in Lévy's solution.

The integration constants A_m , B_m , C_m and D_m can be determined from the boundary conditions at the four edges. A simplification in Lévy's solution can be obtained by making use of the symmetry. If the boundary conditions are symmetric about the X axis, the deflection surface (Fig. 2.3.2) must be an even function of y :

$$w(+y) = w(-y); \quad (2.3.14)$$

consequently, the coefficients C_m and D_m are to be taken equal to zero, which yields a simplified form of Eq. (2.3.13):

$$Y_m(y) = A_m \cosh \frac{m\pi y}{a} + B_m \frac{m\pi y}{a} \sinh \frac{m\pi y}{a}. \quad (2.3.15)$$

Thus, in the case of identical boundary conditions at $y = \pm b/2$, Lévy's solution of the differential equation of the plate can be represented by

$$w(x, y) = \sum_{m=1}^{\infty} W_m \sin \frac{m\pi x}{a} + \sum_{m=1}^{\infty} \left(A_m \cosh \frac{m\pi y}{a} + B_m \frac{m\pi y}{a} \sinh \frac{m\pi y}{a} \right) \sin \frac{m\pi x}{a}. \quad (2.3.16)$$

Summary. Although Lévy's method, which uses a single trigonometric series, is more general than Navier's solution, the former does not have an entirely general character either since in its original form it can be applied only if

1. the two opposite edges of the plate are simply supported (in the solution presented the simple supports were assumed to be at $x = 0$ and $x = a$) and
2. the shape of the loading function is the same for all sections parallel to the direction of the other two edges (parallel to the X axis).

It should be noted, however, that the convergence of Lévy's solution is extremely fast, even in the case of concentrated or line loads. On the other hand, the required

mathematical manipulations can be quite complex. Because of the fast convergence of the solution, in most cases it is satisfactory to consider only the first few terms.

For some plate problems the assumption $b \rightarrow \infty$ tends to be too limiting in the derivation of particular solutions for the Lévy method, since the class of loads that can be accommodated is considerably restricted. To overcome this limitation, we may use the deflection functions of simply supported plates (obtained by Navier's method) for a particular solution, as shown in Sec. 3.1.

ILLUSTRATIVE EXAMPLE I

Let us determine the deflection of a uniformly loaded ($p_z = p_0$) rectangular plate that is simply supported at all four edges using Lévy's method.

Since both the loading and the boundary conditions satisfy the previously discussed requirements for application of Lévy's method and the deflection surface is symmetrical with respect to the X axis, the solution can be represented by Eq. (2.3.16). As the first step in the solution, the uniformly distributed load is expanded into a sine series in accordance with Eq. (2.3.5). The coefficient P_m of the single Fourier series expansion is obtained from the half-range sine series expansion. Equation (A.1.20) yields

$$\begin{aligned} P_m &= \frac{2}{a} \int_0^a p(x) \sin \frac{m\pi x}{a} dx = \frac{2p_0}{a} \int_0^a \sin \frac{m\pi x}{a} dx \\ &= \begin{cases} \frac{4p_0}{m\pi} & \text{for } m = 1, 3, 5, \dots, \\ 0 & \text{for } m = 2, 4, 6, \dots \end{cases} \end{aligned} \quad (2.3.17)$$

Next, the load is expressed in the sine series according to Eq. (2.3.5):

$$p(x) = \frac{4p_0}{\pi} \sum_{m=1,3,5,\dots}^{\infty} \frac{1}{m} \sin \frac{m\pi x}{a}. \quad (2.3.18)$$

Substitution of Eq. (2.3.18) into the differential equation (2.3.1) gives the constants of the trigonometric series expression of the particular solution:

$$W_m = \frac{4p_0 a^4}{\pi^5 D m^5}. \quad (2.3.19)$$

Thus, the particular solution can be written as

$$w_P = \frac{4p_0 a^4}{\pi^5 D} \sum_{m=1,3,5,\dots}^{\infty} \frac{1}{m^5} \sin \frac{m\pi x}{a}. \quad (2.3.20)$$

The homogeneous solution, represented by Eqs. (2.3.9) and (2.3.15), gives

$$w_H = \sum_{m=1}^{\infty} \left(A_m \cosh \frac{m\pi y}{a} + B_m \frac{m\pi y}{a} \sinh \frac{m\pi y}{a} \right) \sin \frac{m\pi x}{a}. \quad (2.3.21)$$

From the boundary conditions of the plate at $y = \pm(b/2)$, which are

$$w = 0 \quad \text{and} \quad \nabla^2 w = 0, \quad (2.3.22)$$

we obtain two equations pertinent to one specific $m = 1, 3, 5, \dots$ value:

$$A_m \cosh \frac{m\pi b}{2a} + B_m \frac{m\pi b}{2a} \sinh \frac{m\pi b}{2a} = -\frac{4p_0 a^4}{\pi^5 m^5 D} \quad (2.3.23)$$

and

$$A_m \frac{m^2 \pi^2}{a^2} \cosh \frac{m\pi b}{2a} + B_m \frac{m^2 \pi^2}{a^2} \left(\frac{m\pi b}{2a} \sinh \frac{m\pi b}{2a} + 2 \cosh \frac{m\pi b}{2a} \right) = 0, \quad (2.3.24)$$

from which A_m and B_m are determined. The sum of the particular solution and the solution of the homogeneous differential equation yields the deflection surface of the plate (2.1.2):

$$\begin{aligned} w(x, y) &= \frac{4p_0 a^4}{\pi^5 D} \sum_{m=1,3,5,\dots} \frac{1}{m^5} \\ &\times \left(1 - \frac{2 \cosh \alpha_m \cosh \eta_m + \alpha_m \sinh \alpha_m \cosh \eta_m - \eta_m \sinh \eta_m \cosh \alpha_m}{1 + \cosh 2\alpha_m} \right) \\ &\times \sin \frac{m\pi x}{a}, \end{aligned} \quad (2.3.25)$$

where

$$\alpha_m = \frac{m\pi b}{2a} \quad \text{and} \quad \eta_m = \frac{m\pi y}{a}. \quad (2.3.26)$$

This series converges extremely rapidly, so that consideration of its first term is sufficient for most practical purposes.

ILLUSTRATIVE EXAMPLE II

A square plate with two opposite edges simply supported and the other two edges clamped is subjected to a partially sinusoidal load (Fig. 2.3.3). Determine the maximum deflection of the plate and the maximum positive movement.

Since two opposite edges ($x = 0, a$) are simply supported and the load intensity is the same along all cross sections parallel to the Y axis, Lévy's method can be used.

Due to the identical boundary conditions at $\bar{y} = \pm(a/2)$, the deflection surface can be represented by Eq. (2.3.16). To find a particular solution, we first, expand $p_z(x) = p_0 \sin(\pi x/a)$ into a single Fourier series. The coefficient of expansion P_m in Eq. (2.3.5) is obtained[†] from

[†] See Appendix A.1.

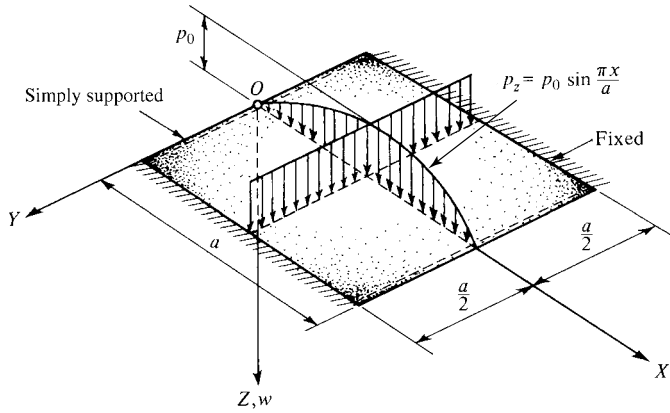


Figure 2.3.3 Plate with opposite edges simply supported and other two fixed.

$$P_m = \frac{2}{a} \int_0^a p_z(x) \sin \frac{m\pi x}{a} dx = \frac{2}{a} \int_0^a p_0 \sin \frac{\pi x}{a} \sin \frac{m\pi x}{a} dx = p_0. \quad (2.3.27)$$

Therefore, the lateral load can be expressed by

$$p_z(x) = p_0 \sin \frac{\pi x}{a}. \quad (2.3.28)$$

In accordance with Eq. (2.3.4), the particular solution using one term is

$$w_P = W_1 \sin \frac{\pi x}{a}. \quad (2.3.29)$$

Substituting Eqs. (2.3.28) and (2.3.29) into the differential equation of the plate strip (2.3.1), we obtain

$$W_1 = \frac{p_0 a^4}{\pi^4 D}; \quad (2.3.30)$$

therefore

$$w_P = \frac{p_0 a^4}{\pi^4 D} \sin \frac{\pi x}{a}. \quad (2.3.31)$$

The boundary conditions

$$(w)_{y=\pm a/2} = 0 \quad \text{and} \quad \left(\frac{\partial w}{\partial y} \right)_{y=\pm a/2} = 0 \quad (2.3.32)$$

yield the equations

$$\begin{aligned} W_1 + A_1 \cosh \alpha_1 + B_1 \alpha_1 \sinh \alpha_1 &= 0, \\ A_1 \sin \alpha_1 + B_1 (\alpha_1 \cosh \alpha_1 + \sinh \alpha_1) &= 0, \end{aligned} \quad (2.3.33)$$

where $\alpha_1 = \pi/2$.

Solving Eq. (2.3.33), we find that

$$\begin{aligned} A_1 &= -\frac{W_1(\alpha_1 \cosh \alpha_1 + \sinh \alpha_1)}{\alpha_1 + \cosh \alpha_1 \sinh \alpha_1}, \\ B_1 &= \frac{W_1 \sinh \alpha_1}{\alpha_1 + \cosh \alpha_1 \sinh \alpha_1}. \end{aligned} \quad (2.3.34)$$

Therefore, the expression (2.3.16) for the deflection surface of the plate becomes

$$\begin{aligned} w(x, y) = w_P + w_H &= \frac{p_0 a^4}{\pi^4 D} \left(1 + \frac{\sinh \alpha_1}{\alpha_1 + \cosh \alpha_1 \sinh \alpha_1} \frac{\pi y}{a} \sinh \frac{\pi y}{a} \right. \\ &\quad \left. - \frac{\alpha_1 \cosh \alpha_1 + \sinh \alpha_1}{\alpha_1 + \cosh \alpha_1 \sinh \alpha_1} \cosh \frac{\pi y}{a} \right) \sin \frac{\pi x}{a}. \end{aligned} \quad (2.3.35)$$

The maximum deflection occurs at $x = a/2$ and $y = 0$; thus we obtain

$$w_{\max} \approx 0.00154 \frac{p_0 a^4}{D}. \quad (2.3.36)$$

Using expression (2.3.35), the bending moments m_x and m_y at the center of the plate are calculated from Eqs. (1.2.26) and (1.2.27); thus at $x = a/2, y = 0$,

$$\begin{aligned} m_x &= \frac{D\pi^2}{a^2} [W_1 + A_1 - \nu(A_1 + 2B_1)], \\ m_y &= -\frac{D\pi^2}{a^2} [A_1 + 2B_1 - \nu(W_1 + A_1)]. \end{aligned} \quad (2.3.37)$$

Using $\nu = 0.3$, these expressions become

$$m_x \approx 0.0223 p_0 a^2 \quad \text{and} \quad m_y \approx 0.0268 p_0 a^2 = +m_{\max}. \quad (2.3.38)$$

References and Bibliography

- [2.3.1] LÉVY, M., "Sur l'équilibre élastique d'une plaque rectangulaire," *C. R. Acad. Sci.*, 129 (1899), 535–539.
- [2.3.2] TÖLKE, F., "Über Spannungszustände in dünnen Rechteckplatten," *Ing.-Arch.*, 5, (1934), 187.
- [2.3.3] NÁDAI, Á., "Die Formänderungen und die Spannungen von rechteckigen elastischen Platten," *Forsch. a. d. Gebiete d. Ingenieurwesens (Berlin)*, Heft Nos. 170 and 171 (1915).
- [2.3.4] LAMBLE, J. H., and LI SHING, "A Survey of Published Works on the Deflection and Stress in Flat Plates Subject to Hydrostatic Loading," *Trans. Inst. Naval Arch.*, 89 (1947), 128–147.
- [2.3.5] GECKELER, J. W., "Elastostatik," in *Handbuch der Physik*, Vol. 6, Springer-Verlag, Berlin, 1928, pp. 141–308.
- [2.3.6] BIEZENO, C. B., and GRAMMEL, R., *Technische Dynamik*, Vol. 1, 2nd ed., Springer-Verlag, Berlin, 1953.
- [2.3.7] L'HERMITE, R., *Résistance des matériaux*, Dunond, Paris, 1954.

- [2.3.8] TIMOSHENKO, S., and WOINOWSKY-KRIEGER, S., *Theory of Plates and Shells*, 2nd ed., McGraw-Hill Book Company, New York, 1959.
 [2.3.9] GIRKMANN, K., *Flächentragwerke*, 6th ed., Springer-Verlag, Vienna, 1963.
 [2.3.10] NÁDAI, Á., *Die elastischen Platten*, 2nd ed., Springer-Verlag, Berlin, 1963.

2.4 Further Examples of Series Solutions

Examples given in this section illustrate both the versatility and limitation of the single and double Fourier series solutions of certain plate problems. Evaluations of the required definite integrals and higher-order partial derivatives are, in general, very time consuming and error prone. Obtaining the results in the traditional manner may take many hours and many pages of paper. Nowadays, with the help of the so-called symbolic mathematics computer programs [2.4.1–2.4.4], however, the computation of such tedious tasks of calculus is quite effortless. In most of these cases we have eliminated the intermediate steps and merely give the end results. Some computer programs[†] offer an additional collection of routines designed to carry out step-by-step solutions of the given problems.

ILLUSTRATIVE EXAMPLE I

A simply supported rectangular plate is subjected to $p_z = p_0(x/a)^2$ lateral load, as shown in Fig. 2.4.1. Let us determine the deflected plate surface $w(x, y)$, the internal moments m_x, m_y, m_{xy} and transverse shear forces q_x, q_y using Navier's method. The obtained results should be checked by Lévy's approach for w, m_x and m_y at the center of the plate assuming that $\nu = 0.3$.

(a) *Navier's Solution.* First, we expand the lateral load into a double Fourier series, as described in Appendix A.1. Using Eq. (A.1.36), we obtain

$$\begin{aligned} P_{mn} &= \frac{4}{ab} \int_0^a \int_0^b p_z(x, y) \sin \frac{m\pi x}{a} \sin \frac{n\pi y}{b} dx dy \\ &= \frac{4p_0}{a^3b} \int_0^a x^2 \sin \frac{n\pi x}{a} dx \int_0^b \sin \frac{m\pi y}{b} dy = \frac{4p_0}{\pi^2 mn} I, \end{aligned} \quad (2.4.1)$$

where

$$\begin{aligned} I &= \left(\frac{2}{m\pi} \sin m\pi + \frac{2}{m^2\pi^2} \cos m\pi - \cos m\pi - \frac{2}{m^2\pi^2} \right) (-\cos n\pi + 1) \\ &\text{for } m, n = 1, 2, 3, \dots \end{aligned} \quad (2.4.2)$$

Equation (2.2.4a) gives

$$W_{mn} = \frac{P_{mn}}{D\pi^4(m^2/a^2 + n^2/b^2)^2} = \frac{4p_0 I}{D\pi^6 mn(m^2/a^2 + n^2/b^2)^2}. \quad (2.4.3)$$

[†] Ref. [2.4.1], for example.

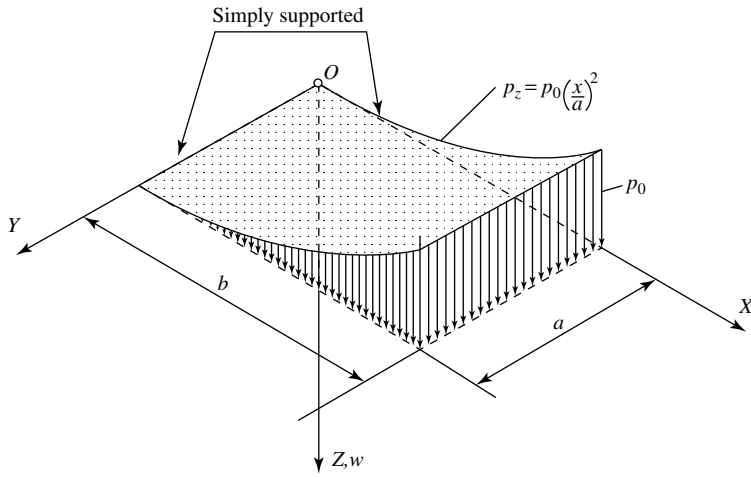


Figure 2.4.1 Simply supported plate subjected to parabolic lateral load.

Thus, the equation of the deflected plate surface (2.2.5) becomes

$$w(x, y) = \frac{4p_0}{D\pi^6} \sum_{m=1}^{\infty} \sum_{n=1}^{\infty} \frac{I}{mn(m^2/a^2 + n^2/b^2)^2} \sin \frac{m\pi x}{a} \sin \frac{n\pi y}{b}. \quad (2.4.4)$$

If $b = a$, the deflection at the center of the plate is

$$w_{x=y=a/2} = 0.001197 \frac{p_0 a^4}{D}. \quad (2.4.5)$$

Equation (2.2.6) gives the following expressions for the internal moments:

$$m_x = \frac{4p_0}{\pi^4} \sum_{m=1}^{\infty} \sum_{n=1}^{\infty} \frac{[(m/a)^2 + \nu(n/b)^2] I}{mn [(m/a)^2 + (n/b)^2]^2} \sin \frac{m\pi x}{a} \sin \frac{n\pi y}{b}, \quad (2.4.6)$$

$$m_y = \frac{4p_0}{\pi^4} \sum_{m=1}^{\infty} \sum_{n=1}^{\infty} \frac{[(n/b)^2 + \nu(m/a)^2] I}{mn [(m/a)^2 + (n/b)^2]^2} \sin \frac{m\pi x}{a} \sin \frac{n\pi y}{b}, \quad (2.4.7)$$

$$m_{xy} = \frac{-4p_0(1-\nu)}{\pi^4} \sum_{m=1}^{\infty} \sum_{n=1}^{\infty} \frac{I}{ab [(m/a)^2 + (n/b)^2]^2} \times \cos \frac{m\pi x}{a} \cos \frac{n\pi y}{b}. \quad (2.4.8)$$

If $b = a$, the internal moments at the center of the plate become

$$m_x \approx 0.0135 p_0 a^2, \quad m_y \approx 0.01375 p_0 a^2 \quad \text{and} \quad m_{xy} = 0. \quad (2.4.9)$$

Equation (2.2.7) yields the transverse shear forces in the form

$$q_x = \frac{4p_0}{\pi^3} \sum_{m=1}^{\infty} \sum_{n=1}^{\infty} \frac{I}{an [(m/a)^2 + (n/b)^2]} \cos \frac{m\pi x}{a} \sin \frac{n\pi y}{b} \quad (2.4.10)$$

and

$$q_y = \frac{4p_0}{\pi^3} \sum_{m=1}^{\infty} \sum_{n=1}^{\infty} \frac{I}{bm [(m/a)^2 + (n/b)^2]} \sin \frac{m\pi x}{a} \cos \frac{n\pi y}{b}. \quad (2.4.11)$$

(b) *Lévy's Approach.* In order to be able to solve the above given plate problem by Lévy's method, first, we must move the X axis to the $y = b/2$ location, as shown in Fig. 2.3.2. Next, we expand the lateral load into a single Fourier series according to Eq. (2.3.5). Thus,

$$p_z(x) = \sum_{m=1}^{\infty} P_m \sin \frac{m\pi x}{a}, \quad (2.4.12)$$

where P_m is obtained from the half-range sine series expansion of the load in the form

$$\begin{aligned} P_m &= \frac{2}{a} \int_0^a p_z(x) \sin \frac{m\pi x}{a} dx = \frac{2p_0}{a^3} \int_0^a x^2 \sin \frac{m\pi x}{a} dx \\ &= \begin{cases} \frac{2p_0}{m^3\pi^3} (m^2\pi^2 - 4) & \text{for } m = 1, 3, 5, \dots, \\ -\frac{2p_0}{m\pi} & \text{for } m = 2, 4, 6, \dots \end{cases} \end{aligned} \quad (2.4.13)$$

Hence, the single series expansion of the load becomes

$$p_z(x) = \frac{2p_0}{\pi^3} \sum_{m=1,3,5,\dots}^{\infty} \frac{1}{m^3} (m^2\pi^2 - 4) \sin \frac{m\pi x}{a} - \frac{2p_0}{\pi} \sum_{m=2,4,6,\dots}^{\infty} \frac{1}{m} \sin \frac{m\pi x}{a}. \quad (2.4.14)$$

Substitution of Eq. (2.4.14) into the differential equation of the plate strip (2.3.1) gives the constant of the trigonometric series expression for the particular solution

$$W_m = \frac{2p_0a^4}{D\pi^7m^7} (m^2\pi^2 - 4) \quad \text{for } m = 1, 3, 5, \dots \quad (2.4.15)$$

and

$$W_m = \frac{-2p_0a^4}{D\pi^5m^5} \quad \text{for } m = 2, 4, 6, \dots \quad (2.4.16)$$

Hence, the particular solution can be written as

$$w_P = \frac{2p_0a^4}{D\pi^7} \sum_{m=1,3,5,\dots}^{\infty} \frac{1}{m^7} (m^2\pi^2 - 4) \sin \frac{m\pi x}{a} - \frac{2p_0a^4}{D\pi^5} \sum_{m=2,4,6,\dots}^{\infty} \frac{1}{m^5} \sin \frac{m\pi x}{a}. \quad (2.4.17)$$

The homogeneous solution has the general form[†]

$$w_H = \sum_{m=1}^{\infty} \left(A_m \cosh \frac{m\pi y}{a} + B_m \frac{m\pi y}{a} \sinh \frac{m\pi y}{a} \right) \sin \frac{m\pi x}{a}. \quad (2.4.18)$$

From the boundary conditions of the plate at $y = \pm(b/2)$, which are

$$w = 0 \quad \text{and} \quad \nabla^2 w = 0, \quad (2.4.19)$$

we obtain two equations pertinent to one specific m value,

$$W_m + A_m \cosh \frac{m\pi b}{2a} + B_m \frac{m\pi b}{2a} \sinh \frac{m\pi b}{2a} = 0, \quad (2.4.20)$$

$$A_m \frac{m^2\pi^2}{a^2} \cosh \frac{m\pi b}{2a} + B_m \frac{m^2\pi^2}{a^2} \left(\frac{m\pi b}{2a} \sinh \frac{m\pi b}{2a} + 2 \cosh \frac{m\pi b}{2a} \right) = 0, \quad (2.4.21)$$

from which

$$A_m = -W_m \frac{1 + (m\pi b/4a) \tanh(m\pi b/2a)}{\cosh(m\pi b/2a)} \quad \text{and} \quad B_m = \frac{W_m}{2 \cosh(m\pi b/2a)}. \quad (2.2.22)$$

Hence, the equation of the deflected plate surface becomes

$$w(x, y) = w_H + w_P = \frac{2p_0a^4}{D\pi^7} \sum_{m=1,3,5,\dots}^{\infty} \frac{1}{m^7} (m^2\pi^2 - 4) F_1 \sin \frac{m\pi x}{a} - \frac{2p_0a^4}{D\pi^5} \sum_{m=2,4,6,\dots}^{\infty} \frac{1}{m^5} F_1 \sin \frac{m\pi x}{a}, \quad (2.4.23)$$

where

$$F_1 = 1 - \frac{2 \cosh \alpha_m \cosh \eta_m + \alpha_m \sinh \alpha_m \cosh \eta_m - \eta_m \sinh \eta_m \cosh \alpha_m}{1 + \cosh 2\alpha_m}, \quad (2.4.24)$$

with

$$\alpha_m = \frac{m\pi b}{2a} \quad \text{and} \quad \eta_m = \frac{m\pi y}{a}. \quad (2.4.25)$$

[†] See Sec. 2.3.

Applying Eq. (1.2.26) and Eq. (1.2.27), we obtain for the bending moments

$$m_x = \frac{2p_0a^2}{\pi^5} \sum_{m=1,3,5,\dots}^{\infty} \frac{1}{m^5} (m^2\pi^2 - 4)(F_1 - \nu F_2) \sin \frac{m\pi x}{a} - \frac{2p_0a^2}{\pi^3} \sum_{m=2,4,6,\dots}^{\infty} \frac{1}{m^3} (F_1 + \nu F_2) \sin \frac{m\pi x}{a} \quad (2.4.26)$$

and

$$m_y = \frac{2p_0a^2}{\pi^5} \sum_{m=1,3,5,\dots}^{\infty} \frac{1}{m^5} (m^2\pi^2 - 4)(F_2 - \nu F_1) \sin \frac{m\pi x}{a} - \frac{2p_0a^2}{\pi^3} \sum_{m=2,4,6,\dots}^{\infty} \frac{1}{m^3} (F_2 + \nu F_1) \sin \frac{m\pi x}{a}, \quad (2.4.27)$$

where

$$F_2 = \frac{\alpha_m \sinh \alpha_m \cosh \eta_m - \eta_m \sinh \eta_m \cosh \alpha_m}{1 + \cosh 2\alpha_m}. \quad (2.4.28)$$

If $b = a$, these expressions give us at the center of the plate the following lateral deflection and bending moments, respectively:

$$w \approx 0.001198 \frac{p_0a^4}{D}, \quad m_x \approx 0.01319 p_0a^2 \quad \text{and} \quad m_y \approx 0.01389 p_0a^2. \quad (2.4.29)$$

A comparison of the so-obtained results shows very little differences between the two approaches, and even these extremely small discrepancies can be eliminated by using more than four terms in the Navier solution. Although Lévy's method yields faster converging expressions, it requires more extensive computations to obtain those fast converging series. Consequently, if the boundary and loading conditions permit, preference should be given to Navier's approach using the classical method in plate analysis.

ILLUSTRATIVE EXAMPLE II

Determine the deflection of a partially loaded, simply supported rectangular plate, shown in Fig. 2.4.2, assuming that the partial load is uniformly distributed ($p_z = p_0$). The constants of the Fourier expansion of the load are

$$P_{mn} = \frac{4p_0}{ab} \int_{\xi-(c/2)}^{\xi+(c/2)} \int_{\eta-(d/2)}^{\eta+(d/2)} \sin \frac{m\pi x}{a} \sin \frac{n\pi y}{b} dx dy = \frac{16p_0}{\pi^2 mn} \sin \frac{m\pi \xi}{a} \sin \frac{n\pi \eta}{b} \sin \frac{m\pi c}{2a} \sin \frac{n\pi d}{2b}. \quad (2.4.30)$$

From Eq. (2.2.4a) the constants of the double series expression of the deflections can be computed:

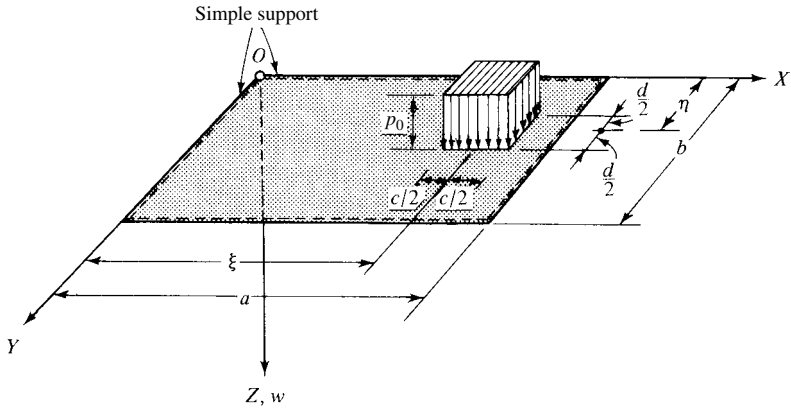


Figure 2.4.2 Uniform load over small rectangular area.

$$W_{mn} = \frac{16p_0 \sin(m\pi\xi/a) \sin(n\pi\eta/b) \sin(m\pi c/2a) \sin(n\pi d/2b)}{D\pi^6 mn[(m^2/a^2) + (n^2/b^2)]^2} \quad (2.4.31)$$

Substituting W_{mn} into Eq. (2.2.2), the equation of the deflection surface of the plate is obtained:

$$w(x, y) = \frac{16p_0}{D\pi^6} \sum_{m=1}^{\infty} \sum_{n=1}^{\infty} \frac{\sin(m\pi\xi/a) \sin(n\pi\eta/b) \sin(m\pi c/2a) \sin(n\pi d/2b)}{mn[(m^2/a^2) + (n^2/b^2)]^2} \\ \times \sin \frac{m\pi x}{a} \sin \frac{n\pi y}{b}. \quad (2.4.32)$$

The convergence of this solution is relatively fast, provided that the ratios a/c and d/b are not too small. The deflections can be obtained with sufficient accuracy by taking the first four terms of the series.

ILLUSTRATIVE EXAMPLE III

Find the deflections of a simply supported rectangular plate subjected to a concentrated lateral force P , as shown in Fig. 2.4.3. The solution is obtained from the previous derivation by introducing

$$p_0 = \frac{P}{cd} \quad (2.4.33)$$

and letting the contact area approach zero by permitting

$$c \rightarrow 0 \quad \text{and} \quad d \rightarrow 0.$$

Thus, Eq. (2.4.30) can be written as

$$P_{mn} = \frac{16P}{\pi^2 mn cd} \sin \frac{m\pi\xi}{a} \sin \frac{n\pi\eta}{b} \sin \frac{m\pi c}{2a} \sin \frac{n\pi d}{2b}. \quad (2.4.34)$$

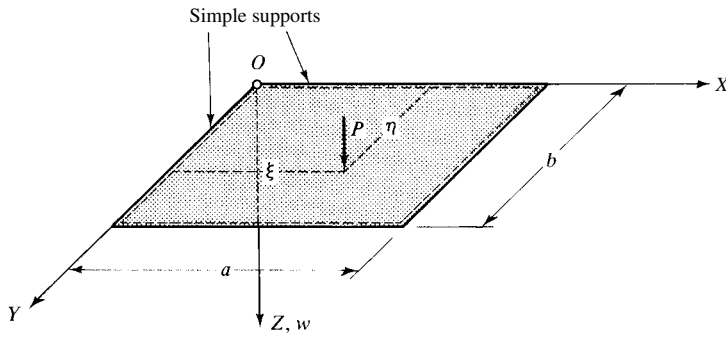


Figure 2.4.3 Rectangular plate loaded by concentrated force.

But, to be able to use the limit approach first, Eq. (2.4.34) must be put into a more suitable form. For this purpose, the right-hand side is multiplied and divided by $a \cdot b$, giving

$$P_{mn} = \lim_{c \rightarrow 0, d \rightarrow 0} \left[\frac{4P}{ab} \sin \frac{m\pi\xi}{a} \sin \frac{n\pi\eta}{b} \times \frac{\sin(m\pi c/2a) \sin(n\pi d/2b)}{(m\pi c/2a) \cdot (n\pi d/2b)} \right]. \quad (2.4.35)$$

Knowing that

$$\lim_{\alpha \rightarrow 0} \frac{\sin \alpha}{\alpha} = \lim_{\alpha \rightarrow 0} \left[\frac{(d/d\alpha) \sin \alpha}{(d/d\alpha) \alpha} \right] = \lim_{\alpha \rightarrow 0} \cos \alpha = 1, \quad (2.4.36)$$

Eq. (2.4.35) becomes

$$P_{mn} = \frac{4P}{ab} \sin \frac{m\pi\xi}{a} \sin \frac{n\pi\eta}{b}, \quad (2.4.37)$$

and the deflection of the plate subjected to a concentrated load is obtained from

$$w(x, y) = \frac{4P}{\pi^4 ab D} \sum_{m=1}^{\infty} \sum_{n=1}^{\infty} \frac{\sin(m\pi\xi/a) \sin(n\pi\eta/b)}{[(m^2/a^2) + (n^2/b^2)]^2} \sin \frac{m\pi x}{a} \sin \frac{n\pi y}{b} \quad (2.4.38)$$

for $m, n = 1, 2, 3, \dots$

The convergence of this series solution is slow in the vicinity of the concentrated load. The second derivatives of Eq. (2.4.38) will even diverge at the point of application of force.

By applying the principle of superposition, the plate deflection due to all types of lateral loading can be computed, provided that the plate is simply supported at all edges.

ILLUSTRATIVE EXAMPLE IV

Determine the deflections of a partially loaded rectangular plate, shown in Fig. 2.4.4, using Lévy's method.

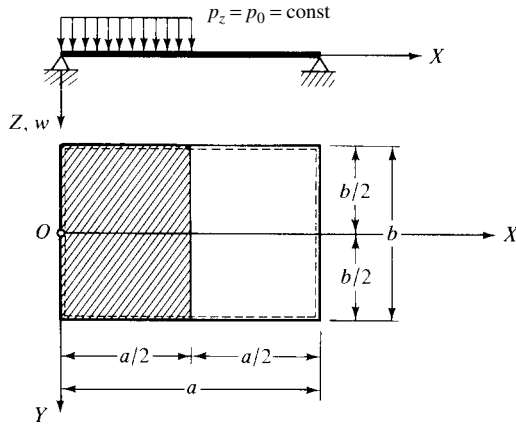


Figure 2.4.4 Partially loaded rectangular plate.

The general solution is sought in the form of Eq. (2.3.6); thus, we can write

$$w(x, y) = w_P + w_H = \sum_{m=1}^{\infty} W_m \sin \frac{m\pi x}{a} + \sum_{m=1}^{\infty} \left(A_m \cosh \frac{m\pi y}{a} + B_m \frac{m\pi y}{a} \sinh \frac{m\pi y}{a} \right) \sin \frac{m\pi x}{a}. \quad (2.4.39)$$

From Eq. (2.3.5),

$$p_z(x) = \sum_{m=1}^{\infty} P_m \sin \frac{m\pi x}{a}, \quad (2.4.40)$$

where P_m is determined using Fourier's expansion as described in Appendix A.1. This gives

$$P_m = \frac{2}{a} \int_0^{a/2} p(x) \sin \frac{m\pi x}{a} dx = \frac{2p_0}{m\pi} \left(1 - \cos \frac{m\pi}{2} \right); \quad (2.4.41)$$

hence

$$P_m = \begin{cases} \frac{2p_0}{m\pi} & \text{for } m = 1, 3, 5, \dots, \\ \frac{4p_0}{m\pi} & \text{for } m = 2, 6, 10, \dots, \\ 0 & \text{for } m = 4, 8, 12, \dots \end{cases} \quad (2.4.42)$$

Thus, the sine series expression for the lateral load ($p_z = p_0$) becomes

$$p_z(x) = \frac{2p_0}{\pi} \sum_{m=1,3,5,\dots} \frac{1}{m} \sin \frac{m\pi x}{a} + \frac{4p_0}{\pi} \sum_{m=2,6,10,\dots} \frac{1}{m} \sin \frac{m\pi x}{a}. \quad (2.4.43)$$

Application of Navier's method to the plate strip (2.3.1) yields

$$W_m = \begin{cases} \frac{2p_0a^4}{D\pi^5m^5} & \text{for } m = 1, 3, 5, \dots, \\ \frac{4p_0a^4}{D\pi^5m^5} & \text{for } m = 2, 6, 10, \dots, \\ 0 & \text{for } m = 4, 8, 12, \dots \end{cases} \quad (2.4.44)$$

Substituting this expression into (2.3.4), the particular solution becomes

$$w_p = \frac{2p_0a^4}{D\pi^5} \sum_{m=1,3,5,\dots}^{\infty} \frac{1}{m^5} \sin \frac{m\pi x}{a} + \frac{4p_0a^4}{D\pi^5} \sum_{m=2,6,10,\dots}^{\infty} \frac{1}{m^5} \sin \frac{m\pi x}{a}. \quad (2.4.45)$$

The constants A_m and B_m in (2.3.16) are determined from the boundary conditions at $y = \pm(b/2)$, which are

$$w = 0 \quad \text{and} \quad \frac{\partial^2 w}{\partial y^2} + \nu \frac{\partial^2 w}{\partial x^2} = \frac{\partial^2 w}{\partial y^2} = 0. \quad (2.4.46)$$

Considering a specific m value, the substitution of (2.4.39) into (2.4.46) gives

$$W_m + A_m \cosh \frac{m\pi b}{2a} + B_m \frac{m\pi b}{2a} \sinh \frac{m\pi b}{2a} = 0 \quad (2.4.47)$$

and

$$(A_m + 2B_m) \frac{m^2\pi^2}{a^2} \cosh \frac{m\pi b}{2a} + B_m \frac{m^3\pi^3b}{2a^3} \sinh \frac{m\pi b}{2a} = 0; \quad (2.4.48)$$

hence

$$\begin{aligned} A_m &= -\frac{W_m}{2 \cosh(m\pi b/2a)} \left(2 + \frac{m\pi b}{2a} \tanh \frac{m\pi b}{2a} \right), \\ B_m &= \frac{W_m}{2 \cosh(m\pi b/2a)}. \end{aligned} \quad (2.4.49)$$

Thus, the solution of the homogeneous plate equation becomes

$$\begin{aligned} w_H &= -\frac{p_0a^4}{D\pi^4} \sum_m^{\infty} \frac{c_m}{m^5} \left[\frac{\cosh \eta_m}{2 \cosh \alpha_m} (2 + \alpha_m \tanh \alpha_m) - \frac{\eta_m}{2 \cosh \alpha_m} \sinh \eta_m \right] \\ &\quad \times \sin \frac{m\pi x}{a}, \end{aligned} \quad (2.4.50)$$

where

$$\eta_m = \frac{m\pi y}{a}, \quad \alpha_m = \frac{m\pi b}{2a}$$

and

$$c_m = \begin{cases} 2 & \text{for } m = 1, 3, 5, \dots, \\ 4 & \text{for } m = 2, 6, 10, \dots, \\ 0 & \text{for } m = 4, 8, 12, \dots \end{cases} \quad (2.4.51)$$

If $a = b$, the deflection at the center of the plate becomes

$$(w)_{x=a, 2, y=0} = 0.002028 \frac{p_0 a^4}{D}. \quad (2.4.52)$$

References

- [2.4.1] MAPLESOFTWARE, *MAPLEV*, Release 4, Waterloo, Ontario, Canada, 1996.
- [2.4.2] WOLFRAM RESEARCH, *Mathematica*, Version 2.0, Champaign, Illinois, 1992.
- [2.4.3] MATHSOFT, Mathcad, Version 6, Cambridge, Massachusetts, 1995.
- [2.4.4] SOFTWAREHOUSE, *DERIVE a Mathematical Assistant for Your Personal Computer*, Version 3, Honolulu, Hawaii, 1995.

2.5 Extensions of Navier's and Lévy's Methods

a. Generalization of Navier's Solution. Lardy extended the use of Navier's solution to rectangular plates clamped along all four edges [2.5.1]. Instead of using trigonometric functions, he introduced the characteristic functions of a freely vibrating beam to obtain an equation of the deflected plate surface. This Navier-type solution converges quickly and—with the help of pertinent tables—is relatively easy to apply. Since Lardy's solution technique is basically the same as the more general approach introduced later by Mukhopadhyay, here we will merely treat the latter in detail.

Mukhopadhyay further extended Lardy's method to cover any type of boundary and loading conditions [2.5.2]. He also used the characteristic functions of freely vibrating uniform beams [2.5.3, 2.5.4] in his Navier-type plate analysis.

The characteristic function $X(x)$ that satisfies the homogeneous differential equation of the freely vibrating uniform beam with span length a ,

$$\frac{d^4}{dx^4} X(x) - \frac{\mu^4}{a^4} X(x) = 0, \quad (2.5.1)$$

can be written in the general form

$$X(x) = K_1 \sin \frac{\mu x}{a} + K_2 \cos \frac{\mu x}{a} + K_3 \sinh \frac{\mu x}{a} + K_4 \cosh \frac{\mu x}{a}, \quad (2.5.2)$$

where the integration constants K_1 , K_2 , K_3 and K_4 are unknowns [2.5.5, 2.5.6]. These constants are determined from the four boundary conditions of the beam. A nontrivial solution, however, is possible only if the circular frequency[†] ω assumes one of the eigenvalues ω_m [2.5.3].

[†] Embedded in μ .

These characteristic functions for simply supported and clamped edges can be directly applied to plate problems having similar boundary conditions. The characteristic function of a beam with free-edges, however, is not directly applicable to plates having free boundaries. We will briefly discuss this problem later.

Similar characteristic functions can be used in the Y direction; hence

$$Y(y) = K_5 \sin \frac{\mu y}{b} + K_6 \cos \frac{\mu y}{b} + K_7 \sinh \frac{\mu y}{b} + K_8 \cosh \frac{\mu y}{b}. \quad (2.5.3)$$

As known, these characteristic functions satisfy the following orthogonality relations:

$$\int_0^a X_m(x) \cdot X_n(x) dx = 0, \quad \int_0^a X_m''(x) \cdot X_n''(x) dx = 0, \quad (2.5.4)$$

$$\int_0^b Y_m(y) \cdot Y_n(y) dy = 0, \quad \int_0^b Y_m''(y) \cdot Y_n''(y) dy = 0, \quad (2.5.5)$$

$$\int_0^a X_m'''' \cdot X_n dx = 0, \quad \int_0^b Y_m'''' \cdot Y_n dy = 0 \quad (2.5.6)$$

for $m \neq n$.

Next, we express the deflection surface of the plate in the form

$$w(x, y) = \sum_{p=1}^r \sum_{s=1}^r W_{ps} X_p(x) \cdot Y_s(y), \quad (2.5.7)$$

where $X_p(x)$ and $Y_s(y)$ are beam characteristic functions along the X and Y axes satisfying the pertinent boundary conditions of the plate and W_{ps} are unknown constants to be determined.

For this purpose, we express the lateral load $p_z(x, y)$ with the help of these characteristic functions in the series form

$$\begin{aligned} p_z(x, y) = \sum_{m=1}^r \sum_{n=1}^r P_{mn} X_m Y_n = P_{11} X_1 Y_1 + P_{12} X_1 Y_2 + \cdots + P_{mn} X_m Y_n \\ + \cdots + P_{rr} X_r Y_r. \end{aligned} \quad (2.5.8)$$

Multiplying both sides of Eq. (2.5.7) by X_m and Y_n and integrating with respect to x and y , from 0 to a and 0 to b , respectively, we can write

$$P_{mn} = \frac{\int_0^a \int_0^b p_z(x, y) \cdot X_m Y_n dx dy}{\int_0^a X_m^2 dx \int_0^b Y_n^2 dy}. \quad (2.5.9)$$

Thus, for the uniformly loaded plate, for instance, we obtain

$$P_{mn} = p_0 \frac{\int_0^a X_m dx \int_0^b Y_n dy}{\int_0^a X_m^2 dx \int_0^b Y_n^2 dy}, \quad (2.5.10)$$

where p_0 represents the constant intensity of the lateral load. Similarly, for a plate subjected to a concentrated load p_0 at coordinates ξ and η , Eq. (2.5.9) gives

$$P_{mn} = \frac{P_0(X_m)_\xi \cdot (Y_n)_\eta}{\int_0^a X_m^2 dx \int_0^b Y_n^2 dy}. \quad (2.5.11)$$

If both ends of the beam are simply supported, the characteristic function has the form

$$X_m(x) = \sin \frac{\mu_m x}{a}, \quad \mu_m = \pi, 2\pi, 3\pi, \dots, m\pi. \quad (2.5.12)$$

If one end is simply supported and the other end is fixed, the pertinent characteristic function is

$$X_m(x) = \sin \frac{\mu_m x}{a} - \alpha_m (\sinh) \frac{\mu_m x}{a}, \quad (2.5.13)$$

where

$$\mu_m = 3.9166, 7.0685, \dots, \frac{(4m+1)\pi}{4}, \quad \alpha_m = \frac{\sin \mu_m}{\sinh \mu_m}. \quad (2.5.14)$$

If both ends are fixed, we should use

$$X_m(x) = \sin \frac{\mu_m x}{a} - \sinh \frac{\mu_m x}{a} - \alpha_m \left(\cos \frac{\mu_m x}{a} - \cosh \frac{\mu_m x}{a} \right), \quad (2.5.15)$$

where

$$\mu_m = 4.712, 7.853, \dots, \frac{1}{2}(2m+1)\pi \quad (2.5.16)$$

and

$$\alpha_m = \frac{\sin \mu_m - \sinh \mu_m}{\cos \mu_m - \cosh \mu_m}. \quad (2.5.17)$$

However, when a free-edge is involved, derivation of characteristic functions for a plate becomes far more complex. That is, the characteristic function for a beam with free-edges cannot directly be applied to plates having a free boundary, since the free-edge boundary condition of beams does not contain the torsional moment embedded in Eqs. (1.3.5) and (1.3.6). Furthermore, such a characteristic function for plates must also contain the effects of the boundary conditions of the two adjoining plate edges, the aspect ratio a/b and the Poisson ratio ν , respectively. Because of these complexities, we do not treat this problem here but refer the reader to the

original paper [2.5.2]. It is evident that more research is required on this subject to simplify this part of the analysis.

Fletcher and Thorne give readily usable Fourier series-type solutions for rectangular plates subjected to any type of transverse loads [2.5.7]. They treat 81 combinations of free, simply supported and fixed boundary conditions.

The method is based on the superposition technique, discussed in detail in Sec. 3.8. With the origin of the coordinate system at the center of the plate, the solution is written in the form

$$w(x, y) = w_1(x, y) + w_2(x, y) + w_3(x, y), \quad (2.5.18)$$

where w_1 is the deflection of a simply supported plate under the lateral load $p_z(x, y)$, w_2 is the deflection of an edge loaded plate such that the deflections and moments on all edges are arbitrary except at the corners where the deflection is zero and w_3 is the deflection of a plate bent by concentrated corner loads. After taking the bending moment boundary equations into account, these individual deflections are

$$w_1(x, y) = \frac{4K}{a^2b} \sum_{m=1}^{\infty} \sum_{n=1}^{\infty} \frac{P_{mn}}{(\alpha^2 + \beta^2)^2} \sin \alpha x \sin \beta y, \quad (2.5.19)$$

$$\begin{aligned} w_2(x, y) = & \frac{4K}{ab} \sum_{m=1}^{\infty} \sum_{n=1}^{\infty} \frac{(-1)^{n+1} \alpha (\alpha^2 + 2\beta^2)}{v\beta^2} + (-1)^n \alpha d_m \\ & + \left[\frac{\alpha (\alpha^2 + 2\beta^2)}{v\beta^2} - \alpha \right] e_m + \left[-\frac{(-1)^m \beta (\beta^2 + 2\alpha^2)}{v\alpha^2} + (-1)^m \beta \right] h_n \\ & + \left[\frac{\beta (\beta^2 + 2\alpha^2)}{v\alpha^2} - \beta \right] i_n \frac{\sin \alpha x \sin \beta y}{(\alpha^2 + \beta^2)^2}, \end{aligned} \quad (2.5.20)$$

$$\begin{aligned} w_3(x, y) = & \frac{4}{ab} \sum_{m=1}^{\infty} \sum_{n=1}^{\infty} [(-1)^{m+1} w(a, b) - (-1)^n w(a, 0) \\ & - (-1)^m w(0, b) + w(0, 0)] \frac{\sin \alpha x \sin \beta y}{\alpha \beta}, \end{aligned} \quad (2.5.21)$$

where $\alpha = n\pi/a$, $\beta = m\pi/b$, $K = p_z a^3/D$ and d_m, e_m, h_m and i_m are undetermined Fourier coefficients arising from the second derivatives of w evaluated along the boundaries. The constants P_{mn} are the conventional Fourier coefficients introduced in Sec. 2.2. Satisfaction of the boundary conditions theoretically leads to an infinite set of equations in infinitely many unknown constants. In practice, however, it is sufficient to consider only a limited number of terms in the series to obtain very usable results. Especially in the case of distributed lateral loads, the convergence of the solution is quite fast. As already mentioned, in Ref. [5.5.7] readily the reader will find usable expressions for all the above-discussed combinations of boundary conditions. Although this method yields very accurate results, its application requires considerable computational efforts.

b. Rationalization of Lévy's Solution. The classical Lévy solution is unique. That is, it can be mathematically proven that rectangular plates not having two opposite

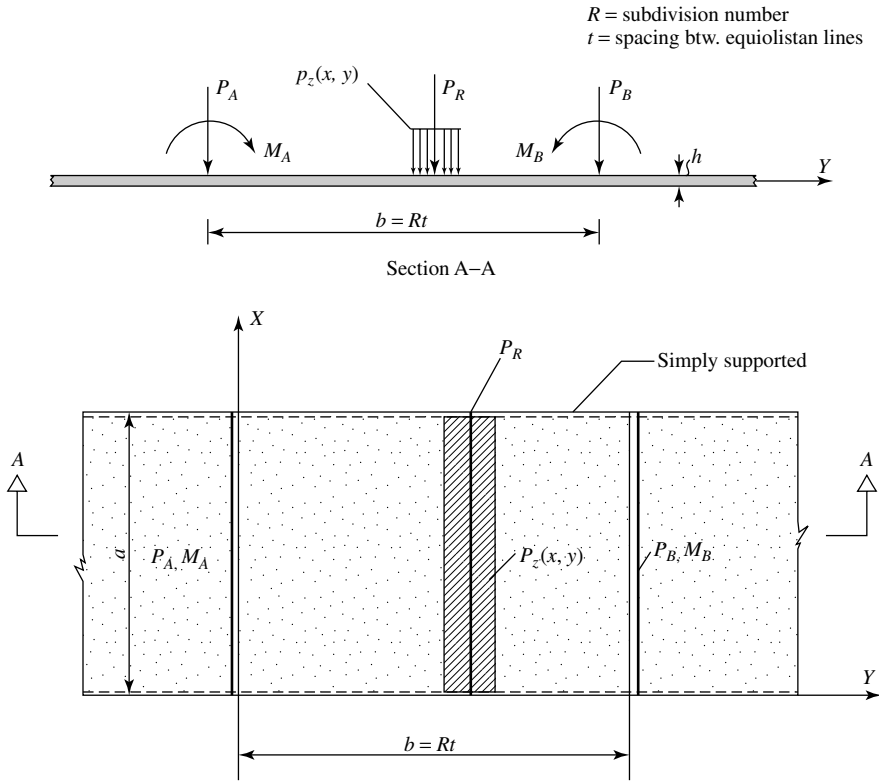


Figure 2.5.1 Finite plate represented by infinite plate strip.

edges simply supported do not admit such a solution. In order to rationalize Lévy's solution, however, Åkkeson introduced an "end-conditioning" technique [2.5.8]. He used the simply supported infinite plate strip shown in Fig. 2.5.1, which carries the lateral load p_z and four external line loads M_A , M_B and P_A , P_B . These boundary line loads are applied just outside of $y = 0$ and $y = b$ boundaries to provide the prescribed boundary conditions along the edges $y = 0, b$. All external loads are replaced by $R + 1$ equidistant line loads P_R . The external load and the boundary forces are expanded into sine series. The deflections and the internal forces are also given in trigonometric series forms. The so-derived expressions are lengthy, but they can be rationalized by applying matrix methods.

References and Bibliography

- [2.5.1] LARDY, P., "Sur une méthode nouvelle de résolution du problème des dalles rectangulaires encastrees," *IABSE Publications*, 13 (1953), 197–220.
- [2.5.2] MUKHOPADHYAY, M., "A General Solution for Rectangular Plate Bending," *Forsch. Ing.-Wes.*, 45 (1979), 111–118.
- [2.5.3] YOUNG, D., and FELGAR, R. P., "Tables of Characteristic Functions Representing Normal Modes of Vibration of a Beam," Report No. 4913, University of Texas, Austin, Texas, 1949.

- [2.5.4] ÅKESSON, B. Å., and TAGNFORS, H., "Tables of Eigenmodes for Vibrating Uniform One-Span Beams," Publication No. 23, Chalmers University of Technology, Gothenburg, Sweden, 1971.
- [2.5.5] TIMOSHENKO, S., and YOUNG, D. H., *Vibration Problems in Engineering*, 3rd ed., D. Van Nostrand Company, Princeton, New Jersey, 1955.
- [2.5.6] BIGGS, J. M., *Introduction to Structural Dynamics*, McGraw-Hill Book Company, New York, 1964.
- [2.5.7] FLETCHER, H. J., and THRONE, C. J., "Bending of Thin Rectangular Plates," in P. Nagdhy (Ed.), *Proceedings of the Second U.S. National Conference of Applied Mathematics*, NAGDHY, American Society of Mechanical Engineers, New York, 1955, pp. 389–406.
- [2.5.8] ÅKESSON, B. Å., "Rationalization of Lévy's Plate Solution," Publication No. 252, Transaction of Chalmers University of Technology, Gothenburg, Sweden, 1961.
- [2.5.9] ÅKESSON, B. Å., "Functions Simplifying the Use of Lévy's Plate Solution," Publication No. 301, Transactions of Chalmers University of Technology, Gothenburg, Sweden, 1965.
- [2.5.10] LEISSA, A. W., et al., "A comparison of Approximate Methods for the Solution of Plate Bending Problems," *AIAAJ*, 7, (1969), 920–928.

2.6 Method of Images

For certain plate problems the solution can be obtained by arbitrary extension of the plate and/or applying fictitious forces to create the desired deflection patterns.[†]

In Fig. 2.6.1a, for instance, a simply supported plate in the form of an isosceles right triangle is shown. This plate is subjected to a concentrated lateral force P . We replace the triangular plate by an *equivalent* square plate upon which two loads, $+P$ and $-P$, are now acting. The point of application of the fictitious load $-P$ is the *mirror* or *image* point of that of the actual load with respect to the diagonal. It is evident by observation that the deflections of the original and equivalent plates are the same. Consequently, a solution of the problem can be obtained by superimposing

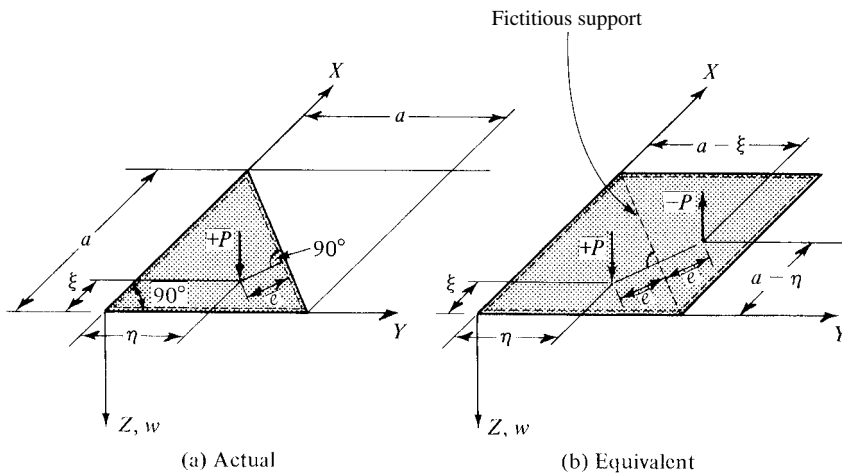


Figure 2.6.1 Method of images.

[†] This method was introduced by Nádai [3].

Navier's solution given in Eq. (2.4.38) using $+P$ and $-P$ forces. Thus, we can write

$$\begin{aligned}
 w = w_1 + w_2 = & \frac{4Pa^2}{\pi^4 D} \sum_{m=1}^{\infty} \sum_{n=1}^{\infty} \frac{\sin(m\pi\xi/a) \sin(n\pi\eta/a)}{(m^2 + n^2)^2} \sin \frac{m\pi x}{a} \sin \frac{n\pi y}{a} \\
 & - \frac{4Pa^2}{\pi^4 D} \sum_{m=1}^{\infty} \sum_{n=1}^{\infty} \frac{\sin\{[m\pi(a-\eta)]/a\} \sin\{[n\pi(a-\xi)]/a\}}{(m^2 + n^2)^2} \\
 & \times \sin \frac{m\pi x}{a} \sin \frac{n\pi y}{a}.
 \end{aligned} \quad (2.6.1)$$

The deflections of a triangular plate subjected to a uniformly distributed load p_0 can be obtained in an analogous manner.

ILLUSTRATIVE EXAMPLE

Determine the deflection surface of a simply supported plate subjected to a concentrated moment at point $A(\xi, \eta)$, as shown in Fig. 2.6.2a.

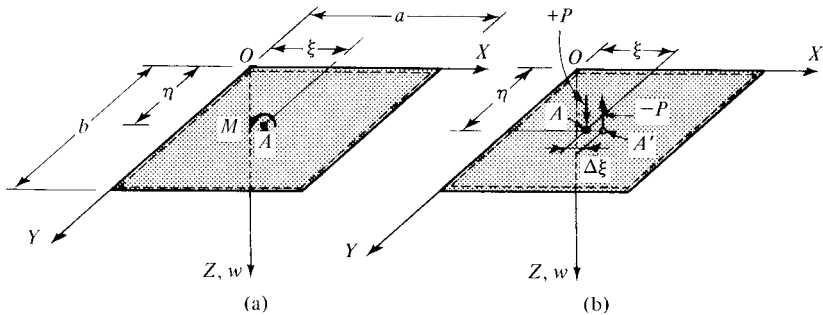


Figure 2.6.2 Concentrated moment.

Replacing the external moment by a couple, $M = P \nabla \xi$, the deflection surface, which corresponds to the action of a concentrated moment, is obtained from

$$w(x, y) = P \lim_{\Delta\xi \rightarrow 0} [f(\xi + \Delta\xi, \eta, x, y) - f(\xi, \eta, x, y)], \quad (2.6.2)$$

where $f(\bullet)$ represents shape functions pertinent to the concentrated forces $+P$ and $-P$ acting at $A(\xi, \eta)$ and $A'(\xi + \Delta\xi, \eta)$, respectively (Fig. 2.6.2b). If we decrease $\Delta\xi$ without limit ($\Delta\xi \rightarrow 0$) while maintaining the original value of $M = P \Delta\xi$, we must proportionally increase P . This process is identical with replacing P by M in Eq. (2.4.38) and differentiating the shape function with respect to ξ . Thus, we can write

$$w(x, y) = M \frac{\partial}{\partial \xi} f(\xi, \eta, x, y), \quad (2.6.3)$$

and we obtain

$$w = \frac{4M}{\pi^3 a^2 b D} \sum_m \sum_n \frac{m}{[(m^2/a^2) + (n^2/b^2)]^2} \times \cos \frac{m\pi\xi}{a} \sin \frac{n\pi\eta}{b} \sin \frac{m\pi x}{a} \sin \frac{n\pi y}{b}. \quad (2.6.4)$$

2.7 Plate Strips

a. Plate Strip Bent to Cylindrical Deflection Surface. If the plate is infinitely long in one direction, the plate becomes a *plate strip* (Fig. 2.7.1). Let us assume that the plate strip has a finite dimension in the X direction and that it is subjected to a lateral load $p_z(x)$ that is uniform at any section parallel to the X direction. In such a case, the deflection of the plate w becomes a function of x only; consequently, all the derivatives with respect to y are zero. Thus, the governing differential equation of the plate (1.2.30) is considerably simplified and takes the form

$$\frac{d^4 w(x)}{dx^4} = \frac{p_z(x)}{D}, \quad (2.7.1)$$

which has a marked similarity to the differential equation of a beam:

$$\frac{d^4 w^*(x)}{dx^4} = \frac{p_z(x)}{EI}, \quad (2.7.2)$$

as already discussed in Sec. 2.3.

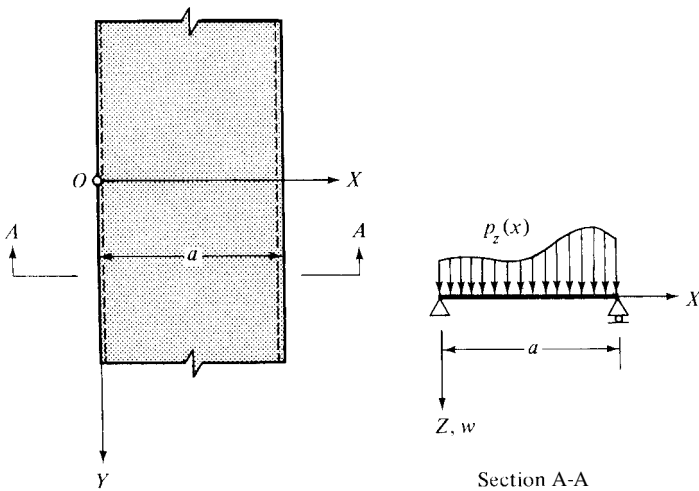


Figure 2.7.1 Plate strip.

Comparing Eqs. (2.7.1) and (2.7.2), it is evident that

$$w = w^*(1 - \nu^2), \quad (2.7.3)$$

from which it follows that due to its two-dimensional action the deflection of a plate strip is somewhat smaller than the corresponding beam deflection.

Solution of the differential equation of a plate strip [Eq. (2.7.1)] can follow Navier's method,[†] provided that the edges of the plate, pertaining to its finite dimensions, are simply supported. Expanding the deflection $w(x)$ and the lateral load $p_z(x)$ into single Fourier series,[‡] we can write

$$\begin{aligned} w(x) &= \sum_m W_m \sin \frac{m\pi x}{a}, \\ p_z &= \sum_m P_m \sin \frac{m\pi x}{a} \quad \text{for } m = 1, 2, 3, \dots \end{aligned} \quad (2.7.4)$$

The substitution of these expressions (pertinent to a specific m value) in Eq. (2.7.1) yields $W_m = a^4 P_m / Dm^4 \pi^4$; hence

$$w(x) = \frac{a^4}{\pi^4 D} \sum_m \frac{P_m}{m^4} \sin \frac{m\pi x}{a} \quad \text{for } m = 1, 2, 3, \dots \quad (2.7.5)$$

If the edges of the plate strip at $x = 0$ and $x = a$ are not simply supported, the integration of the differential equation (2.7.12) and the determination of the four integration constants from the boundary conditions can follow the same technique as that conventionally used in the solution of beam problems [2.7.1, 2.7.2]. But by far the simplest way to obtain a solution for the plate strip is by the use of beam formulas [5, 9, 2.7.3] in connection with the above-discussed relationship between plate and beam deflections (2.7.3). The deflections of plate strips of this type have already been used in Sec. 2.3 for the particular solutions of the governing differential equation of the plate (1.2.30).

Since the deflection $w(x)$ is only a function of x , the curvature of the plate strip in the Y direction is zero; thus

$$\frac{d^2 w}{dy^2} = 0. \quad (2.7.6)$$

Using Eq. (2.7.5), the internal moments can be obtained from Eqs. (1.2.26) and (1.2.27):

$$m_x = -D \frac{d^2 w}{dx^2} \quad (2.7.7)$$

and

$$m_y = -D\nu \frac{d^2 w}{dx^2} = \nu m_x. \quad (2.7.8)$$

[†] See Sec. 2.2.

[‡] See Appendix A.1.

The expression for the twisting moment is

$$m_{xy} = 0. \quad (2.7.9)$$

Similarly, Eqs. (1.2.33a) and (1.2.33b) yield the transverse shear:

$$q_x = -D \frac{d^3 w}{dx^3} \quad \text{and} \quad q_y = 0. \quad (2.7.10)$$

b. Partial Loading. The solution of plate strips loaded with a lateral load uniformly distributed on a subrectangle, as shown in Fig. 2.7.2, is of considerable practical importance. This problem occurs frequently in design of the roadway slabs of reinforced-concrete highway bridges. Since our previous assumptions concerning the load distribution and the shape of the deflected plate surface are no longer valid, the governing differential equation of the plate (1.2.30) must be used instead of the equation of the plate strip (2.7.1).

For long rectangular plates, Navier's solution, as given by Eq. (2.4.32), is applicable, provided that the width-to-length ratio a/b is not zero and that the edges are simply supported. When the plate length increases without limit ($b \rightarrow \infty$), the Fourier series expression of lateral loading and that of the pertinent plate deflections can be transformed into Fourier integral forms [1]. Furthermore, if b becomes infinite, Lévy's solution (Sec. 2.3) can be applied advantageously with some modification.

To show the use of Lévy's method, let us consider first an infinitely long plate loaded with a line load, as shown in Fig. 2.7.3. The solution of the homogeneous

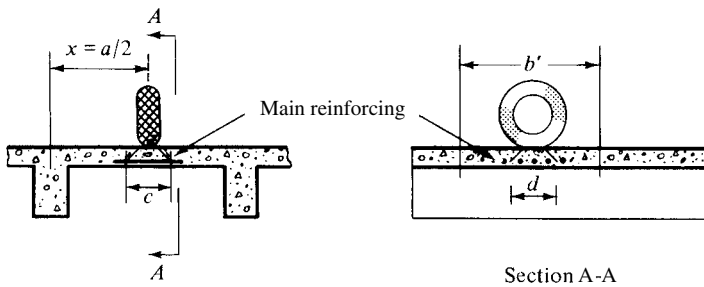


Figure 2.7.2 Roadway slab of a reinforced-concrete highway bridge.

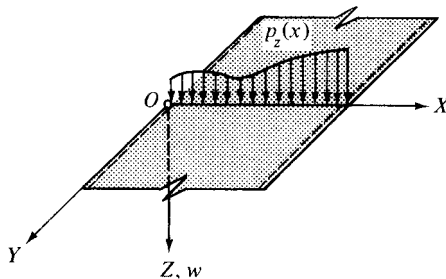


Figure 2.7.3 Line load on plate strip.

form of the plate equation (2.1.1), again, can be written in the form of Eq. (2.3.9). Functions that satisfy the resulting ordinary differential equation (2.3.13) are

$$Y_m(y) = e^{m\pi y/a}, \quad e^{-m\pi y/a}, \quad ye^{m\pi y/a}, \quad ye^{-(m\pi y/a)} \quad (2.7.11)$$

and

$$Y_m(y) = \sinh \frac{m\pi y}{a}, \quad \cosh \frac{m\pi y}{a}, \quad y \sinh \frac{m\pi y}{a}, \quad y \cosh \frac{m\pi y}{a}. \quad (2.7.12)$$

Since the deflections for the plate strip shown in Fig. 2.7.3 vanish at $y = \infty$, of the above given expressions for $Y_m(y)$, only

$$Y_m(y) = \left(A_m + B_m \frac{m\pi y}{a} \right) e^{-(m\pi y/a)} \quad (2.7.13)$$

can be considered. Hence, the solution of Eq. (2.1.1) takes the form

$$w_H = \sum_{m=1}^{\infty} \left(A_m + B_m \frac{m\pi y}{a} \right) e^{-(m\pi y/a)} \sin \frac{m\pi x}{a}. \quad (2.7.14)$$

Furthermore, the apparent symmetry of the deflected middle surface with respect to the X axis requires that, at $y = 0$, $\partial w / \partial y = 0$; this condition is satisfied if $A_m = B_m$. Therefore, Eq. (2.7.14) becomes[†]

$$w_H = \sum_{m=1}^{\infty} A_m \left(1 + \frac{m\pi y}{a} \right) e^{\mp(m\pi y/a)} \sin \frac{m\pi x}{a}. \quad (2.7.15)$$

The integration constant A_m in Eq. (2.7.15) can be determined from the “boundary” condition at $y = 0$. That is, taking a section parallel to the Y axis, we find a discontinuity in the diagram of the transverse shear forces q_y at the point of action of the load. This phenomenon is analogous to the discontinuities found in the shear diagrams of beams subjected to concentrated loads. Consequently, we can state that at $y = 0$ the transverse shear q_y is equal to half the line load. Therefore, if the line load is uniformly distributed along the X axis, using Eq. (1.2.33b), we can write

$$(q_y)_{y=0} = -D \frac{\partial}{\partial y} \nabla^2 w = -\frac{2p_0}{\pi} \sum_m \frac{1}{m} \sin \frac{m\pi x}{a} \quad \text{for } m = 1, 3, 5, \dots, \quad (2.7.16)$$

where the right-hand side of Eq. (2.7.16) represents the Fourier series expression of the line load divided by 2.

The substitution of Eq. (2.7.15) in the left-hand side of Eq. (2.7.16) gives

$$A_m = \frac{p_0 a^3}{\pi^4 m^4 D} \quad \text{for } m = 1, 3, 5, \dots \quad (2.7.17)$$

[†] The negative sign of the exponent is applicable for $+y$, whereas for $-y$ the plus sign should be used.

Since the plate at $y \geq 0$ carries no load, the particular solution of Eq. (1.2.30) is zero. Thus, the expression of the deflection becomes

$$w = w_H = \frac{p_0 a^3}{\pi^4 D} \sum_{m=1}^{\infty} \frac{1}{m^4} \left(1 + \frac{m\pi y}{a}\right) e^{-(m\pi y/a)} \sin \frac{m\pi x}{a} \quad \text{for } m = 1, 3, 5, \dots \quad (2.7.18)$$

A similar approach can be taken if the line load is distributed only along a portion of the X axis, as shown in Fig. 2.7.4. Assuming, for instance, a uniformly distributed partial line load p_0 , the constants of the Fourier expansion of the load are calculated from[†]

$$P_m = \frac{2p_0}{a} \int_{\xi-(c/2)}^{\xi+(c/2)} \sin \frac{m\pi x}{a} dx = \frac{4p_0}{\pi m} \sin \frac{m\pi \xi}{a} \sin \frac{m\pi c}{2a}. \quad (2.7.19)$$

Thus, the partial line load expressed in a sine series can be written as

$$p_z = \frac{4p_0}{\pi} \sum_{m=1}^{\infty} \frac{1}{m} \sin \frac{m\pi \xi}{a} \sin \frac{m\pi c}{2a} \sin \frac{m\pi x}{a}. \quad (2.7.20)$$

From the boundary condition of the transverse shear forces q_y at $y = 0$, the integration constant A_m is obtained in a similar manner, as discussed above, which gives

$$A_m = \frac{p_0 a^3}{m^4 \pi^4 D} \sin \frac{m\pi \xi}{a} \sin \frac{m\pi c}{2a}. \quad (2.7.21)$$

Substituting this expression in Eq. (2.7.15), we obtain

$$w = w_H = \frac{p_0 a^3}{\pi^4 D} \sum_{m=1}^{\infty} \frac{e^{-(m\pi y/a)}}{m^4} \left(1 + \frac{m\pi y}{a}\right) \sin \frac{m\pi \xi}{a} \sin \frac{m\pi c}{2a} \sin \frac{m\pi x}{a} \quad \text{for } m = 1, 2, 3, \dots, y \geq 0. \quad (2.7.22)$$

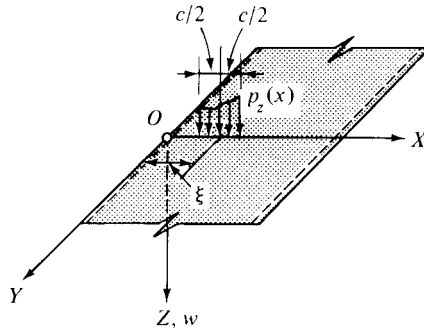


Figure 2.7.4 Partial line load.

[†] See Appendix A.1.

Equation (2.7.22) can be used for solution of plate strips subjected to a concentrated load. For this condition, we substitute $P = p_0 c$ and $\sin(m\pi c/2a) \approx m\pi c/2a$. The resulting deflection is then

$$w = \frac{Pa^2}{2\pi^3 D} \sum_{m=1}^{\infty} \frac{e^{-(m\pi y/a)}}{m^3} \left(1 + \frac{m\pi y}{a}\right) \sin \frac{m\pi \xi}{a} \sin \frac{m\pi x}{a}$$

for $m = 1, 2, 3, \dots, y \geq 0$. (2.7.23)

For problems involving uniform loads acting on a subrectangle, as shown in Fig. 2.7.5, a solution can be obtained by superimposing plate deflections (2.7.22) produced by many partial line loads (Fig. 2.7.5). An analytical expression can be derived by taking an infinitesimal element of $d\eta$ width and integrating Eq. (2.7.22) between the proper limits [1, 2]. Furthermore, using a length-to-width ratio $b/a \leq 4$, Eq. (2.4.32) gives usable results for simply supported boundary conditions. In routine design, however, it is impractical to compute the expressions of the actual deflections and the resulting stress distributions. A simplified method based on the concept of the *effective width in bending* gives usable results for most practical purposes.

c. Effective Width in Bending. The effective width b' in the bending of a plate strip subjected to a partial load uniformly distributed on a rectangular area is obtained by equating the actual moment area for m_x (at $x = a/2$) with that of a fictitious rectangular moment diagram assuming that the maximum moments are the same (Fig. 2.7.6a).

The simplest expression for the effective width is

$$b' = \frac{2}{3}a. \quad (2.7.24)$$

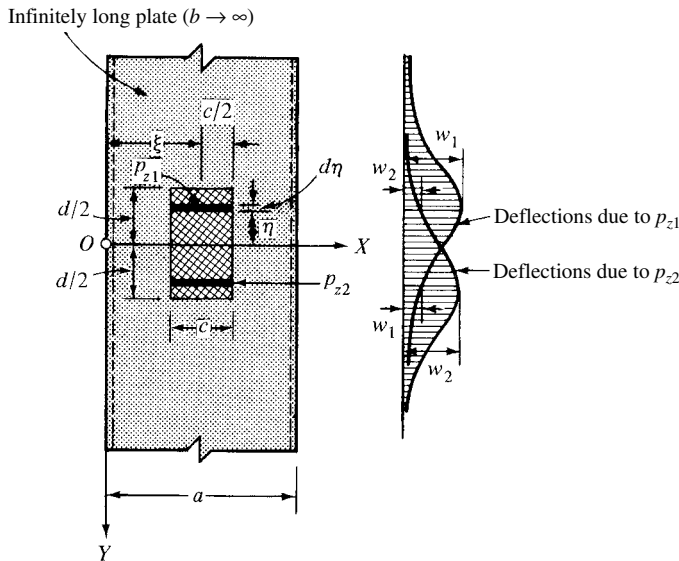


Figure 2.7.5 Partial surface load.

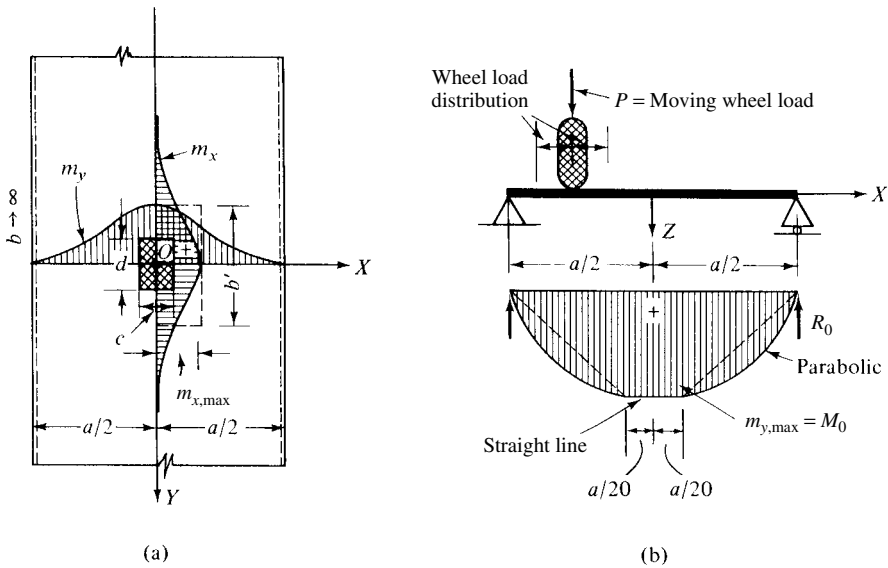


Figure 2.7.6 Wheel load on plate strip.

Holmberg [2.7.5] recommends the use of

$$b' = \frac{Pa}{4m_{x,\max}} \quad (2.7.25)$$

for the effective width, where P is the total wheel load.

Bittner [2.7.11] gives the following values for partial uniform loads distributed on subsquares ($c = d$) assuming simply supported boundary conditions:

$d/a = 0.05$	0.10	0.20	0.30	0.40	0.50	0.60	0.70	0.80	0.90	1.00
$b'/a = 0.75$	0.87	1.04	1.16	1.25	1.33	1.40	1.46	1.52	1.57	1.62

In the case of fixed boundaries at $x = 0$ and $x = a$, the effective width in bending b' can be calculated from

$d/a = 0.05$	0.10	0.20	0.30	0.40	0.50	0.60	0.70	0.80	0.90	1.00
$b'/a = 0.45$	0.55	0.67	0.76	0.84	0.90	0.96	1.01	1.06	1.12	1.18

For simply supported boundary conditions, the curve shown in Fig. 2.7.7 gives good results.

If the plate is continuous in the X direction, approximate values of the maximum moments due to moving wheel load can be obtained from the extensive tables of influence lines of continuous beams computed by Anger [2.7.13]. But in the case of bridges the girders provide elastic supports (Fig. 2.7.8a), the consideration of which can be economically done only by use of high-speed electronic computers, as discussed later. Approximate values for maximum moments and reactions are given

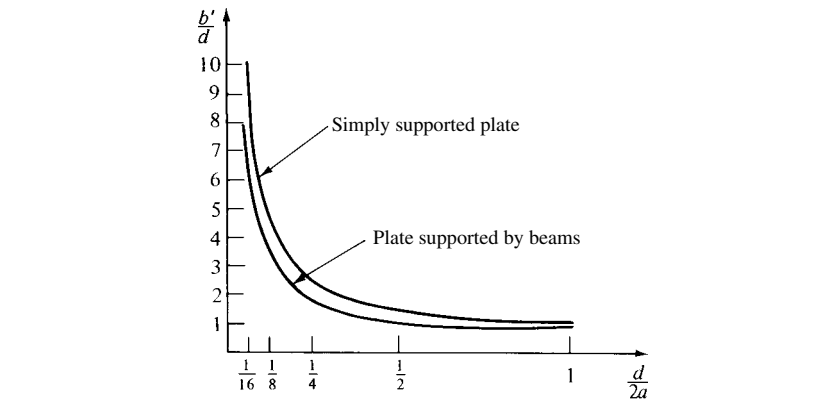


Figure 2.7.7 Diagram of effective widths in bending.

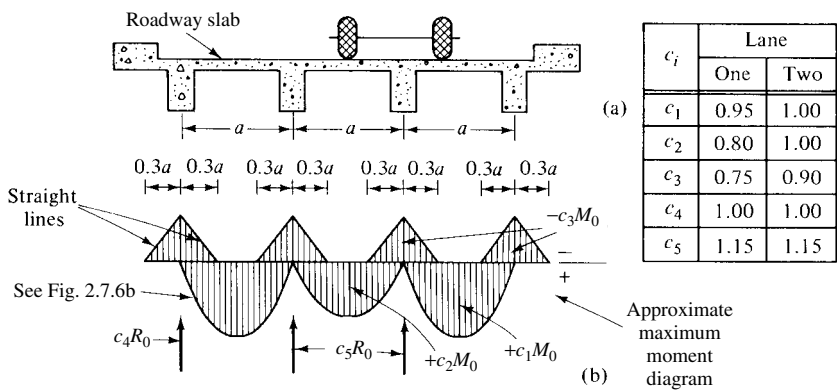


Figure 2.7.8 Continuous one-way bridge slab.

in Fig. 2.7.8b. For simply supported plate strips the maximum moment diagram can be approximated as shown in Fig. 2.7.6b.

Summary. Solutions of long rectangular plates bent to a cylindrical surface are readily obtained from the corresponding beam deflections. The resulting expressions give a particular solution, w_P , of the governing plate equation (1.2.30) when Lévy’s method is used.

Of considerable practical importance are problems involving partial loadings uniformly distributed on a small rectangular area, since they can represent the wheel loads acting on the roadway slabs of certain types of highway bridges. For routine design the use of a simplified method based on the concept of effective width in bending is recommended.

ILLUSTRATIVE EXAMPLE I

A plate strip, shown in Fig. 2.7.9, is simply supported at $x = 0$ and clamped at $x = a$. Determine the negative moments at the fixed edge assuming that the plate strip carries a uniformly distributed load p_0 .

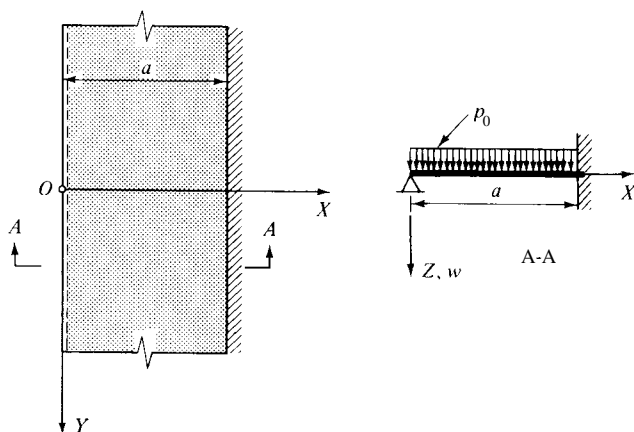


Figure 2.7.9 Plate strip bent to cylindrical surface.

Since the plate strip is bent to a cylindrical surface, the pertinent beam formula can be used for expressing the deflections [2.7.3]. Thus, we can write

$$w(x) = \frac{p_0 a^4}{48D} \left[\frac{x}{a} - 3 \left(\frac{x}{a} \right)^3 + 2 \left(\frac{x}{a} \right)^4 \right]. \quad (2.7.26)$$

The negative moments at the clamped edge are calculated from Eqs. (2.7.7) and (2.7.8), giving

$$(m_x)_{x=a} = -D \left(\frac{d^2 w}{dx^2} \right)_{x=a} = -\frac{p_0 a^2}{8} \quad (2.7.27)$$

and

$$(m_y)_{x=a} = \nu m_x = -\nu \frac{p_0 a^2}{8}. \quad (2.7.28)$$

ILLUSTRATIVE EXAMPLE II

Figure 2.7.10 shows a simply supported infinitely long plate strip carrying a uniformly distributed load p_0 . Determine the maximum deflection and bending moment using Navier's approach. Consider only two terms in the pertinent series expressions.

First, we express the load by a single Fourier series using the half-range expansion[†] to obtain only sine terms. Thus, the period of expansion in this case is $T = 2a$. This gives

$$p_z(x) = \sum_m P_m \sin \frac{m\pi x}{a} \quad \text{for } m = 1, 3, \quad (2.7.29)$$

[†] See Appendix A.1.

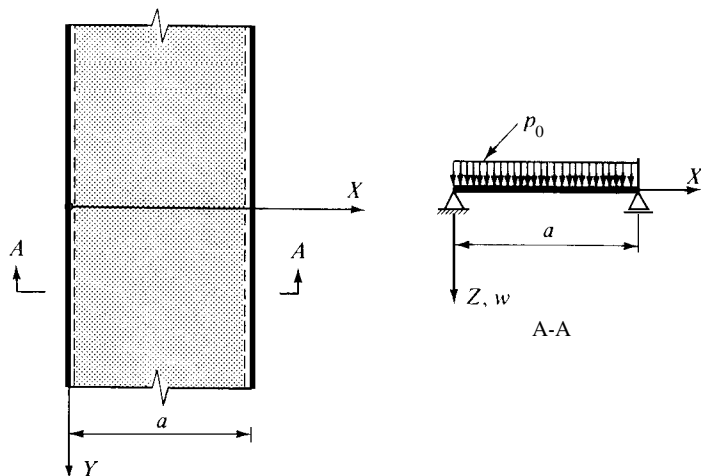


Figure 2.7.10 Simply supported plate strip.

where

$$\begin{aligned} P_m &= \frac{2p_0}{a} \int_0^a \sin \frac{m\pi x}{a} dx = \frac{2p_0}{a} \left(-\frac{a}{m\pi} \right) \left[\cos \frac{m\pi x}{a} \right]_0^a \\ &= \frac{4p_0}{m\pi} \quad \text{for } m = 1, 3; \end{aligned} \quad (2.7.30)$$

hence

$$p_z(x) = \frac{4p_0}{\pi} \sin \frac{\pi x}{a} + \frac{4p_0}{3\pi} \sin \frac{3\pi x}{a}. \quad (2.7.31)$$

Substitution of this expression in Eq. (2.7.5) yields

$$w(x) = \frac{4a^4 p_0}{D\pi^5} \sin \frac{\pi x}{a} + \frac{4a^4 p_0}{3^5 D\pi^5} \sin \frac{3\pi x}{a}. \quad (2.7.32)$$

Equation (2.7.7) gives us the expression for the bending moments in the following form:

$$m_x(x) = -D \frac{d^2 w}{dx^2} = \frac{4a^2 p_0}{\pi^3} \sin \frac{\pi x}{a} + \frac{4a^2 p_0}{3^5 \pi^3} \sin \frac{3\pi x}{a}. \quad (2.7.33)$$

The maximum deflection and bending moment occur at $x = a/2$. They are

$$w_{\max} = 0.01302 p_0 a^4 / D \quad \text{and} \quad m_{x,\max} = 0.12423 p_0 a^2.$$

In this case, the deviation of these values from their “exact” ones is very small. However, if the variation of the loading function is pronounced, more than two terms must be considered in the computation.

ILLUSTRATIVE EXAMPLE III

A simply supported semi-infinite rectangular plate is subjected to a concentrated load P at $x = \xi$ and $y = \eta$ (Fig. 2.7.11a). Determine an expression for the resulting deflections w .

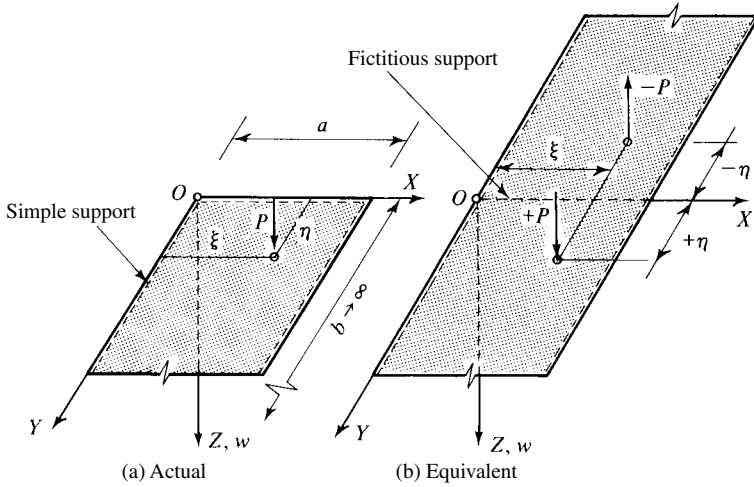


Figure 2.7.11 Concentrated force on a semi-infinite plate strip.

For this condition the method of images, as described in Sec. 2.6, can be used. Consequently, we arbitrarily extend the plate strip in the $-y$ direction and apply a fictitious negative concentrated force $-P$ at $x = \xi$, $y = -\eta$ (Fig. 2.7.11b). Since the deflection patterns of the actual and equivalent plates are the same, solution of the problem is obtained by superimposing the deflections produced by $+P$ and $-P$ forces.

For the region $0 \leq y \leq \eta$, Eq. (2.7.23) gives

$$w = \frac{Pa^2}{2\pi^3 D} \sum_{m=1}^{\infty} \frac{1}{m^3} \left\{ \left[1 + \frac{m\pi(\eta - y)}{a} \right] e^{-[m\pi(\eta - y)/a]} - \left[1 + \frac{m\pi(\eta + y)}{a} \right] e^{-[m\pi(\eta + y)/a]} \right\} \sin \frac{m\pi\xi}{a} \sin \frac{m\pi x}{a}, \quad (2.7.34)$$

and for $y \geq \eta$ we obtain

$$w = \frac{Pa^2}{2\pi^3 D} \sum_{m=1}^{\infty} \frac{1}{m^3} \left\{ \left[1 + \frac{m\pi(y - \eta)}{a} \right] e^{-[m\pi(y - \eta)/a]} - \left[1 + \frac{m\pi(y + \eta)}{a} \right] e^{-[m\pi(y + \eta)/a]} \right\} \sin \frac{m\pi\xi}{a} \sin \frac{m\pi x}{a}. \quad (2.7.35)$$

It should be noted that bending moments calculated from these expressions do not converge rapidly near the point of application of the load.

References and Bibliography

- [2.7.1] TIMOSHENKO, S. P., and YOUNG, D. H., *Theory of Structures*, 2nd ed., McGraw-Hill Book Company, New York, 1965.
- [2.7.2] WANG, CH. K., and ECKEL, C. L., *Elementary Theory of Structures*, McGraw-Hill Book Company, New York, 1957.
- [2.7.3] KLEINLOGEL, A., *Belastungsglieder*, W. Ernst und Sohn, Berlin, 1948.
- [2.7.4] MORRIS, R. M., "Concentrated Loads on Slabs," *Bull. Ohio State Univ. Eng. Exp. Sta.*, No. 80 (Nov. 1933).
- [2.7.5] HOLMBERG, A., "Medverkande bredden hos tvärsidigt upplagda rektangulära plattor av armerad betong," *Betong*, 31 (1946), 124–145.
- [2.7.6] BITTNER, E., *Berechnung von kreuzbewehrten Platten und Behältern aus Eisenbeton*, Springer-Verlag, Berlin, 1962.
- [2.7.7] OLSEN, H., and REINITZHUER, F., *Die zweiseitig gelagerte Platte*, Vol. 1, 3rd ed., Vol. 2, 2nd ed., W. Ernst und Sohn, Berlin, 1959 and 1960.
- [2.7.8] RÜSCH, H., *Fahrbahnplatten von Strassenbrücken*, Heft 106, 5th ed., Deutscher Ausschuss für Stahlbeton, W. Ernst und Sohn, Berlin, 1960.
- [2.7.9] FRITSCH, J., *Massivbrücken*, Franz Deuticke, Vienna, 1948.
- [2.7.10] RITTER, M., "Die Anwendung der Theorie elastischer Platten auf dem Eisenbeton," in *Proceedings of the International Congress for Bridge and Structural Engineering*, held in Vienna 1928, Springer-Verlag, Berlin, 1929.
- [2.7.11] BITTNER, E., *Momententafeln und Einflussflächen für kreuzweise bewehrte Eisenbetonplatten*, Springer-Verlag, Vienna, 1938.
- [2.7.12] FRANZ, G., "Platten, mitwirkende Breite, Berechnungsverfahren," in *Vorträge auf den Betontag 1961*, Deutscher Beton-Verein, Wiesbaden, 1961.
- [2.7.13] ANGER, G., *Zehnteilige Einflusslinien für durchlaufende Träger*, Vol. 3, 7th ed., W. Ernst und Sohn, Berlin, 1949.
- [2.7.14] DÜSTERHÖFT, H., "Modelluntersuchungen schiefer Durchlaufplattenbrücken auf Einzelstützen," *Publ. IABSE*, 23 (1963), 111–126.
- [2.7.15] ABDEL-SAYED, G., "Effective Width of Steel Deck-Plate in Bridges," *J. Struct. Div. Proc. ASCE*, 95, No. ST. 7 (July 1969), 1459–1474.
- [2.7.16] MÜLLER, H., *Mitwirkende Breite des Plattenbalkens; Definitionsgleichungen und Abhängigkeit von der Randquerträgerausbildung*, Wiss. S. T. H., Dresden, 1961.
- [2.7.17] KÖPCKE, W., and DENECKE, G., *Die mitwirkende Breite der Gurte von Plattenbalken*, Deutscher Ausschuss für Stahlbeton, Heft 192, W. Ernst und Sohn, Berlin, 1967.

2.8 Rigorous Solution of Circular Plates Subjected to Rotationally Symmetric Loading

If a circular plate is under the action of lateral loads, which are radially symmetric with respect to the origin of the polar coordinate system, the deflected plate surface is also rotationally symmetric (Fig. 2.8.1), provided that the support has the same type of symmetry. In this case w is independent of ϕ ; thus the Laplacian operator (1.2.31) becomes

$$\nabla_r^2 = \frac{d^2(\bullet)}{dr^2} + \frac{1}{r} \frac{d(\bullet)}{dr}. \quad (2.8.1)$$

Consequently, the differential equation of the circular plate has the following form:[†]

[†] The same expression can be obtained from the equilibrium of the plate element [2]; also see Sec. 3.4.

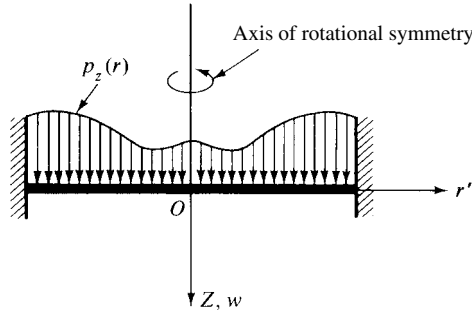


Figure 2.8.1 Rotational symmetry.

$$\nabla_r^2 \nabla_r^2 w(r) = \frac{d^4 w}{dr^4} + \frac{2}{r} \frac{d^3 w}{dr^3} - \frac{1}{r^2} \frac{d^2 w}{dr^2} + \frac{1}{r^3} \frac{dw}{dr} = \frac{p_z(r)}{D}, \quad (2.8.2)$$

where D is the flexural rigidity of the plate given by Eq. (1.2.28).

Since the deflections of the circular plate under radially symmetric loading are independent of ϕ , the expressions of the internal forces given in Sec. 1.4 become

$$m_r = -D \left(\frac{d^2 w}{dr^2} + \frac{\nu}{r} \frac{dw}{dr} \right), \quad (2.8.3)$$

$$m_\phi = -D \left(\nu \frac{d^2 w}{dr^2} + \frac{1}{r} \frac{dw}{dr} \right), \quad (2.8.4)$$

$$m_{r\phi} = m_{\phi r} = 0, \quad (2.8.5)$$

$$q_r = v_r = -D \left(\frac{d^3 w}{dr^3} + \frac{1}{r} \frac{d^2 w}{dr^2} - \frac{1}{r^2} \frac{dw}{dr} \right) \quad \text{and} \quad q_\phi = 0. \quad (2.8.6)$$

The rigorous solution of Eq. (2.8.2) is obtained again as the sum of the solution of the homogeneous differential equation (2.1.1) and one particular solution. Thus, we can write

$$w = w_H + w_P. \quad (2.8.7)$$

The solution of the homogeneous differential equation $\nabla_r^2 \nabla_r^2 w_H = 0$ can be given by

$$w_H = C_1 + C_2 r^2 + C_3 \ln \frac{r}{r_0} + C_4 r^2 \ln \frac{r}{r_0}, \quad (2.8.8)$$

where C_1, C_2, C_3 and C_4 are constants that can be determined from the boundary conditions. If the deflections at the center of the plate are not infinitely large, C_3 and C_4 must be equal to zero, and Eq. (2.8.8) becomes

$$w_H = C_1 + C_2 r^2. \quad (2.8.9)$$

The particular solution w_P is obtained by direct integration of Eq. (2.8.2). For this purpose we split the differential equation into two parts, in a way similar to that described by Eq. (1.2.43) in Sec. 1.2. Let us express first the *moment-sum* in terms of polar coordinates:

$$\mathfrak{M} = \frac{m_r + m_\varphi}{1 + \nu}. \quad (2.8.10)$$

Substituting the expression of the internal moments (2.8.3) and (2.8.4) into Eq. (2.8.10), we obtain

$$\begin{aligned} \mathfrak{M} &= -\frac{D}{1 + \nu} \left(\frac{d^2 w}{dr^2} + \nu \frac{1}{r} \frac{dw}{dr} + \frac{1}{r} \frac{dw}{dr} + \nu \frac{d^2 w}{dr^2} \right) \\ &= -D \left(\frac{d^2 w}{dr^2} + \frac{1}{r} \frac{dw}{dr} \right) = -D \nabla_r^2 w. \end{aligned} \quad (2.8.11)$$

When we apply the differential operator ∇_r^2 to Eq. (2.8.11), a comparison with Eq. (2.8.2) gives

$$\nabla_r^2 \mathfrak{M} = -p_z(r). \quad (2.8.12)$$

Equations (2.8.11) and (2.8.12) can be given in somewhat different forms:

$$\nabla_r^2 \mathfrak{M} = \frac{d^2 \mathfrak{M}}{dr^2} + \frac{1}{r} \frac{d\mathfrak{M}}{dr} = \frac{1}{r} \frac{d}{dr} \left(r \frac{d\mathfrak{M}}{dr} \right) = -p_z(r) \quad (2.8.13)$$

and

$$\nabla_r^2 w_P(r) = \frac{d^2 w_P}{dr^2} + \frac{1}{r} \frac{dw_P}{dr} = \frac{1}{r} \frac{d}{dr} \left(r \frac{dw_P}{dr} \right) = -\frac{\mathfrak{M}}{D}. \quad (2.8.14)$$

Let us integrate Eq. (2.8.13) with respect to r ; this gives

$$\frac{d\mathfrak{M}}{dr} = -\frac{1}{r} \int p_z(r) r \, dr. \quad (2.8.15)$$

The moment-sum is calculated by integrating Eq. (2.8.15):

$$\boxed{\mathfrak{M} = -\int \frac{dr}{r} \int p_z(r) r \, dr.} \quad (2.8.16)$$

Substituting into Eq. (2.8.14) and carrying out the integration, a particular solution is determined:

$$\boxed{w_P = -\frac{1}{D} \int \frac{dr}{r} \int \mathfrak{M} r \, dr.} \quad (2.8.17)$$

ILLUSTRATIVE EXAMPLE I

Determine the internal forces and the deflection of a circular plate, fixed at the edge, loaded with a uniformly distributed load, as shown in Fig. 2.8.2.

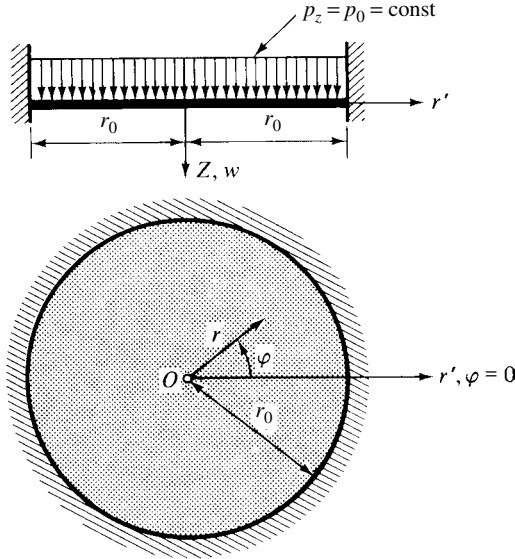


Figure 2.8.2 Uniformly loaded circular plate with fixed boundary.

The moment-sum is determined from Eq. (2.8.16):

$$\mathfrak{M} = -p_0 \int \frac{dr}{r} \int r dr = -\frac{p_0 r^2}{4}. \quad (2.8.18)$$

Equation (2.8.17) gives the particular solution

$$w_P = \frac{p_0}{4D} \int \frac{dr}{r} \int r^3 dr = \frac{p_0 r^4}{64D}. \quad (2.8.19)$$

The solution of the homogeneous form of Eq. (2.8.2) is obtained from Eq. (2.8.9); thus, the general solution is

$$w = w_H + w_P = C_1 + C_2 r^2 + \frac{p_0 r^4}{64D}. \quad (2.8.20)$$

Equation (2.8.20) must satisfy the boundary conditions

$$[w(r)]_{r=r_0} = 0 \quad \text{and} \quad \left(\frac{dw}{dr} \right)_{r=r_0} = 0. \quad (2.8.21)$$

The first equation of the boundary conditions states that the deflection at the edge is zero. This gives

$$[w(r)]_{r=r_0} = 0 = C_1 + C_2 r_0^2 + \frac{p_0 r_0^4}{64}. \quad (2.8.22)$$

From the second equation of the boundary conditions, we obtain

$$\left[\frac{dw(r)}{dr} \right]_{r=r_0} = 0 = 2C_2 r_0 + \frac{p_0 r_0^3}{16D}; \quad (2.8.23)$$

hence

$$C_2 = -\frac{p_0 r_0^2}{32D}. \quad (2.8.24)$$

Substitution of this result into Eq. (2.8.22) yields

$$C_1 = \frac{p_0 r_0^4}{64D}. \quad (2.8.25)$$

Thus, the equation of the deflected plate surface can be written as

$$w(r) = \frac{1}{D} \left(\frac{p_0 r_0^4}{64} - \frac{p_0 r_0^2 r^2}{32} + \frac{p_0 r^4}{64} \right) = \frac{p_0}{64D} (r_0^2 - r^2)^2. \quad (2.8.26)$$

Hence, the maximum deflection at the center of the plate is

$$(w_{\max})_{r=0} = \frac{p_0 r_0^4}{64D}. \quad (2.8.27)$$

From Eqs. (2.8.3), (2.8.4) and (2.8.6) the internal forces are

$$\begin{aligned} m_r &= \frac{p_0}{16} [(1 + \nu)r_0^2 - (3 + \nu)r^2], \\ m_\varphi &= \frac{p_0}{16} [(1 + \nu)r_0^2 - (1 + 3\nu)r^2], \\ q_r &= -\frac{p_0 r_0^2}{2r}. \end{aligned} \quad (2.8.28)$$

ILLUSTRATIVE EXAMPLE II

Determine the equation of the deflected plate surface $w(r)$ of a simply supported circular plate subjected to a rotationally symmetric lateral load that linearly increases from the center of the edge, as shown in Fig. 2.8.3.

From Eq. (2.8.16)

$$\mathfrak{M} = -\frac{p_0}{r_0} \int \frac{dr}{r} \int r^2 dr = -\frac{p_0 r^3}{9r_0}. \quad (2.8.29)$$

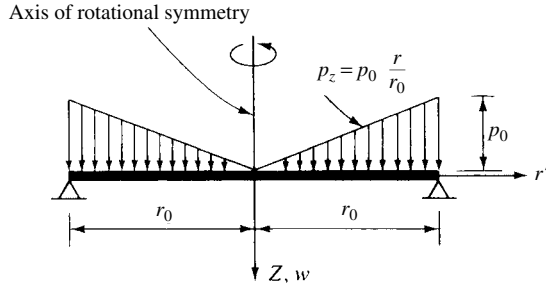


Figure 2.8.3 Circular plate with linearly increasing lateral load.

Substituting this result into Eq. (2.8.17), a particular solution of the governing differential equation of problem (2.8.2) is obtained:

$$w_P = \frac{1}{D} \int \frac{dr}{r} \int \frac{p_0 r^3}{9r_0} r dr = \frac{p_0}{45Dr_0} \int r^4 dr = \frac{p_0 r^5}{225Dr_0}. \quad (2.8.30)$$

Equation (2.8.9) gives the solution for the homogeneous form of the differential equation, $\nabla_r^2 \nabla_r^2 w_H = 0$; thus the general solution of Eq. (2.8.2) can be written as

$$w = w_H + w_P = C_1 + C_2 r^2 + \frac{p_0 r^5}{225Dr_0}. \quad (2.8.31)$$

The unknown constants C_1 and C_2 are determined from the boundary conditions of the problem, which are

$$(w)_{r=r_0} = 0 \quad \text{and} \quad (m_r)_{r=r_0} = 0. \quad (2.8.32)$$

The second boundary condition gives

$$(m_r)_{r_0} = \left[-D \left(\frac{d^2 w}{dr^2} + \frac{\nu}{r} \frac{dw}{dr} \right) \right]_{r=r_0} = 0. \quad (2.8.33)$$

By substituting Eq. (2.8.31) into (2.8.33), the boundary condition becomes the equation of the second:

$$2C_2 + \frac{4p_0 r_0^2}{45D} + 2\nu C_2 + \frac{\nu p_0 r_0^2}{45D} = 0, \quad (2.8.34)$$

from which

$$C_2 = -\frac{p_0 r_0^2}{90D} \left(\frac{4 + \nu}{1 + \nu} \right). \quad (2.8.35)$$

The geometrical boundary condition,

$$(w)_{r=r_0} = C_1 + C_2 r_0^2 + \frac{p_0 r_0^4}{225D} = 0, \quad (2.8.36)$$

yields

$$C_1 = \frac{p_0 r_0^4}{45D} \left[\frac{4 + \nu}{2(1 + \nu)} - \frac{1}{5} \right]. \quad (2.8.37)$$

Equation (2.8.31) with known C_1 and C_2 coefficients defines the deflected plate surface.

Summary. The above-discussed method for rigorous solution of circular plates can be used in most cases with relative ease, provided that the lateral loads and boundary supports are rotationally symmetric with respect to the center of the plate. Consequently, the application of this method is highly recommended. The practical importance of the solution of such problems is especially pronounced in container, pressure vessel, water tank, silo (where they are used as cover plates) and machine design (Fig. 2.8.4).

2.9 Solutions of Membrane Problems

As introduced in Sec. 1.7, the governing differential equation for rectangular membranes is Eq. (1.7.2). For circular plates we derived two differential equations, Eqs. (1.7.4) and (1.7.6). The first one governs the general loading case, and the second one is restricted to rotationally symmetric loads. In both cases, we assumed also rotationally symmetric edge supports. All these differential equations are valid only for small deflections. The large-deflection theory of membranes, which describes the actual membrane behavior more effectively, is treated in Sec. 11.1.

Since for membranes the clamped boundary conditions are analogous to simple supports of thin plates with flexural rigidity, a Navier-type approach, as discussed in Sec. 2.2, can be applied in most cases.

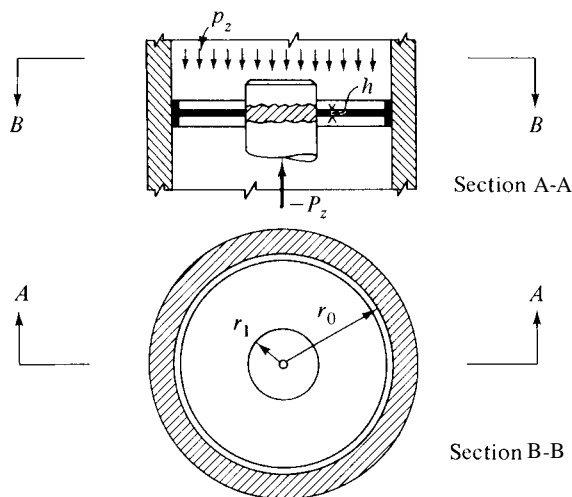


Figure 2.8.4 Use of circular plate in machine design.

Consequently, we express the lateral load in the double Fourier series

$$p_z(x, y) = \sum_{m=1}^{\infty} \sum_{n=1}^{\infty} P_{mn} \sin \frac{m\pi x}{a} \sin \frac{n\pi y}{b}, \quad (2.9.1)$$

where P_{mn} is obtained from Eq. (A.1.36). Expressing the membrane deflections in a similar way, we can write

$$w(x, y) = \sum_{m=1}^{\infty} \sum_{n=1}^{\infty} W_{mn} \sin \frac{m\pi x}{a} \sin \frac{n\pi y}{b}. \quad (2.9.2)$$

The substitution of Eqs. (2.9.1) and (2.9.2) into the governing differential equation of rectangular membranes (1.7.2) yields (for specific m, n values) the amplitude of the deflections:

$$W_{mn} = \frac{P_{mn}}{\pi^2[(m^2/a^2) + (n^2/b^2)]\sigma h}. \quad (2.9.3)$$

Solution of differential equation (1.7.6), which governs the small-deflection theory of circular membranes subjected to rotationally symmetric loads, has the general form

$$w = w_H + w_p, \quad (2.9.4)$$

where

$$w_H = C_1 + C_2 \ln r. \quad (2.9.5)$$

A particular solution is obtained by direct integration of the differential equation (1.7.6):

$$w_p = -\frac{1}{\sigma h} \int \frac{dr}{r} \int p_z(r) dr. \quad (2.9.6)$$

Since the deflection at the center of the plate cannot be infinitely large, we must disregard C_2 in Eq. (2.9.5).

Classical solutions of differential equation (1.7.4) are, however, far more difficult. Although one can transform this partial differential equation into an ordinary differential equation by separating the variables,

$$w(x, \varphi) = R(r) \cdot \Phi(\varphi), \quad (2.9.7)$$

combined with other mathematical manipulations, the exact solutions remain cumbersome. Applying one of the energy methods discussed in Sec. 4.2 and Sec. 4.3, respectively, one can obtain very usable solutions to these problems in analytical forms.

ILLUSTRATIVE EXAMPLE I

Let us determine the equation of small deflections of the rectangular, stretched membrane shown in Fig. 2.9.1. The lateral load p_0 is assumed to be uniformly distributed.

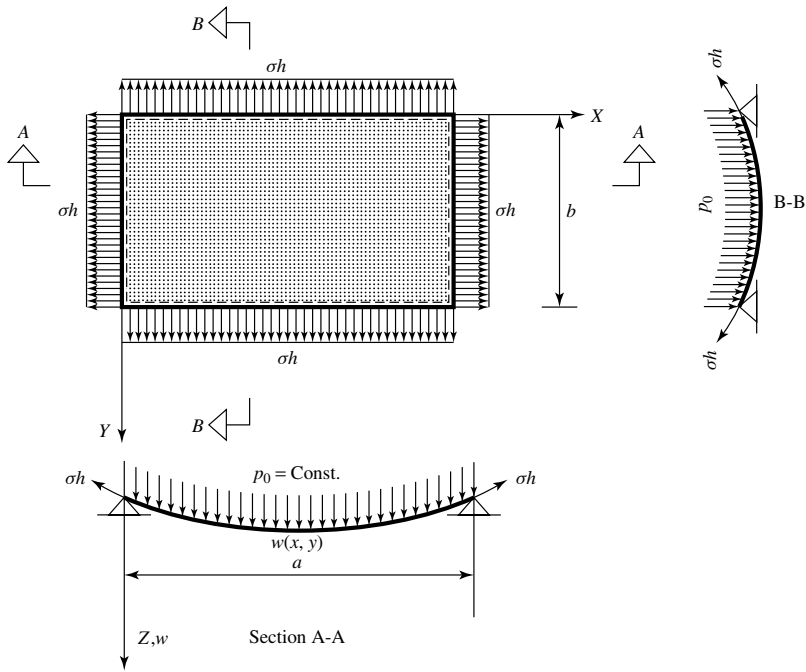


Figure 2.9.1 Stretched rectangular membrane.

We use a Navier-type approach. From Table A.1.1 we obtain

$$P_{mn} = \frac{16p_0}{\pi^2 mn} \quad \text{for } m, n = 1, 3, 5, \dots \quad (2.9.8)$$

Substitution of Eq. (2.9.8) into Eq. (2.9.3) gives

$$W_{mn} = \frac{16p_0}{\pi^4 mn[(m^2/a^2) + (n^2/b^2)]\sigma h}. \quad (2.9.9)$$

Thus the equation of the deflected membrane surface becomes

$$w(x, y) = \frac{16p_0}{\pi^4 \sigma h} \sum_m \sum_n \frac{1}{mn[(m^2/a^2) + (n^2/b^2)]} \quad \text{for } m, n = 1, 3, 5, \dots \quad (2.9.10)$$

ILLUSTRATIVE EXAMPLE II

Find the lateral deflections of a stretched, circular membrane subjected to a lateral load that is linearly increasing from center to edge (Fig. 2.9.2). Assume that the small-deflection theory of membranes is valid.

We seek the general solution of Eq. (1.7.6) in the form

$$w = w_H + w_P. \quad (2.9.11)$$

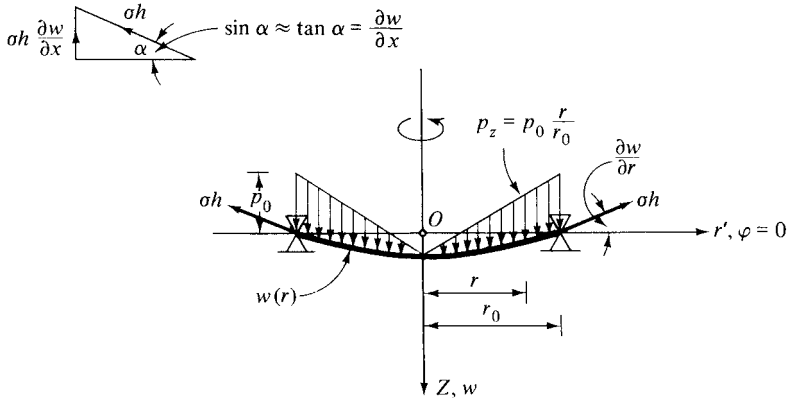


Figure 2.9.2 Stretched circular membrane.

A particular solution w_P is obtained from Eq. (2.9.6); thus

$$w_P = -\frac{p_0}{r_0 \sigma h} \int \frac{dr}{r} \int r^2 dr = -\frac{p_0 r^3}{9 r_0 \sigma h}. \quad (2.9.12)$$

Since the solution of the homogeneous form of Eq. (1.7.6) is

$$w_H = C_1 + C_2 \ln r, \quad (2.9.13)$$

theoretically, the general solution should be written as

$$w = C_1 + C_2 \ln r - \frac{p_0 r^3}{9 r_0 \sigma h}. \quad (2.9.14)$$

However, as already mentioned, the second term on the right-hand side of this equation must be disregarded, since it would create an unwanted singularity in the solution. The remaining constant C_1 is determined from the boundary condition,

$$w(r_0) = C_1 - \frac{p_0 r_0^3}{9 r_0 \sigma h} = 0; \quad (2.9.15)$$

hence

$$C_1 = \frac{p_0 r_0^3}{9 \sigma h r_0} \quad (2.9.16)$$

and

$$w(r) = \frac{p_0}{9 \sigma h r_0} [r_0^3 - r^3] \quad (2.9.17)$$

which gives the required zero deflection at the boundary r_0 .

2.10 Series Solutions of Moderately Thick Plates

a. Navier-Type Approach. Assuming a simply supported rectangular plate of dimensions $a \cdot b$ and h subjected to $p_z(x, y)$ lateral load,[†] we may apply Navier's method to obtain double Fourier series solutions to this problem.

First, the lateral load is expanded in double Fourier series as described in Appendix A.1; thus

$$p_z(x, y) = \sum_{m=1}^{\infty} \sum_{n=1}^{\infty} P_{mn} \sin \frac{m\pi x}{a} \sin \frac{n\pi y}{b}. \quad (2.10.1)$$

Next, the unknown deflections and rotations of the midplane are expressed in similar double Fourier series:

$$w(x, y) = \sum_{m=1}^{\infty} \sum_{n=1}^{\infty} W_{mn} \sin \frac{m\pi x}{a} \sin \frac{n\pi y}{b}, \quad (2.10.2)$$

$$\psi_x(x, y) = \sum_{m=1}^{\infty} \sum_{n=1}^{\infty} A_{mn} \sin \frac{m\pi x}{a} \sin \frac{n\pi y}{b}, \quad (2.10.3)$$

$$\psi_y(x, y) = \sum_{m=1}^{\infty} \sum_{n=1}^{\infty} B_{mn} \sin \frac{m\pi x}{a} \sin \frac{n\pi y}{b}. \quad (2.10.4)$$

Let us consider first Mindlin's plate theory as introduced in Sec. 1.5b. The above given expressions for the kinematic unknowns simultaneously satisfy the differential equations of the moderately thick plate [Eqs. (1.5.19)–(1.5.21)] and the pertinent boundary conditions given in Eq. (1.5.29).

Substitution of these double series expressions into the differential equations of equilibrium gives the Fourier coefficients

$$W_{mn} = \left\{ 1 + \frac{D\pi^2}{\kappa^2 Gh} \left[\left(\frac{m}{a} \right)^2 + \left(\frac{n}{b} \right)^2 \right] \right\} \frac{P_{mn}}{D\pi^4 \left[(m/a)^2 + (n/b)^2 \right]^2}, \quad (2.10.5)$$

$$A_{mn} = - \frac{m P_{mn}}{a D \pi^3 \left[(m/a)^2 + (n/b)^2 \right]^2}, \quad (2.10.6)$$

$$B_{mn} = - \frac{n P_{mn}}{b D \pi^3 \left[(m/a)^2 + (n/b)^2 \right]^2}. \quad (2.10.7)$$

A similar approach can be taken with the sixth-order theory of moderately thick plates developed by Levinson [2.10.1, 2.10.2]. In this case, the differential equations of equilibrium are represented by Eqs. (1.5.33), (1.5.34) and (1.5.35), respectively. The so-obtained improved set of Fourier coefficients are

$$W_{mn} = \left\{ 1 + \frac{6D\pi^2}{5Gh} \left[\left(\frac{m}{a} \right)^2 + \left(\frac{n}{b} \right)^2 \right] \right\} \frac{P_{mn}}{D\pi^4 \left[(m/a)^2 + (n/b)^2 \right]^2}, \quad (2.10.8)$$

[†] For a coordinate system see Fig. 1.1.1.

$$A_{mn} = - \left\{ 1 - \frac{3D\pi^2}{10Gh} \left[\left(\frac{m}{a} \right)^2 + \left(\frac{n}{b} \right)^2 \right] \right\}^2 \frac{m P_{mn}}{a D \pi^3 [(m/a)^2 + (n/b)^2]^2}, \quad (2.10.9)$$

$$B_{mn} = - \left\{ 1 - \frac{3D\pi^2}{10Gh} \left[\left(\frac{m}{a} \right)^2 + \left(\frac{n}{b} \right)^2 \right] \right\}^2 \frac{n P_{mn}}{b D \pi^3 [(m/a)^2 + (n/b)^2]^2}. \quad (2.10.10)$$

In addition, it is worth noting that the simplified Reissner plate theory described by Eq. (1.5.11)—along with other higher-order plate theories derived only in terms of the lateral deflections[†] $w(x, y)$ —lend themselves well to the above-introduced Navier-type solutions [2.10.3], provided that all edges are simply supported.

Furthermore, if we would like to compute only the lateral deflections of a simply supported Mindlin plate, the use of the so-called *conjugate plate analogy* [2.10.4] offers the easiest way. According to this analogy, the deflections $w(x, y)$ obtained by solving the governing differential equation of thin plates (1.2.30) should merely be augmented by a shear deflection component $w_s = \mathfrak{M}/\kappa^2 Gh$, where \mathfrak{M} represents the moment-sum given in Eq. (1.2.42). This moment-sum can readily be computed by solving the differential equation (1.2.43a), which is identical with that of the membranes, that is, (1.7.2). Consequently, the very same Navier solution, discussed in Sec. 2.9, can be applied.

b. Lévy-Type Approach. To obtain Lévy-type solutions of moderately thick plate problems, we must use the uncoupled Mindlin differential equations of equilibrium:

$$D \nabla^4 w(x, y) = \left(1 - \frac{D}{\kappa^2 Gh} \nabla^2 \right) p_z(x, y), \quad (2.10.11)$$

$$D \nabla^4 \psi_x(x, y) = - \frac{\partial p_z(x, y)}{\partial x}, \quad (2.10.12)$$

$$D \nabla^4 \psi_y(x, y) = - \frac{\partial p_z(x, y)}{\partial y}. \quad (2.10.13)$$

As in Sec. 2.3, we assume that the two opposite edges at $x = 0$ and $x = a$ are simply supported and the load is symmetrical about the X axis, as shown in Figs. 2.3.1 and 2.3.2, respectively. The pertinent homogeneous forms of the differential equations are

$$\nabla^4 w(x, y) = \nabla^4 \psi_x(x, y) = \nabla^4 \psi_y(x, y) = 0. \quad (2.10.14)$$

We seek the solution of the transverse displacements in the form

$$w(x, y) = w_H(x, y) + w_P(x, y), \quad (2.10.15)$$

where w_H is the solution of $D \nabla^4 w_H = 0$ and w_P represents a particular solution of the governing differential equation of thin plates (1.2.30).

[†] Listed in the reference part of Sec. 1.5.

The corresponding uncoupled equilibrium equations in Levinson's plate theory [2.10.5] are

$$D\nabla^4 w(x, y) = \left(1 - \frac{6D}{5Gh}\nabla^2\right) p_z(x, y), \quad (2.10.16)$$

$$D\nabla^4 \psi_x(x, y) = -\left(1 + \frac{3D}{10Gh}\nabla^2\right) \frac{\partial p_z(x, y)}{\partial x}, \quad (2.10.17)$$

$$D\nabla^4 \psi_y(x, y) = -\left(1 + \frac{3D}{10Gh}\nabla^2\right) \frac{\partial p_z(x, y)}{\partial y}. \quad (2.10.18)$$

As already mentioned in Sec. 1.5c, the midplane rotations ψ_x and ψ_y are in this case somewhat differently defined from those given by Mindlin.

Expressing the lateral load and the particular solutions of the kinematic unknowns by single Fourier sine series, that is,

$$p_z(x) = \sum_{m=1}^{\infty} P_m(y) \sin \frac{m\pi x}{a}, \quad (2.10.19)$$

$$w_P(x) = \sum_{m=1}^{\infty} W_m(y) \sin \frac{m\pi x}{a}, \quad (2.10.20)$$

$$\psi_{x(P)} = \sum_{m=1}^{\infty} J_m(y) \sin \frac{m\pi x}{a}, \quad (2.10.21)$$

$$\psi_{y(P)} = \sum_{m=1}^{\infty} R_m(y) \sin \frac{m\pi x}{a}, \quad (2.10.22)$$

and substituting these expressions into Mindlin's uncoupled plate equations, we obtain the following set of ordinary differential equations:

$$\begin{aligned} & \frac{d^4 W_m}{dy^4} - 2\left(\frac{m\pi}{a}\right)^2 \frac{d^2 W_m}{dy^2} + \left(\frac{m\pi}{a}\right)^4 W_m \\ &= \frac{1}{D} \left\{ \left[1 + \left(\frac{m\pi}{a}\right)^2 \frac{D}{\kappa^2 Gh} \right] P_m - \frac{D}{\kappa^2 Gh} \frac{d^2 P_m}{dy^2} \right\}, \end{aligned} \quad (2.10.23)$$

$$\begin{aligned} & \frac{d^4 J_m}{dy^4} - 2\left(\frac{m\pi}{a}\right)^2 \frac{d^2 J_m}{dy^2} + \left(\frac{m\pi}{a}\right)^4 J_m \\ &= -\frac{m\pi}{aD} P_m, \end{aligned} \quad (2.10.24)$$

$$\begin{aligned} & \frac{d^4 R_m}{dy^4} - 2\left(\frac{m\pi}{a}\right)^2 \frac{d^2 R_m}{dy^2} + \left(\frac{m\pi}{a}\right)^4 R_m \\ &= -\frac{1}{D} \frac{dP_m}{dy}. \end{aligned} \quad (2.10.25)$$

A similar procedure using Levinson's uncoupled higher-order plate equations [2.10.5] yields

$$\begin{aligned} \frac{d^4 W_m}{dy^4} - 2 \left(\frac{m\pi}{a} \right)^2 \frac{d^2 W_m}{dy^2} + \left(\frac{m\pi}{a} \right)^4 W_m \\ = \frac{1}{D} \left\{ \left[1 + \left(\frac{m\pi}{a} \right)^2 \frac{6D}{5Gh} \right] P_m - \frac{6D}{5Gh} \frac{d^2 P_m}{dy^2} \right\}, \end{aligned} \quad (2.10.26)$$

$$\begin{aligned} \frac{d^4 J_m}{dy^4} - 2 \left(\frac{m\pi}{a} \right)^2 \frac{d^2 J_m}{dy^2} + \left(\frac{m\pi}{a} \right)^4 J_m \\ = -\frac{m\pi}{aD} \left\{ \left[1 - \left(\frac{m\pi}{a} \right)^2 \frac{3D}{10Gh} \right] P_m + \left(\frac{m\pi}{a} \right) \frac{3D}{10Gh} \frac{d^2 P_m}{dy^2} \right\} \end{aligned} \quad (2.10.27)$$

and

$$\begin{aligned} \frac{d^4 R_m}{dy^4} - 2 \left(\frac{m\pi}{a} \right)^2 \frac{d^2 R_m}{dy^2} + \left(\frac{m\pi}{a} \right)^4 R_m \\ = -\frac{1}{D} \left\{ \left[1 - \left(\frac{m\pi}{a} \right)^2 \frac{3D}{10Gh} \right] \frac{dP_m}{dy} + \frac{3D}{10Gh} \frac{d^3 P_m}{dy^3} \right\}. \end{aligned} \quad (2.10.28)$$

Solution of these equations gives the constants W_m , I_m and R_m for a specific m value. The boundary conditions in this case are those of simple supports at edges $x = 0$ and $x = a$.

For solutions of the homogeneous form of both types of plate equations, Cooke and Levinson [2.10.5] derived the following expressions:

$$\begin{aligned} w_H = \sum_{m=1}^{\infty} \left(A_m \cosh \frac{m\pi y}{a} + B_m y \sinh \frac{m\pi y}{a} + C_m \sinh \frac{m\pi y}{a} \right. \\ \left. + D_m y \cosh \frac{m\pi y}{a} \right) \sin \frac{m\pi x}{a}, \end{aligned} \quad (2.10.29)$$

$$\begin{aligned} \psi_{x(H)} = \sum_{m=1}^{\infty} \left(E_m \cosh \frac{m\pi y}{a} - B_m \frac{m\pi y}{a} \sinh \frac{m\pi y}{a} + G_m \sinh \frac{m\pi y}{a} \right. \\ \left. - D_m \frac{m\pi y}{a} \cosh \frac{m\pi y}{a} \right) \cos \frac{m\pi x}{a} \end{aligned} \quad (2.10.30)$$

and

$$\begin{aligned} \psi_{y(H)} = \sum_{m=1}^{\infty} \left[(G_m - D_m) \cosh \frac{m\pi y}{a} - D_m \frac{m\pi y}{a} \sinh \frac{m\pi y}{a} \right. \\ \left. + (E_m - B_m) \sinh \frac{m\pi y}{a} - B_m \cosh \frac{m\pi y}{a} \right] \sin \frac{m\pi x}{a}. \end{aligned} \quad (2.10.31)$$

Using the sums of the pertinent homogeneous and particular solutions, the constants A_m, \dots, G_m are obtained from the six boundary conditions at the edges $y = \pm b/2$. These boundary conditions can be free-edge, simple support or fixed edge, respectively.

Finally, it should be noted that somewhat different Lévy-type solutions of moderately thick, rectangular plates can be found in Refs. [2.10.6] and [2.10.7].

These mathematical operations are extremely tedious and labor intensive. Some relief of the large amount of “longhand” computations can be achieved, however, by utilizing programs of “symbolic mathematics” listed in Appendix A.1 [A.1.18–A.1.21]. If there is a frequent need to solve these equations, one can program the whole procedure. The reader will find some additional information on solutions of moderately thick plates in Refs. [2.10.8–2.10.11].

Summary. In this section the extension of Navier’s solution technique to Mindlin’s and Levinson’s plate theories was demonstrated. Some other higher-order plate theories can also be treated in a similar fashion. The procedure is relatively simple. Further simplification can be obtained by applying the *conjugate plate* analogy. Treating other than simply supported boundary conditions by a Lévy-type approach, however, becomes extremely difficult. The required extensive hand computations can be facilitated, to certain degree, by the use of *symbolic mathematics* programs. This later part is intended mostly for research engineers, who will probably find some inspiration to do further research in this important field.

ILLUSTRATIVE EXAMPLE

Let us determine the deflections of a simply supported, rectangular Mindlin plate of $a \cdot b$ dimensions subjected to uniformly distributed lateral load of constant p_0 intensity.

We apply the above-mentioned conjugate plate analogy, according to which

$$w(x, y) = w_K(x, y) + w_s(x, y), \quad (2.10.32)$$

where w_K represents the Navier solution of Kirchhoff’s plate equation (1.2.30) and w_s is an additional shear contribution [2.10.4] in the form

$$w_s(x, y) = \frac{\mathfrak{M}}{\kappa^2 G h}, \quad (2.10.33)$$

where \mathfrak{M} is the moment-sum given in Eq. (1.2.42) and the constants of the Mindlin plate, κ^2 and G , are defined in Sec. 1.5b.

First, the load is expressed in the double Fourier series

$$p_z(x, y) = \sum_{m=1}^{\infty} \sum_{n=1}^{\infty} P_{mn} \sin \frac{m\pi x}{a} \sin \frac{n\pi y}{b}, \quad (2.10.34)$$

where P_{mn} is obtained from Table A.1.1; hence

$$P_{mn} = \frac{16p_0}{\pi^2 mn} \quad \text{for } m, n = 1, 3, 5, \dots \quad (2.10.35)$$

Expressing the solution w_K in a similar way,

$$w_K(x, y) = \sum_{m=1}^{\infty} \sum_{n=1}^{\infty} W_{mn} \sin \frac{m\pi x}{a} \sin \frac{n\pi y}{b}, \quad (2.10.36)$$

and substituting Eqs. (2.10.34) and (2.10.35) into the governing differential equation of thin plates (1.2.30), we obtain, for a set of m, n values,

$$W_{mn} = \frac{P_{mn}}{D\pi^4 [(m^2/a^2) + (n^2/b^2)]^2}; \quad (2.10.37)$$

hence

$$w_K(x, y) = \sum_{m=1}^{\infty} \sum_{n=1}^{\infty} \frac{P_{mn}}{[(m^2/a^2) + (n^2/b^2)]^2} \sin \frac{m\pi x}{a} \sin \frac{n\pi y}{b}. \quad (2.10.38)$$

We take a similar approach to determine the moment-sum. In this case, the pertinent differential equation (1.2.43a) is

$$\frac{\partial^2 \mathfrak{M}}{\partial x^2} + \frac{\partial^2 \mathfrak{M}}{\partial y^2} = -p_z. \quad (2.10.39)$$

Expressing, again, the moment-sum in the double Fourier series

$$\mathfrak{M}(x, y) = \sum_{m=1}^{\infty} \sum_{n=1}^{\infty} M_{mn} \sin \frac{m\pi x}{a} \sin \frac{n\pi y}{b} \quad (2.10.40)$$

and substituting Eqs. (2.10.34) and (2.10.40) into Eq. (2.10.39) give

$$M_{mn} = \frac{P_{mn}}{\pi^2 [(m^2/a^2) + (n^2/b^2)]}. \quad (2.10.41)$$

Thus, the equation of deflections becomes

$$\begin{aligned} w = & \frac{16p_0}{D\pi^6} \sum_m \sum_n \frac{\sin(m\pi x/a) \sin(n\pi y/b)}{mn[(m^2/a^2) + (n^2/b^2)]^2} \\ & + \frac{16p_0}{\pi^4} \sum_m \sum_n \frac{\sin(m\pi x/a) \sin(n\pi y/b)}{mn[(m^2/a^2) + (n^2/b^2)]} \\ & \text{for } m, n = 1, 3, 5, \dots \end{aligned} \quad (2.10.42)$$

References and Bibliography

- [2.10.1] LEVINSON, M., "An Accurate, Simple Theory of Statics and Dynamics of Elastic Plates," *Mech. Res. Commun.*, 7 (1980), 343–350.
- [2.10.2] LEVINSON, M., and COOKE, D. W., "Thick Rectangular Plates—I: The Generalized Navier Solution," *Int. J. Mech. Sci.*, 25 (1983), 199–205.

- [2.10.3] BALUCH, M. H., and VOYIADJIS, G. Z., "Higher-Order Plate Equations Based on Reissner's Formulation of Plate Problem," *Arab. J. Sci. Eng.*, 5 (1980), 75–80.
- [2.10.4] WANG, C. M., and ALWIS, W. A. M., "Simply Supported Polygonal Mindlin Plate Deflections Using Kirchhoff Plate," *ASCE J. Eng. Mech. Div.*, 121 (1995), 1383–1384.
- [2.10.5] COOKE, D. W., and LEVINSON, M., "Thick Rectangular Plates—II: The Generalized Lévy Solution," *Int. J. Mech. Sci.*, 25 (1983), 207–215.
- [2.10.6] SALERNO, V. L., and GOLDBERG, M. A., "Effect of Shear Deformation on the Bending of Rectangular Plates," *J. Appl. Mech.*, 27 (1950), 54–58.
- [2.10.7] KOELLER, R. C., and ESSENBURG, F., "Shear Deformation in Rectangular Plates," *Proc. 4th U.S. Natl. Congr. Appl. Mech.*, pp. 555–561.
- [2.10.8] WOINOWSKY-KRIEGER, S., "Der Spannungszustand in dicken elastischen Platten," *Ing.-Arch.*, 4 (1933), 203–226.
- [2.10.9] LO, K. H., et al., "A High-Order Theory of Plate Deformation, Part 1: Homogeneous Plates," *J. Appl. Mech.*, 54 (1977), 663–668.
- [2.10.10] SHIRAKAWA, K., "Bending of Plates Based on Improved Theory," *Mech. Res. Commun.*, 10 (1983), 205–211.
- [2.10.11] LEVINSON, M., "A Novel Approach to Thick Plate Theory Suggested by Studies in Foundation Theory," *Int. J. Mech. Sci.*, 26 (1984), 427–436.

2.11 Summary

Of the mathematical methods for solutions of plate problems introduced in this chapter, the rigorous solution of the governing differential equation of thin plates expressed in Cartesian coordinate system is purely of academic interest, since rigorous solutions of Kirchhoff's plate equation can be obtained only in an extremely limited number of cases. For the majority of practical problems, a rigorous solution either cannot be found or is of such complicated structure that it can be applied only with great difficulty in a practical computation. Closed-form solutions for circular plates, however, can be obtained with relative ease, provided that the lateral loads and supports are rotationally symmetric.

For simply supported rectangular thin-plates, Navier's method yields mathematically correct solutions. The convergence of the resulting double Fourier series depends considerably on the continuity of the loading function. Slow convergence, created by discontinuous loading, is especially pronounced in the case of concentrated forces. For continuously distributed lateral loads, however, the convergence of this solution technique is very satisfactory.

The application of Lévy's method based on the use of the single Fourier series is somewhat more complex, but the solution converges very rapidly. In addition, Lévy's method is more general, although it does not have an entirely general character either. It can be used only if two opposite edges of the plate are simply supported and the shape of the loading is the same for all sections parallel to the direction of simply supported edges.

A generalization of Navier's approach has also been introduced. This solution technique can be applied for thin plates with any boundary conditions and subjected to any type of loading. The consideration of free-edge boundary conditions, however, still appears to be somewhat more problematic.

In addition, it should be noted that the applicability of Navier's and Lévy's methods can be considerably extended by means of the *superposition technique*. That is, these results can provide a particular solution for the governing plate equation (1.2.30), upon which the solution of the homogeneous form of the plate equation, representing additional boundary conditions, can be superimposed.

In the classical bending analysis of moderately thick, rectangular plates, again, a Navier-type approach can be applied, provided that the plate is simply supported. In a similar manner, Lévy's classical solution can also be extended to solutions of moderately thick plate problems. But because of its complexity, this approach is recommended only to research engineers.

Finally, it should be mentioned that solutions of very thin plates create no problems if the deflections remain small. For rectangular membranes Navier's approach offers an easy solution technique. Solutions for circular membranes carrying circular symmetrical loads are obtained by direct integration.

All classical solutions presented fall under the classification of boundary value problems of *mathematical physics*. The mastery of the mathematical techniques presented here can be obtained only by practice. Consequently, the study of the illustrative problems is highly recommended. As mentioned, the number of mathematically correct solutions obtainable by the classical methods is limited. Many problems of considerable practical importance either cannot be solved by these methods or the solution obtained is too cumbersome for most practical use. In spite of these shortcomings, the classical methods do have their own merits, which are (1) clearness of the mathematical modeling, (2) application of consistent mathematical science and techniques, (3) yielding of reusable solutions and (4) the provision of important theoretical foundations for almost all approximate and numerical methods. Therefore, it is essential that the reader be introduced to the fundamentals of classical methods in spite of their inherent limitations.

Problems[†]

- 2.2.1. A simply supported rectangular plate is loaded with a uniformly distributed lateral load p_0 . Find the edge reactions and the anchorage forces at the corners.
- 2.2.2. A simply supported square plate is subjected to a sinusoidal-type load in the form $p_z = \sin(\pi x/a) \cdot \sin(\pi x/a)$. Find the deflection and bending moments at the center of the plate.
- 2.2.3. Solve Problem 2.2.1 using a parabolic load distribution.
- 2.2.4. A simply supported rectangular plate carries a hydrostatic load that has its maximum intensity at $x = a$. Determine the equation of the deflected plate surface using Navier's method.
- 2.2.5. Combine a uniformly distributed load with a hydrostatic load and determine the location and magnitude of the maximum deflection.
- 2.2.6. Determine the maximum bending and torsional moments in Problem 2.2.5.
- 2.3.1. Rework Problem 2.2.4 using Lévy's method.
- 2.3.2. Two opposite edges of a rectangular plate are simply supported, and the other two are clamped. Determine the equation of the deflected plate surface by Lévy's method. Assume a uniformly distributed load p_0 .
- 2.3.3. Rework Problem 2.3.2 assuming a square plate and hydrostatic load.
- 2.3.4. Find the maximum bending moments in Problem 2.3.2.

[†] The first two numbers refer to the corresponding section.

- 2.4.1. A rectangular plate is subjected to a uniform line load p_0 at $y = \eta$. Assuming simply supported boundary conditions, determine the equation of the deflected plate surface.
- 2.4.2. Find all internal forces in Problem 2.4.1.
- 2.4.3. A simply supported square plate is subjected to a positive sinusoidal edge moment at $x = a$. Determine the equation of the deflected plate surface.
- 2.8.1. Consider a simply supported circular plate subjected to a rotationally symmetric load in the form of a cone. Determine the equation of the deflected plate surface.
- 2.8.2. Determine the maximum moments and shear forces in Problem 2.8.1.
- 2.8.3. Rework Problem 2.8.1 assuming fixed boundary conditions.
- 2.8.4. Determine the moments and shear forces in Problem 2.8.3.
- 2.8.5. Rework Illustrative Example II given in Sec. 2.8 assuming a parabolic load distribution and a fixed boundary.

3

Further Plate Problems and Their Classical Solutions

3.1 Plates on Elastic Foundation

Many problems of considerable practical importance can be related to the solution of plates on an elastic foundation. Reinforced-concrete pavements of highways and airport runways and foundation slabs of buildings, to name a few, are well-known direct applications. Of equal importance, however, is the lesser known indirect application of this type of plate problem to solution of shallow shells. That is, an analogy exists between the governing differential equation of a shallow shell and that of a plate on an elastic foundation.

To simplify the inherently complex problem, let us assume that the supporting medium is isotropic, homogeneous and linearly elastic. Such a type of subbase is called a *Winkler-type foundation* [3.1.1]. The foundation's reaction $p_z^*(x, y)$ can be described by the relationship

$$p_z^*(x, y) = kw, \quad (3.1.1)$$

where k (in pounds per cubic inch or kilonewtons per cubic centimeter) represents the *bedding constant* of the foundation material [3.1.2].

Numerical values for the bedding constants of various types of soils are given in Ref. [3.1.2]. The hypothesis of linear-elastic, isotropic foundation material of soils is only an approximation of the real condition; thus higher accuracy can be obtained by considering the actual elastoplastic deformations of the soils. Since hand computation tends to be too cumbersome [3.1.4], the use of high-speed electronic computers is recommended [3.1.5, 3.1.6].

When the plate is supported by a continuous elastic foundation, the external load acting in the lateral direction consists of the surface load $p_z(x, y)$ and the reaction of the elastic foundation $p_z^*(x, y)$. Thus, the differential equation of the plate

(1.2.30) becomes

$$\frac{\partial^4 w}{\partial x^4} + 2\frac{\partial^4 w}{\partial x^2 \partial y^2} + \frac{\partial^4 w}{\partial y^4} = \frac{1}{D}[p_z(x, y) - p_z^*(x, y)]. \quad (3.1.2)$$

In this differential equation, the reactive force p_z^* exerted by the subbase is also unknown, since it depends on the lateral displacement $w(x, y)$ of the plate. Substituting Eq. (3.1.1) into (3.1.2), the governing differential equation of a plate on an elastic foundation can be written as

$$D \nabla^2 \nabla^2 w + kw = p_z. \quad (3.1.3)$$

Again, Eq. (3.1.3) can be solved only for relatively few combinations of load and boundary conditions by the *classical* methods.

a. Applications of Navier's Solution. If the edges of a plate on an elastic foundation are simply supported, Navier's method (discussed in Sec. 2.2) can be used with relative ease. The unknown amplitudes of the deflections W_{mn} are obtained by substituting the double trigonometric expression of the deflections [Eq. (2.2.2)] and that of the lateral loads [Eq. (2.2.3)] into the governing differential equation of the problem [Eq. (3.1.3)]. Thus, for a specific set of m and n values we obtain

$$W_{mn} = \frac{P_{mn}}{D\pi^4[(m^2/a^2) + (n^2/b^2)]^2 + k}, \quad (3.1.4)$$

which substituted into (2.2.2) yields

$$w(x, y) = \sum_{m=1}^{\infty} \sum_{n=1}^{\infty} \frac{P_{mn} \sin(m\pi x/a) \sin(n\pi y/b)}{D\pi^4[(m^2/a^2) + (n^2/b^2)]^2 + k}. \quad (3.1.5)$$

The Navier-type boundary condition is more common in the case of shallow shells (Fig. 3.1.1) than in actual foundation problems, since the edge beams or diaphragms are usually weak and permit deformations other than those in their plane.

Let us now consider shallow shells. The differential equation of equilibrium of such structures can be written as [7]

$$D \nabla^2 \nabla^2 w = hk_x \frac{\partial^2 \Phi}{\partial y^2} + hk_y \frac{\partial^2 \Phi}{\partial x^2} + p_z, \quad (3.1.6)$$

where $\Phi(x, y)$ is the Airy-type stress function and k_x and k_y represent the curvature in the X and Y directions, respectively. The compatibility equation of the problem has the form [3.1.1]

$$\frac{1}{E} \nabla^2 \nabla^2 \Phi = -k_x \frac{\partial^2 w}{\partial y^2} - k_y \frac{\partial^2 w}{\partial x^2}. \quad (3.1.7)$$

If the curvature in both directions is the same,

$$k_x = k_y = \frac{1}{R}, \quad (3.1.8)$$

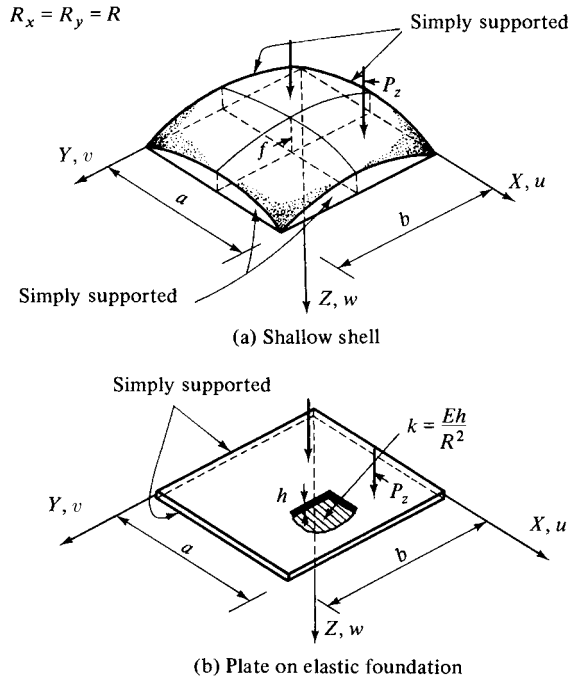


Figure 3.1.1 Analogy between shallow shell and plate on elastic foundation.

then Eq. (3.1.7) becomes

$$\frac{1}{E} \nabla^2 \nabla^2 \Phi + \frac{1}{R} \nabla^2 w = 0. \quad (3.1.9)$$

We can introduce a new scalar function $F(x, y)$ that satisfies the relationships

$$w(x, y) = \nabla^2 \nabla^2 F(x, y), \quad (3.1.10a)$$

$$\Phi(x, y) = -\frac{E}{R} \nabla^2 F(x, y). \quad (3.1.10b)$$

Substituting Eq. (3.1.10) into Eq. (3.1.6), we then obtain

$$D \nabla^2 \nabla^2 \nabla^2 \nabla^2 F + \frac{Eh}{R^2} \nabla^2 \nabla^2 F = p_z. \quad (3.1.11)$$

Or using Eq. (3.1.10a), the differential equation of a shallow shell, which satisfies Eq. (3.1.8), can be written as[†]

$$D \nabla^2 \nabla^2 w + \frac{Eh}{R^2} w = p_z. \quad (3.1.12)$$

[†] Equation (3.1.12) can be utilized for shells in which the rise is not more than one-fifth of the smaller side of the rectangle covered. Strictly speaking, the use of Eq. (3.1.12) should be restricted to the boundary condition $n_x = n_y = 0$ and $w = 0$; for other cases it is merely an approximation. Equation (3.1.15) represents the more exact differential equation of shallow shells.

The introduction of a fictitious bedding constant in the form

$$k = \frac{Eh}{R^2} \quad (3.1.13)$$

makes Eq. (3.1.12) identical to Eq. (3.1.3).

The internal moments m_x , m_y , m_{xy} , m_{yx} and the transverse shear forces q_x and q_y can be computed from the deflection in the same manner as that of the bending of rectangular plates. The in-plane forces n_x , n_y , n_{xy} and n_{yx} can be calculated from the stress function.

By substituting $w(x, y)$, determined from Eq. (3.1.12), into the compatibility equation (3.1.7), the stress function $\Phi(x, y)$ can be calculated either by analytical or by numerical methods. Thus, the membrane forces are

$$n_x = h \frac{\partial^2 \Phi}{\partial y^2}, \quad n_y = h \frac{\partial^2 \Phi}{\partial x^2} \quad \text{and} \quad n_{xy} = n_{yx} = -h \frac{\partial^2 \Phi}{\partial x \partial y}. \quad (3.1.14)$$

Although Marguerre's more exact equation of a rectangular shallow spherical shell [3.1.7, 3.1.8],

$$\nabla^2 \nabla^2 \nabla^2 w + \frac{12(1 - \nu^2)}{R^2 h^2} \nabla^2 w = \frac{\nabla^2 p_z}{D}, \quad (3.1.15)$$

has a different form than the one given above in Eq. (3.1.12), Navier's method can also be used for solution of Marguerre's equation [3.1.9], provided the boundaries are simply supported.

b. Application of Lévy's Solution. If any two opposite edges of the plate on an elastic foundation are simply supported and the shape of the loading is the same for all sections parallel to the direction of the simply supported edges, then Lévy's solution[†] can be applied advantageously.

The general solution of the differential equation of the plate on an elastic foundation (3.1.3) is sought, again, as the sum of a particular solution and the solution of the homogeneous form of Eq. (3.1.3). Thus, we have

$$w = w_p + w_H. \quad (3.1.16)$$

One particular solution is obtained from the application of Navier's method to the differential equation of a plate strip on an elastic foundation (Fig. 3.1.2), which is [3.1.2]

$$D \frac{d^4 w}{dx^4} + kw = p_z(x). \quad (3.1.17)$$

By expressing the load p_z in a single trigonometric series containing sine terms only [Eq. (2.3.5)] and by seeking the solution of Eq. (3.1.17) in a similar type of

[†] See Sec. 2.3.

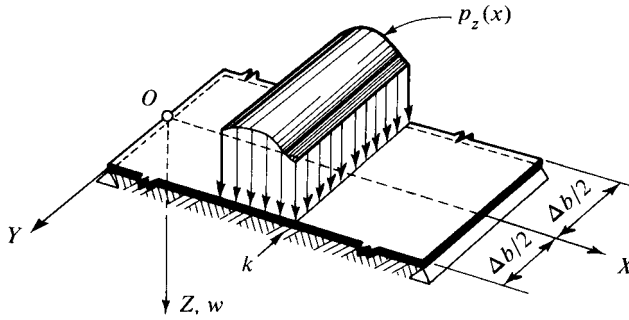


Figure 3.1.2 Elastically supported plate strip.

trigonometric series, we obtain

$$w_P(x) = \frac{1}{D} \sum_{m=1}^{\infty} \frac{P_m \sin(m\pi x/a)}{(m^4\pi^4/a^4) + (k/D)} \quad \text{for } m = 1, 3, 5, \dots \quad (3.1.18)$$

In this solution, we have assumed that the simple supports are at $x = 0$ and $x = a$. The solution of the homogeneous form of Eq. (3.1.3),

$$D \nabla^2 \nabla^2 w + kw = 0, \quad (3.1.19)$$

is sought, again, with the help of Eq. (2.3.9); thus we have

$$w_H = \sum_{m=1}^{\infty} Y_m(y) \sin \frac{m\pi x}{a} \quad \text{for } m = 1, 3, 5, \dots, \quad (3.1.20)$$

where $Y_m(y)$ is a function of a single argument that has to satisfy the *characteristic* equation of (3.1.19). This ordinary differential equation can be written as

$$Y_m^{\text{IV}}(y) - \frac{2m^2\pi^2}{a^2} Y_m''(y) + \left(\frac{m^4\pi^4}{a^4} + \frac{k}{D} \right) Y_m(y) = 0. \quad (3.1.21)$$

The solution of Eq. (3.1.21) has the general form

$$Y_m(y) = e^{C_y}. \quad (3.1.22)$$

Timoshenko [2] gives Eq. (3.1.22) in the form

$$Y_m(y) = A_m e^{\beta_m y} \cos \gamma_m y + B_m e^{-\beta_m y} \cos \gamma_m y + C_m e^{\beta_m y} \sin \gamma_m y + D_m e^{-\beta_m y} \sin \gamma_m y, \quad (3.1.23)$$

where

$$\beta_m = \sqrt{\frac{1}{2} \left(\sqrt{\mu_m^4 + \lambda^4} + \mu_m^2 \right)} \quad (3.1.24)$$

and

$$\gamma_m = \sqrt{\frac{1}{2} \left(\sqrt{\mu_m^4 + \lambda^4} - \mu_m^2 \right)}. \quad (3.1.25)$$

In these equation μ_m and λ represent

$$\mu_m = \frac{m\pi}{a} \quad \text{and} \quad \lambda^4 = \frac{k}{D}, \quad (3.1.26)$$

respectively. The arbitrary constants A_m , B_m , C_m and D_m are calculated from the boundary conditions.

Lévy's solution can also be applied to the problem, shown in Fig. 3.1.3, if we replace the previously discussed particular solution by

$$w_p = \frac{4kw_0}{D\pi} \sum_{m=1,3,5,\dots}^{\infty} \frac{\sin(m\pi x/a)}{m[(m^4\pi^4/a^2) + (k/D)]}, \quad (3.1.27)$$

which represents the deflection of a simply supported plate strip on an elastic foundation. The deflection of the edges, w_0 , is obtained from the assumption that a rigid body is supported on an elastic foundation, in which case the deflection is

$$w_0 = \frac{\sum p_z}{abk}. \quad (3.1.28)$$

The solution of the homogeneous equation, w_H , is identical to the one discussed above.

Doganoff [3.1.9] gives solutions of Marguerre's equation (3.1.15) in a manner basically similar to the one discussed above.

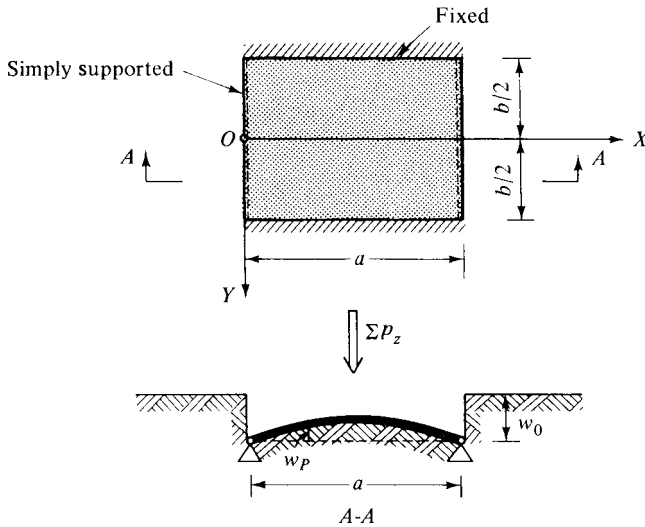


Figure 3.1.3 Foundation plate.

c. *Other Solutions.* Volterra [3.1.10] has obtained a solution of a more general nature by applying a Fourier transformation. Westergaard has investigated the behaviors of concrete road pavements [3.1.11] and those of airport runways [3.1.12]. Schleicher [3.1.13] has solved the problem of circular plates on an elastic foundation by using Bessel functions. Hampe [15] made Schleicher's solution more accessible for practical use by providing extensive tables. All these solutions are mathematically quite involved; consequently, they are beyond the introductory scope of this book.

d. *Other Than Winkler-Type Foundations.* We can consider the Winkler foundation as a series of uncorrelated linear springs that can be subjected to either tension or compression. This assumption is valid for most cases, since cavities between the plate and subgrade due to lateral loadings seldom occur. There are, however, some foundation materials that admit only compressive stresses. For such a foundation, combined with certain types of loadings and plate flexibility, the admission of tensile stresses across the common interface separating the plate from the foundation is *not realistic*. Within the no-contact region the plate lifts up away from the foundation and gaps are created between the plate and the subgrade (Fig. 3.1.4). The task is to determine the conditions under which no-contact regions will form and to compute their locations and extent. The exact solution of such a problem is very difficult and involves intricate dual integral equations [3.1.17]. The mathematical complexity of this problem can be simplified—to some extent—for a concentrated load of magnitude P by introducing a dimensionless ratio $P\beta/q$, where q is the uniform distributed weight of the plate and β represents a characteristic number

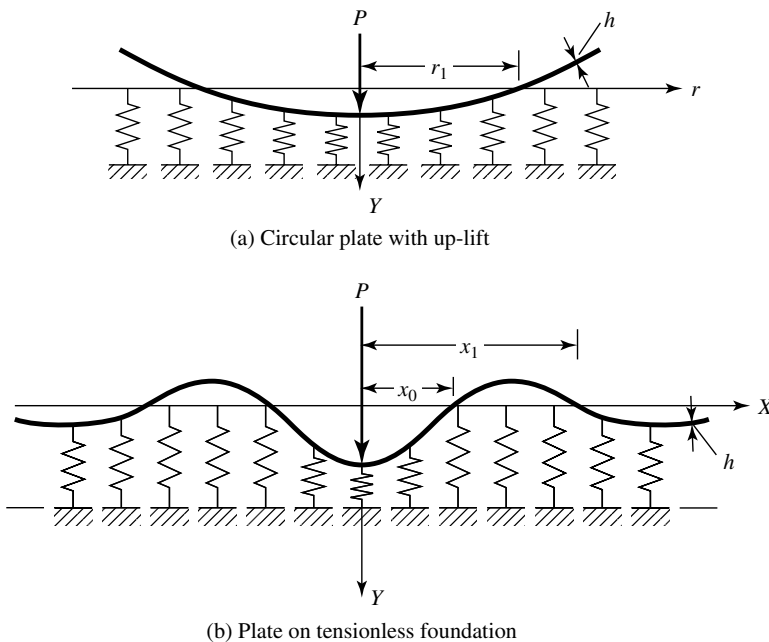


Figure 3.1.4 Plates on foundation that reacts in compression only.

that depends on the mechanical properties of the plate and the tensionless foundation ($\beta^4 = k/4D$). This ratio specifies the extent of the no-contact region under the concentrated force [3.1.18].

For plates with constant thickness under a point load, the range of validity of the Winkler-type foundation can be given by

$$-8 \leq \frac{P}{q\ell^2} \leq 5610,$$

where $\ell^4 = D/k$.

Instead of using the above-described “exact” solution of this difficult problem, one can apply a simple iterative approach that can be employed to establish the location and extent of the no-contact zones with relative ease. In the first step, we determine where the lateral deflections are negative using either the finite difference or finite-element method [3.1.19]. In the second step of computation, this region will not obtain the foundation support whereas the rest of it does. The extent of the no-contact zone can be further refined by repeating the second step.

The Reissner model [3.1.24] is more general than the Winkler-type foundation and, consequently, is more difficult to handle. This model incorporates shear stresses and includes some of the effects of lateral deflections within the foundation. The fundamental assumption made by Reissner is that the normal stresses σ_x and σ_y vanish within the foundation. For additional details the reader should consult Ref. [3.2.25].

ILLUSTRATIVE EXAMPLE I

Let us determine the equation of the lateral deflections of a simply supported plate on a Winkler foundation subjected to a concentrated force, as shown in Fig. 3.1.5.

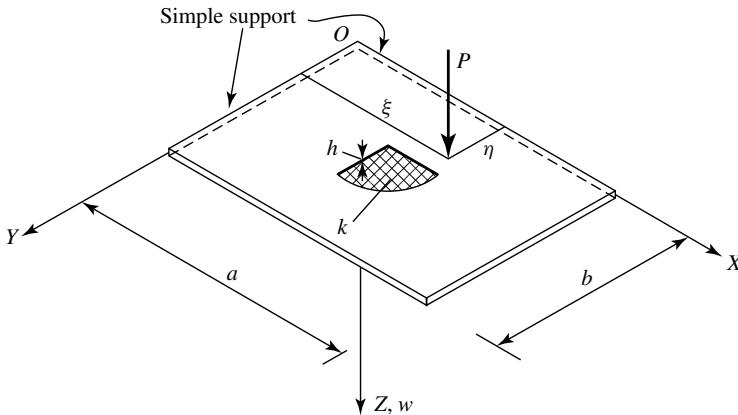


Figure 3.1.5 Simply supported plate on elastic foundation.

The boundary conditions of the plate permit the use of Navier’s method. Thus, following the corresponding standard procedure described in Sec. 2.2,

first, we express the lateral load by a double Fourier series. Hence

$$p_z(x, y) = \sum_m \sum_n P_{mn} \sin \frac{m\pi x}{a} \sin \frac{n\pi y}{b}, \quad (3.1.29)$$

where[†]

$$P_{mn} = \frac{4P}{ab} \sin \frac{m\pi \xi}{a} \sin \frac{n\pi \eta}{b} \quad \text{for } m, n = 1, 2, 3, \dots \quad (3.1.30)$$

Utilizing Eq. (3.1.4), we obtain

$$W_{mn} = \frac{(4P/ab) \sin(m\pi \xi/a) \sin(n\pi \eta/b)}{D\pi^4[(m^2/a^2) + (n^2/b^2)]^2 + k}, \quad (3.1.31)$$

which substituted into the double Fourier series expression of the deflections given by Eq. (2.2.2) gives

$$w(x, y) = \sum_m \sum_n \frac{(4P/ab) \sin(m\pi \xi/a) \sin(n\pi \eta/b)}{D\pi^4[(m^2/a^2) + (n^2/b^2)]^2 + k} \sin \frac{m\pi x}{a} \sin \frac{n\pi y}{b} \quad \text{for } m, n = 1, 2, 3, \dots \quad (3.1.32)$$

ILLUSTRATIVE EXAMPLE II

A rectangular shallow spherical shell is subjected to a uniformly distributed lateral load, as shown in Fig. 3.1.6. Find the lateral deflections of the shell.

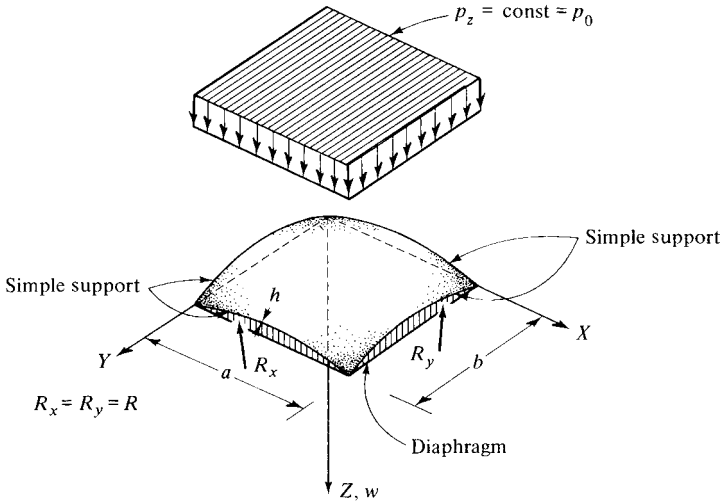


Figure 3.1.6 Uniformly loaded shallow shell.

[†] See Eq. (2.4.37).

The governing differential equation of the problem is Eq. (3.1.12), and the bedding constant of the plate is given by Eq. (3.1.13). The double Fourier series expression of the load [Eq. (2.2.9)] yields

$$p_z(x, y) = \frac{16p_0}{\pi^2} \sum_m \sum_n \frac{1}{mn} \sin \frac{m\pi x}{a} \sin \frac{n\pi y}{b} \quad \text{for } m, n = 1, 3, 5, \dots \quad (3.1.33)$$

We express the plate deflections in a similar form:

$$w(x, y) = \sum_m \sum_n W_{mn} \sin \frac{m\pi x}{a} \sin \frac{n\pi y}{b} \quad \text{for } m, n = 1, 3, 5, \dots \quad (3.1.34)$$

The substitution of Eqs. (3.1.33) and (3.1.34) into (3.1.12) yields, for a set of specific m, n values, the amplitudes of the double Fourier series expression of the deflections:

$$W_{mn} = \frac{16p_0}{\pi^2} \frac{1}{mn \{D[(m\pi/a)^2 + (n\pi/b)^2]^2 + (Eh/R^2)\}}. \quad (3.1.35)$$

Thus, the lateral deflection of the shallow spherical shell can be written as

$$w(x, y) = \frac{16p_0}{\pi^2} \sum_m \sum_n \frac{\sin(m\pi x/a) \sin(n\pi y/b)}{mn \{\pi^4 D[(m^2/a^2) + (n^2/b^2)]^2 + (Eh/R^2)\}} \quad \text{for } m, n = 1, 3, 5, \dots \quad (3.1.36)$$

References and Bibliography

- [3.1.1] VLASOV, V. Z., *General Theory of Shells and Its Applications in Engineering* (translation of *Obshchaya teoriya obolochek i yeye prilozheniya v tekhnike*), NASA TT F-99, National Aeronautics and Space Administration, Washington, D.C., 1964.
- [3.1.2] HETÉNYI, M., *Beams on Elastic Foundation*, University of Michigan Press, Ann Arbor, Michigan, 1961.
- [3.1.3] *Symposium on Load Tests of Bearing Capacity of Soil, June 1947*, ASTM Special Technical Publication No. 79, Philadelphia, 1948.
- [3.1.4] VLASOV, V. Z., and LEONTEV, N. N., *Beams, Plates and Shells on Elastic Foundation* (translation of *Balki, plity, i oblochki na uprugom osnavanii*), NASA TT F-357, National Aeronautics and Space Administration, Washington, D.C., 1966.
- [3.1.5] HUANG, Y. H., "Finite Element Analysis of Nonlinear Soil Media," in *Proceedings of the Symposium on Application of Finite-Element Method in Civil Engineering* (held at Nashville, Tenn., Nov. 13–14, 1969) (W. H. Rowan and R. M. Hackett, eds.), School of Engineering, Vanderbilt University, Nashville, 1969, pp. 663–690.
- [3.1.6] HWANG, C. T., HO, M. K., and WILSON, N. E., "Finite Element in Analysis of Soil Deformations," in *Proceedings of the Symposium on Application of Finite-Element Method in Civil Engineering* (held at Nashville, Tenn., Nov. 13–14, 1969) (W. H. Rowan and R. M. Hackett, eds.), School of Engineering, Vanderbilt University, Nashville, 1969, pp. 729–746.
- [3.1.7] MARGUERRE, K., "Zur Theorie der gekrümmten Platte grosser Formänderung," in *Proceedings 5th International Congress of Applied Mechanics*, held in Cambridge, Mass., 1938, John Wiley & Sons, New York, 1939, pp. 93–101.
- [3.1.8] MARGUERRE, K., *Neue Festigkeitsprobleme des Ingenieurs*, Springer-Verlag, Berlin, 1950.

- [3.1.9] DOGANOFF, I., *Berechnung von Kugelschalen über rechteckigem Grundriss*, Werner-Verlag, Düsseldorf, 1962.
- [3.1.10] VOLTERRA, E., "Sul problema generale della piastra poggiata su suolo elastico," *R. C. Accad. Lincei*, 2 (May 1947), 596–598.
- [3.1.11] WESTERGAARD, H. M., "Stresses in Concrete Pavements Computed by Theoretical Analysis," *Public Roads*, 7 (April 1926), 25–35.
- [3.1.12] WESTERGAARD, H. M., "New Formulas for Stresses in Concrete Pavements for Airfields," *Proc. ASCE*, 73 (May 1947), 687–701.
- [3.1.13] SCHLEICHER, F., *Kreisplatten auf elastischer Unterlage*, Springer-Verlag, Berlin, 1926.
- [3.1.14] GORLOV, A. M., *Avtamatizirovannyi raschet priamougol'nykh plit na uprugom osvannii (Automated Design of Rectangular Plates on Elastic Foundation)*, Sroizdat, Moscow, 1968.
- [3.1.15] KORENEV, B. G., *Raschet plit na uprugom osvannii (Design of Plates on Elastic Foundation)*, Gos. izd-vo lit-ry po stroitel'stvu, arkhitekture i stroit. materialam, Moscow, 1962.
- [3.1.16] PALATNIKOV, E. A., *Priamougol'naia plita na uprugom osvannii (Rectangular Plates on Elastic Foundation)*, Izd-vo lit-ry po stroitel'stvu, Moscow, 1964.
- [3.1.17] HUSSIAN, M. A., et al., "Cavitation at the Ends of an Elliptic Inclusion Inside a Plate Under Tension," *J. Appl. Mech.*, 35 (1968), 505–509.
- [3.1.18] WEITSMAN, Y., "On Foundations That React in Compression Only," *J. Appl. Mech.*, 37 (1970), 1019–1030.
- [3.1.19] CHILTON, D. S., and WEKEZER, J. W., "Plates on Elastic Foundation," *J. Struct. Div., ASCE*, 116 (1990), 3236–3241.
- [3.1.20] WOINOWSKY-KRIEGER, S., "Berechnung einer auf elastischem Halbraum aufliegenden, unendlich erstreckten Platte," *Ing.-Arch.*, 17 (1949), 142–148.
- [3.1.21] HAHN, J., *Durchlaufträger, Rahmen, Platten und Balken auf elastischer Bettung*, 11th ed., Werner-Verlag, Düsseldorf, 1971.
- [3.1.22] SHERIF, G., and KÖNIG, G., *Platten und Balken auf nachgiebigem Baugrund*, Springer-Verlag, Berlin, 1975.
- [3.1.23] RAUHAUS, D., "Tabellen zur Berechnung der Kreisplatte auf elastischer Unterlage," *Bauingenieur*, 52 (1977), 387–392.
- [3.1.24] REISSNER, E., "A Note on Deflections of Plates on a Viscoelastic Foundation," *J. Appl. Mech.*, 25 (1958), 144–145.

3.2 Plates with Variable Flexural Rigidity

a. Rectangular Plates. We assume that the middle surface of the plate is plane and coincides with the XY plane of our Cartesian coordinate system (Fig. 3.2.1). The differential equation for the bending of the plate of variable flexural rigidity $D(x, y)$ is obtained by substituting the expressions of moments given by Eqs. (1.2.26), (1.2.27) and (1.2.29) into the equilibrium equation (1.2.9). Since the flexural rigidity of the plate is now a function of x and y , we obtain

$$\begin{aligned} \frac{\partial^2}{\partial x^2} \left[D \left(\frac{\partial^2 w}{\partial x^2} + \nu \frac{\partial^2 w}{\partial y^2} \right) \right] + 2(1 - \nu) \frac{\partial^2}{\partial x \partial y} \left[D \frac{\partial^2 w}{\partial x \partial y} \right] \\ + \frac{\partial^2}{\partial y^2} \left[D \left(\frac{\partial^2 w}{\partial y^2} + \nu \frac{\partial^2 w}{\partial x^2} \right) \right] = p_z, \end{aligned} \quad (3.2.1)$$

which may be written in the form

$$\boxed{\nabla^2(D \nabla^2 w) - (1 - \nu) \mathcal{L}(D, w) = p_z,} \quad (3.2.2)$$

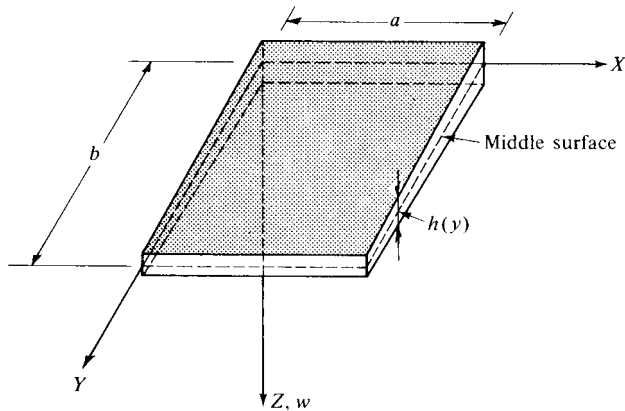


Figure 3.2.1 Rectangular plate with variable thickness.

where $\mathcal{L}(D, w)$ is defined by

$$\mathcal{L}(D, w) = \frac{\partial^2 D}{\partial x^2} \frac{\partial^2 w}{\partial y^2} - 2 \frac{\partial^2 D}{\partial x \partial y} \frac{\partial^2 w}{\partial x \partial y} + \frac{\partial^2 D}{\partial y^2} \frac{\partial^2 w}{\partial x^2}. \quad (3.2.3)$$

Only a limited number of cases [3.2.1, 3.2.2] permit the solution of Eq. (3.2.2) by the classical methods. Provided that the boundary conditions admit the Lévy-type solution,[†] its rectangular plates with variable rigidity yields good accuracy [3.2.2]. The degree of complexity of the analysis, however, depends considerably on the mathematical expressions describing the variation of thickness and flexural rigidity, respectively.

b. Circular Plates. We limit ourselves to rotational symmetric loading and geometry, since this is the type most widely encountered in civil and mechanical engineering. Without this rotational symmetry the classical solutions are quite involved and restricted [3.2.1]. Due to the symmetry, q_ϕ , $m_{\phi r}$ and $m_{r\phi}$ (Fig. 1.4.1b) vanish, and only the internal forces shown in Fig. 3.2.2 act on the plate element.

The sum of the moments of all forces about the Y' axis gives

$$\left(m_r + \frac{dm_r}{dr} dr \right) (r + dr) d\phi - m_r r d\phi - q_r r d\phi dr - m_\phi dr d\phi = 0. \quad (3.2.4)$$

The last term on the left-hand side of Eq. (3.2.4) is due to the resultant moment, shown in Fig. 3.2.2b. After neglecting small quantities of higher-order, Eq. (3.2.4) becomes

$$m_r + \frac{dm_r}{dr} r - m_\phi - q_r r = 0, \quad (3.2.5)$$

or, in a more concise form,

$$m_\phi - \frac{d(m_r r)}{dr} = -q_r r. \quad (3.2.6)$$

[†] See Sec. 2.3.

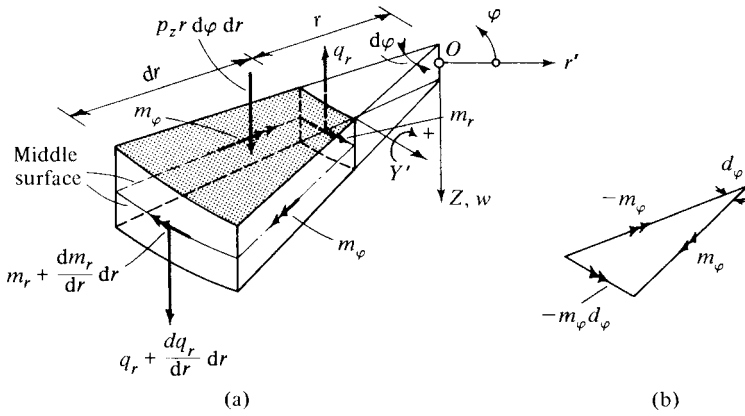


Figure 3.2.2 Plate element.

By introducing the slope of the deflection surface,

$$\vartheta = -\frac{dw}{dr}, \quad (3.2.7)$$

the expressions of the internal moments given in Eqs. (2.8.3) and (2.8.4) become

$$m_r = D(r) \left[\frac{d\vartheta}{dr} + \nu \frac{\vartheta}{r} \right] \quad (3.2.8)$$

and

$$m_\varphi = D(r) \left[\frac{\vartheta}{r} + \nu \frac{d\vartheta}{dr} \right]. \quad (3.2.9)$$

The substitution of these expressions into Eq. (3.2.6) gives

$$D(r) \frac{d}{dr} \left[\frac{d\vartheta}{dr} + \frac{\vartheta}{r} \right] + \frac{dD(r)}{dr} \left[\frac{d\vartheta}{dr} + \nu \frac{\vartheta}{r} \right] = q_r, \quad (3.2.10)$$

or

$$\frac{d^2\vartheta}{dr^2} + \left[\frac{1}{r} + \frac{1}{D(r)} \frac{dD(r)}{dr} \right] \frac{d\vartheta}{dr} + \left[\frac{\nu}{D(r)} \frac{dD(r)}{dr} - \frac{1}{r} \right] \frac{\vartheta}{r} = \frac{q_r}{D(r)}. \quad (3.2.11)$$

The transverse shear can be obtained by the free-body equilibrium (Fig. 3.2.3):

$$q_r = -\frac{1}{2\pi r} \int_0^r p_z(r) \cdot 2\pi r dr = -\frac{1}{r} \int_0^r p_z(r) r dr. \quad (3.2.12)$$

In designing machine parts, circular plates with linearly varying thicknesses are of considerable practical interest. Consequently, let us first consider the case when the thickness of the plate linearly increases with the radius (Fig. 3.2.4a):

$$h = cr. \quad (3.2.13)$$

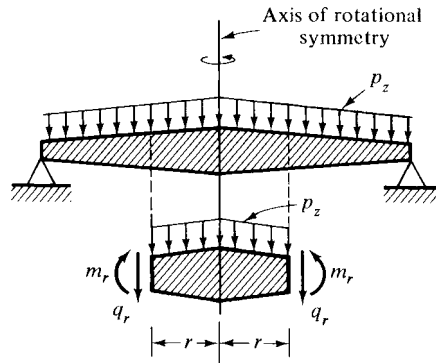
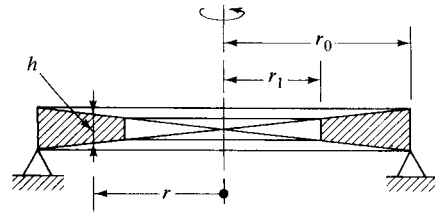
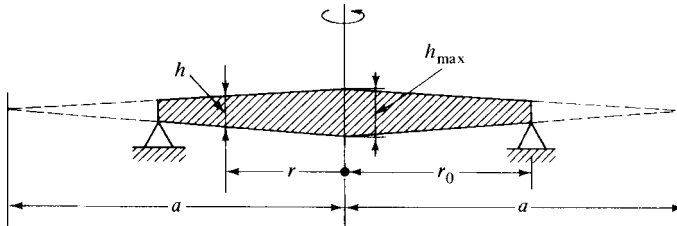


Figure 3.2.3 Determination of transverse shear force.



(a) Case 1



(b) Case 2

Figure 3.2.4 Circular plates with linearly varying thickness.

The flexural rigidity [Eq. (1.2.28)] of the plate becomes

$$D(r) = \frac{Ec^3 r^3}{12(1 - \nu^2)}; \quad (3.2.14)$$

hence

$$\frac{dD(r)}{dr} = \frac{Ec^3 r^2}{4(1 - \nu^2)} \quad \text{and} \quad \frac{1}{D} \frac{dD}{dr} = \frac{3}{r}. \quad (3.2.15)$$

Substituting these values into Eq. (3.2.11), we obtain

$$r^3 \frac{d^2 \vartheta}{dr^2} + 4r^2 \frac{d\vartheta}{dr} - (1 - 3\nu)r\vartheta = \frac{12q_r(1 - \nu^2)}{Ec^3}. \quad (3.2.16)$$

By introducing $\rho = r/r_0$, Eq. (3.2.16) becomes

$$\rho^3 \frac{d^2 \vartheta}{d\rho^2} + 4\rho^2 \frac{d\vartheta}{d\rho} - (1 - 3\nu)\rho\vartheta = \frac{12q_r(1 - \nu^2)}{Ec^3r_0}. \quad (3.2.17)$$

The general solution of this differential equation is sought in two parts:

$$\vartheta = \vartheta_H + \vartheta_P, \quad (3.2.18)$$

where ϑ_H is the solution of the homogeneous form of Eq. (3.2.17) and ϑ_P is a particular solution of (3.2.17), containing the external load [Eq. (3.2.12)]. The solution of the homogeneous differential equation is

$$\vartheta_H = A\rho^{c_1} + B\rho^{c_2}; \quad (3.2.19)$$

where $c_{1,2} = [-3 \pm \sqrt{9 - 4(3\nu - 1)}]/2$ and A and B represent arbitrary constants that can be determined from the boundary conditions of the plate.

The second case of considerable practical interest is illustrated in Fig. 3.2.4b. The maximum thickness of the plate is at the center and is linearly diminishing as the radius r is increasing. Thus, the variation of the thickness of the plate can be written as

$$h = h_{\max} \left(1 - \frac{r}{a}\right), \quad (3.2.20)$$

where a is the altitude of the triangle representing the variation of the thickness, as shown in Fig. 3.2.4b. By introducing $\rho = r/a$, the governing differential equation of the problem (3.2.11) becomes

$$\frac{d^2 \vartheta}{d\rho^2} + \left[\frac{1}{\rho} + \frac{1}{D(\rho)} \frac{dD(\rho)}{d\rho} \right] \frac{d\vartheta}{d\rho} + \left[\frac{\nu}{D(\rho)} \frac{dD(\rho)}{d\rho} - \frac{1}{\rho} \right] \frac{\vartheta}{\rho} = \frac{q_r a^2}{D(\rho)}. \quad (3.2.21)$$

The variation of the flexural rigidity of the plate can be written as

$$D(\rho) = D_{\max}(1 - \rho)^3, \quad (3.2.22)$$

where

$$D_{\max} = \frac{Eh_{\max}^3}{12(1 - \nu^2)}. \quad (3.2.23)$$

Using Eq. (3.2.22) and assuming that $\nu = \frac{1}{3}$, Eq. (3.2.21) becomes

$$\rho^2(1 - \rho)^3 \frac{d^2 \vartheta}{d\rho^2} + \rho(1 - 4\rho)(1 - \rho)^2 \frac{d\vartheta}{d\rho} - (1 - \rho)^2 \vartheta = \frac{q_r a^2 \rho^2}{D_{\max}}. \quad (3.2.24)$$

The solution of the homogeneous form of Eq. (3.2.24) is

$$\vartheta_H = A \left(\frac{1 + 2\rho}{\rho} \right) + B \left[\frac{3\rho - 2\rho^2}{(1 - \rho)^2} \right], \quad (3.2.25)$$

where A and B represent arbitrary constants to be determined from the boundary conditions of the plate. To obtain the general solution of the differential equation of the problem (3.2.24), we must, again, combine ϑ_H with a particular solution ϑ_P of Eq. (3.2.24).

Summary. Variable flexural rigidity creates numerous mathematical problems. The complexity of the exact solution depends considerably on the expressions for the flexural rigidity and that of the applied loading. With the exception of rotationally symmetric circular plates, problems related to plates with variable flexural rigidity seldom can be solved by the classical methods. Consequently, the solutions are usually obtained via approximate and numerical techniques described in Part II.

ILLUSTRATIVE EXAMPLE

Determine the moments m_r and m_φ in a circular plate, shown in Fig. 3.2.5, assuming that the variation of the plate thickness $h = cr$ and that Poisson's ratio $\nu = \frac{1}{3}$.

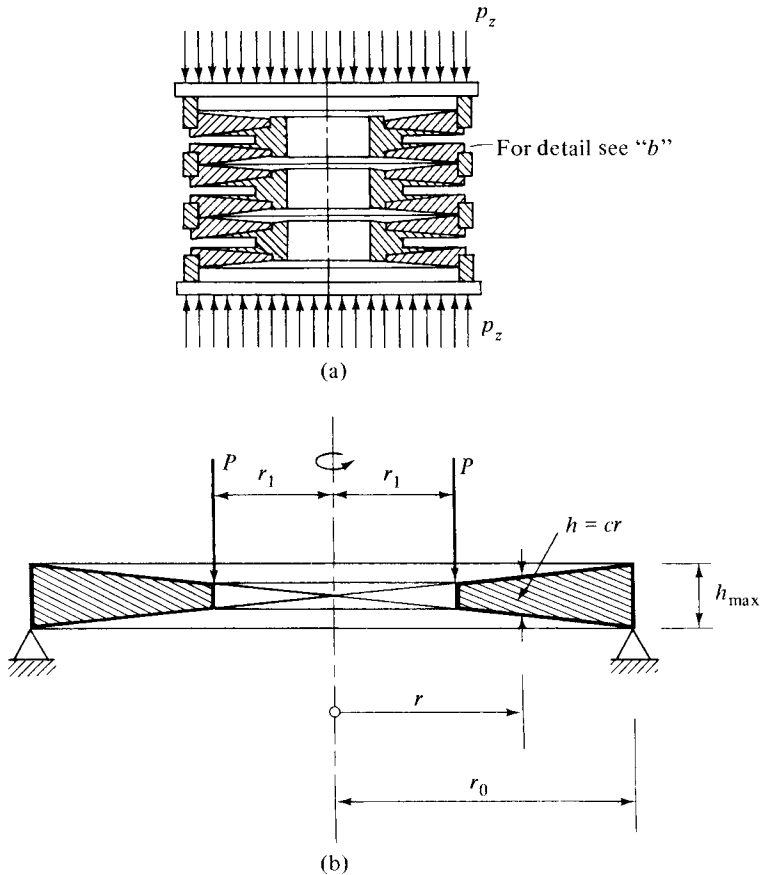


Figure 3.2.5 Spring made of assemblage of plates.

The transverse shear is obtained from Eq. (3.2.12); thus

$$q_r = -\frac{P}{2\pi r}. \quad (3.2.26)$$

Consequently, the differential equation of problem (3.2.17) becomes

$$\rho^4 \frac{d^2 \vartheta}{d\rho^2} + 4\rho^3 \frac{d\vartheta}{d\rho} - (1 - 3\nu)\rho^2 \vartheta = -\frac{6P(1 - \nu^2)}{\pi Ec^3 r_0^2}. \quad (3.2.27)$$

Using $\nu = \frac{1}{3}$, Eq. (3.2.27) can be considerably simplified:

$$\rho^4 \frac{d^2 \vartheta}{d\rho^2} + 4\rho^3 \frac{d\vartheta}{d\rho} = -\frac{16P}{3\pi Ec^3 r_0^2}. \quad (3.2.28)$$

The solution of the homogeneous form of Eq. (3.2.28) is obtained from Eq. (3.2.19); thus

$$\vartheta_H = A + \frac{B}{\rho^3}. \quad (3.2.29)$$

A particular solution of Eq. (3.2.28) is

$$\vartheta_P = -\frac{8}{3} \frac{P}{\pi Ec^3 r_0^2 \rho^2}. \quad (3.2.30)$$

Hence, the general solution of the differential equation of problem (3.2.28) becomes

$$\vartheta = \vartheta_H + \vartheta_P = A + \frac{B}{\rho^3} - \frac{8P}{3\pi Ec^3 r_0^2 \rho^2}. \quad (3.2.31)$$

The boundary conditions of the problem are

$$\begin{aligned} \text{at } r = r_1 : \quad \rho = \frac{r_1}{r_0} = n \quad \text{and} \quad m_r = 0; \\ \text{at } r = r_0 : \quad \rho = 1 \quad \text{and} \quad m_r = 0. \end{aligned} \quad (3.2.32)$$

Substituting Eq. (3.2.31) into Eq. (3.2.8), these boundary conditions yield

$$A = -\frac{40}{3} \frac{P}{\pi Ec^3 r_0^2} \frac{1 - n}{1 - n^3} \quad (3.2.33)$$

and

$$B = \frac{5}{3} \frac{P}{\pi Ec^3 r_0^2} \frac{n(1 - n^2)}{1 - n^3}. \quad (3.2.34)$$

Hence

$$\vartheta = -\frac{8P}{3\pi E c^3 r_0^2} \left[\frac{5(1-n^2)n}{8(1-n^3)\rho^3} - \frac{1}{\rho^2} - \frac{5(1-n)}{1-n^3} \right]. \quad (3.2.35)$$

The bending moments are obtained by substituting (3.2.35) into (3.2.8) and (3.2.9), respectively. Thus

$$m_r = \frac{5P}{12\pi} \left[\frac{(1-n^2)n}{(1-n^3)\rho} - 1 + \frac{(1-n)\rho^2}{1-n^3} \right] \quad (3.2.36)$$

and

$$m_\varphi = \frac{P}{4\pi} \left[\frac{5(1-n)\rho^2}{1-n^3} + \frac{1}{3} \right]. \quad (3.2.37)$$

References and Bibliography

- [3.2.1] MANSFIELD, E. H., "On the Analysis of Elastic Plates of Variable Thickness," *Q. J. Appl. Mech. Appl. Math.*, 15 (1962), 167–192.
- [3.2.2] CONWAY, H. D., "A Lévy-type Solution for a Rectangular Plate of Variable Thickness," *J. Appl. Mech.*, 25 (June 1958), 297–298.
- [3.2.3] FUNG, Y. C., "Bending of Thin Elastic Plates of Variable Thickness," *J. Aeronaut. Sci.*, 20 (1953), 455–468.
- [3.2.4] CONWAY, H. D., "Note on the Bending of Circular Plates of Variable Thickness," *J. Appl. Mech.*, 16 (June 1949), 209–210.
- [3.2.5] FAVRE, H., "Sur un type de plaque circulaire encastree d'épaisseur linéairement variable," *Bull. Tech. Suisse Romande* (Aug. 1949, Dec. 1949).
- [3.2.6] PICHLER, O., *Die Biegung Kreissymmetrischer Platten von veränderlicher Dicke*, Springer-Verlag, Berlin, 1928.
- [3.2.7] CONWAY, H. D., "Closed Form Solutions for Plates of Variable Thickness," *J. Appl. Mech.*, 20 (Dec. 1953), 564–565.
- [3.2.8] CONWAY, H. D., "Axially Symmetrical Plates with Linearly Varying Thickness," *J. Appl. Mech.*, 18, No. 2 (1951), 140–142.
- [3.2.9] CONWAY, H. D., "The Bending of Symmetrically Loaded Circular Plates with Variable Thickness," *J. Appl. Mech.*, 15 (March 1948), 1–6.
- [3.2.10] OLSSON, R. G., "Biegung kreisförmiger Platten von radial veränderlicher Dicke," *Ing.-Arch.*, 8 (1937), 81–98.
- [3.2.11] WORCH, G., "Die Biegung elastischer kreissymmetrischer Platten von veränderlicher Dicke," *Beton und Eisen*, 41 (1942), 34.
- [3.2.12] CRAEMER, H., "Die Beanspruchung von Kreisplatten mit nach dem Rande abnehmender Stärke bei Belastung durch Einzellast und gleichmässig verteiltem Gegendruck (Säulenfundament)," *Beton und Eisen*, 27 (1928), 382.
- [3.2.13] KOVALENKO, A. D., *Kruglye plastiny peremennoi tolshchiny (Circular Plates of Variable Thickness)*, Gos. izd-vo fizikomatematicheskoi lit-ry, Moscow, 1959.
- [3.2.14] FAVRE, H., and GILQ, B., "La plaque rectangulaire flechie d'épaisseur linéairement variable," *Z. Angew. Math. Mech.*, 3 (1952), 354.
- [3.2.15] FERTIS, D. G., and MIJATOV, M. M., "Equivalent Systems for Variable Thickness Plates," *J. Eng. Mech. Div., ASCE*, 115 (1989), 2287–2300.
- [3.2.16] FERTIS, D. G., and LEE, C. T., "Elastic and Inelastic Analysis of Variable Thickness Plates Using Equivalent Systems," *Mech. Struct. Mach.*, 21 (1993), 201–236.
- [3.2.17] LO, W. K., and LEE, L. T., "Equivalent Systems for Variable Thickness Circular Plates," *Comp. Struct.*, 58 (1996), 957–971.

3.3 Simultaneous Bending and Stretching

The derivation of the governing differential equation of the plate, discussed in Sec. 1.2, is based on the assumption that no in-plane forces act on the middle surface of the plate. Occasionally, however, in-plane forces are applied directly at the boundaries or they arise due to temperature variations.[†] Furthermore, in-plane forces can occur when the displacements of the plate parallel to its middle surface are hindered by the supports. This latter type of stretching of the middle surface is generally of a negligible order of magnitude, provided that the lateral deflections are small.

Let us now consider the equilibrium of a $dx\,dy$ element, shown in Fig. 3.3.1, that is subjected to in-plane (membrane) forces n_x , n_y and $n_{xy} = n_{yx}$ per unit length. The increments of these internal forces, acting on the *near sides* of the element, are expressed by the first terms of Taylor's expansion.[‡] Since there are no "body forces," the projection of the membrane forces on the X axis gives[§]

$$\left(n_x + \frac{\partial n_x}{\partial x} dx\right) dy - n_x dy + \left(n_{yx} + \frac{\partial n_{yx}}{\partial y} dy\right) dx - n_{yx} dx = 0, \quad (3.3.1)$$

which after simplification becomes

$$\frac{\partial n_x}{\partial x} + \frac{\partial n_{yx}}{\partial y} = 0. \quad (3.3.2)$$

Similarly, the projection of the in-plane forces on the Y axis gives

$$\frac{\partial n_{xy}}{\partial x} + \frac{\partial n_y}{\partial y} = 0. \quad (3.3.3)$$

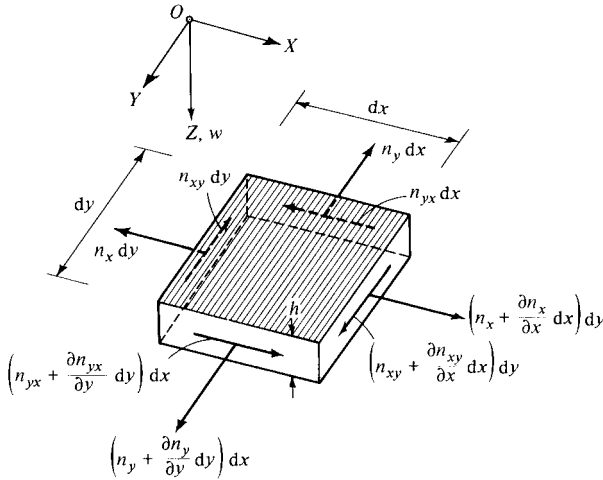


Figure 3.3.1 Membrane forces on plate element.

[†] See Sec. 10.4.

[‡] See Sec. 1.2.

[§] In the summation of forces in the X and Y directions we can neglect the effects of small angles produced by the deformation.

or, using Airy's stress function $\Phi(x, y)$, we can write

$$\frac{D}{h} \nabla^2 \nabla^2 w = \frac{p_z}{h} + \frac{\partial^2 \Phi}{\partial y^2} \frac{\partial^2 w}{\partial x^2} + \frac{\partial^2 \Phi}{\partial x^2} \frac{\partial^2 w}{\partial y^2} - 2 \frac{\partial^2 \Phi}{\partial x \partial y} \frac{\partial^2 w}{\partial x \partial y}. \quad (3.3.7a)$$

If the plate has a small initial curvature w_0 , then Eq. (3.3.7) becomes

$$D \nabla^2 \nabla^2 w = p_z + n_x \frac{\partial^2 (w_0 + w)}{\partial x^2} + n_y \frac{\partial^2 (w_0 + w)}{\partial y^2} + 2n_{xy} \frac{\partial^2 (w_0 + w)}{\partial x \partial y}, \quad (3.3.8)$$

which is basically the same as the differential equation of equilibrium of a shallow shell [3.1.1].

If the *in-plane forces are not known*, the solution of Eq. (3.3.7) can be obtained only when an additional differential equation, which expresses the relationship between lateral displacement w and Airy's stress function Φ , is used. In this case, the problem can be solved by iteration, as discussed in Sec. 11.1. If the in-plane forces expressed by Φ are *independent* of the lateral deflection w , Eq. (3.3.7a) yields the required solution.

Summary. Since Eq. (3.3.7) can be considered as the governing differential equation of the plate (1.2.30), upon which the effect of a fictitious lateral load is superimposed, we can use either Navier's or Lévy's method[†] in our solution. In both cases the magnitude of the in-plane forces should be known.

ILLUSTRATIVE EXAMPLE

A simply supported rectangular plate is simultaneously loaded with a uniform lateral load $p_z = p_0$ and subjected to uniform edge tension $\bar{n}_x = \bar{n}_0$ at edges $x = 0$ and $x = a$, as shown in Fig. 3.3.3. Find the expression of the deflected plate surface.

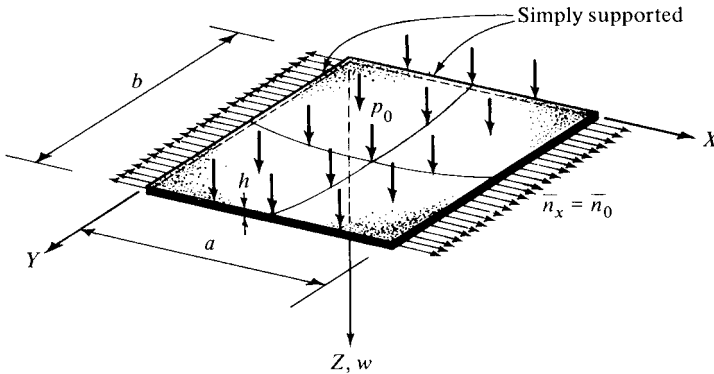


Figure 3.3.3 Plate subjected to lateral and in-plane forces.

[†] See Secs. 2.2 and 2.3, respectively.

Since $n_y = n_{xy} = 0$, Eq. (3.3.7) becomes

$$D \nabla^2 \nabla^2 w = p_z + \bar{n}_0 \frac{\partial^2 w}{\partial x^2}. \quad (3.3.9)$$

The boundary conditions of the problem permit the use of Navier's method; thus, we express the lateral load in a double Fourier series [Eq. (A.1.37)]:

$$p_z = \frac{16p_0}{\pi^2} \sum_m \sum_n \frac{1}{mn} \sin \frac{m\pi x}{a} \sin \frac{n\pi y}{b} \quad \text{for } m, n = 1, 3, 5, \dots \quad (3.3.10)$$

Assuming the deflection in the form of a similar double Fourier series,

$$w(x, y) = \sum_m \sum_n W_{mn} \sin \frac{m\pi x}{a} \sin \frac{n\pi y}{b} \quad \text{for } m, n = 1, 3, 5, \dots, \quad (3.3.11)$$

the substitution of Eqs. (3.3.10) and (3.3.11) into (3.3.9) (using a particular set of m, n values) yields the unknown W_{mn} coefficients:

$$W_{mn} = \frac{16p_0/D\pi^6}{mn\{[(m^2/a^2) + (n^2/b^2)]^2 + (\bar{n}_0 m^2/\pi^2 D a^2)\}}. \quad (3.3.12)$$

Hence

$$w(x, y) = \frac{16p_0}{D\pi^6} \sum_{m=1}^{\infty} \sum_{n=1}^{\infty} \frac{\sin(m\pi x/a) \sin(n\pi y/b)}{mn\{[(m^2/a^2) + (n^2/b^2)]^2 + (\bar{n}_0 m^2/\pi^2 D a^2)\}} \quad (3.3.13)$$

for $m, n = 1, 3, 5, \dots$

References and Bibliography

- [3.3.1] GIRKMANN, K., "Traglasten gedrückter und zugleich querbelasteter Stäbe und Platten," *Der Stahlbau*, 15 (1942), 57.
- [3.3.2] PETTERSSON, O., "Plates Subjected to Compression or Tension and to Simultaneous Transverse Load," *Ingen. Vetensk. Akad. Tidsk. Tekn. Forsk.*, 25 (1954), 78–82.
- [3.3.3] CHANG, C. C., and CONWAY, H. D., "Marcus Method Applied to Solution of Uniformly Loaded and Clamped Rectangular Plate Subjected to Forces in Its Plane," *J. Appl. Mech.*, 19 (1952), 179–184.
- [3.3.4] CONWAY, H. D., "Bending of Rectangular Plates Subjected to a Uniformly Distributed Load and to Tensile or Compressive Forces in the Plane of the Plate," *J. Appl. Mech.*, 17 (Mar. 1950), 99–100.

3.4 Plates of Various Geometrical Forms

The geometrical configuration of certain design problems may force the structural engineer to use other than circular or rectangular plates occasionally. Needless to

say, the analytical approach to the solution of such problems is usually too complicated to be considered for practical use [3.6.1, 3.6.2]. The more general numerical techniques are based either on the finite difference or on the finite-element methods treated in Chapters 5 and 7, respectively. In this section we shall discuss briefly those problems related to plates of various geometrical shapes, the solution of which can be obtained analytically with relative ease. It is assumed that such plates are of constant thickness. Because of the considerable importance of skew plates in bridges and in aeronautical structures (swept wings), they are treated in a more detailed form in Secs. 10.3 and 12.7.2.

a. Elliptical Plates. Elliptical plates with clamped boundary conditions subjected to uniformly distributed lateral loads (Fig. 3.4.1) are one of the few specific problems for which an analytic solution is easily obtainable. The approach is similar to that described in Sec. 2.1.

Let us describe the deflection surface by

$$w(x, y) = C \left(\frac{x^2}{a^2} + \frac{y^2}{b^2} - 1 \right)^2, \quad (3.4.1)$$

where a and b are the semimajor and semiminor axes of the ellipse, respectively. Equation (3.4.1) satisfies the boundary conditions

$$w = 0, \quad \frac{\partial w}{\partial x} = 0 \quad \text{and} \quad \frac{\partial w}{\partial y} = 0. \quad (3.4.2)$$

The constant C is obtained from substituting Eq. (3.4.1) into the differential equation of the plate problem (1.2.30), which gives

$$\nabla^2 \nabla^2 w = 8C \left[3 \left(\frac{1}{a^2} + \frac{1}{b^2} \right)^2 - \frac{4}{a^2 b^2} \right] = \frac{p_0}{D}; \quad (3.4.3)$$

hence

$$C = \frac{p_0}{8D \{ 3[(1/a^2) + (1/b^2)]^2 - (4/a^2 b^2) \}}. \quad (3.4.4)$$

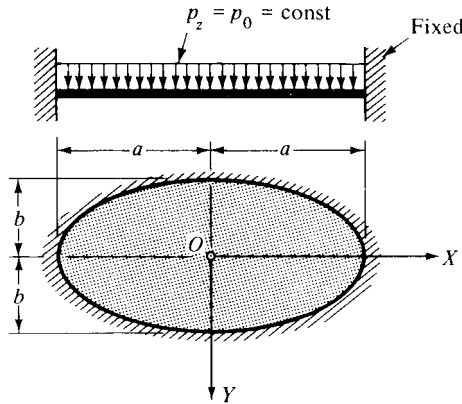


Figure 3.4.1 Clamped elliptical plate.

This expression substituted into Eq. (3.4.1) yields the solution of the problem. More complex boundary and loading conditions are treated by Sengupta [3.4.4] and Perry [3.4.5].

b. Triangular Plates. Solutions for simply supported isosceles triangular plates can be obtained with relative ease by applying the previously described method of images (Sec. 2.6). Basically, the same approach is applicable for uniformly distributed loads. Navier's method applied to this problem provides that simply supported boundary conditions (Fig. 3.4.2) give [3]

$$w(x, y) = \frac{16p_0a^4}{\pi^6 D} \left[\sum_{m=1,3,5,\dots}^{\infty} \sum_{n=2,4,6,\dots}^{\infty} \frac{n \sin(m\pi x/a) \sin(n\pi y/a)}{m(n^2 - m^2)(m^2 + n^2)^2} + \sum_{m=2,4,6,\dots}^{\infty} \sum_{n=1,3,5,\dots}^{\infty} \frac{m \sin(m\pi x/a) \sin(n\pi y/a)}{n(m^2 - n^2)(m^2 + n^2)^2} \right]. \quad (3.4.5)$$

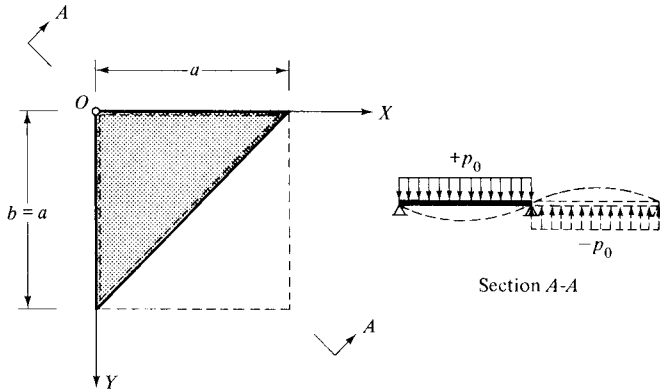


Figure 3.4.2 Isosceles triangular plate.

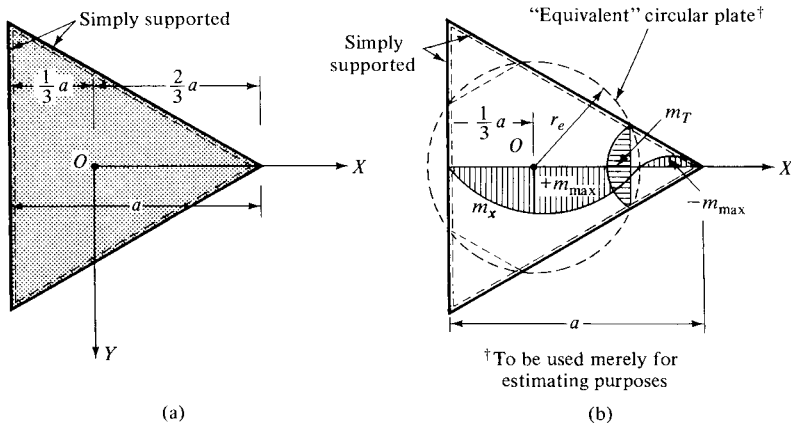


Figure 3.4.3 Equilateral triangular plate.

For simply supported triangular plates under uniform lateral loads, a closed-form solution has been obtained by Woinowsky-Krieger [3.4.6] in the form

$$w(x, y) = \frac{p_0}{64Da} \left(x^3 - x^2a - 3xy^2 - y^2a + \frac{4}{27}a^3 \right) \cdot \left(\frac{4}{9}a^2 - x^2 - y^2 \right) \quad (3.4.6)$$

utilizing a membrane analogy. This method can also be extended to cover the case of concentrated loads.

For *preliminary* design purposes, the simply supported equilateral triangular plate can be replaced by an *equivalent* circular one [3.4.8], as shown in Fig. 3.4.3, which gives approximately the same maximum moments. The radii of the simply supported *equivalent* circular plates are

$$\text{For uniform load :} \quad r_e = 0.35a;$$

$$\text{For concentrated load at the center :} \quad r_e = 0.38a.$$

The approximate value of the maximum negative moments in the line connecting the center and the vertices of the triangle (Fig. 3.4.3b) is given by

$$-m_{\max} \approx -0.25(+m_{\max}). \quad (3.4.7)$$

Furthermore, the transverse moment in the line connecting the points of intersection of the sides of the triangle with the *equivalent* circle can be approximated by

$$m_T \approx +0.25(+m_{\max}). \quad (3.4.8)$$

Similar approximations can be used for irregular triangles also, provided that the length of the sides does not vary considerably.

c. Sector-Shaped Plates. Let us consider a sector plate subjected to uniform load, as shown in Fig. 3.4.4. Again, the solution of the problem is sought in two parts:

$$w = w_H + w_P. \quad (3.4.9)$$

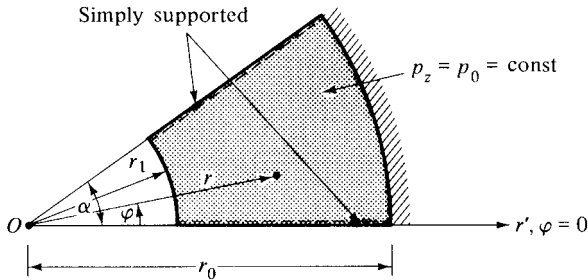


Figure 3.4.4 Sector plate.

By expanding the lateral load into a trigonometric series containing sine terms only,[†] the expression for the load becomes

$$P_z = \frac{4p_0}{\pi} \sum_{m=1,3,5}^{\infty} \frac{1}{m} \sin \frac{m\pi\varphi}{\alpha}. \quad (3.4.10)$$

Utilizing the Clebsch approach, the solution of the homogeneous form of the differential equation of the plate ($\nabla_r^2 \nabla_r^2 w = 0$) can be given by

$$w_H = \Phi_0 + \sum_{m=1}^{\infty} \Phi_m \sin \frac{m\pi\varphi}{\alpha}, \quad (3.4.11)$$

where

$$\Phi_m = C_{1m}\rho^{m\pi/\alpha} + C_{2m}\rho^{-m\pi/\alpha} + C_{3m}\rho^{2+m\pi/\alpha} + C_{4m}\rho^{2-m\pi/\alpha} \quad (3.4.12)$$

and

$$\Phi_0 = C_{10} + C_{20} \ln \rho + C_{30}\rho^2 + C_{40}\rho^2 \ln \rho. \quad (3.4.13)$$

In these expressions, ρ represents $\rho = r/r_0$. The particular solution assumes the form

$$w_P = \frac{4p_0r_0^4}{\pi} \rho^4 \sum_{m=1,3,5}^{\infty} \frac{1}{m(16 - m^2\pi^2/\alpha^2)(4 - m^2\pi^2/\alpha^2)} \sin \frac{m\pi\varphi}{\alpha}. \quad (3.4.14)$$

The coefficients C_{10} , C_{20} , C_{30} , C_{40} and C_{1m} , C_{2m} , \dots are determined from the boundary conditions at $r = r_0$ and $r = r_1$.

If the uniformly loaded plate sector takes the form of a semicircle ($\alpha = \pi$) (Fig. 3.4.5), then the solution assumes the form

$$\begin{aligned} w = & \sum_{m=1,3,5}^{\infty} (C_{1m}r^m + C_{2m}r^{2+m}) \sin m\varphi \\ & + \frac{4p_0r_0^4}{\pi D} \sum_{m=1,3,5}^{\infty} \frac{1}{m(16 - m^2)(4 - m^2)} \sin m\varphi; \end{aligned} \quad (3.4.15)$$

the constants C_{1m} and C_{2m} are obtained from the boundary condition at $r = r_0$.

If the boundary conditions along the arc of the semicircle are those of simple supports, Eq. (3.4.15) becomes [6]

$$\begin{aligned} w = & \frac{p_0r_0^4}{D} \sum_{m=1,3,5}^{\infty} \left\{ 4\rho^4 \frac{1}{m\pi(16 - m^2)(4 - m^2)} \right. \\ & + \rho^m \frac{m + 5 + \nu}{m\pi(16 - m^2)(2 + m)[m + 0.5(1 + \nu)]} \\ & \left. - \rho^{m+2} \frac{m + 3 + \nu}{m\pi(4 + m)(4 - m^2)[m + 0.5(1 + \nu)]} \right\} \sin m\varphi. \end{aligned} \quad (3.4.16)$$

[†] See Appendix A.1 and Sec. 3.6.

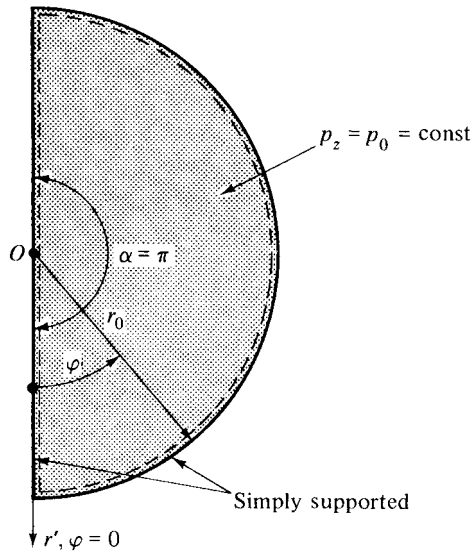


Figure 3.4.5 Semicircular plate.

For any load expressed in single trigonometric series containing sine terms only, a similar approach can be used. The particular solution is obtained from Eq. (2.3.4), expressed in terms of polar coordinates. The prerequisite for the application of this method is that the two straight-line boundaries be simply supported.

Although Clebsch's method, as described in Sec. 3.6, can be applied to sector and wedge-shaped plates with arbitrary boundary conditions, the solutions are invariably difficult and complex. Readers who are interested in the mathematical theory of elasticity should consult Refs. [3.4.10–3.4.13] for further study.

Six combinations of fixed, free and simply supported boundary conditions along the radial edges of sector plates have been investigated by Williams [3.4.13]. The assumed deflection function

$$w(r, \varphi) = r^{\lambda+1} [B_1 \sin(\lambda + 1)\varphi + B_2 \cos(\lambda + 1)\varphi + B_3 \sin(\lambda - 1)\varphi + B_4 \cos(\lambda - 1)\varphi] \quad (3.4.17)$$

contains the usual four (integration) constants B_i and an additional parameter λ . The latter is calculated from the vanishing determinant of the four homogeneous algebraic equations supplied by the boundary conditions of the radial edges, which gives the equation $f(\lambda, \alpha, \nu) = 0$. The four constants B_1, B_2, B_3 and B_4 are evaluated from the boundary conditions along the edges $\varphi = 0$ and $\varphi = \alpha$.

Summary. The analytical solution of plates having other than rectangular or circular forms is usually complicated. Consequently, if solutions are not readily available, the use of numerical methods (Part II) or yield-line analysis (Chapter 13) is recommended. In the case of sector plates, the designer must be aware of the fact that the stress at the apex (origin of the coordinate system) tends to infinity [3.4.13].

References and Bibliography

- [3.4.1] QUINLAN, P. M., "The λ -Method for Polygonal Plates," Scientific Report No. 1, National University of Ireland, University College, Cork, April 1964.
- [3.4.2] KRETTNER, J., "Beitrag zur Berechnung schiefwinkliger Platten," *Ing.-Arch.*, 22 (1954), 47–54.
- [3.4.3] SZILARD, R., and HUBKA, W. F., "Static and Dynamic Analysis of Plates of Arbitrary Shape and Boundary Condition," *Publ. IABSE*, 25 (1965), 317–338.
- [3.4.4] SENGUPTA, H. M., "The Bending of an Elliptic Plate Under Certain Distributions of Load," *Bull. Calcutta Math. Soc.*, 40 (Mar. and June 1948), 17–35, 55–63.
- [3.4.5] PERRY, C. L., "The Bending of Thin Elliptical Plates," *Proc. Symp. Appl. Math.*, 3 (1950), 131–139.
- [3.4.6] WOINOWSKY-KRIEGER, S., "Berechnung der ringsum frei aufliegenden gleichseitigen Dreiecksplatte," *Ing.-Arch.*, 4 (1933), 254–262.
- [3.4.7] CARRIER, G. F., and SHAW, F. S., "Some Problems on the Bending of Thin Plates," *Proc. Symp. Appl. Math.*, 3 (1950), 125–128.
- [3.4.8] GÖTTLICHER, H., "Die ringsum fest eingespannte Dreiecksplatte von gleichbleibender und von veränderlicher Stärke," *Ing.-Arch.*, 8 (1938), 12.
- [3.4.9] MODOR, Z., "Berechnung der Platten in Polygonalform," *Bauingenieur*, 34 (1959), 427–437.
- [3.4.10] CARRIER, G. F., "The Bending of the Clamped Sectorial Plate," *J. Appl. Mech.*, 11 (1944), A-134–A-139–.
- [3.4.11] WOINOWSKY-KRIEGER, S., "The Bending of a Wedge-Shaped Plate," *J. Appl. Mech.*, 20 (1953), 77–81.
- [3.4.12] HASSÉ, H. R., "The Bending of a Uniformly Loaded Clamped Plate in Form of a Circular Sector," *Q. Mech. Appl. Math.*, 3, Pt. 3 (Sept. 1950), 271–278.
- [3.4.13] WILLIAMS, M. L., "Surface Stress Singularities Resulting from Various Boundary Conditions in Angular Corners of Plates under Bending," in *Proceedings of the First U.S. Natl. Congress on Applied Mechanics* (held at the Illinois Institute of Technology, 1951), American Society of Mechanical Engineers, New York, 1952, pp. 325–329.

3.5 Various Types of Circular Plates

a. Annular Plates. The solution of axially symmetric bending of circular plates with central holes (Fig. 3.5.1) may follow a procedure similar to the one described in Sec. 2.8, but one must consider the boundary conditions at the outer ($r = r_0$) as well as at the inner ($r = r_i$) boundaries. For the solution of the homogeneous form of the differential equation, the expression given by Eq. (2.8.8) can be used. By introducing

$$\rho = \frac{r}{r_0}, \quad (3.5.1)$$

the homogeneous solution can be given in the form

$$w_H = C_1 + C_2 \rho^2 + C_3 \ln \rho + C_4 \rho^2 \ln \rho. \quad (3.5.2)$$

A particular solution w_P can be obtained from Eqs. (2.8.16) and (2.8.17) by direct integration, as described in Sec. 2.8. The four constants C_1 , C_2 , C_3 and C_4 are determined from the boundary conditions at the inner and outer edges. The approach is similar when the central hole is replaced by a nondeformable rigid body, as shown in Fig. 3.5.2. Considerable simplification in the solution of these boundary value

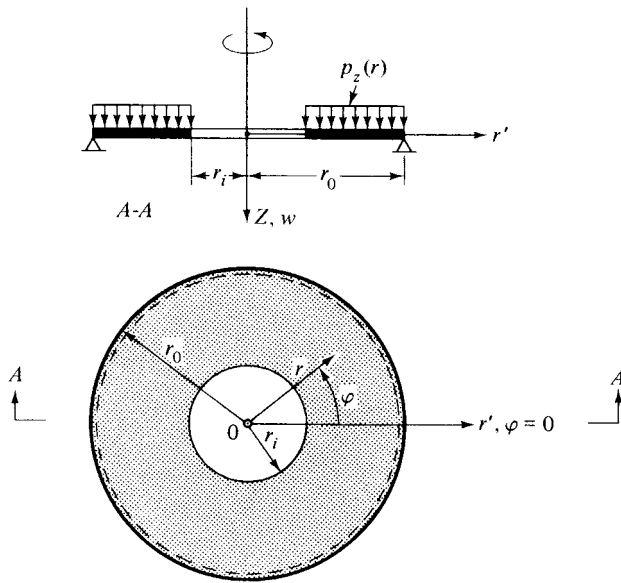


Figure 3.5.1 Circular plate with central hole.

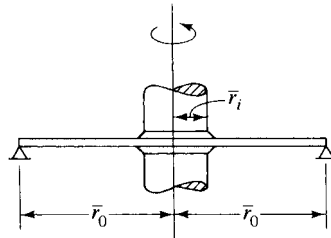


Figure 3.5.2 Annular plate with shaft.

problems can be achieved by assuming that $\nu = 0$. Since the bending of annular plates has important practical applications, especially in machine design, extensive solutions for the most common loading cases are available in Refs. [5], [3.5.1], [3.5.2] and [3.5.3]. The solutions of annular plates loaded with concentrated forces producing arbitrary plate deflections are treated in Refs. [9] and [3.6.4].

b. Antisymmetric Loading. The linearly varying hydrostatic loading (Fig. 3.5.3a) acting on a circular plate can be divided into a uniformly distributed load and an antisymmetric triangular load, as shown in Fig. 3.5.3b. Thus, the expression of the lateral load is

$$p_z(r) = p_0 + p_1 \rho \cos \varphi. \quad (3.5.3)$$

Since the uniform part of the load produces a rotationally symmetric deflection surface, which has been treated in Sec. 2.8, only the case of the triangular loading will be discussed here. The solution of the governing differential equation of a circular

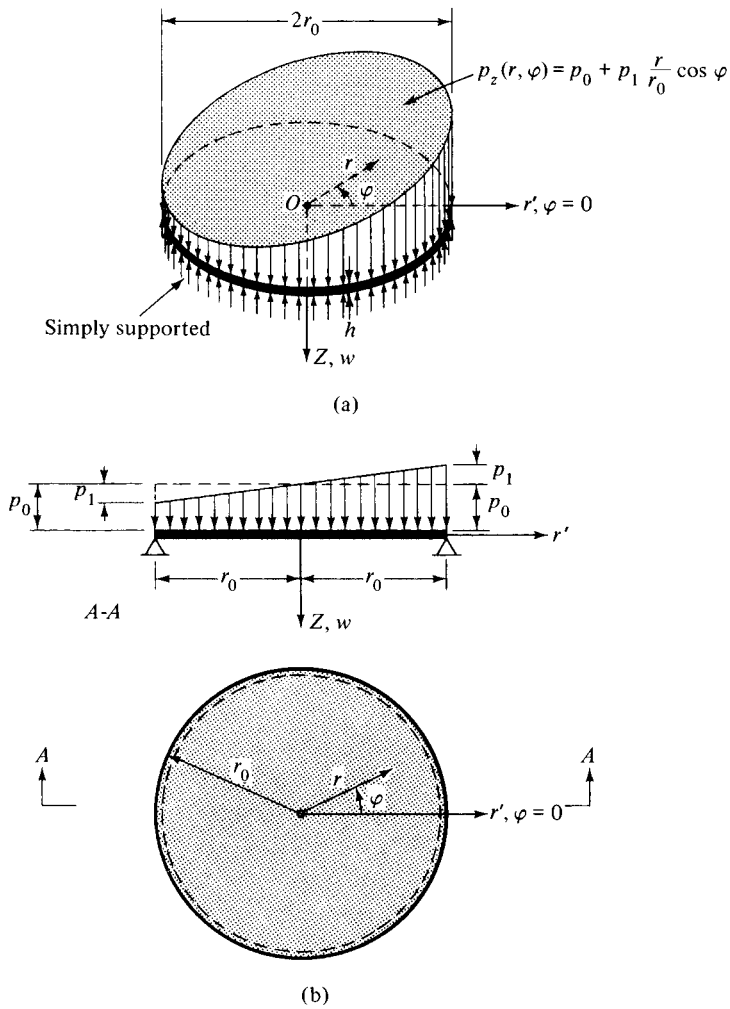


Figure 3.5.3 Hydrostatic load on circular plate.

plate (1.4.11) can, again, be given as the sum of a particular solution and the solution of the homogeneous form of the differential equation; thus,

$$w(r, \varphi) = w_H + w_P. \quad (3.5.4)$$

The particular solution of the nonhomogeneous differential equation (1.11.11),

$$\nabla_r^2 \nabla_r^2 w = \frac{p_1}{D} \rho \cos \varphi, \quad (3.5.5)$$

may be taken in the form

$$w_P = C_P \rho^5 \cos \varphi. \quad (3.5.6)$$

Substituting Eq. (3.5.6) into Eq. (3.5.5), the unknown constant C_P can be determined:

$$C_P = \frac{p_1 r_0^4}{192D}. \quad (3.5.7)$$

The solution of the homogeneous form of the differential equation of the plate can be given as[†]

$$w_H = (C_1 \rho + C_2 \rho^3) \cos \varphi. \quad (3.5.8)$$

The general solution of the deflection of the circular plate, according to Eq. (3.5.4), is

$$w(r, \varphi) = \left(\frac{p_1 r_0^4}{192D} \rho^5 + C_1 \rho + C_2 \rho^3 \right) \cos \varphi. \quad (3.5.9)$$

From the boundary conditions at the edge, the unknown coefficients C_1 and C_2 can be obtained in the usual manner.

Another common type of antisymmetric loading is a moment applied to a rigid disk located at the center of the circular plate, as shown in Fig. 3.5.4. In this case, we may state that there is no external lateral load; thus the solution of the homogeneous form of the differential equation yields the solution of the problem. Consequently, the equation of the deflected plate surface has the form

$$w(r, \varphi) = \left(C_1 \rho + C_2 \frac{1}{\rho} + C_3 \rho^3 + C_4 \rho \ln \rho \right) \cos \varphi. \quad (3.5.10)$$

The constants C_1 , C_2 , C_3 and C_4 are determined from the boundary conditions.

c. Concentrated Load Acting at the Center. A special case of the symmetric bending of circular plates is when the concentrated lateral load acts at the center (Fig. 3.5.5). Because of the discontinuous character of the lateral loading, an approach other than that described in Sec. 2.8 is utilized. The solution in this case is obtained from the equilibrium of the vertical forces, which states that

$$-2\pi r q_r = P_z, \quad (3.5.11)$$

$$M = Pe$$

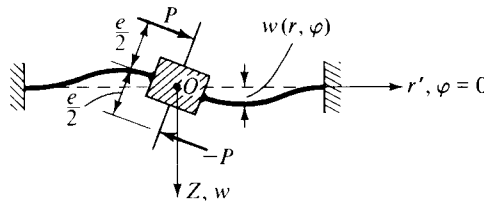


Figure 3.5.4 Circular plate with moment acting at center.

[†] Other types of functions can be obtained from Ref. [14].

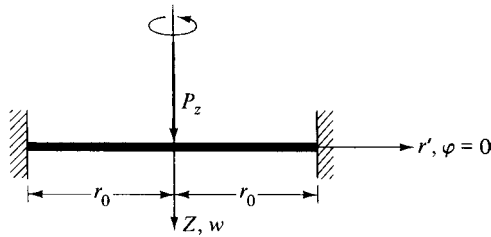


Figure 3.5.5 Concentrated force at center of circular plate.

and by expressing q_r using Eq. (1.4.15); thus, we obtain

$$D \left(\frac{d^3 w}{dr^3} + \frac{1}{r} \frac{d^2 w}{dr^2} - \frac{1}{r^2} \frac{dw}{dr} \right) = D \frac{d}{dr} \left[\frac{1}{r} \frac{d}{dr} \left(r \frac{dw}{dr} \right) \right] = \frac{P_z}{2\pi r}. \quad (3.5.12)$$

Repeated integration of Eq. (3.5.12) yields

$$w(r) = \frac{P_z}{2\pi D} \left(\frac{r^2}{4} \ln r + C_1 r^2 + C_2 \ln r + C_3 \right). \quad (3.5.13)$$

Since for $r = 0$ the deflection should remain finite, we must use $C_2 = 0$. The other two coefficients, C_1 and C_3 , are to be determined from the boundary conditions of the specific problem. In the case of simply supported edges, for instance, the deflection of the plate becomes

$$w(r) = \frac{P_z r_0^2}{16\pi D} \left[\frac{3 + \nu}{1 + \nu} (1 - \rho^2) + 2\rho^2 \ln \rho \right], \quad (3.5.14)$$

whereas for clamped edges we obtain

$$w(r) = \frac{P_z r_0^2}{16\pi D} (1 - \rho^2 + 2\rho^2 \ln \rho). \quad (3.5.15)$$

References and Bibliography

- [3.5.1] WAHL, A. M., and LOBO, G., "Stresses and Deflections in Flat Circular Plates with Central Holes," *Trans. ASME*, 52 (1930), 29–43.
- [3.5.2] TRUMPLER, W. E., "Design Data for Circular Plates with Central Hole," *J. Appl. Mech.*, 10 (Sept. 1943), A173–A175.
- [3.5.3] HOLMBERG, A., "The Effect of Holes in Circular Plates," *Publ. IASBE*, 9 (1949), 213–216.
- [3.5.4] REISSNER, E., "Über die Biegung der Kreisplatte mit exzentrischer Einzellast," *Math. Ann.*, 111 (1935), 777–780.
- [3.5.5] FLÜGGE, W., "Kreisplatten mit linear veränderlichen Belastungen," *Bauingenieur*, 10 (1929), 221–225.
- [3.5.6] REISSNER, H., "Über die unsymmetrische Biegung dünner Kreisringplatten," *Ing.-Arch.*, 1 (1929), 72.
- [3.5.7] BIRGER, I. A., *Kruglye plastinki i obolochki vrashcheniia (Rotationally Symmetrical Plates and Shells)*, Oborongiz, Moscow, 1961.

3.6 Circular Plate Loaded by an Eccentric Concentrated Force

Since any lateral load acting on a plate can be replaced by a finite number of concentrated forces, the solution of the circular plates under an arbitrary concentrated load can be considered one of the fundamental problems in the theory of plates. Although it is assumed that the boundary condition is rotationally symmetric, the analysis of the deflections due to such nonsymmetric loads, as outlined in Sec. 1.4, is quite tedious. Certain simplifications can be achieved, however, by considering that the deflected plate surface is symmetric with respect to the line connecting the origin of the polar coordinate system ($\varphi = 0$) and the point of application, A , of the force (Fig. 3.6.1).

The general solution of the governing differential equation of circular plates (1.4.11) was obtained by Clebsch in the form

$$w(r, \varphi) = w_P + F_0(r) + \sum_{m=1}^{\infty} F_m(r) \cos m\varphi + \sum_{m=1}^{\infty} F'_m(r) \sin m\varphi, \quad (3.6.1)$$

where w_P represents a particular solution of Eq. (1.4.11) and $F_0(r)$, $F_1(r)$, $F_2(r)$, \dots , $F'_1(r)$, $F'_2(r)$, \dots are functions of r only.

Let us divide the circular plate into two cylindrical parts by the radius $\overline{OA} = r_P$. In the case of the outer plate ring, the load P is an edge load; consequently, only the terms that represent the complementary part of the solution[†] must be considered. Furthermore, utilizing the above-mentioned symmetry of the deflected plate surface, Eq. (3.6.1), representing the deflection of the outer part, can be written as

$$w_{H1} = w_1(r, \varphi) = F_0(r) + \sum_{m=1}^{\infty} F_m(r) \cos m\varphi, \quad (3.6.2)$$

where

$$\begin{aligned} F_0(r) &= C_{10} + C_{20}r^2 + C_{30} \ln \frac{r}{r_0} + C_{40}r^2 \ln \frac{r}{r_0}, \\ F_1(r) &= C_{11}r + C_{21}r^3 + C_{31}r^{-1} + C_{41}r \ln \frac{r}{r_0}, \\ &\vdots \\ F_m(r) &= C_{1m}r^m + C_{2m}r^{-m} + C_{3m}r^{m+2} + C_{4m}r^{-m+2} \quad \text{for } m > 1. \end{aligned} \quad (3.6.3)$$

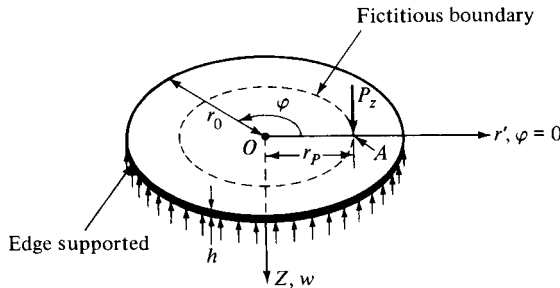


Figure 3.6.1 Eccentric force.

[†] Solution of the homogeneous form of the differential equation.

Similarly, the deflections of the inner part of the plate can be expressed in the form

$$w_{H2} = w_2(r, \varphi) = f_0(r) + \sum_{m=1}^{\infty} f_m(r) \cos m\varphi, \quad (3.6.4)$$

where the functions $f_0(r)$, $f_1(r)$, $f_2(r)$, \dots are similar to those given in Eq. (3.6.3). Thus we may write

$$\begin{aligned} f_0(r) &= c_{10} + c_{20}r^2 + c_{30} \ln \frac{r}{r_0} + c_{40}r^2 \ln \frac{r}{r_0}, \\ f_1(r) &= c_{11}r + c_{21}r^3 + c_{31}r^{-1} + c_{41}r \ln \frac{r}{r_0}, \\ &\vdots \\ f_m(r) &= c_{1m}r^m + c_{2m}r^{-m} + c_{3m}r^{m+2} + c_{4m}r^{-m+2} \quad \text{for } m > 1. \end{aligned} \quad (3.6.5)$$

Since at the center of the plate the deflection, the slope and the internal moments are not infinite, we obtain

$$\begin{aligned} c_{30} &= c_{40} = 0, \\ c_{31} &= c_{41} = 0, \\ &\vdots \\ c_{3m} &= c_{4m} = 0. \end{aligned} \quad (3.6.6)$$

The remaining unknown constants in Eqs. (3.6.3) and (3.6.5) are determined from the boundary conditions of the inner and outer ring plates.

Let us assume, for instance, that the edge of the circular plate is fixed; thus the two boundary conditions are

$$(w_1)_{r=r_0} = 0 \quad \text{and} \quad \left(\frac{\partial w_1}{\partial r} \right)_{r=r_0} = 0. \quad (3.6.7)$$

Because of the continuity of the plate at $r = r_p$, the deflections and the slopes of the inner and outer parts are the same; therefore,

$$(w_1)_{r=r_p} = (w_2)_{r=r_p} \quad \text{and} \quad \left(\frac{\partial w_1}{\partial r} \right)_{r=r_p} = \left(\frac{\partial w_2}{\partial r} \right)_{r=r_p}. \quad (3.6.8)$$

Furthermore, another equation in the form of the compatibility of the internal forces can be used; thus

$$(m_{1r})_{r=r_p} = (m_{2r})_{r=r_p}, \quad (3.6.9)$$

or, in another form,

$$\left(\frac{\partial^2 w_1}{\partial r^2} \right)_{r=r_p} = \left(\frac{\partial^2 w_2}{\partial r^2} \right)_{r=r_p}. \quad (3.6.10)$$

The sixth equation for determination of the unknown constants is obtained by stating that at the point of application of the load the difference of the transverse shear forces is equal to the external load, which gives

$$(q_{1r} - q_{2r})_{r=r_P, \varphi=0} = P, \quad (3.6.11)$$

expressing the discontinuity of the internal shear forces at $r = r_P$ and $\varphi = 0$. This equation is familiar to the readers from elementary treatment of mechanics, since a similar equation is used for construction of the shear diagrams of beams.

To utilize Eq. (3.6.11) effectively, we must now express the concentrated load in a form similar to Eqs. (3.6.2) and (3.6.4), representing a cosine series expansion. In the Fourier series expression of the concentrated load P in polar coordinates, we first replace the concentrated force with a partial line load distributed over an arc of length $r_P 2\Delta\varphi$, as shown in Fig. 3.6.2. The intensity of this line load between $+\Delta\varphi$ and $-\Delta\varphi$ is

$$p_z = \frac{P}{2r_P \Delta\varphi} = \text{const.} \quad (3.6.12)$$

As discussed in Appendix A.1, a cosine series expansion of an arbitrary function can be obtained by making the function even (Fig. 3.6.2b) and using a period of $T = 2L$,

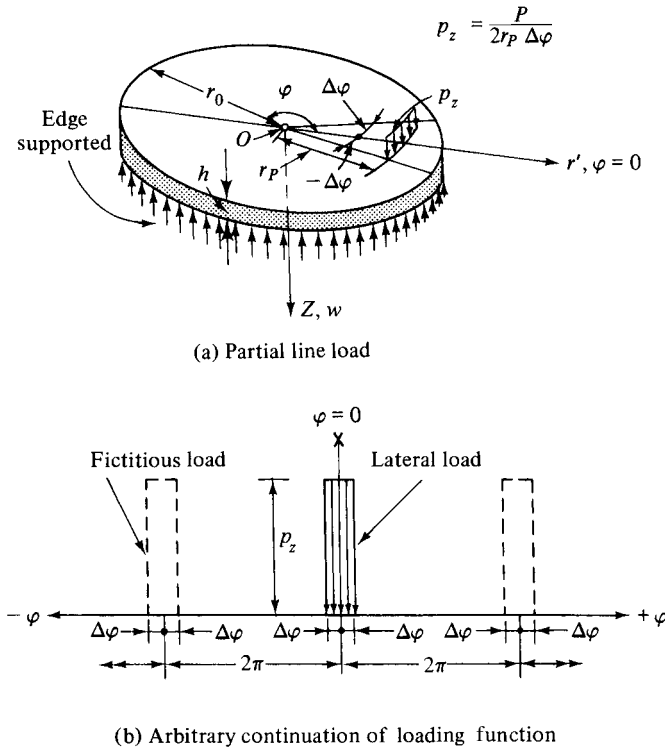


Figure 3.6.2 Arbitrary continuation of loading function.

which, in the case of polar coordinates, becomes $T = 2\pi$. Thus Eq. (A.1.25) can be written in the form

$$p_z(\varphi) = \frac{1}{2}A_0 + \sum_1^{\infty} A_m \cos m\varphi. \quad (3.6.13)$$

Equation (A.1.24) gives

$$A_0 = \frac{2}{\pi} \int_0^{\pi} p_z d\varphi = \frac{2}{\pi} \int_0^{+\Delta\varphi} \frac{P}{2r_P \Delta\varphi} d\varphi = \frac{P}{\pi r_P} \quad (3.6.14)$$

and

$$A_m = \frac{2}{\pi} \int_0^{\pi} p_z \cos m\varphi d\varphi = \frac{2}{\pi} \int_0^{+\Delta\varphi} \frac{P}{2r_P \Delta\varphi} \cos m\varphi d\varphi = \frac{P}{\pi r_P m \Delta\varphi} \sin m \Delta\varphi. \quad (3.6.15)$$

Hence the cosine series expression of the line load in terms of polar coordinates becomes

$$\begin{aligned} p_z(\varphi) &= \frac{P}{2\pi r_P} + \sum_1^{\infty} \frac{P}{\pi r_P m \Delta\varphi} \sin m \Delta\varphi \cos m\varphi \\ &= \frac{P}{\pi r_P} \left(\frac{1}{2} + \sum_1^{\infty} \frac{\sin m \Delta\varphi}{m \Delta\varphi} \cos m\varphi \right). \end{aligned} \quad (3.6.16)$$

If $\Delta\varphi$ is approaching zero, the limit approach, described by Eq. (2.4.36), can be used.

Therefore, Eq. (3.6.16) can be written as

$$p_z(\varphi) = \frac{P}{\pi r_P} \left(\frac{1}{2} + \sum_1^{\infty} \cos m\varphi \right). \quad (3.6.17)$$

Substituting Eq. (3.6.17) into Eq. (3.6.11) and expressing the shear forces in accordance with Eq. (1.4.15), we obtain

$$D \left(\frac{\partial}{\partial r} \nabla_r^2 w_1 - \frac{\partial}{\partial r} \nabla_r^2 w_2 \right) = \frac{P}{\pi r_P} \left(\frac{1}{2} + \sum_1^{\infty} \cos m\varphi \right). \quad (3.6.18)$$

The previously discussed boundary conditions in connection with Eq. (3.6.18) yield all the unknown coefficients in the expression of the plate deflections.

The results of these tedious computations are given in Ref. [14]. Solution for simply supported edge conditions is discussed in Ref. [2]. The maximum deflection for a clamped plate is

$$w_{\max} = w(r_P, 0) = \frac{P}{16\pi D} \frac{(r_0^2 - r_P^2)^2}{r_0^2}. \quad (3.6.19)$$

With $r_P = 0$, Eq. (3.6.19) represents the solution for the concentrated load acting at the center.

A similar approach can be taken to include arbitrary loadings acting on circular and annular plates. This general application of Eq. (3.6.1), however, is more tedious.

Summary. It is evident that the classical solution of circular plate problems, which do not have rotational symmetry, requires extensive mathematical manipulations and can be rather time consuming. Consequently, this approach is not recommended for everyday application by the design engineer.

References and Bibliography

- [3.6.1] MELAN, E., "Die Berechnung einer exzentrisch durch eine Einzellast belasteten Kreisplatte," *Eisenbau*, 11 (1920), 190–192.
- [3.6.2] FLÜGGE, W., *Die strenge Berechnung von Kreisplatten unter exzentrisch angeordneten Lasten*, Springer-Verlag, Berlin, 1928.
- [3.6.3] KUDRIAVTSEV, N. V., "Flexure of a Round Plate with an Eccentric Hole by a Concentrated Load," *C. R. (Doklady) Acad. Sci., U.R.S.S.*, 53, No. 2 (1946), 103–106.
- [3.6.4] FÖPPL, A., "Die Biegung einer kreisförmigen Platte," *Sitzungsberichte Akad. Wiss. Math. Physik. Klasse K1 (München)*, 45 (1912), 155–190.

3.7 Plates with Edge Moments

First, let us consider a rectangular, simply supported plate subjected to an edge moment described by a Fourier sine series,

$$\bar{m}_y = \sum_{m=1}^{\infty} Y_m \sin \alpha_m x, \quad \alpha_m = \frac{m\pi}{a}, \quad (3.7.1)$$

acting along the edge AB , as shown in Fig. 3.7.1a. The pertinent boundary conditions of this plate problem are

$$w(x, y) = 0, \quad m_x = 0 \quad \text{for } x = 0, \quad x = a, \quad (3.7.2a)$$

$$w(x, y) = 0, \quad m_y = \bar{m}_y \quad \text{for } y = 0, \quad (3.7.2b)$$

$$w(x, y) = 0, \quad m_y = 0 \quad \text{for } y = b. \quad (3.7.2c)$$

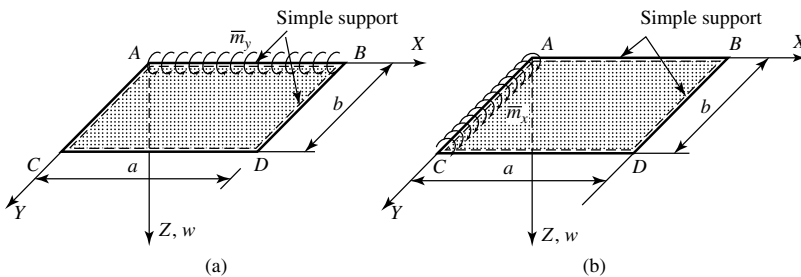


Figure 3.7.1 Plates under distributed edge moments.

The solution $w(x, y)$ must simultaneously satisfy the homogeneous form of the differential equation of the plate,

$$\nabla^4 w(x, y) = 0, \quad (3.7.3)$$

and the above given boundary conditions.

We assume the solution in the form

$$w(x, y) = \sum_{m=1}^{\infty} W_m \sin \alpha_m x, \quad (3.7.4)$$

where

$$W_m = \frac{1}{\alpha_m^2} (C_{1m} \cosh \alpha_m y + \alpha_m y C_{2m} \sinh \alpha_m y + C_{3m} \sinh \alpha_m y + \alpha_m y C_{4m} \cosh \alpha_m y) \quad (3.7.5)$$

and C_{1m} , C_{2m} , C_{3m} and C_{4m} are unknown coefficients to be determined from the boundary conditions.

For a specific m number the boundary conditions expressed by the first requirement of Eqs. (3.7.2b) and (3.7.2c), respectively, give

$$C_{1m} = 0, \quad (3.7.6)$$

$$C_{1m} \cosh \alpha_m b + \alpha_m b C_{2m} \sinh \alpha_m b + C_{3m} \sinh \alpha_m b + \alpha_m b C_{4m} \cosh \alpha_m b = 0. \quad (3.7.7)$$

The second requirement in those two equations can be formulated as

$$-D \left(\frac{\partial^2 w}{\partial y^2} + \nu \frac{\partial^2 w}{\partial x^2} \right)_{y=0} = Y_m \sin \alpha_m x, \quad (3.7.8)$$

$$\left(\frac{\partial^2 w}{\partial y^2} + \nu \frac{\partial^2 w}{\partial x^2} \right)_{y=b} = 0. \quad (3.7.9)$$

Since along the edges y is constant, the corresponding second derivatives, $\partial^2 w / \partial w^2$, are zero. Thus, the two equations given above become

$$-D (C_{1m} + 2 C_{2m}) = Y_m, \quad (3.7.10)$$

$$(C_{1m} + 2 C_{2m}) \cosh \alpha_m b + \alpha_m b C_{2m} \sinh \alpha_m b + (C_{3m} + 2 C_{4m}) \sinh \alpha_m b + \alpha_m b C_{4m} \cosh \alpha_m b = 0. \quad (3.7.11)$$

The solution of these four equations[†] resulting from the boundary conditions yields

$$\begin{aligned} C_{1m} &= 0, & C_{2m} &= -\frac{Y_m}{2D}, \\ C_{3m} &= \frac{Y_m}{2D} \alpha_m b (1 - \coth^2 \alpha_m b), & C_{4m} &= \frac{Y_m}{2D} \coth \alpha_m b. \end{aligned} \quad (3.7.12)$$

[†] Equations (3.7.6), (3.7.7), (3.7.10) and (3.7.11)

The equation of the deflected plate surface is therefore

$$w(x, y) = \frac{1}{2D} \sum_{m=1}^{\infty} \frac{Y_m}{\alpha_m^2 \sinh \alpha_m b} \times \left[\alpha_m y \cosh \alpha_m (b - y) - \alpha_m b \frac{\sinh \alpha_m y}{\sinh \alpha_m b} \right] \sin \alpha_m x. \quad (3.7.13)$$

On the other hand, if the plate is subjected to an edge moment

$$\bar{m}_x = \sum_{m=1}^{\infty} X_m \sin \beta_m y, \quad \beta_m = \frac{m\pi}{b}, \quad (3.7.14)$$

acting along the edge AC (Fig. 3.7.1b), then a similar procedure, as treated above, gives the following expression for the deflections:

$$w(x, y) = \frac{1}{2D} \sum_{m=1}^{\infty} \frac{X_m}{\beta_m^2 \sinh \beta_m a} \times \left[\beta_m x \cosh \beta_m (a - x) - \beta_m a \frac{\sinh \beta_m x}{\sinh \beta_m a} \right] \sin \beta_m y. \quad (3.7.15)$$

Finally, if the rectangular, simply supported plate is subjected to two *symmetrically* distributed edge moments (Fig. 3.7.2)

$$\bar{m}_y = \sum_{m=1}^{\infty} Y_m \sin \alpha_m x, \quad \alpha_m = \frac{m\pi}{a}, \quad (3.7.16)$$

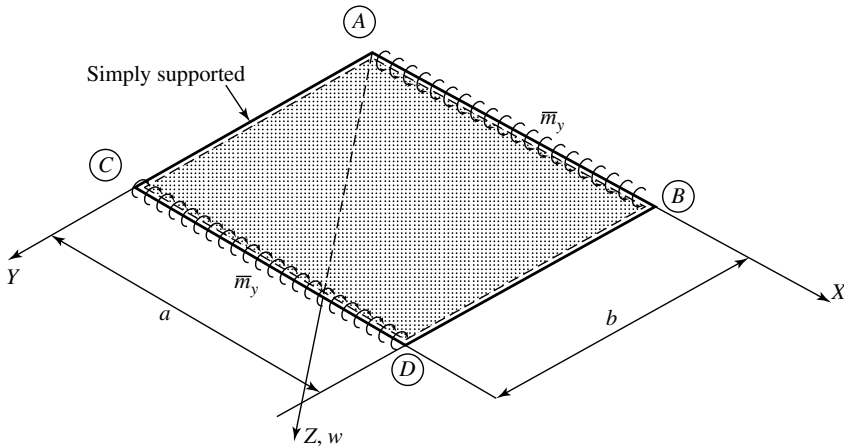


Figure 3.7.2 Two symmetrically distributed edge moments.

then the equation of deflections is readily obtained by replacing y with $b - y$ in Eq. (3.7.13); hence

$$w(x, y) = \frac{1}{2D} \sum_{m=1}^{\infty} \frac{Y_m}{\alpha_m^2 \sinh \alpha_m b} \left[\alpha_m (b - y) \cosh \alpha_m y + \alpha_m y \cosh \alpha_m (b - y) - \alpha_m b \frac{\sinh \alpha_m (b - y) + \sinh \alpha_m y}{\sinh \alpha_m b} \right] \sin \alpha_m x. \quad (3.7.17)$$

We introduced these plate problems and their solutions primarily with regard to their future use in the subsequent Secs. 3.8 and 3.9, respectively.

3.8 Solutions Obtained by Means of Superposition

Since the governing differential equation of thin plates (1.2.30) is linear, we can apply the *principle of superposition* to determine lateral deflections of rectangular plates regardless of the boundary and/or loading conditions. This approach permits us to reduce an initially complex plate problem to several simpler ones that can be solved by either Navier's or Lévy's method. Then, the solutions of these less complex problems are added in such a manner that the boundary conditions of the initial problems are satisfied.

Considerable care must be taken, however, to ensure compatibility of the coordinate systems before the superposition of the deflections is attempted. In most cases just a simple translation of the origins of the coordinate systems is required to obtain compatibility between our standard coordinate system (with the origin in the upper left-hand corner, as shown in Fig. 1.1.1a) and that used by Lévy's approach (Fig. 2.3.1). For example, if we intend to use the previously mentioned "standard" coordinate system for a Lévy-type solution, we must replace y with $y - b/2$. If the lateral load and the boundary conditions both have double symmetry, it is advantageous to transfer the origin of the coordinate systems to the center of the plate. In addition, we should also consider that Lévy's solution with all the combinations of boundary conditions (Fig. 3.8.1) does have an additional requirement of symmetry of the lateral loads with respect to the X axis, as shown in Fig. 2.3.2.

In the following, we briefly *outline* the superposition procedure using a quite difficult plate problem as an example. Let us consider a rectangular plate with all edges clamped. This plate is subjected to a uniformly distributed load p_0 . Since our problem has double symmetry, it is advantageous to move the origin of the coordinate system X, Y, Z to the center of the plate.

Although no *direct* solution exists to this problem that could simultaneously satisfy the governing differential equation (1.2.30) and the boundary conditions, $\partial w / \partial n = 0$, we may obtain the equation of the deflected plate surface, $w(x, y)$, by the superposition of the solution of each of the three simply supported plates shown in Fig. 3.8.2. We observe that the deflected plate surfaces for these three simpler plate problems (w_1, w_2, w_3) are already available, having been obtained without too much difficulty. In this case, the application of the principle of superposition requires four steps.

First, we determine the equation of the deflected plate surface, w_1 , for plate 1, which represents a simply supported rectangular plate subjected to uniformly distributed load p_0 . For this purpose we can use Eq. (2.2.11) in a slightly modified

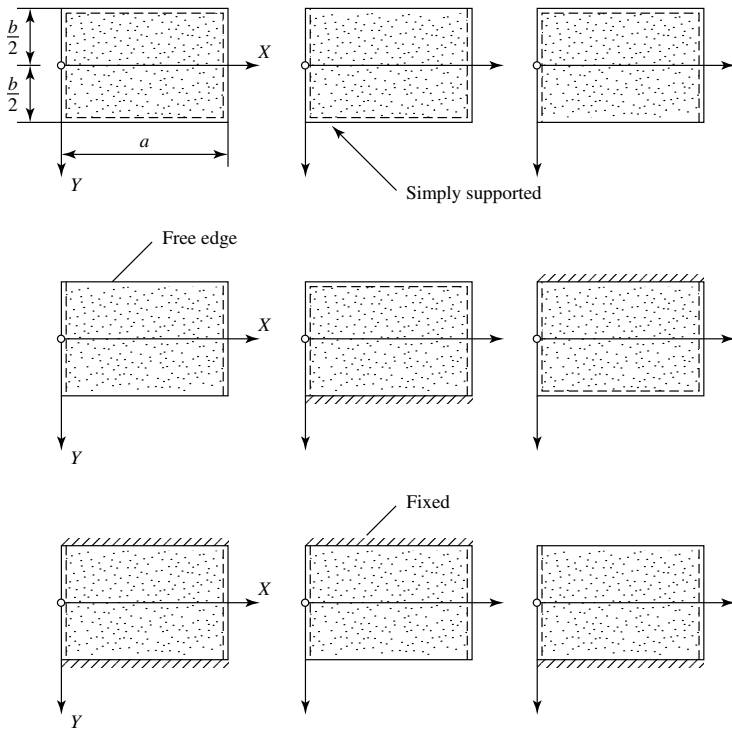


Figure 3.8.1 Boundary conditions for Lévy's solution.

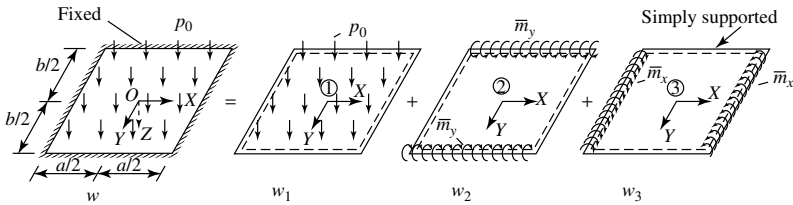


Figure 3.8.2 Graphical representation of principle of superposition.

form, since we have now b instead of $2a$ as plate dimension in the Y direction and, in addition, we have moved the origin of the coordinate system to the center of the plate. Thus, we can write

$$w_1(x, y) = \frac{16p_0}{\pi^6 D} \sum_{m=1}^{\infty} \sum_{n=1}^{\infty} \frac{\sin[m\pi(x + a/2)/a] \sin[n\pi(y + b/2)/b]}{mn[(m^2/a^2) + (n^2/b^2)]^2}. \quad (3.8.1)$$

Next, we obtain the deflected plate surface, w_2 , for plate 2, which is, again, a simply supported plate, but this time the plate is subjected to an edge moment \bar{m}_y . This problem has already been treated in the previous section. Consequently, we may use Eq. (3.7.17) after the required coordinate transformation.

The third step is similar to the second. The equation of the deflected plate surface, w_3 , for plate 3 is, again, obtained from the modified form of Eq. (3.7.17). This modification is carried out in two installments. First, we replace x with Y , a with b and α_m with β_m . Next, we transfer the origin of the coordinate system to the center of the plate, as discussed in the step first of this superposition procedure.

In the fourth step, for a set of m, n values, we fulfill the boundary conditions of the initial plate problem, which are

$$\left(\frac{\partial w_1}{\partial x} + \frac{\partial w_2}{\partial x} + \frac{\partial w_3}{\partial x} = 0 \right)_{x=\pm a/2}, \quad (3.8.2)$$

$$\left(\frac{\partial w_1}{\partial y} + \frac{\partial w_2}{\partial y} + \frac{\partial w_3}{\partial y} = 0 \right)_{y=\pm b/2}. \quad (3.8.3)$$

This gives us two[†] equations, from which the unknown coefficients Y_m and X_m can be calculated. Since all these infinite series converge fast, we need to consider only few terms.

Finally, we can write the solution of our initial plate problem in the form

$$w(x, y) = w_1(x, y) + w_2(x, y) + w_3(x, y). \quad (3.8.4)$$

The lengthy details of the above *outlined* solution can be found in Refs. [3.8.1–3.8.6]. They are, however, too involved to be handled here.

A similar approach can be taken if we have to deal with free (instead of fixed) edges. The reader finds sufficient details concerning such a computational technique in Ref. [3.8.6]. In addition, a noteworthy application of the principle of superposition is given in Ref. [3.8.7], which treats a cantilever plate. At the same time, this paper serves as an example regarding the complexity of such a solution.

Summary. In the hands of competent research engineers, the superposition technique is a very powerful tool to obtain classical solutions to various difficult plate problems that can serve as a benchmark for approximate and numerical analyses. The reader should not be misled, however, by the seemingly simple principle of this computational method (as outlined above), since the mathematical manipulations required to obtain the solution is, in most cases, very lengthy and involved. Furthermore, the final result appears to be quite cumbersome for practical use. As always, some help concerning the lengthy mathematical manipulations can be obtained by using one of the “symbolic mathematics” programs listed in Refs. [A.1.18–A.1.21].

ILLUSTRATIVE EXAMPLE

Let us obtain an analytical solution of the plate problem shown in Fig. 3.8.3 using the superposition technique. This plate has one simple supported edge. The other three edges are fixed.

[†] Two equations are sufficient because of the prevailing double symmetry.

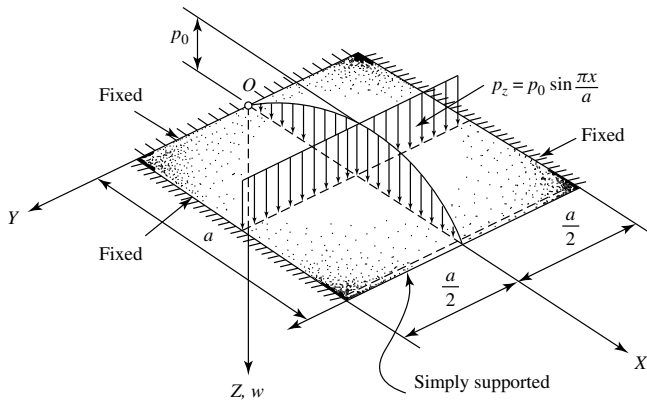
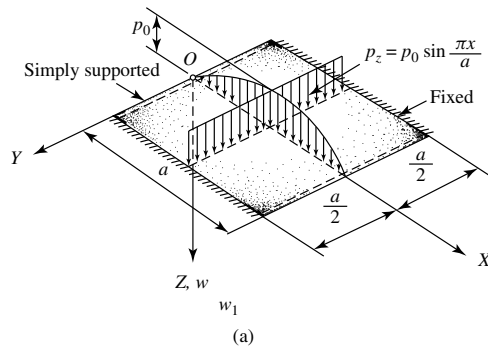
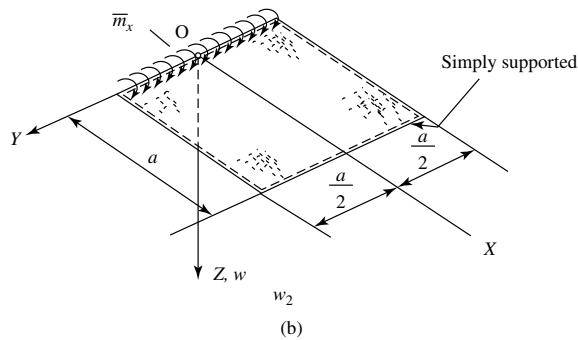


Figure 3.8.3 Plate with three edges fixed and one simply supported.



(a)



(b)

Figure 3.8.4 Superposition of two simpler plate problems.

We begin our computation by reducing this initially complex plate problem to two lesser complex ones for which we have already developed solutions. That is, Eq. (2.3.35) defines the deflected surface w_1 of the plate shown in Fig. 3.8.4a, and Eq. (3.7.15) represents the solution w_2 of the simply supported plate subjected to \bar{m}_x edge moments as illustrated in Fig. 3.8.4b. For the sake of simplicity, in this example we are using only one term in both equations.

The unknown constant X_1 in Eq. (3.7.15) will be determined from the new boundary condition, which requires that the slope of the deflected plate surface becomes zero at the edge $x = 0$. Consequently,

$$\left(\frac{\partial w}{\partial x}\right)_{x=0} = \left(\frac{\partial w_1}{\partial x} + \frac{\partial w_2}{\partial x}\right)_{x=0} = 0. \quad (3.8.5)$$

Since we have elected to use the coordinate system of Lévy's approach (Fig. 2.3.2), the origin of our "standard" coordinate system, used in obtaining Eq. (3.7.15), must be transferred to be compatible with the new coordinate system. This is accomplished by replacing y with $y + b/2$ in Eq. (3.7.15). Consequently, the new form of Eq. (3.7.15) is

$$w_2(x, y) = \frac{1}{2D} \frac{X_1}{\beta_1^2 \sinh \beta_1 a} \left[\beta_1 x \cosh \beta_1 (a - x) - \beta_1 a \frac{\sinh \beta_1 x}{\sinh \beta_1 a} \right] \times \sin \beta_1 \left(\frac{b}{2} + y \right), \quad (3.8.6)$$

where $\beta_1 = \pi/b$. Furthermore, we observe that

$$\sin \frac{\pi}{b} \left(\frac{b}{2} + y \right) = \sin \frac{\pi}{2} \cos \frac{\pi y}{b}. \quad (3.8.7)$$

Thus, the first derivative of w_2 with respect to x at $x = 0$ is

$$\left(\frac{\partial w_2}{\partial x}\right)_{x=0} = X_1 F_2 \sin \beta_1 y, \quad (3.8.8)$$

where

$$F_2 = \frac{1}{2D\beta_1} \left(\coth \beta_1 a - \frac{\beta_1 a}{\sinh^2 \beta_1 a} \right). \quad (3.8.9)$$

Next, we determine the first derivative of w_2 with respect to x at $x = 0$. This gives

$$\left(\frac{\partial w_1}{\partial x}\right)_{x=0} = \frac{p_0 a^3}{\pi^3 D} F_1, \quad (3.8.10)$$

where

$$F_1 = 1 + \frac{\sinh \alpha_1}{\alpha_1 + \cosh \alpha_1 \sin \alpha_1} \left(\frac{\pi y}{a} \right) \sinh \frac{\pi x}{a} - \frac{\alpha_1 \cosh \alpha_1 + \sinh \alpha_1}{\alpha_1 + \cosh \alpha_1 \sin \alpha_1} \cosh \frac{\pi y}{a} \quad (3.8.11)$$

and $\alpha_1 = \pi/2$. Substitution of Eqs. (3.8.8) and (3.8.9) into the boundary condition yields

$$\frac{p_0 a^3}{\pi^3 D} F_1 + X_1 F_2 \sin \beta_1 y = 0, \quad (3.8.12)$$

from which

$$X_1 = - \frac{(p_0 a^3 / \pi^3 D) F_1}{(\sin \beta_1 y) F_2}. \quad (3.8.13)$$

This is substituted into Eq. (3.7.15). Finally, we can write the solution of our initial problem as $w = w_1 + w_2$.

References and Bibliography

- [3.8.1] HENKY, H., *Der Spannungszustand in rechteckigen Platten*, doctoral dissertation, TH München, München, Germany, 1913.
- [3.8.2] TIMOSHENKO, S., and WOINOWSKY-KRIEGER, S., *Theory of Plates and Shells*, 2nd ed., McGraw-Hill Book Company, New York, 1959.
- [3.8.3] BOOBNOV, I. G., *Theory of Ship Structures*, Vol. 2., St. Petersburg, Russia, 1914.
- [3.8.4] L'HERMITE, R., *Résistance des Matériaux*, Dunond, Paris, 1954.
- [3.8.5] GIRKMANN, K., *Flächentragwerke*, 6th ed., Springer-Verlag, Wien, 1963.
- [3.8.6] MCFARLAND, D., et al., *Plate Analysis*, Spartan Books, New York, 1972.
- [3.8.7] CHANG, F. -V., "Bending of a Cantilever Rectangular Plate Loaded Discontinuously," *Appl. Math. Mech.*, 2 (1981), 403–410.

3.9 Continuous Plates

a. Introduction. Rectangular plates that are continuous over one or more intermediate supports are of considerable practical interest, as illustrated in the Introduction of this book. Unfortunately, their classical analysis—with the exception of the simplest cases—is quite cumbersome. Consequently, numerical or engineering methods are used almost exclusively in the praxis to obtain usable approximate solutions of these important plate problems in an economical way. In spite of the mathematical difficulties involved in the classical analysis of continuous plates, we would like to outline some procedures that can be followed by research engineers who seek exact solutions to specific continuous plate problems. As often mentioned in this book, the main purpose of obtaining mathematically exact solutions is to provide a benchmark against which other, less exact, methods can be judged.

In this section, we treat only continuous plates with rigid intermediate supports; that is, the plate has zero lateral deflections at the supports. Furthermore, we assume that the supports do not prevent rotations of the plate. It is noted that there are cases when the supporting beams are relatively flexible; thus, the deflections of the plate along the supports can no longer be neglected. Although this situation can be best handled with numerical methods, the reader will find examples for the classical solution of such a problem in Refs. [3.9.1] and [3.9.2].

Continuous plate problems are externally statically indeterminate. As in the case of other statically indeterminate structures, the classical methods used in the analysis of continuous plates fall into two distinct categories: force and deformation methods. Following either approach, the continuous plate is subdivided along the intermediate supports into individual, single-span panels. The analysis is based on (1) the equilibrium conditions of the individual panels and (2) the compatibility of displacements at the adjoining edges. In this section, we treat only the force method. The deformation method is discussed in Sec. 12.4 in connection with the *moment distribution* technique as applied to continuous plates.

b. Plates Continuous in One Direction. Let us consider a plate that is simply supported at the edges $y = 0$ and $y = b$ and continuous in the X direction (Fig. 3.9.1).

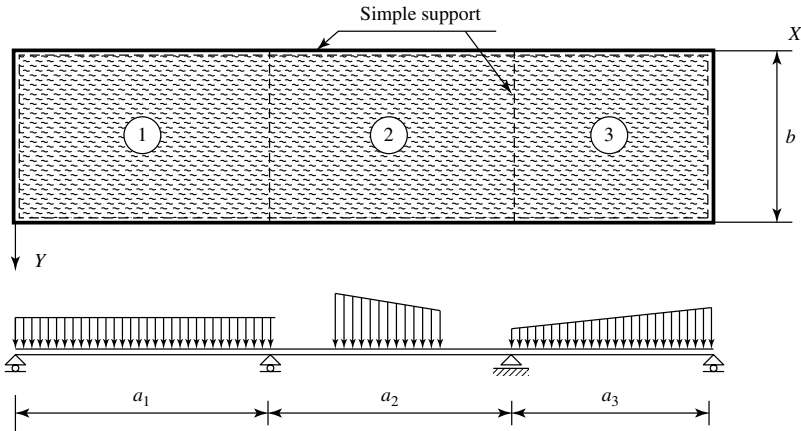


Figure 3.9.1 Plate continuous in one direction.

In applying the force method, we first introduce fictitious hinges above the unyielding intermediate supports. In this way, the redundant external moments are eliminated (Fig. 3.9.2). Similar fictitious hinges should be used at the ends if those supports are fixed. In our further discussion, we assume that the thickness of the plate is constant between supports but the individual panels can have different flexural rigidities. The analysis is based on expressing slope continuity at the adjoining edges, as we do in the classical analysis of continuous beams. This requirement between panels i and $i+1$ at support i (Fig. 3.9.2) gives

$$\left(\frac{\partial w_i}{\partial x} \right)_{x_i=a_i} = \left(\frac{\partial w_{i+1}}{\partial x} \right)_{x_i=0}. \quad (3.9.1)$$

To formulate Eq. (3.9.1), however, it is necessary that we determine the edge slopes of the deflected middle surface of the individual panels i and $i+1$ due to the lateral loads and the rotations produced by the redundant edge moments \bar{m}_{i-1} , \bar{m}_i and \bar{m}_{i+1} .

Applying the principle of superposition,[†] we express the deflected plate surface of the component panel i (Fig. 3.9.2) as

$$w_i = w_{0i} + w_i^I + w_i^{II}, \quad (3.9.2)$$

where w_{0i} is the known Lévy solution of the laterally loaded, simply supported plate expressed in the $(X, Y, Z)_i$ local coordinate system of panel i with its origin at the upper-left corner. This can be written in the form

$$w_{0i} = \sum_{m=1,2,3,\dots} F_{im}(x) \sin \beta_m y, \quad \beta_m = \frac{m\pi}{b}. \quad (3.9.3)$$

[†] See Sec. 3.8.

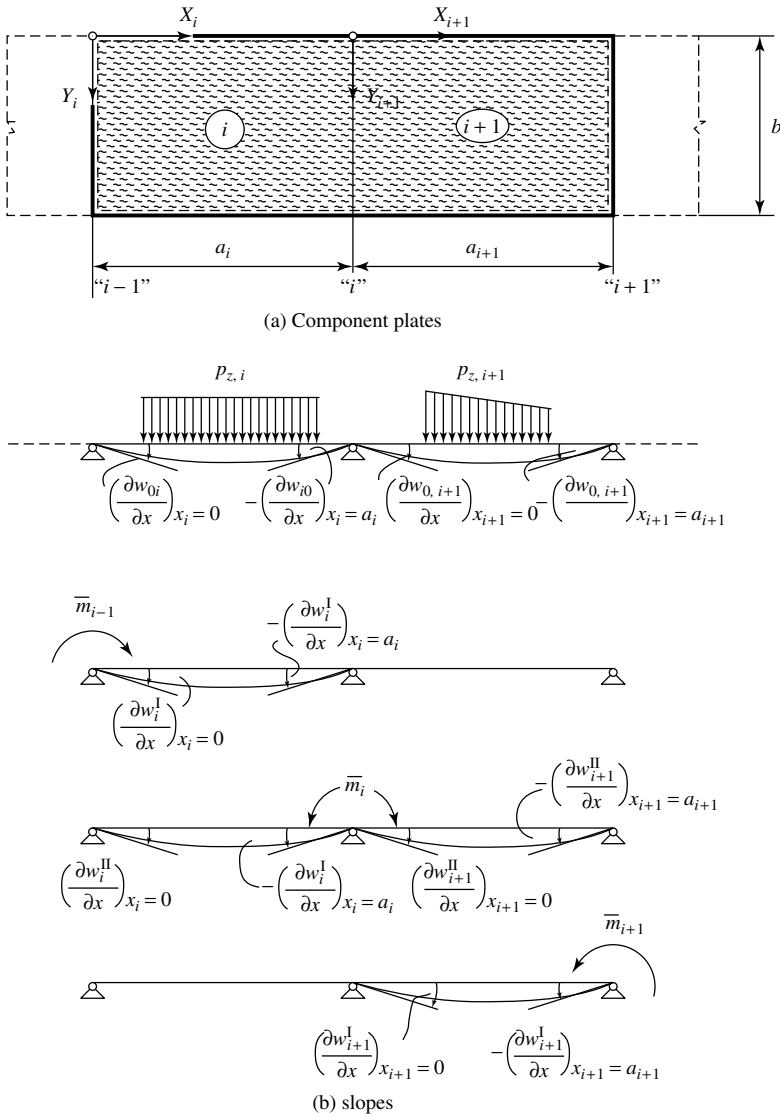


Figure 3.9.2 Deformations of two adjoining panels.

The other two deflection surfaces w_i^I and w_i^{II} represent solutions due to the edge moments \bar{m}_{i-1} and \bar{m}_i acting, again, on the simply supported component panel (i) (Fig. 3.9.2b). Since the Lévy solution usually converges very rapidly, it is sufficient to consider only a few terms in the summation. The slopes of the deflected plate surface w_{0i} along the edges $i-1$ and i can be expressed by the first derivatives of w_{0i} as

$$\left(\frac{\partial w_{0i}}{\partial x} \right)_{x_i=0} = \sum_m \left(\frac{\partial F_{im}}{\partial x} \right)_{x_i=0} \sin \beta_m y \quad (3.9.4)$$

and

$$\left(\frac{\partial w_{0i}}{\partial x} \right)_{x_i=a_i} = \sum_m \left(\frac{\partial F_{im}}{\partial x} \right)_{x_i=a_i} \sin \beta_m y. \quad (3.9.5)$$

The edge moments

$$\bar{m}_{i-1} = \sum_m X_{i-1,m} \sin \beta_m y, \quad \bar{m}_i = \sum_m X_{im} \sin \beta_m y \quad (3.9.6)$$

produce, according to Eq. (3.7.15), the pertinent deflected plate surfaces

$$w_i^I = \frac{1}{2D_i} \sum_m \frac{X_{i-1,m}}{\beta_m^2 \sinh \beta_m a_i} \left[\beta_m x \cosh \beta_m (a_i - x) - \beta_m a_i \frac{\sinh \beta_m x}{\sinh \beta_m a_i} \right] \sin \beta_m y \quad (3.9.7)$$

and

$$w_i^{II} = \frac{1}{2D_i} \sum_m \frac{X_{im}}{\beta_m^2 \sinh \beta_m a_i} \left[\beta_m (a_i - x) \cosh \beta_m x - \beta_m a_i \frac{\sinh \beta_m (x - a_i)}{\sinh \beta_m a_i} \right] \sin \beta_m y. \quad (3.9.8)$$

In these expressions the coefficients $X_{i-1,m}$ and X_{im} are yet unknowns. They will be determined later in the course of the computation using Eq. (3.9.1).

The slopes created by the edge moments \bar{m}_{i-1} and \bar{m}_i are determined by differentiating the corresponding equations of the deflected plate surfaces [Eqs. (3.9.7) and (3.9.8)] with respect to x . Thus, using an abbreviated form, we can write

$$\left[\frac{\partial w_i^I}{\partial x} \right]_{x_i=0} = \sum_m X_{i-1,m} \phi_{xm} \sin \beta_m y, \quad (3.9.9)$$

$$\left[\frac{\partial w_i^I}{\partial x} \right]_{x_i=a_i} = - \sum_m X_{i-1,m} \hat{\phi}_{xm} \sin \beta_m y \quad (3.9.10)$$

and

$$\left[\frac{\partial w_i^{II}}{\partial x} \right]_{x_i=0} = \sum_m X_{im} \hat{\phi}_{xm} \sin \beta_m y, \quad (3.9.11)$$

$$\left[\frac{\partial w_i^{II}}{\partial x} \right]_{x_i=a_i} = - \sum_m X_{im} \phi_{xm} \sin \beta_m y. \quad (3.9.12)$$

We shall treat the component panel $(i+1)$ in a similar way. Now we assume, for the sake of simplicity, that $a_i = a_{i+1} = a$ and $D_i = D_{i+1} = D$. Then, from the requirement of slope continuity at the edge i , as expressed in Eq. (3.9.1), we obtain for a specific m value the so-called *three-moment equation* of continuous plates:

$$X_{i-1,m} + 2X_{im} \frac{\phi_{xm}}{\hat{\phi}_{xm}} + X_{i+1,m} = \frac{1}{\hat{\phi}_{xm}} \left[\left[\frac{dF_{im}}{dx} \right]_{x_i=a_i} - \left[\frac{dF_{i+1}}{dx} \right]_{x_{i+1}=0} \right], \quad (3.9.13)$$

where

$$\phi_{xm} = \frac{1}{2D\beta_m} \left[\coth \beta_m a - \frac{\beta_m a}{\sinh^2 \beta_m a} \right] \quad (3.9.14)$$

and

$$\hat{\phi}_{xm} = \frac{\beta_m a \coth \beta_m a - 1}{2D\beta_m \sinh \beta_m a}. \quad (3.9.15)$$

A similar equation can be written for each immediate support, from which the unknown $X_{i-1,m}$, X_{im} and $X_{i+1,m}$ in the single series expressions of the edge moments can be determined. Needless to say, the amount of the required mathematical operations is very high.

c. Plates Continuous in Two Directions. A procedure analogous to the one used in the foregoing can be applied to plates continuous in both directions (Fig. 3.9.3). For the solution of this complex plate problem Galerkin derived the so-called *seven-moment equation* [3.9.3], which is valid for each intermediate edge. Although it is theoretically possible to also obtain closed-form solutions for plates continuous in two directions [3.9.4, 3.9.5], the required mathematical manipulations become prohibitively extensive. Consequently, the numerical or engineering approximations are used in practice almost exclusively. For this reason, we refer the reader to Parts II

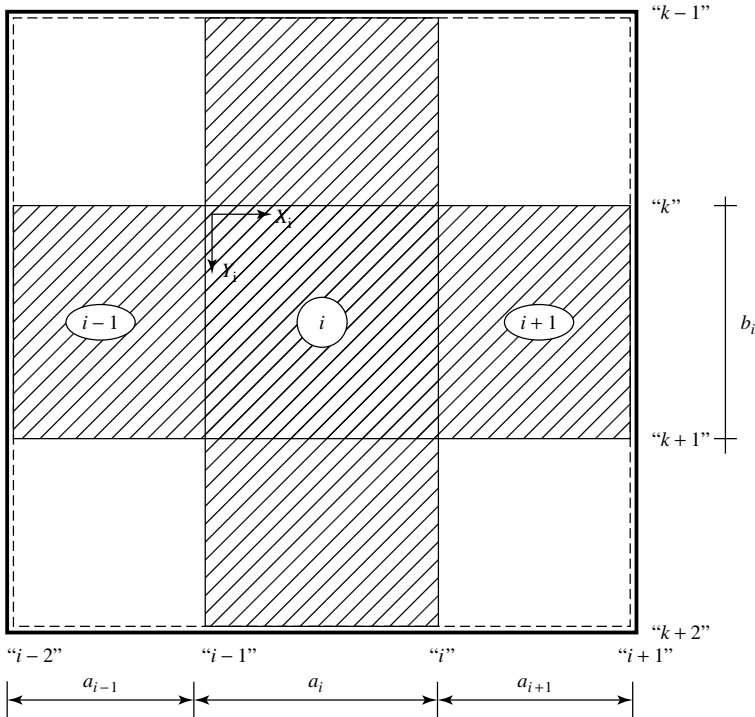


Figure 3.9.3 Plate continuous in two directions.

and IV, where numerous worked examples illustrate the application of these practical approaches. Last but not least, we call the readers' attention to the powerful *WinPlate Primer* computer program,[†] which yields highly accurate results for any continuous plate subjected to various types of lateral forces. For additional readings on analytical solutions of continuous plates, the reader should consult Refs. [3.9.6–3.9.11].

d. Column-Supported Continuous Plates. If large plates are supported by rows of equidistant columns, we speak of *flat plates* (Fig. 3.9.4). We assume that the dimensions of the plate are large in relation to the column spacings and the lateral loads are uniformly distributed over the surface of the whole plate. Additional assumptions are that the cross-sectional areas of the columns are negligibly small and the columns provide unyielding supports without any restraint in plate rotations.

For reinforced-concrete flat plates, the *punching shear* at the face of the supporting columns can be at times critical. For this reason the analyst must always consult the current *Reinforced-Concrete Codes* to obtain the required minimum plate thickness for such constructions. To avoid any punching shear problems and yet maintain a minimum plate thickness at the same time, drop panels around the top of the columns are often used (Fig. 3.9.4). Another solution is increasing the size of the columns near the top to form a mushroom-shaped column capital, as shown in Fig. 3.9.5. For heavy live-loads, flat slabs have long been recognized as the most economical construction. Because of the considerable practical importance of these types of plate structures, we will treat them in more detail in Secs. 10.6 and 12.6.

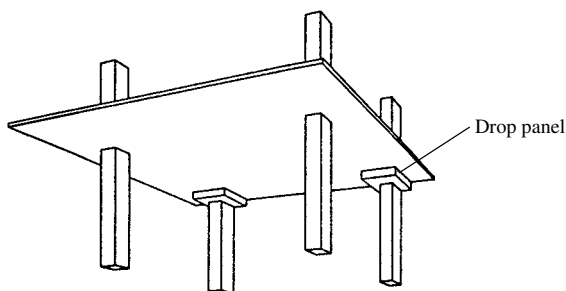


Figure 3.9.4 Flat plate with and without drop panels.

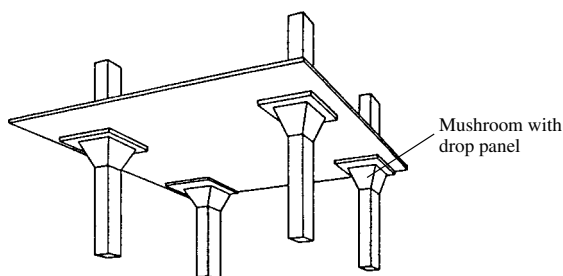


Figure 3.9.5 Flat slab with “mushroom” column heads.

[†] See Sec. A.4.2.

Summary. To obtain closed-form, analytical solutions for the difficult plate problems discussed in this section, an extremely large amount of mathematical manipulations is required. Therefore, we have given only an overview as well as sufficient references covering the presently available computational methods on these subjects. This section is clearly intended for research engineers who want to advance these classical solution techniques. For the practicing engineer, however, we strongly recommend the use of the numerical or approximate methods introduced later in this book.

References and Bibliography

- [3.9.1] MCFARLAND, D., et al., *Analysis of Plates*, Spartan Books, New York, 1972.
- [3.9.2] IHLENBURG, W., "Über elastischen Querträgern durchlaufende Platte," *Der Stahlbau*, 22 (1953), 169.
- [3.9.3] GALERKIN, B. G., *Sobranie socinenij*, Vols. 1 and 2, Acad. Sc. USSR Moscow, 1953.
- [3.9.4] PONOMARJOV, S., et al., *Stress Analysis in Mechanical Engineering* (in Hungarian[†]), Vol. 3, Múszaki Könyvkiadó, Budapest, 1965.
- [3.9.5] WOINOWSKY-KRIEGER, S., "Beiträge zur Theorie der durchlaufenden Platte," *Ing.-Arch.*, 9 (1938), 396.
- [3.9.6] NÁDAI, Á., *Die elastischen Platten*, Springer-Verlag, Berlin, 1925.
- [3.9.7] FLÜGGE, W., *Handbook of Engineering Mechanics*, McGraw-Hill Book Company, New York, 1962.
- [3.9.8] GIRKMANN, K., *Flächentragwerke*, 6th ed., Springer-Verlag, Vienna, 1963.
- [3.9.9] TIMOSHENKO, S., and WOINOWSKY-KRIEGER, S., *Theory of Plates and Shells*, 2nd ed., McGraw-Hill Book Company, New York, 1959.
- [3.9.10] L'HERMITE, R., *Résistance des matériaux*, Dunond, Paris, 1953.
- [3.9.11] BECHERT, H., "Über die Stützenmomente kreuzweise durchlaufender Platten bei vollständiger Lastumordnung," *Die Bautechnik*, 38 (1961), 384–387.

3.10 Summary

Although the material presented in this chapter is of considerable practical importance, a highly mathematically oriented presentation was followed. Development of the mathematical aspects was deliberately pursued for mostly academic reasons. Consequently, all sections of this chapter are written with a reasonably rigorous context to present classical solutions for the plate problems treated. Reasons for such a theoretical approach are manifold. First, the mathematically inclined reader can gain valuable insight into the physical and mathematical aspects of such solution techniques; second, he or she might be inspired to refine or advance such solutions; and finally, mathematically rigorous solutions of the problems presented in this chapter can serve as a benchmark, as mentioned earlier, against which the accuracy of numerical and approximate solutions can be tested.

Again, the classical solutions of these rectangular plates are based mostly on Lévy's approach and to a substantially lesser degree on Navier's method. Both solution techniques are considerably extended by means of the principle of superposition to adapt them to the problems treated here. In the case of circular plates, the solutions are given as the sum of a particular solution and the solution of homogeneous form of the pertinent differential equation, properly expressed in a polar coordinate system.

[†] Translation of the original Russian work.

Unfortunately, the increased sophistication of the plate problems creates increased complexity in their classical analysis and ultimately places a practical limit on their implementation. Therefore, the majority of the classical solutions presented here are far too cumbersome for application in every-day engineering practice. Consequently, the use of numerical and engineering methods, as discussed in Parts II and IV of this book, are not only strongly recommended but should be considered mandatory. Nevertheless, readers with more inquisitive minds should probably compare the results of the here-discussed classical solutions with those obtained numerically and draw their own conclusions with respect to the obtained accuracy and required computational efforts.

Problems[†]

- 3.1.1. Using Illustrative Example I in Sec. 3.1, determine the Winkler modulus k by assuming that $w_{\max} = 0.004$ m, $E = 250$ GPa, $h = 4.0$ mm, $a = 1.0$ m, $b = 1.2$ m and $p_0 = 20$ MPa.
- 3.1.2. Derive the equation of the elastic plate surface of the rectangular plate shown in Fig. 3.1.3 by applying Lévy's method. Assume that the lateral load is uniformly distributed.
- 3.2.1. Determine the bending moments m_r and m_ϕ of the circular plate shown in Fig. 3.2.3. Assume, however, that the variation of plate thickness is $h = cr^2$ and Poisson's ratio is zero.
- 3.2.2. A simply supported rectangular plate is loaded by a concentrated center force P_z and is simultaneously subjected to $n_y = n_0$ uniform edge tension at $y = 0$ and $y = b$. Derive the equation of the deflected plate surface.
- 3.3.1. Redo Problem 3.3.2 by assuming that the lateral load acting on the plate is not a concentrated force but a hydrostatic pressure $p_z = p_0x/a$.
- 3.4.1. Check the accuracy of the *equivalent circular plate* approximation for a simply supported equilateral triangular plate (Fig. 3.4.3.).
- 3.5.1. Determine the bending moments m_r and m_ϕ of a simply supported circular plate with a central hole subjected to a uniformly distributed lateral load.
- 3.5.2. Derive the equation of a deflected plate surface of an annular plate with a center shaft (Fig. 3.5.2). Assume that the plate is subjected to a uniformly distributed lateral load.
- 3.5.3. Assume that a circular plate is subjected to a concentrated moment at its center, as shown in Fig. 3.5.4. Determine the bending moments m_r and m_ϕ if the boundary conditions are simply supported.
- 3.5.4. Redo Problem 3.5.3 by assuming a fixed boundary condition.
- 3.7.1. A simply supported rectangular plate is subjected to an edge moment \overline{m}_y as shown in Fig. 3.7.1a. Determine the bending moments m_x and m_y at the center of the plate.
- 3.7.2. Determine the bending moments m_x and m_y of the plate shown in Fig. 3.7.2.

[†] The first two numbers refer to the corresponding section.

4

Energy and Variational Methods for Solution of Lateral Deflections

4.1 Introduction and Basic Concepts

a. Introduction. Up to this point, we have used—almost exclusively—Newton’s law of equilibrium of forces in the development of differential equations for plates. Yet another approach can also be taken based on Bernoulli’s principle of virtual work, which replaces the force vectors by work and potential energy, both of which are scalar quantities.

The variational methods used in this chapter are among the most powerful analytical tools of mathematical physics for the engineer. Here we deal with the so-called *direct methods* of calculus of variation—commonly called *energy methods*—to obtain analytical solutions for complex plate problems. They comprise a body of *approximate* solution techniques. Although several energy methods have been developed, we restrict ourself to discussion of the most widely used ones in plate analysis. These were introduced by physicists Rayleigh, Ritz, Galerkin, Kantorovich, Lagrange and Trefftz.

There are three reasons why energy methods may be preferable to the more rigorous classical solutions discussed in the foregoing chapters. First, the energy methods are easier, both conceptually and mathematically. Second, they are extremely powerful to obtain reusable analytical solutions, even for plates of arbitrary shape and boundary conditions. Finally, they provide a valuable preparation for understanding the principles of *finite element methods*,[†] which have rapidly become the most dominant numerical methods in structural analysis.

[†] Treated in Sec. 7.3.

b. Basic Concepts. In the preceding sections, plate problems have been represented by a differential equation (1.2.30) derived from the equilibrium condition of internal and external forces. This differential equation, including the boundary conditions of the problem under consideration, can be solved by either classical or numerical methods. Alternative approaches based on certain energy principles are presented in this and subsequent sections. Although the governing plate equation itself can also be derived from energy considerations [4.1.1], we shall use these methods exclusively for obtaining approximate analytic solutions of various plate problems.

When a structure is subjected to external forces, it deforms. During this deformation, the external forces do certain amounts of work. The work of a force is defined as the scalar product of the force vector \mathbf{P} and the *corresponding* displacement vector \mathbf{s} . This scalar quantity is positive if the direction of these two vectors is the same. When the force remains constant, the work becomes $W = \mathbf{P} \cdot \mathbf{s}$; on the other hand, if the force varies during displacement, the work should be calculated from the definite integral $W = \int_{s_1}^{s_2} P \, ds \cos \alpha$.

During deformation of an elastic body the work of the external forces, W_e , is resisted by the work of the internal forces, W_i . These internal forces are *conservative* forces; that is, after removal of the loads the elastic structure returns to its original position and the work of the internal forces is completely recovered. If we define *energy* as the ability to do work, then the *law of conservation of energy* requires that the total internal work be equal and opposite to the total external work; consequently, we can write

$$\boxed{W_e + W_i = 0.} \quad (4.1.1)$$

There are various types of energies called potential, strain, kinetic, and so on. *Potential* energy is defined as the capability of the force to do work because of its *position*. The potential energy of the internal forces is called *strain energy*, U , which is equal to the negative work of the internal forces ($U = -W_i$). The potential of the external forces, V , is defined as the negative work done by the external forces, which remain unchanged in magnitude, between their initial and final positions. The *total potential* Π of a structural system consists of its strain energy plus the potential of the load:

$$\Pi = U + V. \quad (4.1.2)$$

In the analysis of structures by energy methods, we must distinguish between *real* and *virtual work*. To illustrate the fundamental difference between these two concepts, let us consider an elastic spring of one degree of freedom (DOF), as shown in Fig. 4.1.1a.[†] To maintain the static equilibrium of the system, the load must be applied at a slow rate; otherwise vibrations are produced. Such a loading process results in a gradual buildup in the spring force, as illustrated in Fig. 4.1.1b. The work done by stretching the spring is represented by the area of the triangle OAB ; thus

$$W_i = - \int_0^{x_1} (kx) \, dx = - \frac{kx_1^2}{2} = - \frac{1}{2} P_{i \max} x_{\max}. \quad (4.1.3)$$

[†] In simplified statical and dynamic analysis of structures, plates can be approximated by a single mass-spring system [14.1.2].

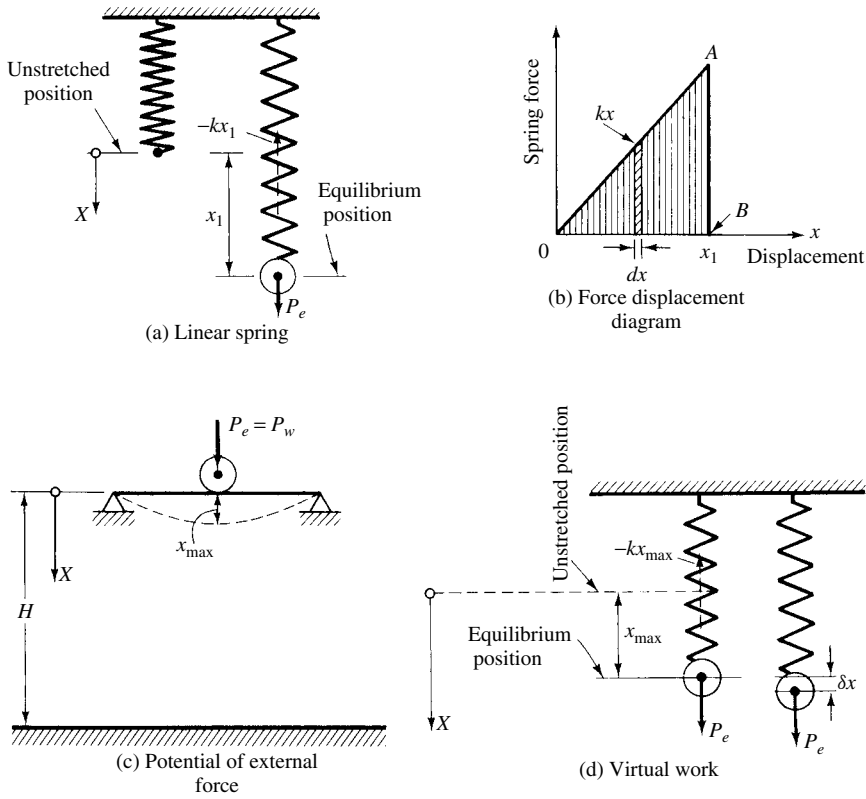


Figure 4.1.1 Illustration of various energy concepts.

Consequently, we can state that the *real internal work* in an elastic system equals half of the product of the final values of the internal forces and corresponding deformations.

Similarly, the real work done by the external force (which has been gradually built up) can be written as

$$W_e = \frac{1}{2} P_e x_{\max}. \quad (4.1.4)$$

Thus, the real work of external forces acting upon an elastic system is half of the product of these forces and the corresponding final displacement components.

To illustrate the concept of potential V of an external force, let us consider the weight of a body, P_w , in the gravitational field of the earth, as shown in Fig. 4.1.1c. If the body is located at datum level H above the earth's surface, then its weight (due to its position) can perform $P_w H$ total work, provided that the supporting structure is removed. Consequently, if the corresponding final deformation of the structure subjected to this load is x_{\max} , the potential of the external force becomes

$$V = -P_e x_{\max}. \quad (4.1.5)$$

The negative sign indicates the loss of potential energy while the force moves from its initial to its final position. It should be noted that in expression (4.1.5) the factor of

$\frac{1}{2}$ is absent, since in computing the potentials of the external forces they are assumed to be kept unchanged during the deformation.

In the case of *virtual* work we deal with an elastic body that is already in equilibrium. Consequently, the body, subjected to the maximum values of static (i.e., slowly piled-up) external forces, has already reached its final state of deformation. Now, we disturb this equilibrium condition by introducing small, arbitrary, but compatible displacements that satisfy the boundary conditions.[†] During these virtual displacements all forces are held constant.

Using, again, the spring-force system with a one-DOF motion (Fig. 4.1.1d) to represent an elastic structure, we introduce the virtual displacement in the form of an incremental[‡] deformation δx ; then the incremental work of the spring becomes

$$\delta W_i = -(kx_{\max})\delta x = -P_{i\max} \delta x. \quad (4.1.6)$$

Similarly, the increment of work done by the external force is

$$\delta W_e = P_e \delta x. \quad (4.1.7)$$

Note that Eqs. (4.1.6) and (4.1.7) do not contain the factor of $\frac{1}{2}$, since we have commenced from the equilibrium conditions and have assumed that during the infinitesimal displacements neither the external nor the internal forces change.

The strain energy, stored in a plate during deformation, is found by integrating (over the entire middle surface) the negative work of internal forces ($U = -W_i$). In general, the strain energy of the plate consists of *bending* (U_b) and *membrane* (U_m) parts, which are

$$U_b = \frac{1}{2} \iint_{(A)} (m_x \kappa_x + m_y \kappa_y + 2m_{xy} \chi) dx dy \quad (4.1.8a)$$

and

$$U_m = \frac{1}{2} \iint_{(A)} (n_x \varepsilon_x + n_y \varepsilon_y + n_{xy} \gamma) dx dy, \quad (4.1.8b)$$

where m_x, m_y, m_{xy} and κ_x, κ_y, χ are the internal force (per unit length) and the corresponding strain components produced by bending, as described in Sec. 1.2. Similarly, n_x, n_y, n_{xy} are the membrane forces (per unit length) and $\varepsilon_x, \varepsilon_y, \gamma$ are the corresponding strains caused by stretching of the plate.[§] In the small-deflection theory of plates, the membrane and bending effects are decoupled; thus, they can be treated separately. Although the transverse shear forces (q_x and q_y) produce additional strain energy, its order of magnitude is very small compared to the bending strain energy; consequently, it is usually neglected.[¶]

[†] As discussed later, there are cases when satisfaction of the geometrical boundary conditions is sufficient.

[‡] The variational symbol δ is used here to express the infinitesimal increment. Since these incremental values are usually represented by the second term of Taylor's series, δ represents a differential operator.

[§] See Secs. 1.1 and 3.3.

[¶] For consideration of the effects of transverse shear deformation, see Secs. 1.5 and 4.7.

Using the definition of potential of external forces, the potential of distributed and concentrated surface forces can be written as

$$V_1 = - \left[\iint_{(A)} (p_x u + p_y v + p_z w) dx dy + \sum_i P_i \Delta_i + \sum_i M_i \theta_i \right], \quad (4.1.9)$$

where u, v, w, Δ_i and θ_i are the corresponding displacement components. A similar expression can be obtained for body forces by replacing the surface integral by a volume integral. In Eq. (4.1.9), however, the potentials of edge forces are not included. These forces have potentials only if compatible boundary displacements are permitted. In such cases, the potentials of edge moments $(\bar{m}_n, \bar{m}_{nt})$ and transverse edge force (\bar{v}_n) can be expressed by

$$V_2 = - \oint \left(\bar{v}_n w + \bar{m}_n \frac{\partial w}{\partial n} + \bar{m}_{nt} \frac{\partial w}{\partial t} \right) ds, \quad (4.1.10)$$

where n and t represent the outward normal and the tangent directions respectively, along the plate boundary, s . Additional expressions for the potential energy of external forces are developed in various sections of this book as need for them arises.

c. Variational Methods. Variational methods are among the most important approximate methods of mathematical physics, used for solution of difficult boundary value problems. In the theory of elasticity the *variational principle*, introduced by Lagrange, is based on the virtual work theorem. The objective of the variational methods is to find from a group of admissible functions those that represent the deflections of the elastic body, pertinent to its stable equilibrium condition, [4.1.2–4.1.7].

The *principle of minimum potential* makes use of the change of the total potential [Eq. (4.1.2)] during arbitrary variation of the deflection. Again, we disturb the equilibrium position of the elastic system by introducing $\delta u, \delta v$ and δw , compatible virtual displacements. The new position $(u + \delta u, v + \delta v, w + \delta w)$ produces an increase in the strain energy stored. The change in the total potential $\delta \Pi$ can be calculated from

$$\delta \Pi = \Pi(u + \delta u, v + \delta v, w + \delta w) - \Pi(u, v, w).$$

Since the equilibrium configuration is represented by those admissible functions that make the total potential of the system minimum, we can write

$$\delta \Pi = \delta U + \delta V = \delta(U + V) = 0. \quad (4.1.11)$$

Components of the *compatible* infinitesimal virtual displacements $(\delta u, \delta v, \delta w)$ must be piecewise continuous functions of x, y and z in the interior domain of the body. In addition, they should satisfy the geometrical boundary condition of the elastic system and be capable of representing all possible displacement patterns. If these admissible displacement functions are chosen properly, very good accuracy can be attained, as is illustrated in this and subsequent sections.

Let us apply Eq. (4.1.11) to the force-spring system shown in Fig. 4.1.1d. The total potential, corresponding to the deflection $x + \delta x$, is

$$\Pi = U + V = (x + \delta x)^2 \frac{k}{2} - P_e(x + \delta x),$$

from which, after neglecting the higher-order quantities such as the square of the virtual displacement δx , we obtain

$$\delta \Pi = kx \delta x - P_e \delta x = (kx - P_e) \delta x = 0;$$

hence

$$kx = P_e.$$

It is evident from this simple case that the virtual work of the internal and external forces also must vanish; hence

$$\boxed{\delta W_i + \delta W_e = 0.} \quad (4.1.12)$$

Equation (4.1.12) represents an alternative formulation of the variational method. We note that if all boundary conditions are satisfied, Eqs. (4.1.11) and (4.1.12) yield the same result. Furthermore, it is of importance to remember that Eqs. (4.1.1) and (4.1.11) represent independent energy principles. That is, while the law of conservation of energy involves real work, the principle of minimum total potential is concerned with virtual work. In addition, the latter deals with the first derivative of the total potential without containing any statement about the total potential itself [4.1.2–4.1.7].

References and Bibliography

- [4.1.1] KIRCHHOFF, G., *Vorlesungen über mathematische Physik, Mechanik*, Teubner, Leipzig, 1876.
- [4.1.2] ARGYRIS, T. H., and KELSEY, S., *Energy Theorems and Structural Analysis*, Butterworth, London, 1960.
- [4.1.3] WASHIZU, K., *Variational Methods in Elasticity and Plasticity*, Pergamon Press, Oxford, 1960.
- [4.1.4] LANGHAAR, H. L., *Energy Methods in Applied Mechanics*, John Wiley & Sons, New York, 1962.
- [4.1.5] MIKHLIN, S. G., *Variational Methods in Mathematical Physics*, McMillan, New York, 1964.
- [4.1.6] SCHECHTER, R. S., *The Variational Methods in Engineering*, McGraw-Hill Book Co., New York, 1967.
- [4.1.7] LANCZOS, C., *The Variational Principles of Mechanics*, 4th ed., University of Toronto Press, Toronto, 1970.
- [4.1.8] RICHARDS, T. H., *Energy Methods in Stress Analysis*, John Wiley & Sons, New York, 1977.
- [4.1.9] REDDY, J. N., *Energy and Variational Methods in Applied Mechanics*, John Wiley & Sons, New York, 1984.
- [4.1.10] DAVIES, G. A. O., *Virtual Work in Structural Analysis*, John Wiley & Sons, New York, 1982.
- [4.1.11] WELLERSTEIN, D. V., *A Variational Approach to Structural Analysis*, John Wiley & Sons, New York, 2001.

4.2 Ritz's Method

a. Ritz Method. An energy method developed by Ritz [4.2.2] applies the principle of minimum potential energy (4.1.11). According to this theorem, as discussed above, of all displacements that satisfy the boundary conditions, those making the total potential energy of the structure a minimum are the sought deflections pertinent to the stable[†] equilibrium conditions.

Let us represent the deflected middle surface in the form of a series [4.2.3]:

$$\begin{aligned} w(x, y) &= c_1 f_1(x, y) + c_2 f_2(x, y) + c_3 f_3(x, y) + \cdots + c_n f_n(x, y) \\ &= \sum_{i=1}^n c_i f_i(x, y), \end{aligned} \quad (4.2.1)$$

where $f_i(x, y)$, $i = 1, 2, 3, \dots, n$, are continuous functions that satisfy *individually* at least the geometrical boundary conditions and are capable of representing the deflected plate surface. The unknown constants $c_1, c_2, c_3, \dots, c_n$ are determined from the minimum potential energy principle; thus

$$\boxed{\frac{\partial \Pi}{\partial c_1} = 0, \quad \frac{\partial \Pi}{\partial c_2} = 0, \dots, \quad \frac{\partial \Pi}{\partial c_n} = 0.} \quad (4.2.2)$$

This minimization procedure yields n simultaneous algebraic equations in the undetermined coefficients $c_1, c_2, c_3, \dots, c_n$, from which the unknown parameters c_i can be calculated. It should be noted that during the partial differentiation all coefficients, except the specific c_i under consideration, are taken constant.

If we substitute into Eq. (4.1.8a) the internal moments expressed in terms of the displacement components,[‡]

$$\begin{aligned} m_x &= -D \left(\frac{\partial^2 w}{\partial x^2} + \nu \frac{\partial^2 w}{\partial y^2} \right), & m_y &= -D \left(\frac{\partial^2 w}{\partial y^2} + \nu \frac{\partial^2 w}{\partial x^2} \right) \\ m_{xy} &= -D(1 - \nu) \frac{\partial^2 w}{\partial x \partial y}, \end{aligned} \quad (4.2.3)$$

and use the following auxiliary functions[§] for expressing the changes of curvature,

$$\kappa_x = -\frac{\partial^2 w}{\partial x^2}, \quad \kappa_y = -\frac{\partial^2 w}{\partial y^2}, \quad \chi = -\frac{\partial^2 w}{\partial x \partial y}, \quad (4.2.4)$$

then the strain energy for the plate in bending can be written as

$$U_b = \frac{1}{2} \iint_{(A)} D \left\{ \left(\frac{\partial^2 w}{\partial x^2} + \frac{\partial^2 w}{\partial y^2} \right)^2 - 2(1 - \nu) \left[\frac{\partial^2 w}{\partial x^2} \frac{\partial^2 w}{\partial y^2} - \left(\frac{\partial^2 w}{\partial x \partial y} \right)^2 \right] \right\} dx dy \quad (4.2.5)$$

[†] Unstable equilibrium conditions are treated in Chapter 16.

[‡] See Sec. 1.2.

[§] See Eq. (1.2.21).

If all edges of the plate are fixed, the second term on the right-hand side of Eq. (4.2.5) becomes zero. Thus, the expression of potential energy becomes simplified:

$$U_b = \frac{1}{2} \iint_{(A)} D \left(\frac{\partial^2 w}{\partial x^2} + \frac{\partial^2 w}{\partial y^2} \right)^2 dx dy. \quad (4.2.6)$$

The same simplification holds for other boundary conditions for rectangular plates, provided that either $w = 0$ or $\partial w / \partial n = 0$, where n represents the outward normal to the boundary.

For the most general case the potential energy of a circular plate, expressed in terms of polar coordinates,[†] has the form

$$U_b = \iint_{(A)} \left\{ \frac{D}{2} \left(\frac{\partial^2 w}{\partial r^2} + \frac{1}{r} \frac{\partial w}{\partial r} + \frac{1}{r^2} \frac{\partial^2 w}{\partial \varphi^2} \right)^2 + 2(1 - \nu) \left[\frac{\partial}{\partial r} \left(\frac{1}{r} \frac{\partial w}{\partial \varphi} \right) \right]^2 \right. \\ \left. - 2(1 - \nu) \frac{\partial^2 w}{\partial r^2} \left(\frac{1}{r} \frac{\partial w}{\partial r} + \frac{1}{r^2} \frac{\partial^2 w}{\partial \varphi^2} \right) \right\} r dr d\varphi, \quad (4.2.7)$$

which, in the case of a fixed edge, becomes

$$U_b = \iint_{(A)} \frac{D}{2} \left(\frac{\partial^2 w}{\partial r^2} + \frac{1}{r} \frac{\partial w}{\partial r} + \frac{1}{r^2} \frac{\partial^2 w}{\partial \varphi^2} \right)^2 r dr d\varphi. \quad (4.2.8)$$

When the deflected middle surface is symmetrical about the center, w is a function of r only. Thus, Eq. (4.2.7) is simplified:

$$U_b = \pi \int_0^{r_0} D \left[\left(\frac{d^2 w}{dr^2} + \frac{1}{r} \frac{dw}{dr} \right)^2 - 2(1 - \nu) \frac{d^2 w}{dr^2} \frac{1}{r} \frac{dw}{dr} \right] r dr. \quad (4.2.9)$$

Similarly, for clamped circular plates with axially symmetric deflections, Eq. (4.2.8) can be written as

$$U_b = \pi \int_0^{r_0} D \left(\frac{d^2 w}{dr^2} + \frac{1}{r} \frac{dw}{dr} \right)^2 r dr, \quad (4.2.10)$$

where r_0 is the radius of the circular plate (Fig. 1.4.1a).

The total potential energy for a rectangular plate subjected to lateral load assumes the following form in a Cartesian coordinate system:

[†] See Sec. 1.4.

$$\Pi = \frac{1}{2} \int_0^a \int_0^b D \left\{ \left(\frac{\partial^2 w}{\partial x^2} + \frac{\partial^2 w}{\partial y^2} \right)^2 - 2(1 - \nu) \times \left[\frac{\partial^2 w}{\partial x^2} \frac{\partial^2 w}{\partial y^2} - \left(\frac{\partial^2 w}{\partial x \partial y} \right)^2 \right] \right\} dx dy - \int_0^a \int_0^b p_z w dx dy. \quad (4.2.11)$$

If the edge forces, including reactions, are able to gain or lose potentials during the deformation, then Eq. (4.2.11) should be augmented by Eq. (4.1.10).

In the case of elastically supported boundaries, the strain energy produced in the edge beam during its deformation is given by

$$U_{b,\text{edge}} = \frac{1}{2} \oint w^2 \rho ds, \quad (4.2.12)$$

where ρ is the spring constant of the edge beam (per unit length), as defined as in Sec. 1.3.

Similarly, if the edge beam is elastically restrained against rotation, the strain energy stored in the edge beam can be written as

$$U_{b,\text{edge}}^* = \frac{1}{2} \oint \left(\frac{\partial w}{\partial n} \right)^2 \rho^* ds, \quad (4.2.13)$$

where ρ^* represents the torsional stiffness (per unit length) of the edge beam.

The membrane part of the strain energy, U_m , is obtained by substituting the pertinent expressions for in-plane strains[†] (ε_x , ε_y and γ) into Eq. (4.1.8b); thus

$$\begin{aligned} U_m &= \frac{1}{2} \iint_{(A)} (n_x \varepsilon_x + n_y \varepsilon_y + n_{xy} \gamma) dx dy \\ &= \frac{1}{2} \iint_{(A)} \left[n_x \frac{\partial u}{\partial x} + n_y \frac{\partial v}{\partial y} + n_{xy} \left(\frac{\partial u}{\partial y} + \frac{\partial v}{\partial x} \right) \right] dx dy. \end{aligned} \quad (4.2.14)$$

This expression can be written in terms of displacement components,

$$\begin{aligned} U_m &= \frac{1}{2} \iint_{(A)} \left\{ \frac{Eh}{1 - \nu^2} \left[\left(\frac{\partial u}{\partial x} + \nu \frac{\partial v}{\partial y} \right) \frac{\partial u}{\partial x} + \left(\frac{\partial v}{\partial y} + \nu \frac{\partial u}{\partial x} \right) \frac{\partial v}{\partial y} \right. \right. \\ &\quad \left. \left. + \frac{1 - \nu}{2} \left(\frac{\partial u}{\partial y} + \frac{\partial v}{\partial x} \right)^2 \right] \right\} dx dy, \end{aligned} \quad (4.2.15)$$

[†] See Sec. 1.6.

or in terms of stress and Airy's stress function,

$$\begin{aligned}
 U_m &= \frac{h}{2E} \iint_{(A)} [(\sigma_x + \sigma_y)^2 - 2(1 + \nu)(\sigma_x \sigma_y - \tau^2)] dx dy \\
 &= \frac{h}{2E} \iint_{(A)} \left\{ \left(\frac{\partial^2 \Phi}{\partial x^2} + \frac{\partial^2 \Phi}{\partial y^2} \right)^2 - 2(1 + \nu) \left[\frac{\partial^2 \Phi}{\partial x^2} \frac{\partial^2 \Phi}{\partial y^2} - \left(\frac{\partial^2 \Phi}{\partial x \partial y} \right)^2 \right] \right\} dx dy.
 \end{aligned} \tag{4.2.16}$$

b. Selection of Proper Shape Functions for Bending. It is evident from the preceding discussion that the solution of plate problems by the Ritz method is reduced to the finding of suitable functions, $f_i(x, y)$, that satisfy the boundary conditions and closely approximate the shape of the actual deflection surface. Satisfaction of the differential equation of the plate (1.2.30) by the assumed series expression (4.2.1), however, is not required. The accuracy of the Ritz method depends considerably on how well the assumed shape functions are capable of describing the actual deflection surface.

Of the several methods available for selecting suitable shape functions, $f_i(x, y)$, for bending analysis of plates by the Ritz method, the use of the trigonometric function and the utilization of beam deflection formulas are considered here. Other alternatives, based on the eigenfunctions of transverse vibrations of beams or on column buckling, are discussed in the subsequent section.

Let us express the lateral displacements in the form of infinite series in which the variables are separated; thus, we can write

$$w(x, y) = \sum_m \sum_n W_{mn} X_m(x) \cdot Y_n(y), \tag{4.2.17}$$

where $X_m(x)$ and $Y_n(y)$ represent the terms in the series expressions that individually satisfy (at least) the geometrical boundary conditions and are functions of either x or y .

In the case of simply supported boundary conditions at $x = 0$ and $x = a$, for instance, a sine series in the form

$$\sum_m W_m \sin \frac{m\pi x}{a} \quad \text{for } m = 1, 2, 3, \dots \tag{4.2.18}$$

can be used advantageously. Similar expressions can be written in the Y direction, provided that the edges at $y = 0$ and $y = b$ are simply supported.

If the edges at $x = 0$ and $x = a$ are fixed, the type of cosine series given as

$$\sum_m \frac{1}{2} W_m \left(1 - \cos \frac{2m\pi x}{a} \right) \quad \text{for } m = 1, 3, 5, \dots \tag{4.2.19}$$

offers a suitable shape function.[†] An analogous expression can also be used in the Y direction, provided that the edges at $y = 0$ and $y = b$ are clamped. Combination of

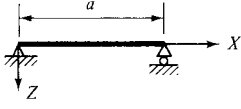
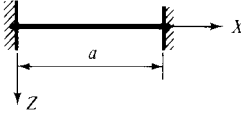
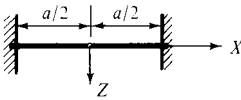
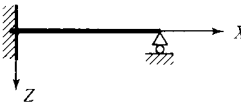
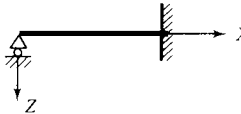
[†] If the origin of the coordinate system coincides with the center of the plate, Eq. (4.2.19) becomes $X_m = \sum_m W_m [1 - (-1)^m \cos(2m\pi x/a)]$ for $m = 1, 3, 5, \dots$

sine and cosine functions in the form

$$w(x, y) = \frac{1}{2} \sum_m \sum_n W_{mn} \sin \frac{m\pi x}{a} \left(1 - \cos \frac{2n\pi y}{b} \right) \quad \text{for } m = 1, 2, 3, \dots; n = 1, 3, 5 \dots \quad (4.2.20)$$

is useful when opposite edges are simply supported and the others are clamped.

Table 4.2.1 Shape Functions for Approximate Analysis of Rectangular Plates

Case	Boundary Conditions	Shape Functions $\sum_m X_m(x)$ in Eq. (4.2.17)
1		$\sum_m X_m = \sum_m \sin \frac{m\pi x}{a}$
2		$\sum_m X_m = \sum_m \frac{1}{2} \left(1 - \cos \frac{2m\pi x}{a} \right)$ for $m = 1, 3, 5, \dots^a$ $\sum_m X_m = \sum_m \sin \frac{\pi x}{a} \sin \frac{m\pi x}{a}$ $\sum_m X_m = \frac{x}{a} \left(\frac{x}{a} - 1 \right)^2 + \sum_m (-1)^m \frac{x^2}{a^2} \left(\frac{x}{a} - 1 \right) - \sum_m \frac{1}{m\pi} \sin \frac{m\pi x}{a}$
3		$\sum_m X_m = \sum_m (a^2 - 4x^2)^2 x^m \quad \text{for } m = 0, 1, 2, 3, \dots$
4		$\sum_m X_m = \frac{x}{a} \left(\frac{x}{a} - 1 \right) \left(\frac{x}{2a} - 1 \right) - \sum_m \frac{1}{m\pi} \sin \frac{m\pi x}{a}$
4a		$\sum_m X_m = \sum_m \frac{x}{2a} \left(\frac{x^2}{a^2} - 1 \right) (-1)^m - \sum_m \frac{1}{m\pi} \sin \frac{m\pi x}{a}$

Note: These expressions for Y_n are analogous; a = span length in X direction. For vibrating beam and column buckling formulas, see Sec. 4.3.

^a An alternate form of this expression is

$$w = W_{11} \left(1 - \cos \frac{2\pi x}{a} \right) \left(1 - \cos \frac{2\pi y}{b} \right) + \left(1 - \cos \frac{2\pi x}{a} \right) \sum_n W_{1n}^* \left(1 - \cos \frac{2n\pi y}{b} \right) + \left(1 - \cos \frac{2\pi y}{b} \right) \sum_m W_{m1}^* \left(1 - \cos \frac{2m\pi x}{a} \right) \quad \text{for } m, n = 2, 3, \dots, r.$$

Trigonometric functions are not the only possible choice for shape functions; they can also be obtained from the static deflection formulas of beams. For this purpose we consider the plane strip (of dy width) as a beam and derive the elastic deflection line by integrating the governing differential equation of beam. Combination of statical deflection formulas with trigonometric series offers another possibility for suitable shape functions. Often-used shape functions for simply supported and fixed boundary conditions are given in Table 4.2.1. These functions are sufficiently general to be able to represent all possible displacement patterns. Additional expressions are given in Sec. 4.4. Although high accuracy can be attained by the Ritz method in the deflection analysis of plates, the accuracy of the internal forces, because second- or third-order derivatives of w are involved in their determination, is usually somewhat reduced.

Summary. Advantages of the Ritz method lie in the relative ease with which complex boundary conditions can be handled. It is a powerful tool yielding high accuracy in the deflection analysis, provided that suitable shape functions are employed. The Ritz method can be used, for example, for plates of various shapes and of variable thicknesses. Since it is essentially an analytical procedure, approximate analytical solutions of complex plate problems can be obtained by this approach. Furthermore, the method merely requires the evaluation of definite integrals of simple functions selected in advance. The crux of the solution of plate problems by this, and by all energy methods, is the selection of the proper shape functions, on which the obtainable accuracy depends. The use of the Ritz method is recommended when computers are not readily available and the solution must be obtained by hand computation. Although the required mathematical operations are relatively simple, they can occasionally be quite lengthy. The Ritz method can be considered as one of the most usable methods of higher analysis for solving complex boundary value problems in mathematical physics.

ILLUSTRATIVE EXAMPLE I

Find the maximum deflection of the simply supported square plate under a lateral load in the form of a triangular prism (Fig. 4.2.1) by the Ritz method.

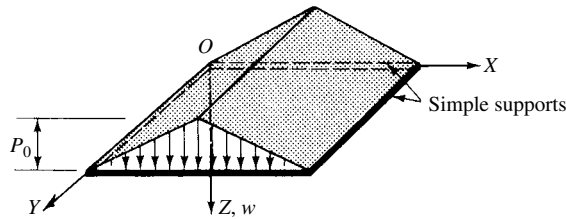


Figure 4.2.1 Simply supported plate loaded in as triangular prism.

Because of the simply supported boundary conditions, a double sine series, restricted to odd numbers, can be used for the deflection surface; thus

$$w(x, y) = \sum_{m=1}^{\infty} \sum_{n=1}^{\infty} W_{mn} \sin \frac{m\pi x}{a} \sin \frac{n\pi y}{a} \quad (4.2.21)$$

for $m, n = 1, 3, 5, \dots$,

where $W_{mn} = c_i$ represents the undetermined constants in Eq. (4.2.1). Mathematical expressions for the lateral load are

$$p_z = \begin{cases} \frac{2p_0x}{a} & \text{for } 0 < x < \frac{a}{2}, \\ 2p_0 - \frac{2p_0x}{a} & \text{for } \frac{a}{2} < x < a. \end{cases} \quad (4.2.22)$$

The potential energy of the lateral load is calculated from Eq. (4.1.9):

$$\begin{aligned} V &= - \iint_{(A)} [p_z(x, y)w(x, y)] dA \\ &= -2 \sum_m \sum_n \int_0^{a/2} \int_0^a \frac{2p_0x}{a} W_{mn} \sin \frac{m\pi x}{a} \sin \frac{n\pi y}{a} dx dy \\ &= - \sum_m \sum_n \frac{8p_0a^2}{m^2n\pi^3} W_{mn} \sin \frac{m\pi}{2}. \end{aligned} \quad (4.2.23)$$

The strain energy, after elimination of all double product terms that do not contribute to the value of U_b , is [Eq. (4.2.6)]:

$$\begin{aligned} U_b &= \frac{D}{2} \int_0^a \int_0^a \sum_m \sum_n \left[W_{mn} \left(\frac{m^2\pi^2}{a^2} + \frac{n^2\pi^2}{a^2} \right) \sin \frac{m\pi x}{a} \sin \frac{n\pi y}{a} \right]^2 dx dy \\ &= \frac{D\pi^4 a^2}{8} \sum_m \sum_n W_{mn}^2 \left(\frac{m^2}{a^2} + \frac{n^2}{a^2} \right)^2. \end{aligned} \quad (4.2.24)$$

Minimization of the total energy (4.2.2),

$$\frac{\partial \Pi}{\partial W_{mn}} = \frac{\partial U_b}{\partial W_{mn}} + \frac{\partial V}{\partial W_{mn}} = 0, \quad (4.2.25)$$

gives, for a specific set of m, n values,

$$\frac{D\pi^4 a^2}{4} W_{mn} \left(\frac{m^2}{a^2} + \frac{n^2}{a^2} \right)^2 - \frac{8p_0a^2}{m^2n\pi^3} \sin \frac{m\pi}{2} = 0; \quad (4.2.26)$$

hence

$$W_{mn} = \frac{32p_0a^4 \sin(m\pi/2)}{m^2n\pi^7 D(m^2 + n^2)^2} \quad (4.2.27)$$

and

$$\begin{aligned} w(x, y) &= \frac{32p_0a^4}{D\pi^7} \sum_{m=1}^{\infty} \sum_{n=1}^{\infty} \frac{\sin(m\pi/2)}{m^2n(m^2 + n^2)^2} \cdot \sin \frac{m\pi x}{a} \sin \frac{n\pi y}{a} \\ &\quad \text{for } m, n = 1, 3, 5, \dots \end{aligned} \quad (4.2.28)$$

The maximum deflection at $x = y = a/2$, using the first three terms ($m = n = 1; m = 1, n = 3; m = 3, n = 1$) of the series expression (4.2.28) is

$$w_{\max} = \frac{7.9289 p_0 a^4}{\pi^7 D} = 0.002625 \frac{p_0 a^4}{D}. \quad (4.2.29)$$

A comparison with the corresponding result of a more exact solution, $w_{\max} = 0.00263 p_0 a^4 / D$, given in Ref. [2], indicates only an insignificant error. This example illustrates the high accuracy obtainable by the Ritz method, provided that proper shape functions are used. Considering more terms, even this relatively small error can be eliminated.

ILLUSTRATIVE EXAMPLE II

Determine the maximum deflection of the clamped rectangular plate shown in Fig. 4.2.2 by the Ritz method. Assume that the plate is subjected to constant lateral load and use $a/b = 1.5$ span ratio.

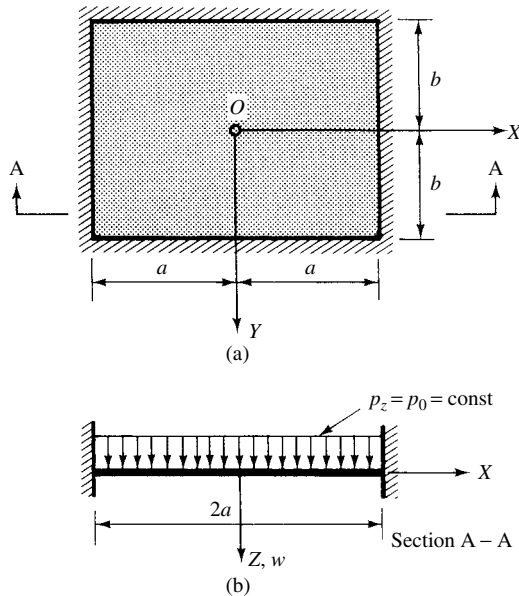


Figure 4.2.2 Rectangular plate with fixed edges.

To utilize the apparent symmetry of the deflected plate surface, we take the coordinate axes through the middle of the plate parallel to the sides. In this case, the deflection given by Eq. (2.5.30) becomes

$$w(x, y) = \sum_m \sum_n \frac{W_{mn}}{4} \left[1 - (-1)^m \cos \frac{m\pi x}{a} \right] \left[1 - (-1)^n \cos \frac{n\pi y}{b} \right]$$

for $m, n = 1, 3, 5, \dots$ (4.2.30)

This series expression satisfies the given boundary conditions

$$\begin{aligned} (w)_{x=\pm a} &= 0, & \left(\frac{\partial w}{\partial x}\right)_{x=\pm a} &= 0; \\ (w)_{y=\pm b} &= 0, & \left(\frac{\partial w}{\partial y}\right)_{y=\pm b} &= 0. \end{aligned} \quad (4.2.31)$$

For the sake of simplicity, let us consider only the first term ($m = n = 1$) in Eq. (4.2.30). Thus, we can write

$$w = \frac{W_{11}}{4} \left(1 + \cos \frac{\pi x}{a}\right) \left(1 + \cos \frac{\pi y}{b}\right). \quad (4.2.31a)$$

Substitution of this expression into Eq. (4.2.6) gives the strain energy of the plate in bending; therefore

$$U_b = \frac{D}{2} \int_{-a}^a \int_{-b}^b (\nabla^2 w)^2 dx dy = \frac{D\pi^4 W_{11}^2}{32} \left(\frac{3b}{a^3} + \frac{3a}{b^3} + \frac{2}{ab}\right). \quad (4.2.32)$$

Similarly, from Eq. (4.1.9), the potential of the external forces is computed:

$$V = -p_0 \int_{-a}^a \int_{-b}^b w(x, y) dx dy = -p_0 W_{11} ab. \quad (4.2.33)$$

Minimization of the total potential,

$$\frac{\partial(U_b + V)}{\partial W_{11}} = 0,$$

yields

$$W_{11} = \frac{16p_0 a^4}{D\pi^4} \frac{1}{3 + 3(a^4/b^4) + 2(a^2/b^2)}. \quad (4.2.34)$$

If $a/b = 1.5$ and $\nu = 0.3$, the maximum deflection at $x = y = 0$ is calculated from Eqs. (4.2.31a) and (4.2.34):

$$w_{\max} = 0.0791 \frac{p_0 a^4}{Eh^3}. \quad (4.2.35)$$

A comparison with the “exact” solution of the problem [2], which is

$$w_{\max} = 0.0760 \frac{p_0 a^4}{Eh^3}, \quad (4.2.36)$$

shows that the approximate solution is accurate enough for most practical purposes. By considering more terms in the series representation of the deflections, a more accurate solution can be obtained.

References and Bibliography

- [4.2.1] KIRCHHOFF, G., *Vorlesungen über mathematische Physik, Mechanik*, B. G. Teubner, Leipzig, 1876.
- [4.2.2] RITZ, W., "Über eine neue Methode zur Lösung gewisser Variationsprobleme der mathematischen Physik," *J. f. Reine u. Angew. Math.*, 135 (1908), 1–61.
- [4.2.3] RITZ, W., *Oeuvres complètes*, Gauthier-Villars, Paris, 1913.
- [4.2.4] HOFF, H. J., *The Analysis of Structures Based on the Minimal Principles and Principle of Virtual Displacements*, John Wiley & Sons, New York, 1956.
- [4.2.5] BERGER, E. R., "Ein Minimalprinzip zur Auflösung der Plattengleichung," *Österr. Ing.-Arch.*, 7 (1953), 39–49.
- [4.2.6] MORLEY, L. S. D., "The Approximate Solution of Plate Problems," *Proc. 9th Int. Congr. Appl. Mech., Brussels*, VI (1956), 22–29.
- [4.2.7] KANTOROVICH, L. V., "Some Remarks on Ritz's Method" (in Russian), *Trudy vysshego voennomorstogo inzhenerno-stroitel'nogo uchilishcha*, Leningrad, No. 3 (1941).
- [4.2.8] LEIBENZON, L. S., *Variatsionnye metody resheniia radach teorii uprugosti (Variational Methods in the Theory of Elasticity)*, Gos. Izd-vo Tekhniko-Teoret. Lit-rv. Moscow, 1943.
- [4.2.9] KRYLOV, N. M., "Sur la solution approchée des problèmes de la physique mathématique et de la science d'ingenieur," *Bull. Acad. Sci.*, URSS, 7 (1930), 1089–1114.
- [4.2.10] ÖDMAN, S. T. A., "Studies of Boundary Value Problems," Pt. I. *Medd.*, No. 20, Swedish Cement and Concrete Research Institute, Royal Institute of Technology, Stockholm, 1953.
- [4.2.11] GIRKMANN, K., and TUNGL, E., "Näherungsweise Berechnung eingespannter Rechteckplatten," *Österr. Bauzeitschr.*, 8 (1953), 47–53.
- [4.2.12] PICKETT, G., "Solution of Rectangular Clamped Plate with Lateral Load by Generalized Energy Method," *J. Appl. Mech.* (Dec. 1939), A–168–170.
- [4.2.13] IGUCHI, S., "Die Knickung der vierseitig eingespannten rechteckigen Platte durch Schubkräfte," *Proc. Phys. Math. Soc. Jpn.*, 20 (Oct. 1938), 814–832.
- [4.2.14] WEINSTEIN, A., "On a Minimal Problem in the Theory of Elasticity," *J. London Math. Soc.*, 10 (1935), 184–192.

4.3 Galerkin's Method and Its Variant by Vlasov

a. Galerkin's Method. The variational principle defined in Sec. 4.1 was reformulated by Galerkin [4.3.1, 4.3.2], who further generalized and simplified the virtual work principle. Galerkin's method can be applied successfully to such diverse types of problems as small- and large-deflection theories, linear and nonlinear vibration and stability problems of plates and shells, provided that differential equations of the problem under investigation have already been determined. Although the mathematical theory behind Galerkin's method is quite complex [4.3.3], its physical interpretation is relatively simple.

We assume that the structural system is in equilibrium. Consequently, the sum of all external and internal forces is zero. The equilibrium condition of an infinitesimal *element* is represented by the pertinent differential equations

$$\begin{aligned}\mathcal{L}_1(u, v, w) - p_x &= 0, \\ \mathcal{L}_2(u, v, w) - p_y &= 0, \\ \mathcal{L}_3(u, v, w) - p_z &= 0,\end{aligned}\tag{4.3.1}$$

which describe the equilibrium of all forces in the X , Y and Z directions, respectively. In Eq. (4.3.1), \mathcal{L}_1 , \mathcal{L}_2 and \mathcal{L}_3 denote differential operators operating on the

displacement functions, while p_x , p_y and p_z are external forces. The equilibrium of the structural system is obtained by integrating these differential equations (4.3.1) over the entire structure.

Let us express the small arbitrary variations of the displacement functions by δu , δv and δw . Although the displacement components are interrelated, their *arbitrary variations are not interrelated*. The *virtual work* of the external and internal forces [Eq. (4.1.12)],

$$\delta W_1 + \delta W_e = \delta(W_1 + W_e) = 0, \quad (4.3.2)$$

is obtained directly from the differential equations of the equilibrium without determining the actual potential energy of the system. Thus, we can write

$$\begin{aligned} \iiint_{(V)} [\mathcal{L}_1(u, v, w) - p_x](\delta u) dV &= 0, \\ \iiint_{(V)} [\mathcal{L}_2(u, v, w) - p_y](\delta v) dV &= 0, \\ \iiint_{(V)} [\mathcal{L}_3(u, v, w) - p_z](\delta w) dV &= 0. \end{aligned} \quad (4.3.3)$$

In a rigorous sense, these variational equations are valid only if the displacement functions u , v and w are the exact solutions of the problem under investigation. As in the case of the Ritz method, we replace the exact solutions for displacements by approximate expressions in the form

$$u = \sum_{i=1}^m a_i \xi_i(x, y, z), \quad v = \sum_{i=1}^n b_i \eta_i(x, y, z), \quad w = \sum_{i=1}^r c_i \zeta_i(x, y, z), \quad (4.3.4)$$

where $\xi_i(x, y, z)$, $\eta_i(x, y, z)$ and $\zeta_i(x, y, z)$ are functions that satisfy all prescribed boundary conditions and a_i , b_i and c_i are undetermined constants. Furthermore, it is required that these displacement functions (4.3.4) should have at least the same order derivatives as called for by the differential operators in Eq. (4.3.3).

Although differential equations are used in the variational equations (4.3.3), it is not required that the assumed approximate displacements satisfy Eq. (4.3.1). Expressing the small arbitrary variations of the displacements by

$$\delta u = \sum_{i=1}^m \xi_i(x, y, z) \delta a_i, \quad \delta v = \sum_{i=1}^n \eta_i(x, y, z) \delta b_i, \quad \delta w = \sum_{i=1}^r \zeta_i(x, y, z) \delta c_i, \quad (4.3.5)$$

the validity of Eq. (4.3.3) is maintained, even for approximate solutions of the displacement functions, provided that the variation of the displacement is carried out

term by term. Thus, the substitution of Eq. (4.3.5) into Eq. (4.3.3) results in

$$\begin{aligned} \sum_{i=1}^m \delta a_i \iiint_{(V)} [\mathcal{L}_1(u, v, w) - p_x] \xi_i(x, y, z) dV &= 0, \\ \sum_{i=1}^n \delta b_i \iiint_{(V)} [\mathcal{L}_2(u, v, w) - p_y] \eta_i(x, y, z) dV &= 0, \\ \sum_{i=1}^r \delta c_i \iiint_{(V)} [\mathcal{L}_3(u, v, w) - p_z] \zeta_i(x, y, z) dV &= 0. \end{aligned} \quad (4.3.6)$$

These equations have to be satisfied for *any small* variations of δu_i , δv_i and δw_i . Thus, the variations of the expansion coefficients δa_i , δb_i , δc_i are arbitrary and not interrelated. This provides $m + n + r$ equations,

$$\begin{aligned} \iiint_{(V)} [\mathcal{L}_1(u, v, w) - p_x] \xi_i(x, y, z) dV &= 0, \\ \iiint_{(V)} [\mathcal{L}_2(u, v, w) - p_z] \eta_i(x, y, z) dV &= 0, \\ \iiint_{(V)} [\mathcal{L}_3(u, v, w) - p_z] \zeta_i(x, y, z) dV &= 0. \end{aligned} \quad (4.3.6a)$$

for the computation of $m + n + r$ unknown coefficients a_i , b_i and c_i .

It should be noted that the differential operators, $\mathcal{L}(\cdot)$, act on the entire series expressions of the displacement components [Eq. (4.3.4)], which in turn are multiplied by the individual terms of functions ξ_i , η_i and ζ_i resulting in simple analytic expressions. By integrating these expressions over the entire structural system, a set of coupled algebraic equations for the undetermined coefficients (a_i , b_i and c_i) is obtained.

In particular, let us investigate the approximate solution of plate bending by Galerkin's method. We select[†] a complete set of independent, continuous functions capable of representing the lateral deflections

$$w(x, y) = \sum_{i=1}^n c_i f_i(x, y). \quad (4.3.7)$$

Each term of this expression must satisfy all boundary conditions of the problem but not necessarily the governing differential equation of the plate (1.2.30). Since the

[†] In selection of suitable shape functions, generally the methods described in Sec. 4.3 are applicable, but with more restrictions. Here we require the satisfaction of the geometrical as well as the statical boundary conditions.

derivation of Eq. (1.2.30) is based on the equilibrium of the internal and external forces in the Z direction, the total work performed by all these forces during a small virtual δw displacement can be expressed by

$$\boxed{\iint_{(A)} [D \nabla^2 \nabla^2 w - p_z(x, y)] (\delta w) dx dy = 0.} \quad (4.3.8)$$

This equation represents the basic *variational equation of plate bending*. Substitution of the series expression of the lateral displacements (4.3.7) into this equation gives

$$\sum_{i=1}^n \delta c_i \iint_{(A)} [D \nabla^2 \nabla^2 w(x, y) - p_z(x, y)] f_i(x, y) dx dy = 0. \quad (4.3.9)$$

Since Eq. (4.3.9) must be satisfied for any values of δc_i it follows that

$$\begin{aligned} \iint_{(A)} (D \nabla^2 \nabla^2 w - p_z) f_1(x, y) dx dy &= 0, \\ \iint_{(A)} (D \nabla^2 \nabla^2 w - p_z) f_2(x, y) dx dy &= 0, \\ &\vdots \\ \iint_{(A)} (D \nabla^2 \nabla^2 w - p_z) f_n(x, y) dx dy &= 0. \end{aligned} \quad (4.3.10)$$

After substituting Eq. (4.3.7) into Eq. (4.3.10), we evaluate the integrals over the entire surface of the plate. In this way, again, the solution of the differential equation of the plate (1.2.30) is reduced to the evaluation of definite integrals of simple functions, selected in advance. From the resulting linear equations the undetermined coefficients ($c_1, c_2, c_3, \dots, c_n$) can easily be calculated.

Since the virtual work of internal forces is obtained directly from the differential equations, without determining the strain energy, Galerkin's method appears to be more general than that of Ritz. The use of Galerkin's method is particularly recommended for solution of differential equations with variable coefficients.

Accuracy of the method depends considerably on the selected shape function, which is the case for all energy approaches. Solutions can also be obtained by satisfying merely the geometrical boundary conditions of the problem by the assumed series expression of the deflected plate surface. In such a case, the edge forces may create additional virtual work, which must be considered. The solution, however, converges much faster when all the boundary conditions are satisfied.

The Galerkin method can be extended for the solution of simply supported plates of general shape [4.3.23]. To express the geometry of the plate in a simple form, however, the use of natural coordinates is recommended. Applying Vlasov's technique,

this approach can be extended to other than simply supported boundary conditions. In this case, however, the required computations “by longhand” can be quite extensive.

b. Vlasov's Method. An important version of Galerkin's method, which can be used for approximate solution of difficult plate and shell problems, was developed by Vlasov [4.3.4, 4.3.5].

Let us express, again, the lateral deflections by infinite series:

$$w(x, y) = \sum_m \sum_n W_{mn} \phi_{mn}(x, y). \quad (4.3.11)$$

Similarly, we may express the lateral loads as

$$p_z(x, y) = \sum_m \sum_n P_{mn} \varphi_{mn}(x, y). \quad (4.3.12)$$

Furthermore, let us represent $\phi_{mn}(x, y)$ and $\varphi_{mn}(x, y)$ as the product of two functions, each of which depends just on a single argument; thus

$$\phi_{mn} = X_m(x) \cdot Y_n(y), \quad (4.3.13)$$

and

$$\varphi_{mn} = X_m(x) \cdot Y_n(y). \quad (4.3.14)$$

Separation of the variables reduces the variational problem to the selection of two linearly independent sets of functions $X_m(x)$ and $Y_m(y)$ that satisfy all boundary conditions. For these functions, Vlasov [4.3.4] used the eigenfunctions of vibrating beams, with boundary conditions similar to those of the plate.

The free vibrations of a single-span[†] beam (of uniform cross section) is described by the partial differential equation

$$\frac{\partial^4 w(x, t)}{\partial x^4} = -\frac{\bar{m}}{EI} \frac{\partial^2 w(x, t)}{\partial t^2}, \quad (4.3.15)$$

where $w(x, t)$ is the time-dependent (t) lateral deflection and \bar{m} is the mass per unit length. We assume the solution of Eq. (4.3.15) in the form

$$w(x, t) = X(x) \sin \omega t, \quad (4.3.16)$$

where ω is the circular frequency[‡] of the free vibration. Substitution of (4.3.16) into (4.3.15) gives

$$\frac{d^4 X(x)}{dx^4} = \frac{\bar{m}\omega^2}{EI} X(x). \quad (4.3.17)$$

[†] For vibrations of structural systems, see Chapters 14 and 15.

[‡] For the definition, see Sec. 14.1.

Upon introduction of the symbol

$$\frac{\lambda^4}{l^4} = \frac{\overline{m}\omega^2}{EI}, \quad (4.3.18)$$

Eq. (4.3.17) becomes

$$X^{IV} = \frac{\lambda^4}{l^4} X, \quad (4.3.19)$$

where λ is the shape parameter and l is the span length.

The general solution of Eq. (4.3.19) is

$$X(x) = C_1 \sin \frac{\lambda x}{l} + C_2 \cos \frac{\lambda x}{l} + C_3 \sinh \frac{\lambda x}{l} + C_4 \cosh \frac{\lambda x}{l}. \quad (4.3.20)$$

The constants C_1 , C_2 , C_3 and C_4 are determined from the boundary conditions, while λ is a root of the characteristic equation. This equation is derived by equating the determinants of the homogeneous boundary equations to zero. Eigenfunctions $X_m(x)$, pertinent to the m th mode of vibration, are obtained by substituting λ_m into Eq. (4.3.20); thus

$$X_m(x) = C_1 \sin \frac{\lambda_m x}{l} + C_2 \cos \frac{\lambda_m x}{l} + C_3 \sinh \frac{\lambda_m x}{l} + C_4 \cosh \frac{\lambda_m x}{l}. \quad (4.3.21)$$

Table 4.3.1 contains expressions of these eigenfunctions for various boundary conditions.

The eigenfunctions and their derivatives satisfy certain important mathematical relations. Let $X_m(x)$ and $X_n(x)$ be any two eigenfunctions of the vibrating beam corresponding to ω_m and ω_n circular frequencies, respectively. Then, for different modes ($m \neq n$), the integral of the following products is zero:

$$\int_0^l X_m(x) X_n(x) dx = 0 \quad \text{and} \quad \int_0^l X_m''(x) X_n''(x) dx = 0. \quad (4.3.22)$$






Thus, the eigenfunctions and their second derivatives are said to be *orthogonal* for some boundary conditions.[†] The same holds for their fourth-order derivatives, while the desirable property $\int_0^l X_m'' X_n dx = 0$, which facilitates the solution, is slightly violated.

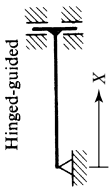

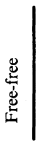

Since the eigenfunctions are orthogonal, we may utilize another useful property common to all orthogonal functions; that is, we may expand the arbitrary load $p_z(x, y)$ in terms of the eigenfunctions. The constants P_{mn} in Eq. (4.3.12) can be expressed in terms of eigenfunctions $X_m(x)$ and $Y_m(y)$ by means of

$$P_{mn} = \frac{\int_0^a \int_0^b p_z(x, y) X_m(x) Y_n(y) dx dy}{\int_0^a \int_0^b X_m^2(x) Y_n^2(y) dx dy}. \quad (4.3.23)$$

[†] Strictly speaking, these functions are only *quasi-orthogonal*. These orthogonality conditions, however, do not hold for free and guided or elastically supported edges.

Table 4.3.1 Frequencies and Eigenfunctions for Uniform Beams

Type	Boundary Conditions	Frequency Equation	Eigenfunction, $X_m(x)$	Roots of Frequency Equation, λ_m
Clamped-clamped 	$X(0) = X'(0) = 0$ $X(l) = X'(l) = 0$	$\cos \lambda \cosh \lambda = 1$	$J\left(\frac{\lambda_m x}{l}\right) - \frac{J(\lambda_m)}{H(\lambda_m)} H\left(\frac{\lambda_m x}{l}\right)$	$\lambda_1 = 4.7300$ $\lambda_2 = 7.8532$ $\lambda_3 = 10.9956$ $\lambda_4 = 14.1372$ For m large, $\lambda_m \approx (2m + 1)\pi/2$
Clamped-hinged 	$X(0) = X'(0) = 0$ $X(l) = X''(l) = 0$	$\tan \lambda = \tanh \lambda$	$J\left(\frac{\lambda_m x}{l}\right) - \frac{J(\lambda_m)}{H(\lambda_m)} H\left(\frac{\lambda_m x}{l}\right)$	$\lambda_1 = 3.9266$ $\lambda_2 = 7.0686$ $\lambda_3 = 10.2102$ $\lambda_4 = 13.3518$ For m large, $\lambda_m \approx (4m + 1)\pi/4$
Clamped-free 	$X(0) = X'(0) = 0$ $X''(l) = X'''(l) = 0$	$\cos \lambda \cosh \lambda = -1$	$J\left(\frac{\lambda_m x}{l}\right) - \frac{G(\lambda_m)}{F(\lambda_m)} H\left(\frac{\lambda_m x}{l}\right)$	$\lambda_1 = 1.8751$ $\lambda_2 = 4.6941$ $\lambda_3 = 7.8548$ $\lambda_4 = 10.9955$ For m large, $\lambda_m \approx (2m - 1)\pi/2$
Clamped-guided 	$X(0) = X'(0) = 0$ $X'(l) = X'''(l) = 0$	$\tan \lambda = -\tanh \lambda$	$J\left(\frac{\lambda_m x}{l}\right) - \frac{F(\lambda_m)}{J(\lambda_m)} H\left(\frac{\lambda_m x}{l}\right)$	$\lambda_1 = 2.3650$ $\lambda_2 = 5.4978$ $\lambda_3 = 8.6394$ $\lambda_4 = 11.7810$ For m large, $\lambda_m \approx (4m - 1)\pi/4$
Hinged-hinged 	$X(0) = X''(0) = 0$ $X(l) = X''(l) = 0$	$\sin \lambda = 0$	$\sin \frac{m\pi x}{l}$	$\lambda_m = m\pi$

	$X(0) = X''(0) = 0$ $X'(0) = X'''(0) = 0$	$\cos \lambda = 0$	$\sin \frac{(2m-1)\pi x}{2l}$	$\lambda_m \approx (2m-1)\pi/2$
	$X'(0) = X'''(0) = 0$ $X'(l) = X'''(l) = 0$	$\sin \lambda = 0$	$\cos \frac{m\pi x}{l}$	$\lambda_m = m\pi$
	$X''(0) = X'''(0) = 0$ $X''(l) = X'''(l) = 0$	$\cos \lambda \cosh \lambda = 1$	$G\left(\frac{\lambda_m x}{l}\right) - \frac{J(\lambda_m)}{H(\lambda_m)} F\left(\frac{\lambda_m x}{l}\right)$ $G\left(\frac{\lambda_m x}{l}\right) - \frac{G(\lambda_m)}{F(\lambda_m)} F\left(\frac{\lambda_m x}{l}\right)$	Same as for clamped-clamped beam Same as for clamped-hinged beam
	$X''(0) = X'''(0) = 0$ $X(l) = X'(l) = 0$	$\tan \lambda = \tanh \lambda$	$G\left(\frac{\lambda_m x}{l}\right) - \frac{J(\lambda_m)}{H(\lambda_m)} F\left(\frac{\lambda_m x}{l}\right)$ $G\left(\frac{\lambda_m x}{l}\right) - \frac{H(\lambda_m)}{F(\lambda_m)} F\left(\frac{\lambda_m x}{l}\right)$	Same as for clamped-guided beam

Notes:

(1) The circular frequency is

$$\omega_m = \frac{\lambda_m}{l^2} \sqrt{\frac{EI}{\bar{m}}}$$

where

EI = bending stiffness

\bar{m} = mass per unit length

l = length of beam

(2) Notation used in expressions for eigenfunctions:

$$F(u) = \sinh u + \sin u$$

$$G(u) = \cosh u + \cos u$$

$$H(u) = \sinh u - \sin u$$

$$J(u) = \cosh u - \cos u$$

$$u = \frac{\lambda_m x}{l}$$

Source: After Ref. [4.3.15].

Let us now express the plate deflection by eigenfunctions in the form

$$w = \sum_m \sum_n W_{mn} \phi_{mn}(x, y) = \sum_m \sum_n W_{mn} X_m(x) Y_n(y) \quad (4.3.24)$$

and use a similar expression for the lateral load [Eq. (4.3.12)]. Then, after substitution of Eqs. (4.3.11) and (4.3.12) into the variational equation of the plate problem (4.3.8), we obtain

$$D \sum_m \sum_n W_{mn} \int_0^a \int_0^b \phi_{ik} \nabla^4 \phi_{mn} dx dy - \sum_m \sum_n P_{mn} \int_0^a \int_0^b \phi_{mn} \phi_{ik} dx dy = 0. \quad (4.3.25)$$

Let us analyze separately the integral terms in this equation. If we use $\phi_{mn} = \phi_{mn} = X_m(x) \cdot Y_n(y)$, then the first integral term in Eq. (4.3.25) can be written as

$$\begin{aligned} \int_0^a \int_0^b \phi_{ik} \nabla^4 \phi_{mn} dx dy &= \int_0^a \int_0^b [X_m^{IV}(x) Y_n(y) X_i(x) Y_k(y) \\ &\quad + 2X_m''(x) Y_n''(y) X_i(x) Y_k(y) \\ &\quad + Y_n^{IV}(y) X_m(x) X_i(x) Y_k(y)] dx dy. \end{aligned} \quad (4.3.26)$$

By neglecting the terms with nonidentical subscripts mi and nk , the error induced is zero or negligible. If we introduce the notation.

$$\begin{aligned} I_1 &= \int_0^a X_m^{IV}(x) X_m(x) dx, & I_2 &= \int_0^b Y_n(y) Y_n(y) dy, \\ I_3 &= \int_0^a X_m''(x) X_m(x) dx, & I_4 &= \int_0^b Y_n''(y) Y_n(y) dy, \\ I_5 &= \int_0^b Y_n^{IV}(y) Y_n(y) dy, & I_6 &= \int_0^a X_m(x) X_m(x) dx, \end{aligned} \quad (4.3.27)$$

then Eq. (4.3.26) can be written as

$$\int_0^a \int_0^b \phi_{ik} \nabla^4 \phi_{mn} dx dy = I_1 I_2 + 2I_3 I_4 + I_5 I_6. \quad (4.3.28)$$

The integrals of the second term in Eq. (4.3.25) are calculated in an analogous manner; thus

$$\int_0^a \int_0^b \phi_{mn} \phi_{ik} dx dy = \int_0^a \int_0^b X_m^2(x) Y_n^2(y) dx dy = I_7 I_8, \quad (4.3.29)$$

where

$$I_7 = \int_0^a X_m^2(x) dx \quad \text{and} \quad I_8 = \int_0^b Y_n^2(y) dy. \quad (4.3.30)$$

Considering a specific set of m, n values, the variational equation of the plate problem can be reduced to

$$DW_{mn}(I_1 I_2 + 2I_3 I_4 + I_5 I_6) - P_{mn} I_7 I_8 = 0. \quad (4.3.31)$$

Therefore, the undetermined expansion coefficients W_{mn} can be calculated from

$$W_{mn} = \frac{P_{mn} I_7 I_8}{(I_1 I_2 + 2I_3 I_4 + I_5 I_6) D}, \quad (4.3.32)$$

which, after substitution of Eq. (4.3.23), becomes,

$$W_{mn} = \frac{\int_0^a \int_0^b p_z(x, y) X_m(x) Y_n(y) dx dy}{(I_1 I_2 + 2I_3 I_4 + I_5 I_6) D}. \quad (4.3.33)$$

In this way, approximate solution of plate bending is reduced to the evaluation of simple definite integrals. Furthermore, the orthogonality (or quasi-orthogonality) of the eigenfunctions reduces the required numerical work significantly. The reader will find usable tables for the eigenfunctions and their derivatives in Refs. [11], [3.1.1], [3.1.4], [4.3.21] and [4.3.22].

A similar approach can be taken with the eigenfunctions of column buckling [4.5.1], the governing differential equation of which is

$$EI \frac{d^4 w}{dx^4} + P \frac{d^2 w}{dx^2} = 0. \quad (4.3.34)$$

Upon introduction of

$$\left(\frac{\lambda}{l}\right)^2 = \frac{P}{EI}, \quad (4.3.35)$$

Eq. (4.3.34) becomes

$$X^{IV} + \left(\frac{\lambda}{l}\right)^2 X'' = 0. \quad (4.3.36)$$

The general solution of Eq. (4.3.36) is

$$X_m = C_1 \sin \frac{\lambda_m x}{l} + C_2 \cos \frac{\lambda_m x}{l} + C_3 \frac{x}{l} + C_4, \quad (4.3.37)$$

where C_1, C_2, C_3 and C_4 represent constants to be found from the boundary conditions of the column, while $\lambda_1, \lambda_2, \lambda_3, \dots$ are the roots of the characteristic equation pertinent to the first, second, third, and so on buckling modes.

A comparison of Eq. (4.3.37) with Eq. (4.3.21) indicates that the eigenfunctions of column buckling are simpler. Consequently, their use may offer considerable advantages in some cases. These functions are also quasi-orthogonal; that is, for $m \neq n$ they satisfy

$$\int_0^l X_m^{IV} X_n dx = 0 \quad \text{and} \quad \int_0^l X_m''' X_n dx = 0, \quad (4.3.38)$$

while

$$\int_0^l X_m X_n dx \neq 0 \quad \text{for } m \neq n. \quad (4.3.39)$$

Again, this violation of the orthogonality requirement (4.3.39) is of negligible order of magnitude.

In the case of orthotropic plates,[†] the eigenfunctions of a vibrating beam may yield better results, provided that the torsional rigidity of the plate is small. On the other hand, if the orthotropic plate has small flexural rigidity in one of the principal directions of orthotropy, the use of the eigenfunctions of column buckling can be more advantageous [24, 4.5.1]. If possible, one should take advantage of the symmetry by moving the origin of the coordinate system to the center of the plate, as shown in Illustrative Example II of Sec. 4.2. In this way the tedious task of calculation of integrals can be mitigated.

Summary. The variational methods introduced in this section are more general than the Ritz method. Consequently, they occupy an important position among the approximate methods for solving static and dynamic plate problems, when classical methods present unsurmountable difficulties. In the final analysis, the problem is reduced to the evaluation of certain definite integrals of simple functions selected in advance. Although these integrals are basically simple, in certain cases, the computation required might be quite lengthy. If possible, advantage should be taken of the symmetry. For the mathematically inclined reader, the use of these methods is highly recommended, especially when computers are not readily available.

The accuracy of variational methods depends considerably on the selection of the shape functions. While variational methods are one of the most recommended computational tools for longhand calculation, they are not suited for automated computer applications. Because of its relative ease in selecting shape functions for almost all boundary conditions encountered in actual practice, Vlasov's method can be considered more universal than the other methods. Further simplification in the numerical computation is due to the quasi-orthogonality of the eigenfunctions of the vibrating beam or those of column buckling.

ILLUSTRATIVE EXAMPLE I

Find an analytical expression by Galerkin's method for the deflection of a uniformly loaded square plate with all edges clamped (Fig. 4.3.1). Use a Cartesian coordinate system with the point of origin located at the upper left-hand corner of the plate.

We select the product of the cosine series given in Eq. (4.2.30) to represent the deflected plate surface; thus

$$w(x, y) = \sum_m \sum_n W_{mn} \frac{1}{4} \left(1 - \cos \frac{2m\pi x}{a} \right) \left(1 - \cos \frac{2n\pi y}{a} \right) \quad \text{for } m, n = 1, 3, 5, \dots, \quad (4.3.40)$$

[†] See Sec. 10.1.

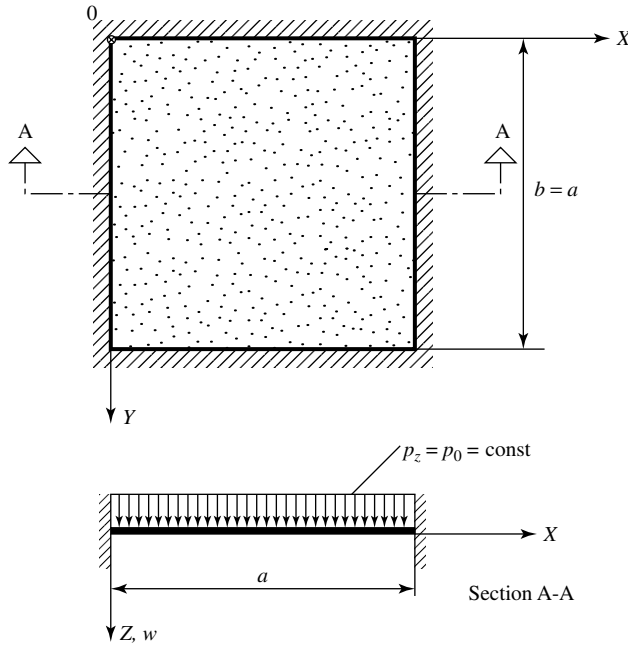


Figure 4.3.1 Clamped square plate.

which satisfies the geometrical boundary conditions

$$w = 0 \quad \text{and} \quad \frac{\partial w}{\partial x} = \frac{\partial w}{\partial y} = 0 \quad (4.3.41)$$

at the edges ($x = 0, a; y = 0, a$).

To simplify the solution, let us consider only the first term ($m = n = 1$) in Eq. (4.3.40). Thus, the variational equation (4.3.9) becomes

$$\int_0^a \int_0^a [DW_{11} \nabla^2 \nabla^2 f_1(x, y) - p_0] f_1(x, y) dx dy = 0, \quad (4.3.42)$$

where

$$f_1 = \frac{1}{4} \left(1 - \cos \frac{2\pi x}{a} \right) \left(1 - \cos \frac{2\pi y}{a} \right). \quad (4.3.43)$$

Substituting (4.3.43) into (4.3.42), the first term becomes

$$\begin{aligned} & W_{11} D \int_0^a \int_0^a [\nabla^2 \nabla^2 f_1(x, y)] f_1(x, y) dx dy \\ &= W_{11} D \int_0^a \int_0^a \left[-\frac{1}{16} \left(\frac{2\pi}{a} \right)^4 \left(1 - \cos \frac{2\pi y}{a} \right) \cos \frac{2\pi x}{a} \right. \end{aligned}$$

$$\begin{aligned}
& + \frac{1}{8} \left(\frac{2\pi}{a} \right)^4 \cos \frac{2\pi x}{a} \cos \frac{2\pi y}{a} \\
& - \frac{1}{16} \left(\frac{2\pi}{a} \right)^4 \left(1 - \cos \frac{2\pi x}{a} \right) \cos \frac{2\pi y}{a} \Bigg] \\
& \quad \times \left(1 - \cos \frac{2\pi x}{a} \right) \left(1 - \cos \frac{2\pi y}{a} \right) dx dy \\
& = W_{11} D \left(\frac{3\pi^4}{4a^2} + \frac{\pi^4}{2a^2} + \frac{3\pi^4}{4a^2} \right) = \frac{2W_{11} D \pi^4}{a^2}. \tag{4.3.44}
\end{aligned}$$

For the second term of Eq. (4.3.42) we obtain

$$\begin{aligned}
p_0 \int_0^a \int_0^a f_1(x, y) dx dy &= \frac{p_0}{4} \int_0^a \int_0^a \left(1 - \cos \frac{2\pi x}{a} \right) \left(1 - \cos \frac{2\pi y}{a} \right) dx dy \\
&= \frac{p_0 a^2}{4}; \tag{4.3.45}
\end{aligned}$$

thus

$$\frac{2W_{11} D \pi^4}{a^2} = \frac{p_0 a^2}{4}; \tag{4.3.46}$$

hence

$$W_{11} = \frac{p_0 a^4}{8D\pi^4}. \tag{4.3.47}$$

To obtain information concerning the accuracy of this solution, let us compare the maximum deflection,

$$(w_{\max})_{x=y=a/2} = \frac{p_0 a^4}{8D\pi^4} = 0.00128 \frac{p_0 a^4}{D}, \tag{4.3.48}$$

with its “exact” value,

$$w_{\max} = 0.00126 \frac{p_0 a^4}{D}, \tag{4.3.49}$$

obtained by a more rigorous approach [2]. Although only one term of the series expression has been used, the error is less than 1.6%.

ILLUSTRATIVE EXAMPLE II

A square plate of side a has simply supported boundary conditions along the edges $x = 0$ and $y = 0$ and is fixed at the other edges (Fig. 4.3.2). The plate is subjected to a uniformly distributed lateral load. Find (1) an approximate expression for the deflected plate surface using Vlasov's method and (2) the maximum deflections.

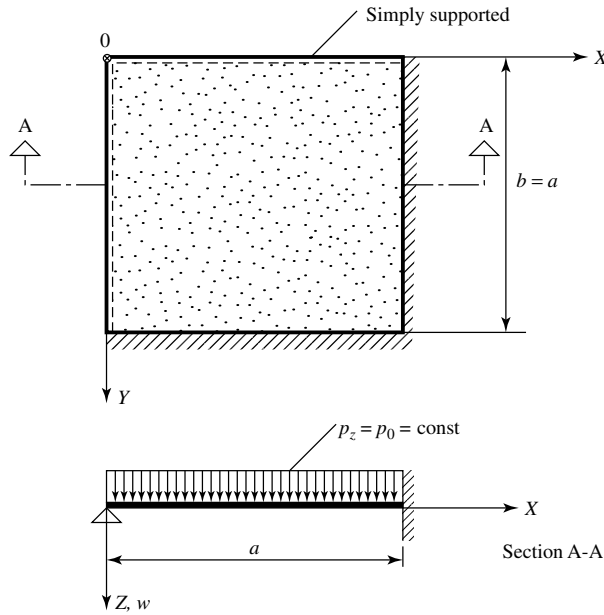


Figure 4.3.2 Square plate with various boundary conditions.

1. The *fundamental functions* of the vibrating beam corresponding to the boundary problem under consideration are given in Table 4.3.1. We express the lateral deflection in the form

$$w(x, y) = \sum_m \sum_n W_{mn} \phi_{mn} = \sum_m \sum_n W_{mn} X_m(x) Y_n(y), \quad (4.3.50)$$

where

$$X_m(x) = \sin \frac{\lambda_m x}{a} - C_m \sinh \frac{\lambda_m x}{a}, \quad (4.3.51)$$

$$Y_n(y) = \sin \frac{\lambda_n y}{a} - C_n \sinh \frac{\lambda_n y}{a} \quad (4.3.52)$$

and

$$C_m = \frac{\sin \lambda_m}{\sinh \lambda_m} \quad \text{and} \quad C_n = \frac{\sin \lambda_n}{\sinh \lambda_n}. \quad (4.3.53)$$

Using only the first term ($m = 1, n = 1$), Eq. (4.3.50) can be written as

$$w = W_{11} X_1(x) Y_1(y) = W_{11} \left(\sin \frac{\lambda_1 x}{a} - C_1 \sinh \frac{\lambda_1 x}{a} \right) \times \left(\sin \frac{\lambda_1 y}{a} - C_1 \sinh \frac{\lambda_1 y}{a} \right), \quad (4.3.54)$$

where

$$C_1 = \frac{\sin \lambda_1}{\sinh \lambda_1} = \frac{\sin 3.9266}{\sinh 3.9266} = -0.0279. \quad (4.3.55)$$

The unknown expansion coefficient W_{11} is calculated from Eq. (4.3.33):

$$W_{11} = \frac{p_0 \int_0^a \int_0^a X_1 Y_1 dx dy}{(I_1 I_2 + 2 I_3 I_4 + I_5 I_6) D}, \quad (4.3.56)$$

where I_1, I_2, \dots, I_6 denote the definite integrals given in Eq. (4.3.27). Substituting Eq. (4.3.54) into the numerator of the right-hand side of Eq. (4.3.56), we obtain

$$\begin{aligned} p_0 \left(\int_0^a X_1(x) dx \right)^2 &= p_0 \left\{ \left[-\frac{a}{\lambda_1} \cos \frac{\lambda_1 x}{a} - \frac{a C_1}{\lambda_1} \cosh \frac{\lambda_1 x}{a} \right]_0^a \right\}^2 \\ &= 0.3695 a^2 p_0. \end{aligned} \quad (4.3.57)$$

The evaluation of the definite integrals I_1, I_2, \dots, I_6 yields

$$\begin{aligned} I_1 &= I_5 = \int_0^a X_1^{\text{IV}} X_1 dx = \left(\frac{\lambda_1}{a} \right)^4 \int_0^a \left(\sin \frac{\lambda_1 x}{a} - C_1 \sinh \frac{\lambda_1 x}{a} \right)^2 dx \\ &= \frac{237.72}{a^4} (0.4364 - 0.0001 + 0.0634) a = \frac{237.72}{a^4} 0.4997 a, \\ I_2 &= I_6 = \int_0^a X_1^2 dx = \int_0^a \left(\sin \frac{\lambda_1 x}{a} - C_1 \sinh \frac{\lambda_1 x}{a} \right)^2 dx = 0.4997 a, \\ I_3 &= I_4 = \int_0^a X_1'' X_1 dx = \left(\frac{\lambda_1}{a} \right)^2 \int_0^a \left(-\sin^2 \frac{\lambda_1 x}{a} + C_1^2 \sinh^2 \frac{\lambda_1 x}{a} \right) dx \\ &= \left(\frac{\lambda_1}{a} \right)^2 \left[-\frac{a}{2} + \frac{a}{4\lambda_1} \sin 2\lambda_1 + C_1^2 \left(\frac{a}{4\lambda_1} \sinh 2\lambda_1 - \frac{a}{2} \right) \right] = -\frac{5.751}{a}. \end{aligned} \quad (4.3.58)$$

Substitution of Eqs. (4.3.57) and (4.3.58) into Eq. (4.3.56) gives

$$W_{11} = \frac{p_0 \times 0.3695 a^4}{D(59.3827 + 66.148 + 59.3718)} = 0.00198 \frac{p_0 a^4}{D}. \quad (4.3.59)$$

Thus, an approximate expression for the deflected middle surface (4.3.50) is

$$\begin{aligned} w(x, y) &= 0.00198 \frac{p_0 a^4}{D} \left(\sin \frac{3.9266x}{a} + 0.0279 \sinh \frac{3.9266x}{a} \right) \\ &\quad \times \left(\sin \frac{3.9266y}{a} + 0.0279 \sinh \frac{3.9266y}{a} \right). \end{aligned} \quad (4.3.60)$$

2. The maximum deflection occurs where the slope ($\partial w/\partial x$ and $\partial w/\partial y$) is zero. The location of the zero slope was found to be at $x = y = 0.3826a$. The deflection of the plate at this point is

$$w_{\max} = 0.002233 \frac{p_0 a^4}{D}. \quad (4.3.61)$$

A comparison of this value with the more rigorous solution [2] indicates an error of 3.3%. If required, the results can be improved by taking more terms in the series expansion of the deflected plate surface (4.3.50) into account. Evaluation of the definite integrals, however, becomes increasingly tedious.

References and Bibliography

- [4.3.1] GALERKIN, B. G., "Series-Solutions of Some Cases of Equilibrium of Elastic Beams and Plates" (in Russian), *Vestnik, Inshenemov.*, 1 (1915), 879–903.
- [4.3.2] GALERKIN, B. G., *Thin Elastic Plates* (in Russian), Gostrojizdat, Leningrad, 1933.
- [4.3.3] RAFAL'SON, Z. KH., "On the Question of Solution of the Biharmonic Equation" (in Russian), *Dokl. Akad. Nauk*, 64, No. 6 (1949), 799–802.
- [4.3.4] VLASOV, V. Z., *Stroitel'naia Mekhanika Tonkostekhnich Prostranstvenich System (Struct. Mech. of Thin-Walled Three-dimen. Systems)*, Gos. Izd-vo Stroit, Lyt.-ry, Moscow, 1949.
- [4.3.5] VLASOV, V. Z., "Some New Problems on Shells and Thin Structures," *Nat. Adv. Comm. Aeron., NACA Tech. Memo*, No. 1204 (March 1949).
- [4.3.6] GALERKIN, B. G., "State of Stress in Bending of Rectangular Plate, According to the Theory of Thick Plates and the Theory of Thin Plates" (in Russian), *Trudy Lenigradskogo Inst. Sooruzhenii*, No. 2 (1935), pp. 3–21.
- [4.3.7] GUZMAN, A. M., and LUISONI, C. J., "Elastizidad y plastizidad de placas oblicuas," *Univ. Nac. La Plata Publ. Fac. Cienc. Fisicomat.*, (2)4, Separ. 1, Rev. Dept. Constr. (June 1953), 452–493.
- [4.3.8] FUNK, P., *Variationsrechnung und ihre Anwendung in Physik und Technik*, 2nd ed., Springer-Verlag, Berlin, 1970.
- [4.3.9] LIUSTERNIK, L. A., and SOBOLEV, V. J., *Elements of Functional Analysis*, F. Ungar Publishing Co., New York, 1961.
- [4.3.10] REISSNER, E., "On a Variational Theorem in Elasticity," *J. Math. Phys.*, 29, No. 2 (July 1950), 90–95.
- [4.3.11] DUNCAN, W. J., "Galerkin's Method in Mechanics and Differential Equations," *Aero. Res. Council (Great Britain), Rep. and Memo.*, No. 1798 (H.M.S.O.) (Aug. 1937).
- [4.3.12] REISSNER, E., and STEIN, M., "Torsion and Transverse Bending of Cantilever Plates," *Nat. Adv. Com. Aeron., National Advisory Committee for Aeronautics NACA Tech. Note*, No. 2639, June 1951.
- [4.3.13] BEREZIN, I. S., and ZHIDKOV, N. P., *Computing Methods*, Vol. II, Pergamon Press, Elmsford, New York, 1965.
- [4.3.14] COURANT, R., and HILBERT, D., *Methoden der mathematischen Physik*, Vol. II, 2nd ed., Springer-Verlag, Berlin, 1965.
- [4.3.15] FLÜGGE, W. (Ed.), *Handbook of Engineering Mechanics*, McGraw-Hill Book Co., New York, 1962.
- [4.3.16] LARDY, P., "Sur une méthode nouvelle de résolution du problème des dalles rectangulaires encastrees," *Publ. Int. Assoc. Bridge Struct. Eng.*, 13 (1953), 197–220.
- [4.3.17] LANZOS, C., *The Variational Principles of Mechanics*, University of Toronto Press, Toronto, 1964.
- [4.3.18] LANGHAAR, H. L., *Energy Methods in Applied Mechanics*, John Wiley & Sons, New York, 1962.

- [4.3.19] MICHLIN, S. G., *Variational Methods in Mathematical Physics*, Pergamon Press, Elmsford, New York, 1964.[†]
- [4.3.20] LEISSA, A. W., et al., "A Comparison of Approximate Methods for the Solution of Plate Bending Problems," *J. AIAA*, 7, No. 5 (May 1969), 920–927.
- [4.3.21] YOUNG, D., and FELGAR, R. P., "Tables of Characteristic Functions Representing Normal Modes of Vibration of a Beam," Publication No. 4913, University of Texas, Austin, July 1949.
- [4.3.22] FELGAR, R. P., "Formulas for Integrals Containing Characteristic Functions of a Vibrating Beam," Circular 14, Bureau of Engineering Research, University of Texas, Austin, 1950.
- [4.3.23] SAADATPOUR, M. M., and AZHARI, M., "The Galerkin Method for Statik Analysis of Simply Supported Plates of General Shape," *Comp. Struct.*, 69 (1998), 1–9.

4.4 Further Variational and Energy Procedures

Besides the Ritz and Galerkin methods, there are a number of approximate ways of solving variational problems related to boundary value problems of plates. Since due to the space limitation we cannot treat them all here, we confine ourselves to those that are—in our opinion—the most effective ones.

a. Ritz Method Combined with Lagrange Multipliers. This variation of Ritz's method was first proposed by Trefftz [4.4.1, 4.4.2] and further developed by Budiansky and co-workers [4.4.3]. Since it is often difficult to construct a series of assumed functions that satisfies all the prescribed boundary conditions of a plate under investigation, the application of Ritz's method is in many cases unnecessarily restricted. With the help of the so-called Lagrange *multipliers*, however, we can enforce those boundary conditions that are not satisfied by our original assumption

$$w(x, y) = c_1 f_1(x, y) + c_2 f_2(x, y) + \cdots + c_n f_n(x, y). \quad (4.4.1)$$

Let us suppose that this equation satisfies all but k boundary conditions or restraints, which may be expressed in terms of the n unknown of the assumed deflection given by Eq. (4.4.1). Thus, we write

$$\begin{aligned} \phi_1[c_1, c_2, \dots, c_n] &= 0, \\ \phi_2[c_1, c_2, \dots, c_n] &= 0, \\ &\vdots \\ \phi_k[c_1, c_2, \dots, c_n] &= 0. \end{aligned} \quad (4.4.2)$$

The stationary value of the total potential requires that

$$\frac{\partial \Pi}{\partial c_1} \delta c_1 + \frac{\partial \Pi}{\partial c_2} \delta c_2 + \cdots + \frac{\partial \Pi}{\partial c_n} \delta c_n = 0. \quad (4.4.3)$$

[†] The German translation of the Russian original (*Variatsionnye metody v matematicheskii fiziki*) is *Variationsmethode der mathematischen Physik*, Akademie-Verlag, Berlin, 1962.

In addition, if we take the first variation of each of the constraints, we have

$$\begin{aligned}
 \frac{\partial \phi_1}{\partial c_1} \delta c_1 + \frac{\partial \phi_1}{\partial c_2} \delta c_2 + \cdots + \frac{\partial \phi_1}{\partial c_n} \delta c_n &= 0, \\
 \frac{\partial \phi_2}{\partial c_1} \delta c_1 + \frac{\partial \phi_2}{\partial c_2} \delta c_2 + \cdots + \frac{\partial \phi_2}{\partial c_n} \delta c_n &= 0, \\
 &\vdots \\
 \frac{\partial \phi_k}{\partial c_1} \delta c_1 + \frac{\partial \phi_k}{\partial c_2} \delta c_2 + \cdots + \frac{\partial \phi_k}{\partial c_n} \delta c_n &= 0.
 \end{aligned} \tag{4.4.4}$$

Now we multiply the first equation given above by the constant λ_1 and the second one by λ_2 and so on. Then we add the results to Eq. (4.4.3). After rearranging the terms, we obtain

$$\begin{aligned}
 &\left[\frac{\partial \Pi}{\partial c_1} + \frac{\partial \phi_1}{\partial c_1} \lambda_1 + \frac{\partial \phi_2}{\partial c_1} \lambda_2 + \cdots + \frac{\partial \phi_k}{\partial c_1} \lambda_k \right] \delta c_1 \\
 &+ \left[\frac{\partial \Pi}{\partial c_2} + \frac{\partial \phi_1}{\partial c_2} \lambda_1 + \frac{\partial \phi_2}{\partial c_2} \lambda_2 + \cdots + \frac{\partial \phi_k}{\partial c_2} \lambda_k \right] \delta c_2 + \cdots \\
 &+ \left[\frac{\partial \Pi}{\partial c_n} + \frac{\partial \phi_1}{\partial c_n} \lambda_1 + \frac{\partial \phi_2}{\partial c_n} \lambda_2 + \cdots + \frac{\partial \phi_k}{\partial c_n} \lambda_k \right] \delta c_n = 0.
 \end{aligned} \tag{4.4.5}$$

The undetermined constants $\lambda_1, \lambda_2, \dots, \lambda_k$ are called *Lagrange multipliers* [4.4.3]. We can determine the values of these constants by using the following conditions:

$$\begin{aligned}
 \frac{\partial \Pi}{\partial c_1} + \frac{\partial \phi_1}{\partial c_1} \lambda_1 + \frac{\partial \phi_2}{\partial c_1} \lambda_2 + \cdots + \frac{\partial \phi_k}{\partial c_1} \lambda_k &= 0, \\
 \frac{\partial \Pi}{\partial c_2} + \frac{\partial \phi_1}{\partial c_2} \lambda_1 + \frac{\partial \phi_2}{\partial c_2} \lambda_2 + \cdots + \frac{\partial \phi_k}{\partial c_2} \lambda_k &= 0, \\
 &\vdots \\
 \frac{\partial \Pi}{\partial c_n} + \frac{\partial \phi_1}{\partial c_n} \lambda_1 + \frac{\partial \phi_2}{\partial c_n} \lambda_2 + \cdots + \frac{\partial \phi_k}{\partial c_n} \lambda_k &= 0.
 \end{aligned} \tag{4.4.6}$$

Equations (4.4.2) and (4.4.6) form a set of $k + n$ independent equations that we must solve for the unknowns c_1, c_2, \dots, c_n and $\lambda_1, \lambda_2, \dots, \lambda_k$.

These equations may also be generated by defining a so-called *modified total potential* Π^* as

$$\begin{aligned}
 \Pi^* &= \Pi(c_1, c_2, \dots, c_n) + \lambda_1 \phi_1(c_1, c_2, \dots, c_n) \\
 &\quad + \lambda_2 \phi_2(c_1, c_2, \dots, c_n) + \cdots + \lambda_k \phi_k(c_1, c_2, \dots, c_n),
 \end{aligned} \tag{4.4.7}$$

or in another form

$$\Pi^* = \Pi^*(c_1, c_2, \dots, c_n, \lambda_1, \lambda_2, \dots, \lambda_k). \tag{4.4.8}$$

The stationary value of this modified total potential requires that

$$\frac{\partial \Pi^*}{\partial c_1} = 0, \quad \frac{\partial \Pi^*}{\partial c_2} = 0, \dots, \quad \frac{\partial \Pi^*}{\partial c_n} = 0 \quad (4.4.9)$$

and

$$\frac{\partial \Pi^*}{\partial \lambda_1} = 0, \quad \frac{\partial \Pi^*}{\partial \lambda_2} = 0, \dots, \quad \frac{\partial \Pi^*}{\partial \lambda_k} = 0, \quad (4.4.10)$$

from which the unknown coefficients c_i and multipliers λ_i can be computed. A Lagrange multiplier λ_i represents the reaction necessary to maintain the constraint to which is associated.

Unfortunately, the solution criteria, as discussed above, are conceptionally more difficult to understand than those of the Galerkin and Ritz methods. In addition, evaluation of the governing equations (4.4.9) and (4.4.10) requires sufficient mathematical facilities, as shown in Illustrative Example I. It is of interest to note that one can achieve almost the same objectives by the very simple error minimization technique, introduced by Szilard [4.5.2].

b. Kantorovich Method. In order to achieve improved accuracy, Kantorovich introduced a solution procedure [4.4.4] that falls between the exact solution of the plate differential equation (1.2.30) and Galerkin's variational approach. By means of separating the variables, the task of solving the partial differential equation of the plate is reduced to solving an ordinary differential equation of fourth order.

The solution is sought in the form

$$w(x, y) = \phi_1(y) \cdot f_1(x) + \phi_2(y) \cdot f_2(x) + \dots + \phi_n(y) \cdot f_n(x), \quad (4.4.11)$$

where $\phi_1, \phi_2, \dots, \phi_n$ are functions of y alone and satisfy the prescribed boundary conditions of the plate in the Y direction. Such functions may be chosen in different ways, as discussed in the foregoing sections. However, if for the sake of simplicity we would like to limit ourselves only to one term, we may use the pertinent beam equations given in Ref. [A.2.1], for instance, by replacing EI with D . Thus, the simplified form of Eq. (4.4.11) is

$$w(x, y) = \phi_1(y) \cdot f_1(x). \quad (4.4.12)$$

Since the dependence upon y is completely known in $\phi_1(y)$, the y variable can be integrated out of Galerkin's variational equation (4.3.8) which, in this case, takes the form

$$\int_0^b [C_1 f^{IV} + C_2 f'' + C_3 f + C_4] \phi_1(y) dy = 0, \quad (4.4.13)$$

where C_1, C_2, C_3 and C_4 are known constants and primes denote differentiation with respect to x . The expression in brackets represents an ordinary nonhomogeneous differential equation whose general solution is

$$f(x) = A_1 \cosh \alpha x \cos \beta x + A_2 \cosh \alpha x \sin \beta x \\ + B_1 \sinh \alpha x \sin \beta x + B_2 \sinh \alpha x \cos \beta x + f_0(x), \quad (4.4.14)$$

where $f_0(x)$ is the particular solution of this differential equation. The constants A_1, A_2, B_1 and B_2 must be determined from the boundary conditions of the plate in the X direction. If the plate problem is symmetrical in the X direction, we can discard the unsymmetrical terms in Eq. (4.4.14) and use the simplified expression

$$f(x) = A_1 \cosh \alpha x \cos \beta x + B \sinh \alpha x \sin \beta x + f_0(x). \quad (4.4.15)$$

As shown above, this method requires reasonably good assumptions of the displacement field only in one independent variable and then generates an ordinary differential equation in the remaining independent variable. After solving this differential equation, we have a fairly reliable assumption in that direction. This improves the overall accuracy of Galerkin's method. Although, in our discussion, we have selected the Y direction for the assumed shape function, there is no reason why the X direction cannot be used for this purpose. Generally speaking, one selects the direction for the assumed function depending on the availability of a suitable shape function. The other independent variable should be reserved for boundary conditions, such as free-edges, that are more difficult to treat.

c. Principle of Conservation of Energy. When the plate is acted upon by *conservative* forces, $p_z(x, y)$, which have potential energy, the conservation-of-energy equation is

$$W_e + W_i = 0. \quad (4.4.16)$$

This equation states that the sum of the real work of the external forces, W_e , and that of the internal forces, W_i , is zero.

Conservative forces are defined as forces whose work done in displacement of a structure is path independent. Since this is the case for the lateral forces that act upon the plate, we can write

$$W_e = \int_0^a \int_0^b p_z(x, y) \cdot w(x, y) dx dy. \quad (4.4.17)$$

The work of the internal forces represents the negative value of the strain energy; thus

$$W_i = -U_b = -\frac{1}{2} \int_0^a \int_0^b (m_x \kappa_x + m_y \kappa_y + m_{xy} \chi) dx dy, \quad (4.4.18)$$

where the bending and torsional moments are given by Eqs. (1.2.26), (1.2.27) and (1.2.29), respectively, while the pertinent strains κ_x, κ_y and χ are defined by Eq. (1.2.21).

Since in this case we have only one energy equation at our disposal, the assumed field of displacements can contain only one unknown constant W_1 ; therefore

$$w(x, y) = W_1 \phi(x, y). \quad (4.4.19)$$

Substitution of this expression into the conservation-of-energy equation (4.4.16) yields the unknown coefficient W_1 in a very simple way. If the assumed deflection field

satisfies all the prescribed boundary conditions of the plate, the so-obtained solutions are surprisingly good. If necessary, however, the error minimization technique described in Sec. 4.5 can further improve the results. Although the concept of conservation of energy is very transparent and the required computational effort is relatively small, for unknown reasons this energy method is seldom used for solution of static plate problems.

d. Finite Element Method.[†] In essence, the FEM[‡] is a piecewise application of the classical Ritz method introduced in Sec. 4.2. As shown therein, central to this classical energy procedure is the assumption of *admissible* displacement fields covering the whole region of the plate. In many practical problems, however, it is quite difficult or even impossible to generate suitable shape functions for plates with complicated geometrical configurations and/or with difficult boundary conditions and supports (Fig. 4.4.1). In contrast to this approach, the FEM deals with shape functions covering only finite sized subdomains called “finite element.” Thus, instead of considering the plate as a continuum, the FEM subdivides the structure into a number of finitely sized and conveniently shaped subregions (Fig. 4.4.2) and considers the plate as an

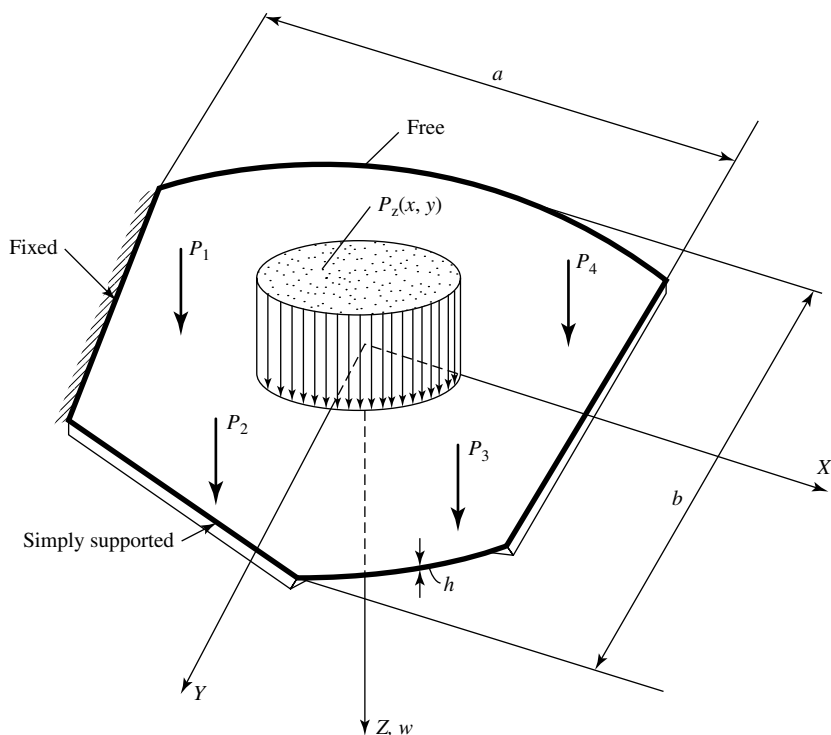


Figure 4.4.1 Plate of arbitrary shape and boundary conditions.

[†] We restrict ourselves here only to the displacement formulation.

[‡] Throughout the book *finite element methods* and *finite element(s)* will be abbreviated as FEM and FE, respectively.

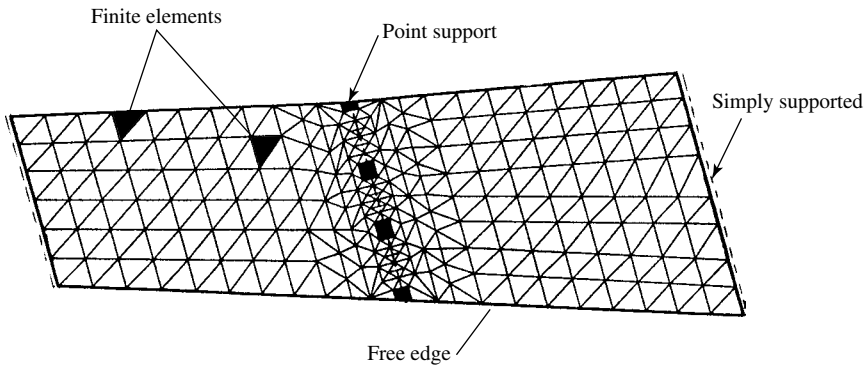


Figure 4.4.2 Finite element representation of plate bridge.

assembly of small elements. As an analogy, we may use the mosaic representation of a painting.

Within these elements we can use relatively simple shape functions. To obtain an acceptable representation of the original continuum, a sufficient number of elements is required. In addition, as a further contrast to the classical Ritz method, in the FEM all mathematical manipulations necessary to obtain the appropriate functional representing the total potential of the system can be evaluated in piecewise manner from element to element with the help of a computer. The total potential is then computed as the sum of the potentials of the individual finite elements. In this piecewise interpretation of the original Ritz method, we also apply the principle of stationary total potential to compute the response of the plate structure. The functions chosen to describe the assumed displacement fields with the subregions must fulfill certain criteria that are discussed later in Sec. 7.4 in detail.

Such a piecewise application of the Ritz method was first proposed by Courant in 1943 [4.4.9]. Since that time the FEM has become one of the most important computer-aided numerical methods for obtaining approximate solutions to a large variety of real-life problems that arise in engineering and mathematical physics. Consequently, a considerable part of this book is devoted to this very important numerical method, which currently appears to monopolize the field of numerical solution techniques.

e. Other Methods. Besides the variational methods discussed in this section, there are a number of other ways for solving boundary value problems of plates by using variational or direct energy methods. Here, we shall confine ourselves simply to the enumeration of these other approaches: the Morley-Trefftz method [4.4.10], the use of a modified Castigliano theorem [4.4.11], the complimentary energy method, an alternative to the FEM [4.4.12], weighted residuals and the Hellinger-Reissner variational principle [4.4.13], to name a few. Of course, this list is not complete.

Summary. As often mentioned previously, the single most important step in all variational and direct energy methods is the selection of admissible shape functions for the displacement fields. While satisfying all the prescribed boundary conditions generally improves the achievable accuracy, this desirable requirement cannot always be satisfied. This limitation can be overcome by applying the Lagrange multipliers in

connection with the Ritz method. Although all methods treated in more detail in this section require quite lengthy mathematical manipulations, the conservation-of-energy procedure combined with the error-minimization technique appears to be the most efficient in this respect. Furthermore, the limitations imposed on the classical energy and variational methods by nonconventional geometrical shapes and odd boundary conditions can be successfully overcome by using simple subdomains for which the generation of shape functions is relatively easy. This technique is provided by the FEM, which is the topic of numerous sections in this book.

ILLUSTRATIVE EXAMPLE I

Figure 4.4.3 shows a square plate subjected to p_0 uniformly distributed lateral force. Three edges of the plate are clamped, while the fourth one is simply supported at $x = a$. To be determined is the deflection at the center of the plate by applying the Lagrangian multiplier approach.

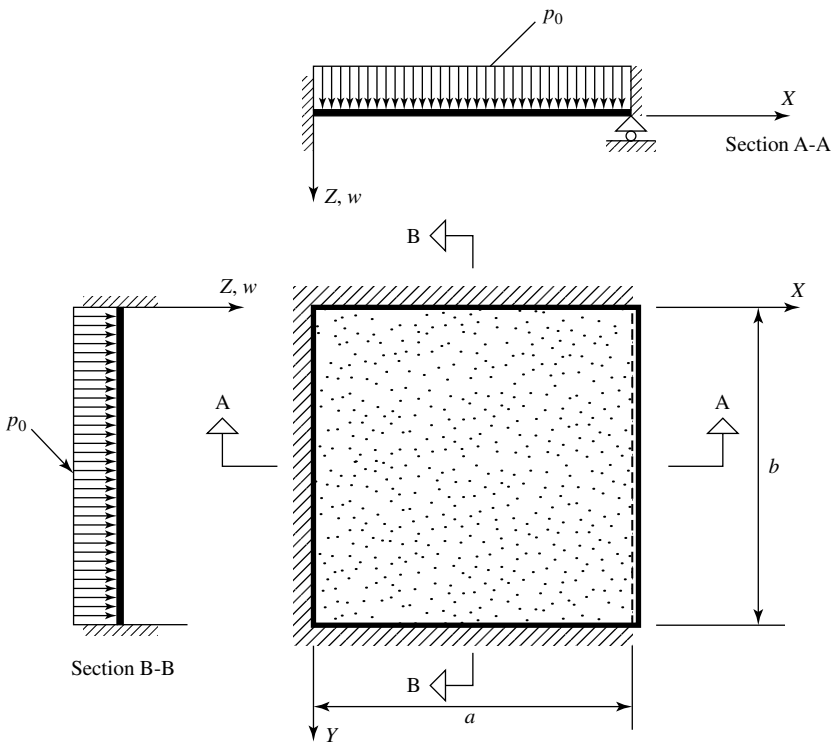


Figure 4.4.3 Square plate with various boundary conditions.

The boundary conditions of the plate are

$$\begin{aligned} w(x, y) &= 0 & \text{at } x = 0, a, \\ \frac{\partial w(x, y)}{\partial x} &= 0 & \text{at } x = 0 \end{aligned} \quad (4.4.20)$$

and

$$w(x, y) = 0, \quad \frac{\partial w(x, y)}{\partial y} = 0 \quad \text{at } y = 0, a. \quad (4.4.21)$$

The equation of the deflected plate surface is approximated by

$$w(x, y) = \sum_{m=1}^{\infty} \sum_{n=1,3,5,\dots}^{\infty} \frac{W_{mn}}{2} \sin \frac{m\pi x}{a} \cdot \left(1 - \cos \frac{2\pi y}{a}\right). \quad (4.4.22)$$

Since this equation does not satisfy the prescribed constraint of zero slope at the edge $x = 0$, we use *Lagrangian multipliers* to also enforce this boundary condition.

In our case, the total potential given in Eq. (4.2.1) becomes simplified; thus we can write

$$\Pi = -\frac{D}{2} \int_0^a \int_0^a \left(\frac{\partial^2 w}{\partial x^2} + \frac{\partial^2 w}{\partial y^2} \right)^2 dx dy + p_0 \int_0^a \int_0^a w(x, y) dx dy. \quad (4.4.23)$$

Since at $x = 0$ the slope must be zero,

$$\frac{\partial w(x, y)}{\partial x} = \frac{\pi}{a} \sum_{m=1}^{\infty} \sum_{n=1}^{\infty} m W_{mn} \frac{\sin n\pi y}{a} = 0, \quad (4.4.24)$$

a sufficient constraint is

$$\sum_{m=1}^{\infty} m W_{mj} = 0 \quad \text{for } j = 1, 2, 3, \dots, \infty. \quad (4.4.25)$$

Thus, we must have an infinite number of constraints to satisfy the zero-slope boundary condition along the edge $x = 0$. Consequently, an infinite number of *Lagrange* multipliers $\lambda_1, \lambda_2, \dots, \lambda_n$ is required. To compute these, we use the *modified total potential* given in Eq. (4.4.7). In our case, this becomes

$$\Pi^* = \Pi + \sum_{m=1}^{\infty} \sum_{n=1}^{\infty} \lambda_n m W_{mn}. \quad (4.4.26)$$

Substituting Eq. (4.4.22) into Eq. (4.4.23) and performing the required differentiations and integrations, we obtain

$$\begin{aligned} \Pi = & - \sum_{m=1}^{\infty} \sum_{n=1}^{\infty} \frac{D\pi^4}{8a^2} \left\{ W_{mn}^2 \left[\frac{m^4}{2} + \frac{(m^2 + 4n^2)^2}{4} \right] \right\} \\ & + \sum_{m=1,3,5,\dots}^{\infty} \sum_{n=1}^{\infty} \frac{p_0 a^2}{\pi} \left(\frac{W_{mn}}{m} \right). \end{aligned} \quad (4.4.27)$$

Substituting this expression into Eq. (4.4.26), we can write

$$\Pi^* = \text{Eq. (4.4.27)} + \sum_{m=1}^{\infty} \sum_{n=1}^{\infty} \lambda_n m W_{mn}. \quad (4.4.28)$$

After performing the differentiations as prescribed in Eq. (4.4.9), we satisfy the stationary values of Π^* for each value of W_{mn} . Consequently, we can write

$$\frac{\partial \Pi^*}{\partial W_{mn}} = -\frac{D\pi^4}{4a^2} \left\{ W_{mn} \left[\frac{m^4}{2} + \frac{(m^2 + 4n^2)^2}{4} \right] \right\} = 0 + \frac{p_0}{\pi} \frac{1}{m} + \lambda_n m = 0, \quad (4.4.29)$$

from which

$$W_{mn} = \frac{p_0 a^4 (4/\pi m) + 4a^2 m \lambda_n}{D\pi^4 [m^4/2 + (m^2 + 4n^2)^2/4]}. \quad (4.4.30)$$

Similarly, Eq. (4.4.10) gives

$$\frac{\partial \Pi^*}{\partial \lambda_n} = \sum_{m=1}^{\infty} m W_{mn} = 0. \quad (4.4.31)$$

Substituting Eq. (4.4.30) into Eq. (4.4.31), we have

$$\begin{aligned} & \frac{4p_0 a^4}{D\pi^5} \sum_{m=1,3,5,\dots}^{\infty} \frac{1}{[m^4/2 + (m^2 + 4n^2)^2/4]} \\ & + \frac{4a^2 \lambda_n}{D\pi^4} \sum_{m=1}^{\infty} \frac{m^2}{[m^4/2 + (m^2 + 4n^2)^2/4]} = 0, \end{aligned} \quad (4.4.32)$$

or, in more compact form,

$$\frac{4p_0 a^4}{D\pi^5} A_{mn}^I + \frac{4a^2 \lambda_n}{D\pi^4} A_{mn}^{II} = 0, \quad (4.4.33)$$

from which

$$\lambda_n = -\frac{p_0 a^2}{\pi} B_n, \quad (4.4.34)$$

where

$$B_n = \frac{A_{mn}^I}{A_{mn}^{II}}. \quad (4.4.35)$$

This constant is calculated by first summing A_{mn}^I in the numerator and A_{mn}^{II} in the denominator separately and then performing the division. To evaluate λ_n ,

we must compute B_n . For B_1 we obtained the approximate value of $B_1 \approx 0.19$. Substituting this into Eq. (4.4.34), Eq (4.4.30) then yields

$$W_{11} = 0.00157 \frac{p_0 a^4}{D}, \quad W_{31} = 0.00007 \frac{p_0 a^4}{D}. \quad (4.4.36)$$

Similarly, with $B_3 \approx 0.033$, we get

$$W_{13} = 0.00004 \frac{p_0 a^4}{D}, \quad W_{33} = 0.00002 \frac{p_0 a^4}{D}. \quad (4.4.37)$$

With these W_{mn} constants, the equation of the deflected plate surface (4.4.22) is now completely defined. For the deflection at the center of the plate, we have obtained

$$[w(x, y)]_{x=a/2, y=b/2} = 0.00152 \frac{p_0 a^4}{D}. \quad (4.4.38)$$

A comparison with the more exact solution of this problem given in Ref. [2] shows an error of approximately 3%. Finally, we would like to mention again that, for the sake of simplicity, we omitted the quite lengthy intermediate mathematical operations.

ILLUSTRATIVE EXAMPLE II

The rectangular plate shown in Fig. 4.4.4 supports a uniformly distributed load p_0 . Its span ratio is $a/b = 1.2$. The plate is clamped on two opposite edges, while the other edges are simply supported. Determine the deflected

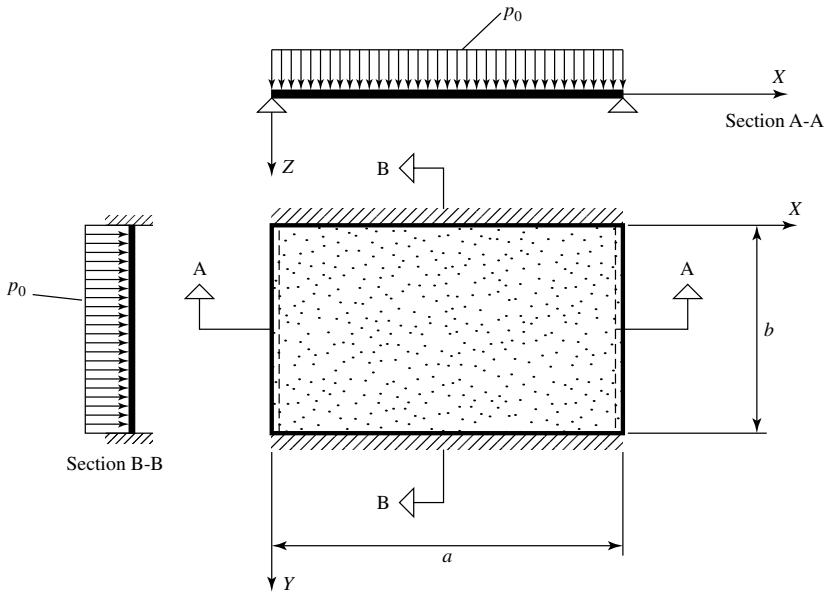


Figure 4.4.4 Rectangular plate with clamped and simply supported boundary conditions.

plate surface using the conservation-of-energy principle. Compare the obtained center deflection with that quoted in Ref. [2].

The prescribed boundary conditions of the plate are

$$\begin{aligned} w(x, y) &= 0 & \text{at } x = 0, a, \quad y = 0, b, \\ \frac{\partial w(x, y)}{\partial y} &= 0 & \text{at } y = 0, b, \\ \frac{\partial^2 w(x, y)}{\partial x^2} &= 0 & \text{at } x = 0, a. \end{aligned} \quad (4.4.39)$$

We select a shape function with just one unknown coefficient, C , which satisfies all the above given boundary conditions. Using only one term in the expressions given in Table 4.2.1, we can write

$$w(x, y) = \frac{C}{2} \sin \frac{\pi x}{a} \left(1 - \cos \frac{2\pi y}{b} \right). \quad (4.4.40)$$

Next, we calculate the work of the internal forces, which in this case has the simplified form

$$W_i = -U_b = -\frac{D}{2} \int_0^a \int_0^b \left(\frac{\partial^2 w}{\partial x^2} + \frac{\partial^2 w}{\partial y^2} \right)^2 dx dy = -11.9244 \frac{C^2 D}{8} \left(\frac{\pi}{a} \right)^4 ab. \quad (4.4.41)$$

The work of the external forces is

$$W_e = \frac{p_0}{2} \int_0^a \int_0^b w(x, y) dx dy = C \frac{ab p_0}{2\pi}. \quad (4.4.42)$$

From the principle of conservation-of-energy,[†]

$$C \frac{ab p_0}{2\pi} = 11.9244 C^2 \frac{D \pi^4}{8a^4} ab, \quad (4.4.43)$$

we obtain

$$C = 0.001098 \frac{p_0 a^4}{D} \quad \text{or} \quad C = 0.0022784 \frac{p_0 b^4}{D}. \quad (4.4.44)$$

Thus the equation of the deflected plate surface becomes

$$w(x, y) = 0.0011392 \frac{p_0 b^4}{D} \left[\sin \frac{\pi x}{a} \left(1 - \cos \frac{2\pi y}{b} \right) \right]; \quad (4.4.45)$$

[†] Given in Eq. (4.4.16).

hence the center deflection is

$$[w(x, y)]_{x=a/2, y=b/2} = 0.0022784 \frac{p_0 b^4}{D}. \quad (4.4.46)$$

A comparison with Timoshenko's more exact value given in Ref. [2]

$$[w(x, y)]_{x=a/2, y=b/2} = 0.00223 \frac{p_0 b^4}{D} \quad (4.4.47)$$

shows an error of only 2.1%. Even this relatively small error can be further reduced by applying the error-minimization technique treated in the next section.

ILLUSTRATIVE EXAMPLE III[†]

Let us consider a rectangular plate clamped all around its edges, as shown in Fig. 4.4.5. This plate is subjected to p_0 uniformly distributed lateral load. Determine the equation of the deflected plate surface by using Kantorovich's method.

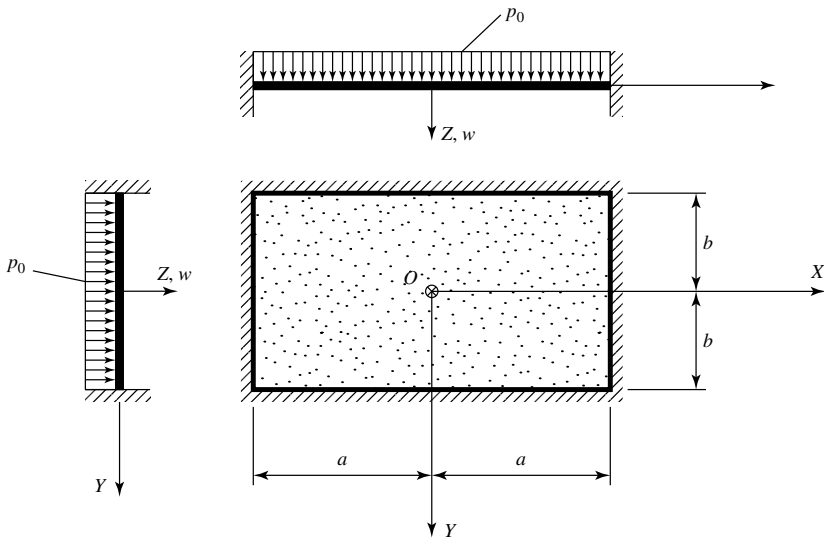


Figure 4.4.5 Clamped rectangular plate.

First, we make a reasonable assumption for the variation of $w(x, y)$ in the Y direction that satisfies the following boundary conditions:

$$w[x, y] = 0 \quad \text{and} \quad \frac{\partial w}{\partial y} = 0 \quad \text{at } y = \pm b. \quad (4.4.48)$$

[†] After Ref. [4.4.4].

Assuming only one term expansion, we write

$$w[x, y] = \phi[y] \cdot f(x) = [y^2 - b^2]^2 f(x). \quad (4.4.49)$$

Applying Galerkin's variational equation,[†]

$$\int_{-b}^b \left[\nabla^4 w[x, y] - \frac{p_0}{D} \right] \cdot \phi[y] dy = 0. \quad (4.4.50)$$

Substituting the assumed shape function into this equation gives

$$\int_{-b}^b \left\{ \left[24f + 2[12y^2 - 4b^2]f'' + [y^2 - b^2]f^{IV} - \frac{p_0}{D} \right] [y^2 - b^2]^2 \right\} dy = 0, \quad (4.4.51)$$

or

$$0.8127b^9 f^{IV} - 1.6254b^7 f'' + 25.6b^5 f = 1.0667 \frac{b^5 p_0}{D}, \quad (4.4.52)$$

where primes denote differentiations with respect to x . Its characteristic equation is

$$0.8127b^9 \lambda^4 - 1.6254b^7 \lambda^2 + 25.6b^5 \lambda = 0, \quad (4.4.53)$$

the roots of which are

$$\lambda_i = [\pm \alpha \pm \beta i] \frac{1}{b}, \quad \alpha = 2.075, \quad \beta = 1.143, \quad i = 1, 2, 3, 4. \quad (4.4.54)$$

The general solution of Eq. (4.4.52) is[‡]

$$f(x) = A \cosh \alpha \frac{x}{b} \cos \beta \frac{x}{b} + B \sinh \alpha \frac{x}{b} \sin \beta \frac{x}{b} + f_0(x), \quad (4.4.55)$$

where

$$f_0 = \frac{p_0}{24D} \quad (4.4.56)$$

represents a particular solution of Eq. (4.4.52).

Applying the boundary conditions at the edges $x = +a$, $x = -a$, we obtain

$$f(a) = A \cosh \alpha \frac{a}{b} \cos \beta \frac{a}{b} + B \sinh \alpha \frac{a}{b} \sin \beta \frac{a}{b} + \frac{p_0}{24D} = 0 \quad (4.4.57)$$

[†] See Sec. 4.3.

[‡] After discarding the unsymmetrical terms.

and

$$\begin{aligned} \left[\frac{df(x)}{dx} \right]_{x=a} &= A \left[\frac{a}{b} \sinh \alpha \frac{a}{b} \cos \beta \frac{a}{b} - \frac{\beta}{b} \cosh \alpha \frac{a}{b} \sin \beta \frac{a}{b} \right] \\ &+ B \left[\frac{\alpha}{b} \cosh \alpha \frac{a}{b} \sin \beta \frac{a}{b} + \frac{\beta}{b} \sinh \alpha \frac{a}{b} \cos \beta \frac{a}{b} \right] = 0. \end{aligned} \quad (4.4.58)$$

The solution of these two equations gives

$$A = \frac{\gamma_1}{\gamma_0} \cdot \frac{p_0}{24D}, \quad B = \frac{\gamma_2}{\gamma_0} \cdot \frac{p_0}{24D}, \quad (4.4.59)$$

where (for $\mu = a/b$)

$$\begin{aligned} \gamma_0 &= \beta \sinh \alpha \mu \cosh \alpha \mu + \alpha \sin \beta \mu \cos \beta \mu, \\ \gamma_1 &= -(\alpha \cosh \alpha \mu \sin \beta \mu + \beta \sinh \alpha \mu \cos \beta \mu), \\ \gamma_2 &= \alpha \sinh \alpha \mu \cos \beta \mu - \beta \cosh \alpha \mu \sin \beta \mu. \end{aligned} \quad (4.4.60)$$

Thus, the final form of the equation of the deflected plate surface will be

$$\begin{aligned} w(x, y) &= \frac{p_0(b^2 - y^2)^2}{24\gamma_0 D} \left(\gamma_1 \cosh \alpha \frac{x}{b} \cos \beta \frac{x}{b} + \gamma_2 \sinh \alpha \frac{x}{b} \sin \beta \frac{x}{b} \right) \\ &+ \frac{p_0(y^2 - b^2)^2}{24D}. \end{aligned} \quad (4.4.61)$$

For $a = b$, the maximum deflection is

$$w(0, 0) = 0.01996 \frac{p_0 b^4}{D}. \quad (4.4.62)$$

The error in this case is between 1 and 2%.

We can improve this result by either using more terms in the assumed shape function

$$\phi_k(y) = (y^2 - b^2)^2 \cdot y^{2k-2} \quad (4.4.63)$$

or applying the obtained result as an assumed shape function now in the X direction and determining $f(y)$ as described above. In both cases, however, the required mathematical operations will be extremely time consuming.

References and Bibliography

- [4.4.1] TREFFTZ, E., "Ein Gegenstück zum Ritzschen Verfahren," *Proc. 2nd Int. Congr. Appl. Mech.*, Zürich (1926), 131–137.
- [4.4.2] TREFFTZ, E., "Die Bestimmung der Knicklast gedrückter, rechteckiger Platten," *ZAMM*, 15 (1935), 359.

- [4.4.3] BUDIANSKY, B., et al., "The Lagrangian Multiplier Method of Finding Upper and Lower Limits to Critical Stresses of Clamped Plates," National Advisory Committee for Aeronautics NACA Report 848, 1946.
- [4.4.4] KANTOROVICH, L. V., and KRYLOV, V. I., *Approximate Methods of Higher Analysis* (in Russian), Interscience Publishers, New York, 1958.
- [4.4.5] REDDY, J. N., *Energy and Variational Methods in Applied Mechanics*, John Wiley & Sons, New York, 1984.
- [4.4.6] DAVIES, G. A. O., *Virtual Work in Structural Analysis*, John Wiley & Sons, New York, 1982.
- [4.4.7] RICHARDS, T. H., *Energy Methods in Stress Analysis*, John Wiley & Sons, New York, 1977.
- [4.4.8] BEREZIN, I. S., and ZHIDKOV, N. P., *Computing Methods*, Vol. 2 (in Russian), Pergamon, Oxford, 1965.
- [4.4.9] COURANT, R., "Variational Methods for the Solution of Problems of Equilibrium and Vibrations," *Bull. Am. Math. Soc.*, 49 (1943), 1–23.
- [4.4.10] MORLEY, L. S., "The Approximate Solution of Plate Problems," *Proc. Ninth Int. Congr. Appl. Mech.*, 6, (1956), 22–29.
- [4.4.11] FU-BAO-LIAN, "On the Modified Castigliano's Theorem," *Chinese Appl. Math. Mech.* (English ed.), 5 (1984), 1263–1272.
- [4.4.12] LIEW, K. M., and WANG, C. M., "pb-2 Rayley-Ritz Method for General Plate Analysis," *Eng. Struct.*, 15 (1993), 55–60.
- [4.4.13] REISSNER, E., "On the Variational Theorems of Elasticity," in *Problems in Continuum Mechanics—Mushkhelishvili Anniversary Volume*, McGraw-Hill Book Co., New York, 1958.
- [4.4.14] SI YUAN, Y. J., and WILLIAMS, F. W., "Bending Analysis of Mindlin Plates by Extended Kantorovich Method," *J. Eng. Mech. Div., ASCE*, 124 (1998), 1339–1345.

4.5 Techniques to Improve Energy Solutions

The success of variational methods, as mentioned earlier, depends principally on the suitable choice of approximate functions, but the nature of the load may also have an influence on convergence of the solution. That is, for obtaining the same accuracy, a distributed load usually requires less terms in the polynomial expression of the deflections than a concentrated force. Accelerated convergence can be attained, however, by replacing the concentrated force with two distributed loads, as shown in Fig. 4.5.1. By superimposing the deflections due to this *equivalent load* system, the deflections of the plate subjected to a concentrated force can be approximated more closely.

Further improvement in the results of energy methods can be accomplished by a generalization of the error distribution principle introduced by Szilard [4.7.2]. Let us assume that an approximation $w_1(x, y)$ to the exact solution has already been found by either Ritz's or Galerkin's method. This first approximation of the deflection surface is expressed in infinite series form:

$$w_1(x, y) = \sum_{i=1}^n W_i f_i(x, y) \quad \text{for } i = 1, 2, 3, \dots, n. \quad (4.5.1)$$

Each term in Eq. (4.5.1) must at least satisfy the geometrical boundary conditions of the plate. If all boundary conditions are satisfied, convergence of the solution is usually improved. Although the latter limitation is required only for Galerkin's

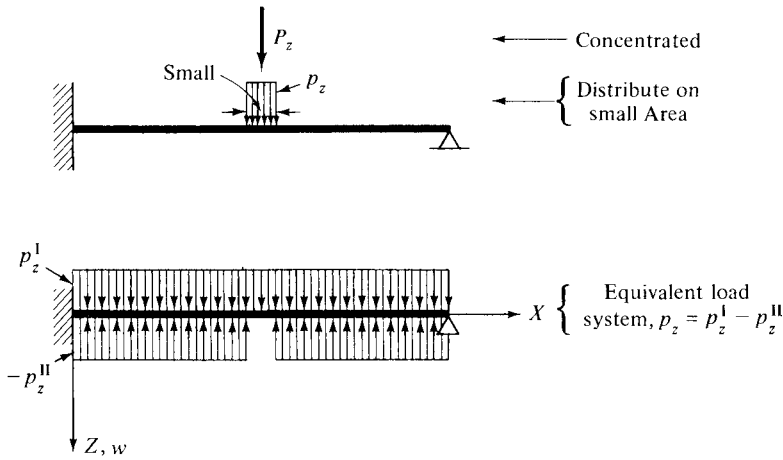


Figure 4.5.1 Equivalent load system for concentrated forces.

method, we assume in the first part of our discussion that all terms in Eq. (4.5.1) satisfy all boundary conditions of the problem.

Since the obtained solution is only an approximation of the actual plate deflections, the insertion of Eq. (4.5.1) into the governing differential equation (1.2.30) yields *residual errors* ε within the interior domain of the plate. Thus, at point, ζ, η , the residual error is

$$(\varepsilon_1)_{\zeta, \eta} = (D \nabla^2 \nabla^2 w_1 - p_z)_{\zeta, \eta}. \quad (4.5.2)$$

The definite integral

$$\varepsilon_1 = \iint_{(A)} (D \nabla^2 \nabla^2 w_1 - p_z) dx dy \neq 0 \quad (4.5.3)$$

represents the total residual error of the first approximate solution.

Next, we select a suitable *error function* $\varepsilon_1(x, y)$. If the edges of the plate have continuous unyielding supports, a parabolic error function, with its apex at the locus of the maximum deflection, usually gives good results. An error function, of course, can also be generated by evaluating Eq. (4.5.2) at numerous points and by curve fitting the results. This approach, however, is more tedious and usually not required.

We write the improved solution in the form

$$w(x, y) = w_1(x, y) + w_2(x, y) + \cdots, \quad (4.5.4)$$

where

$$w_2(x, y) = \sum_{i=1}^m c_i \phi_i(x, y). \quad (4.5.5)$$

Again, each function $\phi_i(x, y)$ in Eq. (4.5.5) must satisfy the geometrical boundary conditions of the problem. The unknown coefficients (c_1, c_2, \dots, c_m) are determined

by the *least-squares method*, which brings the errors toward zero as much as possible. Thus, the necessary minimum conditions are obtained from

$$\frac{\partial}{\partial c_i} \iint_{(A)} [D \nabla^2 \nabla^2 w_2(x, y) - \varepsilon_1(x, y)]^2 dx dy = 0 \quad (4.5.6)$$

for $i = 1, 2, 3, \dots, m$.

This procedure, as in the case of Ritz's method, leads to a set of linear equations in the unknown parameters. The solution of these equations yields the coefficients c_i . When the total residual error is small, the use of one term in Eq. (4.5.5) is usually sufficient. If required, this error distribution procedure can be repeated until the order of the total residual error becomes negligible.

It appears that the least-squares method could also be used for determination of the first approximation, $w_1(x, y)$, to the deflections. This approach, however, as Weber points out [4.5.3], often leads to an entirely incorrect solution, in which the deflections even have wrong signs throughout. The method presented here is quite different, since it consists merely of improving a close approximation by means of minimizing a *small* residual error. On the other hand, when the originally chosen displacement function $w_1(x, y)$ is incapable of further approximation of the exact solution, regardless of the number of terms carried, this simple technique may result in a significant improvement. In fact, in many instances it may be more economical to use a limited number of terms in the first approximation, $w_1(x, y)$, and repeat the error distribution twice.

We may also partition the plate into k subregions, as shown in Fig. 4.5.2. Now the residual first error for each subregion can be determined from

$$\varepsilon_{1,k} = \iint_{(A_k)} D(\nabla^2 \nabla^2 w_1 - p_z) dA_k \neq 0. \quad (4.5.7)$$

If our first approximation, $w_1(xy)$, satisfies only the geometrical boundary conditions, we have to minimize the boundary errors as well as the residual errors of the interior domain [4.5.4]. This alternative procedure, however, tends to be more complex than the one introduced above.

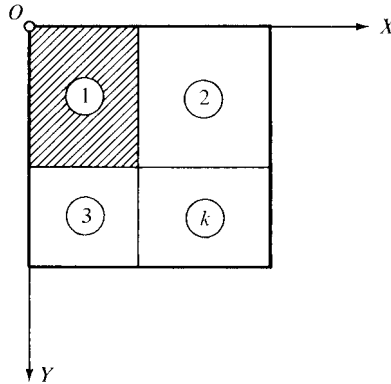


Figure 4.5.2 Subregions.

Summary. As the following example indicates, this simple error distribution technique gives encouraging results when the approximate solution obtained by variational methods is unable to represent the exact deflections beyond a certain degree of accuracy. Since the method makes further use of the differential equation, it is especially recommended for refinement of Galerkin's method. For concentrated loads, accelerated convergence can be attained by introduction of an equivalent load system.

ILLUSTRATIVE EXAMPLE

A clamped square plate of uniform thickness is subjected to a concentrated lateral force P_z at its center. An approximate expression for the deflected plate surface has been obtained by Vlasov's method in the form

$$w_1(x, y) = \frac{P_z a^2}{D} [1.935 \times 10^{-3} X_1(x) \cdot Y_1(y) + 6.1594 \times 10^{-6} X_1(x) \cdot Y_2(y) \\ + 6.1594 \times 10^{-6} X_2(x) \cdot Y_1(y) + 3.3489 \times 10^{-8} X_2(x) \cdot Y_2(y) \\ - 1.3619 \times 10^{-4} X_1(x) \cdot Y_3(y) - 1.3619 \times 10^{-4} X_3(x) \cdot Y_1(y)], \quad (4.5.8)$$

where $X_i(x)$ and $Y_i(y)$ represent the eigenfunctions of clamped beams pertinent to the i th mode. Improve this solution by distributing the residual error using the least-squares approach.

The total residual error is determined from Eq. (4.5.3), yielding

$$\varepsilon_1 = \left(D \int_0^a \int_0^a \nabla^4 w_1 \, dx \, dy \right) - P_z = P_z (2.2534 + 0.00249 + 0.00638 \\ + 0.000008261 - 0.1816 - 0.9824) - P_z = 0.098 P_z. \quad (4.5.9)$$

Let us assume that the error function has the form

$$\varepsilon_1(x, y) = A_0 \sin \frac{\pi x}{a} \sin \frac{\pi y}{a}, \quad (4.5.10)$$

where

$$A_0 \approx \frac{0.098 P_z}{\int_0^a \int_0^a \sin(\pi x/a) \sin(\pi y/a) \, dx \, dy} = \frac{0.098 \pi^2 P_z}{4a^2}. \quad (4.5.11)$$

For $w_2(x, y)$ we introduce a simple one-term expression,

$$w_2(x, y) = \frac{c}{4} \left(1 - \cos \frac{2\pi x}{a} \right) \left(1 - \cos \frac{2\pi y}{a} \right), \quad (4.5.12)$$

which satisfies all boundary conditions of the problem.

Equation (4.5.6) can be written as

$$2 \int_0^a \int_0^a \left\{ [D \nabla^2 \nabla^2 w_2(x, y) - \varepsilon_1(x, y)] \times \frac{\partial}{\partial c_i} [D \nabla^2 \nabla^2 w_2(x, y) - \varepsilon_1(x, y)] \right\} dx dy = 0. \quad (4.5.13)$$

Substitution of Eqs. (4.5.10) and (4.5.11) into this expression gives

$$\begin{aligned} 2 \int_0^a \int_0^a \left\{ \frac{Dc}{4} \left(\frac{2\pi}{a} \right)^4 \left[\cos \frac{2\pi x}{a} \left(\cos \frac{2\pi y}{a} - 1 \right) + 2 \cos \frac{2\pi x}{a} \cos \frac{2\pi y}{a} \right. \right. \\ \left. \left. + \left(\cos \frac{2\pi x}{a} - 1 \right) \cos \frac{2\pi y}{a} \right] \right. \\ \left. - \frac{0.098\pi^2 P_z}{4a^2} \sin \frac{\pi x}{a} \sin \frac{\pi y}{a} \right\} \\ \times \frac{D}{4} \left(\frac{2\pi}{a} \right)^4 \left[\cos \frac{2\pi x}{a} \left(\cos \frac{2\pi y}{a} - 1 \right) + 2 \cos \frac{2\pi x}{a} \cos \frac{2\pi y}{a} \right. \\ \left. + \left(\cos \frac{2\pi x}{a} - 1 \right) \cos \frac{2\pi y}{a} \right] dx dy = 0. \end{aligned} \quad (4.5.14)$$

After simplification, we evaluate the definite integrals in Eq. (4.5.14) and determine the required constant:

$$c = 0.5586 \times 10^{-4} \frac{P_z a^2}{D}. \quad (4.5.15)$$

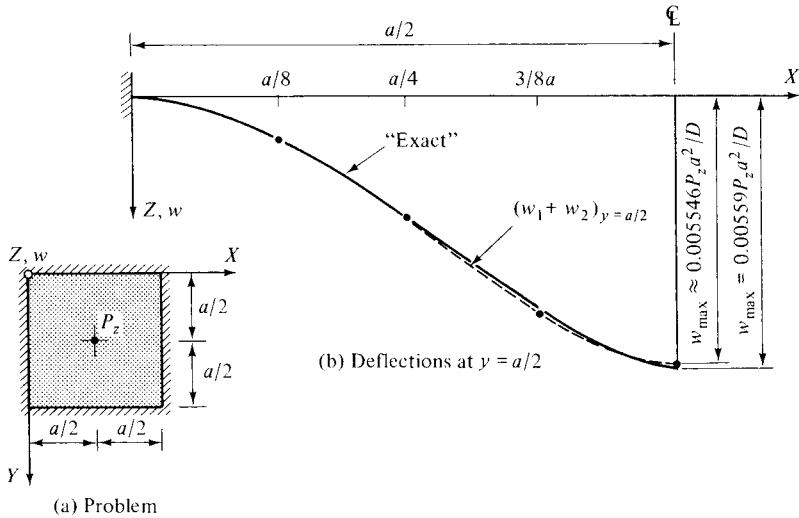


Figure 4.5.3 Exact-vs.-approximate solution.

Hence, the improved expression for the deflections becomes

$$w(x, y) = w_1(x, y) + 0.13965 \times 10^{-4} \frac{P_z a^2}{D} \left(1 - \cos \frac{2\pi x}{a}\right) \left(1 - \cos \frac{2\pi y}{a}\right), \quad (4.5.16)$$

where $w_1(x, y)$ is defined by Eq. (4.5.8).

As Fig. 4.5.3 indicates, by this simple procedure a close approximation of the exact solution for the interior region of the plate has been attained.

References and Bibliography

- [4.5.1] GIENCKE, E., "Reihenansätze zur Lösung von Plattenproblemen," *Z. f. Angw. Math. u. Mech.*, 41, GAMM Tagung, Sonderheft (1961), T86–T88.
- [4.5.2] SZILARD, R., "A Technique to Improve Galerkin's Variational Method," in C. A. Brebbia et al. (Eds.) *Proceedings of the International Conference on Variational Methods in Engineering*, held at the University of Southampton, Southampton, Southampton University Press, Southampton, 1972. Sept. 1972, pp. 6128–6138.
- [4.5.3] WEBER, C., "Über genäherte Lösungen von Differentialgleichungen mit Hilfe von Minimalansätzen," *Z. f. Angw. Math. u. Mech.*, 21, No. 5 (Oct. 1941), 310–311.
- [4.5.4] MORLEY, L. S. D., "The Approximate Solution of Plate Problems," *Proc. 9th Int. Congr. Appl. Mech.*, Université de Bruxelles, Brussels, 1956, 6 (1957), 22–29.
- [4.5.5] TREFFTZ, E., "Ein Gegenstück zum Ritzschen Verfahren," *Verh. 2. Int. Kongress Tech. Mech.*, Zurich (1926), E. Meissner, Zurich, 1927, pp. 131–137.

4.6 Application of Energy Methods to Moderately Thick Plates

a. Galerkin's Method. We can extend here the use of Galerkin's variational approach, treated in Sec. 4.3 for thin plates, to moderately thick plates. We seek, again, approximate solutions for the unknown deflections w and rotations ψ_x and ψ_y in finite linear combinations of shape functions in the form

$$w(x, y) = \sum_{m=1}^m A_i \phi_i(x, y) \quad \text{for } i = 1, 2, \dots, m, \quad (4.6.1a)$$

$$\psi_x(x, y) = \sum_{j=1}^n B_j \phi_j(x, y) \quad \text{for } j = 1, 2, \dots, n \quad (4.6.1b)$$

$$\psi_y(x, y) = \sum_{k=1}^k C_k \phi_k(x, y) \quad \text{for } k = 1, 2, \dots, k, \quad (4.6.1c)$$

where ϕ_i , ϕ_j and ϕ_k are independent, continuous displacement functions that satisfy all prescribed boundary conditions and have at least the same order of derivatives as called for by the differential operators in the governing equations of the moderately thick plates.[†] These differential equations can be written in the following

[†] See Sec. 1.5.

general forms:

$$\mathcal{L}_1(w, \psi_x, \psi_y) - p_z = 0, \quad (4.6.2a)$$

$$\mathcal{L}_2(w, \psi_x, \psi_y) = 0, \quad (4.6.2b)$$

$$\mathcal{L}_3(w, \psi_x, \psi_y) = 0, \quad (4.6.2c)$$

where \mathcal{L}_1 , \mathcal{L}_2 and \mathcal{L}_3 represent differential operators; w , ψ_x , ψ_y are displacement components and p_z is the external load.

The unknown parameters A_i , B_j and C_k in Eq. (4.6.1) are determined from Galerkin's variational equations (4.3.3), which in this case take the following forms:

$$\int_0^a \int_0^b [\text{diff. eq. (4.6.2a)}] \phi_i(x, y) dx dy = 0, \quad (4.6.3a)$$

$$\int_0^a \int_0^b [\text{diff. eq. (4.6.2b)}] \phi_j(x, y) dx dy = 0, \quad (4.6.3b)$$

$$\int_0^a \int_0^b [\text{diff. eq. (4.6.2c)}] \phi_k(x, y) dx dy = 0. \quad (4.6.3c)$$

These equations provide $i + j + k$ linearly independent algebraic equations for the determination of the parameters A_i , B_j and C_k .

However, instead of using Reissner's or Mindlin's three differential equations, we may considerably simplify this variational procedure by utilizing the *simplified* form of the governing equations, as given in Eq. (1.5.11). That is, this differential equation is formulated only in terms of transverse displacement. Consequently, we can write

$$\int_0^a \int_0^b \left[D \left(\nabla^2 w + \frac{h^2(2-\nu)}{10(1-\nu)} \nabla^3 w - p_z \right) \right] \phi_i(x, y) dz dy = 0 \quad (4.6.4)$$

for $i = 1, 2, \dots, m$,

where $\nabla^3 w$ is defined by Eq. (1.5.12). The boundary conditions for the deflections $w(x, y)$ and, consequently, for the shape functions ϕ_i are already discussed in Sec. 1.5.

b. Ritz's Method. We can also use Ritz's method, treated in Sec. 4.2, to obtain approximate, analytical solutions for laterally loaded, moderately thick plates. Again, we express the displacement fields through Eq. (4.6.1). In the case of simply supported rectangular plates, for example, we may use the following expressions for the displacement components:

$$w^*(\xi, \eta) = \sum_{m=1}^{\infty} A_m \sin(m\pi\xi) \sin(\pi\eta), \quad (4.6.5a)$$

$$\psi_x^*(\xi, \eta) = \sum_{m=1}^{\infty} B_m \cos(m\pi\xi) \sin(\pi\eta), \quad (4.6.5b)$$

$$\psi_y^*(\xi, \eta) = \sum_{m=1}^{\infty} C_m \sin(m\pi\xi) \cos(\pi\eta), \quad (4.6.5c)$$

where w^* , ξ and η represent normalized expressions by the plate dimensions, that is,

$$\xi = \frac{x}{a}, \quad \eta = \frac{y}{b}, \quad w^* = \frac{w}{b}. \quad (4.6.6)$$

The bending strain energy for the Mindlin plate can be written [4.6.2] as

$$\begin{aligned} U_b^* = \frac{D}{2} \int_0^1 \int_0^1 \left\{ \left(\frac{1}{a} \frac{\partial \psi_x^*}{\partial \xi} + \frac{1}{b} \frac{\partial \psi_y^*}{\partial \eta} \right)^2 \right. \\ \left. - 2(1-\nu) \left[\frac{1}{ab} \frac{\partial \psi_x^*}{\partial \xi} \cdot \frac{\partial \psi_y^*}{\partial \eta} - \frac{1}{4} \left(\frac{1}{b} \frac{\partial \psi_x^*}{\partial \eta} + \frac{1}{a} \frac{\partial \psi_y^*}{\partial \xi} \right) \right] \right. \\ \left. + \frac{\kappa^2 Gh}{D} \left[\left(\psi_x^* + \frac{b}{a} \frac{\partial w^*}{\partial \xi} \right)^2 + \left(\psi_y^* + \frac{\partial w^*}{\partial \eta} \right)^2 \right] \right\} ab \, d\xi \, d\eta. \end{aligned} \quad (4.6.7)$$

Similarly, the nondimensional form of the potential energy of the external forces becomes

$$V^* = - \int_0^1 \int_0^1 [p_z^*(\xi, \eta) \cdot w^*(\xi, \eta)] ab \, d\xi \, d\eta. \quad (4.6.8)$$

Thus, the total potential of the system, expressed in nondimensional terms, is

$$\Pi^* = U_b^* + V^*. \quad (4.6.9)$$

After substituting the admissible functions of the displacement fields (4.6.5) into Eqs. (4.6.7) and (4.6.8), respectively, we apply the principle of minimum potential energy,

$$\frac{\partial \Pi^*}{\partial A_m} = 0, \quad \frac{\partial \Pi^*}{\partial B_m} = 0, \quad \frac{\partial \Pi^*}{\partial C_m} = 0. \quad (4.6.10)$$

This yields a set of algebraic equations, from which the unknown parameters A^m , B_m and C_m can be determined.

Summary. To obtain approximate, closed-form solutions for the deflections of moderately thick plates, we applied the basic concepts of the Galerkin and Ritz methods in this section. Although the underlying principles of both methods, as discussed in the foregoing sections, are not changed, the required mathematical operations can be quite extensive. For this reason, the use of the simplified form of Reissner's equation for moderately thick plates in connection with Galerkin's variational approach is recommended.

References and Bibliography

- [4.6.1] DOBYNS, A. L., "Analysis of Simply Supported Orthotropic Plate Subjected to Static and Dynamic Loads," *AIAA J.*, 19 (1981), 642–650.
- [4.6.2] ROUFAEL, O. L., and DAWE, D. J., "Raileigh-Ritz Vibration Analysis of Rectangular Mindlin Plate Subjected to Membrane Stresses," *J. Sound and Vibration*, 85 (1982), 263–275.
- [4.6.3] WANG, C. M., et al., "Buckling Formula for Biaxially Loaded Rectangular Mindlin Plates," *Steel Structures*, 4 (1993), 69–77.
- [4.6.4] RÜDIGER, D., "Die Verfahren von Ritz und Trefftz in der Reissnerschen Plattentheorie," *Ing.-Arch.*, 29 (1960), 257–281.

4.7 Summary

As already discussed in Chapters 2 and 3, the more exact classical methods of analytical solutions cannot be applied to plate-bending problems in cases of irregular geometry and boundary conditions or loads. Consequently, approximate analytical approaches must be used if one desires to obtain closed-form solutions to the above-mentioned problems. The energy methods treated in this chapter offer the required flexibility and generality in such cases. Furthermore, some of these techniques can also be applied for solution of vibration and stability problems of plates, as shown in Secs. 14.5 and 16.3. In addition, the basic ideas underlying the Galerkin and Ritz methods also allow their extensions to moderately thick plates [4.6.2, 4.6.3].

An important merit of the energy methods is the relatively uncomplicated way in which they can be applied without actually solving the pertinent differential equations of plates. To obtain realistic results, the most important step in all energy methods is the selection of suitable shape functions. To facilitate such selection, the reader will find numerous usable suggestions (including worked examples) in Tables 4.2.1 and 4.3.1.

Based on the author's experience, the conservation-of-energy principle followed by an error minimization procedure offers the most efficient way to obtain very good results. [4.5.2] Both concepts are quite transparent; consequently, they are easy to learn. Naturally, these comments are valid only for rectangular plates having continuous boundary conditions, as shown in all illustrative examples of this chapter. Finally, it is recommended that in the error minimization technique one should resort to shape functions that are different from the one used in connection with the conservation of energy. In this way, the superposition of the two shape functions, compensating each other, can better approximate the actual deflection field of the plate. In addition, experienced analysts can also select error functions that correspond to the actual error distribution of the problem at hand, thus further improving the achievable accuracy.

Leissa and his co-workers evaluated and compared nine other energy methods using (1) a uniformly loaded, simply supported elliptical plate and (2) a square plate having free-edges supported at four asymmetrically located interior points and loaded by its own weight [4.3.20]. Here, we would like to summarize their most important findings concerning only the Ritz (R), Galerkin (G) and Kantorovich (K) methods, since, of the nine energy methods investigated by them, these three have been treated in this chapter. With regards to their capability in obtaining accurate solutions, the K procedure appears to be the best, including yielding higher derivatives required for the determination of moments and shears in the plate. Since the R and K methods

only require the satisfaction of the essential boundary conditions, they are more effective in treating free boundary conditions than the G method. All three methods are difficult to apply in the case of curvilinear boundaries. Concerning the ease in learning to understand and use these methods by practicing engineers, the K and G methods are conceptually more difficult, since they require the understanding of variational calculus. Furthermore, the K method is often beyond the grasp of the average engineer.

The disadvantage of all energy methods is the fact that the solution procedure cannot be automated. Therefore, a large portion of the computation must be carried out by "longhand." Although the required differentiations and integrations are relatively simple, they become quite lengthy. Nowadays, however, this tedious task can be reduced to a large degree by using programs of "symbolic mathematics" [A.1.18–A.1.21]. In addition, the resulting algebraic equations can also be solved with the help of these programs. Finally, it should be mentioned that some of the more sophisticated, programmable calculators offer, to somewhat lesser degree, similar services at far more acceptable price.

Problems†

- 4.2.1.** Determine an approximate expression for the deflections of the plate shown in Fig. 4.4.4, applying the Ritz method. Assume a span ratio of $a/b = 1.2$. Compute the center deflection and compare your value with the results given in Illustrative Example II of Sec. 4.4.
- 4.2.2.** Figure 4.2.2 shows a clamped rectangular plate subjected to a uniform load p_0 . Determine an approximate equation for the deflections using the Ritz method. Assume only a one-term shape function in form

$$w(x, y) = c(x^2 - a^2)^2(y^2 - b^2)^2.$$

Compare the so-obtained center deflection with that given in Eq. (2.2.29).

- 4.2.3.** Find an approximate equation for the elastic surface of a rectangular plate, shown in Fig. 2.3.3, using Ritz's method. Determine the moments m_x and m_y at the center of the plate.
- 4.2.4.** A simply supported rectangular plate carries a concentrated load P_z at $x = a/2$ and $y = b/2$, as shown in Fig. 2.1.2. Using Ritz's method, determine an approximate expression for the deflections. Evaluate the maximum deflection.
- 4.2.5.** A uniformly loaded rectangular plate is simply supported at the edges $y = 0, b$. The edge $x = 0$ is clamped, while the fourth side of the plate at $x = a$ is free. Assuming a one-term shape function in the form

$$w(x, y) = c \left(\frac{a}{x} \right)^2 \sin \left(\frac{b}{\pi y} \right),$$

determine the deflection at the center of the plate.

† The first two numbers refer to the corresponding section.

- 4.3.1. Solve the problem given in problem 4.2.2 but this time applying Galerkin's variational approach. Compare the two methods for their efficiency and accuracy.
- 4.3.2. Redo problem 4.2.5 using Galerkin's method.
- 4.3.3. Figure 2.4.1 shows a simply supported plate subjected to a parabolic load. Determine the center deflection using Galerkin's method.
- 4.3.4. Using Galerkin's method, redo problem 2.2.4.
- 4.4.1. Using the conservation-of-energy principle (CEP), find a one-term approximation for the plate problem shown in Fig. 4.3.2.
- 4.4.2. Redo problem 4.2.2 using the CEP.
- 4.4.3. A simply supported rectangular plate is subjected to a hydrostatic load, as shown in Fig. 2.2.2. Determine an approximate expression for the deflections using the CEP.
- 4.4.4. Using the CEP, determine the elastic surface of the plate shown in Fig. 2.3.3.
- 4.5.1. Improve the solution obtained in problem 4.4.2 by using the error minimization technique (EMT), treated in Sec. 4.5.
- 4.5.2. Using the EMT, obtain an improved result for the deflected plate surface obtained in the solution of problem 4.4.1.
- 4.5.3. Improve the solution of problem 4.2.4 by applying the EMT.
- 4.5.4. Using the EMT, improve the solution obtained in problem 4.4.4.

Part II

Numerical Methods for Solution of Static, Linear-Elastic Plate Problems

As we have already discussed and illustrated in the Introduction to this book, structural plates have a multitude of applications in extremely diverse fields of the industry. Consequently, economical and reliable analyses of various types of plate structures are of great interest to civil, architectural, mechanical and aeronautical engineers and naval architects.

In Chapter 1, we formulated the flexural behaviors of various plate types, introducing mathematically correct partial differential equations. Unfortunately, the analytical solutions of these differential equations have been limited to homogeneous plates of relatively simple geometry and loading and boundary conditions. Even when analytical solutions could be found, they were often too difficult and cumbersome to use in everyday engineering practice. Thus, general solution techniques are required that are applicable to plates of arbitrary geometry and loadings and can handle various boundary conditions with relative ease. In addition, their concept should be transparent and their technique easy to learn. The numerical methods treated in this book satisfy most of these practical requirements.

The aim of all these numerical methods is to provide suitable computational algorithms for obtaining approximate numerical solutions to difficult problems of mathematical physics. The numerical techniques introduced in Part II of the book are the so-called *discrete* methods. That is, the continuum of the plate or its boundary is discretized either mathematically or physically. Here we will treat the following numerical methods for the solution of various, often very difficult, plate problems:

- (a) finite difference methods (FDMs),
- (b) gridwork method (GWM),
- (c) finite element method (FEM),

- (d) finite strip method (FSM) and
- (e) boundary element method (BEM).

Of these five methods the FDM and BEM are based on mathematical discretization of the plate continuum or its boundary, respectively, while the others employ various types of physical discretization techniques.

Although we intend to solve here only linear-elastic bending problems of plates, in subsequent parts of the book the reader will find extensions of these numerical methods to special plates, including treatments of various dynamic and stability problems.

a. Finite Difference Methods. These are the oldest—but still very viable—numerical methods and are especially suited for the solutions of various plate problems. As already mentioned, the FDM is based on a mathematical discretization of the plate continuum. For this purpose, the plate is covered by a two-dimensional *mesh* (Fig. Ov.1). Next, the partial derivatives in the governing plate equation (1.1.30) are replaced by corresponding finite difference quotients at each *mesh point*. In this way, we transform the differential equation governing the displacements $w(x, y)$ into algebraic equations. The finite difference expressions for the interior points are conveniently given in so-called *stencil* forms, which represent graphical representations of the pertinent finite difference expressions. These stencils must usually be modified at the boundaries in order to satisfy the prescribed boundary conditions. Since the FDM gives an algebraic equation at each mesh point, the solution of these coupled equations yields the displacement w_i at each mesh point “ i .”

A considerable improvement in accuracy over the above-discussed ordinary FDM can be obtained by approximating the governing differential equation at several mesh points. This approach, however, can be quite involved. Thus, these so-called *multi-local* methods should only be used when pertinent stencils are readily available.

Although currently the FEM has achieved an almost exclusive dominance in the numerical analysis of surface structures, it would be shortsighted not to consider

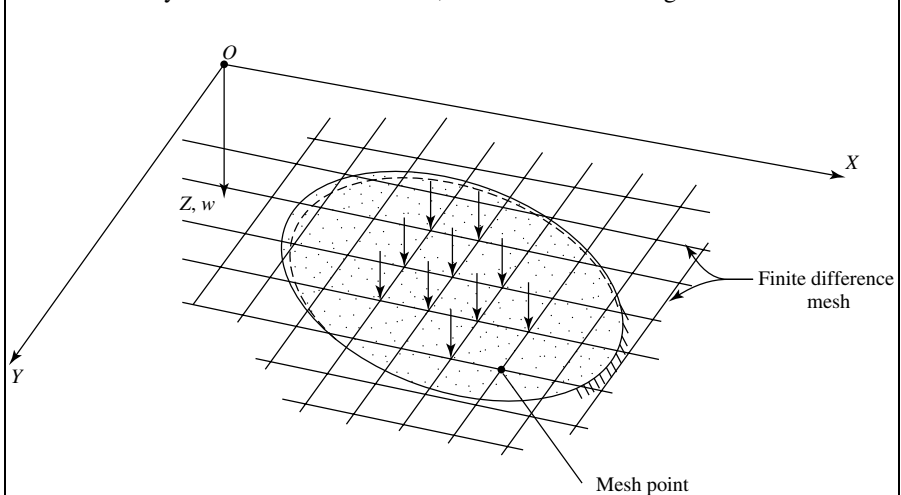


Figure Ov.1 Finite difference discretization of plate.

the FDM as viable alternatives in plate analysis. That is, the FDM may offer the following advantages over the FEM:

1. The procedure is simple and entirely transparent to the user. Consequently, there is no “black-box” mentality involved, since the analyst is always in command.
2. The use of the FDM does not require elaborate program systems with input and output procedures that are often difficult to learn.
3. The only computer program required is an algorithm for the solution of a set of algebraic equations that is readily available and very simple to use.
4. The number of equations is considerably reduced. For the use of the multilocal approach, for instance, not even a computer is required, since the limited number of equations generated by this highly accurate method can also be solved by some upscale scientific calculators with built-in equation solvers.

b. Gridwork Method. This powerful numerical method for the analysis of surface-type structures, such as plates and shells, was the forerunner of the now more popular FEM. Consequently, it exhibits many affinities with the FEM. Using the GWM, we replace the continuum of the plate by an *equivalent* gridwork of beams. Thus, this approach is based on physical instead of mathematical discretization. To determine the required equivalent bending and torsional stiffness of these beams, we may use one of the following procedures:

1. State the equivalence of the strain energies of the plate and gridwork.
2. Use the equivalence of the stress conditions between the original continuum and its substitute system.
3. Employ a limit approach of the corresponding finite difference equation of a substitute system. That is, by introducing infinitely small mesh widths, the finite difference equation of the substitute system should pass into the differential equation of the plate. From this requirement, equivalent values for bending and torsional stiffness can be determined.

Analysis of the substitute gridwork of beams (Fig. Ov.2) follows the matrix displacement method of three-dimensional framed structures that is currently familiar to

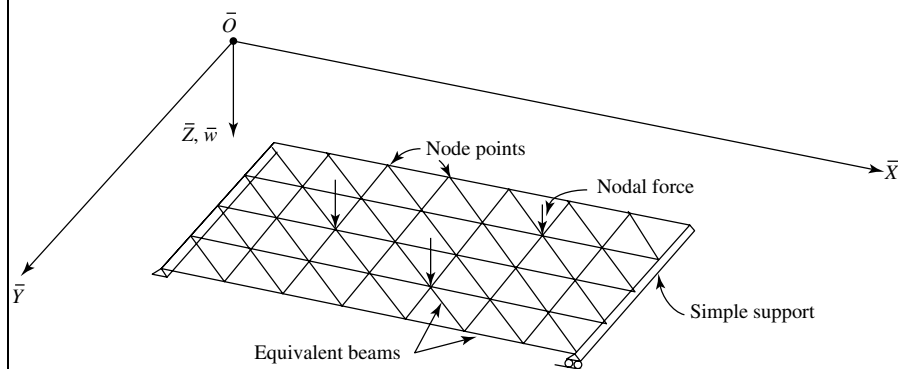


Figure Ov.2 Gridwork representation of plate bridge.

all structural engineers. Furthermore, *all pertinent computer programs can be used* for the analysis of diverse plate problems. This is one of the most important advantages of the GWM. Analysis of the substitute beam structure yields the nodal displacements, that is, one translation and two rotations. As with the matrix displacement method, treatment of the boundary conditions is relatively simple. This is not always the case with the determination of the internal forces of the plate based on the displacement field of the substitute structure. The FDM offers a welcome help in this respect.

Taking patterns from the FEM, we can also create so-called gridwork cells having three, four or more nodal points. These gridwork cells are, for all practical purposes, equivalent to finite elements; thus, they can be used in any finite element program. Furthermore, it is often easier to create so-called *conforming*[†] framework cells than to create their finite element counterparts. Consequently, the convergence characteristics of such conforming framework cells in elastic stability analysis, for instance, are superior to those of nonconforming finite elements.

c. Finite Element Method. The FEM is currently the most powerful and versatile numerical technique for the solution of structural-mechanical problems. The FEM applies a physical discretization in which the actual continuum is replaced by an assembly of discrete elements (Fig. Ov.3), referred to as finite elements, connected together to form a two- or three-dimensional structure.

Several types of FEMs have been developed for analyzing various plate problems. The three major categories are (a) FEM based on displacements, (b) mixed or hybrid FEM and (c) equilibrium-based FEM. Of the three approaches, the displacement method is the most natural and therefore the most used in engineering. Hence, in this book we deal exclusively with the displacement-type of FEM.

As already mentioned in Sec. 4.4c, in the FEM the continuum of plate is replaced by an assembly of a number of individual elements connected only at a limited

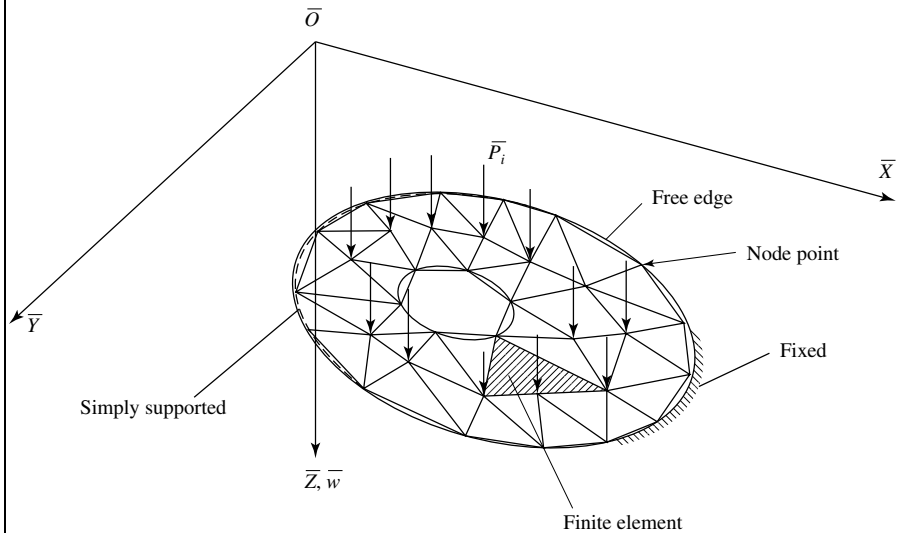


Figure Ov.3 Arbitrary plate discretized by triangular finite elements.

[†] For a definition see Secs. 7.2 and 7.4.

number of so-called *node points*. The method assumes that if the load deformation characteristics of each element can be defined, then by assembling the elements the load deflection behavior of the plate can be approximated. Mathematically, the FEM is based on the Ritz variational approach. In this case, however, we apply this classical energy method piecewise over the plate, as already discussed in Sec. 4.4c.

The practical analysis of a plate using the FEM consists of a six-stage process:

1. discretization of the continuum,
2. formulation of the element stiffness matrix,
3. assembly of the individual elements into a plate structure,
4. imposition of the prescribed boundary conditions,
5. solution of the resulting matrix displacement equations and
6. evaluation of the results.

Once the second stage has been completed, the solution technique follows the standard matrix displacement approach used in the analysis of framed structures. Thus, here we need only elaborate on the discretization and element formulation processes.

In the *discretization* of the plate, we idealize its continuum by using imaginary lines to divide it into a number of two-dimensional finite elements. These elements are assumed to be interconnected at their nodal points. The displacements of these nodal points are the basic unknowns, similar to the matrix displacement analysis of framed structures.

In the *formulation of element stiffness matrices*, shape functions are chosen to uniquely define the state of displacements within each element in terms of nodal displacements. This is done by selecting shape functions to specify the pattern in which the elements are to deform. Using these shape functions, the element stiffness matrices are derived by applying either the principle of minimum potential energy or that of virtual work.

Like its forerunner, the matrix displacement method, the FEM is also extremely well suited to computer applications. That is, because of the matrix structure of its formulation, most of the subroutines of a finite element program is based on matrix manipulations. Pertinent algorithms are, however, mostly provided in permanent library forms of all scientific computer languages. In addition, the reader can find some books that exclusively deal with the programming aspects of the FEM. These books[†] are often accompanied with diskettes that contain the necessary algorithms in prerecorded form, further facilitating their applications.

There are also numerous, commercially available finite element program systems that can deal with various plate problems. Such widely used program systems include ADINA, ANSYS, ASKA, MARC, NASTRAN, STRUDL and SAP, to name a few. Since they are too general, these very *large* program systems are relatively cumbersome to use for the solution of a specific plate problem. In addition, their learning curves are quite steep. To avoid such difficulties, program systems (such as WinPlate Primer[‡]) were developed that are devoted exclusively to the solution of various plate problems. In choosing a finite element package, one should consider the convergence

[†] For the list of them see Sec. 7.13.

[‡] See Section A.4.2.

characteristics of the program, the ease in generating the input data and the way one can evaluate the results. (These considerations are discussed in detail in the pertinent sections of Chapter 7).

d. Finite Strip Method. This method represents a semianalytical, seminumerical process that offers substantial computational advantages for a *specific* class of plate problems by drastically reducing the number of equations to be solved. The FSM was originally presented as an extension of the FEM for rectangular plate bending in which two opposite ends in one (usually in the longitudinal) direction are assumed to be simply supported while the other two edges can have arbitrary boundary conditions. We subdivide the plate into a small number of strips each of constant thickness (Fig. Ov.4). These strips represent two-dimensional finite elements having simple polynomial functions in one direction and a continuously differentiable smooth series in the other. Thus, the FSM can be considered as a special case of the FEM.

The FSM was considerably improved after its initial introduction in 1968. Now, boundary conditions other than simple supports in the longitudinal directions can be used. Furthermore, the method was also extended to cover vibration and stability analyses of thin and even moderately thick plates. The FSM can be employed advantageously in static, dynamic and stability analysis of rectangular plates, bridge slabs, box-girder bridges and shear wall-frame systems in multistory buildings.

e. Boundary Element Method. In recent years, the BEM has emerged as a powerful alternative to the FDM and FEM. While these and all other previously discussed numerical solution techniques require the discretization of the entire plate domain, the BEM applies discretization only at the boundary of the continuum (Fig. Ov.5).

Boundary element methods are usually divided into two categories: direct and indirect BEMs. The direct BEM formulates the problem in terms of variables that have definite physical meanings, such as displacements of the boundary nodes of the plate. In contrast, the indirect BEM uses variables whose physical meanings cannot always be clearly specified. Consequently, the direct BEM is more transparent. For this reason, the direct BEM is preferred by engineers and, thus, will be treated exclusively in this book. The indirect BEM still remains very much the province of applied mathematicians.

The essential feature of this method is that the governing differential equation of the plate is transformed into a set of integral equations on the boundary using Galerkin's

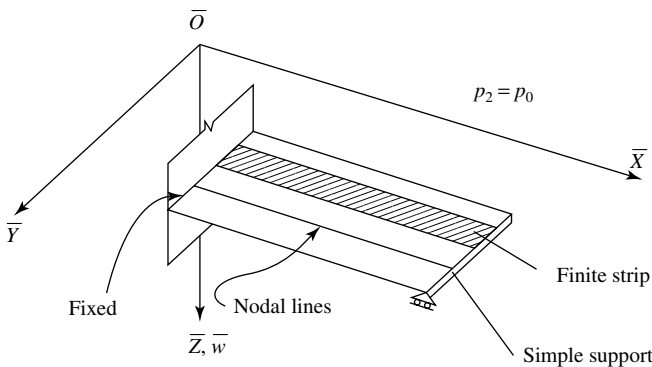


Figure Ov.4 Uniformly loaded plate represented by finite strips.

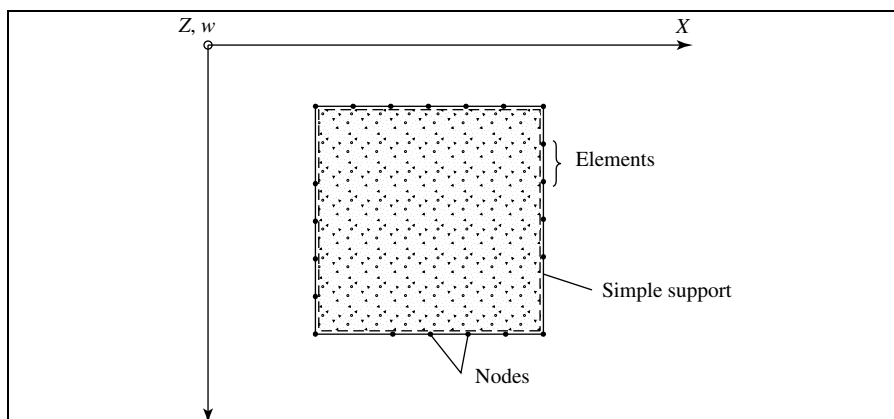


Figure Ov.5 Uniformly loaded plate discretized by using linear boundary elements.

variational approach. The so-obtained integral equations are then discretized by the help of so-called fundamental solutions of the related field equation, thus creating a finite number of elements around the external boundary of the plate. These discretized equations include nodal unknowns at the boundary of the plate alone. The prescribed boundary conditions are then used to connect the unknown boundary values to the known ones.

Mathematically, the direct version of the BEM is closely related to the collocation method and as such is not extremely difficult to relate to other domain-type methods. Thus, in many cases, it appears to be advantageous to combine the BEM with the FEM.

Several interesting advantages can be attributed to the BEM. The most important of these are

1. simplified analysis by reduction of the size of the problem to be handled and
2. ease of treatment of infinite and semi-infinite domains, such as for plate-soil interactions

In contrast to the FDM and FEM, currently the BEM is not a general-purpose numerical approach but is under rapid development. While the FEM can use, for instance, very sophisticated computer power in its preprocessing and postprocessing phase, the BEM begins with elementary solutions and uses computer implementation mostly in the very last stage. Although the mathematical requirements for the use of the BEM are much higher than in other numerical methods discussed here, anyone acquainted with influence lines or influence surfaces and superposition of unit solutions will find the main ideas of the BEM not too difficult to understand. The future of the BEM lies in making the method more accessible to the practicing engineers.

Examples. The numerical examples given in this book are solely for illustrating the applications of the various methods. Consequently, the subdivisions used are often very crude. Of course, by applying finer discretizations, the obtainable accuracy can be increased up to certain point. That is, after the convergence curve flattens out, a finer subdivision merely creates more work—and even divergence caused by roundoff

errors—instead of providing the desired higher accuracy. Thus, it is important that the user know the *convergence characteristics* of the numerical method he or she intends to use and plan the discretization of the plate structure accordingly.

Finally, the analyst should be aware of some pitfalls of the numerical computations. *Gross errors* can be caused by human or mechanical mistakes that are often very difficult to detect. For this reason, it is recommended that the computation be independently checked by another person using a different solution technique. The engineering methods treated in Part IV, for instance, offer easy-to-use alternatives for such quick checking. These approximate methods mostly require only manual computations. Of course, the results of a finite element analysis can also be independently checked by either the GWM or the FDM using computerized approaches.

Roundoff errors may also distort the end results. These errors are created by not using a sufficient number of digits in the computation. Another source of error is *truncation error*, which occurs when an originally infinite process is truncated after a finite number of steps. Sometimes even the *algorithms* used in the numerical process are *unstable*. In such case, a “small perturbation” in a single coefficient changes the process from one that yields a unique solution to one that gives an infinite number of solutions to the same problem.

A very important source of error can be an *ill-conditioned* coefficient matrix of a system of algebraic equations. Such ill-conditioned systems are characterized by the fact that the determinant of the coefficient matrix is small in magnitude relative to certain cofactors of elements of the matrix. This is often encountered in the stability analysis of plates, because large numbers occur next to relatively very small numbers in the main diagonal of the coefficient matrix. The large numbers represent the resistance of the plate to axial compression, while the small numbers are pertinent to its much smaller bending stiffness. Increasing the significant figures used in the computation often eliminates this very disturbing error that may render the results of the whole computation entirely useless.

Remember that in the engineering application of plate analysis we are usually dealing with *inaccurate input data*. In the first place, the external loads are known only with a certain degree of accuracy. In addition, the material properties, such as the modulus of elasticity E and Poisson’s ratio ν , can contain certain inaccuracies. Furthermore, the actual boundary conditions are merely approximations of the theoretical ones. Consequently, even an “exact” solution can only approximate the real behavior of a plate. The error caused by these inherent inaccuracies of the input is called *error of data*.

The above-mentioned *errors of calculation* introduced in our numerical computation must always be smaller than the data errors. As a rule, it is desirable that the errors of calculation have less than $\pm 5\%$ discrepancy in comparison with the mathematically exact solution of a given plate problem.

Last, but not least, the emotional state of the analyst should not be neglected, since it is frequently a source of human error. Consequently, any haste in computation should be avoided. No calculation should be attempted when the analyst is upset, depressed or overly excited. Without a “cool head” for logical thinking, any type of computation is virtually impossible. A clear and systematic presentation of each computational step not only permits an easier independent check by other persons but also mitigates the chances for human error.

Summary. The interest of engineers in numerical methods has grown exponentially in the last decades for various reasons. First, high-capacity personal computers are

now mass produced and, thus, are available for a very reasonable price. Second, these computers combined with commercially available subroutines or complete program systems make it possible to obtain numerical results for complex, “real-world” plate problems in engineering practice for which analytical solutions are not available. Third, most numerical processes can be handled by engineers with somewhat limited training in higher mathematics.

These conditions not only explain the popularity of numerical methods in plate analysis but also emphasize the need for extensive training of students in these disciplines in colleges and universities. Therefore, a comprehensive and systematic presentation of the most important numerical methods—briefly introduced above—occupies a significant part of this book. A large number of worked numerical examples are also given in order to facilitate the understanding and practical applications of these methods.

5

Finite Difference Methods

5.1 Ordinary Finite Difference Methods

a. Introduction. In the previous chapters, plate problems were solved by means of various analytical approaches. Due to their inherent mathematical difficulties, however, such analytical solutions are restricted to simple plate geometry, loading and boundary conditions. As mentioned earlier, for many plate problems of considerable practical interest, analytical solutions to the governing differential equations cannot be found; thus, numerical methods must be engaged to obtain approximate solutions. Among the numerical techniques presently available for solutions of various plate problems, the *finite difference method* (FDM) is probably the most transparent and the most general. Especially, plate bending analysis is a classical field of the FDM. Today, despite the existence of numerous finite element-based software packages, the FDM can still be regarded as a numerical method that has merit due to its straightforward approach and a minimum requirement on hardware. In applying the FDM, the derivatives in the governing differential equations are replaced by difference quantities at some selected points of the plate. These points are located at the joints of a square, rectangular, triangular or other reference network, called a *finite difference mesh*. Consequently, if some static, dynamic or elastic stability problem of a plate can be described by a differential equation, we can replace it at each mesh point by an equivalent finite difference equation. A similar approach is taken with the expressions describing the boundary conditions. Thus, the FDM applies a mathematical discretization of the plate continuum yielding a set of algebraic equations, from which the plate deflections at the mesh points can be obtained.

b. Finite Difference Expressions. In the ordinary FDM, we replace the differential operators d and ∂ by suitable *difference operators* Δ . Let us first consider the one-dimensional case. To obtain finite difference expressions for derivatives, we approximate the function $y = f(x)$ a given interval by an *interpolating polynomial* $\phi(x)$ and accept $\phi'(x), \phi''(x), \phi'''(x), \dots$ in place of $f'(x), f''(x), f'''(x), \dots$. It is evident that a better polynomial approximation of the original function $f(x)$ at the

so-called *pivotal* point m yields better finite difference expressions and therefore improved accuracy.

The simplest way of obtaining usable finite difference expressions for the first and second derivatives of a function $y = f(x)$ at a pivotal point m is by substituting for $f(x)$ a second-order parabola through a number of equally placed points, as shown in Fig. 5.1.1. This *collocating* polynomial using Δx intervals between points can be expressed by

$$\phi(x) = y_m + \frac{y_{m+1} - y_{m-1}}{2(\Delta x)} \cdot x + \frac{y_{m+1} - 2y_m + y_{m-1}}{(\Delta x)^2} \cdot \frac{x^2}{2}; \quad (5.1.1)$$

therefore

$$\phi'(x) = \frac{y_{m+1} - y_{m-1}}{2(\Delta x)} + \frac{y_{m+1} - 2y_m + y_{m-1}}{(\Delta x)^2} \cdot x. \quad (5.1.2)$$

Since the pivotal point m is located at $x_m = 0$, the first derivative of the original function can be approximated by

$$\left(\frac{dy}{dx} \right)_m \approx \left(\frac{\Delta y}{\Delta x} \right)_m = [\phi'(x)]_m = \frac{1}{2(\Delta x)} (y_{m+1} - y_{m-1}). \quad (5.1.3)$$

Similarly, the finite difference expression for the second derivative is

$$\left(\frac{d^2y}{dx^2} \right)_m = \left[\frac{d}{dx} \left(\frac{dy}{dx} \right) \right]_m \approx \left(\frac{\Delta^2 y}{\Delta x^2} \right)_m = \phi''(x)_m = \frac{1}{(\Delta x)^2} (y_{m+1} - 2y_m + y_{m-1}). \quad (5.1.4)$$

A procedure identical to that used above yields the higher-order derivatives

$$\begin{aligned} \left(\frac{d^3y}{dx^3} \right)_m &\approx \left[\frac{\Delta}{2(\Delta x)} \left(\frac{\Delta^2 y}{\Delta x^2} \right) \right]_m = \frac{1}{2(\Delta x)^3} (\Delta^2 y_{m+1} - \Delta^2 y_{m-1}) \\ &= \frac{1}{2(\Delta x)^3} (y_{m+2} - 2y_{m+1} + 2y_{m-1} - y_{m-2}) \end{aligned} \quad (5.1.5)$$

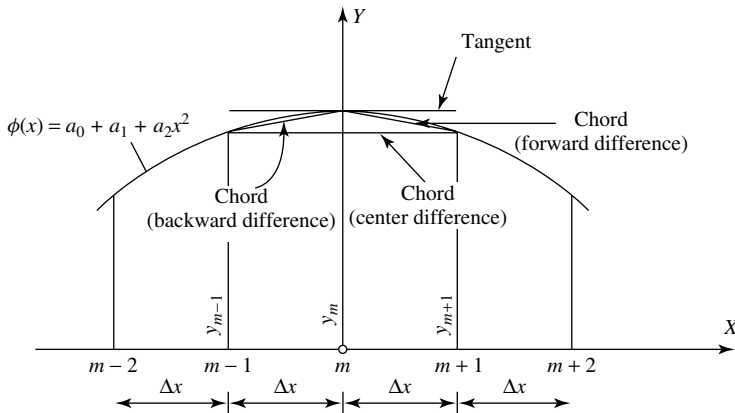


Figure 5.1.1 Graphical representation of finite differences.

and

$$\begin{aligned}
 \left(\frac{d^4 y}{dx^4}\right)_m &\approx \left(\frac{\Delta^4 y}{\Delta x^4}\right)_m = \left[\frac{\Delta}{\Delta x} \left(\frac{\Delta^3 y}{\Delta x^3}\right)\right]_m = \frac{1}{(\Delta x)^4} (\Delta^3 y_{m+1/2} - \Delta^3 y_{m-1/2}) \\
 &= \frac{1}{(\Delta x)^4} (\Delta^2 y_{m+1} - 2 \Delta^2 y_m + \Delta^2 y_{m-1}) \\
 &= \frac{1}{(\Delta x)^4} (y_{m+2} - 4y_{m+1} + 6y_m - 4y_{m-1} + y_{m-2}), \quad (5.1.6)
 \end{aligned}$$

These expressions are called *central differences*, since they can also be obtained by advancing centrally in the table of differences with discrete points located symmetrically with respect to the pivotal point m , as shown in Table 5.1.1. These finite difference expressions are schematically represented in Table 5.1.2, including the first *error terms* ε_1 obtained by using the Taylor series approach, discussed later.

The physical meaning of central differences is also shown in Fig. 5.1.1. That is, using a second-order parabola for interpolating polynomials, the slope of the chord line from point x_{m-1} to point x_{m+1} becomes identical to that of the tangent at point x_m . Similarly, we can interpret the meaning of the first *forward difference*

$$\left(\frac{dy}{dx}\right)_m \approx \left(\frac{\Delta y}{\Delta x}\right)_m = \frac{y_{m+1} - y_m}{\Delta x} \quad (5.1.7)$$

and that of the first *backward difference*

$$\left(\frac{dy}{dx}\right)_m \approx \left(\frac{\Delta y}{\Delta x}\right)_m = \frac{y_m - y_{m-1}}{\Delta x}. \quad (5.1.8)$$

We shall thereafter consider only central differences because of their higher accuracy.

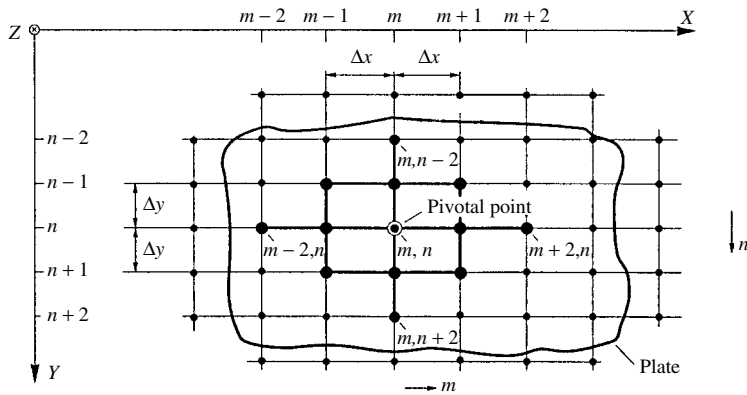
C. Finite Difference Representation of Plate Equation. Let us restrict our derivation to equally spaced square mesh. Introducing a $\Delta x = \Delta y = \lambda$ mesh width (Fig. 5.1.2.), the finite difference expressions for the fourth-order derivatives of

Table 5.1.1 “Central” Differences

x	y	Δy	$\Delta^2 y$	$\Delta^3 y$	$\Delta^4 y$
x_{m-2}	y_{m-2}				
		$\Delta y_{m-(3/2)}$			
x_{m-1}	y_{m-1}		$\Delta^2 y_{m-1}$		
		$\Delta y_{m-(1/2)}$		$\Delta^3 y_{m-(1/2)}$	
x_m	y_m		$\Delta^2 y_m$		$\Delta^4 y_m$
		$\Delta y_{m+(1/2)}$		$\Delta^3 y_{m+(1/2)}$	
x_{m+1}	y_{m+1}		$\Delta^2 y_{m+1}$		
		$\Delta y_{m+(3/2)}$			
x_{m+2}	y_{m+2}				

Table 5.1.2 Schematic Representation of Derivatives by Central Differences

$y_m^{(k)}$	Coefficients	First Error Term
y'_m	$\left[\begin{array}{ccccc} \ominus & & & & \oplus \end{array} \right] \frac{1}{2(\Delta x)}$	$-\frac{1}{6}(\Delta x)^2 y_m'''$
y''_m	$\left[\begin{array}{ccccc} \oplus & - & \ominus & - & \oplus \end{array} \right] \frac{1}{(\Delta x)^2}$	$-\frac{1}{12}(\Delta x)^2 y_m^{IV}$
y'''_m	$\left[\begin{array}{ccccc} \ominus & - & \oplus & & \ominus & - & \oplus & & \ominus \end{array} \right] \frac{1}{2(\Delta x)^3}$	$-\frac{1}{4}(\Delta x)^2 y_m^V$
y_m^{IV}	$\left[\begin{array}{ccccc} \oplus & - & \ominus & - & \oplus & - & \ominus & - & \oplus \end{array} \right] \frac{1}{(\Delta x)^4}$	$-\frac{1}{6}(\Delta x)^2 y_m^{VI}$
Point	$\begin{array}{ccccccccc} \ominus & \ominus & \ominus & \ominus & \ominus \\ m-2 & m-1 & m & m+1 & m+2 \end{array}$	ε_1

**Figure 5.1.2** Plate covered by rectangular mesh.

Eq. (1.2.30) can be written as

$$\begin{aligned} \left(\frac{\partial^4 w}{\partial x^4} \right)_{m,n} &\approx \frac{1}{\lambda^4} (w_{m+2,n} - 4w_{m+1,n} + 6w_{m,n} - 4w_{m-1,n} + w_{m-2,n}), \\ \left(\frac{\partial^4 w}{\partial y^4} \right)_{m,n} &\approx \frac{1}{\lambda^4} (w_{m,n+2} - 4w_{m,n+1} + 6w_{m,n} - 4w_{m,n-1} + w_{m,n-2}). \end{aligned} \quad (5.1.9)$$

Similarly, the finite difference expression of the *mixed* fourth derivative $\partial^4 w / (\partial x^2 \partial y^2)$ is derived by using the same approach as described above for the fourth derivatives; thus

$$\begin{aligned} \left(\frac{\partial^4 w}{\partial x^2 \partial y^2} \right)_{m,n} &\approx \left\{ \frac{\Delta^2}{(\Delta y)^2} \left[\frac{\Delta^2 w}{(\Delta x)^2} \right] \right\}_{m,n} \\ &= \frac{1}{(\Delta y)^2} \left\{ \left[\frac{\Delta^2 w}{(\Delta x)^2} \right]_{m,n+1} - 2 \left[\frac{\Delta^2 w}{(\Delta x)^2} \right]_{m,n} + \left[\frac{\Delta^2 w}{(\Delta x)^2} \right]_{m,n-1} \right\} \end{aligned}$$

$$= \frac{1}{\lambda^4} [4w_{m,n} - 2(w_{m+1,n} + w_{m-1,n} + w_{m,n+1} + w_{m,n-1}) + w_{m+1,n+1} + w_{m+1,n-1} + w_{m-1,n+1} + w_{m-1,n-1}]. \quad (5.1.10)$$

Therefore, the finite difference representation of Eq. (1.2.30) at pivotal point m, n is

$$(D \nabla^2 \nabla^2 w)_{m,n} \approx \frac{D}{\lambda^4} [20w_{m,n} - 8(w_{m+1,n} + w_{m-1,n} + w_{m,n+1} + w_{m,n-1}) + 2(w_{m+1,n+1} + w_{m-1,n+1} + w_{m+1,n-1} + w_{m-1,n-1}) + w_{m+2,n} + w_{m-2,n} + w_{m,n+2} + w_{m,n-2}] + \varepsilon(\lambda^2) = (p_z)_{m,n},$$

(5.1.11)

where $\varepsilon(\lambda^2)$ is the *error term* describing the discrepancy between the exact expression of the biharmonic operator (∇^4 operating on w) and its finite difference representation. The accuracy of the finite difference method can be improved by reducing the error term, as described in Sec. 5.2. In Fig. 5.1.3, Eq. (5.1.11) is given in a diagrammatic form. Again, using the m, n pivotal point, the finite difference expressions for the internal forces and moments are

$$\begin{aligned} (m_x)_{m,n} &\approx -D \left[\frac{\Delta^2 w}{(\Delta x)^2} + \nu \frac{\Delta^2 w}{(\Delta y)^2} \right]_{m,n} \\ &= -\frac{D}{\lambda^2} [(w_{m+1,n} - 2w_{m,n} + w_{m-1,n}) + \nu(w_{m,n+1} - 2w_{m,n} + w_{m,n-1})], \end{aligned} \quad (5.1.12)$$

$$\begin{aligned} (m_y)_{m,n} &\approx -D \left[\frac{\Delta^2 w}{(\Delta y)^2} + \nu \frac{\Delta^2 w}{(\Delta x)^2} \right]_{m,n} \\ &= -\frac{D}{\lambda^2} [(w_{m,n+1} - 2w_{m,n} + w_{m,n-1}) + \nu(w_{m+1,n} - 2w_{m,n} + w_{m-1,n})], \end{aligned} \quad (5.1.13)$$

$$\begin{aligned} (m_{xy})_{m,n} = (m_{yx})_{m,n} &\approx -(1-\nu)D \left\{ \frac{\Delta}{2(\Delta x)} \left[\frac{\Delta w}{2(\Delta y)} \right] \right\}_{m,n} \\ &= -\frac{(1-\nu)D}{4\lambda^2} (w_{m+1,n+1} - w_{m+1,n-1} - w_{m-1,n+1} + w_{m-1,n-1}), \end{aligned} \quad (5.1.14)$$

$$\begin{aligned} (q_x)_{m,n} &\approx -D \left\{ \frac{\Delta}{2(\Delta x)} \left[\frac{\Delta^2 w}{(\Delta x)^2} + \frac{\Delta^2 w}{(\Delta y)^2} \right] \right\}_{m,n} \\ &= -\frac{D}{2\lambda} \left\{ \left[\left(\frac{\Delta^2 w}{(\Delta x)^2} \right)_{m+1,n} - \left(\frac{\Delta^2 w}{(\Delta x)^2} \right)_{m-1,n} \right] \right. \\ &\quad \left. + \left[\left(\frac{\Delta^2 w}{(\Delta y)^2} \right)_{m+1,n} - \left(\frac{\Delta^2 w}{(\Delta y)^2} \right)_{m-1,n} \right] \right\} \end{aligned}$$

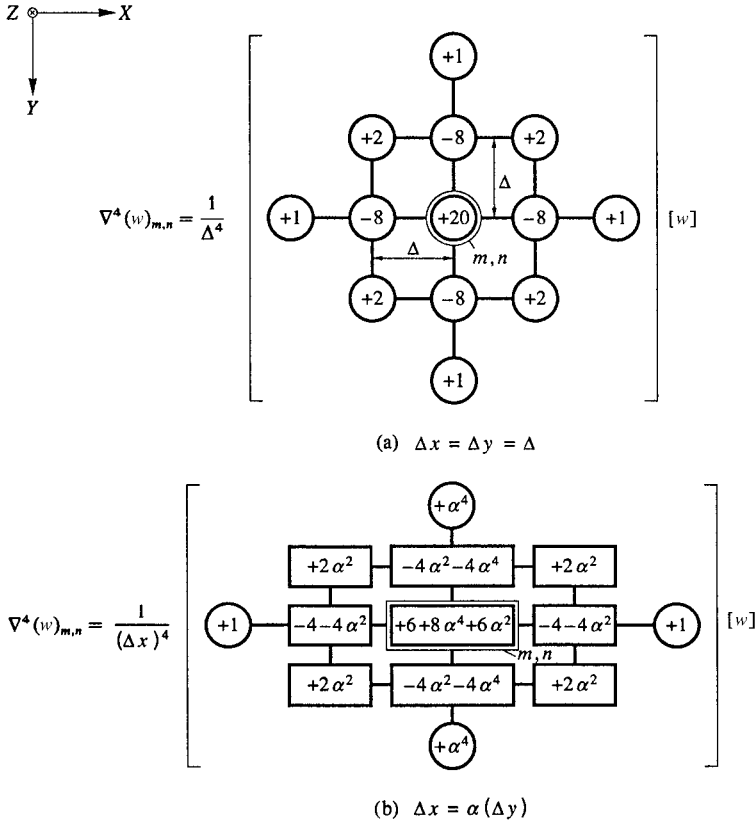


Figure 5.1.3 Stencils for interior mesh points.

$$\begin{aligned}
 &= -\frac{D}{2\lambda^3} [(w_{m+2,n} - 2w_{m+1,n} + 2w_{m-1,n} - w_{m-2,n}) \\
 &\quad + (w_{m+1,n+1} - 2w_{m+1,n} + w_{m+1,n-1} - w_{m-1,n+1} \\
 &\quad + 2w_{m-1,n} - w_{m-1,n-1})], \quad (5.1.15)
 \end{aligned}$$

$$\begin{aligned}
 (q_y)_{m,n} &\approx -D \left\{ \frac{\Delta}{2(\Delta y)} \left[\frac{\Delta^2 w}{(\Delta x)^2} + \frac{\Delta^2 w}{(\Delta y)^2} \right] \right\}_{m,n} \\
 &= -\frac{D}{2\lambda} \left\{ \left[\left(\frac{\Delta^2 w}{(\Delta x)^2} \right)_{m,n+1} - \left(\frac{\Delta^2 w}{(\Delta x)^2} \right)_{m,n-1} \right] \right. \\
 &\quad \left. + \left[\left(\frac{\Delta^2 w}{(\Delta y)^2} \right)_{m,n+1} - \left(\frac{\Delta^2 w}{(\Delta y)^2} \right)_{m,n-1} \right] \right\} \\
 &= -\frac{D}{2\lambda^3} [(w_{m+1,n+1} - 2w_{m,n+1} + w_{m-1,n+1} - w_{m+1,n-1} \\
 &\quad + 2w_{m,n-1} - w_{m-1,n-1}) \\
 &\quad + (w_{m,n+2} - 2w_{m,n+1} + 2w_{m,n-1} - w_{m,n-2})]. \quad (5.1.16)
 \end{aligned}$$

The pattern of coefficients for these finite difference approximations of the stress resultants is given in Fig. 5.1.4.

d. Boundary Conditions. Solution of the governing plate equation (1.2.30) by the finite difference method also requires proper finite difference representation of the boundary conditions. Consequently, we replace the derivatives in the mathematical expressions of various boundary conditions (discussed in Sec. 1.3) with the pertinent finite difference expressions. When central differences are used, however, the introduction of fictitious points outside of the plate is required.

The finite difference expression of Eq. (1.3.1), describing a fixed boundary condition along a grid line parallel to the X axis (Fig. 5.1.5a), gives

$$w_{m,n} = 0 \quad \text{and} \quad \left(\frac{\partial w}{\partial x} \right)_{m,n} \approx \frac{1}{2\lambda} (w_{m+1,n} - w_{m-1,n}) = 0, \quad (5.1.17)$$

which represents zero deflection and slope at pivotal point m, n . Therefore, from Eq. (5.1.17) it follows that

$$w_{m+1,n} = w_{m-1,n}. \quad (5.1.18)$$

Although a fictitious point $(m-1, n)$ has been introduced to express the boundary condition by central differences, no additional deflection ordinate is carried in the computation.

The boundary condition representing a simple support (Fig. 5.1.5b) can be treated in a similar manner. The finite difference form of Eq. (1.3.7) gives

$$w_{m,n} = 0 \quad \text{and} \quad \left(\frac{\partial^2 w}{\partial x^2} + \nu \frac{\partial^2 w}{\partial y^2} \right)_{m,n} \approx w_{m+1,n} + w_{m-1,n} = 0; \quad (5.1.19)$$

hence

$$w_{m+1,n} = -w_{m-1,n}. \quad (5.1.20)$$

The treatment of a free boundary condition by central differences is somewhat more involved. If the pivotal point (m, n) is at the boundary, we must introduce four fictitious points outside of the plate (Fig. 5.1.6a). Again, deflections at these fictitious points can be expressed in terms of deflections of the mesh points located on the plate. For this purpose, we specify that the edge force and edge moment at the pivotal point are zero. Using notations of Fig. 5.1.6a, the finite difference form of Eqs. (1.3.2) and (1.3.3) becomes

$$(m_y)_{m,n} \approx -(2 + 2\nu)w_{m,n} + w_{m,n-1} + w_{m,n+1} + \nu(w_{m-1,n} + w_{m+1,n}) = 0, \quad (5.1.21)$$

$$\begin{aligned} (v_y)_{m,n} &\approx (6 - 2\nu)(w_{m,n-1} - w_{m,n+1}) + (2 - \nu) \\ &\quad \times (w_{m+1,n+1} + w_{m-1,n+1} - w_{m-1,n-1} - w_{m+1,n-1}) \\ &\quad - w_{m,n-2} + w_{m,n+2} = 0. \end{aligned} \quad (5.1.22)$$

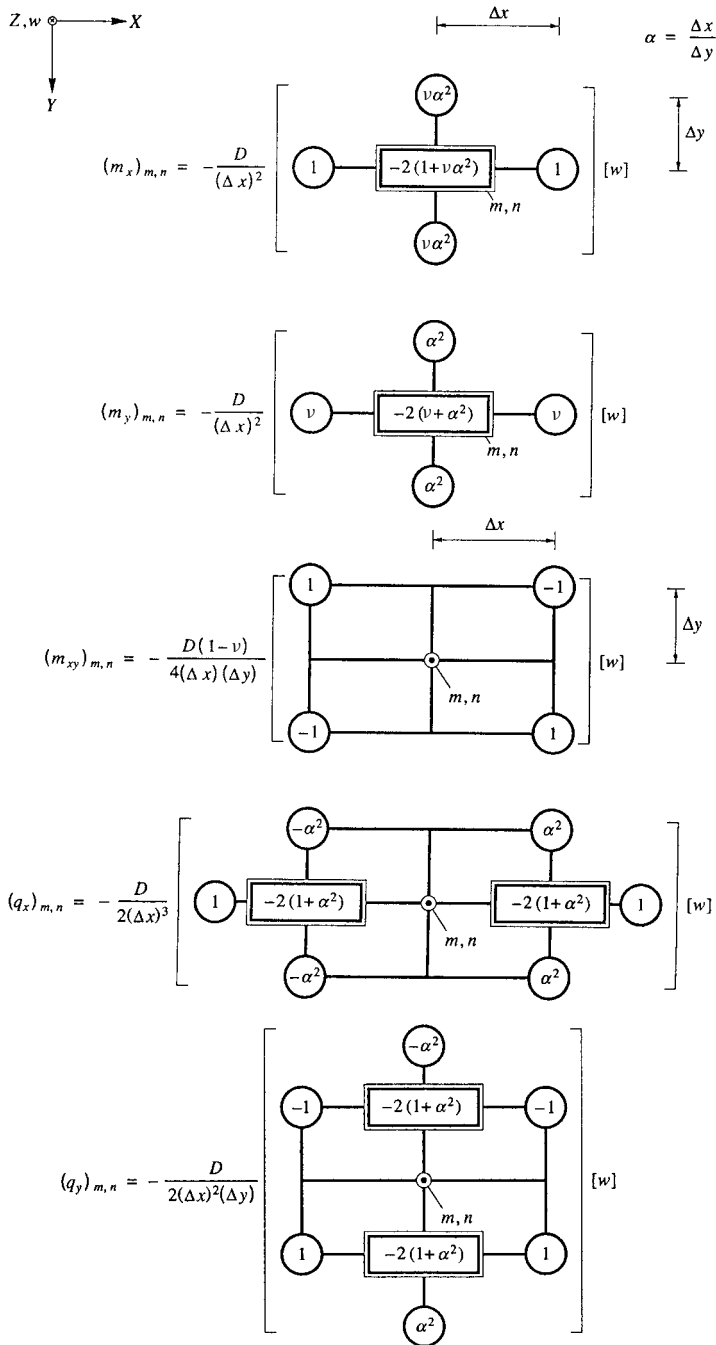


Figure 5.1.4 Stencils for moments and lateral shear forces.

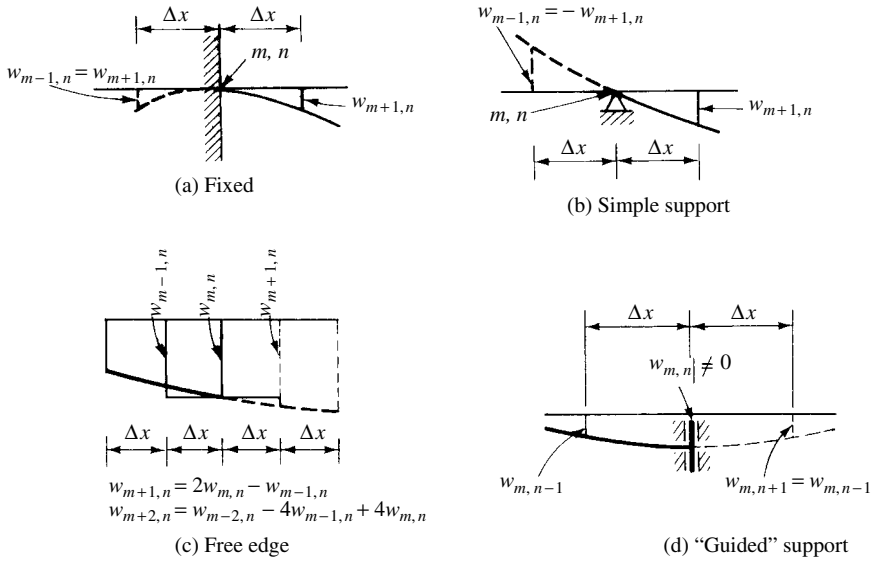


Figure 5.1.5 Representation of boundary conditions for ordinary FDM.

The two additional equations required to eliminate the deflections of the fictitious points from Eq. (5.1.21) are

$$(m_y)_{m-1,n} \approx -2(1+\nu)w_{m-1,n} + w_{m-1,n-1} + w_{m-1,n+1} + \nu(w_{m-2,n} + w_{m,n}) = 0 \quad (5.1.23)$$

and

$$(m_y)_{m+1,n} \approx -(2+2\nu)w_{m+1,n} + w_{m+1,n-1} + w_{m+1,n+1} + \nu(w_{m+2,n} + w_{m,n}) = 0. \quad (5.1.24)$$

Eliminating $w_{m,n+2}$, $w_{m-1,n+1}$, $w_{m,n+1}$ and $w_{m+1,n+1}$ from these equations and substituting the result into Eq. (5.1.21), the finite difference representation of the free-edge condition is obtained. This is schematically shown in Fig. 5.1.6b.

When the pivotal point is at distance λ from the free-edge (Fig. 5.1.7a), the deflection of the fictitious mesh point $m, n+2$ can be eliminated by stating that the m_y moment at this point is zero. The finite difference form of this boundary condition is

$$(m_y)_{m,n+2} \approx -\frac{D}{2\lambda^2}[(w_{m,n+2} - 2w_{m,n+1} + w_{m,n}) + \nu(w_{m+1,n+1} - 2w_{m,n+1} + w_{m-1,n+1})] = 0, \quad (5.1.25)$$

from which

$$w_{m,n+2} = 2w_{m,n+1}(1+\nu) - w_{m,n} - (w_{m+1,n+1} + w_{m-1,n+1})\nu. \quad (5.1.26)$$

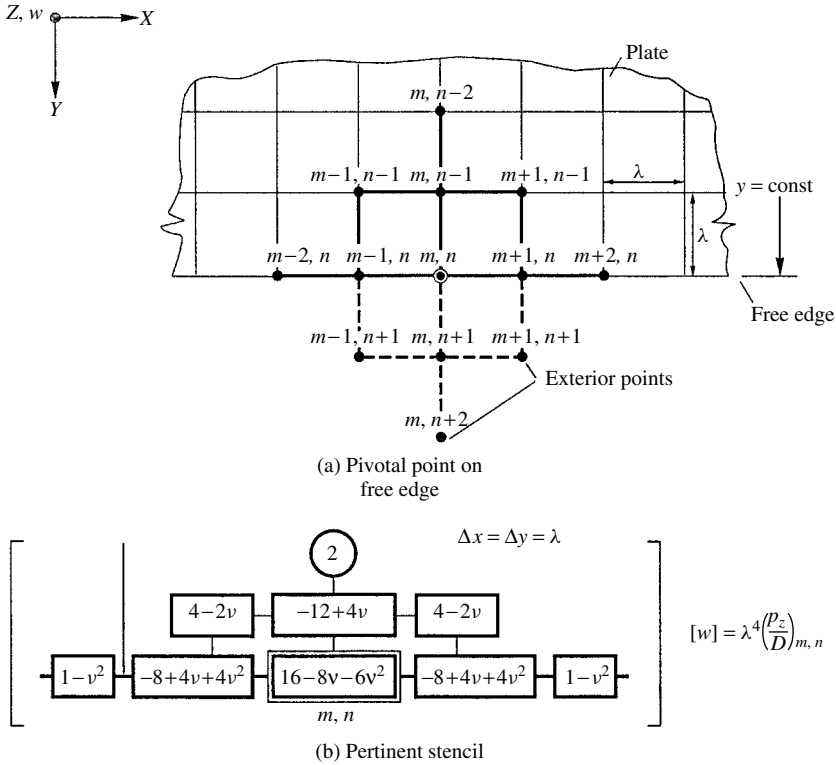


Figure 5.1.6 Finite difference representation of free edge.

Substituting this expression into Eq. (5.1.11), we obtain the finite difference representation of this condition, which is schematically shown in Fig. 5.1.7b.

At a *corner* where two free-edges parallel to the X and Y axes meet, we first apply the free-edge boundary condition to all mesh points on the edge parallel to the X axis. Then, we apply similar equations to the mesh points on the edge parallel to the Y axis. In addition, we state that at the corner the torsional moment $m_{xy} = 0$. The obtained finite difference patterns are schematically shown in Fig. 5.1.8. In the case of rectangular mesh, stencils pertinent to various free-edge conditions are given in Fig. 5.1.9. It is obvious that the axes could be rotated for all the preceding finite difference patterns.

When the plate is continuous over beam supports, we may follow three different approaches in the analysis. First, if the beams are small and closely spaced, such a plate and beam assembly can be considered an orthotropic plate, the analysis of which is discussed in detail in Sec. 10.1. If the supporting beams are large and relatively widely spaced, we may either apply the readily usable stencils given in Refs. [5.1.13] and [5.1.14] or carry out the following simple iteration: We begin this iterative cycle by assuming that the beams represent rigid supports. Next the reactive forces acting on these beams are calculated. Then we load the beams with these reactive forces, making them active, and calculate the beam deflections at each mesh point. In doing so, however, we must consider in the moment of inertia the

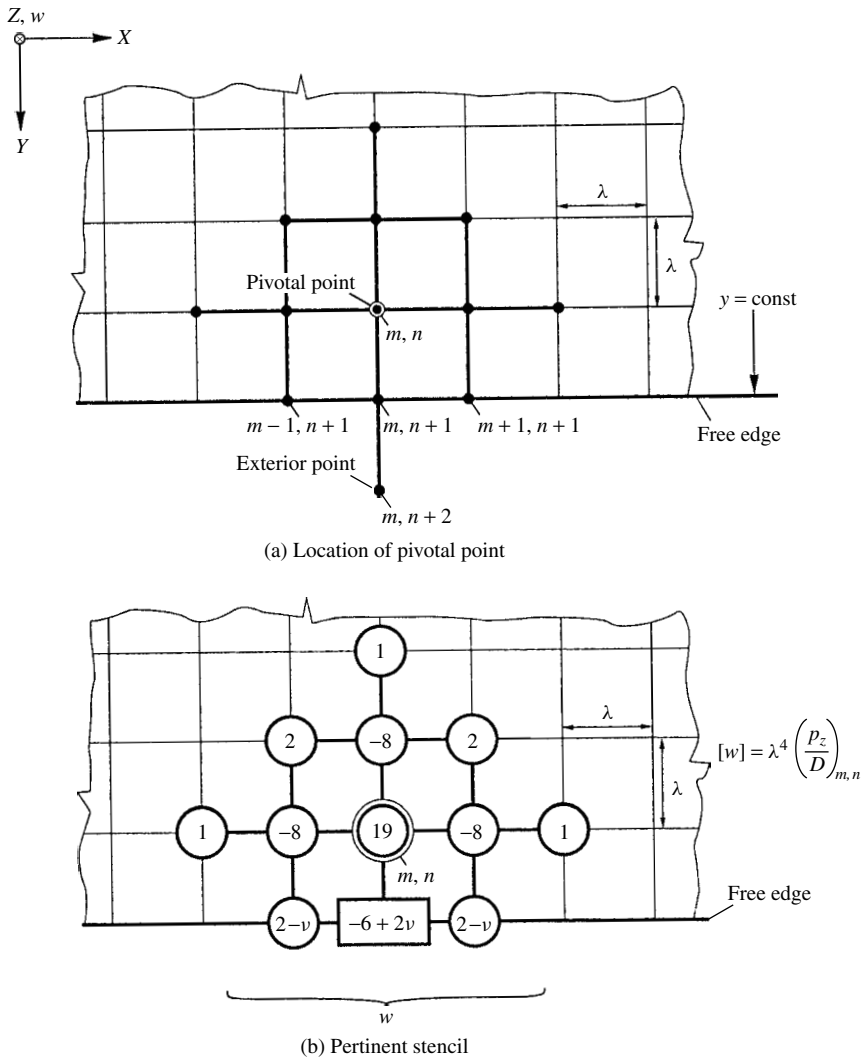


Figure 5.1.7 Pivotal point near edge of plate.

effective width[†] of the plate that acts together with the beam. In the last step, the calculated deflections are introduced into the finite difference analysis of the plate as known values. If necessary, this iterative cycle can be repeated until convergence is achieved. However, a second iterative cycle is only seldom required.

Curved boundaries may require an unevenly spaced finite difference mesh. In this case, the derivation of ordinary finite difference expressions remains fundamentally the same, but the resulting expressions [5.1.4] are cumbersome to handle. Consequently, it is more economical to approximate the plate geometry by equally placed

[†] For definition and approximate values see Sec. 16.10.

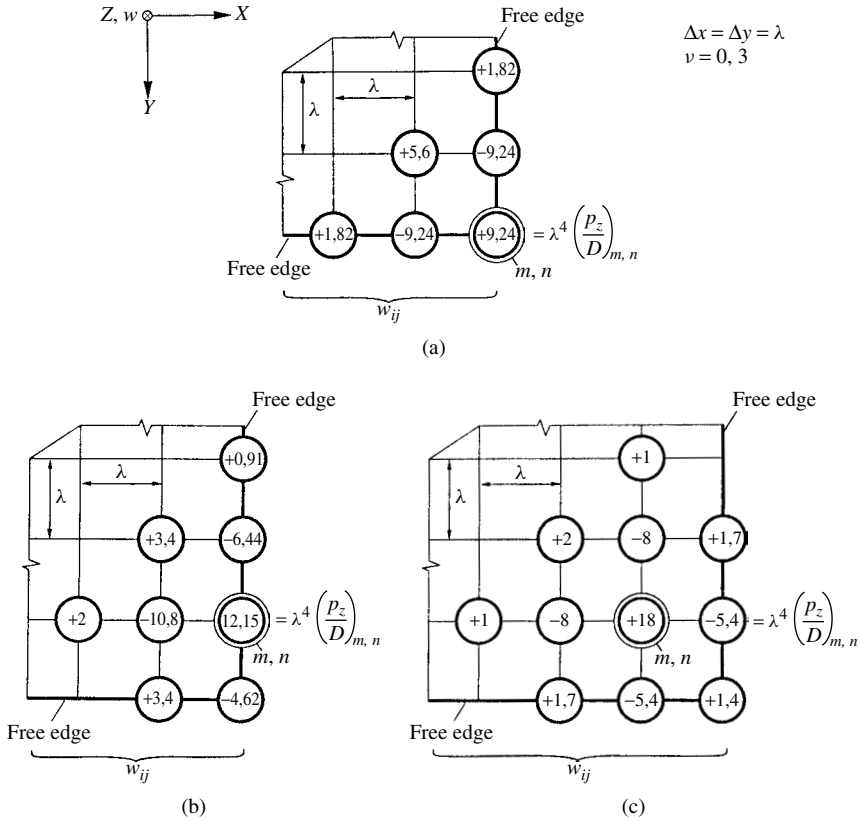


Figure 5.1.8 Finite difference stencils at free corner.

mesh points, as shown in Fig. 5.1.10. Such a practical approximation is discussed in more detail later in this section.

By representing the governing differential of the plate and the equations defining the prescribed boundary conditions of a given problem by finite difference expressions, we replace the continuum of the plate with a pattern of discrete points. Consequently, the original problem of solving the plate equation has been transformed into the solution of a set of simultaneous algebraic equations in the form

$$\mathbf{A}\mathbf{w} = \mathbf{p}, \quad (5.1.27)$$

where \mathbf{A} symbolizes the resulting coefficient matrix, \mathbf{w} is the vector of the unknown mesh-point displacements and \mathbf{p} represents the vector of the loads acting on the mesh points (to be discussed next). The solution of this matrix equation can be easily accomplished by personal computers or one of the more advanced programmable calculators with a built-in equation solver.

e. Load Representation. If the lateral load p_z is uniformly distributed, its value can be readily substituted into the right-hand side of Eq. (5.1.11). This method can

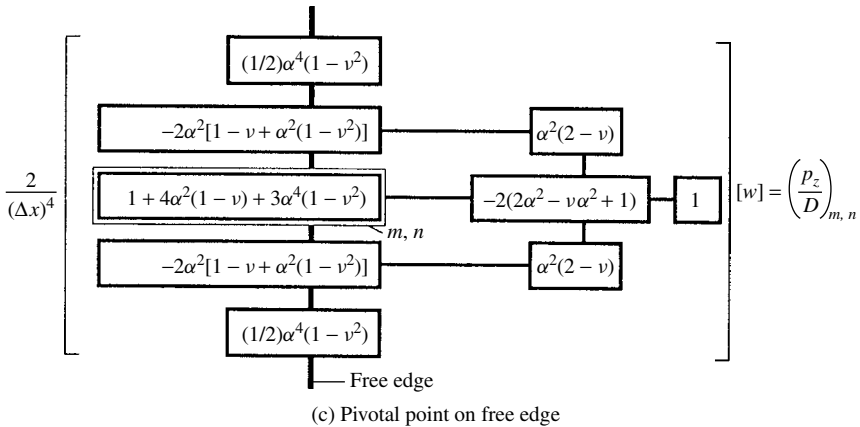
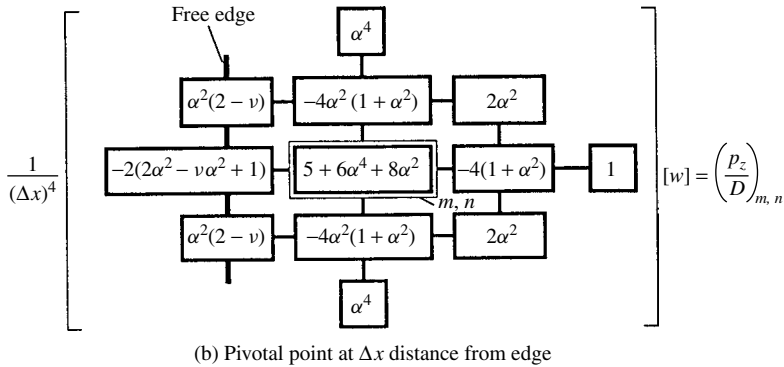
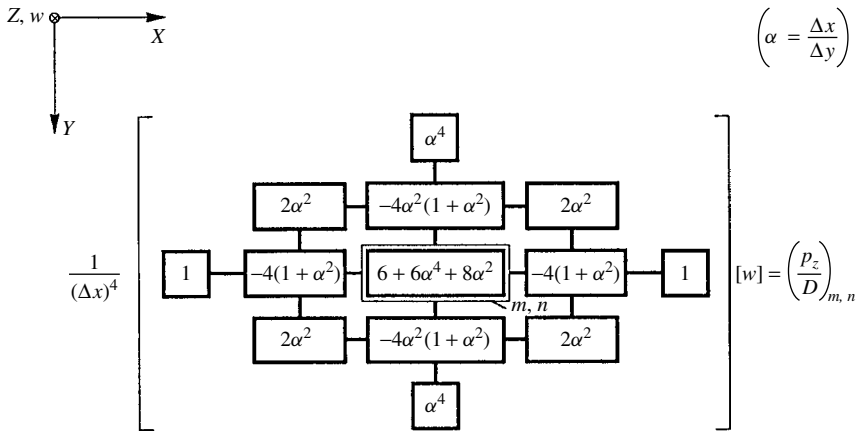


Figure 5.1.9 Finite difference patterns with various locations of pivotal point m, n .

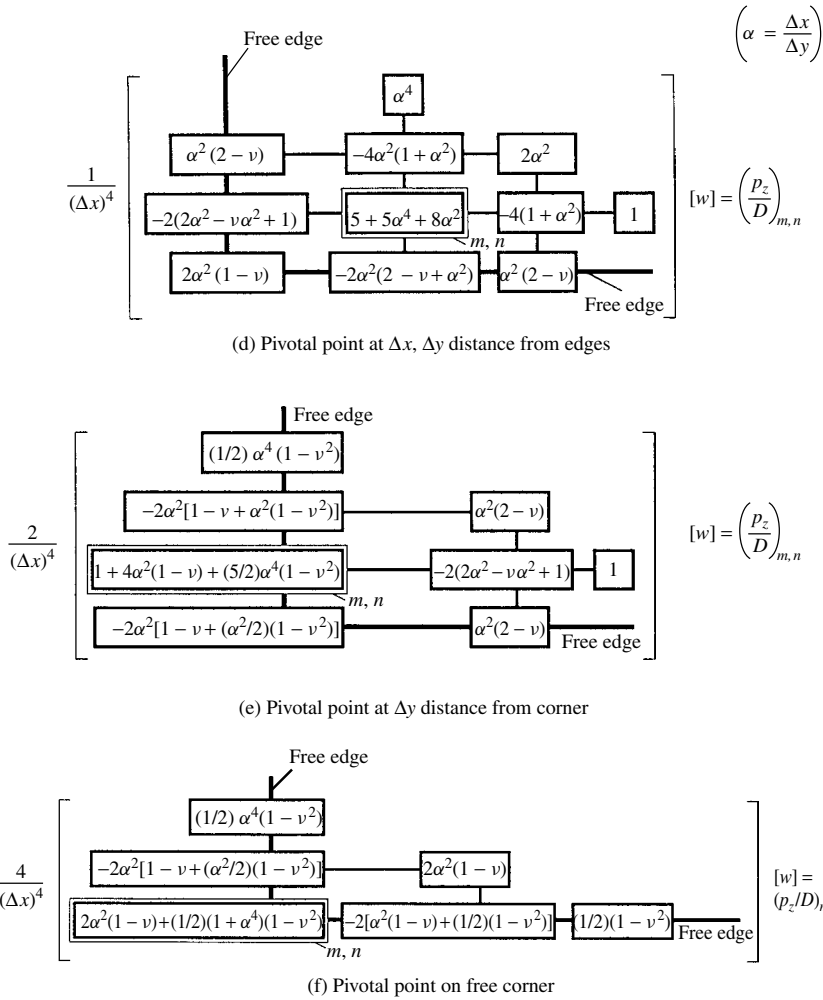


Figure 5.1.9 (continued)

be extended to other types of distributed lateral loads, $p_z(x, y)$, provided that the variation of the load intensity from mesh point to mesh point is not excessive. This type of load representation results in a *stepped distribution* (Fig. 5.1.11), which, in a general case, can yield good results only if the width of the mesh (λ) is relatively small. This statement is especially true for the representation of concentrated loads by stepped distribution in the form

$$(p_z)_{m,n} = \left[\frac{P_z}{(\Delta x)(\Delta y)} \right]_{m,n}, \quad (5.1.28)$$

which in the extreme case ($\lambda \rightarrow 0$) can create a singularity ($w_{m,n} \rightarrow \infty$) in the solution. This problem can easily be overcome by expressing the concentrated load by an equivalent load system, as shown in Sec. 4.5.

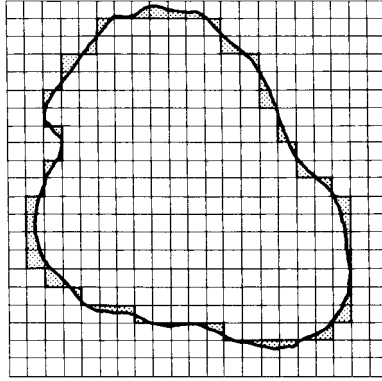


Figure 5.1.10 Approximation of irregular boundary line by square mesh.

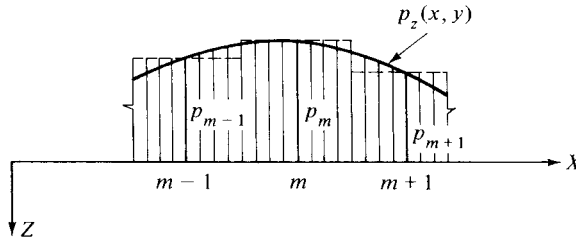


Figure 5.1.11 "Stepped" representation of distributed load.

If the intensity of the lateral load varies considerably from mesh point to mesh point, a *weighted value* of this quantity should be used. There are several ways to obtain such a weighted representation of the lateral load. One of the simplest ways is to use a straight-line distribution between the gridwork points. Dealing first with a one-dimensional case, as shown in Fig. 5.1.12a, the equivalent concentrated force P_m , at pivotal point m , can be obtained by introducing a fictitious load-supporting structure in the form of simply supported beams. The sum of the reactions of two adjoining beams is

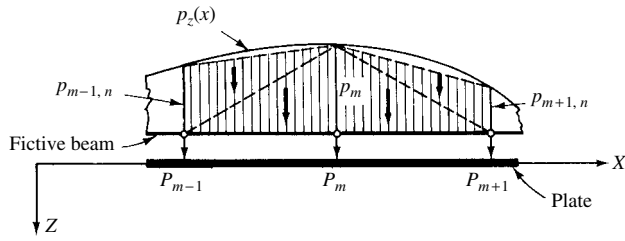
$$\begin{aligned} P_m(x) &= \left(\frac{1}{2} p_{m-1,n} \right) \frac{\Delta x}{3} + (p_{m,n}) \frac{2 \Delta x}{3} + \left(\frac{1}{2} p_{m+1,n} \right) \frac{\Delta x}{3} \\ &= \frac{\Delta x}{6} (p_{m-1,n} + 4p_{m,n} + p_{m+1,n}); \end{aligned} \quad (5.1.29)$$

hence

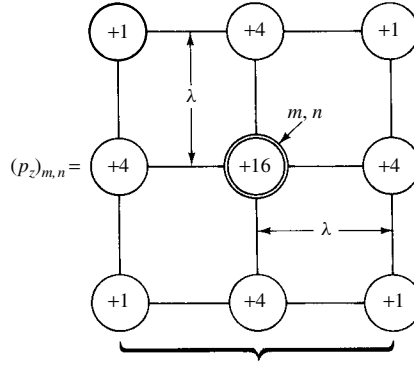
$$(p_z)_m = \frac{P_m(x)}{\Delta x} = \frac{1}{6} (p_{m-1,n} + 4p_{m,n} + p_{m+1,n}). \quad (5.1.30)$$

For square mesh, this one-dimensional load-averaging rule becomes two dimensional by creating a *Cartesian product* with a similar expression in the Y direction.[†] Thus

[†] This expression is equivalent to Simpson's one-third rule of numerical integration for four squares.



(a) One-dimensional case



(b) Stencil for two-dimensional load averaging

Figure 5.1.12 “Straight-line” load-averaging method.

the weighted value of the lateral load at the pivotal point becomes

$$(p_z)_{m,n} = \frac{1}{36} \times \left\{ \begin{array}{l} p_{m-1,n-1} + 4p_{m,n-1} + p_{m+1,n-1} \\ + 4p_{m-1,n} + 16p_{m,n} + 4p_{m+1,n} \\ + p_{m-1,n+1} + 4p_{m,n+1} + p_{m+1,n+1} \end{array} \right\}. \quad (5.1.31)$$

Schematic representation of this load-averaging rule is given in Fig. 5.1.12b. An improved expression, which uses a second-order parabola instead of a straight line for the development of the lower-dimensional rules, is discussed in Sec. 5.2.

f. Two-Stage Solution. The accuracy obtainable by the ordinary finite difference method can be increased by lowering the order of the derivatives using Eq. (1.2.43) instead of Eq. (1.2.30). The finite difference expressions of the two coupled second-order partial differential equations are

$$\begin{aligned} (\nabla^2 \mathfrak{M})_{m,n} &\approx \left[\frac{\Delta^2 \mathfrak{M}}{(\Delta x)^2} \right]_{m,n} + \left[\frac{\Delta^2 \mathfrak{M}}{(\Delta y)^2} \right]_{m,n} \\ &= \frac{1}{(\Delta x)^2} (\mathfrak{M}_{m+1,n} - 2\mathfrak{M}_{m,n} + \mathfrak{M}_{m-1,n}) \\ &\quad + \frac{1}{(\Delta y)^2} (\mathfrak{M}_{m,n+1} - 2\mathfrak{M}_{m,n} + \mathfrak{M}_{m,n-1}) = -(p_z)_{m,n} \end{aligned} \quad (5.1.32)$$

and

$$\begin{aligned} (\nabla^2 w)_{m,n} &\approx \frac{1}{(\Delta x)^2} (w_{m+1,n} - 2w_{m,n} + w_{m-1,n}) \\ &+ \frac{1}{(\Delta y)^2} (w_{m,n+1} - 2w_{m,n} + w_{m,n-1}) = -(p_z^*)_{m,n}, \end{aligned} \quad (5.1.33)$$

where

$$(p_z^*)_{m,n} = \left(\frac{\mathfrak{M}}{D} \right)_{m,n} \quad (5.1.34)$$

is a fictitious lateral load and \mathfrak{M} represents the *moment-sum* in accordance with Eq. (1.2.42). Both differential equations [(5.1.32) and (5.1.34)] are of the Poisson type. To be able to solve Eq. (5.1.32), however, we must know the boundary conditions for \mathfrak{M} . In the case of simple support, \mathfrak{M} is zero at the boundary. Representation of the real and fictitious lateral loads in these equations can follow either of the above-described load representation methods, depending on the type of load and the required accuracy of the solution. When the boundary values of \mathfrak{M} are not directly obtainable, the two-stage method tends to be more involved. Marcus [5.1.15] extended the application of the two-stage methods to flat plates. Other investigators [5.1.2, 2.2.16] have treated continuous plates and plates of various geometrical form by this *two-stage* approach.

g. Error of Finite Difference Approximation. To determine the error involved in representing the derivatives of the original function $f^{(k)}(x)$ by those of the interpolating polynomial $\phi^{(k)}(x)$, we use Taylor's series, which is considered to be the ultimate in osculation. That is, Taylor's expansion of a function $f(x)$ not only represents the curve going through the same collocation points but also has the same geometrical properties (tangent, curvature, etc.) as the original function.

Taylor's expansion of $f(x)$ in the vicinity of mesh point $x = x_m + \Delta x$ gives

$$\begin{aligned} y_{m+1} = f(x_m + \Delta x) &= y(x)_m + \frac{\Delta x}{1!} y'(x)_m + \frac{(\Delta x)^2}{2!} y''(x)_m \\ &+ \frac{(\Delta x)^3}{3!} y'''(x)_m + \cdots = \sum_{k=0}^{\infty} \frac{(\Delta x)^k}{k!} y^{(k)}(x)_m, \end{aligned} \quad (5.1.35)$$

from which

$$\begin{aligned} y'(x)_m &= \left(\frac{dy}{dx} \right)_m \approx \frac{y_{m+1} - y_m}{\Delta x} - \frac{\Delta x}{2} y''(x)_m - \frac{(\Delta x)^2}{6} y'''(x)_m + \cdots \\ &= \frac{y_{m+1} - y_m}{\Delta x} + \varepsilon(\Delta x), \end{aligned} \quad (5.1.36)$$

where $\varepsilon(\Delta x) = \varepsilon_1 + \varepsilon_2 + \cdots$ is the *error term*, representing the truncation error of all neglected terms. Error terms for higher derivatives can be derived similarly [5.1.20]. In general, the error involved by expressing the k th derivative by finite difference

approximation is

$$f^{(k)}(x)_m = \frac{\Delta^{(k)} y_m}{(\Delta x)^k} + \varepsilon_k(\Delta x). \quad (5.1.37)$$

In this expression ε_k does not vanish when $\Delta x \rightarrow 0$. Unfortunately, the accuracy of ordinary finite difference expressions gets progressively lower as the order of the derivative is increased. Consequently, results obtained from ordinary finite difference solution of higher than fourth-order differential equations should be viewed with some skepticism.

h. Recommended Procedures. In planning the analysis of a plate by means of the ordinary FDM, one must first consider the convergence characteristics of this numerical procedure. As Fig. 5.1.13 indicates, the ordinary FDM converges relatively fast toward the exact solution of a given plate problem, provided that the finite difference mesh is not too fine. When using very small subdivisions, the convergence becomes quite slow. In addition, the number of equations to be solved increases exponentially. Furthermore, an extremely fine mesh and the resulting large number of simultaneous equations may create roundoff errors in their solution that adversely affect its accuracy. Thus, the use of an iterative approach is recommended.

In setting up the finite difference equations, the first mesh can be relatively crude, say $(\Delta x)^{(1)} = a/4$ and $(\Delta y)^{(1)} = b/4$, respectively. To facilitate this procedure, the plate and the finite difference mesh are drawn to a convenient scale. Next, the mesh points are numbered in such a manner that the resulting coefficient matrix **A** in Eq. (5.1.27) will have a band structure and the so-created bandwidth of the matrix will be relatively small. In the process of numbering the mesh points, we must also

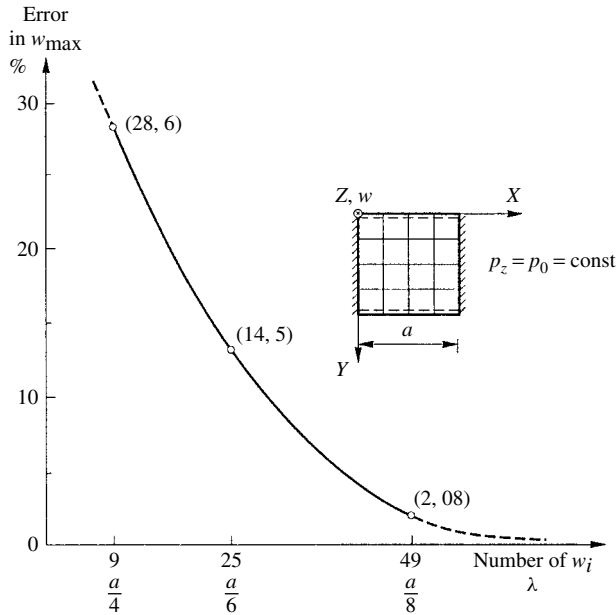


Figure 5.1.13 Convergence of ordinary FDM.

consider the prescribed boundary conditions as previously described in Sec. 5.1d. Of course, if the structure and the loads are symmetrical, we should utilize the prevailing symmetry, since it can considerably reduce the required computational effort. In the third step, we draw the stencil representing the finite difference form of the biharmonic operator ∇^4 (Fig. 5.1.3) on a piece of transparent paper using the same scale as for the first finite difference mesh. It is recommended that for the stencil on transparent paper we use a different color, say red, in order to clearly distinguish it from the finite difference mesh in the following step. Now, by superimposing at each mesh point this stencil for ∇^4 upon the mesh covering the plate, we can write the corresponding finite difference equations with relative ease. However, an independent check for this procedure is highly recommended. Such a computation that tests the correctness of the resulting algebraic equations should be performed, if possible, by another person.

Next, we repeat the above-described procedure, this time using *half* of the previously applied mesh size. Following the recommendation given above, the refined mesh sizes should now be $(\Delta x)^{(2)} = a/8$ and $(\Delta y)^{(2)} = b/8$, for instance. The so-obtained more accurate values for the mesh-point deflections $w_i^{(2)}$ can be further improved by using Richardson's powerful extrapolation formula

$$w_i^{(3)} = w_i^{(2)} + \frac{w_i^{(2)} - w_i^{(1)}}{2^\mu - 1}, \quad (5.1.38)$$

where $w_i^{(1)}$ is the lateral deflection of mesh point i obtained from the first finite difference solution of the plate problem with $(\Delta x)^{(1)}$ and $(\Delta y)^{(1)}$ mesh sizes and $w_i^{(2)}$ represents the results of the second computation with $(\Delta x)^{(2)} = (\Delta x)^{(1)}/2$ and $(\Delta y)^{(2)} = (\Delta y)^{(1)}/2$, respectively. The value of the exponent μ depends on the convergence characteristics of the numerical method applied. For the ordinary FDM $\mu = 2$. It should be noted, however, that if the results of the second solutions already fall into the flat region of the convergence curve (Fig. 5.1.13), Robinson's extrapolation formula may even *overcorrect* the end results, since in such a case $\mu \neq 2$.

The second refined finite difference mesh introduces additional mesh-point deflections that were not computed in the first solution of the problem. To be able to use the above given extrapolation formula for these points, we apply a quadratic interpolation

$$w_j = w_{i,\ell} + w_{i,c} = \frac{1}{2}(w_i + w_{i+1}) - 0.125(w_i - 2w_{i+1} + w_{i+2}), \quad (5.1.39)$$

where the first term is obviously the linear part of the interpolation and the second term represents the quadratic correction, as illustrated in Fig. 5.1.14. Equation (5.1.39) can be derived from Newton-Gregory's interpolating formula for equally spaced arguments. Logically, this interpolation formula can also be used in a diagonal direction between the mesh points.

If the plates are of arbitrary shape—instead of triangular, trapezoidal, hexagonal or other finite difference nets—we should try to match the geometrical boundaries with either a proper square or an equally spaced rectangular mesh, as shown in Fig. 5.1.15, which also illustrates the right and wrong ways of such an approximation. Of course, some manipulations are usually required until a desirable fit is achieved. Experience shows that even with a moderately fine subdivision satisfactory results can be obtained. Such an approach is straightforward and can be applied for almost all

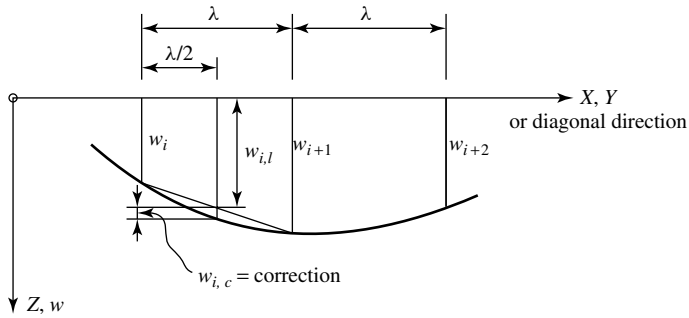


Figure 5.1.14 Linear and quadratic interpolations.

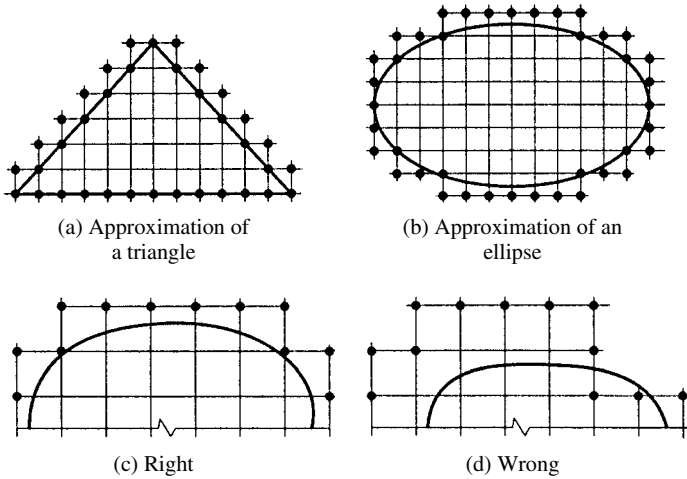


Figure 5.1.15 Approximation of plates of arbitrary shape.

arbitrary boundary shapes. Using this approximation, the above given finite difference patterns are still applicable; thus, the need for lengthy derivations of new stencils are completely eliminated.

In the vicinity of openings in the plate or column supports, for instance, the use of finer meshes is recommended (Figs. 5.1.16 and 5.1.17) in order to deal with the stress concentration associated with such locations. Assuming that a finer mesh is used, additional points $a \rightarrow q$ must be locally added to accommodate the pertinent stencil of the biharmonic operator ∇^4 (Fig. 5.1.18). Again, we can apply the interpolation formula (5.1.38) to incorporate these additional points into the coefficient matrix \mathbf{A} .

Summary. The ordinary FDM is one of the most general numerical methods used in structural mechanics. It is especially suited for solutions of a wide variety of plate problems, as illustrated throughout this book. As shown above, the FDM transforms the governing plate equations—along with the prescribed boundary conditions—into a set of simultaneous algebraic equations the solution of which is obtained by using either computers or one of the more advanced scientific calculators. Thus, the method is based on a combination of manual and computer operations.

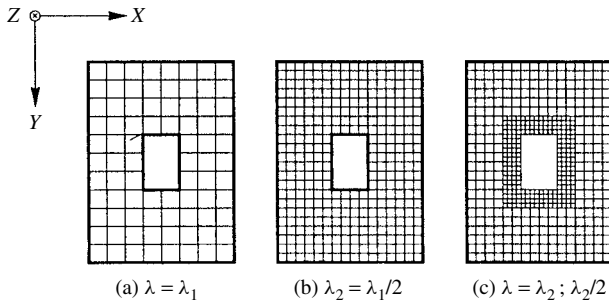


Figure 5.1.16 Mesh refinements in vicinity of opening.

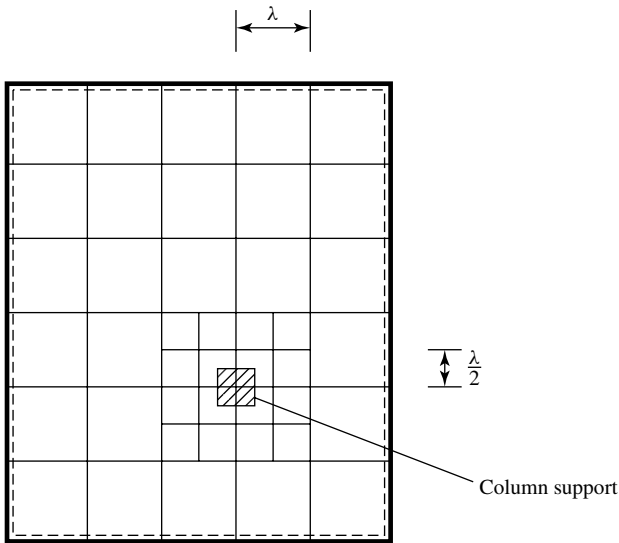


Figure 5.1.17 Finer mesh for column support.

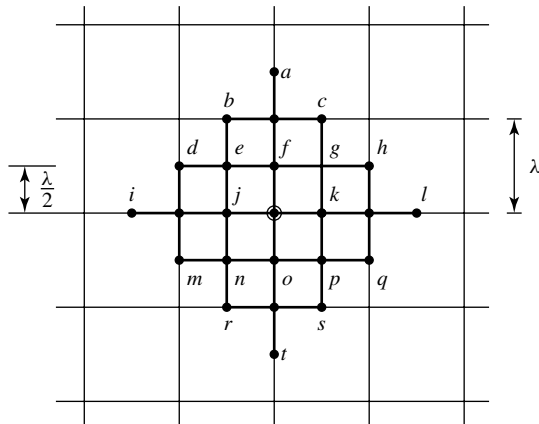


Figure 5.1.18 Additional points required by $\lambda/2$ subdivision.

The *advantages* of the ordinary FDM are as follows:

1. It is simple and transparent in its operations.
2. It has readily usable and reusable finite difference patterns (stencils).
3. Since only the deflection ordinates w_i are the unknowns, the size of the coefficient matrix is much smaller in comparison to that of the FEM.
4. It is versatile. That is, basically the same technique can be applied for the solution of dynamic and elastic stability problems of plates.
5. Using the above-described and recommended procedure, acceptable accuracy for all technical purposes can be achieved with relative ease.
6. There is no need for computers or pertinent program systems since the resulting simultaneous algebraic equation, in most of the cases, can also be solved by advanced scientific calculators with built-in equation solvers. Moreover, computer programs for the solution of this task are plentiful and readily available.

The *disadvantages* of the FDM are as follows:

- (a) Since the FDM—as described above and illustrated by the numerical examples below—is partially a “longhand” operation, it is not well suited for solution of very large plate systems involving hundreds or even thousands of equations.
- (b) Automation of the FDM by development of pertinent computer programs is not an easy task.
- (c) Beyond certain mesh widths, convergence of the solution becomes slow.
- (d) In most cases, the resulting coefficient matrix, \mathbf{A} is not symmetrical.
- (e) Using FDM is not recommended when higher than fourth-order derivatives are involved.

ILLUSTRATIVE EXAMPLE I

Determine the maximum deflection of a simply supported square plate subjected to a distributed load in the form of a triangular prism, as shown in Fig. 5.1.19a.

Because of the simply supported boundary conditions, the two-stage solution can be applied. Numbering of the mesh points (utilizing the apparent symmetry) is shown in Fig. 5.1.19b. With a stepped-load representation, Eq. (5.1.32) yields

$$\begin{aligned}
 \text{At point 1:} \quad 2\mathfrak{M}_2 + 2\mathfrak{M}_3 - 4\mathfrak{M}_1 &= -p_0 \left(\frac{a^2}{16} \right); \\
 \text{At point 2:} \quad \mathfrak{M}_1 + 2\mathfrak{M}_4 - 4\mathfrak{M}_2 &= -p_0 \left(\frac{a^2}{16} \right); \\
 \text{At point 3:} \quad \mathfrak{M}_1 + 2\mathfrak{M}_4 - 4\mathfrak{M}_3 &= -\frac{p_0}{2} \left(\frac{a^2}{16} \right); \\
 \text{At point 4:} \quad \mathfrak{M}_2 + \mathfrak{M}_3 - 4\mathfrak{M}_4 &= -\frac{p_0}{2} \left(\frac{a^2}{16} \right).
 \end{aligned} \tag{5.1.40}$$

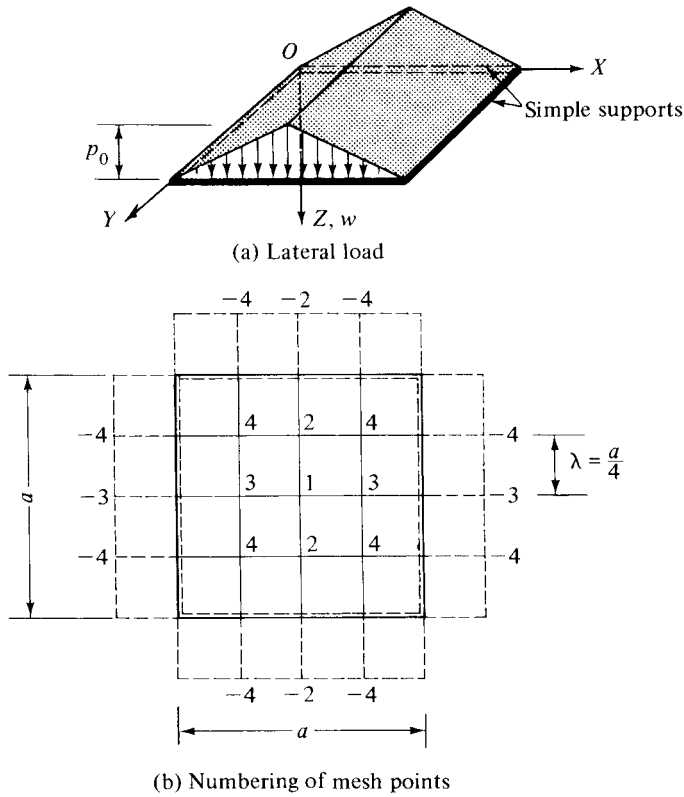


Figure 5.1.19 Simply supported plate subjected to triangular prismatic load.

Solutions of these equations are

$$\begin{aligned} \mathfrak{M}_1 &= +\frac{14}{256} p_0 a^2, & \mathfrak{M}_2 &= +\frac{11}{256} p_0 a^2, \\ \mathfrak{M}_3 &= +\frac{9}{256} p_0 a^2, & \mathfrak{M}_4 &= +\frac{7}{256} p_0 a^2. \end{aligned} \quad (5.1.41)$$

To obtain deflections at the mesh points, we apply Eq. (5.1.33) in a similar manner:

$$\begin{aligned} \text{At point 1:} \quad & \frac{16}{a^2} (2w_2 + 2w_3 - 4w_1) = -\frac{14}{256} \frac{p_0 a^2}{D}; \\ \text{At point 2:} \quad & \frac{16}{a^2} (w_1 + 2w_4 - 4w_2) = -\frac{11}{256} \frac{p_0 a^2}{D}; \\ \text{At point 3:} \quad & \frac{16}{a^2} (w_1 + 2w_4 - 4w_3) = -\frac{9}{256} \frac{p_0 a^2}{D}; \\ \text{At point 4:} \quad & \frac{16}{a^2} (w_2 + w_3 - 4w_4) = -\frac{7}{256} \frac{p_0 a^2}{D}. \end{aligned} \quad (5.1.42)$$

Solution of these equations yields

$$\begin{aligned} w_1 &= +0.00293 \frac{p_0 a^4}{D} = w_{\max}, & w_2 &= +0.00214 \frac{p_0 a^4}{D}, \\ w_3 &= +0.00202 \frac{p_0 a^4}{D}, & w_4 &= +0.00148 \frac{p_0 a^4}{D}. \end{aligned} \quad (5.1.43)$$

ILLUSTRATIVE EXAMPLE II

Find approximate values of displacements of a continuous plate, shown in Fig. 5.1.20, by the ordinary FDM.

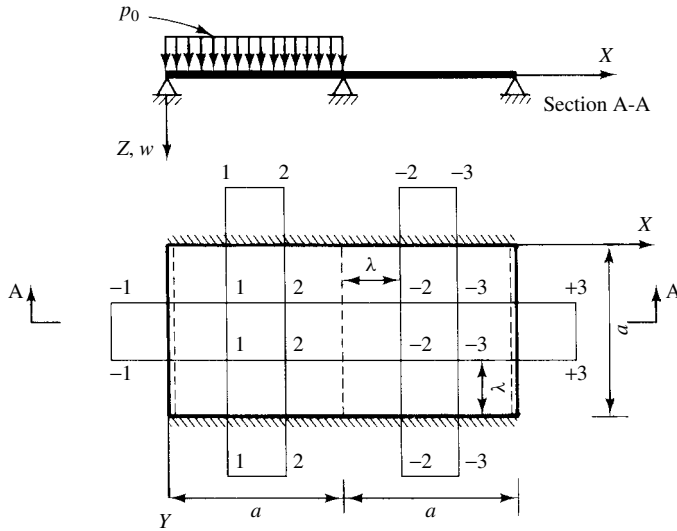


Figure 5.1.20 Continuous plate.

To satisfy the boundary conditions, we use Eqs. (5.1.18) and (5.1.20) at the fixed and simply supported boundaries, respectively. From the stencil given in Fig. 5.1.3, the finite difference equations in matrix form are

$$\begin{bmatrix} 12 & -6 & 0 \\ -6 & 12 & 0 \\ 0 & -6 & 12 \end{bmatrix} \begin{Bmatrix} w_1 \\ w_2 \\ w_3 \end{Bmatrix} = \frac{\lambda^4 p_0}{D} \begin{Bmatrix} 1 \\ 1 \\ 0 \end{Bmatrix}. \quad (5.1.44)$$

Solution of these simultaneous equations yields

$$w_1 = w_2 = \frac{\lambda^4 p_0}{6D} = \frac{p_0 a^4}{486D} \quad \text{and} \quad w_3 = \frac{\lambda^4 p_0}{12D} = -\frac{p_0 a^4}{972D}. \quad (5.1.45)$$

These approximate values can be improved using a finer mesh.

ILLUSTRATIVE EXAMPLE III

Find the maximum deflection and negative moment of the uniformly loaded square plate shown in Fig. 5.1.21a using the *recommended procedures* discussed in Sec. 5.1h.

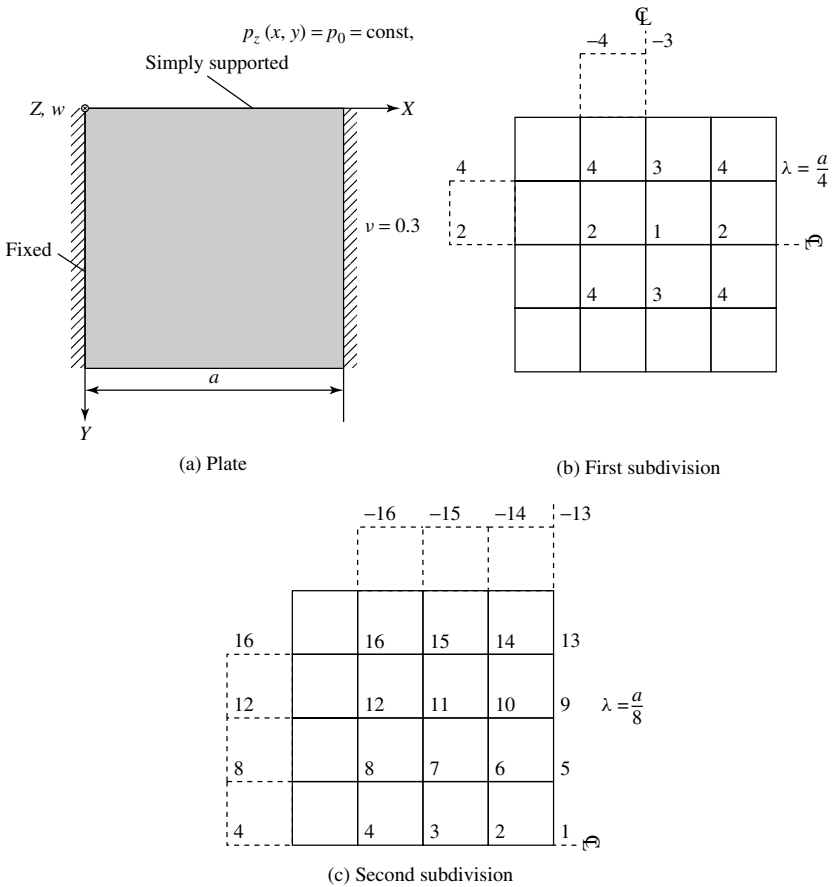


Figure 5.1.21 Square plate with two opposite edges fixed and two edges simply supported.

First, we select a relatively coarse finite difference mesh with $\lambda = a/4$. In numbering the mesh points, the apparent double symmetry of the plate is considered (Fig. 5.1.21b). From the clamped boundary conditions it follows that the fictitious points outside the domain of the plate are the same as the corresponding points within the plate proper. Similarly, the simply supported boundary conditions require that the pertinent fictitious mesh-points outside the plate should have a negative sign, according to Eq. 5.1.20.

By applying the stencil of the biharmonic operator ∇^4 (Fig. 5.1.20) at each interior mesh-point, we obtain the following simultaneous equations given in

matrix form:

$$\begin{bmatrix} 20 & -16 & -16 & 8 \\ 8 & 22 & 4 & -16 \\ -8 & 4 & 20 & -16 \\ 2 & -8 & -8 & 22 \end{bmatrix} \cdot \begin{Bmatrix} w_1^{(1)} \\ w_2^{(1)} \\ w_3^{(1)} \\ w_4^{(1)} \end{Bmatrix} = \begin{Bmatrix} p_0 \\ p_0 \\ p_0 \\ p_0 \end{Bmatrix} \frac{a^4}{256 D}, \quad (5.1.46)$$

the solution of which gives the first approximation of the deflection ordinates at the mesh points,

$$\{w^{(1)}\} = \{247 \quad 162 \quad 182 \quad 121\} \cdot \frac{a^4 p_0 \times 10^{-5}}{D}. \quad (5.1.47)$$

Next, we use smaller mesh widths, $\lambda = a/8$, as shown in Fig. 5.1.21c. Now, the coefficient matrix $\mathbf{A}^{(2)}$ in the matrix equation of the problem

$$\mathbf{A}^{(2)} \mathbf{w}^{(2)} = \mathbf{p}^{(2)} \quad (5.1.48)$$

becomes

$$\mathbf{A}^{(2)} = \begin{pmatrix} 1 & 2 & 3 & 4 & 5 & 6 & 7 & 8 & 9 & 10 & 11 & 12 & 13 & 14 & 15 & 16 \\ 20 & -16 & 2 & -16 & 8 & & & & 2 & & & & & & & \\ -8 & 21 & -8 & 1 & 4 & -16 & 4 & & & 2 & & & & & & \\ 1 & -8 & 20 & -8 & & 4 & -16 & 4 & & & 2 & & & & & \\ & 1 & -8 & 21 & & & 4 & -16 & & & & 2 & & & & \\ -8 & 4 & & & 21 & -16 & 2 & & -8 & 4 & & & 1 & & & \\ 2 & -8 & 2 & & -8 & 22 & -8 & 1 & 2 & -8 & 2 & & & 1 & & \\ & 2 & -8 & 2 & 1 & -8 & 21 & -8 & & 2 & -8 & 2 & & & 1 & \\ & & 2 & -8 & & 1 & -8 & 22 & & & 2 & -8 & & & & 1 \\ 1 & & & & -8 & 4 & & & 20 & -16 & 2 & & -8 & 4 & & \\ & 1 & & & 2 & -8 & 2 & & -8 & 21 & -8 & 1 & 2 & -8 & 2 & \\ & & 1 & & 2 & -8 & 2 & 1 & -8 & 20 & -8 & & 2 & -8 & 2 & \\ & & & 1 & & 2 & -8 & & 1 & -8 & 21 & & & 2 & -8 & \\ & & & & 1 & & & & -8 & 4 & & & 19 & -16 & 2 & \\ & & & & & 1 & & & 2 & -8 & 2 & & -8 & 20 & -8 & 1 \\ & & & & & & 1 & & & 2 & -8 & 2 & 1 & -8 & 19 & -8 \\ & & & & & & & 1 & & & 2 & -8 & & 1 & -8 & 20 \end{pmatrix} \quad \begin{matrix} 1 \\ 2 \\ 3 \\ 4 \\ 5 \\ 6 \\ 7 \\ 8 \\ 9 \\ 10 \\ 11 \\ 12 \\ 13 \\ 14 \\ 15 \\ 16 \end{matrix} \quad (5.1.49)$$

The corresponding vector of the loads is

$$\{p\} = \{1 \quad 1 \quad 1 \quad 1 \quad 1 \quad 1 \quad 1 \quad 1 \quad 1 \quad 1 \quad 1 \quad 1 \quad 1 \quad 1 \quad 1 \quad 1\} \cdot \frac{p_0 a^4}{4096 D}. \quad (5.1.50)$$

The solution of Eq. (5.1.48) is

$$\begin{aligned} \mathbf{w}^{(2)} = \{ & 0.2088 \quad 0.1868 \quad 0.1272 \quad 0.0507 \quad 0.1952 \quad 0.1748 \quad 0.1193 \\ & 0.0478 \quad 0.1543 \quad 0.1385 \quad 0.0951 \quad 0.0387 \quad 0.0871 \quad 0.0784 \\ & 0.0543 \quad 0.0226 \} \cdot \frac{p_0 a^4 \times 10^{-2}}{D}. \end{aligned} \quad (5.1.51)$$

By using Richardson's extrapolation formula [Eq. (5.1.38)], the improved value of the maximum deflection becomes

$$w_{\max} = w_1^{(3)} = w_1^{(2)} + \frac{w_1^{(2)} - w_1^{(1)}}{3} = \frac{0.002215 p_0 a^4}{D} \quad (\text{error: } 2\%). \quad (5.1.52)$$

In a similar fashion, we can improve the values obtained for the maximum negative moment. The first analysis with the coarse mesh ($\lambda = a/4$) gave

$$-m_{\max}^{(1)} = -\frac{D}{\lambda^2}(2w_2) = -0.05184 p_0 a^2 \quad (\text{error: } -25\%). \quad (5.1.53)$$

With the refined mesh ($\lambda = a/8$) we obtained

$$-m_{\max}^{(2)} = -\frac{D}{\lambda^2}(2w_4) = -0.06489 p_0 a^2 \quad (\text{error: } -7\%). \quad (5.1.54)$$

Thus, the extrapolation yields

$$-m_{\max}^{(3)} = m_{\max}^{(2)} + \frac{m_{\max}^{(2)} - m_{\max}^{(1)}}{3} = -0.0694 p_0 a^2 \quad (\text{error: } -0.4\%). \quad (5.1.55)$$

A comparison with the analytical solution of this problem [2] indicates only a relatively small discrepancy of 0.4%. This and the other results of this computation are listed in Table 5.1.3.

Table 5.1.3 Summary of Results

Deflection and Moments	$\lambda^{(1)} = a/4$	%	$\lambda^{(2)} = a/8$	%	Extrapolated	%	Factor
w_1	0.00247	+28.6	0.002088	+8.3	0.001958	+2.0	$p_0 a^4 / D$
$m_{x,1}$	0.03344	+ 0.7	0.03338	+0.5	0.03336	+0.4	$p_0 a^2$
$m_{y,2}$	0.02896	-18.7	0.02586	+6.0	0.02467	+1.1	$p_0 a^2$
$-m_{\max}$	-0.0518	-25	-0.06489	-7.0	-0.0694	-0.4	$p_0 a^2$

ILLUSTRATIVE EXAMPLE IV

Figure 5.1.22a shows a simply supported triangular plate subjected to a uniformly distributed load p_0 . Let us determine the maximum deflection ordinate w_{\max} and the maximum moments $m_{x,\max}$, $m_{y,\max}$ of the plate by the ordinary FDM.

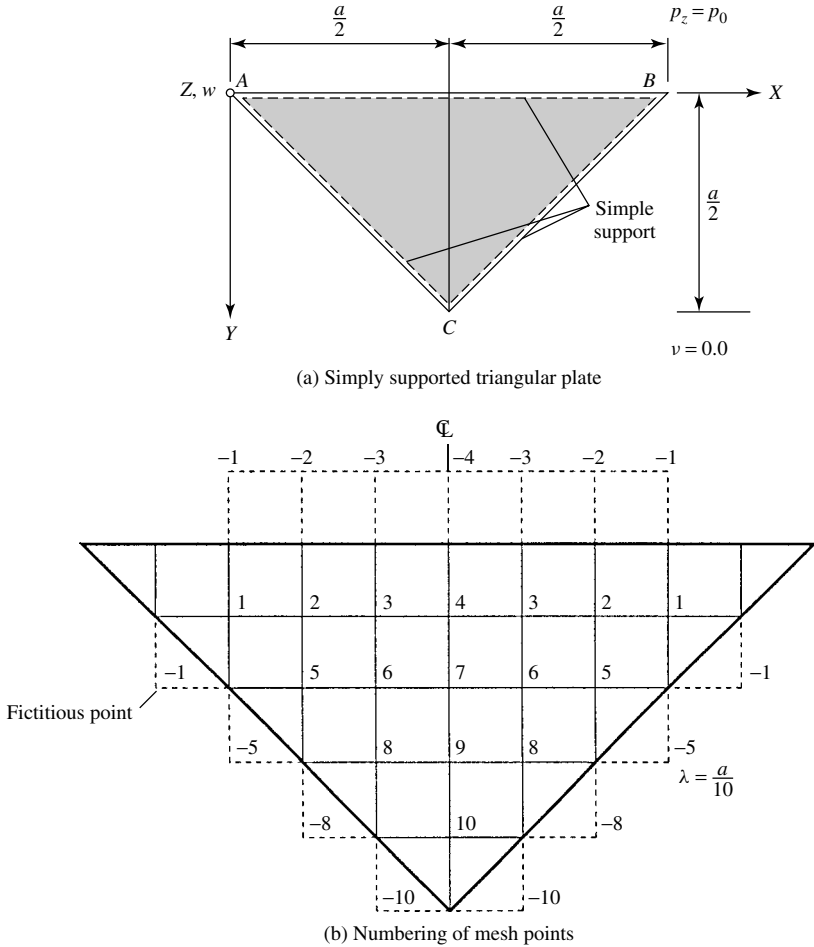


Figure 5.1.22 Approximation of oblique boundaries of triangular plate.

Applying a square mesh with $\lambda = a/2$ subdivisions, we approximate boundaries of the two oblique edges by zigzag lines, as shown in Fig. 5.1.22b. In numbering the mesh points, we have considered the apparent symmetry of the structure and the simply supported boundary conditions according to Fig. 5.1.5. Using the stencil for the biharmonic operator ∇^4 given in Fig. 5.1.3a, we obtain

the coefficient matrix

$$\mathbf{A} = \begin{bmatrix} 17 & -8 & 1 & 0 & 1 & 0 & 0 & 0 & 0 & 0 \\ -8 & 19 & -8 & 1 & -8 & 2 & 0 & 0 & 0 & 0 \\ 1 & -8 & 20 & -8 & 2 & -8 & 2 & 1 & 0 & 0 \\ 0 & 2 & -16 & 19 & 0 & 4 & -8 & 0 & 1 & 0 \\ 1 & -8 & 2 & 0 & 18 & -8 & 1 & 1 & 0 & 0 \\ 0 & 2 & -8 & 2 & -8 & 21 & -8 & -8 & 2 & 0 \\ 0 & 0 & 4 & -8 & 2 & -16 & 20 & 4 & -8 & 1 \\ 0 & 0 & 1 & 0 & 1 & -8 & 2 & 19 & -8 & 1 \\ 0 & 0 & 0 & 1 & 0 & 4 & -8 & -16 & 20 & -8 \\ 0 & 0 & 0 & 0 & 0 & 0 & 1 & 2 & -8 & 16 \end{bmatrix} \quad (5.1.56)$$

of the simultaneous algebraic equations, while the vector of the loads becomes

$$\mathbf{p} = \left\{ 1 \quad 1 \quad 1 \quad 1 \quad 1 \quad 1 \quad 1 \quad 1 \quad 1 \quad 1 \right\} \frac{p_0 \lambda^4}{D}. \quad (5.1.57)$$

The solution of the matrix equation

$$\mathbf{w} = \mathbf{A}^{-1} \mathbf{p} \quad (5.1.58)$$

gives

$$\mathbf{w} = \{ 0.305894 \quad 0.765854 \quad 1.165164 \quad 1.322904 \quad 0.761478 \\ 1.493077 \quad 1.793943 \quad 0.934673 \quad 1.354966 \quad 0.511027 \} \frac{12 p_0 a^4}{10^4 E h^3}. \quad (5.1.59)$$

Hence, the maximum deflection ordinate of the plate is

$$w_{\max} = w_7 = 0.00215316 \frac{p_0 a^4}{E h^3} \quad (\text{error: } 1.3\%). \quad (1.5.60)$$

Using the stencils given in Fig. 5.1.4, we also calculate the maximum moments. At mesh point 9, we obtain

$$m_{x, \max} = -\frac{E h^3}{\lambda^2} (w_8 - 2w_9 + w_8) = \frac{p_0 a^2}{100} 0.840586 \quad (\text{error: } 3.7\%), \quad (5.1.61)$$

while the maximum moment

$$m_{y, \max} = -\frac{E h^3}{\lambda^2} (w_4 - 2w_7 + w_9) = \frac{p_0 a^2}{100} 0.910016 \quad (\text{error: } 3.2\%) \quad (5.1.62)$$

occurs at mesh point 7. The above given errors represent the deviations from the finite difference solution of the same problem but using a triangular mesh instead of a square one. The so-obtained accuracy can be, of course, further increased by using a finer mesh. This example shows that the approximation of the oblique boundaries by a zigzag line not only simplifies the calculation but also gives quite usable results.

References and Bibliography

- [5.1.1] NÁDAI, Á., *Die elastischen Platten*, Springer-Verlag, Berlin, 1925.
- [5.1.2] BEYER, K., *Die Statik im Stahlbetonbau*, Springer-Verlag, Berlin, 1948.
- [5.1.3] LEVY, H., and BAGOTT, E. A., *Numerical Solutions of Differential Equations*, Dover Publications, New York, 1950.
- [5.1.4] SALVADORI, M. G., and BARON, M. L., *Numerical Methods in Engineering*, 2nd ed., Prentice-Hall, Englewood Cliffs, New Jersey, 1961.
- [5.1.5] SZILARD, R., *Theory and Analysis of Plates: Classical and Numerical Methods*, Prentice-Hall, Englewood Cliffs, New Jersey, 1974.
- [5.1.6] GHALI, A., and NEVILLE, A. M., *Structural Analysis: A Unified Classical and Matrix Approach*, 2nd ed., Chapman & Hall, London, 1978.
- [5.1.7] DANKERT, J., *Numerische Methoden der Mechanik*, Springer-Verlag, Vienna, 1977.
- [5.1.8] MARSAL, D., *Die numerische Lösung partieller Differentialgleichungen*, B. I. Wissenschaftsverlag, Zürich, 1976.
- [5.1.9] FLORIN, G., *Slabs and Plates*, Trans Tech Publications, Rockport, Massachusetts, 1979.
- [5.1.10] MARSAL, D., *Finite Differenzen und Elemente*, Springer-Verlag, Berlin, 1989.
- [5.1.11] SZILARD, R., *Finite Berechnungsmethoden der Strukturmechanik*, Vol. 2, Ernst & Sohn, Berlin, 1990.
- [5.1.12] LEVY, H., and LESSMAN, F., *Finite Difference Equations*, Dover Publications, New York, 1992.
- [5.1.13] WOOD, R. H., *Plastic and Elastic Design of Slabs and Plates*, Ronald Press Co., New York, 1961.
- [5.1.14] STIGLAT, K., *Rechteckige und schiefe Platten mit Randbalken*, W. Ernst und Sohn, Berlin, 1962.
- [5.1.15] MARCUS, H., *Die Theorie elastischer Gewebe und ihre Anwendung auf die Berechnung biegsamer Platten*, Springer-Verlag, Berlin, 1924.
- [5.1.16] OHLIG, R., "Zwei- und vierseitig aufgelagerte Rechteckplatten unter Einzelkraftbelastung," *Ing.-Arch.*, 16 (1947), 51–71.
- [5.1.17] FORSYTHE, G., and WASOW, R. W., *Finite Difference Methods for Partial Differential Equations*, John Wiley & Sons, New York, 1959.
- [5.1.18] WANG, P. CH., *Numerical and Matrix Methods in Structural Mechanics*, John Wiley & Sons, New York, 1966.
- [5.1.19] HEINS, C. P., "Bridge Tests Predicted by Finite Difference Plate Theory," *J. Struct. Div.*, ASCE, 95 (Feb. 1969), 249–265.
- [5.1.20] SOARE, M., *Application des equations aux differences finies au calcul des coques*, Edition Eyrolles, Paris, 1962.

5.2 Improved Finite Difference Methods

a. Need for Improvements. While the use of an ordinary finite difference technique is very simple and the method is quite general, it is characterized by slow convergence. Furthermore, when higher-order derivatives and a large number of

mesh points are involved, the solution, due to machine errors, may converge to a wrong number. One of the reasons for such convergence characteristics is that the *collocating polynomials* used in deriving finite difference expressions agree only in value with the exact function at the mesh points and their derivatives do not match. Additional sources of error are the approximation of boundary conditions and the use of the usually coarse load-averaging rules. Furthermore, extremely fine mesh, and the resulting large number of simultaneous equations, may create roundoff errors in computer solutions and adversely affect the accuracy and economy of the method. Consequently, when high accuracy in the finite difference solution of plate problems is required, improved finite difference techniques should be applied.

Refinements in the finite difference method usually come from three sources: (1) replacement of the individual derivatives by expressions obtained from *osculating* polynomials (which also collocate, up to some higher order, the derivatives of the exact function), (2) refined representation of the actual boundary conditions and (3) improved load-averaging techniques.

b. Method of Higher Approximation. The general tool for derivation of improved derivatives is the Taylor expansion, which not only collocates a function by going through the same points but also has the same geometrical properties (e.g., tangent, curvature) in the vicinity of a given point. To obtain improved finite difference expansions, we consider additional mesh points in the vicinity of the pivotal point m .

Suppose that we want to derive an improved expression for the second derivative. For this purpose let us expand the function $y(x)$ at point $m + 1$ and $m - 1$ into a Taylor series. This yields

$$\begin{aligned} y_{m+1} = y(x_m + \Delta x) &= y(x_m) + \frac{\Delta x}{1!} y'(x_m) + \frac{(\Delta x)^2}{2!} y''(x_m) \\ &+ \frac{(\Delta x)^3}{3!} y'''(x_m) + \cdots + \frac{(\Delta x)^k}{k!} y^{(k)}(x_m) + \cdots \end{aligned} \quad (5.2.1)$$

and

$$\begin{aligned} y_{m-1} = y(x_m - \Delta x) &= y(x_m) - \frac{\Delta x}{1!} y'(x_m) + \frac{(\Delta x)^2}{2!} y''(x_m) \\ &- \frac{(\Delta x)^3}{3!} y'''(x_m) + \cdots + \frac{(-\Delta x)^k}{k!} y^{(k)}(x_m) + \cdots \end{aligned} \quad (5.2.2)$$

Adding Eqs. (5.2.1) and (5.2.2), we can write

$$\begin{aligned} y_m'' &= \frac{1}{(\Delta x)^2} (y_{m+1} - 2y_m + y_{m-1}) - \frac{(\Delta x)^2}{12} y_m^{IV} - \frac{(\Delta x)^4}{360} y_m^{VI} + \cdots \\ &= \left[\frac{\Delta^2 y}{(\Delta x)^2} \right]_m + \varepsilon_1 + \varepsilon_2 + \cdots, \end{aligned} \quad (5.2.3)$$

where ε_1 and ε_2 represent the error terms. By expressing the fourth-order derivative y_m^{IV} in ε_1 using central differences, we obtain

$$\begin{aligned} \left(\frac{d^2 y}{dx^2} \right)_m = y_m'' &= \frac{1}{12(\Delta x)^2} (-y_{m+2} + 16y_{m+1} - 30y_m + 16y_{m-1} - y_{m-2}) \\ &+ \frac{(\Delta x)^4}{90} y_m^{VI} + \cdots \end{aligned} \quad (5.2.4)$$

The order of magnitude of the error in this expression (given in Δx) is $(\Delta x)^4$, compared with $(\Delta x)^2$ in the corresponding ordinary finite difference expressions obtained from central differences. Thus, the accuracy of this finite difference expression [Eq. (5.2.4)] has been considerably increased.

Improved finite difference quantities for other derivatives can be derived in a similar manner. These sharpened finite difference expressions are schematically given in Table 5.2.1. Operators for mixed derivatives can be calculated from one-dimensional expressions, as discussed in Sec. 5.1.1. The corresponding improved finite difference patterns are given in Fig. 5.2.1. Sharpened finite difference expressions for the Laplacian and biharmonic operators, obtained through the method of higher approximation, are given in Fig. 5.2.2. Although these expressions have a higher degree of accuracy, they require more mesh points, a pronounced disadvantage of this technique, especially when boundary conditions are evaluated. That is, to simplify the relatively complex treatments of boundary conditions by improved finite differences, one often applies the less accurate approximations shown in Fig. 5.1.5. Such an approach is, in most cases, just “barely sufficient.” Consequently, special attention should always be paid to the boundaries since the accuracy gained can easily be lost by less accurate representation of the boundary conditions. Furthermore, the use of these improved operators should be accompanied by better load-averaging techniques, already discussed in Sec. 5.1.1.

c. Multilocal Method (Hermitian Method). The German and French terms for the multilocal method are *Mehrstellenverfahren* and *méthode plurilocale*, respectively. In the pertinent English language literature this method is often called the *Hermitian method*, although this sharpened finite difference technique was not originated by Hermite. The improved accuracy is obtained, again, by expanding the function into the Taylor series at points $m + 1$ and $m - 1$, as discussed above. If we want to derive an improved expression for the second derivative, for instance, we write the fourth derivative of the error term, ε_1 , (5.2.3) in terms of the second derivatives; thus

$$y_m^{IV} = \left(\frac{d^4 y}{dx^4} \right)_m = \left[\frac{d^2}{dx^2} \left(\frac{d^2 y}{dx^2} \right) \right]_m \approx \left(\frac{\Delta^2 \eta}{\Delta x^2} \right)_m, \quad (5.2.5)$$

Table 5.2.1 Schematic Representation of Higher-Order Finite Difference Expressions

$y_m^{(k)}$	Coefficients	First Error Term
y'_m	$\left[\begin{array}{ccccccc} (-1) & - & (+8) & \text{---} & (-8) & - & (+1) \end{array} \right] \frac{1}{12(\Delta x)}$	$+\frac{1}{30}(\Delta x)^4 y_m^{V}$
y''_m	$\left[\begin{array}{ccccccc} (-1) & - & (+16) & - & (-30) & - & (+16) & - & (-1) \end{array} \right] \frac{1}{12(\Delta x)^2}$	$+\frac{1}{90}(\Delta x)^4 y_m^{VI}$
y'''_m	$\left[\begin{array}{ccccccc} (-1) & - & (+8) & - & (-13) & \text{---} & (+13) & - & (-8) & - & (+1) \end{array} \right] \frac{1}{8(\Delta x)^3}$	$+\frac{7}{120}(\Delta x)^4 y_m^{VII}$
y_m^{IV}	$\left[\begin{array}{ccccccc} (-1) & - & (+12) & - & (-39) & - & (+56) & - & (-39) & - & (+12) & - & (-1) \end{array} \right] \frac{1}{6(\Delta x)^4}$	$+\frac{7}{240}(\Delta x)^4 y_m^{VIII}$
Point	$\begin{array}{ccccccc} \circ & \circ & \circ & \circ & \circ & \circ & \circ \\ m+3 & m+2 & m+1 & m & m-1 & m-2 & m-3 \end{array}$	ε_1

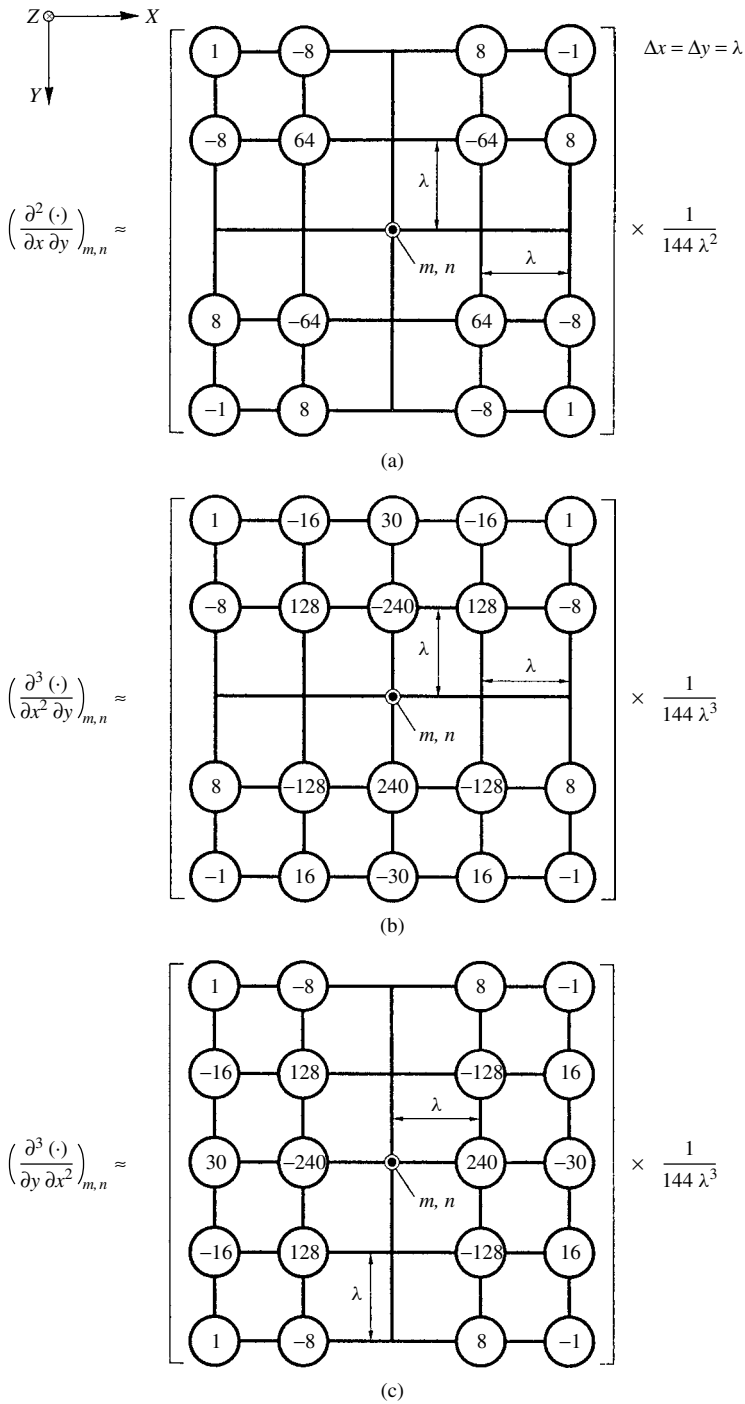
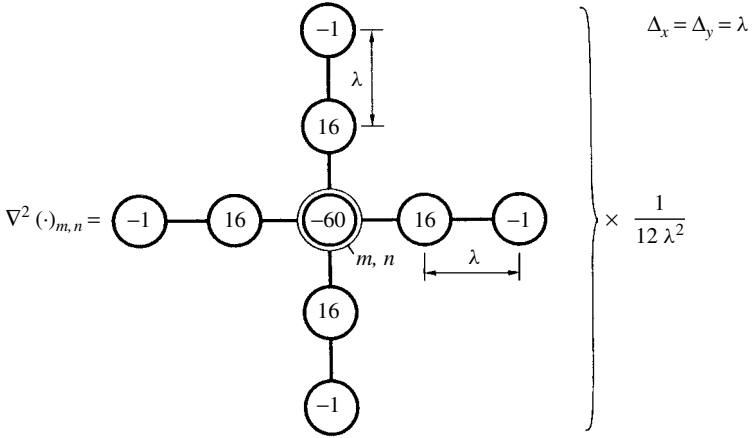
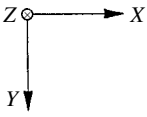
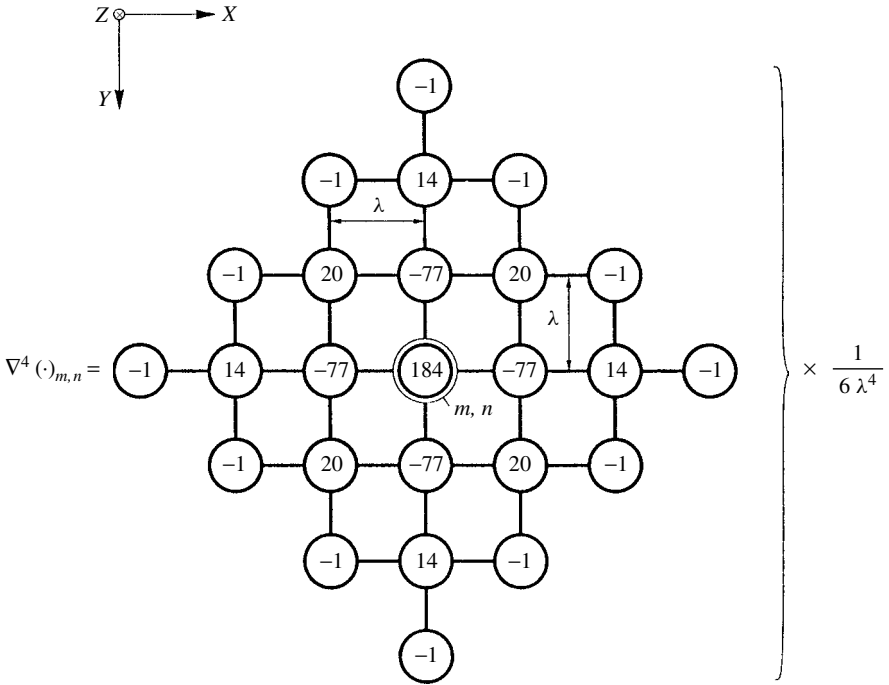


Figure 5.2.1 Stencils for mixed derivatives of higher order.



(a) Laplacian operator



(b) Biharmonic operator

Figure 5.2.2 Improved ∇^2 and ∇^4 operators.

where $\eta = y''$. Using only the first error term, Eq. (5.2.3) gives

$$\eta_m'' = \frac{1}{(\Delta x)^2}(\eta_{m-1} - 2\eta_m + \eta_{m+1}) - \frac{(\Delta x)^2}{12}\eta_m^{IV} - \dots, \quad (5.2.6)$$

or, in another form,

$$y_m^{IV} = \frac{1}{(\Delta x)^2}(y_{m-1}'' - 2y_m'' + y_{m+1}'') - \frac{(\Delta x)^2}{12}y_m^{VI} + \dots \quad (5.2.7)$$

Substitution of this expression into Eq. (5.2.3) yields

$$\begin{aligned} \frac{1}{(\Delta x)^2}(y_{m-1} - 2y_m + y_{m+1}) &= \frac{1}{12}(y_{m-1}'' + 10y_m'' + y_{m+1}'') \\ &\quad - \frac{(\Delta x)^4}{240}y_m^{VI} + \dots \end{aligned} \quad (5.2.8)$$

Equations (5.2.4) and (5.2.8) have errors of the same order of magnitude, but the latter requires fewer mesh points than the expression previously obtained through higher-order approximation.

Similar expressions in which, in addition to the ordinates, the derivatives of the function appear at various mesh points[†] can be derived for other derivatives. Equation (5.2.8) can be written in the more general form

$$y_m^{(k)} = \sum_{i=-\kappa}^{i=+\kappa} (a_{m+i} y_{m+i}) + \sum_{i=-1}^{i=+1} (A_{m+i} y_{m+i}^{(k)}) + \varepsilon \quad \text{for } \kappa = \frac{k}{2}, \frac{k+1}{2}, \quad (5.2.9)$$

where k represents the order of derivative and the error term is usually neglected.[‡]

Let us consider, for instance, a linear differential equation in the form

$$y^{(k)} = f(x, y, y', \dots, y^{(k-2)}, y^{(k-1)}) \quad (5.2.10)$$

in which we have expressed the derivative $y^{(k)}$ in terms of lower derivatives ($k-1, k-2, \dots, 2, 1$). The substitution of (5.2.10) into the right-hand side of (5.2.9) gives, for each pivotal point, x_m , an equation that contains the unknowns $y_{m+1}^{(s)}$, where $0 \leq s \leq k-1$. Additional equations of the form (5.2.9) for each $y_m^{(s)}$ result in the following system of equations:

$$\begin{aligned} \sum_{i=-\kappa}^{i=\kappa} [a_{m+i}^{(1)} y_{m+i} + A_{m+i}^{(1)} y_{m+i}^{(k-1)}] &= 0, \\ \sum_{i=-\kappa}^{i=\kappa} [a_{m+i}^{(2)} y_{m+i} + A_{m+i}^{(2)} y_{m+i}^{(k-2)}] &= 0, \\ &\vdots \\ \sum_{i=-\kappa}^{i=\kappa} [a_{m+i}^{(k-1)} y_{m+i} + A_{m+i}^{(k-1)} y_{m+i}'] &= 0. \end{aligned} \quad (5.2.11)$$

[†] Hence the name *multilocal*.

[‡] The first term on the right-hand side of Eq. (5.2.9) represents the central difference operator.

In these equations the ordinates and the derivatives of the functions are unknown. Using additional statements about the boundary conditions involving higher derivatives, a sufficient number of equations for the solution can be obtained. Furthermore, a successive elimination of the unknown derivatives from Eq. (5.2.11) yields finite difference expressions in terms of the y_{m+1} , y_m , and y_{m-1} ordinates for the specific differential equation (5.2.10) in consideration.

Collatz [5.2.1, 5.2.2] extended this concept to the governing differential equation of the plate (1.2.30) utilizing two-dimensional Taylor series expansion that has the general form

$$w(x - \Delta x, y - \Delta y) = w_{m,n} + \sum_{j=1}^{\infty} \left[\frac{(-1)^j}{j!} \left(\Delta x \frac{\partial}{\partial x} + \Delta y \frac{\partial}{\partial y} \right)^j w \right]_{m,n} \quad (5.2.12)$$

Stencils for schematic representation of the governing differential equation (1.2.30) are given in Fig. 5.2.3. The derivation of such improved finite difference operators is usually tedious and involved. Therefore, it should not be attempted routinely but only when the elaborate derivations required are justified by repeated reuse of the improved finite difference expressions. Zurmühl [5.2.4] has derived extensive formulas for the treatment of various boundary conditions by the multilocal method, the most important of which are given Figs. 5.2.4–5.2.10. In addition, the reader finds in Zurmühl's paper very useful expressions for the internal forces expressed by the *multilocal* technique, further contributing to the practical applicability of this method. Other applications of this improved finite difference technique can be found in the references listed at the end of this section.

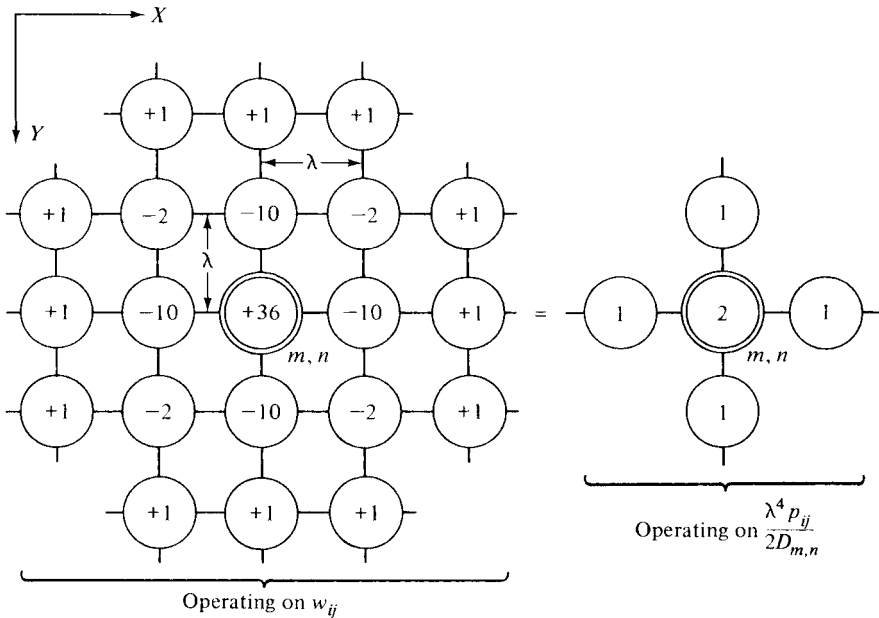
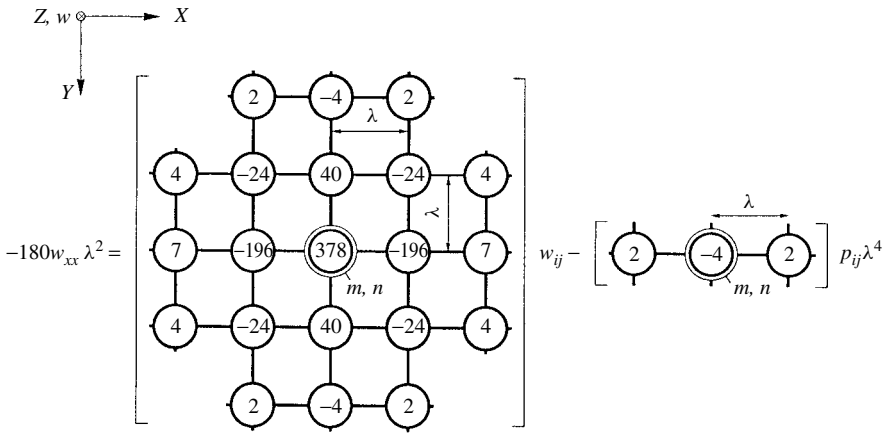
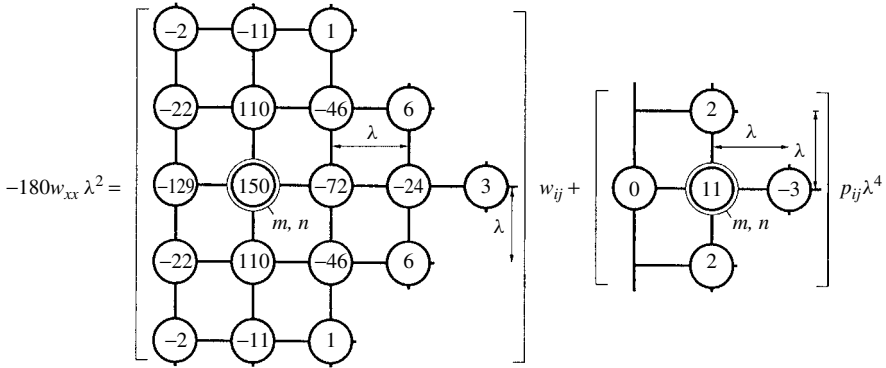
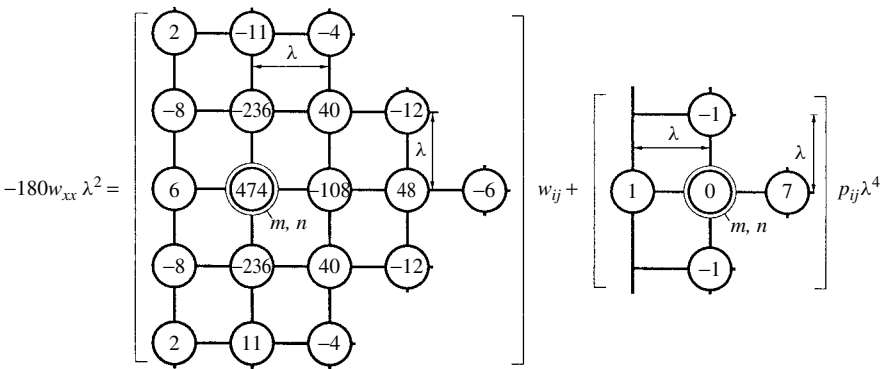


Figure 5.2.3 General stencil for multilocal method.



(a) For interior points

(b) Pivotal point a λ distance from edge(c) Pivotal point of λ distance from edge**Figure 5.2.4** Multilocal stencils for second derivatives.

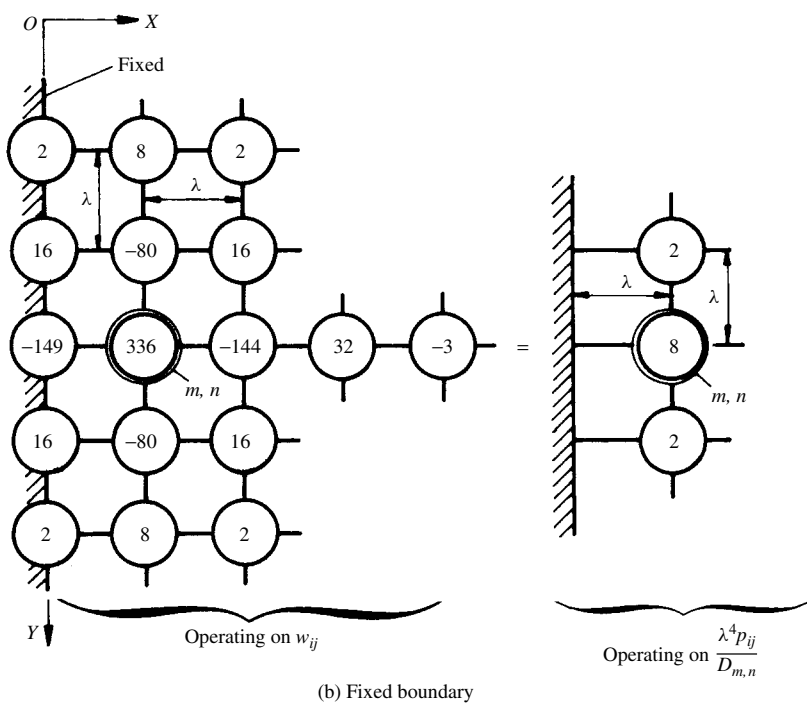
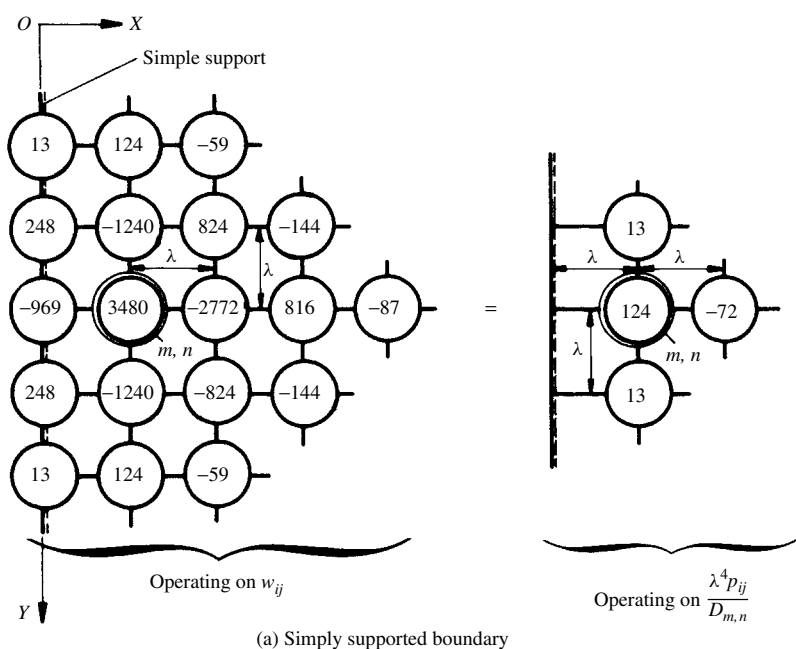


Figure 5.2.5 Pivotal point m, n next to boundaries.

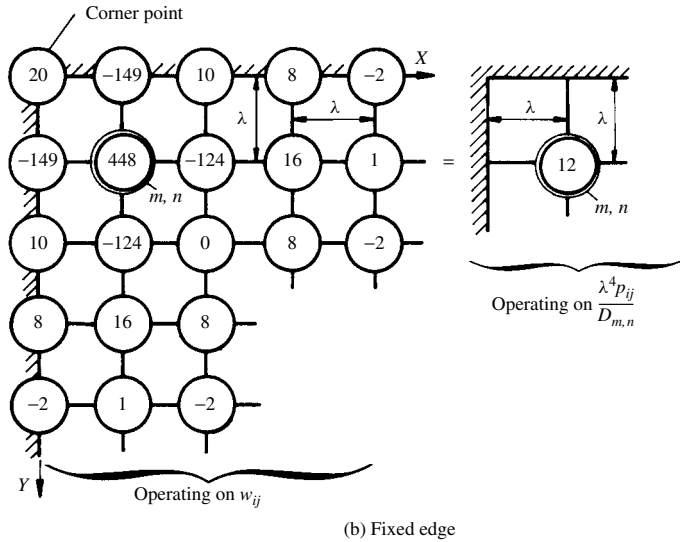
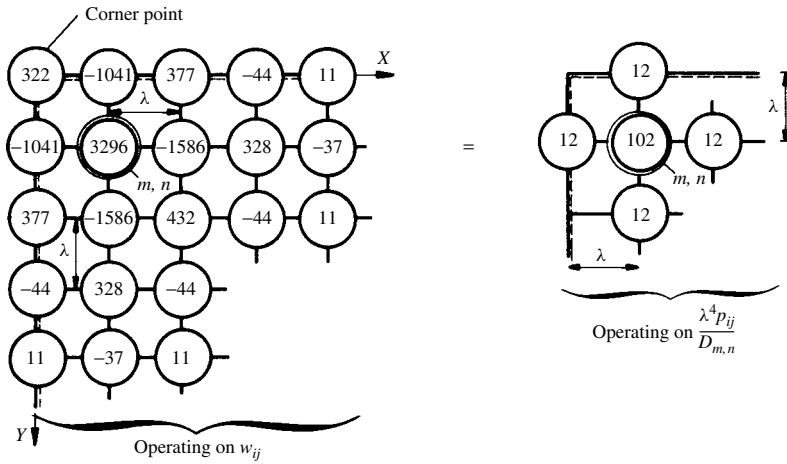


Figure 5.2.6 Stencils for simply supported and fixed corner points.

d. Funicular Polygon Method (Variation of the Hermitian Method). The funicular polygon method represents a sharpened finite difference technique introduced by Stüssi [5.2.5, 5.2.6] and extended by Dubas [5.2.7]. It is based on a relationship that exists in the field of structural mechanics between a function y and its second derivative y'' .

The fourth-order differential equation of a plate strip (2.7.1) can be written in terms of two second-order differential equations:

$$\frac{d^2 M(x)}{dx^2} = -p_z(x) \quad (5.2.13)$$

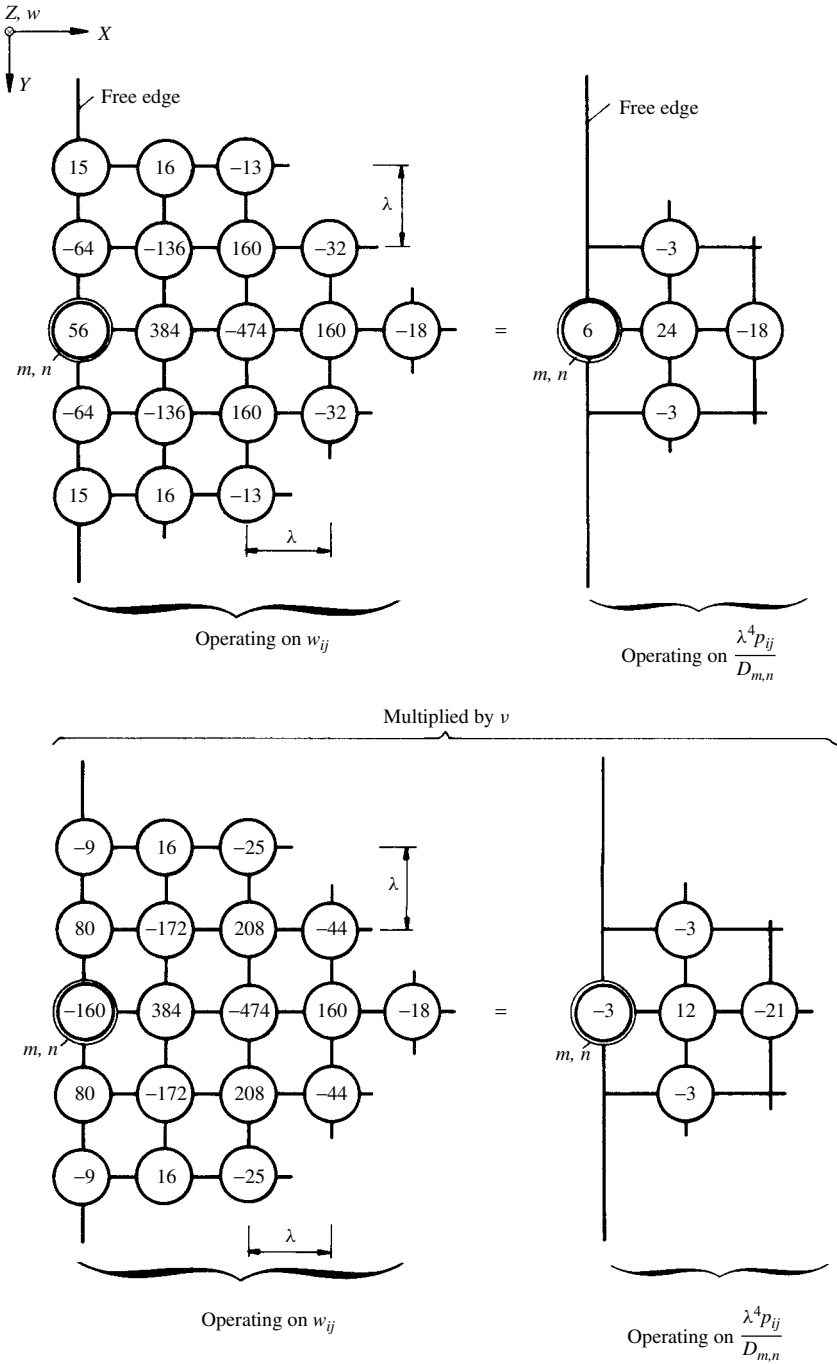


Figure 5.2.7 Stencils for free-edge conditions. These two stencils must be used jointly.

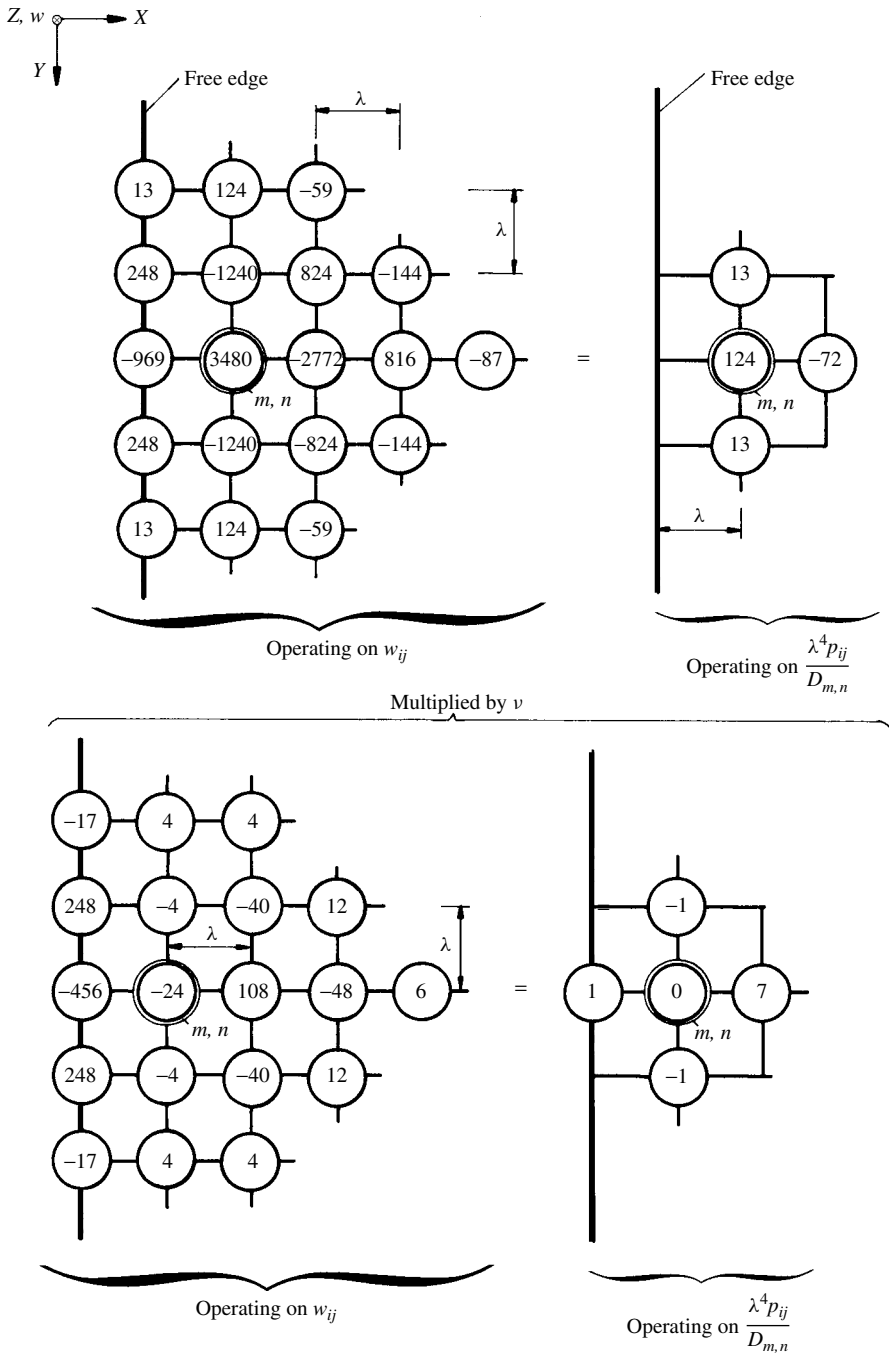


Figure 5.2.8 Pivotal point m, n at λ distance from free edge. These two stencils must be used jointly.

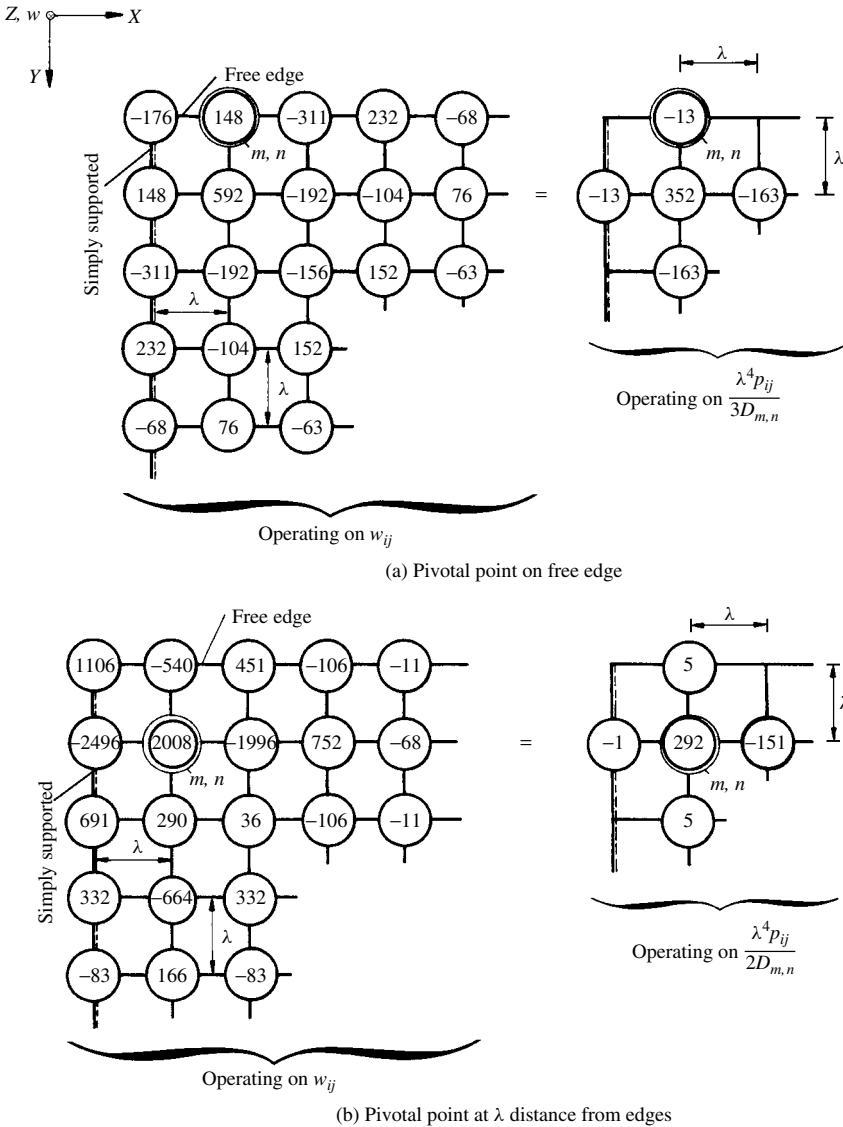


Figure 5.2.9 Stencils for corner of simply supported and free edges.

and

$$\frac{d^2 w}{dx^2} = -\frac{M}{D}. \quad (5.2.14)$$

Assuming, again (as we did for the straight-line representation of the load in Sec. 5.1), that the lateral load at the mesh points is transmitted by a series of fictive simply supported beams (Fig. 5.2.11), the equivalent concentrated load (P_m) is obtained by computing the reactions of these beams using a second-order parabola for

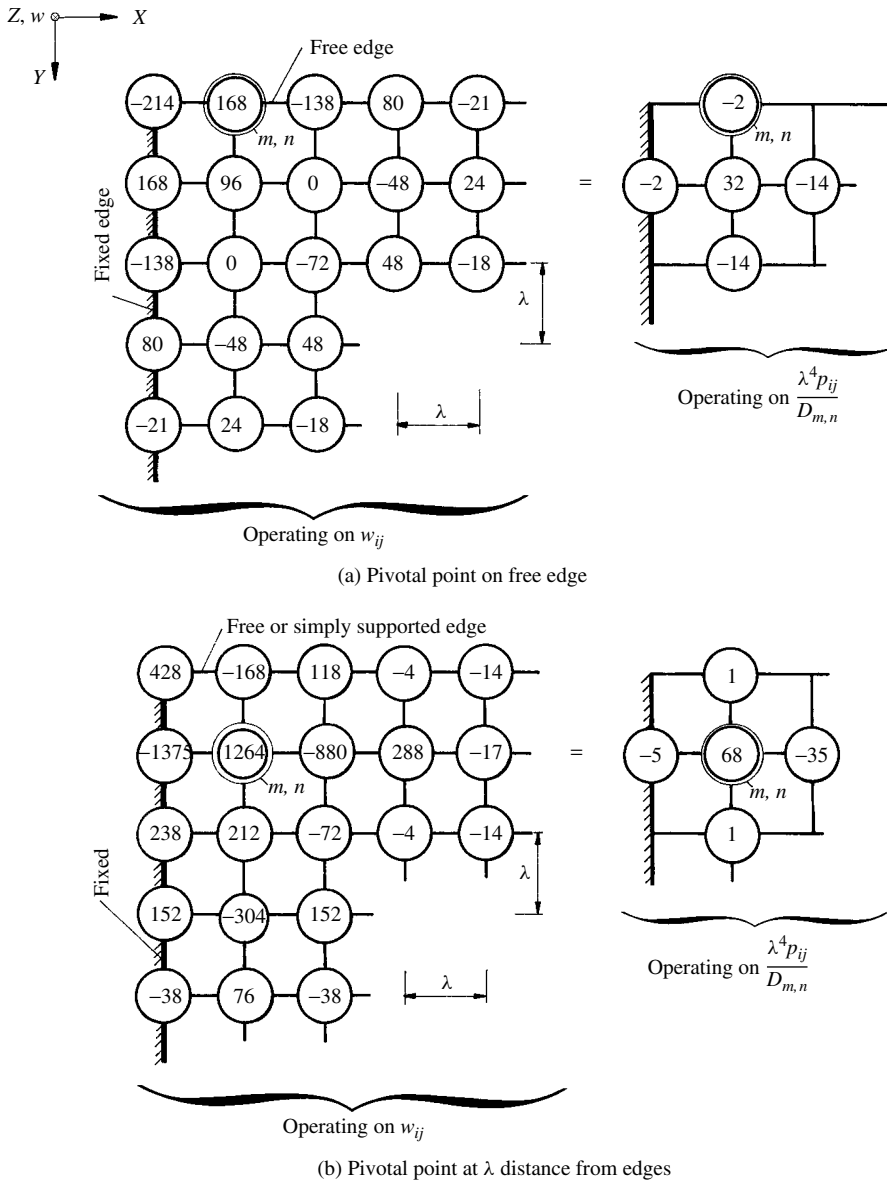


Figure 5.2.10 Additional multilocal patterns for edge regions.

the representation of the load distribution. This requires the superposition of the reactions created by the shaded area in Fig. 5.2.11 upon the already derived *equivalent joint load* (5.1.29) pertinent to the assumption of the straight-line load distribution. This yields

$$P_m = \frac{\Delta x}{12} (p_{m-1} + 10p_m + p_{m+1}). \quad (5.2.15)$$

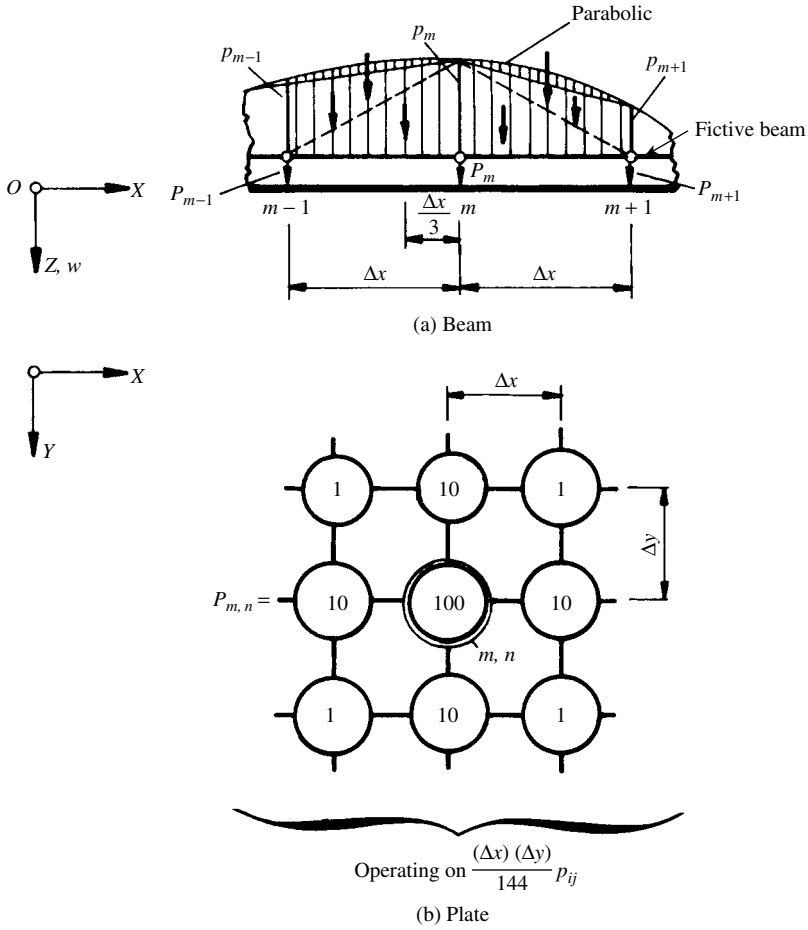


Figure 5.2.11 Improved load averaging.

Expressing Eq. (5.2.13) by central differences, we can write

$$M_{m-1} - 2M_m + M_{m+1} = -\frac{P_m(\Delta x)^2}{\Delta x} = -\frac{(\Delta x)^2}{12}(p_{m-1} + 10p_m + p_{m+1}). \quad (5.2.16)$$

By introducing

$$M = \eta \quad \text{and} \quad \eta'' = \frac{d^2 M}{dx^2} = -p_z, \quad (5.2.17)$$

a more general form of Eq. (5.2.16) is obtained:

$$\eta_{m-1} - 2\eta_m + \eta_{m+1} = \frac{(\Delta x)^2}{12}(\eta''_{m-1} + 10\eta''_m + \eta''_{m+1}) = (\Delta x)P_m(\eta''), \quad (5.2.18)$$

which is called the *funicular polygon equation*, since it corresponds to the equation of the funicular polygon of the equivalent joint forces P_m . Equation (5.2.18), with the exception of the error term, is identical to the previously derived Eq. (5.2.8). The advantage of the structural mechanics analogy used in the derivation of the funicular polygon equation lies in the fact that the usability of Eq. (5.2.18) is extended to discontinuous functions, since the equivalent joint load of any function can be obtained by applying the above-described procedure.

Equation (5.2.18) gives a mathematical relationship between a function and its second derivative, which can be used for solving second- and fourth-order differential equations, since it permits the substitution of the second and fourth derivatives by the function itself or by lower-order derivatives, respectively. The finite difference solution of the differential equation of the plate (1.2.30) by this improved finite difference method is based on the same principle; that is, the derivatives are expressed by suitable combinations of the *joint loads*. For this purpose we express the two-dimensional lateral load $p_z(x, y)$ as the *Cartesian product* of two one-dimensional load-averaging rules. This operation yields

$$P_{m,n} = \frac{(\Delta x)(\Delta y)}{144} \left\{ \begin{array}{l} p_{m-1,n-1} + 10p_{m,n-1} + p_{m+1,n-1} \\ + 10p_{m-1,n} + 100p_{m,n} + 10p_{m+1,n} \\ + p_{m-1,n+1} + 10p_{m,n+1} + p_{m+1,n+1} \end{array} \right\}. \quad (5.2.19)$$

Next, an analogous expression is constructed from the joint loads:

$$\left\{ \begin{array}{l} P_{m-1,n-1} + 10P_{m,n-1} + P_{m+1,n-1} \\ + 10P_{m-1,n} + 100P_{m,n} + 10P_{m+1,n} \\ + P_{m-1,n+1} + 10P_{m,n+1} + P_{m+1,n+1} \end{array} \right\}. \quad (5.2.20)$$

To formulate the partial derivatives of the differential equation of the plate (1.2.30) in terms of joint loads, first, the *funicular polygon equation* (5.2.18) is written for the X and Y directions:

$$\Delta x P_{m,n}(w'') = w_{m-1,n} - 2w_{m,n} + w_{m+1,n} \quad (5.2.21)$$

and

$$\Delta y P_{m,n}(\ddot{w}) = w_{m,n-1} - 2w_{m,n} + w_{m,n+1}, \quad (5.2.22)$$

where $P_{m,n}$ is a joint load [Eq. (5.2.19)]. Similarly,

$$\Delta x P_{m,n}(w^{IV}) = w''_{m-1,n} - 2w''_{m,n} + w''_{m+1,n}, \quad \text{etc.} \quad (5.2.23)$$

Now all terms of the differential equation of the plate (1.2.30) can be expressed by joint loads that have the general form of (5.2.20). Then, using Eqs. (5.2.21), (5.2.22) and (5.2.23), all derivatives of w are eliminated in two subsequent operations [5.2.7]. The results of these mathematical manipulations are given in diagrammatic form

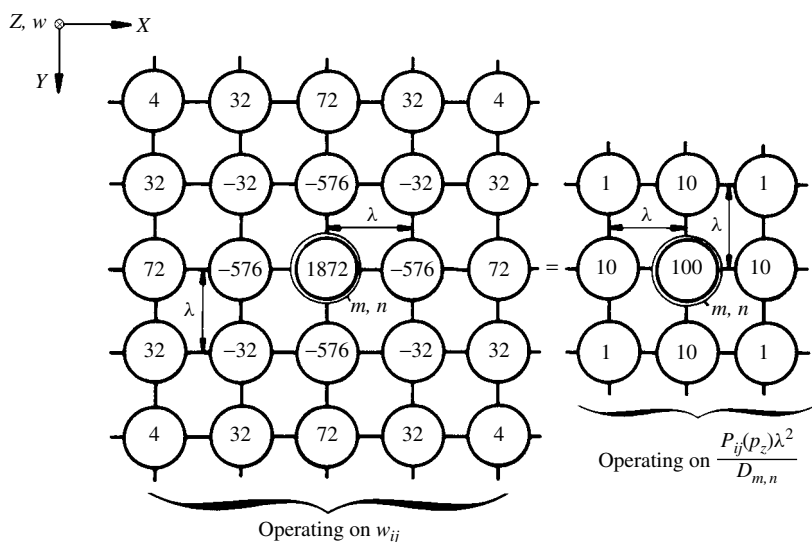


Figure 5.2.12 General stencils for funicular polygon method.

in Fig. 5.2.12. Stencils for the various edge conditions are shown in Figs. 5.2.13 and 5.2.14.

In the previous subsection we gave multilocal stencils for rectangular plates covering practically all edge and corner conditions. Here—to save space—we have restricted ourselves to the most commonly used edge supports. Readers who are interested in obtaining additional readily usable finite difference patterns for the funicular polygon method are referred to Ref. [5.2.7]. The convergence characteristics of this improved FDM is illustrated in Fig. 5.2.15.

e. Successive Approximation. Other ways for improving on the accuracy of ordinary finite difference solutions are based on error minimizations combined with iteration.

First, we obtain a solution $w^{(0)}(x, y)$ using ordinary finite difference techniques and an improved load-averaging rule. For a quadratic mesh ($\Delta x = \Delta y = \lambda^{(0)}$), the magnitude of the error can be expressed by $\varepsilon^{(0)} = F(x, y)(\lambda^{(0)})^\mu$, where μ represents the order of error and $F(x, y)$ is a function that is independent of mesh size. The order of error for the biharmonic operator, calculated from central difference, is $\mu = 2$.

Next, decreasing the mesh width to $\lambda^{(1)} = \lambda^{(0)}/2$, a new solution $w^{(1)}(x, y)$ is obtained. We estimate the error of this second solution by *Runge's principle*, which gives

$$\varepsilon_{m,n}^{(1)} \approx \frac{w_{m,n}^{(0)} - w_{m,n}^{(1)}}{2^\mu - 1} = \frac{w_{m,n}^{(0)} - w_{m,n}^{(1)}}{3}. \quad (5.2.24)$$

An improved solution is sought in the form

$$w(x, y) = w^{(1)}(x, y) + c_1 \phi_1(x, y) + \cdots, \quad (5.2.25)$$

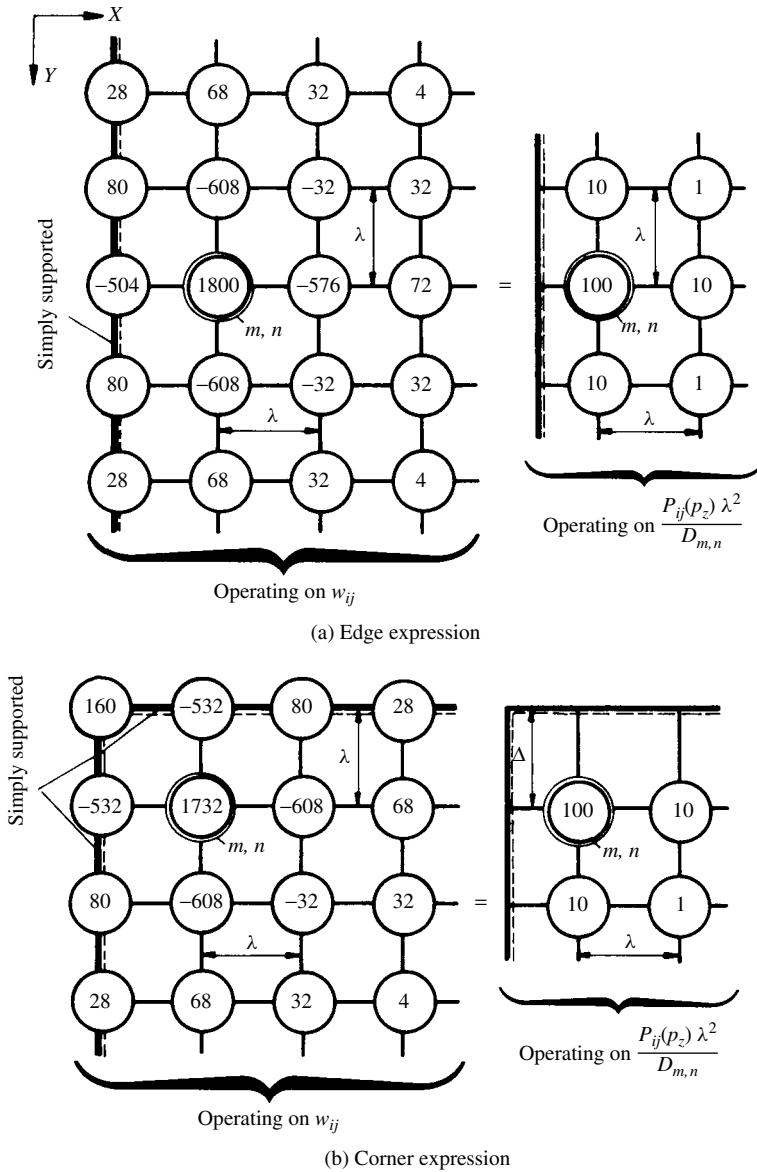
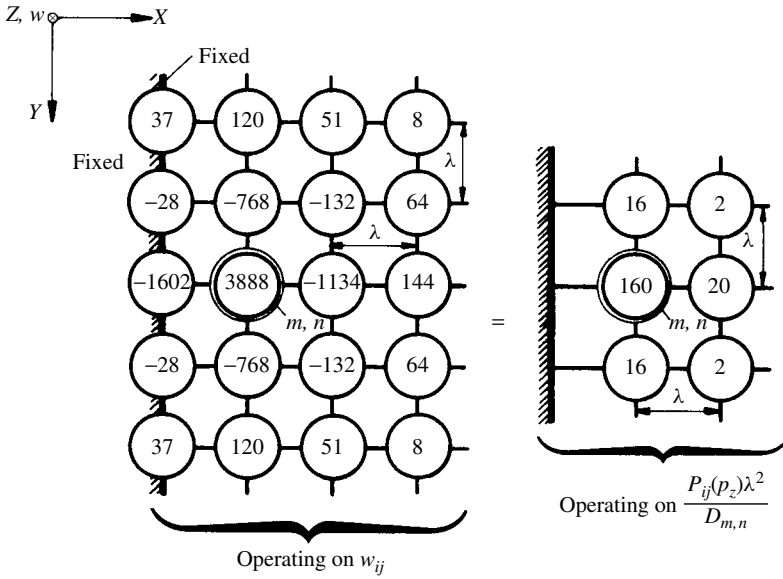
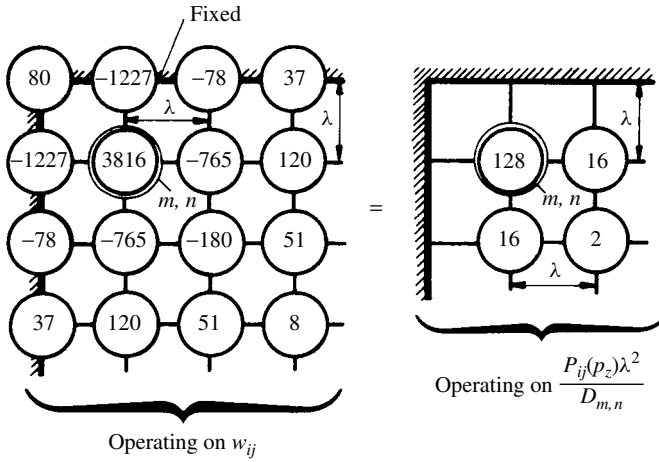


Figure 5.2.13 Stencils for simple supported edges (funicular polygon method).

where $\phi_1(x, y)$ is a function affine to $w^{(1)}(x, y)$. The product of the corresponding beam deflections in the X and Y directions, for instance, provides very usable shape functions. In a computerized solution, the deflected plate surface can easily be *curve fitted*, yielding the best choice for $\phi_1(x, y)$. Other suitable expressions can be found in Secs. 4.2 and 4.3. The unknown constant c_1 in Eq. (5.2.25) is determined from minimizing the error $\varepsilon^{(1)}$. If the exact solution is $w(x, y)$, the square of the error sum



(a) Edge expression



(b) Corner expression

Figure 5.2.14 Stencils for fixed edges (funicular polygon method).

of the improved solution [Eq. (5.2.25)] is

$$\begin{aligned}
 (s^{(1)})^2 &= \sum_{i=1}^k [w_{m,n} - w_{m,n}^{(1)} - c_1 \phi_1(x, y)_{m,n} - \dots]^2 \\
 &\approx \sum_{i=1}^k [\varepsilon_{m,n}^{(1)} - c_1 \phi_1(x, y)_{m,n}]^2,
 \end{aligned} \tag{5.2.26}$$

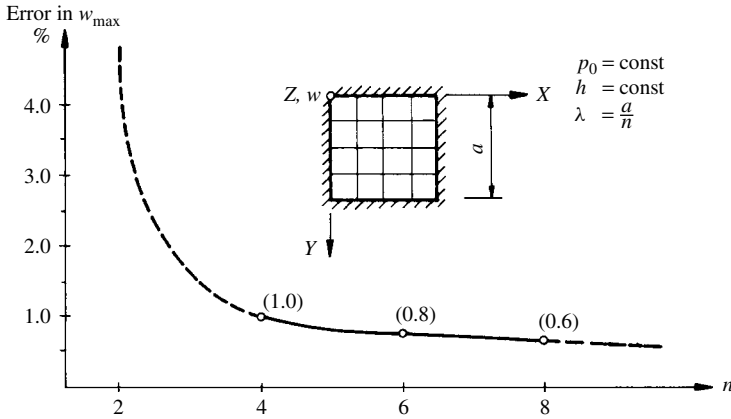


Figure 5.2.15 Convergence characteristics of funicular polygon method.

where $i = 1, 2, 3, \dots, k$ represents the number of mesh points. The minimum principle gives

$$\frac{\partial [s^{(1)}]^2}{\partial c} = 2 \sum_{i=1}^k \{ [c_1 \phi_1(x, y)_{m,n} - \varepsilon_{m,n}^{(1)}] \phi_1(x, y)_{mn} \} = 0; \quad (5.2.27)$$

hence

$$c_1 = \frac{\sum_{i=1}^k \varepsilon_{mn}^{(1)} \phi_1(x, y)_{m,n}}{\sum_{i=1}^k [\phi_1(x, y)_{m,n}]^2} \quad (5.2.28)$$

This cycle can be repeated. The least-squares method, used in this error distribution process, usually yields better estimates of the derivatives, because it provides a “smoothing” effect.

Since it is usually inconvenient to use $\lambda^{(2)} = \lambda^{(0)}/4$ for the second cycle, we may estimate the maximum error for rectangular plates from

$$\varepsilon_{\max}^{(2)} = c_2 = \frac{1.5(w_{\max}^{(2)} - w_{\max}^{(1)})}{(1/M^2) + (1/N^2)}, \quad (5.2.29)$$

where M and N represent the number of mesh widths between the location of $w_{\max}^{(2)}$ and the nonyielding ($w = 0$) boundaries. Equation (5.2.29) assumes that the maximum deflection occurs close to the center of the plate and that the error function is

$$\phi_2(x, y) = c_2 \left(1 - \frac{x^2}{M^2 \lambda^2} \right) \left(1 - \frac{y^2}{N^2 \lambda^2} \right). \quad (5.2.30)$$

This simple iterative technique results in an especially fast convergence to the exact solution when sharpened biharmonic operators are used, but without the benefit of improved expressions for the boundary conditions. In such a case $\mu = 4$ for interior

mesh points [Eq. (5.2.24)], while $\mu = 2$ (or another pertinent number) is applicable at the boundaries. Usually one cycle gives sufficiently improved results.

Summary. Sharpened FDMs are very powerful tools in the hands of a competent analyst. Improved finite difference expressions are generally obtained from Taylor series expansion, used to satisfy the differential equation at several points for each finite difference expression. Special attention should be paid to (1) load representation and (2) the boundary value problems. Inaccurate formulas used at the boundaries considerably reduce the accuracy gained at interior points. Although, with the same mesh size, these improved techniques require more work, in general, they prove to be more economical than ordinary FDMs. That is, a relatively coarse mesh is sufficient for good accuracy. Since the method of higher approximation requires more mesh points, preference should be given to the so-called Hermitian methods (multilocal and funicular polygon). In fact, these methods are recommended most by the author for “hand” computation and for the use with programmable desk-top calculators, provided that appropriate stencils are readily available. Derivation of improved formulas can be quite involved; consequently, a simple error distribution technique has been developed for solution of complicated differential equations by the ordinary FDM. The iteration converges quickly to the exact solution when the derivatives at the interior region are expressed by the method of higher approximation and the boundary errors are minimized.

ILLUSTRATIVE EXAMPLE I

Let us solve the problem shown in Fig. 5.1.19a using the funicular polygon method. The joint-point loads are determined from Eq. (5.2.19); thus we can write

$$P_1 = P_2 = \frac{\lambda^2}{144} \left(24 \frac{p_0}{2} + 120 p_0 \right) = 0.916 \lambda^2 p_0,$$

$$P_3 = P_4 = \frac{\lambda^2}{144} \left(120 \frac{p_0}{2} + 12 p_0 \right) = 0.500 \lambda^2 p_0.$$

The finite difference equations at each of the grid points are calculated using the stencils shown in Figs. 5.2.12 and 5.2.13:

$$\begin{aligned} \text{At point 1:} \quad & 1872w_1 - 1152w_2 - 1152w_3 - 128w_4 \\ & = \frac{\lambda^4 p_0}{D} (24 \times 0.5 + 120 \times 0.916) = 122 \frac{\lambda^4 p_0}{D}; \end{aligned}$$

$$\begin{aligned} \text{At point 2:} \quad & -576w_1 + 1872w_2 - 64w_3 - 1152w_4 \\ & = \frac{\lambda^4 p_0}{D} (22 \times 0.5 + 110 \times 0.916) = 112 \frac{\lambda^4 p_0}{D}; \end{aligned}$$

$$\begin{aligned} \text{At point 3:} \quad & -576w_1 - 64w_2 + 1872w_3 - 1152w_4 \\ & = \frac{\lambda^4 p_0}{D} (120 \times 0.5 + 12 \times 0.916) = 71 \frac{\lambda^4 p_0}{D}; \end{aligned}$$

At point 4: $-32w_1 - 576w_2 - 576w_3 + 1872w_4$

$$= \frac{\lambda^4 p_0}{D} (110 \times 0.5 + 11 \times 0.916) = 65.1 \frac{\lambda^4 p_0}{D}.$$

The solution of this system of linear algebraic equations gives

$$\begin{aligned} w_1 &= 0.00265 \frac{a^4 p_0}{D}, & w_2 &= 0.00193 \frac{a^4 p_0}{D}, \\ w_3 &= 0.00185 \frac{a^4 p_0}{D}, & w_4 &= 0.00132 \frac{a^4 p_0}{D}. \end{aligned}$$

Since the analytically obtained maximum deflection [2] is $w_1 = w_{\max} = 0.00263a^4 p_0/D$, the discrepancy between the “exact” and the improved finite difference solutions is only 0.76%. A comparison with the relatively accurate two-step finite difference solution (error 5%), discussed in the previous section, clearly illustrates the advantages of this powerful tool in analyzing plate problems. If we compare the results obtainable using the central difference expressions for the biharmonic operator with those of the funicular polygon method, we can state that, applying the same mesh size, the latter method reduces the error by more than an order of magnitude. On the other hand, the increase of additional effort required is relatively small.

ILLUSTRATIVE EXAMPLE II

The problem shown in Fig. 5.1.19a is to be solved by the multilocal method. Using the stencils given in Figs. 5.2.3 and 5.2.8a, the following set of equations can be written:

At point 1: $36w_1 - 20w_2 - 20w_3 - 8w_4$

$$= \left[2p_0 + 2p_0 + 2 \left(\frac{1}{2} p_0 \right) \right] \frac{\lambda^4}{D} = 2.5 \frac{p_0}{D} \lambda^4;$$

At point 2: $-2772w_1 + 4296w_2 + 1648w_3 - 2768w_4$

$$= \left[124p_0 + 13 \times 2 \left(\frac{1}{2} p_0 \right) - 72p_0 \right] \frac{\lambda^4}{D} = 65 \frac{p_0}{D} \lambda^4;$$

At point 3: $-2772w_1 + 1648w_2 + 4296w_3 - 2768w_4$

$$= \left[124 \left(\frac{1}{2} p_0 \right) + 13 \times 2 \left(\frac{1}{2} p_0 \right) - 72p_0 \right] \frac{\lambda^4}{D} = \frac{3p_0}{D} \lambda^4;$$

At point 4: $432w_1 - 1630w_2 - 1630w_3 + 3952w_4$

$$= \left[102 \left(\frac{1}{2} p_0 \right) + 12 \times 2 \left(\frac{1}{2} p_0 \right) + 12p_0 \right] \frac{\lambda^4}{D} = 75 \frac{p_0}{D} \lambda^4.$$

$$\begin{aligned}
 -8w_1^{(0)} + 4w_2^{(0)} + 20w_3^{(0)} - 16w_4^{(0)} &= \frac{p_0 a^4}{256D}, \\
 +2w_1^{(0)} - 8w_2^{(0)} - 8w_3^{(0)} + 22w_4^{(0)} &= \frac{p_0 a^4}{256D}.
 \end{aligned}$$

Solution of these equations yields

$$\begin{aligned}
 w_1^{(0)} &= 0.63129 \frac{p_0 a^4}{256D}, & w_2^{(0)} &= 0.41449 \frac{p_0 a^4}{256D}, \\
 w_3^{(0)} &= 0.46630 \frac{p_0 a^4}{256D}, & w_4^{(0)} &= 0.30835 \frac{p_0 a^4}{256D}
 \end{aligned}$$

and

$$w_{\max}^{(0)} = w_1^{(0)} = 0.00247 \frac{p_0 a^4}{D}.$$

This result compared with the “exact” solution, $0.00192 p_0 a^4 / D$, shows an error of 28.6%.

Next, we decrease the mesh width to $\lambda^{(1)} = a/8$ and calculate an improved solution $w^{(1)}$. The estimated error of this solution, based on Eq. (5.2.24), is

$$\begin{aligned}
 \varepsilon_1^{(1)} &= \frac{0.53446 - 0.63129}{3} \cdot \frac{p_0 a^4}{256D} = -0.03228 \frac{p_0 a^4}{256D}, \\
 \varepsilon_2^{(1)} &= \frac{0.32560 - 0.41449}{3} \cdot \frac{p_0 a^4}{256D} = -0.02963 \frac{p_0 a^4}{256D}, \\
 \varepsilon_3^{(1)} &= \frac{0.39514 - 0.46630}{3} \cdot \frac{p_0 a^4}{256D} = -0.02372 \frac{p_0 a^4}{256D}, \\
 \varepsilon_4^{(1)} &= \frac{0.24338 - 0.30835}{3} \cdot \frac{p_0 a^4}{256D} = -0.02168 \frac{p_0 a^4}{256D}.
 \end{aligned}$$

Assuming an error function for $w^{(1)}$ in the form

$$\varepsilon_1(x, y) = c_1 \phi_1(x, y) = \frac{c_1}{2} \left(1 - \cos \frac{2\pi x}{a} \right) \sin \frac{\pi y}{a},$$

we obtain the unknown coefficient c_1 from Eq. (5.2.28):

$$\begin{aligned}
 c_1 &= -\frac{p_0 a^4}{256D} \\
 &\times \frac{0.03228 \times 1 + 0.02963 \times 0.5 + 0.02372 \times 0.70711 + 0.02168 \times 0.35355}{1 + 0.25 + 0.5 + 0.125} \\
 &= -0.03815 \frac{p_0 a^4}{256D};
 \end{aligned}$$

Table 5.2.2 Summary of Results

Cycle Number	$w_{\max}^{(i)} = (w)_{x=y=a/2}^{(i)}$	Percentage Error
1	$w^{(0)} = 0.00247 p_0 a^4 / D$	28.6
2	$w^{(1)} = 0.00208 p_0 a^4 / D$	8.33
3	$w^{(2)} = w^{(1)} + c_1 \phi_1$	
	$= 0.0019388 p_0 a^4 / D$	0.98
4	$w^{(3)} = w^{(1)} + c_1 \phi_1 + c_2 \phi_2$	
	$= 0.001925 p_0 a^4 / D$	0.26

therefore

$$w_{\max}^{(2)} = [w^{(1)} + c_1 \phi_1(x, y)]_{x=y=a/2} = 0.00193880 \frac{p_0 a^4}{D}.$$

Repetition of the same procedure gives $w_{\max} = 0.001925 p_0 a^4 / D$. The results of this successive approximation are summarized in Table 5.2.2. Although the deflections converge rapidly to their exact values, this is not always the case with the internal moments and shear forces, especially if the assumed $\phi_1(x, y)$, $\phi_2(x, y)$, ... error functions are not affine to the exact deflected place surface. In such a case, we may use the errors $\varepsilon_1, \varepsilon_2, \dots, \varepsilon_n$ associated with each mesh point as fictitious loads $p_1^*, p_2^*, \dots, p_n^*$ to obtain the required corrections by the finite difference technique. Then we proceed with the final cycle of approximation, as indicated in Sec. 5.2e. When high accuracy is required, improved operators should be used for the interior mesh points and for determination of the internal forces.

ILLUSTRATIVE EXAMPLE IV

Assume, again, that the edges $x = 0$ and $x = a$ of a square plate are fixed and the other two edges are simply supported. The plate carries a uniformly distributed lateral load p_0 . Determine the maximum deflection and moments of this plate using the method of higher approximation, introduced in Sec. 5.2b.

Since in this case we do not have readily usable stencils for the boundary conditions, we try to extend the simplified assumptions, given in Fig. 5.1.5, to deal with the simply supported and clamped boundaries of this plate. The finite difference mesh and the numbering of the corresponding mesh points are shown in Fig. 5.2.17.

Employing the improved biharmonic operator given in Fig. 5.2.2b and using the above-mentioned simplifications for the boundaries, we obtain the coefficient matrix

$$\mathbf{A} = \begin{bmatrix} 184 & -154 & 28 & -154 & 8 & -4 & 28 & -4 & 0 \\ -77 & 198 & -79 & 40 & -156 & 40 & -2 & 28 & -2 \\ 14 & -79 & 198 & -2 & 40 & -156 & 0 & -2 & 28 \\ -77 & 40 & -2 & 198 & -156 & 28 & -77 & 40 & -2 \\ 2 & -78 & 20 & -78 & 212 & -80 & 20 & -78 & 20 \\ -1 & 20 & -78 & 14 & -80 & 212 & -1 & 20 & -78 \\ 14 & -2 & 0 & -77 & 40 & -2 & 170 & -152 & 28 \\ -1 & 14 & -1 & 20 & -78 & 20 & -76 & 184 & -78 \\ 0 & -1 & 14 & -1 & 20 & -78 & 14 & -78 & 184 \end{bmatrix}$$

for the matrix equation $\mathbf{Aw} = \mathbf{p}$. The corresponding load vector is

$$\mathbf{p} = \{1 \quad 1 \quad 1 \quad 1 \quad 1 \quad 1 \quad 1 \quad 1 \quad 1\} \frac{6\lambda^4 p_0}{D}.$$

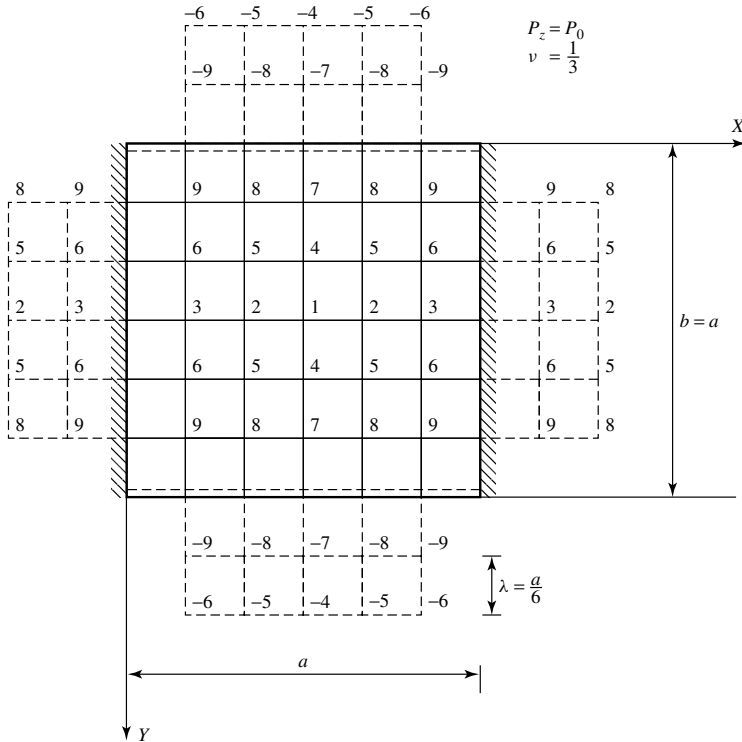


Figure 5.2.17 Square plate with two opposite edges simply supported and other two clamped.

Solution of our matrix equation yields the vector of displacements

$$\mathbf{w} = \begin{Bmatrix} 1.933 \\ 1.568 \\ 0.685 \\ 1.706 \\ 1.386 \\ 0.610 \\ 1.030 \\ 0.842 \\ 0.377 \end{Bmatrix} \frac{p_0 a^4 10^{-3}}{D}.$$

Since the maximum displacement occurs at the center of the plate, $w_1 = w_{\max} = 0.001933 p_0 a^4 / D$. A comparison of this result with its analytically obtained more exact value [2] indicates only a negligible error of 0.5%.

The case with the maximum positive moment is similar. Using

$$(m_x)_{m,n} = \frac{D}{12\lambda^2} [w_{m-2,n} - 16w_{m-1,n} + 30w_{m,n} - 16w_{m+1,n} + w_{m+2,n} + v(w_{m,n-2} - 16w_{m,n-1} + 30w_{m,n} - 16w_{m,n+1} + w_{m,n+2})], \quad (a)$$

we obtain

$$(m_x)_{x=y=a/2} = 0.03301 p_0 a^2,$$

which also shows only a negligible error.

But the finite difference equation

$$(m_y)_{m,n} = \frac{D}{12\lambda^2} [w_{m,n-2} - 16w_{m,n-1} + 30w_{m,n} - 16w_{m,n+1} + w_{m,n+2} + v(w_{m-2,n} - 16w_{m-1,n} + 30w_{m,n} - 16w_{m+1,n} + w_{m+2,n})] \quad (b)$$

gives

$$(m_y)_{x=0,y=a/2} = -0.05635 p_0 a^2.$$

This result compared with its analytically obtained value of $-0.0697 p_0 a^2$ [2] shows an unacceptable error of -19.2% . Consequently, we can state that, while the approximation of the simply supported boundaries using Fig. 5.1.5b may occasionally be acceptable, we must use a better approach than given in Fig. 5.5.1a when we are dealing with clamped edges in connection with any of the improved FDMs.

References and Bibliography

- [5.2.1] COLLATZ, L., *The Numerical Treatment of Differential Equations*, 3rd ed., Springer-Verlag, Berlin, 1966.
- [5.2.2] COLLATZ, L., "Das Mehrstellenverfahren bei Plattenaufgaben," *Z. f. Angew. Math. u. Mech.*, 30 (Nov.-Dec. 1950), 385-388.
- [5.2.3] COLLATZ, L., *Eigenwertaufgaben mit technischen Anwendungen*, Akad. Verlagsges., Leipzig, 1949, p. 350.
- [5.2.4] ZURMÜHL, R., "Behandlung der Plattenaufgaben nach dem verbesserten Differenzenverfahren," *Z. f. Angew. Math. u. Mech.*, 37 (Jan.-Feb. 1957), 1-16.
- [5.2.5] STÜSSI, F., "Numerische Lösung von Randwertproblemen mit Hilfe der Seilpolygongleichung," *Z. f. Angew. Math. u. Phys.*, 1 (1950), 53-80.
- [5.2.6] STÜSSI, F., "Ausgewählte Kapitel aus der Theorie des Brückenbaues," in *Taschenbuch für Bauingenieure*, 2nd ed., Springer-Verlag, Berlin, 1955, pp. 905-963.
- [5.2.7] DUBAS, P., "Calcul numérique des plaques et des parois minces," Ph.D. Dissertation, Publication de l'Institut de Statique Appliquée de l'Ecole Polytechnique Fédérale de Zurich, No. 27, 1955.

5.3 Finite Difference Analysis of Moderately Thick Plates

As was already discussed in Sec. 1.5, neglecting the effects of transverse shear deformation in moderately thick plates causes error in computation of deflections and stress resultants of such plates. In addition, in some cases transverse direct stress may also influence results. To consider these effects, which are neglected in classical plate theory, we can follow three different approaches. The selection of the most suitable one depends, on the one hand, on the accuracy we seek and, on the other hand, on the effort we are willing to put in such a numerical analysis. The three approaches are (a) correction to classical finite difference solutions, (b) direct finite difference formulation of the problem, and (c) finite difference representation of three-dimensional elasticity. Here, we will treat only the first two methods in detail, since they are quite usable in everyday engineering practice. In dealing with the third technique, however, we restrict ourselves to an introductory presentation because its application is more involved and requires special, not readily available computer programs.

a. Correction to Classical Finite Difference Solutions. This is, by far, the simplest and most economical method to approximate the additional shear deformation effects in moderately thick plates. First, we perform a finite difference analysis based on the classical Kirchhoff's plate theory obtaining the deflections w_K . Next, we augment the so-obtained results with deflections revised with a correction factor in the form of Cw_K .

For *simply supported* Mindlin plates of various shapes, we can use the discrete form of the *conjugate plate analogy* mentioned in Sec. 2.10. In the first step of such a numerical analysis of moderately thick plates, we can use any of the already introduced FDMs to obtain $w_{K,i}$ at each mesh point. In the second step, we calculate the additional deflections caused by the transverse shear using

$$w_{s,i} = \frac{\mathfrak{M}_i}{\kappa^2 G h_i} = \frac{(m_x + m_y)_i}{(1 + \nu) \kappa^2 G h_i}, \quad (5.3.1)$$

where \mathfrak{M}_i is the so-called *moment-sum* (1.2.42) at mesh point i and $\kappa^2 = \frac{5}{6}$ represents the shear correction factor. Thus, for simply supported Mindlin plates the deflection at each mesh point can be calculated from

$$w_{M,i} = w_{K,i} + w_{s,i}. \quad (5.3.2)$$

This represents the exact relationship between the deflection values of Mindlin and Kirchhoff plates [5.3.1]. With the so-augmented deflections, we can also *estimate* the stress resultants using the corresponding finite difference expressions introduced in Secs. 5.1 and 5.2, respectively. However, a more exact approach leads to utilization of the stencils developed for the direct finite difference analysis, discussed in Section 5.3b.

For other not simply supported boundaries, we may apply a similar approach developed by Donnell [5.3.2] that also considers the additional effect caused by direct stress. His *approximation* of the deflected plate surface is

$$w_{mt}(x, y) \approx w_K(x, y) - \frac{(8 - 3\nu)h^2}{40(1 - \nu)} \nabla^2 w_K(x, y), \quad (5.3.3)$$

where w_K represents, again, the solution for the Kirchhoff plate obtained from a previously introduced finite difference procedure. The second term on the right-hand side of Eq. (5.3.3) can also be given in a discrete form by applying the finite difference patterns of ∇^2 operating on the already calculated deflections $w_{K,i}$. Thus, using ordinary finite differences, we can write

$$\begin{aligned} (\nabla^2 w_K)_{m,n} &= \left(\frac{\partial^2 w_K}{\partial x^2} + \frac{\partial^2 w_K}{\partial y^2} \right)_{m,n} \\ &\approx \frac{1}{(\Delta x)^2} [(w_K)_{m-1,n} - 2(w_K)_{m,n} + (w_K)_{m+1,n}] \\ &\quad + \frac{1}{(\Delta y)^2} [(w_K)_{m,n-1} - 2(w_K)_{m,n} + (w_K)_{m,n+1}]. \end{aligned} \quad (5.3.4)$$

A corresponding stencil for ∇^2 but expressed by higher-order finite differences is given in Fig. 5.2.2a.

b. Direct Finite Difference Formulation. Despite their wide use in the solution of plate problems related to their classical theory, FDMs have been very sparingly utilized for the analysis of moderately thick plates. Speare applies the ordinary FDM to Reissner's plate theory [5.2.3]. We consider here only the simplified version of the pertinent differential equation (1.5.11), since in this case only one variable, w , is involved in the analysis. The ordinary finite difference representation of Eq. (1.5.11) developed by Speare is given in Fig. 5.3.1, and the finite difference patterns of the stress resultants[†] m_x , m_z and q_x are shown in Figs. 5.3.2–5.3.4 [5.2.3].

The boundary conditions to be satisfied are as follows:

$$\begin{array}{ll} \text{Simply supported :} & w = m_n = \phi_t = 0, \\ \text{Fixed :} & w = \phi_n = \phi_t = 0, \\ \text{Free :} & m_n = m_{nt} = q_n = 0, \end{array}$$

where

$$\phi_n = -\frac{\partial w}{\partial n} + \frac{12(1+\nu)}{5Eh}q_n, \quad \phi_t = -\frac{\partial w}{\partial t} + \frac{12(1+\nu)}{5Eh}q_t.$$

Subscripts n and t refer to the normal and tangential directions, respectively. The finite difference forms of these equations can be derived using stencils of the corresponding stress resultants (Figs. 5.3.2–5.3.4).

A closer inspection of all the above-introduced stencils reveals that certain values of plate thickness h will make some terms zero or very small. If this occurs, the mesh length λ should be changed. Furthermore, it should be noted that the use of the general stencil (Fig. 5.3.1) in combination with the simplified boundary conditions (Fig. 5.1.5) gives completely erroneous results.

To increase the accuracy of this finite difference procedure, we may apply the *successive approximation* technique introduced in Sec. 5.2e. In selecting the first mesh size, $\lambda^{(0)} = L/(4 \rightarrow 6)$ is recommended, while the subsequent subdivision should

[†] See Eqs. (1.5.13)–(1.5.17).

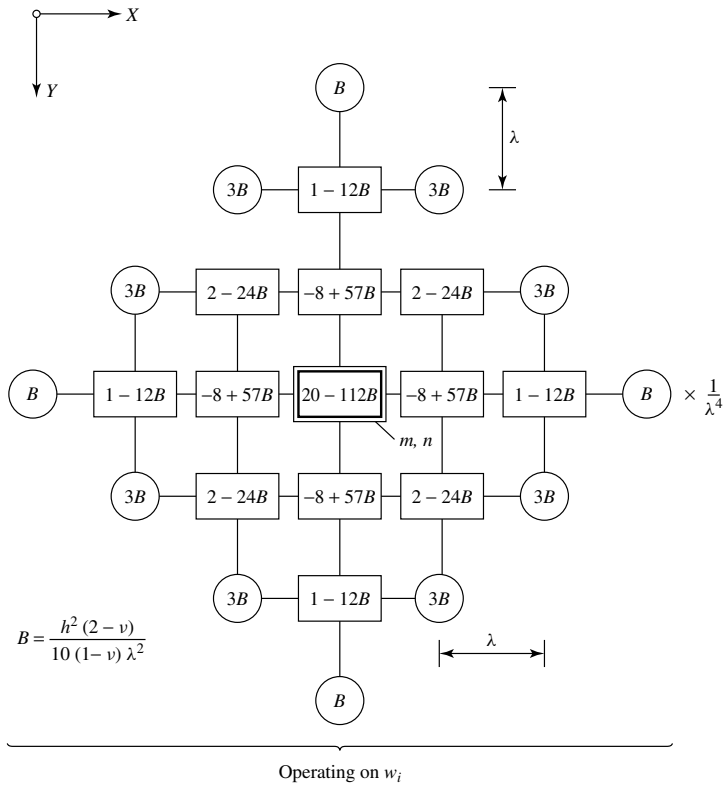


Figure 5.3.1 Finite difference representation of left-hand side of differential Equation (1.5.11).

be half of the first one. Here L represents the shortest span length of the plate. For the treatment of oblique plates and other irregular plate geometry, the approximation recommended in Sec. 5.1 can be used. Even without the above-mentioned iterative improvements, this versatile direct FDM shows acceptable accuracy and good convergence characteristics, in comparison with the more exact series solutions of certain test problems [5.3.2]. Its use, however, is not simple because of the relatively complex handling of the boundary conditions.

c. Finite Difference Representation of Three-Dimensional Elasticity. Ng and Bencharif [5.3.4] simplified Lamé's differential equations of three-dimensional elasticity (1.6.2) using three principal planes at the elevations $z = 0$ and $z = \pm h/2$ and applied them to moderately thick plates in the following form:

$$\begin{aligned}
 (\lambda + 2G) \frac{\partial^2 u}{\partial x^2} + G \frac{\partial^2 u}{\partial y^2} + (\lambda + G) \frac{\partial^2 v}{\partial x \partial y} &= 0, \\
 (\lambda + G) \frac{\partial^2 u}{\partial x \partial y} + G \frac{\partial^2 v}{\partial x^2} + (\lambda + 2G) \frac{\partial^2 v}{\partial x \partial y} &= 0, \\
 \nabla^4 w &= \frac{p_z(x, y)}{D},
 \end{aligned}
 \tag{5.3.5}$$

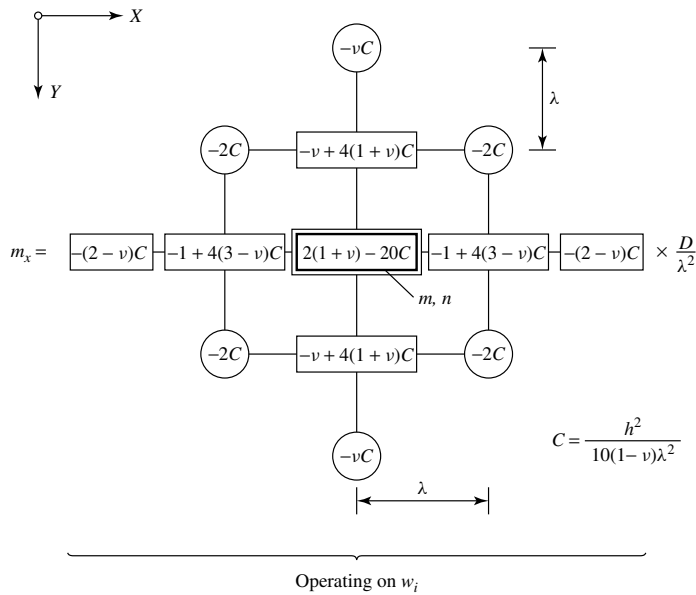


Figure 5.3.2 Stencil for bending moment m_x , Eq. (1.5.13).

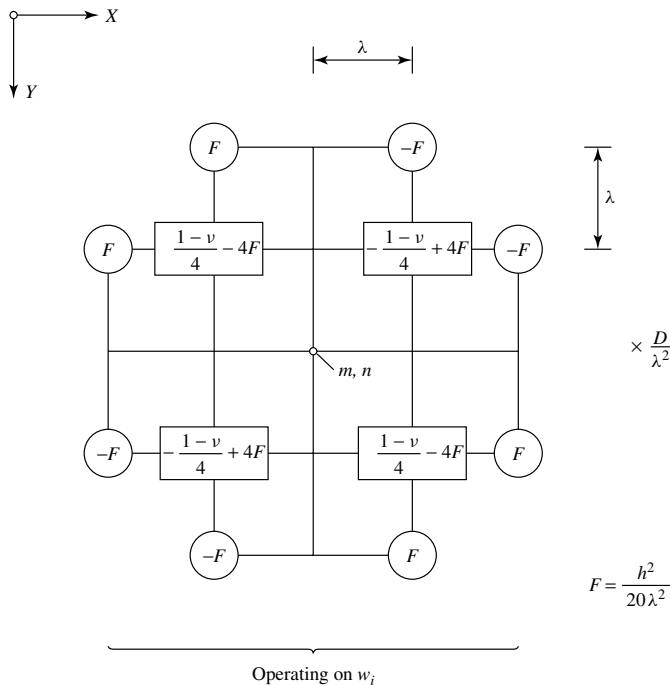


Figure 5.3.3 Finite difference patterns for torsional moment m_{xy} , Eq. (1.5.15).

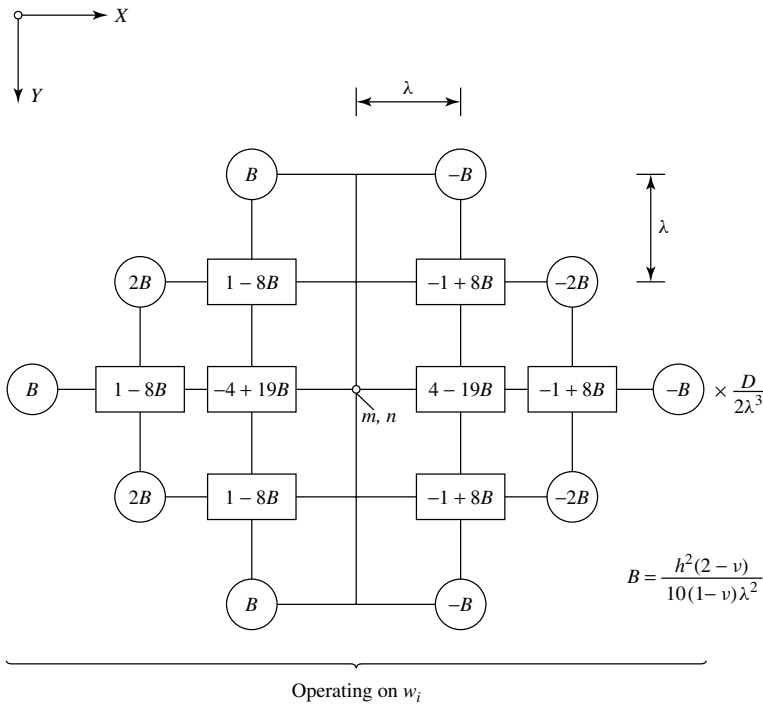


Figure 5.3.4 Stencil for q_x , Eq. (1.5.16).

where λ is defined by Eq. (1.6.4). These differential equations are then expressed in finite difference form at each mesh point of the middle surface of the plate using a three-dimensional finite difference mesh. The two most important boundary conditions of rectangular, moderately thick plates[†] are as follows:

For clamped plates:

$$\begin{aligned}
 x = \pm \frac{a}{2}: \quad u &= 0, & v &= 0, & w &= 0; \\
 y = \pm \frac{b}{2}: \quad u &= 0, & v &= 0, & w &= 0; \\
 z = \pm \frac{h}{2}: \quad \tau_{xz} &= 0, & \tau_{yz} &= 0, & \sigma_z &= \pm \frac{p_z}{2}.
 \end{aligned} \tag{5.3.6}$$

For simply supported plates:

$$\begin{aligned}
 x = \pm \frac{a}{2}: \quad \sigma_x &= 0, & \tau_{xy} &= 0, & w &= 0; \\
 y = \pm \frac{b}{2}: \quad \sigma_y &= 0, & \tau_{xy} &= 0, & w &= 0; \\
 z = \pm \frac{h}{2}: \quad \tau_{xz} &= 0, & \tau_{yz} &= 0, & \sigma_z &= \pm \frac{p_z}{2}.
 \end{aligned} \tag{5.3.7}$$

[†] The origin of the Cartesian coordinate system is at the center of the plate.

To use this alternative three-dimensional finite difference approach for the analysis of moderately thick plates effectively, however, one needs a readily usable computer program. For more details on this method the reader is referred to Ref. [5.3.5].

Summary. To compute the deflections of simply supported moderately thick plates, utilization of the effortless conjugate plate analogy is the most effective. In addition, using this approach, one can apply stencils of the direct finite difference approach for determination of stress resultants without creating any incompatibility, since in both methods w is the only variable. For consideration of more general plate geometry and boundary conditions, application of the direct finite difference approach combined with the iterative *successive approximation* technique is recommended. It should be noted, however, that handling of the boundary conditions is not always a simple task. For approximate results, Donnell's simplified approach is the most suitable. When the problem is on the border line between moderately thick and thick plates, researchers may find the three-dimensional elasticity approach to be the most exact and, therefore, the most appealing.

ILLUSTRATIVE EXAMPLE I

Let us determine the maximum deflection of a simply supported rectangular plate subjected to a $p_z = p_0$ uniformly distributed lateral load. This moderately thick reinforced concrete (RC) plate has the following dimensions:

$$a = 10 \text{ m}, \quad \frac{b}{a} = \frac{3}{4}, \quad h = 2 \text{ m}, \quad E = 30,000 \text{ MN/m}^2, \quad \nu = 0.3.$$

Due to the double symmetry of this plate problem, we can work with a quarter plate. With a mesh size of $\lambda = a/6 = b/8$, only 12 mesh-point deflections have to be found. The numbering of these mesh points is shown in Fig. 5.3.5.

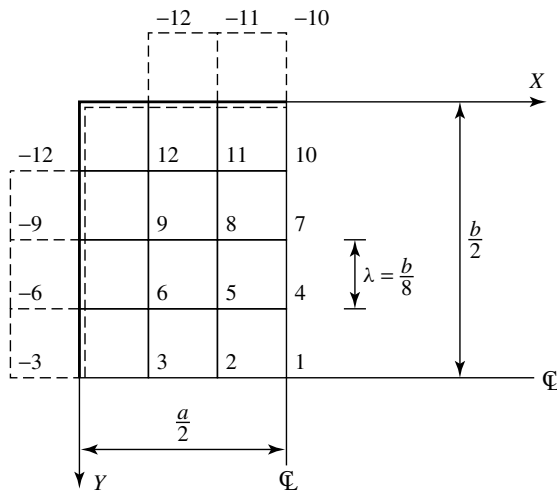


Figure 5.3.5 Mesh-point numbering of quarter plate.

Since the plate is simply supported, we can apply the conjugate plate analogy discussed above. In the first step, deflections of the Kirchhoff plate are determined using the ordinary finite difference technique. Consequently, the pertinent stencil to be applied is given in Fig. 5.1.3a. Similarly, the boundary conditions can be approximated according to Fig. 5.1.5. The obtained coefficient matrix of the coupled linear equations $\mathbf{Aw} = \mathbf{p}$ becomes

$$\mathbf{A} = \begin{bmatrix} 20 & -16 & 2 & -16 & 8 & 0 & 2 & 0 & 0 & 0 & 0 & 0 \\ -8 & 21 & -8 & 4 & -16 & 4 & 0 & 2 & 0 & 0 & 0 & 0 \\ 1 & -8 & 19 & 0 & 4 & -16 & 0 & 0 & 2 & 0 & 0 & 0 \\ -8 & 4 & 0 & 21 & -16 & 2 & -8 & 4 & 0 & 1 & 0 & 0 \\ 2 & -8 & 2 & -8 & 22 & -8 & 2 & -8 & 2 & 0 & 1 & 0 \\ 0 & 2 & -8 & 1 & -8 & 20 & 0 & 2 & -8 & 0 & 0 & 1 \\ 1 & 0 & 0 & -8 & 4 & 0 & 20 & -16 & 2 & -8 & 4 & 0 \\ 0 & 1 & 0 & 2 & -8 & 2 & -8 & 21 & -8 & 2 & -8 & 2 \\ 0 & 0 & 1 & 0 & 2 & -8 & 1 & -8 & 19 & 0 & 2 & -8 \\ 0 & 0 & 0 & 1 & 0 & 0 & -8 & 4 & 0 & 19 & -16 & 2 \\ 0 & 0 & 0 & 0 & 1 & 0 & 2 & -8 & 2 & -8 & 20 & -8 \\ 0 & 0 & 0 & 0 & 0 & 1 & 0 & 2 & -8 & 1 & -8 & 18 \end{bmatrix}. \quad (5.3.8)$$

The corresponding vector of the loads is

$$\mathbf{p} = \{1 \quad 1 \quad 1 \quad 1 \quad 1 \quad 1 \quad 1 \quad 1 \quad 1 \quad 1 \quad 1 \quad 1\} \frac{p_0 \lambda^4}{D}. \quad (5.3.9)$$

Solution of the above given matrix equation gives

$$\mathbf{w}_K = \begin{bmatrix} 8.5941 \\ 7.5014 \\ 4.4178 \\ 8.0250 \\ 7.0070 \\ 4.1303 \\ 6.3246 \\ 5.5279 \\ 3.2678 \\ 3.5580 \\ 3.1152 \\ 1.8511 \end{bmatrix} \frac{p_0 \lambda^4}{D} = \begin{bmatrix} 6.6312 \\ 5.7881 \\ 3.4088 \\ 6.1921 \\ 5.4066 \\ 3.1869 \\ 4.8801 \\ 4.2653 \\ 2.5214 \\ 2.7454 \\ 2.4037 \\ 1.4283 \end{bmatrix} \frac{10^{-3} p_0 a^4}{D}. \quad (5.3.10)$$

With

$$\begin{aligned} D &= \frac{Eh^3}{12(1-\nu^2)} = \frac{30000 \times 2^3}{12(1-0.3^2)} \\ &= 21,978 \quad \text{and} \quad G = \frac{E}{2(1+\nu)} = 11,538.5, \end{aligned} \quad (5.3.11)$$

the maximum deflection of the Kirchhoff plate is

$$w_{K,1} = \frac{6.6312 \times 10^{-3} \times 10^4 p_0}{21,978} = 0.00317 p_0. \quad (5.3.12)$$

To obtain the additional deflection $w_{s,1}$ caused by transverse shear, we use Eq. (5.3.1), which requires determination of $m_{x,1}$ and $m_{y,1}$. These are calculated as

$$m_{x,1} = -\frac{D}{\lambda^2} [2(w_2 - w_1) + 2\nu(w_4 - w_1)] = 2.5268 p_0 \lambda^2, \quad (5.3.13)$$

$$m_{y,1} = -\frac{D}{\lambda^2} [2(w_4 - w_1) + 2\nu(w_2 - w_1)] = 1.7938 p_0 \lambda^2. \quad (5.3.14)$$

Consequently,

$$w_{s,1} = \frac{m_{x,1} + m_{y,1}}{(1 + \nu)\kappa^2 G h} = \frac{(2.5268 + 1.7938)(10/6)^2 p_0}{1.3(5/6)11,538.5 \times 2} = 0.00048 p_0. \quad (5.3.15)$$

Thus, the maximum deflection of the Mindlin plate is

$$w_{M,\max} = w_{M,1} + w_{s,1} = 0.00365 p_0. \quad (5.3.16)$$

The result shows that for this moderately thick plate consideration of transverse shear increases the maximum deflection by approximately 15%. A similar approach should be taken if we want to determine the increased deflections of other mesh points.

ILLUSTRATIVE EXAMPLE II

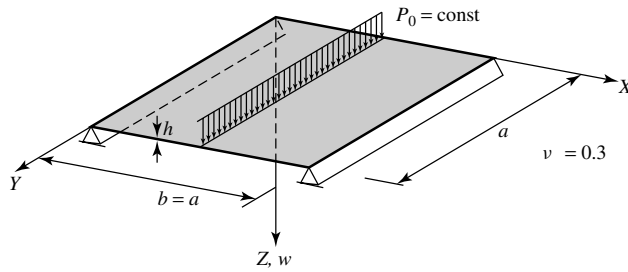
Figure 5.3.6a shows a moderately thick square plate with two opposite edges simply supported while the other two edges are free. The plate is subjected to a uniformly distributed line load p_0 acting at half of the span between the two supports. Dimensions and elastic properties of this RC plate are

$$a = 10.0 \text{ m}, \quad h = 1.2 \text{ m}, \quad E = 30,000 \text{ MN/m}^2, \quad \nu = 0.3,$$

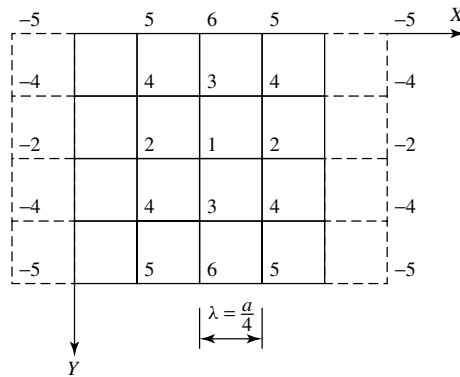
$$D = \frac{Eh^3}{12(1 - \nu^2)} = 4747.2 \text{ Mnm}, \quad G = \frac{E}{2(1 + \nu)} = 11538.5 \text{ MN/m}^2.$$

Determine the maximum deflection using Donnell's *approximation* in connection with the ordinary FDM.

Utilizing the double symmetry of this plate problem, the mesh points are numbered as shown in Fig. 5.3.6b. First, we determine the maximum deflection of the Kirchhoff plate according to Eq. (5.3.3). For this purpose, we apply the general stencil given in Fig. 5.1.3a. Boundary conditions of the two simply supported edges are approximated using Fig. 5.1.5b. Stencils pertinent to the free edges are given in Figs. 5.1.6 and 5.1.7.



(a) Moderately thick plate



(b) Numbering of mesh points

Figure 5.3.6 Moderately thick plate with two simply supported and two free-edges.

Consequently, the ordinary FDM yields the following coefficient matrix:

$$\mathbf{A} = \begin{bmatrix} 20 & -16 & -16 & 8 & 0 & 2 \\ -8 & 20 & 4 & -16 & 2 & 0 \\ -8 & 4 & 20 & -16 & 3.4 & -5.4 \\ 2 & -8 & -8 & 20 & -5.4 & 1.7 \\ 0 & 2 & 3.4 & -10.8 & 13.06 & -6.44 \\ 2 & 0 & -10.8 & 6.8 & -12.88 & 13.06 \end{bmatrix}. \quad (5.3.17)$$

With the pertinent load vector

$$\mathbf{p} = \{1 \quad 0 \quad 1 \quad 0 \quad 0 \quad 1\} \frac{p_0 a^3}{64D}, \quad (5.3.18)$$

solution of the matrix equation $\mathbf{Aw} = \mathbf{p}$ becomes

$$\mathbf{w} = \begin{Bmatrix} 0.02357 \\ 0.01573 \\ 0.02419 \\ 0.01616 \\ 0.01787 \\ 0.02680 \end{Bmatrix} \frac{p_0 a^3}{D} \begin{matrix} (12.6\%) \\ (9.2\%) \\ (12.5\%) \\ (9.2\%) \\ (8.3\%) \\ (11.6\%) \end{matrix}. \quad (5.3.19)$$

In this case $w = w_K$ represents deflections of the Kirchhoff plate. Percentages in parentheses in the above equation indicate deviations from the more exact analytical solution obtained by Lévy's approach. These discrepancies, of course, can be reduced considerably by using smaller mesh sizes combined with the techniques discussed in Secs. 5.1 and 5.2, respectively.

To approximate the effect of the transverse shear on the lateral deflection, the second term on the right-hand side of Eq. (5.3.3) must be evaluated. This gives

$$\begin{aligned} w_{s,1} &= -\frac{(8-3\nu)h^2}{40(1-\nu)} \nabla^2 w_{K,1} \\ &= -0.36514 \left[\frac{1}{\lambda^2} (2w_2 - 2w_1) + \frac{1}{\lambda^2} (2w_3 - 2w_1) \right] \\ &= 0.194 \times 10^{-3} p_0. \end{aligned} \quad (5.3.20)$$

Hence, the approximate value of the maximum deflection becomes

$$w_{\max} = w_1 = w_{K,1} + w_{s,1} \approx 5.16 \times 10^{-3} p_0. \quad (5.3.21)$$

This indicates merely a 4% increase over the classical solution of this plate problem. With $h = 2.0$ m, however, this difference becomes approximately 10%. The same approach can be applied to calculate all mesh-point deflections. A similar technique can also be used in connection with the improved FDMs.

References and Bibliography

- [5.3.1] WANG, C. M., and ALWIS, W. A. M., "Simply Supported Polygonal Mindlin Plate Deflections Using Kirchhoff Plates," *J. Eng. Mech. Div., ASCE*, 121 (1995), 1383–1385.
- [5.3.2] DONNEL, L. H., *Beams, Plates and Shells*, McGraw-Hill Book, Co., New York, 1976.
- [5.3.3] SPEARE, P. R. S., "Numerical Methods and Refined Plate Theories," *Comp. Struct.*, 15 (1982), 351–358.
- [5.3.4] NG, S. F., and BENCHARIF, N., "Finite Difference Computer Programs for the Modelling of Thick Rectangular Plates," *Comp. Struct.*, 33 (1989), 1011–1016.
- [5.3.5] BENCHARIF, N., "Application of Finite Difference Method to Deflections of Clamped and Simply Supported Rectangular Thick Plates," M.A.Sc. Thesis, Ottawa University, Ottawa, Canada, 1988.

5.4 Advances in Finite Difference Methods

Although nowadays the bulk of innovative research in numerical analysis of surface structures is devoted to FDMs, there are some noteworthy exceptions.

For instance, Reddy and Gera introduced an alternate formulation to the ordinary FD method to improve its accuracy [5.4.1]. Their approach is based on elimination of the biharmonic plate equation (1.2.30) by replacing it with two bending moment relations given in Eqs. (1.2.26) and (1.2.27) and by formulating the equilibrium equation in the form

$$\frac{\partial^2 m_x}{\partial x^2} - 2D(1-\nu) \frac{\partial^4 w}{\partial x^2 \partial y^2} + \frac{\partial^2 m_y}{\partial y^2} = -p_z(x, y). \quad (5.4.1)$$

Then, applying the ordinary FDM, the bending moment relations are expressed in finite difference forms as given in Eqs. (5.1.12) and (5.1.13), respectively. Similarly, using finite difference approximations, Eq. (5.4.1) becomes

$$-L_x^2(m_x) + 2D(1 - \nu)L_{xy}^4(w) - L_y^2(m_y) = p_{m,n}, \quad (5.4.2)$$

where the finite difference operators L_x^2 and L_{xy}^4 are represented by Eqs. (5.1.4) and (5.1.10), respectively. An analogous finite difference expression can be written for L_y^2 .

After imposing appropriate boundary conditions, Eqs. (5.1.12), (5.1.13) and (5.4.2) are solved *simultaneously* for the three unknowns w , m_x and m_y . This approach results in more accurate moments than those obtained by using the OFD method [5.4.1].

For distributed lateral loads, accuracy of this FDM can be further improved by applying their weighted representations as given in Eq. (5.1.31) and simultaneously using a similar straight-line averaging technique for the two moments. Thus, for each pivotal point m , n we can write

$$\begin{aligned} [S](m_x) &= -D[L_x^2(w) + \nu L_y^2(w)], \quad [S](m_y) = -D[L_y^2(w) + \nu L_x^2(w)], \\ -L_x^2(m_x) + 2D(1 - \nu)L_{xy}^4(w) - L_y^2(m_y) &= [S](p), \end{aligned} \quad (5.4.3)$$

where $[S]$ represents the matrix operator schematically given in Fig. 5.1.12.

Another improvement in the ordinary FD method is due to the *finite difference energy approach*. So far, we have been using the traditional FDMs by replacing the differential quantities in the governing differential equation of the plate by difference quantities. The finite difference energy method uses the expressions of strain energy and expresses these by finite difference quantities. Such an approach was originally introduced by Courant [5.4.2] and Forsyth et al. [5.4.3]. Minimization of these potential energy expressions yields a set of algebraic equations that can be solved for the unknowns. This type of FDM is equivalent to a constant-strain FEM with slope discontinuities at the element edges.[†] If the displacement w_i are expressed as unknowns at the mesh points of the finite difference grid, then we speak of a “whole-station” scheme. In contrast, in the “half-station” scheme, the energy due to bending is integrated over the shaded area shown in Fig. 5.4.1. The functional values and derivations of displacements are evaluated at the centroid of this area. Using this approach, a comprehensive computer program system for linear and nonlinear analysis of surface structures was developed at Lockheed Palo Alto Research Laboratory [5.4.4].

Giencke improved the multilocal FDM by using a different energy approach [5.4.5]. That is, in the classical higher-order FDMs, the internal forces are calculated as difference quantities of the lateral displacements $w(x, y)$. This creates an undesirable loss of accuracy in the results. To avoid such a loss, Giencke introduced the bending curvatures[‡] as unknowns in plate bending problems, from which the bending and twisting moments can be calculated directly.[§] Equations for these unknowns are derived using the principles of virtual forces and displacements simultaneously. In this way, a type of multilocal finite difference equation is created [5.4.6].

[†] See Sec. 7.6.

[‡] See Eq. (1.2.21).

[§] See Eqs. (1.2.26), (1.2.27) and (1.2.29).

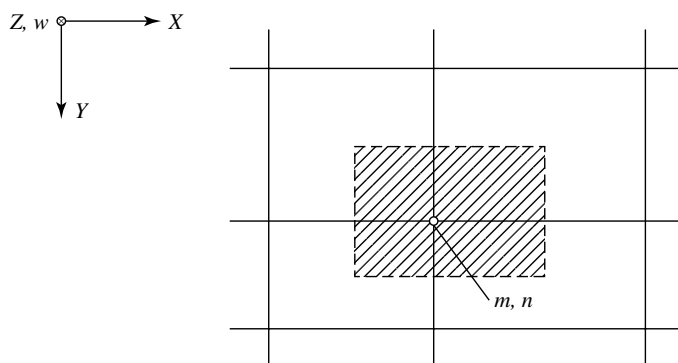


Figure 5.4.1 Half-station technique.

For mathematically inclined research engineers, the study of Refs. [5.4.7] and [5.4.8] is highly recommended. These very accurate higher-order finite difference techniques, however, should be considerably simplified and made more accessible to engineers.

References and Bibliography

- [5.4.1] REDDY, J. N., and GERA, R., "An Improved Finite-Difference Analysis of Bending of Thin Rectangular Elastic Plates," *Comp. Struct.*, 10 (1979), 431–438.
- [5.4.2] COURANT, R., FRIEDRICH, K., and LEWY, H., "Über die partiellen Differenzengleichungen der mathematischen Physik," *Math. Ann.*, 100 (1928), 32–74.
- [5.4.3] FORSYTH, G. E., and WASOW, W. R., *Finite Difference Methods for Partial Differential Equations*, John Wiley & Sons, New York, 1960.
- [5.4.4] BUSHNELL, D., and ALMROTH, B. O., "Finite Difference Energy Method for Nonlinear Shell Analysis," in *Proceedings of the Conference on Computer Oriented Analyses of Shell Structures*, Lockheed Palo Research Laboratory, Palo Alto, California, 1970.
- [5.4.5] GIENCKE, E., "The Mechanical Interpretation of High Accuracy Multipoint Difference Methods for Plates and Shells," in *Proceedings of IUTAM Symposium on High Speed Computing of Elastic Structures*, Vol. 2, held in Liegè, Aug. 23–28, 1970, University Liegè, 1971, pp. 809–836.
- [5.4.6] GIENCKE, E., "Ein einfaches und genaues finites Verfahren von orthotropen Scheiben und Platten," *Stahlbau*, 36 (1967), 268–276, 303–315.
- [5.4.7] USMANI, R. A. "An $O(h^6)$ Finite Difference Analogue for the Solution of Some Differential Equations Occurring in Plate Deflection Theory," *J. Inst. Math. Appl.*, 20 (1977), 331–333.
- [5.4.8] PAKALIA TAKIS, G., and SIMOS, T. E., "A Finite Difference Method for the Numerical Solution of Fourth-Order Differential Equations with Engineering Applications," *Comp. Struct.*, 65 (1997), 491–495.

5.5 Summary and Conclusions

For fairly simple plate geometry, loading and boundary conditions, the FDMs discussed in this chapter offer valuable alternatives in the numerical analysis of plate problems. In addition, the FDMs can be used for *independent* checks of the results obtained by other numerical or analytical analysis techniques.

The FDMs are based on *mathematical* discretization of the plate continuum. In their classical forms, the differential quantities in the governing differential equations are replaced by finite difference expressions at each mesh point of the fine difference grid that is laid over the plate domain. Since only one unknown, w_i , is used at each mesh point, the size of the resulting coefficient matrix as well as its bandwidth is greatly reduced. Consequently, the obtained set of a few linear algebraic equations can be solved even by some advanced scientific calculators with preprogrammed equation solvers.

The procedure required for the solution of various plate problems is transparent. If readily usable stencils for the plate domain and prescribed boundary conditions are available, generation of the required finite difference equations is simple and involves only “longhand” operations. In most cases, a computer is not required. With improved FDMs, the obtained accuracy is remarkably good even with relatively coarse mesh. Furthermore, the FDM is highly versatile. That is, basically the same approach can be used to solve dynamic and elastic stability plate problems, as shown in Secs. 15.1 and 16.4.

The most significant drawbacks of the FDM are as follows:

- The FDMs—with the notable exception of the finite difference energy method—are ill-suited for automated procedures, since their programming is cumbersome. Consequently, it is not recommended for the analysis of large plate structures.
- Handling of irregular geometry, loads and boundary conditions can be quite difficult.
- If suitable finite difference stencils are not readily available, their development is generally time consuming.

Although at present the FEM dominates the field of numerical analysis of plates, at times, as shown in this chapter, FD methods can offer significant advantages over other numerical solution techniques. Unfortunately, research in this field has been neglected to a large extent. Currently the finite difference energy approach appears to be the most promising to compete successfully with the all-dominating FEM, especially if it is combined with the method of higher approximation.

Problems[†]

- 5.1.1.** Find the maximum deflection of a simply supported rectangular plate subjected to $p_z = p_0$ uniformly distributed lateral load. Assume the following values for the plate: $a = 10$ m, $b/a = \frac{4}{3}$ and a mesh size of $\lambda = a/6 = b/8$. Apply the two-stage approach in connection with the ordinary FDM.
- 5.1.2.** Determine the convergence characteristics of the two-stage approach using problem 5.1.1 and $\lambda_1 = a/4$, $\lambda_2 = a/6$ and $\lambda_3 = a/8$ mesh sizes.
- 5.1.3.** Find (a) the maximum deflection and (b) the maximum negative and positive bending moments of a uniformly loaded square plate using the ordinary FDM. Assume fixed boundary conditions.

[†] The first two numbers refer to the corresponding section.

- 5.1.4. Re-solve problem 5.1.3, but assume this time that a square opening the size of $a/6 \times a/6$ is located at the center of the plate.
- 5.1.5. Obtain an approximate solution for the maximum positive moment in the lock-gate, shown in Fig. 1.1.1c. Use a $b/a = \frac{4}{2}$ span ratio and the ordinary FDM.
- 5.1.6. Re-solve problem 5.1.5, but assume that the thickness of the plate varies linearly from the bottom to the top of the plate.
- 5.1.7. A square plate with two opposite edges simply supported and the other two clamped carries a concentrated load P_z at its center. Determine the maximum positive and negative moments by the ordinary FDM. Use an equivalent load representation according to Fig. 4.5.1.
- 5.1.8. A rectangular plate shown in Fig. 2.3.1 carries a distributed load $p_z = p_0 \sin(\pi x/a)$. Determine the maximum moments in the plate using the ordinary FDM. Assume a $b/a = \frac{4}{3}$ span ratio and use $\lambda = a/6 = b/8$ mesh size.
- 5.2.1. Determine the maximum deflection of the plate shown in Fig. 5.2.16 by the multilocal method.
- 5.2.2. Use the successive approximation technique described in Sec. 5.2.e to improve the results obtained by solving problem 5.1.3.
- 5.2.3. Determine the deflections of the plate shown in Fig. 5.3.6 by the multilocal method, but assume that the plate is thin rather than moderately thick.
- 5.2.4. Determine the maximum positive and negative deflections of the continuous plate shown in Fig. 5.1.20 by the multilocal method. Use $\lambda = a/5$ for the mesh size.
- 5.2.5. A square clamped plate is subjected to a concentrated load at its center. Find the deflections of the plate using the funicular polygon method. The concentrated force can be represented by the equivalent load system shown in Fig. 4.5.1. In addition, determine the maximum positive and negative moments either by the method of higher approximation or by applying the stencils given in Fig. 5.2.4.
- 5.2.6. Re-solve problem 5.2.5, this time using the multilocal method, and compare the obtained two sets of results for accuracy.
- 5.3.1. A simply supported moderately thick rectangular plate carries a hydrostatic load. Determine the deflections by means of the conjugate plate analogy. Use $h = a/5$ for the plate thickness.
- 5.3.2. A moderately thick clamped square plate carries a uniformly distributed load. Determine its deflections.

6

Gridwork and Framework Methods

6.1 Basic Concepts

Already at the beginning of the twentieth century it was established that analogies exist between the behavior of plates in flexure or tension and that of a gridwork [6.1.1, 6.1.2]. A gridwork is a plane, two-dimensional structure consisting of intersecting rigidly jointed beams, as shown in Fig. 6.1.1. The framework, in comparison with the gridwork, represents a space frame, that is, a three-dimensional assemblage of interconnecting bars and/or beams (Fig. 6.1.2). In general, we can state that the stress and strain distributions in elastic continua can be approximated to a high degree of accuracy by equivalent gridworks or frameworks depending on the type of the actual surface structure. The basic requirement for such a *lattice analogy* is that the strain energy of the continuum should be represented as accurately as possible by that of the substitute system. If this requirement is satisfied, stiffness of the actual system can be replaced by that of an *equivalent* grid- or framework. For such an analogy, in the case of plates the required equivalent axial, flexural and torsional rigidities of the corresponding beam structure can be derived by using one of the following approaches:

- (a) *Comparison of Differential Equations.* After a limit approach, concerning the distances between beams, we compare the differential equation for deflections of the gridwork with that of the plate. This relatively difficult procedure yields the required equivalent cross-sectional properties of the gridwork in the most exact forms. It can be used for rectangular as well as triangular beam assemblages [6.1.3, 6.1.4].
- (b) *Equivalence of Displacement Fields.* We assume that the plate is divided into discrete rectangular elements. With each plate element we associate an equivalent gridwork model consisting of rigidly jointed beams. The equivalent cross-sectional properties of these beams are obtained by equating the

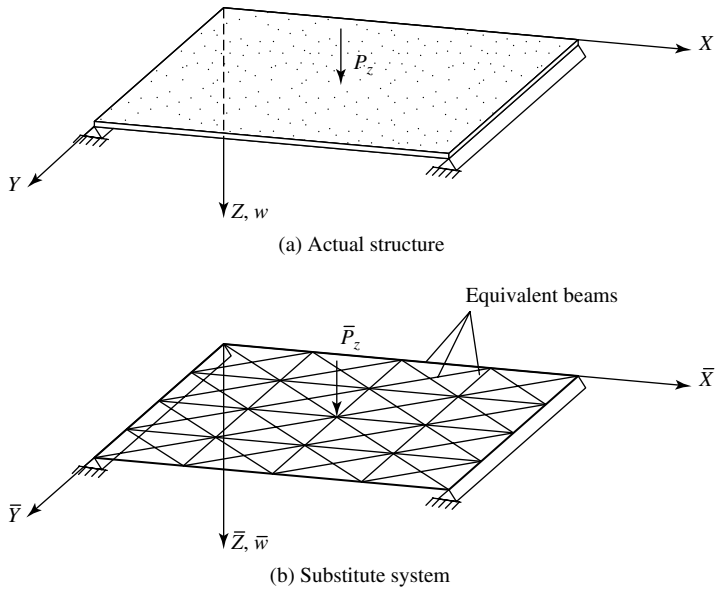


Figure 6.1.1 Gridwork representation of plate.

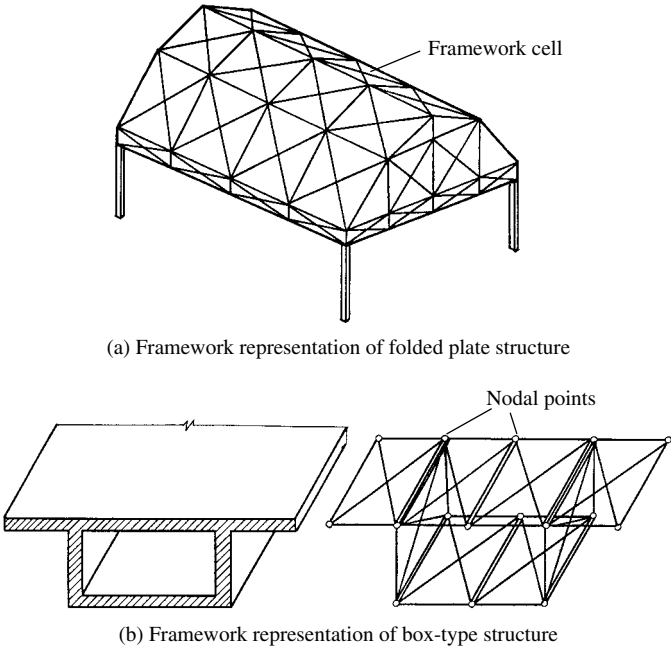


Figure 6.1.2 Three-dimensional frameworks.

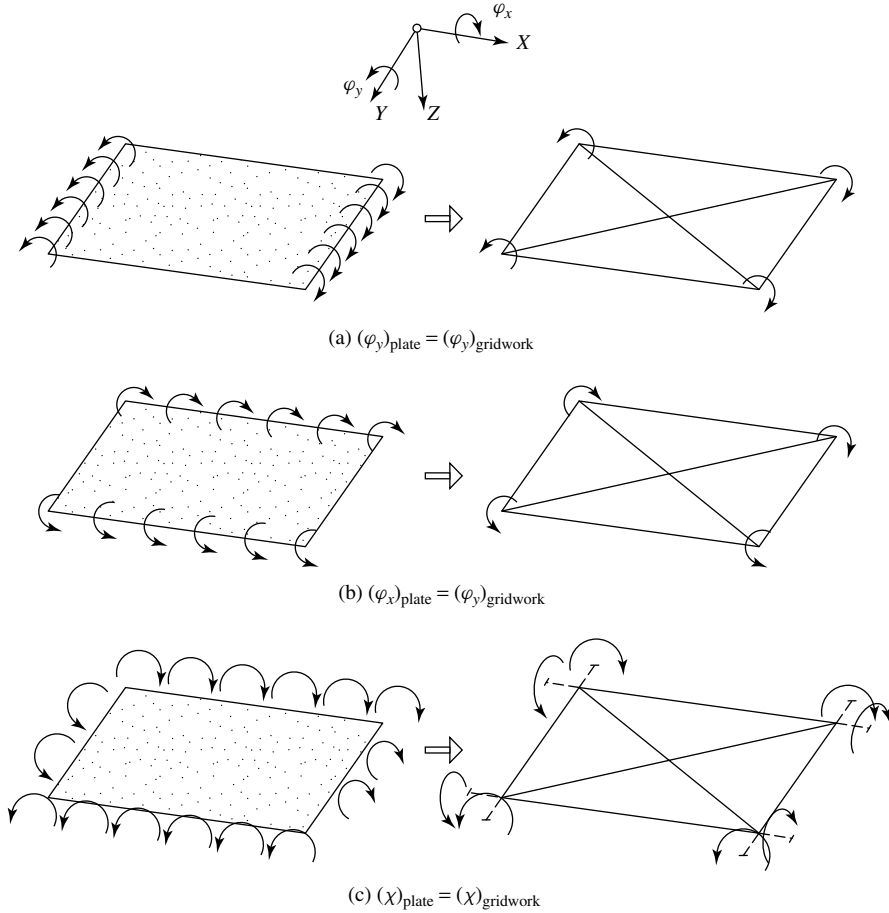


Figure 6.1.3 Equivalent displacements.

rotations of the nodes of the gridwork with those of the plate element of equal size when both are subjected to statically equivalent moments, as shown in Fig. 6.1.3. Logically, a similar approach can be used in the case of axial tensions and in-plane shear deformations [6.1.5].

- (c) *Equivalence of Strain Energies.* We use the same technique described above, but this time the strain energies of the plate element are simply equated with those of the gridwork model. This is a straightforward and relatively simple method, as demonstrated in Sec. 6.2.

To obtain the required equivalent cross-sectional properties, in all these approaches we apply *physical* discretization techniques instead of the mathematical ones used in FDMs.

In determining the equivalent cross-sectional properties, however, one should clearly distinguish between discretized continuum (Fig. 6.1.1) and cell models (Fig. 6.1.3) in future applications of the obtained results. For instance, using the

first method discussed above, we derive equivalent cross-sectional properties for the interior region of the plate. Thus, for equivalent beam members at the boundaries or at the edges of grid- or framework cells, only half of the obtained values should be used in the computation. On the other hand, if we apply the equivalent cross-sectional properties derived from gridwork cells in a three-dimensional framework computer program, values obtained for the edge members of the cell must be added to those of the adjoining ones. This is, however, not the case if they are used in a finite element program since we deal here with stiffness coefficients that must be added at any rate at the joints.

It is apparent that there is a close connection between the gridwork-framework method and the FEM. Consequently, this discrete analysis technique can be considered as a special case of the FEM. Although in recent years the FEM has achieved almost exclusive dominance in the field of numerical analysis of surface structures, there are cases when the grid- and framework methods can offer distinct advantages over the FEM. The most significant advantage of the former is that plates can be analyzed by standard computer programs developed for gridworks or three-dimensional frameworks.

References and Bibliography

- [6.1.1] KLEIN, F., and WIEGHARDT, K., "Über Spannungsflächen und reziproke Diagramme, mit besonderer Berücksichtigung der MAXWELLSchen Arbeiten," *Arch. Math. Phys. Dritte Reihe*, 8 (1904), 1–10, 95–119.
- [6.1.2] WIEGHARDT, K., "Über einen Grenzübergang der Elastizitätslehre und seine Anwendung auf die Statik hochgradig statisch unbestimmter Fachwerke," *Verhandlungen des Vereins z. Förderung Gewerbeleisses*, 85 (1906), 139–176.
- [6.1.3] HRENNIKOFF, A., "Plane Stress and Bending of Plates by Method of Articulated Framework," Ph.D. Thesis, Massachusetts Institute of Technology, Cambridge, Massachusetts, 1940.
- [6.1.4] SALONEN, E.-M., "A Gridwork Method for Plates in Bending," *Acta Polytec. Scand.*, Civil Engineering and Building Construction Series No. 8. (1969), 1–31.
- [6.1.5] YETTRAM, A. L., and HUSAIN, M. H., "Grid- Framework Method for Plates in Flexure," *J. Eng. Mech., ASCE*, 91 (June 1965), 53–64.
- [6.1.6] SPIERIG, S., "Beitrag zur Lösung von Scheiben-, Platten- und Schalenproblemen mit Hilfe von Gitterrostmodellen," *Abhandlungen der Braunschweigischen Wissenschaftlichen Gesellschaft*, 15 (1963), 133–165.
- [6.1.7] BENARD, E. F., "A Study of the Relationship between Lattice and Continuous Structures," Ph.D. Thesis, University of Illinois, Urbana, Illinois, 1965.

6.2 Equivalent Cross-Sectional Properties

a. Articulated Continuum. This method for derivation of equivalent cross-sectional properties consists of replacing the continuum of the plate by a gridwork whose rigidly jointed beams are arranged in a definite pattern. The gridwork is given the same geometrical outline and boundary conditions as the plate. It is assumed that the statically equivalent lateral loads act only on the nodal points. If these beams are endowed with suitable equivalent cross-sectional rigidities, then the deflections of the gridwork will closely resemble those of the original plate.

Hrennikoff has proposed several gridwork patterns [6.2.1]. The one discussed here is shown in Fig. 6.2.1. Although it is valid only for Poisson's ratio $\nu = \frac{1}{3}$, with the

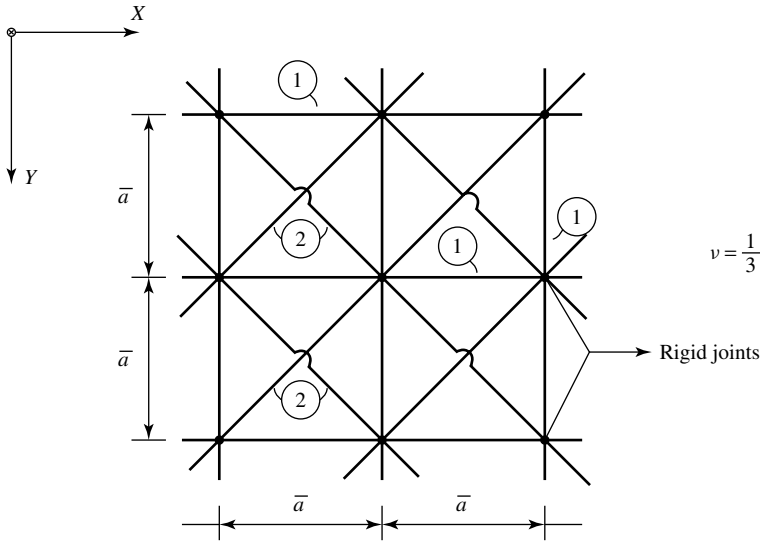


Figure 6.2.1 Hrennikoff's square gridwork pattern.

help of the conversion formulas given in Appendix A.2, however, its applicability can be extended to any value of ν .

The equivalent flexural properties of these beams are obtained from the equality of deformations for bending of the plate (1.2.30) with those of the square gridwork of unit size. This comparison gives the equivalent moment of inertias

$$I_1 = \frac{\bar{a}h^3}{12(1+\nu)} \quad \text{and} \quad I_2 = \frac{\bar{a}h^3}{12\sqrt{2}(1+\nu)}. \quad (6.2.1)$$

A basically similar approach is used for stretching the plate. This gives the following areas of the equivalent bars:

$$A_1 = \frac{3}{4}\bar{a}h \quad \text{and} \quad A_2 = \frac{3}{4\sqrt{2}}\bar{a}h. \quad (6.2.2)$$

As already mentioned above, in both cases Poisson's ratio is $\nu = \frac{1}{3}$. Edge members, however, should be endowed only with $I_1/2$ and $A_1/2$ cross-sectional properties.

Most researchers who have studied plate bending problems using the *lattice analogy* introduced rectangular beam patterns in their analysis. Practical applications of such gridworks are, however, restricted if plates of arbitrary shape are to be analyzed. To overcome this restriction, Salonen [6.2.2] proposed a more general triangular shape in his gridwork pattern (Fig. 6.2.2). In deriving the corresponding differential equation, he assumed that the gridwork is constructed of identical triangular units with equally spaced parallel bars. Furthermore, these bars have constant and identical bending and torsional rigidities.[†] Using these assumptions, Salonen obtained the

[†] These assumptions were required only for deriving the differential equation.

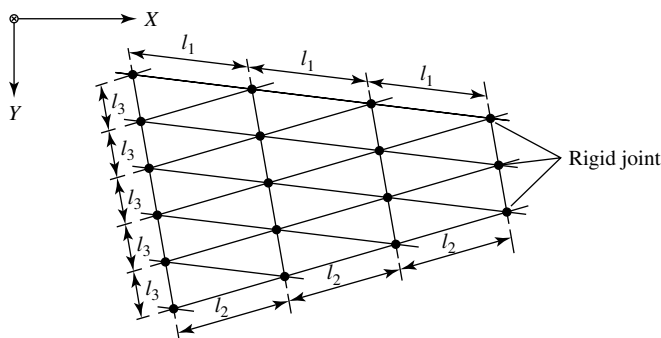


Figure 6.2.2 Salonen's triangular pattern.

following differential equation for triangular gridworks:

$$\sum_{i=1}^3 \left(B_i \frac{\partial^4 w}{\partial x_i^4} + C_i \frac{\partial^4 w}{\partial x_i^2 \partial y_i^2} \right) \ell_i = P_{z,i}, \quad (6.2.3)$$

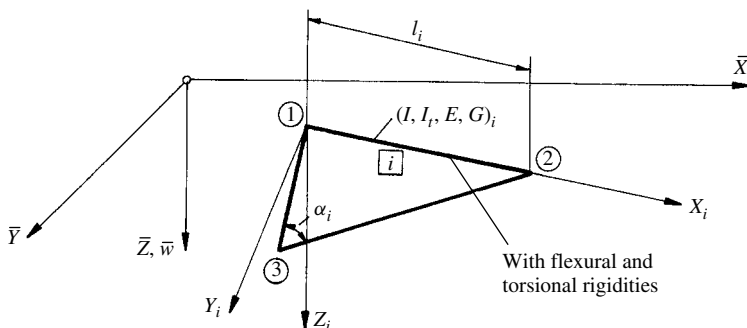
where B_i is the bending stiffness of the i th beam parallel to X_i axis and C_i represents its torsional rigidity. The beam length is denoted by ℓ_i , and $P_{z,i}$ represents the concentrated joint force. Equation (6.2.3) was derived in a manner similar to that presented in Ref. [6.2.3]. Assuming that the distance between beams becomes infinitely small, the requirement that differential equation (6.2.3) must be identical with the differential equation of the plate (1.2.30) gives the equivalent cross-sectional properties of the i th beam,

$$B_i = C_i = D \ell_i \frac{c_i}{s_i}, \quad (6.2.4)$$

where

$$c_i = \cos \alpha_i \quad \text{and} \quad s_i = \sin \alpha_i \quad (6.2.5)$$

and α_i is an angle corresponding to the beam and ℓ_i represents its length (Fig. 6.2.3). The indices $i = 1, 2, 3$ are cyclicly permuted.

Figure 6.2.3 Beam i of triangular gridwork.

Equation (6.2.4) can be written in a slightly different form

$$(EI)_i = (GI_t)_i = D\ell_i \cot \alpha_i, \quad (6.2.6)$$

where $(EI)_i$ represents the equivalent bending rigidity of the i th interior beam in the gridwork and $(GI_t)_i$ denotes its torsional rigidity. Again, stiffness values of the exterior beams are half of the interior ones. Strictly speaking, Eqs. (6.2.4) and (6.2.6) are valid only for $\nu = 0$, but with the help of the conversion formulas given in Appendix A.2, any ν value can be considered. Furthermore, some plate problems permit the use of arbitrary Poisson ratios. Fixed boundary conditions of arbitrary shape and simply supported straight boundaries are examples of such cases, provided that the thickness of the plate is constant or varies linearly in the X and Y directions.

The usefulness of this simple but effective gridwork method can be considerably extended by employing rectangular grids in connection with triangular ones. The equivalent cross-sectional properties of a rectangular unit (shown in Fig. 6.2.4) constructed from two triangular ones are

$$(EI)_1 = (GI_t)_1 = D\ell_y \quad \text{and} \quad (EI)_2 = (GI_t)_2 = D\ell_x. \quad (6.2.7)$$

It is of interest to note that these values are identical with those given in Ref. [6.1.5], although their derivation is quite different.

As mentioned above, we can effectively combine the triangular and rectangular gridworks. In such a case, however, care should be taken in determining the equivalent cross-sectional properties at the connecting lines of the two patterns. Nevertheless, a simple approximation can yield usable results. That is, we calculate the average value of the two *exterior* beam properties and use the so-obtained cross-sectional properties for the beams where the two patterns meet. As will be illustrated[†] in Sec. 6.3, the convergence characteristics of these gridwork methods are quite different. That is, Hrennikoff's square model approaches the exact solution from below, while that of

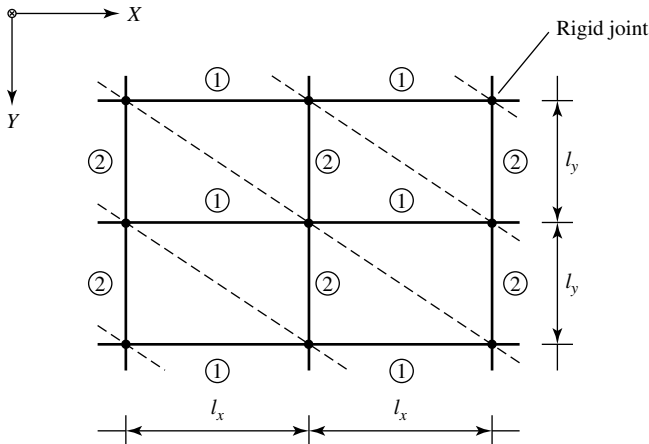


Figure 6.2.4 Rectangular gridwork constructed from triangular units.

[†] See Fig. 6.3.7.

Salonen approaches from above. Consequently, their weighted averages give quite reliable results. Both methods can be used in connection with commercially available gridwork or framework programs.

b. Equivalence of Strain Energies. The most effective general tool for obtaining equivalent cross-sectional properties of gridworks is the energy method. In this approach we state that the strain energy of a plate element is equal to the strain energy of the gridwork cell,[†] assuming that both elements have the same geometrical configurations. Thus, we write

$$\overline{U}_e = \overline{U}_g, \quad (6.2.8)$$

where \overline{U}_e is the strain energy of the plate element and \overline{U}_g represents the strain energy of the equivalent gridwork. Both energies are expressed in a global $\overline{X}, \overline{Y}, \overline{Z}$ reference system (Fig. 6.2.5). We can express the strain energy of the plate in the slightly different form

$$\overline{U}_e = A_e \overline{U}_0, \quad (6.2.9)$$

where A_e represents the surface area of the plate element and \overline{U}_0 is the strain energy density per unit area:

$$\overline{U}_0 = \frac{D}{2} \left\{ \left(\frac{\partial^2 \overline{w}}{\partial \overline{x}^2} \right)^2 + \left(\frac{\partial^2 \overline{w}}{\partial \overline{y}^2} \right)^2 + 2 \left(\frac{\partial^2 \overline{w}}{\partial \overline{x} \partial \overline{y}} \right)^2 - 2\nu \left[\left(\frac{\partial^2 \overline{w}}{\partial \overline{x} \partial \overline{y}} \right)^2 - \frac{\partial^2 \overline{w}}{\partial \overline{x}^2} \cdot \frac{\partial^2 \overline{w}}{\partial \overline{y}^2} \right] \right\}. \quad (6.2.10)$$

The bending moment of an exterior beam i of a gridwork cell can be expressed in its local X, Y coordinate system (Fig. 6.2.6) as

$$M_i = EI_i \frac{\partial^2 w}{\partial x^2}. \quad (6.2.11)$$

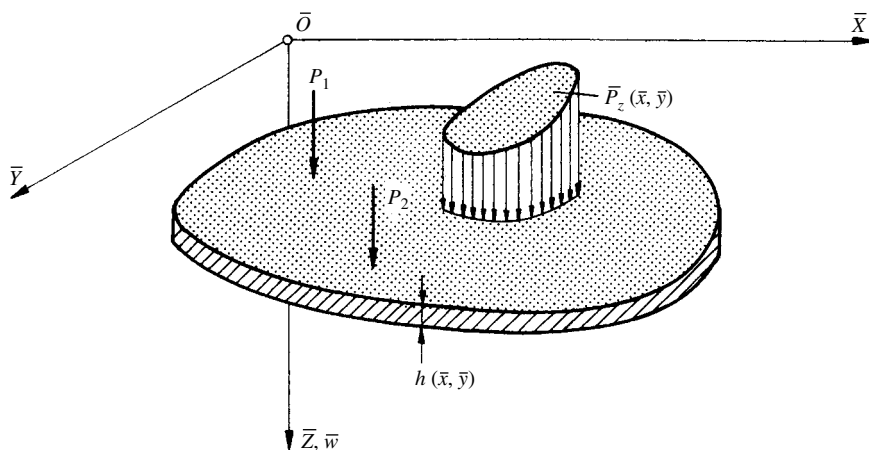
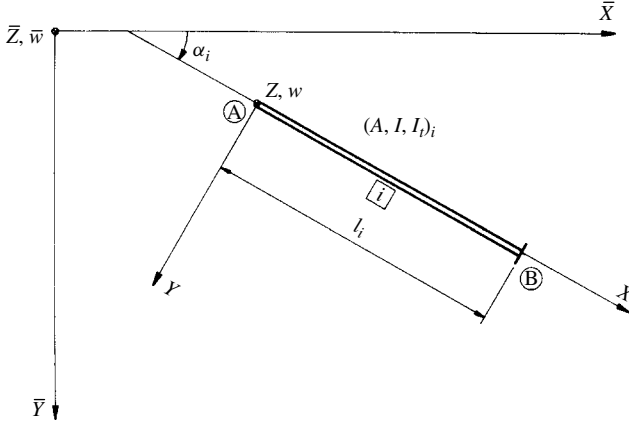


Figure 6.2.5 Plate in global coordinate system.

[†] A gridwork cell is an isolated gridwork unit.


 Figure 6.2.6 Beam in X, Y plane.

Using the pertinent transformation relationship

$$\frac{\partial^2 w}{\partial x^2} = \frac{\partial^2 \bar{w}}{\partial \bar{x}^2} \cos^2 \alpha_i + 2 \frac{\partial^2 \bar{w}}{\partial \bar{x} \partial \bar{y}} \sin \alpha_i \cos \alpha_i + \frac{\partial^2 \bar{w}}{\partial \bar{y}^2} \sin^2 \alpha_i, \quad (6.2.12)$$

we can transform the strain energy of the beam from the local coordinate system into the global reference system

$$\begin{aligned} (U_b)_i &= \frac{1}{2} M_i \frac{\partial^2 w}{\partial x^2} l_i = \frac{1}{2} E (I l)_i \left(\frac{\partial^2 w}{\partial x^2} \right)^2 \\ &= \frac{1}{2} \rho'_i \left(\frac{\partial^2 \bar{w}}{\partial \bar{x}^2} \cos^2 \alpha_i + 2 \frac{\partial^2 \bar{w}}{\partial \bar{x} \partial \bar{y}} \sin \alpha_i \cos \alpha_i + \frac{\partial^2 \bar{w}}{\partial \bar{y}^2} \sin^2 \alpha_i \right)^2, \end{aligned} \quad (6.2.13)$$

where

$$\rho'_i = E (I l)_i. \quad (6.2.14)$$

We can follow a similar approach for torsion as described above for bending. If the exterior beam i of a gridwork cell has a torsional rigidity $GI_{t,i}$, the strain energy of this beam subjected to torsional moment M_t expressed in its local coordinate system X, Y is

$$(U_t)_i = \frac{1}{2} GI_{t,i} M_t \frac{\partial^2 w}{\partial x \partial y} l_i = \frac{1}{2} G [I_t l]_i \left(\frac{\partial^2 w}{\partial x \partial y} \right)^2. \quad (6.2.15)$$

Using, again, a corresponding coordinate transformation

$$\frac{\partial^2 w}{\partial x \partial y} = \left(\frac{\partial^2 \bar{w}}{\partial \bar{y}^2} - \frac{\partial^2 \bar{w}}{\partial \bar{x}^2} \right) \sin \alpha_i \cos \alpha_i + \frac{\partial^2 \bar{w}}{\partial \bar{x} \partial \bar{y}} (\cos^2 \alpha_i - \sin^2 \alpha_i), \quad (6.2.16)$$

we can express Eq. (6.2.15) in the global reference system $\bar{X}, \bar{Y}, \bar{Z}$ as

$$(\bar{U}_i)_i = \frac{1}{2} \gamma_i \left[\frac{1}{2} \left(\frac{\partial^2 \bar{w}}{\partial \bar{y}^2} - \frac{\partial^2 \bar{w}}{\partial \bar{x}^2} \right) \sin 2\alpha_i + \frac{\partial^2 \bar{w}}{\partial \bar{x} \partial \bar{y}} \cos 2\alpha_i \right]^2, \quad (6.2.17)$$

where

$$\gamma_i = G[I_i l]_i. \quad (6.2.18)$$

c. Equivalence of Displacement Fields. Since this approach to determine equivalent cross-sectional properties is restricted to rectangular units, it is not as general as the two other methods discussed above; consequently, it is not treated here in detail. Interested readers are referred to Ref. [6.1.5].

Summary. The gridwork method constitutes a physical discretization technique of the plate continuum by replacing it with specially arranged beams. To obtain the corresponding equivalent cross-sectional properties of these beams, we introduced three different approaches from which the equivalence of strain energies appears to be the most usable one. In any case, deriving these equivalent properties is, in general, not an easy task. Consequently, when such information is not readily available, the reader should first conduct an extensive library research before embarking on such a tedious project, since a number of additional equivalent cross-sectional properties will be found in the pertinent literature.

ILLUSTRATIVE EXAMPLE

Let us determine the equivalent cross-sectional properties of the rectangular gridwork cell shown below in Fig. 6.3.1. We assume that the beams are rigidly jointed together and can be subjected as well to bending as to torsion. Furthermore, to simplify the derivation, let us assume that Poisson's ratio $\nu = 0$.

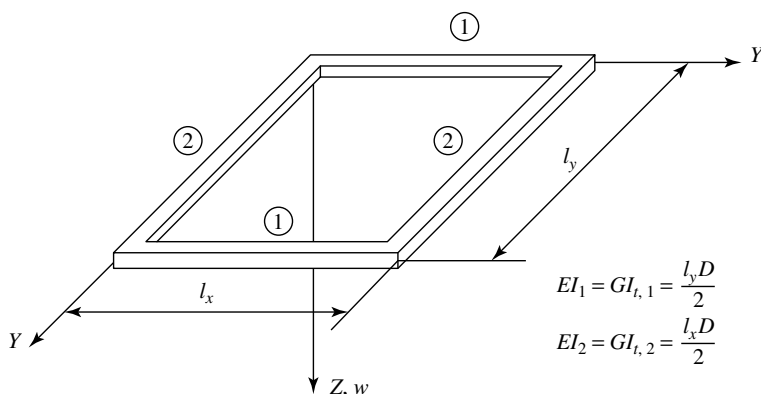


Figure 6.3.1 Rectangular gridwork cell.

In this case, the strain energy of the corresponding plate element, given in Eq. (6.2.10), becomes

$$\bar{U}_e = A_e \bar{U}_0 = \ell_x \ell_y \frac{D}{2} \left[\left(\frac{\partial^2 \bar{w}}{\partial \bar{x}^2} \right)^2 + \left(\frac{\partial^2 \bar{w}}{\partial \bar{y}^2} \right)^2 + 2 \left(\frac{\partial^2 \bar{w}}{\partial \bar{x} \partial \bar{y}} \right)^2 \right], \quad (6.2.19)$$

whereas the strain energy of the equivalent gridwork cell can be expressed by

$$\bar{U}_b = 2(\bar{U}_b + \bar{U}_t)_1 + 2(\bar{U}_b + \bar{U}_t)_2. \quad (6.2.20)$$

With $\alpha_1 = 0$ and $\alpha_2 = 90^\circ$, Eqs. (6.2.13) and (6.2.17) become

$$(\bar{U}_b)_1 = \frac{1}{2} \rho'_1 \left(\frac{\partial^2 \bar{w}}{\partial \bar{x}^2} \right)^2, \quad (\bar{U}_t)_1 = \frac{1}{2} \gamma_1 \left(\frac{\partial^2 \bar{w}}{\partial \bar{x} \partial \bar{y}} \right)^2 \quad (6.2.21)$$

and

$$(\bar{U}_b)_2 = \frac{1}{2} \rho'_2 \left(\frac{\partial^2 \bar{w}}{\partial \bar{y}^2} \right)^2, \quad (\bar{U}_t)_2 = \frac{1}{2} \gamma_2 \left(\frac{\partial^2 \bar{w}}{\partial \bar{x} \partial \bar{y}} \right)^2. \quad (6.2.22)$$

Substituting these equations into Eq. (6.2.20), the strain energy of the gridwork cell can be expressed by

$$\bar{U}_b = \rho'_1 \left(\frac{\partial^2 \bar{w}}{\partial \bar{x}^2} \right)^2 + \rho'_2 \left(\frac{\partial^2 \bar{w}}{\partial \bar{y}^2} \right)^2 + (\gamma_1 + \gamma_2) \left(\frac{\partial^2 \bar{w}}{\partial \bar{x} \partial \bar{y}} \right)^2. \quad (6.2.23)$$

Since equivalence of the strain energies requires that

$$\begin{aligned} & \rho'_1 \left(\frac{\partial^2 \bar{w}}{\partial \bar{x}^2} \right)^2 + \rho'_2 \left(\frac{\partial^2 \bar{w}}{\partial \bar{y}^2} \right)^2 + (\gamma_1 + \gamma_2) \left(\frac{\partial^2 \bar{w}}{\partial \bar{x} \partial \bar{y}} \right)^2 \\ &= \ell_x \ell_y \frac{D}{2} \left[\left(\frac{\partial^2 \bar{w}}{\partial \bar{x}^2} \right)^2 + \left(\frac{\partial^2 \bar{w}}{\partial \bar{y}^2} \right)^2 + 2 \left(\frac{\partial^2 \bar{w}}{\partial \bar{x} \partial \bar{y}} \right)^2 \right], \end{aligned} \quad (6.2.24)$$

by identifying the corresponding terms in this equation of equivalence, we obtain

$$\rho'_1 = \rho'_2 = \frac{1}{2} (\gamma_1 + \gamma_2) = \ell_x \ell_y \frac{D}{2}. \quad (6.2.25)$$

It follows from Eq. (6.2.15) that

$$EI_1 = \frac{\ell_y D}{2} \quad \text{and} \quad EI_2 = \frac{\ell_x D}{2}. \quad (6.2.26)$$

Furthermore,

$$G[I_t]_1 = \frac{\ell_y D}{2} \quad \text{and} \quad G[I_t]_2 = \frac{\ell_x D}{2}, \quad (6.2.27)$$

since they also satisfy the equation of equivalence (6.2.20).

As mentioned repeatedly, isolated gridwork cells must be juxtaposed to replace the plate, as shown in Fig. 6.3.2. Consequently, the cross-sectional properties of adjacent beams must be added. Thus, the so-obtained results are logically equivalent to those given in Eq. (6.2.7).

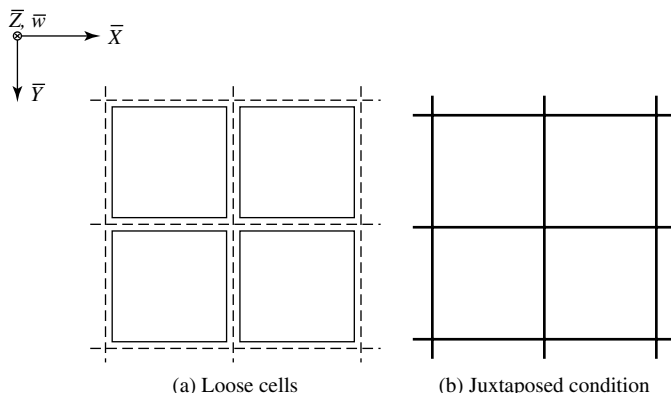


Figure 6.3.2 Juxtaposing adjacent gridwork cells.

References and Bibliography

- [6.2.1] HRENNIKOFF, A., "Solution of Problems of Elasticity by the Framework Method," *J. Appl. Mech.*, ASME, 8 (Dec. 1941), A169–A175.
- [6.2.2] SALONEN, E.-M., "A Gridwork Method for Plates in Bending," *Civil Eng. Build. Construc. Ser.*, No. 8 (1969), 1–31.
- [6.2.3] WOINOWSKY-KIEGER, S., "Zur Theorie schiefwinkliger Trägerroste," *Ing. Archiv*, 25 (1957), 350–358.
- [6.2.4] AVRAM, C., et al., *Numerical Analysis of Reinforced Concrete Structures*, Elsevier, Amsterdam, 1993.
- [6.2.5] ABSI, E., "La théorie des équivalences et son application a l'étude des ouvrages d'art," *Annales de Inst. Tech. du Batiment et Travaux Publics*, 298 (1972), 58–80.
- [6.2.6] ABSI, E., *Méthodes de calcul numérique*, Eyrolles, Paris, 1978.
- [6.2.7] SZILARD, R., *Finite Berechnungsmethoden der Strukturmechanik*, Vol. 2: *Flächentragwerke im Bauwesen*, Ernst & Sohn, Berlin, 1990.

6.3 Gridwork Cells and Their Stiffness Matrices

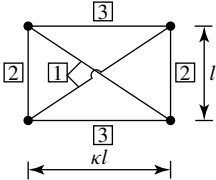
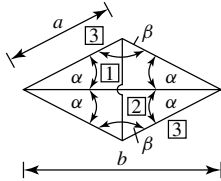
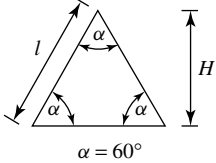
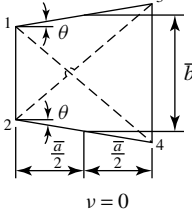
By isolating a unit from the equivalent gridwork structure of the plate, we obtain a *gridwork cell*; an example of it is shown in Fig. 6.3.1. The equivalent cross-sectional properties of such gridwork cells are determined by using one of the methods described in the foregoing section. Next, we apply the superposition technique

(illustrated in Fig. 6.3.2) to assemble the complete lattice structure from these individual cells. Consequently, if a commercially available computer program for gridworks is utilized to analyze such a substitute structure, the equivalent cross-sectional properties pertinent to the adjacent exterior beams of each cell must be added.

In addition to the two gridwork models, already introduced Table 6.3.1 provides further equivalent cross-sectional properties pertinent to other rectangular and triangular gridwork cells.

There are instances, however, when a finite element program is more readily available than that of a gridwork or the reader intends to write his or her own computer codes for the analysis of the equivalent lattice structure utilizing gridworks. In such cases, we must first determine the stiffness matrix of these gridwork cells in order

Table 6.3.1 Additional Gridwork Cells

Gridwork Cell	Beam Number	EI_i	$GI_{t,i}$	Reference
	1	$\frac{lh^3}{24} \frac{(1 + \kappa^2)^{3/2}}{\kappa}$ $\times \frac{vE}{1 - v^2}$	0	[6.3.3]
	2	$\frac{lh^3}{24} \cdot \frac{(\kappa^2 - v)E}{\kappa(1 - v^2)}$	$\frac{lh^3}{24} \cdot \frac{\kappa(1 - 3v)E}{(1 - v^2)}$	
	3	$\frac{lh^3}{24} \cdot \frac{(1 - \kappa^2 v)E}{1 - v^2}$	$\frac{lh^3}{24} \cdot \frac{(1 - \kappa^2 v)E}{(1 - v^2)}$	
	1	0	$\frac{ah^3}{12} \cdot \frac{(1 - 4 \cos^2 \alpha)E}{\cos \alpha(1 - v^2)}$	[6.3.4]
	2	$\frac{bh^3 \cot \beta}{12} \cdot \frac{E}{1 - v}$	$\frac{ah^3}{12}$ $\times \frac{(\sin^2 \alpha - \cos^2 \alpha - 2v \sin^2 \alpha)E}{\sin \alpha(1 - v^2)}$	
	3	$\frac{ah^3 \cot \alpha}{24} \cdot \frac{E}{1 - v}$	$\frac{ah^3 \cot \alpha}{24} \cdot \frac{(1 - v \tan^2 \alpha)E}{(1 - v^2)}$	
 $\alpha = 60^\circ$	All beams	$\frac{Hh^3}{36} \cdot \frac{E}{1 - v}$	$\frac{Hh^3}{36} \cdot \frac{(1 - 3v)E}{(1 - v^2)}$	[6.3.5]
 $v = 0$	1-2	$D \frac{\bar{a}}{2} \left(1 + \frac{\bar{b}}{\bar{a}} \tan \theta \right)$	$D \frac{\bar{a}}{2} \left(1 + \frac{\bar{b}}{\bar{a}} \tan \theta \right)$	[6.2.2]
	3-4	$D \frac{\bar{a}}{2} \left(1 - \frac{\bar{b}}{\bar{a}} \tan \theta \right)$	$D \frac{\bar{a}}{2} \left(1 - \frac{\bar{b}}{\bar{a}} \tan \theta \right)$	
	1-3	$D \frac{\bar{b}}{2} \sec \theta$	$D \frac{\bar{b}}{2} \sec \theta$	
	2-4	$D \frac{\bar{b}}{2} \sec \theta$	$D \frac{\bar{b}}{2} \sec \theta$	

to replace it with the stiffness matrix of the corresponding finite elements. To obtain the stiffness matrix of the total substitute structure, we simply add these individual stiffness matrices, as discussed in Sec. 6.4.

To generate the flexural part of the gridwork cell stiffness coefficients, we apply the so-called *direct* procedure similar to that used in obtaining stiffness coefficients for beams. That is, we introduce unit motions, one at the time, along the displacement components of the nodal points and calculate the required active force that creates the unit displacement and the resulting reactive forces and moments along the other displacement coordinates that are prevented from motion. This procedure is illustrated in Fig. 6.3.3.

If all beam elements of the gridwork cells are parallel to the local coordinate axes X, Y , determination of the stiffness coefficients is relatively simple. That is, after renumbering the stiffness matrices of the individual beams of the gridwork cells, we add those stiffness coefficients that have the same indices. Thus

$$K_{ij} = \sum k_{ij}. \quad (6.3.1)$$

The stiffness matrix of the i th member of the gridwork cell N in its local x, y, z coordinate system (Fig. 6.3.4) is

$$\mathbf{K}_b^{(i)} = \begin{bmatrix} GI_t/L & 0 & 0 & -GI_t/L & 0 & 0 \\ 0 & 12EI_y/L^3 & -6EI_y/L^2 & 0 & -12EI_y/L^3 & -6EI_y/L^2 \\ 0 & -6EI_y/L^2 & 4EI_y/L & 0 & 6EI_y/L^2 & 2EI_y/L^2 \\ -GI_t/L & 0 & 0 & GI_t/L & 0 & 0 \\ 0 & -12EI_y/L^3 & 6EI_y/L^2 & 0 & 12EI_y/L^3 & 6EI_y/L^2 \\ 0 & -6EI_y/L^2 & 2EI_y/L & 0 & 6EI_y/L^2 & 4EI_y/L \end{bmatrix}^{(i)}, \quad (6.3.2)$$

where GI_t and EI_y represent the equivalent cross-sectional properties of the beam.

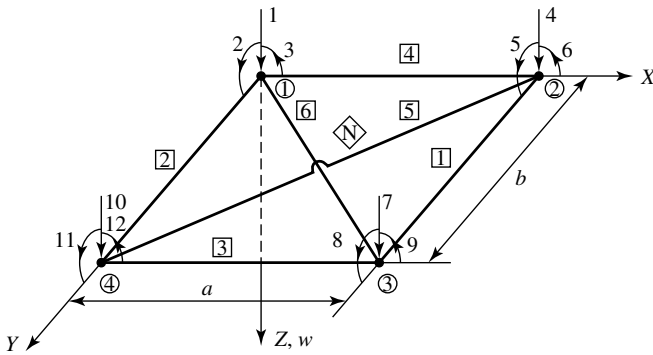
By comparing this stiffness matrix with that of a plane frame member [6.3.7], the similarity is striking, since a gridwork cell resembles a plane frame structure in many respects. Both structures can be considered as plane frames. The only difference is the nature of their loading.

For beams having a general position in the X, Y plane, we must first rotate their local coordinate system x, y, z into a X', Y', Z' position that is parallel to the X, Y, Z axes (Fig. 6.3.5) before we can add the corresponding stiffness coefficients according to Eq. (6.3.1). The corresponding matrix operation is

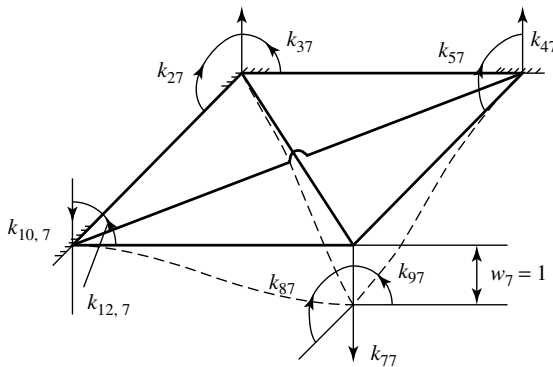
$$\mathbf{K}_b'^{(i)} = \mathbf{T}^{(i)} \mathbf{K}_b^{(i)} (\mathbf{T}^{(i)})^T, \quad (6.3.3)$$

where the transformation matrix \mathbf{T} has the form

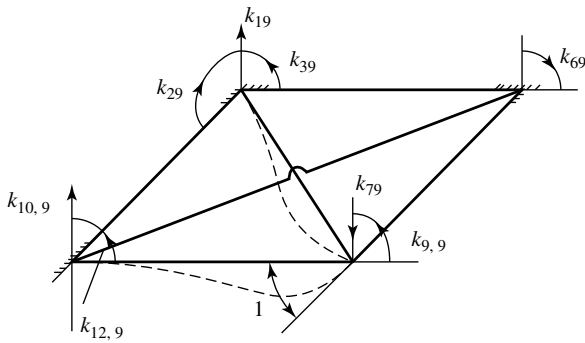
$$\mathbf{T}^{(i)} = \begin{bmatrix} c & s & 0 & 0 & 0 & 0 \\ -s & c & 0 & 0 & 0 & 0 \\ 0 & 0 & 1 & 0 & 0 & 0 \\ 0 & 0 & 0 & c & s & 0 \\ 0 & 0 & 0 & -s & c & 0 \\ 0 & 0 & 0 & 0 & 0 & 1 \end{bmatrix}^{(i)}. \quad (6.3.4)$$



(a) Sign convention and numbering system



(b) Unit translation



(c) Unit rotation

Figure 6.3.3 Generation of flexural stiffness coefficients.

In this equation c and s represent $\cos \beta$ and $\sin \beta$, respectively. Equation (6.3.4) is obtained by applying the above-mentioned analogy between gridworks and plane frame structures. It is of basic importance, however, to note that the angle β is measured from the local x axis of the beam to the intermediate X' axis, as shown in Fig. 6.3.5.

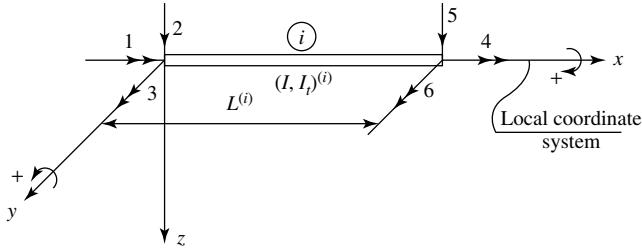


Figure 6.3.4 Beam element of gridwork cell.

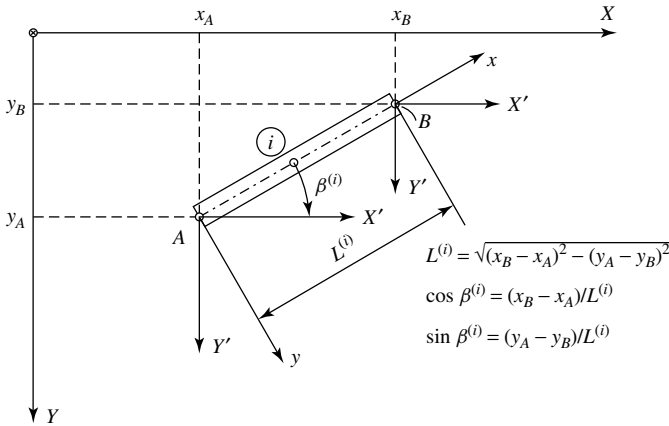


Figure 6.3.5 Orientation of beam in X, Y plane.

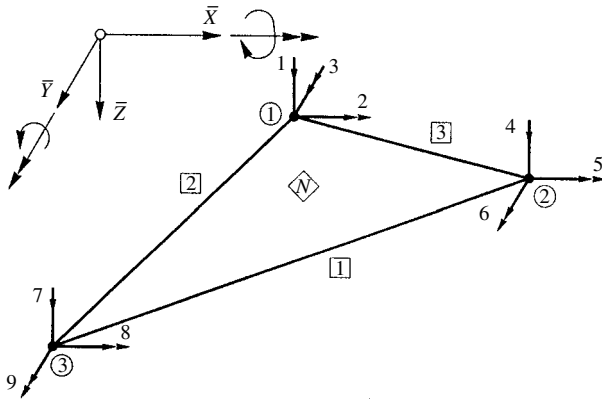


Figure 6.3.6 Triangular gridwork cell.

The so-obtained stiffness matrices for two rectangular gridwork cells are given in Tables 6.3.2 and 6.3.3, respectively. The stiffness matrix for a gridwork cell of general triangular shape (Fig. 6.3.6) can be found in explicit form in Ref. [6.3.1], but it is not reproduced here since its application is somewhat cumbersome. Consequently, if the plate geometry requires triangular discretization, use of the pertinent equivalent

Table 6.3.2 Stiffness Matrix of Gridwork Cell Shown in Fig. 6.3.3a

1	2	3	4	5	6	1	2	3	4	5	6
Symmetric	$6(3 \tan \delta - \cot \delta \cdot 3 \cot^3 \delta)$	$-9 \cot^2 \delta$	$-9 \tan \delta$	$-6 \cot \delta (3 \cot^2 \delta - 1)$	$3(3 \cot^2 \delta - 1)$	0	1				
		$6 \cot \delta$	-2	$-3(3 \cot^2 \delta - 1)$	$3 \cot \delta - \tan \delta$	0	2				
			$6 \tan \delta$	0	0	0	3				
				$6(3 \delta - \cot \delta - 3 \cot^3 \delta)$	$-9 \cot^2 \delta$	$-9 \tan \delta$	4				
					$6 \cot \delta$	2	5				
					$6 \tan \delta$	$6 \tan \delta$	6				
7	8	9	10	11	12	11	12				
$[K]^{(N)} = \frac{Eh^3}{32}$	$-6 \cot \delta$	3	$-3 \cot \delta$	$-6(3 \tan \delta - \cot \delta)$	0	$-3(3 \tan \delta - \cot \delta)$	1 (N)				
	-3	$\tan \delta$	-1	0	0	0	2				
	$3 \cot \delta$	-1	$\cot \delta$	$3(3 \tan \delta - \cot \delta)$	0	$3 \tan \delta - \cot \delta$	3				
	$-6(3 \tan \delta - \cot \delta)$	0	$-3(3 \tan \delta - \cot \delta)$	$-6 \cot \delta$	-3	$-3 \cot \delta$	4				
	0	0	0	3	$\tan \delta$	1	5				
	$3(3 \tan - \cot \delta)$	0	$3 \tan \delta - \cot \delta$	$3 \cot \delta$	1	$\cot \delta$	6				
	$6(3 \tan \delta - \cot \delta + 3 \cot^3 \delta)$	$-9 \cot^2 \delta$	$9 \tan \delta$	$-6 \cot \delta (3 \cot^2 \delta - 1)$	$-3(3 \cot^2 \delta - 1)$	0	7				
		$6 \cot \delta$	-2	$3(3 \cot^2 \delta - 1)$	$3 \cot \delta - \tan \delta$	0	8				
			$6 \tan \delta$	0	0	0	9				
	Symmetric			$6(3 \tan \delta - \cot \delta - \cot \delta + 3 \cot^3 \delta)$	$9 \cot^2 \delta$	$9 \tan \delta$	10				
					$6 \cot \delta$	2	11				
						$6 \tan \delta$	$6 \tan \delta$	12			

Note: $\tan \delta = a/b$ and $\nu = \frac{1}{3}$.

Table 6.3.3 Stiffness Matrix of Rectangular Gridwork Cell

1	2	3	4	5	6	7	8	9	10	11	12
$12 \frac{D_x b^3 + D_y a^3}{a^3 b^3}$	$\frac{D_x b + 4 D_y a}{ab}$	$\frac{4 D_x b + D_y a}{ab}$	$\frac{D_x b^3 + D_y a^3}{12 a^3 b^3}$	$\frac{D_x b + 4 D_y a}{ab}$	$\frac{4 D_x b + D_y a}{ab}$	$\frac{D_x b^3 + D_y a^3}{12 a^3 b^3}$	$\frac{D_x b + 4 D_y a}{ab}$	$\frac{4 D_x b + D_y a}{ab}$	$\frac{D_x b^3 + D_y a^3}{12 a^3 b^3}$	$\frac{D_x b + 4 D_y a}{ab}$	$\frac{4 D_x b + D_y a}{ab}$
$6 \frac{D_y}{b^2}$	0	$\frac{4 D_x b + D_y a}{ab}$	$\frac{D_x}{6 \frac{a^2}{b^2}}$	$\frac{D_x b + 4 D_y a}{ab}$	$\frac{4 D_x b + D_y a}{ab}$	$\frac{D_x}{6 \frac{a^2}{b^2}}$	$\frac{D_x b + 4 D_y a}{ab}$	$\frac{4 D_x b + D_y a}{ab}$	$\frac{D_x}{6 \frac{a^2}{b^2}}$	$\frac{D_x b + 4 D_y a}{ab}$	$\frac{4 D_x b + D_y a}{ab}$
$-6 \frac{D_x}{a^2}$	0	$\frac{4 D_x b + D_y a}{ab}$	$\frac{D_x}{6 \frac{a^2}{b^2}}$	0	0	$\frac{D_x}{6 \frac{a^2}{b^2}}$	$\frac{D_x b + 4 D_y a}{ab}$	0	0	$\frac{D_x}{6 \frac{a^2}{b^2}}$	$\frac{D_x b + 4 D_y a}{ab}$
$-12 \frac{D_x}{a^3}$	0	$\frac{D_x}{a}$	0	$\frac{D_x}{6 \frac{a^2}{b^2}}$	0	$\frac{D_x}{6 \frac{a^2}{b^2}}$	0	0	$\frac{D_x}{6 \frac{a^2}{b^2}}$	0	0
0	$-\frac{D_x}{a}$	0	0	0	0	0	0	0	0	0	0
$-6 \frac{D_x}{a^2}$	0	$2 \frac{D_x}{a}$	$6 \frac{D_x}{a^2}$	0	0	$12 \frac{D_x b^3 + D_y a^3}{a^3 b^3}$	$\frac{D_x b + 4 D_y a}{ab}$	0	$\frac{D_x b^3 + D_y a^3}{12 a^3 b^3}$	$\frac{D_x b + 4 D_y a}{ab}$	$\frac{4 D_x b + D_y a}{ab}$
0	0	0	$-12 \frac{D_x}{b^3}$	$-6 \frac{D_x}{b^2}$	0	$\frac{D_x b^3 + D_y a^3}{12 a^3 b^3}$	$\frac{D_x b + 4 D_y a}{ab}$	0	$\frac{D_x b^3 + D_y a^3}{12 a^3 b^3}$	$\frac{D_x b + 4 D_y a}{ab}$	$\frac{4 D_x b + D_y a}{ab}$
0	0	0	$6 \frac{D_y}{b^2}$	$2 \frac{D_y}{b}$	0	$-\frac{D_y}{b}$	0	$\frac{D_x b + 4 D_y a}{ab}$	$\frac{D_x b^3 + D_y a^3}{12 a^3 b^3}$	$\frac{D_x b + 4 D_y a}{ab}$	$\frac{4 D_x b + D_y a}{ab}$
0	0	0	0	0	$-\frac{D_y}{b}$	$6 \frac{D_y}{a^2}$	0	$\frac{D_x b + 4 D_y a}{ab}$	$\frac{D_x b^3 + D_y a^3}{12 a^3 b^3}$	$\frac{D_x b + 4 D_y a}{ab}$	$\frac{4 D_x b + D_y a}{ab}$
$-12 \frac{D_x}{b^3}$	$-\frac{D_x}{b^2}$	0	0	0	0	$-12 \frac{D_x}{a^3}$	0	0	$\frac{D_x b^3 + D_y a^3}{12 a^3 b^3}$	$\frac{D_x b + 4 D_y a}{ab}$	$\frac{4 D_x b + D_y a}{ab}$
$6 \frac{D_y}{b^2}$	$2 \frac{D_x}{b}$	0	0	0	0	$6 \frac{D_y}{a^2}$	$-\frac{D_x}{a}$	0	$-\frac{D_x}{a}$	$-\frac{D_y}{b^2}$	$\frac{D_x}{a^2}$
0	0	$-\frac{D_x}{b}$	0	0	0	$\frac{D_x}{a^2}$	0	$-\frac{D_x}{a}$	$-\frac{D_y}{b^2}$	$\frac{D_x}{a^2}$	$\frac{D_x}{a^2}$

$[k]^{(N)} =$

$D_x = \frac{E b h^3}{24(1 - \nu^2)}$ $D_y = \frac{E a h^3}{24(1 - \nu^2)}$ $\nu = 0$

Note: Obtained by adding two Salonen units (see Fig. 6.2.4).

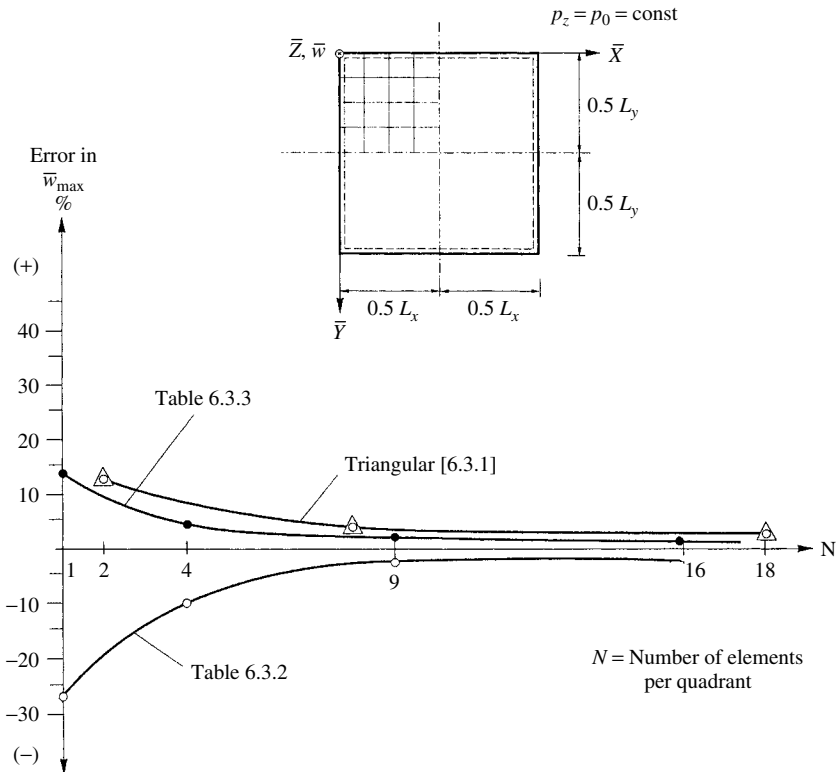


Figure 6.3.7 Convergence characteristics of gridwork cells.

cross-sectional properties in connection with a computer program for gridwork is preferable. The convergence characteristics of these gridwork cells are graphically illustrated in Fig. 6.3.7. Additional gridwork cells pertinent to orthotropic plates are treated in Sec. 10.1.

Any calculation error in these stiffness matrices can easily be detected by checking the *macroscopic* equilibrium of the gridwork cell. Since, by definition, the elements of a column or row in the stiffness matrix represent active or reactive forces and moments produced by unit motion of a nodal point (Fig. 6.3.3), the corresponding equations of equilibrium within a column or row must be satisfied. Thus, we require that

$$\sum M_x = 0, \quad \sum M_y = 0, \quad \sum P_z = 0. \quad (6.3.5)$$

Summary. Provided that the equivalent cross-sectional properties of gridworks are already determined, calculation of the stiffness matrices corresponding to rectangular gridwork cells is a relatively straightforward procedure, since gridworks resemble plane frames. Such a simple approach is, however, not the case with triangular cells because of their inherently more complex geometry. Gridwork cells can be effectively used in Finite element programs by replacing rectangular finite elements. Besides

having reasonable good convergence characteristics, they are always “conformable,”[†] which is important in the finite element stability analysis of plates. Furthermore, the use of rectangular gridwork cells is especially advantageous for orthotropic and ribbed plates, as discussed in Sec. 10.1.

References and Bibliography

- [6.3.1] SZILARD, R., *Finite Berechnungsmethoden der Strukturmechanik*, Vol. 2: *Flächentragwerke im Bauwesen*, Ernst & Sohn, Berlin, 1990.
- [6.3.2] AVRAM, C., et al., *Numerical Analysis of Reinforced Concrete Structures*, Elsevier, Amsterdam, 1993.
- [6.3.3] SZILARD, R., and POWELL, R. O., “Dynamic Stability Analysis of Prismatic Shells by Framework Method,” in Krapenbauer, R. (ed.), *Proceedings of IASS Symposium on Folded Plates and Prismatic Structures*, Vol. 1, Vienna, 1970.
- [6.3.4] YETTRAM, A. I., and HUSSAIN, H. M., “Gridwork Method for Plates in Flexure,” *J. Struct. Div., ASCE*, 97 (1971), 149–153.
- [6.3.5] BENARD, E. F., “A Study of the Relationship between Lattice and Continuous Structures,” Ph.D. Thesis, University of Illinois, Urbana, Illinois, 1965.
- [6.3.6] KNAPP, R. H., and SZILARD, R., “Nonlinear Stability Analysis of Pseudo-Cylindrical Shells,” *Acta Sci. Hung.*, 86 (1978), 9–41.
- [6.3.7] SZILARD, R., *Finite Berechnungsmethoden der Strukturmechanik*, Vol. 1: *Stabwerke*, Ernst & Sohn, Berlin, 1982.
- [6.3.8] WEAVER, W., JR., and GERE, J. M., *Matrix Analysis of Framed Structures*, 3rd ed., Van Nostrand Reinhold, New York, 1990.
- [6.3.9] HARRISON, H. B., *Structural Analysis and Design*, Pergamon Press, Oxford, 1990.
- [6.3.10] TEZCAN, S. S., “Nonlinear Analysis of Thin Plates by Framework Method,” *AIAA J.*, 5 (1967), 1890–1892.

6.4 Computational Procedures for Gridworks

Introduction. The gridwork analysis treated here is based on the *matrix displacement* method of computerized structural analysis techniques, which is most commonly used in design and analysis of rigid-frame structures. This computational approach is also often called the *direct stiffness method* in the pertinent literature. The unknown quantities are the joint displacements, that is, translation w and rotations φ_x and φ_y . An advantage of this method is that it is extremely well suited for matrix-type formulation and, thus, for computer programming. In addition, it is of importance that the analyst can more easily visualize the deflected plate surface than the stresses created by the loads. The same statement is valid for the kinematic boundary conditions.

As mentioned in Sec. 6.3, a grillage-type structure resembles a plane frame in many respects. First, all rigidly connected beams of both types lie in a plane. Second, bending of these beams plays the dominant role in carrying the external loads in both structures. In gridworks, the effects of torsional moments are of secondary importance. Similarly, the axial stresses are mostly of negligible order in planar frames. The most important difference, however, is the way external loads are applied to these structures. That is, external forces in gridworks act normal to its own plane, whereas forces applied to planar rigid-frames lie in their planes. Furthermore, vectors of

[†] For a definition see Sec. 7.4.

the internal moments lie in the plane of the gridwork, whereas internal moments in the planar rigid-frames have their vectors normal to the plane of the structure. Consequently, we may state that a gridwork is a special case of plane frames.

Based on the analogy discussed above between gridworks and planar rigid-frames, we may assume that most readers will find the following treatment of gridwork analysis quite familiar. Thus, we can concentrate on the salient features of the computational approach emphasizing the specific highlights pertinent to gridworks and refer to the numerous textbooks on matrix displacement analysis of framed structures [6.4.1–6.4.12][†] for more details.

In addition, it should be mentioned that the gridwork representation of plates provides a relatively smooth transition between the basic structural analysis of frames and the more advanced treatment of surface-type structures such as plates.

In the following, we will treat the computational procedures for gridworks in two parts. First, commercially available computer programs for analysis of gridworks or frameworks are plentiful. Thus, we will concentrate on their use as related to plate analysis. Next, in isolated cases, the engineer must write his or her own program. So the reader is provided with sufficient guidance to accomplish such a task.

Finally, an often neglected phase in the procedures of numerical analysis of plates must be mentioned. That is, before any computation can proceed, we must have a good assumption concerning the thickness of the plate. For this purpose, a paper-and-pencil approach using one of the simple *engineering methods* treated in this book is the most useful. Furthermore, such approximations by longhand computation can also be used for predicting maximum deflections, critical stresses and regions of stress concentration. Hence, they will help in the discretization process and may render the first independent check of computer results.

6.4.1 Procedures Using Commercially Available Programs

Computational procedures using commercially available software for gridwork analysis can be divided into three parts:

1. preprocessing,
2. analysis and
3. postprocessing.

A flow chart shown in Fig. 6.4.1 shows the various processing phases in more detail.

a. Preprocessing. The first step in analyzing a plate structure using the gridwork method is selection of the global *Cartesian* coordinate system \bar{X} , \bar{Y} , \bar{Z} . The plate should lie in the \bar{X} , \bar{Y} plane and the applied forces should act parallel to the \bar{Z} axis, as illustrated in Fig. 6.1.1a. If rectangular units are used, the axes \bar{X} and \bar{Y} should be parallel to the corresponding local axes of these units. Next, we replace the plate with an equivalent gridwork (Fig. 6.1.1b). In this step (except in the simplest cases), some modeling skill is expected from the engineer, which can be acquired mostly by experience. However, as mentioned above, a preliminary computation by hand using one of the engineering approaches discussed in Part IV can give some guidance in this respect. Areas of stress concentrations, for instance, require finer

[†] Listed in chronological order.

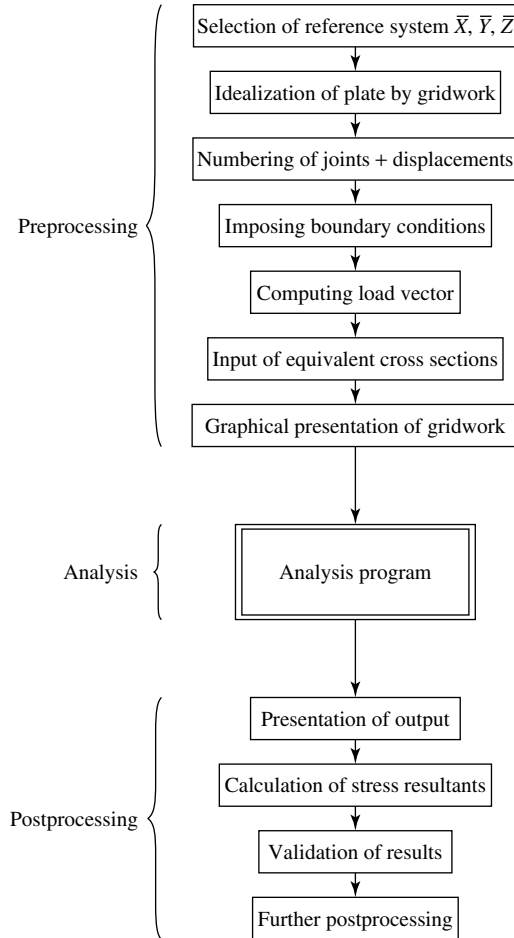


Figure 6.4.1 Phases of gridwork analysis process.

grids than the rest of the plate. Furthermore, since the gridwork method requires that concentrated external forces must act on joints, we must construct the grillage accordingly. A similar consideration applies to line loads. That is, they also must act on grid members. In addition, the total number of joints to be used in the computation should depend on the convergence characteristics of the specific schemes applied and on the required accuracy of the final results.

Nowadays, using up-to-date software for grillage analysis, the automatic mesh generator also assigns numbers to the joints when the grid is created. If this is not the case, the analyst should refer to Fig. 6.4.2, which shows effective and ineffective joint-numbering sequences. The simplest rule is to keep the maximum joint point difference as small as possible when the numbering is based on joints, since this procedure influences the structure of the stiffness matrix of the total gridwork system and may affect the efficiency of the solution of the resulting set of equations. This is especially true when very large gridwork systems are analyzed. The location of the

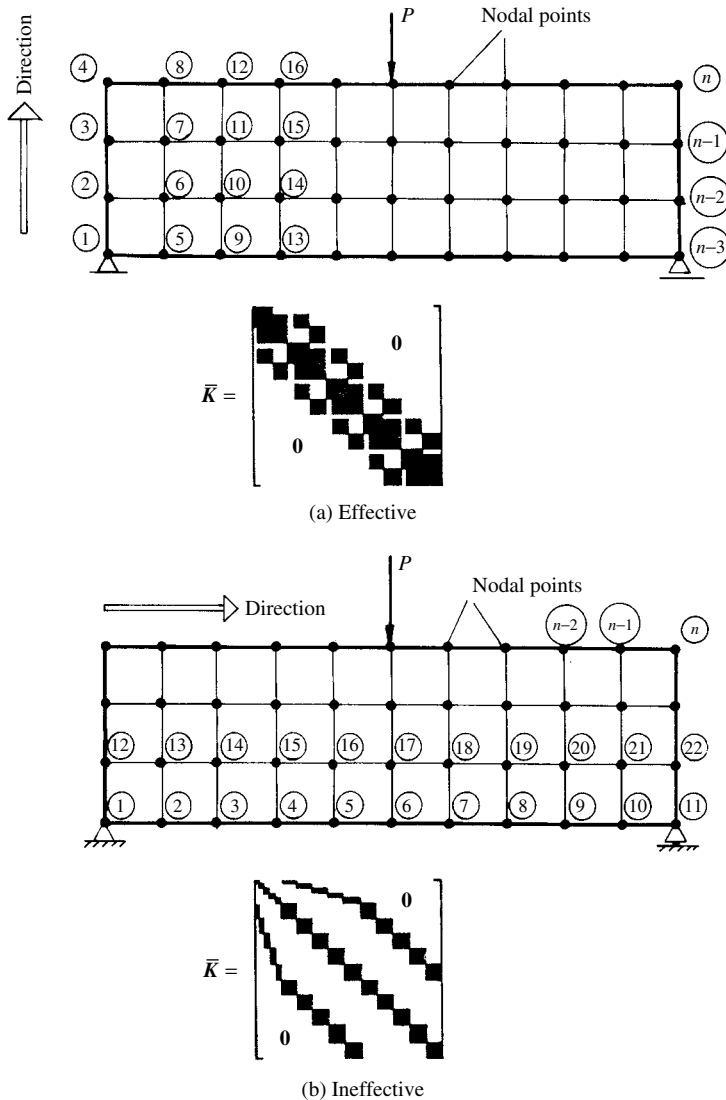


Figure 6.4.2 Effect of joint numbering on stiffness matrix.

joints must be defined by specifying their coordinates in the global reference system. Since a gridwork is essentially a two-dimensional structure, only the input of two coordinates \bar{x}_i and \bar{y}_i are required. Usually, numbering of the joints automatically takes care of identifying the individual members in the grid. As already mentioned, there are three significant displacement components at each joint: translation in the \bar{Z} direction and rotation about the \bar{X} and \bar{Y} axes, respectively. The numbering sequence for these displacements usually follows the above given order. Their sign convention, however, must be clearly specified in the program; otherwise serious mistakes can occur when interpreting the results. The most common practice in this respect is to

assign positive signs for the translation vectors that point in the positive direction of the \bar{Z} axis. For the vectors of rotations, the so-called right-hand screw sign convention is most frequently used, as discussed in Sec. 6.4.2.

Treating the *boundary conditions* in the matrix displacement method is extremely simple. That is, we strike out—either on a local or on a global level—those rows and columns in the element stiffness matrices or in the stiffness of the total structure that correspond to the “locked” displacement components. More will be said on this important subject in Sec. 6.4.2. Handling the boundary conditions is, again, automatic by using commercially available programs. We are merely required to input the pertinent joint data.

Loads on the gridwork can have a variety of sources. Some examples are

1. externally applied forces and moments,
2. body forces created by the gravity,
3. prescribed boundary displacements,
4. temperature changes[†] and
5. initial-strain and stress.

Concentrated point loads and moments are directly applied to the joints. Consequently, during discretization of the plate, joints should be assigned to the points where they act. Since gridworks can carry only joint loads, surface loads must be converted to *equivalent joint loads*. These can be obtained by calculating the static equivalent forces of the surface loads. The simplest way is to lump the distributed loads at the joints. This can give an acceptable approximation, provided that a relatively fine subdivision has been used. Alternatively, one can calculate the equivalent joint loads by equating the work expressions for the equivalent joint loads with those created by distributed surface or body forces. This is the most exact way of handling distributed loads and will be discussed in more detail in the pertinent section dealing with the FEM. For triangular units or cells, the equivalent joint loads can be approximated by creating partial loading areas, as shown in Fig. 6.4.3. This gives

$$\bar{P}_j = \bar{p}_z(x, y) \Delta A_j \quad \text{for } j = 1, 2, 3. \quad (6.4.1)$$

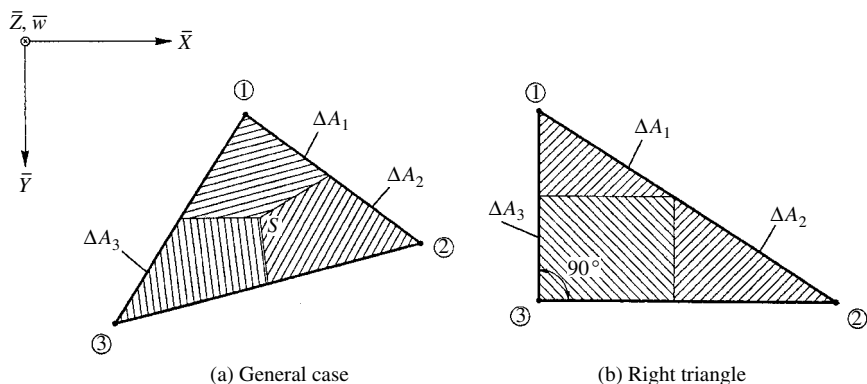


Figure 6.4.3 Loading areas for triangular gridworks.

[†] To be treated in Secs. 10.4 and 16.8

As already mentioned, line loads require “supporting” beams in the discretization process. The corresponding fixed-end reactions with opposite signs should be used as equivalent joint loads.

Before analysis of the gridwork can start, checking the validity of the input data is mandatory. This time-consuming task can be helped considerably by using interactive graphic displays. This gives the user immediate feedback as to the validity of the grid generated. These programs also can display the joint loads and the boundary conditions.

b. Analysis. The mathematical task associated with analysis of equivalent gridwork structures consists of solving the matrix displacement equation

$$\bar{\mathbf{K}}\bar{\mathbf{p}} = \bar{\mathbf{d}} \quad (6.4.2)$$

for its unknown displacement vector $\bar{\mathbf{d}}$. In this equation $\bar{\mathbf{K}}$ is the stiffness matrix of the total structure and $\bar{\mathbf{p}}$ represents the load vector. This task constitutes the single most computer-time-intensive phase of the analysis. For this reason, considerable efforts have been undertaken to develop special solution algorithms that require a minimum number of operations to obtain the required solution. In programs for the analysis of gridwork or framework structures the equation solver is usually embedded in the “black box” and consequently remains hidden from the user. Here we will list briefly the most-often-used equation solver algorithms.

Since $\bar{\mathbf{K}}$ in Eq. (6.4.2) is always a square, symmetric and positive-definite matrix, the Cholesky *square-root*[†] technique of matrix decomposition is particularly well suited as an equation solver in matrix analysis of structures. This method is more economical concerning computer time than other elimination processes. It has already been mentioned that the joint numbering sequence is quite significant since it determines the bandwidth of the coefficient matrix $\bar{\mathbf{K}}$. That is, by properly numbering the joints and hence the unknown displacements, the bandwidth is kept small. Thus, the computational effort needed for equation solution is often near a minimum.

The Gauss elimination scheme is often the equation solver used in various programs. This approach in effect factorizes or triangularizes the coefficient matrix during the forward elimination process. Furthermore, it is characteristic of the Gauss algorithm applied to sparsely populated matrices that only part of the matrix is affected by elimination of one unknown.

These elimination methods, including their variations and various other equation-solving techniques, are well documented in Refs. [6.4.11–6.4.16]. Some of these references also contain readily usable FORTRAN programs, as discussed in Sec. 6.4.2.

c. Postprocessing. The above-discussed analysis phase of the program yields the deformations of the equivalent gridwork structure. The postprocessing phase of the so-obtained results consists of the following steps:

1. presentation of the output,
2. calculation of the stress resultants,
3. validation of the results and
4. further processing steps (if required).

[†] Also known as Crout’s method.

Commercially available gridwork programs generate considerable data concerning the deformation of the structure, part of which is, for instance, joint rotations, of secondary interest to the analyst. Consequently, only the lateral displacements of the joints expressed in global coordinates should be documented in a well-organized manner. In addition, use of the computer graphics showing the deflected gridwork (Fig. 6.4.4) proves to be an ideal combination in connection with the tabular output.

Before computing the stress resultants of the original plate, the analyst should become familiar with the sign convention of the program given in the user's manual. Unfortunately, this is often not clearly defined. When in doubt, the analyst should run a small comparative study using a simple plate problem with known "exact" solution, as given in Chapter 2, to eliminate any ambiguity in this respect.

The computer program gives the displacements at each joint point of the equivalent structure. The engineer, however, is usually more interested in distributions of moments and shear forces throughout the plate. For rectangular gridwork patterns, use of the finite difference stencils given in Fig. 5.1.4 offers the simplest and most reliable way to calculate the stress resultants. In addition to the displacements, the program commonly gives the bending and torsional moments along with the transverse shears at the joint point of the gridwork. To obtain good results using these outputs, it is often advantageous to evaluate the stress resultants at the midpoints of the equivalent beams. For a triangular gridwork pattern, determination of stress resultants in the plate is not a trivial matter. That is, although the internal forces given in the local coordinate system of the beams can be easily computed from [6.2.2]

$$m_{x,i} = \frac{D}{B_i} M_i, \quad m_{xy,i} = \frac{D}{C_i} M_{t,i}, \quad (6.4.3)$$

they must be transferred from their local coordinate system to the global reference system of the plate. In the above equation B_i and C_i represent the equivalent bending and torsional rigidities of beam i as previously defined in Eq. (6.2.4). If the gridwork is formed using rectangular units (Fig. 6.2.4), the stress resultant can be evaluated (even for an arbitrary value of ν) from

$$m_x = \frac{M_1}{\ell_y} + \nu \frac{M_2}{\ell_x}, \quad m_y = \frac{M_2}{\ell_x} + \nu \frac{M_1}{\ell_y} \quad (6.4.4a)$$

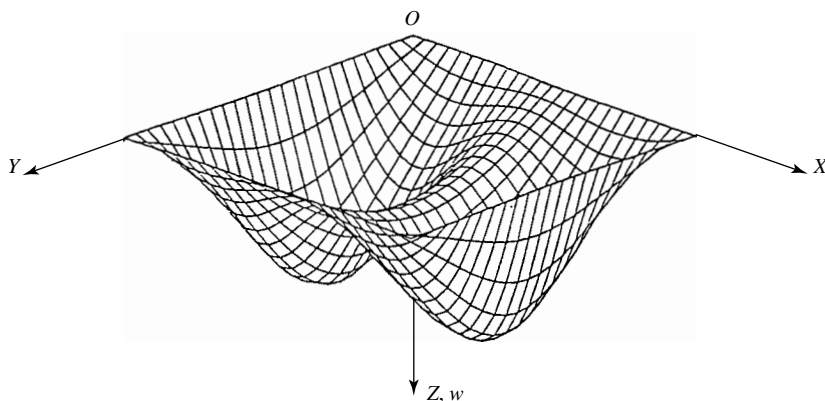


Figure 6.4.4 Three-dimensional representation of deflected plate surface.

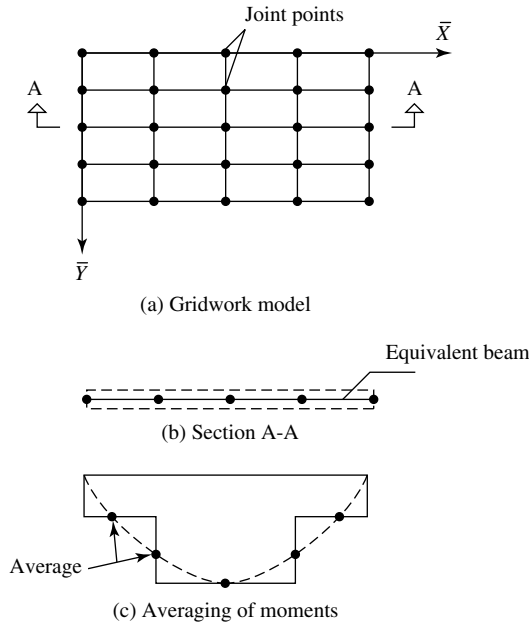


Figure 6.4.5 Stress resultant averaging.

and

$$m_{xy} = (1 - \nu) \frac{M_{r,1}}{\ell_y}, \quad m_{yx} = (1 - \nu) \frac{M_{r,2}}{\ell_x}. \quad (6.4.4b)$$

The approximate nature of the gridwork method manifests itself clearly in that the internal forces in adjacent units show some discrepancies at the common joint points that can be removed by averaging them (Fig. 6.4.5).

The final step in postprocessing is validation and verification of the results. The analyst should run a small (if possible similar) test example with known exact or reliable results to build confidence in the program system. It is false to assume that all commercial runs yield useful results! The most fundamental check involves an equilibrium check. That is, all externally applied forces must be in equilibrium with the obtained reactions. As mentioned earlier, engineers experienced in plate analysis can use the graphic image of the deflected plate surface to detect further discrepancies. For instance, instead of smooth continuous lines, wavy lines may indicate numerical instability in the analysis that can be eliminated by prescribing “double precision” in the equation-solving algorithm. In addition, the reasonableness of the solution can be established by applying one of the engineering methods treated in Part IV. If an *entirely independent* check is required, a separate computation with the help of the FDM should be considered.

6.4.2 Guidance for Gridwork Programming

The development of a program for matrix analysis of gridwork structures is no simple undertaking by any means. Consequently, the engineer should write his or her own

program only if a definite need for it exists and the program will be reused many times. Otherwise, the FDM offers a considerably simpler way for plate analysis, since requires an equation solver that is readily available even in some advanced scientific calculators rather than a computer program.

The first step in writing a computer program includes selecting a suitable programming language. The recommended choice in this respect is FORTRAN, since it is still the dominant programming language in science and engineering, and many usable subroutines are written in this language. Other programming languages such as PASCAL and the new and improved versions of BASIC or C++ may also qualify if the analyst is more familiar with them.

Next, a library research should be conducted as to whether such a program exists in the literature because modifying an existing program for gridworks to suit some specific individual need is far easier than writing one from “scratch.” References [6.4.11–6.4.14] provide such codes written in FORTRAN. In addition, engineers can apply the so-called building block strategy to write their own computer program for matrix displacement analysis of gridworks. That is, as its name implies, this procedure mainly involves manipulations of matrices. A collection of FORTRAN subroutines that perform these functions can be found in Refs. [6.4.15–6.4.23]. These can be used directly by readers to assemble their own computer program.

Procedures of program development can be divided into three phases: (1) preprocessing, (2) analysis and (3) postprocessing. Most of what was said about these phases in the previous subsection retains its validity here, so we will only emphasize the differences. The general statement in this respect is, however, that the program should be considerably simpler than those commercially distributed, since it is intended for personal or internal use and not for general distribution and/or sale.

a. Preprocessing. Generation of a gridwork model can be considered a six-step procedure:

1. definition of plate geometry, including boundary and loading conditions;
2. discretization of the plate continuum by using an equivalent gridwork structure;
3. numbering of joint points, displacement and load components;
4. definition and input of joint coordinates;
5. input of equivalent cross-sectional and material properties of each beam and
6. input of loads acting on the joints.

These steps do not need to be as elaborate and sophisticated as we are accustomed to when using commercially distributed programs. The mesh generation, for instance, can be accomplished without a mesh generator program and corresponding graphic display. Although the creation of gridwork models by hand is a simple and straightforward process, it can be occasionally quite time consuming, especially when dealing with very large plate structures. That is, the gridwork models are hand drawn by the analyst laying out the mesh on paper. The analyst must number all joints and displacement components on this drawing by hand following the recommendations and sequences already discussed in Sec. 6.4.1. Since the input of the global joint coordinates along with all other inputs should be *interactive*, it is important that during this input process the user be guided by appropriate comments concerning each step.

b. Analysis. As already mentioned, the analysis of grid structures resembles that of plane frames in many respects. Hence, the required computational procedures for the latter are readily available in numerous textbooks on matrix displacement analysis of structures [6.4.1–6.4.12] and can be used as samples in writing such programs. Furthermore, the reader will find complete FORTRAN codes for static gridwork analysis in Refs. [6.4.11–6.4.12]. Consequently, it appears to be sufficient if we briefly concentrate here on the steps required after the preprocessing phase is already completed.

The closed-form expression for the stiffness matrix of an individual beam element is given in Eq. (6.3.2). This is valid only in the local X, Y, Z coordinate system of the beam (Fig. 6.3.4). If the axes of the local and global coordinate systems are parallel, computing the stiffness matrix of the structure, $\bar{\mathbf{K}}$, from stiffness matrices of individual beams, $\mathbf{K}_b^{(i)}$, requires only simple additions. That is, after the beam matrices are renumbered following the new global numbering system of the structure, the elements $\bar{K}_{i,j}$ of the stiffness matrix $\bar{\mathbf{K}}$ are obtained by adding element stiffness coefficients having the same subscripts, as shown in Eq. (6.3.1).

However, if the local coordinate axes are not parallel to those of the global reference system, rotation of X, Y, Z axes into a parallel position with the global axes is required before additions of element stiffness coefficients can be carried out. Such a rotation according to Eq. (6.3.3) yields

$$\mathbf{K}_b^{(i)} = \begin{bmatrix} Ac^2 + Bs^2 & -Asc + Bsc & -Cs & -Ac^2 - Bs^2 & Asc - Bsc & -Cs \\ -Asc + Bsc & As^2 + Bc^2 & -Cc & Asc - Bsc & -As^2 - Bc^2 & -Cc \\ -Cs & -Cc & D & Cs & Cc & E \\ -Ac^2 - Bs^2 & Asc - Bsc & Cs & Ac^2 + Bs^2 & -Asc + Bsc & Cs \\ Asc - Bsc & -As^2 - Bc^2 & Cc & -Asc + Bsc & As^2 + Bc^2 & Cc \\ -Cs & -Cc & E & Cs & Cc & D \end{bmatrix}, \quad (6.4.5)$$

where $s = \sin \beta$, $c = \cos \beta$ and

$$A = \frac{GI_t}{\ell}, \quad B = \frac{12EI_y}{\ell^3}, \quad C = \frac{6EI_y}{\ell^2}, \quad D = \frac{4EI_y}{\ell}, \quad E = \frac{2EI_y}{\ell}. \quad (6.4.6)$$

Equation (6.4.5) is valid if the angle β is measured from the intermediate X' axis into the direction of the local X axis. Otherwise, the transposed relationship

$$\mathbf{K}_b^{(i)} = (\mathbf{T}^{(i)})^T \mathbf{K}_b^{(i)} \mathbf{T}^{(i)} \quad (6.4.7)$$

must be used.

In addition to the joint coordinates and beam properties, the analysis part of the program must give detailed information for each joint concerning the degrees of freedom that are constrained to take care of the boundary conditions. This can be easily accomplished by numbering the local and global displacements. Those displacement components that are constrained do not receive any number during the numbering process of the displacement components. Consequently, these degrees of freedom

must be eliminated either from the beam matrices[†] on the local level or from the stiffness matrix of the structure on the global level.

The structure stiffness matrix $\bar{\mathbf{K}}$ has the following three important properties, which can be advantageously utilized in solving the governing matrix equation of the structure $\bar{\mathbf{K}}\bar{\mathbf{p}} = \bar{\mathbf{d}}$:

1. Since $\bar{\mathbf{K}}$ is symmetric, only half of the matrix needs to be assembled and stored in the computer. This very desirable property of the matrix also reduces the equation solution effort by about one-half.
2. The structure matrix $\bar{\mathbf{K}}$ is always positive definite, since the strain energy stored in the joints is always positive.
3. The matrix $\bar{\mathbf{K}}$ is a spare matrix, that is, most of its elements are zero. Furthermore, by properly numbering the displacements, we obtain a band matrix with relatively small bandwidth. This property also reduces the effort required for solving the governing matrix equation.

Once the global equation of equilibrium in form

$$\bar{\mathbf{K}}\bar{\mathbf{p}} = \bar{\mathbf{d}} \quad (6.4.8)$$

has been assembled and appropriate boundary conditions have been applied, either Cholesky's or Gauss's method is normally used to solve Eq. (6.4.8) for n displacements.

In writing a program for the above-discussed analysis phase, the reader should apply the previously mentioned building block technique; that is, by combining the readily available pertinent FORTRAN subroutines [6.4.15–6.4.21], the programming effort can be considerably reduced. The final analysis program should also have sufficient embedded "comment statements" by the programmer that will help in remembering what he or she has done on a later reading and help others to understand the program.

c. Postprocessing. The first and most important step in this phase is validation of the newly created program. For this purpose, the analyst should solve a few of the plate problems with known exact or series solutions[‡] using subsequently reduced mesh widths. If the so-obtained approximate results are satisfactory, the next step should concern the presentation of the results. In this respect, we refer to the corresponding part of Sec. 3.4.1. However, two additional comments are appropriate. The first one concerns the often misleading differences in the commonly used notations and sign conventions that, unfortunately, exist between the matrix displacement method and classical plate theory. These are illustrated in Fig. 6.4.6. Thus, in evaluating the obtained results, these differences must be taken into account; otherwise, serious errors can occur. The second comment deals with the highly desirable graphical presentation of the results. The best course in this respect is, of course, to use one of the many commercially available "plot" programs. If the analyst wants to write a graphic program, the FORTRAN subroutine given in Ref. [6.4.23]

[†] This is the preferred way.

[‡] See Chapter 2.

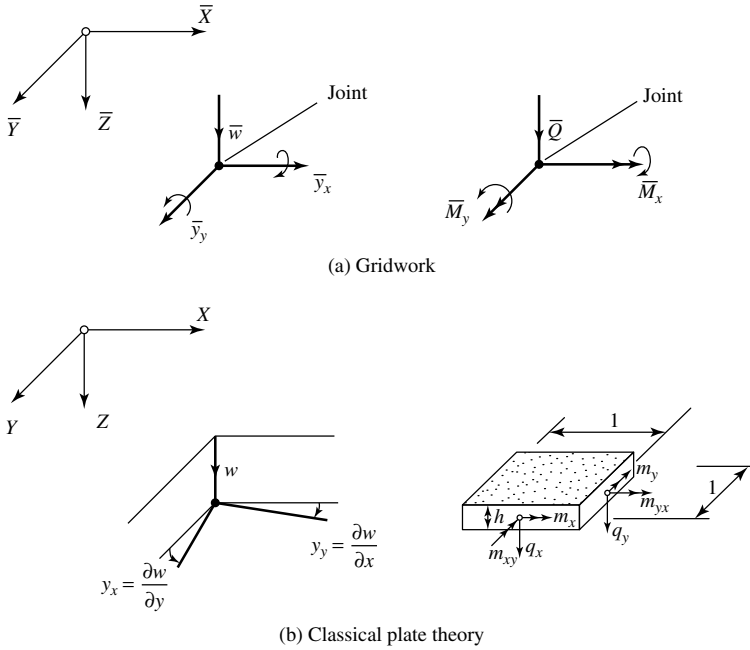


Figure 6.4.6 Different notations and sign convention.

will be of great help to code contour line displays for joint displacements and stress resultants.

When *gridwork cells* are employed in plate analysis, the required steps are identical to those used in the FEM. Consequently, it is sufficient to refer here only to Sec. 7.13, where the guidelines for finite element programming are treated in detail. For solutions of smaller plate problems, however, use of the *stiffness method* combined with the *code number technique* can be of advantage, since this approach requires only very limited computer programming efforts. In view of an abundant literature available for the stiffness analysis of structures [6.4.1–6.4.15], the most important steps are summarized below:

1. We start out, again, with a line drawing of the substitute structure numbering every joint and cell. On this drawing only the allowed displacements are also shown and globally numbered. To obtain the stiffness matrix $\bar{\mathbf{K}}$ of the total structure having the narrowest bandwidth possible, we should follow the previously given recommendations on this subject.
2. Next, we numerically evaluate the stiffness matrices for each cell. In the case of triangular cells, a transformation of these matrices from their local coordinate system to the global reference system is also required.
3. The indices of all stiffness coefficients k_{ij} of each cell are now renumbered using the code number technique to conform to the previously selected global numbering system [6.4.25]. Thus, we obtain \bar{k}_{ij} . In the next step, all stiffness coefficients with the same subscripts are simply added to obtain the stiffness matrix $\bar{\mathbf{K}}$ of the total substitute structure.

4. As already discussed, all loads must be reduced to the joints creating the load vector $\bar{\mathbf{p}}$. We also combine the unknown displacements into a column vector $\bar{\mathbf{d}}$. Solution of the obtained algebraic equations, $\bar{\mathbf{K}}\bar{\mathbf{p}} = \bar{\mathbf{d}}$, yields the joint deformations $\bar{\mathbf{d}}$.
5. Once these joint displacements are determined, the internal stress resultants can be computed using either the ordinary or the improved FDMs.

The only programming required in this case involves steps 3 and 4, for which, however, computer programs are readily available. Thus, analysts must only combine them to suit their purpose. See Illustrative Examples III and IV for the application of this stiffness method.

Summary. Since gridworks closely resemble planar frame structures, using the matrix displacement analysis with which most readers are already familiar, treating a plate as an articulated continuum by means of an equivalent plate structure does not create considerable difficulties for the analyst. If possible, commercially available gridwork programs should be used. Most of the difficulties, however, usually arise in the interpretation of the results concerning the stress resultants, since notations and sign conventions are different from those accustomed to in the analytical part of the plate analysis. In addition, an averaging method is required to obtain continuously smooth values for the stress resultants.

If possible, the reader should not attempt to write a computer program for gridwork method, since this is by no means an easy task. Work in this respect, however, can be considerably helped by using available subroutines.

ILLUSTRATIVE EXAMPLE I

Let us determine the deflected plate surface $w(x, y)$ and the maximum bending moment m_{\max} of the square plate shown in Fig. 6.4.7a by using the gridwork method. The elastic properties of this plate are

$$E = 30,000,000 \text{ kN/m}^2, \quad \nu = 0.3, \quad G = 11,540,000 \text{ kN/m}^2.$$

First, we substitute the plate continuum by an equivalent gridwork system. Utilizing the existing double symmetry of the structure and load, our computational model becomes a quarter of the total system, as shown in Fig. 6.4.7b. Based on Eq. (6.2.7), the equivalent cross-sectional properties of the interior beams are, for $i = 4, 6, 7, 9$,

$$\begin{aligned} I_i &= \frac{D\ell}{E} = \frac{h^3\ell}{12(1-\nu^2)} = 0.1099 \times 10^{-2} \text{ m}^4, \\ I_{i,t} &= \frac{D\ell}{G} = \frac{h^3\ell}{6(1-\nu)} = 0.2857 \times 10^{-2} \text{ m}^4. \end{aligned} \quad (6.4.9)$$

Since the exterior beams have only half of the above given values, we obtain

$$\begin{aligned} I_e &= \frac{I_i}{2} = 0.5495 \times 10^{-3}, \quad I_{e,t} = \frac{I_{i,t}}{2} = 0.1429 \times 10^{-2} \\ &\text{for } e = 1, 2, 3, 5, 8, 10, 11, 12. \end{aligned} \quad (6.4.10)$$

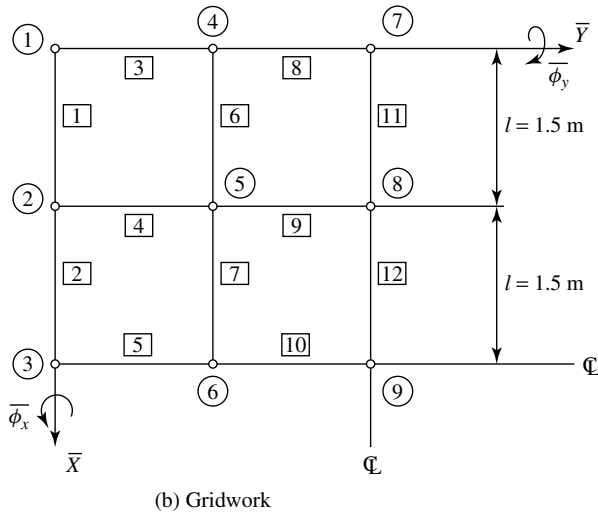
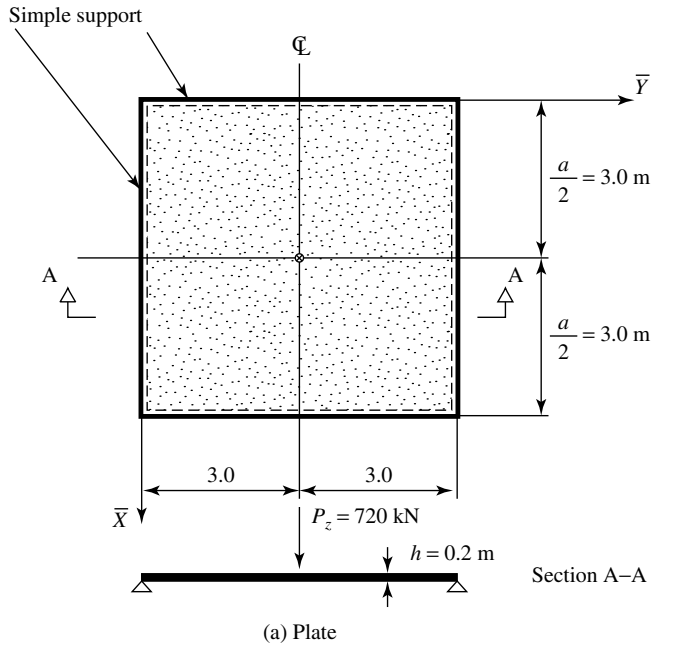


Figure 6.4.7 Gridwork representation of square plate.

Coordinates of the joints in the \bar{X} , \bar{Y} , \bar{Z} reference system are given in Table 6.4.1. Numbering of the beams, including their joint points and types, is given in Table 6.4.2.

The pertinent boundary conditions of the joints are tabulated in Table 6.4.3, where “y” indicating yes and “n” denoting no refer to the displacements that can or cannot take place, respectively.

Table 6.4.1 Coordinates

<i>Joint</i>	\bar{x}	\bar{y}	<i>Joint</i>	\bar{x}	\bar{y}
1	0.0	0.0	6	3.0	1.5
2	1.5	0.0	7	0.0	3.0
3	3.0	0.0	8	1.5	3.0
4	0.0	1.5	9	3.0	3.0
5	1.5	1.5			

Table 6.4.2 Identification of Beams

<i>Beam</i>	<i>Joints</i>	<i>Type</i>	<i>Beam</i>	<i>Joints</i>	<i>Type</i>
1	1–2	e	7	5–6	i
2	2–3	e	8	4–7	e
3	1–4	e	9	5–8	i
4	2–5	i	10	6–9	e
5	3–6	e	11	7–8	e
6	4–5	i	12	8–9	e

Note: i = interior, e = exterior.

Table 6.4.3 Boundary Conditions

<i>Joints</i>	\bar{w} <i>Locked</i>	$\bar{\phi}_x$ <i>Locked</i>	$\bar{\phi}_y$ <i>Locked</i>
1	y	y	y
2	y	n	y
3	y	n	y
4	y	y	n
6	n	n	y
7	y	y	n
8	n	y	n
9	n	y	y

Our gridwork program [6.4.24] gave the following vertical displacements of the joints in meters:

$$\bar{w} = \begin{Bmatrix} 0.0000 \\ 0.0000 \\ 0.0000 \\ 0.0000 \\ 0.0059 \\ 0.0088 \\ 0.0000 \\ 0.0088 \\ 0.0143 \end{Bmatrix} \quad \text{m.} \quad (6.4.11)$$

A comparison of the maximum vertical displacement with its more exact analytical solution

$$\bar{w}_{\max} = 0.01160 \frac{P_z a^2}{D} = 0.0137 \text{ m} \quad (6.4.12)$$

gives an error of 4.3% in spite of the relatively crude subdivision. To obtain the maximum bending moment m_{\max} , we use Eq. (5.1.12), which gives

$$m_{\max} = -\frac{D}{\ell^2}[2\bar{w}_6 - 2(1 + \nu)\bar{w}_9 + 2\nu\bar{w}_8] = 139.68 \text{ kN-m/m} \quad (6.4.13)$$

ILLUSTRATIVE EXAMPLE II

Figure 6.4.8a shows a simply supported triangular plate subjected to a uniformly distributed lateral load $p_z = p_0 = 100 \text{ kN/m}^2$. By means of the gridwork method, let us determine (a) the deflected plate surface, (b) the maximum lateral deflection and (c) the maximum bending moment.

The elastic properties of the plate are

$$E = 30,000,000 \text{ kN/m}^2, \quad G = 15,000,000 \text{ kN/m}^2, \quad \nu = 0.$$

By utilizing the apparent symmetry of the structure and the load, it is sufficient to treat only one-half of the plate if we introduce a “guided”[†] boundary condition along the symmetry line. To take care of the oblique edge of the triangular plate, we combine triangular units with the rectangular ones, as shown in Fig. 6.4.8b. With a grid size $\ell = 1.00 \text{ m}$, Eq. (6.2.7) gives the following cross-sectional properties for the interior beams of rectangular units:

$$\begin{aligned} I_1 &= \frac{D\ell}{E} = \frac{h^3\ell}{12} = 8333 \text{ cm}^4, \\ I_{t,1} &= \frac{D\ell}{G} = \frac{h^3\ell}{6} = 16,666 \text{ cm}^4. \end{aligned} \quad (6.4.14)$$

As mentioned in Sec. 6.4.2, we should use only one-half of the above given values for the exterior beams of rectangular units; thus

$$I_2 = \frac{I_1}{2} = 4166 \text{ cm}^4 \quad \text{and} \quad I_{t,2} = \frac{I_{t,1}}{2} = 8333 \text{ cm}^4. \quad (4.4.15)$$

The equivalent cross-sectional properties of the diagonal members of triangular units [Eq. (6.4.6)] are

$$I_3 = \frac{D\ell}{2E} \cot 90^\circ = 0 \quad \text{and} \quad I_{t,3} = \frac{D\ell}{G} \cot 90^\circ = 0. \quad (6.4.16)$$

To avoid divisions by zero, we substitute 0 by 1, which represents a very small number in relation to the cross-sectional properties of the other beams. Consequently, we can approximate $I_3 = I_{t,3} \approx 1$.

It is of interest to note that the remaining two types of equivalent beams can be reduced to types 1 and 2, respectively. Hence

[†] See Fig. 5.1.5d.

$$I_4 = I_2 + \frac{D\ell}{2E} \cot 45^\circ = 4166 + 4166 = 8333 \text{ cm}^4 = I_1, \quad (6.4.17)$$

$$I_{t,4} = I_{t,2} + \frac{D\ell}{2G} \cot 45^\circ = 8333 + 8333 = 16,666 \text{ cm}^4 = I_{t,1}$$

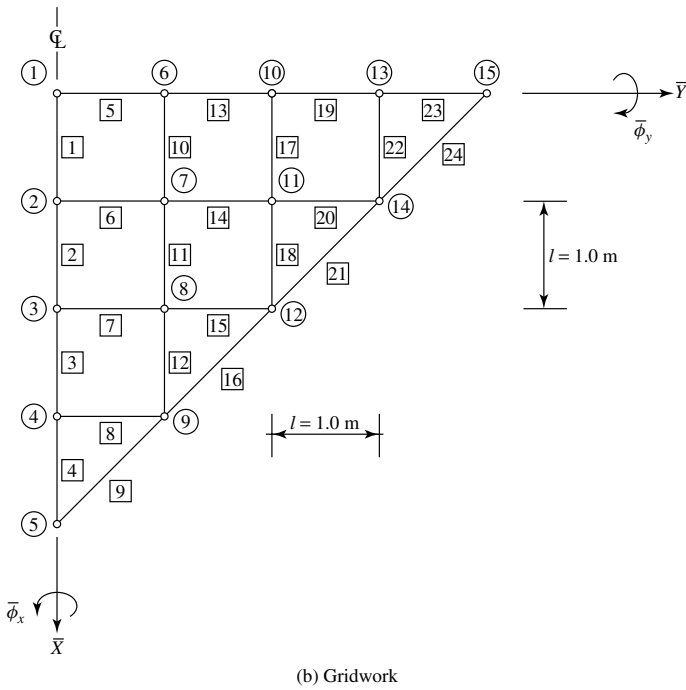
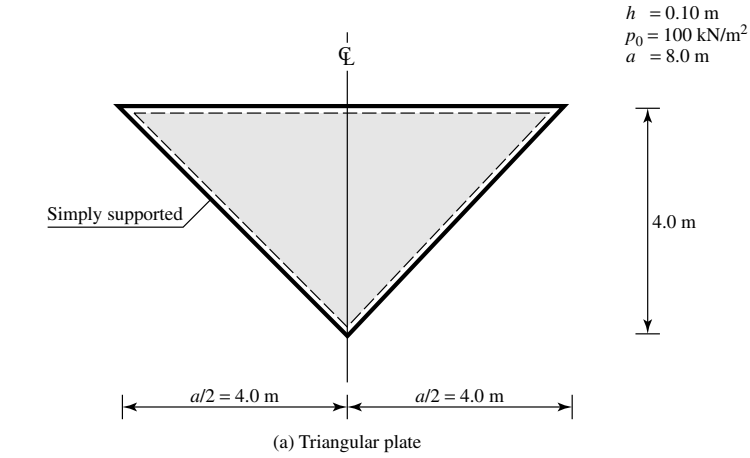


Figure 6.4.8 Gridwork representation of triangular plate.

and

$$I_5 = \frac{D\ell}{2E} \cot 45^\circ = 4166 \text{ cm}^4 = I_2,$$
$$I_{t,5} = \frac{D\ell}{2G} \cot 45^\circ = 8333 \text{ cm}^4 = I_{t,2}.$$

(6.4.18)

Coordinates of the joint points are listed in Table 6.4.4. Identification of the equivalent beams and their specific types, which include information concerning their equivalent cross-sectional properties, is given in Table 6.4.5. Boundary conditions of the joint points are given in Table 6.4.6. The joint loads are summarized in Table 6.4.7. In this case the “statically equivalent” load approximation was applied. Furthermore, loads acting on joints without freedom in the lateral direction have been eliminated, since they do not influence the deflection pattern.

Table 6.4.4 Coordinates

<i>Joint</i>	\bar{x}	\bar{y}	<i>Joint</i>	$\bar{\psi}$	\bar{y}
1	0.00	0.00	9	3.00	1.00
2	1.00	0.00	10	0.00	2.00
3	2.00	0.00	11	1.00	2.00
4	3.00	0.00	12	2.00	2.00
5	4.00	0.00	13	0.00	3.00
6	0.00	1.00	14	1.00	3.00
7	1.00	1.00	15	0.00	4.00
8	2.00	1.00			

Our gridwork program [6.4.24] has yielded the following joint point displacements:

$$\bar{\mathbf{w}} = \left\{ \begin{array}{c} 0.000 \\ 2.515 \\ 2.759 \\ 1.271 \\ 0.000 \\ 0.000 \\ 2.035 \\ 1.915 \\ 0.000 \\ 0.000 \\ 0.919 \\ 0.000 \\ 0.000 \\ 0.000 \\ 0.000 \end{array} \right\} \text{ cm.}$$

(6.4.19)

Table 6.4.5 Identification of Beams

<i>Beam</i>	<i>Joints</i>	<i>Type</i>	<i>Beam</i>	<i>Joints</i>	<i>Type</i>
1	1–2	2	13	6–10	2
2	2–3	2	14	7–11	1
3	3–4	2	15	8–12	1
4	4–5	2	16	9–12	3
5	1–6	2	17	10–11	1
6	2–7	1	18	11–12	1
7	3–8	1	19	10–13	2
8	4–9	1	20	11–14	1
9	5–9	3	21	12–14	3
10	6–7	1	22	13–14	1
11	7–8	1	23	13–15	2
12	8–9	1	24	14–15	3

Table 6.4.6 Boundary Conditions

<i>Joint</i>	\bar{w} Locked	$\bar{\phi}_x$ Locked	$\bar{\phi}_y$ Locked
1	y	y	n
2	n	y	n
3	n	y	n
4	n	y	n
5	y	y	n
6	y	y	n
9	y	n	n
10	y	y	n
12	y	n	n
13	y	y	n
14	y	n	n
15	y	y	n

Note: y = yes; n = no.

Table 6.4.7 Joint Loads

<i>Joint</i>	P_x	M_x	M_y
1	0.00	–6.25	6.25
2	50.00	–12.50	0.00
3	50.00	–12.50	0.00
4	50.00	–12.50	0.00
5	0.00	–2.10	–4.17
6	0.00	0.00	12.50
7	100.00	0.00	0.00
8	100.00	0.00	0.00
9	50.00	6.50	6.50
10	0.00	0.00	12.50
11	100.00	0.00	0.00
12	50.00	6.50	6.50
13	0.00	0.00	12.50
14	50.00	6.50	6.50
15	0.00	0.00	2.10

A comparison of the computed maximal lateral deflection $\bar{w}_3 = 2.759$ cm with its more exact analytically obtained value of $\bar{w}_{\max} = 2.662$ cm shows a relatively small error of 3.6%. The maximum bending moment[†] that occurs at point 2 has been computed, again, using the ordinary FDM. This gives

$$m_{x,\max} = -\frac{D}{\ell^2} (-2\bar{w}_2 + \bar{w}_3) = 56.77 \text{ kN-m/m.} \quad (6.4.20)$$

This moment has a still acceptable error of -5% . Using smaller mesh widths, of course, even these small errors will also decrease.

ILLUSTRATIVE EXAMPLE III

Let us consider a uniformly loaded square plate with simply supported edges as shown in Fig. 6.4.9a. Using the gridwork cell given in Table 6.3.2 with $a = b = L/4 = 0.75$ m grid size, let us determine the deflected plate surface $w(x, y)$ at various joint points and compute the maximum bending moment m_{\max} . Poisson's ratio $\nu = \frac{1}{3}$.

Since both the structure and load have double symmetry, we can analyze only one-quarter of the plate by assigning *guided*[‡] boundary conditions at the planes of symmetry. The unknown displacements $\bar{\mathbf{d}}$ that can occur at the joint points of the quarter plate are shown and numbered in Fig. 6.4.9b.

For a square gridwork cell ($a = b$) the element stiffness matrix becomes

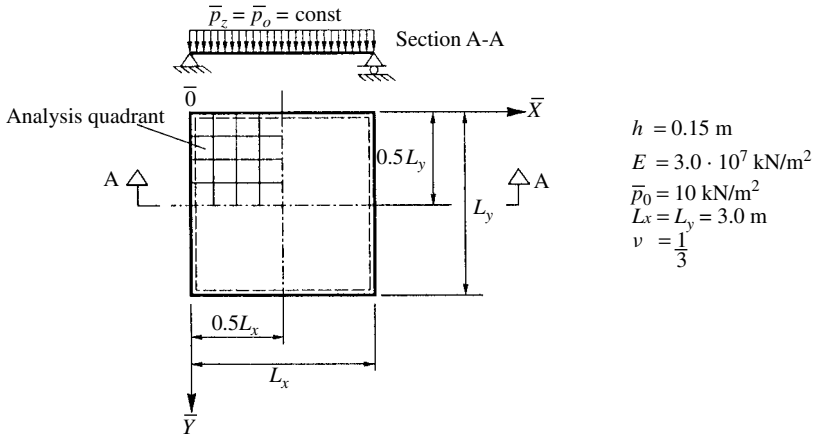
$$\bar{\mathbf{K}}_e^{(N)} = \frac{Eh^3}{12(1+\nu)} \times \begin{bmatrix} 15/a^2 & & & & & & & & & & \\ 4.5/a & 3.0 & & & & & & & & & \\ -4.5/a & -1.0 & 3.0 & & & & & & & & \\ -6./a^2 & 0.0 & 3/a & 15/a^2 & & & & & & & \\ 0.0 & 0.0 & 0.0 & 4.5/a & 3.0 & & & & & & \\ -3/a & 0.0 & 1.0 & 4.5/a & 1.0 & 3.0 & & & & & \\ -3/a^2 & -1.5/a & 1.5/a & -6/a^2 & -3/a & 0.0 & 15/a^2 & & & & \\ 1.5/a & 0.5 & -0.5 & 3/a & 1.0 & 0.0 & -4.5/a & 3.0 & & & \\ -1.5/a & -0.5 & 0.5 & 0.0 & 0.0 & 0.0 & 4.5/a & -1.0 & 3.0 & & \\ -6/a^2 & -3/a & 0.0 & -3/a^2 & -1.5/a & -1.5/a & -6/a^2 & 0.0 & -3/a & 15/a^2 & \\ 3/a & 1.0 & 0.0 & 1.5/a & 0.5 & 0.5 & 0.0 & 0.0 & 0.0 & -4.5/a & 3.0 \\ 0.0 & 0.0 & 0.0 & 1.5/a & 0.5 & 0.5 & 3/a & 0.0 & 1.0 & -4.5/a & 1.0 & 3.0 \end{bmatrix} \quad (6.4.21)$$

Next, we substitute the given value for a into this matrix, and using the *code number technique*, we renumber the joint displacements to conform to the global numbering shown in Fig. 6.4.9b. This gives

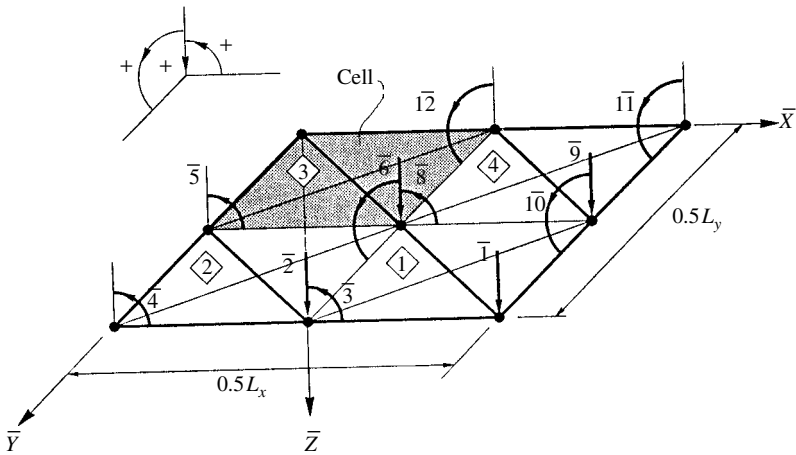
[†] In the subscript, we used the notation of classical plate theory.

[‡] See Fig. 5.1.5d.

Cell Number	1	2	3	4	5	6	7	8	9	10	11	12	Local number
1	$\bar{6}$	$\bar{7}$	$\bar{8}$	$\bar{9}$	$\bar{10}$	$\bar{0}$	$\bar{1}$	$\bar{0}$	$\bar{0}$	$\bar{2}$	$\bar{0}$	$\bar{3}$	Global number
2	$\bar{0}$	$\bar{0}$	$\bar{5}$	$\bar{6}$	$\bar{7}$	$\bar{8}$	$\bar{2}$	$\bar{0}$	$\bar{3}$	$\bar{0}$	$\bar{0}$	$\bar{4}$	
3	$\bar{0}$	$\bar{0}$	$\bar{0}$	$\bar{0}$	$\bar{12}$	$\bar{0}$	$\bar{6}$	$\bar{7}$	$\bar{8}$	$\bar{0}$	$\bar{0}$	$\bar{5}$	
4	$\bar{0}$	$\bar{12}$	$\bar{0}$	$\bar{0}$	$\bar{11}$	$\bar{0}$	$\bar{9}$	$\bar{10}$	$\bar{0}$	$\bar{6}$	$\bar{7}$	$\bar{8}$	



(a) Plate problem



(b) Substitute system

Figure 6.4.9 Plate and its substitute system.

During this renumbering process, those displacements that cannot take place on the substitute structure have obtained *zero* designations, indicating that their corresponding rows and columns should be struck from the pertinent element stiffness matrices. Adding the element stiffness coefficients that have the same global subscripts, the stiffness matrix of the total structure is determined. Now, if we lump the uniformly distributed load at the joints, we obtain the governing matrix equation of this problem:

$$\frac{Eh^3}{12(1+\nu)} \begin{bmatrix} 6.6667 & & & & & & & & & & & \\ -2.6667 & 13.3333 & & & & & & & & & & \\ 2.0 & 0 & 6.0 & & & & & & & & & \\ 0 & 2.0 & 1.0 & 3.0 & & & & & & & & \\ 0 & 1.0 & 0.5 & 0 & 6.0 & & & & & & & \\ -1.3333 & -5.3333 & 0 & 1.0 & 4.0 & 26.6667 & & & & & & \\ -1.0 & -4.0 & 0 & 0.5 & 0 & 0 & 12.0 & & & & & \\ 1.0 & 0 & 0 & 0.5 & 2.0 & 0 & 0 & 12.0 & & & & \\ -2.6667 & -1.3333 & 1.0 & 0 & 0 & -5.3333 & 0 & 4.0 & 13.3333 & & & \\ -2.0 & -1.0 & 0.5 & 0 & 0 & 0 & 0 & 0 & 0 & 6.0 & & \\ 0 & 0 & 0 & 0 & 0 & -1.0 & 0.5 & 0.5 & -2.0 & 1.0 & 3.0 & \\ 0 & 0 & 0 & 0 & 0.5 & -4.0 & 2.0 & 0 & -1.0 & 0.5 & 0 & 6.0 \end{bmatrix} \begin{Bmatrix} \bar{d}_1 \\ \bar{d}_2 \\ \bar{d}_3 \\ \bar{d}_4 \\ \bar{d}_5 \\ \bar{d}_6 \\ \bar{d}_7 \\ \bar{d}_8 \\ \bar{d}_9 \\ \bar{d}_{10} \\ \bar{d}_{11} \\ \bar{d}_{12} \end{Bmatrix} = \begin{Bmatrix} 5.625 \\ 11.25 \\ 0 \\ -1.40625 \\ -2.8125 \\ 22.5 \\ 0 \\ 0 \\ 11.25 \\ 0 \\ 1.40625 \\ 2.8125 \end{Bmatrix} \begin{matrix} \bar{1} \\ \bar{2} \\ \bar{3} \\ \bar{4} \\ \bar{5} \\ \bar{6} \\ \bar{7} \\ \bar{8} \\ \bar{9} \\ \bar{10} \\ \bar{11} \\ \bar{12} \end{matrix} \quad (6.4.22)$$

The solution of Eq. (6.4.22) gives the column matrix of the joint displacements:

$$\bar{\mathbf{d}} = \begin{Bmatrix} 5.55766 \\ 4.02009 \\ 1.99195 \\ 3.06314 \\ 2.23316 \\ 2.91894 \\ 1.43098 \\ -1.43098 \\ 4.02009 \\ 1.99195 \\ 3.06314 \\ 2.23316 \end{Bmatrix} \times 10^{-3} \text{ m and rad.} \quad (6.4.23)$$

The deflected plate surface is shown in Fig. 6.4.10. The obtained maximum deflection \bar{w}_1 has an error of merely 0.3%. The maximum bending moment is calculated using the ordinary FDM. Equation (5.1.12) gives

$$\begin{aligned}
 \max m_x &= -\frac{3 \times 10^7 \times 0.15^3}{12[1 - (1/3)^2]} \frac{1}{1.5^2} [(4.02009 - 5.55766) \times 10^{-3} \\
 &\quad + 2\frac{1}{3}(4.02009 - 5.55766) \times 10^{-3}] \\
 &= 4218.75(-3.07514 - \frac{1}{3}3.07514) \times 10^{-3} \\
 &= 17.298 \text{ kNm/m} \quad (\text{error: } 0.31\%). \quad (6.4.24)
 \end{aligned}$$

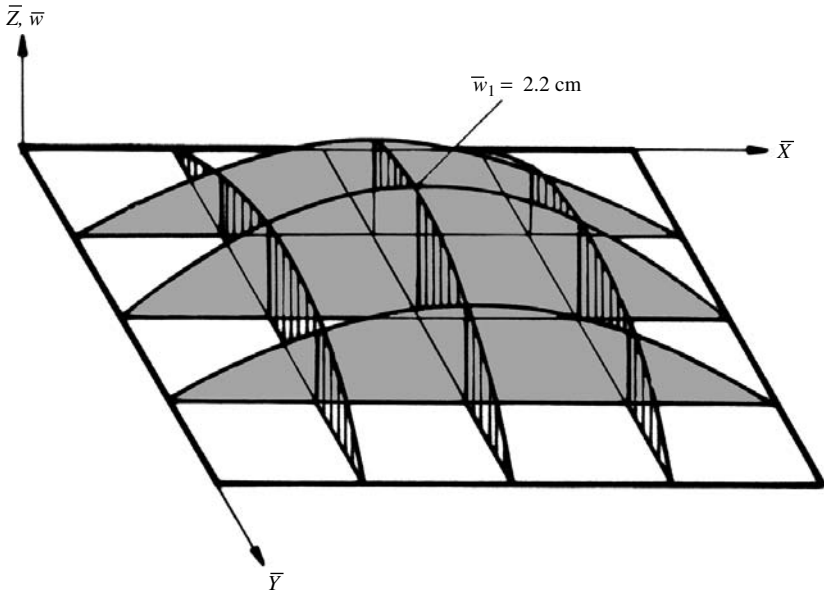


Figure 6.4.10 Deflected plate surface.

Again, a comparison with its analytically obtained more exact value shows only a negligible discrepancy of 0.31%.

ILLUSTRATIVE EXAMPLE IV

Let us solve the preceding plate problem again, but this time we use the gridwork cell given in Table 6.3.3. In this case, the element stiffness matrix becomes

$\mathbf{K}_e^{(N)} =$

1	50,612											
2	18,979	23,724										
3	-18,979	0	23,724									
4	-25,306	0	18,979	50,612								
5	0	-4744	0	18,979	23,724							
6	-18,979	0	9489	18,979	0	23,724						
7	0	0	0	-25,306	-18,979	0	50,612					
8	0	0	0	18,979	9489	0	-18,979	23,724				
9	0	0	0	0	0	-4744	18,979	0	23,724			
10	-25,306	-18,979	0	0	0	0	-25,306	0	-18,979	50612		
11	18,979	9489	0	0	0	0	0	-4744	0	-18,979	23,724	
12	0	0	-4744	0	0	0	18,979	0	9489	-18,979	0	23,724
	1	2	3	4	5	6	7	8	9	10	11	12

Symmetric

$E = 3 \times 10^7 \text{ kN/m}^2$
 $\nu = 0.33$
 $h = 0.15 \text{ m}$

(6.4.25)

Using the same code numbers as in Illustrative Example III, the stiffness matrix of the substitute structure becomes

$\bar{\mathbf{K}} =$

1	50,612											
2	-25,306	101,224										
3	18,979	0	47,449									
4	0	18,979	9489	23,724								
5	0	0	0	-4744	47,449							
6	0	-50,612	0	0	37,959	202,449						
7	0	-37,959	0	0	0	0	94,898					
8	0	0	-9489	0	18,979	0	0	94,898				
9	-25,306	0	0	0	0	-50,612	0	37,959	101,224			
10	-18,979	0	0	0	0	0	-9489	0	0	47,449		
11	0	0	0	0	0	0	0	0	-18,979	9489	23,724	
12	0	0	0	0	0	-37,959	18,979	0	0	0	-4744	47,449
	1	2	3	4	5	6	7	8	9	10	11	12

Symmetric

(6.4.26)

Since the column vector of the loads also remains the same as in Eq. (6.4.23), solution of the governing matrix equation yields the following displacement components:

$$\bar{\mathbf{d}} = \begin{Bmatrix} 0.00580 \\ 0.00420 \\ -0.00199 \\ -0.00306 \\ -0.00223 \\ 0.00303 \\ 0.00143 \\ -0.00143 \\ 0.00420 \\ 0.00199 \\ 0.00306 \\ 0.00223 \end{Bmatrix} \begin{matrix} \bar{1} \\ \bar{2} \\ \bar{3} \\ \bar{4} \\ \bar{5} \\ \bar{6} \\ \bar{7} \\ \bar{8} \\ \bar{9} \\ \bar{10} \\ \bar{11} \\ \bar{12} \end{matrix} \quad \text{m and rad.} \quad (6.4.27)$$

The maximum lateral displacement $\bar{w}_{\max} = \bar{w}_1 = 0.0058 \text{ m}$ (error 2.3.%) and using the ordinary FDM the computed maximum bending moment show only relatively small errors.

$$\begin{aligned} m_x, \max &= -4218.75[2(4.2 - 5.8)10^{-3} + \frac{2}{3}(4.2 - 5.8)10^{-3}] \\ &= 18.0 \left[\frac{\text{kN}}{\text{m}} \right] \quad (\text{error: 4.4\%}). \end{aligned} \quad (6.4.28)$$

References and Bibliography

- [6.4.1] PRZEMIENIECKI, J. S., *Theory of Matrix Structural Analysis*, McGraw-Hill Book Co., New York, 1968.
- [6.4.2] BEAUFAT, F. W., et al., *Computer Methods of Structural Analysis*, Prentice-Hall, Englewood Cliffs, New Jersey, 1970.
- [6.4.3] MEEK, J. L., *Matrix Structural Analysis*, McGraw-Hill Book Co., New York, 1971.
- [6.4.4] AZAR, J. J., *Matrix Structural Analysis*, Pergamon Press, New York, 1972.
- [6.4.5] VANDERBILT, M. D., *Matrix Structural Analysis*, Quantum Publishers, New York, 1974.
- [6.4.6] KARDESTUNCER, H., *Elementary Matrix Analysis of Structures*, MacGraw-Hill Book Co., New York, 1974.
- [6.4.7] NORRIS, C. H., et al., *Elementary Structural Analysis*, 3rd ed., MacGraw-Hill Book Co., New York, 1976.
- [6.4.8] WILLEMS, N., and LUCAS, W. M., *Structural Analysis for Engineers*, MacGraw-Hill Book Co., New York, 1978.
- [6.4.9] GHALI, A., and NEVILLE, A. M., *Structural Analysis: A Unified Classical and Matrix Approach*, 2nd ed., Chapman & Hall, London, 1978.
- [6.4.10] MEYERS, V. J., *Matrix Analysis of Structures*, Harper & Row, New York, 1983.
- [6.4.11] WEAVER, W., and GERE, J. M., *Matrix Analysis of Framed Structures*, 3rd ed., Van Nostrand Reinhold, New York, 1990.
- [6.4.12] HARRISON, H. B., *Structural Analysis and Design*, 2nd ed., Pergamon Press, Oxford, 1990.
- [6.4.13] SMITH, I. M., and GRIFFITHS, D. V., *Programming the Finite Element Method*, 2nd ed., John Wiley & Sons, Chichester, United Kingdom, 1988.

- [6.4.14] SCHWARZ, H. R., *FORTRAN-Programme zur Methode der finiten Elemente*, 3rd ed., Teubner, Stuttgart, 1991.
- [6.4.15] SZILARD, R., *Finite Berechnungsmethoden der Strukturmechanik*, Vol. 1: *Stabwerke*, Ernst & Sohn, Berlin, 1982.
- [6.4.16] PRESS, W. H., et al., *Numerical Recipes in FORTRAN: The Art of Scientific Computing*, 2nd ed., Cambridge University Press, Cambridge, Massachusetts, 1992.
- [6.4.17] BATHE, K.-J., and WILSON, E. L., *Numerical Methods in Finite Element Analysis*, Prentice-Hall, Englewood Cliffs, New Jersey, 1976.
- [6.4.18] GRIFFITHS, D. V., and SMITH, G. M., *Numerical Methods for Engineers*, CRC Press, Boca Raton, Florida, 1991.
- [6.4.19] BATHE, K.-J., *Finite Element Procedures in Engineering Analysis*, Prentice-Hall, Englewood Cliffs, New Jersey, 1982.
- [6.4.20] BREBBIA, C. A., and FERRANTE, A. J., *Computational Methods for the Solution of Engineering Problems*, 2nd ed., Pentech Press, London, 1979.
- [6.4.21] JAMES, M. L., SMITH, G. M., and WOLFORD, J. C., *Applied Numerical Methods for Digital Computation with FORTRAN and CSMP*, 2nd ed., Individual Education Plan, New York, 1977.
- [6.4.22] RALSTON, A., and WILF, H. S., *Mathematical Methods for Digital Computers*, John Wiley & Sons, New York, 1964.
- [6.4.23] MORO, D. M., *FORTRAN 77*, Edward Arnold, London, 1982.
- [6.4.24] SZILARD, R., et al., *Turbo-Basic Programme für Baumechanik und Statik*, Ernst & Sohn, Berlin, 1989.
- [6.4.25] TEZCAN, S. S., "Discussion of the Simplified Formulation of Stiffness Matrices," *J. Struct. Div., ASCE*, 89 (1963), 445–449.
- [6.4.26] WEST, R., *Recommendations on the Use of Grillage Analysis for Slab and Pseudo-Slab Bridges*, Cement & Concrete Association, London, 1973.
- [6.4.27] COPE, R. J., and CLARK, L. A., *Concrete Slabs: Analysis and Design*, Elsevier, London, 1984.
- [6.4.28] HABLY, E. C., *Bridge Deck Behaviour*, Chapman & Hall, London, 1991.
- [6.4.29] NATIONAL INSTITUTE OF SCIENCE AND TECHNOLOGY, *CMLIB, Core Mathematics Library*, <http://gams.nist.gov>.
- [6.4.30] NUMERICAL ALGORITHMS GROUP, *Libraries and Programs*, Mayfield House, Oxford, United Kingdom, 1999.
- [6.4.31] ROSS, C. T. F., *Finite Element Programs in Structural Engineering and Continuum Mechanics*, Albion Publishing, Chister, United Kingdom, 1996.

6.5 Summary and Conclusions

The gridwork method presented in this chapter is a simple, very transparent and yet highly versatile numerical technique for the analysis of diverse plate problems. The method replaces the continuum of plates by a system of interconnected beams endowed with *equivalent* cross-sectional properties. For determination of these properties, one of the following approaches can be applied: (a) comparing the differential equation of plates with that of the equivalent gridwork systems, (b) equating the strain energy expressions of plates and gridworks and (c) employing the equal deformation principle for the two systems. In any case, determination of these equivalent cross-sectional properties often involves tedious high-level research. Consequently, it should not be routinely attempted by the analyst unless a definite need exists for it. For instance, derivation of such properties for moderately thick plates could be considered a worthwhile but time-consuming undertaking.

Fortunately, a sufficient number of equivalent cross-sectional properties are readily available in the pertinent literature. Thus, their determination is seldom required. With

these known beam properties, the analysis procedure follows either the well-known matrix displacement method for framed structures or the equally familiar stiffness approach combined with the code number technique if *gridwork cells* are employed in the computation.[†] Gridwork cells represent finite beam units of various geometrical configurations. The beams in these cells are interconnected at their joints. In the analysis, we use the stiffness matrices of such cells, which can also be substituted for element stiffness in a corresponding finite element computer programs. In both cases, all lateral loads must be reduced to equivalent joint loads.

Various gridwork models were presented in this chapter. Their merits are simplicity, versatility and efficiency. That is, plates of arbitrary shape, loadings and boundary conditions can be easily analyzed by applying conventionally available computer programs for gridworks or three-dimensional frames. In particular, Salonen's rectangular and triangular models are noteworthy, since they provide rapid and fairly accurate solutions for many difficult plate problems. It is recommended that in the case of arbitrary plate geometry the interior domain should be discretized by using rectangular units, while at the edges triangular units should be employed. With the decrease of mesh sizes, the method produces solutions approaching the exact values. Last, but not least, the gridwork method can provide an entirely independent check of the results of other numerical methods.

Finally, we should also mention the few minor drawbacks associated with the gridwork method:

- (a) While the deflected plate surface can be determined with relative ease, this is not the case when it is necessary to also compute the stress resultants. As demonstrated, the FDM offers a valuable alternative to mitigate this problem.
- (b) Computer programs for either gridwork or finite element analysis are required. An exception to this is the solution of a relatively simple plate problem employing the stiffness matrices of gridwork cells. In this case, only an equation solver is required.
- (c) Strictly speaking, the various equivalent cross-sectional properties are valid for a fixed Poisson ratio ($\nu = \frac{1}{3}$ or $\nu = 0$). In general, this restriction does not create major problems in practical plate analysis, since clamped arbitrarily shaped and simply supported straight boundaries are independent of ν . In addition, with the formulas given in Section A.2, one can also approximate the effects of other Poisson ratios.
- (d) Since at each joint three displacement components are considered, the resulting matrix displacement equations are considerably greater than in the FDM.

Problems‡

- 6.3.1.** Verify the value of the stiffness coefficient k_{11} in Table 6.3.3. Assume that $D_x = D_y = D$.
- 6.3.2.** Verify the value of the stiffness coefficient k_{13} in Table 6.3.3.
- 6.4.1.** Using a computer program for gridworks in combination with Eq. (6.2.7), determine the deflected plate surface and the maximum positive bending

[†] As demonstrated in Illustrative Examples III and IV.

[‡] The first two numbers refer to the corresponding section.

moment of a uniformly loaded square plate. Assume the following dimensions and elastic properties for the plate: $p_0 = 50 \text{ kN/m}^2$, $h = 0.2 \text{ m}$, $E = 30,000,000 \text{ kN/m}^2$ and $\nu = 0$.

- 6.4.2.** Re-solve problem 6.4.1, this time using the equivalent cross-sectional properties given in Eq. (6.2.1).
- 6.4.3.** Solve the plate problem shown in Fig. 5.2.17 by means of the gridwork method. Use a computer program for gridworks and Eq. (6.2.6) for the equivalent cross-sectional properties.
- 6.4.4.** Select a uniformly loaded, simply supported plate of triangular shape. Determine the maximum lateral deflection of this plate by the gridwork method. Use a computer program for gridworks and Eq. (6.2.6) for the equivalent cross-sectional properties.
- 6.4.5.** Solve problem 6.4.4 but assume that the plate boundaries are fixed.
- 6.4.6.** Determine the deflected plate surface and the maximum positive and negative bending moments of the continuous plate shown in Fig. 5.1.20. Use Eq. (6.2.6) and a computer program for gridworks.
- 6.4.7.** Determine the maximum lateral deflection of the square plate shown in Fig. 5.1.19. Use the gridwork cell given in Table 6.3.3.
- 6.4.8.** Solve the plate problem shown in Fig. 5.2.16 using the stiffness coefficients of a square gridwork cell given in Eq. (6.4.21). Determine the maximum bending moment by means of the FDM.
- 6.4.9.** Design a continuous reinforced-concrete plate bridge with two equal spans. Assume that four concentrated forces represent the moving truck load. This structure should be analyzed by the gridwork method using Eq. (6.2.7) and a computer program for gridworks. Determine the maximum negative and positive moments with the help of the ordinary FDM.

7

Finite Element Method

7.1 Introduction and Brief History of the Method

During the past three decades, the *finite element method* (FEM) has rapidly become the most dominant numerical technique in almost all fields of engineering and applied science. Its present popularity can be attributed to the following major factors:

- It is *familiar* to engineers. That is, the FEM evolved as an extension of the earlier established matrix displacement analysis of framed structures, in which the structure is represented as an assemblage of bar and beam elements. The same concepts and matrix operations are used in the FEM. But instead of beam elements, discrete pieces of continua are employed to represent the surface-type structural system.
- The FEM used in computation closely represents the actual continuum and thus is *easy to visualize*. The same can be said for the support and load conditions. Such essential *simplicity* in modeling greatly contributes to its popularity.
- The general availability and greatly increased power of *personal computers* have facilitated the use of numerical methods in everyday engineering analysis. These personal computers with their unprecedented memory and speed have brought the FEM within the reach of every engineer.
- Once a general computer *program* for displacement analysis[†] of structures is written, it can be easily modified to solve diverse problems in continuum mechanics, since the basic matrix operations—for which subroutines are readily available—remain the same. Furthermore, the simple logic of the FEM makes it ideally suited for “structured” computer programming. Consequently, numerous FEM programs are commercially available.
- The FEM is *versatile and flexibility*. That is, the continuum may have arbitrary shape, supports and loading conditions. Even in such a complex case, the FEM

[†] In this book we deal exclusively with the finite element displacement method, since it is the most widely used finite element technique.

delivers a realistic solution. Common applications include linear and nonlinear static, dynamic and stability problems in the fields of structural, mechanical, naval, mining, and aerospace engineering.

The classical methods discussed in the first part of this book consider plates as a continua, the behaviors of which are governed by corresponding partial differential equations (PDEs). Analytical solutions of these PDEs, however, are limited to the simplest cases. But in engineering practice, the shape of the plates and their support and loading conditions are often arbitrary. Analytical solutions of such “real-life” problems are mostly very difficult or even impossible. The FEM, on the other hand, considers the continuum of a plate as an assembly of finite size particles, and the overall response of such a system is obtained by formulating simultaneous algebraic equations that can be readily solved by a computer. An unsophisticated analogy of the FEM is a comparison with the mosaic technique used for discrete representation of pictures. In our case, the finite size particles of the continuum are called *finite elements*. The behavior of each such element is described in a simple way. These elements are reconnected by *nodes* that act as a binding mechanism to hold the discretized system together. A more sophisticated description of the FEM considers it as a *piecewise polynomial interpolation* used in connection with energy theorems, as treated in subsequent sections.

In the application of the FEM for the analysis of any problems of physical continua, the following steps are routinely applied:

1. discretization of the continuum,
2. selection of suitable shape functions,
3. element formulation,
4. treatment of the boundary conditions and loads,
5. assembly of the discretized system,
6. solution of the resulting system of equations and
7. computation of the stress resultants.

We may use the FEM in three ways: (a) setting up a relatively simple plate problem “by hand” and solving the resulting simultaneous equations with the help of an advanced scientific calculator with built-in equation solver, (b) generating and writing the required computer codes employing available subroutines and (c) using commercially available finite element program systems.

The origins of the FEM are well known by now. This important numerical technique first appeared in the 1950s for the stress analysis of aircraft structures. Long before this, however, the mathematician Courant introduced [7.1.1] a *piecewise polynomial* solution of St.-Venant torsional problems applying an energy theorem in combination with triangular elements. He assumed a linear distribution of the warping functions among these elements. This approach can be viewed as an extension of the Rayleigh-Ritz method. Consequently, Courant was the first to establish the *mathematical foundation* of the method. Unfortunately, this important work was unnoticed by engineers, since the procedure appeared to be impractical at the time due to the lack of digital computers, which are required for solution of the resulting large number of simultaneous algebraic equations.

Prior to that, most of the essential ideas of the FEM can be found in Hrennikoff's framework solution of stress problems related to elastic continua [7.1.2, 7.1.3]. Using the "lattice analogy" that replaces the original continuum by a system of elastic bars and beams, Hrennikoff extended the well-established method for matrix displacement analysis of framed structures to plates and shells. But instead of an infinite number of displacement components as are present in the original system, the substitute framework deals only with a finite number of degrees of freedom. Based on the equivalent elastic properties of such bars and beams in the substitute structure, the displacements of the framework can closely approximate those of the original continuum. Furthermore, if we consider the use of framework cells as described in the previous chapter, we can state that the *forerunner* of the FEM was the framework approach to stress problems of continua.

As its framework counterpart, the FEM grew out of the matrix displacement method for structural analysis. Instead of bars and beams, this time an assembly of small particles of the continuum was used to obtain the overall response of the original system. During its early development for stress analysis of aircraft structures, the method relied heavily on engineering intuitions. The continuum was assumed to be composed of small (finite) *elements* physically connected only at a number of *nodal* points. The comprehensive treatment of energy theorems by Argyris [7.1.4, 7.1.5] established the foundation for the derivation of an element stiffness matrix for rectangular panels under plane stress. Clough and his co-workers, employing a direct engineering analogy between a framed structure and a discretized continuum, introduced the method to practicing structural engineers. Their classical paper [7.1.6] describes the FEM for analyzing delta wings of airplanes. The term "finite element method" was coined in 1960. Later, Melosh established the connection between the FEM and certain energy approaches [7.1.7]. In 1967 Zienkiewicz and Cheung published the first book on the FEM [7.1.8]. Since then, the method has become firmly established as an indispensable tool for engineers and scientists. Besides its original structural-mechanical applications, the FEM is now used for solution of such diverse problems as steady-state heat conduction, fluid dynamics and numerical solution of PDEs of mathematical physics, to name a few.

During the decade 1960–1970, further development of the FEM emphasized the improvement of various elements combined with the creation of large general-purpose computer program systems. By mid-1990, roughly 40,000 papers and more than a hundred books had been published about the method. Of these books, 87 are listed here [7.1.8–7.1.95] approximately in chronological order.

References and Bibliography

- [7.1.1] COURANT, R., "Variational Methods for the Solution of Problems of Equilibrium and Vibration," *Bull. Am. Math. Soc.*, 49 (1943), 1–23.
- [7.1.2] HRENNIKOFF, A., "Plane Stress and Bending of Plates by Articulated Framework," Ph.D. Thesis, Massachusetts Institute of Technology, Boston, Massachusetts, 1940.
- [7.1.3] HRENNIKOFF, A., "Solution of Problems of Elasticity by Framework Method," *J. Appl. Mech.*, 8 (1941), A169–A175.
- [7.1.4] ARGYRIS, J. H., and KELSEY, S., *Energy Theorems and Structural Analysis*, Butterworths, London, 1960.
- [7.1.5] ARGYRIS, J. H., and KELSEY, S., *Modern Fuselage Analysis and the Elastic Aircraft*, Butterworths, London, 1963.

- [7.1.6] TURNER, M. J., CLOUGH, R. W., MARTIN, H. C., and TOPP, L. J., "Stiffness and Deflection Analysis of Complex Structures," *J. Aeronaut. Sci.*, 23 (1956), 805–824.
- [7.1.7] MELOSH, R. J., "Development of Stiffness Method to Bound Elastic Behavior of Structures," Ph.D. Thesis, University of Washington, Seattle, Washington, 1962.
- [7.1.8] ZIENKIEWICZ, O. C., and CHEUNG, Y. K., *The Finite Element Method in Structural and Continuum Mechanics*, McGraw-Hill Book Co., London, 1967.
- [7.1.9] HOLLAND, I., and BELL, K. (Eds.), *Finite Element Methods in Stress Analysis*, Tapir, Trondheim, Norway, 1967.
- [7.1.10] ROWAN, W. H., and HACKETTS, R. M. (Eds.), *Application of Finite Element Methods in Civil Engineering*, Vanderbilt University Press, Nashville, Tennessee, 1969.
- [7.1.11] TOTTENHAM, H., and BREBBIA, C. (Eds.), *Finite Element Techniques in Structural Mechanics*, Stress Analysis Publ., Southampton, United Kingdom, 1970.
- [7.1.12] ZIENKIEWICZ, O. C., *The Finite Element Method in Engineering Science*, McGraw-Hill Book Co., London, 1971.
- [7.1.13] SMITH, G. N., *An Introduction to Matrix Finite Element Methods in Civil Engineering*, Applied Science Publ., London, 1971.
- [7.1.14] ODEN, J. T., *Finite Elements of Nonlinear Continua*, McGraw-Hill Book Co., New York, 1972.
- [7.1.15] DESAI, C. S., and ABEL, J., *Introduction to the Finite Element Method*, Van Nostrand Reinhold Co., New York, 1972.
- [7.1.16] AZIZ, A. K. (Ed.), *The Mathematical Foundation of the Finite Element Method with Applications to Partial Differential Equations*, Academic Press, New York, 1972.
- [7.1.17] URAL, O., *Finite Element Method*, Intex Ed. Publ., New York, 1973.
- [7.1.18] ROBINSON, J., *Integrated Theory of Finite Element Methods*, John Wiley & Sons, London, 1973.
- [7.1.19] BUCK, K. E., et al. (Eds.), *Finite Elemente in der Statik*, W. Ernst & Sohn, Berlin, 1973.
- [7.1.20] MARTIN, H. C., and CAREY, G. F., *Introduction to the Finite Element Analysis*, McGraw-Hill Book Co., New York, 1973.
- [7.1.21] ODEN, J. T., and OLIVEIRA, E. R. A. (Eds.), *Lectures on Finite Element Methods in Continuum Mechanics*, University of Alabama, Huntsville, Alabama, 1973.
- [7.1.22] STRANG, G., and FIX, G. J., *An Analysis of the Finite Element Method*, Prentice-Hall, Englewood Cliffs, New Jersey, 1973.
- [7.1.23] NORRIE, D. H., and DE URIES, G., *The Finite Element Method: Fundamentals and Applications*, Academic Press, New York, 1973.
- [7.1.24] COOK, R. D., *Concepts and Applications of Finite Element Analysis*, John Wiley & Sons, New York, 1974.
- [7.1.25] BREBBIA, C. A., and CONNOR, J. J., *Fundamentals of Finite Element Techniques*, John Wiley & Sons, New York, 1974.
- [7.1.26] HUEBNER, K., *The Finite Element Method for Engineers*, John Wiley & Sons, New York, 1975.
- [7.1.27] GALLAGHER, R. H., *Finite Element Analysis Fundamentals*, Prentice-Hall, Englewood Cliffs, New Jersey, 1975.
- [7.1.28] KOLAR, V., et al., *Berechnungen von Flächen- und Raumtragwerken nach der Methode der finiten Elemente*, Springer-Verlag, Berlin, 1975.
- [7.1.29] HAHN, H. G., *Methode der finiten Elemente in der Festigkeitslehre*, Akademische Verlagsgesellschaft, Wiesbaden, 1975.
- [7.1.30] ASHWELL, D. G., and GALLAGHER, R. H. (Eds.), *Finite Elements for Thin Shells and Curved Members*, John Wiley & Sons, London, 1976.
- [7.1.31] SEGERLUND, L. J., *Applied Finite Element Analysis*, John Wiley & Sons, New York, 1976.
- [7.1.32] BATHE, K.-J., and WILSON, E. L., *Numerical Methods in Finite Element Analysis*, Prentice-Hall, Englewood Cliffs, New Jersey, 1976.
- [7.1.33] ZIENKIEWICZ, O. C., *The Finite Element Method*, 3rd ed., McGraw-Hill Book Co., Maidenhead, United Kingdom, 1977.

- [7.1.34] MITCHELL, A. R., and WAIT, R., *The Finite Element Method in Partial Differential Equations*, Albion Publishing, Chichester, United Kingdom, 1977.
- [7.1.35] HINTON, E., and OWEN, D. R., *Finite Element Programming*, Academic Press, London, 1977.
- [7.1.36] TONG, P., and ROSETTOS, J. N., *Finite Element Methods: Basic Technique and Interpretation*, MIT Press, Cambridge, Massachusetts, 1977.
- [7.1.37] BERGAN, P. G., et al. (Eds.), *Finite Elements in Nonlinear Mechanics*, Vols. 1 and 2, Tapir, Trondheim, Norway, 1978.
- [7.1.38] CHUNG, T. J., *Finite Element Analysis in Fluid Dynamics*, McGraw-Hill Book Co., New York, 1978.
- [7.1.39] Ciarlet, P. G., *The Finite Element Method for Elliptic Problems*, North-Holland, Amsterdam, 1978.
- [7.1.40] PAHL, J., et al. (Eds.), *Finite Elemente in der Baupraxis*, W. Ernst & Sohn, Berlin, 1978.
- [7.1.41] HINTON, E., and OWEN, D. R., *An Introduction to the Finite Element Computation*, Pineridge Press, Swansea, 1979.
- [7.1.42] DESAI, C. S., *Elementary Finite Element Method*, Prentice-Hall, Englewood Cliffs, New Jersey, 1979.
- [7.1.43] DAVIS, A. J., *The Finite Element Method: A First Approach*, Oxford University Press, Oxford, 1980.
- [7.1.44] OWEN, D. R. J., and HINTON, E., *Finite Elements in Plasticity*, Pineridge Press, Swansea, United Kingdom, 1980.
- [7.1.45] OWEN, D. R. J., and HINTON, E., *A Simple Guide to Finite Elements*, Pineridge Press, Swansea, United Kingdom, 1980.
- [7.1.46] BECKER, E. B., et al., *Finite Elements—An Introduction*, Vol. 1, Prentice-Hall, Englewood Cliffs, New Jersey, 1981.
- [7.1.47] BATHE, K.-J., *Finite Element Procedures in Engineering Analysis*, Prentice-Hall, Englewood Cliffs, New Jersey, 1982.
- [7.1.48] KARDESTUNGER, H. (Ed.), *Proceedings on the Unification of Finite Elements—Finite Differences—and Calculus of Variation*, University of Connecticut Publication, Storrs, Connecticut, 1982.
- [7.1.49] HUEBNER, K. H., and THORNTON, E. A., *The Finite Element Method for Engineers*, John Wiley & Sons, New York, 1982.
- [7.1.50] ASCE STRUCTURAL DIVISION, *Finite Element Analysis of Reinforced Concrete*, American Society of Chemical Engineers, New York, 1982.
- [7.1.51] LIVESLEY, R. K., *Finite Elements: An Introduction for Engineers*, Cambridge University Press, Cambridge, 1983.
- [7.1.52] CAREY, G. F., and ODEN, J. T., *Finite Elements—A Second Course*, Vol. II, Prentice-Hall, Englewood Cliffs, New Jersey, 1983.
- [7.1.53] CAREY, G. F., and ODEN, J. T., *Finite Elements—Computational Aspects*, Vol. III, Prentice-Hall, Englewood Cliffs, New Jersey, 1984.
- [7.1.54] WEAVER, W., and JOHNSTON, P. R., *Finite Elements for Structural Analysis*, Prentice-Hall, Englewood Cliffs, New Jersey, 1984.
- [7.1.55] REDDY, J. N., *An Introduction to the Finite Element Method*, McGraw-Hill Book Co., New York, 1984.
- [7.1.56] ROSS, C. T. F., *Finite Element Programs for Axisymmetrical Problems in Engineering*, Albion Publishing, Chichester, United Kingdom, 1984.
- [7.1.57] KARDESTUNGER, H. (Ed.), *Unification of Finite Element Methods*, North-Holland, Amsterdam, 1984.
- [7.1.58] HUSTON, R. L., and PASSERELLO, CH. E., *Finite Element Methods: An Introduction*, Marcel Dekker, New York, 1984.
- [7.1.59] LINK, M., *Finite Elemente der Statik und Dynamik*, Teubner, Stuttgart, 1984.
- [7.1.60] AXELSSON, O., and BARKER, V. A., *Finite Element Solution of Boundary Value Problems—Theory and Computation*, Academic Press, Orlando, Florida, 1984.

- [7.1.61] GRUNDMANN, H., STEIN, E., and WUNDERLICH, W. (Eds.), *Finite Elemente Anwendung in der Baupraxis*, Ernst & Sohn, Berlin, 1985.
- [7.1.62] WAIT, R., and MITCHELL, A. R., *Finite Element Analysis and Applications*, John Wiley & Sons, New York, 1985.
- [7.1.63] GOULD, P. L., *Finite Element Analysis of Shells of Revolution*, Pitman, Boston, 1985.
- [7.1.64] ALLAIRE, P. E., *Basics of the Finite Element Method—Solid Mechanics, Heat Transfer and Fluid Mechanics*, William C. Brown, Dubuque, Iowa, 1985.
- [7.1.65] WHITE, R. E., *An Introduction to the Finite Element Method with Applications to Non-Linear Problems*, Wiley-Interscience, New York, 1985.
- [7.1.66] YANG, T. Y., *Finite Element Structural Analysis*, Prentice-Hall, Englewood Cliffs, New Jersey, 1986.
- [7.1.67] CRISFIELD, M. A., *Finite Elements and Solution Procedures for Structural Analysis*, Pineridge Press, Swansea, United Kingdom, 1986.
- [7.1.68] AKIN, J. E., *Finite Element Analysis for Undergraduates*, Academic Press, London, 1986.
- [7.1.69] BURNETT, D. S., *Finite Element Analysis*, Addison-Wesley Publ. Co., Reading, Massachusetts, 1987.
- [7.1.70] MEYER, CH. (Ed.), *Finite Element Idealization*, ASCE Press, New York, 1987.
- [7.1.71] HUGHES, T. J. R., *The Finite Element Method*, Prentice-Hall, Englewood Cliffs, New Jersey, 1987.
- [7.1.72] KARDESTUNGER, H., and NORRIE, D. H. (Eds.), *Finite Element Handbook*, McGraw-Hill Book Co., New York, 1987.
- [7.1.73] SMITH, I. M., and GRIFFITHS, D. V., *Programming the Finite Element Method*, John Wiley & Sons, Chichester, 1988.
- [7.1.74] MEISSNER, U., and MENZEL, A., *Die Methode der finiten Elemente*, Springer-Verlag, Berlin, 1989.
- [7.1.75] RAO, S. S., *Finite Element Method in Engineering*, 2nd ed., Pergamon Press, Oxford, 1989.
- [7.1.76] COOK, R. D., et al., *Concepts and Applications of Finite Element Analysis*, 3rd ed., John Wiley & Sons, New York, 1989.
- [7.1.77] MELOSH, R. J., *Structural Engineering Analysis by Finite Elements*, Prentice-Hall, London, 1990.
- [7.1.78] BRICKFORD, W. B., *A First Course in the Finite Element Method*, Irwin, Homewood, Illinois, 1990.
- [7.1.79] SZILARD, R., *Finite Berechnungsmethoden der Strukturmechanik*, Vol. 2: *Flächentragwerke im Bauwesen*, Ernst & Sohn, Berlin, 1990.
- [7.1.80] SZABO, B., and BABUŠKA, I., *Finite Element Analysis*, John Wiley & Sons, New York, 1991.
- [7.1.81] CHANDRUPATLA, T. R., and BELEGUNDU, A. D., *Introduction to Finite Elements in Engineering*, Prentice-Hall, Englewood Cliffs, New Jersey, 1991.
- [7.1.82] SCHWARZ, H. R., *Methode der finiten Elemente*, 3rd ed., Teubner, Stuttgart, 1991.
- [7.1.83] CRISFIELD, M. A., *Nonlinear Finite Element Analysis*, John Wiley & Sons, New York, 1991.
- [7.1.84] BEER, G., and WATSON, J. O., *Introduction to Finite and Boundary Element Methods for Engineers*, John Wiley & Sons, New York, 1992.
- [7.1.85] MOHR, G. A., *Finite Elements for Solids, Fluids and Optimization*, Oxford University Press, New York, 1992.
- [7.1.86] AKIN, J. E., *Finite Elements for Analysis and Design*, Academic Press, San Diego, California, 1994.
- [7.1.87] ZIENKIEWICZ, O. C., and TAYLOR, R. L., *The Finite Element Method*, 4th ed., Vols. 1 and 2, McGraw-Hill Book Co., London, 1994.
- [7.1.88] COOK, R. D., *Finite Element Stress Analysis*, John Wiley & Sons, New York, 1995.
- [7.1.89] SPYRAKOS, C. C., *Finite Element Modeling in Engineering Practice*, Algor Publ. Div., Pittsburgh, Pennsylvania, 1996.
- [7.1.90] BITTNER, Z., and ŠEJNOHA, J., *Numerical Methods in Structural Mechanics*, ASCE Press, New York, 1996.

- [7.1.91] CHEUNG, Y. K., LO, S. H., and LEUNG, A. Y. T., *Finite Element Implementation*, Blackwell Science, Oxford, 1996.
- [7.1.92] PRATHAP, G., *The Finite Element Method in Structural Mechanics*, Kluwer Academic Publisher, Dordrecht, The Netherlands, 1993.
- [7.1.93] CROLL, W. F., *A Primer for Finite Elements in Elastic Structures*, John Wiley & Sons, New York, 1998.
- [7.1.94] DESAI, S. C., and KUNDU, T., *Introductory Finite Element Method*, CRC Press, Boca Raton, Florida, 2001.
- [7.1.95] COCK, R. F., et al., *Concepts and Applications of Finite Element Analysis*, 4th ed., John Wiley & Sons, New York, 2001.

7.2 Engineering Approach to the Method

As already mentioned, the precursor of the FEM was the matrix displacement method for the analysis of framed structures. Thus, we may also consider the FEM as an extension of this familiar technique, in a similar way, as the first originators of the method used it in connection with the analysis of delta-wing panels [7.1.6]. Consequently, in applying a piecewise approach to the approximate solution of complex plate problems, the required procedures are analogous to those described in the foregoing chapter that dealt with the gridwork method. Therefore, we intend to treat the basic principles and steps of this numerical solution technique by extending the familiar engineering approach for framed structures to plates. In the subsequent section, however, the rigorous mathematical foundation of the FEM will also be introduced. Naturally, because of the close similarity between the gridwork and finite element methods, some overlap, and hence repetition, is unavoidable.

Similar to the gridwork method, the FEM uses local approximate solutions to build the solution for the entire plate problem. In applying a piecewise approximation, first the continuum of the plate is subdivided into a finite number of subregions called *finite elements*. The elements may be straight-sided or curvilinear triangles or quadrilaterals (Fig. 7.2.1). These elements do not overlap and are connected only through their *nodal points*. This first step in the finite element procedure is called *discretization*. For smaller problems, the discretization is usually done “by hand.” For larger plate systems, this procedure becomes nearly impossible. Consequently, automatic mesh generation algorithms capable of discretizing a given plate geometry into efficient finite element mesh are employed [7.2.1–7.2.3].

The number of elements to be used is determined, to a large extent, by the convergence characteristics of the selected elements. In addition, one must consider smaller mesh sizes in the vicinity of expected stress concentrations, such as point supports, or cut-outs, as shown in Fig. 7.2.2.

In connection with the discretization procedure, an efficient *node-numbering scheme* must be adopted in the global \bar{X} , \bar{Y} , \bar{Z} reference system. As stated in Sec. 6.4, this determines the bandwidth of the global stiffness matrix. Since in our case the number of degrees of freedom (DOF) per node[†] is 3 and the stiffness matrix is symmetrical, the half bandwidth, BW, can be calculated from

$$BW = 3(d + 1), \quad (7.2.1)$$

[†] See Fig. 6.4.6.

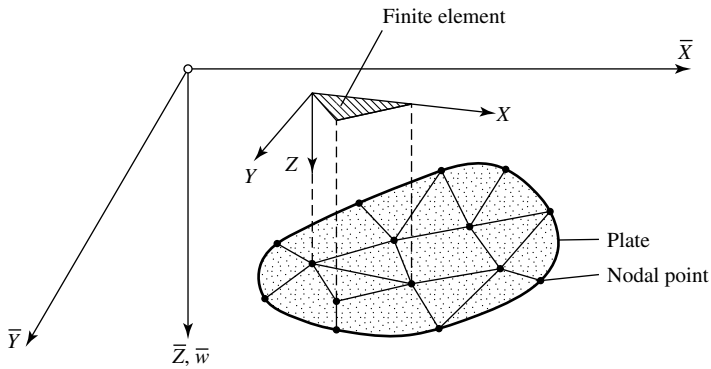


Figure 7.2.1 Discretization of plate continuum.

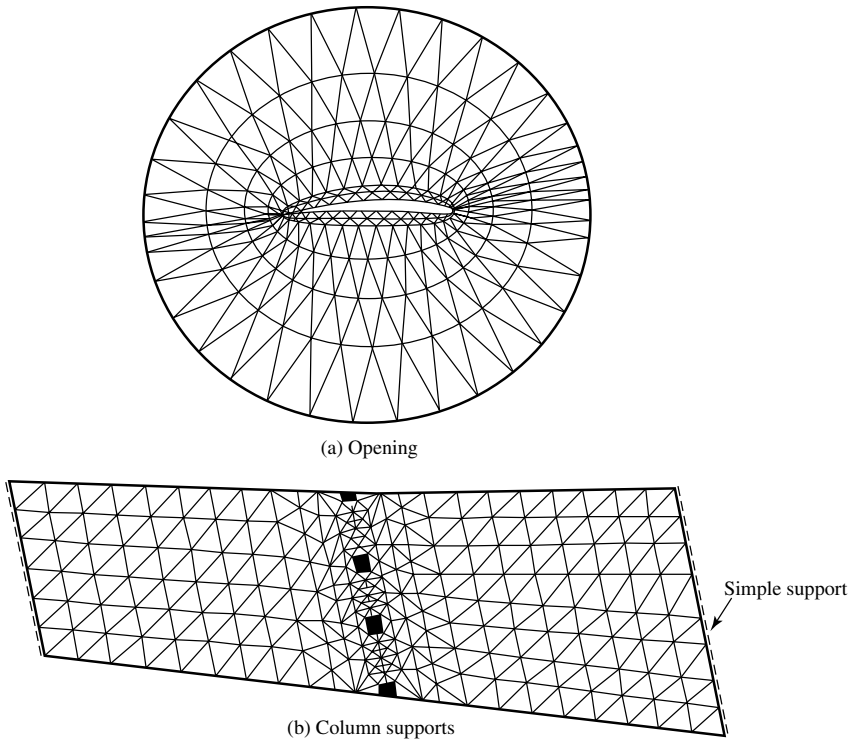


Figure 7.2.2 Finer subdivision in vicinity of stress concentrations.

where d is the maximum largest difference in the node numbers occurring for all elements of the assemblage. The above equation indicates that d must be small in order to obtain the optimum half bandwidth. Thus, the smallest bandwidth can be achieved simply by numbering the nodes across the shortest dimension of the plate. By reducing the bandwidth, the storage requirements in the computer and the solution time of the governing matrix equation are equally reduced. Simultaneous with the node

numbering, the displacements at each node are numbered according to the following sequence: (1) translation, (2) rotation around the \bar{X} axis and (3) rotation around the \bar{Y} axis. This numbering process results in $\bar{1}, \bar{2}, \bar{3}, \dots, \bar{n}$ nodal displacements that actually can take place.

The next step involves the calculation of the *element stiffness matrix* $\mathbf{K}_e^{(N)}$, which relates a displacement at a nodal point to the so-created forces at the other nodes. According to the engineering definition of the coefficients k_{ij} of the element stiffness matrix, they represent active or reactive forces caused by a unit displacement of one node while the other nodes are kept fixed. Thus, for the rectangular plate element shown in Fig. 7.2.3, the general form of the element stiffness matrix—expressed in its local X, Y, Z coordinate system—becomes

$$\mathbf{K}_e^{(N)} = \begin{bmatrix} k_{11} & k_{12} & k_{13} & \dots & k_{1,10} & k_{1,11} & k_{1,12} \\ & k_{22} & k_{23} & \dots & k_{2,10} & k_{2,11} & k_{2,12} \\ & & k_{33} & \dots & k_{3,10} & k_{3,11} & k_{3,12} \\ & & & \ddots & \vdots & \vdots & \vdots \\ \text{Symmetric} & & & & k_{10,10} & k_{10,11} & k_{10,12} \\ & & & & & k_{11,11} & k_{11,12} \\ & & & & & & k_{12,12} \end{bmatrix}^{(N)} \quad (7.2.2)$$

Using the principle of virtual displacement [7.2.4], the individual coefficients of the element stiffness matrix can be computed [7.2.5] from

$$k_{ij}1 = \iiint_V \sigma_i^T \epsilon_j dV = \iint_A \mathbf{m}_i^T \kappa_j dA, \quad (7.2.3)$$

where \mathbf{m}_i is the vector of the stress resultants created by the unit displacement on the coordinate i . Thus, we can write

$$\mathbf{m}_i = \begin{Bmatrix} m_{x,i} \\ m_{y,i} \\ m_{xy,i} \end{Bmatrix} = D \begin{bmatrix} 1 & \nu & 0 \\ \nu & 1 & 0 \\ 0 & 0 & (1-\nu)/2 \end{bmatrix} \begin{Bmatrix} -\frac{\partial^2}{\partial x^2} w_i \\ -\frac{\partial^2}{\partial y^2} w_i \\ -2\frac{\partial^2}{\partial x \partial y} w_i \end{Bmatrix}, \quad (7.2.4)$$

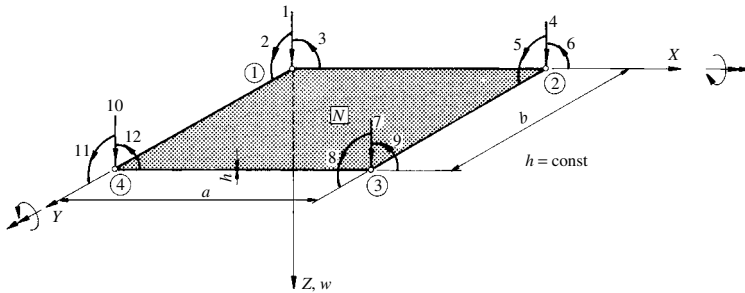


Figure 7.2.3 Rectangular element.

and

$$\kappa_j = \begin{Bmatrix} \kappa_{x,j} \\ \kappa_{y,j} \\ 2\kappa_{xy,j} = 2\chi_j \end{Bmatrix} = \begin{Bmatrix} -\frac{\partial^2 w_j}{\partial x^2} \\ -\frac{\partial^2 w_j}{\partial y^2} \\ -2\frac{\partial^2 w_j}{\partial x \partial y} \end{Bmatrix} \quad (7.2.5)$$

represents the vector of curvatures created by a unit displacement on coordinate j .

The substitution of Eqs. (7.2.4) and (7.2.5) into Eq. (7.2.3) gives the general equation for evaluation of stiffness coefficients in the form

$$k_{ij} = D \cdot \iint_A \begin{Bmatrix} \frac{\partial^2 w_i}{\partial x^2} \\ \frac{\partial^2 w_i}{\partial y^2} \\ \frac{\partial^2 w_i}{\partial x \partial y} \end{Bmatrix}^T \begin{bmatrix} 1 & \nu & 0 \\ \nu & 1 & 0 \\ 0 & 0 & 2(1-\nu) \end{bmatrix} \begin{Bmatrix} \frac{\partial^2 w_j}{\partial x^2} \\ \frac{\partial^2 w_j}{\partial y^2} \\ \frac{\partial^2 w_j}{\partial x \partial y} \end{Bmatrix} dA. \quad (7.2.6)$$

The assumed displacement functions $w_i(x, y)$ and $w_j(x, y)$, which are chosen to describe the displacement patterns in the plate element, must meet certain strict criteria to obtain convergence to the exact solutions of plate problems. These important requirements for obtaining suitable finite elements will be discussed extensively in Sec. 7.4. These assumed displacement functions represent, in general, only approximately the displacements in the plate elements. For this purpose polynomial and trigonometric functions are most commonly used.

Employing an engineering approach, we can create an *exact* displacement function for the lateral nodal displacements of a rectangular plate element. For this purpose we use a plate of $2a \times 2b$ dimensions with clamped edges under a load $P = 1$ concentrated at the center (Fig. 7.2.4). The mathematically exact solution of this problem is given in Ref. [7.2.6]. Since we require a unit amplitude for the lateral displacement at the center, the result w_{\max}^* must be normalized accordingly. In this way, the displacement function $\phi^i = w_i(x, y)$ for unit translation on coordinate 7 (Fig. 7.2.5a) can be determined. Obviously, the same function can also be used for the translation of the other nodes with appropriate modifications.

However, it is much more difficult to derive a *compatible* displacement function for the unit rotation on coordinate 9 (Fig. 7.2.5b). We can circumvent this problem to a certain extent by using the normalized derivatives of ϕ_i with respect to x and y , respectively. Again, the same displacement functions can be employed, after appropriate modifications, for the unit rotations of the other nodes. The obtained displacements, however, violate the slope continuity at the far end of the plate element. Experience shows, nonetheless, that good results can be obtained with such slightly *nonconforming* shape functions, provided that they are used in static (versus stability) analysis of plates.

On the other hand, *Cartesian products* of the displacement functions of beam elements give conforming shape functions that satisfy all continuity requirements

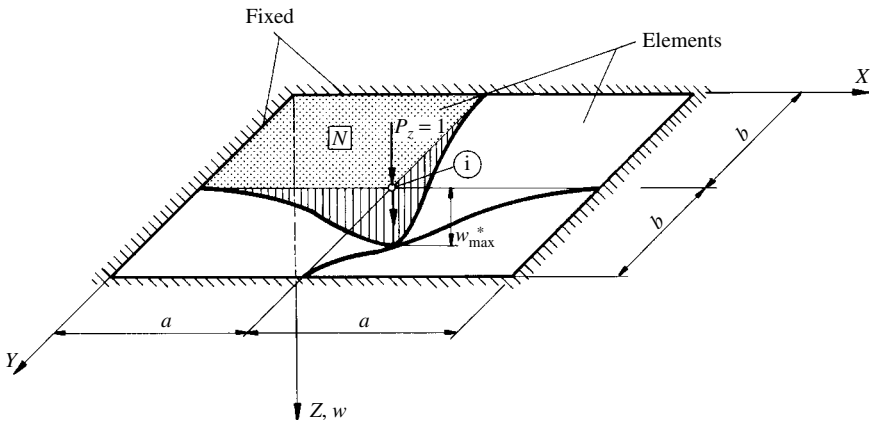


Figure 7.2.4 Generation of displacement functions for translations of nodal points.

between elements. Thus, the deflection pattern produced by normalized unit translation of the node located at $x = a$ and $y = b$ distance can be approximated by

$$\phi_i(x, y) = \left[3 \left(\frac{x}{a} \right)^2 - 2 \left(\frac{x}{a} \right)^3 \right] \left[3 \left(\frac{y}{b} \right)^2 - 2 \left(\frac{y}{b} \right)^3 \right]. \quad (7.2.7)$$

Similarly, the deflection pattern due to a normalized rotation around the Y axis of the same nodal point, for example, can be approximately described by

$$\phi_j(x, y) = \left[a \left(\frac{x}{a} \right)^2 \left(1 - \frac{x}{a} \right) \right] \left[3 \left(\frac{y}{b} \right)^2 - 2 \left(\frac{y}{b} \right)^3 \right]. \quad (7.2.8)$$

Although these shape functions satisfy all continuity requirements at the boundaries as well as within the element domain, their convergence characteristics are not satisfactory. That is, computations with the derived elements yield approximately 5–7% smaller deflections compared to the exact solutions [7.2.7]. These discrepancies are created by the fact that the elements do not deform similarly to the actual deformations developed in the plate.

As was the case with gridwork cells, any calculation error in computing the element stiffness matrix can be detected by checking the equilibrium of the element. Consequently, equations of equilibrium[†] must be satisfied for each column or row in the matrix.

The next step involves conversion of all external forces to equivalent *joint loads*. Since all loads must act on joints, we assign nodes to concentrated forces and moments during the discretization process. Distributed lateral loads $p_z(x, y)$ can easily be converted to joint loads by employing their statically equivalent forces. More exact results can be obtained by using the approximate displacement functions introduced above in connection with the principle of virtual work. Thus, we

[†] See Eq. (6.3.5).

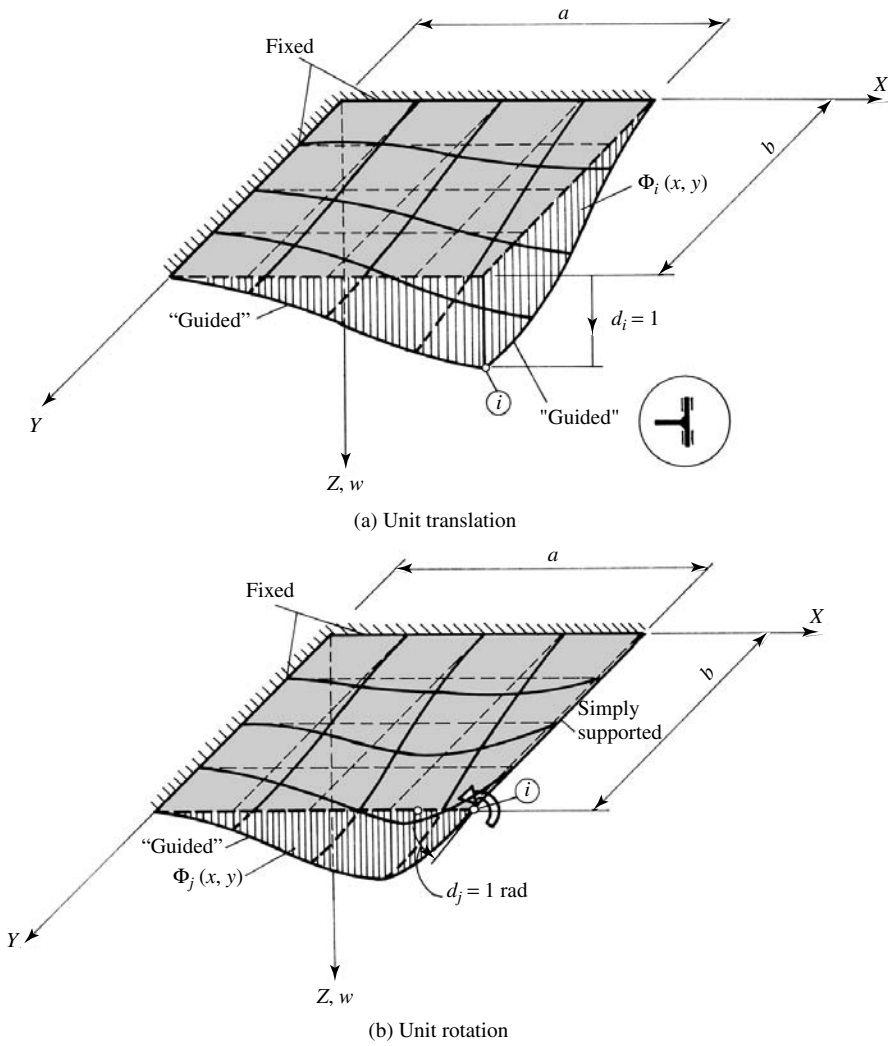


Figure 7.2.5 Shape functions due to unit displacements.

can write

$$P_i = \iint_A \phi_i(x, y) \cdot p_z(x, y) \, dA, \quad (7.2.9)$$

$$M_i = \iint_A \phi_j(x, y) \cdot p_z(x, y) \, dA.$$

Similar expressions can be used for triangular elements. One can also apply the approximations given in Fig. 6.4.3.

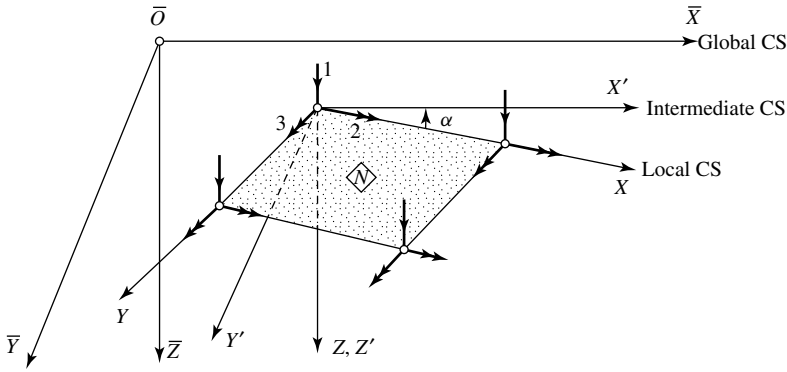


Figure 7.2.6 Rotation of local coordinate system (CS).

Since the element stiffness matrices and the equivalent joint loads are determined in local coordinate systems X, Y, Z , they must be rotated into an intermediate system X', Y', Z' (Fig. 7.2.6) before assemblage. The axes of this intermediate system are parallel to those of the global reference system $\bar{X}, \bar{Y}, \bar{Z}$. This coordinate rotation is expressed by

$$(\mathbf{K}'_e)^{(N)} = (\mathbf{T}\mathbf{K}_e\mathbf{T}^T)^{(N)}, \quad (7.2.10)$$

where the transformation matrix $\mathbf{T}^{(N)}$ has the form

$$\mathbf{T}^{(N)} = \begin{bmatrix} \mathbf{R}_1 & & & \\ & \mathbf{R}_2 & & \\ & & \mathbf{R}_3 & \\ & & & \mathbf{R}_4 \end{bmatrix}^{(N)} \quad (7.2.11)$$

and the rotation matrix for the nodal point (i) is

$$\mathbf{R}_i^{(N)} = \begin{bmatrix} 1 & 0 & 0 \\ 0 & \cos \alpha & \sin \alpha \\ 0 & -\sin \alpha & \cos \alpha \end{bmatrix}^{(N)} \quad (7.2.12)$$

A similar approach can be taken to transfer the vectors of the external joint loads to the intermediate coordinate system. Very often, however, such coordinate transformations are not necessary, since the axes of the local and global coordinate systems are generally parallel.

It is important to remember that Eq. (7.10) is valid only if the angle of rotation α in Eq. (7.2.12) is measured from the local X axis of the element toward the intermediate X' axis, as shown in Fig. 7.2.6. Otherwise a transposed relationship in Eq. (7.2.10) is applicable.

To solve a plate problem, it is necessary to combine the individual stiffness matrices $\bar{\mathbf{K}}_e^{(N)}$ into the overall stiffness matrix $\bar{\mathbf{K}}$ of the plate structure. Similarly, the individual nodal forces $\bar{\mathbf{p}}_i^{(N)}$ must also be combined to form the vector of the nodal forces, $\bar{\mathbf{p}}$, acting on the whole structure. For this purpose, we have to *renumber* the nodal displacements of the elements, $\mathbf{d}_i^{(N)}$, by replacing the local numbers $1, 2, \dots, 12$

with their equivalent global numbers $\bar{1}, \bar{2}, \bar{3}, \dots, \bar{n}$. This is accomplished by using the *index number technique*,[†] which is already familiar to most engineers from the analysis of framed structures. A similar procedure is followed for the nodal forces to obtain the vector $\bar{\mathbf{p}}$, which represents all nodal forces acting upon the whole structure expressed in the global reference system. In connection with this renumbering process, we can also impose the boundary conditions of the plate. That is, those displacements that cannot take place receive $\bar{0}$ numbers. The zero number indicates that the pertinent rows and columns must be eliminated from the element stiffness matrices. Then, the obtained reduced stiffness matrices must be shrunk to a smaller size. An alternative procedure for dealing with the boundary conditions are given in Sec. 7.3.

The *assembly* of the governing matrix equation for the whole structure includes building up the global stiffness matrix $\bar{\mathbf{K}}$ of the plate from the stiffness matrices $\bar{\mathbf{K}}_e^{(N)}$ of the individual elements N and creating the overall global forces or load vector $\bar{\mathbf{p}}$. The most common technique builds up $\bar{\mathbf{K}}$ by simply adding the stiffness coefficients of the elements having the same subscripts. Hence,

$$\bar{\mathbf{K}}_{ij} = \sum_N \bar{k}_{e,ij}^{(N)}, \quad (7.2.13)$$

where the summation is taken over all elements and $k_{e,ij}^{(N)}$ represents the coefficient of the element stiffness matrix. Similarly, by

$$\bar{\mathbf{p}}_i = \sum_N p_i^{(N)}, \quad (7.2.14)$$

we obtain the global load vector. This process is graphically presented in Fig. 7.2.7.

The resulting system of simultaneous algebraic equations

$$\boxed{\bar{\mathbf{K}} \bar{\mathbf{d}} = \bar{\mathbf{p}}} \quad (7.2.15)$$

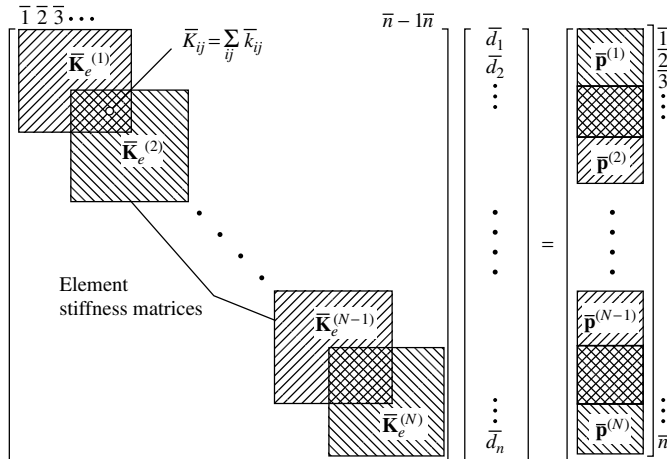


Figure 7.2.7 Assembly of governing equation.

[†] See, for instance, Illustrative Example III in Sec. 6.4.

is solved for the unknown nodal displacements $\bar{\mathbf{d}}$. Once these are known, the assumed shape functions define the displacements throughout the assemblage of elements.

Finally, subsidiary quantities such as moments and shear forces are evaluated for each element nodal point (i) . That is, once the nodal displacements are known, the stress resultants of the N th element can be found from

$$\mathbf{m}_i = (\mathbf{S}_e \mathbf{d}_e)_i^{(N)} \quad \text{and} \quad \mathbf{q}_i = (\mathbf{Q}_e \mathbf{d}_e)_i^{(N)}, \quad (7.2.16)$$

where $\mathbf{S}_e^{(N)}$ and $\mathbf{Q}_e^{(N)}$ are the so-called element *stress matrices*. Since in these expressions we deal with element displacements $\mathbf{d}_e^{(N)}$, the pertinent displacement vectors must be transformed back to their local coordinate systems. Hence

$$\mathbf{d}_e^{(N)} = \{(\mathbf{T})^T \bar{\mathbf{d}}_e\}^{(N)}, \quad (7.2.17)$$

The *general* expression for the stress matrices is

$$\sigma_i^{(N)} = \left\{ \begin{matrix} \mathbf{m}_i \\ \mathbf{q}_i \end{matrix} \right\}^{(N)} = (\mathbf{E} \mathbf{D} \mathbf{N} \mathbf{d}_e)_i^{(N)}, \quad (7.2.18)$$

where \mathbf{E} is the elasticity matrix, \mathbf{D} represents a matrix of differential operators and \mathbf{N} stands for the matrix of the shape functions.

An important item that the structural engineer, wishes to determine in an analysis is the stress pattern induced in the plate by the external loads. Since this knowledge is probably more important than the displacements, we devote a separate section[†] to cover this subject.

ILLUSTRATIVE EXAMPLE

To determine the stiffness coefficient k_{77} of the rectangular plate element shown in Fig. 7.2.3, we use Eq. (7.2.6). The assumed displacement functions w_i and w_j required for evaluation of this equation are approximated by

$$w_i = w_j = w_7 = \left[3 \left(\frac{x}{a} \right)^2 - 2 \left(\frac{x}{a} \right)^3 \right] \cdot \left[3 \left(\frac{y}{b} \right)^2 - 2 \left(\frac{y}{b} \right)^3 \right], \quad (7.2.19)$$

which represents the *Cartesian* product of the corresponding beam functions. In this case, Eq. (7.2.6) becomes

$$\begin{aligned} k_{77} = D \int_0^b \int_0^a & \left[\left(\frac{\partial^2 w_7}{\partial x^2} \right)^2 + \left(\frac{\partial^2 w_7}{\partial y^2} \right)^2 + 2\nu \frac{\partial^2 w_7}{\partial x^2} \cdot \frac{\partial^2 w_7}{\partial y^2} \right. \\ & \left. + 2(1 - \nu) \left(\frac{\partial^2 w_7}{\partial x \partial y} \right)^2 \right] dx dy. \end{aligned} \quad (7.2.20)$$

[†] See Sec. 7.8.

Substitution of Eq. (7.2.19) into this expression gives

$$\begin{aligned}
 k_{77} = D \int_0^b \int_0^a \left\{ \frac{36}{a^4} \left[1 - 2\frac{x}{a} \right]^2 \left[3 \left(\frac{y}{b} \right)^2 - 2 \left(\frac{y}{b} \right)^3 \right]^2 \right. \\
 + 2\nu \frac{6}{a^2} \left[1 - 2\frac{x}{a} \right] \left[3 \left(\frac{y}{b} \right)^2 - 2 \left(\frac{y}{b} \right)^3 \right] \\
 \times \left[3 \left(\frac{x}{a} \right)^2 - 2 \left(\frac{x}{a} \right)^3 \right] \cdot \frac{6}{b^2} \left[1 - 2\frac{y}{b} \right] \\
 + \left[3 \left(\frac{x}{a} \right)^2 - 2 \left(\frac{x}{a} \right)^3 \right]^2 \cdot \frac{36}{b^4} \left[1 - 2\frac{y}{b} \right]^2 \\
 \left. + 2(1 - \nu) \frac{36}{a^2} \left[\frac{x}{a} - \left(\frac{x}{a} \right)^2 \right]^2 \frac{36}{b^2} \left[\frac{y}{b} - \left(\frac{y}{b} \right)^2 \right]^2 \right\} dx dy
 \end{aligned} \quad (7.2.21)$$

and

$$\begin{aligned}
 k_{77} = D \int_0^b \int_0^a \left\{ \frac{36}{a^4} \left[1 - 4\frac{x}{a} + 4 \left(\frac{x}{a} \right)^2 \right] \left[9 \left(\frac{y}{b} \right)^4 - 12 \left(\frac{y}{b} \right)^5 + 4 \left(\frac{y}{b} \right)^6 \right] \right. \\
 + \frac{72\nu}{a^2 b^2} \left[3 \left(\frac{x}{a} \right)^2 - 2 \left(\frac{x}{a} \right)^3 - 6 \left(\frac{x}{a} \right)^3 + 4 \left(\frac{x}{a} \right)^4 \right] \\
 \times \left[3 \left(\frac{y}{b} \right)^2 - 2 \left(\frac{y}{b} \right)^3 - 6 \left(\frac{y}{b} \right)^3 + 4 \left(\frac{y}{b} \right)^4 \right] \\
 + \frac{36}{b^4} \left[1 - 4\frac{y}{b} + 4 \left(\frac{y}{b} \right)^2 \right] \left[9 \left(\frac{x}{a} \right)^4 - 12 \left(\frac{x}{a} \right)^5 + 4 \left(\frac{x}{a} \right)^6 \right] \\
 + 2592(1 - \nu) \left[\left(\frac{x}{a} \right)^2 - 2 \left(\frac{x}{a} \right)^3 + \left(\frac{x}{a} \right)^4 \right] \\
 \left. \times \left[\left(\frac{y}{b} \right)^2 - 2 \left(\frac{y}{b} \right)^3 + \left(\frac{y}{b} \right)^4 \right] \right\} dx dy.
 \end{aligned} \quad (7.2.22)$$

After performing the integration, we obtain

$$\begin{aligned}
 k_{77} = D \left\{ \frac{36}{a^4} \left[a - 2a + \frac{4a}{3} \right] \left[b - \frac{b}{2} \right] \right. \\
 + \frac{72\nu}{a^2 b^2} \left[\frac{3a}{2} - \frac{a}{2} - \frac{3a}{2} + \frac{4a}{5} \right] \left[b - \frac{b}{2} - \frac{3b}{2} + \frac{4b}{5} \right] \\
 + \frac{36}{b^4} \left[b - 2b + \frac{4b}{3} \right] \left[\frac{9a}{5} - 2a + \frac{4a}{7} \right] \\
 \left. + \frac{2592}{a^2 b^2} (1 - \nu) \left[\frac{a}{3} - \frac{a}{2} + \frac{a}{5} \right] \left[\frac{b}{3} - \frac{b}{2} + \frac{b}{5} \right] \right\}, \quad (7.2.23)
 \end{aligned}$$

or in more condensed form

$$\begin{aligned}
 k_{77} &= D \left(\frac{156}{35} \frac{b}{a^3} + \frac{156}{35} \frac{a}{b^3} + \frac{72}{25} \frac{1}{ab} \right) \\
 &= \frac{Eh^3}{12(1-\nu^2)} \cdot \frac{1}{ab} \left[\frac{156}{35} \left(\frac{b}{a} \right)^2 + \frac{156}{35} \left(\frac{a}{b} \right)^2 + \frac{72}{25} \right]. \quad (7.2.24)
 \end{aligned}$$

Remarks: Since the application of the FEM by longhand is identical to that of the gridwork method using framework cells, we refer the reader to Illustrative Examples III and IV in Sec. 6.4. The only difference in the two approaches involves the element stiffness matrices, but the computational sequence remains the same. In addition, the reader will find a few corresponding examples in subsequent sections.

References and Bibliography

- [7.2.1] IMAFUKU, I., et al., "A Generalized Automatic Mesh Generation Scheme for Finite Element Method," *Int. J. Num. Meth. Eng.*, 15 (1980), 713–731.
- [7.2.2] SADEK, E. A., "A Scheme for Automatic Generation of Triangular Finite Elements," *Int. J. Num. Meth. Eng.*, 15 (1980), 1813–1822.
- [7.2.3] LO, S. H., "A New Mesh Generation Scheme for Arbitrary Planar Domain," *Int. J. Num. Meth. Eng.*, 21 (1985), 1403–1426.
- [7.2.4] DAVIS, G. A., *Virtual Work in Structural Analysis*, John Wiley & Sons, Chester, United Kingdom, 1982.
- [7.2.5] ARGYRIS, J. H., and KELSEY, S., *Energy Theorems and Structural Analysis*, Butterworths, London, 1960.
- [7.2.6] TIMOSHENKO, S., and WOINOWSKY-KIEGER, S., *Theory of Plates and Shells*, McGraw-Hill Book Co., New York, 1959.
- [7.2.7] SZILARD, R., *Theory and Analysis of Plates*, Prentice-Hall, Englewood Cliffs, New Jersey, 1974.
- [7.2.8] SZILARD, R., *Finite Berechnungsmethoden der Strukturmechanik*, Vol. 2: *Flächentragwerke im Bauwesen*, Ernst & Sohn, Berlin, 1990.

7.3 Mathematical Formulation of Finite Element Method

7.3.1 Consideration of Total System

In Sec. 7.2, the displacement approach of the FEM was introduced as an intuitively conceived direct *extension* of the familiar matrix displacement analysis technique used for framed structures. Here, we are concerned with the stricter mathematical formulation of this method.

From a mathematical standpoint, the displacement version of the FEM can be considered as a *special case* of the Ritz method discussed in Sec. 4.2. That is, both methods are essentially equal, since each uses a set of assumed displacement functions for obtaining approximate solutions to given plate problems. Furthermore, the *principle of minimum potential energy* is applied by both methods to make these functions stationary. The major difference between the two approaches is that the assumed displacement functions in the FEM are not defined over the whole domain

of the plate, since they represent *piecewise* trial functions that must satisfy certain continuity and completeness conditions to be discussed later. The principle of minimum potential energy ensures that, if the selected displacement fields satisfy the above-mentioned conditions, the total potential energy of the discrete structure will be greater than the energy of the corresponding exact deformation of the plate. In addition, as the number of elements is increased, the FEM solution will converge to its correct value [7.3.1, 7.3.2].

For a linear-elastic plate defined in a global coordinate system $\bar{X}, \bar{Y}, \bar{Z}$ and subjected to $\bar{\mathbf{p}}$ external forces, we seek a solution $\bar{\boldsymbol{\phi}} = \bar{\mathbf{F}} \bar{\mathbf{a}}$ that makes the total potential of the system minimum:

$$\bar{\Pi} = \bar{\Pi}_{\text{int}} + \bar{\Pi}_{\text{ext}}. \quad (7.3.1)$$

Following the classical Ritz method, this requirement can be formulated as

$$\left\{ \begin{array}{c} \frac{\partial \bar{\Pi}}{\partial \bar{a}_1} \\ \frac{\partial \bar{\Pi}}{\partial \bar{a}_2} \\ \vdots \\ \frac{\partial \bar{\Pi}}{\partial \bar{a}_m} \end{array} \right\} = \{0\}, \quad (7.3.2)$$

where $\bar{a}_1, \bar{a}_2, \dots, \bar{a}_m$ are unknown coefficients of the assumed global displacement functions

$$\bar{\boldsymbol{\phi}} = \bar{\mathbf{F}} \bar{\mathbf{a}}, \quad (7.3.3)$$

which satisfy the prescribed boundary conditions of the plate as already discussed in Sec. 4.2. Equation (7.3.2) gives m simultaneous algebraic equations from which the unknown coefficients $\bar{\mathbf{a}}$ are determined. Unfortunately, we can find suitable displacement functions only for the simplest geometry, load and boundary conditions. To eliminate such serious restrictions in solving plate problems, we are using here a *piecewise* approximation that enables us to solve more general plate problems that are of considerable practical interest. For this purpose, the plate is discretized by using a finite number of elements, as shown in Fig. 7.2.1.

The assumed displacement functions of the element N with r nodal points can be written as

$$\mathbf{f}_e^{(N)} = (\mathbf{N}_e \mathbf{d}_e)^{(N)}, \quad (7.3.4)$$

where

$$\mathbf{d}_e^{(N)} = \left\{ \begin{array}{c} \mathbf{d}_1 \\ \mathbf{d}_2 \\ \mathbf{d}_3 \\ \vdots \\ \mathbf{d}_r \end{array} \right\}^{(N)} \quad (7.3.5)$$

is the vector of nodal displacements and

$$\mathbf{N}_e^{(N)} = [\mathbf{N}_1 \quad \mathbf{N}_2 \quad \mathbf{N}_3 \quad \dots \quad \mathbf{N}_r]^{(N)} \quad (7.3.6)$$

represents the matrix of the assumed shape functions that must satisfy certain requirements to be discussed in Sec. 7.4.

The total potential of the continuum can be approximated as the sum of the potential energies of the individual finite elements:

$$\bar{\Pi} \approx \sum_{N=1}^M (\Pi_{\text{int}} + \Pi_{\text{ext}})_e^{(N)}. \quad (7.3.7)$$

The strain energy of the N th element evaluated in its local X, Y, X coordinate system can be written as

$$\Pi_{\text{int},e}^{(N)} = \frac{1}{2} \left(\int_V \boldsymbol{\varepsilon}^T \boldsymbol{\sigma} dV \right)^{(N)} = \frac{1}{2} \left(\int_V \boldsymbol{\varepsilon}^T \mathbf{E} \boldsymbol{\varepsilon} dV \right)^{(N)}, \quad (7.3.8)$$

where \mathbf{E} represents the elasticity matrix and $\boldsymbol{\varepsilon}$ is the strain vector. Furthermore, we can express the strain vector through pertinent differentiation of the assumed shape functions \mathbf{N} combined with the nodal displacements of the elements \mathbf{d}_e in the form

$$\boldsymbol{\varepsilon}^{(N)} = (\mathbf{D} \mathbf{d}_e)^{(N)}, \quad (7.3.9)$$

where the matrix \mathbf{D} is obtained by corresponding differentiation of the shape functions \mathbf{N} . By substituting Eq. (7.3.9) into Eq. (7.3.8), we obtain

$$\Pi_{\text{int},e}^{(N)} = \frac{1}{2} \left(\int_V \mathbf{d}_e^T \mathbf{D}^T \mathbf{E} \mathbf{D} \mathbf{d}_e dV \right)^{(N)} = \frac{1}{2} (\mathbf{d}_e^T \mathbf{K}_e \mathbf{d}_e)^{(N)}, \quad (7.3.10)$$

where

$$\boxed{\mathbf{K}_e^{(N)} = \left(\int_V \mathbf{D}^T \mathbf{E} \mathbf{D} dV \right)^{(N)}} \quad (7.3.11)$$

represents the stiffness matrix of the N th element. A more elaborate form of this equation is already given by Eq. (7.2.6).

Since the element stiffness matrix $\mathbf{K}_e^{(N)}$ was determined in its local coordinate system X, Y, Z , it must be subsequently transferred to the global reference system X, Y, Z of the plate. This can be accomplished by using the already familiar transformation relationship

$$\bar{\mathbf{K}}_e^{(N)} = (\mathbf{T} \mathbf{K}_e \mathbf{T}^T)^{(N)}. \quad (7.3.12)$$

The size of the transformation matrix $\mathbf{T}^{(N)}$ depends on the number of nodal points of the element and that of its allowed DOF allowed at each node.

Next, we can express the total potential energy of the external and internal forces in the global coordinate system in the form

$$\bar{\Pi} = \bar{\Pi}_{\text{int}} + \bar{\Pi}_{\text{ext}} = \frac{1}{2} \bar{\mathbf{d}}^T \left(\sum_{N=1}^M \bar{\mathbf{K}}_e^{(N)} \right) \bar{\mathbf{d}} - \bar{\mathbf{d}}^T \bar{\mathbf{p}}, \quad (7.3.13)$$

where $\bar{\mathbf{d}}$ represents the vector of the unknown nodal displacements. Since the sum

$$\sum_{N=1}^M \bar{\mathbf{K}}_e^{(N)} = \bar{\mathbf{K}} \quad (7.3.14)$$

symbolizes the stiffness matrix of the whole system, the principle of minimum potential energy yields

$$\frac{\partial \bar{\Pi}}{\partial \bar{\mathbf{d}}} = \frac{\partial}{\partial \bar{\mathbf{d}}} \left(\frac{1}{2} \bar{\mathbf{d}}^T \bar{\mathbf{K}} \bar{\mathbf{d}} - \bar{\mathbf{d}}^T \bar{\mathbf{p}} \right) = \{0\}, \quad (7.3.15)$$

the *governing matrix equation* of the finite element in the already familiar form

$$\bar{\mathbf{K}} \bar{\mathbf{d}} - \bar{\mathbf{p}} = \{0\}, \quad (7.3.16)$$

or

$$\boxed{\bar{\mathbf{d}} = \bar{\mathbf{K}}^{-1} \bar{\mathbf{p}}.} \quad (7.3.17)$$

7.3.2 Formulation of Element Stiffness Matrices[†]

A general approach to formulate the element stiffness matrices is the application of one of the following *variational principles*:

- principle of virtual work,
- minimum principle of potential energy,
- minimum principle of complimentary energy,
- *Castigliano's* second theorem and
- unit displacement method.

Here we will only deal with the first two methods since they are most commonly used in structural mechanics.

a. Application of Virtual Work. The virtual work of the external forces, \mathbf{p} , acting on the nodal points of the element is

$$\delta W_{\text{ext}} = \delta \mathbf{d}^T \mathbf{p}, \quad (7.3.18)$$

[†] To simplify notation, in this section we are omitting the subscripts and superscripts that refer to elements, since all matrix operations are carried out on the element level.

where δ represents the conventional variation notation [7.3.5] and \mathbf{d} is the vector of nodal displacements as defined in Eq. (7.3.5). Variation of the corresponding strain energy can be written as

$$\delta W_{\text{int}} = \delta \boldsymbol{\varepsilon}^T \boldsymbol{\sigma} dV. \quad (7.3.19)$$

The virtual work of the external forces must equal that of the strain energy, hence

$$\delta W_{\text{ext}}^{(N)} = \delta W_{\text{int}}^{(N)}; \quad (7.3.20)$$

therefore

$$\delta \mathbf{d}^T \mathbf{p} = \int_V \delta \boldsymbol{\varepsilon}^T \boldsymbol{\sigma} dV. \quad (7.3.21)$$

where $\boldsymbol{\varepsilon}$ represents the strain vector according to Eq. (7.3.9) and $\boldsymbol{\sigma}$ denotes the pertinent stress vector

$$\boldsymbol{\sigma} = \mathbf{E} \boldsymbol{\varepsilon}. \quad (7.3.22)$$

The matrix \mathbf{E} is the elasticity matrix for elastic and isotropic materials. By substituting Eqs. (7.3.9) and (7.3.22) into Eq. (7.3.21), we obtain

$$\delta \mathbf{d}^T \mathbf{p} = \int_V \delta \mathbf{d}^T \mathbf{D}^T \mathbf{E} \mathbf{D} \mathbf{d} dV. \quad (7.3.23)$$

Since this equation is valid for any variation of the nodal point displacements, we can write

$$\mathbf{p} = \int_V \mathbf{D}^T \mathbf{E} \mathbf{D} \mathbf{d} dV, \quad (7.3.24)$$

or

$$\mathbf{p} = \mathbf{K}_e \mathbf{d}, \quad (7.3.25)$$

where

$$\boxed{\mathbf{K}_e = \int_V \mathbf{D}^T \mathbf{E} \mathbf{D} dV} \quad (7.3.26)$$

represents the stiffness matrix of the finite element.

b. Principle of Minimum Potential Energy. We define the elastic potential of a finite element as

$$\Pi = \Pi_{\text{int}} + \Pi_{\text{ext}} = \frac{1}{2} \int_V \boldsymbol{\varepsilon}^T \boldsymbol{\sigma} dV - \mathbf{d}^T \mathbf{p}, \quad (7.3.27)$$

or

$$\Pi = \frac{1}{2} \int_V \boldsymbol{\varepsilon}^T \mathbf{E} \boldsymbol{\varepsilon} dV - \mathbf{d}^T \mathbf{p}. \quad (7.3.28)$$

By substituting Eq. (7.3.9) into this expression, we obtain

$$\Pi = \frac{1}{2} \mathbf{d}^T \int_V (\mathbf{D}^T \mathbf{E} \mathbf{D} dV) \mathbf{d} - \mathbf{d}^T \mathbf{p}. \quad (7.3.29)$$

The necessary condition for Π to have a stationary value is that

$$\frac{\partial \Pi}{\partial \mathbf{d}} = \{0\}. \quad (7.3.30)$$

This requirement yields

$$\left(\int_V \mathbf{D}^T \mathbf{E} \mathbf{D} dV \right) \mathbf{d} - \mathbf{p} = \{0\}, \quad (7.3.31)$$

or since

$$\boxed{\mathbf{K}_e = \int_V \mathbf{D}^T \mathbf{E} \mathbf{D} dV} \quad (7.3.32)$$

represents, again, the element stiffness matrix, we obtain the governing FEM equation for the N th element in the form

$$\mathbf{K}_e \mathbf{d} = \mathbf{p}. \quad (7.3.33)$$

It is evident by now that Eq. (7.3.32) is identical with Eqs. (7.3.11) and (7.3.26). Again, we want to point out that a more elaborate form of these equations is given in Eq. (7.2.6).

c. Alternative Formulation. We can also express the internal displacements $\mathbf{f}(x, y)$ in terms of the displacement functions $\mathbf{M}(x, y)$:

$$\mathbf{f} = \mathbf{M} \boldsymbol{\alpha}, \quad (7.3.34)$$

where $\boldsymbol{\alpha}$ denotes the column matrix of the amplitudes of the displacement functions. These *unknown coefficients* are represented by **generalized coordinates**. The number of independent functions in matrix \mathbf{M} , however, should equal that of the independent nodal displacement components d_i , which are given in terms of generalized coordinates:

$$\mathbf{d} = \mathbf{A} \boldsymbol{\alpha}. \quad (7.3.35)$$

The matrix \mathbf{A} is obtained by substituting the coordinates of the nodal points into the square matrix \mathbf{M} . The unknown coefficients are determined from

$$\boldsymbol{\alpha} = \mathbf{A}^{-1} \mathbf{d}. \quad (7.3.36)$$

Using this formulation, the vector of the element strains becomes

$$\boldsymbol{\varepsilon} = \mathbf{L}\boldsymbol{\alpha}. \quad (7.3.37)$$

The matrix \mathbf{L} in this equation is obtained by appropriate differentiation of the displacement functions. The corresponding element stresses are

$$\boldsymbol{\sigma} = \mathbf{E}\boldsymbol{\varepsilon} = \mathbf{E}\mathbf{L}\boldsymbol{\alpha}, \quad (7.3.38)$$

where \mathbf{E} represents, again, the elasticity matrix of the finite element material.

Applying the principle of virtual displacements, the virtual work of the external and internal forces using generalized coordinates may be written as

$$\delta\boldsymbol{\alpha}^T \boldsymbol{\beta} = \int_V \delta\boldsymbol{\varepsilon}^T \boldsymbol{\sigma} \, dV = \int_V \delta\boldsymbol{\alpha}^T \mathbf{L}^T \mathbf{E} \mathbf{L} \boldsymbol{\alpha} \, dV, \quad (7.3.39)$$

where $\boldsymbol{\beta}$ represents the vector of the generalized nodal forces corresponding with displacements $\boldsymbol{\alpha}$. From Eq. (7.3.39) we obtain

$$\boldsymbol{\beta} = \left(\int_V \mathbf{L}^T \mathbf{E} \mathbf{L} \, dV \right) \boldsymbol{\alpha}. \quad (7.3.40)$$

The term in parentheses represents the generalized coordinate stiffness matrix of the finite elements:

$$\boxed{\tilde{\mathbf{K}}_e = \int_V \mathbf{L}^T \mathbf{E} \mathbf{L} \, dV}. \quad (7.3.41)$$

Since

$$\boldsymbol{\varepsilon} = \mathbf{B}\mathbf{d} = \mathbf{L}\boldsymbol{\alpha}, \quad (7.3.42)$$

we can write

$$\mathbf{K}_e = \int_V (\mathbf{L}\mathbf{A}^{-1})^T \mathbf{E} \mathbf{L} \mathbf{A}^{-1} \, dV = \boxed{(\mathbf{A}^{-1})^T \tilde{\mathbf{K}}_e \mathbf{A}^{-1}}. \quad (7.3.43)$$

The right-hand side of this equation represents a coordinate transformation in which the transformation matrix \mathbf{A}^{-1} relates the generalized coordinates $\boldsymbol{\alpha}$ to the nodal point displacements \mathbf{d} , as given in Eq. (7.3.35).

ILLUSTRATIVE EXAMPLE

Let us apply the *general* relationships introduced above to the rectangular plate element shown in Fig. 7.2.3.

The lateral deflections of the element may be represented by

$$w(x, y) = \mathbf{N}^T \mathbf{d}, \quad (7.3.44)$$

where \mathbf{N} is the shape function matrix and \mathbf{d} represents the vector of nodal point displacements. A more detailed expression for this equation is

$$w(x, y) = [\mathbf{N}_{(1)} \quad \mathbf{N}_{(2)} \quad \mathbf{N}_{(3)} \quad \mathbf{N}_{(4)}] \begin{Bmatrix} \mathbf{d}_{(1)} \\ \mathbf{d}_{(2)} \\ \mathbf{d}_{(3)} \\ \mathbf{d}_{(4)} \end{Bmatrix}. \quad (7.3.45)$$

Here the subscripts refer to the nodal points $(i) = (1), (2), (3), (4)$. At each nodal point three displacement components (Fig. 7.3.1a) are to be considered:

$$\mathbf{d}_{(i)} = \begin{Bmatrix} w \\ \theta_x \\ \theta_y \end{Bmatrix}_{(i)} = \begin{Bmatrix} w \\ \frac{\partial w}{\partial y} \\ -\frac{\partial w}{\partial x} \end{Bmatrix}_{(i)} \quad \text{for } i = 1, 2, 3, 4. \quad (7.3.46)$$

The corresponding nodal forces (Fig. 7.3.1b) are

$$\mathbf{f}_{(i)} = \begin{Bmatrix} Q \\ M_x \\ M_y \end{Bmatrix}_{(i)} \quad \text{for } i = 1, 2, 3, 4. \quad (7.3.47)$$

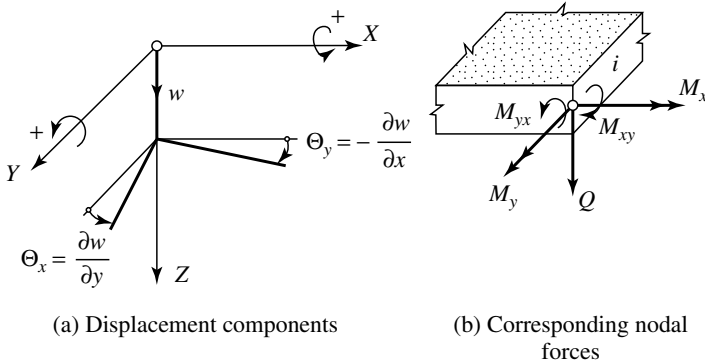


Figure 7.3.1 Nodal forces and displacements.

It should be pointed out, again, that contrary to the classical plate theory θ_y represents a negative slope in the FEM. Furthermore, the concentrated nodal point moments rotate around the X and Y axis, respectively. That is, they are not obtained by integrating the σ_x and σ_y stresses as discussed in Sec. 1.2. Their sign conventions follow also that of the FEM and are shown in Fig. 7.3.1b.[†]

[†] See also Fig. 6.4.6, which represents a similar case.

The shape functions pertinent to a nodal point ① have the general form

$$\mathbf{N}_{\textcircled{1}} = \begin{Bmatrix} \phi_1(x, y) \\ \phi_2(x, y) \\ \phi_3(x, y) \end{Bmatrix}_{\textcircled{1}}^T, \quad (7.3.48)$$

where ϕ_1 , ϕ_2 and ϕ_3 are assumed displacement functions corresponding to d_1 , d_2 and d_3 nodal displacements (Fig. 7.3.1a).

The stain vector $\boldsymbol{\varepsilon}$ is defined as

$$\boldsymbol{\varepsilon} = \mathbf{D}\mathbf{d}, \quad (7.3.49)$$

where \mathbf{D} in this case is

$$\mathbf{D} = [\mathbf{D}_{\textcircled{1}} \quad \mathbf{D}_{\textcircled{2}} \quad \mathbf{D}_{\textcircled{3}} \quad \mathbf{D}_{\textcircled{4}}], \quad (7.3.50)$$

with

$$\mathbf{D}_{\textcircled{i}} = \begin{Bmatrix} -\frac{\partial^2 \mathbf{N}_{\textcircled{i}}}{\partial x^2} \\ -\frac{\partial^2 \mathbf{N}_{\textcircled{i}}}{\partial y^2} \\ -2\frac{\partial^2 \mathbf{N}_{\textcircled{i}}}{\partial x \partial y} \end{Bmatrix}. \quad (7.3.51)$$

For elastic isotropic plate, the elasticity matrix is

$$\mathbf{E} = \frac{Eh^2}{12(1-\nu^2)} \begin{bmatrix} 1 & \nu & 0 \\ \nu & 1 & 0 \\ 0 & 0 & \frac{1}{2}(1-\nu) \end{bmatrix}. \quad (7.3.52)$$

Thus, the element stiffness matrix according to Eq. (7.3.32) becomes

$$\mathbf{K}_e = \int_0^b \int_0^a \mathbf{D}^T \mathbf{E} \mathbf{D} \, dx \, dy. \quad (7.3.53)$$

By substituting Eqs. (7.3.51) and (7.3.52) into this equation, we obtain an explicit expression for the stiffness coefficients

$$k_{ij} = D \int_0^b \int_0^a \begin{Bmatrix} \frac{\partial^2 \phi_i}{\partial x^2} \\ \frac{\partial^2 \phi_i}{\partial y^2} \\ 2\frac{\partial^2 \phi_i}{\partial x \partial y} \end{Bmatrix}^T \begin{bmatrix} 1 & \nu & 0 \\ \nu & 1 & 0 \\ 0 & 0 & \frac{1}{2}(1-\nu) \end{bmatrix} \begin{Bmatrix} \frac{\partial^2 \phi_j}{\partial x^2} \\ \frac{\partial^2 \phi_j}{\partial y^2} \\ 2\frac{\partial^2 \phi_j}{\partial x \partial y} \end{Bmatrix}, \quad (7.3.54)$$

where ϕ_i and ϕ_j represent shape functions at a specific nodal point. These shape functions have unit values at the nodal point in question and zero values at other nodal points, as shown in Fig. 7.2.5. Equation (7.3.54) is, for all practical purposes, identical with Eq. (7.2.6).

In Sec. 7.6.1 the *alternative approach* will be used to derive explicit expressions for a nonconforming stiffness matrix.

References and Bibliography

- [7.3.1] RICHARDS, T. H., *Energy Methods in Stress Analysis*, John Wiley & Sons, New York, 1977.
- [7.3.2] DAVIS, G. A. O., *Virtual Work in Structural Analysis*, John Wiley & Sons, New York, 1982.
- [7.3.3] ARGYRIS, J. H., and KELSEY, S., *Energy Theorems and Structural Analysis*, Butterworths, London, 1960.
- [7.3.4] ARGYRIS, J. H., and KELSEY, S., *Modern Fuselage Analysis and the Elastic Aircraft*, Butterworths, London, 1963.
- [7.3.5] WASHIZU, K., *Variational Methods in Elasticity and Plasticity*, 2nd ed., Pergamon Press, Oxford, 1973.
- [7.3.6] PILKEY, W. D., and WUNDERLICH, W., *Mechanics of Structures: Variational and Computational Methods*, CRC Press, Boca Raton, Florida, 1994.
- [7.3.7] ZIENKIEWICZ, O. C., *The Finite Element Method*, 3rd ed., McGraw-Hill Book Co., Maidenhead, Berkshire, United Kingdom, 1977.
- [7.3.8] KARDESTUNGER, H., and NORRIE, D. H. (Eds.), *Finite Element Handbook*, McGraw-Hill Book Co., New York, 1987.

7.4 Requirements for Shape Functions

The process of creating a finite element displacement model was treated in the foregoing sections. There we stated that the FEM is a special case of Ritz's energy-based solution technique. The essential difference of the FEM lies in the special nature of the assumed displacement functions, since they are *local* rather than global. Consequently, it is assumed that the finite element solutions of plate problems can be obtained in functional forms element by element across the whole domain; that is, they can be defined *piecewise* over the plate.

As is the case with all energy methods, the accuracy of the solution depends considerably on the quality of the assumed displacement functions. The functions defined over each element are called *shape functions*. *The shape function N_i for node i must assume unit value at node i and must be zero at all other nodes of the element and along all sides of the element that do not contain node i .* These fundamental requirements are depicted in Fig. 7.2.5.

Within an element, the lateral deflections can be described by a linear combination of shape functions N_1, N_2, \dots, N_r . These functions, however, must meet certain requirements if convergence to the true solution is to be obtained as the number of elements is increased. These basic convergence requirements are

1. continuity within the element,
2. continuity across element boundaries,
3. compatibility between elements,
4. rigid-body motions that must be represented,

5. invariability by rigid-body motions,
6. ability to represent constant curvatures,
7. invariability by coordinate transformations and
8. close approximation of true plate deflections due to unit motions of nodes (Fig. 7.2.5).

Condition 1 guarantees that the displacement field within the element and certain of its derivatives will be continuous since discontinuity will cause infinite strains. Condition 1 will also ensure that all integrals necessary for computation of element stiffness coefficients k_{ij} are well defined.

Condition 2 deals with compatibility at element interfaces. In general, the shape functions should provide interelement compatibility up to the order $n - 1$, where n is the highest-order derivative in the energy functional used to generate element stiffness coefficients. Shape functions that satisfy these conditions of compatibility are called *conformable*. In the pertinent technical literature the degree of continuity is usually expressed by $C^{(n)}$. Thus, $C^{(0)}$ implies continuity of lateral deflections w , $C^{(1)}$ indicates additional continuity of the first derivatives of w , and $C^{(2)}$ implies continuity even of the second derivatives of w . Consequently, for bending of plates $C^{(1)}$ continuity is required. To satisfy this requirement, we have to ensure continuity of w as well as its normal derivatives $\partial w / \partial n$ along the element boundaries. However, this is not always an easy task! Thus, this requirement is often violated by many successful *nonconforming* elements. Their good performance must be contributed to the fact that, as the element approaches constant-curvature condition, interelement compatibility can be approximated.

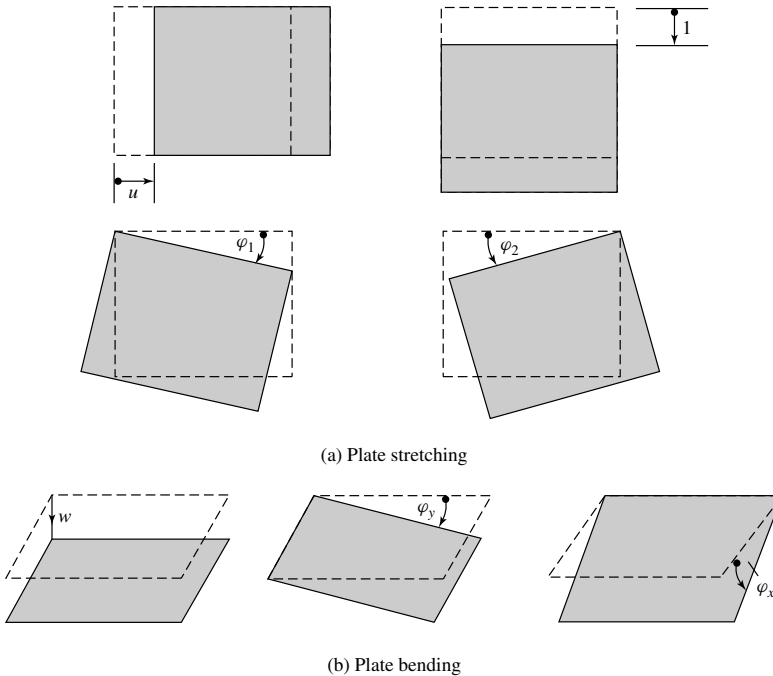


Figure 7.4.1 Rigid-body motions.

Rigid-body motion without strain must be represented. That is, when nodal element displacement components are given unit values corresponding to rigid-body motion (Fig. 7.4.1), the elements must exhibit zero strains and zero nodal forces. In addition, the element must be invariable by such rigid-body motion.

As the size of the elements decreases, the derivatives appearing in the functional of the variational expression should tend to have constant values. Consequently, when the nodal displacements are given values corresponding to the state of constant-curvatures, the shape functions must produce constant strains throughout the element. Since a constant-curvature condition automatically ensures $C^{(1)}$ continuity as the

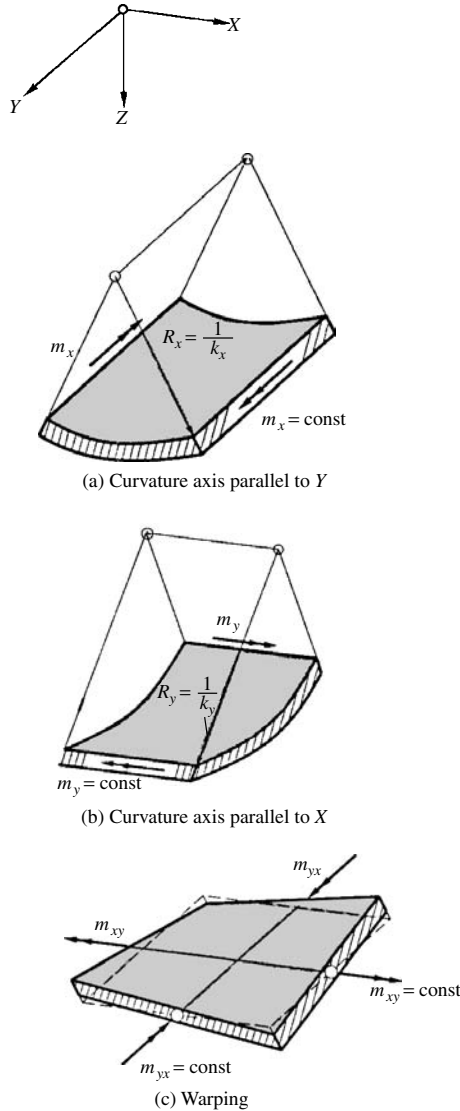


Figure 7.4.2 Constant-curvatures.

element size decreases, it is necessary to include terms in the shape functions that represent this very important state of strains (Fig. 7.4.2).

Finally, we require that the shape functions do not change when we transform them from a *Cartesian* coordinate system to another one. When symmetrical polynomials are used, the expressions of the polynomials should be complete to a required degree to satisfy this requirement. Incomplete polynomials should contain, at least, symmetrical terms.

Requirement 8 is often overlooked. Although some shape functions, such as those obtained using beam functions, may satisfy all previously discussed requirements, the solution will not converge to its true value [7.4.1]. The reason for such discrepancy is easy to comprehend when one graphically compares the displacement fields obtained by unit nodal motions with those of the exact solution of such plate problems[†].

In addition to the *mathematical* requirements discussed above for appropriate shape functions, one should consider two other *physical* requirements:

9. the shape of the element and
10. the number of the nodal points.

Many types of functions could serve as shape functions for plate bending. Polynomials are currently the most widely used [7.4.2]. The reason for this is that polynomials are relatively easy to integrate and differentiate. Trigonometric functions also possess these properties, but they are seldom used [7.4.3, 7.4.4].

Selection of proper shape functions and generating pertinent element stiffness matrices are very difficult tasks requiring plenty of devotion, time and work. Consequently, such an assignment should not be routinely undertaken but left to mathematically inclined research engineers or Ph. D. Candidates.

References and Bibliography

- [7.4.1] SZILARD, R., *Theory and Analysis of Plates*, Prentice-Hall Englewood, Cliffs, New Jersey, 1974.
- [7.4.2] KARDESTUNGER, H., and NORRIE, D. H. (Eds.), *Finite Element Handbook*, McGraw-Hill Book Co., New York, 1987.
- [7.4.3] KRAHULA, J., and POLHEMUS, J., "Use of Fourier Series in the Finite Element Method," *AIAA J.*, 6 (1968), 726–728.
- [7.4.4] CHAKRABARTI, S., "Trigonometric Function Representations for Rectangular Plate Bending Elements," *Int. J. Num. Meth. Eng.*, 3, No. 2 (1971).

7.5 Various Shape Functions and Corresponding Element Families[‡]

One of the most difficult tasks facing an analyst is element selection. An area for which this problem is quite pronounced is that of plate bending, since there is a bewildering array of plate elements that have resulted from approximately 40 years of research activities in this field [7.5.1–7.5.3].

[†] See Fig. 7.2.4.

[‡] To eliminate the discrepancy in sign conventions between the FEM and classical plate theory concerning the rotation Θ_y , either we use directly $-\partial w/\partial x$ or it must be assumed that the pertinent shape function has a negative sign.

The critical step, which largely controls the accuracy of the finite element solution, is the selection of appropriate shape functions. To achieve convergence to the true solutions, the selected shape function must satisfy the requirements introduced in Sec. 7.4. It is not very difficult to achieve $C^{(0)}$ continuity. The degree of difficulty, however, considerably increases when higher-order continuity such as $C^{(1)}$ is required.

In this section we give a brief overview of the most frequently employed shape functions and their corresponding element families. By *element families* we mean finite elements that are constructed by using certain related groups of shape functions.

7.5.1 Polynomials and Their Element Families

Polynomial series expressions in x and y form the basis of several shape functions used in constructing finite elements for plate analysis. One of the reasons for their popularity is that they can be easily integrated and differentiated. As stated previously, accuracy of the finite element solutions directly depends upon the extent to which the assumed shape function can approximate the true deflection of the plate. With polynomials, we can state that the higher the degree, the better is this approximation. Such polynomials of high degree, however, create some problems of their own, which we will be pointed out later.

The polynomial form of shape functions for plate elements is

$$w(x, y) = [1 \quad x \quad y \quad x^2 \quad xy \quad y^2 \quad x^3 \quad x^2y \quad xy^2 \quad y^3 \dots] \begin{Bmatrix} \alpha_1 \\ \alpha_2 \\ \alpha_3 \\ \alpha_4 \\ \vdots \end{Bmatrix}, \quad (7.5.1)$$

where α_i represents *generalized coordinates*, the definition of which was already introduced in Sec. 7.3.

The terms of successive-degree polynomials can be represented by Pascal's triangle:

				1					
				x		y			
			x^2		xy		y^2		
		x^3		x^2y		xy^2		y^3	
	x^4		x^3y		x^2y^2		xy^3		y^4
x^3		x^4y		x^3y^2		x^2y^3		xy^4	y^5

(7.5.2)

which is the product of a column and row matrix:

$$\begin{Bmatrix} 1 \\ x \\ x^2 \\ x^3 \\ \vdots \end{Bmatrix} [1 \quad y \quad y^2 \quad y^3 \quad \dots] = \begin{bmatrix} 1 & y & y^2 & y^3 & \dots \\ x & xy & xy^2 & xy^3 & \dots \\ x^2 & x^2y & x^2y^2 & x^2y^3 & \dots \\ x^3 & x^3y & x^3y^2 & x^3y^3 & \dots \\ \vdots & \vdots & \vdots & \vdots & \vdots \end{bmatrix}. \quad (7.5.3)$$

In choosing the order of the polynomial, the following considerations should be taken into account:

- The polynomial should satisfy the requirements listed in Sec. 7.4.
- The number of generalized coordinates α_i should be equal to the number of nodal DOF of the element.
- Polynomials of order n that are *complete* are invariant to transformation from one *Cartesian* coordinate system to another one.
- Polynomial of order n that are *incomplete* yet contain appropriate terms to preserve symmetry are also invariant during coordinate transformation. Thus, the polynomials should not only include terms containing x and y but always both.

Schemes of complete and incomplete polynomials for triangular and rectangular elements are graphically depicted in Fig. 7.5.1.

Since plate deformations involve second derivatives of $w(x, y)$, interelement compatibility requires continuity of the normal derivatives $\partial w / \partial n$ as well as continuity of the deflections w . Furthermore, to satisfy the requirement for constant-curvatures and that of rigid-body motion, the polynomial representation of the shape function must contain a complete second-degree polynomial in x and y , as shown in the equation

$$w(x, y) = \alpha_1 + \alpha_2 x + \alpha_3 y + \alpha_4 x^2 + \alpha_5 xy + \alpha_6 y^2 + \cdots \quad (7.5.4)$$

a. Polynomials for Triangular Elements. By selecting a cubic polynomial with 10 terms,

$$w(x, y) = [1 \quad x \quad y \quad x^2 \quad xy \quad y^2 \quad x^3 \quad x^2y \quad xy^2 \quad y^3] \begin{Bmatrix} \alpha_1 \\ \alpha_2 \\ \alpha_3 \\ \alpha_4 \\ \alpha_5 \\ \alpha_6 \\ \alpha_7 \\ \alpha_8 \\ \alpha_9 \\ \alpha_{10} \end{Bmatrix}, \quad (7.5.5)$$

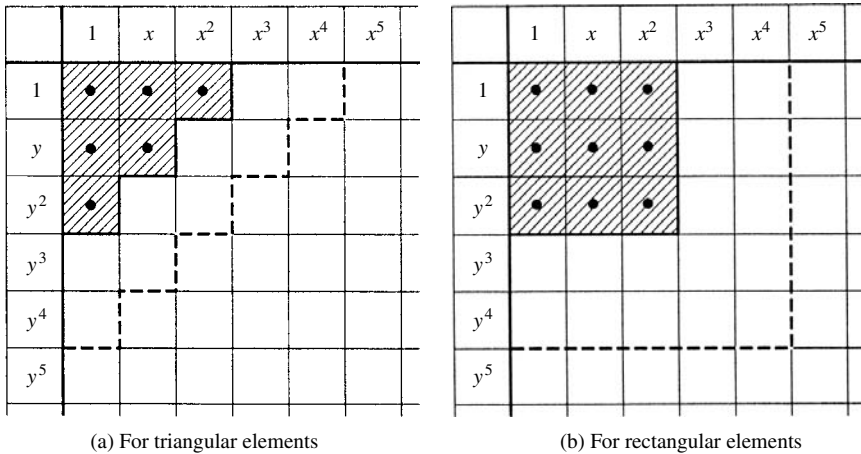


Figure 7.5.1 Polynomials in context in Pascal's triangle.

we cannot uniquely define its 10 unknown α_i coefficients with only three nodal points having three displacement quantities at each nodal point (Fig. 7.5.2a). Consequently, we must introduce an additional node located at the centroid of the triangle. While dealing with this center node creates certain computational difficulties, it is desirable to eliminate this additional nodal point. To reduce the number of coefficients in Eq. (7.5.5) to nine, Tocher collected the two terms x^2y and xy^2 by taking $\alpha_8 = \alpha_9$ [7.5.5]. The resulting shape function is not invariant to coordinate transformation and the convergence characteristics of the element formulated with it is not always monotone. To eliminate these problems, Bazeley and co-workers introduced $\alpha_2 = 0.5$ in the polynomial expression [7.5.6]. With this assumption, based on certain mathematical considerations, all other parameters could now be uniquely defined. The convergence characteristics of the formulated element are also quite satisfactory [7.5.7].

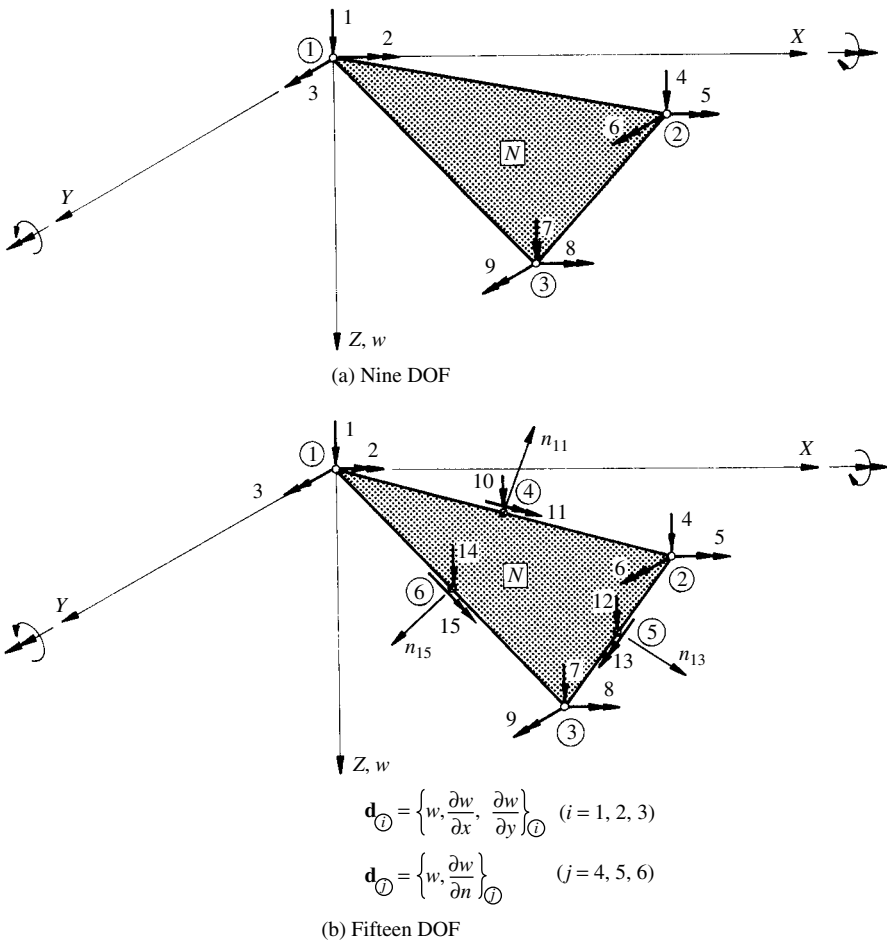


Figure 7.5.2 Triangular elements with 9 and 15 DOF.

With a complete polynomial of fourth degree,

$$w(x, y) = [1 \quad x \quad y \quad x^2 \quad xy \quad y^2 \quad \dots \quad xy^3 \quad y^4] \begin{Bmatrix} \alpha_1 \\ \alpha_2 \\ \alpha_3 \\ \vdots \\ \alpha_{15} \end{Bmatrix}, \quad (7.5.6)$$

we introduce 15 unknown coefficients α_i that again require an equal number of nodal DOF to be uniquely defined. An obvious choice for additional nodal displacements is the midpoint of each side of the triangle, as shown in Fig. 7.5.2b. Unfortunately, the required slope continuity along the sides is not yet satisfied with this shape function.

The next approach is the selection of a complete quintic polynomial,

$$w\{x, y\} = [1 \quad x \quad y \quad x^2 \quad xy \quad y^2 \quad \dots \quad x^2y^3 \quad xy^4 \quad y^5] \begin{Bmatrix} \alpha_1 \\ \alpha_2 \\ \alpha_3 \\ \vdots \\ \alpha_{21} \end{Bmatrix}, \quad (7.5.7)$$

with 21 coefficients α_i . By introducing six displacements per corner nodes,

$$\mathbf{d}_{\odot} = \left\{ w \quad \frac{\partial w}{\partial x} \quad \frac{\partial w}{\partial y} \quad \frac{\partial^2 w}{\partial x^2} \quad \frac{\partial^2 w}{\partial x \partial y} \quad \frac{\partial^2 w}{\partial y^2} \right\}_{\odot} \quad \text{for } i = 1, 2, 3, \quad (7.5.8)$$

and three additional displacement quantities in form of normal slopes at the midpoints of the sides,

$$\mathbf{d}_{\odot} = \left(\frac{\partial w}{\partial n} \right)_{\odot} \quad \text{for } j = 4, 5, 6, \quad (7.5.9)$$

as shown in Fig. 7.5.3, we can uniquely define the 21 parameters α_i in Eq. (7.5.7). Triangular elements formulated with this polynomial yields excellent results [7.5.3]. Finally, in Fig. 7.5.4 we give a brief overview of the possibilities one can have for creating shape functions with polynomials for triangular plate elements [7.5.8].

b. Polynomials for Rectangular Elements. Numerous plate elements have rectangular geometry. Since in such a case the element sides are parallel to the local *Cartesian* coordinate system, it is more convenient to formulate a finite element of rectangular shape than a triangular one. A typical rectangular element with four corner nodes is shown in Fig. 7.5.5a. At each node three displacements are introduced:

$$\mathbf{d}_{\odot} = \left\{ \begin{array}{c} w \\ \frac{\partial w}{\partial x} \\ \frac{\partial w}{\partial y} \end{array} \right\}_{\odot} \quad \text{for } i = 1, 2, 3, 4. \quad (7.5.10)$$

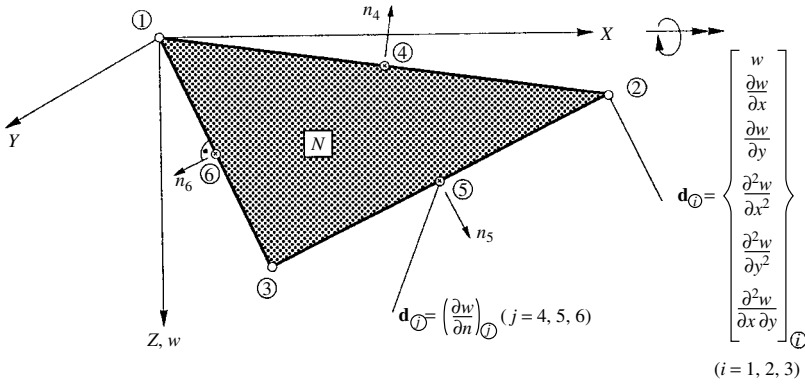


Figure 7.5.3 Triangular element based on complete quintic polynomial.

The polynomial expression that defines the corresponding shape function is

$$w(x, y) = [1 \quad x \quad y \quad x^2 \quad xy \quad y^2 \quad x^3 \quad x^2y \quad xy^2 \quad y^3 \quad x^3y \quad xy^3] \begin{Bmatrix} \alpha_1 \\ \alpha_2 \\ \alpha_3 \\ \vdots \\ \alpha_{12} \end{Bmatrix}. \quad (7.5.11)$$

This is an incomplete fourth-order polynomial in x and y with x^4 , x^2y^2 and y^4 terms missing, as shown in Fig. 7.5.5b. Furthermore, because the normal slopes $\partial w / \partial n$ are not compatible, slope discontinuities occur at the adjacent edges. The corresponding element was originally developed by Melosh, Zienkiewicz and Cheung [7.5.9, 7.5.10] and is therefore referred to in the pertinent literature as the MCZ rectangle. However, the explicit form for the pertinent stiffness matrix was derived by Aldini, Clough and Melosh; consequently, this element is sometimes also labeled as ACM. Although the derived element is not conforming, it delivers satisfactory results, as discussed in Sec. 7.6.1. The reason for its good performance is manifold. First, the presence of 1 , x , y , x^2 , xy and y^2 terms in Eq. (7.5.11) guarantees rigid-body motion and constant-curvature states of deformations. Second, with the fourth-order terms x^3y and xy^3 the governing differential equation of the plate is satisfied when a and b are approaching zero.

To obtain a conforming rectangular plate element, we add the second-order twist derivative $\partial^2 w / \partial x \partial y$ as the nodal DOF. Thus, the displacements for a typical corner node i , as shown in Fig. 7.5.6a, are

$$\mathbf{d}_i = \begin{Bmatrix} w \\ -\frac{\partial w}{\partial x} \\ \frac{\partial w}{\partial y} \\ \frac{\partial^2 w}{\partial x \partial y} \end{Bmatrix}_{\text{at node } i} \quad \text{for } i = 1, 2, 3, 4. \quad (7.5.12)$$

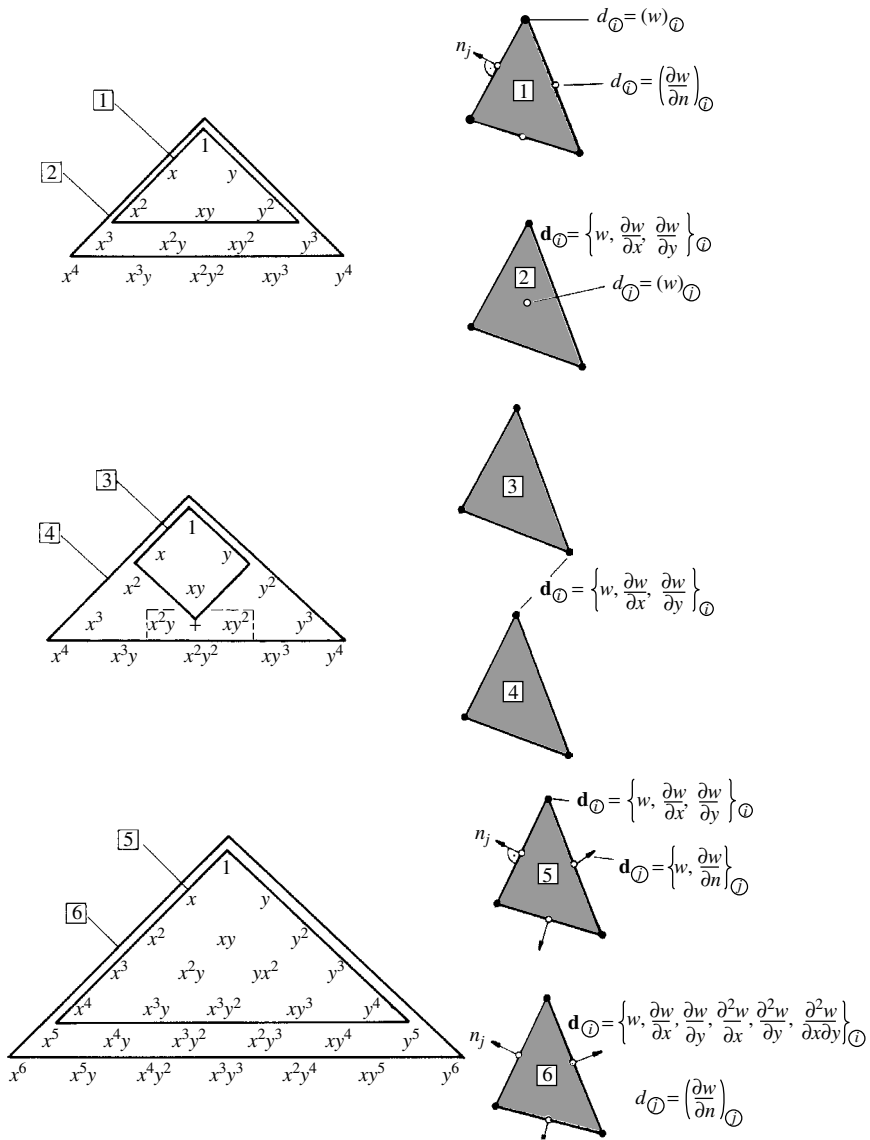
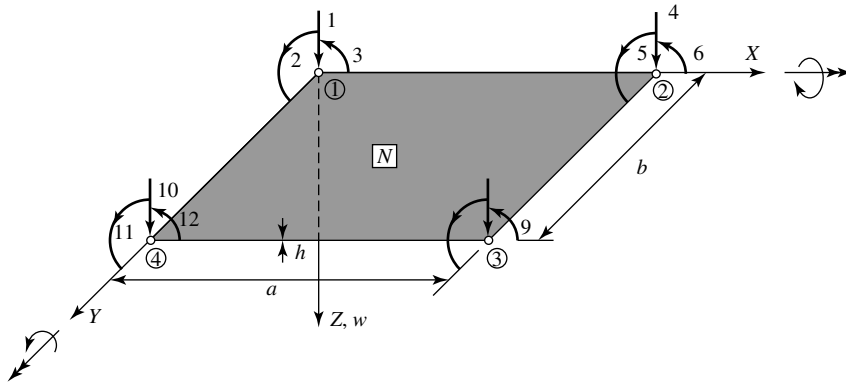


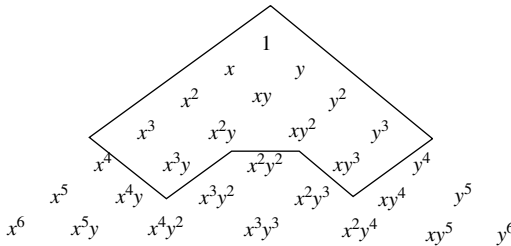
Figure 7.5.4 Overview of triangular elements in polynomial element family.

In this case, the shape function contains 16 terms of the complete sixth-order polynomial (Fig. 7.5.6b)

$$\begin{aligned}
 w(x, y) = & \alpha_1 + \alpha_2 x + \alpha_3 y + \alpha_4 x^2 + \alpha_5 xy + \alpha_6 y^2 + \alpha_7 x^3 + \alpha_8 x^2 y + \alpha_9 xy^2 \\
 & + \alpha_{10} y^3 + \alpha_{11} x^3 y + \alpha_{12} x^2 y^2 + \alpha_{13} xy^3 + \alpha_{14} x^4 y^2 \\
 & + \alpha_{15} x^2 y^3 + \alpha_{16} x^3 y^3,
 \end{aligned} \tag{7.5.13}$$



(a) Element



(b) Terms used in Pascal's triangle

Figure 7.5.5 Nonconforming rectangular element with 12 DOF.

achieving compatible slope conditions at all four edges. The convergence characteristics of the obtained rectangular element are very good. The above given shape function can also be written in terms of a bicubic *Hermitian* polynomial, as shown in the subsequent section.

Bogner and his co-workers developed a more refined shape function [7.5.11] based on a biquintic polynomial (Fig. 7.5.7). The corresponding rectangular element with four corner nodes has the following nine nodal displacements:

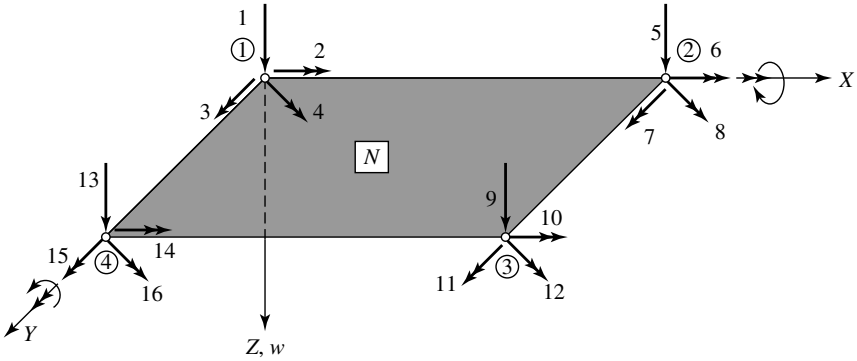
$$\mathbf{d}_{\odot} = \left\{ w \quad \frac{\partial w}{\partial x} \quad \frac{\partial w}{\partial y} \quad \frac{\partial^2 w}{\partial x^2} \quad \frac{\partial^2 w}{\partial y^2} \quad \frac{\partial^2 w}{\partial x \partial y} \quad \frac{\partial^3 w}{\partial x^2 \partial y} \quad \frac{\partial^3 w}{\partial x \partial y^2} \quad \frac{\partial^4 w}{\partial x^2 \partial y^2} \right\}. \quad (7.5.14)$$

As expected, on the one hand, such a plate element has superior convergence characteristics but, on the other hand, its complexity creates certain computational difficulties.

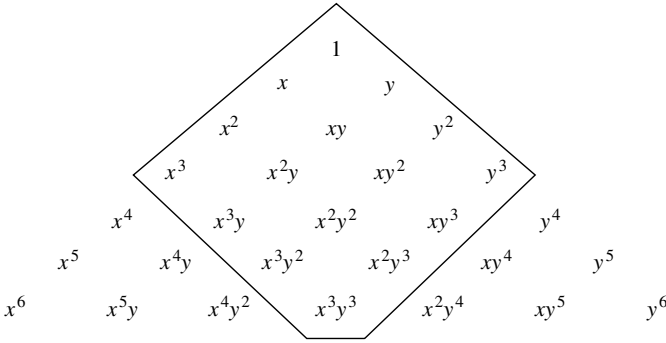
7.5.2 Hermitian Elements

Shape functions in polynomial form, in general, do not provide constant twist modes; thus, the convergence of such elements to the correct solutions is not always guaranteed. To overcome this problem, we already introduced a polynomial[†] with 16

[†] See Eq. (7.5.13).



(a) Element



(b) Terms used in Pascal's triangle

Figure 7.5.6 Conforming rectangular element with 16 DOF.

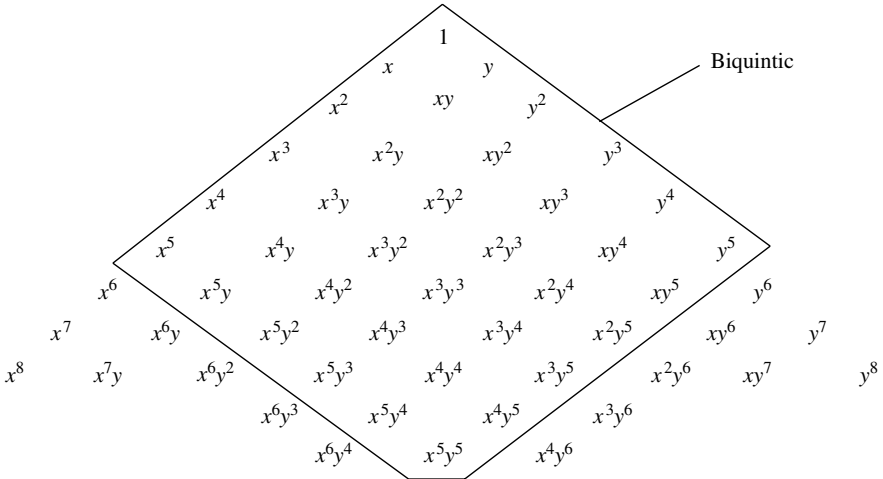


Figure 7.5.7 Terms used in Pascal's triangle for high-precision rectangular element.

constants—equal to the number of nodal displacements—that includes the twisting freedom $\partial^2 w / \partial x \partial y$ into the vector of nodal displacements, \mathbf{d}_e , given in Eq. (7.5.12). An alternative approach is the use of *Hermitian* polynomials.

First, we introduce the one-dimensional *Hermitian cubic* polynomial

$$w(\xi) = d_1 N_1(\xi) + d_2 N_2(\xi) + d_3 N_3(\xi) + d_4 N_4(\xi), \quad (7.5.15)$$

where $\xi = x/l$ and

$$\begin{aligned} N_1(\xi) &= 1 - 3\xi^2 + 2\xi^3, \\ N_2(\xi) &= (\xi - 2\xi^2 + \xi^3)l, \\ N_3(\xi) &= 3\xi^2 - 2\xi^3, \\ N_4(\xi) &= -(\xi^2 + \xi^3)l. \end{aligned} \quad (7.5.16)$$

These shape functions are depicted in Fig. 7.5.8. The reader will readily recognize them as the equations of deflected shape of a beam to which unit translations and rotations have been applied at the ends. These shape functions have the required features: That is, either the function or its derivative takes the value of unity at one end and both are zero at the other end.

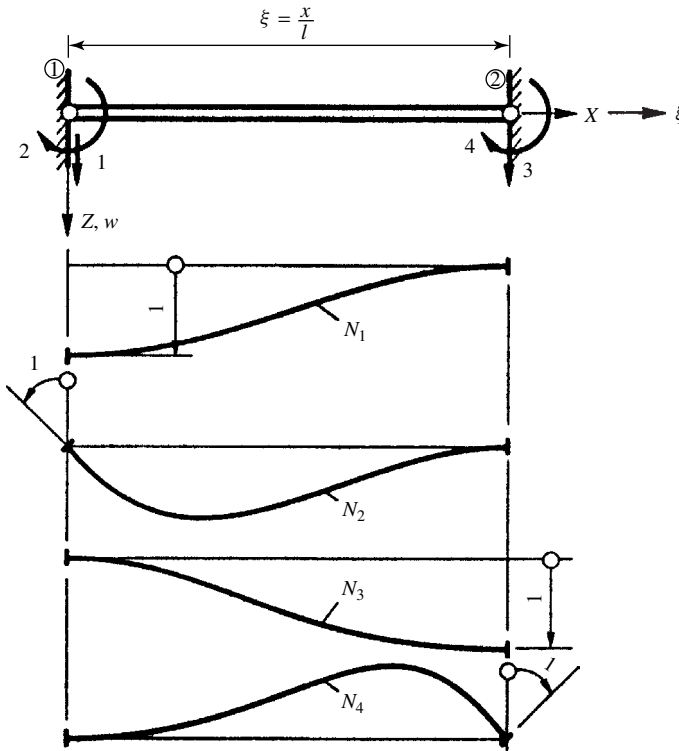


Figure 7.5.8 Shape functions of beam.

Next, we can form the products of these one-dimensional expressions to obtain the two-dimensional case. Thus,

$$\begin{aligned} \{N\}_{\textcircled{1}} &= \begin{Bmatrix} N_1(\xi) & N_1(\eta) \\ N_1(\xi) & N_2(\eta) \\ -N_2(\xi) & N_1(\eta) \\ N_2(\xi) & N_2(\eta) \end{Bmatrix}_{\textcircled{1}}, & \{N\}_{\textcircled{2}} &= \begin{Bmatrix} N_3(\xi) & N_1(\eta) \\ N_3(\xi) & N_2(\eta) \\ N_4(\xi) & N_1(\eta) \\ N_4(\xi) & N_2(\eta) \end{Bmatrix}_{\textcircled{2}}, \\ \{N\}_{\textcircled{3}} &= \begin{Bmatrix} N_3(\xi) & N_3(\eta) \\ N_3(\xi) & N_4(\eta) \\ N_4(\xi) & N_3(\eta) \\ N_4(\xi) & N_4(\eta) \end{Bmatrix}_{\textcircled{3}}, & \{N\}_{\textcircled{4}} &= \begin{Bmatrix} N_1(\xi) & N_3(\eta) \\ N_1(\xi) & N_4(\eta) \\ N_2(\xi) & N_3(\eta) \\ N_2(\xi) & N_4(\eta) \end{Bmatrix}_{\textcircled{4}}, \end{aligned} \quad (7.5.17)$$

where

$$\begin{aligned} N_1(\xi) &= 1 - \xi^2 + 2\xi^3, & N_1(\eta) &= 1 - \eta^2 - 2\eta^3, \\ N_2(\xi) &= (\xi - 2\xi^2 + \xi^3)a, & N_2(\eta) &= (\eta - 2\eta^2 + \eta^3)b, \\ N_3(\xi) &= 3\xi^2 - 2\xi^3, & N_3(\eta) &= 3\eta^2 - 2\eta^3, \\ N_4 &= (-\xi^2 + \xi^3)a, & N_4(\eta) &= (-\eta^2 + \eta^3)b, \end{aligned} \quad (7.5.18)$$

and

$$\begin{aligned} l &= a, & \xi &= \frac{x}{a}, \\ l &= b, & \eta &= \frac{y}{b}. \end{aligned} \quad (7.5.19)$$

Hence the two-dimensional form of the Hermitian shape functions can be written as

$$w(x, y) = \begin{bmatrix} \{N_1\}^T & \{N_2\}^T & \{N_3\}^T & \{N_4\}^T \end{bmatrix} \begin{Bmatrix} d_1 \\ d_2 \\ d_3 \\ \vdots \\ d_{15} \\ d_{16} \end{Bmatrix}. \quad (7.5.20)$$

The corresponding functions associated with four DOF at the corner node $\textcircled{1}$ are depicted in Fig. 7.5.9.

These types of Hermitian shape functions were first introduced by Bogner and his co-workers to formulate a rectangular plate element with $C^{(1)}$ continuity [7.5.13]. An explicit expression for the derived stiffness matrix \mathbf{K}_e is given in Sec. 7.7.1. A similar approach, but with some improvements, has been taken in Ref. [7.5.13].

To seek a more accurate solution, one can also consider a fifth-order Hermitian polynomials. Once again, Fig. 7.5.10 shows such a plate element and the one introduced above in the context of Pascal's triangle.

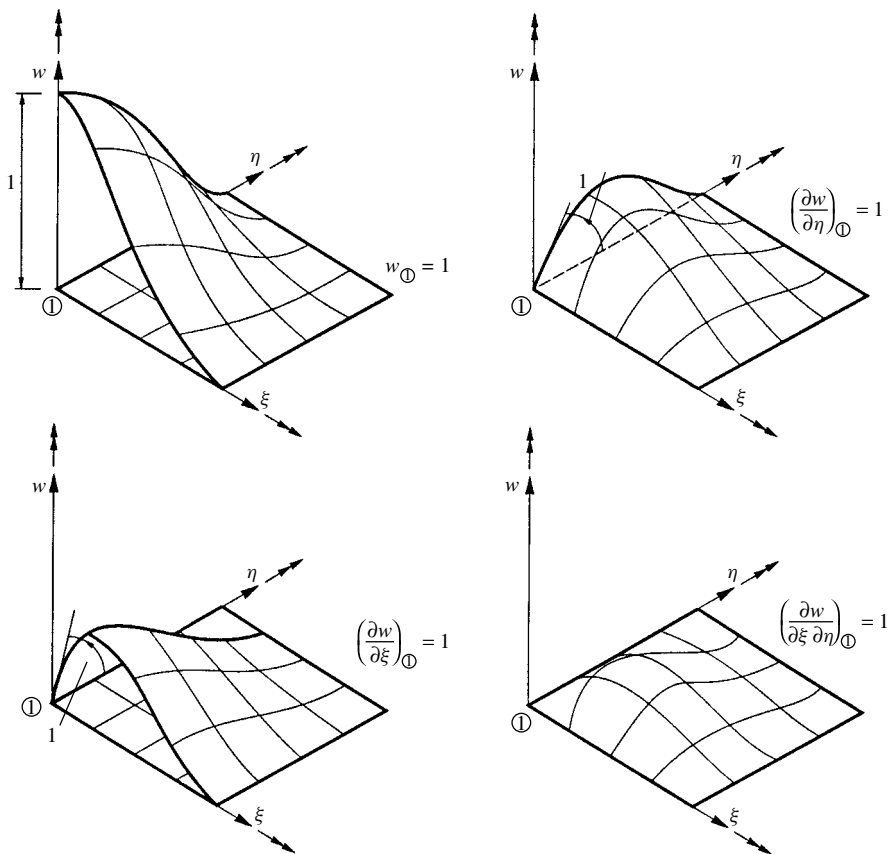


Figure 7.5.9 Shape functions at node 1 of rectangular plate.

7.5.3 Other Element Families

In this section we intend to give only a brief summary of some additional element families that are used in the finite element analysis of plates. Interested readers should refer to the pertinent literature for more details [7.5.14].

a. Lagrangian Elements. These elements are characterized by using nodal displacements for values of dependent variables. The two-dimensional *Lagrangian* interpolation functions are obtained from the *Cartesian* products of one-dimensional equations. A rectangular element with complete quadratic representation, for instance, contains nine parameters and hence nine nodes. Consequently, an internal node is required to be able to uniquely define these parameters. The usefulness of this element family is limited by (a) a number of internal nodes that usually must be eliminated and (b) its poor curve-fitting properties.

b. Serendipity Elements. This element family is actually a Lagrangian element and is characterized by omission of internal nodes. The interpolation functions of *serendipity* elements are not complete since the last terms are omitted, as illustrated

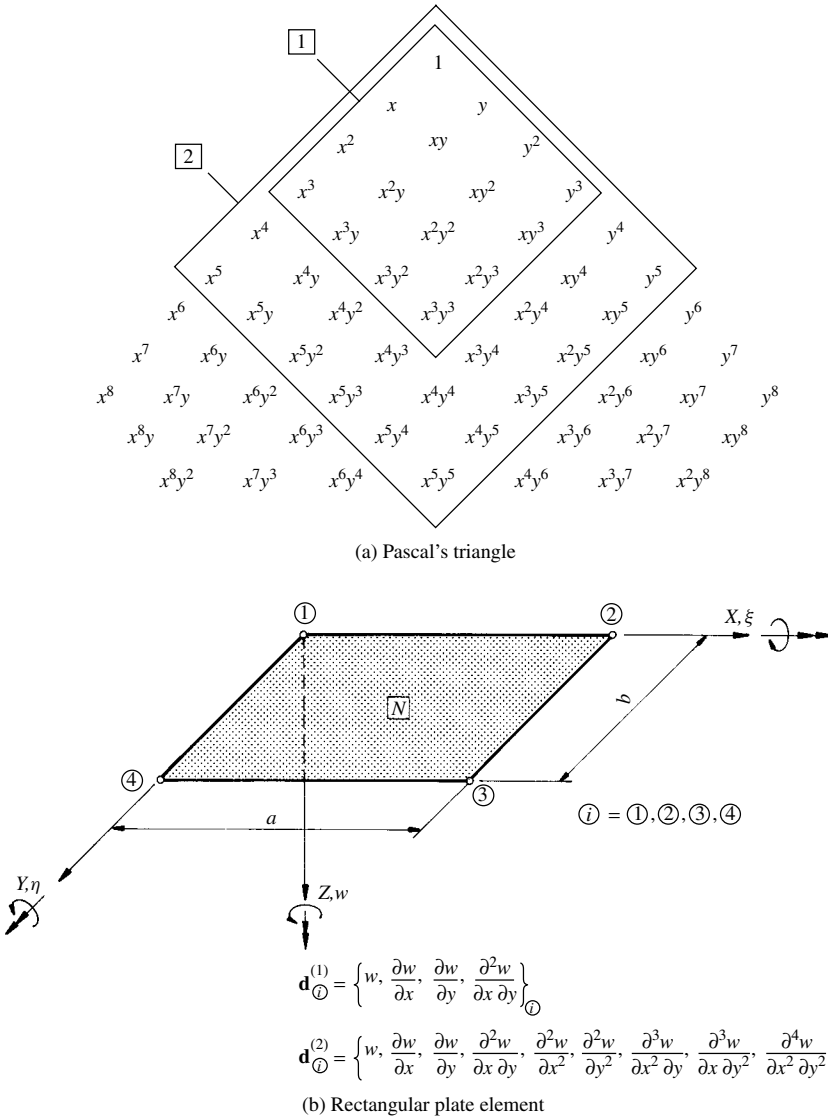


Figure 7.5.10 Hermitian elements in context of Pascal's triangle.

in the context of Pascal's triangle (Fig. 7.5.11). We are referring here only to two variants of rectangular serendipity elements: one with four corner nodes and another with eight nodes. In both cases the DOF per node points are one translation w and two rotations $\partial w / \partial x$ and $\partial w / \partial y$. These elements have been proven to be effective in plate analysis.

c. Hierarchical Elements. Recently some alternate types of interpolation functions have become popular for formulating plate elements. They are called *hierarchical*

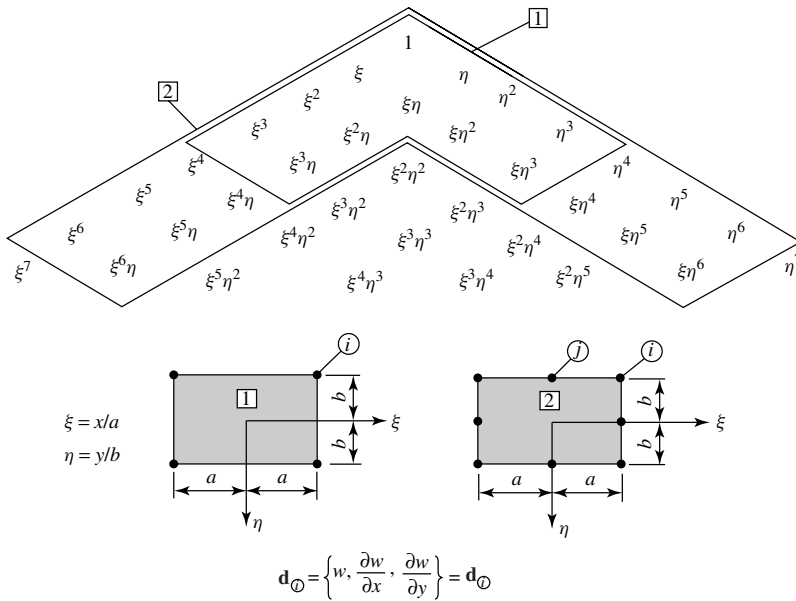


Figure 7.5.11 Serendipity elements in context of Pascal's triangle.

functions. The unique feature of these polynomials is that the higher-order polynomials contain the lower-order ones.

d. Heterosis Elements. These elements—used mostly for moderately thick plates—represent a synthesis of selectively integrated nine-node Lagrangian elements and eight-node serendipity elements. The name *heterosis* (used mostly in genetics) refers to improvement in characteristics exhibited by hybrids over those of their parents. The selective integration technique will be treated later.

Summary. In this section a number of shape functions and corresponding element families were introduced with the sole purpose of illustrating the predominant complexity associated with the element selection procedure. While formulation of element stiffness matrices is a relatively standard approach, selection of appropriate shape functions, which guarantee monotonic convergence to the correct solution, represents a difficult task requiring experience, time and even a certain amount of serendipity. Thus, it is best left to qualified research engineers. In subsequent sections, the reader will find readily usable stiffness matrices with proven convergence characteristics in explicit form for triangular and rectangular plate bending elements.

References and Bibliography

- [7.5.1] HRABOK, M. M., and HRUDEY, T. M., "A Review of Catalogue of Plate Bending Elements," *Comp. Struct.*, 19 (1984), 479–495.
- [7.5.2] BELL, K., "Triangular Plate Bending Elements," in *Finite Element Methods*, Tapir, Trondheim, 1969, pp. 213–261.
- [7.5.3] HRABOK, M. M., and HRUDEY, T. M., "Finite Element Analysis in Design of Floor Systems," *J. Struct. Eng., ASCE*, 109 (1983), 909–925.

- [7.5.4] CLOUGH, R. W., and TOCHER, J. L., "Finite Element Stiffness Matrices for Analysis of Plate Bending," in *Proceedings of the First Conference on Matrix Methods in Structural Mechanics*, AF Publ. No. AFFDL TR-6680, Wright-Patterson Air Force Base, Dayton, Ohio, 1965, pp. 515–546.
- [7.5.5] TOCHER, J. L., "Analysis of Plate Bending Using Triangular Elements," Ph.D. Thesis, University of California, Berkeley, 1962.
- [7.5.6] BAZELEY, G. P., et al., "Triangular Elements in Plate Bending," in *Proceedings of the First Conference on Matrix Methods in Structural Mechanics*, AF Publ. No. AFFDL TR-6680, Wright-Patterson Air Force Base, Dayton, Ohio, 1965, pp. 547–576.
- [7.5.7] SZILARD, R., et al., *BASIC-Programme für Baumechanik und Statik*, Ernst & Sohn, Berlin, 1986.
- [7.5.8] AVRAM, C., et al., *Numerical Analysis of Reinforced Concrete Structures*, Elsevier Science, Amsterdam, 1993.
- [7.5.9] MELOSH, R. J., "Basis of Derivation of Matrices for Direct Stiffness Method," *J. AIAA*, 1 (1963), 1631–1637.
- [7.5.10] ZIENKIEWICZ, O. C., and CHEUNG, Y. K., "The Finite Element Method for Analysis of Elastic Isotropic and Orthotropic Slabs," *Proc. Inst. Civil Eng.*, 28 (1964), 471–488.
- [7.5.11] BOGNER, F. K., et al., "The Generation of Interelement Compatible Stiffness and Mass Matrices by Use of Interpolation Formulas," in *Proceedings of the First Conference on Matrix Methods in Structural Mechanics*, AF Publ. No. AFFDL TR-6680, Wright-Patterson Air Force Base, Dayton, Ohio, 1965, pp. 397–443.
- [7.5.12] GALLAGHER, R. H., "Analysis of Plate and Shell Structures," in *Proceedings of Symposium on Application of Finite Element Methods in Civil Engineering*, Vanderbilt University, Nashville, Tennessee, 1969, pp. 155–205.
- [7.5.13] BUFLER, H., and STEIN, E., "Zur Plattenberechnung mittels finiter Elemente," *Ing. Arch.*, 39 (1970), 248–260.
- [7.5.14] KARDESTUNGER, H., and NORRIE, D. H. (Eds.), *Finite Element Handbook*, McGraw-Hill Book Co., New York, 1987.
- [7.5.15] REDDY, J. N., *An Introduction to the Finite Element Method*, McGraw-Hill Book Co., New York, 1993.

7.6 Simple Plate Elements

In this section low-order rectangular and triangular plate bending elements are introduced. Applying the *alternative formulation* technique described in Sec. 7.3c, *explicit* expressions for the stiffness matrix of the rectangular element are presented. Although these relatively simple elements have merely $C^{(0)}$ continuity, usable results can be obtained with them, as their practical applications demonstrate [7.6.1].

7.6.1 Rectangular Element with Four Corner Nodes

Let us consider the rectangular element shown in Fig. 7.6.1. For the nodal displacements, we choose one lateral displacement and two rotations; thus we can write

$$\mathbf{d}_{\odot} = \left\{ \begin{array}{c} w \\ \theta_x \\ \theta_y \end{array} \right\}_{\odot} \quad \text{for } \odot = 1, 2, 3, 4. \quad (7.6.1)$$

In this case, we select the polynomial expression given in Eq. (7.5.11) to define the displacement field of the element. As Fig. 7.5.5b illustrates, certain terms are omitted

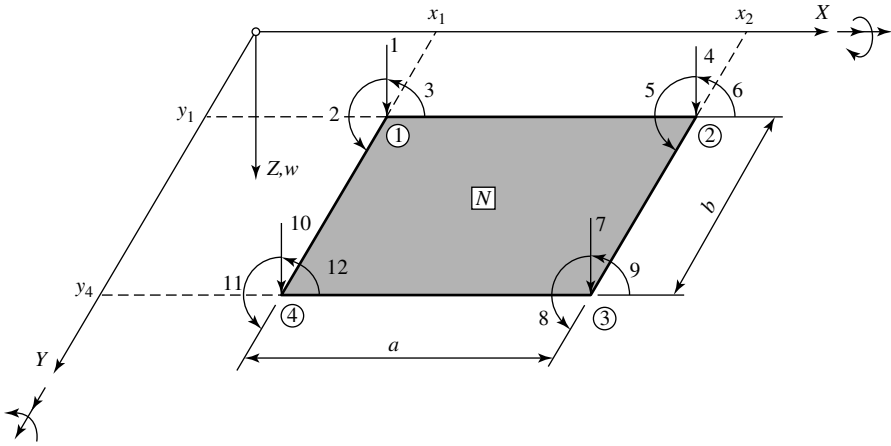


Figure 7.6.1 Rectangular element with four corner nodes.

from the complete fourth-order polynomial to be able determine the 12 parameters α_i in the shape function

$$w(x, y) = \alpha_1 + \alpha_2 x + \alpha_3 y + \alpha_4 x^2 + \alpha_5 xy + \alpha_6 y^2 + \alpha_7 x^3 + \alpha_8 x^2 y + \alpha_9 xy^2 + \alpha_{10} y^3 + \alpha_{11} x^3 y + \alpha_{12} xy^3 = \mathbf{w}^T \boldsymbol{\alpha} \quad (7.6.2)$$

with the help of 12 displacement components,

$$\mathbf{d}_e = \{d_1 \quad d_2 \quad d_3 \quad \cdots \quad d_{11} \quad d_{12}\}. \quad (7.6.3)$$

Before we demonstrate how this can be accomplished, let us first investigate this shape function more closely. In particular, at $x = 0$, the shape function becomes

$$w(y)_{x=0} = \alpha_1 + \alpha_3 y + \alpha_6 y^2 + \alpha_{10} y^3, \quad (7.6.4)$$

which permits its unique definition with the four nodal displacements d_1, d_2, d_{10} and d_{11} , but the pertinent slope equation

$$\left(\frac{\partial w}{\partial x} \right)_{x=0} = \alpha_2 + \alpha_5 y + \alpha_9 y^2 + \alpha_{12} y^3 \quad (7.6.5)$$

with four unknowns cannot be uniquely determined with only d_3 and d_{12} displacement components. Consequently, discontinuity of the normal slope will occur. The case at the other element boundaries at $x = a, y = 0$ and $y = b$ is similar. Hence this element is nonconforming and has only $C^{(0)}$ continuity. In spite of this apparent weakness, this simple element delivers good results. The reasons for this relatively good performance were already discussed in Sec. 7.5.1b.

The rotation about the X axis of nodal point \textcircled{i} is obtained from

$$(\theta_x)_{\textcircled{i}} = \left(\frac{\partial w}{\partial y} \right)_{\textcircled{i}} = \alpha_3 + \alpha_5 x + 2\alpha_6 y + \alpha_8 x^2 + 2\alpha_9 xy + 3\alpha_{10} y^2 + \alpha_{11} x^3 + 3\alpha_{12} xy^2. \quad (7.6.6)$$

Similarly, the rotation about the Y axis is calculated from

$$(\theta_y)_{\textcircled{1}} = - \left(\frac{\partial w}{\partial x} \right)_{\textcircled{1}} = -\alpha_2 - 2\alpha_4 x - \alpha_5 y - 3\alpha_7 x^2 - 2\alpha_8 xy - \alpha_9 y^2 - 3\alpha_{11} x^2 y - \alpha_{12} y^3. \quad (7.6.7)$$

The minus sign in this equation is due to the already discussed[†] differences in sign conventions used in classical plate theory and FEMs, respectively.

To determine the unknown parameters α_i in Eq. (7.6.2), we substitute the nodal point coordinates x_i and y_i into Eqs. (7.6.2), (7.6.6) and (7.6.7). Thus, we can write

$$\mathbf{d}_e = \begin{Bmatrix} w_{\textcircled{1}} \\ \theta_{x\textcircled{1}} \\ \theta_{y\textcircled{1}} \\ w_{\textcircled{2}} \\ \theta_{x\textcircled{2}} \\ \theta_{y\textcircled{2}} \\ w_{\textcircled{3}} \\ \theta_{x\textcircled{3}} \\ \theta_{y\textcircled{3}} \\ w_{\textcircled{4}} \\ \theta_{x\textcircled{4}} \\ \theta_{y\textcircled{4}} \end{Bmatrix} = \mathbf{A} \begin{Bmatrix} \alpha_1 \\ \alpha_2 \\ \alpha_3 \\ \alpha_4 \\ \alpha_5 \\ \alpha_6 \\ \alpha_7 \\ \alpha_8 \\ \alpha_9 \\ \alpha_{10} \\ \alpha_{11} \\ \alpha_{12} \end{Bmatrix}, \quad (7.6.8)$$

where the explicit form of matrix \mathbf{A} is

$$\mathbf{A} = \begin{array}{c} \begin{array}{cccccccccccc} 1 & 2 & 3 & 4 & 5 & 6 & 7 & 8 & 9 & 10 & 11 & 12 \end{array} \\ \left[\begin{array}{ccc|ccc|ccc|ccc} 1 & x_1 & y_1 & x_1^2 & x_1 y_1 & y_1^2 & x_1^3 & x_1^2 y_1 & x_1 y_1^2 & y_1^3 & x_1^3 y_1 & x_1 y_1^3 \\ 0 & -1 & 0 & -2x_1 & -y_1 & 0 & -3x_1^2 & -2x_1 y_1 & -y_1^2 & 0 & -3x_1^2 y_1 & -y_1^3 \\ 0 & 0 & 1 & 0 & x_1 & 2y_1 & 0 & x_1^2 & 2x_1 y_1 & 3y_1^2 & x_1^3 & 3x_1 y_1^2 \end{array} \right\} \textcircled{1} \\ \hline \left[\begin{array}{ccc|ccc|ccc|ccc} 1 & x_2 & y_2 & x_2^2 & x_2 y_2 & y_2^2 & x_2^3 & x_2^2 y_2 & x_2 y_2^2 & y_2^3 & x_2^3 y_2 & x_2 y_2^3 \\ 0 & -1 & 0 & -2x_2 & -y_2 & 0 & -3x_2^2 & -2x_2 y_2 & -y_2^2 & 0 & -3x_2^2 y_2 & -y_2^3 \\ 0 & 0 & 1 & 0 & x_2 & 2y_2 & 0 & x_2^2 & 2x_2 y_2 & 3y_2^2 & x_2^3 & 3x_2 y_2^2 \end{array} \right\} \textcircled{2} \\ \hline \left[\begin{array}{ccc|ccc|ccc|ccc} 1 & x_3 & y_3 & x_3^2 & x_3 y_3 & y_3^2 & x_3^3 & x_3^2 y_3 & x_3 y_3^2 & y_3^3 & x_3^3 y_3 & x_3 y_3^3 \\ 0 & -1 & 0 & -2x_3 & -y_3 & 0 & -3x_3^2 & -2x_3 y_3 & -y_3^2 & 0 & -3x_3^2 y_3 & -y_3^3 \\ 0 & 0 & 1 & 0 & x_3 & 2y_3 & 0 & x_3^2 & 2x_3 y_3 & 3y_3^2 & x_3^3 & 3x_3 y_3^2 \end{array} \right\} \textcircled{3} \\ \hline \left[\begin{array}{ccc|ccc|ccc|ccc} 1 & x_4 & y_4 & x_4^2 & x_4 y_4 & y_4^2 & x_4^3 & x_4^2 y_4 & x_4 y_4^2 & y_4^3 & x_4^3 y_4 & x_4 y_4^3 \\ 0 & -1 & 0 & -2x_4 & -y_4 & 0 & -3x_4^2 & -2x_4 y_4 & -y_4^2 & 0 & -3x_4^2 y_4 & -y_4^3 \\ 0 & 0 & 1 & 0 & x_4 & 2y_4 & 0 & x_4^2 & 2x_4 y_4 & 3y_4^2 & x_4^3 & 3x_4 y_4^2 \end{array} \right\} \textcircled{4} \end{array} \quad (7.6.9)$$

[†] See Figs. 6.4.6 and 7.3.1a.

Since

$$\mathbf{d}_e = \mathbf{A}\boldsymbol{\alpha} \quad \text{and} \quad \boldsymbol{\alpha} = \mathbf{A}^{-1}\mathbf{d}_e, \quad (7.6.10)$$

the shape function can be obtained from

$$w(x, y) = \mathbf{w}^T \boldsymbol{\alpha} = \mathbf{w}^T \mathbf{A}^{-1} \mathbf{d}_e = \{\mathbf{N}\}^T \mathbf{d}_e. \quad (7.6.11)$$

Aldini and Clough [7.6.2] were the first to derive explicit expressions for the element stiffness matrix \mathbf{K}_e in the form

$$\mathbf{K}_e^{(N)} = \frac{Eh}{180(1-\nu^2)} \begin{bmatrix} 1 & 2 & 3 & 4 & 5 & 6 & 7 & 8 & 9 & 10 & 11 & 12 \\ F & G & -H & L & -M & -N & O & -P & -Q & I & J & -K & 1 \\ & R & -Z & -M & T & \phi & P & U & \phi & -J & S & \phi & 2 \\ & & V & N & \phi & X & Q & \phi & Y & -K & \phi & W & 3 \\ & & & F & G & H & I & J & K & O & -P & Q & 4 \\ & & & & R & Z & -J & S & \phi & P & U & \phi & 5 \\ & & \text{Symmetric} & & & V & K & \phi & W & -Q & \phi & Y & 6 \\ & & & & & & F & -G & H & L & M & N & 7 \\ & & & & & & & R & -Z & M & T & \phi & 8 \\ & & & & & & & & V & -N & \phi & X & 9 \\ & & & & & & & & & F & -G & -H & 10 \\ & & & & & & & & & & R & Z & 11 \\ & & & & & & & & & & & V & 12 \end{bmatrix}, \quad (7.6.12)$$

where the individual stiffness coefficients are

$$\begin{aligned} F &= \frac{(42 - 12\nu + 60\rho^2 + 60\rho^{-2})h^2}{ab}, & Q &= \frac{[15\rho^{-1} - 3(1 - \nu)\rho]h^2}{a}, \\ G &= \frac{(30\rho + 3\rho^{-1} + 12\nu\rho^{-1})h^2}{b}, & R &= [20\rho + 4(1 - \nu)\rho^{-1}]h^2, \\ H &= \frac{(30\rho^{-1} + 3\rho + 12\nu\rho)h^2}{a}, & S &= [10\rho - (1 - \nu)\rho^{-1}]h^2, \\ I &= \frac{(-42 + 12\nu - 60\rho^2 + 30\rho^{-2})h^2}{ab}, & T &= [10\rho - 4(1 - \nu)\rho^{-1}]h^2, \end{aligned}$$

$$\begin{aligned}
 J &= \frac{[30\rho + 3(1-\nu)\rho^{-1}]h^2}{b}, & U &= [5\rho + (1-\nu)\rho^{-1}]h^2, \\
 K &= \frac{(15\rho^{-1} - 3\rho - 12\nu\rho)h^2}{a}, & V &= [20\rho^{-1} + 4(1-\nu)\rho]h^2, \\
 L &= \frac{(-42 + 12\nu - 60\rho^{-2} + 30\rho^2)h^2}{ab}, & W &= [10\rho^{-1} - 4(1-\nu)\rho]h^2, \\
 M &= \frac{(-15\rho + 3\rho^{-1} + 12\nu\rho^{-1})h^2}{b}, & X &= [10\rho^{-1} - (1-\nu)\rho]h^2, \\
 N &= \frac{[30\rho^{-1} + 3(1-\nu)\rho]h^2}{a}, & Y &= [5\rho^{-1} + (1-\nu)\rho]h^2, \\
 O &= \frac{(42 - 12\nu - 30\rho^2 - 30\rho^{-2})h^2}{ab}, & Z &= (15\nu h^2), \\
 P &= \frac{[-15\rho + 3(1-\nu)\rho^{-1}]h^2}{b}, & \phi &= 0, \\
 \rho &= \frac{a}{b} \quad \text{and} \quad \rho^{-1} = \frac{b}{a}.
 \end{aligned} \tag{7.6.13}$$

Similar expressions can be found in Refs. [7.6.3–7.6.6]. The good monotonic convergence characteristics of this bending plate element are shown in Fig. 7.6.2. As mentioned in connection with gridwork cells, it is always advisable to check the macroscopic equilibrium of each column in a stiffness matrix to detect any printing errors. That is, the stiffness coefficients k_{ij} represent active or reactive nodal forces

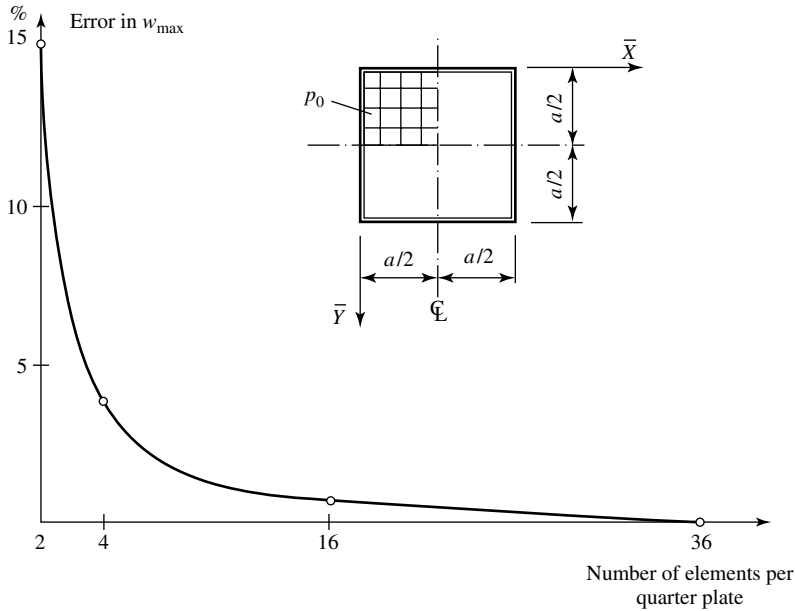


Figure 7.6.2 Convergence characteristics of nonconforming rectangular element.

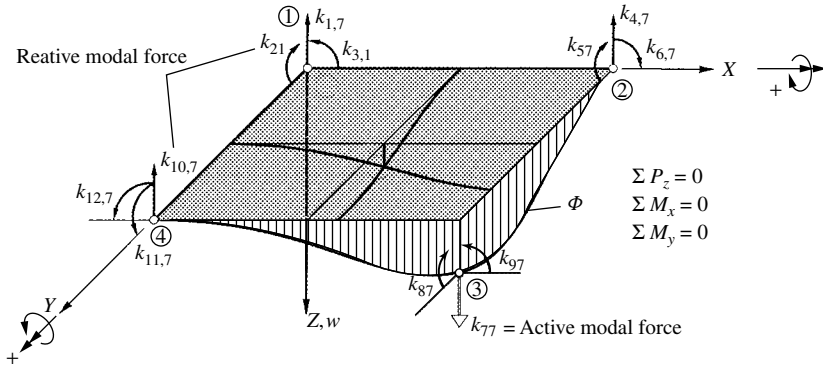


Figure 7.6.3 Equilibrium of stiffness coefficients.

created by unit displacement of one node while all other displacements are prevented from taking place, as illustrated in Fig. 7.6.3. These nodal forces must be in equilibrium.

7.6.2 Triangular Element with Three Corner Nodes

In most engineering applications, triangular plate elements are more attractive than rectangular ones, since it is easier to treat irregular boundaries with triangular shapes. In addition, it is also easier to vary element sizes in the vicinity of stress concentration. Against these obvious advantages of triangular bending elements, one must consider considerably increased difficulties encountered in generating element stiffness matrices. Therefore, it is extremely rare to find triangular element stiffness matrices in explicit forms. In most cases, however, FORTRAN or BASIC subroutines are available [7.6.1, 7.6.8].

As mentioned in Sec. 7.5.1a, it is not possible to uniquely define the 10 parameters in the cubic polynomial

$$w(x, y) = \alpha_1 + \alpha_2 x + \alpha_3 y + \alpha_4 x^2 + \alpha_5 xy + \alpha_6 y^2 + \alpha_7 x^3 + \alpha_8 x^2 y + \alpha_9 xy^2 + \alpha_{10} y^3 \quad (7.6.14)$$

with merely nine DOF. To eliminate this problem, Tocher [7.6.7] set $\alpha_8 = \alpha_9$ and obtained the shape function

$$w(x, y) = \mathbf{w}^T \boldsymbol{\alpha}, \quad (7.6.15)$$

with

$$\mathbf{w}^T = [1 \quad x \quad y \quad x^2 \quad xy \quad y^2 \quad x^3 \quad (x^2y + xy^2) \quad y^3] \quad (7.6.16a)$$

and

$$\boldsymbol{\alpha} = \begin{Bmatrix} \alpha_1 \\ \alpha_2 \\ \alpha_3 \\ \vdots \\ \alpha_9 \end{Bmatrix}. \quad (7.6.16b)$$

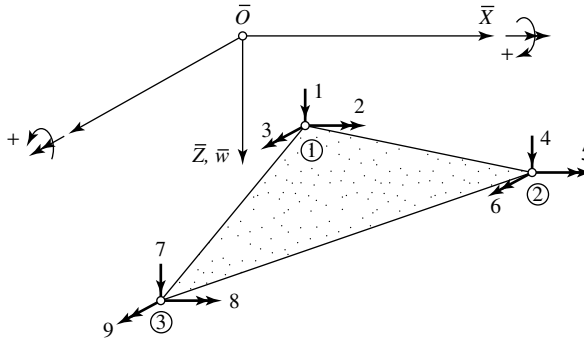


Figure 7.6.4 Triangular element of arbitrary shape.

For each node point \textcircled{i} , the transverse displacements and rotations about the X and Y axes are taken as DOF, as shown in Fig. 7.6.4, thus

$$\mathbf{d}_{\textcircled{i}} = \begin{Bmatrix} w \\ \theta \\ \theta_y \end{Bmatrix}_{\textcircled{i}} = \begin{Bmatrix} w \\ \frac{\partial w}{\partial y} \\ -\frac{\partial w}{\partial x} \end{Bmatrix}_{\textcircled{i}} \quad \text{for } \textcircled{i} = 1, 2, 3. \quad (7.6.17)$$

The minus sign for the third DOF indicates that if we take a positive dw displacement at the distance dx , the rotation dw/dx about the Y axis will be opposite to the corresponding direction of the rotation used in the FEM.

To derive the element stiffness matrix, we apply again the alternative formulation described in Sec. 7.3.2c. By substituting Eq. (7.6.16) into Eq. (7.6.17), we obtain

$$\begin{Bmatrix} w \\ \frac{\partial w}{\partial y} \\ -\frac{\partial w}{\partial x} \end{Bmatrix} = \begin{bmatrix} 1 & x & y & x^2 & xy & y^2 & x^3 & (x^2y + xy^2) & y^3 \\ 0 & 0 & 1 & 0 & x & 2y & 0 & (x^2 + 2xy) & 3y^2 \\ 0 & -1 & 0 & -2x & -y & 0 & -3x^2 & -(2xy + y^2) & 0 \end{bmatrix} \begin{Bmatrix} \alpha_1 \\ \alpha_2 \\ \vdots \\ \alpha_9 \end{Bmatrix}. \quad (7.6.18)$$

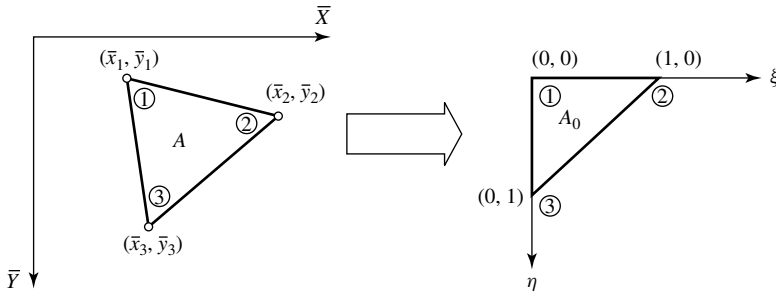


Figure 7.6.5 “Mapping” of arbitrary triangle into unit triangle.

The parameters $\alpha_1, \alpha_2, \dots, \alpha_9$ are calculated from

$$\boldsymbol{\alpha} = \mathbf{A}^{-1} \mathbf{d}_e, \quad (7.6.19)$$

where \mathbf{A} represents the transformation matrix that relates the generalized coordinates $\boldsymbol{\alpha}$ to the nodal point displacements \mathbf{d}_e in the form

$$\mathbf{A} = \begin{bmatrix} 1 & x_1 & y_1 & x_1^2 & x_1 y_1 & y_1^2 & x_1^3 & (x_1^2 y_1 + x_1 y_1^2) & y_1^3 \\ 0 & 0 & 1 & 0 & x_1 & 2y_1 & 0 & (x_1^2 + 2x_1 y_1) & 3y_1^2 \\ 0 & -1 & 0 & -2x_1 & -y_1 & 0 & -3x_1^2 & -(2x_1 y_1 + y_1^2) & 0 \\ 1 & x_2 & y_2 & x_2^2 & x_2 y_2 & y_2^2 & x_2^3 & (x_2^2 y_2 + x_2 y_2^2) & y_2^3 \\ 0 & 0 & 1 & 0 & x_2 & 2y_2 & 0 & (x_2^2 + 2x_2 y_2) & 3y_2^2 \\ 0 & -1 & 0 & -2x_2 & -y_2 & 0 & -3x_2^2 & -(2x_2 y_2 + y_2^2) & 0 \\ 1 & x_3 & y_3 & x_3^2 & x_3 y_3 & y_3^2 & x_3^3 & (x_3^2 y_3 + x_3 y_3^2) & y_3^3 \\ 0 & 0 & 1 & 0 & x_3 & 2y_3 & 0 & (x_3^2 + 2x_3 y_3) & 3y_3^2 \\ 0 & -1 & 0 & -2x_3 & -y_3 & 0 & -3x_3^2 & -(2x_3 y_3 + y_3^2) & 0 \end{bmatrix} \quad (7.6.20)$$

and

$$\mathbf{d}_e = \begin{Bmatrix} d_1 \\ d_2 \\ d_3 \\ \vdots \\ d_9 \end{Bmatrix} \quad (7.6.21)$$

are the nodal displacements of the element.

The element stiffness matrix is calculated from[†]

$$\mathbf{K}_e = (\mathbf{A}^{-1})^T \tilde{\mathbf{K}}_e \mathbf{A}^{-1} \quad \text{with} \quad \tilde{\mathbf{K}}_e = \int_A \mathbf{L}^T \mathbf{E} \mathbf{L} dA, \quad (7.6.22)$$

which require differentiation in matrix \mathbf{L} and integration over the area of the triangle, A . To facilitate these mathematical manipulations, the triangle is usually *mapped* into a rightangled, isosceles *unit* triangle in the ξ, η coordinate system, as shown in Fig. 7.6.5. Using the notation

$$\bar{x}_{ij} = \bar{x}_i - \bar{x}_j \quad \text{and} \quad \bar{y}_{ij} = \bar{y}_i - \bar{y}_j, \quad (7.6.23)$$

the correspondence between \bar{x}, \bar{y} coordinates and the new ξ, η coordinates can be expressed by

$$\bar{x} = \bar{x}_1 + \bar{x}_{21}\xi + \bar{x}_{31}\eta \quad \text{and} \quad \bar{y} = \bar{y}_1 + \bar{y}_{21}\xi + \bar{y}_{31}\eta. \quad (7.6.24)$$

Conversely,

$$\xi = \frac{1}{2A} [\bar{y}_{31}\bar{x} + \bar{x}_{13}\bar{y} + (\bar{x}_3\bar{y}_1 - \bar{x}_1\bar{y}_3)] \quad (7.6.25a)$$

[†] See Eqs. (7.3.41)–(7.3.43).

and

$$\eta = \frac{1}{2A} [\bar{y}_{12}\bar{x} + \bar{x}_{21}\bar{y} + (\bar{x}_1\bar{y}_2 - \bar{x}_2\bar{y}_1)]. \quad (7.6.25b)$$

Differentiation with respect to ξ and η may be expressed as

$$\begin{Bmatrix} \frac{\partial}{\partial \xi} \\ \frac{\partial}{\partial \eta} \end{Bmatrix} = \begin{bmatrix} \frac{\partial \bar{x}}{\partial \xi} & \frac{\partial \bar{y}}{\partial \xi} \\ \frac{\partial \bar{x}}{\partial \eta} & \frac{\partial \bar{y}}{\partial \eta} \end{bmatrix} = \mathbf{J} \begin{Bmatrix} \frac{\partial}{\partial \bar{x}} \\ \frac{\partial}{\partial \bar{y}} \end{Bmatrix}. \quad (7.6.26)$$

The elements of the Jacobian matrix \mathbf{J} are

$$\mathbf{J} = \begin{bmatrix} \bar{x}_{21} & \bar{y}_{21} \\ \bar{x}_{31} & \bar{y}_{31} \end{bmatrix}. \quad (7.6.27)$$

The inverse relation of Eq. (7.6.26) is

$$\begin{Bmatrix} \frac{\partial}{\partial \bar{x}} \\ \frac{\partial}{\partial \bar{y}} \end{Bmatrix} = \mathbf{J}^{-1} \begin{Bmatrix} \frac{\partial}{\partial \xi} \\ \frac{\partial}{\partial \eta} \end{Bmatrix}, \quad (7.6.28)$$

where

$$\mathbf{J}^{-1} = \frac{1}{2A} \begin{bmatrix} \bar{y}_{31} & \bar{y}_{12} \\ \bar{x}_{13} & \bar{x}_{21} \end{bmatrix}. \quad (7.6.29)$$

The integral of polynomial terms in ξ and η over the triangular area may be computed from

$$I_{pq} = \int_A \xi^p \eta^q dA = 2A \int_{A_0} \xi^p \eta^q dA_0 = 2A \frac{p!q!}{(p+q+2)!}. \quad (7.6.30)$$

Although symmetry is maintained by combining two of the cubic terms in Eq. (7.6.14), a lack of invariance has been introduced into this equation. Consequently, for certain orientations of the element sides with respect to the global coordinate axes \bar{X} , \bar{Y} , the matrix \mathbf{A} becomes singular and cannot be inverted. In spite of this shortcoming, this triangular element has been extensively used in the past, since reasonable good results could be obtained with it.

Zienkiewicz and his co-workers succeeded in constructing a more satisfactory stiffness matrix for simple triangular elements [7.6.10]. They also used the complete 10-term polynomial displacement expression given in Eq. (7.6.14) but reduced it to a 9-DOF expression by setting $\alpha_2 = 0.5$, thus eliminating the problem of invariance. This element is in principle similar to the one discussed above. Again, in formulating the element stiffness matrix, the procedure described above of *mapping* the general triangle into a unit triangle is used. Pertinent BASIC and FORTRAN programs for plate analysis can be found in Refs. [7.6.1] and [7.6.8], respectively. This element performs satisfactorily for all element orientations.

Summary. In this section nonconforming, low-order rectangular and triangular elements for plate bending analysis with the FEM are presented. While the stiffness matrix of the quite usable rectangular element could be formulated in explicit form, unfortunately, this was not the case for elements of general triangular shape. However, the procedure of generating stiffness matrices for triangular elements by employing the so-called *alternative formulation* technique is also explained in detail. For practical computation with triangular elements, the reader is referred to Sec. 7.7.2, where an explicitly formulated stiffness matrix for a higher-order triangular element is introduced. In addition, one can find an explicitly given stiffness matrix for a triangular element in Refs. [7.6.6] and [7.6.9].

ILLUSTRATIVE EXAMPLE

Let us determine the maximum displacement w_{\max} of the clamped rectangular plate shown in Fig. 7.6.6a by using the FEM in connection with the stiffness matrix given in Eq. (7.6.12). This procedure is fundamentally the same as the one previously employed in connection with framework cells.

Utilizing the apparent double symmetry of the structure and load, it is sufficient to deal only with a quarter plate, provided that “guided” boundary

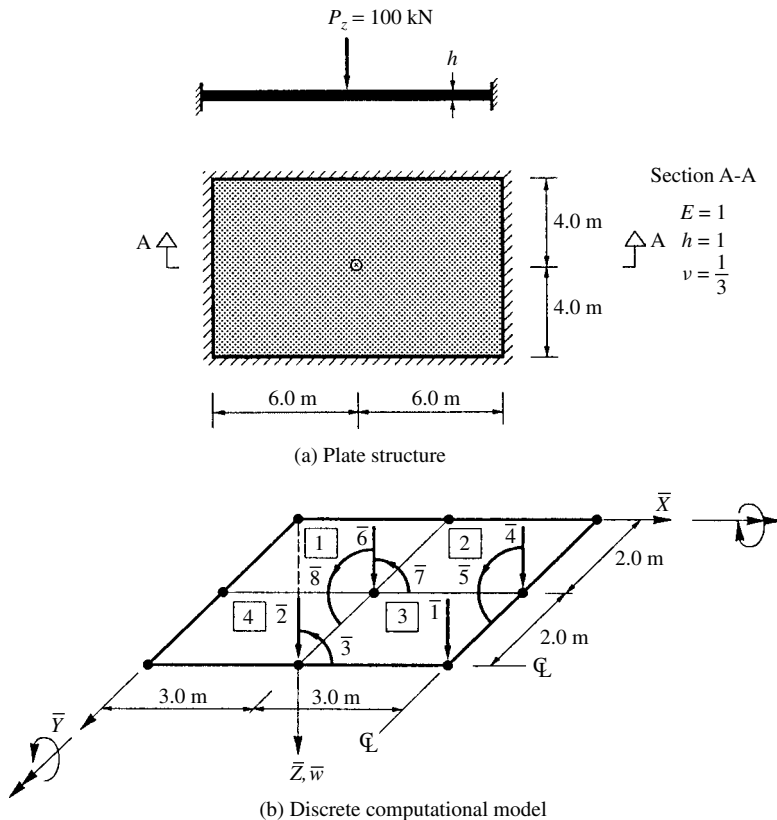


Figure 7.6.6 Rectangular plate with fixed edges under central load.

conditions are introduced at the symmetry lines. Using a crude subdivision of $2 \times 2 = 4$, the corresponding finite element computational model is shown in Fig. 7.6.6b. Employing the already familiar code-numbering technique, the following correspondence exists between the local and global numbers of the displacement components:

Element	1	2	3	4	5	6	7	8	9	10	11	12	Local numbers
1	$\bar{0}$	$\bar{0}$	$\bar{0}$	$\bar{0}$	$\bar{0}$	$\bar{0}$	$\bar{6}$	$\bar{8}$	$\bar{7}$	$\bar{0}$	$\bar{0}$	$\bar{0}$	Global numbers
2	$\bar{0}$	$\bar{0}$	$\bar{0}$	$\bar{0}$	$\bar{0}$	$\bar{0}$	$\bar{4}$	$\bar{5}$	$\bar{0}$	$\bar{6}$	$\bar{8}$	$\bar{7}$	
3	$\bar{6}$	$\bar{8}$	$\bar{7}$	$\bar{4}$	$\bar{5}$	$\bar{0}$	$\bar{1}$	$\bar{0}$	$\bar{0}$	$\bar{2}$	$\bar{0}$	$\bar{3}$	
4	$\bar{0}$	$\bar{0}$	$\bar{0}$	$\bar{6}$	$\bar{8}$	$\bar{7}$	$\bar{2}$	$\bar{0}$	$\bar{3}$	$\bar{0}$	$\bar{0}$	$\bar{0}$	

The stiffness matrix of the total structure obtained from elements 1 to 4 is

$$\bar{\mathbf{K}} = \frac{Eh}{180(1-\nu^2)} \begin{bmatrix} \bar{1} & \bar{2} & \bar{3} & \bar{4} & \bar{5} & \bar{6} & \bar{7} & \bar{8} \\ F & L & N & I & -J & O & Q & P \\ & 2F & 0 & O & P & 2I & 0 & -2J \\ & & 2V & Q & 0 & 0 & 2W & 0 \\ & & & 2F & 0 & 2L & 2N & 0 \\ & & & & 2R & 0 & 0 & 2T \\ & & & & & 4F & 0 & 0 \\ & & & & & & 4V & 0 \\ & & & & & & & 4R \end{bmatrix} \begin{matrix} \bar{1} \\ \bar{2} \\ \bar{3} \\ \bar{4} \\ \bar{5} \\ \bar{6} \\ \bar{7} \\ \bar{8} \end{matrix} \quad (7.6.31)$$

Substitution of the numerical values gives

$$\bar{\mathbf{K}} = \frac{1}{160} \begin{bmatrix} \bar{1} & \bar{2} & \bar{3} & \bar{4} & \bar{5} & \bar{6} & \bar{7} & \bar{8} \\ 33.278 & 0.472 & 7.667 & -26.611 & -23.167 & -7.139 & 2.333 & -10.583 \\ & 66.555 & 0 & -7.139 & -10.583 & -53.222 & 0 & -46.333 \\ & & 34.667 & 2.333 & 0 & 0 & 5.333 & 0 \\ & & & 66.555 & 0 & 0.944 & 15.333 & 0 \\ & & & & 63.555 & 0 & 0 & 26.444 \\ & & & & & 133.111 & 0 & 0 \\ & & & & & & 69.333 & 0 \\ & & & & & & & 127.111 \end{bmatrix} \begin{matrix} \bar{1} \\ \bar{2} \\ \bar{3} \\ \bar{4} \\ \bar{5} \\ \bar{6} \\ \bar{7} \\ \bar{8} \end{matrix} \quad (7.6.32)$$

With the load vector

$$\bar{\mathbf{p}} = \{25 \quad 0 \quad 0 \quad 0 \quad 0 \quad 0 \quad 0 \quad 0\}, \quad (7.6.33)$$

solution of the governing matrix equation $\bar{\mathbf{K}}\bar{\mathbf{d}} = \bar{\mathbf{p}}$ yields the displacement components

$$\bar{\mathbf{d}} = \begin{Bmatrix} 524.57 \\ 180.41 \\ -122.95 \\ 246.45 \\ 192.37 \\ 98.52 \\ -62.70 \\ 69.42 \end{Bmatrix}. \quad (7.6.34)$$

A comparison of the obtained maximum deflection $w_{\max} = \bar{w}_1 = 524.57$ with its “exact” value of $w_{\max} = 489.94$ indicates an error of 8.8%. Using a $4 \times 4 = 16$ -element subdivision, we obtain a much more improved value for the maximum deflection, $w_{\max} = 498.58$. A further improvement can be achieved by employing Richardson’s extrapolation formula[†] with $\mu = 2$. This gives

$$w_{\max} = 498.58 + \frac{498.58 - 524.57}{(3.0/1.5)^2 - 1} = 489.92 \quad (\text{error} \approx 0\%). \quad (7.6.35)$$

References and Bibliography

- [7.6.1] SZILARD, R., *BASIC-Programme für Baumechanik und Statik*, Ernst & Sohn, Berlin, 1986.
- [7.6.2] ALDINI, A., and CLOUGH, R., “Analysis of Plate Bending by Finite Element Method,” Report. No. G7337, National Science Foundation, Washington, D.C., 1960.
- [7.6.3] ZIENKIEWICZ, O. C., “Finite Element Procedures in the Solution of Plate and Shell Problems,” in Zienkiewicz, U. C., and Holister, G. S. (Eds.), *Stress Analysis*, John Wiley & Sons, London, 1965, pp. 120–144.
- [7.6.4] ZIENKIEWICZ, O. C., and CHEUNG, Y. K., “Finite Element Method of Analysis for Arch Dam Shells and Comparison with Finite Difference Procedures,” in Rydzewski, J. R. (Ed.), *Theory of Arch Dams*, Pergamon Press, Oxford, 1965, pp. 123–140.
- [7.6.5] PRZEMIENIECKI, J. S., *Theory of Matrix Structural Analysis*, McGraw-Hill Book Co., New York, 1968.
- [7.6.6] TUNA, J. J., *Handbook of Structural and Mechanical Matrices*, McGraw-Hill, New York, 1987.
- [7.6.7] TOCHER, J. L., “Analysis of Plate Bending Using Triangular Elements,” Ph.D. Dissertation, Department of Civil Engineering, University of California, Berkeley, 1962.
- [7.6.8] SCHWARZ, H. R., *FORTRAN-Programme zur Methode der finiten Elemente*, 3rd ed., Teubner, Stuttgart, 1991.
- [7.6.9] HOLLAND, I., and BELL, K. (Eds.), *Finite Element Methods in Stress Analysis*, Tapir, Trondheim, Norway, 1969.
- [7.6.10] BAZELEY, G. P., CHEUNG, Y. K., IRONS, B. M., and ZIENKIEWICZ, O. S., “Triangular Elements in Plate Bending: Conforming and Non-conforming Solution,” in *Proceedings of the First Conference on Matrix Methods in Structural Mechanics*, AF Publ. No. AFFDL TR-6680, Wright-Patterson Air Force Base, Dayton, Ohio, 1965, pp. 547–576.

[†] See Eq. (5.1.38).

7.7 Higher-Order Plate Elements

7.7.1 Rectangular Element with 16 DOF

Formulating a plate bending element that is continuous in deflections w and normal derivatives $\partial w/\partial x$ and $\partial w/\partial y$ along the element boundaries is far more difficult than constructing an element with only $C^{(0)}$ continuity. As already mentioned, the *Cartesian* products of beam functions represent conforming shape functions with $C^{(1)}$ continuity. Unfortunately, since the constant twist is missing in such shape functions, elements formulated with them are too “stiff”; that is, the obtained deflections are smaller than the actual ones.

Attempts to achieve $C^{(1)}$ continuity at the element boundaries encounter the fundamental difficulty that the twist can not be uniquely defined at the corners. This difficulty was overcome by Bogner and his co-workers [7.7.1] by adding twist $\partial^2 w/\partial x \partial y$ to the list of nodal DOF. Hence at each corner node the displacements are

$$\mathbf{d}_{\textcircled{i}} = \begin{Bmatrix} w \\ \theta_x \\ \theta_y \\ \theta_{xy} \end{Bmatrix}_{\textcircled{i}} = \begin{Bmatrix} w \\ \frac{\partial w}{\partial y} \\ -\frac{\partial w}{\partial x} \\ \frac{\partial^2 w}{\partial x \partial y} \end{Bmatrix}_{\textcircled{i}} \quad \text{for } \textcircled{i} = 1, 2, 3, 4. \quad (7.7.1)$$

The formulated 16-DOF conforming element is shown in Fig. 7.7.1. The corresponding shape function in polynomial form is

$$w(x, y) = \mathbf{w}^T \boldsymbol{\alpha} = \text{Eq. (7.6.11)}. \quad (7.7.2)$$

The parameters α_i in this equation can be uniquely determined by using the so-called *alternative formulation* procedure[†] for element stiffness matrices. Consequently, the

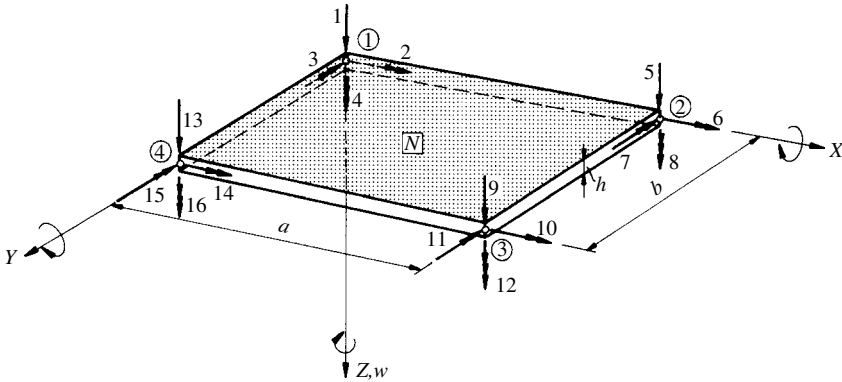


Figure 7.7.1 Conforming element with 16 DOF (CS = coordinate system).

[†] See Sec. 7.3.2c.

strategy is the same as the one already introduced in connection with the 12-DOF nonconforming rectangular element.

This shape function fulfills all the criteria for monotonic convergence listed in Sec. 7.4. Furthermore, it can be shown that interelement compatibility in deflections and in normal slopes along the element boundaries is satisfied. Therefore the element formulated with Eq. (7.7.2) is conforming and has $C^{(1)}$ continuity.

In computing the pertinent element stiffness matrix \mathbf{K}_e , one of the two equations (7.3.32) or (7.3.43) can be used. Although the shape functions given in Eqs. (7.5.17) and (7.5.18) can be conveniently used for computational manipulations, it appears to be easier to obtain an explicit expression for stiffness coefficients by hand computations if the physical interpretation of the beam shape functions are preserved. That is, as usual,

$$w(x, y) = [N_1 \quad N_2 \quad N_3 \quad \cdots \quad N_{16}] \begin{Bmatrix} d_1 \\ d_2 \\ d_3 \\ \vdots \\ d_{16} \end{Bmatrix}, \quad (7.7.3)$$

defining

$$\begin{aligned} p_1 &= \frac{1}{a^3}(a^3 - 3ax^2 + 2x^3), & q_1 &= \frac{1}{b^3}(b^3 - 3by^2 + 2y^3), \\ p_2 &= \frac{1}{a^2}(a^2x - 2ax^2 + x^3), & q_2 &= \frac{1}{b^2}(b^2y - 2by^2 + y^3), \\ p_3 &= \frac{1}{a^3}(3ax^2 - 2x^3), & q_3 &= \frac{1}{b^3}(3by^2 - 2y^3), \\ p_4 &= \frac{1}{a^2}(x^3 - ax^2), & q_4 &= \frac{1}{b^2}(y^3 - by^2). \end{aligned} \quad (7.7.4)$$

Hence the shape functions N_i for the 16 nodal displacements become

$$\begin{aligned} N_1 &= p_1q_1, & N_9 &= p_3q_3, \\ N_2 &= p_2q_1, & N_{10} &= p_4q_3, \\ N_3 &= p_1q_2, & N_{11} &= p_3q_4, \\ N_4 &= p_2q_2, & N_{12} &= p_4q_4, \\ N_5 &= p_1q_3, & N_{13} &= p_3q_1, \\ N_6 &= p_2q_3, & N_{14} &= p_4q_1, \\ N_7 &= p_1q_4, & N_{15} &= p_3q_2, \\ N_8 &= p_2q_4, & N_{16} &= p_4q_2 \end{aligned} \quad (7.7.5)$$

The stiffness coefficients k_{ij} of the element stiffness matrix \mathbf{K}_e can be computed from

$$k_{ij} = D \int_0^b \int_0^a \left[\frac{\partial^2 N_i}{\partial x^2} \frac{\partial^2 N_j}{\partial x^2} + \nu \frac{\partial^2 N_i}{\partial x^2} \frac{\partial^2 N_j}{\partial y^2} + \nu \frac{\partial^2 N_j}{\partial x^2} \frac{\partial^2 N_i}{\partial y^2} \right]$$

$$+ \frac{\partial^2 N_i}{\partial y^2} \frac{\partial^2 N_j}{\partial y^2} + 2(1 - \nu) \frac{\partial^2 N_i}{\partial x \partial y} \frac{\partial^2 N_j}{\partial x \partial y} \Big] dx dy. \quad (7.7.6)$$

Expressed in a more general form, this equation becomes

$$k_{ij} = \frac{Eh^3}{12ab(1 - \nu^2)} \left[\beta_1 \left(\frac{b}{a} \right) + \beta_2 \left(\frac{a}{b} \right)^2 + \beta_3 + \beta_4 \nu \right] a^{\beta_5} b^{\beta_6}, \quad (7.7.7)$$

where the constants $\beta_1, \beta_2, \dots, \beta_6$ are given in Table 7.7.1. Fortunately, it is not required to determine all the coefficients of the element stiffness matrix, since it is sufficient to determine only the first four columns in this matrix. That is, by adequately changing the indices i, j and also the sign if required, all other stiffness coefficients can be readily determined. These required changes are listed in Table 7.7.2.

Table 7.7.1 Constants β_i for Eqs. (7.7.7) and (15.2.29)

j	i	β_1	β_2	β_3	β_4	β_5	β_6	β_7
1	1	$\frac{156}{35}$	$\frac{156}{35}$	$\frac{72}{25}$	0	0	0	169
1	2	$\frac{22}{35}$	$\frac{78}{35}$	$\frac{6}{25}$	$\frac{6}{5}$	0	1	$\frac{143}{6}$
1	3	$\frac{78}{35}$	$\frac{22}{35}$	$\frac{6}{25}$	$\frac{6}{5}$	1	0	$\frac{143}{6}$
1	4	$\frac{11}{35}$	$\frac{11}{35}$	$\frac{1}{50}$	$\frac{1}{5}$	1	1	$\frac{121}{36}$
1	5	$-\frac{156}{35}$	$\frac{54}{35}$	$-\frac{72}{25}$	0	0	0	$\frac{117}{2}$
1	6	$-\frac{22}{35}$	$\frac{27}{35}$	$-\frac{6}{25}$	$-\frac{6}{5}$	0	1	$\frac{33}{4}$
1	7	$\frac{78}{35}$	$-\frac{13}{35}$	$\frac{6}{25}$	0	1	0	$-\frac{169}{12}$
1	8	$\frac{11}{35}$	$-\frac{13}{70}$	$\frac{1}{50}$	$\frac{1}{10}$	1	1	$-\frac{143}{75}$
1	9	$-\frac{54}{35}$	$-\frac{54}{35}$	$\frac{72}{25}$	0	0	0	$\frac{81}{4}$
1	10	$\frac{13}{35}$	$\frac{27}{35}$	$-\frac{6}{25}$	0	0	1	$-\frac{39}{8}$
1	11	$\frac{27}{35}$	$\frac{13}{35}$	$-\frac{6}{25}$	0	1	0	$-\frac{39}{8}$
1	12	$-\frac{13}{70}$	$-\frac{13}{70}$	$\frac{1}{50}$	0	1	1	$\frac{169}{144}$
1	13	$\frac{54}{35}$	$-\frac{156}{35}$	$-\frac{72}{25}$	0	0	0	$\frac{117}{2}$
1	14	$-\frac{13}{35}$	$\frac{78}{35}$	$\frac{6}{25}$	0	0	1	$-\frac{169}{12}$
1	15	$\frac{27}{35}$	$-\frac{22}{35}$	$-\frac{6}{25}$	$-\frac{6}{5}$	1	0	$\frac{33}{4}$
1	16	$-\frac{13}{70}$	$\frac{11}{35}$	$\frac{1}{50}$	$\frac{1}{10}$	1	1	$-\frac{143}{72}$

Table 7.7.1 (continued)

j	i	β_1	β_2	β_3	β_4	β_5	β_6	β_7
2	2	$\frac{4}{35}$	$\frac{52}{35}$	$\frac{8}{25}$	0	0	2	$\frac{13}{3}$
2	4	$\frac{2}{35}$	$\frac{22}{105}$	$\frac{2}{75}$	$\frac{2}{15}$	1	2	$\frac{11}{18}$
2	6	$-\frac{4}{35}$	$\frac{18}{35}$	$-\frac{8}{25}$	0	0	2	$\frac{3}{2}$
2	8	$\frac{2}{35}$	$-\frac{13}{105}$	$\frac{2}{75}$	0	1	2	$-\frac{13}{36}$
2	10	$\frac{3}{35}$	$\frac{9}{35}$	$\frac{2}{25}$	0	0	2	$-\frac{9}{8}$
2	12	$-\frac{3}{10}$	$-\frac{13}{210}$	$-\frac{1}{150}$	0	1	2	$\frac{13}{48}$
2	14	$-\frac{3}{35}$	$\frac{26}{35}$	$-\frac{2}{25}$	0	0	2	$-\frac{13}{4}$
2	16	$-\frac{3}{70}$	$\frac{11}{105}$	$-\frac{1}{150}$	$-\frac{1}{30}$	1	2	$-\frac{11}{24}$
3	2	$\frac{11}{35}$	$\frac{11}{35}$	$\frac{1}{50}$	$\frac{6}{5}$	1	1	$\frac{121}{36}$
3	3	$\frac{52}{35}$	$\frac{4}{35}$	$\frac{8}{25}$	0	2	0	$\frac{13}{3}$
3	4	$\frac{22}{105}$	$\frac{2}{35}$	$\frac{2}{75}$	$\frac{2}{15}$	2	1	$\frac{11}{18}$
3	6	$-\frac{11}{35}$	$\frac{13}{70}$	$-\frac{1}{50}$	$-\frac{1}{10}$	1	1	$\frac{143}{72}$
3	7	$\frac{26}{35}$	$-\frac{3}{35}$	$-\frac{2}{25}$	0	2	0	$-\frac{13}{4}$
3	8	$\frac{11}{105}$	$-\frac{3}{70}$	$-\frac{1}{150}$	$-\frac{1}{30}$	2	1	$-\frac{11}{24}$
3	10	$\frac{13}{70}$	$\frac{13}{70}$	$-\frac{1}{50}$	0	1	1	$-\frac{169}{144}$
3	11	$\frac{9}{35}$	$\frac{3}{35}$	$\frac{2}{25}$	0	2	0	$-\frac{9}{8}$
3	12	$-\frac{13}{210}$	$-\frac{3}{70}$	$-\frac{1}{150}$	0	2	1	$\frac{13}{48}$
3	14	$-\frac{13}{70}$	$\frac{11}{35}$	$\frac{1}{50}$	$\frac{1}{10}$	1	1	$-\frac{141}{72}$
3	15	$\frac{18}{35}$	$-\frac{4}{35}$	$-\frac{8}{25}$	0	2	0	$\frac{3}{2}$
3	16	$-\frac{13}{105}$	$\frac{2}{35}$	$\frac{2}{75}$	0	2	1	$-\frac{13}{36}$
4	4	$\frac{4}{105}$	$\frac{4}{105}$	$\frac{8}{225}$	0	2	2	$\frac{1}{9}$
4	8	$\frac{2}{105}$	$-\frac{1}{35}$	$-\frac{2}{225}$	0	2	2	$-\frac{1}{12}$
4	12	$-\frac{1}{70}$	$-\frac{1}{70}$	$\frac{1}{450}$	0	2	2	$\frac{1}{16}$
4	16	$-\frac{1}{35}$	$\frac{2}{105}$	$-\frac{2}{225}$	0	2	2	$-\frac{1}{12}$

Notes: i = row, j = column.

As shown in Fig. 7.7.2, the convergence properties of this higher-order element are *excellent*. In the same figure, we also compared the convergence characteristics of the 12-DOF nonconforming element with those of the 16-DOF conforming element introduced in this section. It is evident that using the same subdivision the conforming element approaches the exact solution faster than the nonconforming one. Furthermore, one is converging from “above” and the other one from “below”.

Table 7.7.2 Index Scheme i, j for Evaluation of k_{ij}

$$k_{ij} = (\pm) \frac{Eh^3}{12ab(1-\nu^2)} \left[\beta_1 \left(\frac{b}{a} \right)^2 + \beta_2 \left(\frac{a}{b} \right)^2 + \beta_3 + \beta_4 \nu \right] a^{\beta_5} b^{\beta_6}$$

1	1,1															
2	2,1	2,2														
3	3,1	3,2	3,3													
4	4,1	4,2	4,3	4,4												
5	5,1	6,1	(-)	(-)												
6	6,1	6,2	6,3	8,2	2,1	2,2										
7	7,1	(-)			(-)	(-)	3,3									
8	8,1	8,2	8,3	8,4	(-)	(-)	4,3	4,4								
9	9,1	(-)	(-)			(-)	(-)		1,1							
10	10,1	10,2	10,3	(-)			(-)	(-)	(-)	2,2						
11	11,1	10,3	11,3	(-)	(-)	14,3	15,3	16,3	3,1	2,3	3,3					
12	12,1	12,2	12,3	12,4	(-)	(-)		16,4	4,1	4,2	4,3	4,4				
13	13,1	(-)		(-)		(-)		(-)		(-)	(-)		1,1			
14	14,1	14,2	14,3	16,2	10,1	10,2	10,3	12,2	6,1	6,2	6,3	8,2	2,1	2,2		
15	15,1	(-)		(-)	(-)	(-)		(-)	(-)	(-)	7,3	8,3	3,1	2,3	3,3	
16	16,1	16,2	16,3	16,4	(-)	(-)		12,3		(-)	(-)	(-)	4,1	4,2	4,3	4,4
	1	2	3	4	5	6	7	8	9	10	11	12	13	14	15	16

Symmetric

Note: The notation (–) indicates change of sign for the corresponding stiffness coefficients.

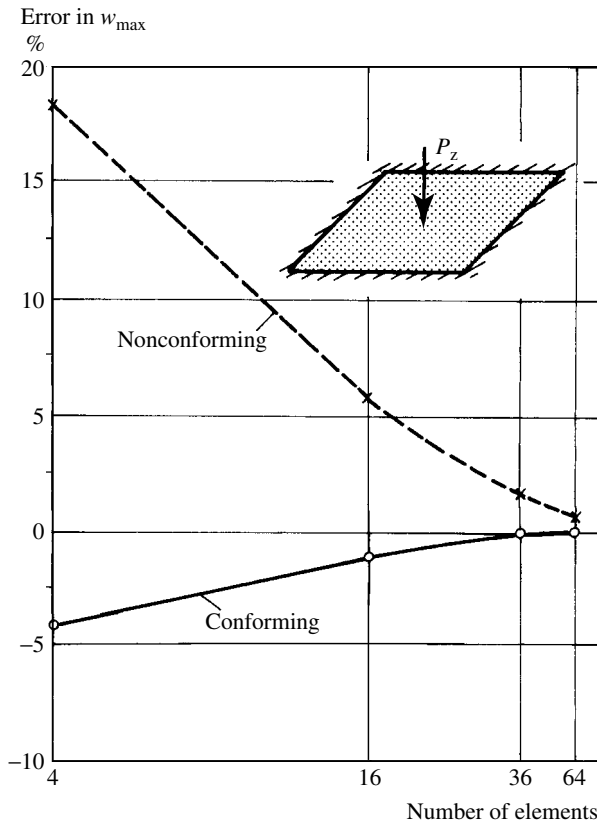


Figure 7.7.2 Convergence characteristics of conforming and nonconforming elements.

7.7.2 Discrete Kirchhoff Triangular Element

This viable alternative approach for formulating triangular bending elements for thin plates is based on the so-called *discrete KIRCHHOFF theory*. The resulting element is known as the discrete Kirchhoff triangular (DKT) element.

The DKT approach was proposed in 1969 by Dhatt et al. [7.7.2] and somewhat later by Kikuchi [7.7.3], but wider acceptance of this new formulation came only 10 years later, mostly due to the continuous efforts of Batoz et al. [7.7.4–7.7.8]. In the meantime, the DKT element was extensively tested for its convergence properties. Because of its proven excellence, it remains one of the best triangular elements for plate bending.

It is apparent from reading the foregoing sections that by using only a single polynomial expression for the transverse deflections w , it is extremely difficult to formulate a *compatible* triangular element with 9 DOF for plate bending. The alternative DKT approach uses the Reissner-Mindlin theory for moderately thick plates and assumes that the nodal deflections and rotations are independent from each other. In this way, the shape functions for the displacement components can be made continuous at the interelement boundaries. Since the plate to be analyzed is not moderately thick but thin, the transverse shear strain must be zero at specific discrete points.

Consequently, the corresponding terms in the energy functional for moderately thick plates can be neglected. Kirchhoff's thin-plate theory is then imposed at particular points to relate rotations and transverse displacements. The shape functions for w , θ_x and θ_y maintain compatibility at the boundaries of the element; therefore, the DKT element is *conforming*.

Since it is beyond the scope of this book to engage in lengthy derivation leading to the explicit formulation of the DKT element, it was omitted here. Interested readers are referred to Refs. [7.7.4] and [7.7.5] to obtain more details on this subject. Here we give only a brief summary of the essential steps required to formulate the element stiffness matrix.

The DKT element uses the same nodal displacement components, w , θ_x and θ_y , for each of the three corner nodes (Fig. 7.7.3) as the simple triangular element introduced in the foregoing section. The starting point for the element formulation is, however, an *initial* element with corner and midside nodes, as shown in Fig. 7.7.4a:

- First, the rotations θ_x and θ_y are approximated by

$$Q_x = \sum_{i=1}^6 N_i \theta_{xi} \quad \text{and} \quad Q_y = \sum_{i=1}^6 N_i \theta_{yi} \quad (7.7.8)$$

using N_i complete quadratic polynomials for the shape functions expressed in area coordinates ξ_1 , ξ_2 and ξ_3 , as shown in Fig. 7.7.4b. These assumed shape functions are

$$\begin{aligned} N_1 &= \xi_1(2\xi_1 - 1), & N_2 &= \xi_2(2\xi_2 - 1), & N_3 &= \xi_3(2\xi_3 - 1), \\ N_4 &= 4\xi_1\xi_2, & N_5 &= 4\xi_2\xi_3, & N_6 &= 4\xi_3\xi_1. \end{aligned} \quad (7.7.9)$$

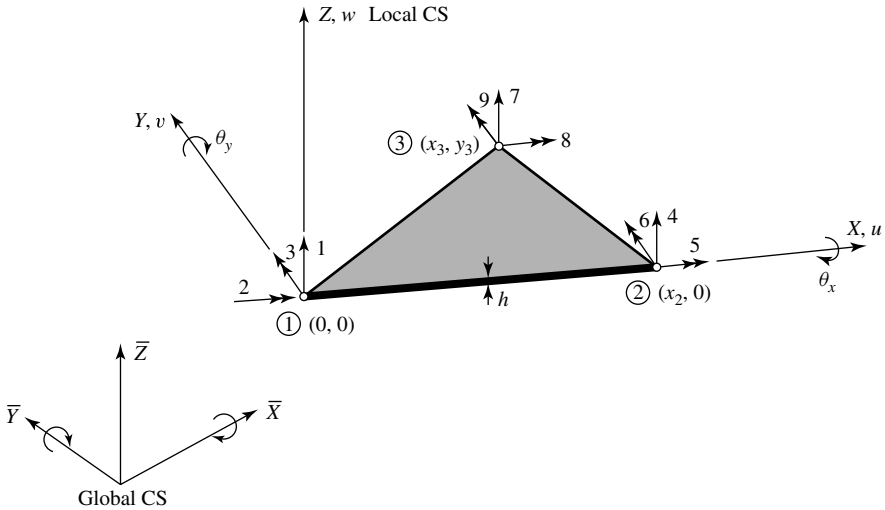


Figure 7.7.3 Explicitly formulated DKT element.

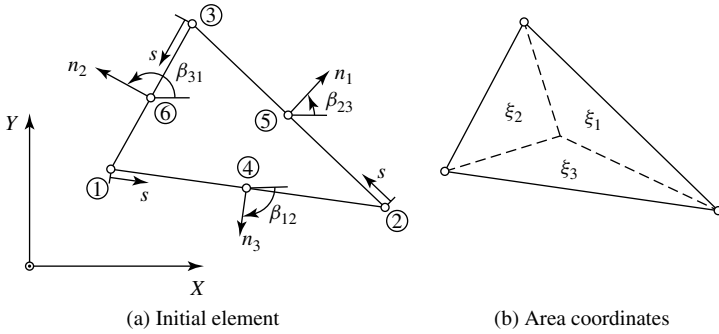


Figure 7.7.4 Development of DKT element.

- The transverse displacements w along the edges are represented by cubic polynomials in the edge tangent coordinate s . Thus, along the edges the rotation $\partial w / \partial s$ at midpoint \textcircled{k} is

$$\left. \frac{\partial w}{\partial s} \right|_k = -\frac{3}{2l_{ij}} w_i - \frac{1}{4} \frac{\partial w_i}{\partial s} + \frac{3}{2l_{ij}} w_j - \frac{1}{4} \frac{\partial w_j}{\partial s} \quad \text{for } k = 4, 5, 6, \quad (7.7.10)$$

where l_{ij} denotes the length of the side \overline{ij} with corner nodes \textcircled{i} and \textcircled{j} and the corresponding midpoint is \textcircled{k} .

- According to the classical theory of thin plates, the rotations at the corner nodes are

$$\theta_{xi} = \left. \frac{\partial w}{\partial y} \right|_i \quad \text{and} \quad \theta_{yi} = - \left. \frac{\partial w}{\partial x} \right|_i \quad \text{for } i = 1, 2, 3. \quad (7.7.11)$$

- Similarly, we impose this classical plate theory approach also at the midpoints. Thus, we can write

$$\theta_s|_k = \left. \frac{\partial w}{\partial s} \right|_k \quad \text{for } k = 4, 5, 6. \quad (7.7.12)$$

- Furthermore, if we assume that the normal slopes vary linearly along the element sides, then we obtain

$$\begin{aligned} \theta_n|_4 &= \frac{1}{2} \left[\left(\frac{\partial w}{\partial n} \right)_1 + \left(\frac{\partial w}{\partial n} \right)_2 \right], \\ \theta_n|_5 &= \frac{1}{2} \left[\left(\frac{\partial w}{\partial n} \right)_2 + \left(\frac{\partial w}{\partial n} \right)_3 \right], \\ \theta_n|_6 &= \frac{1}{2} \left[\left(\frac{\partial w}{\partial n} \right)_3 + \left(\frac{\partial w}{\partial n} \right)_1 \right]. \end{aligned} \quad (7.7.13)$$

- To acquire a relationship between the 12 nodal rotations and the 9 nodal DOF, the following transformation is required for each side:

$$\begin{Bmatrix} \theta_x \\ \theta_y \end{Bmatrix} = \begin{bmatrix} \cos \beta_{ij} & -\sin \beta_{ij} \\ \sin \beta_{ij} & \cos \beta_{ij} \end{bmatrix} \begin{Bmatrix} \theta_n \\ \theta_s \end{Bmatrix}, \quad \begin{Bmatrix} \frac{\partial w}{\partial s} \\ \frac{\partial w}{\partial n} \end{Bmatrix} = \begin{bmatrix} \cos \beta_{ij} & \sin \beta_{ij} \\ \sin \beta_{ij} & -\cos \beta_{ij} \end{bmatrix} \begin{Bmatrix} \theta_x \\ \theta_y \end{Bmatrix}, \quad (7.7.14)$$

where the angle β_{ij} is defined in Fig. 7.7.4a.

- The stiffness matrix of the DKT element is now expressed in the standard form[†]

$$\mathbf{K}_e = \iint_A \mathbf{D}^T \mathbf{E} \mathbf{D} \, dx \, dy \quad (7.7.15)$$

for which Batoz [7.7.5] introduced the explicit form

$$\mathbf{K}_e = \frac{1}{2A} [\alpha]^T \mathbf{E} [\alpha], \quad (7.7.16)$$

where A represents the area of the triangle and \mathbf{E} denotes the matrix of homogeneous isotropic elastic material given by

$$\mathbf{E} = \frac{1}{24} \begin{bmatrix} D\mathbf{R} & \nu D\mathbf{R} & 0 \\ \nu D\mathbf{R} & D\mathbf{R} & 0 \\ 0 & 0 & \frac{D(1-\nu)}{2}\mathbf{R} \end{bmatrix}. \quad (7.7.17)$$

In this matrix D stands for the flexural rigidity of the plate given by Eq. (1.2.28) and

$$\mathbf{R} = \begin{bmatrix} 2 & 1 & 1 \\ 1 & 2 & 1 \\ 1 & 1 & 2 \end{bmatrix}. \quad (7.7.18)$$

Table 7.7.3 provides explicit expressions for the matrix $[\alpha]$. In addition, a FORTRAN subroutine for generating the above DKT stiffness matrix is listed in Appendix A.4.2. In addition, in Ref. [7.7.7] the reader will find pertinent FORTRAN coding. Figures 7.7.5 and 7.7.6 demonstrate the excellent convergence characteristics of this unique plate bending element.

Summary and Conclusions. In the past decades, a large number of plate bending elements have been developed. This area of research is still active, and we may anticipate additional developments in the future. While in the foregoing section we dealt with relatively simple—yet quite usable—plate elements with $C^{(0)}$ continuity, here we introduced two higher-order conforming elements. According to the convergence requirements stated in Sec. 7.4, the shape functions must contain constant-curvatures $\partial^2 w / \partial x^2$ and $\partial^2 w / \partial y^2$ and constant twist $\partial^2 w / \partial x \partial y$. In addition, continuity not

[†] See Eq. (7.3.32).

Table 7.7.3 Explicit Form of Matrix $[\alpha]$

Global CS

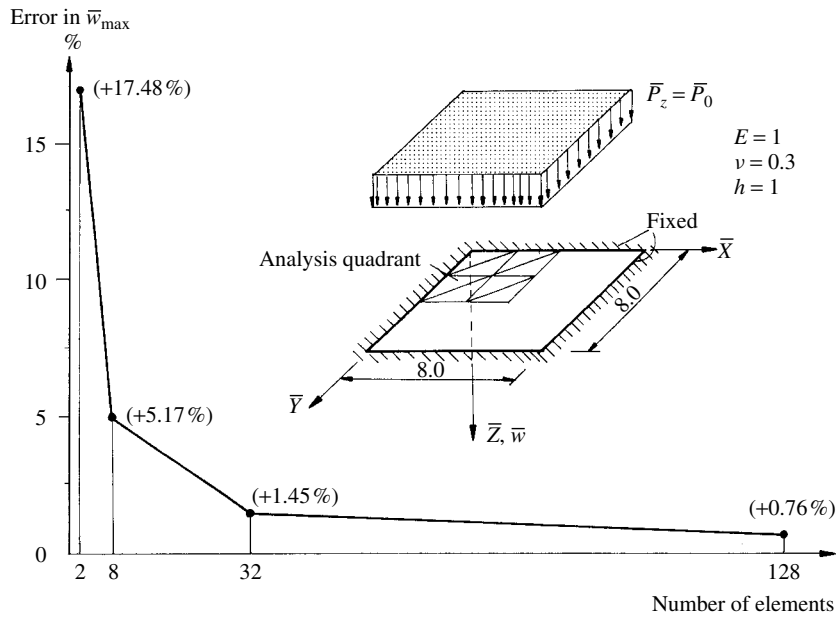
Local CS $\mathbf{d}_{e,i} = \begin{Bmatrix} w_x \\ w_y \end{Bmatrix} = \begin{Bmatrix} \theta_x \\ \theta_y \end{Bmatrix}$ $i = 1, 2, 3$.

$$[\alpha] = \begin{bmatrix} y_3 p_6 & 0 & -4y_3 & 0 & -2y_3 & 0 & 0 & 0 \\ -y_3 p_6 & 0 & 2y_3 & 0 & 4y_3 & 0 & 0 & 0 \\ y_3 p_5 & -y_3 q_5 & y_3(2-r_5) & y_3 q_4 & y_3(r_4-2) & -y_3(p_4+p_5) & y_3(q_4-q_5) & y_3(r_4-r_5) \\ -x_2 f_5 & x_{23} + x_2 r_5 & -x_2 q_5 & 0 & x_3 & x_2 f_5 & x_2(r_5-1) & -x_2 q_5 \\ 0 & x_{23} & 0 & x_2 t_4 & x_3 + x_2 r_4 & -x_2 q_4 & x_2(r_4-1) & -x_2 q_4 \\ x_{23} f_5 & x_{23}(1-r_5) & x_{23} q_5 & -x_3 t_4 & x_3(1-r_4) & -x_{23} f_5 + x_3 t_4 & -x_{23} r_5 - x_3 r_4 - x_2 & x_3 q_4 + x_{23} q_5 \\ -x_3 p_6 - x_2 p_5 & x_2 q_5 + y_3 & -4x_{23} + x_2 r_5 & x_3 p_6 & -y_3 & 2x_3 & x_2 p_5 & (r_5-2)x_2 \\ -x_{23} p_6 & y_3 & 2x_{23} & x_{23} p_6 + x_2 p_4 & -y_3 + x_2 q_4 & -4x_3 + x_2 r_4 & -x_2 p_4 & (r_4-2)x_2 \\ x_{23} p_5 & -x_{23} q_5 & (2-r_5)x_{23} & -x_3 p_4 & (r_4-1)y_3 & -x_{23} p_5 + x_3 p_4 & -x_{23} q_5 - x_3 q_4 & -x_{23} r_5 - x_3 r_4 \\ +y_3 f_5 & +(1-r_5)y_3 & +y_3 q_5 & +y_3 t_4 & -x_3 q_4 & -(4+t_5)y_3 & +(r_4-r_5)y_3 & +4x_2 + (q_5-q_4)y_3 \end{bmatrix}$$

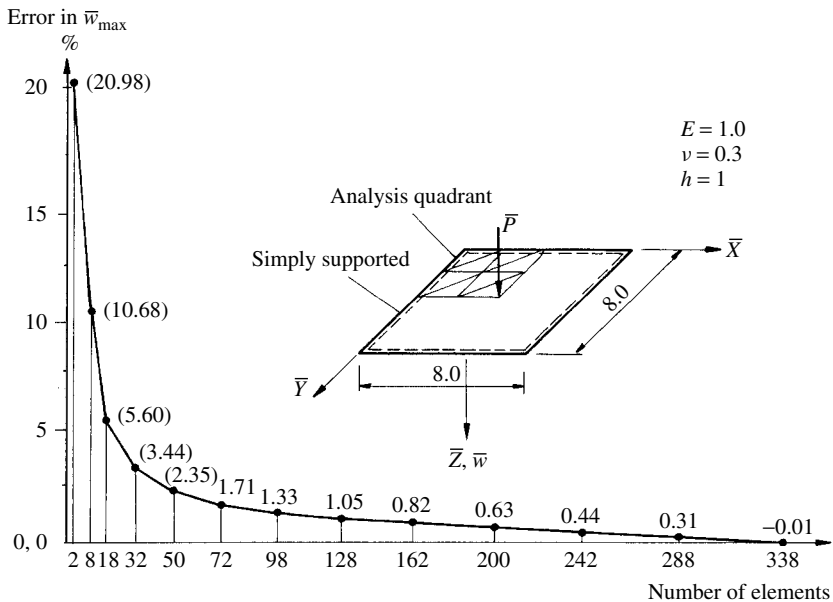
with

$$\begin{aligned} x_{ij} &= x_i - x_j & y_{ij} &= y_i - y_j & l_{ij}^2 &= x_{ij}^2 + y_{ij}^2 \\ p_4 &= -6x_{23}/l_{23}^2 & p_5 &= -6x_3/l_{31}^2 & p_6 &= -6x_{12}/l_{12}^2 \\ t_4 &= -6y_{23}/l_{23}^2 & t_5 &= -6y_3/l_{31}^2 & q_4 &= 3x_{23}y_{23}/l_{23}^2 \\ q_5 &= 3x_3y_3/l_{31}^2 & r_4 &= 3y_{23}^2/l_{23}^2 & r_5 &= 3y_{31}^2/l_{31}^2 \end{aligned}$$

Note: CS = Coordinate System. From Ref. [7.7.5].



(a) Uniformly distributed load



(b) Concentrated force

Figure 7.7.5 Convergence studies for DKT element.

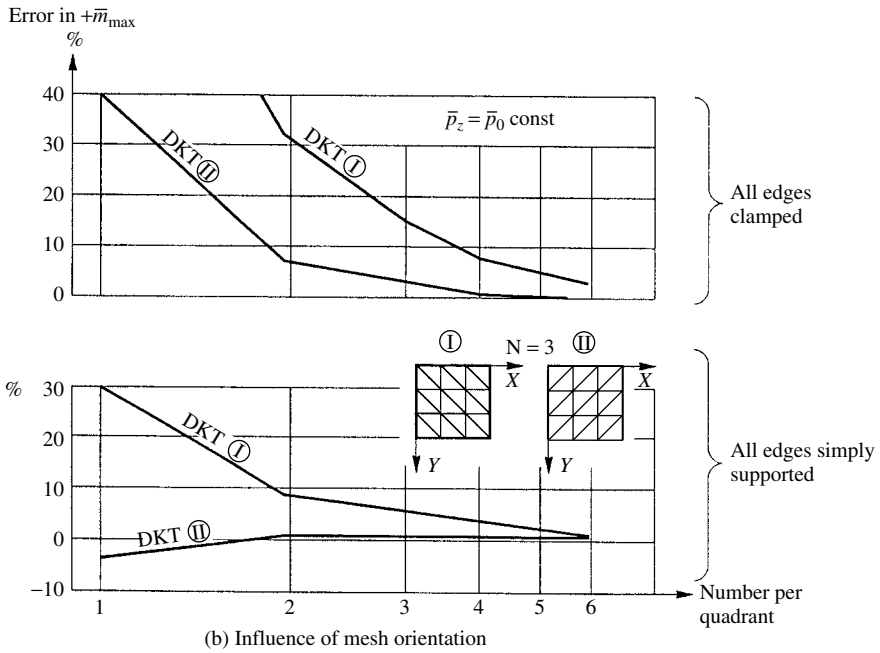
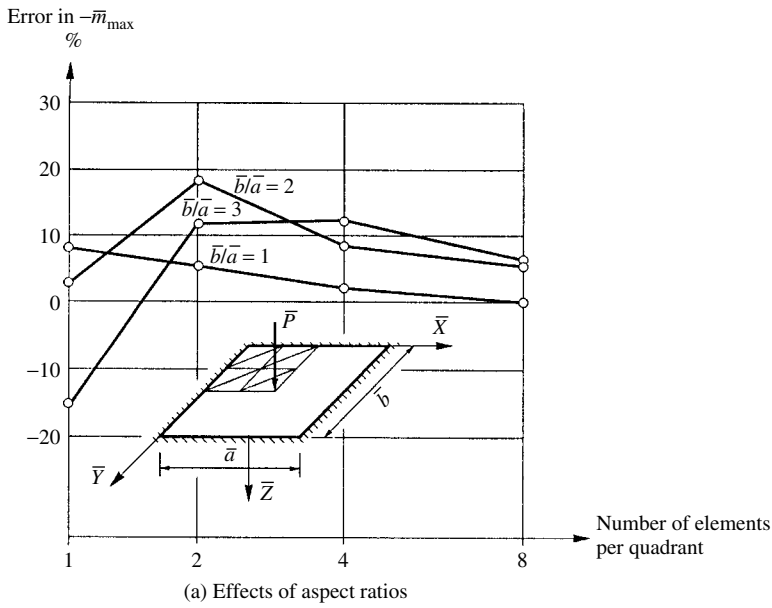


Figure 7.7.6 Further convergence studies.

only in displacements w but also in its derivatives must be maintained between adjacent elements. Our selection from the presently available numerous plate bending elements was based on (a) conformity, (b) accuracy and (c) relative ease in applications. To satisfy the last requirement, the stiffness matrices of both elements presented in this section are given *explicitly*. Furthermore, their convergence properties are excellent. These criteria are especially important for practical applications of these elements. To facilitate their use in practice, FORTRAN subroutines for formulating the corresponding stiffness matrices are given in Appendix A.4.2. In addition, Refs. [7.7.10] and [7.7.11] provide complete FORTRAN programs for static analysis of plates using the rectangular element with 16 DOF. Finally, we call the reader's attention to some other very good elements listed in Refs. [7.7.9] and [7.7.12–7.7.14]. Unfortunately, their practical applications are not that easy.

ILLUSTRATIVE EXAMPLE I

Let us consider the analysis of a clamped square plate subjected to a concentrated center force $P_z = 1000$ kN, as shown in Fig. 7.7.7a. We apply the 16-DOF rectangular plate bending element to determine the maximum lateral deflection w_{\max} . For the discretization, we use only four elements (Fig. 7.7.7b). Utilizing the apparent double symmetry of the structure and load, we can deal only with one element (Fig. 7.7.7c). The corresponding element stiffness matrix is given in Table 7.7.1. Between the local and global numbering of the lateral deflection, the following relationship exists: $9 \rightarrow \bar{1}$. Thus, using Eq. (7.7.7), we obtain

$$k_{11} = \bar{\mathbf{K}} = \frac{D}{(a/2)^2} \left(\frac{156}{35} + \frac{156}{35} + \frac{72}{25} \right) = 11.7943 \frac{D}{(a/2)^2}, \quad (7.7.19)$$

or with

$$D = \frac{Eh^3}{12(1-\nu^2)} = 9272 \text{ m-kN} \quad \text{and} \quad a = 4.00 \text{ m} \quad (7.7.20)$$

the stiffness coefficient becomes $k_{11} = 27,339$. Consequently, the maximum lateral deflection is

$$\bar{\mathbf{d}} = \bar{\mathbf{K}}^{-1} \bar{\mathbf{p}} = \bar{d}_1 = \frac{P_z/4}{k_{11}} = \frac{250}{27,339} = 0.00914 \text{ m} \quad (\text{error} : -5.8\%). \quad (7.7.21)$$

ILLUSTRATIVE EXAMPLE II

Let us compare the efficiency of the triangular DKT element with that of the conforming 16-DOF rectangular element. For this purpose, we use a simply supported square plate subjected to a center load as shown in Fig. 7.7.8a.

Utilizing the apparent double symmetry of the structure and load, our first discretization scheme involves four rectangular elements per quarter plate (Fig. 7.7.8b). Our computer program [7.7.15] gave the following displacement components:

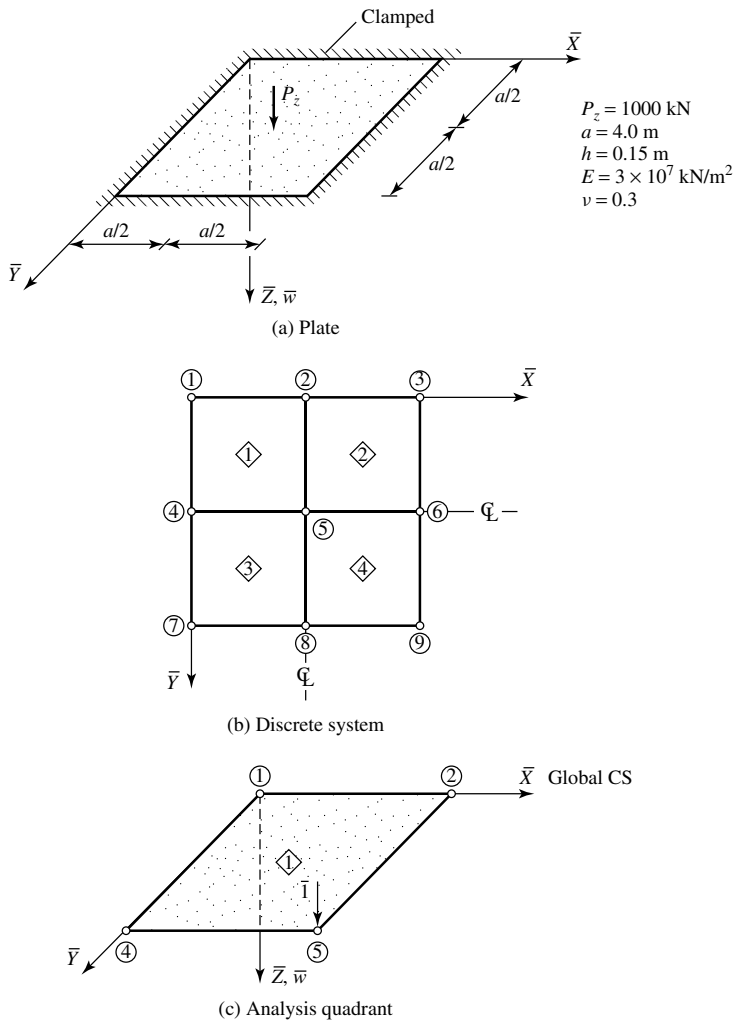
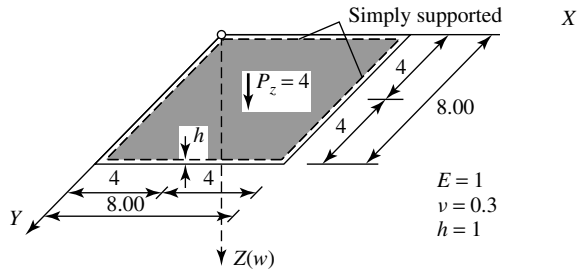
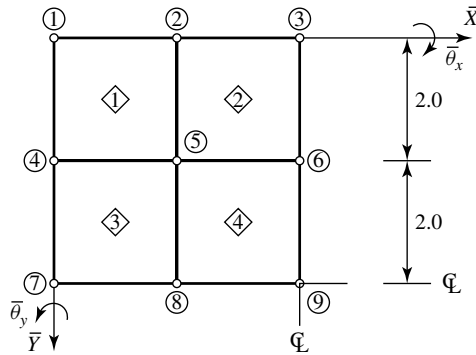


Figure 7.7.7 Clamped square plate under central load.

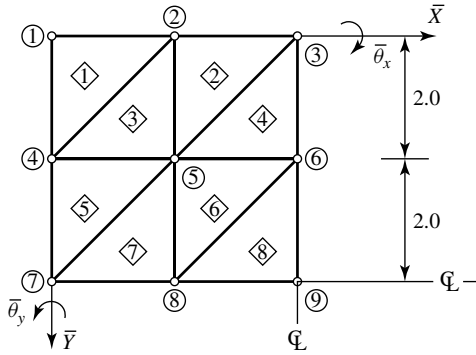
Node Number	\bar{w}	$\bar{\Theta}_x$	$\bar{\Theta}_y$	$\bar{\Theta}_{xy}$
1	.0000D + 00	.0000D + 00	.0000D + 00	.3819D + 01
2	.0000D + 00	.0000D + 00	.7064D + 01	.2977D + 01
3	.0000D + 00	.0000D + 00	.1033D + 02	.0000D + 00
4	.0000D + 00	.7064D + 01	.0000D + 00	.2977D + 01
5	.1334D + 02	.5805D + 01	.5805D + 01	.2822D + 01
6	.1992D + 02	.0000D + 00	.9066D + 01	.0000D + 00
7	.0000D + 00	.1033D + 02	.0000D + 00	.0000D + 00
8	.1992D + 02	.9066D + 01	.0000D + 00	.0000D + 00
9	.3207D + 02	.0000D + 00	.0000D + 00	.0000D + 00



(a) Plate



(b) Discretization I



(c) Discretization II

Figure 7.7.8 Simply supported square plate under central load.

A comparison of the obtained maximum deflection[†] $w_{\max} = 32.07$ with its “exact” value $w_{\text{exact}} = 32.43$ [2] shows only a very small percentage error of -1.1% , which can be neglected for all practical purposes.

Next, we use the DKT triangular element for the analysis quadrant, as shown in Fig. 7.7.8c. Our computer program [7.7.15] gave the flowing displacement components:

[†] Dimensionless value.

Node Number	\bar{w}	$\bar{\Theta}_x$	$\bar{\Theta}_y$
1	.0000D + 00	.0000D + 00	.0000D + 00
2	.0000D + 00	.7253D + 01	.0000D + 00
3	.0000D + 00	.1061D + 02	.0000D + 00
4	.0000D + 00	.0000D + 00	-.7253D + 01
5	.1379D + 02	.5616D + 01	-.5616D + 01
6	.2133D + 02	.1022D + 02	.0000D + 00
7	.0000D + 00	.0000D + 00	-.1061D + 02
8	.2133D + 02	.0000D + 00	-.1022D + 02
9	.3589D + 02	.0000D + 00	.0000D + 00

Since in this case the procentual error is +10.1%, we can state that the rectangular element has better convergence properties.

References and Bibliography

- [7.7.1] BOGNER, F. K., et al., "The Generation of Interelement Compatible Stiffness and Mass Matrices by Use of Interpolation Formulas," in *Proceedings of the First Conference on Matrix Methods in Structural Mechanics*, AF Publ. No. AFFDL-TR-6680, Wright Patterson Air Force Base, Dayton, Ohio, 1965, 397–443.
- [7.7.2] DHATT, G., et al., "Numerical Analysis of Thin Shells by Curved Triangular Elements Based on Discrete Kirchhoff Hypothesis," in *Proceedings of the ASCE Symposium on Application of FEM in Civil Engineering*, Vanderbilt University, Nashville, Tennessee, 1969, pp. 255–278.
- [7.7.3] KIKUCHI, F., "On the Finite Element Scheme Based on the Discrete Kirchhoff Assumption," *Num. Math.*, 24 (1975), 2005–2029.
- [7.7.4] BATOZ, J. L., BATHE, J.-K., and HO, L., "A Study of Three-Node Triangular Plate Bending Elements," *Int. J. Num. Meth. Eng.*, 15 (1980), 1771–1812.
- [7.7.5] BATOZ, J. L., "An Explicit Formulation for an Efficient Triangular Plate Bending Element," *Int. J. Num. Meth. Eng.*, 18 (1982), 1077–1089.
- [7.7.6] BATOZ, J. L., and TAHAR, M. B., "Evaluation of a New Quadrilateral Thin Plate Bending Element," *Int. J. Num. Meth. Eng.*, 18 (1982), 1655–1677.
- [7.7.7] JEYACHANDRABOSE, C., KIRHOPE, J., and BABU, C. R., "An Alternative Formulation for DKT Plate Bending Element," *Int. J. Num. Meth. Eng.*, 21 (1985), 1289–1293.
- [7.7.8] DHATT, G., et al., "New Triangular Discrete Kirchhoff Plate/Shell Element," *Int. J. Num. Meth. Eng.*, 23 (1986), 453–470.
- [7.7.9] TORRES, J., et al., "A $C^{(1)}$ Finite Element Family for Kirchhoff Plate Bending," *Int. J. Num. Meth. Eng.*, 24 (1986), 2005–2029.
- [7.7.10] SMITH, I. M., and GRIFFITHS, D. V., *Programming the Finite Element Method*, 2nd ed., John Wiley & Sons, New York, 1988.
- [7.7.11] SCHWARZ, H. R., *FORTTRAN-Programme zur Methode der finiten Elemente*, 3rd ed., Teubner, Stuttgart, 1991.
- [7.7.12] BELL, K., "On the Quintic Triangular Plate Bending Element," Report No. 72-2, Institutt for Statikk, Norwegian Institute of Technology, Trondheim, Norway, 1972.
- [7.7.13] ANDERHEGGEN, E., "A Conforming Triangular Bending Solution," *Int. J. Num. Meth. Eng.*, 2 (1970), 259–264.
- [7.7.14] BIRKHOFF, G., and MASFIELD, L., "Compatible Triangular Finite Elements," *J. Math. Anal. Appl.*, 47 (1974), 531–553.
- [7.7.15] SZILARD, R., and DUNAI, L., *FlächES, Berechnung von Flächentragwerken*, Version 1.5, Ernst & Sohn, Berlin, 1994.

7.8 Computation of Loads and Stress Resultants

a. Loads. In the FEM, the right-hand side, $\bar{\mathbf{p}}$, of its governing matrix equation (7.2.15) represents the column vector of forces acting on the nodal points expressed in the global reference system of the plate structure. Five different types of loading conditions can occur in practice: (1) concentrated forces and moments acting at a point, (2) distributed loads, (3) prescribed boundary displacements, (4) body force loadings and (5) thermal loadings.

A *concentrated load* may be applied as a force or moment at a point. It must be assigned directly to a node of the discretized structure. It is obvious that such a moment load can only be assigned to a node that has corresponding rotational DOF in the stiffness formulation. If the nodes have only translational DOF, we apply the moments as couples of lateral forces. Furthermore, it is required that when we subdivide the plate into elements, we must select nodal locations that coincide with the location of concentrated forces. It is also of importance, as discussed earlier, that in the vicinity of concentrated forces finer subdivisions are used. Since in most cases the Z axes of the local and global coordinate systems are parallel, no transformation of lateral forces from the local coordinate system to the global reference system is required.

Distributed loads on the plate act between nodes; thus, they must be converted to direct nodal forces. This conversion can be accomplished by applying one of the following approaches: *direct method*, lumped loads based on *static equivalencies* of the forces and *consistent load* representations.

The direct method of formulation considers the distributed loads on an element based on their tributary area. This is the simplest approach. In rectangular elements, for instance, the total distributed lateral load on the element is assigned as four equal concentrated forces acting on the nodes. For the triangular element N , the assigned forces at nodal point \textcircled{i} are

$$P_{\textcircled{i}}^{(N)} = \iint_A p_z(x, y) \Delta A \approx p_0 A_j \quad \text{for } j = 1, 2, 3, \quad (7.8.1)$$

where A_j represents the corresponding tributary areas according to Fig. 6.4.3. Since the FEM is not overly sensitive to representation of the lateral loads, the direct method yields quite acceptable results, provided that the element size is reasonably small.

An somewhat more refined approach uses statically equivalent lumped nodal forces and corresponding moments of these concentrated forces rotating about the nodal point.

The most exact formulation of distributed loads involves the consistent load approach based on virtual work. That is, we state that during a virtual displacement the work of the concentrated nodal force and that of the actual distributed load must be equal. Thus, the consistent load acting at node i of element N is obtained from

$$1 \cdot P_{\textcircled{i}}^{(N)} = 1 \cdot \iint \phi_i^{(N)}(x, y) \cdot p_z(x, y) dx dy, \quad (7.8.2)$$

$$1 \cdot M_{\textcircled{i}}^{(N)} = 1 \cdot \iint \phi_j^{(N)}(x, y) \cdot p_z(x, y) dx dy,$$

where ϕ_i and ϕ_j represent the Cartesian products of corresponding beam shape functions given in Eqs. (7.2.7) and (7.2.8), respectively. Strictly speaking, however, we should have used the actual shape functions N of the pertinent finite element. Logically, the same approach can be applied to line loads. Since, as mentioned above, the FEM is not overly sensitive to representations of lateral loads, Eq. (7.8.2) yields very good results for all practical purposes.

Such insensitivity in load representation, however, is not the case for *prescribed displacements*. Therefore, it is of importance that such displacements be described with high precision because even small changes can produce large differences in stress response. To account for prescribed nodal displacements, the expanded system equation

$$\begin{bmatrix} \bar{k}_{11} & \bar{k}_{12} & \bar{k}_{13} & \cdots & \bar{k}_{1n} \\ \bar{k}_{21} & \bar{k}_{22} & \bar{k}_{23} & \cdots & \bar{k}_{2n} \\ \bar{k}_{31} & \bar{k}_{32} & \bar{k}_{33} & \cdots & \bar{k}_{3n} \\ \vdots & \vdots & \vdots & \ddots & \vdots \\ \bar{k}_{n1} & \bar{k}_{n2} & \bar{k}_{n3} & \cdots & \bar{k}_{nn} \end{bmatrix} \begin{Bmatrix} \bar{d}_1 \\ \bar{d}_2 \\ \bar{d}_3 \\ \vdots \\ \bar{d}_n \end{Bmatrix} = \begin{Bmatrix} \bar{P}_1 \\ \bar{P}_2 \\ \bar{P}_3 \\ \vdots \\ \bar{P}_n \end{Bmatrix} \quad (7.8.3)$$

is modified according to one of the following computational methods:

1. To illustrate the first approach, let us assume that the prescribed displacement component corresponding to \bar{d}_2 is δ . To obtain this $\bar{d}_2 = \delta$ value and the other displacements, we multiply the corresponding coefficient in the main diagonal of the stiffness matrix $\bar{\mathbf{K}}$ by a very large number, say 10^{10} , and replace the \bar{P}_2 nodal force by $\bar{k}_{22}10^{10}\delta$. Thus, we obtain

$$\begin{bmatrix} \bar{k}_{11} & \bar{k}_{12} & \bar{k}_{13} & \cdots & \bar{k}_{1n} \\ \bar{k}_{21} & 10^{10}\bar{k}_{22} & \bar{k}_{23} & \cdots & \bar{k}_{2n} \\ \bar{k}_{31} & \bar{k}_{32} & \bar{k}_{33} & \cdots & \bar{k}_{3n} \\ \vdots & \vdots & \vdots & \ddots & \vdots \\ \bar{k}_{n1} & \bar{k}_{n2} & \bar{k}_{n3} & \cdots & \bar{k}_{nn} \end{bmatrix} \begin{Bmatrix} \bar{d}_1 \\ \bar{d}_2 \\ \bar{d}_3 \\ \vdots \\ \bar{d}_n \end{Bmatrix} = \begin{Bmatrix} \bar{P}_1 \\ \bar{k}_{22}10^{10}\delta \\ \bar{P}_3 \\ \vdots \\ \bar{P}_n \end{Bmatrix}. \quad (7.8.4)$$

Now, it is relatively easy to prove that

$$\frac{\bar{k}_{21}}{\bar{k}_{22}}10^{-10}\bar{d}_1 + \bar{d}_2 + \frac{\bar{k}_{23}}{\bar{k}_{22}}10^{-10}\bar{d}_3 + \cdots + \frac{\bar{k}_{2n}}{\bar{k}_{22}}10^{-10}\bar{d}_n = \delta; \quad (7.8.5)$$

therefore

$$\bar{d}_2 \approx \delta. \quad (7.8.6)$$

2. Assuming, again, that the prescribed displacement component is $d_2 = \delta$, we rearrange Eq. (7.8.3) as follows:

$$\begin{bmatrix} \bar{k}_{11} & 0 & \bar{k}_{13} & \cdots & \bar{k}_{1n} \\ 0 & 1 & 0 & \cdots & 0 \\ \bar{k}_{31} & 0 & \bar{k}_{33} & \cdots & \bar{k}_{3n} \\ \vdots & \vdots & \vdots & \ddots & \vdots \\ \bar{k}_{n1} & 0 & \bar{k}_{n3} & \cdots & \bar{k}_{nn} \end{bmatrix} \begin{Bmatrix} \bar{d}_1 \\ \bar{d}_2 \\ \bar{d}_3 \\ \vdots \\ \bar{d}_n \end{Bmatrix} = \begin{Bmatrix} \bar{P}_1 - \bar{k}_{12}\delta \\ \delta \\ \bar{P}_3 - \bar{k}_{32}\delta \\ \vdots \\ \bar{P}_n - \bar{k}_{n2}\delta \end{Bmatrix}. \quad (7.8.7)$$

Solution of these equations gives us anew not only the prescribed displacement component $\bar{d}_2 = \delta$ but also its effect on the other displacements.

For *thick* plates, another possible load can be *body force* loading, which acts at every material point of the plate rather than on its surface. Such body forces include self-weight (gravity) loading. They are best handled by the direct method discussed above using concentrated forces lumped at the nodal points. In other than thick plates, gravity forces can be treated as surface loads.

Finally, we should mention *thermal loading*. Because of its importance in the engineering practice, a separate section[†] is devoted to this loading condition.

b. Stresses and Stress Resultants. Stresses are usually computed at the nodal points of the elements. If the state of deformations $\bar{\mathbf{d}}$ of the plate is known, we have to transform first the element displacements $\bar{\mathbf{d}}_e^{(N)}$ from the global reference system back to their individual local coordinate system. This is accomplished by

$$\mathbf{d}_e^{(N)} = (\mathbf{T}^T \bar{\mathbf{d}}_e)^{(N)}, \quad (7.8.8)$$

where $\bar{\mathbf{d}}_e^{(N)}$ represents a subset of the global displacement vector $\bar{\mathbf{d}}$ corresponding to element N . It should be noted that this subset contains not only the nodal displacements of the element but also its boundary conditions. After these local DOF are computed, we calculate the stresses by means of the *general* equation

$$\boldsymbol{\sigma}^{(N)} = (\mathbf{E}\boldsymbol{\epsilon})^{(N)} = (\mathbf{E}\mathbf{D}\mathbf{d}_e)^{(N)} = (\mathbf{E}\mathbf{D}\mathbf{N}\mathbf{d}_e)^{(N)} = (\mathbf{S}_e\mathbf{d}_e)^{(N)}. \quad (7.8.9)$$

All notation used in this equation was defined in Secs. 7.2 and 7.3. First, we are interested in obtaining the stress resultants of the plate from which the corresponding stress components can be calculated. Referring to Eq. (7.2.16), we can write the stress resultants at nodal point \textcircled{i} as

$$\mathbf{m}_{\textcircled{i}}^{(N)} = \begin{Bmatrix} m_x \\ m_y \\ m_{xy} \end{Bmatrix}_{\textcircled{i}}^{(N)} \quad \text{and} \quad \mathbf{q}_{\textcircled{i}}^{(N)} = \begin{Bmatrix} q_x \\ q_y \end{Bmatrix}_{\textcircled{i}}^{(N)}, \quad (7.8.10)$$

and for the N th element

$$\mathbf{m}_e^{(N)} = (\mathbf{S}_e\mathbf{d}_e)^{(N)} \quad \text{and} \quad \mathbf{q}_e^{(N)} = (\mathbf{Q}_e\mathbf{d}_e)^{(N)}, \quad (7.8.11)$$

where $\mathbf{S}_e^{(N)}$ and $\mathbf{Q}_e^{(N)}$ are the *stress matrices* due to bending and transverse shearing of the plate, respectively. A more explicit expression of the stress matrix for bending is

$$\mathbf{m}_{\textcircled{i}}^{(N)} = (\mathbf{E}\mathbf{D}\mathbf{N}\mathbf{d}_e)_{\textcircled{i}}^{(N)} = \mathbf{E} \begin{bmatrix} -\frac{\partial^2}{\partial x^2} \mathbf{N}^T \\ -\frac{\partial^2}{\partial y^2} \mathbf{N}^T \\ -2\frac{\partial}{\partial x} \frac{\partial}{\partial y} \mathbf{N}^T \end{bmatrix}_{\textcircled{i}}^{(N)} \cdot \mathbf{d}_e^{(N)}, \quad (7.8.12)$$

[†] See Sec. 10.4.

where \mathbf{N} is the column matrix of the corresponding shape functions and \mathbf{E} represents the elasticity matrix for isotropic homogeneous plates:

$$\mathbf{E} = D \begin{bmatrix} 1 & \nu & 0 \\ \nu & 1 & 0 \\ 0 & 0 & (1 - \nu)/2 \end{bmatrix}. \quad (7.8.13)$$

Similarly, the stress matrix for transverse shearing can be written as

$$\mathbf{Q}_i^{(N)} = -D \begin{bmatrix} \frac{\partial^3}{\partial x^3} & \frac{\partial^3}{\partial x \partial y^2} \\ \frac{\partial^3}{\partial y^3} & \frac{\partial}{\partial x^2 \partial y} \end{bmatrix} \left\{ \begin{matrix} \mathbf{N}^T \\ \mathbf{N}^T \end{matrix} \right\}_{\textcircled{1}}^{(N)}. \quad (7.8.14)$$

Consequently, the matrix expressions for a rectangular plate with four corner nodes become

$$\mathbf{m}_e^{(N)} = [\mathbf{S}_1 \quad \mathbf{S}_2 \quad \mathbf{S}_3 \quad \mathbf{S}_4]^{(N)} \left\{ \begin{matrix} \mathbf{d}_1 \\ \mathbf{d}_2 \\ \mathbf{d}_3 \\ \mathbf{d}_4 \end{matrix} \right\}^{(N)} = (\mathbf{S}_e \mathbf{d}_e)^{(N)} \quad (7.8.15)$$

and

$$\mathbf{q}_e^{(N)} = [\mathbf{Q}_1 \quad \mathbf{Q}_2 \quad \mathbf{Q}_3 \quad \mathbf{Q}_4]^{(N)} \left\{ \begin{matrix} \mathbf{d}_1 \\ \mathbf{d}_2 \\ \mathbf{d}_3 \\ \mathbf{d}_4 \end{matrix} \right\}^{(N)} = (\mathbf{Q}_e \mathbf{d}_e)^{(N)}. \quad (7.8.16)$$

Explicit expressions of the stress matrices $\mathbf{S}_e^{(N)}$ and $\mathbf{Q}_e^{(N)}$ for the simple rectangular element shown in Fig. 7.6.1 are given in Tables 7.8.1 and 7.8.2, while the corresponding stiffness matrices can be found in Eqs. (7.6.12) and (7.6.13), respectively.

Since the stress resultants are computed at the nodal points of each element, these procedures usually result in considerable discrepancies at the common nodes. Such discrepancies are commonly resolved by averaging the stress resultants in all elements joined at the same node, as illustrated in Fig. 6.4.6.

For triangular finite elements, the procedure used to compute stress resultants is the same as the one discussed above. Such an approach, however, will be far more efficient if the general triangular shape of the element is mapped into an equivalent unit triangle [7.8.3, 7.8.4], as shown in Fig. 7.8.1. For this purpose, we need the Jacobi determinant

$$|J| = \begin{vmatrix} x_2 - x_1 & y_2 - y_1 \\ x_3 - x_1 & y_3 - y_1 \end{vmatrix} \quad (7.8.17)$$

and the partial derivatives

$$\begin{aligned} \xi_{,x} &= \frac{y_3 - y_1}{|J|}, & \eta_{,x} &= -\frac{y_2 - y_1}{|J|}, \\ \xi_{,y} &= \frac{x_3 - x_1}{|J|}, & \eta_{,y} &= \frac{x_2 - x_1}{|J|}. \end{aligned} \quad (7.8.18)$$

Table 7.8.1 Stress Matrix for Bending Corresponding to Stiffness Matrix Given in Eq. (7.6.12)

1	2	3	4	5	6	7	8	9	10	11	12	
$6\rho + 6\nu\rho^{-1}$	$4a$	$-4\nu b$	$-6\nu\rho^{-1}$	0	$-2\nu b$	0	0	0	-6ρ	$2a$	0	①
$6\nu\rho + 6\rho^{-1}$	$4\nu a$	$-4b$	$-6\rho^{-1}$	0	$-2b$	0	0	0	$-6\nu\rho$	$2\nu a$	0	
$-(1-\nu)$	$-(1-\nu)b$	$(1-\nu)a$	$1-\nu$	$(1-\nu)b$	0	$-(1-\nu)$	0	0	$1-\nu$	0	$-(1-\nu)a$	
$-6\nu\rho^{-1}$	0	$2\nu b$	$6\rho + 6\nu\rho^{-1}$	$4a$	$4\nu b$	-6ρ	$2a$	0	0	0	0	②
$-6\rho^{-1}$	0	$2b$	$6\nu\rho + 6\rho^{-1}$	$4\nu a$	$4b$	$-6\nu\rho$	$2\nu a$	0	0	0	0	
$-(1-\nu)$	$-(1-\nu)b$	0	$1-\nu$	$(1-\nu)b$	$(1-\nu)a$	$-(1-\nu)$	0	$-(1-\nu)a$	$1-\nu$	0	0	
0	0	0	-6ρ	$-2a$	0	$6\rho + 6\nu\rho^{-1}$	$-4a$	$4\nu b$	$-6\nu\rho^{-1}$	0	$2\nu b$	③
0	0	0	$-6\nu\rho$	$-2\nu a$	0	$6\nu\rho + 6\rho^{-1}$	$-4\nu a$	$4b$	$-6\rho^{-1}$	0	$2b$	
$-(1-\nu)$	0	0	$1-\nu$	0	$(1-\nu)a$	$-(1-\nu)$	$(1-\nu)b$	$-(1-\nu)a$	$1-\nu$	$-(1-\nu)b$	0	
-6ρ	$-2a$	0	0	0	0	$-6\nu\rho^{-1}$	0	$-2\nu b$	$6\rho + 6\nu\rho^{-1}$	$-4a$	$-4\nu b$	④
$-6\nu\rho$	$-2\nu a$	0	0	0	0	$-6\rho^{-1}$	0	$-2b$	$6\nu\rho + 6\rho^{-1}$	$-4\nu a$	$-4b$	
$-(1-\nu)$	0	$(1-\nu)a$	$1-\nu$	0	0	$-(1-\nu)$	$(1-\nu)b$	0	$1-\nu$	$-(1-\nu)b$	$-(1-\nu)a$	

$$S_e^{(N)} = \frac{D}{ab}$$

$$\rho = a/b$$

Source: From Ref. [7.8.1]. For numbering of DOF, see Fig. 7.6.1.

Table 7.8.2 Stress Matrix for Shear Corresponding to Stiffness Matrix given in Eq. (7.6.12)

1	2	3	4	5	6	7	8	9	10	11	12	
$-\frac{12}{a^3} - \frac{6}{b^2a}$	$\frac{4}{-ab}$	$\frac{6}{-a^2}$	$\frac{12}{a^3} + \frac{6}{b^2a}$	$\frac{4}{ab}$	$\frac{6}{-a^2}$	$-\frac{6}{b^2a}$	$\frac{2}{ab}$	0	$\frac{6}{b^2a}$	$-\frac{2}{ab}$	0	q_x
$-\frac{12}{b^3} - \frac{6}{ba^2}$	$\frac{6}{-b^2}$	$\frac{4}{-ab}$	$\frac{6}{ba^2}$	0	$-\frac{2}{ab}$	$-\frac{6}{ba^2}$	0	$\frac{2}{ab}$	$\frac{12}{b^3} + \frac{6}{ba^2}$	$-\frac{6}{b^2}$	$\frac{4}{ab}$	q_y
$-\frac{12}{a^3} - \frac{6}{b^2a}$	$\frac{4}{-ab}$	$\frac{6}{-a^2}$	$\frac{12}{a^3} + \frac{6}{b^2a}$	$\frac{4}{ab}$	$\frac{6}{-a^2}$	$-\frac{6}{b^2a}$	$\frac{2}{ab}$	0	$\frac{6}{b^2a}$	$-\frac{2}{ab}$	0	q_x
$-\frac{12}{b^3} - \frac{6}{ba^2}$	0	$\frac{2}{ab}$	$-\frac{12}{b^3} - \frac{6}{ba^2}$	$\frac{6}{-b^2}$	$\frac{4}{ab}$	$\frac{12}{b^3} + \frac{6}{ba^2}$	$-\frac{6}{b^2a}$	$-\frac{4}{ab}$	$-\frac{6}{ba^2}$	0	$\frac{2}{-ab}$	q_y
$\frac{6}{ba^2}$	$\frac{2}{ab}$	0	$-\frac{6}{b^2a}$	$\frac{2}{-ab}$	0	$\frac{12}{a^3} + \frac{6}{b^2a}$	$-\frac{4}{ab}$	$\frac{6}{-a^2}$	$-\frac{12}{a^3} - \frac{6}{b^2a}$	$\frac{4}{ab}$	$-\frac{6}{-a^2}$	q_x
$\frac{6}{ba^2}$	0	$\frac{2}{ab}$	$-\frac{12}{b^3} - \frac{6}{ba^2}$	$\frac{6}{-b^2}$	$\frac{4}{ab}$	$\frac{12}{b^3} + \frac{6}{ba^2}$	$-\frac{6}{b^2}$	$-\frac{4}{ab}$	$-\frac{6}{ba^2}$	0	$\frac{2}{-ab}$	q_y
$\frac{6}{b^2a}$	$\frac{2}{ab}$	0	$-\frac{6}{b^2a}$	$\frac{2}{-ab}$	0	$\frac{12}{a^3} + \frac{6}{b^2a}$	$-\frac{4}{ab}$	$\frac{6}{-a^2}$	$-\frac{12}{a^3} - \frac{6}{b^2a}$	$\frac{4}{ab}$	$-\frac{6}{-a^2}$	q_x
$\frac{6}{ba^2}$	0	$\frac{2}{ab}$	$-\frac{12}{b^3} - \frac{6}{ba^2}$	$\frac{6}{-b^2}$	$\frac{4}{ab}$	$\frac{12}{b^3} + \frac{6}{ba^2}$	$-\frac{6}{b^2}$	$-\frac{4}{ab}$	$-\frac{6}{ba^2}$	0	$\frac{2}{-ab}$	q_y
$\frac{6}{b^2a}$	$\frac{2}{ab}$	0	$-\frac{6}{b^2a}$	$\frac{2}{-ab}$	0	$\frac{12}{a^3} + \frac{6}{b^2a}$	$-\frac{4}{ab}$	$\frac{6}{-a^2}$	$-\frac{12}{a^3} - \frac{6}{b^2a}$	$\frac{4}{ab}$	$-\frac{6}{-a^2}$	q_x
$-\frac{12}{b^3} - \frac{6}{ba^2}$	$\frac{6}{-b^2}$	$\frac{4}{-ab}$	$\frac{6}{ba^2}$	0	$-\frac{2}{ab}$	$-\frac{6}{ba^2}$	0	$\frac{2}{ab}$	$\frac{12}{b^3} + \frac{6}{ba^2}$	$-\frac{6}{b^2}$	$\frac{4}{ab}$	q_y

$Q_e = D$

Source: From Ref. [7.8.4]. For numbering of DOF, see Fig. 7.6.1.

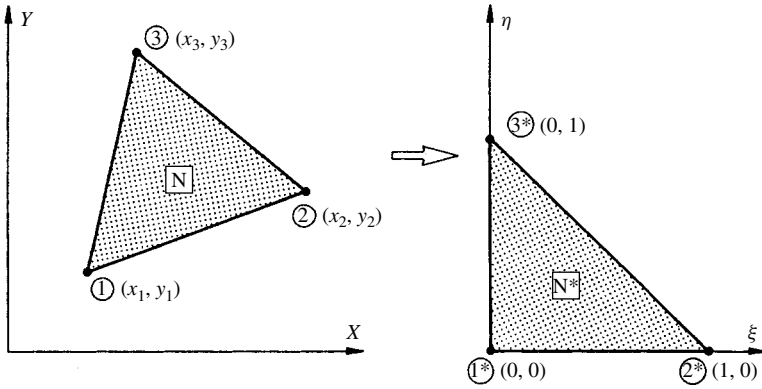


Figure 7.8.1 Mapping of triangular element.

The corresponding nodal displacements of the element that has now the shape of a unit triangle are

$$\delta_e^* = \begin{bmatrix} w_1 \\ (w_{\textcircled{1},x}\eta_{,y} - w_{\textcircled{1},y}\eta_{,x}) \cdot |J| \\ (w_{\textcircled{1},y}\xi_{,x} - w_{\textcircled{1},x}\xi_{,y}) \cdot |J| \\ w_2 \\ (w_{\textcircled{2},x}\eta_{,y} - w_{\textcircled{2},y}\eta_{,x}) \cdot |J| \\ (w_{\textcircled{2},y}\xi_{,x} - w_{\textcircled{2},x}\xi_{,y}) \cdot |J| \\ w_3 \\ (w_{\textcircled{3},x}\eta_{,y} - w_{\textcircled{3},y}\eta_{,x}) \cdot |J| \\ (w_{\textcircled{3},y}\xi_{,x} - w_{\textcircled{3},x}\xi_{,y}) \cdot |J| \end{bmatrix}_e \begin{matrix} 1^* \\ 2^* \\ 3^* \\ 4^* \\ 5^* \\ 6^* \\ 7^* \\ 8^* \\ 9^* \end{matrix} \quad (7.8.19)$$

The partial derivatives required for computation of the bending and twisting moments can be written as

$$\begin{aligned} w_{,\xi\xi}^{\textcircled{i}^*} &= \sum_{j=1^*}^{9^*} N_{j,\xi\xi}^{\textcircled{i}^*} \delta_j^*, \\ w_{,\eta\eta}^{\textcircled{i}^*} &= \sum_{j=1^*}^{9^*} N_{j,\eta\eta}^{\textcircled{i}^*} \delta_j^*, \\ w_{,\xi\eta}^{\textcircled{i}^*} &= \frac{1}{2} \sum_{j=1^*}^{9^*} N_{j,\xi\eta}^{\textcircled{i}^*} \delta_j^* \end{aligned}$$

$$\text{for } \textcircled{i}^* = \textcircled{1}^*, \textcircled{2}^*, \textcircled{3}^*, j = 1^*, 2^*, 3^*, \dots, 9^*, \quad (7.8.20)$$

where the superscript \textcircled{i}^* refers to the nodal points of the unit triangle. In order to transfer Eq. (7.8.20) back to the coordinate system x, y, z of the original triangular

element, we use the relationships

$$\begin{aligned} w_{,xx}^{(i)} &= w_{,\xi\xi}^{(i)} \xi_{,x}^2 + 2w_{,\xi\eta}^{(i)} \xi_{,x} \eta_{,x} + w_{,\eta\eta}^{(i)} \eta_{,x}^2, \\ w_{,yy}^{(i)} &= w_{,\xi\xi}^{(i)} \xi_{,y}^2 + 2w_{,\xi\eta}^{(i)} \xi_{,y} \eta_{,y} + w_{,\eta\eta}^{(i)} \eta_{,y}^2, \\ w_{,xy}^{(i)} &= w_{,\xi\xi}^{(i)} \xi_{,x} \xi_{,y} + w_{,\xi\eta}^{(i)} (\xi_{,x} \eta_{,y} + \xi_{,y} \eta_{,x}) + w_{,\eta\eta}^{(i)} \eta_{,x} \eta_{,y}, \end{aligned} \quad (7.8.21)$$

where the superscript (i) refers now to the nodes of the general triangular element. A similar approach can be used to compute the transverse shearing forces. In Ref. [7.8.4] the reader will find usable BASIC programs for all these somewhat tedious mathematical operations.

For the DKT triangular plate element, explicit expressions for bending and twisting moments are given in Ref. [7.8.5]. Knowing the nodal displacements \mathbf{d}_e of the element in its local coordinate system, the moments can be computed from

$$\mathbf{m}_e^{(N)}(\xi, \eta) = \left\{ \begin{matrix} m_x \\ m_y \\ m_{xy} \end{matrix} \right\}^{(N)} = \frac{1}{24} \mathbf{E}_b (\mathbf{L} \boldsymbol{\alpha} \mathbf{d}_e)^{(N)}, \quad (7.8.22)$$

where \mathbf{E}_b is the elasticity matrix given in Eq. (7.8.13) and

$$\mathbf{L} = \begin{bmatrix} \langle I \rangle & \langle 0 \rangle & \langle 0 \rangle \\ \langle 0 \rangle & \langle I \rangle & \langle 0 \rangle \\ \langle 0 \rangle & \langle 0 \rangle & \langle I \rangle \end{bmatrix} \quad (7.8.23)$$

with

$$\langle 0 \rangle = \begin{pmatrix} 0 & 0 & 0 \end{pmatrix} \quad \text{and} \quad \langle I \rangle = (1 - \xi - \xi \eta). \quad (7.8.24)$$

An explicit expression for matrix $\boldsymbol{\alpha}$ in Eq. (7.8.22) is given in Table 7.7.3. Since matrix \mathbf{L} depends upon ξ and η , computation of moments at several points of the element is possible.

Summary and Conclusions. Since the FEM is not overly sensitive to load representation, use of the direct approach is recommended in most cases, provided the finite element mesh is relatively fine. Thus we may lump the distributed forces at the nodes using the pertinent tributary areas. Consideration of prescribed displacements, however, requires more attention.

The stress resultants at the nodes are calculated using the nodal displacements and the appropriate derivatives of the shape functions. This procedure is quite tedious by longhand computation; thus one should utilize computerized approaches. The obtained stress resultants may differ substantially between adjacent elements if coarse idealization is used. These differences decrease as the finite element mesh is refined. Acceptable results are obtained if the stress resultants are averaged. Finally, we should mention that, in rectangular elements, the FDM can give a simple alternative approach for calculating stress resultants.

ILLUSTRATIVE EXAMPLE I

Let us compute the bending and twisting moments at the center of the plate shown in Fig. 7.6.6a.

The displacement field of this plate was already determined in the Illustrative Example of Sec. 7.6.[†] For this purpose, the explicit expressions[‡] of the simple rectangular element with four corner nodes (Fig. 7.6.1) are used. The corresponding stress matrix $\mathbf{S}_e^{(N)}$ for the moments is also presented in explicit form in Table 7.8.1. To utilize this stress matrix, however, we must first change the numbering of the DOF for element [3] from the global to the local system. This constitutes an inverse process of the index number technique applied in the original Illustrative Example of Sec. 7.6. Thus, under consideration of the prescribed boundary conditions, we obtain the displacement vector of element [3] as

$$\mathbf{d}_e^{(3)} = \begin{Bmatrix} \mathbf{d}_1 \\ \mathbf{d}_2 \\ \mathbf{d}_3 \\ \mathbf{d}_4 \end{Bmatrix}^{(3)} = \begin{Bmatrix} d_1 \\ d_2 \\ d_3 \\ d_4 \\ d_5 \\ d_6 \\ d_7 \\ d_8 \\ d_9 \\ d_{10} \\ d_{11} \\ d_{12} \end{Bmatrix}^{(3)} = \begin{Bmatrix} 98.5184 \\ 69.4160 \\ -62.6984 \\ 246.4504 \\ 192.3716 \\ 0.0000 \\ 524.5735 \\ 0.0000 \\ 0.0000 \\ 180.4093 \\ 0.0000 \\ -122.9534 \end{Bmatrix}^{(3)}. \quad (7.8.25)$$

“Long-hand” multiplication of the first three rows in Table 7.8.1 with the above given vector of element displacements gives

$$\begin{aligned} m_y^{(3)} &= \frac{1}{64} (-9 \times 246.4504 - 6 \times 192.3716 + 10 \frac{1}{3} 524.5735 \\ &\quad - \frac{1}{3} 180.4093 - \frac{1}{3} 122.9534) = 25.6848, \\ m_x^{(3)} &= \frac{1}{64} (-3 \times 264.4504 - 2 \times 192.3716 + 7 \times 524.5735 \\ &\quad - 4 \times 180.4093 - 4 \times 122.9534) = 20.85, \\ m_{xy}^{(3)} &= \frac{1}{64} (-\frac{2}{3} 98.5184 + \frac{2}{3} 246.4504 \\ &\quad - \frac{2}{3} 524.5735 + \frac{2}{3} 180.4093) = -2.0441. \end{aligned} \quad (7.8.26)$$

These results are verified by computer results with a corresponding BASIC program for plates [7.8.4].

ILLUSTRATIVE EXAMPLE II

To demonstrate in detail the computation of stress resultants using triangular finite elements, we refer again to the plate problem shown in Fig. 7.6.6a. This time, however, an alternative form of idealization is employed (Fig. 7.8.2b). The computation is based on nonconforming triangular elements. In Eq. (7.6.14), following the recommendation of Bazeley [7.5.6], we set $\alpha_2 = 0.5$.

[†] The pertinent finite element idealization the plate is shown in Fig. 7.6.6b.

[‡] See Eqs. (7.6.12) and (7.6.13).

The obtained column matrix of the shape functions is

$$\mathbf{N}^{(N)} = \left\{ \begin{array}{l} N_1(\xi, \eta) = 1 - 3\xi^2 - 4\xi\eta - 3\eta^2 + 2\xi^3 + 4\xi^2\eta + 4\xi\eta^2 + 2\eta^3 \\ N_2(\xi, \eta) = \xi - 2\xi^2 - \frac{3}{2}\xi\eta + \xi^3 + \frac{3}{2}\xi^2\eta + \frac{1}{2}\xi\eta^2 \\ N_3(\xi, \eta) = \eta - \frac{3}{2}\xi\eta - 2\eta^2 + \frac{1}{2}\xi^2\eta + \frac{3}{2}\xi\eta^2 + \eta^3 \\ \hline N_4(\xi, \eta) = 3\xi^2 + 2\xi\eta - 2\xi^3 - 2\xi^2\eta - 2\xi\eta^2 \\ N_5(\xi, \eta) = -\xi^2 - \xi\eta + \xi^3 + \xi^2\eta + \xi\eta^2 \\ N_6(\xi, \eta) = \frac{1}{2}\xi\eta + \frac{1}{2}\xi^2\eta - \frac{1}{2}\xi\eta^2 \\ \hline N_7(\xi, \eta) = 2\xi\eta + 3\eta^2 - 2\xi^2\eta - 2\xi\eta^2 - 2\eta^3 \\ N_8(\xi, \eta) = \frac{1}{2}\xi\eta - \frac{1}{2}\xi^2\eta + \frac{1}{2}\xi\eta^2 \\ N_9(\xi, \eta) = -\xi\eta - \eta^2 + \xi^2\eta + \xi\eta^2 + \eta^3 \end{array} \right\}^{(N)}, \quad (7.8.27)$$

where ξ and η represent the coordinates in the unit triangle, displayed in Fig. 7.8.1. The local numbering of the DOF corresponds to that shown in Fig. 7.8.2a.

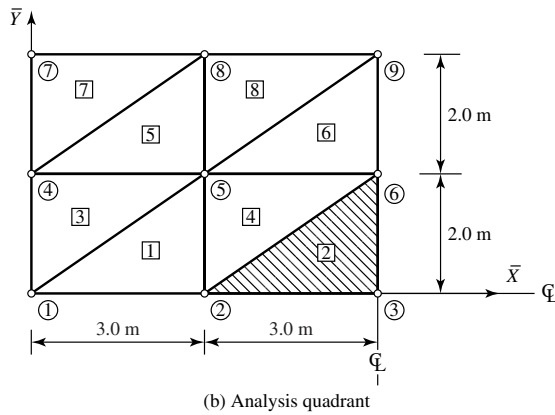
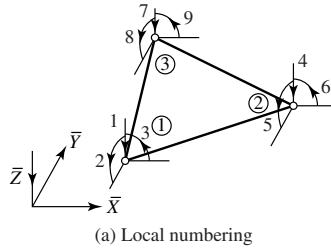


Figure 7.8.2 Alternative discretization of plate shown in Fig. 7.6.6a.

Utilizing the apparent double symmetry of the plate structure and its loading, we subdivide the quarter plate into eight triangular elements (Fig. 7.8.2b). Since we would like to compute only the maximum moments, it is sufficient to restrict our investigation to element [2] and node [3].

A computer analysis based on the above triangular plate element [7.8.4] gives the following displacement components for the element [2], expressed in

the global reference system of the plate:

$$\bar{\mathbf{d}}_e^{(2)} = \begin{Bmatrix} 230.3 \\ 144.3 \\ 0.0 \\ 635.5 \\ 0.0 \\ 0.0 \\ 285.0 \\ 0.0 \\ -218.7 \end{Bmatrix}^{(2)} . \quad (7.8.28)$$

As required, the prescribed boundary conditions are also incorporated into this displacement vector. By comparing Fig. 7.8.2a with Fig. 7.8.2b, the following relationship between the global and local numbering of the nodes can be established:

$$\begin{array}{cc} \text{Local} & \text{global} \\ 1 & \bar{2} \\ 2 & \bar{3} \\ 3 & \bar{6} \end{array} . \quad (7.8.29)$$

Thus, we can write

$$\begin{array}{lll} x_1 = 3, & x_2 = 6, & x_3 = 6, \\ y_1 = 0, & y_2 = 0, & y_3 = 2. \end{array} \quad (7.8.30)$$

Based on these coordinates, the Jacobian determinant becomes

$$|\mathbf{J}| = (x_2 - x_1)(y_3 - y_1) - (x_3 - x_1)(y_2 - y_1) = 6. \quad (7.8.31)$$

The derivatives required for mapping element [2] into a unit triangle are

$$\begin{aligned} \xi_{,x} &= \frac{y_2 - y_1}{|\mathbf{J}|} = 0.33, & \xi_{,y} &= -\frac{x_3 - x_1}{|\mathbf{J}|} = -0.5, \\ \eta_{,x} &= -\frac{y_2 - y_1}{|\mathbf{J}|} = 0.0, & \eta_{,y} &= \frac{x_2 - x_1}{|\mathbf{J}|} = 0.5. \end{aligned} \quad (7.8.32)$$

Now, we can express the displacement vector of element [2] in terms of the unit triangle. This calculation gives

$$\delta_e^{*(2)} = \begin{Bmatrix} 230.3 \\ 144.3 \times 0.5 |\mathbf{J}| \\ -144.3(-0.5) |\mathbf{J}| \\ 635.5 \\ 0.0 \\ 0.0 \\ 285.0 \\ 0.0 \\ -218.7 \times 0.33 |\mathbf{J}| \end{Bmatrix} = \begin{Bmatrix} 230.3 \\ 432.8 \\ 432.8 \\ 635.5 \\ 0.0 \\ 0.0 \\ 285.0 \\ 0.0 \\ -433.0 \end{Bmatrix} . \quad (7.8.33)$$

Next, the required partial derivatives of the shape functions are determined using Eq. (7.8.20). Some of these are

$$\begin{aligned} N_{1,\xi\xi} &= -6 + 12\xi + 8\eta, & N_{2,\xi\xi} &= -4 - 6\xi + 3\eta, \\ N_{1,\eta\eta} &= -6 + 8\xi + 12\eta, & N_{2,\eta\eta} &= \xi, \\ N_{1,\xi\eta} &= -4 + 8\xi + 8\eta, & N_{2,\xi\eta} &= -\frac{3}{2} + 3\xi + \eta, \end{aligned} \quad (7.8.34)$$

The lengthy longhand computation yields the following results for Eq. (7.8.20):

$$w_{,\xi\xi}^{(3*)} = -1565, \quad w_{,\eta\eta}^{(3*)} = -1511.4, \quad w_{,\xi\eta}^{(3*)} = -924.1. \quad (7.8.35)$$

By applying Eq. (7.8.21), these results are transferred back to the original coordinate system of element [2]. Hence

$$w_{,xx}^{(2)} = -173.9, \quad w_{,yy}^{(2)} = -307.1, \quad w_{,xy}^{(2)} = 106.9. \quad (7.8.36)$$

Finally, to obtain the moments in the center of the plate, we substitute these second derivatives into the corresponding equations of classical plate theory[†]; this gives

$$m_x^{(2)} = 14.49, \quad m_y^{(2)} = 25.59, \quad m_{xy}^{(2)} = -8.9. \quad (7.8.37)$$

It is apparent that the procedure introduced above is not suited for hand computation, since it is intended exclusively for computer use. Consequently, this example serves merely to clarify, up to a certain extent, the individual steps discussed in the descriptive part of this section. However, the reader will find BASIC and FORTRAN programs for plate analysis utilizing this type of triangular element in Refs. [7.8.4] and [7.8.6], respectively. Needless to say, in this case application of the FDM for determination of the maximum moments would be far superior to the longhand approach used here.

References and Bibliography

- [7.8.1] ZIENKIEWICZ, O. C., "Finite Element Procedures in the Solution of Plate and Shell Problems," in Zienkiewicz, O. C., and Holister, G. S. (Eds.), *Stress Analysis*, John Wiley & Sons, London, 1965.
- [7.8.2] ZIENKIEWICZ, O. C., and CHEUNG, Y. K., "Finite Element Method of Analysis for Arch Dam Shells and Comparison with Finite Difference Procedures," in Rydzewski, J. R. (Ed.), *Theory of Arch Dams*, Pergamon Press, Oxford, 1965.
- [7.8.3] SCHWARZ, H. R., *Methode der finiten Elemente*, 3rd ed., Teubner, Stuttgart, 1991.
- [7.8.4] SZILARD, R., et al., *BASIC-Programme für Baumechanik und Statik*, Ernst & Sohn, Berlin, 1986.
- [7.8.5] BATOZ, J. L., "An Explicit Formulation for an Efficient Triangular Plate-Bending Element," *Int. J. Num. Meth. Eng.*, 18 (1982), 1077–1069.
- [7.8.6] SCHWARZ, H. R., *FORTTRAN-Programme zur Methode der finiten Elemente*, Teubner, Stuttgart, 1981.
- [7.8.7] ZIENKIEWICZ, O. C., *The Finite Element Method*, 3rd ed., McGraw-Hill Book Co., London, 1977.

[†] Eqs. (1.2.26), (1.2.27) and (1.2.29).

7.9 Moderately Thick Plate Elements

The finite element analysis of moderately thick plates with $h/L \geq \frac{1}{10} - \frac{1}{5}$ ratios must consider additional deformations of the plate caused by transverse shearing. The corresponding Reissner-Mindlin plate theories were treated in Sec. 1.5. These theories have been used in a variety of ways for generating rectangular [7.9.1–7.9.8] and triangular [7.9.9–7.9.13] finite elements.

Applying the first-order shear theory from Mindlin, the displacement components are expressed using Eq. (1.5.18) as

$$u = z\psi_x(x, y), \quad v = z\psi_y(x, y), \quad w = w(x, y), \quad (7.9.1)$$

where ψ_x and ψ_y are rotations of the normal in the X, Z and Y, Z planes, respectively. The Mindlin plate model is shown in Fig. 7.9.1a. In this plate theory w , ψ_x and ψ_y are independent variables. Consequently, finite elements based on Mindlin's theory require only $C^{(0)}$ continuity in the lateral displacements and rotations.

The strains due to bending of the plate are

$$\kappa = \begin{Bmatrix} \kappa_x \\ \kappa_y \\ \phi \end{Bmatrix} = \begin{Bmatrix} \frac{\partial \psi_x}{\partial x} \\ \frac{\partial \psi_y}{\partial y} \\ \frac{\partial \psi_x}{\partial x} + \frac{\partial \psi_y}{\partial y} \end{Bmatrix}. \quad (7.9.2)$$

In addition, we must consider the strains due to transverse shear, which are calculated from

$$\gamma = \begin{Bmatrix} \gamma_x \\ \gamma_y \end{Bmatrix} = \begin{Bmatrix} \frac{\partial w}{\partial x} + \psi_x \\ \frac{\partial w}{\partial y} + \psi_y \end{Bmatrix}. \quad (7.9.3)$$

The corresponding stress resultants can be written as

$$\mathbf{m} = \begin{Bmatrix} m_x \\ m_y \\ m_{xy} \end{Bmatrix} = \mathbf{E}_b \kappa \quad \text{and} \quad \mathbf{q} = \begin{Bmatrix} q_x \\ q_y \end{Bmatrix} = \mathbf{E}_s \gamma, \quad (7.9.4)$$

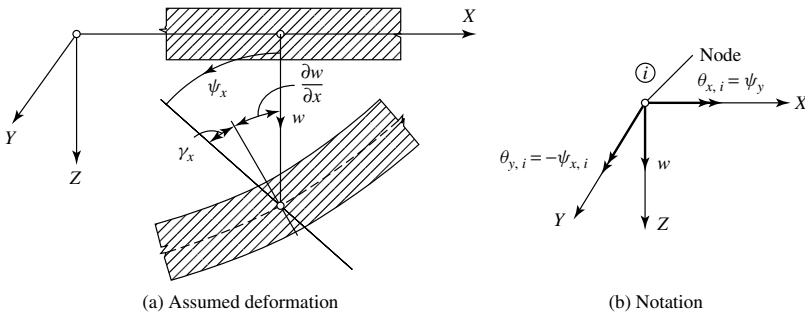


Figure 7.9.1 Moderately thick plate model.

where \mathbf{E}_b and \mathbf{E}_s represent the elasticity matrices for bending and shear, respectively:

$$\mathbf{E}_b = \text{Eq. (7.8.13)} \quad \text{and} \quad \mathbf{E}_s = \frac{Eh\alpha}{2(1+\nu)} \begin{bmatrix} 1 & 0 \\ 0 & 1 \end{bmatrix}, \quad (7.9.5)$$

where $\alpha = \kappa^2$ is the shear modification number usually taken as $\frac{5}{6}$ for homogeneous isotropic plates.[†]

The stress resultants given in Eqs. (1.5.23)–(1.5.27) for moderately thick plates of uniform thickness may be written in a simplified matrix form as

$$\begin{Bmatrix} \mathbf{m} \\ \mathbf{q} \end{Bmatrix} = \frac{Eh}{12(1-\nu^2)} \begin{bmatrix} h^2 & \nu h^2 & 0 & 0 & 0 \\ \nu h^2 & h^2 & 0 & 0 & 0 \\ 0 & 0 & \frac{h^2(1-\nu)}{2} & 0 & 0 \\ 0 & 0 & 0 & 5(1-\nu) & 0 \\ 0 & 0 & 0 & 0 & 5(1-\nu) \end{bmatrix} \begin{Bmatrix} \kappa_x \\ \kappa_y \\ \phi \\ \gamma_x \\ \gamma_y \end{Bmatrix}. \quad (7.9.6)$$

The internal strain energy of the element is

$$\Pi_{\text{int},e} = \frac{1}{2} \iint \boldsymbol{\kappa}^T \mathbf{m} \, dA + \frac{1}{2} \iint \boldsymbol{\gamma}^T \mathbf{q} \, dA. \quad (7.9.7)$$

Since the strain due to bending and shear may be expressed in terms of nodal displacements \mathbf{d}_e , by performing the operations indicated in Eqs. (7.9.2) and (7.9.3), we can write

$$\boldsymbol{\kappa} = \mathbf{D}_b \mathbf{d}_e \quad \text{and} \quad \boldsymbol{\gamma} = \mathbf{D}_s \mathbf{d}_e, \quad (7.9.8)$$

where \mathbf{D}_b and \mathbf{D}_s represent the differentiations of the shape functions \mathbf{N} , as indicated in Eqs. (7.9.2) and (7.9.3).

Substituting Eqs. (7.9.4) and (7.9.5) into Eq. (7.9.7), the strain energy of the element becomes

$$\Pi_{\text{int},e} = \frac{1}{2} \iint \mathbf{d}_e^T \mathbf{D}_b^T \mathbf{E}_b \mathbf{D}_b \mathbf{d}_e \, dA + \frac{1}{2} \iint \mathbf{d}_e^T \mathbf{D}_s^T \mathbf{E}_s \mathbf{D}_s \mathbf{d}_e \, dA, \quad (7.9.9)$$

or in a more concise form

$$\Pi_{\text{int},e} = \frac{1}{2} \mathbf{d}_e^T \mathbf{K}_e \mathbf{d}_e, \quad (7.9.10)$$

in which \mathbf{K}_e is the stiffness matrix for the moderately thick plate element and includes bending and transverse shear effects.

Using the shape functions

$$\begin{aligned} w &= a_1 + a_2x + a_3y + a_4xy + a_5x^2 + a_6y^2 + a_7x^2y + a_8xy^2, \\ \psi_x &= b_1 + b_2x + b_3y + b_4xy, \quad \psi_y = c_1 + c_2x + c_3y + c_4xy \end{aligned} \quad (7.9.11)$$

[†] See Sec. 1.5.

and applying the restrictions of constant shear strain

$$\frac{\partial \psi_x}{\partial x} = 0 \quad \text{and} \quad \frac{\partial \psi_y}{\partial y} = 0, \quad (7.9.12)$$

we obtain [7.9.8]

$$a_5 = \frac{1}{2}b_2, \quad a_6 = \frac{1}{2}c_3, \quad a_7 = \frac{1}{2}b_4, \quad a_8 = \frac{1}{2}c_4. \quad (7.9.13)$$

Since now the number of unknowns is reduced to 12, the element has the same nodal DOF as the simple nonconforming rectangular element with four corner nodes shown in Fig. 7.6.1.

A very usable alternative approach based on Reissner's theory is offered by Pryor et al. [7.9.7]. The chosen displacement function for $w(x, y)$ is the same as used in Eq. (7.6.2) in connection with the simple rectangular thin-plate element. The assumed displacement functions for the rotations correspond to those in Eq. (7.9.11). Thus, we can superimpose the stiffness matrix listed in Eq. (7.6.12) and the stiffness matrix containing the shear terms represented by the second right-hand side term of Eq. (7.9.9). Consequently, Eq. (7.9.10) can be written as

$$\Pi_{\text{int},e} = \frac{1}{2} \mathbf{d}_e^T (\mathbf{K}_{e,b} + \mathbf{K}_{e,s}) \mathbf{d}_e \quad (7.9.14)$$

Furthermore, the shape functions for rotations caused by transverse shear are the same as those used in computing stiffness matrices for bilinear plane stress elements [7.9.15–7.9.17]. The derivation of element stiffness matrices for moderately thick plates follows the standard procedures already introduced for Kirchhoff plates. It is important to realize, however, that the subscript notation and sign conventions in the classical and improved plate theories sometimes differ from those used in the finite element approach (Fig. 7.9.2b), as was already pointed out. Of course, in formulating the stiffness matrix containing the additional transverse shear effects $\mathbf{K}_{e,s}$, one must use the expressions introduced above in the procedure. It means that in the strain vector $\boldsymbol{\gamma}$ only the additional strain produced by transverse shear can be considered. The obtained rectangular plate element with 20 DOF is shown in Fig. 7.9.2.

In addition, one should be also aware of the fact that the boundary conditions in the present approach are not always the same as those of the Reissner theory given in

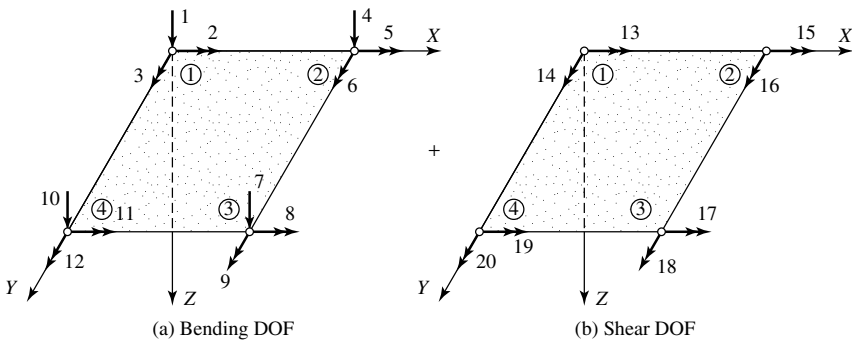


Figure 7.9.2 Moderately thick plate element.

Eqs. (1.5.8)–(1.5.10). That is, boundary conditions for finite element analysis of moderately thick plates must satisfy the prescribed displacement conditions at the plate edges. These can be satisfied, however, only approximately. The vanishing twisting moment condition, for example, could not be fulfilled because the appropriate DOF is not included in the displacement-based FEM. However, the formulation presented above has the ability to satisfy zero shear resultant condition along a free edge, since the rotation γ (caused by the transverse shear) is specified to vanish at two end nodal points. Thus, there will be no transverse shear deformation along the free edge. The most common boundary conditions encountered in practice are given as follows for $x = \text{const}$:

$$\text{Simply supported:} \quad \bar{w} = 0, \quad \bar{\psi}_x \neq 0, \quad \bar{\theta}_x \neq 0; \quad (7.9.15a)$$

$$\text{Clamped:} \quad \bar{w} = 0, \quad \bar{\psi}_x = 0, \quad \bar{\theta}_x = 0; \quad (7.9.15b)$$

$$\text{Free:} \quad \bar{w} \neq 0, \quad \bar{\psi}_x \neq 0, \quad \bar{\theta}_x = 0. \quad (7.9.15c)$$

As Fig. 7.9.3 shows, the accuracy of the FE procedure presented here is good.

To compute the stress resultants, one should follow logically the standard finite element procedures as described in the foregoing section. For this purpose, however, an additional stress matrix $\mathbf{S}_{e,s}$ containing the transverse shear effects must be generated.

It is much more difficult to develop stiffness matrices of triangular elements for moderately thick plates. Consequently, only relatively few triangular elements are presently available. The principal difficulty appears to be that there are only two expressions for the average shear strains without the coupling strain $\partial u/\partial y + \partial v/\partial x$ for plane stress. This sometimes leads to numerical difficulties.

In most cases, numerical integration is used for generating element stiffness matrices. This approach may lead to the so-called locking behavior, resulting in overstiff

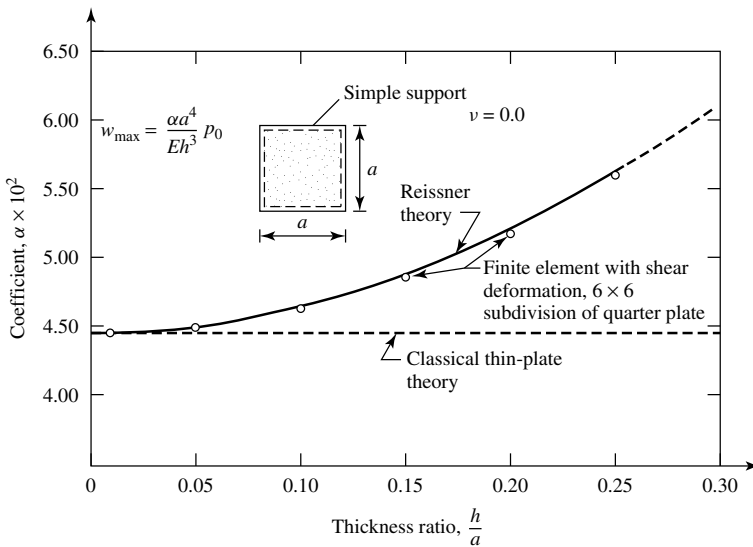


Figure 7.9.3 Accuracy of 20-DOF element [7.8.7].

solutions. Selective or reduced integration[†] may overcome this difficulty. With highly constrained plate boundaries, however, over stiff solutions may still occur. In recent years much research activity has been directed to eliminate this problem [7.9.12, 7.9.14].

Finally, we should mention the *conjugate plate analogy* introduced in Sec.5.3. This simple approach to the analysis of simply supported moderately thick plates of polygonal shape eliminates the need for more complicated finite element analysis. That is, this analogy presents a relationship between the deflections of Kirchhoff and Mindlin plates and therefore allows speedy and accurate computation of deflections of moderately thick plates from the corresponding Kirchhoff solution. For other than simply supported boundary conditions, application of Donnel's correction factor[‡] to the classical deflections is recommended. While the conjugate beam analogy yields exact results, this correction factor gives only usable approximations.

Summary. Classical plate theory neglects the transverse shear deformations. However, the effects of these additional deformations on moderately thick plates can be of importance, especially if the ratio of thickness to span length (h/L) is approaching $\frac{1}{5}$ value. An expanded FEM based on the Reissner-Mindlin theory is presented herein and is applied to a 4-node, 12-DOF rectangular plate element. By separating the bending effects of classical plate theory from the effects of transverse shearing, it is possible to superimpose the stiffness matrix of the simple rectangular plate bending element and that of a matrix obtained from the transverse shearing terms. In this way, a finite element of 20 DOF is obtained.

References [7.9.2] and [7.9.14] give FORTRAN programs for generating stiffness matrices for moderately thick plates that can facilitate the reader in writing a computer program.

ILLUSTRATIVE EXAMPLE

Figure 7.9.4a shows a square rectangular plate with simply supported boundary conditions subjected to uniformly distributed load p_0 . To be determined are (a) the maximum lateral deflection and (b) the maximum bending moment. Since the thickness-to-span ratio of the plate is $h/a \approx \frac{1}{5}$, the effects of transverse shear must be considered in the analysis.

The simply supported boundary conditions permit the use of the conjugate plate analogy. Thus, in the first part of the analysis we compute the deflections w_K of the corresponding Kirchhoff plate. For this purpose the stiffness matrix of the simple rectangular plate element with four corner nodes—explicitly given in Eqs. (7.6.12) and (7.6.13)—is used. Figure 7.9.4b shows the finite element idealization of the analysis quadrant. A computer program based on this plate element gives the following maximum lateral deflection and moment at the nodal point (16):

$$\bar{w}_{K,16} = 0.0112 \text{ m} \quad (\text{error} : 2.2\%) \quad \text{and} \quad \bar{m}_{K,16} = 12318 \text{ m-kN/m} \quad (7.9.16)$$

[†] See Sec. 7.11.

[‡] See Eq. (5.3.3).

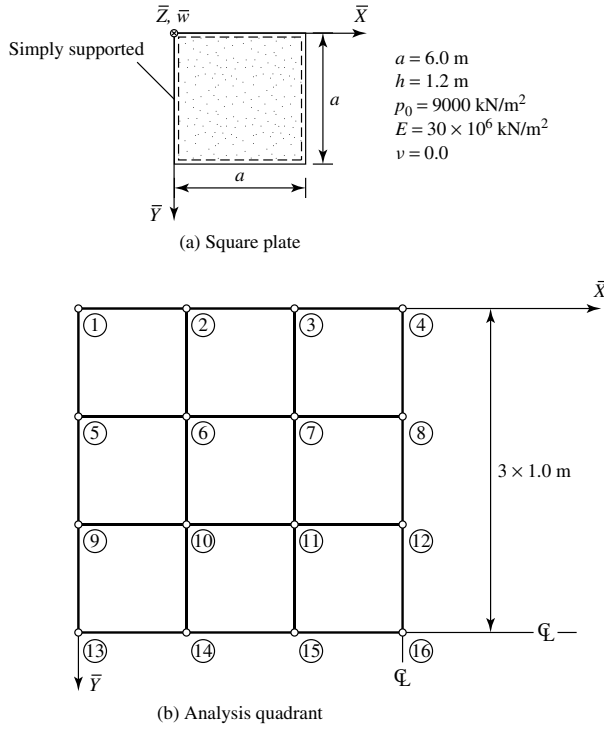


Figure 7.9.4 Moderately thick plate.

Next, we calculate the additional maximum deflection caused by the transverse shear by applying Eq. (5.3.1). Thus, we can write

$$\bar{w}_{s,16} = \frac{2 \bar{m}_{K,16}}{\kappa^2 G h} = \frac{2 \times 12318}{0.8333 \times 15 \times 10^6 \times 1.2} = 0.0164 \text{ m.} \quad (7.9.17)$$

Hence, the total maximum deflection of the plate including the effect of shear deformation becomes

$$\bar{w}_{t,16} = \bar{w}_{K,16} + \bar{w}_{s,16} = 0.01284 \text{ m.} \quad (7.9.18)$$

This represents an approximate 14% increase over the finite element solution based on classical plate theory. The same approach can be taken for the other nodal points.

A comparison with maximum deflection obtained from the Reissner theory for moderately thick plates,

$$\bar{w}_{R,\max} = 0.05217 \frac{p_0 a^4}{E h^3} = 0.0117 \text{ m,} \quad (7.9.19)$$

shows an error of 9%. Interpreting this result, however, one must consider the approximate nature of the FEM used in the computation and the relatively

coarse subdivision of the finite element idealization. These errors are carried over into Eq. (7.9.18). Consequently, the inherent error of this computation due to the finite element approach can be estimated as 5–6%. By increasing the number of elements, this error will get subsequently smaller.

To calculate the maximum positive moment at the center of the plate, we utilize the corresponding finite difference equation (5.1.12), which with $v = 0$ becomes

$$\bar{m}_{t,\max} \approx -\frac{D}{(\Delta x)^2}(2\bar{w}_{t,15} - 2\bar{w}_{t,16}). \quad (7.9.20)$$

To evaluate this equation, we also require the total plate deflection at node (15). We obtain this by the procedure used above for nodal point (16). Thus, we can write

$$\bar{w}_{t,15} = \bar{w}_{K,15} + \frac{(\bar{m}_{x,15} + \bar{m}_{y,15})_K}{\kappa^2 Gh} = 0.0098 + \frac{11,636 + 10,705}{14.9994 \times 10^6} = 0.0113, \quad (7.9.21)$$

Consequently, the approximate value of the maximum moment is

$$\bar{m}_{t,\max} \approx -4.32 \times 10^6 \times 2(0.113 - 0.01284) = 13306 \text{ m-kN/m}. \quad (7.9.22)$$

References and Bibliography

- [7.9.1] BATHE, K. J., and DVORKIN, E. N., "A Four-Node Plate Bending Element Based on Mindlin/Reissner Plate Theory and Mixed Interpolation," *Int. J. Num. Meth. Eng.*, 21 (1985), 367–383.
- [7.9.2] CRISFIELD, M. A., "A Quadratic Mindlin Element Using Shear Constraints," *Comp. Struct.*, 18 (1984), 833–852.
- [7.9.3] HUANG, H. C., and HINTON, E., "A Nine Node Lagrangian Mindlin Plate Element with Enhanced Shear Interpolation," *Eng. Comput.*, 1 (1984), 369–379.
- [7.9.4] HINTON, E., and HUANG, H. C., "A Family of Quadrilateral Mindlin Plate Elements with Substitute Shear Strain Fields," *Comp. Struct.*, 23 (1986), 409–431.
- [7.9.5] TESSLER, T. J. R., and HUGHES, T. J. R., "An Improved Treatment of Transverse Shear in the Mindlin-Type Four- Node Quadrilateral Element," *Comp. Meth. Appl. Mech. Eng.*, 39 (1983), 311–335.
- [7.9.6] VOYIADIS, G. Z., and PECQUET, R. W., "Isotropic Plate Element with Shear and Normal Strain Deformations," *Int. J. Num. Meth. Eng.*, 24 (1987), 1671–1695.
- [7.9.7] PRYOR, C. W., et al., "Finite Element Bending Analysis of Reissner Plates," *J. Eng. Mech. Div., ASCE*, 96 (1970), 967–982.
- [7.9.8] LINN, P. P., and DHILLON, B. S., "Triangular Thick Plate Bending Element," Paper No. M 61–365, in *Proceedings of the First International Conference on Structural Mechanics in Reactor Technology*, Vol. 6, Berlin, 1970.
- [7.9.9] GRIEMANN, L. F., and LINN, P. P., "Finite Element Analysis of Plate Bending with Transverse Shear Deformation," *Nucl. Eng. Des.*, 14 (1970), 223.
- [7.9.10] RAO, G. V., et al., "A High Precision Triangular Plate Bending Element for the Analysis of Thick Plates," *Nucl. Eng. Des.*, 30 (1974), 408.
- [7.9.11] MOHR, G. A., "A Triangular Element for Thick Slabs," *Comp. Struct.*, 9 (1978), 595–598.
- [7.9.12] ZIENKIEWICZ, O. C., and LEFEBRE, D., "A Robust Triangular Plate Bending Element of the Reissner-Mindlin Type," *Int. J. Num. Meth. Eng.*, 26 (1988), 1169–1181.

- [7.9.13] KABIR, H. R. H., "A Shear Locking Free Three-Node Triangular Element for Moderately Thick and Thin Plates," *Int. J. Num. Meth. Eng.*, 35 (1992), 503–519.
- [7.9.14] HINTON, E., *Numerical Methods and Software for Dynamic Analysis of Plates and Shells*, Pineridge Press, Swansea, United Kingdom, 1988.
- [7.9.15] HAHN, H. G., *Methode der finiten Elemente in der Festigkeitslehre*, 2nd ed., Akademische Verlagsgesellschaft, Wiesbaden, 1982.
- [7.9.16] AVRAM, C., et al., *Numerical Analysis of Reinforced Concrete Structures*, Elsevier, Amsterdam, 1993.
- [7.9.17] SZILARD, R., *Finite Berechnungsmethoden der Struktur mechanik*, Vol. 2, Ernst & Sohn, Berlin, 1990.
- [7.9.18] BATOZ, J. L., and LARDEUR, D., "A Discrete Triangular Nine d.o.f. Element for the Analysis of Thick to Very Thin Plates," *Int. J. Num. Meth. Eng.*, 31 (1982), 1–18.
- [7.9.19] KANT, T., "Numerical Analysis of Thick Plates," *Comp. Meth. Appl. Eng.*, 26 (1982), 1–18.
- [7.9.20] KANT, T., et al., "A Refined Higher Order C^0 Plate Bending Element," *Comp. Struct.*, 15 (1982), 177–183.

7.10 Thick-Plate Elements

When the thickness-to-span ratio h/L exceeds approximately 2.0, a plate problem becomes a corresponding problem of three-dimensional elasticity. In Sec. 1.6 we introduced the governing differential equations of three-dimensional elasticity in a Cartesian coordinate system; its solution, however, can rarely be obtained analytically. Even the application of the FDM is extremely cumbersome. Consequently, it is natural that we extend the versatile FEM to, thick-plate problems. The finite element procedure in this case follows, again, the standard approach introduced in the foregoing sections. The main difference is that idealization of the thick plate is now three dimensional, as shown in Fig. 7.10.1. However, creating a corresponding

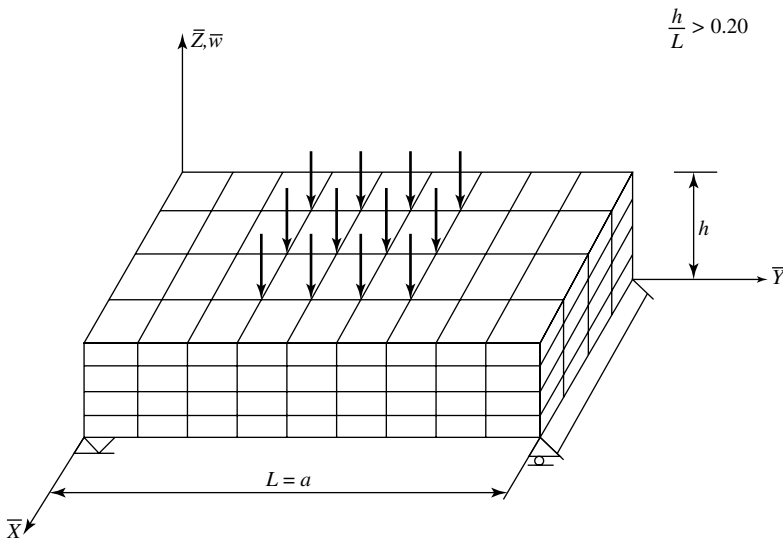


Figure 7.10.1 Three-dimensional idealization of a thick plate.

finite element mesh can be involved, particularly in terms of proper numbering of the nodes.

To formulate finite elements for thick plates, first we express the three-dimensional *strain-displacement relationship* in matrix form as

$$\boldsymbol{\varepsilon} = \begin{Bmatrix} \varepsilon_x \\ \varepsilon_y \\ \varepsilon_z \\ \gamma_{xy} \\ \gamma_{yz} \\ \gamma_{zx} \end{Bmatrix} = \begin{Bmatrix} \frac{\partial u}{\partial x} \\ \frac{\partial v}{\partial y} \\ \frac{\partial w}{\partial z} \\ \frac{\partial u}{\partial y} + \frac{\partial v}{\partial x} \\ \frac{\partial v}{\partial z} + \frac{\partial w}{\partial y} \\ \frac{\partial w}{\partial x} + \frac{\partial u}{\partial z} \end{Bmatrix}, \quad (7.10.1)$$

where u , v and w represent the displacements at any point of the three-dimensional continuum. Thus, the *strain-displacement operator* becomes

$$\mathbf{B} = \begin{bmatrix} \frac{\partial}{\partial x} & 0 & 0 \\ 0 & \frac{\partial}{\partial y} & 0 \\ 0 & 0 & \frac{\partial}{\partial z} \\ \frac{\partial}{\partial y} & \frac{\partial}{\partial x} & 0 \\ 0 & \frac{\partial}{\partial z} & \frac{\partial}{\partial y} \\ \frac{\partial}{\partial z} & 0 & \frac{\partial}{\partial x} \end{bmatrix}, \quad (7.10.2)$$

Hence, the *stress-strain relationship* for a homogeneous isotropic material can be written as

$$\boldsymbol{\sigma} = \mathbf{E}\boldsymbol{\varepsilon}, \quad (7.10.3)$$

where the stress vector is

$$\boldsymbol{\sigma} = \{ \sigma_x \quad \sigma_y \quad \sigma_z \quad \tau_{xy} \quad \tau_{yz} \quad \tau_{zx} \} \quad (7.10.4)$$

and \mathbf{E} represents the corresponding elasticity matrix. By expanding Eq. (7.10.3), we obtain

$$\begin{Bmatrix} \sigma_x \\ \sigma_y \\ \sigma_z \\ \tau_{xy} \\ \tau_{yz} \\ \tau_{zx} \end{Bmatrix} = \frac{E}{1 - \nu - 2\nu^2} \times \begin{bmatrix} 1 - \nu & \nu & \nu & 0 & 0 & 0 \\ \nu & 1 - \nu & \nu & 0 & 0 & 0 \\ \nu & \nu & 1 - \nu & 0 & 0 & 0 \\ 0 & 0 & 0 & \frac{1 - 2\nu}{2} & 0 & 0 \\ 0 & 0 & 0 & 0 & \frac{1 - 2\nu}{2} & 0 \\ 0 & 0 & 0 & 0 & 0 & \frac{1 - 2\nu}{2} \end{bmatrix} \begin{Bmatrix} \varepsilon_x \\ \varepsilon_y \\ \varepsilon_z \\ \tau_{xy} \\ \tau_{yz} \\ \tau_{zx} \end{Bmatrix} \quad (7.10.5)$$

The strain energy part of the total potential of the system is

$$\Pi_{\text{int}} = \frac{1}{2} \int_V \boldsymbol{\varepsilon}^T \mathbf{E} \boldsymbol{\varepsilon} dV. \quad (7.10.6)$$

As in previous sections, it is convenient to write some element displacement fields in terms of nodal displacements \mathbf{d} . In such a case the *strain vector* can be written as

$$\boldsymbol{\varepsilon} = \mathbf{D} \mathbf{d} \quad (7.10.7)$$

Thus, the strain energy can be expressed in the form

$$\Pi_{\text{int}} = \frac{1}{2} \mathbf{d}^T \int_V (\mathbf{D}^T \mathbf{E} \mathbf{D} dV) \mathbf{d}, \quad (7.10.8)$$

or

$$\Pi_{\text{int}} = \frac{1}{2} \mathbf{d}^T \mathbf{K}_e \mathbf{d}, \quad (7.10.9)$$

with

$$\mathbf{K}_e = \int_V \mathbf{D}^T \mathbf{E} \mathbf{D} dV, \quad (7.10.10)$$

which represents the stiffness matrix of the three-dimensional finite element. We may also use the *alternative* approach discussed in Sec. 7.3c by employing *generalized coordinates*. In such a case, the element stiffness matrix is Eq. (7.3.43).

a. Rectangular Hexahedronal Element. In this subsection we shall only consider the simplest hexahedronal element having eight corner nodes with three DOF u, v, w

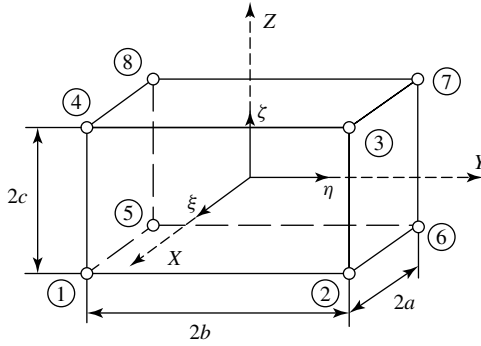


Figure 7.10.2 Simple hexahedronal thick-plate element.

per node. Such a three-dimensional finite element (often called “brick”) is shown in Fig. 7.10.2. We assume the following displacement functions:

$$\begin{aligned}
 u(x, y, z) &= \alpha_1 + \alpha_2 x + \alpha_3 y + \alpha_4 z + \alpha_5 xy + \alpha_6 xz + \alpha_7 yz + \alpha_8 xyz \\
 v(x, y, z) &= \alpha_9 + \alpha_{10} x + \alpha_{11} y + \alpha_{12} z + \alpha_{13} xy + \alpha_{14} xz + \alpha_{15} yz + \alpha_{16} xyz \\
 w(x, y, z) &= \alpha_{17} + \alpha_{18} x + \alpha_{19} y + \alpha_{20} z + \alpha_{21} xy \\
 &\quad + \alpha_{22} xz + \alpha_{23} yz + \alpha_{24} xyz.
 \end{aligned} \tag{7.10.11}$$

It is often convenient to use dimensionless local coordinates ξ, η, ζ with their origin at the centroid of the element. With the introduction of

$$\xi = \frac{x}{a}, \quad \eta = \frac{y}{b}, \quad \zeta = \frac{z}{c}, \tag{7.10.12}$$

the displacement functions for u, v and w may also be written in the form of shape functions:

$$N_i = \frac{1}{8}(1 + \xi\xi_i)(1 + \eta\eta_i)(1 + \zeta\zeta_i) \quad \text{for } i = 1, 2, \dots, 8. \tag{7.10.13}$$

Consequently, the displacement fields can be expressed as

$$u = [N]\mathbf{u}, \quad v = [N]\mathbf{v}, \quad w = [N]\mathbf{w}, \tag{7.10.14}$$

with

$$\begin{aligned}
 [N] &= [N_1, N_2, \dots, N_i, \dots, N_8], \\
 \mathbf{u} &= \{u_1, u_2, \dots, u_8\}, \quad \mathbf{v} = \{v_1, v_2, \dots, v_8\}, \\
 \mathbf{w} &= \{w_1, w_2, \dots, w_8\}
 \end{aligned} \tag{7.10.15}$$

Formulating the element stiffness matrix \mathbf{K}_e follows the standard procedure described above and in the foregoing sections. An *explicit* form of the obtained stiffness matrix is given in Ref. [7.10.1].

Higher-order rectangular hexahedral elements can also be formulated by employing the *Lagrangian* interpolation techniques. This approach, however, creates additional difficulties due to the presence of nodal points within the volume of the element. More sophisticated representations of three-dimensional finite elements can be found in Ref. [7.10.4]. Furthermore, computer programs for three-dimensional finite element analysis of solids are published in Ref. [7.10.5].

b. Thick-Plate Elements of Various Shapes. Use of the simple hexahedral elements discussed above is restricted to thick plates of regular boundaries, as shown in Fig. 7.10.1. Somewhat more flexible is the wedge-shaped element obtained from a hexahedral element by cutting it diagonally along the 14–67 plane (Fig. 7.10.2). Such an element can be efficiently combined with the simple parallelepiped elements to accommodate more complex plate geometry [7.10.7].

The most flexible thick-plate element appears to be the tetrahedron-shaped three-dimensional element. Its drawback, however, is the large number of elements required for proper idealization of thick plates. Furthermore, the so-created finite element mesh is hard to visualize.

The isoparametric elements [7.10.8, 7.10.9] represent some improvement in this respect, since they make it possible to treat thick plates with curved boundaries with smaller numbers of elements.

A detailed discussion of these elements is out of the scope of this book. Interested readers are referred to the pertinent literature for further study [7.10.6–7.10.10].

Summary and Conclusions. The FEM is a powerful numerical technique for the analysis of thick plates. Theoretically, one can also employ the standard finite element procedures in this case. A serious drawback of its practical application, however, is that the required very large amount of data usually exceed the storage capacities of desktop computers. In addition, the necessary computer time can be excessive. Consequently, one is forced to use the more powerful “mainframes”. Other difficulties lie in the mesh generation, especially if tetrahedron elements are used.

References and Bibliography

- [7.10.1] MELOSH, R. J., “Structural Analysis of Solids,” *J. Struct. Div., ASCE, ST-4*, 89 (1963), 205–223.
- [7.10.2] ARGYRIS, J. H., “Matrix Analysis of Three-Dimensional Elastic Media Small and Large Displacements,” *AIAA J.*, 3 (1965), 45–51.
- [7.10.3] CLOUGH, R. W., “A Comparison of Three-Dimensional Finite Elements,” in *Proceedings of the Symposium on Application of Finite Elements in Civil Engineering*, Vanderbilt University, Nashville, Tennessee, 1969, pp. 1–26.
- [7.10.4] RASHID, Y., “Three-Dimensional Analysis of Elastic Solids,” *Int. J. Solids Struct.*, Part I, 5 (1969), 1311–1332; Part II, 6 (1970), 195–207.
- [7.10.5] ANONYMOUS, “*Three-Dimensional Computer Programs for Structural Analysis*,” ASME Special Publication, American Society of Mechanical Engineers, New York, 1972.
- [7.10.6] AVRAM, C., et al., *Numerical Analysis of Reinforced Concrete Structures*, Elsevier, Amsterdam, 1993.
- [7.10.7] HAHN, H. G., *Methode der finiten Elemente*, 2nd ed., Akademische Verlagsgesellschaft, Frankfurt, 1982.
- [7.10.8] ZIENKIEWICZ, O. C., et al., “Isoparametric Element Families for Two- and Three-Dimensional Analysis,” in Holland, I., and Bell, K. (Eds.), *Finite Element Methods in Stress Analysis*, Tapir, Trondheim, Norway, 1969, pp. 383–432.

- [7.10.9] ZIENKIEWICZ, O. C., *Finite Element Method*, 3rd ed., McGraw-Hill Book Co., London, 1977.
- [7.10.10] FIELD, S. A., "Three-Dimensional Theory of Elasticity," in I. Holland and K. Bell (Eds.), *Finite Element Methods in Stress Analysis*, Tapir, Trondheim, Norway, 1969, pp. 333–363.

7.11 Numerical Integration

The determination of element stiffness matrix coefficients k_{ij} requires evaluation of certain definite integrals. In the foregoing sections, we introduced some explicitly given stiffness coefficients obtained by performing closed-form analytical integrations throughout the element areas. For some elements, however, analytical integration is either impossible or too cumbersome to perform economically. Consequently, the recent trend in formulating finite element matrices is to use numerical integration procedures that can be carried out efficiently by computer. This is also true with consistent load representations and evaluating the elements of mass matrices.[†]

In numerical integration techniques, the integral is approximated by the sum of values of the integrand at a number of selected points that are multiplied by a numerical factor W_i , known as the *weight coefficient*.

Although a wide variety of numerical integration schemes exist, here we will only treat the *Gaussian quadrature* in more detail, since it is the most frequently used numerical integration technique yielding on average very good accuracy. For the other numerical integration procedures (e.g., Simpson's two-dimensional rule and the Newton-Cotes method), we refer the reader to Refs. [7.11.1–7.11.5].

For the integration of a function over a *rectangular area*, we employ a coordinate transformation to obtain an equivalent unit square with the limits of integration ± 1 in each direction (Fig. 7.11.1). The corresponding relationships are:

$$x = \frac{a}{2}\xi + \frac{a}{2} \quad y = \frac{b}{2}\eta + \frac{b}{2}. \quad (7.11.1)$$

The integral

$$\int_0^a \int_0^b \psi(x, y) dx dy = \int_{-1}^{+1} \int_{-1}^{+1} \psi(x, y) d\xi d\eta \quad (7.11.2)$$

can be evaluated by using the two-dimensional *Gaussian quadrature*

$$\int_{-1}^{+1} \int_{-1}^{+1} \psi(x, y) \approx \sum_{i=1}^m \sum_{j=1}^m \psi(\xi_i, \eta_j) W_i W_j, \quad (7.11.3)$$

where W_i and W_j are the weight coefficients. Furthermore, ξ_i and η_j represent coordinates of the *sampling points*, and m is the number of the points. Care must be taken to find the correct locations of these points. They cannot be located, for instance, at the boundaries of the unit square. Table 7.11.1 contains sampling points and corresponding weight coefficients in the ξ direction [7.11.6]. Since the boundaries of

[†] See Sec. 15.2.2.

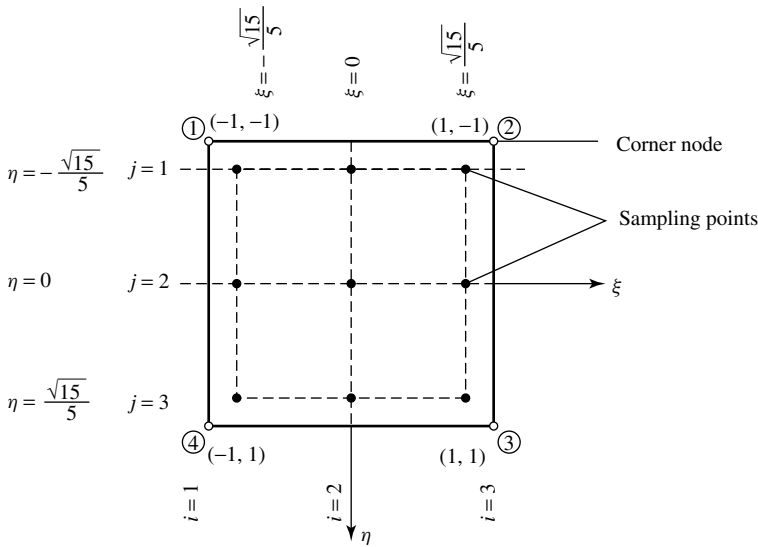


Figure 7.11.1 Gaussian quadrature with nine sampling points.

Table 7.11.1 Gaussian Quadrature in ξ Direction, $\int_{-1}^{+1} \psi(\xi) d\xi \approx \sum_{i=1}^m W_i \psi(\xi_i)$

$\pm \xi_i$ Coordinates			m	Weight Coefficient, W_i		
0.57735	0.02691	0.89626	2	1.00000	0.00000	0.00000
0.00000	0.00000	0.00000	3	0.88888	0.88888	0.88889
0.77459	0.66692	0.41483		0.55555	0.55555	0.55556
0.33998	0.10435	0.84856	4	0.65214	0.51548	0.62546
0.86113	0.63115	0.94053		0.34785	0.48451	0.37454
0.00000	0.00000	0.00000	5	0.56888	0.88888	0.88889
0.53846	0.93101	0.05683		0.47862	0.86704	0.99366
0.90617	0.98459	0.38664		0.23692	0.68850	0.56189
0.23861	0.91860	0.83197	6	0.46791	0.39345	0.72691
0.66120	0.93864	0.66265		0.36076	0.15730	0.48139
0.93246	0.95142	0.03152		0.17132	0.44923	0.79170
0.00000	0.00000	0.00000	7	0.41795	0.91836	0.73469
0.40584	0.51513	0.77397		0.38183	0.00505	0.05119
0.74153	0.11855	0.99394		0.27970	0.53914	0.89277
0.94910	0.79123	0.42759		0.12948	0.49661	0.68870
0.18343	0.46424	0.95650	8	0.36268	0.37833	0.78362
0.52553	0.24099	0.16329		0.31370	0.66458	0.77887
0.79666	0.64774	0.13627		0.22238	0.10344	0.53374
0.96028	0.98564	0.97536		0.10122	0.85362	0.90376

the unit square are parallel to the Cartesian coordinate axis ξ , η , the variables are uncoupled. Consequently, we can logically use the same data for the η direction.

Use of the standard Gaussian quadrature over triangular areas is also possible. In this case, we consider the triangle as a degenerated rectangle, as shown in Fig. 7.11.2.

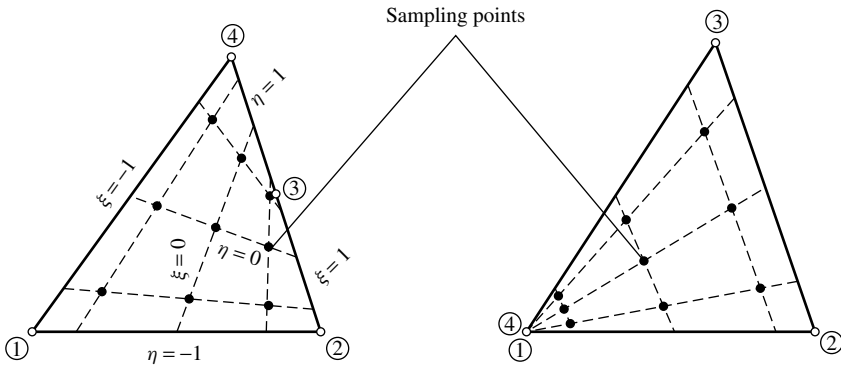


Figure 7.11.2 Triangles represented as degenerated rectangles.

It is, however, more common to employ special coordinate systems for this purpose. The triangular element, for instance, can also be presented in *area coordinates* through the introduction of

$$\xi_1 = \frac{A_1}{A}, \quad \xi_2 = \frac{A_2}{A}, \quad \xi_3 = \frac{A_3}{A}, \quad (7.11.4)$$

where A represents the area of the triangle and A_1, A_2, A_3 are subareas pertinent to the centroid P of the triangle, as shown in Fig. 7.11.3a. Let

$$A_1 + A_2 + A_3 = A; \quad (7.11.5)$$

then

$$\xi_1 + \xi_2 + \xi_3 = 1, \quad (7.11.6)$$

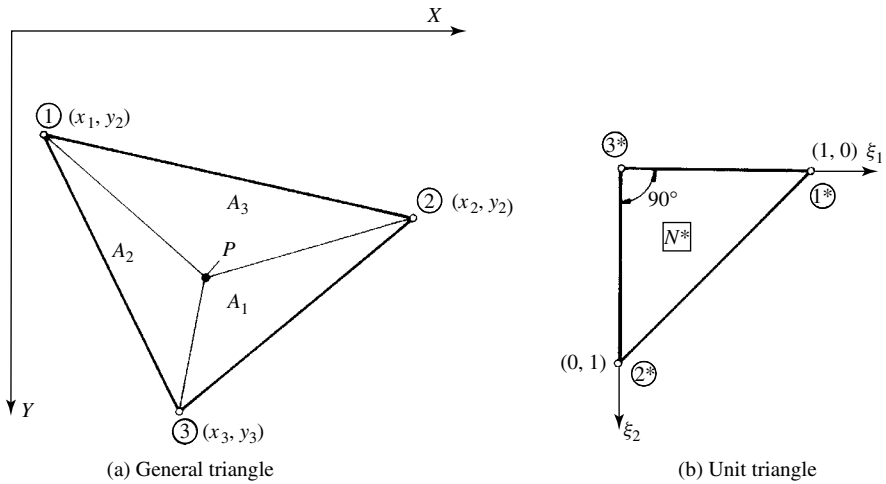


Figure 7.11.3 Area coordinates used in mapping.

and consequently,

$$\xi_3 = 1 - \xi_1 + \xi_2. \quad (7.11.7)$$

The linear relationship with the Cartesian coordinates can be written as

$$x = x_1\xi_1 + x_2\xi_2 + x_3\xi_3, \quad y = y_1\xi_1 + y_2\xi_2 + y_3\xi_3. \quad (7.11.8)$$

where (x_1, y_1) , (x_2, y_2) and (x_3, y_3) represent the coordinates of the corner nodes in the X, Y coordinate system.

Numerical integration over triangular regions can be simplified by the use of Hammer's formula [7.11.4], which takes the general form

$$\int_0^1 \int_0^{1-\xi_1} \psi(\xi_1, \xi_2) d\xi_2 d\xi_1 \approx \frac{1}{2} \sum_{i=1}^m W_i(\xi_1^{(i)}, \xi_2^{(i)}), \quad (7.11.9)$$

where W_i is the weight coefficient corresponding to the sampling points $\xi_1^{(i)}, \xi_2^{(i)}$ and m represents the number of sampling points. Typical values of W_i and sampling points are given in Table 7.11.2.

General quadrilateral elements can also be mapped into a unit square (Fig. 7.11.4) by using the bilinear function

$$\phi = \begin{Bmatrix} (1-\xi)(1-\eta) \\ \xi(1-\eta) \\ \xi\eta \\ (1-\xi)\eta \end{Bmatrix} \quad (7.11.10)$$

In this case, the transformation relationships are

$$x = \mathbf{x}^T \phi(\xi, \eta) \quad \text{and} \quad y = \mathbf{y}^T \phi(\xi, \eta), \quad (7.11.11)$$

where

$$\mathbf{x}^T = \{x_1 \quad x_2 \quad x_3 \quad x_4\}^T \quad \text{and} \quad \mathbf{y}^T = \{y_1 \quad y_2 \quad y_3 \quad y_4\}^T. \quad (7.11.12)$$

Full numerical integration of bending and transverse shear terms in the stiffness matrix expressions for moderately thick plates may lead to the so-called shear-locking behavior. That is, if we examine the deflection patterns of moderately thick plates for different stiffness-to-span ratios, we observe over stiff results for thinner plates. This

Table 7.11.2 Coordinates and Weights in Eq. (7.11.9)

m	$\xi_1^{(i)}$	$\xi_2^{(i)}$	W_i
1	$\frac{1}{3}$	$\frac{1}{3}$	1
3	$\frac{1}{2}$	$\frac{1}{2}$	$\frac{1}{3}$
	$\frac{1}{2}$	0	$\frac{1}{3}$
	0	$\frac{1}{2}$	$\frac{1}{3}$

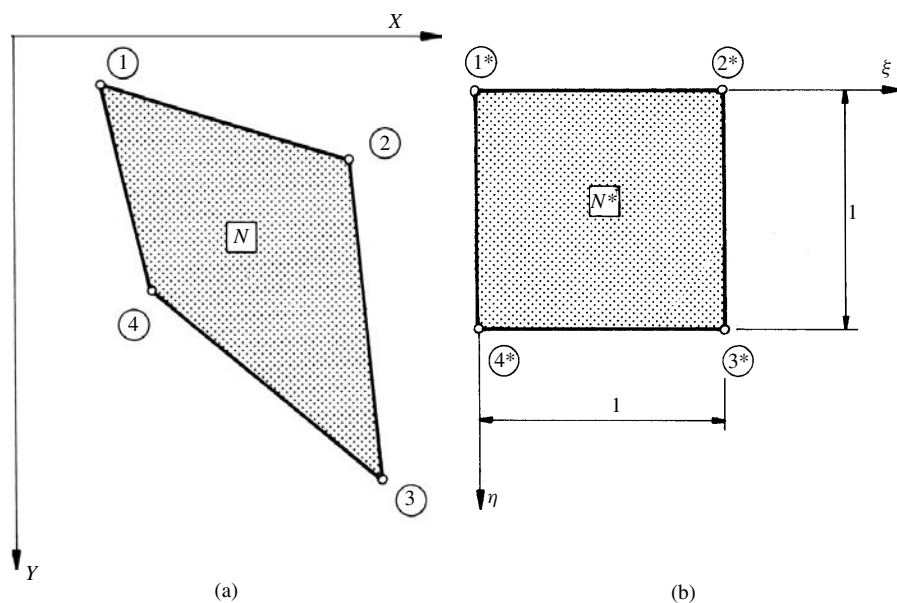


Figure 7.11.4 Mapping of general rectangle.

is due to the imposition of excessive number of shear restraints. To overcome this difficulty, reduced or selected integration techniques are introduced. In this approach, $\mathbf{K}_{e,s}$, representing the transverse shear terms, is deliberately underintegrated. In some cases with lightly restrained boundaries, however, the solution may fail if such elements are employed. Interested readers should consult Refs. [7.11.9–7.11.11] for further study of this subject.

References and Bibliography

- [7.11.1] IRONS, B. M., "Engineering Application of Numerical Integration in Stiffness Methods," *AIAA J.*, 4 (1966), 2035–2037.
- [7.11.2] ABRAMOWITZ, M., and STEGAN, I. A., *Handbook of Mathematical Functions*, McGraw-Hill Book Co., New York, 1970.
- [7.11.3] BATHE, K. J., *Finite Element Procedures*, Prentice-Hall, Upper Saddle River, New Jersey, 1996.
- [7.11.4] MAMMER, P. C., and STROUD, A. H., "Numerical Evaluation of Multiple Integrals," *Math. Tables Other Aids Comput.*, 12 (1958), 272–280.
- [7.11.5] GRIFFITHS, D. V., and SMITH, I. M., *Numerical Methods for Engineers*, CRC Press, Boca Raton, Florida, 1991.
- [7.11.6] DAVIS, P., and RABANOWITZ, P., "Abcissas and Weights for Gaussian Quadrature," *J. Res. Nat. Bur. Stand.*, 56 (1956), RP 2645.
- [7.11.7] YING, L. A., "Some Special Interpolation Formulae for Triangular and Quadrilateral Elements," *Int. J. Num. Meth. Eng.*, 18 (1982), 959–966.
- [7.11.8] SMITH, I. M., and GRIFFITHS, D. V., *Programming the Finite Element Methods*, 2nd ed., John Wiley & Sons, Chichester, 1988.
- [7.11.9] ZIENKIEWICZ, O. C., et al., "Reduced Integration Technique in General Analysis of Plates and Shells," *Int. J. Num. Meth. Eng.*, 3 (1971), 275–290.

- [7.11.10] HUGHES, T. J. R., et al., "Reduced and Selective Integration Techniques in the Finite Element Analysis of Plates," *Nucl. Eng. Des.*, 46 (1976), 203–222.
- [7.11.11] MACNEAL, R. H., "Simple Quadrilateral Shell Element," *Comp. Struct.*, 8 (1978), 175–183.

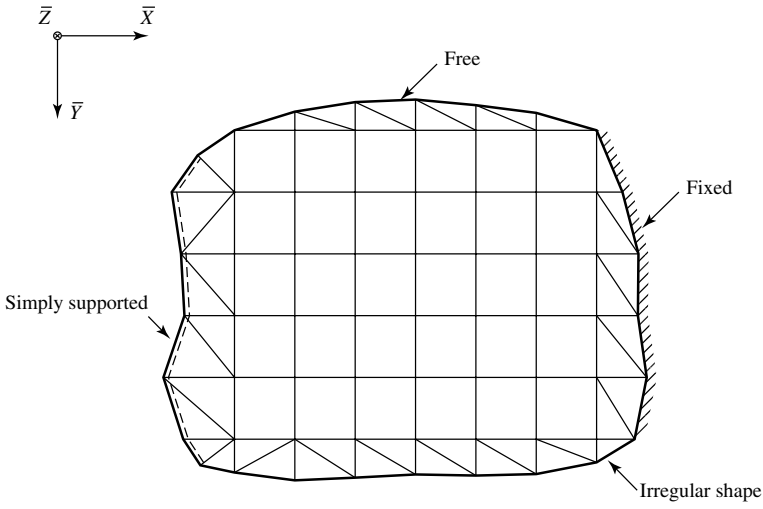
7.12 Modeling Finite Element Analysis

Creating a suitable computational model is the first important step in a finite element analysis of plates. Before embarking on modeling, however, the geometry and boundary conditions of the structure along with the applied loads must be clearly defined. A proper modeling starts with a good conceptual understanding of the physical behavior of the plate, which includes the anticipated stress and deflection patterns. As a prerequisite, it is expected that the analyst has a clear understanding of the underlying plate and finite element theories. The engineering approximations treated in Part IV of this book offer valuable help in this respect. In addition, these simple procedures can also be used to determine the first estimate of the required plate thickness, which represents an important input data in the finite element analysis.

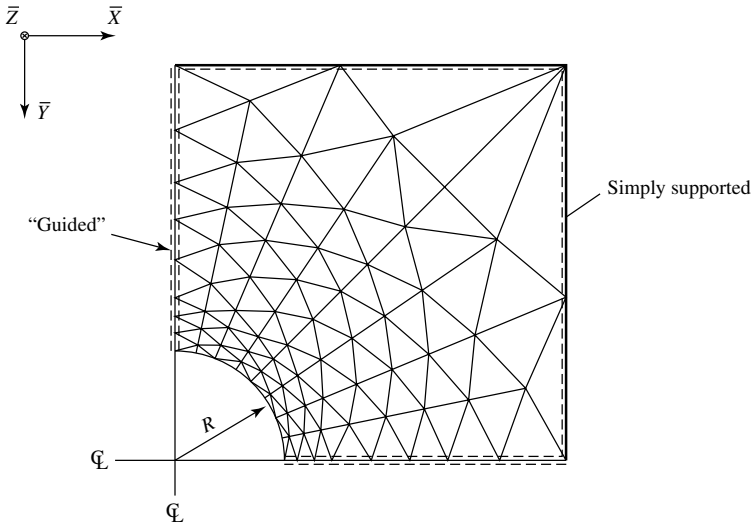
The next step involves the discretization of the plate continuum by using properly selected finite elements. These plate elements are connected only at a discrete number of nodal points along their periphery. In this way, a finite element mesh representing a substitute structure is created. For smaller projects, the mesh is hand generated by laying it out on paper and numbering the elements and their nodal points. To minimize the bandwidth of the global stiffness matrix of the plate, the procedure discussed in Sec. 6.4 in connection with the gridwork method is applied. For larger projects, mostly automated mesh generation techniques are used. These procedures afford the user to create a large number of elements quickly, as discussed in subsequent sections.[†] In both cases, the following guidelines are to be followed:

1. Whenever possible, the finite element mesh should be relatively uniform. However, in the vicinity of rapid changes in geometry and loading, finer mesh subdivisions are required (Fig. 7.12.1b). Special caution should be exercised in transition from coarse to finer mesh.
2. The use of rectangular elements should be preferred, except where triangular elements are required to model irregular boundaries and loadings.
3. The aspect ratio between the element's longest and shortest dimensions should not be excessive. The optimum aspect ratio is close to unity. As a general rule, however, it is desirable to keep the aspect ratios under 3–4. Illegal element shapes must be avoided. For triangular elements acute angles less than 30° are not desirable.
4. If rectangular elements are combined with triangular ones, elements with corner nodes are preferred. In addition, all these elements must have the same nodal DOF.
5. Selection of element-types should be governed by the geometrical requirements of the plate and the convergence characteristics of the element. In most cases, the conforming rectangular element with 16 DOF combined with the triangular

[†] See also Sec. 6.4.1.



(a) Combination of rectangular and triangular elements



(b) Plate with hole

Figure 7.12.1 Some mesh patterns.

DKT element[‡] represents a good choice. In real-life structures, such as bridges, often more than one type of element must be selected to properly idealize the structure. That is, plate elements model the bridge deck, while beam elements represent the girders. In such cases, however, special elements with proper interface between plate and beam must be employed.

[‡] See Sec.7.7.

6. Since large stiffness variations between elements can lead to an *ill-conditioned* stiffness matrix of the total structure, rendering meaningless results, such conditions must be avoided by all means.
7. Concentrated external forces and column supports cause high stresses in the vicinity of their point actions. Thus, a relatively fine mesh is required to obtain sufficiently accurate stresses in such regions. Similarly, openings in the plate also call for mesh refinements to obtain detailed stress information in their regions.
8. For one-way symmetry of the structure and its loading, it is sufficient to analyze half of the plate by assuming “guided” boundary conditions at the symmetry line. For double symmetry, the quarter plate represents the analysis quadrant. Again, at the lines of symmetry guided boundary conditions must be used. Certain triangular elements, however, may exhibit unsymmetrical response. The analyst should be aware of such troubling possibilities.
9. Needless to say, moderately thick plates should not be modeled by plate elements that do not include the effects of transverse shear in their stiffness matrix formulation. Similarly, moderately thick-plate elements are unsuitable for modeling thick plates, since thick plate theory belongs to the three-dimensional stress analysis category.

Summary. In this section, some fundamental aspects of the finite element modeling of a plate structure are addressed. It is of basic importance that the structure and its supports and loads are well defined before actual modeling takes place. In creating a finite element computational model, we replace the actual continuum by a substitute discrete system consisting of rectangular and triangular plate elements connected only at their nodal points. In selecting suitable element-types, one should strive for accuracy and computational efficiency. The understanding of the structural behavior of the plate cannot be overemphasized. For this purpose, simple *engineering methods* can provide valuable information and furnish, at the same time, a rough approximate check of the finite element solution.

References and Bibliography

- [7.12.1] MEYER, C. (Ed.), *Finite Element Idealization*, ASCE Publication, New York, 1987.
- [7.12.2] BASU, P. K., and LAMPRECHT, R. M., “Some Trends in Computerized Stress Analysis,” in *Proceedings of the Seventh Conference on Electronic Computation*, ASCE Publication, New York, 1979.
- [7.12.3] MEYER, C., and SCORDELIS, A. C., “Computer Program for Non-Prismatic Folded Plates with Plate and Beam Elements,” Structures and Material Research Report No. UC SESM 71-23, Department of Civil Engineering, University of California, Berkeley, 1971.
- [7.12.4] DUNDER, V., et al., “Practical Applications of the Finite Element Method,” *J. Struct. Div., ASCE*, 104 (1978), ST1 9–21.

7.13 Programming Finite Element Analysis

In general, the reader will resort to the use of commercially available large-scale program systems for the finite element analysis of plate structures. Application of such programs is, however, not without problems, as discussed in the next section. There

are, nevertheless, some isolated instances—such as dealing with unique plate problems or preparing a master of science thesis or even a doctoral dissertation—when one must develop a *specialized* finite element program. Since such relatively small-scale programs are intended mostly for research rather than for repeated commercial use, priority in programming should be given to *readability*. This can be achieved, among other items, by using a *structured* programming style and by including numerous *comment statements*. In general, elaborate input and output schemes are not required for such research-oriented programs, but it is highly desirable that the user be *guided* during program execution by appropriate comments appearing on the screen calling for the next step to be taken. The reader will find our WinPlatePrimer program system FORTRAN source codes that represents a good model to emulate. Larger programs might follow a similar approach, provided that more efficient storage schemes and data management techniques are incorporated.

In programming the FEM, the first step involves the selection of a suitable language. Since nearly all finite element software, independent subroutines for numerical analysis and codes listed in various text and reference books are written in FORTRAN, this high-level programming language should be the primary choice. No language has yet been devised that is better suited for numerical analysis. Furthermore, its syntax of file-handling operations is clear and well established. In addition, since FORTRAN is so entrenched in structural engineering applications, programs written in this language assure maximum leadership and portability. Of course, the programmer should always employ the latest version of FORTRAN, which usually incorporates numerous new and useful features. It is of special importance that such a new version always maintain compatibility with its earlier editions. Other high-level languages worth considering are PASCAL, ALGOL, C++, ADA and various new and improved versions of BASIC.

Programming the FEM involves three distinct stages: (a) preprocessing, (b) analysis to determine the structural response and (c) postprocessing. *Preprocessing* consists of data preparation such as nodal coordinates, boundary conditions, loading, material information and mesh generation, as described in the foregoing section. The *analysis* part deals with generation of element stiffness matrices, their transformation from local to global coordinate system, assembly of the stiffness matrix of the total structure, imposing the prescribed boundary conditions and solution of the governing matrix equation $\bar{\mathbf{K}}\bar{\mathbf{d}} = \bar{\mathbf{p}}$. The *Postprocessing* stage manages the results obtained from the analysis, which typically involves presentation of the deflection pattern of the plate, distribution of the internal stress resultants and validation of the results. These processing phases are graphically illustrated in Fig. 7.13.1. In the following some additional comments are given to elaborate these steps.

Although preprocessing is the least technologically demanding aspect of finite element programming, its execution requires considerable effort and time. Since the input phase is highly error prone, a significant amount of time must be spent on checking the input data. Consequently, it is advisable that the program contain numerous *diagnostic* messages that call the user's attention to erroneous inputs. The highly crucial modeling phase has already been treated in the foregoing section in detail. Similarly, computation of the loads has already been discussed in Sec. 7.8a. The final step in preprocessing should be a plot graph of the computational model that can help in detecting some input errors.

The analysis stage represents the core of the finite element procedure. First, by using appropriate subroutines, stiffness matrices of all elements are generated. If the

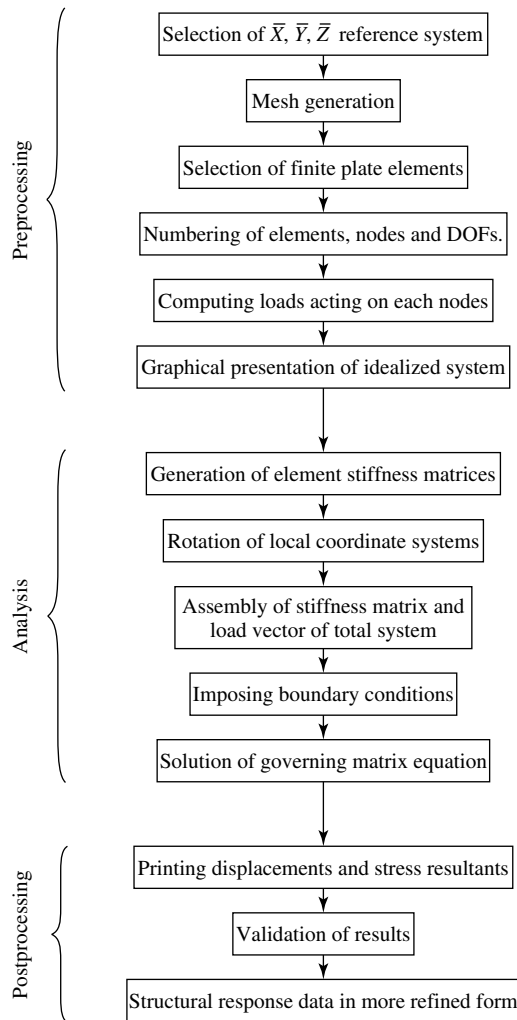


Figure 7.13.1 Processing phases of finite element analysis.

axes of the local coordinates are not parallel to those of the global reference system, they must be rotated into a parallel position. Next, the stiffness matrix and the load vector of the system are assembled[†] to obtain the governing matrix equation $\bar{\mathbf{K}}\bar{\mathbf{d}} = \bar{\mathbf{p}}$. Before solution of this equation can be attempted, however, boundary conditions must be incorporated into the stiffness matrix. In the displacement-based FEM, the boundary conditions are represented by certain zero-displacement components. Hence, appropriate information must be given in the assembly routine that prevents these components from being assembled in the total system. This can be achieved by simply striking out the rows and columns in the system equation that are associated with zero displacements. The most obvious approach to the solution of

[†] See Sec. 7.2.

the governing matrix equation would be $\bar{\mathbf{d}} = \bar{\mathbf{K}}^{-1} \bar{\mathbf{p}}$, requiring matrix inversion. Such a solution not only requires a time-consuming matrix operation but, also destroys the important band structure of the stiffness matrix by creating a fully populated inverted matrix. Consequently, its use is not recommended. *Cholesky* factorization [7.13.1–7.13.8] represents a far more economical solution technique. Since the stiffness matrix $\bar{\mathbf{K}}$ is always positive-definite and symmetrical, this method is extensively used in the finite element analysis of structures. If the main random-access memory of the personal computer does not have sufficient storage capacity, the *frontal solution* technique [7.13.9] may offer a usable alternative.

The *Postprocessing* phase involves selection, display and validation of the results. The output of the finite element analysis consists of numbers. These represent nodal displacements and stress resultants presented in suitable table forms. Since the finite element program generates a very large amount of numbers, a function of postprocessing should be to relate only the important information and filter out the rest. A very efficient and attractive way to present the results graphically is using appropriate contour lines in the X, Y plane. Reference [7.13.15] provides a FORTRAN program for the generation of such contour lines. Needless to say, for proper interpretation of the obtained results, experience with plate structures is required on the part of the analyst. Finally, the results should be verified. The deflected plate surface offers the first check. The experienced analyst can detect coarse errors by simply viewing the deformed structure. The next check should be an equilibrium check of the external forces and the reactions at the supports. It is also recommended to include in the program computation of the work of the external and internal forces. The sum of the work of the external and internal forces must be, of course, approximately zero. When applicable, some *engineering methods*[†] can also offer valuable approximate checks. To obtain a truly independent validation of the results, the computation must be repeated using, for instance, the gridwork method or another finite element program.

The building blocks of structured computer programs are the individual *subroutines*. Again, one of the important advantages of FORTRAN is the ready availability of such subroutines. For instance, Refs. [7.13.1–7.13.8], give FORTRAN libraries of matrix operations, solutions of simultaneous linear equations, numerical differentiations and integrations and so on. Thus, the finite element programming may consist of merely incorporating these subroutines in proper sequence in the new program system. Furthermore, in Refs. [7.13.10–7.13.14] complete finite element programs written in FORTRAN are listed that can either be used directly or modified to suit some individual needs. Finally, the reader's attention should be called to the fact that modern pre- and postprocessing codes with graphical interfaces are also commercially available [7.3.15].

Summary. Programming the finite element plate analysis is usually a tedious and time-consuming assignment requiring not only fundamental knowledge in plate and finite element theories but also good programming skills. Consequently, it should only be undertaken when a definite need for a specialized plate program exists. Otherwise, one should use one of the commercially available large program systems[‡] that also deal with the analysis of plate structures. If for some reason programming is required, the recommended computer language is FORTRAN, since many

[†] See Part IV.

[‡] See Sec. 7.14.

of the required subroutines—and even small program systems—are available in the pertinent literature. The finite element program should be *structured*. The available FORTRAN subroutines should be the building blocks from which the program should be constructed.

References and Bibliography

- [7.13.1] TEUKOLSKY, S. A., et al., *Numerical Recipes in FORTRAN: The Art of Scientific Computing*, Cambridge University Press, New York, 1992.
- [7.13.2] VETTERING, W. T., *Numerical Recipes Example Book (FORTRAN)*, 2nd ed., Cambridge University Press, New York, 1993.
- [7.13.3] GRIFFITHS, D. V., and SMITH, I. M., *Numerical Methods for Engineers*, CRC Press, Boca Raton, Florida, 1991.
- [7.13.4] SCHWARZ, H. R., *FORTRAN-Programme zur Methode der finiten Elemente*, 3rd ed., Teubner, Stuttgart, 1991.
- [7.13.5] FORD, B., and SAYERS, D. K., “Developing a Single Numerical Algorithm Library for Different Machine Ranges,” *ACM Trans. Math. Software*, 2 (1976), 115.
- [7.13.6] MCCORMICK, J. M., and SALVADOR, M. G., *Numerical Methods in FORTRAN*, Prentice-Hall, Englewood Cliffs, New Jersey, 1965.
- [7.13.7] CANAHAM, B., et al., *Applied Numerical Methods*, John Wiley & Sons, New York, 1969.
- [7.13.8] JAMES, M. L., SMITH, G. M., and WOLFORD, J. C., *Applied Numerical Methods for Digital Computation with FORTRAN and CSMP*, 2nd ed., IEP Publisher, New York, 1977.
- [7.13.9] IRONS, B. M., “A Frontal Solution Program for Finite Element Analysis,” *Int. J. Num. Meth. Eng.*, 2 (1970), 5–32.
- [7.13.10] SMITH, I. M., and GRIFFITHS, D. V., *Programming the Finite Element Method*, 2nd ed., John Wiley & Sons, New York, 1988.
- [7.13.11] HINTON, E., and OWENS, D. R., *An Introduction to Finite Element Computations*, Pineridge Press, Swansea, United Kingdom, 1979.
- [7.13.12] CRISFIELD, M. A., *Finite Elements and Solution Procedures for Structural Analysis*, Pineridge Press, Swansea, United Kingdom, 1986.
- [7.13.13] BREBBIA, C. A., and FERRANTE, A. J., *Computational Methods for the Solution of Engineering Problems*, Pentech Press, London, 1978.
- [7.13.14] HINTON, E., and OWEN, D. R. J., *Finite Element Software for Plates and Shells*, Pineridge Press, Swansea, United Kingdom, 1984.
- [7.13.15] *FEMAP*, Enterprise Software Products, Exton, Pennsylvania.

7.14 Commercial Finite Element Codes

Nowadays many general-purpose, large-scale finite element program systems are commercially available. A few of them are listed in alphabetical order at the end of this section in Refs. [7.14.1–7.14.14]. Due to the prevailing high volatility of the computer hardware and software market, some of these program systems will certainly disappear in time; on the other hand, we will also see interesting newcomers presenting valuable innovative features. Although most of these programs were originally developed for mainframe computers, they can now run on powerful workstations and personal computers that have sufficiently fast CPU processors, adequate random-access memory and large-capacity hard disks. These large-scale, general-purpose program systems do have, among numerous other features, plate analysis capabilities. It should be noted, however, that most sophisticated program systems lose their large built-in potential in the hands of inexperienced users. As already

emphasized, without true understanding of the physical behavior of plate structures and funded knowledge in FEMs, the user cannot properly model the actual structural systems, thus rendering the resulting finite elements computation mostly meaningless.

Supplying a user-friendly interface between the analyst and computer in the form of *interactive computer graphics* considerably simplifies the otherwise tedious pre- and postprocessing procedures. In *Preprocessing*, for instance, automatic mesh generation can be achieved by using only a relatively small amount of input information in the form of plotting the boundaries of the plate. With a similar approach, mesh refinements can be obtained in the vicinity of stress concentrations. Furthermore, the created mesh can automatically assign the element numbers, their nodal points and corresponding DOF and even compute the global coordinates of the nodes. Some other required features of user-friendly preprocessing are as follows:

- menu system with submenus (if required);
- screen instructions concerning the next steps to be executed by the user;
- extensive “help” information;
- diagnostic error messages;
- easy way to correct erroneous inputs;
- load generator program creating nodal loads;
- graphical display of the generated finite element mesh showing elements, node numbers and nodal restrains and
- element library that contains the following finite elements: rod, bar, beam, shear panel, membrane, plane strain, thin and thick and laminated plates, shell, wedge, “brick” and tetrahedrons.

The *Analysis Phase* deals with extensive computations of the input data obtained from the preprocessing part of the program[†]. The most important portion of this stage is solution of the governing matrix equation. Unfortunately, the user very seldom knows which method has been used to solve the large number of simultaneous equations created by the program.

Postprocessing involves the selection and display of input data and the obtained results. More sophisticated program systems may also give some estimate of the accuracy. A quasi-independent check of the obtained results for plates, however, may be achieved by repeating the computation using the folded plate, cylindrical shell or general shell analysis part of the program system. The printable portion of the output contains most of the input data for checking purposes and the computed displacements and stresses at the nodes. The most attractive and efficient way of presenting the results of the analysis is to display them graphically. The *interactive graphic* postprocessing program displays the deformed geometry of the structure and various stress contours. To obtain smooth contour lines, the stress values at the nodes are always averaged. A built-in “zoom” capability allows the user to view details at close range. A very effective way to call the user’s attention to the zones of critical stresses is to paint it with red color.

All general-purpose, large-scale finite element program systems share the following drawbacks:

[†] See corresponding part of flow chart in Fig. 7.13.1.

- Since the source codes are not given, these programs always represent “black boxes” for the analyst. That is, the user is in no position to know and/or control the individual computer operations. Consequently, he or she cannot change the program to suit his or her special needs.
- General-purpose program systems are *ab ovo* very large. Thus, it takes considerable effort and time to learn their proper use.
- In general, the plate analysis section is only a small portion of the total program systems. Hence, the analyst has to first study the total “user’s manual” before applying the program to a plate problem. This can be very time consuming and frustrating. In this respect smaller program systems devoted exclusively to the solution of plate problems (the so-called “program-packages” that deal individually with framed structures, plates, shells and three-dimensional stress problems) are much more effective.

Since all commercially marketed large, general-purpose finite element program systems are relatively expensive, the engineer must have some guidelines for their efficient evaluation in order to avoid costly mistakes by purchasing the wrong one. Some guidelines for rating such program systems are as follows:

- The distributor must be a reputable firm whose employees consist of highly trained structural engineers with extensive experience in the field of FEMs.
- A well-written user’s manual that contains on-line training in the form of numerous worked examples and clear step-by-step instructions is essential.
- The manual should be accompanied by a well-designed “demo” disk. This combination should enable the engineer to a large extent to evaluate the whole program system before purchasing it.
- Built-in convergence and/or error estimation is highly desirable.
- The program system should not contain expensive items—such as fluid dynamics, for instance—which a structural engineer, in general, does not need.
- Last, but not least, the engineer should obtain pertinent references and recommendations from the users concerning the specific software.

Summary. The analysis of large plate structures undoubtedly requires the employment of large-scale commercial software. However, without good background in plate theory and the FEM proper modeling of the structure and right interpretation of the obtained results are not possible. In selecting a suitable program system, user friendliness and accuracy of the results should be the primary concerns of the engineer. In addition, it is recommended that he or she follow the guidelines given above to avoid costly mistakes in purchasing a commercial finite element code that does not live up to expectations.

References and Bibliography

- [7.14.1] *ABAQUS*, Hibbit, Karlson & Sorensen, Providence, Rhode Island.
- [7.14.2] *ADINA*, Adina R & D, Watertown, Massachusetts.
- [7.14.3] *ALGOR*, Algor Interactive System, Pittsburgh, Pennsylvania.
- [7.14.4] *ANSYS*, Swanson Analysis Systems, Houston, Pennsylvania.

- [7.14.5] COSMOS, Structural Research and Analysis, Santa Monica, California.
- [7.14.6] MARC, Marc Software International, Palo Alto, California.
- [7.14.7] NASTRAN, MacNeal-Schwendler, Los Angeles, California.
- [7.14.8] SAFE, Computers & Structures, Berkeley, California.
- [7.14.9] SAP7, Structural Mechanics Computer Lab., University of Southern California, Los Angeles California.
- [7.14.10] SAP86, Number Cruncher Microsystems, San Francisco, California.
- [7.14.11] MTAB*STRESS, Structural Analysis, Austin, Texas.
- [7.14.12] SAP90, Computers & Structures, Berkeley, California.
- [7.14.13] STAAD-III, Research Engineers, Yorba Linda, California.
- [7.14.14] WinSTRUDL, Computer Aided Structural Technology, Fremont, California.
- [7.14.15] FONG, H. H., "Interactive Graphics and Commercial Finite Element Codes," *Mech. Eng.*, 106, No. 5 (1984), 18–27.
- [7.14.16] FALK, H., and BEARDSLEY, C. W., "Finite Element Analysis Packages for Personal Computers," *Mech. Eng.*, 107, No. 1 (1985), 54–71.
- [7.14.17] BAUGH, J. W., "Using Formal Methods to Specify the Functional Properties of Engineering Software," *Comp. Struct.*, 45 (1992), 557–570.
- [7.14.18] SZILARD, R., "Anforderungen an Software für die Tragwerksanalyse," *Bautechnik*, 70 (1993), 70–77.

7.15 Summary and Conclusions

In the last four decades, methods of numerical plate analysis have undergone an unprecedented development. Three separate but interrelated factors contributed to this remarkable progress:

1. introduction of the matrix analysis of structures,
2. development of the FEM and
3. progress in computer technology and proliferation of relatively inexpensive workstations and personal computers.

The development of the FEM can be considered one of the most significant achievements in the field of structural analysis. It provides a convenient and powerful technique to solve problems covering the whole spectrum of structural engineering. One of the greatest advantages of the FEM is its *versatility*; that is, the same *unified* approach is employed in analyzing deflections and stresses of any type of structure. The geometrical configuration, boundary conditions and loading may be completely arbitrary.

The main characteristics of the FEM are as follows:

- The finite element approach considers the plate structure to be an assembly of finite-sized units by applying a physical discretization technique. Consequently, the plate problem is not stated in terms of partial differential equations of the continuum.
- The plate problem is solved by using variational formulation in the form of minimizing the total potential of the assembled substitute structure with respect to nodal displacements.
- The analysis involves subdivision of the plate domain into finite elements and the evaluation of the elastic properties of each element. This results in element

stiffness matrices that express the relationship between element nodal forces and displacements. By applying an appropriate superposition technique and imposing the prescribed boundary conditions, the stiffness matrix $\bar{\mathbf{K}}$ of the total structure is obtained.

- The equilibrium of the plate is expressed in terms of the stiffness matrix of the total structure, resulting in the simultaneous algebraic equations $\bar{\mathbf{K}}\bar{\mathbf{d}} = \bar{\mathbf{p}}$. Formulation of this governing matrix equation and its solution requires, however, extensive computer-based matrix operations.

Since the achievable accuracy of the FEM depends to a large degree on the element shape functions, a fairly extensive survey of these functions, including methods of their generation, has been included in this chapter. The perplexing array of shape functions and their corresponding elements raises the valid question: Which are the best elements? We were trying to answer this undoubtedly difficult question by taking into account the introductory nature of our treatment of the FEM in this book. Thus, we recommend that use of the conforming rectangular element with 16 DOF and that of the DKT triangular element. The reason for this recommendation is the corresponding stiffness matrices are given in explicit forms, which assures their relatively easy application. In addition, the convergence characteristics of both elements are excellent or very good, respectively.

As mentioned before, only the *displacement-based* FEM was treated in this chapter, since it is currently the most popular and widely used model. There are, however, other finite element approaches also worth mentioning. The so-called *hybrid method*, for instance, uses separate shape-functions for the displacements and stresses in the finite elements. Although this reduces the problem of enforcing compatibility conditions, the number of unknowns in the governing matrix equation is considerably increased.

Finally, it may be of interest to the reader if we compare the two most widely used numerical techniques for solution of plate problems: the finite difference and finite element methods. Although the two methods appear superficially different, they have many similarities. That is, both discretize the plate continuum and generate simultaneous algebraic equations to be solved for mesh-point or nodal displacements. Furthermore, The FDM can be used to generate the flexibility matrix of the total structure, the inversion of which leads to the stiffness matrix $\bar{\mathbf{K}}$. On the other hand, the FEM can also be used to create governing differential equations for structures. Consequently, these two most important numerical methods in structural analysis are related, especially if one considers the energy-based variety of the FDM. However, there are also significant differences between the two methods. The FDM uses mathematical discretization based on the partial differential equations, while finite element discretization is strictly physical and applies the minimum principle of the total potential to obtain the governing matrix equation. Furthermore, the finite difference stencils overlap one another and may have points outside the plate boundaries. The finite elements do not overlap and have no nodes outside the plate boundaries. Since in the FDM the unknowns are only the lateral mesh-point displacements, the number of equations to be solved, assuming the same mesh for both, is merely a fraction of that required for the FEM. In addition, application of the FDM does not need a special computer program. The only requirement is an equation solver. Consequently, for small-scale and relatively “regular” plate problems, the FDM may have distinct advantages over the FEM. On the other hand, for solution of large plate

structures of arbitrary shape and boundary conditions having variable thickness and various types of loading, the FEM is far better suited than the FDM, provided that a corresponding finite element computer program is readily available. Since writing and testing a finite element code for plate analysis is a very tedious and time-consuming task requiring solid programming experience, such an undertaking should be reserved only for special cases.

Problems[†]

- 7.2.1. Determine the stiffness coefficient k_{78} of the rectangular plate element shown in Fig. 7.2.3 by using Eq. (7.2.6). The pertinent shape functions should be approximated by appropriate cross products of the beam functions given in Eqs. (7.2.7) and (7.2.8), respectively. Follow the Illustrative Example in Sec. 7.2.
- 7.6.1. Find the center deflection of the plate shown in Fig. 7.7.7a by employing the nonconforming rectangular plate element with 12 DOF. The corresponding stiffness matrix is given in Eqs. (7.6.12) and (7.6.13).
- 7.6.2. Repeat problem 7.6.1 but with a 2×2 subdivision of the analysis quadrant.
- 7.7.1. Verify the results obtained in Illustrative Example II of Sec. 7.7 by using the conforming rectangular plate element with 16 DOF.
- 7.7.2. Obtain an expression for the stiffness coefficient k_{77} of the DKT plate element.
- 7.8.1. Compute the maximum bending moment of problem 7.6.1. Use Table 7.8.1 for the corresponding stress matrix.
- 7.8.2. Determine the internal stress resultants in problem 7.6.2.
- 7.9.1. Compute the maximum deflection of a simply supported moderately thick square plate subjected to $P_0 = 400,000$ kN concentrated force at its center by using the conjugate beam analogy[‡]. The plate dimensions are given in Fig. 7.9.4a. The subdivision of the analysis quadrant should be 2×2 .
- 7.9.2. Repeat problem 7.9.1 assuming clamped boundary conditions. Use *Donnel's* approximation

$$w \approx \left[1 - \frac{1.065h^2}{6(1-\nu)} \nabla^2 \right] w_K,$$

where w_K represents *Kirchhoff's* classical solution of the given plate problem obtained by FEM analysis. The harmonic operator ∇^2 in this equation may be approximated by a corresponding finite difference expression.

- 7.13.1. Write a *simple* finite element program for plate analysis. Use the sample program given in Appendix A.4.2 as your guide.
- 7.13.2. Determine the convergence characteristics of the plate element used in your finite element program.

[†] The first two numbers refer to the corresponding section.

[‡] See Sec. 2.10.

8

Classical Finite Strip Method

8.1 Introduction and Basic Concepts

Although, the FEM is a very powerful and highly versatile tool for the analysis of diverse plate problems, it becomes uneconomical with simple rectangular plates. Since rectangular plates are used frequently either as plate structures or structural components in various branches of engineering, a more economical treatment of such plates is needed. For this purpose the *finite strip method* (FSM) was developed. The *classical* FSM can be considered as a simplified extension of the FEM for the analysis of Kirchhoff's plates in which two opposite edges in the longitudinal direction are assumed to be either simply supported or fixed. However, the two other edges in the transverse direction can have arbitrary boundary conditions. The FSM represents a semianalytical, seminumerical *hybrid* process that has important advantages for plates with fairly simple geometry.

The classical FSM was first introduced by Cheung [8.1.1] for the analysis of rectangular plates with two opposite edges simply supported. A similar—but quite independent—approach was also published by Powell and Odgen [8.1.2] at a later date.

Basically, the classical FSM involves an approximation of the mathematically exact solution of a plate problem by using a continuous harmonic function series that satisfies the boundary conditions in the longitudinal direction and a piecewise interpolation polynomial in the transverse direction. As already mentioned, the boundary conditions in the transverse direction can be arbitrary. This approach permits the discretization of the rectangular plates in finite longitudinal *strips*, as shown on Fig. 8.1.1. These strips are connected to one another along the *nodal lines*. Displacements and rotations represent the degrees of freedom of each nodal line. Stiffness and load matrices of the individual strips are determined either by virtual work or by using the minimum of the potential energy principle. These matrices of the finite strips are assembled in the usual way to form the stiffness and load matrices of the total structure. Consequently, the steps to be followed are generally similar to those of the FEM.

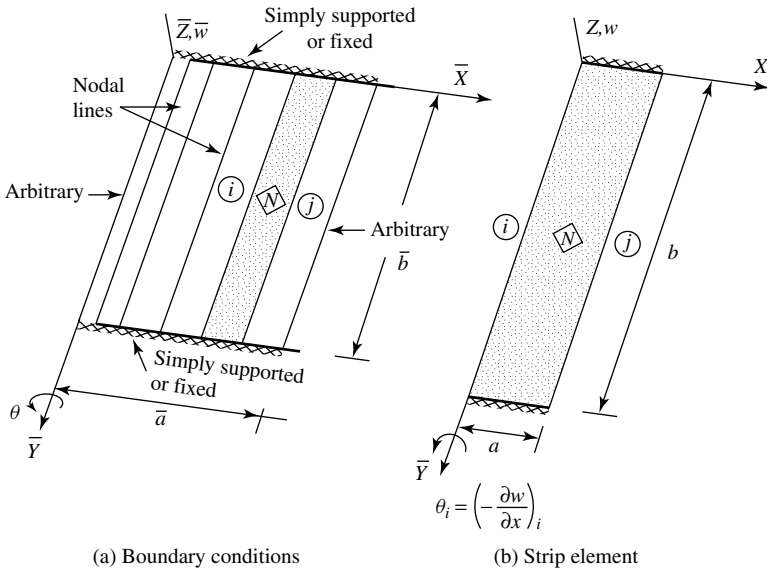


Figure 8.1.1 Plate bending using classical FSM.

The displacement function for each finite strip is chosen in the general form

$$w(x, y) = \sum_{n=1}^{\infty} X_n(x) \cdot Y_n(y), \quad (8.1.1)$$

which represents in effect Kantorovich's technique of separation of variables treated in Sec. 4.4. The simply supported boundary conditions in the longitudinal direction call for a $Y_n(y) = \sin n\pi y/b$ smooth and differentiable trigonometric function, while $X_n(x)$ in the transverse direction may represent simple polynomials corresponding to the n terms of the series Y_n . As in the case of the FEM, the selection of a suitable shape function is of primary importance concerning the convergence characteristics of the method.

While in the FEM each nodal point has at least three degrees of freedom, the FSM replaces numerous elements by a single strip with just two degrees of freedom at the nodal lines. Consequently, the number of unknown displacements is drastically reduced. Furthermore, the classical FSM takes advantage of the orthogonality of the harmonic functions in the stiffness matrix formulation, resulting in a block diagonal stiffness matrix of the plate. This approach not only simplifies the data manipulation in forming the assembled stiffness matrix of the structure but also reduces its bandwidth. Thus, considerable economy in the solution is achieved.

In the last decades, static solutions to thin-plate problems using the FSM have been developed extensively. For instance, the method has been extended to cover other than simply supported edges in the longitudinal direction [8.1.3], which includes clamped and simply supported and clamped boundary conditions. In addition, the recently developed spline and "computed" shape functions[†] further increase the applicability

[†] See Sec. 10.8.

of the FSM [8.1.4]. Free vibrations and elastic stability problems of rectangular plates can also be solved economically by the FSM.

While the above-mentioned solutions have been based entirely on Kirchhoff's plate theory, recently, moderately thick plate theories are also being used to include the effect of transverse shear. This effort has resulted in moderately thick finite strip solutions discussed later detail.

References and Bibliography

- [8.1.1] CHEUNG, Y. K., "The Finite Strip Method in the Analysis of Elastic Plates with Two Opposite Simply Supported Ends," *Proc. Inst. Civ. Eng.*, 40 (1968), 1–7.
- [8.1.2] POWELL, G. H., and OGDEN, D. W., "Analysis of Orthotropic Bridge Decks," *J. Struct. Div., ASCE*, 95 (1969), 909–923.
- [8.1.3] CHEUNG, Y. K., "The Flexural Vibration of Rectangular and Other Polygonal Plates," *J. Eng. Mech. Div., ASCE*, 97 (1971), 391–411.
- [8.1.4] CHEUNG, Y. K., and THAM, L. G., *Finite Strip Method*, CRC Press, Boca Raton, Florida, 1998.

8.2 Displacement Functions for Classical FSM

As with the FEM, selection of suitable displacement functions for the strip elements is the most important part of the analysis, since it greatly influences the quality of the obtained results. Consequently, *great care* should be exercised in selecting suitable displacement functions to achieve convergence to the exact solutions of plate problems. Since the FSM can be considered an extension of the FEM, it can also be mathematically classified as a variation of Ritz's energy approach with piecewise approximation of the displacement field. The types of displacement functions to be used for the finite strips, however, are different from those employed for the finite elements. That is, while the FEM uses mostly polynomials in both directions, the classical FSM utilizes trigonometric series in the longitudinal (Y) direction and employs polynomials in the transverse (X) direction. The most general requirement to achieve convergence to the exact solution is that the strain should remain finite at the interfaces between strips in the Ritz-type energy formulation of the plate problem.

Selection of suitable displacement functions for the finite strip elements is based on the separation of variables, as indicated in Eq. (8.1.1). Convergence to the right solutions can be assured if the following three conditions are satisfied:

1. The basic function $Y_n(y)$ should be represented by trigonometric series that satisfy the boundary conditions of the plate in the Y direction.
2. The transverse part of the displacement function $X_n(x)$ should be a polynomial satisfying the constant-strain conditions in the X direction. It should be noted that the strain vector ϵ is obtained by differentiating the displacement function, as discussed in Sec. 8.3.
3. The displacements w , $\theta_x = \partial w / \partial x$ must be compatible along the nodal lines.

a. Basic Functions in Longitudinal Direction. For the series representation of the basic function $Y_n(y)$, the *classical* FSM employs mostly eigenfunctions of vibrating

beams or those of beam buckling. Although the recently developed spline and “computed” shape functions can replace the series by polynomials [8.2.1], treatment of these alternatives is discussed later in connection with the advanced topics of the FSM.

The general form of the eigenfunctions of a vibrating beam has the general form

$$Y_n(y) = C_1 \sin \frac{\lambda_n y}{b} + C_2 \cos \frac{\lambda_n y}{b} + C_3 \sinh \frac{\lambda_n y}{b} + C_4 \cosh \frac{\lambda_n y}{b}, \quad (8.2.1)$$

where λ_n is a parameter to be determined according to the end supports and b represents the length of the strip element (Fig. 8.1.1b). The coefficients C_1 , C_2 , C_3 and C_4 should be determined from the boundary conditions in the Y direction. The use of the eigenfunctions of vibrating beams in connection with Galerkin’s solution of plate and shell problems was first suggested by Vlasov [8.2.2, 8.2.3] and was treated in Sec. 4.3.

The following particular shapes of the basic function $Y_n(y)$ can be used in FSM to solve the most common plate problems:

1. Both ends are simply supported (Fig. 8.2.1). The boundary conditions can be written as

$$Y_n(0) = Y_n''(0) = 0 \quad \text{and} \quad Y_n(b) = Y_n''(b) = 0; \quad (8.2.2)$$

hence

$$Y_n(y) = \sin \frac{\lambda_n y}{b}, \quad \lambda_n = \pi, 2\pi, 3\pi, \dots \quad (8.2.3)$$

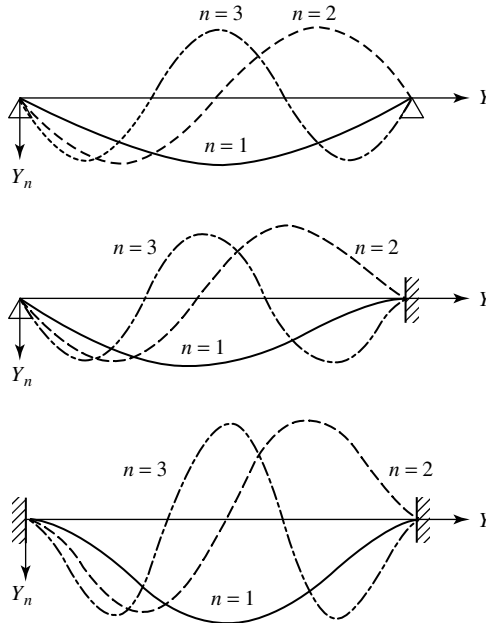


Figure 8.2.1 Shapes of vibrating beams.

2. One end is simply supported while the other is fixed.
The boundary conditions in this case are

$$Y_n(0) = Y_n''(0) = 0 \quad \text{and} \quad Y_n(b) = Y_n'(b) = 0, \quad (8.2.4)$$

and the corresponding eigenfunction becomes

$$\begin{aligned} Y_n(y) &= \sin \frac{\lambda_n y}{b} - c_n \sinh \frac{\lambda_n y}{b}, \\ \lambda_n &= \frac{4n+1}{4}\pi \quad \text{for } n = 1, 2, 3, \dots, \\ c_n &= \frac{\sin \lambda_n}{\sinh \lambda_n}. \end{aligned} \quad (8.2.5)$$

3. Both ends are fixed, having the pertinent boundary conditions

$$Y_n(0) = Y_n'(0) = 0 \quad \text{and} \quad Y_n(b) = Y_n'(b) = 0. \quad (8.2.6)$$

Thus, the corresponding eigenfunction is

$$\begin{aligned} Y_n(y) &= \sin \frac{\lambda_n y}{b} - \sinh \frac{\lambda_n y}{b} - c_n \left(\cos \frac{\lambda_n y}{b} - \cosh \frac{\lambda_n y}{b} \right), \\ \lambda_n &= \frac{2n+1}{2}\pi \quad \text{for } n = 1, 2, 3, \dots, \\ c_n &= \frac{\sin \lambda_n - \sinh \lambda_n}{\cos \lambda_n - \cosh \lambda_n}. \end{aligned} \quad (8.2.7)$$

For the other boundary conditions, such as free-free, fixed-free and simply supported-free, we merely refer to Ref. [8.2.4], which also contains valuable data concerning their integrals to be used in formulating the finite strip procedures.

Another valuable source for basic functions $Y_n(y)$ can be the eigenfunctions of column buckling [8.2.5]. The general form of these equations is

$$Y_n(y) = C_1 \sin ky + C_2 \cos ky + C_3 y + C_4, \quad (8.2.8)$$

where C_1, C_2, C_3 and C_4 are constants and k represents a parameter; their values are found by considering the boundary conditions of the finite strip in the Y direction.

If both ends are simply supported, Eq. (8.2.8) becomes

$$Y_n(y) = C_1 \sin \frac{n\pi y}{b} \quad \text{for } n = 1, 2, 3, \dots, \quad (8.2.9)$$

where C_1 represents the undetermined amplitude of the buckled shape. For our purpose C_1 can be taken as $C_1 = 1$. Consequently, Eqs. (8.2.3) and (8.2.9) become identical.

For fixed end columns, for example, the equation of the deflection curve is

$$Y_n(y) = \cos \frac{2n\pi y}{b} - 1. \quad (8.2.10)$$

For a plate strip fixed at $y = 0$ and free at the other end, the eigenfunction of the buckled column becomes

$$Y_n(y) = 1 - \cos \frac{(2n-1)\pi y}{2b}. \quad (8.2.11)$$

The reader will find additional deflection curves of column buckling in most standard textbooks on elastic stability. For stability analysis of elastic plates, for example, these functions give more exact results than the eigenfunctions of vibrating beams.

Finally, it should be noted that all these basic functions are *orthogonal*. Consequently, for $m \neq n$

$$\int_0^b Y_m Y_n = 0 \quad \text{and} \quad \int_0^b Y_m'' \cdot Y_n'' = 0. \quad (8.2.12)$$

Due to these valuable properties of orthogonality, computation of integrals required in formulating the finite strip procedures becomes simpler, as discussed in Sec.8.3.

b. Shape Functions in Transverse Direction. For the $X_n(x)$ part of the displacements [Eq. (8.1.1)], polynomials can be used. For this purpose, we can employ the well-known beam functions[†] that represent the deflection curves of a fixed beam subjected subsequently to unit translations and rotations, respectively, at each end (Fig. 8.2.2). Thus for a typical strip element with sides \textcircled{i} and \textcircled{j} (Fig. 8.1.1), the displacement function can be written as

$$\begin{aligned} w(x, y) = \sum_{n=1}^r \left[\left(1 - \frac{3x^2}{a^2} + \frac{2x^3}{a^3} \right) w_{in} + \left(-x + \frac{2x^2}{a} - \frac{x^3}{a^2} \right) \theta_{in} \right. \\ \left. + \left(\frac{3x^2}{a^2} - \frac{2x^3}{a^3} \right) w_{jn} + \left(\frac{x^2}{a} - \frac{x^3}{a^2} \right) \theta_{jn} \right] Y_n(y), \end{aligned} \quad (8.2.13)$$

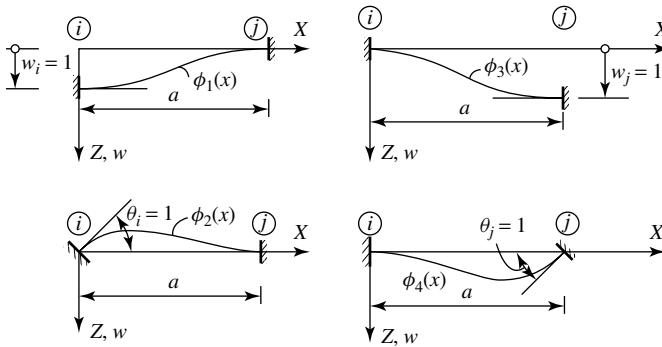


Figure 8.2.2 Fixed beam subjected to unit displacements.

[†] See Refs. [6.4.1–6.4.15].

where w_{in} , w_{jn} and θ_{in} , θ_{jn} are translations and rotations, respectively, corresponding to the nodal lines \textcircled{i} and \textcircled{j} .

We can also express the displacement function $w(x, y)$ in a more general form by using polynomials

$$w(x, y) = \sum_{n=1}^r (\alpha_1 + \alpha_2 x + \alpha_3 x^2 + \alpha_4 x^3) Y_n, \quad (8.2.14)$$

where $\alpha_1, \dots, \alpha_4$ are parameters to be expressed in terms of the nodal-line displacements. Equation (8.2.14) can be written in a more concise form as

$$w(x, y) = \sum_{n=1}^r [\mathbf{C}_i \quad \mathbf{C}_j] \begin{Bmatrix} \delta_i \\ \delta_j \end{Bmatrix} Y_n, \quad (8.2.15)$$

where \mathbf{C}_i and \mathbf{C}_j are matrices associated with δ_i and δ_j nodal-line displacements (deflection and rotation) and n denotes the number of terms in series Y_n .

Although the shape functions $X_n(x)$ and $Y_n(y)$ introduced here are capable of giving good results in most of cases, they nevertheless have some shortcomings. For instance, because the beam functions are continuously differentiable, it is difficult to use them to simulate abrupt changes of bending moments at internal supports or in the vicinity of concentrated forces. In addition, they are not too exact at the free-edges of the plates. These difficulties, however, can be overcome by using refined shape functions [8.2.1].

References and Bibliography

- [8.2.1] CHEUNG, Y. K., and THAM, L. G., *Finite Strip Method*, CRC Press, Boca Raton, Florida, 1998.
- [8.2.2] VLASOV, V. Z., *General Theory of Shells and Its Applications in Engineering* (translation of Russian original by NASA), N64-19883, Office of Technical Service, Washington, D.C., 1949.
- [8.2.3] WLASSOW, W. S., *Allgemeine Schalentheorie und ihre Anwendung in der Technik* (German translation of Russian original), Akademie-Verlag, Berlin, 1958.
- [8.2.4] FELGAR, R. P., "Formulas Containing Characteristic Functions of a Vibrating Beam," Circular 14, University of Texas, Austin, Texas, 1950.
- [8.2.5] TIMOSHENKO, S. P., and GERE, J. M., *Theory of Elastic Stability*, 2nd ed., McGraw-Hill Book Co., New York, 1961.

8.3 Formulation of the Method

The nodal displacements of a rectangular strip element corresponding to the n th term in the series Y_n are

$$\delta_n = \left\{ w_i, \left(\frac{\partial w}{\partial x} \right)_i, w_j, \left(\frac{\partial w}{\partial y} \right)_j \right\}_n^T = \begin{Bmatrix} w_{in} \\ \theta_{in} \\ w_{jn} \\ \theta_{jn} \end{Bmatrix} = \begin{Bmatrix} \delta_{in} \\ \delta_{jn} \end{Bmatrix}. \quad (8.3.1)$$

Consequently, the displacements w_i, w_j and the rotations θ_i, θ_j along the nodal lines i and j are:

$$\begin{Bmatrix} w_i \\ \theta_i \\ w_j \\ \theta_j \end{Bmatrix} = \sum_{n=1}^r \{w_{in}, \theta_{in}, w_{jn}, \theta_{jn}\}^T Y_n = \begin{Bmatrix} \delta_i \\ \delta_j \end{Bmatrix}. \quad (8.3.2)$$

The displacement field given previously in Eq. (8.2.13) can be rewritten in the more concise matrix form

$$w(x, y) = \sum_{n=1}^r \mathbf{L}_n \delta_n = \mathbf{N} \delta, \quad (8.3.3)$$

where

$$\mathbf{L}_n = \left[\left(1 - \frac{3x^2}{a^2} + \frac{2x^3}{a^3} \right), \left(-x + \frac{2x^2}{a} - \frac{x^3}{a^2} \right), \left(\frac{3x^2}{a^2} - \frac{2x^3}{a^3} \right), \left(\frac{x^2}{a} - \frac{x^3}{a^2} \right) \right] Y_n \quad (8.3.4)$$

and

$$\delta = \begin{Bmatrix} \delta_1 \\ \delta_2 \\ \vdots \\ \delta_r \end{Bmatrix}. \quad (8.3.5)$$

The strain vector ϵ is obtained by differentiating the displacement function w with respect to the x and y coordinates. Hence

$$\epsilon = \begin{Bmatrix} -\frac{\partial^2 w}{\partial x^2} \\ -\frac{\partial^2 w}{\partial y^2} \\ 2\frac{\partial^2 w}{\partial x \partial y} \end{Bmatrix} = \sum_{n=1}^r \mathbf{B}_n \delta_n = \mathbf{B} \delta, \quad (8.3.6)$$

where \mathbf{B} represents the strain matrix. Its submatrix \mathbf{B}_n corresponding to the n th term of the series Y_n is defined as

$\mathbf{B}_n =$

$$\begin{bmatrix} \left(\frac{6}{a^2} - \frac{12x}{a^3} \right) Y_n & \left(-\frac{4}{a} + \frac{6x}{a^2} \right) Y_n & \left(\frac{12x}{a^3} - \frac{6}{a^2} \right) Y_n & \left(-\frac{2}{a} + \frac{6x}{a^2} \right) Y_n \\ -\left(1 - \frac{3x^2}{a^2} + \frac{2x^3}{a^3} \right) Y_n'' & \left(x - \frac{2x^2}{a} + \frac{x^3}{a^2} \right) Y_n'' & -\left(\frac{3x^2}{a^2} - \frac{2x^3}{a^3} \right) Y_n'' & \left(\frac{x^3}{a^2} - \frac{x^2}{a} \right) Y_n'' \\ \left(-\frac{12x}{a^2} + \frac{12x^2}{a^3} \right) Y_n' & \left(-2 + \frac{8x}{a} - \frac{6x^2}{a^2} \right) Y_n' & \left(\frac{12x}{a^2} - \frac{12x^2}{a^3} \right) Y_n' & \left(-\frac{6x^2}{a^2} + \frac{4x}{a} \right) Y_n' \end{bmatrix}. \quad (8.3.7)$$

In this equation Y_n , Y'_n and Y''_n are series defining the strip displacements in the Y direction[†] and its first and second derivatives, respectively.

Similarly, the stress vector is

$$\boldsymbol{\sigma} = \begin{Bmatrix} m_x \\ m_y \\ m_{xy} \end{Bmatrix} = \mathbf{D}\boldsymbol{\varepsilon} = \mathbf{D}\mathbf{B}\boldsymbol{\delta} = \mathbf{D} \sum_{n=1}^r \mathbf{B}_n \boldsymbol{\delta}_n, \quad (8.3.8)$$

where \mathbf{D} represents the elastic matrix

$$\mathbf{D} = D \begin{bmatrix} 1 & \nu & 0 \\ \nu & 1 & 0 \\ 0 & 0 & (1 - \nu)/2 \end{bmatrix} \quad \text{and} \quad D = \frac{Eh^3}{12(1 - \nu^2)}. \quad (8.3.9)$$

To derive the *stiffness matrix* \mathbf{K}_e for the finite strip element, we use—as in the FEM—the minimum principle of the total potential energy. This is given as

$$\Pi = U + W, \quad (8.3.10)$$

where U is the strain energy of the elastic strip,

$$U = \frac{1}{2} \int_0^b \int_0^a \boldsymbol{\varepsilon}^T \boldsymbol{\sigma} \, dx \, dy = \frac{1}{2} \int_0^b \int_0^a \boldsymbol{\sigma}^T \mathbf{B}^T \mathbf{D} \mathbf{B} \boldsymbol{\delta} \, dx \, dy, \quad (8.3.11)$$

and W represents the work done by the load vector on the displacement field $w = \mathbf{N}\boldsymbol{\delta}$. Thus, we can write

$$W = - \int_0^b \int_0^a \boldsymbol{\delta}^T \mathbf{N}^T \mathbf{p} \, dx \, dy, \quad (8.3.12)$$

where \mathbf{N} denotes the shape function defined in Eq. (8.3.3) and \mathbf{p} is the load vector.

The principle of the minimum potential energy requires that

$$\frac{\partial \Pi}{\partial \boldsymbol{\delta}} = \frac{\partial (U + W)}{\partial \boldsymbol{\delta}} = \{0\}. \quad (8.3.13)$$

After performing the partial differentiations in Eq. (8.3.11), we obtain

$$\frac{\partial \Pi}{\partial \boldsymbol{\delta}} = \int_0^b \int_0^a \mathbf{B}^T \mathbf{D} \mathbf{B} \boldsymbol{\delta} \, dx \, dy - \int_0^b \int_0^a \mathbf{N}^T \mathbf{p} \, dx \, dy = \{0\}; \quad (8.3.14)$$

hence

$$\mathbf{K}_e \boldsymbol{\delta} - \mathbf{f}_p = \{0\}, \quad (8.3.15)$$

where

$$\mathbf{K}_e = \int_0^b \int_0^a \mathbf{B}^T \mathbf{D} \mathbf{B} \, dx \, dy \quad (8.3.16)$$

[†] See Sec. 8.2.

represents the stiffness matrix of the rectangular finite strip and

$$\mathbf{f}_p = \int_0^b \int_0^a \mathbf{N}^T \mathbf{p} \, dx \, dy \quad (8.3.17)$$

denotes the consistent load vector.

We recall that the displacement function $w(x, y)$ is expressed as a series; thus, Eq. (8.3.16) can be written in the more expanded form

$$\begin{aligned} \mathbf{K}_e &= \int_0^b \int_0^a \mathbf{B}^T \mathbf{D} \mathbf{B} \, dx \, dy = \int_0^b \int_0^a [\mathbf{B}_1 \, \mathbf{B}_2 \cdots \mathbf{B}_r]^T \mathbf{D} [\mathbf{B}_1 \, \mathbf{B}_2 \cdots \mathbf{B}_r] \, dx \, dy \\ &= \int_0^b \int_0^a \begin{bmatrix} \mathbf{B}_1^T \mathbf{D} \mathbf{B}_1 & \mathbf{B}_1^T \mathbf{D} \mathbf{B}_2 & \cdots & \mathbf{B}_1^T \mathbf{D} \mathbf{B}_r \\ \mathbf{B}_2^T \mathbf{D} \mathbf{B}_1 & \mathbf{B}_2^T \mathbf{D} \mathbf{B}_2 & \cdots & \mathbf{B}_2^T \mathbf{D} \mathbf{B}_r \\ \vdots & \vdots & \ddots & \vdots \\ \mathbf{B}_r^T \mathbf{D} \mathbf{B}_1 & \mathbf{B}_r^T \mathbf{D} \mathbf{B}_2 & \cdots & \mathbf{B}_r^T \mathbf{D} \mathbf{B}_r \end{bmatrix} dx \, dy. \end{aligned} \quad (8.3.18)$$

Thus, the stiffness matrix of the finite plate strip becomes

$$\mathbf{K}_e = \begin{bmatrix} \mathbf{K}_{11} & \mathbf{K}_{12} & \cdots & \mathbf{K}_{1r} \\ \mathbf{K}_{21} & \mathbf{K}_{22} & \cdots & \mathbf{K}_{2r} \\ \vdots & \vdots & \ddots & \vdots \\ \mathbf{K}_{r1} & \mathbf{K}_{r2} & \cdots & \mathbf{K}_{rr} \end{bmatrix}, \quad (8.3.19)$$

with the current term

$$\mathbf{K}_{ij, mn} = \int_0^b \int_0^a \mathbf{B}_m^T \mathbf{D} \mathbf{B}_n \, dx \, dy = \begin{bmatrix} \mathbf{K}_{ii} & \mathbf{K}_{ij} \\ \mathbf{K}_{ji} & \mathbf{K}_{jj} \end{bmatrix}_{mn}. \quad (8.3.20)$$

If both ends of the finite strip are simply supported in the longitudinal direction, the basic function and its first and second derivatives are involved in the evaluation of the stiffness matrix. These are

$$\mathbf{Y}_n = \sin \frac{n\pi y}{b}, \quad \mathbf{Y}'_n = \frac{n\pi}{b} \cos \frac{n\pi y}{b}, \quad \mathbf{Y}''_n = -\left(\frac{n\pi}{b}\right)^2 \sin \frac{n\pi y}{b}. \quad (8.3.21)$$

Thus we have

$$\int_0^b Y'_m Y'_n \, dy = \begin{cases} \left(\frac{m\pi}{b}\right) \left(\frac{n\pi}{b}\right) \int_0^b \cos \frac{m\pi y}{b} \cos \frac{n\pi y}{b} \, dy = 0 & \text{for } m \neq n, \\ \frac{n^2 \pi^2}{2b} & \text{for } m = n \end{cases} \quad (8.3.22)$$

and

$$\int_0^b Y_m Y''_n \, dy = \begin{cases} -\frac{n^2 \pi^2}{b^2} \int_0^b \sin \frac{m\pi y}{b} \sin \frac{n\pi y}{b} \, dy = 0 & \text{for } m \neq n, \\ -\frac{n^2 \pi^2}{2b} & \text{for } m = n. \end{cases} \quad (8.3.23)$$

Therefore, for $m \neq n$ Eq. (8.3.20) becomes zero. For $m = n$ the elements of the stiffness matrix

$$\mathbf{K}_{e,n} = D \begin{bmatrix} k_{11} & k_{12} & k_{13} & k_{14} \\ k_{21} & k_{22} & k_{23} & k_{24} \\ k_{31} & k_{32} & k_{33} & k_{34} \\ k_{41} & k_{42} & k_{43} & k_{44} \end{bmatrix} \quad (8.3.24)$$

corresponding to simply supported rectangular plate strips (Fig. 8.1.1b) are given in Table 8.3.1.[†] Numbering of the nodal line displacement components is defined in Fig. 8.3.1. Similarly, the elements of the stiffness matrix $\mathbf{K}_{e,mn}$ covering general boundary conditions in the Y direction are listed in Table 8.3.2.[‡] Expressions for the definite integrals in this table are (if $m \neq n$ and $I_1 = I_4 = 0$)

$$\begin{aligned} I_1 &= \int_0^b Y_m Y_n \, dy, & I_2 &= \int_0^b Y_m'' \cdot Y_n \, dy, & I_3 &= \int_0^b Y_m Y_n'' \, dy, \\ I_4 &= \int_0^b Y_m'' \cdot Y_n'' \, dy, & I_5 &= \int_0^b Y_m' \cdot Y_n' \, dy. \end{aligned} \quad (8.3.25)$$

Table 8.3.1 Stiffness Matrix Coefficients of Simply Supported Strip^a

$k_{11} = \frac{6b}{a^3} + \frac{13ab}{70}c^2 + \frac{6b}{5a}cv + \frac{6b(1-\nu)}{5a}c$
$k_{21} = -\frac{3b}{a^2} - \frac{11a^2b}{420}c^2 - \frac{3b}{5}cv - \frac{b(1-\nu)}{10}c = k_{12}$
$k_{31} = -\frac{6b}{a^3} + \frac{9ab}{140}c^2 - \frac{6b}{5a}cv - \frac{6b(1-\nu)}{5a}c = k_{13}$
$k_{41} = -\frac{3b}{a^2} + \frac{13a^2b}{840}c^2 - \frac{b}{10}cv - \frac{b(1-\nu)}{10}c = k_{41}$
$k_{22} = \frac{2b}{a} + \frac{ba^3}{210}c^2 + \frac{2ab}{15}cv + \frac{2ab(1-\nu)}{15}c$
$k_{32} = \frac{3b}{a^2} - \frac{13a^2b}{840}c^2 + \frac{b}{10}cv + \frac{b(1-\nu)}{10}c = k_{23}$
$k_{42} = \frac{1}{a} - \frac{a^3b}{280}c^2 - \frac{ab}{30}cv - \frac{ab(1-\nu)}{30}c = k_{24}$
$k_{33} = \frac{6b}{a^3} + \frac{13ab}{70}c^2 + \frac{6b}{5a}cv + \frac{6b(1-\nu)}{5a}c$
$k_{43} = \frac{3b}{a^2} + \frac{11a^2b}{420}c^2 + \frac{3b}{5}cv + \frac{b(1-\nu)}{10}c = k_{34}$
$k_{44} = \frac{2b}{a} + \frac{a^3b}{210}c^2 + \frac{2ab}{15}cv + \frac{2ab(1-\nu)}{15}c$
$c = \frac{n^2\pi^2}{b^2}$

^aEq. (8.3.24).

[†] See also Refs. [8.3.1] and [8.3.2].

[‡] See also Refs. [8.3.3] and [8.3.4].

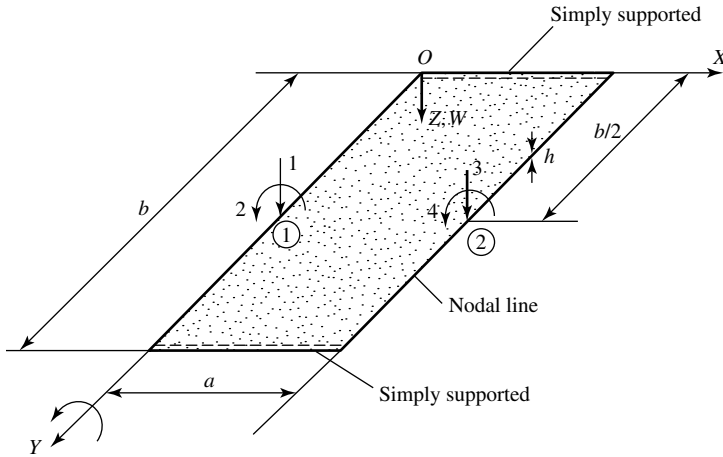


Figure 8.3.1 Simply supported plate strip.

Table 8.3.2 Stiffness Matrix for General Boundary Conditions^a

$k_{11} = \left[\frac{12}{a^3} I_1 - \frac{6\nu}{5a} [I_2 + I_3] + \frac{39a}{105} I_4 + \frac{12(1-\nu)}{5b} I_5 \right] D$
$k_{21} = \left[-\frac{6}{a^2} I_1 - \frac{\nu}{10} [I_2 + 11I_3] + \frac{11a^2}{210} I_4 + \frac{1-\nu}{5} I_5 \right] D = k_{12}$
$k_{31} = \left[-\frac{12}{a^3} I_1 + \frac{6\nu}{3a} [I_2 + I_3] + \frac{27a}{210} I_4 - \frac{12(1-\nu)}{5a} I_5 \right] D = k_{13}$
$k_{41} = \left[\frac{6}{a^2} I_1 - \frac{\nu}{10} [I_2 + I_3] - \frac{13a^2}{420} I_4 + \frac{1-\nu}{5} I_5 \right] D = k_{14}$
$k_{22} = \left[\frac{4}{a} I_1 - \frac{2a\nu}{15} [I_2 + I_3] + \frac{a^3}{105} I_4 + \frac{4a(1-\nu)}{15} I_5 \right] D$
$k_{32} = \left[-\frac{6}{a^2} I_1 - \frac{\nu}{10} [I_2 + I_3] + \frac{13a^2}{420} I_4 - \frac{1-\nu}{5} I_5 \right] D = k_{23}$
$k_{42} = \left[\frac{2}{a} I_1 + \frac{7a\nu}{210} [I_2 + I_3] - \frac{a^3}{140} I_4 - \frac{a(1-\nu)}{15} I_5 \right] D = k_{24}$
$k_{33} = \left[\frac{12}{a^3} I_1 - \frac{6\nu}{5a} [I_2 + I_3] + \frac{39a}{105} I_4 + \frac{12(1-\nu)}{5a} I_5 \right] D$
$k_{43} = \left[-\frac{6}{a^2} I_1 + \frac{\nu}{10} [I_2 + I_3] - \frac{11a^2}{210} I_4 - \frac{1-\nu}{5} I_5 \right] D = k_{34}$
$k_{44} = \left[\frac{4}{a} I_1 - \frac{2a\nu}{15} [I_2 + I_3] + \frac{a^3}{105} I_4 + \frac{4a(1-\nu)}{15} I_5 \right] D$

^aIn the Y direction.

In the FEM one way of checking the correctness of the element stiffness matrix \mathbf{K}_e is by calculating the sums of all stiffness coefficients in each column. For a correct element stiffness matrix these sums must be zero. Unfortunately, such a simple way for checking the stiffness matrices given in Tables 8.3.1 and 8.3.2 is no longer valid in the FSM, since supporting forces exist that are not included in these matrices.

For determination of the *consistent load vector* \mathbf{f}_p , we first refer to Eq. (8.3.17), which can be rewritten as

$$\mathbf{f}_p = \int_0^b \int_0^a \begin{bmatrix} \mathbf{N}_1 \\ \mathbf{N}_2 \\ \vdots \\ \mathbf{N}_r \end{bmatrix} (P_1 Y_1 + P_2 Y_2 + \cdots + P_r Y_r) dx dy, \quad (8.3.26)$$

where the expression in parentheses represents a series-type expansion[†] using the selected basic function Y_n . Consequently, the external lateral load is expressed as

$$p = P_1 Y_1 + P_2 Y_2 + \cdots + P_r Y_r = \sum_{n=1}^r P_n Y_n. \quad (8.3.27)$$

The coefficient P_n can be obtained by multiplying Eq. (8.3.27) by Y_n and integrating it between zero and b . Thus, we have

$$\begin{aligned} \int_0^b p Y_n dy &= P_1 \int_0^b Y_1 Y_n dy + P_2 \int_0^b Y_2 Y_n dy + \cdots \\ &+ P_n \int_0^b Y_n^2 dy + \cdots + P_r \int_0^b Y_r Y_n dy. \end{aligned} \quad (8.3.28)$$

Because of the already discussed orthogonality of the basic functions, Eq. (8.3.28) gives

$$P_n = \frac{\int_0^b p Y_n dy}{\int_0^b Y_n^2 dy}. \quad (8.3.29)$$

In a similar way, the expansion coefficient P_n can be determined for various load distributions. For a locally distributed load, for instance, Cheung [8.3.5] gives

$$P_n = \frac{\int_c^d p Y_n dy}{\int_0^b Y_n^2 dy}, \quad (8.3.29a)$$

[†] See Appendix A.1 for Fourier-type series expansion.

and for a concentrated load P_0 acting on a nodal line[†] at $y = c$ distance,

$$P_n = \frac{P_0 Y_n(c)}{\int_0^b Y_n^2 dy} \quad (8.3.29b)$$

Due to the orthogonality of the basic function Y_n , Eq. (8.3.26) can be written as

$$\mathbf{f}_p = \int_0^b \int_0^a \begin{bmatrix} \mathbf{N}_1 P_1 Y_1 \\ \mathbf{N}_2 P_2 Y_2 \\ \vdots \\ \mathbf{N}_r P_r Y_r \end{bmatrix} dx dy = \begin{Bmatrix} \mathbf{f}_{p,1} \\ \mathbf{f}_{p,2} \\ \vdots \\ \mathbf{f}_{p,r} \end{Bmatrix}, \quad (8.3.30)$$

where

$$\mathbf{f}_{p,n} = \int_0^b \int_0^a \mathbf{N}_n P_n Y_n dx dy. \quad (8.3.31)$$

For simply supported strips subjected to uniformly distributed loads, Eq. (8.3.31) becomes

$$\mathbf{f}_{p,n} = \frac{P_n b}{2} \begin{Bmatrix} a/2 \\ -a^2/12 \\ a/2 \\ a^2/2 \end{Bmatrix}. \quad (8.3.32)$$

Similarly, for a concentrated force P_0 acting on the nodal line i , we obtain

$$\mathbf{f}_{p,n} = P_0 Y_n(c) \begin{Bmatrix} 1 \\ 0 \\ 0 \\ 0 \end{Bmatrix}. \quad (8.3.33)$$

From the previous equations, it is clear that the accuracy obtained by the FSM in a given plate problem depends not only on the shape function but also on how closely the external load can be approximated by the first few terms of the series expansion. Furthermore, it is evident that with different basic functions we obtain different stiffness matrices as well as different consistent load vectors for the finite strips, as shown in Refs. [8.3.1–8.3.4].

References and Bibliography

- [8.3.1] CHEUNG, Y. K., *Finite Strip Method in Structural Analysis*, Pergamon Press, Oxford, 1976.
- [8.3.2] GHALI, A., et al., *Structural Analysis: A Unified Classical and Matrix Approach*, 2nd ed., Chapman & Hall, London, 1978.
- [8.3.3] AVRAM, C., et al., *Numerical Analysis of Reinforced Concrete Structures*, Elsevier, Amsterdam, 1993.

[†] It is advised to put a nodal line under each concentrated load, if possible, to increase accuracy.

- [8.3.4] CHEUNG, Y. K., and THAM, L. G., *Finite Strip Method*, CRC Press, Boca Raton, Florida, 1998.
- [8.3.5] CHEUNG, M. S., et al., *Finite Strip Analysis of Bridges*, E&F Spon, London, 1996.

8.4 Outline of Computational Procedures

The analysis of a rectangular plate by the classical FSM follows, in general, the already familiar matrix displacement approach by solving a system of algebraic equations pertinent to the n th term of the series expansion.

First, the plate is discretized by a suitable number of strips connected to each other by the longitudinal nodal lines, as shown in Fig. 8.4.1b. It is advisable to assign a nodal line to each concentrated force acting on the plate proper. Although the reader will find in Refs. [8.3.3] and [8.3.4] expressions for dealing with concentrated forces acting in the domain of a strip, experience shows that the former approach gives better accuracy.

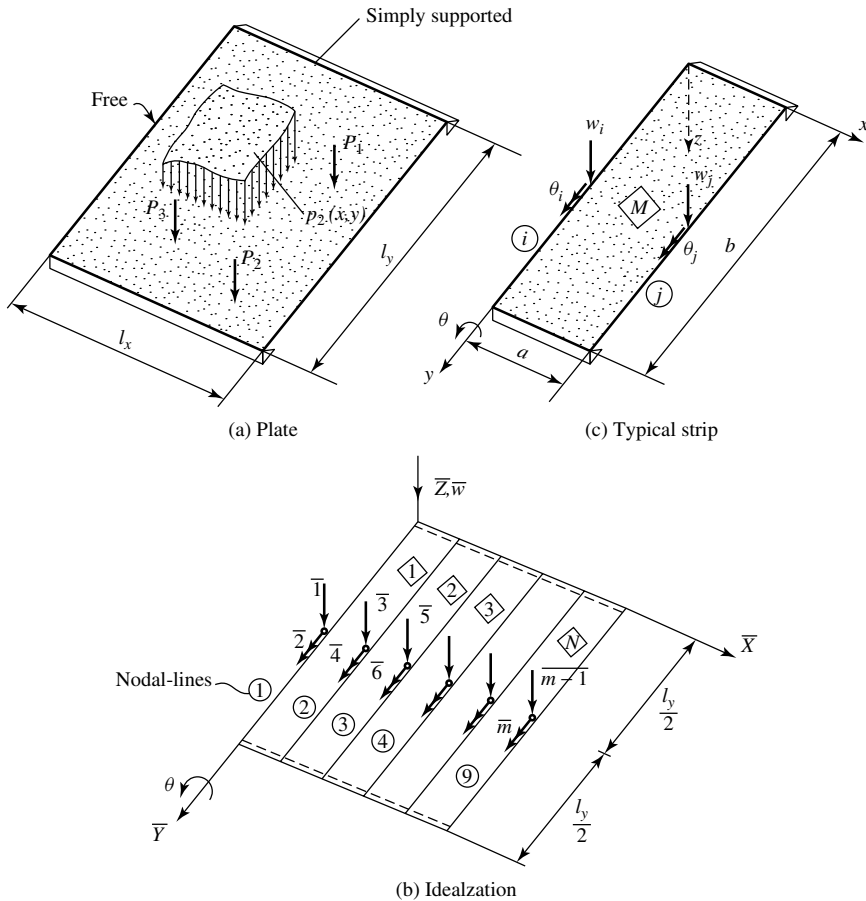


Figure 8.4.1 Idealization of plate by finite strips.

Next, the admissible displacement components of each nodal line are numbered with reference to the global $\bar{X}, \bar{Y}, \bar{Z}$ coordinate system of the structure. As in the closely related FEM, nodal-line displacements, which are restrained, receive no numbers.

For each strip (Fig. 8.4.1c) we compute the element stiffness matrix $\mathbf{K}_{e,n}$ and consistent load vector $\mathbf{f}_{p,n}$ corresponding to the n th term of the series expansion. If the plate is simply supported in the Y direction, we use Table 8.3.1 and Eqs. (8.3.32) and (8.3.33), respectively. These matrices are relevant to the local coordinate system X, Y, Z of each strip. Due to the orthogonality of the selected basic function Y_n , all terms in the stiffness matrix of the strip are uncoupled. Consequently, Eq. (8.3.19) becomes a block diagonal matrix

$$\mathbf{K}_e = \begin{bmatrix} \mathbf{K}_{11} & 0 & \cdots & 0 \\ 0 & \mathbf{K}_{22} & \cdots & 0 \\ \vdots & \vdots & \ddots & \vdots \\ 0 & 0 & 0 & \mathbf{K}_{rr} \end{bmatrix}. \quad (8.4.1)$$

Assemblage of the stiffness matrix $\bar{\mathbf{K}}_n$ of the total structure corresponding to the n th term of the series expansion follows along the same line as that of the FEM, discussed in Sec. 7.2. Since in this case the axes of the global and local coordinate systems are parallel, no rotations of the local coordinate systems are required. In the next step, the coefficients k_{ij} of the strip matrices will be renumbered based on the global numbering of the discretized system by applying the *code number* technique; this gives \bar{k}_{ij} . Since the restrained nodal-line displacements do not receive any global numbers, the corresponding rows and columns are eliminated in the stiffness matrices of the plate strips. Now the stiffness matrix of the total structure, $\bar{\mathbf{K}}_n$, is assembled using the familiar additive approach.

Solution of the uncoupled system of equilibrium equations

$$\bar{\mathbf{K}}_n \bar{\mathbf{f}}_{p,n} = \bar{\boldsymbol{\delta}}_n \quad \text{for } n = 1, 2, \dots, r \quad (8.4.2)$$

gives the nodal-line displacements δ_n pertinent to the n th term of the series expansion, and the sum of these,

$$\bar{\boldsymbol{\delta}} = \sum_{n=1}^r \bar{\boldsymbol{\delta}}_n, \quad (8.4.3)$$

yields the final nodal-line displacement vector.

According to Eq. (8.3.8), the moments are related to the strain, while D contains all the material properties in the form of E and ν , respectively. The matrix of the moments for the midpoint of the two longitudinal sides of the strip for the n th term of the series expansion is

$$\mathbf{m}_n = \begin{Bmatrix} m_{x,i} \\ m_{y,i} \\ m_{xy,i} \\ m_{x,j} \\ m_{y,j} \\ m_{xy,j} \end{Bmatrix}_n = D \begin{bmatrix} \mathbf{B}_i \\ \mathbf{B}_j \end{bmatrix}_n \begin{Bmatrix} \delta_i \\ \delta_j \end{Bmatrix}_n. \quad (8.4.4)$$

Again, the sum of these results,

$$\mathbf{m} = \sum_{n=1}^r \mathbf{m}_n = \left\{ \begin{array}{c} m_{x,i} \\ m_{y,i} \\ m_{xy,i} \\ m_{x,j} \\ m_{y,j} \\ m_{xy,j} \end{array} \right\}_n, \quad (8.4.5)$$

yields the final moments for the nodal lines \textcircled{i} and \textcircled{j} , respectively. The excellent convergence characteristics of the FSM are demonstrated by numerous examples in Ref. [8.1.1].

As is the case with the FEM, we obtain slightly different values at both sides of the nodal lines. By averaging these two values and using a parabolic interpolation between the nodal lines, moments at the middle of the strip can be calculated.

ILLUSTRATIVE EXAMPLE

Let us compute the deflections and the moments of the square reinforced-concrete slab shown in Fig. 8.4.2a using the FSM. The slab carries a concentrated load $P_0 = 1$ at its midpoint. Poisson's ratio of the concrete is assumed to be $\nu = 0.15$. To make the computation easier to follow, let us use only one term ($n = 1$) in the series expansion.

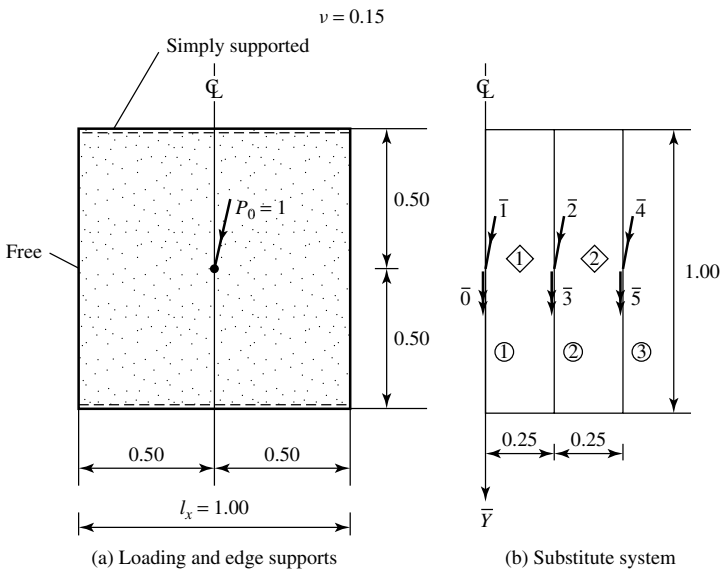


Figure 8.4.2 Square plate with two opposite edges supported and other two edges free.

Because of the symmetry, only one-half of the plate is used. This half plate is divided by lines parallel to the Y axis into only two strips. The five admissible nodal-line displacements (lateral translations and rotations) are numbered as shown in Fig. 8.4.2b.

The stiffness matrix of a simply supported strip (Fig. 8.4.1c) is calculated using the explicit expressions given in Table 8.3.1. Hence, for the first term ($n = 1$) of the series expression, we obtain

$$\mathbf{K}_{e,1} = D \begin{bmatrix} 435.89/b^2 & & \text{Symmetric} & & \\ -49.89/b^2 & 8.34 & & & \\ -429.81/b^2 & 48.89 & 435.89/b^2 & & \\ -48.89/b^2 & 3.912 & 49.89/b^2 & 8.34 & \end{bmatrix}_{n=1}, \quad (8.4.6)$$

and with $b = 1$, the corresponding stiffness matrix of one-half of the slab becomes

$$\bar{\mathbf{K}}_1 = D \begin{bmatrix} 435.89 & & & & \\ -429.81 & 871.79 & & \text{Symmetric} & \\ -48.89 & 0.00 & 16.67 & & \\ 0.00 & -429.81 & 48.89 & 435.89 & \\ 0.00 & -48.89 & 3.91 & 49.89 & 8.34 \end{bmatrix}_1. \quad (8.4.7)$$

From Eq. (8.3.33) the consistent load vector is

$$\mathbf{f}_{p,1} = \begin{Bmatrix} 0.50 \\ 0.00 \\ 0.00 \\ 0.00 \\ 0.00 \end{Bmatrix}_1. \quad (8.4.8)$$

Solution of the matrix equation

$$\bar{\mathbf{K}}_1 \bar{\mathbf{f}}_{p,1} = \bar{\boldsymbol{\delta}}_1 \quad (8.4.9)$$

gives

$$\bar{\boldsymbol{\delta}}_1 = D \begin{Bmatrix} 22.46 \\ 20.33 \\ 11.29 \\ 18.21 \\ 4.93 \end{Bmatrix} 10^{-3}. \quad (8.4.10)$$

According to Eqs. (8.3.7) and (8.4.4), the moment (stress) matrix for the mid-points of the two sides of a strip is

$$\begin{Bmatrix} m_{x,i} \\ m_{y,i} \\ m_{xy,i} \\ \cdots \\ m_{x,j} \\ m_{y,j} \\ m_{xy,j} \end{Bmatrix} = D \begin{bmatrix} (96 + \pi^2)/b^2 & -16/b & -96/b^2 & -8/b \\ (96 + \pi^2)/b^2 & -16/b & -96/b^2 & -8/b \\ 0.00 & 0.00 & 0.00 & 0.00 \\ \cdots & \cdots & \cdots & \cdots \\ -96/b^2 & 8/b & (96 + \pi^2)/b^2 & 16/b \\ -96/b^2 & 8/b & (96 + \pi^2)/b^2 & 16/b \\ 0.00 & 0.00 & 0.00 & 0.00 \end{bmatrix} \begin{Bmatrix} \delta_i \\ \delta_j \end{Bmatrix}, \quad (8.4.11)$$

or

$$\begin{Bmatrix} m_{x,i} \\ m_{y,i} \\ m_{xy,i} \\ - \\ m_{x,j} \\ m_{y,j} \\ m_{xy,j} \end{Bmatrix} = D \begin{bmatrix} 97.48/b^2 & -16/b & -96/b^2 & -8b \\ 24.27/b^2 & -2.4/b & -14.4/b^2 & 4.2/b \\ 0.00 & 0.00 & 0.00 & 0.00 \\ \hline -96/b^2 & 8/b & 97.48/b^2 & 16/b \\ -14.4/b^2 & 1.2/b & 24.27/b^2 & 2.4/b \\ 0.00 & 0.00 & 0.00 & 0.00 \end{bmatrix} \begin{Bmatrix} \delta_i \\ - \\ \delta_j \end{Bmatrix}. \quad (8.4.12)$$

Thus, moments at the midpoint i of strip \diamondsuit_1 are

$$\begin{Bmatrix} m_{x,i} \\ m_{y,i} \\ m_{xy,i} \end{Bmatrix}_{\diamondsuit_1} = D \begin{bmatrix} 97.48 & -16 & -96 & -8 \\ 24.27 & -2.4 & -14.4 & -1.2 \\ 0.00 & 0.00 & 0.00 & 0.00 \end{bmatrix} \begin{Bmatrix} 22.46 \\ 0.00 \\ 20.33 \\ 11.29 \end{Bmatrix} 10^{-3}$$

$$= D \begin{Bmatrix} 147.3 \\ 238.8 \\ 0.00 \end{Bmatrix} 10^{-3}. \quad (8.4.13)$$

Similarly, the moments at the midpoint j of strip \diamondsuit_1 become

$$\begin{Bmatrix} m_{x,j} \\ m_{y,j} \\ m_{xy,j} \end{Bmatrix}_{\diamondsuit_1} = D \begin{bmatrix} -96 & 8 & 97.48 & 16 \\ -14.4 & 12 & 24.27 & 2.4 \\ 0.00 & 0.00 & 0.00 & 0.00 \end{bmatrix} \begin{Bmatrix} 22.46 \\ 0.00 \\ 20.33 \\ 11.29 \end{Bmatrix} 10^{-3}$$

$$= D \begin{Bmatrix} 6.3 \\ 197.1 \\ 0.00 \end{Bmatrix} 10^{-3}. \quad (8.4.14)$$

Using the same approach for strip \diamondsuit_2 , we obtain

$$\begin{Bmatrix} m_{x,i} \\ m_{y,i} \\ m_{xy,i} \end{Bmatrix}_{\diamondsuit_2} = D \begin{bmatrix} 97.48 & -16 & -96 & -8 \\ 24.27 & -2.4 & -14.4 & -1.2 \\ 0.00 & 0.00 & 0.00 & 0.00 \end{bmatrix} \begin{Bmatrix} 20.33 \\ 11.29 \\ 18.21 \\ 4.93 \end{Bmatrix} 10^{-3}$$

$$= D \begin{Bmatrix} 13.1 \\ 198.1 \\ 0.00 \end{Bmatrix} 10^{-3} \quad (8.4.15)$$

and

$$\begin{aligned} \begin{Bmatrix} m_{x,j} \\ m_{y,j} \\ m_{xy,j} \end{Bmatrix}_1^{\diamond} &= D \begin{bmatrix} -96 & 8 & 97.48 & 16 \\ -14.4 & 1.2 & 24.27 & 2.4 \\ 0.00 & 0.00 & 0.000 & 0.00 \end{bmatrix} \begin{Bmatrix} 20.33 \\ 11.29 \\ 18.21 \\ 4.93 \end{Bmatrix} 10^{-3} \\ &= D \begin{Bmatrix} -6.9 \\ 174.7 \\ 0.00 \end{Bmatrix} 10^{-3}. \end{aligned} \quad (8.4.16)$$

To determine the deflected plate surface, we utilize the already computed lateral translations $\delta_{1,1}$, $\delta_{2,1}$ and $\delta_{4,1}$ as amplitudes for the sine functions used in this case for Y_n . A basically similar approach can be taken for the determination of the moment diagrams. As mentioned earlier, we obtained two values for the moments at the nodal line ②. Consequently, their average values should be considered as amplitudes for the pertinent second derivatives of the basic function Y_n .

Although we used only a very crude discretization, in combination with a fairly difficult load and merely one term in the series expansion, the obtained maximum deflection of the plate shows only 6.4% error in comparison with a corresponding FEM solution. In this independent check, the conforming rectangular plate element with 16 DOF and a 2×2 subdivision were employed.

8.5 Summary and Conclusions

The *classical* FSM is a semianalytical, seminumerical technique for the analysis of plates. This approach is particularly suited to accurate and efficient solutions of single, rectangular Kirchhoff plates of simple boundary conditions subjected to quasi-regular transverse forces.

Since the FSM can also be mathematically classified as an energy approach, special attention must be paid to the selection of suitable shape functions, which greatly influences its convergence characteristics. The method utilizes series of orthogonal functions in the longitudinal direction combined with conventional beam functions in the transverse direction. By taking advantage of the orthogonality of the harmonic functions, the FSM yields a block diagonal structure of the assembled stiffness matrix, resulting in greatly simplified data manipulation and drastically reduced computer storage and running time with respect to other numerical methods. These advantageous characteristics of the FSM, combined with the fact that it transforms the two-dimensional plate problems into one-dimensional analysis, permit even the use of advanced scientific calculators in the solution of single plates.

Against the above-mentioned advantages of the classical FSM, however, the analyst must carefully weigh the following disadvantages before applying it:

1. Because of the semianalytical nature of the FSM, its mathematical requirements are generally higher than those for the other numerical techniques treated so far.

2. The method is not always quite transparent. Consequently, its study curve is steeper than usual.
3. If stiffness matrices and load vectors are not readily available in explicit forms, their computation by long hand requires elaborate differentiations and integrations of the shape functions. Symbolic mathematical programs such as MAPLE and MATHEMATICA[†], however, can eliminate much of these tedious computations. Generally, we need pertinent subroutines in our computer programs to generate these inputs.
4. The classical FSM is limited to rectangular plates and relatively simple boundary conditions.
5. Highly irregular loads are difficult, or even impossible, to handle.

Most of these limitations of the classical FSM, however, have been overcome by recent developments and extensions of the method. Now the FSM can deal effectively with circular and continuous plates, plates with arbitrary geometrical shapes, dynamic and stability plate problems, moderately thick plates, and so on. These advances are treated under Extensions of the Classical FSM in Sec. 10.3.

Problems[‡]

- 8.4.1.** Rework the Illustrative Example in Sec. 8.4 using a uniformly distributed load and three strips.
- 8.4.2.** A uniformly loaded square plate has fixed boundary conditions. Calculate the maximum deflection of the plate by using the FSM. Use three strips for the half plate and only one term in the series. Take the Poisson ratio $\nu = 0.3$.
- 8.4.3.** Repeat problem 8.4.2 for the next two terms.
- 8.4.4.** A simply supported rectangular plate with the side ratio of 1/1.5 carries a concentrated force at its midpoint. Calculate moments in the plate using the FSM. Assume that the Poisson ratio $\nu = 0.25$. Use only three-strip idealization and one term in the series expansion.
- 8.4.5.** Repeat problem 8.4.4, but assume that one side of the plate is fixed.
- 8.4.6.** Repeat problem 8.4.4, but assume a partially distributed lateral load that is symmetrically located with respect to the center of the plate.

[†] See References in Sec. 2.4.

[‡] The first two numbers refer to the corresponding section.

9

Boundary Element Method

9.1 Introduction

In recent years, a new numerical method has attracted much attention from applied mathematicians and mathematically inclined structural engineers. This currently emerging numerical solution technique—called the *boundary element method* (BEM)—proceeded from the highly mathematical theory of integral equations. The principal feature of the BEM is that the governing differential equation of plates (1.2.30) is transformed into a set of integral equations on the plate boundary and then these equations are discretized by introducing a finite number of elements located only on the boundary. Consequently, element approximations are made only at the boundary of the plate. At every interior point of the plate, the governing differential equation (1.2.30) is satisfied. Therefore, no interior discretization of the plate is required. In this way, the whole domain of the plate becomes large “finite element” (Fig. 9.1.1a). This leads to a considerable reduction of the unknowns and therefore to reduced computer time.

Although the BEM is now slowly gaining acceptance in structural analysis, it still remains mostly the providence of applied mathematicians and mathematically well trained engineers. The reason for its relatively modest gain in popularity among practicing engineers is partially well founded. That is, in spite of its mathematically elegant formulation, its practical implementation for plate analysis remains quite problematic. In addition, it is difficult write a computer program for the BEM.

Three formulations have been proposed for the BEM: direct, semidirect and indirect. These three types are derived in different way. In the direct formulation, the unknowns are real physical quantities such as displacement components. Mathematically, the direct BEM formulation, which is briefly presented here, can be classified as a special case of the *weighted residuals* technique [9.1.5]. In this case, the discretized boundary element equations are formulated with the help of the so-called *fundamental solution* of the plate differential equation, as discussed in the subsequent section.

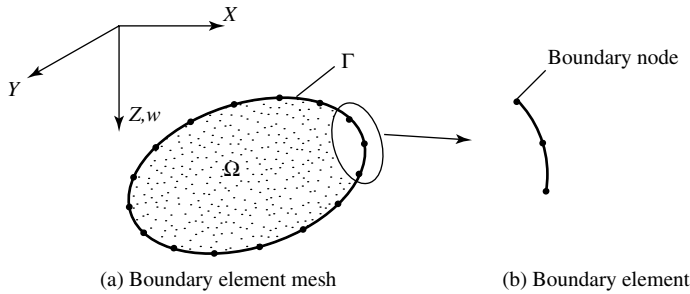


Figure 9.1.1 Discretization of plate boundary.

References and Bibliography

- [9.1.1] BREBBIA, C. A. (Ed.), *Recent Advances in Boundary Element Method, Proceedings of the First Conference on Boundary Element Methods*, Pentech Press, London, 1978.
- [9.1.2] BREBBIA, C. A., and WALKER, S., *Boundary Element Techniques in Engineering*, Newness-Butterworths, London, 1980.
- [9.1.3] BANERJEE, P. K., and BUTTERFIELD, R., *Boundary Element Methods in Engineering Science*, McGraw-Hill Book Co., London, 1981.
- [9.1.4] CHEN, C., and ZHOU, J., *Boundary Element Methods*, Academic Press, London, 1992.
- [9.1.5] BREBBIA, C. A., and DOMINGUEZ, J., *Boundary Elements: An Introductory Course*, 2nd ed., McGraw-Hill Book Co., New York, 1992.
- [9.1.6] BECKER, A. A., *The Boundary Element Method in Engineering*, McGraw-Hill Book Co., London, 1992.
- [9.1.7] BEER, G., and WATSON, J. O., *Introduction to Finite and Boundary Element Methods for Engineers*, John Wiley & Sons, New York, 1992.
- [9.1.8] KANE, J. H., *Boundary Element Analysis in Engineering Continuum Mechanics*, Prentice-Hall, Englewood Cliffs, New Jersey, 1994.
- [9.1.9] KYTHE, P. K., *An Introduction to Boundary Element Methods*, CRC Press, Boca Raton, Florida, 1995.
- [9.1.10] GAUL, L., and FIEDLER, C., *Methode der Randelemente in Statik und Dynamik*, Vieweg Verlag, Wiesbaden, 1997.

9.2 Basic Concepts of Boundary Element Method

To be able to apply the BEM, the *fundamental solution* of the governing differential equation must be known. The fundamental solution is represented by Green's function for infinite domain. By the Green's function we mean the solution of a linear partial differential equation whose nonhomogeneous term has been replaced by a product of delta functions, so as to represent the effect of a concentrated forcing function. Consequently, the fundamental solution is a function that satisfies the governing differential equation at every point of an infinite domain, except at one point called the *load* or *source point*. At this point the differential equation should exhibit singularity; that is, it will tend to become infinite.

Formulation of the direct BEM is based on the Maxwell-Betti reciprocal theorem, which describes the relationships between two distinct equilibrium states in an elastic

structure. This is the same theorem that is used in computation of influence lines and influence surfaces[†].

a. BEM Applied to Beams. To introduce the basic concepts of the BEM, we select first an elastic beam whose second-order differential equation is

$$\frac{d^2 w(x)}{dx^2} + \frac{M(x)}{EI} = 0. \quad (9.2.1)$$

The fundamental solution of this differential equation can be written as

$$w^*(x, y) = \frac{1}{2}|x - y|, \quad (9.2.2)$$

which represents the deflection of the beam at point x caused by the unit moment applied at point y .

Substitution of Eq. (9.2.2) into Eq. (9.2.1) gives

$$\frac{d^2 w^*(x, y)}{dx^2} + \delta(x, y) = 0, \quad (9.2.3)$$

where $\delta(x, y)$ is the Dirac delta function that can represent the concentrated unit moment with the fundamental property

$$\int_{-\infty}^{\infty} \delta(x, y) dx = 1. \quad (9.2.4)$$

In the direct BEM, we use an identity produced by multiplying Eq. (9.2.1) with the fundamental solution and integrate it over the span l of the beam. This gives

$$\int_0^l \left[\frac{d^2 w(x)}{dx^2} + \frac{M(x)}{EI} \right] w^*(x, y) dx = 0. \quad (9.2.5)$$

Carrying out the integration by parts and applying the property of the Dirac delta function, we obtain the following *boundary integral equation*:

$$\begin{aligned} w(y) &= [\theta(l)w^*(l, y) - w(l)\theta^*(l, y)] - [\theta(0)w^*(0, y) - w(0)\theta^*(0, y)] \\ &+ \int_0^l \frac{M(x)}{EI} w^*(x, y) dx, \end{aligned} \quad (9.2.6)$$

where

$$\theta(x) = \frac{dw(x)}{dx} \quad \text{and} \quad \theta^*(x, y) = \frac{dw^*(x, y)}{dx}. \quad (9.2.7)$$

Letting $y \mapsto 0$ and $y \mapsto l$ in Eq. (9.2.6), we obtain

$$\mathbf{A} \begin{Bmatrix} w(0) \\ \theta(0) \end{Bmatrix} + \mathbf{B} \begin{Bmatrix} w(l) \\ \theta(l) \end{Bmatrix} = \int_0^l \frac{1}{EI} \begin{Bmatrix} M(x)w^*(x, 0) \\ M(x)w^*(x, l) \end{Bmatrix} dx. \quad (9.2.8)$$

[†] See Sec. 10.5.

This equation, with known coefficient matrices **A** and **B**, provides two equations for the four boundary values $w(0)$, $\theta(0)$, $w(l)$ and $\theta(l)$. Since we can prescribe two of these boundary conditions, Eq. (9.2.8) can be solved for the remaining two. Consequently, solution of the boundary integral equation immediately yields the desired results at the boundary. In a similar manner, the results at the interior points can be obtained, but in this case the source point of the fundamental solution must be located at the interior point.

b. BEM Applied to Plates. An approach similar to the one used above for beams can be taken when the BEM is applied to plates. However, the corresponding formulation is far more complex. Essentially, the direct boundary element formulation for plates is based upon the same two theorems employed for beams: (a) a fundamental solution of the governing plate equation and (b) the Maxwell-Betti reciprocity theorem. In addition, however, a third theorem in the essence of Gauss-Green must also be applied. This theorem expresses an identity that relates an area integral of a derivative of a function to a line integral of that function around the boundary of that area.

To briefly introduce the reader to the inherently difficult formulation of the BEM as applied to plate bending problems, our short description here is partially based, with some appropriate modifications, on the paper written by Hu and Hartley [9.2.6]. This short summary should serve merely as an introduction illustrating the mathematical complexity of this type of numerical solution of plate problems. A more extensive discussion of the BEM would be outside the scope of this book. For further studies, the reader is referred to the references listed at the end of this and the previous section.

The plate deflection problem is governed by the already introduced plate equation (1.2.30):

$$D \nabla^4 w(x, y) = p(x, y). \quad (9.2.9)$$

The fundamental solution of this fourth-order partial differential equation is given as

$$w^*(P, Q) = \frac{r^2}{8\pi D} \ln(r), \quad (9.2.10)$$

where Q represents a field point and P denotes the source or load point where the unit load is acting (Fig. 9.2.1). The distance between these two points is r . In this case, the meaning of the fundamental solution is the deflection w^* at field point Q

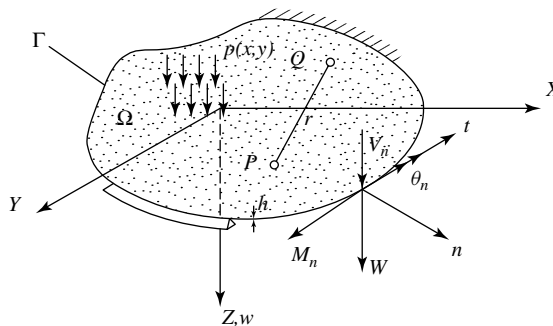


Figure 9.2.1 Relevant notation.

caused by the unit force acting at point P . By employing this fundamental solution of an infinite plate under unit concentrated force, the plate equation is transformed into

$$D \nabla^4 w^*(x, y) = \delta(P, Q), \quad (9.2.11)$$

where $\delta(\bullet)$ denotes, again, the Dirac *delta* function, which tends to approach infinity at point Q and is equal to zero anywhere else.

Next, we utilize the Gauss-Green identity for the biharmonic operator in the form

$$\iint_{\Omega} (u \nabla^4 v - v \nabla^4 u) d\Omega = \int_{\Gamma} \left(u \frac{\partial \nabla^2 v}{\partial n} - \frac{\partial u}{\partial n} \nabla^2 v - v \frac{\partial \nabla^2 u}{\partial n} + \frac{\partial v}{\partial n} \nabla^2 u \right) d\Gamma, \quad (9.2.12)$$

where u and v are two functions having fourth-order derivatives inside of the plate domain, Ω , and third-order derivatives at the boundary Γ . If $u = w$ and $v = w^*$, then we obtain

$$\begin{aligned} & \iint_{\Omega} w \delta(P, Q) d\Omega - \iint_{\Omega} p w^* d\Omega \\ &= D \int_{\Gamma} \left(w \frac{\partial \nabla^2 w^*}{\partial n} - \frac{\partial w}{\partial n} \nabla^2 w^* - w^* \frac{\partial \nabla^2 w}{\partial n} + \frac{\partial w^*}{\partial n} \nabla^2 w \right) d\Gamma. \end{aligned} \quad (9.2.13)$$

This equation represents the *general* integral equation of the plate bending problems. We want, however, to express Eq. (9.2.13) in terms of the normal moment M_n^* , equivalent shear force V_n^* and corner force T_i^* (Fig. 9.2.2) along the boundary corresponding to the fundamental solution given in Eq. (9.2.6). After some mathematical

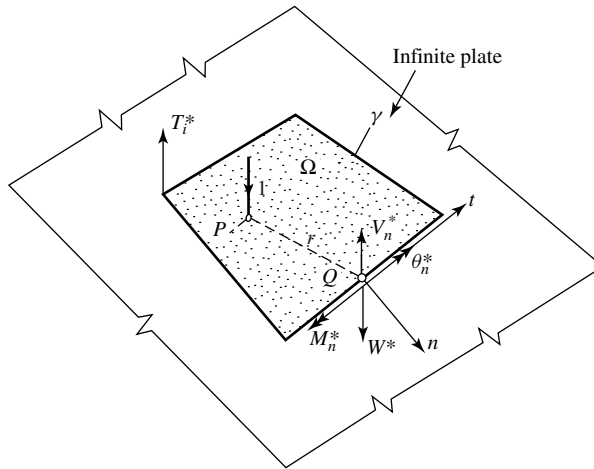


Figure 9.2.2 Fundamental solution.

manipulations, the following equation for the free boundary condition is obtained:

$$Cw(P) - \int_{\Gamma} (M_n^* \theta_n + V_n^* W) d\Gamma - \sum_{i=1}^{N_c} W_i T_i^* = \iint_{\Omega} pw^* d\Omega, \quad (9.2.14)$$

where W , θ_n are deflections and normal rotations, respectively, along the plate boundary and N_c represents the number of boundary corners. Furthermore, the factor C in this equation equals unity if the point P is located inside the plate domain and zero if P is located outside of it. The plate deflection at point P is represented by $w(P)$.

In this formulation of the integral equation, the deflections W and normal rotations at the boundary θ_n are the unknowns. Consequently, for two unknowns to be determined, we need two boundary integral equations: One is the fundamental equation (9.2.14) and the other one is a complementary equation obtained by differentiating the fundamental equation with respect to the boundary normal n at point P . This gives

$$C \frac{\partial w(P)}{\partial n} - \int_{\Gamma} \left(\frac{\partial M_n^*}{\partial n} \theta_n + \frac{\partial V_n^*}{\partial n} W \right) d\Gamma - \sum_{i=1}^{N_c} W_i \frac{\partial T_i^*}{\partial n} = \iint_{\Omega} p \frac{\partial w^*}{\partial n} d\Omega, \quad (9.2.15)$$

where $\partial w(P)/\partial n$ is the normal rotation at point P .

Equations (9.2.14) and (9.2.15) represent the integral formulation of the free boundary condition of the plate. The obvious approach for their solution would be to integrate them analytically. Since analytical integrations are not feasible because of their complexity, we must resort to numerical solution techniques. To be able to solve these two boundary integral equations numerically, however, discretization of the plate boundary is required. The discretization should start from some corner point with jumps in the boundary curvature forming a number of boundary segments. One of the strengths of the BEM is a theoretically unlimited choice of boundary elements. The most common types, however, are constant, linear, quadratic and some higher-order elements. In Fig. 9.2.3 a few boundary elements with appropriate number of nodes—as used in discretization of the boundary—are shown. The unknown functions within each boundary element are the boundary displacements $W(\Gamma)$ and normal boundary rotations $\theta(\Gamma)_n$. Within each element these unknown functions

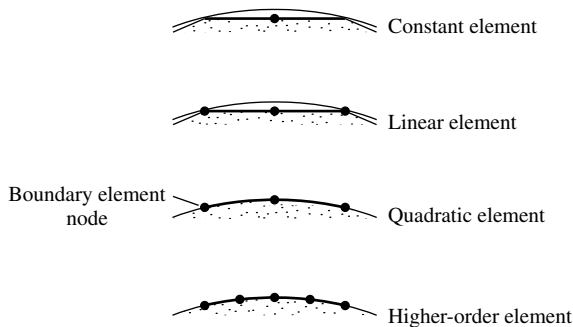


Figure 9.2.3 Different types of boundary elements.

are usually approximated by polynomials. In our case, we use the Lagrange-type shape function.

After the boundary is discretized into boundary elements and the boundary functions are interpolated, the problem reduces to the task to determine the nodal values of the unknown functions. Consequently, the integral equations (9.2.14) and (9.2.15) become

$$Cw(P) - \sum_{i=1}^{N_e} \sum_{j=1}^{N_i} \left[\int_{\Gamma_i} M_n^* L_{ij}(\Gamma) d\Gamma \right] \theta_{nij} - \sum_{i=1}^{N_e} \sum_{j=1}^{N_i} \left[\int_{\Gamma_i} V^* L_{ij}(\Gamma) d\Gamma \right] W_{ij} - \sum_{i=1}^{N_e} W_i T_i^* = \iint_{\Omega} p w^* d\Omega \quad (9.2.16)$$

and

$$C \frac{\partial w(P)}{\partial n} - \sum_{i=1}^{N_e} \sum_{j=1}^{N_i} \left[\int_{\Gamma_i} \frac{\partial M_n^*}{\partial n} L_{ij}(\Gamma) d\Gamma \right] \theta_{nij} - \sum_{i=1}^{N_e} \sum_{j=1}^{N_i} \left[\int_{\Gamma_i} \frac{\partial V^*}{\partial n} L_{ij}(\Gamma) d\Gamma \right] W_{ij} - \sum_{i=1}^{N_e} W_i \frac{\partial T_i^*}{\partial n} = \iint_{\Omega} p \frac{\partial w^*}{\partial n} d\Omega, \quad (9.2.17)$$

where N_e is the number of boundary elements, N_i is the number of nodes within the i th element, L_{ij} represents the *Lagrangian* shape function and W_{ij} , θ_{nij} are the unknown values at the boundary nodes j of the boundary element i .

After the analytical evaluation of the integrals in this equation, we obtain a set of algebraic equations

$$\mathbf{A}\mathbf{x} = \mathbf{b}, \quad (9.2.18)$$

where the coefficient matrix \mathbf{A} depends only on geometrical and material parameters. The column matrix \mathbf{x} contains the unknown boundary values, and the applied loads are represented by the vector \mathbf{b} . It should be noted that the fully populated coefficient matrix \mathbf{A} is unsymmetric.

Once the boundary values are determined, we can compute the internal stress resultants m_x , m_y and m_{xy} of the plate. For this purpose Eq. (9.2.14) is rewritten using $C = 1$. This gives the expression of the plate deflection at point P . The curvatures required for the computation of the internal moments[†] are obtained from

$$\begin{Bmatrix} \frac{\partial^2 w}{\partial x^2} \\ \frac{\partial^2 w}{\partial y^2} \\ \frac{\partial^2 w}{\partial x \partial y} \end{Bmatrix} = \iint_{\Omega} \begin{Bmatrix} \frac{\partial^2 w^*}{\partial x^2} \\ \frac{\partial^2 w^*}{\partial y^2} \\ \frac{\partial^2 w^*}{\partial x \partial y} \end{Bmatrix} p d\Omega + \sum_{i=1}^{N_e} \sum_{j=1}^{N_i} \left[\int_{\Gamma_i} \begin{Bmatrix} \frac{\partial^2 M_n^*}{\partial x^2} \\ \frac{\partial^2 M_n^*}{\partial y^2} \\ \frac{\partial^2 M_n^*}{\partial x \partial y} \end{Bmatrix} L_{ij}(\Gamma) d\Gamma \right] \theta_{nij}$$

[†] See Sec. 1.2.

$$+ \sum_{i=1}^{N_e} \sum_{j=1}^{N_i} \left[\int_{\Gamma_i} \begin{Bmatrix} \frac{\partial^2 V_n^*}{\partial x^2} \\ \frac{\partial^2 V_n^*}{\partial y^2} \\ \frac{\partial^2 V_n^*}{\partial x \partial y} \end{Bmatrix} L_{ij}(\Gamma) d\Gamma \right] W_{ij} + \sum_{i=1}^{N_e} W_i \begin{Bmatrix} \frac{\partial^2 T_i^*}{\partial x^2} \\ \frac{\partial^2 T_i^*}{\partial y^2} \\ \frac{\partial^2 T_i^*}{\partial x \partial y} \end{Bmatrix} \quad (9.2.19)$$

c. Concluding Remarks. Recently, the BEM has emerged as a powerful numerical method in engineering applications. Although the principles of the BEM are mathematically elegant, its practical implementation remains highly problematic. Its accuracy depends largely upon the choice of load points, which is usually beyond the competence of the average user. Furthermore, it is difficult to automate the required procedures within a computer program. As was shown in this section, there are many of complexities in the analysis that require considerable simplifications before the BEM will be as enthusiastically accepted by structural engineers as the FEM for numerical analysis of plates. Until such simplification occurs, the BEM remains mostly the tool of mathematically well versed research engineers.

References and Bibliography

- [9.2.1] TOTTENHAM, H., "The Boundary Element Method for Plates and Shells", in Banerjee, P. K., and Butterfield, R. (Eds.), *Developments in Boundary Element Method Applied Science*, London, 1979.
- [9.2.2] ALERCÓN, E., and PARIS, F., "Boundary Elements in Potential and Elasticity Theory," *Comp. Struct.*, 10 (1979), 351–362.
- [9.2.3] DU, Q., YAO, Z., and SONG, G., "Solution of Some Plate Bending Problems Using the Boundary Element Method," *Appl. Math. Modeling*, 8 (1984), 15–22.
- [9.2.4] HARTMANN, F., and ZOTEMANTEL, R., "The Direct Boundary Element Method in Plate Bending," *Int. J. Num. Meth. Eng.*, 23 (1986), 2049–2069.
- [9.2.5] YE, T. Q., and LIU, Y., "Finite Deflection Analysis of Elastic Plates by Boundary Element Method," *Appl. Math. Modeling*, 9 (1985), 183–188.
- [9.2.6] HU, C., and HARTLEY, G. A., "Analysis of a Thin Plate on Elastic Half-Space," *Comp. Struct.*, 52 (1994), 227–235.
- [9.2.7] EL-ZARANY, A., FADHIL, S., and DEBBIH, M., "An Efficient Approach for Boundary Element Bending Analysis of Thin and Thick Plates," *Comp. Struct.*, 56 (1995), 565–576.
- [9.2.8] BINGNAN, S., JINCHUN, T., and YUYIN, X., "A New Off-Boundary Element Method for Analyzing Plate and Shallow Shell Bending," *Comp. Struct.*, 60 (1996), 297–304.
- [9.2.9] ALIABADI, M. H. (Ed.), *Plate Bending Analysis with Boundary Elements*, Computational Mechanics, Billerica, Massachusetts, 1998.
- [9.2.10] JAWSON, M. A., and MAITI, M., "An Integral Equation Formulation of Plate Bending Problems," *J. Eng. Mat.*, 2 (1968), 83–93.
- [9.2.11] WU, B. C., and ALTIERO, N. J., "A Boundary Integral Method Applied to Plates of Arbitrary Plan Form and Arbitrary Boundary Conditions," *Comp. Struct.*, 10 (1979), 703–707.
- [9.2.12] BENZINE, G., "Boundary Integral Formulation for Plate Flexure with Arbitrary Boundary Conditions," *Mech. Res. Commun.*, 5 (1978), 197–206.
- [9.2.13] STERN, M., "A General Boundary Integral Formulation for the Numerical Solution of Plate Bending Problems," *Int. J. Solids Struct.*, 15 (1979), 769–782.

- [9.2.14] KATSIKADELIS, J. T., and ARMENAKAS, A. E., "Plates on Elastic Foundation by BTE Method," *J. Eng. Mech. Div., ASCE*, 110 (1984), 1086–1105.
- [9.2.15] ALIABADI, M. M. (Ed.), *Plate Bending Analysis with Boundary Elements*, WIT Press, Southampton, United Kingdom, 1998.
- [9.2.16] RASHED, Y. F., *Boundary Element Formulation for Thick Plates*, WIT Press, Southampton, United Kingdom, 1999.

Part III

Advanced Topics

10

Linear Considerations

10.1 Orthotropic Plates

a. General Concepts. In the preceding chapters of this book, it was always assumed that the plate material is homogeneous and isotropic in all directions. In many practical applications of plate structures, however, it is often necessary to consider directional-dependent bending stiffness. If the structural properties of the plate differ in two mutually perpendicular directions, the plate is described as orthogonally anisotropic or, in short, *orthotropic*. Such *structural* anisotropy can be introduced by ribs, corrugations or beam stiffeners (Fig. 10.1.1a), to name a few. In some other cases, the structural material itself is inherently orthotropic. Two-way reinforced-concrete slabs are prime examples of such *natural* anisotropy.

Orthotropic plate structures are very common in present-day engineering. In architectural engineering, for instance, reinforced-concrete slabs with one-way or two-way joists are often used for floor systems in buildings. In civil engineering, the high-way bridge decks usually consist of plates stiffened with rectangular, triangular or trapezoidal ribs. The use of stiffened plates is especially indispensable in ship and aerospace structures. That is, the hull of a ship, its deck, its bottom and superstructure (Fig. 1.2b) may be considered as orthotropic plates. Similarly, in flight structures the wings and fuselage consist of skin with an array of stiffening ribs (Fig. 1.2c).

Although the actual structural behavior of plate stiffener assemblies cannot completely be replaced by that of orthotropic plates, experimental data indicate good agreement with such idealization, provided that the relatively small stiffeners are uniform and closely spaced. The basic idea of this approximation is to convert the stiffened plate into an equivalent orthotropic plate by “smearing out” the stiffeners. Such an approximation, however, cannot be justified if the stiffeners are large (Fig. 10.1.2). In this case, the FEM may be used for the analysis of such a plate-grid structure subjected to lateral loading. The plate should be independently divided into elements, and the corresponding stiffeners must be treated as beam elements with *imposed compatibility* along the lines of beam-plate junctions. Another—probably more economical approach—uses macro-plate-beam elements. The stiffness matrix of such an assembly can be computed by applying the engineering approach already demonstrated in connection with gridwork cells (Sec. 6.3). Consequently, the stiffness coefficients of such large elements can be computed by superimposing the already

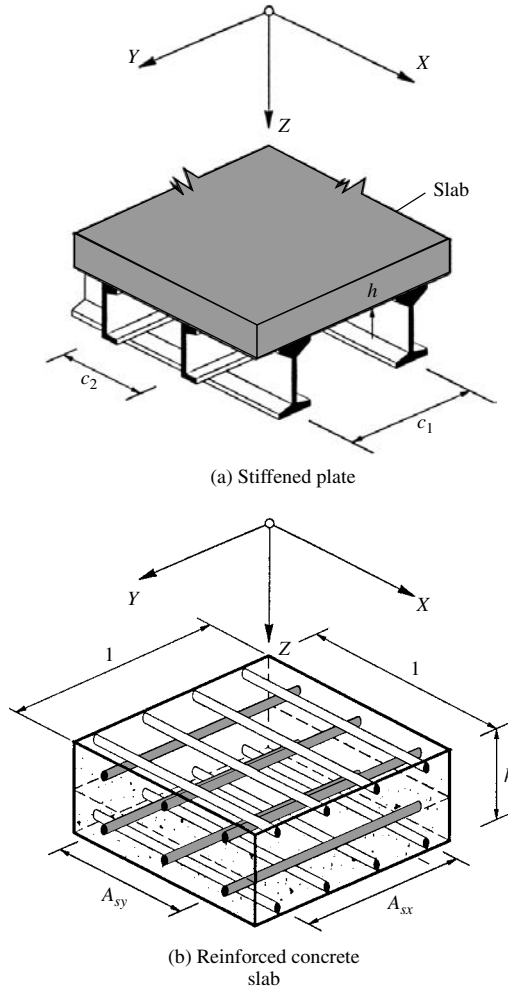


Figure 10.1.1 Examples of structural and natural orthotropy.

available plate and beam stiffness coefficients. Again, compatibility along the lines of beam-plate junctions must be maintained by using appropriate element stiffness matrices.

b. Theory. In the derivation of Kirchhoff's small-deflection plate theory, the number of independent elastic constants was two (E, ν). If we assume that the principal directions of orthotropy coincide with the X and Y coordinate axes, it becomes evident that four elastic constants (E_x, E_y, ν_x, ν_y) are required for the description of the orthotropic stress-strain relationships:

$$\varepsilon_x = \frac{\sigma_x}{E_x} - \nu_y \frac{\sigma_y}{E_y}, \quad \varepsilon_y = \frac{\sigma_y}{E_y} - \nu_x \frac{\sigma_x}{E_x}, \quad \gamma = \frac{\tau}{G_{xy}}, \quad (10.1.1)$$

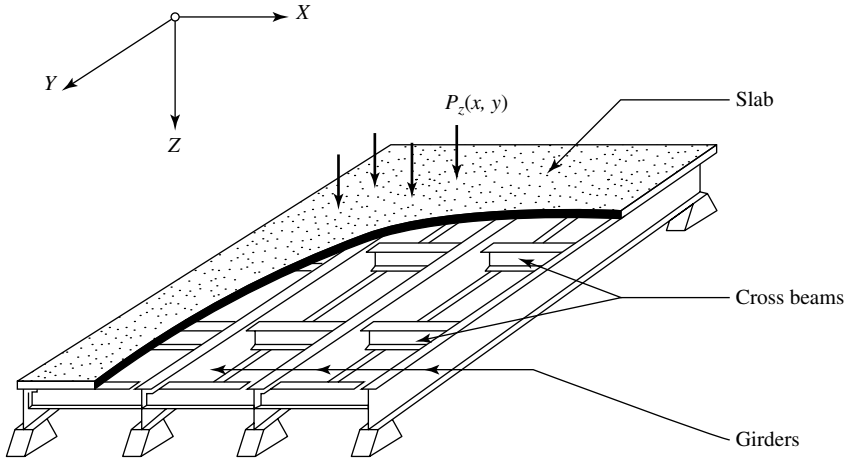


Figure 10.1.2 Plate-grid assembly.

where the shear modulus G_{xy} of the orthotropic material can be expressed in terms of E_x and E_y as follows:

$$G_{xy} \approx \frac{\sqrt{E_x E_y}}{2(1 + \sqrt{\nu_x \nu_y})} \approx \frac{E}{2(1 + \sqrt{\nu_x \nu_y})}.$$

Solving Eq. (10.1.1) for σ_x , σ_y and τ , we find

$$\begin{aligned} \sigma_x &= \frac{E_x}{1 - \nu_x \nu_y} (\varepsilon_x + \nu_y \varepsilon_y), \\ \sigma_y &= \frac{E_y}{1 - \nu_x \nu_y} (\varepsilon_y + \nu_x \varepsilon_x), \\ \tau &= G_{xy} \gamma. \end{aligned} \quad (10.1.2)$$

Next, we express the strains in terms of the lateral deflection, as described in Sec. 1.2. The substitution of these relations into Eqs. (1.2.22) and (1.2.23) gives

$$\begin{aligned} m_x &= -D_x \left(\frac{\partial^2 w}{\partial x^2} + \nu_y \frac{\partial^2 w}{\partial y^2} \right), \\ m_y &= -D_y \left(\frac{\partial^2 w}{\partial y^2} + \nu_x \frac{\partial^2 w}{\partial x^2} \right), \\ m_{xy} &= -2D_t \frac{\partial^2 w}{\partial x \partial y}, \end{aligned} \quad (10.1.3)$$

where

$$D_x = \frac{E_x h^3}{12(1 - \nu_x \nu_y)} \quad \text{and} \quad D_y = \frac{E_y h^3}{12(1 - \nu_x \nu_y)} \quad (10.1.4a)$$

are the flexural rigidities of the orthotropic plate, while

$$2D_t = (1 - \sqrt{\nu_x \nu_y}) \sqrt{D_x D_y} = (1 - \nu_{xy}) D_{xy} \quad (10.1.4b)$$

represents its torsional rigidity. For an orthotropic plate of uniform thickness, the torsional rigidity can be written as

$$D_t = G_{xy} \frac{h^3}{12}. \quad (10.1.5)$$

The substitution of Eq. (10.1.3) into the equilibrium equation of a plate element (1.2.9) yields the governing differential equation of orthotropic plates[†]:

$$\boxed{D_x \frac{\partial^4 w}{\partial x^4} + 2B \frac{\partial^4 w}{\partial x^2 \partial y^2} + D_y \frac{\partial^4 w}{\partial y^4} = p_z(x, y),} \quad (10.1.6)$$

where

$$B = \frac{1}{2}(\nu_y D_x + \nu_x D_y + 4D_t) \quad (10.1.7)$$

is called the *effective torsional rigidity* of the orthotropic plate. Based on Betti's reciprocal theorem, we can write

$$\nu_x E_y = \nu_y E_x \quad \text{or} \quad \nu_x D_y = \nu_y D_x; \quad (10.1.8)$$

therefore, another form for Eq. (10.1.7) is

$$B = \nu_x D_y + 2D_t = \nu_y D_x + 2D_t \approx \nu_{xy} D_{xy} + 2D_t. \quad (10.1.9)$$

Equation (10.1.8) can be used to determine the Poisson ratios due to structural orthotropy. It should be pointed out that in the latter case ν_y and ν_x are not material properties, but rather are elastic constants corresponding to the geometrical configuration of the structural system.

By substituting Eq. (10.1.3) into Eqs. (1.2.5) and (1.2.6), we find the shear forces:

$$\begin{aligned} q_x &= -\frac{\partial}{\partial x} \left(D_x \frac{\partial^2 w}{\partial x^2} + B \frac{\partial^2 w}{\partial y^2} \right), \\ q_y &= -\frac{\partial}{\partial y} \left(D_y \frac{\partial^2 w}{\partial y^2} + B \frac{\partial^2 w}{\partial x^2} \right). \end{aligned} \quad (10.1.10)$$

Similarly, the expressions of the lateral edge forces (1.3.3) become

$$\begin{aligned} v_x &= -D_x \left[\frac{\partial^3 w}{\partial x^3} + \left(\frac{4D_t}{D_x} + \nu_y \right) \frac{\partial^3 w}{\partial x \partial y^2} \right], \\ v_y &= -D_y \left[\frac{\partial^3 w}{\partial y^3} + \left(\frac{4D_t}{D_y} + \nu_x \right) \frac{\partial^3 w}{\partial x^2 \partial y} \right]. \end{aligned} \quad (10.1.11)$$

[†] Often called *Huber's equation* [10.1.3].

If the orthotropic plate is subjected to simultaneous bending and stretching, the governing equation of equilibrium of the isotropic case should also be modified,

$$D_x \frac{\partial^4 w}{\partial x^4} + 2B \frac{\partial^4 w}{\partial x^2 \partial y^2} + D_y \frac{\partial^4 w}{\partial y^4} = p_z(x, y) + n_x \frac{\partial^2 w}{\partial x^2} + 2n_{xy} \frac{\partial^2 w}{\partial x \partial y} + n_y \frac{\partial^2 w}{\partial y^2}, \quad (10.1.12)$$

which will be used in Sec. 16.7 for the elastic stability analysis of orthotropic plates.

The nonlinear differential equations of the large-deflection orthotropic plate theory can be derived in a manner analogous to isotropic plates, with the exception that, in this case, the orthotropic stress-strain relationships (10.1.2) are valid. The governing equations, deduced by Rostovtsev [10.1.5], are

$$\frac{D_x}{h} \frac{\partial^4 w}{\partial x^4} + 2 \frac{B}{h} \frac{\partial^4 w}{\partial x^2 \partial y^2} + \frac{D_y}{h} \frac{\partial^4 w}{\partial y^4} = \frac{\partial^2 \Phi}{\partial y^2} \frac{\partial^2 w}{\partial x^2} - 2 \frac{\partial^2 \Phi}{\partial x \partial y} \frac{\partial^2 w}{\partial x \partial y} + \frac{\partial^2 \Phi}{\partial x^2} \frac{\partial^2 w}{\partial y^2} + \frac{p_z}{h} \quad (10.1.13a)$$

and

$$\frac{1}{E_y} \frac{\partial^4 \Phi}{\partial x^4} + \left(\frac{1}{G_{xy}} - 2 \frac{\nu_x}{E_x} \right) \frac{\partial^4 \Phi}{\partial x^2 \partial y^2} + \frac{1}{E_x} \frac{\partial^4 \Phi}{\partial y^4} = \left(\frac{\partial^2 w}{\partial x \partial y} \right)^2 - \frac{\partial^2 w}{\partial x^2} \frac{\partial^2 w}{\partial y^2}. \quad (10.1.13b)$$

The more rigorous differential equation of the orthogonally stiffened plate [10.1.4, 10.1.18] is

$$D_1 \frac{\partial^8 w}{\partial x^8} + D_2 \frac{\partial^8 w}{\partial x^6 \partial y^2} + D_3 \frac{\partial^8 w}{\partial x^4 \partial y^4} + D_4 \frac{\partial^8 w}{\partial x^2 \partial y^6} + D_5 \frac{\partial^8 w}{\partial y^8} = p_z(x, y), \quad (10.1.14)$$

where the constants D_1, \dots, D_5 express the elastic rigidities of the plate and stiffeners.

c. Determination of Principal Flexural Rigidities. Since the accuracy of the analysis of orthotropic plates depends, to a large extent, on the expressions used for the sectional properties, direct tests, if possible, should be applied to determine the actual flexural and torsional rigidities. Of these, the value of the torsional rigidity is usually the most difficult to obtain. Based on certain analytic considerations, however, reasonable approximations can be introduced. In determining these values, it should always be kept in mind that all sectional properties are defined per unit length.

A suitable formula for the effective torsional rigidity of two-way reinforced-concrete slabs of uniform thickness is

$$B = \sqrt{D_x D_y}. \quad (10.1.15)$$

If a *reinforced-concrete, slab-girder* configuration (Fig. 10.1.3) should be approximated by an *equivalent* isotropic plate, the flexural rigidities can be defined by

$$D_x = \frac{EI_x}{c_1} \quad (10.1.16a)$$

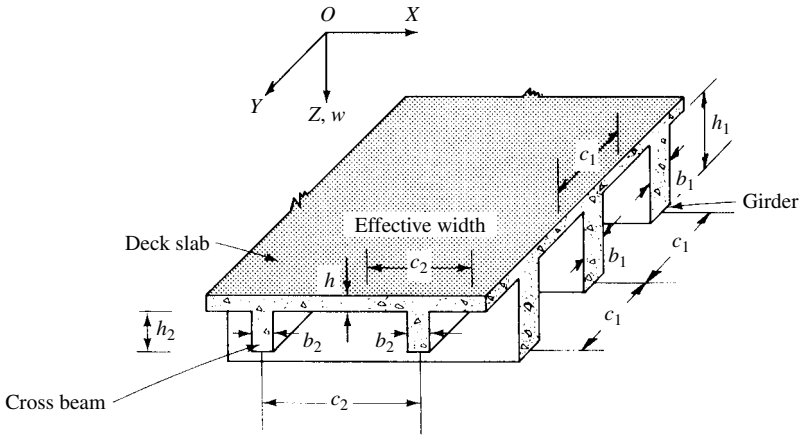


Figure 10.1.3 Reinforced-concrete slab stiffened by orthogonal ribs.

and

$$D_y = \frac{EI_y}{c_2}, \quad (10.1.16b)$$

where I_x and I_y are the moments of inertia of the section with respect to the neutral axis[†] and c_1 and c_2 denote the spacing of the beams. For more rigorous calculation the portion of the cross section formed by the slab should be divided by[‡] $1 - \nu_{xy}^2$. For the effective width of the T sections the use of c_1 and c_2 beam spacings (instead of their code values) is recommended.

In calculating the effective torsional rigidity of such a deck-girder assemblage (Fig. 10.1.3), we usually separate the beam and slab portions; thus

$$B = \frac{Eh^3}{12(1 - \nu_{xy}^2)} + \frac{G_{xy}}{2} \left(\frac{h_1 b_1^3 \eta_1}{c_1} k_1 + \frac{h_2 b_2^3 \eta_2}{c_2} k_2 \right), \quad (10.1.17)$$

where η_i is a numerical factor depending on the ratio h_i/b_i . Some values of η_i are:

h_i/b_i	1.0	1.2	1.5	2.0	2.5	3.0	4.0	6.0	8.0	10.0	∞
η_i	0.140	0.166	0.196	0.229	0.249	0.263	0.281	0.299	0.307	0.313	0.333

Since the torsional rigidities of reinforced-concrete beams are, in general, considerably diminished after cracks have been developed in the concrete [10.1.23], it is recommended that the terms representing the beam portions in Eq. (10.1.17) should be reduced. The magnitude of such a reduction factor, k_i , depends on the reinforcing h_i/b_i ratio and on the ratio of the torsional moment to the simultaneously acting bending moment. Research on this subject has been carried out at the University

[†] For moments of inertia the same subscript notation is used as for flexural rigidities and internal forces (see Sec. 1.2).

[‡] $\nu_{xy}^2 = \nu_x \nu_y$.

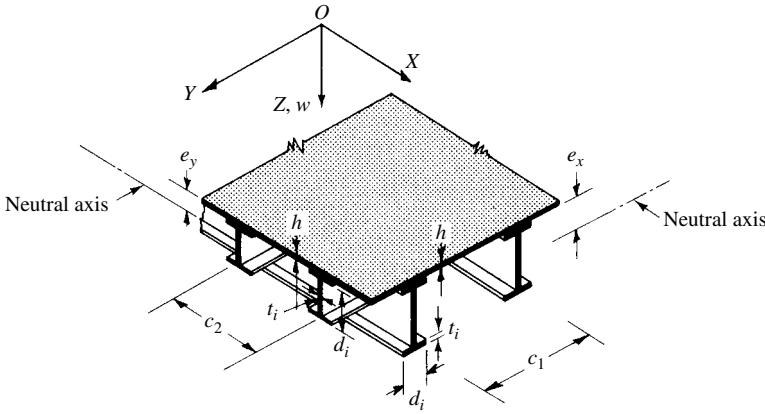


Figure 10.1.4 Steel deck-plate.

of Stuttgart (F. Leonhardt) and at the Swiss Federal Institute of Technology, Zurich (B. Thürlimann).

A similar approach can be used for estimating the equivalent sectional properties of *steel deck plates* (Fig. 10.1.4). In this case the flexural properties can be expressed as

$$D_x = \frac{Eh^3}{12(1 - \nu_{xy}^2)} + \frac{Ehe_x^2}{1 - \nu_{xy}^2} + \frac{EI_{0x}}{c_1}, \quad (10.1.18)$$

$$D_y = \frac{Eh^3}{12(1 - \nu_{xy}^2)} + \frac{Ehe_y^2}{1 - \nu_{xy}^2} + \frac{EI_{0y}}{c_2}, \quad (10.1.19)$$

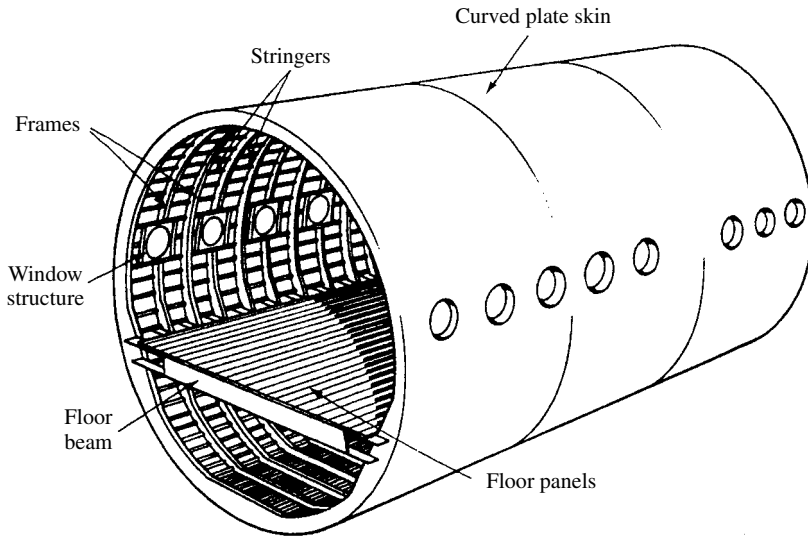
$$B = \frac{Eh^3}{12(1 - \nu_{xy}^2)} + \frac{G_{xy}}{6} \left(\frac{\sum d_t t_t^3}{c_1} + \frac{\sum d_t t_t^3}{c_2} \right), \quad (10.1.20)$$

where I_{0x} and I_{0y} denote the moments of inertia of the stiffeners with respect to their neutral axis in the X and Y directions, respectively, while e_x and e_y represent the distance of the neutral axes from the middle plane of the plate. These formulas can also be used for composite (i.e., concrete-steel; Fig. 10.1.5b) deck slabs by transforming the concrete part of the section into an equivalent steel plate.

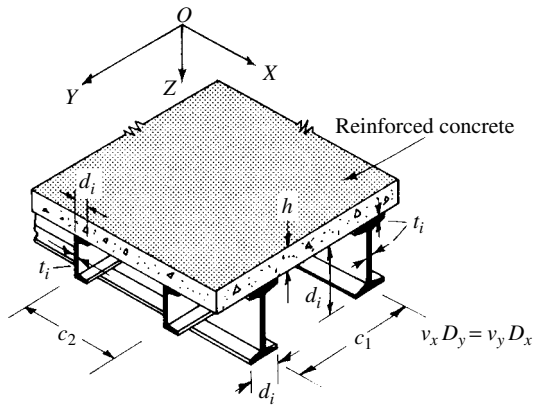
If *open gridworks* (Fig. 10.1.6a) are to be approximated by an equivalent orthotropic plate, provided that the parallel beams are closely spaced at equal distances, the use of the following sectional properties is recommended:

$$D_x = \frac{EI_x}{c_1}, \quad D_y = \frac{EI_y}{c_2} \quad \text{and} \quad B = \frac{G_{xy}}{2} \left(\frac{I_{tx}}{c_1} + \frac{I_{ty}}{c_2} \right), \quad (10.1.21)$$

where I_x , I_y , I_{tx} and I_{ty} represent the moments of inertia and the geometrical torsional rigidities of the beams. In this case we have assumed that $\nu_{xy} D_{xy} = 0$. This assumption is justified, since there is no slab between the beams.



(a) Flight structure

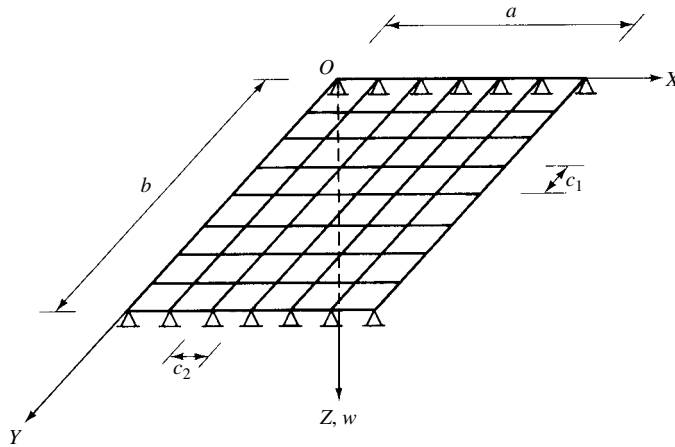
(b) Composite beam gridwork
(close spacings)**Figure 10.1.5** Typical orthotropic plate structures.

For *corrugated plates* made of isotropic materials with corrugation in the X direction, as shown in Fig. 10.1.6b, the principal rigidities can be estimated from

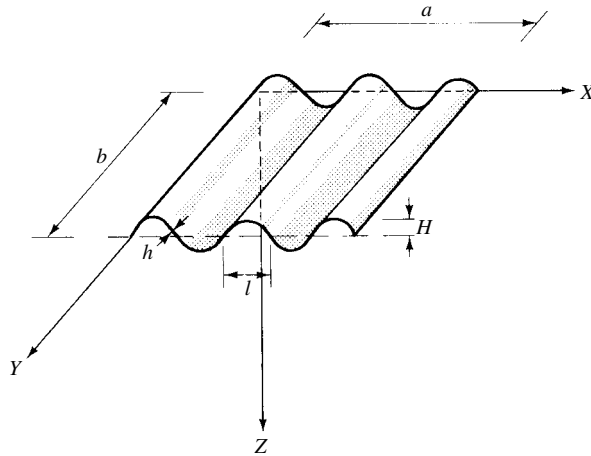
$$D_x = \frac{l}{s} \frac{Eh^3}{12(1-\nu^2)}, \quad D_y = EI, \quad B = \frac{s}{l} \frac{Eh^3}{12(1+\nu^2)}, \quad (10.1.22)$$

where

$$s = l \left(1 + \frac{\pi^2 H^2}{4l^2} \right) \quad \text{and} \quad I = 0.5H^2h \left[1 - \frac{0.81}{1 + 2.5(H/2l)^2} \right]. \quad (10.1.23)$$



(a) Closely spaced open gridwork



(b) Corrugated plate

Figure 10.1.6 Orthotropic plate approximations.

d. Analysis Procedures. Most analytical and numerical solution techniques already introduced in the previous chapters for isotropic plates can be logically applied to the solutions of orthotropic plate problems. Simply supported rectangular orthotropic plates, for instance, can be conveniently analyzed by Navier's method. Similarly, Lévy's solution can be used for rectangular orthotropic plates that are simply supported on two opposite sides and arbitrarily supported on the two opposite sides. Since the governing differential equation for orthotropic plates is available, Galerkin's variational technique can be readily applied to almost any boundary condition of rectangular orthotropic plates. The required procedure remains the same as described in Sec. 4.3 for isotropic plates.

If the plate geometry and its boundary and loading conditions are quite arbitrary, numerical methods must be used. The extension of the *ordinary finite difference*

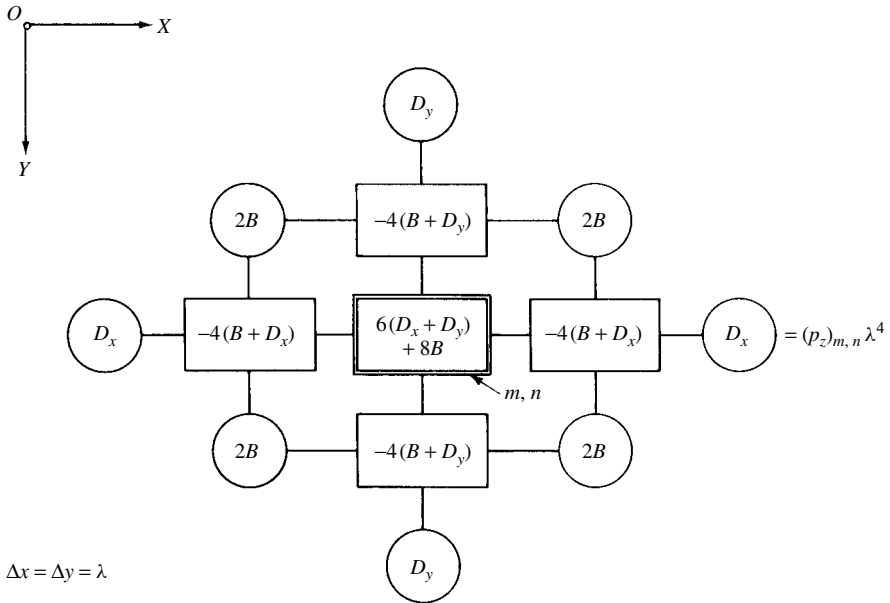


Figure 10.1.7 Coefficient pattern for finite difference expression of orthotropic plate equation (10.1.6).

method to orthotropic plates is straightforward. The corresponding coefficient pattern is given in Fig. 10.1.7. Simply supported and fixed boundary conditions can be treated as described in Sec. 5.1d. For the more difficult case of free edge, a readily usable stencil is provided in Fig. 10.1.8.

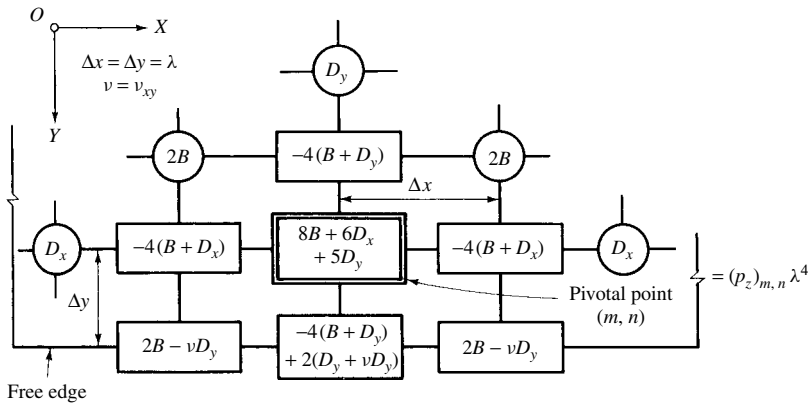
By its very nature, the *gridwork method* discussed in Chapter 6 is well suited for the analysis of many orthotropic plate problems. The analysis procedure is identical with that already discussed in Chapter 6. Let us now consider an orthotropic gridwork cell shown in Fig. 10.1.9. The required equivalent sectional properties were obtained by equating the strain energy of the orthotropic plate element with that of the beams of the gridwork cell [10.1.32]. This resulted in

$$\begin{aligned} I_{AB} = I_{CD} &= \frac{D_x}{2E_x} b, & I_{AC} = I_{BD} &= \frac{D_y}{2E_y} a, \\ J_{AB} = J_{CD} &= \frac{D_t}{G} b, & J_{AC} = J_{BD} &= \frac{D_t}{G} a. \end{aligned} \quad (10.1.24)$$

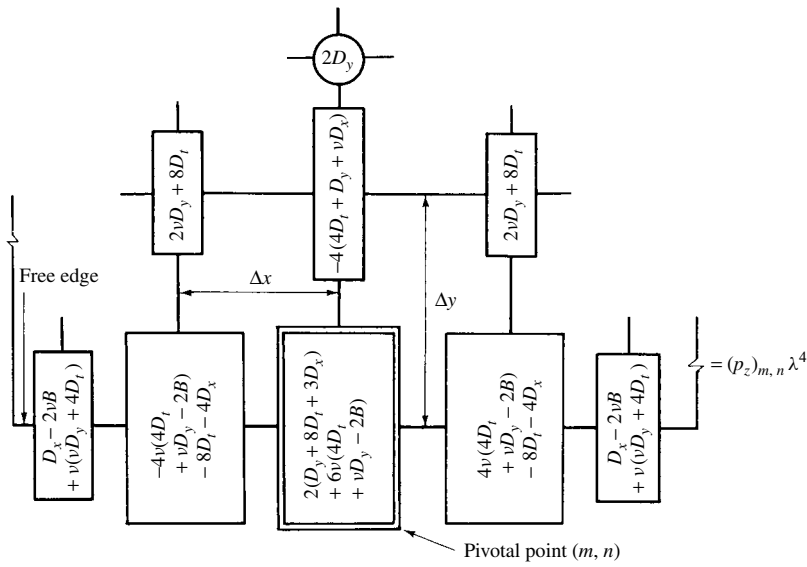
One can use these values in combination with any commercially available computer program developed for grillage analysis.

The stiffness matrix of a somewhat more complex gridwork was derived by Hussein and Morsi [10.1.32]. Although working with this gridwork cell requires more computational effort, it provides rapid convergence and satisfactory accuracy (Fig. 10.1.10).

The *finite element method* treated extensively in Chapter 7 can also be extended to orthotropic plates without any additional difficulty by using appropriate orthotropic stress-strain relationships. For a rectangular plate element in which the local coordinate directions coincide with the principal directions of orthotropy, we rewrite



(a) Point adjacent to free edge



(b) Point on free edge

Figure 10.1.8 Stencils for free edge.

Eq. (7.2.6) as

$$k_{ij} = \iint \left\{ \begin{array}{c} \frac{\partial^2 w_i}{\partial x^2} \\ \frac{\partial^2 w_i}{\partial y^2} \\ \frac{\partial^2 w_i}{\partial x \partial y} \end{array} \right\}^T \left[\begin{array}{ccc} D_x & D_1 & 0 \\ D_1 & D_y & 0 \\ 0 & 0 & D_t \end{array} \right] \left\{ \begin{array}{c} \frac{\partial^2 w_j}{\partial x^2} \\ \frac{\partial^2 w_j}{\partial y^2} \\ \frac{\partial^2 w_j}{\partial x \partial y} \end{array} \right\} dA, \quad (10.1.25)$$

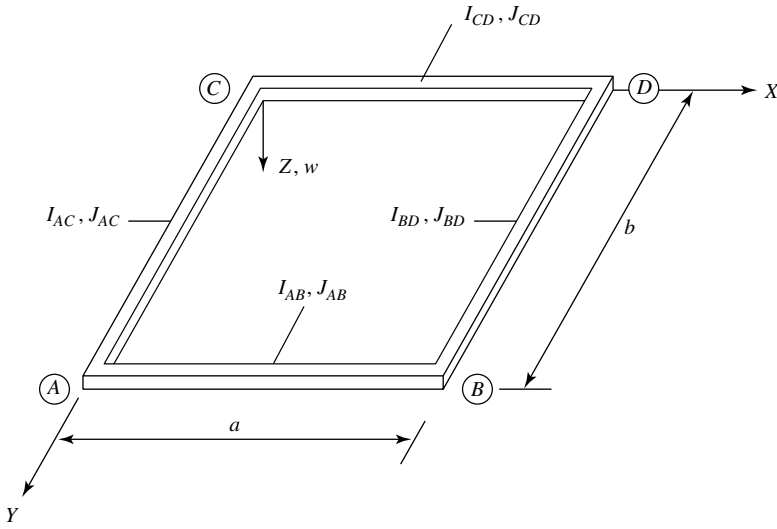


Figure 10.1.9 Gridwork for analysis of orthotropic plates.

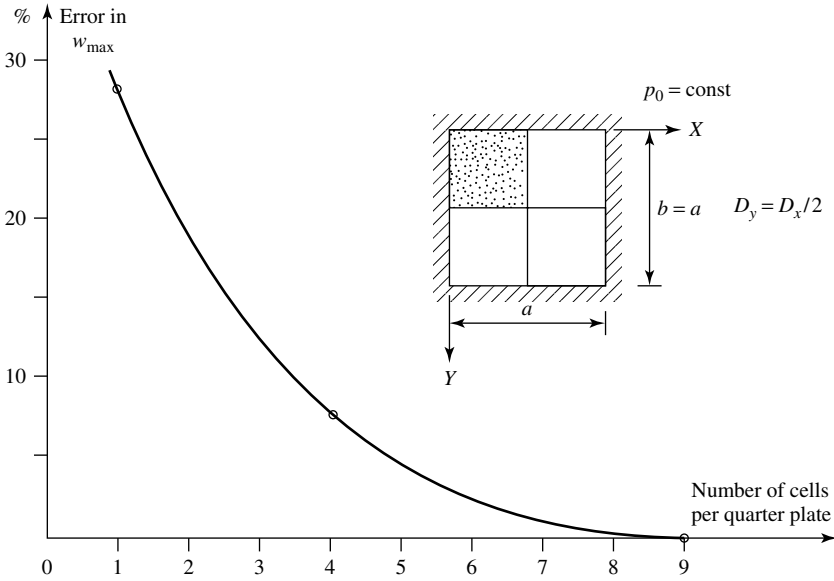


Figure 10.1.10 Convergence characteristics of gridwork cell given in Ref. [10.1.32].

where D_x , D_y and D_t are defined by Eqs. (10.1.4a) and (10.1.5), respectively, and

$$D_1 = \nu_y D_x = \nu_x D_y. \quad (10.1.26)$$

By formulating the stiffness matrix for a rectangular orthotropic plate element, Zienkiewicz and Cheung [10.1.26] applied the same technique as described in

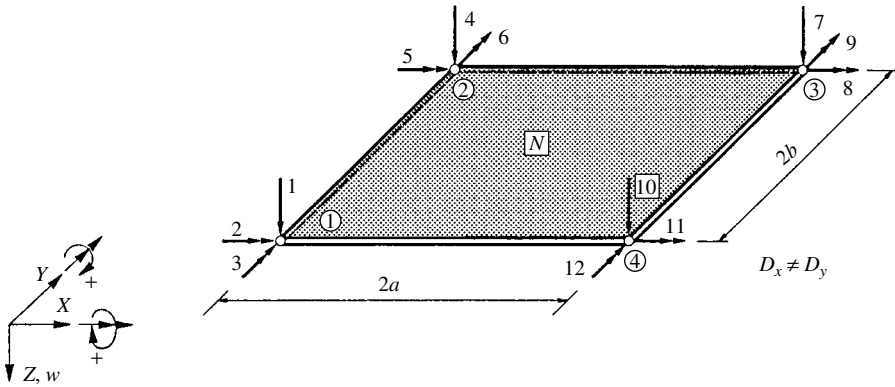


Figure 10.1.11 Orthotropic plate element.

Sec. 7.6.1. The corresponding four-node finite element with three degrees of freedom at each node is shown in Fig. 10.1.11. The polynomial expression selected for the displacement functions is similar to that given in Eq. (7.6.2). The explicit form of this stiffness matrix as supplied in Ref. [10.1.35] is

$$\mathbf{K}_e^{(N)} = \frac{1}{60ab} \mathbf{A} (D_x \mathbf{K}_1 + D_y \mathbf{K}_2 + D_1 \mathbf{K}_3 + D_{xy} \mathbf{K}_4) \mathbf{A}, \quad (10.1.27)$$

where

$$\mathbf{A} = \begin{bmatrix} \alpha & 0 & 0 & 0 \\ 0 & \alpha & 0 & 0 \\ 0 & 0 & \alpha & 0 \\ 0 & 0 & 0 & \alpha \end{bmatrix} \quad \text{with} \quad \alpha = \begin{bmatrix} 1 & 0 & 0 \\ 0 & 2b & 0 \\ 0 & 0 & 2a \end{bmatrix} \quad \text{and} \quad D_{xy} = \frac{Gh^3}{12}, \quad (10.1.28)$$

and the matrices \mathbf{K}_i ($i = 1, 2, 3, 4$) are listed in Table 10.1.1. The corresponding stress matrix \mathbf{S}_e is given in Table 10.1.2. The convergence characteristics of this finite element is shown in Fig. 10.1.12.

For naturally orthotropic plates, D_t is defined in Eq. (10.1.4). If the sectional properties must be related to those of an equivalent plate, as in the case of structural orthotropy such as shown in Fig. 10.1.3, it is probably more convenient to use Eq. (10.1.9) in the form

$$B = v_{xy} D_{xy} + 2D_t = \sqrt{v_x v_y} \sqrt{D_x D_y} + \left[2G_{xy} \frac{h^3}{12} + \frac{G_{xy}}{2} \left(\frac{I_{t1}}{c_1} + \frac{I_{t2}}{c_2} \right) \right], \quad (10.1.29)$$

where the expression in brackets represents $2D_t$. Thus, with the torsional rigidity of the plate given in Eq. (10.1.5), the torsional rigidities of the beam portions of the section (without the plate) have been superimposed. If Eq. (10.1.29) proves to be too difficult to evaluate, we may assume that $v_{xy} = 0$; therefore,

$$B \approx 2D_t, \quad (10.1.30)$$

Table 10.1.2 Stress Matrix for Element Shown in Fig. 10.1.11

$\mathbf{S}_e =$		$= \frac{1}{4ab}$												$\begin{Bmatrix} d_1 \\ d_2 \\ d_3 \\ \vdots \\ d_{11} \\ d_{12} \end{Bmatrix}$											
$m_x \textcircled{1}$	$m_y \textcircled{1}$	$m_{xy} \textcircled{1}$	$m_x \textcircled{2}$	$m_y \textcircled{2}$	$m_{xy} \textcircled{2}$	$m_x \textcircled{3}$	$m_y \textcircled{3}$	$m_{xy} \textcircled{3}$	$m_x \textcircled{4}$	$m_y \textcircled{4}$	$m_{xy} \textcircled{4}$	$6p^{-1}D_x + 6pD_1$	$-8aD_1$	$8bD_x$	$-6pD_1$	$-4aD_1$	0	$-6p^{-1}D_x$	0	$4bD_x$	0	0	0	0	d_1
												$6pD_y + 6p^{-1}D_1$	$-8aD_y$	$8bD_1$	$-6pD_y$	$-4aD_y$	0	$-6p^{-1}D_1$	0	$4bD_1$	0	0	0	0	d_2
												$-2D_{xy}$	$4bD_{xy}$	$-4aD_{xy}$	$2D_{xy}$	0	$4aD_{xy}$	$2D_{xy}$	$-4bD_{xy}$	0	$-2D_{xy}$	0	0	0	d_3
												$-6p^{-1}D_x + 6pD_1$	$8aD_1$	$8bD_x$	0	0	0	0	$-6p^{-1}D_x$	0	$4bD_x$	0	$4bD_x$	0	d_4
												$6pD_y + 6p^{-1}D_1$	$8aD_y$	$8bD_1$	0	0	0	0	$-6p^{-1}D_1$	0	$4bD_1$	0	$4bD_1$	0	d_5
												$2D_{xy}$	$4bD_{xy}$	$4aD_{xy}$	$2D_{xy}$	0	0	$2D_{xy}$	$-4bD_{xy}$	0	$-2D_{xy}$	0	$-4bD_{xy}$	0	d_6
												$-6p^{-1}D_x$	0	$-4bD_x$	0	0	0	$6p^{-1}D_x + 6pD_1$	$-8bD_x$	$-4aD_1$	0	$-4aD_1$	0	d_7	
												$-6p^{-1}D_1$	0	$-4bD_1$	0	0	0	$6pD_y + 6p^{-1}D_1$	$-8bD_1$	$-4aD_y$	0	$-4aD_y$	0	d_8	
												$-2D_{xy}$	$4bD_{xy}$	0	$2D_{xy}$	$4bD_{xy}$	0	$2D_{xy}$	$-4bD_{xy}$	$-4aD_{xy}$	$-4bD_{xy}$	$4aD_{xy}$	$4aD_{xy}$	d_9	
												0	0	0	$-6p^{-1}D_x$	0	$-4bD_x$	$-6pD_1$	0	$8aD_1$	$-8bD_x$	$-8bD_1$	$-8bD_x$	$-8bD_1$	d_{10}
												0	0	0	$-6p^{-1}D_1$	0	$-4bD_1$	$-6pD_y$	0	$8aD_y$	$-8bD_y$	$-8bD_1$	$-8bD_y$	$-8bD_1$	d_{11}
												$-2D_{xy}$	0	0	$2D_{xy}$	$4bD_{xy}$	0	$2D_{xy}$	$-4aD_{xy}$	$-4bD_{xy}$	$-4bD_{xy}$	$4aD_{xy}$	$4aD_{xy}$	$4aD_{xy}$	d_{12}

$(p = \frac{a}{b})$

$$\left(p = \frac{a}{b} \right)$$

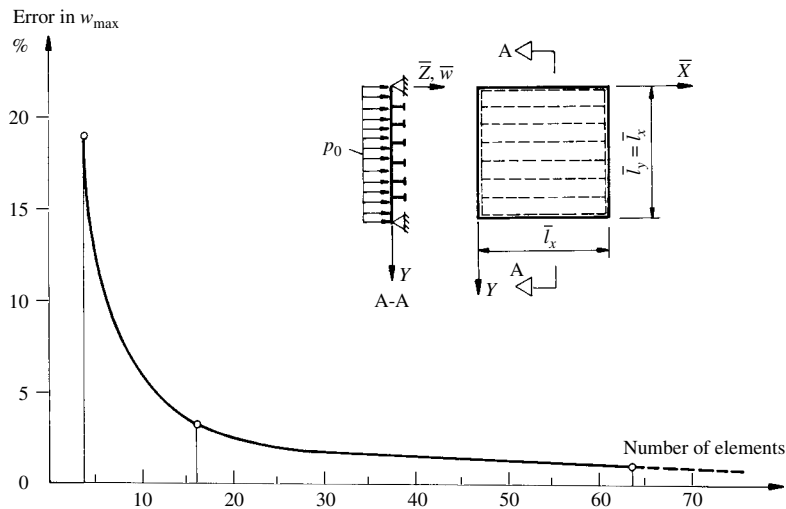
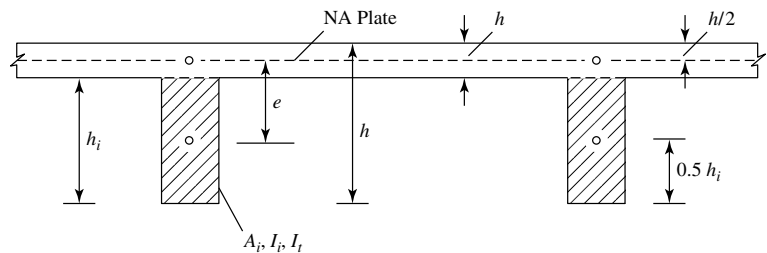
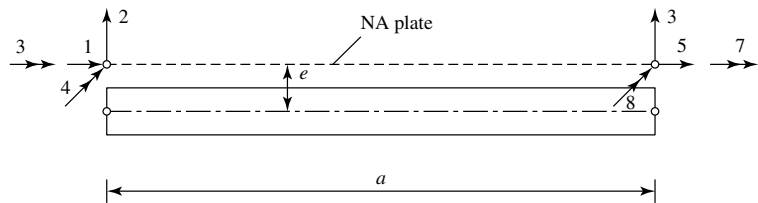


Figure 10.1.12 Convergence characteristics of finite element given in Eqs. (10.1.27)–(10.1.32).



(a) RC Plate and beam assembly



(b) Beam

$$\mathbf{K}_{e, \text{ beam}} = \begin{bmatrix} EA/a & 0.0 & 0.0 & -ES/a & -EA/a & 0.0 & 0.0 & ES/a \\ 0.0 & 12EI/a^3 & 0.0 & -6EI/a^2 & 0.0 & -12EI/a^3 & 0.0 & -6EI/a^2 \\ 0.0 & 0.0 & GI_i/a & 0.0 & 0.0 & 0.0 & -GI_i/a & 0.0 \\ 4EI/a & ES/a & 6EI/a^2 & 0.0 & 0.0 & 0.0 & 0.0 & 2EI/a \\ Symmetric & EA/a & 12EI/a^3 & 0.0 & 0.0 & 0.0 & 0.0 & -ES/a \\ 0.0 & 0.0 & 0.0 & 0.0 & 0.0 & 0.0 & 0.0 & 6EI/a^2 \\ 0.0 & 0.0 & 0.0 & 0.0 & 0.0 & 0.0 & 0.0 & 0.0 \\ 0.0 & 0.0 & 0.0 & 0.0 & 0.0 & 0.0 & 0.0 & 4EI/a \end{bmatrix}$$

$$S = A_i e, \quad I = I_i + A_i e^2$$

(c) Stiffness matrix of beam

Figure 10.1.13 Approximate treatment of RC slab-beam interaction [10.1.36].

from which the required D_t can be calculated. Again, the principal directions of orthotropy must coincide with those of the local coordinate axis. Since symmetry of the stiffness matrix is usually an essential requirement for efficient computations, especially when large matrices are involved, $v_y D_x$ must equal $v_x D_y$ in Eq. (10.1.26). If this is not the case, it can be accomplished by using average values in the form of $v_{xy} D_{xy}$.

Summary. Readers who have already mastered the previously treated Kirchhoff plate theory and its analytical and numerical solution techniques will not find any difficulty in extending them to orthotropic plates. Based on the author's experience, the recommended methods for solution of "real-life" orthotropic plate problems are the finite difference, gridwork and finite element methods. Arbitrary geometry can also be approximated by zigzag lines without losing too much accuracy provided a relatively small mesh size is used. For smaller problems, the application of the FDM offers definite advantages. Among other items, there is no need for a computer program. The only requirement for a finite difference solution is that of an equation solver. Since the number of the generated algebraic equations is usually small, even a high-powered scientific calculator will be sufficient for this purpose. A final reminder: Plate-girder assemblies usually cannot be treated as orthotropic plates! Thus, the FEM must be applied, with certain restrictions, as mentioned in the introduction of this section. The approximation shown in Fig. 10.1.13 may simplify such an approach. It is of importance, however, that degrees of freedom of the plate stiffness matrix and those of the beams have the same directions.

ILLUSTRATIVE EXAMPLE I

Determine an expression for the deflected middle surface of a rectangular orthotropic plate subjected to a uniformly distributed load $p_z = p_0$. The edges of the plate are simply supported. Assume that the principal directions of orthotropy are parallel with those of the edges.

Because of the simply supported boundary conditions, Navier's method can be applied. The double Fourier series of the load[†] is

$$p_0 = \frac{16p_0}{\pi^2} \sum_m \sum_n \frac{1}{mn} \sin \frac{m\pi x}{a} \sin \frac{n\pi y}{b}$$

for $m = 1, 3, 5, \dots, n = 1, 3, 5, \dots$ (10.1.31)

We seek the solution of Eq. (10.1.6) also in form of a double trigonometric series; thus

$$w(x, y) = \sum_m \sum_n W_{mn} \sin \frac{m\pi x}{a} \sin \frac{n\pi y}{b}$$

for $m = 1, 3, 5, \dots, n = 1, 3, 5, \dots$ (10.1.32)

The unknown coefficient W_{mn} for a specific set of m and n is found by substituting Eqs. (10.1.31) and (10.1.32) into the governing differential equation of

[†] See Appendix A.1.

orthotropic plate (10.1.6), which gives

$$W_{mn} = \frac{16p_0}{\pi^6} \frac{1}{mn[D_x(m^4/a^4) + 2B(m^2n^2/a^2b^2) + D_y(n^4/b^4)]}$$

for $m = 1, 3, 5, \dots, n = 1, 3, 5, \dots$

(10.1.33)

By substituting this expression into Eq. (10.1.32), we obtain the required expression for the deflected plate surface. In the case of isotropy, this solution becomes equal to that obtained in Sec. 2.2.

ILLUSTRATIVE EXAMPLE II

Let us solve the governing differential equation (10.1.6) for a plate that is simply supported on opposite edges and clamped on the other two. The plate is subjected to a distributed lateral load $p_z(x, y)$, as shown in Fig. 10.1.14. Because of the prescribed boundary conditions, Lévy's method[†] can be applied. Accordingly, we assume that the solution consists of two parts:

$$w(x, y) = w_H(x, y) + w_P(x, y), \quad (10.1.34)$$

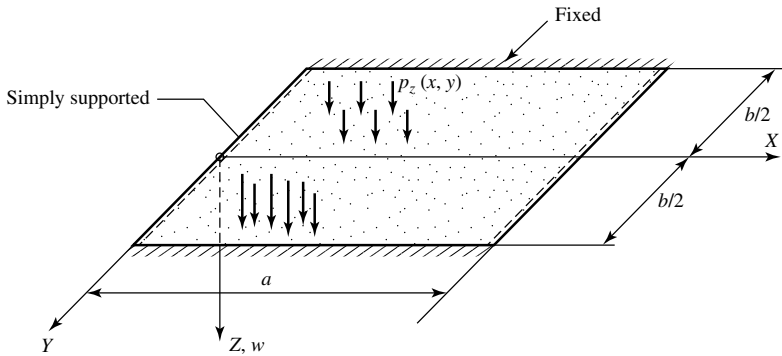


Figure 10.1.14 Orthotropic plate with Lévy's boundary conditions.

where $w_H(x, y)$ represents the solution of the homogeneous form of Eq. (10.1.6) and $w_P(x, y)$ is a particular solution of the governing equation. The homogeneous form of Eq. (10.1.6) is

$$D_x \frac{\partial^4 w_H}{\partial x^4} + 2B \frac{\partial^4 w_H}{\partial x^2 \partial y^2} + D_y \frac{\partial^4 w_H}{\partial y^4} = 0. \quad (10.1.35)$$

Solution of this equation can be expressed by the single trigonometric series

$$w_H(x, y) = \sum_{m=1}^{\infty} Y_m(y) \sin \frac{m\pi x}{a}, \quad (10.1.36)$$

[†] See Sec. 2.3.

which satisfies the boundary conditions at the simply supported edges. Substitution of Eq. (10.1.36) into Eq. (10.1.35) gives

$$\sum_{m=1}^{\infty} \left[D_x \left(\frac{m\pi}{a} \right)^4 Y_m(y) - 2B \left(\frac{m\pi}{a} \right)^2 \frac{\partial^2 Y(y)}{\partial y^2} + D_y \frac{\partial^4 Y_m(y)}{\partial y^4} \right] \sin \frac{m\pi x}{a} = 0. \quad (10.1.37)$$

Equation (10.1.37) is an ordinary homogeneous differential equation of fourth order. Consequently, its solution may be sought in the form

$$Y_m(y) = C e^{\lambda y} \quad (10.1.38)$$

in which C and λ are constants. Substituting Eq. (10.1.38) into Eq. (10.1.37), we obtain the characteristic equation

$$D_x \left(\frac{m\pi}{a} \right)^4 - 2B\lambda^2 \left(\frac{m\pi}{a} \right)^2 + D_y \lambda^4 = 0, \quad (10.1.39)$$

the roots of which are

$$\begin{aligned} \lambda_1 &= \frac{m\pi}{a} \sqrt{\frac{1}{D_y} \left(B + \sqrt{B^2 - D_x D_y} \right)}, \\ \lambda_2 &= \frac{m\pi}{a} \sqrt{\frac{1}{D_y} \left(B - \sqrt{B^2 - D_x D_y} \right)}, \\ \lambda_3 &= -\frac{m\pi}{a} \sqrt{\frac{1}{D_y} \left(B + \sqrt{B^2 - D_x D_y} \right)}, \\ \lambda_4 &= -\frac{m\pi}{a} \sqrt{\frac{1}{D_y} \left(B - \sqrt{B^2 - D_x D_y} \right)}. \end{aligned} \quad (10.1.40)$$

Thus, the general form of the homogeneous solution can be written as

$$w_H(x, y) = \sum_{m=1}^{\infty} (C_1 e^{\lambda_1 y} + C_2 e^{\lambda_2 y} + C_3 e^{\lambda_3 y} + C_4 e^{\lambda_4 y}) \sin \frac{m\pi x}{a}. \quad (10.1.41)$$

Now, we express the loading in terms of sine series,

$$p(x) = P_m \sin \frac{m\pi x}{a}, \quad (10.1.42)$$

in which

$$P_m = \frac{2}{a} \int_0^a p(x) \sin \frac{m\pi x}{a} dx. \quad (10.1.43)$$

Consequently, we can assume the particular solution to be of the form

$$w_P(x, y) = \sum_{m=1}^{\infty} A_m(y) \sin \frac{m\pi x}{a}. \quad (10.1.44)$$

Substitution of $w_P(x, y)$ into the differential equation (10.1.6) yields

$$\sum_{m=1}^{\infty} \left[D_x \left(\frac{m\pi}{a} \right)^4 A_m - 2B \left(\frac{m\pi}{a} \right)^2 \frac{d^2 A_m}{dy^2} + D_y \frac{d^4 A_m}{dy^4} - P_m \right] \sin \frac{m\pi x}{a} = 0. \quad (10.1.45)$$

Hence

$$A_m = \frac{P_m}{D_x} \left(\frac{a}{m\pi} \right)^4; \quad (10.1.46)$$

thus

$$w_P(x, y) = \sum_{m=1}^{\infty} \frac{P_m}{D_x} \left(\frac{a}{m\pi} \right)^4 \sin \frac{m\pi x}{a}, \quad (10.1.47)$$

and the general form of the total solution becomes

$$w(x, y) = \sum_{m=1}^{\infty} \left[C_1 e^{\lambda_1 y} + C_2 e^{\lambda_2 y} + C_3 e^{\lambda_3 y} + C_4 e^{\lambda_4 y} + \frac{P_m}{D_x} \left(\frac{a}{m\pi} \right)^4 \right] \sin \frac{m\pi x}{a}. \quad (10.1.48)$$

The unknown constants C_1 , C_2 , C_3 and C_4 in this equation are determined from the boundary conditions at the two clamped edges, which are

$$(w)_{y=\pm b/2} = 0 \quad \text{and} \quad \left(\frac{\partial w}{\partial y} \right)_{y=\pm b/2} = 0. \quad (10.1.49)$$

ILLUSTRATIVE EXAMPLE III

A square orthotropic plate with fixed boundary conditions is subjected to $p_z = p_0 = \text{constant}$ lateral load. Find approximate values of the deflection by the ordinary FDM. Assume that the principal directions of natural orthotropy are parallel with the plate edges. The *arbitrarily* assumed flexural rigidities of the plate are D_x , $D_y = 0.5D_x$ and $2B = 2.496D_x$, $\nu_x = \nu_y = 0.3$.

Using these flexural rigidities, the governing differential equation (10.1.6) becomes

$$D_x \frac{\partial^4 w}{\partial x^4} + 2.4296D_x \frac{\partial^4 w}{\partial x^2 \partial y^2} + 0.5D_x \frac{\partial^4 w}{\partial y^4} = p_0. \quad (10.1.50)$$

Since the plate is orthotropic, the finite difference equation given in Fig. 10.1.7 should be employed. Thus, we obtain

$$\begin{aligned}
& \frac{D_x}{\lambda^4} (w_{m+2,n} - 4w_{m+1,n} + 6w_{m,n} - 4w_{m-1,n} + w_{m-2,n}) \\
& + \frac{2.4296 D_x}{\lambda^4} [4w_{m,n} - 2(w_{m+1,n} + w_{m-1,n} + w_{m,n+1} + w_{m,n-1}) \\
& \quad + w_{m+1,n+1} + w_{m+1,n-1} + w_{m-1,n+1} + w_{m-1,n-1}] \\
& + \frac{0.5 D_x}{\lambda^4} (w_{m,n+2} - 4w_{m,n+1} + 6w_{m,n} - 4w_{m,n-1} + w_{m,n-2}) = p_0
\end{aligned} \tag{10.1.51}$$

Using only a very coarse subdivision $\lambda = a/4$, as shown in Fig. 10.1.15, and applying the above expression at various mesh points, we obtain

$$\begin{bmatrix} 18.7184 & -17.7184 & -13.7184 & 9.7194 \\ -8.8592 & 20.7184 & 4.8592 & -13.7184 \\ -6.8592 & 4.8592 & 19.7184 & -17.7184 \\ 2.4296 & -6.8592 & -8.8592 & 21.7184 \end{bmatrix} \begin{Bmatrix} w_1 \\ w_2 \\ w_3 \\ w_4 \end{Bmatrix} = \begin{Bmatrix} p_0 \\ p_0 \\ p_0 \\ p_0 \end{Bmatrix} \frac{\lambda^4}{D_x}. \tag{10.1.52}$$

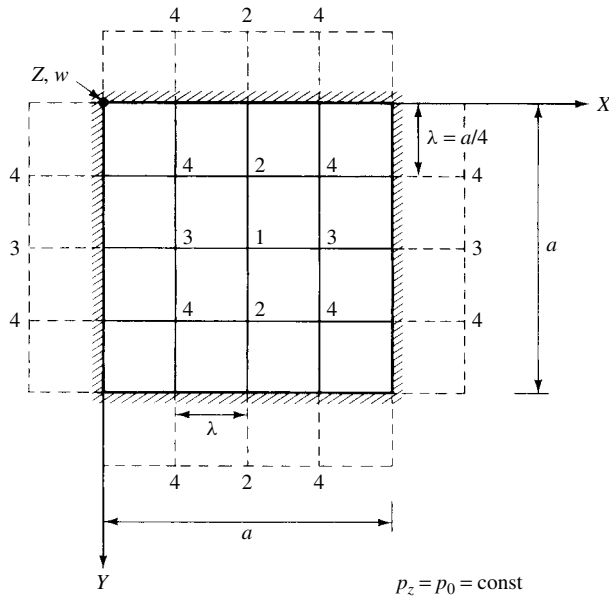


Figure 10.1.15 Numbering of mesh points.

Solution of these algebraic equations gives

$$\mathbf{w} = \begin{Bmatrix} w_1 \\ w_2 \\ w_3 \\ w_4 \end{Bmatrix} = \begin{Bmatrix} 0.4963 \\ 0.3392 \\ 0.3592 \\ 0.2412 \end{Bmatrix} \frac{p_0 \lambda^4}{D_x}. \tag{10.1.53}$$

Since there is no “exact” solution of this problem, we must use an approximate value to judge the obtained accuracy. Thus, a comparison of the approximate center deflection $w_{\max} \approx 0.0019 p_0 a^4 / D_x$ with its energy solution [10.1.6] counterpart

$$w_{\max} \approx 0.003418 \frac{p_0 a^4}{D_x + 0.5714B + D_y} = 0.001544 \frac{p_0 a^4}{D_x} \quad (10.1.54)$$

shows an error of 23%. In this comparison, however, one must weigh the fact that the ordinary FDM gives lower-bound solutions, while an approximate solution based on energy consideration approaches the exact solution from above. Consequently, the actual error will be less than the value given above. By using a finer mesh combined with Richardson’s extrapolation technique, the results can be considerably improved.

ILLUSTRATIVE EXAMPLE IV

Solve the problem in Illustrative Example III by the FEM, assuming that $B = 2D_t$ and $v_{xy}D_{xy} = 0$. Use Table 10.1.1 for the element stiffness matrix.

Let us subdivide the plate into four elements, as shown in Fig. 10.1.16. Considering only those displacements that can take place, the element stiffness matrix becomes

$$\mathbf{K}_e = \frac{D_x}{a^2} \begin{bmatrix} 51.2115 & & \text{Symmetric} \\ 5.94368 & 5.25824 & \\ -9.94364 & 0.00000 & 7.92491 \end{bmatrix}. \quad (10.1.55)$$

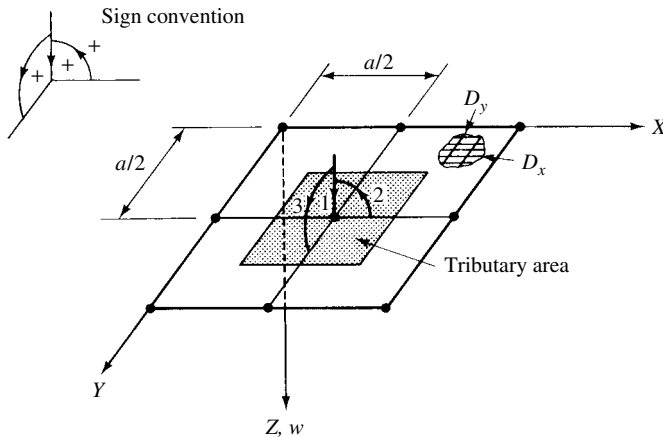


Figure 10.1.16 Finite element representation of clamped orthotropic plate.

Utilizing the apparent double symmetry of the structure and load, it is sufficient to consider only one quarter plate. Hence, the matrix displacement equation of

this plate problem can be written as

$$\bar{\mathbf{d}} = \begin{Bmatrix} \bar{d}_1 \\ \bar{d}_2 \\ \bar{d}_3 \end{Bmatrix} = \begin{bmatrix} 204.846 & 0.0 & 0.0 \\ 0.0 & 21.033 & 0.0 \\ 0.0 & 0.0 & 31.699 \end{bmatrix}^{-1} \begin{Bmatrix} 0.25 \\ 0.0 \\ 0.0 \end{Bmatrix} \frac{p_0 a^4}{D_x}. \quad (10.1.56)$$

Solution of this equation gives $\bar{d}_1 = w_{\max} = 0.00123 p_0 a^4 / D_x$, which in comparison with the approximate energy solution of the problem shows an error of 21%. However, by increasing the number of elements, this error can be substantially reduced.

References and Bibliography

- [10.1.1] PELIKAN, W., and ESSLINGER, M., "Die Stahlfahrbahn, Berechnung und Konstruktion," *Forschungsheft*, No. 7 Maschinenfabrik, Augsburg-Nürnberg, 1957.
- [10.1.2] VITOLS, V., and CLIFTON, R. J., "Analysis of Composite Beam Bridges by Orthotropic Plate Theory," *Proc. ASCE J. Struct. Div.*, 89, Pt. I, ST. 4 (Aug. 1963), 71–94.
- [10.1.3] HUBER, M. T., "Die Theorie der kreuzweise bewehrten Eisenbetonplatten," *Der Bauingenieur*, 4 (1923), 354–392.
- [10.1.4] PFLÜGER, A., "Die orthotrope Platte mit Hohlsteifen," *Österr. Ing.-Arch.*, 2 (1955), 199.
- [10.1.5] ROSTOVTSSEV, G. G., "Calculation of a Thin Plan Sheeting Supported by Ribs" (in Russian), *Trudy Leningrad. Inst. Inzhenerov Grazhdanskogo Vozdushnogo Flota*, No. 20, 1940.
- [10.1.6] LEKHNITSKII, S. G., *Anisotropic Plates* (English translation of the original Russian work), Gordon & Breach, Science Publishers, New York, 1968.
- [10.1.7] HUBER, M. T., "Probleme der Statik technisch wichtiger orthotroper Platten," in *Timoshenko Anniversary Volume*, Macmillan Company, New York, 1938, p. 89.
- [10.1.8] *Design Manual for Orthotropic Steel Plate Deck Bridges*, American Institute of Steel Construction, New York, 1963.
- [10.1.9] SEYDEL, E. B., "Schubknickversuche mit Wellblechtafeln," *Jahrbuch d. Deutsch. Versuchsanstalt für Luftfahrt*, e. V. München und Berlin, 1931, pp. 233–235.
- [10.1.10] BARES, R., and MASSONET CH., *Analysis of Beam Grids and Orthotropic Plates*, Frederick Ungar Publishing Co., New York, 1968.
- [10.1.11] GUYON, Y., "Calcul des ponts larges à poutres multiples solidarisées par les entretoises," *Ann. Ponts et Chaussées*, 116, No. 5 (Sept.–Oct. 1946), 553–612.
- [10.1.12] KRUG, S., and STEIN, P., *Influence Surfaces of Orthogonal-Anisotropic Plates*, Springer-Verlag, Berlin, 1961.
- [10.1.13] HUFFINGTON, N. J., "Theoretical Determination of Rigidity Properties of Orthogonally Stiffened Plates," *J. Appl. Mech.*, 23, No. 1 (March 1956), 15–20.
- [10.1.14] KUO, S. S., *The Computer Analysis of Orthotropic Steel Plate Superstructure for Highway Bridges*, Report prepared for United States Bureau of Public Roads, Contract No. CPR 11-9736, Vols. I–IV, University of New Hampshire, Durham, 1965.
- [10.1.15] AALAMI, B., and CHAPMAN, J. C., "Large Deflexion Behaviour of Rectangular Orthotropic Plates under Transverse and In-Plane Loads," *Proc. Inst. Civil Eng.*, 42 (Mar. 1969), 347–382.
- [10.1.16] HEINS, P. C., and YOO, C. H., "Grid Analysis of Orthotropic Bridges," *Publ. Int. Assoc. Bridge Struct. Eng.*, 30, Pt. I (1970), 73–92.
- [10.1.17] SZILARD, R., "A Practical Method for Torsion Analysis of Gridworks," R. Szilard, P. Zia, and G. Fisher (Eds.), *Analysis of Structural Systems for Torsion* ACI SP-35, American Concrete Institute, Detroit, Michigan, 1973, pp. 117–154.
- [10.1.18] GIENCKE, E., "Die Grundgleichungen für die orthotrope Platte mit exzentrischen Steifen," *Der Stahlbau*, 24 (June 1955), 128–129.

- [10.1.19] TROITSKY, M. S., *Orthotropic Bridges: Theory and Design*, James F. Lincoln Arc Welding Foundation, Cleveland, Ohio, 1967.
- [10.1.20] ZIENKIEWICZ, O. C., and CHEUNG, Y. K., "The Finite Element Method for Analysis of Elastic Isotropic and Orthotropic Slabs," *Proc. Inst. Civil Eng.*, 28 (1964), 471–488.
- [10.1.21] BÜRGERMEISTER, G., et al., "Stahlbrückenbau," in *Ingenieur Taschenbuch Bauwesen*, Vol. II, Pt. 2, Teubner Verlagsgesellschaft, Leipzig, 1970, pp. 478–635.
- [10.1.22] SAVIN, G. N., and FLEISHMAN, N. P., "Rib-Reinforced Plates and Shells" (translated from Russian), NASA-TT-F-427, U.S. Department of Commerce, Clearinghouse for Federal Scientific and Technical Information, Springfield, Virginia, 1967.
- [10.1.23] LAMPERT, P., "Postcracking Stiffness of Reinforced Concrete Beams in Torsion and Bending," in R. Szilard, P. Zia, and G. Fisher (Eds.), *Analysis of Structural Systems for Torsion*, ACI SP-35, American Concrete Institute, Detroit, Michigan, 1973.
- [10.1.24] LEONHARDT, F., "Zur Frage der Übereinstimmung von Berechnung und Wirklichkeit bei Tragwerken aus Stahlbeton und Spannbeton," in K. H. Laerman (Ed.), *Konstruktiver Ingenieurbau*, Werner-Verlag, Düsseldorf, 1967.
- [10.1.25] CHEUNG, Y. K., KING, I. P., and ZIENKIEWICZ, O. C., "Slab Bridges with Arbitrary Shape and Support Conditions—A General Method of Analysis Based on Finite Elements," *Proc. Inst. Civ. Eng.*, 40 (1968), 9–36.
- [10.1.26] ZIENKIEWICZ, O. C., and CHEUNG, Y. K., "Finite Element Method for Analysis of Elastic and Orthotropic Plates," *Proc. Inst. Civ. Eng.*, 28 (1964), 471–478.
- [10.1.27] TROITSKY, M. S., *Stiffened Plates: Bending, Stability and Vibration*, Elsevier, New York, 1976.
- [10.1.28] GANGARAO, H. V. S., ELMEGED, A. A., and CHAUDHARY, V. K., "Macroapproach for Ribbed and Grid Plate Systems," *J. Eng. Mech. Div., ASCE*, 101 (1975), 25–39.
- [10.1.29] JIANG, W., BAO, G., and ROBERTS, J. C., "Finite Element Modeling of Stiffened and Unstiffened Orthotropic Plates," *Comp. Struct.*, 63 (1997), 105–117.
- [10.1.30] KUKRETI, A. R., and RAJAPAKSA, Y., "Analysis Procedure for Ribbed and Grid Plate Systems," *J. Struct. Div., ASCE*, 116 (1990), 372–391.
- [10.1.31] MUKHOPADHYAY, M., and SATSANGI, S. K., "Isoparametric Stiffened Plate Bending Element for the Analysis of Ship Structures," *Trans. R. Inst. Naval Arch.*, 126 (1984), 141–151.
- [10.1.32] HUSSEIN, R., and MORSI, M., "Framework Methods for Orthotropic Plates," *Comp. Struct.*, 22 (1986), 99–113.
- [10.1.33] MUKHOPADHYAY, M., "Stiffened Plates in Bending," *Comp. Struct.*, 50 (1994), 541–548.
- [10.1.34] ALY, A., and KENNEDY, J. B., "Rigidities of Horizontally Curved Flat Structures," *J. Struct. Div., ASCE*, 119 (1993), 2513–2532.
- [10.1.35] ZIENKIEWICZ, O. C., *The Finite Element Method*, 3rd ed., McGraw-Hill Book Co., London, 1977.
- [10.1.36] AVRAM, C., et al., *Numerical Analysis of Reinforced Concrete*, Elsevier, Amsterdam, 1993.

10.2 Laminated and Sandwich Plates

In recent years the use of laminated composite and sandwich plates has considerably increased. They are used especially in aerospace and naval structures, but nowadays their frequent applications can also be found in the automobile industry and building construction in the form of prefabricated and mobile homes and floors made of plywood laminates. Their popularity arises from the fact that, due to their light weight and high strength, they can be used very efficiently.

The term *laminated* refers to a composite structural material that is formed by combining two or more materials that are bonded together by strong adhesives (Fig. 10.2.1a). Consequently, they are by their very nature *anisotropic*. Unlike

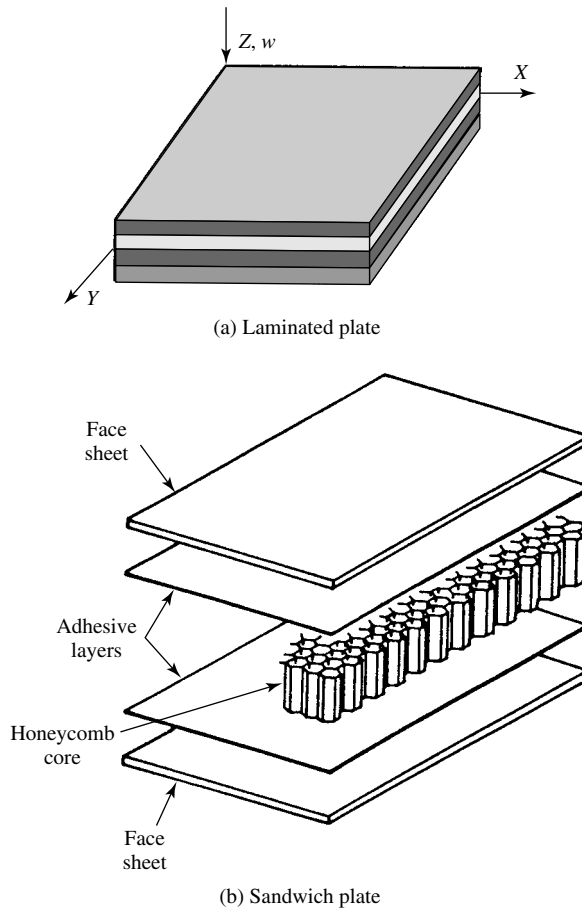


Figure 10.2.1 Laminated and sandwich plates.

isotropic materials, anisotropic materials exhibit complicated mechanical behaviors that do not admit exact solutions very easily. Thus, the analyst must rely mostly on representative approximations to obtain solutions of their boundary value, stability and dynamic problems. *Sandwich*-type construction refers to laminates that consist of two layers of strong materials on the outer faces and a relatively weak core between them (Fig. 10.2.1b). Such sandwich plates offer high bending stiffness for a small weight penalty.

With increasing use of such composite materials, the need for practical methods of analysis is obvious. Laminated plate analysis is based on two types of theories: (1) classical Kirchhoff plate theory and (2) Reissner-Mindlin shear deformation theory for moderately thick plates.

10.2.1 Classical Laminated Plate Theory

Classical laminated plate theory is a direct extension of Kirchhoff's theory for thin plates, which does not account for the effects of transverse shear and strain components

in the plate. However, this assumption is not applicable to moderately thick plates, as discussed in Sec. 1.5. Consequently, classical laminated plate theory is only adequate for the analysis of relatively thin plates when transverse deformation can be neglected.

Structural anisotropy in laminated plates is created by constructing plates of two or more thin bonded layers of isotropic or anisotropic materials. In formulating the governing differential equation, we assume that the individual layers are isotropic and that sliding between them is prevented.

Using the assumptions of classical plate theory, the strain-displacement relationships for the k th layer (Fig. 10.2.2) can be written[†] as

$$\varepsilon_x^{(k)} = -z_k \frac{\partial^2 w}{\partial x^2}, \quad \varepsilon_y^{(k)} = -z_k \frac{\partial^2 w}{\partial y^2}, \quad \gamma_{xy}^{(k)} = -2z_k \frac{\partial^2 w}{\partial x \partial y}. \quad (10.2.1)$$

From Hooke's law we obtain

$$\begin{aligned} \sigma_x^{(k)} &= \frac{E_k}{1 - \nu_k^2} (\varepsilon_x^{(k)} + \nu_k \varepsilon_y^{(k)}), & \sigma_y^{(k)} &= \frac{E_k}{1 - \nu_k^2} (\varepsilon_y^{(k)} + \nu_k \varepsilon_x^{(k)}), \\ \tau_{xy}^{(k)} &= \frac{E_k}{2(1 + \nu_k)} \gamma_{xy}^{(k)}. \end{aligned} \quad (10.2.2)$$

By substituting the appropriate expressions of Eq. (10.2.1) into Eq. (10.2.2) and integrating the latter over each layer, the sum of these results yields the bending and twisting moments,[‡] respectively; thus

$$m_x, m_y, m_{xy} = \sum_k \int_{z_{k-1}}^{z_k} (\sigma_x, \sigma_y, \tau_{xy})^{(k)} z \, dz. \quad (10.2.3)$$

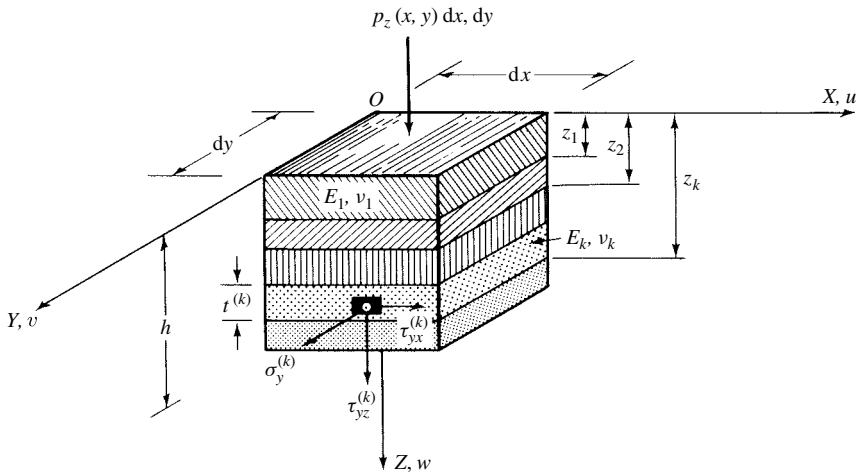


Figure 10.2.2 Multilayered plate element.

[†] See Sec. 1.2.

[‡] See Sec. 1.2.

The governing differential equation of laminated plates is derived in the same manner as described in Sec. 1.2. Thus, we can write

$$D^* \nabla^2 \nabla^2 w(x, y) = p_z(x, y), \quad (10.2.4)$$

where the *transformed flexural rigidity* of the laminated plate is given by Pister and Dong [10.2.1] in the form

$$D^* = \frac{AC - B^2}{A}. \quad (10.2.5)$$

The additional elastic constants in Eq. (10.2.5) are

$$A = \sum_k \frac{E_k}{1 - \nu_k^2} (z_k - z_{k-1}), \quad B = \sum_k \frac{E_k}{1 - \nu_k^2} \frac{z_k^2 - z_{k-1}^2}{2} \quad (10.2.6)$$

and

$$C = \sum_k \frac{E_k}{1 - \nu_k^2} \cdot \frac{z_k^3 - z_{k-1}^3}{3}. \quad (10.2.7)$$

As Eq. (10.2.4) indicates, the flexural behavior of a laminated plate is analogous to that of a homogeneous plate, provided that in Eq. (1.2.30) a transformed flexural rigidity D^* is used.

The deflected plate surface $w(x, y)$ is determined by the same analytical and numerical methods used for homogeneous plates. When $w(x, y)$ is known, the stress components in the k th layer can be calculated from

$$\begin{aligned} \sigma_k^{(k)} &= -z \frac{E_k}{1 - \nu_k^2} \left(\frac{\partial^2 w}{\partial x^2} + \nu_k \frac{\partial^2 w}{\partial y^2} \right), \\ \sigma_y^{(k)} &= -z \frac{E_k}{1 - \nu_k^2} \left(\frac{\partial^2 w}{\partial y^2} + \nu_k \frac{\partial^2 w}{\partial x^2} \right), \\ \tau_{xy}^{(k)} &= -z \frac{E_k}{1 + \nu_k} \frac{\partial^2 w}{\partial x \partial y}. \end{aligned} \quad (10.2.8)$$

Finally, a simplified engineering approach often used for approximation of transformed flexural rigidities of laminated plates should be mentioned. In this approximation, we assume that the Poisson ratios of the layers are nearly the same; thus their average value, ν_a , gives sufficient accuracy. Using the largest Young's modulus of elasticity E_0 as reference value, the expression for the transformed flexural rigidity is

$$D^* \approx \frac{E_0 I^*}{1 - \nu_a^2}, \quad (10.2.9)$$

where

$$I^* \approx \int_{-h_2}^{h_1} \frac{E_k}{E_0} z^2 dz. \quad (10.2.10)$$

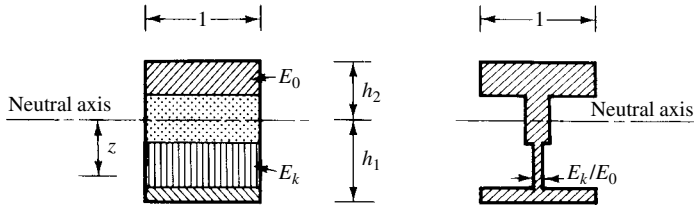


Figure 10.2.3 Transformed section.

In Eq. (10.2.10), z represents the distance of fibers from the neutral axis of the cross section having transformed widths E_k/E_0 (Fig. 10.2.3). A similar approach can be taken to determine the transformed extensional rigidity, which gives

$$K^* \approx \frac{EA^*}{1 - \nu_a^2} = \frac{E_0}{1 - \nu_a^2} \sum_k \frac{E_k}{E_0} t_k, \quad (10.2.11)$$

where A^* is the transformed area of the cross section per unit length.

10.2.2 Sandwich Plates

First, we will treat sandwich plates with cores of metallic honeycomb or of equivalent structural materials, as shown in Fig. 10.2.1b. Next, we will introduce a numerical approach to *steel* sandwich plates, which are depicted in Fig. 10.2.4. Sandwich plates with really *soft* cores will not be covered here since they require special considerations to prevent premature failure at a load level much lower than the one determined using the theory presented in this section.

The classical small-deflection theory of sandwich plates generally uses *variational principles* to derive the governing differential equations, taking into account the

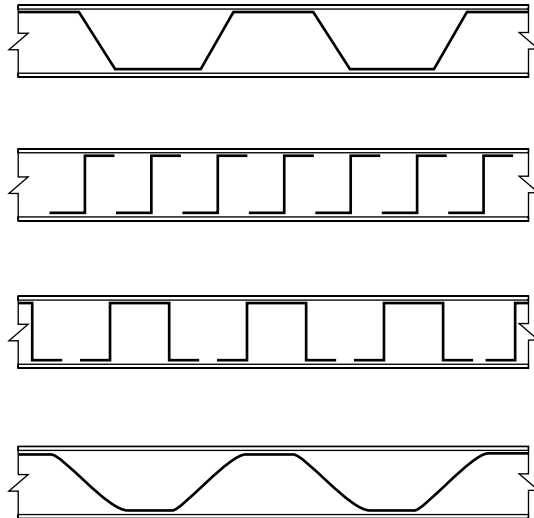


Figure 10.2.4 Steel sandwich plates with various core shapes.

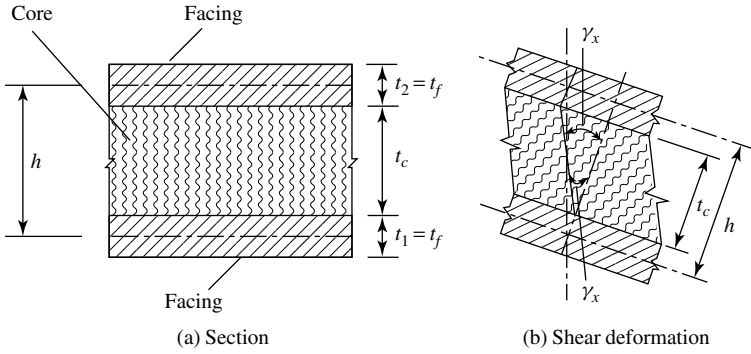


Figure 10.2.5 Notation used in analysis.

effect of transverse shear. These differential equations are based on the following assumptions:

- The thickness of the two outer faces is equal ($t_f = t_1 = t_2$), and they are thin in comparison with the overall plate thickness $h = t_c + t_f$ (Fig. 10.2.5a).
- The in-plane stress in the core is negligible.
- The normals to the midplane remain straight after deformation.
- The materials are linear elastic.

Using the somewhat modified strain energy functional given by Reissner [10.2.13–10.2.17], we can write

$$U = \frac{1}{2} \int_f \sum_{i=1}^2 \left[t_i \left(\frac{\sigma_{xi}^2}{E_{xi}} + \frac{\sigma_{yi}^2}{E_{yi}} - \frac{2\nu_{xyi}}{E_{xi}} \sigma_{xi} \sigma_{yi} + \frac{\tau_{xyi}^2}{G_i} \right) \right] dA + \frac{1}{2} \int_c \left(\frac{\tau_{xz}^2}{G_{xz}} + \frac{\tau_{yz}^2}{G_{yz}} \right) dV, \quad (10.2.12)$$

where f and c refer to the facing and core, respectively. The subscripts $i = 1, 2$ denote the upper and lower facings. Furthermore, τ_{xz} , τ_{yz} and G_{xz} , G_{yz} denote the shear stresses and shear moduli of the core, respectively.

Applying Castigliano's second theorem, the differential equations of isotropic sandwich plates become [10.2.14]

$$\nabla^2 \nabla^2 w^* = \frac{p_z}{D^*} - \frac{1}{S} \nabla^2 p_z, \quad (10.2.13a)$$

$$\frac{1-\nu}{2} \nabla^2 \gamma_x - \frac{S}{D^*} \gamma_x = \frac{\partial}{\partial x} \nabla^2 w^* + \frac{1+\nu}{2S} \frac{\partial p_z}{\partial x}, \quad (10.2.13b)$$

$$\frac{1-\nu}{2} \nabla^2 \gamma_y - \frac{S}{D^*} \gamma_y = \frac{\partial}{\partial y} \nabla^2 w^* + \frac{1+\nu}{2S} \frac{\partial p_z}{\partial y}, \quad (10.2.13c)$$

where

$$D^* = \frac{E_f t_f}{2(1-\nu^2)} h^2, \quad S = \frac{h^2}{t_c} G_c, \quad \nu = \nu_{xy1} = \nu_{xy2} \quad (10.2.14)$$

and γ_x and γ_y are shear deformations in the X and Y directions, respectively, as shown in Fig. 10.2.5b.

Since we have assumed that the behavior of the sandwich plate is linear elastic, the total deflection w^* can be given as the sum of the bending and shear deflections. Consequently, Eq. (10.2.13a) can be split into two:

$$\nabla^2 \nabla^2 w_b = \frac{p_z}{D^*} \quad \text{and} \quad \nabla^2 \nabla^2 w_s = -\frac{1}{S} \nabla^2 p_z, \quad (10.2.15)$$

where w_b denotes the bending part of the total deflections and w_s represents the other part caused by the transverse shear. The bending and twisting moments are calculated from

$$\begin{aligned} m_x &= -D^* \left(\frac{\partial \theta_x}{\partial x} + \nu \frac{\partial \theta_y}{\partial y} \right), & m_y &= -D^* \left(\frac{\partial \theta_y}{\partial y} + \nu \frac{\partial \theta_x}{\partial x} \right), \\ \theta_x &= \frac{\partial w^*}{\partial x} - \gamma_x, & \theta_y &= \frac{\partial w^*}{\partial y} - \gamma_y \end{aligned} \quad (10.2.16)$$

and

$$m_{xy} = -0.5D^*(1 - \nu) \left(\frac{\partial \theta_x}{\partial y} + \frac{\partial \theta_y}{\partial x} \right). \quad (10.2.17)$$

Similarly, the shearing forces are obtained from

$$q_x = G_c \frac{h^2}{t_c} \gamma_x \quad \text{and} \quad q_y = G_c \frac{h^2}{t_c} \gamma_y. \quad (10.2.18)$$

Consequently, the corresponding bending and shearing stresses can be expressed by:

$$\sigma_x = \frac{m_x}{ht_f}, \quad \sigma_y = \frac{m_y}{ht_f}, \quad \tau_{xy} = \frac{m_{xy}}{ht_f}, \quad \tau_x = \frac{q_x}{h}, \quad \tau_y = \frac{q_y}{h}. \quad (10.2.19)$$

If the boundary conditions of the sandwich plates are simply supported, we can use Navier's method to obtain solutions for the governing differential equations (10.2.13a)–(10.2.13c). However, either the ordinary FDM or its improved versions offer much more convenient and general solution techniques covering all boundary conditions, arbitrary geometry and even continuous composite plates. In both cases, the two differential equations given in Eq. (10.2.15) must be solved first to obtain the total lateral deflection field $w^* = w_b + w_s$. From the computed lateral deflections, the bending and twisting moments can be evaluated. In the next step, the shear deformations γ_x and γ_y should be determined if calculation of the shearing forces is also required.

Sandwich plates constructed from steel facing plates with stiff steel cores of various types (Fig. 10.2.4) can be efficiently analyzed by the gridwork method, provided the equivalent sectional properties are available. The rigid attachment between facing and core can be welding, rivets or screws.

into account the bending and shear deformations, can be expressed by [10.2.17]

$$\mathbf{K}_e = \begin{bmatrix} \frac{12EI_x}{(1+\alpha_x)l_x^3} & \frac{6EI_x}{(1+\alpha_x)l_x^2} & 0 & -\frac{12EI_x}{(1+\alpha_x)l_x^3} & \frac{6EI_x}{(1+\alpha_x)l_x^2} & 0 \\ \frac{6EI_x}{(1+\alpha_x)l_x^2} & \frac{(4+\alpha_x)EI_x}{(1+\alpha_x)l_x} & 0 & -\frac{6EI_x}{(1+\alpha_x)l_x^2} & \frac{(4+\alpha_x)EI_x}{(1+\alpha_x)l_x} & 0 \\ 0 & 0 & \frac{(GI_t)_x}{l_x} & 0 & 0 & -\frac{(GI_t)_x}{l_x} \\ -\frac{12EI_x}{(1+\alpha_x)l_x^3} & -\frac{6EI_x}{(1+\alpha_x)l_x^2} & 0 & \frac{12EI_x}{(1+\alpha_x)l_x^3} & \frac{6EI_x}{(1+\alpha_x)l_x^2} & 0 \\ \frac{6EI_x}{(1+\alpha_x)l_x^2} & \frac{(2-\alpha_x)EI_x}{(1+\alpha_x)l_x} & 0 & -\frac{6EI_x}{(1+\alpha_x)l_x^2} & \frac{(4+\alpha_x)EI_x}{(1+\alpha_x)l_x} & 0 \\ 0 & 0 & -\frac{(GI_t)_x}{l_x} & 0 & 0 & \frac{(GI_t)_x}{l_x} \end{bmatrix} \quad \text{Symmetric} \quad (10.2.20)$$

The same element stiffness matrix can be used in the Y direction by simply changing the subscript x to y .

However, to be able to use this element stiffness matrix for the proposed gridwork analysis, its elastic constants must be replaced by those pertinent to steel sandwich plates. In this respect, the following relationships apply:

$$\begin{aligned} EI_x &= I_y D_y, & (GI_t)_x &= I_y D_{xy}, \\ EI_y &= I_x D_y, & (GI_t)_y &= I_x D_{xy}. \end{aligned} \quad (10.2.21)$$

In addition, the shear stiffness of the sandwich plate can be calculated from D_{qx} and D_{qy} per unit length, respectively. The required expressions D_x , D_y , D_{xy} , D_{qx} and D_{qy} vary according to the types of core stiffeners used and can be derived from the procedures applied in Ref. [10.2.19]. The shear deformation constants α_x and α_y are expressed as

$$\alpha_x = \frac{12D_x}{l_x^2 D_{qx}} \quad \text{and} \quad \alpha_y = \frac{12D_y}{l_y^2 D_{qy}}. \quad (10.2.22)$$

As usual, these values are valid only for the internal beams. For external beams, these values must be reduced by 2, as already discussed in Chapter 6. Finally, it should be noted that basically the same approach can be used for other types of composite laminates, provided the corresponding bending and torsional stiffness values can be computed or experimentally determined.

In addition to the two relatively simple numerical solution techniques discussed above, the versatile FEM is also widely applied to solve plate problems related to composite laminates [10.2.20, 10.2.21]. Several finite element computer programs covering such plate problems have also been written [10.2.22–10.2.24]. For a detailed treatment of finite element modeling of laminated plates, we refer the reader to Ref. [10.2.25]. Furthermore, all major commercially available finite element codes, such as ABAQUS, NASTRAN, and SAFE, do have laminated plate elements in their extensive element library. Each layer in such an element can represent different materials, including its specific orientation. In many cases, even the material angle

can be rotated. Some finite elements program systems support up to 50 layers of a laminated plate. Since the use of these codes is basically the same as that of programs written for isotropic plates, it is sufficient here to refer to Chapter 7 in general and Sec. 7.14, in particular.

10.2.3 Moderately Thick Laminated Plates

To predict accurately the structural behavior of moderately thick multilayered composite plates, many different high-order theories have been proposed with the intent to improve the classical laminated plate theory by accounting for transverse shear deformation in a more rigorous way than the approximations discussed above. The simplest of all high-order theories are the ones based on the assumption of a single-layer plate combined with a first-order shear deformation theory of the form

$$\begin{aligned} u &= u_0(x, y) + z\psi_x(x, y), \\ v &= v_0(x, y) + z\psi_y(x, y), \\ w &= w_0(x, y) + z\psi_z(x, y), \end{aligned} \quad (10.2.23)$$

where the subscript zero refers to the displacements obtained from the classical solution and the terms ψ_x , ψ_y and ψ_z , representing the effect of shear deformation, are directly specified as derivatives of w . This approach, however, gives only moderate improvement over the classical laminated plate theory and practically no improvements over the two approximate solution techniques discussed above.

Consequently, still in the spirit of single-layer plate theory, second-order displacement fields

$$\begin{aligned} u &= u_0(x, y) + z\psi_x(x, y) + z^2\zeta_x(x, y), \\ v &= v_0(x, y) + z\psi_y(x, y) + z^2\zeta_y(x, y), \\ w &= w_0(x, y) + z\psi_z(x, y) + z^2\zeta_z(x, y) \end{aligned} \quad (10.2.24)$$

or even third-order displacement fields

$$\begin{aligned} u &= u_0(x, y) + z\psi_x(x, y) + z^2\zeta_x(x, y) + z^3\phi_x(x, y), \\ v &= v_0(x, y) + z\psi_y(x, y) + z^2\zeta_y(x, y) + z^3\phi_y(x, y), \\ w &= w_0(x, y) + z\psi_z(x, y) + z^2\zeta_z(x, y) + z^3\phi_z(x, y) \end{aligned} \quad (10.2.25)$$

are assumed. Such an approach represents the extension of the moderately thick plate theory introduced in Sec. 1.5 for homogeneous isotropic plates. Since in the third-order theory the displacement field accommodates cubic variations of transverse shear strain, there is no need to use a shear correction factor. Needless to say, all these high-order theories considerably complicate the analysis procedures and, therefore, cannot be treated in the framework of this book. For a more detailed study of this interesting subject, the reader is referred to the books written by Reddy [2.10.25–2.10.27].

Unlike the single-layer theories, the layerwise theories assume separate displacement fields within each layer. Again, numerous displacement-based theories have been proposed. The ultimate refinement of the analysis includes three-dimensional elastic models that give the most accurate prediction of stresses and

displacements through the thickness of the multilayered plates. The reader is referred to Refs. [10.2.28] and [10.2.29] for extensive lists of publications related to laminated plate theories.

Summary. The use of laminated composite plates has increased steadily during the past decades, since they exhibit high strength-to-weight and stiffness-to-weight ratios. Classical laminated plate theory, based on Kirchhoff's hypotheses, yields sufficiently accurate results only for thin composite layered plates when the effect of transverse shear deformation can be neglected. Since classical laminated plate theory represents only an extension of Kirchhoff's plate theory for homogeneous isotropic plates, all previously introduced analytical and numerical solution techniques can be applied, provided the properly determined transformed rigidities are used. Several approaches have been proposed to account for transverse shear flexibility, neglected in classical laminated plate theory. Differential equations of sandwich plates, for instance, that take into account the effect of transverse shear can be solved either analytically or numerically by means of various FDMs. Furthermore, a variation of the simple gridwork method not only can be used for the solution of steel sandwich plates but also can be logically extended to other types of laminated plates. First-order single-layer laminate theories are quite adequate if proper correction factors are used. Second- and third-order theories, however, are free from such factors. Considering laminates made of dissimilar materials, layerwise theories in combination with the FEM offer the most accurate results. For detailed studies of these more refined and quite complex theories, the reader is directed to the pertinent literature.

ILLUSTRATIVE EXAMPLE I

A simply supported sandwich plate with dimensions a and b carries a uniformly distributed load p_0 . Let us determine the equation of the deflected plate surface $w^*(x, y)$ and corresponding expressions for the internal stress resultants m_x, m_y, m_{xy}, q_x and q_y .

Since the simply supported boundary conditions

$$w^* = \begin{cases} m_x = \gamma_y = 0 & \text{for } x = 0, x = a \\ m_y = \gamma_x = 0 & \text{for } y = 0, y = b. \end{cases} \quad (10.2.26)$$

permit the application of Navier's method to solve the governing differential equations (10.2.13a)–(10.2.13c) of the sandwich plate, we can express the deflected plate surface in our standard coordinate system[†] as:

$$w^*(x, y) = \sum_{m=1}^{\infty} \sum_{n=1}^{\infty} W_{mn} \sin \alpha_m x \sin \beta_n y, \quad (10.2.27)$$

where

$$\alpha_m = \frac{m\pi}{a} \quad \text{and} \quad \beta_n = \frac{n\pi}{b}. \quad (10.2.28)$$

and W_{mn} represents the unknown coefficient of the Fourier series expansion.

[†] See Table A.1.1, for instance.

Next, we express the lateral load by a similar double *sine* series,

$$p(x, y) = \sum_{m=1}^{\infty} \sum_{n=1}^{\infty} P_{mn} \sin \alpha_m x \sin \beta_n y, \quad (10.2.29)$$

where the coefficient of the expansion according to Table A.1.1 is $P_{mn} = 16p_0/\pi^2 mn$ for $m, n = 1, 3, 5, \dots$

The unknown coefficient W_{mn} in Eq. (10.2.27) is determined by substituting Eqs. (10.2.27) and (10.2.29) into Eq. (10.2.27) and (10.2.29) into Eq. (10.2.13a). This gives

$$W_{mn} = \frac{(1/D^*) + [(\alpha_m^2 + \beta_n^2)/S]}{(\alpha_m^2 + \beta_n^2)^2} P_{mn}. \quad (10.2.30)$$

Consequently, the equation of the deflected plate surface becomes

$$w^*(x, y) = \sum_{m=1}^{\infty} \sum_{n=1}^{\infty} P_{mn} \frac{(1/D^*) + [(\alpha_m^2 + \beta_n^2)/S]}{(\alpha_m^2 + \beta_n^2)^2} \sin \alpha_m x \sin \beta_n y. \quad (10.2.31)$$

A similar approach is taken to determine the shear deformations. The pertinent Fourier series expressions for the shear deformations [10.2.25, 10.2.30] are

$$\begin{aligned} \gamma_x(x, y) &= \sum_{m=1}^{\infty} \sum_{n=1}^{\infty} \Gamma_{x,mn} \cos \alpha_m x \sin \beta_n y, \\ \gamma_y(x, y) &= \sum_{m=1}^{\infty} \sum_{n=1}^{\infty} \Gamma_{y,mn} \sin \alpha_m x \cos \beta_n y, \end{aligned} \quad (10.2.32)$$

where the unknown coefficients of expansion are determined from Eqs. (10.2.13a) and (10.2.13b), respectively. Thus, we can write

$$\Gamma_{x,mn} = \frac{m\pi P_{mn}}{aS(\alpha_m^2 + \beta_n^2)} \quad \text{and} \quad \Gamma_{y,mn} = \frac{n\pi P_{mn}}{bS(\alpha_m^2 + \beta_n^2)}. \quad (10.2.33)$$

Next, we obtain the expressions for the bending moments by substituting Eq. (10.2.31) into Eq. (10.2.16). This results in

$$\begin{aligned} m_x &= \sum_{m=1}^{\infty} \sum_{n=1}^{\infty} P_{mn} \frac{\alpha_m^2 + \nu\beta_n^2}{(\alpha_m^2 + \beta_n^2)^2} \sin \alpha_m x \sin \beta_n y, \\ m_y &= \sum_{m=1}^{\infty} \sum_{n=1}^{\infty} P_{mn} \frac{\beta_n^2 + \nu\alpha_m^2}{(\alpha_m^2 + \beta_n^2)^2} \sin \alpha_m x \sin \beta_n y. \end{aligned} \quad (10.2.34)$$

In a similar way, the twisting moment is determined from Eq. (10.2.17). This gives

$$m_{xy} = (1 - \nu) \sum_{m=1}^{\infty} \sum_{n=1}^{\infty} \frac{mn\pi^2 P_{mn}}{ab(\alpha_m^2 + \beta_n^2)^2} \cos \alpha_m x \cos \beta_n y. \quad (10.2.35)$$

Finally, the expressions for the shear forces are determined by substituting Eqs. (10.2.32) and (10.2.33) into Eq. (10.2.18), and we obtain

$$q_x = \sum_{m=1}^{\infty} \sum_{n=1}^{\infty} \frac{m\pi P_{mn}}{a(\alpha_m^2 + \beta_n^2)} \cos \alpha_m x \sin \beta_n y,$$

$$q_y = \sum_{m=1}^{\infty} \sum_{n=1}^{\infty} \frac{n\pi P_{mn}}{b(\alpha_m^2 + \beta_n^2)} \sin \alpha_m x \cos \beta_n y.$$
(10.2.36)

Finally, it should be noted that the equations derived above are quite general. That is, by using an appropriate P_{mn} coefficient, other loading conditions can be considered. For the most common lateral loads, this coefficient is listed in Table A.1.1.

ILLUSTRATIVE EXAMPLE II

A rectangular fixed sandwich plate with side ratio $b/a = \frac{4}{3}$ and fixed boundary conditions carries a uniformly distributed lateral load $p_z = p_0$ (Fig. 10.2.8a). Determine the deflected plate surface.

Due to the fixed boundary conditions, we must resort in this case to the ordinary FDM to obtain the required results. The double symmetry of the structure and load allows us to consider only one-quarter of the plate. Using the finite difference mesh shown in Fig. 10.2.8b, only 12 deflection ordinates, w_1^*, \dots, w_{12}^* , have to be found. Making use of the two-stage solution technique given in Eq. (10.2.15), the bending part of the total deflections is obtained from

$$\nabla^2 \nabla^2 w_b = \frac{p_0}{D^*}. \quad (10.2.37)$$

By applying the stencil given in Fig. 5.1.3a, the resulting matrix equation becomes

$$\mathbf{A} \mathbf{w}_b = \mathbf{b}_b, \quad (10.2.38)$$

where the coefficient matrix with mesh width $\lambda = a/6$ is

$$\mathbf{A} = \begin{bmatrix} 20 & -16 & 2 & -16 & 8 & 0 & 2 & 0 & 0 & 0 & 0 & 0 \\ -8 & 21 & -8 & 4 & -16 & 4 & 0 & 2 & 0 & 0 & 0 & 0 \\ 1 & -8 & 21 & 0 & 4 & -16 & 0 & 0 & 2 & 0 & 0 & 0 \\ -8 & 4 & 0 & 21 & -16 & 2 & -8 & 4 & 0 & 1 & 0 & 0 \\ 2 & -8 & 2 & -8 & 22 & -8 & 2 & -8 & 2 & 0 & 1 & 0 \\ 0 & 2 & -8 & 1 & -8 & 22 & 0 & 2 & -8 & 0 & 0 & 1 \\ 1 & 0 & 0 & -8 & 4 & 0 & 20 & -16 & 2 & -8 & 4 & 0 \\ 0 & 1 & 0 & 2 & -8 & 2 & -8 & 21 & -8 & 2 & -8 & 2 \\ 0 & 0 & 1 & 0 & 2 & -8 & 1 & -8 & 21 & 0 & 2 & -8 \\ 0 & 0 & 0 & 1 & 0 & 0 & -8 & 4 & 0 & 21 & -16 & 2 \\ 0 & 0 & 0 & 0 & 1 & 0 & 2 & -8 & 2 & -8 & 22 & -8 \\ 0 & 0 & 0 & 0 & 0 & 1 & 0 & 2 & -8 & 1 & -8 & 22 \end{bmatrix} \quad (10.2.39)$$

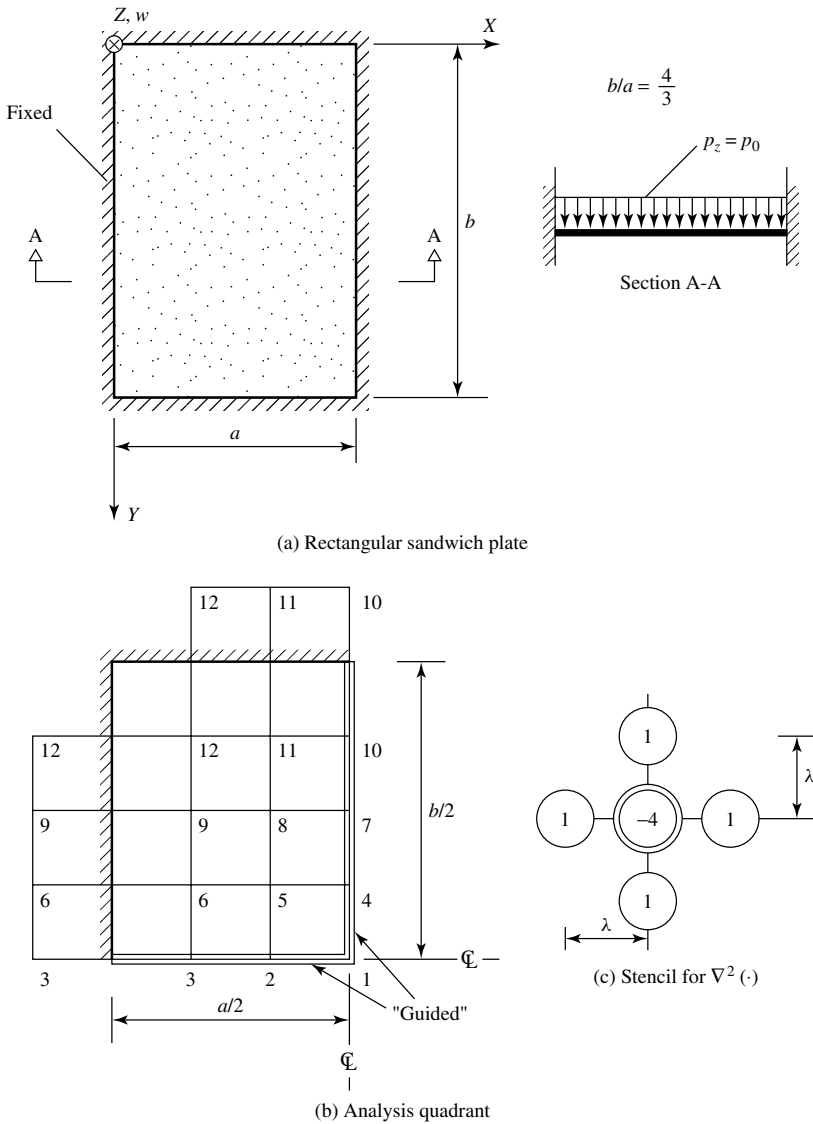


Figure 10.2.8 Analysis of sandwich plate by FDM.

and

$$\mathbf{b}_b = \begin{Bmatrix} 1 \\ 1 \\ 1 \\ \vdots \\ 1 \end{Bmatrix} \frac{\lambda^4 p_0}{D^*} \quad \text{for } \lambda = a/6 \quad (10.2.40)$$

represents the corresponding load vector. Solution of this matrix equation (10.2.38) gives the following bending deflection ordinates at the mesh points:

$$\mathbf{w}_b = \begin{Bmatrix} 234.09 \\ 192.20 \\ 88.60 \\ 214.27 \\ 176.18 \\ 81.62 \\ 156.11 \\ 128.92 \\ 60.62 \\ 70.25 \\ 58.48 \\ 28.19 \end{Bmatrix} \frac{p_0 a^4}{1296 D^*}. \quad (10.2.41)$$

In a similar manner, the shear deflections can be computed from the second expression of Eq. (10.2.15) which, in our special case, is simplified as

$$\nabla^2 w_s = -\frac{p_0}{S} \quad (10.2.42)$$

or in matrix form

$$\mathbf{B} \mathbf{w}_s = - \begin{Bmatrix} 1 \\ 1 \\ 1 \\ \vdots \\ 1 \end{Bmatrix} \frac{a^2 p_0}{36 S}, \quad (10.2.43)$$

where the coefficient matrix \mathbf{B} is obtained by applying the finite difference form of the Laplacian operator $\nabla^2(\cdot)$, given in Fig. 10.2.8c, at each mesh point. To avoid negative values in the main diagonal of matrix \mathbf{B} , however, Eq. (10.2.42) was multiplied by -1 . This gives the coefficient matrix

$$\mathbf{B} = \begin{bmatrix} 4 & -2 & 0 & -2 & 0 & 0 & 0 & 0 & 0 & 0 & 0 & 0 \\ -1 & 4 & -1 & 0 & -2 & 0 & 0 & 0 & 0 & 0 & 0 & 0 \\ 0 & -1 & 4 & 0 & 0 & -2 & 0 & 0 & 0 & 0 & 0 & 0 \\ -1 & 0 & 0 & 4 & -2 & 0 & -1 & 0 & 0 & 0 & 0 & 0 \\ 0 & -1 & 0 & -1 & 4 & -1 & 0 & -1 & 0 & 0 & 0 & 0 \\ 0 & 0 & -1 & 0 & -1 & 4 & 0 & 0 & -1 & 0 & 0 & 0 \\ 0 & 0 & 0 & -1 & 0 & 0 & 4 & -2 & 0 & -1 & 0 & 0 \\ 0 & 0 & 0 & 0 & -1 & 0 & -1 & 4 & -1 & 0 & -1 & 0 \\ 0 & 0 & 0 & 0 & 0 & -1 & 0 & -1 & 4 & 0 & 0 & -1 \\ 0 & 0 & 0 & 0 & 0 & 0 & -1 & 0 & 0 & 4 & -2 & 0 \\ 0 & 0 & 0 & 0 & 0 & 0 & 0 & -1 & 0 & -1 & 4 & -1 \\ 0 & 0 & 0 & 0 & 0 & 0 & 0 & 0 & -1 & 0 & -1 & 4 \end{bmatrix}. \quad (10.2.44)$$

Solution of the altered Eq. (10.2.43) yields

$$\mathbf{w}_s = \begin{Bmatrix} 3.3236 \\ 2.9798 \\ 1.9092 \\ 3.1674 \\ 2.8432 \\ 1.8286 \\ 2.6596 \\ 2.3971 \\ 1.5618 \\ 1.6768 \\ 1.5238 \\ 1.0214 \end{Bmatrix} \frac{a^2 p_0}{36S}, \quad (10.2.45)$$

which represents the vector of shear deformations. The total deflections are obtained from

$$\mathbf{w}^* = \mathbf{w}_b + \mathbf{w}_s = \text{Eq. (10.2.41)} + \text{Eq. (10.2.45)}. \quad (10.2.46)$$

References and Bibliography

- [10.2.1] PISTER, K. S., and DONG, S. B., "Elastic Bending of Layered Plates," *Proc. ASCE*, 84, *J. Eng. Mech. Div.* (Oct. 1959), 1–10.
- [10.2.2] AMBARTSUMYAN, S. A., *Theory of Anisotropic Plates* (translation from the Russian), Technomic Publishing Co., Stamford, Connecticut, 1970.
- [10.2.3] REISSNER, E., "Finite Deflections of Sandwich Plates," in *Proceedings of the First U.S. National Congress of Applied Mechanics*, held in Chicago, June 1951, American Society of Mechanical Engineers, New York, 1952.
- [10.2.4] SMITH, C. B., "Some New Types of Orthotropic Plates Laminated of Orthotropic Materials," *J. Appl. Mech., Trans. ASME*, 20, No. 2 (1953), 286–288.
- [10.2.5] GOLDBERG, M. A., NEWMAN, M., and FORREY, M. J., "Stresses in a Uniformly Loaded Two-Layer Circular Plate," *Proc. ASCE*, 91, *J. Eng. Mech. Div.* (June 1965), 13–31.
- [10.2.6] GRIGOLYUK, E. I., "Theory of Bimetallic Plates and Shells" (in Russian), *Inzhenernyi Sbornik, Inst. Mekhaniki, Akad. Nauk. SSSR*, 17 (1953), 69–120.
- [10.2.7] KOROLEV, V. I., "Thin Double-Layer Plates and Shells" (in Russian), *Inzhenernyi Sbornik, Inst. Mekhaniki, Akad. Nauk. SSSR*, 22 (1955), 98–110.
- [10.2.8] ALLEN, H. G., *Analysis and Design of Structural Sandwich Panels*, Pergamon Press, Elmsford, New York, 1969.
- [10.2.9] ASHTON, J. E., and WHITNEY, J. M., *Theory of Laminated Plates*, Technomic Publishing Co., Stamford, Connecticut, 1970.
- [10.2.10] SCHMIT, L. A., and MONFORTON, G. R., "Finite Deflection Discrete Element Analysis of Sandwich Plates and Cylindrical Shells with Laminated Faces," *AIAA J.*, 8, No. 8 (Aug. 1970), 1454–1461.
- [10.2.11] ALEKSANDROV, A. I., *Raschet trekhsvinykh panelei* (Design of Three-Layered Panels), Gosudarstvennoe Nauchno-tekhnicheskoe Izdatelstvo, Oborongiz, Moscow, 1960.
- [10.2.12] PRYOR, C. W., and BARKER, R. M., "A Finite Element Analysis Including Transverse Shear Effects to Laminated Plates," *AIAA J.*, 9 (May 1971), 912–917.
- [10.2.13] REISSNER, E., "On Bending of Elastic Plates," *Quart. Appl. Mech.*, 5 (1947), 55–68.

- [10.2.14] UENG, C. E. S., and LIN, U. J., "On Bending of Orthotropic Sandwich Plates," *AIAA J.*, 4 (1966), 2241–2242.
- [10.2.15] HUSSEIN, R. M., *Composite Panels/Plates: Analysis and Design*, Technomic Publishing Co., Lancaster, Pennsylvania, 1986.
- [10.2.16] ALLEN, H. G., *Analysis Design of Structural Sandwich Plates*, Pergamon Press, London, 1969.
- [10.2.17] GHALI, A., and NEVILLE, A. M., *Structural Analysis: A Unified Classical and Matrix Approach*, 2nd ed., Chapman & Hall, London, 1978.
- [10.2.18] MONTAGUE, P., "Simple Grillage Analogy for the Analysis of Steel Sandwich Plates with Penetrations," *Struct. Eng.*, 69 (1991), 271–276.
- [10.2.19] LIBOVE, C., and HUBKA, R. E., "Elastic Constants for Corrugated Core Sandwich Plates," NACA Tech. Note 2289, Langley Field, Virginia, 1951.
- [10.2.20] MCGLENN, J., and HARTZ, B., "Finite Element Analysis of Plywood Plates," *J. Struct. Div.*, ASCE, 94 (1968), 551–565.
- [10.2.21] MONFORTON, G. R., "Finite Element Analysis of Skew Sandwich Plates," *J. Eng. Mech.*, ASCE, 98 (1972), 763–769.
- [10.2.22] HA, H. K., "Analysis of Three-Dimensional Orthotropic Sandwich Plate Structures by Finite Element Method," Ph.D. Thesis, Sir George Williams University, Montreal, Canada, 1972.
- [10.2.23] MORTON, G. R., and SCHMIT, L. A., "Finite Element Analysis of Sandwich Plates," in *Proceedings of the Conference on Matrix Methods in Structural Mechanics*, AF Publ. No. TR-68-150, Wright-Patterson Air Force, Dayton, Ohio, 1968.
- [10.2.24] ENTERPRISE SOFTWARE PRODUCTS, *Finite Element Modeling and Postprocessing (FEMAP)*, version 4.3, Exton, Pennsylvania, 1994.
- [10.2.25] OCHOA, O. O., and REDDY, J. N., *Finite Element Analysis of Composite Laminates*, Kluwer Academic Publishers, Dordrecht, 1992.
- [10.2.26] REDDY, J. N. and MIRAVETE, A., *Practical Analysis of Composite Laminates*, CRC Press, Boca Raton, Florida, 1995.
- [10.2.27] REDDY, J. N., *Mechanics of Laminated Composite Plates*, CRC Press, Boca Raton, Florida, 1996.
- [10.2.28] NOOR, A. K., and BRTON, W. S., "Assessment of Shear Deformation Theories for Multilayered Composite Plates," *Appl. Mech. Rev.*, 42 (1989), 1–12.
- [10.2.29] REDDY, J. N., "A Review of Refined Theories of Laminated Composite Plates," *Shock Vib. Dig.*, 22, No. 7. (1990), 3–17.
- [10.2.30] RAY, D. P., and SINHA, P. K., "On the Flexural Behavior of Orthotropic Sandwich Plates," *Build. Sci.*, 8 (1973).
- [10.2.31] VINSON, J. R., *Behavior of Sandwich Structures of Isotropic and Composite Materials*, Technomic Publishing Co., Lancaster, Pennsylvania, 1999.
- [10.2.32] MATTEWS, G. A. O., et al., *Finite Element Modeling of Composite Materials and Structures*, CRC Press, Boca Raton, Florida, 2001.

10.3 Analysis of Skew Plates

Skew plates are of considerable practical importance, since they are often used in civil, mechanical, aeronautical and marine engineering. Continuous skew plate structures are especially important in the design of bridges for oblique-angle crossings (Fig. 10.3.1). In addition, reinforced-concrete skew slabs also find extensive applications in building floor systems. Skew plates can be analyzed using either analytical or numerical solution techniques, introduced in previous chapters. Owing to its mathematical complexity, analytical methods often fail to provide adequate solutions; thus,

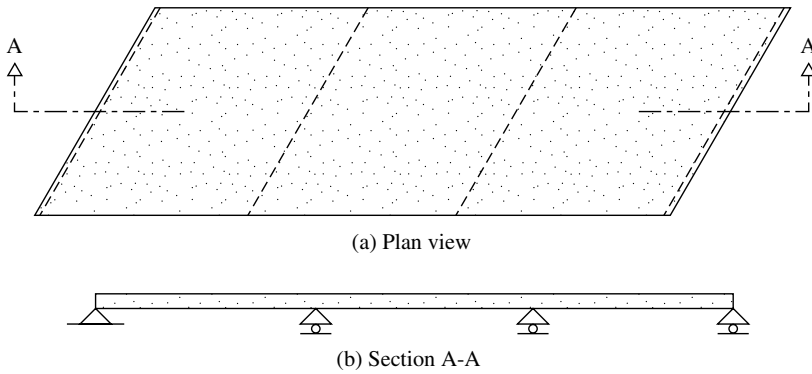


Figure 10.3.1 Skew slab bridge.

numerical techniques such as the finite difference, gridwork and finite element methods are the most commonly used procedures for the bending analysis of skew plates.

a. Analytical Methods. The governing differential equation for isotropic skew plates can be conveniently obtained by introducing an *oblique* coordinate system, as shown in Fig. 10.3.2. The coordinates of the rectangular (X, Y, Z) and oblique (\bar{X}, \bar{Y}, Z) systems are related by

$$\bar{x} = x - y \tan \varphi \quad \text{and} \quad \bar{y} = \frac{1}{\cos \varphi} y. \quad (10.3.1)$$

Substitution of these expressions into Eq. (1.2.31) transforms the Laplacian operator from the rectangular to the oblique coordinate system. Thus, we have

$$\nabla^2 = \frac{1}{\cos^2 \varphi} \left(\frac{\partial^2}{\partial x^2} - 2 \sin \varphi \frac{\partial^2}{\partial \bar{x} \partial \bar{y}} + \frac{\partial^2}{\partial \bar{y}^2} \right). \quad (10.3.2)$$

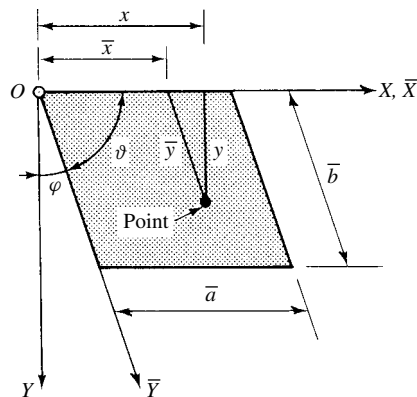


Figure 10.3.2 Oblique coordinate system.

Therefore, the governing plate equation (1.2.30) expressed in terms of the oblique coordinates is

$$\frac{D}{\cos^4 \varphi} \left[\frac{\partial^4 \bar{w}}{\partial \bar{x}^4} + 2(1 + 2 \sin^2 \varphi) \frac{\partial^4 \bar{w}}{\partial \bar{x}^2 \partial \bar{y}^2} - 4 \sin \varphi \left(\frac{\partial^4 \bar{w}}{\partial \bar{x}^3 \partial \bar{y}} + \frac{\partial^4 \bar{w}}{\partial \bar{x} \partial \bar{y}^3} \right) + \frac{\partial^4 \bar{w}}{\partial \bar{y}^4} \right] = \bar{p}_z(\bar{x}, \bar{y}), \quad (10.3.3)$$

or, more concisely,

$$\boxed{D \bar{\nabla}^2 \bar{\nabla}^2 \bar{w}(\bar{x}, \bar{y}) = \bar{p}_z(\bar{x}, \bar{y})}. \quad (10.3.4)$$

For convenience, the boundary conditions should also be expressed in terms of oblique coordinates parallel to edges. A similar procedure can be applied to the governing equation (10.1.6) of orthotropic plates.

The analytical solution of Eq. (10.3.4) becomes complicated by the absence of orthogonal relationships. Consequently, rigorous solutions are quite difficult and thus rarely obtained [10.3.3, 10.3.4]. In addition, special problems arising at corners with acute and obtuse angles make exact solutions even more difficult.

Since the differential equation of skew plates is available, in the case of simple loading and boundary conditions Galerkin's variational process can be employed to obtain deflections and moments. Equation (10.3.1) will also transform the expressions for moments and shears, given in Eqs. (1.2.26), (1.2.27) and (1.2.23), into oblique coordinates. The problem of clamped oblique plates subjected to uniform lateral load, for instance, can be analyzed by using the displacement function

$$\bar{w}(\bar{x}, \bar{y}) = \frac{\bar{W}}{4} \left(1 - \cos \frac{2\pi x}{a} \right) \left(1 - \cos \frac{2\pi y}{b} \right) \quad (10.3.5)$$

expressed in terms of oblique coordinates. In more general cases, however, even such an approximate solution becomes very tedious. For solutions of skew plate problems, frequently occurring in bridge design, extensive tables and graphs are available to practicing engineers [10.3.4–10.3.11, 10.3.19, 10.3.20].[†] Morley has presented in Ref. [10.3.1] a detailed overview of the analytical methods discussed above.

Another analytical approach applies *geometrical mapping*. The skew plate (Fig. 10.3.3a) can be mapped into a unit-square region (Fig. 10.3.3b) in the ξ - η plane by using the transformation relationships

$$x = a\xi + b\kappa\eta \quad \text{and} \quad y = b\eta, \quad (10.3.6)$$

where

$$\kappa = \frac{\cos \theta}{\sin \theta}. \quad (10.3.7)$$

Since such a mapping process requires extensive mathematical manipulations, its treatment is beyond the scope of this book.

[†] Also see the references on influence surfaces for skew plates given in Sec. 10.5

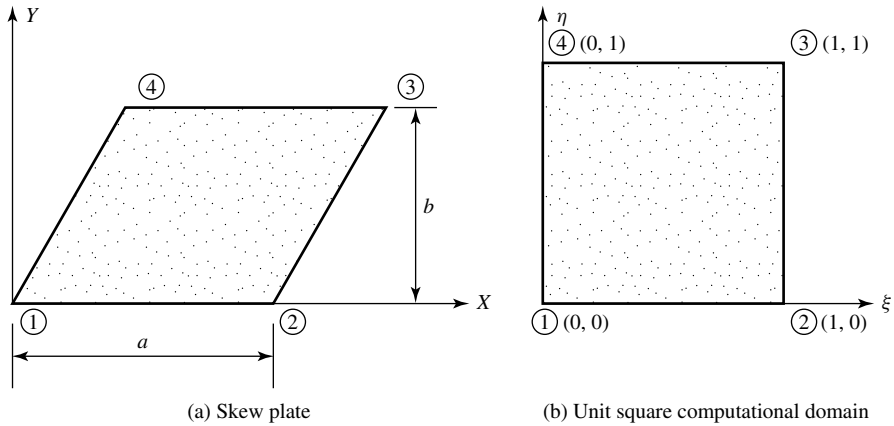


Figure 10.3.3 Mapping of skew plate.

b. Numerical Methods. When analytical methods fail to provide solutions to problems of skew plates, numerical methods must be applied. Although the ordinary FDM described in Sec. 5.1 can easily be extended to oblique or triangular meshwork, the user of this simple technique must be aware of the following problems created by oblique plate shapes:

1. Increase in the skew angle φ adversely influences convergence of the solution.
2. Singularities at corners with obtuse angles cannot be properly accounted for. Additional problems arise at corners with acute angles.
3. Complete satisfaction of the boundary conditions at free edges is difficult.
4. Since moments and shears depend upon differences between the deflection values, it is of basic importance that deflections are determined with a good degree of accuracy.

In spite of these and other limitations of this simple numerical technique, the method yields acceptable results for most practical design purposes. That is, with sufficiently fine subdivisions the oblique boundary can be approximated with a rectangular mesh, as shown in Fig. 5.1.2, thus eliminating the need for oblique or triangular meshwork. Furthermore, the reader will find finite difference solutions of skew plates in Refs. [10.3.12–10.0.15]. Coefficient values for maximum moments along the edge beams were determined by Stiglat using the finite difference technique [10.3.24].

The ordinary finite difference expression for the Laplacian operator ∇^2 is given in Fig. 10.3.4. This operator can be directly utilized in the two-stage solution of the governing differential equation. For simply supported pales, Marcus's method[†] splits the governing fourth-order differential equation (10.3.4) into the two second-order differential equations

$$\begin{aligned}\nabla^2 \overline{m} &= -\overline{p}_z(\overline{x}, \overline{y}), \\ \nabla^2 w &= -\frac{\overline{m}}{D},\end{aligned}\tag{10.3.8}$$

[†] See Eqs. (1.2.43a) and (1.2.43b).

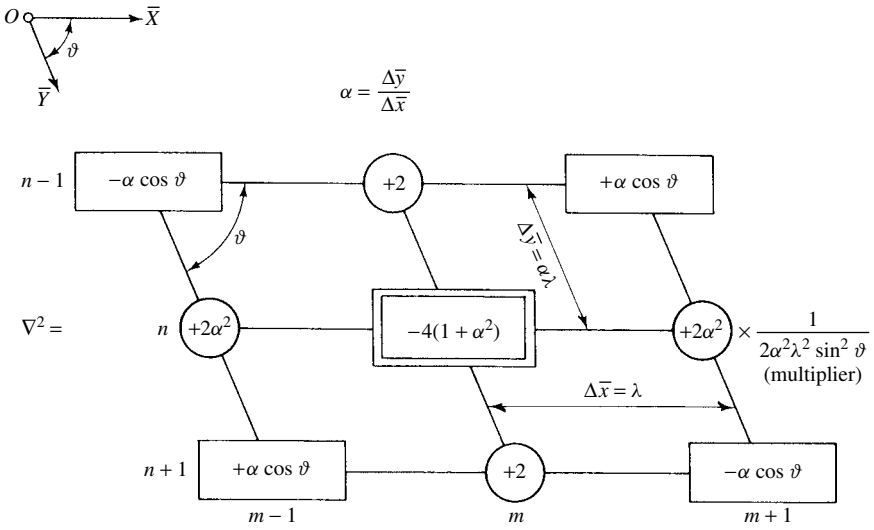


Figure 10.3.4 Stencil for ∇^2 operator in oblique coordinate system.

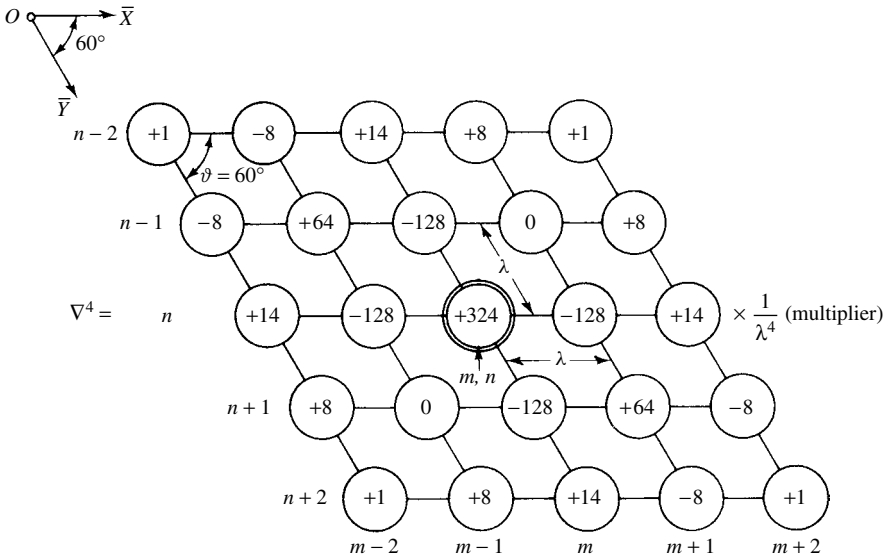


Figure 10.3.5 Stencil for operator ∇^4 in oblique coordinate system ($\vartheta = 60^\circ$).

where $\overline{\mathfrak{M}}$ is the so-called *moment-sum* expressed in the oblique coordinate system. In this way, the loads can be expressed in terms of $\overline{\mathfrak{M}}$ and subsequently are related to the deflections w . Figure 10.3.5 shows a readily usable finite difference stencil for the biharmonic operator in an oblique coordinate system.

The *gridwork method* discussed in Chapter 2 is well suited for the bending analysis of skew plates. In this case, especially, Salonen's approach appears to have certain advantages over the other gridwork approximations, since it can be directly used in a commercially available grillage program. After the deflections of the joint points are determined, the moments and shears can be calculated using the pertinent ordinary finite difference approximations in the oblique coordinate system.

The great versatility of the FEM permits, among other items, consideration of variable thickness, orthotropy and even interactions between spandrel beams and columns with the plate by utilizing the corresponding stiffness matrices of the individual structural members. The *discrete Kirchhoff triangular* (DKT) plate element has already been treated in Sec. 7.7.2. Because of its excellent convergence characteristics, it should be the prime choice for analyzing skew plates by the FEM. Here, again, singularities may create problems in the solution. For instance, in the case of obtuse corners bound by fixed and free-edges, infinite stresses occur whenever the corner angle exceeds approximately 95° . Furthermore, the effect of singularity increases with the increase of skew angles. To partly offset such localized stress irregularities, a fine subdivision should be used in such regions.

Finally, it should be mentioned that the bending behavior of moderately thick skew Reissner-Mindlin plates has also recently been investigated [10.3.25]. In certain cases, the newly introduced spline finite strip element method [10.3.26] can offer a usable alternative to the FEM.

c. Behavior of Skew Plates at Certain Corner Points. Since classical plate theory per se cannot satisfy all boundary conditions, Kirchhoff replaced the torsional moments at the plate edges with equivalent *supplementary forces* to eliminate this mathematical problem, as discussed in Sec. 1.3. There are, however, certain boundary

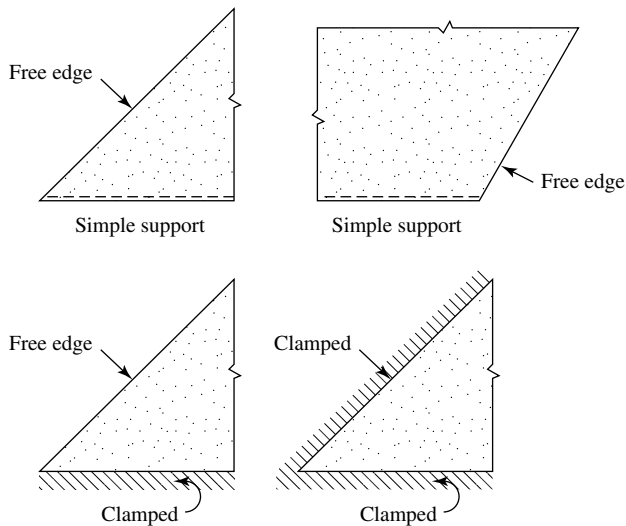


Figure 10.3.6 Plate corners without twisting moments and corner forces.

configurations where the torsional edge moments and corresponding corner forces vanish at the corners [10.3.27]. Such corners with acute and obtuse angles are shown in Fig. 10.3.6 [10.3.29].

Summary. The problems associated with skew plates are discussed in this section considering the available analytical and numerical methods of solution. Again, the shortcomings of the analytical methods are underscored, while the potentials of the numerical methods are emphasized. For smaller skew plate problems, the FDM yields satisfactory results in a simple way. For larger problems, the ease with which the gridwork method can be applied and the versatility of the FEM are demonstrated below in Illustrative Examples II and III, respectively. Special attention is paid to the assessment of skew plate behaviors at corners with acute or obtuse angles.

ILLUSTRATIVE EXAMPLE I

Let us consider a simply supported skew plate with $\bar{a} = \bar{b}$, $\vartheta = 60^\circ$ ($\varphi = 30^\circ$) and $\alpha = 1$. In this case, the Laplacian operator $\bar{\nabla}^2$ becomes the operator shown in Fig. 10.3.7. Determine the maximum deflection \bar{w}_{\max} of this plate subjected to uniformly distributed load p_0 .

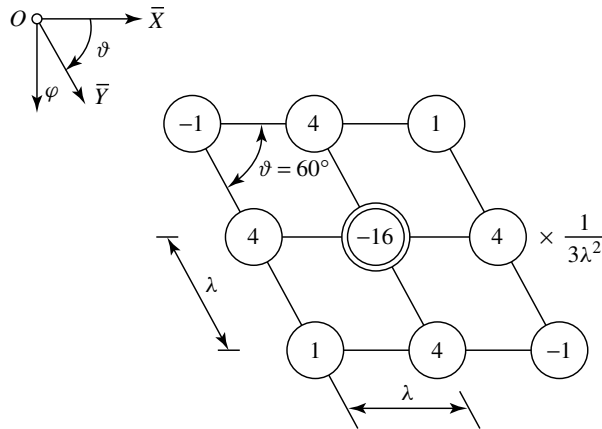


Figure 10.3.7 Operator $\bar{\nabla}^2$ with $\vartheta = 60^\circ$ ($\varphi = 30^\circ$).

The simply supported boundary conditions

$$\bar{w} = 0 \quad \text{and} \quad \bar{m}_x = \bar{m}_y = 0 \quad (10.3.9)$$

permit the use of the two-stage solution technique. However, to avoid negative definite coefficient matrices in the solutions, we multiply both equations in Eq. (10.3.8) by -1 .

First, we use a very crude finite difference mesh with $\lambda = \bar{a}/2$. Thus, the first equation of Eq. (10.3.8) gives

$$\frac{16\overline{\mathfrak{M}}_1}{3\lambda^2} = p_0; \quad \therefore \overline{\mathfrak{M}}_1 = \frac{3\overline{a}^2 p_0}{64} = 0.04688\overline{a}^2 p_0. \quad (10.3.10)$$

From the second Eq. (10.3.8) we obtain

$$\frac{16\overline{w}_1}{3\lambda^2} = \frac{3\overline{a}^2 p_0}{64D}; \quad \therefore \overline{w}_1 = \overline{w}_{\max}^{(1)} = \frac{9\lambda^2 \overline{a}^2 p_0}{16 \times 64D} = 0.0022 \frac{\overline{a}^4 p_0}{D}. \quad (10.3.11)$$

Next, we refine the finite difference mesh by using $\lambda = \overline{a}/4$. Numbering of the mesh points is shown in Fig. 10.3.8. By applying the ∇^2 operator at each numbered mesh point, we obtain the following simultaneous algebraic equations for the moment-sums:

$$\{\overline{\mathfrak{M}}\} = \begin{bmatrix} 16 & -4 & 0 & -4 & 1 & 0 & 0 & 0 & 0 \\ -4 & 16 & -4 & -1 & -4 & 1 & 0 & 0 & 0 \\ 0 & -4 & 16 & 0 & -1 & -4 & 0 & 0 & 0 \\ -4 & -1 & 0 & 16 & -4 & 0 & -4 & 1 & 0 \\ 1 & -4 & -1 & -4 & 16 & -4 & -1 & -4 & 1 \\ 0 & 1 & -4 & 0 & -4 & 16 & 0 & -1 & -4 \\ 0 & 0 & 0 & -4 & -1 & 0 & 16 & -4 & 0 \\ 0 & 0 & 0 & 1 & -4 & -1 & -4 & 16 & -4 \\ 0 & 0 & 0 & 0 & 1 & -4 & 0 & -4 & 16 \end{bmatrix}^{-1} \begin{Bmatrix} 1 \\ 1 \\ 1 \\ 1 \\ 1 \\ 1 \\ 1 \\ 1 \\ 1 \end{Bmatrix} \\ \times 0.1875 \overline{a}^2 p_0 = \mathbf{A}^{-1} \mathbf{b}, \quad (10.3.12)$$

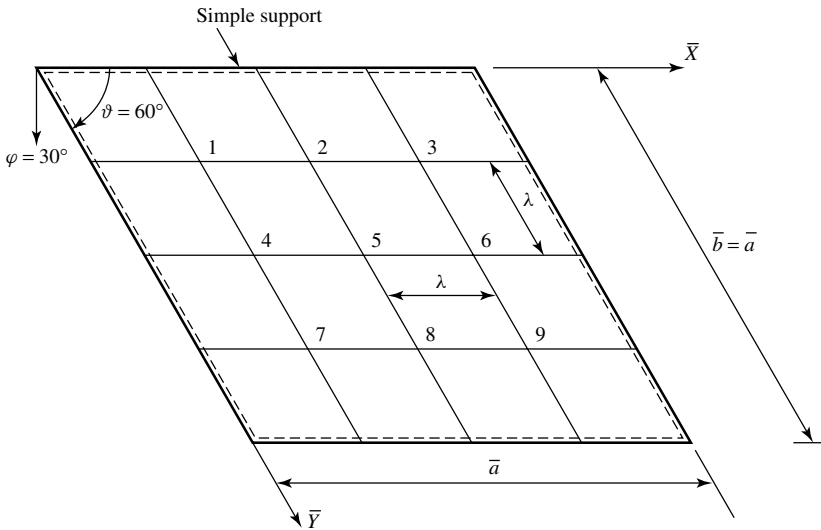


Figure 10.3.8 Oblique finite difference mesh for $\lambda = a/4$.

which gives

$$\{\overline{\mathfrak{M}}\} = \begin{Bmatrix} 0.155 \\ 0.221 \\ 0.191 \\ 0.221 \\ 0.288 \\ 0.221 \\ 0.191 \\ 0.221 \\ 0.155 \end{Bmatrix} 0.1875 \overline{a}^2 p_0. \quad (10.3.13)$$

Using the same coefficient matrix **A** as given above, the second equation of Eq. (10.3.8) now becomes

$$\mathbf{A}\mathbf{w} = \{\overline{\mathfrak{M}}\} \frac{0.1875 \overline{a}^2 p_0 3\lambda^2}{D}; \quad (10.3.14)$$

hence

$$\mathbf{w} = \mathbf{A}^{-1} \{\overline{\mathfrak{M}}\} \frac{0.03516 \overline{a}^4 p_0}{D}. \quad (10.3.15)$$

Solution of this matrix equation yields

$$\overline{\mathbf{w}} = \begin{Bmatrix} 0.0295 \\ 0.0481 \\ 0.0402 \\ 0.0481 \\ 0.0674 \\ 0.0481 \\ 0.0402 \\ 0.0481 \\ 0.0295 \end{Bmatrix} 0.03516 \frac{\overline{a}^4 p_0}{D}. \quad (10.3.16)$$

Consequently,

$$\overline{w}_5 = \overline{w}_{\max}^{(2)} = 0.0674 \times 0.03516 \frac{\overline{a}^4 p_0}{D} = 0.002369 \frac{\overline{a}^4 p_0}{D}. \quad (10.3.17)$$

Applying Eq. (5.1.38), Richardson's extrapolation formula gives

$$\overline{w}_{\max}^{(3)} = \left(0.002369 + \frac{0.002369 - 0.0022}{3} \right) \frac{\overline{a}^4 p_0}{D} = 0.00243 \frac{\overline{a}^4 p_0}{D}, \quad (10.3.18)$$

which is already reasonably close to the difficult analytical solution of this plate problem. Of course, we can further increase the accuracy of this finite difference solution by using $\lambda = a/8$ subdivisions and a repeated extrapolation.

ILLUSTRATIVE EXAMPLE II

Figure 10.3.9 shows a simple-span, reinforced-concrete, skew bridge subjected to $P_z = 100$ kN concentrated force acting at the center of the bridge. Determine the maximum deflection \bar{w}_{\max} and the maximum moments $\bar{m}_{x,\max}$ and $\bar{m}_{y,\max}$ of the bridge by using the gridwork method (GWM).

Applying Salonen's[†] lattice analogy, we introduce a substitute gridwork system consisting of 56 beams, as shown in Fig. 10.3.10. The *equivalent cross-sectional properties* I , I_t are calculated from Eq. (6.2.6). In this case

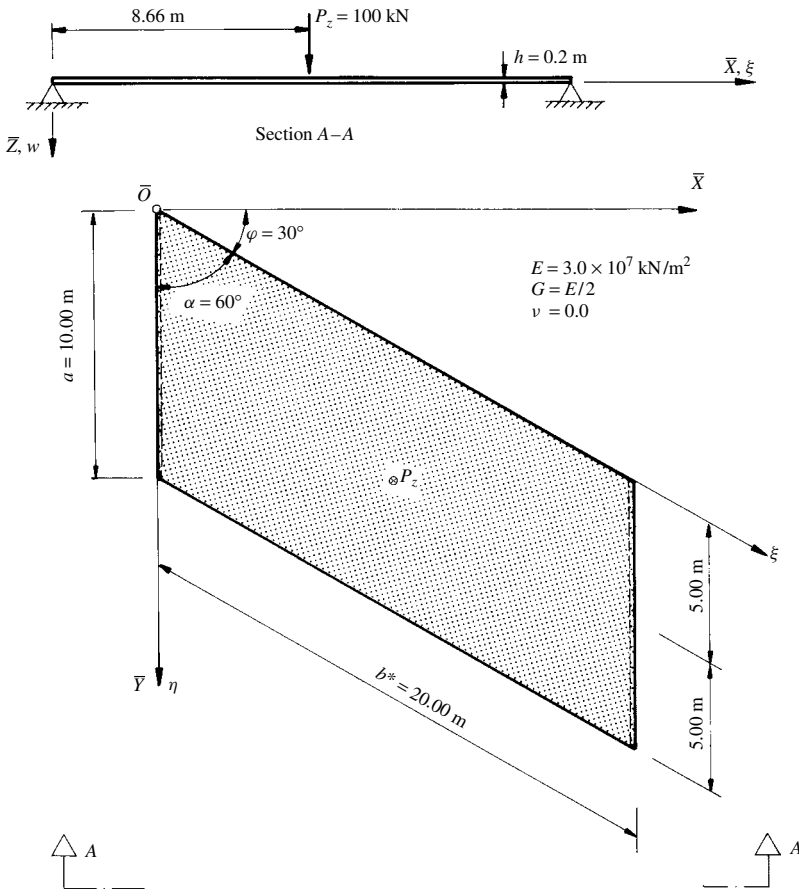


Figure 10.3.9 Skew plate in parallelogram shape.

[†] See Sec. 6.2.

we deal with five beam types. Their equivalent sectional properties are listed in Table 10.3.1

Beams with the corresponding types are listed in Table 10.3.2. The boundary conditions of each joint located at the periphery of the plate are given in Table 10.3.3.

With these values, our gridwork program [10.3.30] yielded $\bar{w}_{\max} = 0.062$ m at joint (13), while the same problem solved utilizing the ordinary FDM gave $\bar{w}_{\max} = 0.066$ m [10.3.9]. Thus, the difference between these two approximate results is merely 6%. Since the convergence characteristics of the GWM is

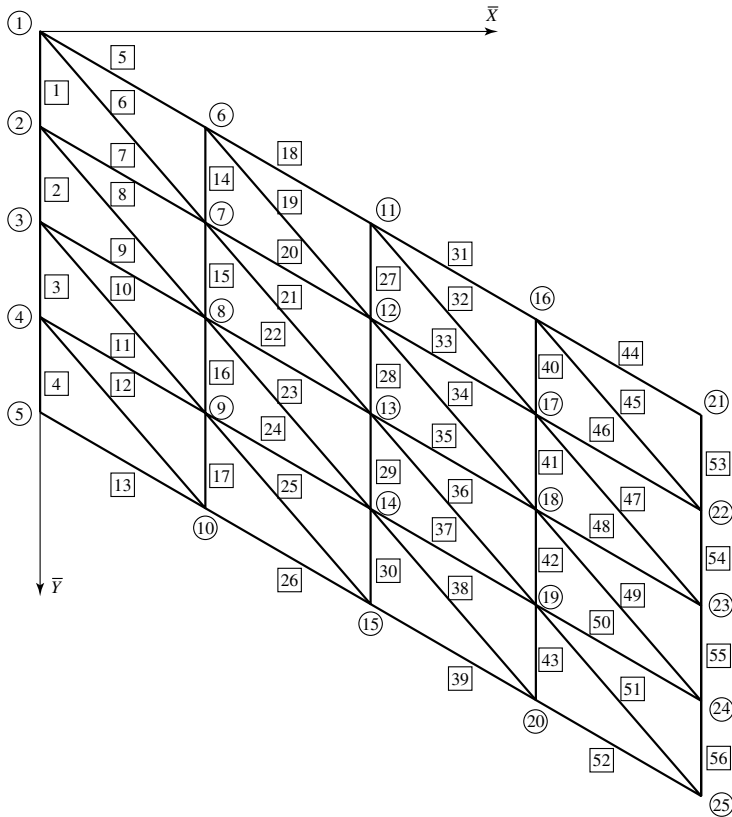


Figure 10.3.10 Substitute gridwork system.

Table 10.3.1 Beam Types

Type	$l^{(N)}$ (m)	$\alpha^{(N)}$ (deg)	$\cot \alpha^{(N)}$	$I^{(N)}$ (m ⁴)	$I_t^{(N)}$ (m ⁴)	Beam
1	2.5	19.1074	2.887	2.406	4.812	1
2	5.00	40.8926	1.1547	1.9245	3.849	5
3	6.61	120	-0.577	-2.543	-5.0883	6
4	5.00	40.8926	1.1547	3.849	7.698	7
5	2.5	19.1074	2.887	4.8116	9.6233	14

Table 10.3.2 Partial List of Beam Data

<i>Beam Number</i>	<i>Joint Number</i>	<i>Type</i>
1	1-2	1
2	2-3	1
3	3-4	1
4	4-5	1
5	1-6	2
6	1-7	3
7	2-7	4
8	2-8	3
9	3-8	4
10	3-9	3
11	4-9	4
12	4-10	3
13	5-10	2
14	6-7	5
15	7-8	5
16	8-9	5
17	9-10	5
18	6-11	2
19	6-12	3
20	7-12	4

Table 10.3.3 Partial List of Boundary Conditions

<i>Joint Number</i>	<i>w Locked</i>	<i>Θ_x Locked</i>	<i>Θ_y Locked</i>
1	Y	Y	N
2	Y	Y	N
3	Y	Y	N
4	Y	Y	N
5	Y	Y	N
6	N	N	N
10	N	N	N
11	N	N	N
15	N	N	N
16	N	N	N
20	N	N	N
21	Y	Y	N
22	Y	Y	N
23	Y	Y	N
24	Y	Y	N
25	Y	Y	N

Note: Y = yes; N = no.

better than those of the FDM and, in addition, the subdivision was finer, we may consider the solution obtained by the GWM as more accurate. The maximum moments, expressed in the oblique coordinate system, can be approximated by

$$\begin{aligned}\bar{m}_{x,\max} &\approx \frac{D}{(EI)_{13}} \bar{M}_{13}^{(22)} = \frac{8}{12 \times 3.849} 250.7 = 43.42 \text{ kN/m}, \\ \bar{m}_{y,\max} &\approx \frac{D}{(EI)_{13}} \bar{M}_{13}^{(29)} = \frac{8}{12 \times 4.8116} 86.9 = 11.90 \text{ kN/m},\end{aligned}\quad (10.3.19)$$

where \bar{M} represents the moment of the corresponding beam at joint point (13). Since the above-mentioned gridwork program gave all joint-point deflections, we could also have calculated these maximum bending moments by applying the pertinent expressions of the FDM expressed in the oblique coordinate system \bar{X}, \bar{Y} .

ILLUSTRATIVE EXAMPLE III

Let us now analyze the continuous plate bridge shown in Fig. 10.3.11 using the versatile FEM. The two abutments at the ends of the bridge represent simple supports, while the interior supports are provided by columns. This reinforced-concrete bridge carries its dead load of $p_z = 3 \text{ kN/m}^2$ along with a live load in the form of four concentrated forces $P_z = 100 \text{ kN}$, which may symbolize the wheel loads of a truck. We will determine (a) the deflected midsurface of the plate and (b) the stresses σ_y in the longitudinal direction.

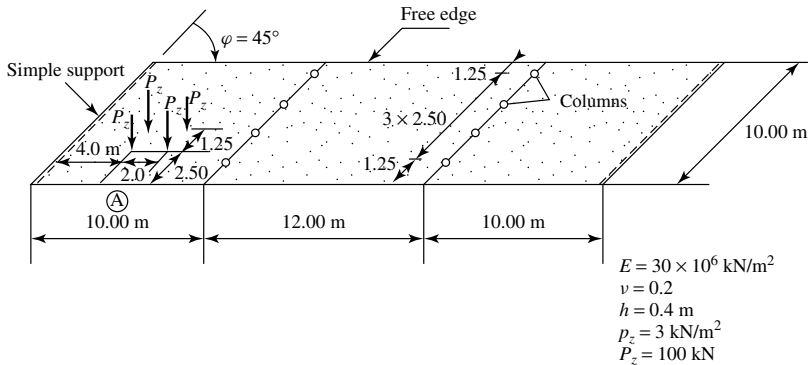


Figure 10.3.11 Continuous skew plate.

To solve this “real live” plate problem, we subdivide the bridge into 512 DKT elements. With this relatively fine subdivision, our pertinent finite element computer program [10.3.31] computed $w_A = 0.00097 \text{ m}$ lateral deflection under the dead load at reference point (A). A check of this result with Ref. [10.3.20] reveals merely 3% discrepancy. The contour lines of the deflected plate surface and those of the σ_y stresses in the vicinity of the truck load are shown in Fig. 10.3.12. The dimensions are in meters and kilonewtons per meters squared, respectively.

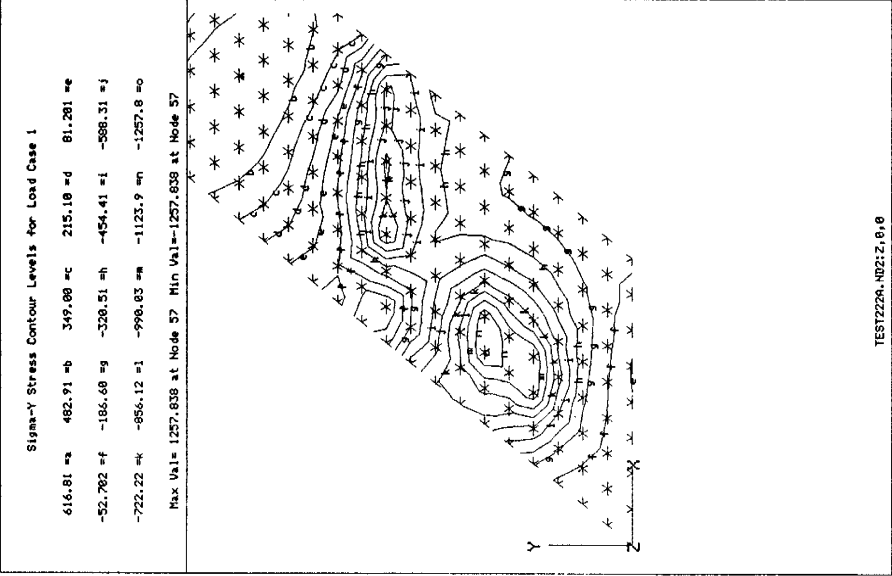
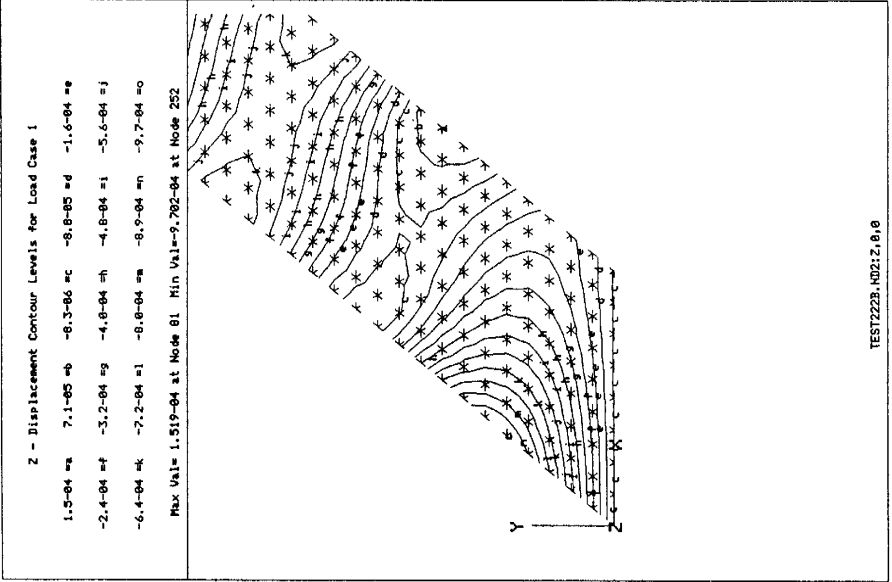


Figure 10.3.12 Graphical display of results.

References and Bibliography

- [10.3.1] MORLEY, L. S. D., *Skew Plates and Structures*, Macmillan Company, New York, 1963.
- [10.3.2] KENNEDY, J. B., and TAMBERG, K. G., "Problems of Skew in Concrete Bridge Design," Report No. RR144, Department of Highways, Downsview, Ontario, Canada, March 1969.
- [10.3.3] KRETTNER, J., "Beitrag zur Berechnung schiefwinkliger Platten," *Ing.-Arch.*, 22 (1954), 47–54.
- [10.3.4] LARDY, P., "Die strenge Lösung des Problems der schiefwinkligen Platte," *Schweiz. Bauzeitung*, 67 (Apr. 1949), 207–209.
- [10.3.5] FAVRE, H., "Contribution à l'étude des plaques obliques," *Schweiz. Bauzeitung*, 120, Nos. 5 and 6 (July–Aug. 1942), 35–36, 51–54.
- [10.3.6] KENNEDY, J. B., and HUGGINS, M. V., "Series Solution of Skewed Stiffened Plates," *Proc. ASCE*, 90, *J. Eng. Mech. Div.*, No. EM1 (Feb. 1964), 1–22.
- [10.3.7] RÜSCH, H., "Berechnungstafeln für schiefwinklige Fahrbahnplatten von Strassenbrücken," *Deutscher Ausschuss für Stahlbeton*, Heft 166, W. Ernst & Sohn, Berlin, 1967.
- [10.3.8] HOMBERG, H., and MARX, K., *Schiefe Stäbe und Platten*, Werner-Verlag, Düsseldorf, 1958.
- [10.3.9] BARES, R., *Tables for the Analysis of Plates, Slabs and Diaphragms Based on the Elastic Theory: Berechnungstafeln für Platten und Wandscheiben* (German-English edition), Bauverlag GmbH, Wiesbaden, 1969.
- [10.3.10] RÜSCH, H., and HERGENRODER, A., *Einflussfelder der Momente schiefwinkliger Platten*, Selbstverlag des MPA Bauwesen der Technischen Hochschule, Munich, 1964.
- [10.3.11] VOGT, H., "Die Berechnung schiefwinkliger Platten und plattenartiger Brückensysteme," *Beton und Eisen*, 39, No. 17 (Sept. 1940), 243–245.
- [10.3.12] JENSEN, V. P., "Analysis of Skew Slabs," *Univ. Illinois Eng. Exp. Stat. Bull.*, 332 (Sept. 1941).
- [10.3.13] JENSEN, V. P., and ALLEN, J. W., "Studies of Highway Skew Slab-Bridges with Curbs, Pt. I: Results of Analyses," *Univ. Illinois Eng. Exp. Sta. Bull.*, 369 (Sept. 1947).
- [10.3.14] NARUOKA, M., and OMURA, H., "Digital Computer Analysis of Influence Coefficients for Deflection and Bending Moment of Orthotropic Parallelogram Plates," *Mem. Fac. Eng. Kyoto Univ.*, 21, Pt. 2 (1959) 103–127.
- [10.3.15] GHALI, A., "Analysis of Continuous Skew Concrete Bridges," in *Proceedings of the First International Symposium on Concrete Bridge Design, Toronto, 1967*, American Concrete Institute, Detroit, Michigan, 1969.
- [10.3.16] CHEUNG, Y. K., et al., "Slab Bridges with Arbitrary Shape and Support Conditions: A General Method of Analysis based on Finite Elements," *Proc. Inst. Civil Eng.*, 40 (May 1968), 11–36.
- [10.3.17] MONFORTON, G. R., and SCHMIT, L. A., Jr., "Finite Element Analysis of Skew Plates in Bending," *AIAA J.*, 6, No. 6 (June 1968), 1150–1152.
- [10.3.18] BÖLCSKEI, E., *Beton-Vasbeton és Feszítettbeton Hidak* (Concrete, Reinforced and Prestressed Concrete Bridges), Tankönyvkiadó, Budapest, 1968.
- [10.3.19] JÁVOR, T., *Simké doskové a roštové mosty: tabuľky vplyvových plôch—Skew Slab and Gridwork Bridges: Tables of Influence Surfaces* (in Slovak, English, German and Russian), Slovenské Vydavateľstvo Tech. Lit., Bratislava, 1967.
- [10.3.20] SCHLEICHER, C., and WEGENER, B., *Durchlaufende schiefe Platten: Continuous Skew Slabs* (in German, Russian and English), VEB Verlag für Bauwesen, Berlin, 1968.
- [10.3.21] SAWKO, F., and COPE, R. J., "The Analysis of Skew Bridge Decks—A New Finite Element Approach," *Struct. Eng.*, 47 (June 1969), 215–224.
- [10.3.22] RAMSTADT, H., "Parallelogram Elements in Bending; Accuracy and Convergence of Results," *Div. Struct. Mech. Tech. Univ. Norway* (Oct. 1967).
- [10.3.23] YEGINOBALI, A., "Continuous Skewed Slabs," *Bull. Eng. Exp. Sta. Ohio State Univ.*, 178 (Nov. 1959), 1–221.
- [10.3.24] STIGLAT, K., *Rechteckige und schiefe Platten mit Randbalken*, Wilhelm Ernst & Sohn, Berlin, 1962.

- [10.3.25] LIEW, K. M., and HAN, J.-B., "Bending Analysis of Shear Deformable Skew Plates," *J. Eng. Mech., ASCE*, 123 (1997), 214–221.
- [10.3.26] THAM, L. G., et al., "Bending of Skew Plates by Spline-Finite-Strip Method," *Comp. Struct.*, 22 (1986), 31–38.
- [10.3.27] WOJNOWSKY-KRIEGER, S., "Über Anwendung der Mellin-Transformation zur Lösung einer Aufgabe der Plattenbiegung," *Ing.-Arch.*, 20 (1952), H.6., 391.
- [10.3.28] RUMPEL, G., "Über das Verhalten dünner Platten in den Eckpunkten," *Der Bauingenieur*, 33 (1958), H.2, 50–54.
- [10.3.29] HANUSKA, A., and BALAS, J., "Hauptbiegungsmomentenlinien schiefer Platten," *Der Bauingenieur*, 40 (1965), 265–267.
- [10.3.30] SZILARD, R., et al., *TURBO-Basic Programme für Baumechanik und Statik*, Ernst & Sohn, Berlin, 1989.
- [10.3.31] SZILARD, R., and DUNAI, L., *FlächES Berechnung von Flächentragwerken*, Ernst & Sohn, Berlin, 1993.

10.4 Thermal Bending of Plates

Temperature variations often represent serious loading conditions, since they may produce excessive deflections and/or high stresses. If the temperature of the plate is uniformly raised or lowered, the plate expands or contracts, respectively. In addition, nonuniform temperature fields create temperature gradients between the top and bottom surfaces of the plate, producing curvature changes and thus rotations (Fig. 10.4.1). Under the influence of T_{av} , the plate remains flat. However, if the unrestrained plate is subjected to ΔT temperature differences between the top and bottom, the plate would assume a spherical shape, as shown in Fig. 10.4.2. When a free plate is heated or cooled uniformly, no normal stresses, just normal strains, are present. Nevertheless, if expansions or rotations are restrained—by boundary conditions or other suitable forces—*thermal stresses* will occur in the plate. Another cause of thermal stresses is *nonuniform* temperature change. In such a case, the individual laminae cannot expand or contract freely across the plate thickness. That is, the various layers tend to expand or contract but the restriction of continuity prevents their free movement. Although the plate may be physically free to move at the boundaries, its laminae may be unable to expand or contract freely in a manner compatible with the temperature distribution through the plate thickness, thus producing *self-equilibrated*[†] thermal stresses. Therefore, we should distinguish these two different sets of circumstances under which thermal stresses occur.

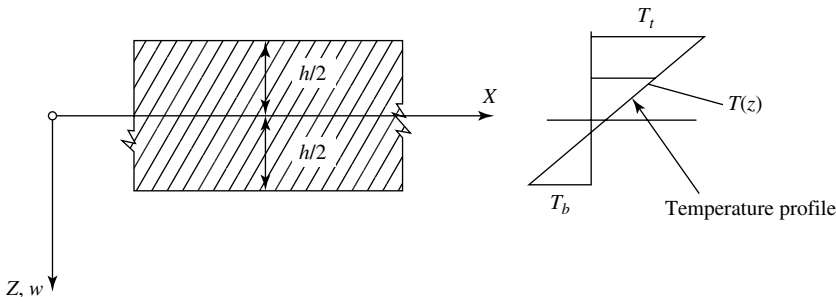


Figure 10.4.1 Linear temperature distribution through thickness of plate ($T_t > T_b$).

[†] That is, no reactions appear at the boundaries.

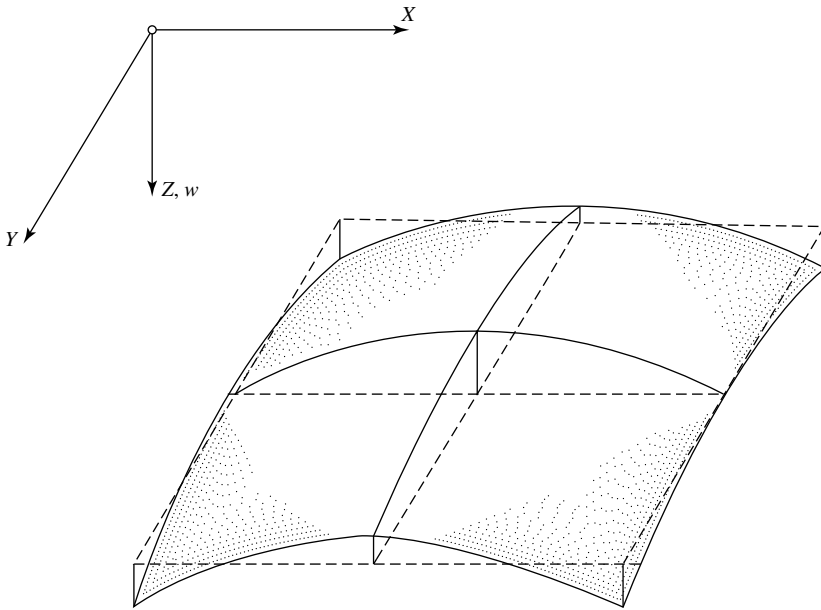


Figure 10.4.2 Deformation of unrestrained rectangular plate temperature gradient.

A practical example of thermal bending of plates includes slab bridges, which are subject to intensive solar radiation in addition to daily change of ambient temperature. The so-created temperature gradients produce thermal stresses, the magnitude of which depends upon the temperature distribution, the boundary conditions and the thermal coefficients of the materials used in construction of the bridge. Thin plates are particularly susceptible to buckling failure induced by thermal or combined lateral and thermal forces, as treated in Sec. 16.8.

Problems involving flexure of plates constructed of isotropic, homogeneous materials subjected to thermal loadings are discussed in this section. Various analytical and numerical solution techniques based upon Kirchhoff's classical plate theory are briefly treated. For moderately thick plates, for which the effect of shear deformation can be significant, we give only the governing differential equations and refer otherwise to the pertinent literature [10.4.15–10.4.18].

a. Governing Equations. With changing temperature, expansion and contraction of the plate occur. For most structural materials, these movements are directly proportional to the change of temperature. Within a certain temperature range, such linear relationships can be expressed by the *coefficient of thermal expansion* α_T , which represents the change in unit length caused by a one-degree ($T = 1^\circ\text{C}$) change of temperature. In SI units, α_T is expressed in meters per degree Celsius. Stresses owing to temperature variations are called *temperature stresses*. As mentioned above, thermal stresses σ_T in a plate are generally present if the movements produced by temperature changes are restricted; otherwise only thermal strains ε_T occur.

Solution for the deflection and stresses in plates due to temperature variations requires augmentation of the previously introduced stress-strain relationships by the

thermal strain. Thus, we can write

$$\begin{aligned}\varepsilon_x &= \frac{1}{E}(\sigma_x - \nu\sigma_y) + \alpha_T T(z), & \varepsilon_y &= \frac{1}{E}(\sigma_y - \nu\sigma_x) + \alpha_T T(z), \\ \gamma_{xy} &= \frac{1}{E}2(1 + \nu)\tau_{xy}.\end{aligned}\quad (10.4.1)$$

It should be noted that temperature change has no effect on the shear-strain component. The quantity of $T(z)$ in Eq. (10.4.1), assuming a linear variation of the temperature gradient, can be expressed by

$$T(z) = \frac{T_t + T_b}{2} + \frac{T_t - T_b}{h}z = T_{av} + \frac{\Delta T}{h}z, \quad (10.4.2)$$

where ΔT represents the difference in temperature between the top and bottom faces of the plate, as shown in Fig. 10.4.1. The temperature gradient between the top and bottom faces is assumed to be linear. An increase in ΔT is considered algebraically positive.

From Eq. (10.4.1) we obtain the corresponding stress components given by

$$\begin{aligned}\sigma_x &= \frac{E}{1 - \nu^2}(\varepsilon_x + \nu\varepsilon_y) - \frac{E}{1 - \nu}\alpha_T T(z), \\ \sigma_y &= \frac{E}{1 - \nu^2}(\varepsilon_y + \nu\varepsilon_x) - \frac{E}{1 - \nu}\alpha_T T(z), \\ \tau_{xy} &= \frac{E}{2(1 + \nu)}\gamma_{xy}.\end{aligned}\quad (10.4.3)$$

In the case of bending, we express the strains by the second derivatives of the deflections, w , as discussed in Sec. 1.2. Thus, integration of the stresses gives

$$m_{x,y} = \int_{-h/2}^{+h/2} \sigma_{x,y} z \, dz \quad \text{and} \quad m_{xy} = \int_{-h/2}^{+h/2} \tau_{xy} z \, dz \quad (10.4.4)$$

or, in more detailed form,

$$\begin{aligned}m_x &= -D \left[\frac{\partial^2 w}{\partial x^2} + \nu \frac{\partial^2 w}{\partial y^2} + \alpha_T \frac{\Delta T}{h}(1 + \nu) \right] = m_{x,b} - m_T, \\ m_y &= -D \left[\frac{\partial^2 w}{\partial y^2} + \nu \frac{\partial^2 w}{\partial x^2} + \alpha_T \frac{\Delta T}{h}(1 + \nu) \right] = m_{y,b} - m_T, \\ m_{xy} &= -D(1 - \nu) \frac{\partial^2 w}{\partial x \partial y},\end{aligned}\quad (10.4.5)$$

where

$$m_T = \frac{\alpha_T E}{1 - \nu} \int_{-h/2}^{+h/2} (\Delta T) z \, dz = D\alpha_T \frac{T_t - T_b}{h}(1 + \nu) \quad (10.4.6)$$

represents the *thermal equivalent* bending moment per unit length. In addition to the above given equations for moments, expressions for the lateral shearing forces are also needed for description of the boundary conditions. These are

$$q_x = -D \frac{\partial}{\partial x} \nabla^2 w - \frac{\partial m_T}{\partial x} \quad \text{and} \quad q_y = -D \frac{\partial}{\partial y} \nabla^2 w - \frac{\partial m_T}{\partial y}. \quad (10.4.7)$$

Similarly, the edge forces can be expressed as

$$\begin{aligned} v_x &= -D \left[\frac{\partial^3 w}{\partial x^3} + (2 - \nu) \frac{\partial^3 w}{\partial x \partial y^2} \right] - \frac{\partial m_T}{\partial x}, \\ v_y &= -D \left[\frac{\partial^3 w}{\partial y^3} + (2 - \nu) \frac{\partial^3 w}{\partial y \partial x^2} \right] - \frac{\partial m_T}{\partial y}. \end{aligned} \quad (10.4.8)$$

Substitution of Eq. (10.4.5) into Eq. (1.2.9), which represents the equilibrium of the infinitesimal plate element in the Z direction, results in

$$\frac{\partial^2 m_x}{\partial x^2} + 2 \frac{\partial^2 m_{xy}}{\partial x \partial y} + \frac{\partial^2 m_y}{\partial y^2} = -p_z + \nabla^2 m_T. \quad (10.4.9)$$

Hence, the extended governing differential equation becomes

$$D \nabla^2 \nabla^2 w = p_z + p_T, \quad (10.4.10)$$

or, in the absence of lateral forces ($p_z = 0$), we obtain the differential equation of *thermoelastic bending* of plates:

$$D \nabla^4 w_T = -\nabla^2 m_T = p_T, \quad (10.4.11)$$

where p_T represents the *equivalent transverse thermal load*.

As usual in classical plate theory, a solution of the governing equation (10.4.11) must satisfy the differential equation as well as the prescribed boundary conditions. In this case, the boundary conditions of a rectangular plate at edge $x = a$ are[†]

- For simply supported edge:

$$w = 0 \quad \text{and} \quad \frac{\partial^2 w}{\partial x^2} = -\frac{m_T}{D}. \quad (10.4.12)$$

- For fixed edge:

$$w = 0 \quad \text{and} \quad \frac{\partial w}{\partial x} = 0. \quad (10.4.13)$$

- For free- edge:

$$\frac{\partial^2 w}{\partial x^2} = -\frac{m_T}{D} \quad \text{and} \quad v_x = 0. \quad (10.4.14)$$

Consequently, not all boundary conditions are homogeneous.

[†] See Fig. 2.4.3, for instance.

A similar approach can be taken for moderately thick plates. Again, with

$$m_T(x, y) = \frac{\alpha_T E}{1 - \nu} \int_{-h/2}^{+h/2} T(x, y, z) z \, dz \quad (10.4.15)$$

the governing differential equations for the *Reissner* plate, for instance, are given in [10.4.16] as

$$\begin{aligned} q_x &= \frac{h^2}{10} \nabla^2 q_x - \frac{\partial m_{Tx}}{\partial x} - D \frac{\partial}{\partial x} \nabla^2 w, \\ q_y &= \frac{h^2}{10} \nabla^2 q_y - \frac{\partial m_{Ty}}{\partial y} - D \frac{\partial}{\partial y} \nabla^2 w, \\ D \nabla^4 w &= -\nabla^2 m_T. \end{aligned} \quad (10.4.16)$$

All the above equations consider only the pure thermal bending of plates. However, if in connection with thermal bending thermal stretching occurs, we must also augment the in-plane force components of two-dimensional stress problems[†] with a corresponding *thermal stress resultant* n_T .

These in-plane force components are expressed by

$$\begin{Bmatrix} n_x \\ n_y \\ n_{xy} \end{Bmatrix} = \int_{-h/2}^{+h/2} \begin{Bmatrix} \sigma_x \\ \sigma_y \\ \tau_{xy} \end{Bmatrix} dz \quad (10.4.17)$$

or in more detailed form by

$$\begin{aligned} n_x &= \frac{Eh}{1 - \nu^2} \left(\frac{\partial u}{\partial x} + \nu \frac{\partial v}{\partial y} \right) - \frac{n_T}{1 - \nu}, \\ n_y &= \frac{Eh}{1 - \nu^2} \left(\frac{\partial v}{\partial y} + \nu \frac{\partial u}{\partial x} \right) - \frac{n_T}{1 - \nu}, \\ n_{xy} &= \frac{E}{2(1 + \nu)} \left(\frac{\partial u}{\partial y} + \frac{\partial v}{\partial x} \right), \end{aligned} \quad (10.4.18)$$

where u and v are displacement components in the X and Y directions, respectively, and

$$n_T = \alpha_T E \int_{-h/2}^{+h/2} \Delta T \, dz \quad (10.4.19)$$

represents the in-plane *thermal stress resultant*.

[†] This is, however, a subject of the *theory of elasticity* and thus cannot be treated here in detail. Consequently, the reader is referred to the pertinent textbooks.

By considering simultaneous thermal bending and stretching, the governing differential equation (10.4.10) must be augmented by

$$\begin{aligned}\frac{Eh}{1-\nu^2}\nabla^4 u &= \frac{1}{1-\nu}\frac{\partial}{\partial x}(\nabla^2 n_T), \\ \frac{Eh}{1-\nu^2}\nabla^4 v &= \frac{1}{1-\nu}\frac{\partial}{\partial y}(\nabla^2 n_T).\end{aligned}\tag{10.4.20}$$

These relations show that the thermal bending and stretching are decoupled in the small-displacement theory.

b. Methods of Solution. Although problems related to thermal stresses in plates have received considerable attention in the past [10.4.19], still only relatively few analytical solutions are known. One of the reasons for this is that by solving linear partial differential equations, separation of variables cannot be used when nonhomogeneous boundary conditions are present.

Focusing our attention first on problems involving only the flexural response of plates, it is evident that they are governed by the differential equation (10.4.11). Closed-form solutions can only be found for special plate geometry and boundary conditions. Two such solutions are given at the end of this section as examples. It is apparent from Eq. (10.4.11) that by introducing a fictitious lateral force in the form $p_T = -\nabla^2 m_T$, the problem can be reduced to the solution of the corresponding isothermal plate problem, provided the boundary conditions are modified according to Eqs. (10.4.12) and (10.4.14), respectively. Consequently, with the exception of the fixed boundary condition, the thermal equivalent moment m_T must be included in the formulation of all other boundary conditions.

As for the solution of the corresponding isothermal plate problems, approximate or numerical methods are mostly used in the determination of thermal flexural responses. Since the governing differential equation is given, Galerkin's method is a logical choice for obtaining analytical expressions for the thermally induced deflections w_T . In the case of arbitrary geometry and boundary conditions of the plate, use of one of the previously introduced numerical methods (FDM, GWM, FEM, FSM) is recommended. Again, in applying these numerical methods, the thermal boundary conditions must be considered. It is of basic importance to remember that the above-treated analogy yields only the deflections w_T .

A more general approach that includes the combined effect of thermal stretching and bending was introduced by Zienkiewicz and his co-worker Cruz [10.4.5]. The fundamental idea of this so-called equivalent load method consists in first determining a force system that prevents any motions caused by temperature change and then computing the deformations after these forces are removed.

The required steps for this procedure are as follows:

1. The plate is restrained against any movement by a suitable force system.
2. The obtained restraining forces with reversed signs are applied to the plate as active forces.
3. The results of step 2 give the lateral deflections, while superposition of the results obtained from steps 1 and 2 yields the stresses.

If any expansions due to temperature rise $\Delta T(x, y, z)$ are prevented, this creates

$$D^* \nabla^2 \nabla^2 w(x, y) = p_z(x, y), \quad (10.4.21)$$

compressive stresses and the corresponding thermal stress resultants

$$\begin{aligned} m_{T,x} = m_{T,y} &= \int_{-h/2}^{+h/2} \frac{E\alpha_T(\Delta T)}{1-\nu} z \, dz, \\ n_{T,x} = n_{T,y} &= - \int_{-h/2}^{+h/2} \frac{E\alpha_T(\Delta T)}{1-\nu} \, dz. \end{aligned} \quad (10.4.22)$$

in the X and Y directions, respectively. The equilibrium of the vertical forces acting on a plate element,

$$\frac{\partial^2 m_{T,x}}{\partial x^2} + 2 \frac{\partial^2 m_{xy}}{\partial x \partial y} + \frac{\partial^2 m_{T,y}}{\partial y^2} = -q_T(x, y), \quad (10.4.23)$$

requires a lateral force q_T to restrain the plate from vertical deflections. In addition, the in-plane forces, which restrain the expansion of the plate, can be computed from

$$n_{r,x} = -\frac{\partial n_{T,x}}{\partial x} \quad \text{and} \quad n_{r,y} = -\frac{\partial n_{T,y}}{\partial y}. \quad (10.4.24)$$

Next, the plate will be subjected to these restraining forces but with reversed signs. Consequently, the lateral thermal deflections are obtained by solving the differential equation

$$D \nabla^4 w_T(x, y) = -q_T. \quad (10.4.25)$$

Similarly, the pertinent two-dimensional stress problem must be solved by assuming that the plate is subjected to $-n_{r,x}$ and $-n_{r,y}$ body forces. The final thermal stresses are obtained by superposition of the stresses due to thermal bending and stretching. It is evident from Eq. (10.4.23) that if the thermal moments $m_{T,x}$ and $m_{T,y}$ do not vary over the plate domain, the lateral force q_T is zero.

Although the solution of Eq. (10.4.25) and that of the corresponding two-dimensional stress problem can be achieved analytically, the versatile finite difference and finite element methods offer much more ease in obtaining usable results in the case of real-life problems. To apply these two numerical methods to two-dimensional stress problems, the reader is referred to Ref. [5.3.1], for instance, or to any other textbook treating these numerical techniques.

Summary. The methods presented in this section are directed primarily to obtaining lateral deflections of thermally loaded plates. It is evident from Eq. (10.4.11) that, by introducing a fictitious lateral force $p_T = -\nabla^2 m_T$, the problems can be reduced to those of Kirchhoff plates, provided the properly augmented boundary conditions are considered. Consequently, all previously introduced analytical and numerical solution techniques can be logically applied to obtain the deflection patterns caused by temperature gradients. However, the solution procedure is much more involved if the

computation of thermal stresses is also required. In such a case, the generalized formulation of thermal stress problems introduced in Ref. [10.4.5] permits the reduction of these relatively complex problems to those of externally loaded plates. It should be noted that to treat such relatively difficult problems in real-life applications, great reliance must be placed on such numerical solution techniques as the finite difference and finite element and other numerical methods. This is the direction on which future research efforts should concentrate.

ILLUSTRATIVE EXAMPLE I

Consider a rectangular plate with fixed boundary conditions subjected to non-uniform heating ΔT (Fig. 10.4.3). Compute the temperature stresses in the plate.

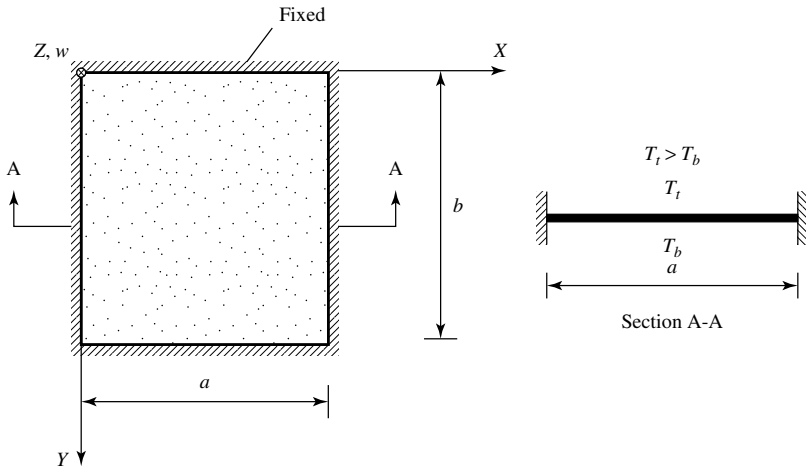


Figure 10.4.3 Clamped plate under nonuniform temperature change.

First we assume that the edges of the plate are free to slide but they restrained against rotation. In such a case, we have a similar condition to that of pure bending of the plate by uniformly distributed edge moments. The edge moments required to restore the originally plane condition are the same, but with opposite signs, as the moments due to the temperature gradient given in Eq. (10.4.6). Consequently,

$$m_T = -\frac{D\alpha_T(\Delta T)}{h}(1 + \nu), \quad (10.4.26)$$

and the corresponding maximum stresses are

$$\sigma_{\max, b} = \pm \frac{6m_T}{h^2}. \quad (10.4.27)$$

However, if the edges are also prevented from in-plane movements, to the stresses produced by bending we must add the created additional normal

stresses, which are

$$\begin{aligned}\sigma_x &= \frac{1}{h} \left(n_{r,x} - \frac{n_T}{1-\nu} \right) - \frac{\alpha_T E (\Delta T)}{1-\nu}, \\ \sigma_y &= \frac{1}{h} \left(n_{r,y} - \frac{n_T}{1-\nu} \right) - \frac{\alpha_T E (\Delta T)}{1-\nu}, \\ \tau_{xy} &= \frac{n_{xy}}{h}.\end{aligned}\quad (10.4.28)$$

ILLUSTRATIVE EXAMPLE II

Let us determine the deflections $w_T(x, y)$ of the simply supported rectangular plate shown in Fig. 10.4.4, assuming that the temperature of its top surface is higher than that of the bottom one ($\Delta T = T_t - T_b$).

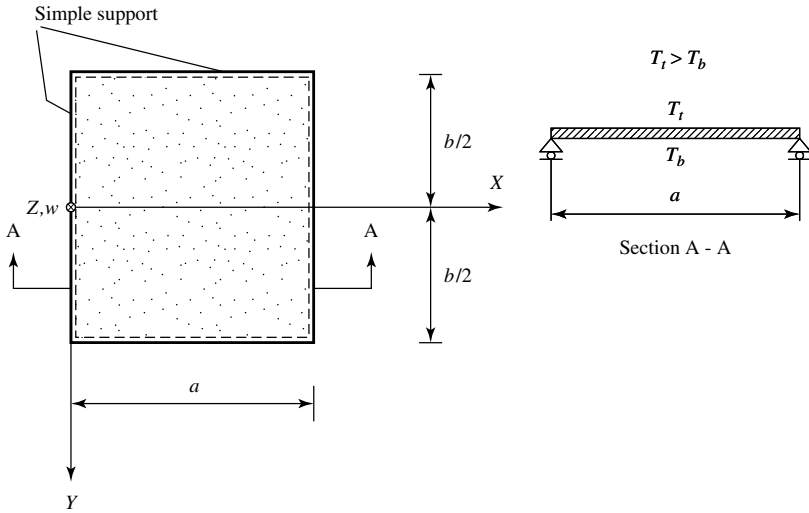


Figure 10.4.4 Simply supported plate subjected to thermally induced bending.

First, we assume that the boundaries of the plate are fixed. According to Eq. (10.4.6), this condition produces uniformly distributed edge moments[†] in the amount of

$$m_{T,n} = \frac{D\alpha_T(\Delta T)}{h}(1+\nu). \quad (10.4.29)$$

Next, we superpose on these moments the moments produced in a simply supported plate, $-m_{T,n}$, acting on the edges. Thus, at the boundaries we have

$$\frac{m_{T,x} + m_{T,y}}{1+\nu} = -\frac{D\alpha_T(\Delta T)}{h}(1+\nu). \quad (10.4.30)$$

[†] The subscript n refers to the normal direction.

In this case, we can replace the fourth-order differential equation of plates (1.2.30) by two second-order differential equations. This approach represents the one already introduced in Sec. 1.2f. Now, for the interior domain of the plate we can write

$$\frac{\partial^2 w_T}{\partial x^2} + \frac{\partial^2 w_T}{\partial y^2} = \frac{\alpha_T(\Delta T)}{h}(1 + \nu). \quad (10.4.31)$$

This equation is analogous to that of a uniformly stretched and uniformly loaded membrane. According to Timoshenko [2], we can express the deflected plate surface as a sum,

$$w_T = w_1 + w_2, \quad (10.4.32)$$

where

$$w_1 = -\frac{\alpha_T(\Delta T)(1 + \nu)}{h} \frac{4a^2}{\pi^3} \sum_{m=1,3,5,\dots}^{\infty} \frac{\sin(m\pi x/a)}{m^3} \quad (10.4.33)$$

and

$$w_2 = \sum_{m=1,3,5,\dots}^{\infty} Y_m \sin \frac{m\pi x}{a}, \quad (10.4.34)$$

with

$$Y_m = A_m \sinh \frac{m\pi y}{a} + B_m \cosh \frac{m\pi y}{a}. \quad (10.4.35)$$

With the help of the boundary conditions, we can determine the constants A_m and B_m . Thus, the final expression for the thermally induced bending is

$$w_T = -\frac{\alpha_T(\Delta T)(1 + \nu)4a^2}{\pi^3 h} \sum_{m=1,3,5,\dots}^{\infty} \frac{\sin(m\pi x/a)}{m^3} \left(1 - \frac{\cosh(m\pi y/a)}{\cosh(m\pi b/2a)} \right). \quad (10.4.36)$$

References and Bibliography

- [10.4.1] BOLEY, B. A., and WEINER, J. H., *Theory of Thermal Stresses*, John Wiley & Sons, New York, 1960.
- [10.4.2] JOHNS, D. J., *Thermal Stress Analysis*, Pergamon Press, Elmsford, New York 1965.
- [10.4.3] MELAN, E., and PARKUS, H., *Wärmespannungen infolge stationärer Temperaturfelder*, Springer-Verlag, Vienna, 1953.
- [10.4.4] GATEWOOD, B. E., *Thermal Stresses*, McGraw-Hill Book Co., New York, 1957.
- [10.4.5] ZIENKIEWICZ, O. C., and CRUZ, C., "The Equivalent Load Method for Elastic Thermal Stress Problems with Particular Reference to Arch Dams," *Proc. Inst. Civil Eng.*, 23 (1962), 15–34.
- [10.4.6] PARKUS, H., *Instationäre Wärmespannungen*, Springer-Verlag, Vienna, 1959.
- [10.4.7] NOWACKI, W., "The State of Stress in Thin Plate Due to the Action of Sources of Heat," *Publ. Int. Asc. Bridge Struct. Eng.*, 16 (1956), 373–398.

- [10.4.8] MENDELSON, A., and HIRSCHBERG, M., "Analysis of Elastic Thermal Stress in Thin Plates with Spanwise and Chordwise Variation of Temperature and Thickness," Tech. Note No. 3778. National Advisory Committee for Aeronautics, Washington, D.C., 1956.
- [10.4.9] HOFF, N. J., "High Temperature Effects on Aircraft Structures," *AGARDograph* 28, Pergamon Press, Elmsford, New York, 1958.
- [10.4.10] OGIBALOV, P. M., and GRIBANOV, V. F., *Termostoichivost' plastin i obolochek* (Thermal Stresses in Plates and Shells), Izd. Mosk. Un-ta, Moscow, 1968.
- [10.4.11] AMES, W. F., *Nonlinear Partial Differential Equations in Engineering*, Vols. 1 and 2, Academic Press, New York, 1965 and 1972.
- [10.4.12] MAULBETSCH, J. L., "Thermal Stresses in Plates," *J. Appl. Mech.*, 2 (1935), A141–A146.
- [10.4.13] WAH, T., "Thermal Stresses in Elastic Plates," *J. Struct. Mech.*, 12 (1984), 59–77.
- [10.4.14] EL-HAWARY, M. M., et al., "Behavior Investigation of Concrete Slabs Subjected to High Temperatures," *Comp. Struct.*, 61 (1996), 345–360.
- [10.4.15] ARIMAN, T., "Thick Elastic Plates on Elastic Foundation Subjected to Steady Temperature Distribution," *Recent Adv. Eng. Sci.*, 2 (1965), 353–369.
- [10.4.16] DAS, Y. C., and RATH, B. K., "Thermal Bending of Moderately Thick Plates," *AIAA J.*, 10 (1972), 1349–1351.
- [10.4.17] BAPU-RAO, M. N., "Thermal Bending of Thick Rectangular Plates," *Nucl. Eng. Des.*, 54 (1979), 115–118.
- [10.4.18] REDDY, J. N., et al., "Thermal Bending of Thick Rectangular Plates of Bimodulus Composite Materials," *J. Mech. Eng. Sci.*, 22 (1980), 297–304.
- [10.4.19] TAUCHERT, T. R., "Thermally Induced Flexure, Buckling, and Vibration of Plates," *Appl. Mech. Rev.*, 44 (1991), 347–360.

10.5 Influence Surfaces

In bridge design one is often confronted with the problem of placing a group of moving loads,[†] representing vehicles, in such a position that maximum stresses will occur in the deck slabs. Although this task can be accomplished by trial and error, the use of *influence surfaces* eliminates the ambiguity of such procedure and may offer considerable time savings.

Influence surfaces of plates are two-dimensional counterparts of *influence lines* used extensively for analysis of girder, arch and truss bridges; consequently, they indicate how the changing of position for a unit load influences such important design parameters as bending moments, shear forces, reactions and deflections. An ordinate of moment influence surface $w(x, y)$ represents, for instance, the moment produced at the *observation point* (ξ, η) when the unit load $P = 1$ is located at point (x, y) , as shown in Fig. 10.5.1. Such influence surfaces are generally represented by contour lines, or as profiles, drawn at certain intervals (Fig. 10.5.2).

The use of influence surfaces is simple and economical. Let us assume, for instance, that P_1, P_2, \dots, P_n concentrated loads are acting at points $(x_1, y_1), (x_2, y_2), \dots, (x_n, y_n)$; then the total particular effect, say moment m_x , at the observation point (ξ, η) is

$$(m_x)_{\xi, \eta} = \sum_{i=1}^n P_i w_i. \quad (10.5.1)$$

[†] The dynamic effects produced by moving loads are not considered here; hence the analysis is quasi-static; thus, the results should be multiplied by appropriate dynamic load factors, as discussed in Sec. 14.1.

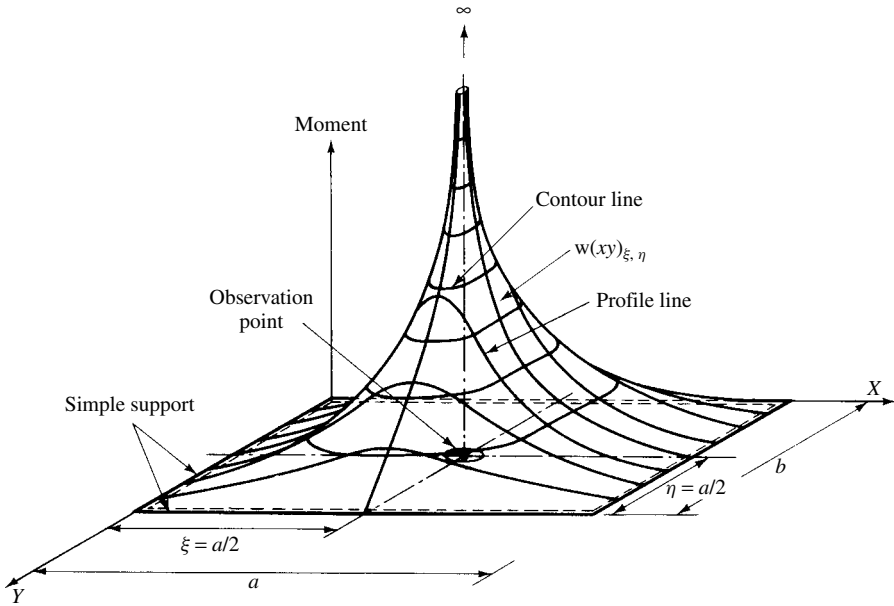


Figure 10.5.2 Influence surface for moment at point $\xi = a/2$, $\eta = b/2$.

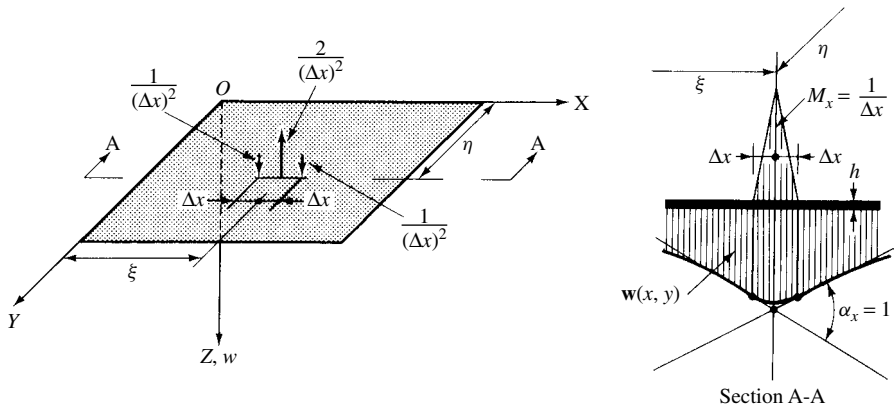


Figure 10.5.3 System of forces to produce $\alpha_x = 1$.

create the desired change of the slope within the interval $\xi - \Delta x$ to $\xi + \Delta x$, since the total moment area of these external forces (which represents the diagram of imposed slopes) is unity:

$$\int_{\xi - \Delta x}^{\xi + \Delta x} M_x dx = 1. \quad (10.5.4)$$

Letting Δx approach zero but maintaining the same value for the integral [Eq. (10.5.4)], the distributed slopes will approach the required concentrated $\alpha_x = 1$ at

the observation point (ξ, η) . This limit approach, however, creates *load singularity*. That is, as Δx approaches zero, the load must approach infinity to satisfy Eq. (10.5.4).

In the analytic approach, the particular solution w_P of Eq. (1.2.30) should contain the required singularity, while the solution of the homogeneous plate equation, w_H , helps to fulfill the requirements of the boundary conditions.

The singular solution in a modified form, given in Eq. (2.1.8),

$$w_P^{(i)} = \frac{P_i}{16\pi D} [(\xi - x)^2 + (\eta - y)^2] \ln[(\xi - x)^2 + (\eta - y)^2], \quad (10.5.5)$$

can be used for P_i individual forces of the appropriate load groups. The superposition of these particular solutions, in connection with the appropriate complimentary solutions, gives

$$\mathbf{w}(x, y)_{\xi, \eta} = \sum w_P^{(i)} + \sum w_H^{(k)}. \quad (10.5.6)$$

In a similar manner, influence surfaces for twisting moment m_{xy} or shear forces q_x, q_y may be obtained. In Fig. 10.5.4 additional load groups capable of producing the required concentrated affine motions at the observation point are shown. In all these cases, these highly concentrated, self-equilibrated loads produce only the desired deformations [10.5.3].

Although generation of influence surfaces by the above-described analytic method is usually tedious, either finite difference [10.5.4] or finite element methods can be used economically. In both these numerical approaches the required affine motions can be introduced directly or indirectly, that is, by employing the appropriate load groups.

Summary. Influence surfaces for particular effects can be obtained based on Maxwell's reciprocity law as deflections of the plate due to a certain system of loads that produce the required affine motions at the observation point. For cases most frequently used in bridge design, influence diagrams are readily available in the German technical literature [10.5.1, 10.5.5, 10.5.6, 10.5.9]. While the analytic approach is generally tedious, numerical methods yield economical solutions.

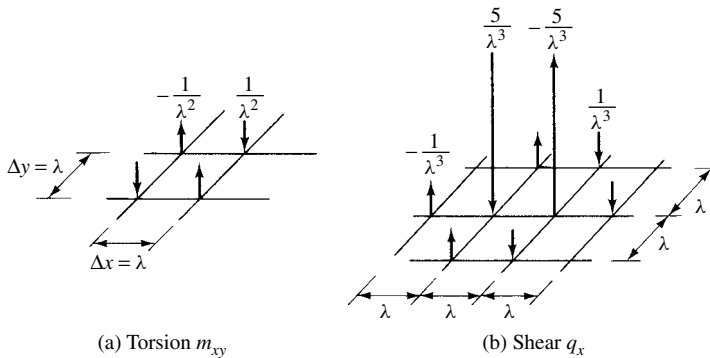


Figure 10.5.4 Load groups for generation of additional influence surfaces.

ILLUSTRATIVE EXAMPLE I

Let us determine an influence surface for the lateral deflections of the simply supported rectangular plate shown in Fig. 10.5.5a. We assume that the observation point is located at $\xi = 2/3a$ and $\eta = 1/4b$.

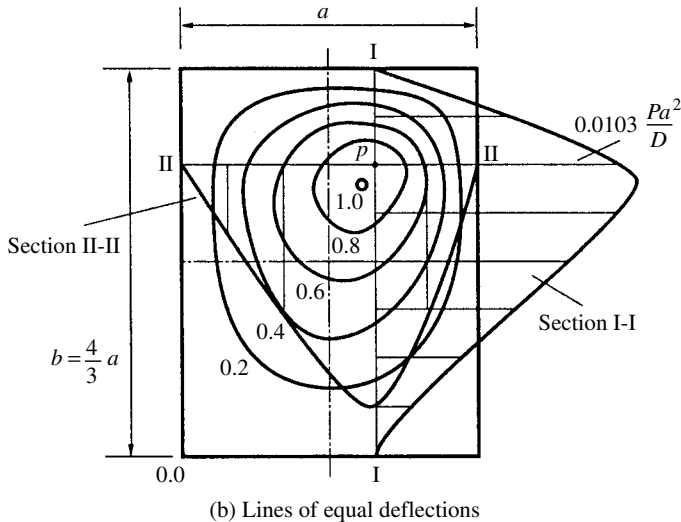
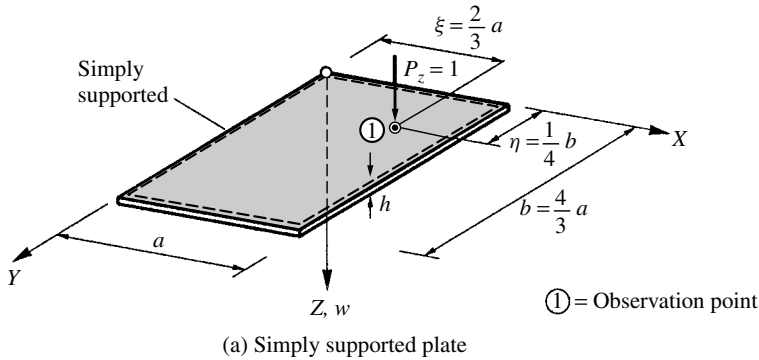


Figure 10.5.5 Generation of influence surface for deflection w_1 .

To generate the required influence surface, we use Maxwell's law of reciprocity. That is, instead of calculating the deflections at the observation point (1) when the moving load $P_z = 1$ is at various points on the plate, we introduce a unit lateral displacement at the observation point and determine the deflections produced at each point of the plate. Therefore, we can state that

$$w_{12}(x, y) = w_{21}(x, y). \quad (10.5.7)$$

The deflected plate surface due to a unit lateral displacement is obtained from Eq. (2.4.38) if we divide this expression by P ; thus, we can write

$$w_{12}(x, y) = \frac{4}{\pi^4 ab D} \sum_{m=1}^{\infty} \sum_{n=1}^{\infty} \frac{\sin(m\pi \xi/a) \sin(n\pi \eta/b)}{((m^2/a^2) + (n^2/b^2))^2} \sin \frac{m\pi x}{a} \sin \frac{n\pi y}{b}. \quad (10.5.8)$$

The influence surface obtained is shown in Fig. 10.5.5b. Although Eq. (10.5.8) does not contain singularity at the observation point, it gives a quite usable approximation for the sought influence surface. However, the convergence of this expression is relatively slow.

ILLUSTRATIVE EXAMPLE II

Let us find the influence surface of bending moment m_y at point (A) of the simply supported continuous plate shown in Fig. 10.5.6. Assume the following dimensionless properties for the plate: $E = 10.0$, $h = 1$ and $\nu = 0.0$.

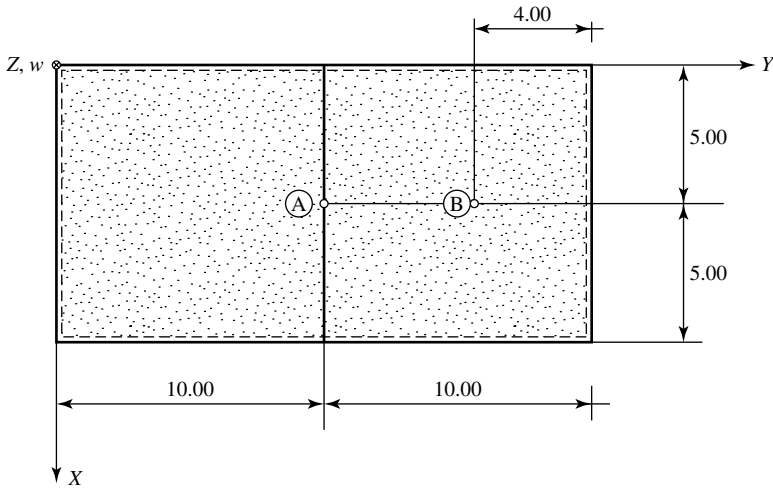


Figure 10.5.6 Plate continuous over two spans.

Since it is very difficult and time consuming to obtain an analytical solution for this problem, we selected a numerical approach in the form of the versatile FEM. Consequently, the plate is subdivided into 200 conforming rectangular finite elements with 16 DOFs[†], as shown in Fig. 10.5.7. With the help of the pertinent group forces (Fig. 10.5.3), we are able to approximate the required singularity and produce $\alpha_A \approx 1$ at the observation point (A).

With $\lambda = 1$ in this case, we apply $P_z = 1$ lateral forces at nodal points 105 and 127, respectively, while $P_z = -2$ acts at nodal point 116, which represents our observation point (A). Our computer program [10.3.31] produced the contour lines of the influence surface, as depicted in Fig. 10.5.8. To check the

[†] See Sec. 7.7.1.

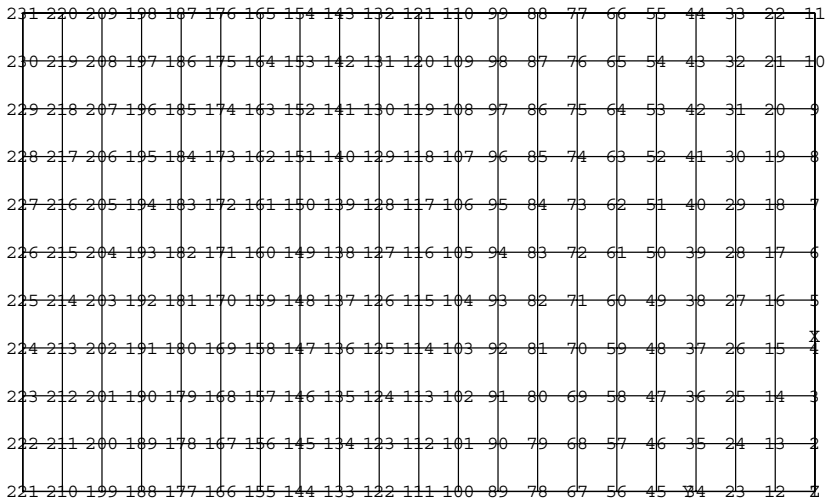


Figure 10.5.7 Numbering of nodal points.

Z - Displacement Contour Levels for Load Case 1

0.1121 = a 0.1040 = b 0.0960 = c 0.0880 = d 0.0800 = e
 0.0720 = f 0.0640 = g 0.0560 = h 0.0480 = i 0.0400 = j
 0.0320 = k 0.0240 = l 0.0160 = m 8.0-03 = n 0 = o
 Max Val = 0.112103 at Node 94 Min Val = 0 at Node 1

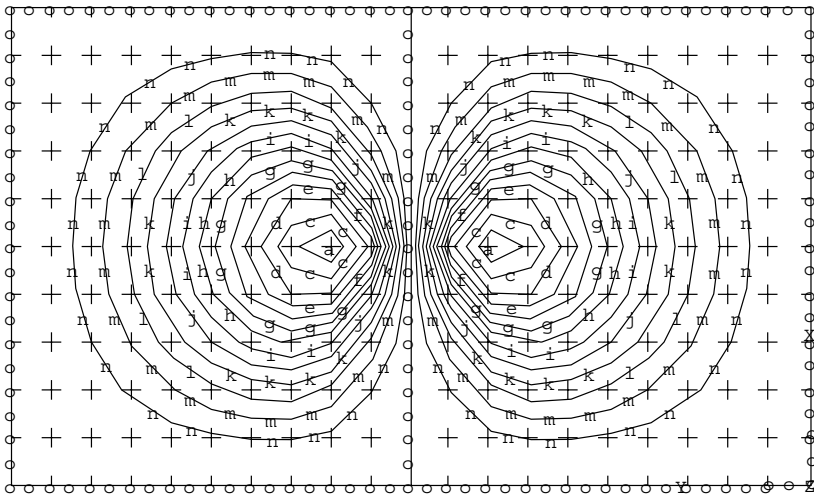


Figure 10.5.8 Influence surface for bending moment $m_{y,A}$.

validity of our solution, we selected the deflection ordinate at point (B) ($x = 5.00$, $y = 16.00$) for which we obtained the value $w_{50} = 0.0605$. A comparison with its analytically determined counterpart $w_B = 0.0597$ [10.5.5] shows a good agreement.

References and Bibliography

- [10.5.1] PUCHER, A., *Einflussfelder elastischer Platten*, Springer-Verlag, Vienna, 1951.
- [10.5.2] BARON, F., "Influence Surfaces for Stress in Slabs," *J. Appl. Mech., Trans. ASME*, 8 (Mar. 1941), A-3–A-13.
- [10.5.3] FLÜGGE, W., "Influence Diagrams," in W. Flügge (Ed.), *Handbook of Engineering Mechanics* McGraw-Hill Book Co., New York, 1962, pp. 28–1–28-11.
- [10.5.4] NEWMARK, N. M., "Note on Calculation of Influence Surfaces in Plates by Use of Difference Equations," *J. Appl. Mech., Trans. ASME*, 8 (1941), A–92.
- [10.5.5] HOELAND, G., *Stützenmomenten-Einflussfelder durchlaufender Platten*, Springer-Verlag, Berlin, 1957.
- [10.5.6] BITTNER, E., *Momententafeln und Einflussflächen für kreuzweise bewehrte Eisenbetonplatten*, Springer-Verlag, Vienna, 1938.
- [10.5.7] WESTERGAARD, H. M., "Computations of Stresses in Bridge Slabs Due to Wheel Loads," *Public Roads*, 11, No. 1 (Mar. 1930), 1–23.
- [10.5.8] OLSEN H., and REINITZHUBER, F., *Die zweiseitig gelagerte Platte*, Vols. 1 and 2, 2nd ed., W. Ernst & Sohn, Berlin, 1951 and 1952.
- [10.5.9] KRUG, S., and STEIN, P., *Einflussfelder orthogonal anisotroper Platten* (German-English ed.), Springer-Verlag, Berlin, 1961.
- [10.5.10] RUSHTON, K. R., "The Representation of Singularities in Field Problems on an Analogue Computer," in *Proceedings of the 4th International Analogue Computation Meeting, Brighton, 1964*, Presses Académiques Europeennes, Brussels, 1966.
- [10.5.11] BALAS, J., and HANUSKA, A., *Influence Surfaces of Skew Plates (Bridge-Types)*, [Vplyvové plochy sikmých dosak (mostné typy)], Vydavateľ'stvo Slovenskej Akademie Vied, Bratislava, 1964.
- [10.5.12] STIGLAT, K., *Einflussfelder rechteckiger und schiefer Platten*, W. Ernst & Sohn, Berlin, 1965.

10.6 Continuous Plates Supported by Rows of Columns

a. Introduction. When two-way reinforced-concrete slabs are not supported by beams, the lateral loads are transferred directly to the columns, and the plates are referred to as flat plates of flat slabs (Fig. 10.6.1). Due to the absence of supporting

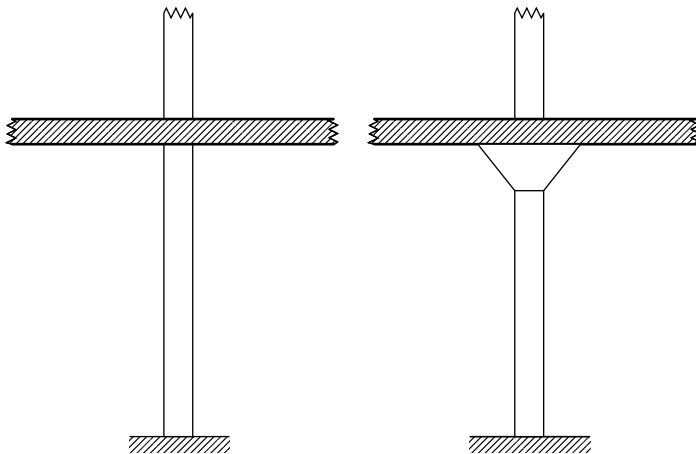


Figure 10.6.1 Column-supported plates.

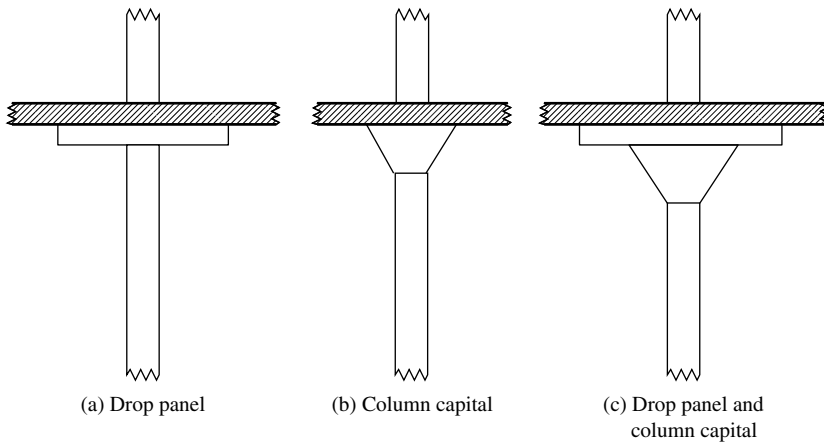


Figure 10.6.2 Various flat-slab configurations.

beams, the columns tend to punch through the slab, as discussed later in detail. To prevent such so-called *punching shear* failures, the thickness of the slabs is usually increased around the columns by rectangular or square *drop panels* (Fig. 10.6.2a). Another approach to reducing such punching shear failures is the use of *column capitals*. In this case, the top of the columns flare out to a shape somewhat similar to an inverted cone (Fig. 10.6.2b), rendering a mushroom-type of appearance to the columns. The column capital gives a wider support, thus reducing the shear and bending stresses in the slab. Furthermore, column capitals and drop panels are often effectively combined (Fig. 10.6.2c). This type of reinforced-concrete floor system is referred to as a *flat slab*. If neither drop panels nor column capitals are used and the slab is of uniform depth, we call such a floor system a *flat plate*. In this case, special shear reinforcement, for instance in form of I-beams embedded into the concrete, is required to increase the shear resistance of the plate. Flat plates are generally used in engineering practice for light loads.

For heavy loads mostly flat slabs are employed, since they offer numerous advantages over an ordinary beam-and-girder floor system. The most important of these are as follows:

- For heavy loads, a flat slab is more economical than other types of floor systems.
- A flat slab results in a more rigid structure.
- The formwork is simpler.
- More clear heights can be obtained in multistory buildings.

For the recommended plate thickness, column spacings and size of drop panels and/or column capitals, the reader should always consult current local building codes such as the Building Code of the American Concrete Institute, the Euro Design Code, the German Industry Norms (DIN) or similar building codes.

b. Analysis of Flat Plates. We assume that the column dimensions are small in relation to the other plate dimensions. Consequently, the infinitely large plate can be regarded as being point supported. Furthermore, we assume that the lateral load p_0

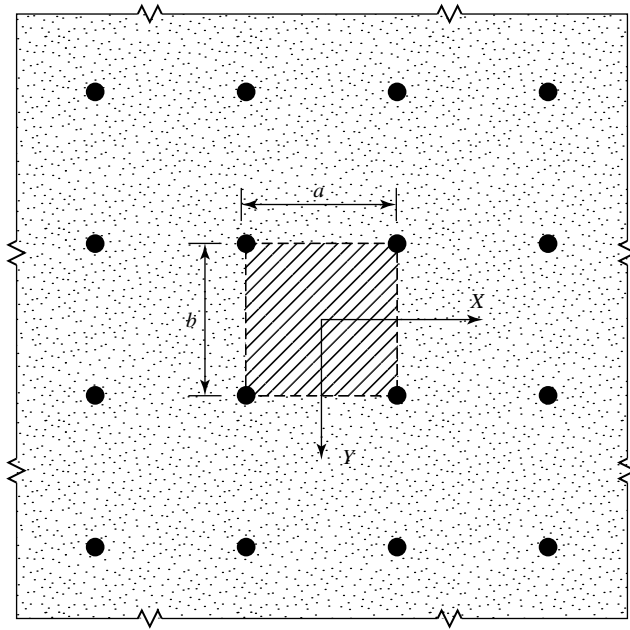


Figure 10.6.3 Interior panel of flat plate.

is uniformly distributed. Using these assumptions, it is sufficient to limit our analysis to one typical interior panel. The origin of the reference coordinate system X, Y, Z is placed at the center of this interior panel, as shown in Fig. 10.6.3. According to Refs. [1–3], the deflections may be expressed as

$$w(x, y) = \frac{p_0 b^4}{384D} \left(1 - \frac{4y^2}{b^2}\right)^2 + A_0 + \frac{p_0 a^3 b}{2\pi^3 D} \sum_{m=2,4,\dots}^{\infty} \frac{(-1)^{m/2} \cos(m\pi x/a)}{m^3 \sinh \alpha_m \tanh \alpha_m} \\ \times \left[\tanh \alpha_m \frac{m\pi y}{a} \sinh \frac{m\pi y}{a} - (\alpha_m + \tanh \alpha_m) \cosh \frac{m\pi y}{a} \right], \quad (10.6.1)$$

where

$$A_0 = -\frac{p_0 a^3 b}{2\pi^3 D} \sum_{m=2,4,\dots}^{\infty} \frac{1}{m^3} \left(\alpha_m - \frac{\alpha_m + \tanh \alpha_m}{\tanh^2 \alpha_m} \right) \quad (10.6.2)$$

and

$$\alpha_m = \frac{m\pi b}{2a}. \quad (10.6.3)$$

By setting $x = y = 0$ and inserting $w(x, y)$ into Eqs. (1.2.26) and (1.2.27), respectively, we obtain the maximum positive bending moments at the center of the plate in the following form

$$m_{x,\max} = c_1 p_0 b^2 \quad \text{and} \quad m_{y,\max} = c_2 p_0 b^2. \quad (10.6.4)$$

The constants c_1 and c_2 are listed in Table 10.6.1 for different span ratios b/a using the value $\nu = 0.2$. Similarly, the maximum deflection at the center of the interior plate is

$$w_{\max} = c_3 \frac{p_0 b^4}{D}. \quad (10.6.5)$$

Again, the coefficients c_3 for different span ratios and $\nu = 0.2$ are listed in Table 10.6.1.

Formulas for calculating the negative moments at the columns ($x = a/2$, $y = b/2$) are

$$\begin{aligned} m_{x,\text{col}} &= -\frac{p_0 ab}{4\pi} \left[(1 + \nu) \ln \frac{a}{d} - (c_4 + c_5 \nu) \right], \\ m_{y,\text{col}} &= -\frac{p_0 ab}{4\pi} \left[(1 + \nu) \ln \frac{a}{d} - (c_5 + c_4 \nu) \right]. \end{aligned} \quad (10.6.6)$$

The coefficients c_4 and c_5 for different span ratios and $\nu = 0.2$ are given in Table 10.6.2. The value d represents the diameter of circular columns. In the case of square or rectangular columns the value of d can be approximated by

$$d \approx 0.57C \quad \text{with} \quad C = \frac{1}{2}(u + v), \quad (10.6.7)$$

where u and v are the cross-sectional dimensions of the column. However, the moments obtained by using Eq. (10.6.6) should be reduced, as shown in Fig. 10.6.4.

Since the deflections of the plate are known, the shearing forces can be calculated using Eq. (1.2.3). This relatively tedious computation, however, can be circumvented by treating a portion of the plate as a circular plate that is fixed at the periphery of the column (Fig. 10.2.5). Such an approximation is justified as long as the panels are nearly square. The free-body of this substitute plate is loaded by a uniformly distributed load p_0 , shearing forces q_p around its periphery and the reactive forces

Table 10.6.1 Values of Coefficients c_1 and c_2

b/a	c_1	c_2	c_3
1.0	0.0331	0.0331	0.00581
1.1	0.0261	0.0352	0.00487
1.2	0.0210	0.0363	0.00428
1.3	0.0175	0.0375	0.00387
1.4	0.0149	0.0384	0.00358
1.5	0.0131	0.0387	0.00337
2.0	0.0092	0.0411	0.00292
∞	0.0083	0.0417	0.00260

Table 10.6.2 Values of Coefficients c_4 and c_5

b/a	1.0	1.1	1.2	1.3	1.4	1.5	2.0
c_4	0.811	0.822	0.829	0.833	0.835	0.836	0.838
c_5	0.811	0.698	0.588	0.481	0.374	0.268	-0.256

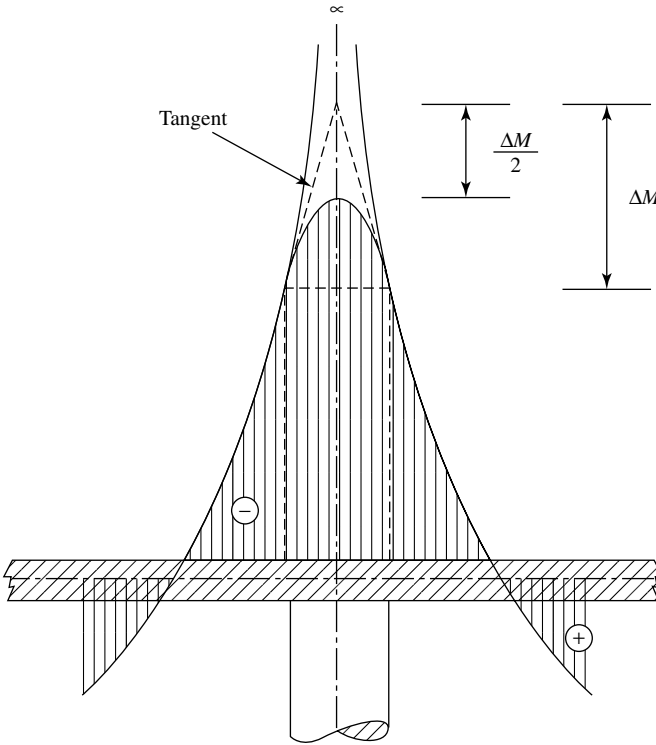


Figure 10.6.4 Reduction of maximum negative moments.

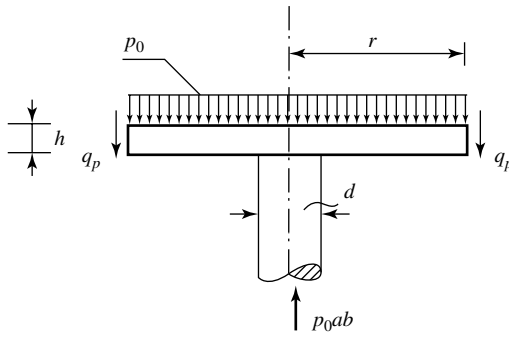


Figure 10.6.5 Substitute circular plate.

p_0ab at the inner fixed boundary, as shown in Fig. 10.6.5. The radius of this circular plate and the shear force per unit length is given by Nádai [3] as

$$r \approx 0.22a \quad \text{and} \quad q_p = 0.723p_0b - 0.11p_0a. \quad (10.6.8)$$

To obtain the maximum negative moments acting at the columns, we load the entire area with uniformly distributed load p_0 . On the other hand, to calculate the

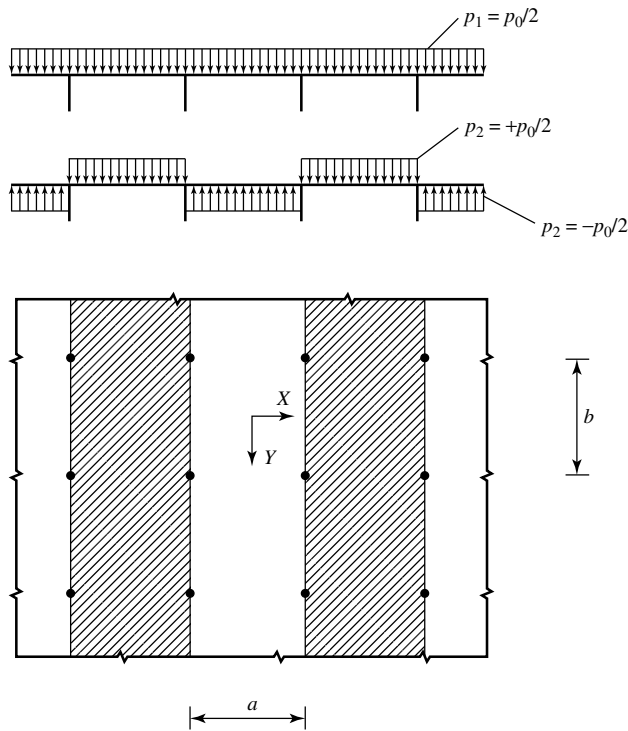


Figure 10.6.6 Loading for maximum field moments.

maximum positive moments in the midspan regions, the loading should be arranged according to Fig. 10.6.6. Thus, we use a uniformly distributed load $p_1 = p_0/2$ in combination with the load $p_2 = \pm p_0/2$ by changing its direction from each bay to the next (Fig. 10.6.7). This second type of loading produces a deflected plate surface similar to that of a uniformly loaded simply supported plate strip of width a .

If only one panel is loaded while the four adjacent panels do not carry any load, we can analyze such a condition by superposition of the loads $p_1 = +p_0/2$ and $p_2 = -p_0/2$ in a chess-board fashion (Fig. 10.6.7). Under such loading conditions, each panel behaves as a simply supported plate; thus we can use Navier's method in the analysis.

c. Analysis of Flat Slabs. In the foregoing treatment of infinitely large plates supported by rows of columns, we assumed that the plate is point supported. This is, however, not the case with flat slabs since the column reactions are distributed over the column capitals. Lewy [10.6.1] assumed a uniform distribution of these reactions (Fig. 10.6.8) in the form

$$p_1 = \frac{p_0 ab}{4cd}. \quad (10.6.9)$$

Consequently, the total lateral forces acting on the flat plate are

$$p(x, y) = p_0 - p_1(x, y) \quad (10.6.10)$$

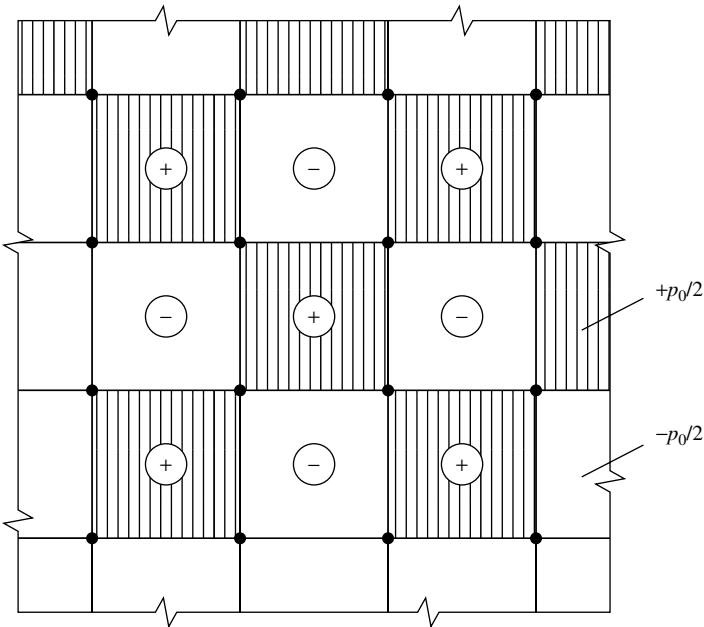


Figure 10.6.7 Chess-board-type surface loading.

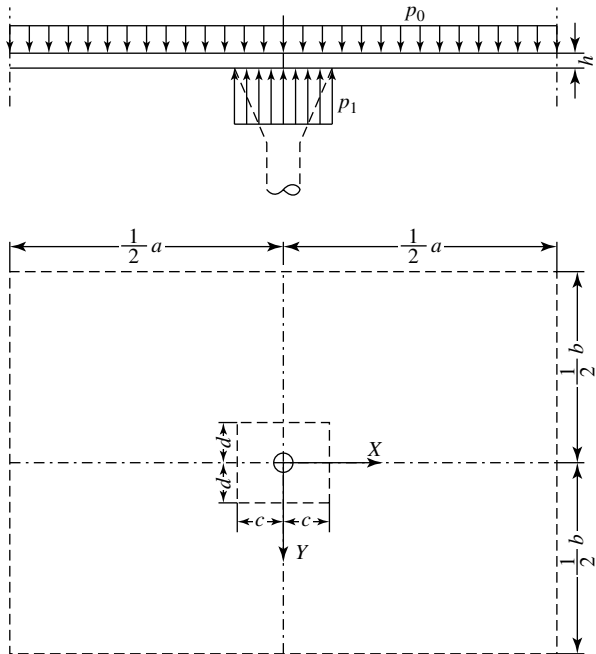


Figure 10.6.8 Assumed distribution of column reactions.

This equation can be written in more detailed form by using Fourier series expansion; thus

$$p(x, y) = -\frac{p_0 a}{\pi c} \sum_m \frac{1}{m} \sin \alpha_m c \cos \alpha_m x - \frac{p_0 b}{\pi d} \sum_n \frac{1}{n} \sin \beta_n d \cos \beta_n y \\ - \frac{p_0 ab}{\pi^2 cd} \sum_m \sum_n \frac{1}{mn} \sin \alpha_m c \sin \beta_n d \cos \alpha_m x \cos \beta_n y \\ \text{for } m, n = 1, 2, 3, \dots, \quad (10.6.11)$$

where

$$\alpha_m = \frac{2m\pi}{a} \quad \text{and} \quad \beta_n = \frac{2n\pi}{b} \quad (10.6.12)$$

Under these combined loads the equation of the deflected plate surface becomes

$$w = A_0 - \frac{p(x, y)}{16D\pi^5} \left(\frac{a^5}{c} \sum_m \frac{1}{m^5} \sin \alpha_m c \cos \alpha_m x + \frac{b^5}{d} \sum_n \frac{1}{n^5} \sin \beta_n d \cos \beta_n y \right) \\ - \frac{p(x, y)a^5b^5}{16cdD\pi^6} \sum_m \sum_n \frac{\sin \alpha_m c \sin \beta_n d \cos \alpha_m x \cos \beta_n y}{mn(m^2b^2 + n^2a^2)^2} \\ \text{for } m, n = 1, 2, 3, \dots \quad (10.6.13)$$

The constant A_0 in this equation can be determined from the boundary condition at $x = y = 0$ where $w = 0$. The stress resultants m_x , m_y and q can be calculated from the corresponding equations given in Sec. 1.2. Unfortunately, is not only this procedure tedious but the convergence of the resulting expressions is quite slow.

Soinier's approach [10.6.2] appears to be somewhat simpler. In this case, the expression for deflections takes the form

$$w(x, y) = \frac{2p_0}{\pi^4 D} \sum_m \frac{a^4}{m^4} \frac{\sin m\pi\alpha}{m\pi\alpha} (1 - \cos m\pi\xi) + \sum_n \frac{b^4}{n^4} \frac{\sin n\pi\beta}{n\pi\beta} (1 - \cos n\pi\eta) \\ + 2 \sum_m \sum_n \frac{\sin m\pi\alpha \cdot \sin n\pi\beta}{m\pi\alpha \cdot n\pi\beta} \left[\frac{1 - \cos m\pi\xi \cdot \cos n\pi\eta}{(m^2/a^2 + n^2/b^2)^2} \right], \quad (10.6.14)$$

where $\xi = x/a$ and $\eta = y/b$. The constants α and β in this equation determine the supporting area of the column capital in terms of the column spacings a and b , as defined in Fig. 10.6.9. Again, the stress resultants can be computed using the pertinent expressions given in Sec. 1.2. Critical loading patterns for the maximum positive and negative moments are the same as discussed above for flat slabs. To facilitate such otherwise tedious computations, the maximum values for moments and shear forces are given in Table 10.6.3 for $\alpha = \beta$ and $\nu = 0.3$. It should be noted that the maximum negative moments can be reduced according to Fig. 10.6.10.

Very noteworthy is the analytical solution of this complex plate problem by Pfaffinger and Thürlimann [10.6.11], since due to the accompanying numerous tables, it is well suited for hand computation. A single series solution was employed for the

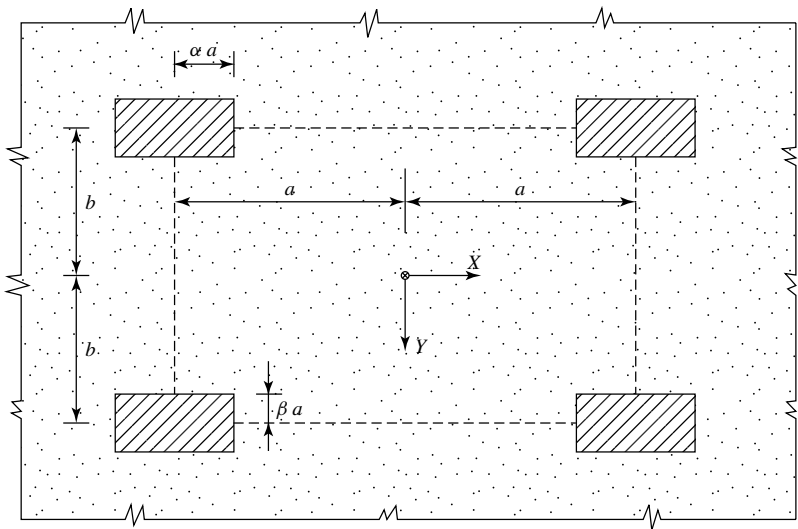


Figure 10.6.9 Top view of flat slab with column capitals.

Table 10.6.3 Design Coefficients for Stress Resultants

β	0	0.1	0.2	0.3	0.4
m_{col}/p_0a^2	$-\infty$	-0.206	-0.142	-0.101	-0.0735
m_{center}/p_0a^2	0.0359	0.0356	0.0348	0.0334	0.0313
q/p_0a	∞	2.73		0.842	

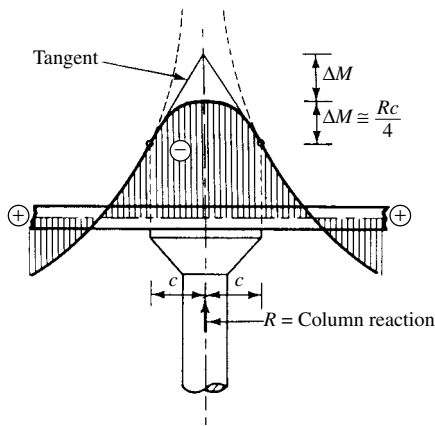


Figure 10.6.10 Reduction of moment above column.

governing plate equation (1.2.3) along with various practical boundary conditions. As already mentioned, extensive tables facilitate the otherwise time-consuming analysis. For instance, values of bending moments are given for the quarter points of the panels; thus the user can easily draw the corresponding moment diagrams required in design for the arrangement of reinforcing bars. In addition, the twisting and principal

moments[†] and their corresponding directions are also listed. The required parameters cover most practical situations. The limitations of these otherwise excellent tables are as follows:

- (a) The structural system must have double symmetry.
- (b) Simply supported boundary conditions at the opposite edges are required.
- (c) For corner panels other boundary conditions as shown cannot be used.

A closer investigation, however, reveals that the influence of the boundary conditions of one panel on the next is negligibly small. Consequently, use of these tables can be further extended.

d. Numerical Analysis. In the foregoing analytical treatments of flat-plate and flat-slab problems, we were forced to use mostly idealized conditions to obtain some usable results. In real life, however, the plates are not infinitely large and the columns are not always equally spaced in the X and Y directions. In discussing the bending of flat slabs, it was also assumed that the column reactions are uniformly distributed over the column capitals. As a rule, however, flat slabs are rigidly connected to their supporting columns. In addition, edge and corner panels are often cantilevered and/or supported by edge beams. Furthermore, in most cases the individual panels have numerous small or large openings and the lateral loads can also be partial loadings or even concentrated forces. Since the analytical methods introduced above are completely unsuited to deal with such real problems of engineering practice, numerical methods must be applied to obtain usable results.

When dealing with such complex flat-plate problems, the various finite difference methods can be effectively employed, provided the supporting columns are relatively weak in bending. Consequently, their bending rigidity in comparison with that of the plate is of negligible order.

For a realistic flat-slab analysis, however, application of the various gridwork or finite element methods is recommended since both numerical techniques can account for the interaction between slab and columns in bending and can also consider the above-mentioned nonclassical geometrical configurations and nonuniform loadings with relative ease. In the FEM approximation of quasi-rigid drop panels or its combination with column capitals, sufficiently small subdivision should be used covering the pertinent areas.

e. Punching Shear. Reinforced-concrete flat-plates may fail by punching shear when the columns suddenly perforate the slab. Such failures are highly localized, involving tangential and radial cracks in the concrete. Consequently, the regions around the columns pose a critical analysis problem since bending moments and shear forces are concentrated in these regions. In addition, because of their interaction, they cannot be treated separately. Punching shear failures are due to tensile failure of the concrete along the developed cracks; hence, a sufficient amount of flexural reinforcement is of primary importance. Readily applicable design formulas for estimating punching shear strength are given in building codes [10.6.12, 10.6.13]. Although these formulas are simple and, hence, convenient to use, they are based on empirical

[†] See Eq. (1.2.39).

findings. Recent research efforts, however, try to correlate two- three-dimensional finite element predictions with experimental results [10.6.14–10.6.17].

Summary. Although applications of the analytical approaches introduced here to flat-plate and flat-slab problems are seriously limited by the idealized conditions presented, they can serve extremely well as benchmarks when the accuracy and effectiveness of the more productive numerical methods are tested. For analysis of relatively small practical problems involving flat plates, the FDMs give good results in a simple way. Unfortunately, commercially available program systems employing finite difference approaches are extremely rare; consequently, the use of the finite difference approach is restricted to relatively small problems that still can be handled by a combination of hand and computer computations, as discussed in Chapter 2. On the other hand, the readily available gridwork and finite element program systems can deal with all complex flat-plate and flat-slab problems encountered in engineering practice.

Finally, the reader should note that the yield-line method (Sec. 11.6) and the engineering approximation of flat-slab problems by using substitute rigid frames (Sec. 12.6) can yield practical approximations to these complex problems in a relatively simple way. Furthermore, the results obtained can provide valuable independent checks for the more sophisticated finite difference, gridwork or finite element analyses.

ILLUSTRATIVE EXAMPLE

Determine the maximum deflection, bending moments and critical shear forces in a typical interior panel of an infinitely large reinforced-concrete flat-plate (Fig. 10.6.3) subjected to $p_0 = 25 \text{ kN/m}^2$ uniformly distributed lateral forces. Assume that the center spacings of the columns are $a = b = 7.0 \text{ m}$. These supporting columns are of square cross-sectional shape with the dimension $d = 0.4 \text{ m}$. Additional properties of the plate are $h = 0.25 \text{ m}$, $E = 30,000,000 \text{ kN/m}^2$ and $\nu = 0.2$.

Since we are dealing here with the idealized conditions introduced above, we can use the pertinent formulas developed for such cases. Consequently, with

$$D = \frac{Eh^3}{12(1 - \nu^2)} = \frac{30 \times 10^6 \times 0.25^3}{12(1 - 0.2^2)} = 40,690 \text{ kNm}, \quad (10.6.15)$$

the bending stiffness of the plate, Eq. (10.6.5) gives the maximum deflection as

$$w_{\max} = c_3 \frac{p_0 b^4}{D} = 0.00581 \frac{25 \times 7.0^4}{40,690} = 0.0086 \text{ m}. \quad (10.6.16)$$

Similarly, from Eq. (10.6.4) we obtain the maximum positive bending moment

$$m_{x,\max} = m_{y,\max} = c_1 p_0 b^2 = 0.0331 \times 25 \times 7.0^2 = 40.55 \text{ kN-m/m}. \quad (10.6.17)$$

In addition, Eq. (10.6.6) yields the maximum negative moments above the columns of interior panels:

$$\begin{aligned} m_{x,\text{col}} &= -\frac{p_0 a^2}{4\pi} \left[(1 + \nu) \ln \frac{a}{d} - (c_4 + c_5 \nu) \right] \\ &= -\frac{25 \times 7.0^2}{4\pi} \left[(1 + 0.2) \ln \frac{7.0}{0.4} - (0.811 + 0.811 \times 0.2) \right] \\ &= -186.95 \text{ kN-m/m.} \end{aligned} \quad (10.6.18)$$

This peak value, however, should be reduced in accordance with Fig. 10.6.4. The value of the critical shear is computed from Eq. (10.6.8), which gives

$$q_p = 0.723 p_0 a - 0.11 p_0 a = 107.27 \text{ kN/m.} \quad (10.6.19)$$

A similar approach can be taken for the interior panels of infinitely large reinforced-concrete flat slabs.

References and Bibliography

- [10.6.1] LEWE, V., *Pilzdecken*, W. Ernst & Sohn, Berlin, 1926.
- [10.6.2] SOINIER, P., *Tables pour le calcul rationnel des planchers sans nervure, et dalles rectangulaires*, Dunond, Paris, 1929.
- [10.6.3] HAJNAL-KÖNYI, K., *Die Berechnung von kreisförmig begrenzten Pilzdecken bei zentral-symmetrischer Belastung*, Springer-Verlag, Berlin, 1929.
- [10.6.4] GREIN, K., *Pilzdecken, Theorie und Berechnung*, 3rd ed., W. Ernst & Sohn, Berlin, 1948.
- [10.6.5] WOJNOWSKY-KRIEGER, S., "On Bending of Flat Slab Supported by Square Shape Columns and Clamped," *J. Appl. Mech., Trans. ASME*, 21 (1954), 263–270.
- [10.6.6] BROTHIE, J. F., and BERESFORD, F. D., "Experimental Study of a Prestressed Concrete Flat Plate Structure," *Civil Eng., Trans. Inst. Eng. Australia*, CE-9 (Oct. 1967), 276–282.
- [10.6.7] MORRIS, D., "Design Coefficients for Flat Slab Structures with Drop Panels," *J. ACI*, 66 (Oct. 1969), 820–822.
- [10.6.8] MAST, P. E., "Stresses in Flat Plates Near Columns," *J. ACI*, 67 (Oct. 1970), 820–822.
- [10.6.9] BRETTTHAUER, G., and SEILER, H. F., "Die Pilzdecke ohne verstärkte Säulenköpfe (Flachdecke)," *Beton- und Stahlbetonbau*, 9 (1966), 229 and 279.
- [10.6.10] BRETTTHAUER, G., and NÖTZHOLD, F., "Zur Berechnung von Pilzdecken," *Beton- und Stahlbetonbau*, 10 (1968), 221–227.
- [10.6.11] PFAFFINGER, D., and THÜRLIMANN, B., *Tabellen für unterzoglose Decken*, Verlags AG. der akad. techn. Vereine, Zürich.
- [10.6.12] ACI COMMITTEE 318, Building-Code Requirements for Reinforced Concrete, American Concrete Institute, Detroit, Michigan 1995.
- [10.6.13] COMITÉ EURO-INTERNATIONAL DU BETON (CEB), *CEB-FIP Model Code*, Bull. d'Information. Swiss Federal Institute of Technology, Lausanne, Switzerland, 1990.
- [10.6.14] LOO, Y-C., and GUAN, H., "Cracking and Punching Shear of RC Flat Plates," *J. Struct. Eng., ASCE*, 123 (1997), 1321–1329.
- [10.6.15] MENÉTREY, P., et al., "Simulation of Punching Failure in Reinforced Concrete Structures," *J. Struct. Eng., ASCE*, 123 (1997), 652–659.
- [10.6.16] PETROU, M. F., et al., "Punching Shear Failures in Concrete Decks as Snap-Through Instability," *J. Struct. Eng., ASCE*, 122 (1996), 998–1005.

10.7 Additional Topics Related to FEM

10.7.1 Various Convergence Tests

There is only one *exact* solution to a given plate problem. Considering the approximate nature of the FEM, however, the resulting numerical solution after we successively refine the element mesh can

- converge to the exact solution,
- converge to a wrong number,
- or diverge entirely.

The subject of convergence of any approximate solution of a plate problem involves several abstract mathematical concepts requiring highly sophisticated analyses. Such rigorous treatment is in the realm of functional analysis and therefore outside the scope of this book.

The discretization error that has the most pronounced influence on the convergence of a finite element solution depends mostly on the following four parameters:

- the shape functions used in generating the element stiffness coefficients,
- the mesh size,
- boundary conditions and
- representation of the external loads.

As already discussed in Sec. 7.3.1, the FEM can be considered a special case of the Ritz energy method. Consequently, to obtain convergence in the finite element solution of a plate problem, we must require that the total potential of the external and internal forces of the substitute system must be equal to that of the original continuum [10.7.1]. This *necessary* requirement for convergence can be expressed by

$$\bar{\Pi} = \bar{\Pi}_{\text{int}} + \bar{\Pi}_{\text{ext}} = \frac{1}{2} \bar{\mathbf{d}}^T \left(\sum_{N=1}^{\infty} \mathbf{K}_e^{(N)} \right) \bar{\mathbf{d}} - \bar{\mathbf{d}}^T \bar{\mathbf{p}}. \quad (10.7.1)$$

For this purpose we can use certain plate problems for which an exact solution is available.[†]

To ensure convergence to the exact solution of the finite element results when the mesh is refined, the shape functions must satisfy all the criteria introduced in Sec. 7.4. Observance of the criterion concerning nonstraining of the element is of basic importance to avoid divergence. As already discussed, straining of the element occurs when all nodal points are subjected to rigid-body displacements. This case can be tested by solving a set of eigenvalue equations for the element, which can be formulated as

$$(\mathbf{K}_e - \omega^2 \mathbf{I}) \mathbf{d}_e = \{0\}, \quad (10.7.2)$$

[†] See Fig. 2.1.1, for instance.

where \mathbf{I} is the identity matrix and ω represents the corresponding eigenvalues. For plate elements, there are three rigid-body modes: a transverse displacement and rotations about the X and Y axes, respectively. Solution of Eq. (10.7.2) must include all rigid-body modes corresponding to zero ω_i frequencies.

To evaluate the convergence characteristics of finite elements, the so-called *patch test* [10.7.2] is used most frequently in engineering practice. The patch represents a small assembly of finite elements. These elements are subjected to either a set of displacements or boundary forces that produce constant-curvatures at each point of the patch. Thus, we require that

$$\bar{\kappa} = \begin{Bmatrix} \bar{\kappa}_x \\ \bar{\kappa}_y \\ \bar{\chi} \end{Bmatrix} = \begin{Bmatrix} -\frac{\partial^2 \bar{w}}{\partial \bar{x}^2} \\ -\frac{\partial^2 \bar{w}}{\partial \bar{y}^2} \\ -\frac{\partial^2 \bar{w}}{\partial \bar{x} \partial \bar{y}} \end{Bmatrix} = \text{const.} \quad (10.7.3)$$

Consequently, we can state that the patch test is passed for a given plate assembly if the above given constant-curvatures are produced under a certain set of displacement or boundary forces. If boundary forces are used, for instance, the boundary forces shown in Fig. 10.7.1 produce the required constant state of curvatures. By applying the bending moments $\bar{m}_x = \bar{M}_0$ at two opposite edges of the plate assembly as shown in Fig. 10.7.1a, the moments $\bar{m}_y = \bar{m}_{xy}$ become zero. Thus, from the corresponding equations for moments[†] we obtain

$$\frac{\partial^2 \bar{w}}{\partial \bar{y}^2} = -\nu \frac{\partial^2 \bar{w}}{\partial \bar{x}^2} = -\frac{12\nu \bar{M}_0}{Eh^3} \quad \text{and} \quad \frac{\partial^2 \bar{w}}{\partial \bar{x} \partial \bar{y}} = 0. \quad (10.7.4)$$

To generate constant warping in the plate assembly, we now apply the boundary forces shown in Fig. 10.7.1b. A closer investigation of the obtained deflection shape reveals that due to the antisymmetry of the given plate configuration and its deflected condition, there are no deflections in the line of the X and Y axes. Furthermore, the free-body equilibrium of a plate quadrant requires that the quadrant must be balanced by four corner forces in the same manner as the whole plate assembly maintains its equilibrium. Subsequent subdivision of this quadrant into four quadrants leads to an infinitesimal element of size $d\bar{x} d\bar{y}$ subjected to the same type of corner forces. To produce corresponding twisting moments, we split each of the four corner forces into halves. Under this condition, the whole plate assembly is subjected to constant twisting moments in the size of $\bar{P}_z d\bar{x}/2$ and $\bar{P}_z d\bar{y}/2$, respectively. Next, we apply the reverse concept of Kirchhoff's supplementary forces[‡] and transform the corner forces into constant twisting moments acting on the edges. Consequently, we can write

$$\frac{\bar{P}_z d\bar{x}}{2 d\bar{x}} = \frac{\bar{P}_z}{2} = \bar{m}_{xy} = \text{const.} \quad (10.7.5)$$

[†] See Sec. 1.2.

[‡] See Sec. 1.3.

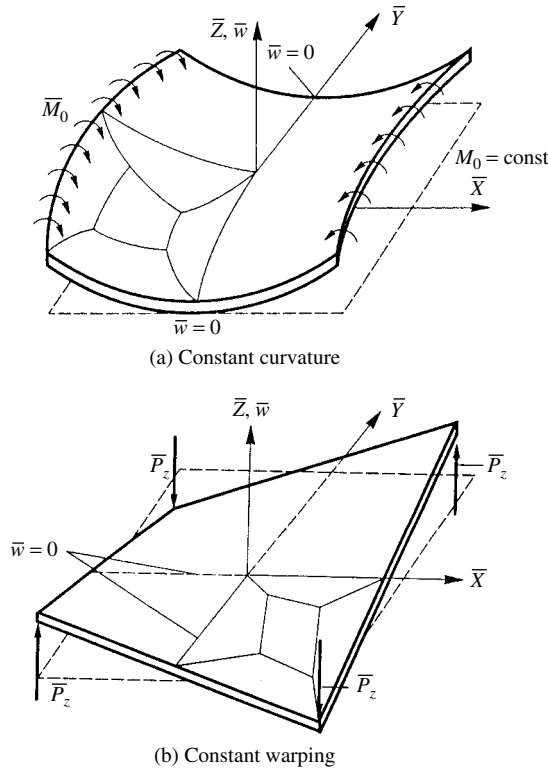


Figure 10.7.1 Patch test for plate bending elements.

Solving the pertinent moment equations by assuming that $\bar{m}_x = \bar{m}_y = 0$ and $\bar{m}_{xy} = \bar{P}_z/2$, we obtain

$$\frac{\partial^2 \bar{w}}{\partial \bar{x}^2} = \frac{\partial^2 \bar{w}}{\partial \bar{y}^2} = 0 \quad \text{and} \quad \frac{\partial^2 \bar{w}}{\partial \bar{x} \partial \bar{y}} = \frac{6\bar{P}_z(1+\nu)}{Eh^3}. \quad (10.7.6)$$

It is recommended that for patch tests relatively simple geometrical configurations be used. However, it is often desirable that the elements be of irregular shape, since some quadrilateral elements may pass the patch test when used as rectangles but fail when used in general quadrilateral form.

Assume the plate element in question satisfies the following criteria:

- state of constant strains,
- rigid-body modes without straining and
- interelement compatibility.

Then, passing the patch test indicates that the finite element solution will converge to the exact value when increasingly finer mesh is used.

Robinson introduced a single-element test [10.7.5] to judge a priori the element performances in bending analysis of plates. He used only a single rectangular plate

element with three edges free and one built in. In the test, the element in question will be subjected to various loading conditions, as shown in Fig. 10.7.2. If the results of the finite element computations correspond to the analytical solutions of the pertinent plate problems, the element will also yield satisfactory results in the finite element analysis of various plate problems. To test triangular elements, a rectangular element must be formed using two such elements.

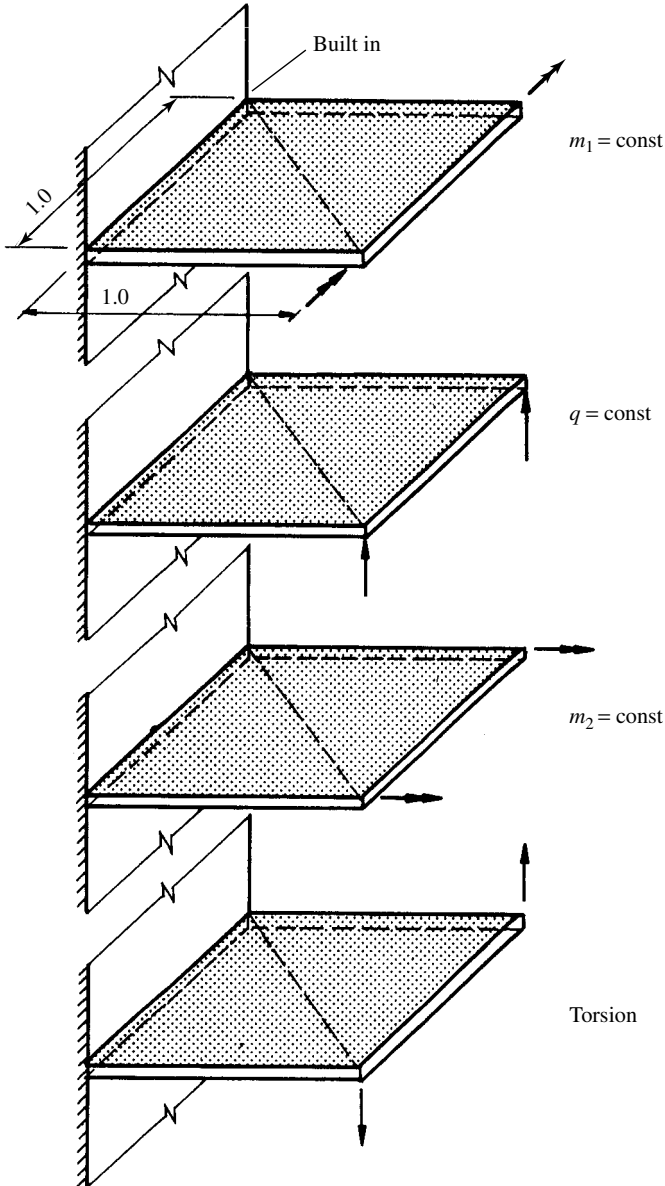


Figure 10.7.2 Robinson's single-element test.

10.7.2 Elements with Curved Sides

In most practical applications of the FEM, we can subdivide the interior domain of plates into rectangular elements and approximate the curved boundaries by a number of straight-sided triangular elements. There are, however, some relatively rare plate problems with highly irregular boundaries. In such cases, a large number of straight-sided elements may be required to satisfactorily model the plate geometry. The number of required finite elements, however, can be considerably reduced by using elements with curved sides. For instance, if the boundary shape is similar to a parabolic curve, we can use a second-order quadratic mapping function to approximate that boundary.

While in some of the previous sections we employed mapping techniques for elements of various shapes to obtain simple squares or triangles, now another mapping concept will be used to provide rectangles and triangles with curved sides. To obtain curved-element boundaries, however, the mapping function must be at least quadratic or even of higher order.

One of these mapping techniques is called *isoparametric*, where the Greek word *iso* means “equal,” referring to the fact that the mapping functions for the joint-point coordinates are chosen to be the same as the shape functions $N_i(x, y)$, which define the displacement fields of the same finite element. The word *parametric* refers to the use of parameters. If the mapping functions employed in the procedure are of lower order than functions describing the displacement fields, we call the obtained element *subparametric*. On the other hand, if the mapping functions are of higher-order than the shape functions of the displacements, we speak of *superparametric* elements.

For the so-called *parent* element, we usually select fairly regular shapes such as squares, rectangles or right and equilateral triangles. To avoid numerical problems when mapping plate elements, the following rules should be observed:

- The parent element should be straight sized.
- For quadrilateral elements, the corner angle should be close to 90° . Similarly, the corner angle for triangular elements should be in the vicinity of 60° .
- If side nodes are used, the length between nodes should be equal.
- The node numbers should be stated in a specific order.

As already mentioned, the isoparametric formulation employs the same functions, $N_i(x, y)$, for mapping as the ones used for generating the element stiffness matrix \mathbf{K}_e . But we can, of course, also use other types of mapping functions to obtain curve-sided elements. In the following, we intend to give merely a short outline of such mapping processes. Because of the relative complexity inherent in the generation of curve-sided plate elements, a detailed handling of this advanced topic is considered to be outside the scope of this book. For more information, the reader is referred to the pertinent literature.

First, a *master* set of mapping functions $f_i(\xi, \eta)$ are developed. Then, we map the local dimensionless coordinates ξ, η of the parent element into curved coordinates $\bar{\xi}, \bar{\eta}$, referred in the global coordinate system, \bar{X}, \bar{Y} , as shown in Fig 10.7.3. Since in many cases the shape functions $N_i(\xi, \eta)$ used in the transformation process are implicitly defined, there is a great need for corresponding numerical procedures when they are applied in isoparametric mapping. Furthermore, it is of basic importance that two adjacent elements satisfy the continuity requirements between them. This

can always be achieved if the shape functions of the parent element also satisfy this requirement.

The main concept underlying the development of curve-sided elements centers on transforming simple geometrical shapes of parent elements given in the local coordinate system into elements with curved edges expressed in the global reference system \bar{X}, \bar{Y} (Fig. 10.7.3). The N nodes of the element given in the local coordinate system may be mapped into corresponding nodes in the global system by

$$\bar{x} = \sum_{i=1}^N f_i(\xi, \eta) \xi_i, \quad \bar{y} = \sum_{i=1}^N f_i(\xi, \eta) \eta_i, \quad (10.7.7)$$

where N represents the total number of nodes, $f_i(\xi, \eta)$ is the mapping function and ξ_i, η_i are coordinates of the nodes. As already mentioned, the mapping functions must be at least quadratic to obtain elements with curved boundaries.

After having described the new element shape via Eq. (10.7.7) in the global reference system, we now face the task of determining the corresponding element stiffness matrix $\bar{\mathbf{K}}_e$ by carrying out the required differentiations and integration. In differentiations the chain rule must be applied, which gives the relations

$$\frac{\partial}{\partial \xi} = \frac{\partial}{\partial \bar{x}} \frac{\partial \bar{x}}{\partial \xi} + \frac{\partial}{\partial \bar{y}} \frac{\partial \bar{y}}{\partial \xi} \quad \text{and} \quad \frac{\partial}{\partial \eta} = \frac{\partial}{\partial \bar{x}} \frac{\partial \bar{x}}{\partial \eta} + \frac{\partial}{\partial \bar{y}} \frac{\partial \bar{y}}{\partial \eta}. \quad (10.7.8)$$

In general, the element stiffness matrix is calculated from[†]

$$\mathbf{K}_e = \iint_A (\mathbf{D}^T \mathbf{E} \mathbf{D}) dA, \quad (10.7.9)$$

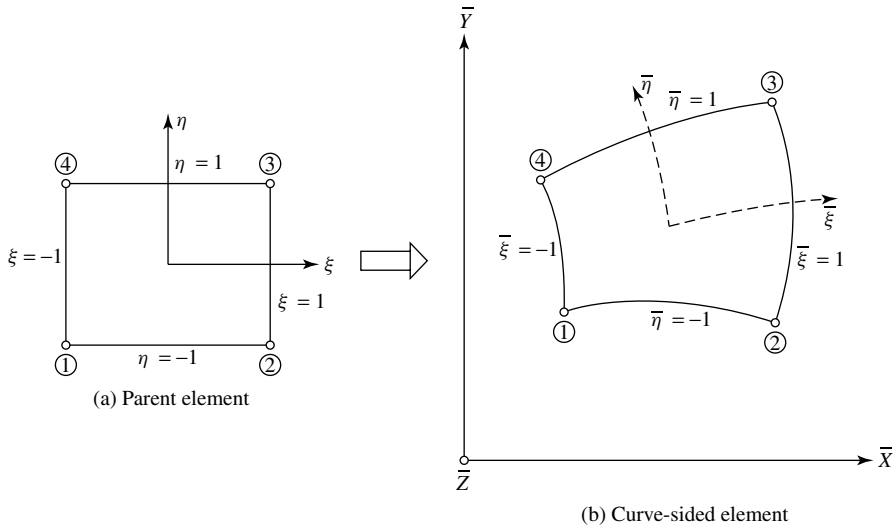


Figure 10.7.3 Mapping straight-sided element into element with curved edges.

[†] See Eq. (7.3.51).

where \mathbf{D} is the matrix defined by Eq. (7.3.51) and \mathbf{E} represents the elasticity matrix as specified in Eq. (7.3.52). The stiffness matrix of the curved element in the global reference system is usually expressed with the help of the Jacobian matrix \mathbf{J} . Thus, we can write

$$\bar{\mathbf{K}}_e = \int_{-1}^1 \int_{-1}^1 (\bar{\mathbf{B}}^T \mathbf{E} \bar{\mathbf{B}}) \det \bar{\mathbf{J}} d\bar{\xi} d\bar{\eta}. \quad (10.7.10)$$

Since the matrix product in parentheses, in general, cannot be expressed in explicit form, we must resort to numerical integration to calculate $\bar{\mathbf{K}}_e$. It is apparent that this procedure is rather complicated even for the simplest case. However, the reader will find detailed description of this process accompanied by a corresponding FORTRAN program in Ref. [10.7.6].

Summary. Nowadays, engineers are seldom required to test plate elements for convergence, since most of the plate elements given in this book converge relatively well or, in some cases, even extremely well. The same can be said concerning plate elements used in commercially available finite element programs. Probably, the only exception is when research engineers are engaged in developing new elements. In such circumstances, comparison of the energy of a test problem having an *exact* solution with that of the finite element system is the most recommended technique to obtain reliable results. Of course, the other convergence testing method can also be used, but one must consider that this method delivers the *necessary* but not *sufficient* part of the convergence requirement. Thus, its reliability is not as high as that of the energy method.

Although the highly flexible subdivision of a plate by straight-sided triangular elements can approximate quite well curved plate edges, there are some plate problems with highly irregular boundaries that may require the application of curve-sided elements. However, to determine the curved shapes of the elements and the corresponding stiffness matrices, a relatively involved mapping process is required. In this section, only the basic concepts of this procedure were briefly described. For more detailed studies of this subject, the reader is referred to the pertinent literature.

References and Bibliography

- [10.7.1] GLAHN, H., "Zur Konvergenz einiger finiter Elementen Methoden," *Ing. Arch.*, 53 (1983), 329–336.
- [10.7.2] IRONS, B. M., and RAZZAQUE, A., "Experience with Patch Test for Convergence of Finite Element Method," in A. K. Aziz (Ed.), *The Mathematical Foundation of the Finite Element Method with Application to Partial Differential Equations*, Academic Press, New York, 1972, pp. 557–587.
- [10.7.3] DEARRANTES OLIVEIRA, E. R., "Results of Convergence of Finite Element Method in Structural and Non-Structural Cases," in J. Pulmano and A. P. Kabaila (Eds.), *Finite Element Methods in Engineering*, University of New South Wales Sydney, Australia, 1974, pp. 3–14.
- [10.7.4] JOHNSON, M. W., and MCLAY, R. W., "Convergence of Finite Element Method in Theory of Elasticity," *Appl. Mech.*, ASME, 35 (1968), 274–278.
- [10.7.5] ROBINSON, J., "A Single Element Test," *Comp. Meth. Appl. Mech. Eng.*, 7 (1976), 191–200.
- [10.7.6] ROBINSON, J., *Integrated Theory of Finite Element Methods*, John Wiley & Sons, New York, 1973.

- [10.7.7] IRONS, B., "Engineering Applications of Numerical Integration in Stiffness Methods," *AIAA J.*, 4 (1966), 2035–2037.
- [10.7.8] FRIED, I., "Accuracy and Condition of Curved (Isoparametric) Elements," *J. Sound Vibr.*, 31 (1973), 345–355.
- [10.7.9] ZLAMAL, M., "Curved Elements in Finite Element Methods," *SIAM J. Num. Anal.*, 11 (1974), 347–362.
- [10.7.10] ZIENKIEWICZ, O. C., *The Finite Element Method*, 3rd ed., McGraw-Hill Book Co., London, 1977.
- [10.7.11] ZIENKIEWICZ, O. C., and PHILLIPS, D. U., "An Automatic Mesh Generation Scheme for Plane and Curved Element Domains," *Int. J. Num. Meth. Eng.*, 3 (1971), 519–528.
- [10.7.12] GORDON, W. J., and HALL, C. A., "Construction of Curvilinear Coordinate Systems and Application to Mesh Generation," *Int. J. Num. Meth. Eng.*, 7 (1973), 461–477.
- [10.7.13] EGRATOUDIS, I., et al., "Curved Isoparametric Quadrilateral Elements for Finite Element Analysis," *Int. J. Sol. Struct.*, 4 (1968), 31–42.
- [10.7.14] IRONS, B. M., "Economic Computer Techniques for Numerically Integrated Finite Elements," *Int. J. Num. Meth. Eng.*, 1 (1969), 201–203.

10.8 Extensions of Classical Finite Strip Method

The *classical finite strip method* introduced by Cheung in 1968 was originally intended only for the analysis of rectangular plates with two opposite simply supported ends. In the meantime, restrictions concerning the boundary conditions have been eliminated by employing various types of beam functions, as demonstrated in Chapter 8.

Unfortunately, the use of the classical FSM still has some shortcomings and may even lead to some difficulties in its practical applications. For instance, when the lateral load acting on the plate is highly irregular, the number of nodes required for the analysis sharply increases. In addition, since the functions used in the longitudinal strip direction are continuously differentiable, they cannot represent satisfactorily abrupt changes in bending moments at interior point supports and at the vicinity of concentrated loads. Other shortcomings of the classical FSM are related to handling of continuous spans, mixed boundary conditions in the longitudinal strip direction and dealing with arbitrary plate geometry. Finally, the classical FSM is applicable only for Kirchhoff's plates; thus it is not suited for the analysis of moderately thick plates.

However, in recent years the classical FSM has been substantially improved. Through the efforts of dedicated researchers the difficulties associated with the classical FSM are now mostly eliminated. One of the mathematical "tools" used to overcome the above-mentioned problems is the application of the *B3-spline function* for longitudinal displacement function. This approach creates the *spline finite strip* alternative. So far, this analysis technique could be successfully applied to a wide variety of plate problems [10.8.1]. It should be mentioned that the cubic spline function has $C^{(2)}$ continuity. In addition, it permits the use of arbitrary boundary conditions in the longitudinal strip direction. It is also applicable to the analysis of rectangular plates with cut-outs or to flat plates with drop panels and even to column-supported continuous plate bridges. Recent studies extend the *spline finite strip* method to moderately thick plates by considering the effect of transverse shear. The other mathematical tool used to overcome the difficulties of the classical FSM is based on the so-called *computed shape function*. These recent developments further increase the flexibility in the choice of interpolating functions. Consequently, the classical FSM is now substantially improved.

10.8.1 Spline Finite Strip Method

a. Spline Functions. The spline functions are piecewise interpolating functions. The term *spline* derives from the drafting tool used by naval architects in laying out curved ship hull contours. The *cubic spline* ($n = 3$) is especially important since it is almost exclusively employed in the spline FSM. It represents the equation of beam deflections when the clamped beam is subjected to a concentrated force. A cubic spline function is a piecewise polynomial that is continuously differentiable over the entire domain of interpolation. Another favorable property of this function is that it breaks the continuous domain into small intervals, and constraints placed in one region have no effects in regions far removed. In addition, the cubic spline function has accuracy in derivatives coupled with good convergence characteristics [10.8.2–10.8.4]. Furthermore, it can be easily adapted to fit various boundary conditions, as illustrated below. A typical cubic spline function is shown in Fig. 10.8.1. Its use as a displacement function in the longitudinal strip direction with fixed and free boundary conditions and equally spaced nodal points is shown in Fig. 10.8.2.

The cubic B3-spline function for equally placed sections is expressed as

$$Y(y) = \sum_{i=-1}^{m+1} \alpha_i \phi_i = \{\phi\}^T \{\alpha\}, \quad (10.8.1a)$$

in which ϕ_i has nonzero values over four consecutive sections. The section ϕ_i with the section knot $y = y_i$ as center is given as

$$\phi_i = \frac{1}{6h^3} \begin{cases} 0 & \text{for } y < y_{i-2}, \\ (y - y_{i-2})^3 & \text{for } y_{i-2} \leq y \leq y_{i-1}, \\ h^3 + 3h^2(y - y_{i-1}) + 3h(y - y_{i-1})^2 & \text{for } y_{i-1} \leq y \leq y_i, \\ -3(y - y_{i-1})^3 & \text{for } y_i \leq y \leq y_{i+1}, \\ h^3 + 3h^2(y_{i+1} - y) + 3h(y_{i+1} - y)^2 & \text{for } y_{i+1} \leq y \leq y_{i+2}, \\ -3(y_{i+1} - y)^3 & \text{for } y < y_{i+2}, \\ 0 & \text{for } y < y_{i+2}. \end{cases} \quad (10.8.1b)$$

The corresponding unknown parameters are represented by α_i . Unequally spaced nodal points can also be used. In this case, however, expression for the function becomes more elaborate.

The treatment of various boundary conditions at the ends of the strip can be easily accomplished by amending the B3-spline function at the corresponding boundaries. Due to the localized nature of the spline functions, only three local boundary splines have to be amended at each end, that is,

$$\{\phi\}^T = \{\tilde{\phi}_{-1} \quad \tilde{\phi}_0 \quad \tilde{\phi}_1 \quad \phi_2 \quad \phi_3 \quad \dots \quad \phi_{m-2} \quad \tilde{\phi}_{m-1} \quad \tilde{\phi}_m \quad \tilde{\phi}_{m+1}\}^T, \quad (10.8.2)$$

where ϕ_i represents standard local splines and $\tilde{\phi}_i$ denotes amended local splines. Consequently, the function $Y(y)$ can be written as

$$Y(y) = \{\phi\}^T \{\alpha\}, \quad (10.8.3)$$

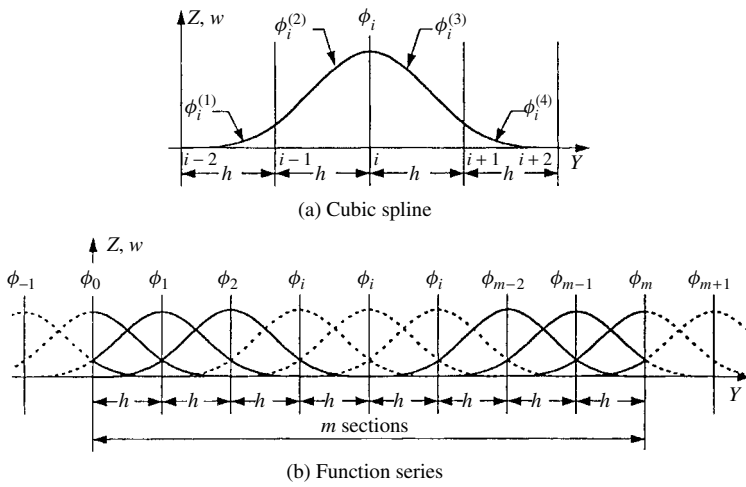


Figure 10.8.1 Cubic spline displacement function.

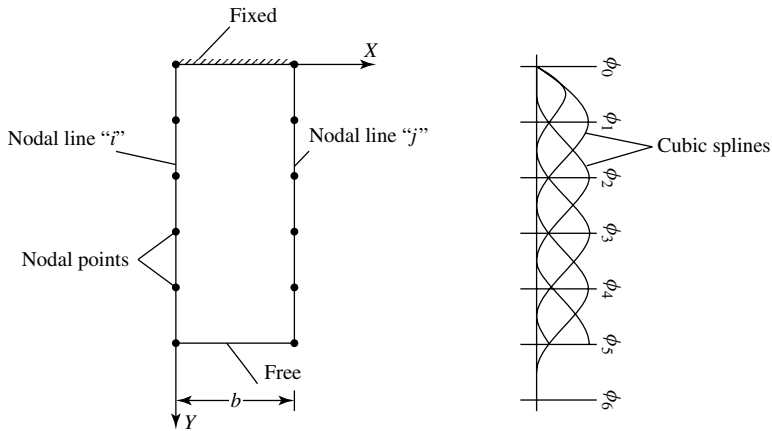


Figure 10.8.2 Displacement function for strip.

where the vector of the displacement parameters is

$$\{\alpha\} = \begin{Bmatrix} \alpha_{-1} \\ \alpha_0 \\ \alpha_1 \\ \alpha_2 \\ \alpha_3 \\ \vdots \\ \alpha_{m-2} \\ \alpha_{m-1} \\ \alpha_m \\ \alpha_{m+1} \end{Bmatrix}. \quad (10.8.4)$$

To incorporate the kinematic boundary conditions, zero values are used in Eq. (10.8.4) for the restrained degrees of freedom. Thus, the corresponding local splines are eliminated in Eqs. (10.8.2) and (10.8.3), respectively. For example, if the boundary is clamped at $y = 0$, we can write

$$Y(y) = \{ \tilde{\phi}_{-1} \quad \tilde{\phi}_0 \quad \tilde{\phi}_1 \quad \phi_2 \quad \phi_3 \quad \dots \}^T \left\{ \begin{array}{c} 0 \\ 0 \\ \alpha_1 \\ \alpha_2 \\ \alpha_3 \\ \vdots \end{array} \right\} . \tag{10.8.5}$$

A similar approach can be used at the $y(l)$ end. Table 10.8.1 shows other amendment schemes of practical interest.

b. Finite Strip Formulation. The displacement field of a strip is expressed as the product of the cubic spline function with equally spaced nodes in the longitudinal strip direction and conventional beam functions in the other. These functions are

$$\{N\}^T = \left\{ \begin{array}{l} N_1 = 1 - 3\left(\frac{x}{b}\right)^2 + 2\left(\frac{x}{b}\right)^3 \\ N_2 = x \left[1 - \frac{2x}{b} + \left(\frac{x}{b}\right)^2 \right] \\ N_3 = 3\left(\frac{x}{b}\right)^2 - 2\left(\frac{x}{b}\right)^3 \\ N_4 = x \left[\left(\frac{x}{b}\right)^2 - \frac{x}{b} \right] \end{array} \right\}^T . \tag{10.8.6}$$

Table 10.8.1 Amended Boundary Spline Functions at End Support

<i>Boundary Condition</i>	<i>Modified Local Spline Functions</i>		
	$\tilde{\phi}_{-1}$	$\tilde{\phi}_0$	$\tilde{\phi}_1$
Free	$\tilde{\phi}_{-1}$	$\tilde{\phi}_0$	$\tilde{\phi}_1$
Simply supported	Eliminated	$\tilde{\phi}_0 - 4\tilde{\phi}_{-1}$	$\tilde{\phi}_1 - \tilde{\phi}_{-1}$
Clamped	Eliminated	Eliminated	$\tilde{\phi}_1 - \frac{1}{2}\tilde{\phi}_0 + \tilde{\phi}_{-1}$
Sliding clamped supported	Eliminated	$\tilde{\phi}_0$	$\tilde{\phi}_1 + \tilde{\phi}_{-1}$
Continuous	$\tilde{\phi}_{-1} - \frac{1}{4}\tilde{\phi}_0$	Eliminated	$\tilde{\phi}_1 - \frac{1}{4}\tilde{\phi}_0$

Note: From Ref. [10.8.1].

They connect each nodal line with two degrees of freedom, that is, the transverse displacement w_i and its corresponding rotation θ_i . Thus,

$$\{N_1 \quad N_2 \quad N_3 \quad N_4\}^T \begin{Bmatrix} w_i \\ \theta_i \\ w_j \\ \theta_j \end{Bmatrix}, \quad (10.8.7)$$

where i and j represent the nodal lines. Consequently, as shown in Fig. 10.8.3, the displacement function for a plate strip can be given as

$$\{w\} = \{N_1 \quad N_2 \quad N_3 \quad N_4\}^T \begin{bmatrix} \{\phi_{w_i}\}^T & \{\phi_{\theta_i}\}^T & & \\ & & \{\phi_{w_j}\}^T & \\ & & & \{\phi_{\theta_j}\}^T \end{bmatrix} \begin{Bmatrix} \{w_i\} \\ \{\theta_i\} \\ \{w_j\} \\ \{\theta_j\} \end{Bmatrix}, \quad (10.8.8)$$

where $\{\phi_i\}^T$ and $\{\phi_j\}^T$ are row matrices in terms of B3 splines and $\{w_i\}$, $\{\theta_i\}$, $\{w_j\}$ and $\{\theta_j\}$ are the vectors of the corresponding displacements for nodal lines i and j , respectively.

Now, since the displacement functions representing the shape functions for the strip element have been determined, we can use the standard procedure described in Sec. 7.3.2 to obtain the corresponding stiffness matrix \mathbf{K}_e . For this purpose, we must

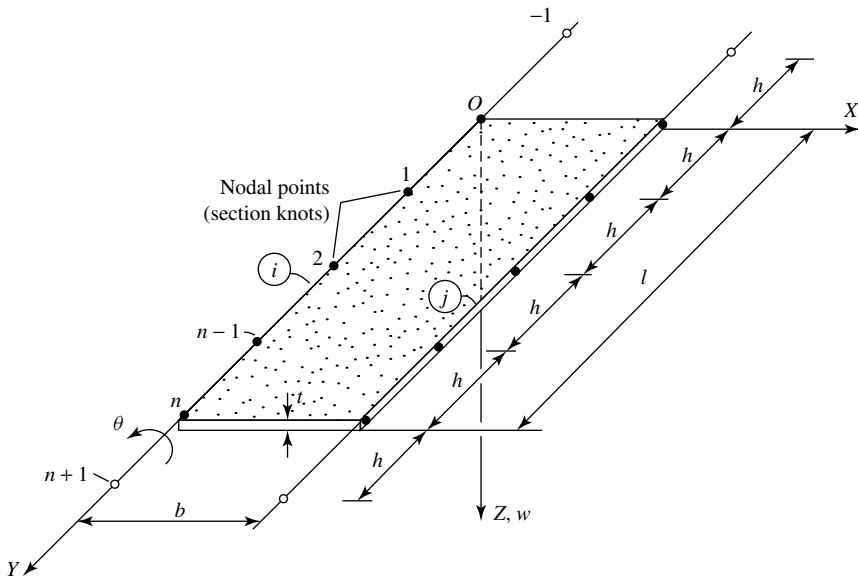


Figure 10.8.3 Typical plate strip.

first establish the strain-displacement relationship, which can be written as

$$\kappa = \begin{Bmatrix} \kappa_x \\ \kappa_y \\ \chi \end{Bmatrix} = \begin{Bmatrix} -\frac{\partial^2 w}{\partial x^2} \\ -\frac{\partial^2 w}{\partial y^2} \\ 2\frac{\partial^2 w}{\partial x \partial y} \end{Bmatrix} = \begin{bmatrix} -\{N''\}^T & 0 & 0 \\ 0 & -\{N\}^T & 0 \\ 0 & 0 & 2\{N'\}^T \end{bmatrix} \begin{Bmatrix} \{\phi\} \\ \{\phi''\} \\ \{\phi'\} \end{Bmatrix} \{d\} = \mathbf{D}d, \quad (10.8.9)$$

where

$$\begin{aligned} \{N'\}^T &= \frac{\partial}{\partial x} \{N\}^T, & \{N''\}^T &= \frac{\partial^2}{\partial x^2} \{N\}^T, \\ \{\phi'\}^T &= \frac{\partial}{\partial y} \{\phi\}, & \{\phi''\} &= \frac{\partial^2}{\partial y^2} \{\phi\} \end{aligned} \quad (10.8.10)$$

represent differentiations of pertinent functions with respect to x and y , respectively.

Thus, the stiffness matrix of the strip element is obtained from

$$\mathbf{K}_e = \int_V \mathbf{D}^T \mathbf{E} \mathbf{D} dV, \quad (10.8.11)$$

or in a more detailed form [10.8.5]

$$\begin{aligned} \mathbf{K}_e &= \int_V \begin{Bmatrix} \{\phi\}^T & \{\phi''\}^T & \{\phi'\}^T \end{Bmatrix} \begin{bmatrix} -\{N''\}^T & 0 & 0 \\ 0 & -\{N\}^T & 0 \\ 0 & 0 & 2\{N'\}^T \end{bmatrix} \\ &\times \mathbf{E} \begin{bmatrix} -\{N''\} & 0 & 0 \\ 0 & -\{N\} & 0 \\ 0 & 0 & 2\{N'\} \end{bmatrix} \begin{Bmatrix} \{\phi\} \\ \{\phi''\} \\ \{\phi'\} \end{Bmatrix} dV. \end{aligned} \quad (10.8.11a)$$

The elasticity matrix \mathbf{E} for an orthotropic plate, for instance, can be written as

$$\mathbf{E} = \begin{bmatrix} D_x & D_1 & 0 \\ D_1 & D_y & 0 \\ 0 & 0 & D_{xy} \end{bmatrix}, \quad (10.8.12)$$

where $D_{xy} = D_t$ represents the torsional rigidity and $D_1 = \nu_x D_y = \nu_y D_x$. This along with the bending rigidities of the plate is defined in Sec. 10.1.

Fan [10.8.5] derived the bending stiffness matrix of a typical plate strip (Fig. 10.8.3) in the following explicit form:

$$\mathbf{K}_e = \frac{1}{420b^3} \begin{bmatrix} 5040D_x I_{111} & 2520bD_x I_{112} & -5040D_x I_{113} & 2520bD_x I_{114} & \vdots & \vdots & \vdots & \vdots \\ -504b^2 D_1 I_{211} & -462b^3 D_1 I_{212} & +504b^2 D_1 I_{213} & -42b^3 D_1 I_{214} & \vdots & \vdots & \vdots & \vdots \\ -504b^2 D_1 I_{311} & -42b^3 D_1 I_{312} & +504b^2 D_1 I_{313} & -42b^3 D_1 I_{314} & \vdots & \vdots & \vdots & \vdots \\ +156b^4 D_y I_{411} & +22b^5 D_y I_{412} & +54b^4 D_y I_{413} & -13b^5 D_y I_{414} & \vdots & \vdots & \vdots & \vdots \\ +2016b^2 D_{xy} I_{511} & +168b^3 D_{xy} I_{512} & -2016b^2 D_{xy} I_{513} & +168b^3 D_{xy} I_{514} & \vdots & \vdots & \vdots & \vdots \\ \hline \vdots & 5040b^2 D_x I_{122} & -2520bD_x I_{123} & 840b^2 D_x I_{124} & \vdots & \vdots & \vdots & \vdots \\ \vdots & -504b^3 D_1 I_{222} & +42b^3 D_1 I_{223} & +14b^3 D_1 I_{224} & \vdots & \vdots & \vdots & \vdots \\ \vdots & -504b^4 D_1 I_{322} & +42b^3 D_1 I_{323} & +14b^4 D_1 I_{324} & \vdots & \vdots & \vdots & \vdots \\ \vdots & +156b^6 D_y I_{422} & +13b^5 D_y I_{423} & -3b^6 D_y I_{424} & \vdots & \vdots & \vdots & \vdots \\ \vdots & +2016b^4 D_{xy} I_{522} & -168b^3 D_{xy} I_{523} & -56b^4 D_{xy} I_{524} & \vdots & \vdots & \vdots & \vdots \\ \hline \vdots & \vdots & 5040D_x I_{133} & -2520bD_x I_{134} & \vdots & \vdots & \vdots & \vdots \\ \vdots & \vdots & -504b^2 D_1 I_{233} & +462b^3 D_1 I_{234} & \vdots & \vdots & \vdots & \vdots \\ \vdots & \vdots & -504b^2 D_1 I_{333} & +42b^3 D_1 I_{334} & \vdots & \vdots & \vdots & \vdots \\ \vdots & \vdots & +156b^4 D_y I_{433} & -22b^5 D_y I_{434} & \vdots & \vdots & \vdots & \vdots \\ \vdots & \vdots & +2016b^2 D_{xy} I_{533} & -168b^3 D_{xy} I_{534} & \vdots & \vdots & \vdots & \vdots \\ \hline \text{Symmetric} & \vdots & \vdots & \vdots & \vdots & \vdots & \vdots & \vdots \\ \vdots & \vdots & \vdots & \vdots & \vdots & \vdots & 5040b^2 D_x I_{144} & \vdots \\ \vdots & \vdots & \vdots & \vdots & \vdots & \vdots & -504b^3 D_1 I_{244} & \vdots \\ \vdots & \vdots & \vdots & \vdots & \vdots & \vdots & -504b^4 D_1 I_{344} & \vdots \\ \vdots & \vdots & \vdots & \vdots & \vdots & \vdots & +156b^6 D_y I_{444} & \vdots \\ \vdots & \vdots & \vdots & \vdots & \vdots & \vdots & +2016b^4 D_{xy} I_{544} & \vdots \end{bmatrix}, \quad (10.8.13)$$

where

$$\begin{aligned} I_{1ij} &= \int_0^l t \{\phi\}_i^T \{\phi\}_j dy, & I_{2ij} &= \int_0^l t \{\phi''\}_i^T \{\phi\}_j dy, & I_{3ij} &= \int_0^l t \{\phi\}_i^T \{\phi''\}_j dy, \\ I_{4ij} &= \int_0^l t \{\phi''\}_i^T \{\phi''\}_j dy, & I_{5ij} &= \int_0^l t \{\phi'\}_i^T \{\phi'\}_j dy. \end{aligned} \quad (10.8.14)$$

It is important to note that the stiffness matrix given in Eq. (10.8.13) is of a general form for a plate strip having any number of sections. That is, the size of the matrix depends on the size of the above integrals of spline vectors or their derivatives.

As usual, the internal stress resultants[†] can be obtained from

$$\sigma = \begin{Bmatrix} m_x \\ m_y \\ m_{xy} \end{Bmatrix} = \mathbf{E} \begin{Bmatrix} -\frac{\partial^2 w}{\partial x^2} \\ -\frac{\partial^2 w}{\partial y^2} \\ 2\frac{\partial^2 w}{\partial x \partial y} \end{Bmatrix}. \quad (10.8.15)$$

[†] See also Secs. 1.2 and 10.1.

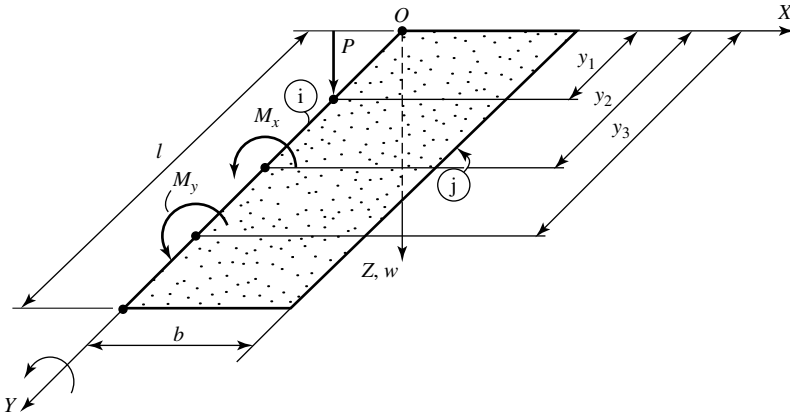


Figure 10.8.4 Concentrated forces acting on nodal line i .

c. Formulation of Load Vector. It is recommended that a nodal line and nodal point should be assigned to each concentrated force (Fig.10.8.4). Needless to say, concentrated forces acting on a common nodal line should not be considered twice when the load matrix of the total structure is compiled. Since there are only four local splines with nonzero values at their specific location, the vector of concentrated forces and moments acting on an strip element should be formulated as

$$\mathbf{p}_e = \{\phi(y_1)\}^T \begin{Bmatrix} P \\ 0 \\ 0 \\ 0 \end{Bmatrix} + \{\phi(y_2)\}^T \begin{Bmatrix} 0 \\ M_x \\ 0 \\ 0 \end{Bmatrix} + \{\phi'(y_3)\}^T \begin{Bmatrix} M_y \\ 0 \\ 0 \\ 0 \end{Bmatrix}. \quad (10.8.16)$$

Because the FSM, similar to other FEM, is not overly sensitive to the way distributed loads are represented, it is in most cases satisfactory to allocate statically equivalent concentrated forces and moments to the corresponding nodal points.

d. Computational Procedures. The required steps follow, in general, those of the standard FEM described in Sec. 7.1.3:

- A Cartesian global reference system $\bar{X}, \bar{Y}, \bar{Z}$ is selected.
- Discretization of the plate is performed by a suitable number of longitudinal strips connected to each other by nodal lines. These strips are further subdivided into a group of nodal sections by equally spaced section knots (nodal points).
- For each strip the plate thickness h , Young's modulus of elasticity E and Poisson's ratio ν must be defined.
- The selected spline representation for each nodal line must satisfy the prescribed boundary conditions in the longitudinal strip direction.
- The displacement function for a strip is expressed as a product of longitudinal spline functions and transverse beam functions.
- The displacements of the nodal lines are defined by the lateral displacements w_i and transverse rotations θ_i of the section knots. These unknowns are separately numbered in the local and global coordinate systems, respectively.

- The element stiffness matrix \mathbf{K}_e and the load vector \mathbf{p}_e are computed in the local coordinate system X, Y, Z of the strip element.
- In the stiffness matrices \mathbf{K}_e , and load vectors \mathbf{p}_e , the local numbering is replaced by its global equivalent.
- The global stiffness matrix $\bar{\mathbf{K}}$ relevant to the degrees of freedom of the nodal lines is computed from the stiffness matrices \mathbf{K}_e of the individual strips according to the additive technique. The same goes for the load vector $\bar{\mathbf{p}}$ of the total system using the vectors \mathbf{p}_e of the strips.
- By solving the governing matrix equation $\bar{\mathbf{K}} \bar{\mathbf{d}} = \bar{\mathbf{p}}$, the tridiagonal block structure of the global stiffness matrix can be utilized.
- With known displacement vector $\bar{\mathbf{d}}$, the internal stress resultants can be determined through the kinematic and constitutive equations.

10.8.2 Computed Shape Functions

If the plate thickness varies significantly along the longitudinal strip direction Y , the use of the so-called *computed shape functions* may save considerable computational efforts, since the degrees-of-freedom can be substantially reduced [10.8.1, 10.8.9]. Applying this approach, a plate strip with varying thickness along the strip direction Y is considered as a beam with the same *boundary conditions* and variation of thickness as the plate strip (Fig. 10.8.5a). This equivalent beam is divided into beam elements representing the various plate rigidities (Fig. 10.8.5b). To compute the longitudinal shape functions $Y_m(y)$, a number of *joint points* are assigned for each beam section. Next, we determine the influence lines for lateral deflections at each node m by imposing a unit translation at the node point in question, while the other nodes have zero deflections (Fig. 10.8.5c). These influence lines for a continuous beam can easily be determined by either the FEM or the FDM. In this way, a total of r computed shape functions are obtained. Again, the shape function of a typical *plate strip* bounded by lines ① and ② can be written as

$$w(x, y) = \sum_{m=1}^r Y_m(y) \{N(x)\}^T \{d\}_m, \quad (10.8.17)$$

where $Y_m(y)$ is the *computed shape function* at the nodal point and m and r represent the number of these points. In addition, $\{N(x)\}^T$ symbolizes a row matrix containing the usual beam shape functions in the X direction as already given in Eq. (10.8.6) and

$$\{d\}_m = \begin{Bmatrix} w_1 \\ \theta_1 \\ w_2 \\ \theta_2 \end{Bmatrix}_m \quad (10.8.18)$$

is the vector of displacement components at nodal point m along the nodal lines ① and ②.

Since the shape function is now known, we can follow the same procedures as used in connection with the classical FSM[†] to obtain the stiffness matrix of all plate

[†] See Sec. 8.3.

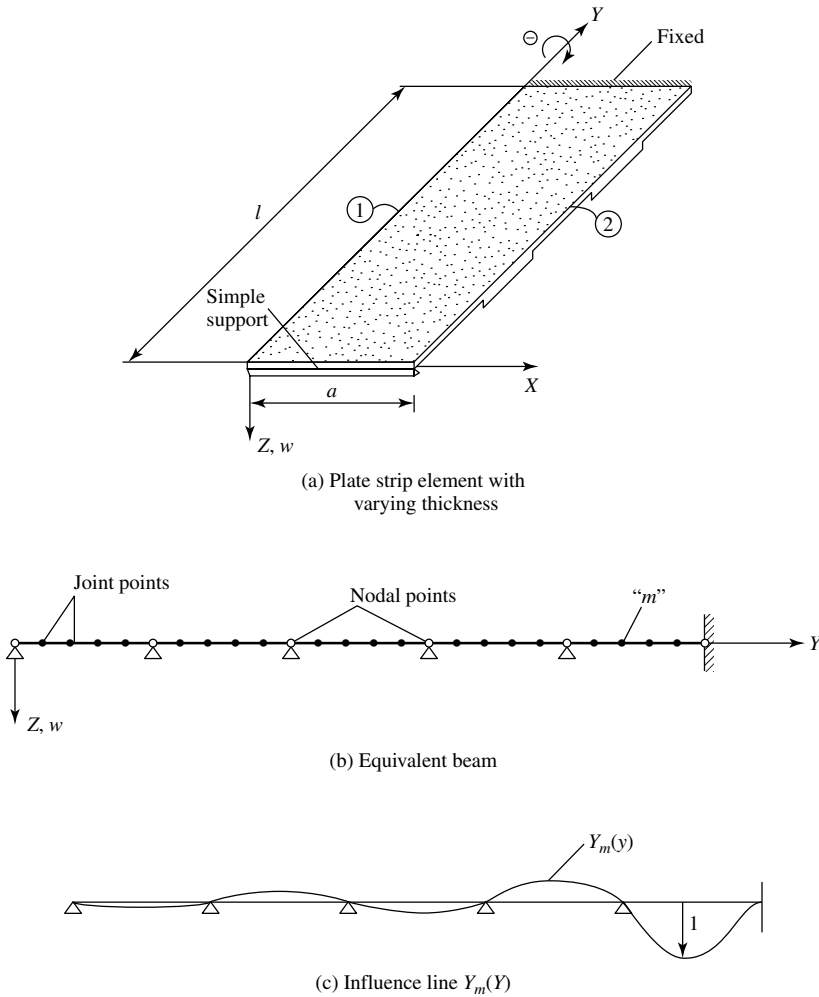


Figure 10.8.5 Concept of computed shape function $Y_m(y)$.

strips and subsequently that of the complete plate structure. Again, the computational algorithm remains the same as the one used for the classical FSM. As mentioned before, all FEMs are not sensitive to the manner of load representation. Thus, we may apply the simple "tributary load" approximations for distributed loads, as already discussed in connection with gridwork and finite element methods. However, if a more exact load representation technique is needed, it can be found in Ref. [10.8.9]. Concentrated loads, as usual, require the assignment of individual nodal lines and nodal points.

10.8.3 Finite Strip Formulation of Moderately Thick Plates

So far, we have limited the applications of the FSM to Kirchhoff plates. Recently, however, the FSM was also extended to the analysis of moderately thick

plates by using first- (and even higher) order Mindlin or Reissner plate theories [10.8.10–10.8.14] introduced in Sec. 1.5. Applying Mindlin's first-order theory, the displacement vector can be written as

$$\begin{Bmatrix} u \\ v \\ w \end{Bmatrix} = \begin{Bmatrix} -z\psi_x(x, y) \\ -z\psi_y(x, y) \\ w(x, y) \end{Bmatrix}, \quad (10.8.19)$$

where $w(x, y)$ represents the transverse displacements and $\psi_x(x, y)$, $\psi_y(x, y)$ denote the section rotations illustrated in Fig. 10.8.6.

We express, again, the functions for deflections and rotations as products of the $Y_m(y)$ and $N_k(x)$ shape functions

$$\begin{aligned} w(x, y) &= \sum_{m=1}^r \sum_{k=1}^s Y_m(y) N_k(x) w_{km}, \\ \psi_x(x, y) &= \sum_{m=1}^r \sum_{k=1}^s Y_m(y) N_k(x) \psi_{x,km}, \\ \psi_y(x, y) &= \sum_{m=1}^r \sum_{k=1}^s Y_m(y) N_k(x) \psi_{y,km}, \end{aligned} \quad (10.8.20)$$

where $Y_m(y)$ represents the *classical* shape functions introduced in Sec. 8.2 and $N_k(x)$ denotes the beam functions given in Eq. (10.8.6). For nondominant shear effects, however, it is often sufficient to use straight-line shape functions with two nodes (Fig. 10.8.7), which are expressed by

$$N_1(x) = 1 - \frac{x}{b} \quad \text{and} \quad N_2(x) = \frac{x}{b} \quad (10.8.21)$$

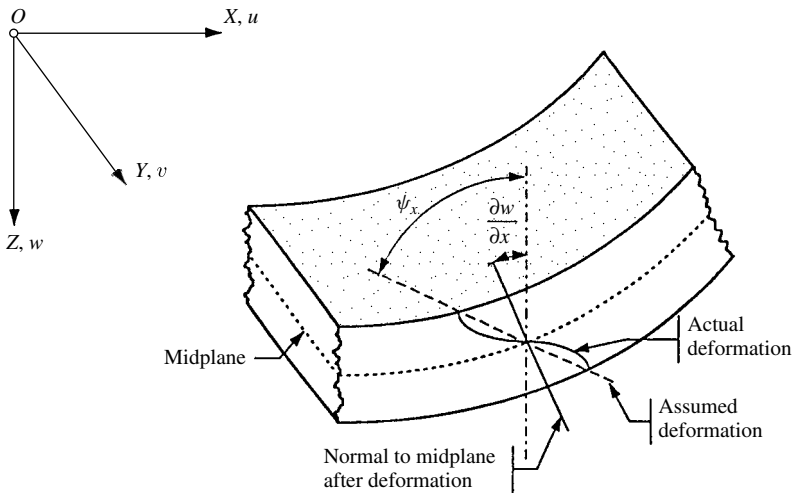


Figure 10.8.6 Cross-sectional deformation of moderately thick plate.

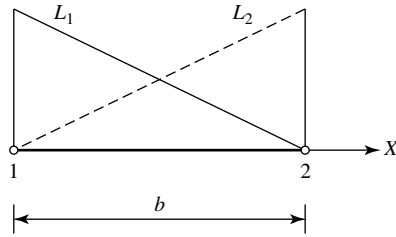


Figure 10.8.7 Straight-line function with two nodes.

The strain-displacement relationships required for generating element stiffness coefficients are

$$\begin{Bmatrix} \epsilon_b \\ \epsilon_s \end{Bmatrix} = \begin{Bmatrix} \epsilon_x \\ \epsilon_y \\ \gamma_{xy} \\ \gamma_{xz} \\ \gamma_{yz} \end{Bmatrix} = \begin{Bmatrix} -z \frac{\partial \psi_x}{\partial x} \\ -z \frac{\partial \psi_y}{\partial y} \\ -z \left(\frac{\partial \psi_x}{\partial y} + \frac{\partial \psi_y}{\partial x} \right) \\ \frac{\partial w}{\partial x} - \psi_x \\ \frac{\partial w}{\partial y} - \psi_y \end{Bmatrix}, \quad (10.8.22)$$

in which ϵ_b represents strains produced by bending and ϵ_s denotes the part of the strain vector due to shear effects.

Substituting Eq. (10.8.20) into Eq. (10.8.22) and following the standard procedures for generating element stiffness matrices, we obtain

$$\mathbf{K}_e = \mathbf{K}_{e,b} + \mathbf{K}_{e,s} = \int_0^l \int_0^b \mathbf{D}_b^T \mathbf{E}_b \mathbf{D} \, dx \, dy + \int_0^l \int_0^b \mathbf{D}_s^T \mathbf{E}_s \mathbf{D}_s \, dx \, dy, \quad (10.8.23)$$

where \mathbf{D}_b and \mathbf{D}_s represent matrices containing the corresponding differentiations of the shape functions and \mathbf{E}_b and \mathbf{E}_s are elasticity matrices for bending and shear, respectively, as defined in Sec. 7.9. The computational procedures are similar to those given in Sec. 7.8.1.

However, the relative simplicity of the above given outline should not mislead the reader, since the actual programming of these procedures requires quite a bit of expertise.

Furthermore, it should be noted that as the plate thickness becomes small, the influence of the shear terms tends to dominate. Consequently, numerical solutions of the plate problems may yield unsatisfactory (i.e., overstiff) results. This *shear locking* phenomenon is well known for plates analyzed using refined plate theories. The problem is similar to that already discussed in connection with the FEM. The use of deliberate under integration is one of the methods often practiced. Namely, a reduction of the order of numerical integration leads to considerably improved accuracy.

Summary. To overcome the shortcomings of the *classical* FSM, the *spline finite strip* approach was introduced by Fan [10.8.5]. Unlike its classical counterpart, this new technique employs B3-spline functions for displacements in the longitudinal strip direction and uses cubic polynomials in the transverse direction for shape functions. The general form of the displacement function is given as their product. The developed spline FSM possesses the combined advantages of the FEM and the classical FSM. Consequently, this new approach may emerge, in some cases, as a viable alternative numerical procedure for plate analysis. A similar approach was taken by using *computed shape functions* instead of splines. Furthermore, to treat even arbitrarily shaped general plates, a mapping procedure was introduced that transforms the arbitrary shapes into unit squares. Thus skew and curved plates can be analyzed with relative ease [10.8.16, 10.8.17]. The spline FSM was also extended to solution of such diverse plate problems as plates with varying rigidities and flat plates, to name a few. Unfortunately, the number of commercially available computer programs using the spline FSM is still relatively small, in spite of its merit of considerably reducing the unknowns required in the computation. Thus, the method still remains mostly within the realm of mathematically inclined engineers with good computer programming background. For further study, the reader will find in Ref. [10.8.20] an extensive chronological listings of publications treating all versions of the FSM.

ILLUSTRATIVE EXAMPLE

Let us determine a spine shape function with only two consecutive sections (i.e., $m = 2$). This function can be written as

$$Y(y) = \sum_{-1}^3 \alpha_i \phi_i(y) = \{ \phi_{-1} \quad \phi_0 \quad \phi_1 \quad \phi_2 \quad \phi_3 \}^T \begin{Bmatrix} \alpha_{-1} \\ \alpha_0 \\ \alpha_1 \\ \alpha_2 \\ \alpha_3 \end{Bmatrix} \quad (10.8.24)$$

with the locations at y_0 , y_1 and y_2 taken as nodal points and denoted by 0, 1 and 2, respectively. A transformation procedure is now applied to express Eq. (10.8.24) in terms of a set of functions and a corresponding set of nodal parameters. By choosing f_0 , f'_0 , f_1 , f_2 and f'_2 as nodal parameters in which f_i and f'_i are the functional value and the value of its first derivative with respect to y , respectively, at node (i) , the following expression can be written:

$$\begin{Bmatrix} f_0 \\ f'_0 \\ f_1 \\ f_2 \\ f'_2 \end{Bmatrix} = \begin{bmatrix} \phi_{-1}(y_0) & \phi_0(y_0) & \phi_1(y_0) & \phi_2(y_0) & \phi_3(y_0) \\ \phi'_{-1}(y_0) & \phi'_0(y_0) & \phi'_1(y_0) & \phi'_2(y_0) & \phi'_3(y_0) \\ \phi_{-1}(y_1) & \phi_0(y_1) & \phi_1(y_1) & \phi_2(y_1) & \phi_3(y_1) \\ \phi_{-1}(y_2) & \phi_0(y_2) & \phi_1(y_2) & \phi_2(y_2) & \phi_3(y_2) \\ \phi'_{-1}(y_2) & \phi'_0(y_2) & \phi'_1(y_2) & \phi'_2(y_2) & \phi'_3(y_2) \end{bmatrix} \begin{Bmatrix} \alpha_{-1} \\ \alpha_0 \\ \alpha_1 \\ \alpha_2 \\ \alpha_3 \end{Bmatrix} = [C]\{\alpha\}. \quad (10.8.25)$$

Inverting the matrix $[C]$, we obtain

$$\begin{Bmatrix} \alpha_{-1} \\ \alpha_0 \\ \alpha_1 \\ \alpha_2 \\ \alpha_3 \end{Bmatrix} = [C]^{-1} \begin{Bmatrix} f_0 \\ f'_0 \\ f_1 \\ f_2 \\ f'_2 \end{Bmatrix}. \quad (10.8.26)$$

Substituting Eq. (10.8.26) into Eq. (10.8.24), the expression for the spline function becomes

$$\begin{aligned} Y(y) &= \{\phi_{-1} \quad \phi_0 \quad \phi_1 \quad \phi_2 \quad \phi_3\}^T [C]^{-1} \begin{Bmatrix} f_0 \\ f'_0 \\ f_1 \\ f_2 \\ f'_2 \end{Bmatrix} \\ &= \{F_{01} \quad F_{02} \quad F_{11} \quad F_{21} \quad F_{22}\}^T \begin{Bmatrix} f_0 \\ f'_0 \\ f_1 \\ f_2 \\ f'_2 \end{Bmatrix}, \end{aligned} \quad (10.8.27)$$

in which F_{01} , F_{02} , F_{11} , F_{21} and F_{22} are linear combinations of ϕ_i . They represent functions corresponding to the nodal parameters. It can be shown that

$$\begin{aligned} F_{01} &= -\frac{1}{2}\phi_{-1} + \frac{7}{4}\phi_0 - \frac{1}{2}\phi_1 + \frac{1}{4}\phi_2 - \frac{1}{2}\phi_3, \\ F_{02} &= h \left[-\frac{13}{6}\phi_{-1} + \frac{7}{12}\phi_0 - \frac{1}{6}\phi_1 + \frac{1}{12}\phi_2 - \frac{1}{6}\phi_3 \right], \\ F_{11} &= 2\phi_{-1} - \phi_0 + 2\phi_1 - \phi_2 + 2\phi_3, \\ F_{21} &= -\frac{1}{2}\phi_{-1} + \frac{1}{4}\phi_0 - \frac{1}{2}\phi_1 + \frac{7}{4}\phi_2 - \frac{1}{2}\phi_3, \\ F_{22} &= h \left[\frac{1}{6}\phi_{-1} - \frac{1}{12}\phi_0 + \frac{1}{6}\phi_1 - \frac{7}{12}\phi_2 + \frac{13}{6}\phi_3 \right]. \end{aligned} \quad (10.8.28)$$

References and Bibliography

- [10.8.1] CHEUNG, Y. K., and THAM, L. G., *Finite Strip Method*, CRC Press, Boca Raton, Florida, 1998.
- [10.8.2] AHBERG, J. H., et al., *The Theory of Splines and Their Applications*, Academic Press, New York, 1967.
- [10.8.3] GREVILLE, T. N. E. (Ed.), *Theory and Applications of Spline Functions*, Academic Press, New York, 1969.
- [10.8.4] BRIKHOFF, G., and DEBOOR, C., "Error Bounds for Cubic Spline Interpolation," *J. Math. Mech.*, 13 (1964), 827–835.
- [10.8.5] FAN, S. C., "Spline Finite Strip Method in Structural Analysis," Ph.D. thesis, Department of Civil Engineering, University of Hong Kong, 1982.
- [10.8.6] FAN, S. C., et al., "Spline Finite Strip in Structural Analysis," in H. Guaguian and Y. K. Cheung (Eds.), *Proceedings of the International Conference on Finite Element Methods, Shanghai*, Gordon & Breach, New York, 1982, pp. 702–709.

- [10.8.7] LI, W. Y., et al., "Finite Strip Analysis of General Plates," *J. Eng. Mech. Div., ASCE*, 112, No. 1 (1986), 43–54.
- [10.8.8] CHEUNG, Y. K., and FAN, S. C., "Spine Finite Strip in Structural Analysis," in *Proceedings of the International Conference on Computing Methods*, Word Scientific Publishing Co., Singapore, 1992, pp. 704–708.
- [10.8.9] CHEUNG, Y. K., et al., "Structural Analysis by Finite Strip Method Using Computed Shape Functions," in *Proceedings of the International Conference on Computing Methods*, Word Scientific Publishing Co., Singapore, 1992, pp. 1140–1144.
- [10.8.10] CANISIUS, T. D. G., and FOSCHI, R. O., "Mindlin Finite Strip Analysis of Structures with Localized Loads," *Comp. Struct.*, 48 (1993), 935–942.
- [10.8.11] KONG, J., and CHEUNG, Y. K., "Application of the Spline Finite Strip to the Analysis of Shear-Deformable Plates," *Comp. Struct.*, 46 (1993), 985–988.
- [10.8.12] MAWENYA, A. S., and DAVIS, J. D., "Finite Strip Analysis of Plate Bending Including Transverse Shear Effects," *Build. Sci.*, 9 (1974), 175–180.
- [10.8.13] AKHRAS, G., et al., "Finite Strip Analysis of Anisotropic Laminated Composite Plates Using Higher Order Shear Deformation Theory," *Comp. Struct.*, 52 (1994), 471–477.
- [10.8.14] NG, S. F., and CHEN, X., "Analysis of Arbitrary Mindlin Plates or Bridge Decks by Spline Finite Strip Method," *Comp. Struct.*, 54 (1995), 111–118.
- [10.8.15] GAGNON, P., et al., "A Finite Strip Element for the Analysis of Variable Thickness Rectangular Thick Plates," *Comp. Struct.*, 63 (1997), 349–362.
- [10.8.16] THAM, L. G., et al., "Bending of Skew Plates by Spline Finite Strip Method," *Comp. Struct.*, 22 (1986), 31–37.
- [10.8.17] CHEUNG, Y. K., et al., "Application of Finite-Strip-Method in the Analysis of Curved Slab Bridges," *Proc. Inst. Civil Eng.*, 81 (1986), 111–124.
- [10.8.18] LOO, Y. C., and CUSENS, A. R., "A Refined Finite Strip Method for the Analysis of Orthotropic Plates," *Proc. Inst. Civil Eng.*, 48 (1971), 85–91.
- [10.8.19] FAN, S. C., and LUAN, M. H., "A New Spline Finite Element for Plate Bending," *J. Eng. Mech. Div., ASCE*, 118 (1992), 1065–1081.
- [10.8.20] FRIEDRICH, R., "Finite Strip Method: 30 Years: A Bibliography (1968–1998), *Eng. Comp.*, 17 (2000), 92–111.

10.9 Summary and Conclusions

This chapter contains a compilation of several advanced topics related to the linear static analysis of various plate problems of considerable practical interest. To limit the size of the book, however, each topic has been treated in a relatively condensed form. Accordingly, corresponding presentations emphasize fundamentals and practical applications of the methods discussed. For further study of the individual subjects, quite an extensive list of references and pertinent literature is given at the end of each section. Because of the advanced nature of the topics treated in this chapter, the mathematical requirements are somewhat higher than usual. Again, the FDM and FEM combined with computer support are in most cases the recommended solution techniques. To facilitate practical applications of these computer based approaches, readily usable finite difference stencils and element stiffness matrices are given in explicit forms. Furthermore, numerous work examples should also contribute to the understanding of the solution procedures. At the end of this chapter, the recently developed spline strip method is briefly introduced. This improved FSM makes it relatively convenient to treat complex plate structures with various edge restraints and loading conditions by using computers of small capacity, since it considerably reduces the number of DOFs required in computation. Its application is, however, not as straightforward as that of the FDM or FEM.

Problems[†]

- 10.1.1. An orthotropic square reinforced concrete slab with simply supported boundary conditions is subjected to a concentrated center force P_z . Using Navier's method, determine expressions for (a) a deflected plate surface and (b) bending moments m_x . Employ the double trigonometric series expression given in Table A.3.1.
- 10.1.2. Determine the values of the unknown coefficients C_1 , C_2 , C_3 and C_4 in Illustrative Example II in Sec. 10.1.
- 10.1.3. A rectangular plate with fixed boundaries carries a uniformly distributed load $p_z = p_0$. Using Galerkin's approach, determine the equation of the deflected plate surface by retaining only the first term in the series expression.
- 10.1.4. Determine the validity of the results obtained from problem 10.1.3. Use the ordinary FDM with a mesh width $\lambda = \bar{a}/8$.
- 10.1.5. Solve the problem given in Illustrative Example IV of Sec. 10.1 by the FEM. Subdivide the plate into eight finite elements.
- 10.2.1. Consider a square honeycomb sandwich plate with simply supported boundaries subjected to hydrostatic pressure. Using Table A.3.1, determine an analytic expression for the deflected plate surface.
- 10.2.2. A continuous sandwich plate consisting of two square panels of equal span carries a uniformly distributed load $p_z = p_0$ on both panels. Assuming simply supported boundary conditions, determine (a) the deflected plate surface and (b) the maximum positive and negative moment by using the ordinary FDM.
- 10.2.3. Repeat problem 10.2.2, but this time use the funicular polygon method treated in Sec. 5.2.
- 10.2.4. Consider a rectangular steel sandwich plate of 6×3 m dimension subjected to $p_z = p_0 = 20$ kN/m² distributed load. Assuming simple supports along all four boundaries, determine the maximum deflection w_{\max} via the GWM. The steel plate has a depth of 200 mm with 15 mm-thick top and bottom panels and a corrugated core 5 mm thick. The corresponding expressions for bending and twisting stiffness should be taken from Ref. [10.2.19].
- 10.3.1. Derive a generally valid finite difference stencil for the differential operator $\nabla^4(\cdot)$ in an oblique coordinate system. Check your result for $\vartheta = 60^\circ$ against the stencil given in Fig. 10.3.5.
- 10.3.2. Check the validity of Eq. (10.3.3) by applying the stencil given in Fig. 10.3.5. The mesh width is $\lambda = \bar{a}/8$.
- 10.3.3. Check the validity of Eq. (10.3.19) by applying Salonen's lattice analogy.
- 10.3.4. For the maximum deflection of the skew plate shown in Fig. 10.3.9, a value of $w_{\max} = 0.062$ m was obtained via the GWM. Check this result by (a) the ordinary FDM and (b) the finite element program described in Appendix A.4.2.
- 10.4.1. Consider a clamped square steel plate of sides a subjected to linear temperature variation through its thickness $h = 10$ mm. The top surface of the plate is heated to 50°C , while the temperature of its bottom surface

[†] The first two numbers refer to the corresponding section.

remains at 20°C . Compute the thermal stress resultants m_T and n_T . Assume $E = 21 \times 10^4 \text{ N/mm}^2$, $\nu = 0.33$ and $\alpha_T = 12 \times 10^{-6} \text{ m/C}^\circ$.

- 10.4.2.** Determine the maximum deflection w_{\max} of a clamped square plate of sides a under an equivalent transverse thermal loading $p_T(x, y)$ using the FDM. Consider a parabolic variation of p_T according to Fig. 2.4.1.
- 10.4.3.** Solve Illustrative Example II in Sec. 10.4 by using a Fourier series approximation for the thermal load, deflections and moments.
- 10.5.1.** Determine the influence surface for the maximum bending moment m_y of a simply supported square plate by using the ordinary FDM. Assume that the observation point is at the center of the plate. Use $\lambda = \bar{a}/10$ and utilize the apparent symmetry.
- 10.5.2.** Redo problem 10.5.1 by using the FEM.
- 10.5.3.** Determine the influence surface for the maximum negative moment of a square clamped plate. Assume that the observation point is at $x = 0$ and $y = \bar{a}/2$. Employ either the FDM or the FEM.
- 10.6.1.** Rework the Illustrative Example in Sec. 10.6 by assuming a flat-slab configuration. Use $\beta = 0.2$.
- 10.6.2.** Using a finite element approach, verify the results obtained in the Illustrative Example in Sec. 10.6.
- 10.7.1.** Using the patch test for plate bending, investigate the finite element given in Eq. (7.6.12) for its convergence.
- 10.7.2.** Redo problem 10.7.1 by applying Robinson's single-element test.
- 10.9.1.** Solve the plate problem given in Fig. 8.4.2a by using the spline FSM.

11

Nonlinear Aspects

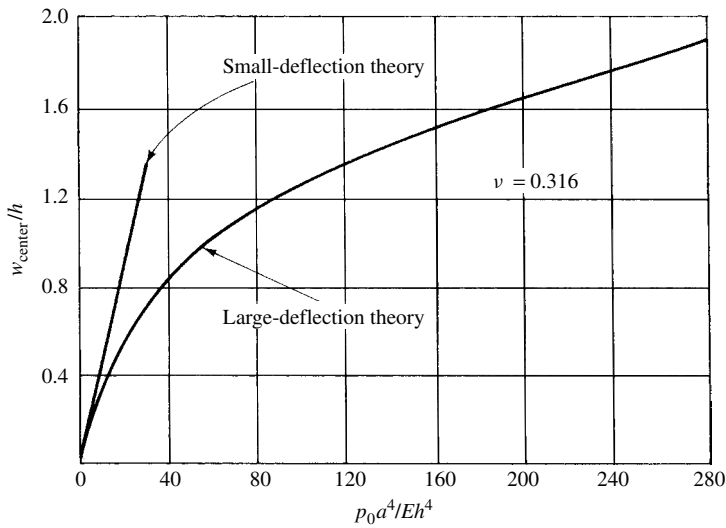
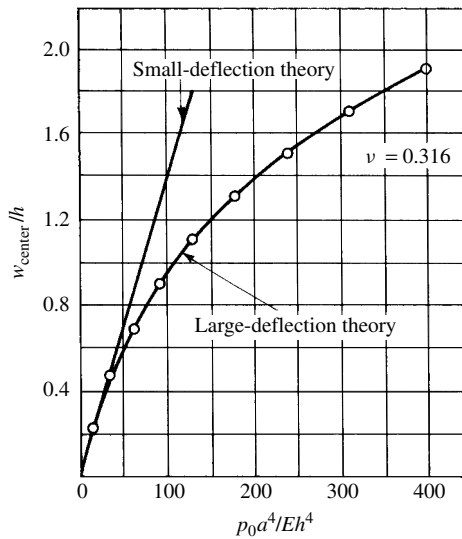
11.1 Large-Deflection Analysis

a. Introduction. In all previous discussions we tacitly assumed that the deflections are small in comparison with the plate thickness ($w \leq 0.2 h$). There are, however, some applications of plate structures, especially in naval and aerospace engineering, where the deflections are no longer small; thus the analysis must be extended to include the additional effects produced by large deflections. By increasing the magnitude of the deflections beyond a certain level ($w \geq 0.3 h$), the relation between external load and deflection is no longer linear. Due to the large deflections, the middle plane stretches, developing tensile membrane forces that can add considerably to the load-carrying capacity of the plate (Fig. 11.1.1).

In this respect, the boundary conditions have a pronounced effect upon the magnitude of the membrane forces developed during the large-deflection process. In the case of simply supported edges, where rotary supports permit rotations but restrain any horizontal displacements ($u = v = 0$), the edges will be free of stress in the direction normal to the boundaries, while other points within the plate will develop tensile stresses. These stresses increase with the distance from the plate edges. However, the situation with fixed boundaries is quite different. That is, at clamped edges tangential and normal stresses occur simultaneously. This is the reason that only in the case of fixed edges can these tensile stresses be fully utilized to carry some part of the lateral load. In general, we can state that middle plane strain will develop whenever the plate is deformed into a nondevelopable surface.

If the plate is permitted to deform beyond half its thickness, its load capacity is already significantly increased. When the magnitude of the maximum deflection reaches the order of the plate thickness ($w_{\max} \approx h$), the membrane action becomes comparable to that of the bending. Beyond this ($w_{\max} > h$), the membrane action predominates. Consequently, for such plate problems, the use of *large-deflection theory*, which accounts for the created membrane forces, is mandatory.

Although the large-deflection theory of plates assumes that the deflections are equal or larger than the plate thickness, these deflections should remain small compared to the other dimensions (a, b) of the plate.

(a) At edges, $u = v = 0$, simply supported [3.1.1]

(b) Fixed [3.1.8]

Figure 11.1.1 Deflections of square plate under constant lateral load.

b. Governing Differential Equations. Considering the simultaneous effects of bending and stretching, the differential equation (3.3.7), which describes the lateral equilibrium of the external and internal forces acting on an infinitesimal plate element, is also applicable for the large-deflection theory. In this case, however, the in-plane forces $[n_x(\Phi), n_y(\Phi)$ and $n_{xy}(\Phi)]$ are produced by large deflections. Since Eq. (3.3.7a) contains two unknowns (w, Φ), an additional equation that relates the deflections and the stress function is required. This is obtained in the form of a

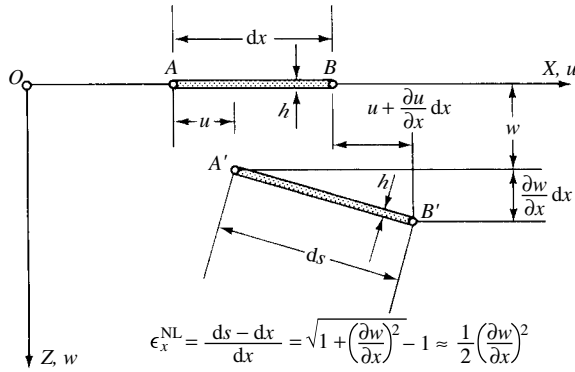


Figure 11.1.2 Strain ϵ_x due to large deflections.

compatibility equation, in which the nonlinear terms in the large-deflection strain-displacement expression (Fig. 11.1.2) are also considered. Thus we can write

$$\begin{aligned}\epsilon_x &= \epsilon_x^{\text{L}} + \epsilon_x^{\text{NL}} = \frac{\partial u}{\partial x} + \frac{1}{2} \left(\frac{\partial w}{\partial x}\right)^2 = \frac{1}{Eh} (n_x - \nu n_y), \\ \epsilon_y &= \epsilon_y^{\text{L}} + \epsilon_y^{\text{NL}} = \frac{\partial v}{\partial y} + \frac{1}{2} \left(\frac{\partial w}{\partial y}\right)^2 = \frac{1}{Eh} (n_y - \nu n_x), \\ \gamma &= \gamma^{\text{L}} + \gamma^{\text{NL}} = \frac{\partial u}{\partial y} + \frac{\partial v}{\partial x} + \frac{\partial w}{\partial x} \frac{\partial w}{\partial y} = \frac{2(1+\nu)}{Eh} n_{xy}.\end{aligned}\quad (11.1.1)$$

If we eliminate, by successive derivation, the displacement components and replace the membrane forces by

$$n_x = h \frac{\partial^2 \Phi}{\partial y^2}, \quad n_y = h \frac{\partial^2 \Phi}{\partial x^2}, \quad n_{xy} = -h \frac{\partial^2 \Phi}{\partial x \partial y}, \quad (11.1.2)$$

where $\Phi(x, y)$ represents an Airy-type stress function, the pertinent compatibility equation is obtained:

$$\nabla^4 \Phi = E \left[\left(\frac{\partial^2 w}{\partial x \partial y} \right)^2 - \frac{\partial^2 w}{\partial x^2} \frac{\partial^2 w}{\partial y^2} \right]. \quad (11.1.3)$$

Using Eqs. (3.3.7a) and (11.1.3), the governing differential equation of large-deflection theory can be written in a more condensed form:

$$\boxed{\frac{D}{h} \nabla^4 w(x, y) = \mathcal{L}(w, \Phi) + \frac{p_z}{h}}, \quad (11.1.4a)$$

$$\boxed{\frac{1}{E} \nabla^4 \Phi(x, y) = -\frac{1}{2} \mathcal{L}(w, w)}, \quad (11.1.4b)$$

where the differential operator $\mathcal{L}(\cdot)$ applied to w and Φ represents

$$\mathcal{L}(w, \Phi) = \frac{\partial^2 w}{\partial x^2} \frac{\partial^2 \Phi}{\partial y^2} + \frac{\partial^2 w}{\partial y^2} \frac{\partial^2 \Phi}{\partial x^2} - 2 \frac{\partial^2 w}{\partial x \partial y} \frac{\partial^2 \Phi}{\partial x \partial y}, \quad (11.1.5)$$

and $\mathcal{L}(w, w)$ is obtained by replacing Φ with w in Eq. (11.1.5).

Equations (11.1.4a) and (11.1.4b) are coupled, nonlinear, partial differential equations of fourth order. The *geometrical nonlinearities* are caused either by higher-order terms of derivatives or by their products. These equations, in the form given above, were first derived by *von Kármán* in 1910 [II.17].

For circular plates, the governing differential equations of large-deflection theory (11.1.4) are usually expressed in polar coordinates, r, φ . Thus, using the coordinate transformation described in Sec. 1.4, we can write

$$\begin{aligned} \frac{D}{h} \nabla_r^2 \nabla_r^2 w(r, \varphi) &= \mathcal{L}_r(w, \Phi) + \frac{p_z}{h}, \\ \frac{1}{E} \nabla_r^2 \nabla_r^2 \Phi(r, \varphi) &= -\frac{1}{2} \mathcal{L}_r(w, w), \end{aligned} \quad (11.1.6)$$

where

$$\begin{aligned} \mathcal{L}_r(w, \Phi) &= \frac{\partial^2 w}{\partial r^2} \left(\frac{1}{r} \frac{\partial \Phi}{\partial r} + \frac{1}{r^2} \frac{\partial^2 \Phi}{\partial \varphi^2} \right) + \left(\frac{1}{r} \frac{\partial w}{\partial r} + \frac{1}{r^2} \frac{\partial^2 w}{\partial \varphi^2} \right) \frac{\partial^2 \Phi}{\partial r^2} \\ &\quad - 2 \frac{\partial}{\partial r} \left(\frac{1}{r} \frac{\partial \Phi}{\partial \varphi} \right) \frac{\partial}{\partial r} \left(\frac{1}{r} \frac{\partial w}{\partial \varphi} \right). \end{aligned} \quad (11.1.7)$$

From this expression $\mathcal{L}_r(w, w)$ can be obtained by substituting w for Φ .

c. Analytical Methods of Solution.[†] Exact solutions of the two simultaneous nonlinear differential equations introduced above are very rare, but a number of indirect analytical methods have been developed that give very satisfactory results to these difficult plate problems. The most important of these are

- double Fourier series approximation,
- Galerkin's energy method,
- Ritz's energy method and
- step-by-step iteration technique.

Whether one uses equilibrium or energy methods for the solution, it is important that proper boundary conditions are considered in the analysis. That is, solution of the large displacement $w(x, y)$ and that of the stress function $\Phi(x, y)$ must satisfy the governing differential equations and the prescribed boundary conditions. The flexural boundary conditions were already treated in Sec. 1.3, but here we resummize and augment them with the corresponding boundary conditions of the membrane stresses. For this purpose, we employ our standard image of rectangular plates, as shown

[†] For numerical solution techniques see Sec. 11.2.

in Fig. 1.1.1a. We limit ourselves to the plate edges at $x = 0$ and $x = a$. Boundary conditions for the two other edges at $y = 0$ and $y = b$ can be obtained by simply replacing x with y and a with b .

The most important boundary conditions encountered in engineering practice are as follows:

- Rigidly clamped edge:

$$w = \frac{\partial w}{\partial x} = u = v = 0. \quad (11.1.8)$$

- Clamped edge but not rigidly fixed:

$$w = \frac{\partial w}{\partial x} = n_x = n_{xy} = 0. \quad (11.1.9)$$

- Simply supported edge with no sliding in the X direction:

$$w = m_x = u = v = 0. \quad (11.1.10)$$

- Simply supported edge with sliding in the X direction:

$$w = m_x = n_x = n_{xy} = 0. \quad (11.1.11)$$

- Free-edge:

$$m_x = v_x = n_x = n_{xy} = 0. \quad (11.1.12)$$

Since the governing equations (11.1.4a) and (11.1.4b) are defined in terms of $w(x, y)$ and $\Phi(x, y)$, we must express the boundary conditions by using the same variables. Consequently, for m_x and v_x we apply the corresponding equations given in Sec. 1.3. For the membrane forces n_x and n_{xy} , we utilize Eq. (11.1.2), which defines them in terms of the stress function $\Phi(x, y)$. For example, Eq. (11.1.11) can be written in the form

$$w = 0, \quad \frac{\partial^2 w}{\partial x^2} + \nu \frac{\partial^2 w}{\partial y^2} = 0, \quad \frac{\partial^2 \Phi}{\partial y^2} = 0, \quad \frac{\partial^2 \Phi}{\partial x \partial y} = 0. \quad (11.1.11a)$$

To obtain the in-plane displacements u and v in terms of w and Φ , the procedure is somewhat more involved. For this purpose, we use Eq. (11.1.1), from which

$$\frac{\partial u}{\partial x} = \varepsilon_x - \frac{1}{2} \left(\frac{\partial w}{\partial x} \right)^2. \quad (11.1.13)$$

Now, if we express ε_x with the help of the stress function, we obtain

$$\frac{\partial u}{\partial x} = \frac{1}{E} \frac{\partial^2 \Phi}{\partial y^2} - \frac{\nu}{E} \frac{\partial^2 \Phi}{\partial x^2} - \frac{1}{2} \left(\frac{\partial w}{\partial x} \right)^2. \quad (11.1.14)$$

Integration of this equation with respect to x gives

$$u = \int_0^a \frac{\partial u}{\partial x} dx. \quad (11.1.15)$$

A similar procedure can be applied for v .

If the boundary conditions permit the use of double Fourier series, then the solution can be sought in the form

$$\begin{aligned} w(x, y) &= \sum_{m=1}^{\infty} \sum_{n=1}^{\infty} W_{mn} X_m(x) \cdot Y_n(y), \\ \Phi(x, y) &= \sum_{p=1}^{\infty} \sum_{q=1}^{\infty} F_{pq} X_p(x) \cdot Y_q(y). \end{aligned} \quad (11.1.16)$$

Simultaneously, the lateral load must be expressed as

$$p_z(x, y) = \sum_{m=1}^{\infty} \sum_{n=1}^{\infty} P_{mn} X_m(x) \cdot Y_n(y), \quad (11.1.17)$$

where

$$P_{mn} = \frac{1}{ab} \int_0^a \int_0^b p_z(x, y) X_m(x) Y_n(y) dx dy. \quad (11.1.18)$$

For $X(x)$ and $Y(y)$ we may select the eigenfunctions of vibrating beams. The solution procedure becomes quite similar to that used by Vlasov in connection with small-deflection analysis of plates, as discussed in Sec. 4.3. Consequently, we select a pair of mn and pq values and substitute the obtained Eqs. (11.1.16) and (11.1.17) into the differential equations (11.1.4a) and (11.1.4b). This gives us two simultaneous nonlinear equations from which the unknowns W_{mn} and F_{pq} can be determined. This procedure is repeated for another set of mn and pq values until convergence in the solution is achieved. Although the use of this double Fourier series approach is straightforward, it is evident that “long-hand” computation of each step becomes quite cumbersome. However, using some “symbolic mathematic” programs, such as Maple or Mathematica, the required computational effort can be considerably reduced.

By applying the Galerkin-Vlasov method[†] to the governing differential equations, their variational expressions become

$$\int_0^a \int_0^b \left[\frac{D}{h} \nabla^4 w - \mathcal{L}(w, \Phi) - \frac{p_z}{h} \right] \delta w dx dy = 0 \quad (11.1.19a)$$

and

$$\int_0^a \int_0^b \left[\frac{1}{E} \nabla^4 \Phi + \frac{1}{2} \mathcal{L}(w, w) \right] \delta \Phi dx dy = 0. \quad (11.1.19b)$$

[†] See Sec. 4.3.

It should be noted that in a variation of the equilibrium equation (11.1.19a), a small virtual displacement δw has been used. In a variation of the compatibility equation (11.1.19b), however, a small virtual change of the stress function $\delta \Phi$ has been applied. These variations are *not interrelated*.

Again, let us represent the lateral deflection $w(x, y)$ and the corresponding stress function $\Phi(x, y)$ with the eigenfunctions of vibrating beams, as stipulated by Eq. (11.1.16). Then the analysis procedure will be quite similar to that used in Sec. 4.3. for small deflections of plates.

The second energy method often used in large-deflection analysis of plates is based on Ritz's principle of minimum potential energy. In this case, however, the strain energy becomes

$$U = U_m + U_b, \quad (11.1.20)$$

where U_m represents the membrane part of the total strain energy and U_b stands for the bending part.

The membrane part of the strain energy, which is due to the stretching of the middle surface of the plate, can also be expressed in terms of the stress functions:

$$\begin{aligned} U_m &= \frac{1}{2} \int_0^a \int_0^b (n_x \varepsilon_x + n_y \varepsilon_y + n_{xy} \gamma_{xy}) dx dy \\ &= \frac{h}{2E} \int_0^a \int_0^b \left\{ \left(\frac{\partial^2 \Phi}{\partial x^2} + \frac{\partial^2 \Phi}{\partial y^2} \right)^2 - 2(1 + \nu) \left[\frac{\partial^2 \Phi}{\partial x^2} \frac{\partial^2 \Phi}{\partial y^2} - \left(\frac{\partial^2 \Phi}{\partial x \partial y} \right)^2 \right] \right\} dx dy; \end{aligned} \quad (11.1.21)$$

the strain energy due to bending has already been given by Eq. (4.2.5). The potential of the lateral forces remains

$$V = \int_0^a \int_0^b [p_z(x, y)w(x, y)] dx dy. \quad (11.1.22)$$

Thus, the total potential of the plate becomes

$$\Pi = U_m + U_b + V. \quad (11.1.23)$$

In the case of homogeneous boundary conditions, Eq. (11.1.23) can be written as

$$\begin{aligned} \Pi &= \frac{1}{2} \int_0^a \int_0^b \left\{ \frac{D}{2} [(\nabla^2 w)^2 - (1 - \nu) \mathcal{L}(w, w)] \right. \\ &\quad \left. - \frac{h}{2E} [(\nabla^2 \Phi)^2 - (1 + \nu) \mathcal{L}(\Phi, \Phi)] \right. \\ &\quad \left. - \frac{h}{2} \Phi \mathcal{L}(w, w) \right\} dx dy - \int_0^a \int_0^b p_z w dx dy, \end{aligned} \quad (11.1.24)$$

where the differential operator $\mathcal{L}(\cdot)$ represents

$$\mathcal{L}(\cdot, \cdot) = \frac{\partial^2(\cdot)}{\partial x^2} \frac{\partial^2(\cdot)}{\partial y^2} + \frac{\partial^2(\cdot)}{\partial y^2} \frac{\partial^2(\cdot)}{\partial x^2} - 2 \frac{\partial^2(\cdot)}{\partial x \partial y} \frac{\partial^2(\cdot)}{\partial x \partial y}. \quad (11.1.25)$$

The unknown constants W_{mn} and F_{pq} in the series expressions can be determined by applying the principle of minimum potential. Hence

$$\frac{\partial \Pi}{\partial W_{mn}} = 0 \quad \text{and} \quad \frac{\partial \Pi}{\partial F_{pq}} = 0. \quad (11.1.26)$$

As in the case of small deflections, Eq. (11.1.26) yields a set of nonlinear simultaneous equations, the solution of which determines these unknowns. Again, we may state that the procedure using long-hand computation is quite tedious.

Probably, the step-by-step iteration offers, in combination with some computer use, the simplest approach to large-deflection analysis of plates.

In the *first* step, we reduce the governing differential equations to

$$D \nabla^2 \nabla^2 w_1 = p_z, \quad \nabla^2 \nabla^2 \Phi_1 = 0. \quad (11.1.27)$$

In the *second* step, we substitute the obtained first approximations into the right-hand sides of Eqs. (11.1.4a) and (11.1.4b). Therefore, the second approximations are obtained from

$$\begin{aligned} \frac{D}{h} \nabla^2 \nabla^2 w_2 &= \mathcal{L}(w_1, \Phi_1) + \frac{p_z}{h}, \\ \frac{1}{E} \nabla^2 \nabla^2 \Phi_2 &= -\mathcal{L}(w_1, w_1). \end{aligned} \quad (11.1.28)$$

Following this procedure, general expressions for these approximations become

$$\begin{aligned} \frac{D}{h} \nabla^2 \nabla^2 w_{n+1} &= \mathcal{L}(w_n, \Phi_n) + \frac{p_z}{h}, \\ \frac{1}{E} \nabla^2 \nabla^2 \Phi_{n+1} &= -\frac{1}{2} \mathcal{L}(w_n, w_n). \end{aligned} \quad (11.1.29)$$

Convergence of this iterative solution can be accelerated by applying the *energy-balancing* principle discussed in the following section.

Summary. When plates undergo large deflections, the lateral loads are carried by simultaneous bending and stretching actions. In this way, important weight reduction can be achieved, provided such large deflections are not objectionable on other grounds. The large-deflection theory of plates leads to *geometrically* nonlinear differential equations, the solution of which by hand is generally very tedious. Although all analysis techniques for large deflections follow the same patterns as those already introduced in connection with small-deflection plate problems, the required computational efforts are considerably higher. However, the drudgery of long-hand computations can be greatly mitigated by employing a combination of a long-hand and computer-aided approach. In this respect, the use of computer programs offering “symbolic mathematics” can be of great advantage.

For further study of this relatively difficult subject, the books written by Cia [11.1.19] or by Donnel [11.1.21] (along with the other references) are recommended.

ILLUSTRATIVE EXAMPLE

Let us determine, based on large-deflection theory, the center deflection of a simply supported square plate subjected to $p_z = p_0$ uniformly distributed lateral load. Let us assume sliding edges and hence zero membrane forces at the edges ($\bar{n}_x = \bar{n}_y = 0$). The corners of the plate, however, should be restrained against in-plane displacements.

To solve this plate problem, Galerkin's method is used in combination with the step-by-step iterative procedure.

Let us represent the lateral deflections $w(x, y)$ and the stress function $\Phi(x, y)$ as infinite series (for $m, n = 1, 3, 5, \dots$),

$$\begin{aligned} w(x, y) &= \sum_m \sum_n W_{mn} \sin \frac{m\pi x}{a} \sin \frac{n\pi y}{b}, \\ \Phi(x, y) &= \sum_m \sum_n F_{mn} \sin \frac{m\pi x}{a} \sin \frac{n\pi y}{b}, \end{aligned} \quad (11.1.30)$$

which satisfy the prescribed boundary conditions

$$\bar{w} = 0, \quad \bar{m}_x = \bar{m}_y = 0, \quad \bar{n}_x = \bar{n}_y = 0. \quad (11.1.31)$$

To simplify the solution, only the first term in the infinite series expressions for the deflections and stress function will be used in our computation. Thus, for square plates Eq. (11.1.30) can be written as

$$w = W_n \sin \alpha x \sin \alpha y, \quad (11.1.32a)$$

$$\Phi = F_n \sin \alpha x \sin \alpha y, \quad (11.1.32b)$$

where $\alpha = \pi/a = \pi/b$.

Assuming that $\Phi_1 = 0$, the first approximation of the deflection, w_1 , is obtained from Navier's solution of Eq. (1.2.30); thus

$$w_1 = W_1 \sin \alpha x \sin \alpha y = \frac{4p_0}{D\pi^2\alpha^4} \sin \alpha x \sin \alpha y. \quad (11.1.33)$$

Substituted into the second equation of (11.1.28), this solution gives

$$\begin{aligned} \int_0^a \int_0^a [F_2 4\alpha^4 \sin \alpha x \sin \alpha y + E W_1^2 \alpha^4 \sin^2 \alpha x \sin^2 \alpha y \\ - E W_1^2 \alpha^4 \cos^2 \alpha x \cos^2 \alpha y] \sin \alpha x \sin \alpha y \, dx \, dy = 0. \end{aligned} \quad (11.1.34)$$

The further solution of this variational equation is not difficult, since it has been reduced to evaluation of definite integrals of simple trigonometric functions. From Eq. (11.1.34) the second approximation for the expansion coefficient of the stress function, F_2 , is obtained. Thus, we can write

$$\Phi_2(x, y) = F_2 \sin \alpha x \sin \alpha y = -\frac{4E W_1^2}{3a^2\alpha^2} \sin \alpha x \sin \alpha y. \quad (11.1.35)$$

Substitution of this expression and that of the first approximation of the deflection (11.1.33) into Eq. (11.1.28) gives

$$\int_0^a \int_0^a \left[\nabla^4 w_2 - \frac{h}{D} \left(\frac{\partial^2 \Phi_2}{\partial y^2} \frac{\partial^2 w_1}{\partial x^2} + \frac{\partial^2 \Phi_2}{\partial x^2} \frac{\partial^2 w_1}{\partial y^2} - 2 \frac{\partial^2 \Phi_2}{\partial x \partial y} \frac{\partial^2 w_2}{\partial x \partial y} \right) - \frac{p_0}{D} \right] \times \sin \alpha x \sin \alpha y \, dx \, dy = 0, \quad (11.1.36)$$

from which, after evaluation of the definite integrals of trigonometric functions, an improved coefficient, W_2 , for the deflections is obtained. Thus, the second approximation of the deflections becomes

$$w_2 = W_2 \sin \alpha x \sin \alpha y = \frac{4p_0}{D\pi^2\alpha^4 + (1536Eha^4p_0^2/27D^2\pi^{10})} \sin \alpha x \sin \alpha y. \quad (11.1.37)$$

Using a pressure ratio $p_0 a^4 / Eh^4 = 110$, for instance, this simplified solution shows only 6% error in center deflection when compared with Levy's "exact" result [11.1.1]. By continuing the iteration, the accuracy can be further improved.

References and Bibliography

- [11.1.1] LEVY, S., "Bending of Rectangular Plates with Large Deflections," NACA Report 737, National Advisory Committee for Aeronautics, Washington, D.C., 1942.
- [11.1.2] WAY, S., "Large Deflections of Uniformly Loaded Rectangular Plates," in *Proceedings of the Fifth International Congress on Applied Mechanics* (held in Cambridge, Mass.), John Wiley & Sons, New York, 1938.
- [11.1.3] HENCKY, H., "Berechnung dünner rechteckigen Platten," *Z. f. Angew. Math. u. Mech.*, 1 (1921), 81 and 423 (discussion).
- [11.1.4] WAY, S., "Bending of Circular Plates with Large Deflections," *Trans. ASME*, 56, No. 8 (Aug. 1934), 627–636.
- [11.1.5] GREEN, J. R., and SOUTHWELL, R. V., "Relaxation Applied to Engineering Problems VIII A: Problems Relating to Large Transverse Displacements of Thin Elastic Plates," *Phil. Trans.*, 239, Ser. A (1945), 539.
- [11.1.6] SONNTAG, G., "Einfluss einer Nachgiebigkeit der Randeinspannung auf die Durchbiegung und Spannungen bei Platten grosser Durchbiegung," *Z. f. Angew. Math. u. Mech.*, 35, No. 9/10 (1955), 356–358.
- [11.1.7] LEVY, S., "Large Deflection Theory for Rectangular Plates," (Proc. Symp. on Non-linear Problems), *Symp. Appl. Math.*, 1 (1947), 197–210.
- [11.1.8] LEVY, S., "Square Plates with Clamped Edges Under Normal Pressure," NACA Report 740, National Advisory Committee for Aeronautics, Washington, D.C., 1942.
- [11.1.9] YAGHMAI, S., "Incremental Analysis of Large Deformations in Mechanics of Solids with Applications to Axisymmetric Shells of Revolution," Report No. CR-1350, National Aeronautics and Space Administration, Washington, D.C., June 1969.
- [11.1.10] MYSZKOWSKI, J., *Nichtlineare Probleme der Plattentheorie*, F. Vieweg und Sohn, Braunschweig, 1969.
- [11.1.11] OHASHI, Y., and KAMIYA, N., "Large Deflections of a Supported Plate Having a Non-Linear Stress-Strain Relation," *Z. f. Angew. Math. u. Mech.*, 48, No. 3 (1968), 159–171.
- [11.1.12] BAUER, F., et al., "Bending of Rectangular Plate with Finite Deflections," *J. Appl. Mech.*, *Trans. ASME*, 32 (1965), 821–825.

- [11.1.13] SUNDARA RAJA IYENGAR, K. T., and MATIN NAQUI, M., "Large Deflection of Rectangular Plates," *Int. J. Non-Linear Mech.*, 1 (1966), 109–122.
- [11.1.14] WANG, C. T., "Non-Linear Large-Deflection Boundary-Value Problems of Rectangular Plates," NACA TN 1425, National Advisory Committee for Aeronautics, Washington, D.C., 1948.
- [11.1.15] KORNISHIN, M. S., *Nelineinye zadachi teorii plastin i pologikh obolochek* (Nonlinear Problems in the Theory of Plates and Shallow Shells, and Methods of Solution), Nauka, Moscow, 1964.
- [11.1.16] SHIL'KRUT, D. I., *Nektorye zadachi nelineinoi teorii obolochek i plastin* (Some Problems in Nonlinear Plate and Shell Theory and Their Solution), Redaktsionnoizdatel'skikh otel Akad. Nauka Moldavskoi SSR, Kishinev, 1967.
- [11.1.17] BIEGER, K. W., and WALTERSDORF, K., *Beitrag zur Frage konsistenter geometrisch nichtlinearer Theorien dünner elastischer Flächentragwerke*, Werner-Verlag, Düsseldorf, 1972.
- [11.1.18] ODEN, J. T., *Finite Elements of Nonlinear Continua*, McGraw-Hill Book Co., New York, 1972.
- [11.1.19] CHIA, CH-Y., *Nonlinear Analysis of Plates*, McGraw-Hill Book Co., New York, 1980.
- [11.1.20] CHIA, CH-Y., "Geometrically Nonlinear Behavior of Composite Plates," *Appl. Mech. Rev.*, 41 (1988), 439–450.
- [11.1.21] DONNEL, L. H., *Beams, Plates and Shells*, McGraw-Hill, Book Co., New York, 1976.
- [11.1.22] LADEVEZE, P., et al., *Nonlinear Computational Structural Methods*, Springer, New York, 1999.

11.2 Numerical Methods for Geometrically Nonlinear Analysis

It is obvious from the foregoing section that analytical solution methods for nonlinear plate problems have serious limitations. Therefore, their use is mostly restricted to solve problems that are merely of academic interest. But during the last decades the recent development of nonlinear numerical analysis has assumed quite an importance, since it is realized that numerous real-life plate problems are in fact nonlinear. In addition, the application of new lightweight materials combined with higher than conventional loadings makes nonlinear analysis of such structures mandatory. Nowadays, parallel developments in computer hardware and software have made it possible to obtain solutions to practical nonlinear plate problems at a reasonable cost and time. A large variety of nonlinear solution techniques have been developed, but here we will treat only the most commonly used numerical solution techniques.

a. Application of Finite Difference Method. If the nonlinear plate problem is relatively small, one may apply the ordinary FDM. Using the square mesh ($\Delta x = \Delta y = \lambda$) shown in Fig. 11.2.1, the corresponding finite difference expressions for the governing geometrically nonlinear differential equations (11.1.1a) and (11.1.1b) at the pivotal point m, n can be written as

$$\begin{aligned}
 &D[20w_{m,n} - 8(w_{m-1,n} + w_{m+1,n} + w_{m,n+1} + w_{m,n-1}) \\
 &\quad + 2(w_{m-1,n+1} + w_{m+1,n+1} + w_{m-1,n-1} + w_{m+1,n-1}) \\
 &\quad + (w_{m-2,n} + w_{m+2,n} + w_{m,n+2} + w_{m,n-2})]
 \end{aligned}$$

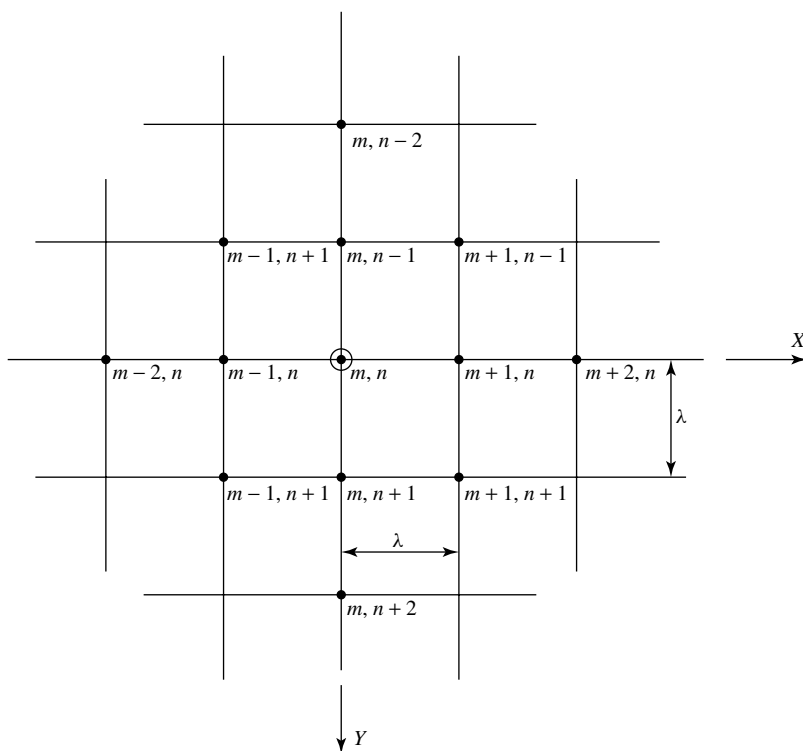


Figure 11.2.1 Numbering of mesh points.

$$\begin{aligned}
 & -h \left[(\Phi_{m,n+1} - 2\Phi_{m,n} + \Phi_{m,n-1})(w_{m-1,n} - 2w_{m,n} + w_{m+1,n}) \right. \\
 & \quad + (\Phi_{m-1,n} - 2\Phi_{m,n} + \Phi_{m+1,n})(w_{m,n+1} - 2w_{m,n} + w_{m,n-1}) \\
 & \quad - \frac{1}{8}(\Phi_{m-1,n+1} + \Phi_{m+1,n-1} - \Phi_{m+1,n+1} - \Phi_{m-1,n-1}) \\
 & \quad \left. \times (w_{m-1,n+1} + w_{m+1,n-1} - w_{m+1,n+1} - w_{m-1,n-1}) \right] - p_z \lambda^4 = 0 \quad (11.2.1)
 \end{aligned}$$

and

$$\begin{aligned}
 & 20\Phi_{m,n} - 8(\Phi_{m-1,n} + \Phi_{m+1,n} + \Phi_{m,n+1} + \Phi_{m,n-1}) \\
 & + 2(\Phi_{m-1,n+1} + \Phi_{m+1,n+1} + \Phi_{m-1,n-1} + \Phi_{m+1,n-1}) \\
 & + (\Phi_{m-2,n} + \Phi_{m+2,n} + \Phi_{m,n+2} + \Phi_{m,n-2}) \\
 & - E \left[\frac{1}{16}(w_{m-1,n+1} + w_{m+1,n-1} - w_{m+1,n+1} - w_{m-1,n-1})^2 \right. \\
 & \quad \left. - (w_{m-1,n} - 2w_{m,n} + w_{m+1,n})(w_{m,n+1} - 2w_{m,n} + w_{m,n-1}) \right] = 0. \quad (11.2.2)
 \end{aligned}$$

The procedures to be applied to solve nonlinear plate problems using the ordinary FDM are identical with those introduced in Sec. 5.1 in connection with linear plate problems. Considering treatments of the boundary conditions, we refer to the

foregoing section and, again, to Sec. 5.1. Although this numerical procedure appears to be simple, solution of the obtained large set of coupled nonlinear equations can be problematic, since it requires special algorithms to solve such problems. In this respect, probably the direct iteration technique is the most commonly used procedure. Convergence of the solution can be accelerated by either applying Richardson's extrapolation formula[†] or improving the first approximation by a correction factor C obtained by balancing the energy of the system. That is, we require that the work of the external forces must be the same as that of the internal forces represented by the strain energy. Since this is usually not the case, we must use a correction factor for the deflections to approximate the required equality of works. Thus, the improved deflections are

$$\mathbf{d}^{(2)} = C\mathbf{d}^{(1)} \quad \text{with} \quad C = \frac{W_{\text{ext}}^{(1)}}{W_{\text{int}}^{(1)}}. \quad (11.2.3)$$

The work of the external forces is expressed by multiplying Eq. (11.1.22) by $\frac{1}{2}$. This multiplier represents the difference between the potential and actual work of the external forces, as discussed in Sec. 4.1. However, the work of the internal forces remains the same as the strain energy. Consequently,

$$W_{\text{ext}}^{(1)} = \frac{1}{2} V^{(1)} \quad \text{and} \quad W_{\text{int}}^{(1)} = U_m^{(1)} + U_b^{(1)}, \quad (11.2.4)$$

where $U_m^{(1)}$ and $U_b^{(1)}$ have been defined in analytical form by Eqs. (4.2.5) and (11.1.21), respectively. However, to determine the required correction factor C numerically, these equations must also be expressed in finite difference forms. In addition, the definite integrations must be carried out numerically.

b. Application of FEM to Nonlinear Problems. Stiffness matrices of nonlinear problems depend on displacements. This creates nonlinearity in the solution. Therefore, the governing matrix equation for a system in equilibrium exhibiting geometrically nonlinear behavior has the form

$$[\bar{\mathbf{K}}^L + \bar{\mathbf{K}}^{\text{NL}}(d)]\bar{\mathbf{d}} = \bar{\mathbf{p}}, \quad (11.2.5)$$

where $\bar{\mathbf{K}}^L$ is the linear part of the stiffness matrix of the system and $\bar{\mathbf{K}}^{\text{NL}}$ represents the displacement-dependent nonlinear part. In writing Eq. (12.1.5), we have assumed that the external forces acting on the plate are not dependent on the displacements. This assumption is valid until the deflections become quite excessive.

The nonlinear part of element stiffness matrix \mathbf{K}_e^{NL} is often referred to in the pertinent literatures as the *geometric* stiffness matrix $\mathbf{K}_{g,e}$, since it contains the geometrically nonlinear effects. To derive \mathbf{K}_e^{NL} , we must consider the nonlinear in-plane strains in the element. Using the second terms in Eq. (11.1.1), we can write

$$\varepsilon_x^{\text{NL}} = \frac{1}{2} \left(\frac{\partial w}{\partial x} \right)^2, \quad \varepsilon_y^{\text{NL}} = \frac{1}{2} \left(\frac{\partial w}{\partial y} \right)^2, \quad \gamma^{\text{NL}} = \frac{\partial w}{\partial x} \frac{\partial w}{\partial y}. \quad (11.2.6)$$

[†] See Eq. (5.1.38).

Consequently, the nonlinear part of the potential energy of a rectangular finite element becomes

$$\begin{aligned}\Pi_e^{\text{NL}} &= \int_0^a \int_0^b (n_x \varepsilon_x^{\text{NL}} + n_y \varepsilon_y^{\text{NL}} + n_{xy} \gamma^{\text{NL}}) dx dy \\ &= \frac{1}{2} \int_0^a \int_0^b \begin{bmatrix} \frac{\partial w}{\partial x} \\ \frac{\partial w}{\partial y} \end{bmatrix}^T \begin{bmatrix} n_x & n_{xy} \\ n_{xy} & n_y \end{bmatrix} \begin{bmatrix} \frac{\partial w}{\partial x} \\ \frac{\partial w}{\partial y} \end{bmatrix} dx dy, \quad (11.2.7)\end{aligned}$$

where n_x , n_y and n_{xy} represent the membrane forces produced by large deflections. Now, the total potential energy of the element can be expressed by

$$\Pi_e = \Pi_e^{\text{L}} + \Pi_e^{\text{NL}}. \quad (11.2.8)$$

Applying the principle of minimum potential energy,

$$\frac{\partial \Pi_e}{\partial \mathbf{d}_e} = 0, \quad (11.2.9)$$

which gives

$$\mathbf{K}_e \mathbf{d}_e = \mathbf{p}_e, \quad (11.2.10)$$

where

$$\mathbf{K}_e = \mathbf{K}_e^{\text{L}} + \mathbf{K}_e^{\text{NL}}, \quad (11.2.11)$$

and with $w = \mathbf{N}^T \mathbf{d}_e$, we obtain

$$\mathbf{K}_e^{\text{NL}} = \int_0^a \int_0^b \begin{bmatrix} \frac{\partial \mathbf{N}_i}{\partial x} \\ \frac{\partial \mathbf{N}_i}{\partial y} \end{bmatrix}^T \begin{bmatrix} n_x & n_{xy} \\ n_{xy} & n_y \end{bmatrix} \begin{bmatrix} \frac{\partial \mathbf{N}_j}{\partial x} \\ \frac{\partial \mathbf{N}_j}{\partial y} \end{bmatrix} dx dy, \quad (11.2.12)$$

where \mathbf{N}_i and \mathbf{N}_j represent the matrices of the shape functions.

Equation (11.2.12) depends on the numerical values of the membrane forces, which are assumed to be constant for a small load increment. In evaluating the nonlinear element stiffness matrices, all definitions and procedures used previously in Chapter 7 apply. Therefore we do not repeat them here.

For the nonconforming rectangular plate element with 12 DOF[†], explicit expressions of $\mathbf{K}_{e,x}^{\text{NL}}$, $\mathbf{K}_{e,y}^{\text{NL}}$ and $\mathbf{K}_{e,xy}^{\text{NL}}$ are given in Table 11.2.1. Similarly, the nonlinear elements k_{ij}^{NL} of the geometric stiffness matrix corresponding to the four-node rectangular plate element with 16 DOF[‡] [7.7.1, 11.2.3] are explicitly defined as

$$k_{ij}^{\text{NL}} = \left[\beta_1 \left(\frac{b}{a} \right) n_x + \beta_2 \left(\frac{a}{b} \right) n_y + \beta_3 n_{xy} \right] a^{\beta_4} b^{\beta_5}. \quad (11.2.13)$$

[†] See Sec. 7.6.

[‡] See Sec. 7.7.

Table 11.2.1 Nonlinear Stiffness Matrix Corresponding to Nonconforming Element with 12 DOF^a

$$[K_e^{NL}]_x^{(N)} = \frac{n_x b}{1260a}$$

552													(N)
-66b	12b ²												1
42a	0	56a ²											2
-552	66b	-42a	552										3
66b	-12b ²	0	-66b	12b ²									4
42a	0	-14a ²	-42a	0	56a ²								5
-204	39b	-21a	204	-39b	-21a	552							6
-39b	9b ²	0	39b	-9b ²	0	66b	12b ²						7
21a	0	-7a ²	-21a	0	28a ²	-42a	0	56a ²					8
204	-39b	21a	-204	39b	21a	-552	-66b	42a	552				9
39b	-9b ²	0	-39b	9b ²	0	-66b	-12b ²	0	66b	12b ²			10
21a	0	28a ²	-21a	0	-7a ²	-42a	0	-14a ²	42a	0	56a ²		11
1	2	3	4	5	6	7	8	9	10	11	12		12

Symmetric

$$[K_e^{NL}]_y^{(N)} = \frac{n_y a}{1260b}$$

552													(N)
-42b	56b ²												1
66a	0	12a ²											2
204	-21b	39a	552										3
-21b	28b ²	0	-42b	56b ²									4
-39a	0	-9a ²	-66a	0	12a ²								5
-204	21b	-39a	-552	42b	66a	552							6
-21b	-7b ²	0	-42b	-14b ²	0	42b	56b ²						7
39a	0	9a ²	66a	0	-12a ²	-66a	0	12a ²					8
-552	42b	-66a	-204	21b	39a	204	21b	-39a	552				9
-42b	-14b ²	0	-21b	-7b ²	0	21b	28b ²	0	42b	56b ²			10
-66a	0	-12a ²	-39a	0	9a ²	39a	0	-9a ²	66a	0	12a ²		11
1	2	3	4	5	6	7	8	9	10	11	12		12

Symmetric

$$[K_e^{NL}]_{xy}^{(N)} = \frac{n_{xy}}{360}$$

180													(N)
0	0												1
0	-5ab	0											2
0	-36b	0	-180										3
36b	0	5ab	0	0									4
0	5ab	0	0	-5ab	0								5
-180	36b	-36a	0	0	36a	180							6
-36b	6b ²	-5ab	0	0	5ab	0	0						7
36a	-5ab	6a ²	-36a	5ab	0	0	-5ab	0					8
0	0	36a	180	-36b	-36a	0	36b	0	-180				9
0	0	5ab	36b	-6b ²	-5ab	-36b	0	5ab	0	0			10
-36a	5ab	0	36a	-5ab	-6a ²	0	5ab	0	0	-5ab	0		11
1	2	3	4	5	6	7	8	9	10	11	12		12

Symmetric

^a See Sec. 7.6.

Table 11.2.2 Index Scheme for Evaluation of Eq. (11.2.13)

[illegible]

Note: (–) indicates negative $k_{i,j}$.

A pertinent scheme for the indices (i, j) is provided in Table 11.2.2. The coefficients $\beta_1, \beta_2, \dots, \beta_5$ in this equation are listed in Table 11.2.3. The same nonlinear element stiffness matrices are also used in Sec. 16.5 in connection with the elastic stability analysis of plates. It should be noted, however, that whereas with large deflections the in-plane forces are positive tension forces, they are negative compressive forces in the stability analysis.

c. Determination of \mathbf{K}_e^{NL} for Gridwork Cells. Due to the nature of the gridwork representation of the plate continuum, we must now take an approach that is quite different from the one discussed above for finite elements. That is, to determine the nonlinear stiffness matrix $\mathbf{K}_{e,x}^{\text{NL}}$ of a square gridwork cell (Fig. 11.2.2) subjected

Table 11.2.3 Coefficients in Eq. (11.2.13)

i	j	β_1	β_2	β_3	β_4	β_5
1	1	$\frac{78}{175}$	$\frac{78}{175}$	$\frac{1}{2}$	0	0
2	1	$\frac{11}{175}$	$\frac{13}{350}$	0	0	1
3	1	$\frac{13}{350}$	$\frac{11}{175}$	0	1	0
4	1	$\frac{11}{2100}$	$\frac{11}{2100}$	$-\frac{1}{50}$	1	1
5	1	$-\frac{78}{175}$	$\frac{27}{175}$	0	0	0
6	1	$-\frac{11}{175}$	$\frac{9}{700}$	$-\frac{1}{10}$	0	1
7	1	$\frac{13}{350}$	$-\frac{13}{350}$	0	1	0
8	1	$\frac{11}{2100}$	$-\frac{13}{4200}$	$\frac{1}{50}$	1	1
9	1	$-\frac{27}{175}$	$-\frac{27}{175}$	$-\frac{1}{2}$	0	0
10	1	$\frac{13}{350}$	$\frac{9}{700}$	$\frac{1}{10}$	0	1
11	1	$\frac{9}{700}$	$\frac{13}{350}$	$\frac{1}{10}$	1	0
12	1	$-\frac{13}{4200}$	$-\frac{13}{4200}$	$-\frac{1}{50}$	1	1
13	1	$\frac{27}{175}$	$-\frac{78}{175}$	0	0	0
14	1	$-\frac{13}{350}$	$\frac{13}{350}$	0	0	1
15	1	$-\frac{9}{700}$	$\frac{11}{175}$	$\frac{1}{10}$	1	0
16	1	$-\frac{13}{4200}$	$\frac{11}{2100}$	$\frac{1}{50}$	1	1
2	2	$\frac{2}{175}$	$\frac{26}{525}$	0	0	2
4	2	$\frac{1}{1050}$	$\frac{11}{1575}$	0	1	2
6	2	$-\frac{2}{175}$	$\frac{3}{175}$	0	0	2
8	2	$\frac{1}{1050}$	$-\frac{13}{3150}$	0	1	2
10	2	$\frac{3}{350}$	$-\frac{3}{700}$	$\frac{1}{60}$	0	2
12	2	$-\frac{1}{1400}$	$\frac{13}{12600}$	$-\frac{1}{300}$	1	2
14	2	$-\frac{3}{350}$	$-\frac{13}{1050}$	0	0	2
16	2	$-\frac{1}{1400}$	$-\frac{11}{6300}$	$\frac{1}{300}$	1	2
4	3	$\frac{11}{1575}$	$\frac{1}{1050}$	0	2	1
6	3	$-\frac{11}{2100}$	$\frac{13}{4200}$	$-\frac{1}{50}$	1	1
8	3	$-\frac{11}{6300}$	$-\frac{1}{1400}$	$\frac{1}{300}$	2	1
10	3	$\frac{13}{4200}$	$\frac{13}{4200}$	$\frac{1}{50}$	1	1
12	3	$\frac{13}{12600}$	$-\frac{1}{1400}$	$-\frac{1}{300}$	2	1
14	3	$-\frac{13}{4200}$	$\frac{11}{2100}$	$-\frac{1}{50}$	1	1
16	3	$-\frac{13}{3150}$	$\frac{1}{1050}$	0	2	1
2	3	$\frac{11}{2100}$	$\frac{11}{2100}$	$\frac{1}{50}$	1	1
3	3	$\frac{26}{525}$	$\frac{2}{175}$	0	2	0

Table 11.2.3 (continued)

i	j	β_1	β_2	β_3	β_4	β_5
7	3	$-\frac{13}{1050}$	$-\frac{3}{350}$	0	2	0
11	3	$-\frac{3}{700}$	$\frac{3}{350}$	$\frac{1}{60}$	2	0
15	3	$\frac{3}{175}$	$-\frac{2}{175}$	0	2	0
4	4	$\frac{2}{1575}$	$\frac{2}{1575}$	0	2	2
8	4	$-\frac{1}{3150}$	$-\frac{1}{1050}$	0	2	2
12	4	$\frac{1}{4200}$	$\frac{1}{4200}$	$-\frac{1}{1800}$	2	2
16	4	$-\frac{1}{1050}$	$-\frac{1}{3150}$	0	2	2
2	5	$-\frac{11}{175}$	$\frac{9}{700}$	$-\frac{1}{10}$	0	1
4	5	$-\frac{11}{2100}$	$\frac{13}{4200}$	$\frac{1}{50}$	1	1
5	5	$\frac{78}{150}$	$\frac{78}{175}$	$-\frac{1}{2}$	0	0
8	5	$-\frac{11}{2100}$	$-\frac{11}{2100}$	$-\frac{1}{50}$	1	1
9	5	$\frac{27}{150}$	$-\frac{78}{175}$	0	0	0
11	5	$-\frac{9}{700}$	$\frac{11}{175}$	$-\frac{1}{10}$	1	0
12	5	$\frac{13}{4200}$	$-\frac{11}{2100}$	$\frac{1}{50}$	1	1
13	5	$-\frac{27}{150}$	$-\frac{27}{175}$	$\frac{1}{2}$	0	0
14	5	$\frac{13}{350}$	$\frac{9}{700}$	$-\frac{1}{10}$	0	1
15	5	$-\frac{9}{700}$	$\frac{13}{350}$	$\frac{1}{10}$	1	0
16	5	$\frac{13}{4200}$	$\frac{13}{4200}$	$-\frac{1}{50}$	1	1
12	6	$\frac{1}{1400}$	$\frac{11}{6300}$	$\frac{1}{300}$	1	2
14	6	$\frac{3}{350}$	$-\frac{3}{700}$	$-\frac{1}{60}$	0	2
16	6	$\frac{1}{1400}$	$-\frac{13}{12600}$	$-\frac{1}{300}$	1	2
2	7	$\frac{11}{2100}$	$-\frac{13}{4200}$	$-\frac{1}{50}$	1	1
4	7	$-\frac{11}{6300}$	$-\frac{1}{1400}$	$-\frac{1}{300}$	2	1
6	7	$-\frac{11}{2100}$	$-\frac{11}{2100}$	$\frac{1}{50}$	1	1
10	7	$\frac{13}{4200}$	$-\frac{11}{2100}$	$-\frac{1}{50}$	1	1
11	7	$\frac{3}{175}$	$-\frac{2}{175}$	0	2	0
12	7	$-\frac{13}{3150}$	$\frac{1}{1050}$	0	2	1
14	7	$-\frac{13}{4200}$	$-\frac{13}{4200}$	$\frac{1}{50}$	1	1
15	7	$-\frac{3}{700}$	$\frac{3}{350}$	$-\frac{1}{60}$	2	0
16	7	$\frac{13}{12600}$	$-\frac{1}{1400}$	$\frac{1}{300}$	2	1
16	8	$\frac{1}{4200}$	$\frac{1}{4200}$	$\frac{1}{1800}$	2	2

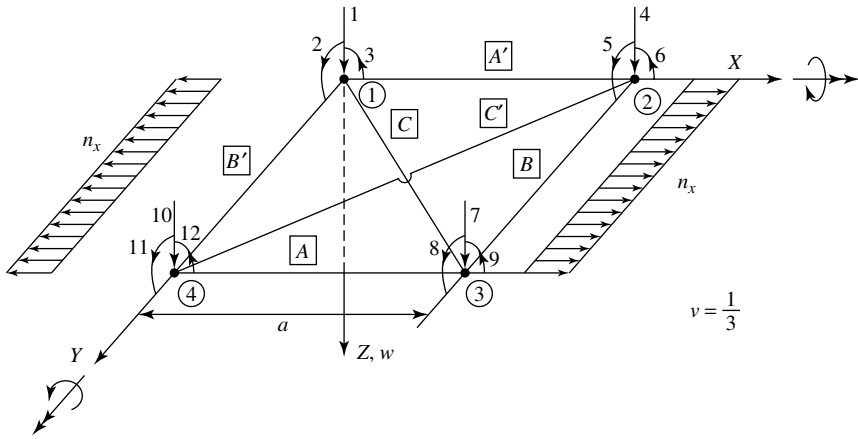


Figure 11.2.2 Gridwork cell subjected to constant n_x tensile forces.

to a constant tensile in-plane force n_x , for instance, we apply the classical matrix displacement method used for beam structures by considering the pertinent nonlinear effects [11.2.4].

Since we are dealing de facto with a bending problem of this gridwork cell, we should introduce a unit translation at each nodal point and determine the produced axial forces in each of the beams. Subjecting, for instance, node ③ to a unit translation according to Fig. 6.3.3b, only beams \boxed{A} , \boxed{B} and \boxed{C} participate in this motion. Consequently, the nodal forces produced by the tensile force n_x (Fig. 11.2.3b) will be carried only by these beams. By solving the created *statically undetermined truss* problem, we obtain the following axial forces:

$$\begin{aligned} P^{(A)} &= \frac{2}{3} \frac{n_x a}{2} = \frac{n_x a}{3}, & P^{(B)} &= -\frac{1}{3} \frac{n_x a}{2} = -\frac{n_x a}{6}, \\ P^{(C)} &= \frac{\sqrt{2}}{3} \frac{n_x a}{2} = \frac{n_x a}{3\sqrt{2}}. \end{aligned} \quad (11.2.14)$$

Next, we use the nonlinear stiffness matrix of a beam undergoing large deflections (Fig. 11.2.4), which has the general form

$$[K_e^{NL}] = \frac{P}{L} \begin{bmatrix} 0 & 0 & 0 & 0 & 0 & 0 \\ 0 & \frac{6}{5} & \frac{1}{10}L & 0 & -\frac{6}{5} & \frac{1}{10}L \\ 0 & \frac{1}{10}L & \frac{2}{15}L^2 & 0 & -\frac{1}{10}L & -\frac{1}{30}L^2 \\ 0 & 0 & 0 & 0 & 0 & 0 \\ 0 & -\frac{6}{5} & -\frac{1}{10}L & 0 & \frac{6}{5} & -\frac{1}{10}L \\ 0 & \frac{1}{10}L & -\frac{1}{30}L^2 & 0 & -\frac{1}{10}L & \frac{2}{15}L^2 \end{bmatrix}, \quad (11.2.15)$$

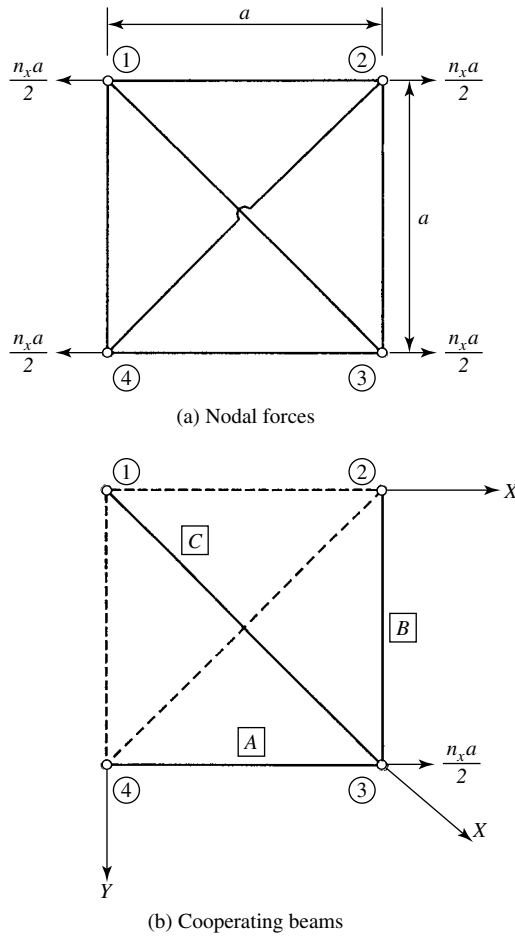


Figure 11.2.3 Gridwork cell subjected to tensile nodal forces.

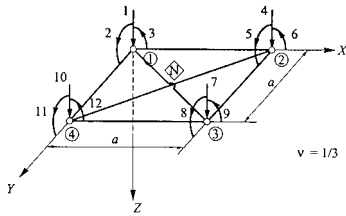
Now, we substitute directly $P^{(A)}$ and $P^{(B)}$ into Eq. (11.2.15) and change the numbering of the DOF of the beam to correspond to numbering of the gridwork cell given in Fig. 11.2.2. In the case of the diagonal beam \boxed{C} , however, we need a coordinate transformation of the displacement vectors from the beam coordinate system to the X, Y, Z coordinate system of the gridwork cell before renumbering the displacement components. We also repeat this procedure for the other nodal points. As usual, by adding the obtained stiffness coefficients k_{ij} , having the same indices, we obtain $\mathbf{K}_{e,x}^{\text{NL}}$, which is given in Table 11.2.4. A similar approach in the Y direction yields $\mathbf{K}_{e,y}^{\text{NL}}$ listed in Table 11.2.5.

If the plate is subjected to n_{xy} shearing forces, only the beams \boxed{C} and $\boxed{C'}$ participate in the load-carrying action (Fig. 11.2.5c). In this case, the corresponding axial forces in these beams become

$$P^{(C)} = -P^{(C')} = -\sqrt{2} \frac{n_{xy}a}{2} = -\frac{n_{xy}a}{\sqrt{2}}. \quad (11.2.16)$$

Table 11.2.5 Nonlinear Stiffness Matrix $\mathbf{K}_{e,y}^{\text{NL}}$ of Gridwork Cell Subjected to n_y Tensile Forces

$$[\mathbf{K}_{e,y}^{\text{NL}}]_y^{(N)} = n_y \times$$



$\frac{2}{5}$												
$\frac{a}{20}$	$\frac{a^2}{15}$											
0	$-\frac{a^2}{45}$	0										
$\frac{1}{5}$	0	$-\frac{a}{60}$	$\frac{2}{5}$									
0	0	0	$\frac{a}{20}$	$\frac{a^2}{15}$								
$\frac{a}{60}$	0	$-\frac{a^2}{180}$	0	$\frac{a^2}{45}$	0							
$-\frac{1}{5}$	$-\frac{a}{60}$	$\frac{a}{60}$	$-\frac{2}{5}$	$-\frac{a}{30}$	0	$\frac{2}{5}$						
$\frac{a}{60}$	$-\frac{a^2}{180}$	$\frac{a^2}{180}$	$\frac{a}{30}$	$-\frac{a^2}{90}$	0	$-\frac{a}{20}$	$\frac{a^2}{15}$					
$-\frac{a}{60}$	$\frac{a^2}{180}$	$-\frac{a^2}{180}$	0	0	0	0	$-\frac{a^2}{45}$	0				
$-\frac{2}{5}$	$-\frac{a}{30}$	0	$-\frac{1}{5}$	$-\frac{a}{60}$	$-\frac{a}{60}$	$\frac{1}{5}$	0	$\frac{a}{60}$	$\frac{2}{5}$			
$\frac{a}{30}$	$-\frac{a^2}{90}$	0	$\frac{a}{60}$	$-\frac{a^2}{180}$	$-\frac{a^2}{180}$	0	0	0	$-\frac{a}{20}$	$\frac{a^2}{15}$		
0	0	0	$\frac{a}{60}$	$-\frac{a^2}{180}$	$-\frac{a^2}{180}$	$-\frac{a}{60}$	0	$\frac{a^2}{180}$	0	$\frac{a^2}{45}$	0	
1	2	3	4	5	6	7	8	9	10	11	12	

Symmetric

Again, we substitute these axial forces into Eq. (11.2.15) and transform the corresponding displacement vectors from their beam coordinate system to the X, Y, Z coordinate system of the gridwork cell. This procedure is repeated for the other nodal points. After proper renumbering of the indices of the individual element stiffness coefficients k_{ij} and adding those that have the same indices, we obtain the $\mathbf{K}_{e,xy}^{\text{NL}}$ stiffness matrix given in Table 11.2.6. Now, we can express the total stiffness matrix of this gridwork cell in the form

$$\mathbf{K}_e = \mathbf{K}_e^{\text{L}} + (\mathbf{K}_{e,x} + \mathbf{K}_{e,y} + \mathbf{K}_{e,xy})^{\text{NL}}. \quad (11.2.17)$$

Hrennikoff's gridwork model is well suited for large-deflection analysis of plates, since the membrane forces at the nodal points of each cell can be determined by using the deflected shape of the plate, as subsequently discussed. In the case of arbitrary plate geometry, we may approximate the irregular boundaries by "zigzag" lines, as shown in Chapters 7 and 8.

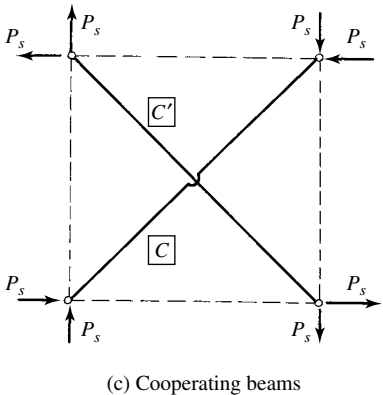
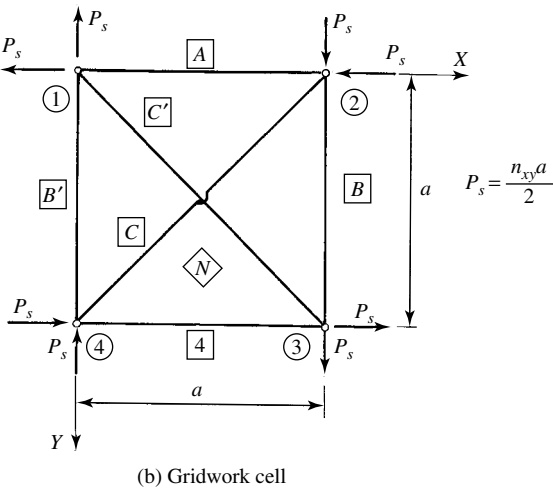
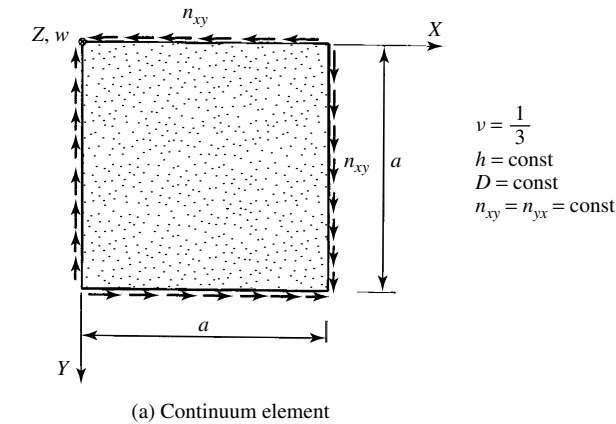
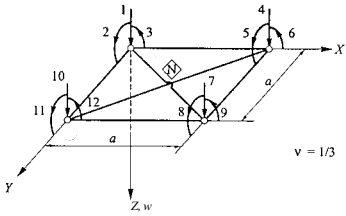


Figure 11.2.5 Gridwork cell subjected to shear forces.

Table 11.2.6 Nonlinear Stiffness Matrix $\mathbf{K}_{e,xy}^{\text{NL}}$ of Gridwork Cell Subjected to n_{xy} Shearing Forces

$$[\mathbf{K}_e^{\text{NL}}]_{xy}^{(N)} = 3n_{xy} \times$$



$\frac{1}{5}$											
$\frac{a}{60}$	$\frac{a^2}{45}$										
$-\frac{a}{60}$	$-\frac{a^2}{45}$	$\frac{a^2}{45}$									
0	0	0	$-\frac{1}{5}$								
0	0	0	$-\frac{a}{60}$	$-\frac{a^2}{45}$							
0	0	0	$-\frac{a}{60}$	$-\frac{a^2}{45}$	$-\frac{a^2}{45}$						
$-\frac{1}{5}$	$-\frac{a}{60}$	$\frac{a}{60}$	0	0	0	$\frac{1}{5}$					
$\frac{a}{60}$	$-\frac{a^2}{180}$	$\frac{a^2}{180}$	0	0	0	$-\frac{a}{60}$	$\frac{a^2}{45}$				
$-\frac{a}{60}$	$\frac{a^2}{180}$	$-\frac{a^2}{180}$	0	0	0	$\frac{a}{60}$	$-\frac{a^2}{45}$	$\frac{a^2}{45}$			
0	0	0	$\frac{1}{5}$	$\frac{a}{60}$	$\frac{a}{60}$	0	0	0	$-\frac{1}{5}$		
0	0	0	$-\frac{a}{60}$	$\frac{a^2}{180}$	$\frac{a^2}{180}$	0	0	0	$\frac{a}{60}$	$-\frac{a^2}{45}$	
0	0	0	$-\frac{a}{60}$	$\frac{a^2}{180}$	$\frac{a^2}{180}$	0	0	0	$\frac{a}{60}$	$-\frac{a^2}{45}$	$-\frac{a^2}{45}$
1	2	3	4	5	6	7	8	9	10	11	12

Symmetric

11.2.1 Various Finite Element Procedures[†]

As already mentioned, geometric nonlinearity results in two classes of plate problems: large deflections and stability. Here, we are concerned only with the large-deflection analysis of plates. Problems related to plate stability are treated extensively in Part VI of this book. In every-day engineering practice, solutions of nonlinear plate problems are usually carried out in the framework of the versatile FEM. However, finite element solutions of nonlinear problems create additional difficulties because larger than usual computational resources, in the form of high clock speed and large memory capacity, are required.

In general, three basic numerical solution techniques can be applied to large-deflection analysis based on the finite element approach: (a) incremental, (b) iterative and (c) combined incremental and iterative procedures. In all these procedures the following standard assumptions are used:

[†] Also logically applicable to the gridwork method.

- The displacements are computed in a Lagrangian reference system with nonmoving $\bar{X}, \bar{Y}, \bar{Z}$ coordinate axes of the undeformed state.
- The strains are represented by Green's strain tensor.
- The strains are small in comparison to unity.
- The material is linear elastic.
- The external loads are static and conservative; that is, their magnitude is unchanged during the deformation process.

a. Incremental (or Euler) Procedure. One of the strongest recommendations for the incremental procedure is its “relatively” easy applicability to nonlinear problems created by large displacements. As introduced in the previous section, these nonlinear problems are characterized by the dependence of the stiffness matrix upon the displacement vector. Thus, the governing matrix equation of equilibrium becomes

$$\bar{\mathbf{K}}(d)\bar{\mathbf{d}} = [\bar{\mathbf{K}}^L + \bar{\mathbf{K}}^{NL}(d)]\bar{\mathbf{d}} = \bar{\mathbf{p}}, \quad (11.2.18)$$

where the linear and nonlinear stiffness matrices of the total structure are obtained by the usual additive process

$$\bar{\mathbf{K}}^L = \sum_{i=1}^M \bar{\mathbf{K}}_{e,i}^L \quad \text{and} \quad \bar{\mathbf{K}}^{NL}(d) = \sum_{i=1}^M \bar{\mathbf{K}}_{e,i}^{NL}(d). \quad (11.2.19)$$

We divide the total external load $\bar{\mathbf{p}}$ into $\Delta\bar{\mathbf{p}}_m$ increments. The *starting* vector of the displacements is obtained from the linear solution of the problem

$$\Delta\bar{\mathbf{d}}_1^{(0)} = (\bar{\mathbf{K}}^L)_1^{-1} \Delta\bar{\mathbf{p}}_1, \quad (11.2.20)$$

where the superscript (0) indicates the initial cycle of the corrective procedure. By checking the state of equilibrium, however, we obtain an unbalanced *residual* load vector

$$[\bar{\mathbf{K}}^L + \bar{\mathbf{K}}^{NL}]_1^{(j)} \Delta\bar{\mathbf{d}}_1^{(j)} = \bar{\mathbf{r}}_1^{(j)} \quad \text{for } j = 1, 2, 3, \dots, \quad (11.2.21)$$

which creates additional small displacements

$$\Delta\bar{\mathbf{d}}_1^{(j+1)} = (\bar{\mathbf{K}}^{(j)})_1^{-1} \bar{\mathbf{r}}_1^{(j)} \quad \text{for } j = 1, 2, 3, \dots \quad (11.2.22)$$

Thus, the improved final displacements vector $\Delta\bar{\mathbf{d}}_1^{(f)}$ due to the first load increment becomes

$$\Delta\bar{\mathbf{d}}_1^{(f)} = \Delta\bar{\mathbf{d}}_1^{(0)} + \sum_{j=1}^n \Delta\bar{\mathbf{d}}_1^{(j)} \quad \text{for } j = 1, 2, 3, \dots \quad (11.2.23)$$

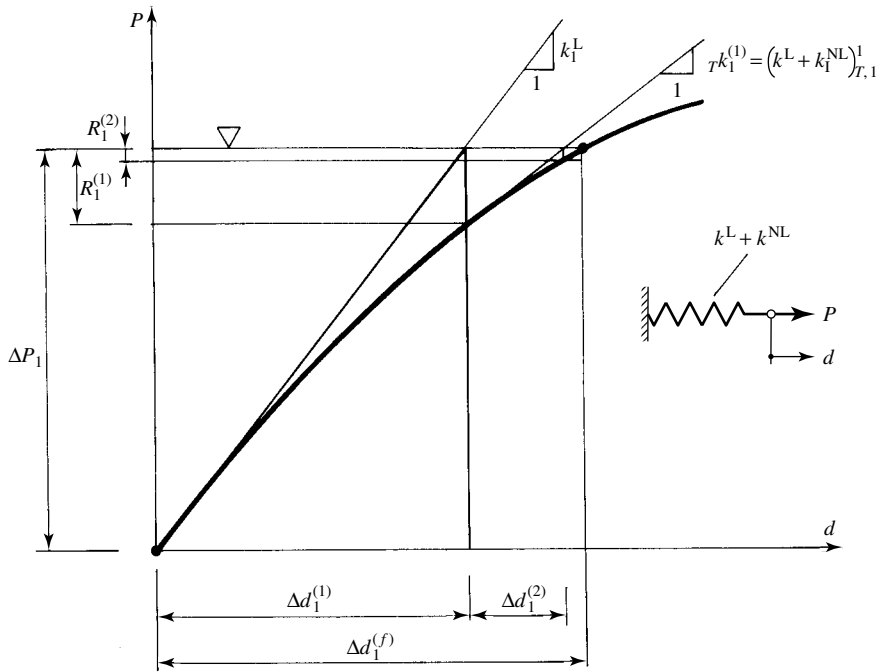


Figure 11.2.6 Schematic illustration of starting process.

This correction procedure should be continued until the residual load vector becomes approximately zero. Figure 11.2.6 illustrates this starting process.

In computing the first residual load, however, difficulty arises in determining the membrane forces, which are essential parts of nonlinear element stiffness matrices. The first approximations for them may be obtained from Eq. (11.1.1) by writing

$$n_1^{(1)} \approx \frac{Eh}{2} \left(\frac{\partial w}{\partial x} \right)^2, \quad n_{y,1}^{(1)} \approx \frac{Eh}{2} \left(\frac{\partial w}{\partial y} \right)^2, \quad n_{xy,1}^{(1)} \approx \frac{Eh}{2(1+\nu)} \left(\frac{\partial w}{\partial x} \frac{\partial w}{\partial y} \right). \quad (11.2.24)$$

In the course of subsequent equilibrium corrections, we should also use the in-plane displacements \bar{u}, \bar{v} in computing the membrane forces of the plate according to Eq. (11.1.1).

After obtaining the first final solution of displacements corresponding to the first load increment, we normally engage the *tangent* stiffness matrix $\bar{\mathbf{K}}_T$ for all other load increments $\Delta \bar{\mathbf{p}}_m$. Thus, at all higher load levels

$$\bar{\mathbf{p}}_{m+1} = \bar{\mathbf{p}}_m + \Delta \bar{\mathbf{p}}_{m+1} \quad \text{for } m = 1, 2, 3, \dots, \quad (11.2.25)$$

we assume that the equilibrium conditions corresponding to the previous load level $\bar{\mathbf{p}}_m$ are already satisfied. Consequently, the tangent stiffness matrix of the total system pertinent to this load level,

$$\bar{\mathbf{K}}_{T,m}^{(f)} = [\bar{\mathbf{K}}^L + \bar{\mathbf{K}}^{NL}]_m^{(f)} = \bar{\mathbf{K}}_{T,m+1}^{(f)}, \quad (11.2.26)$$

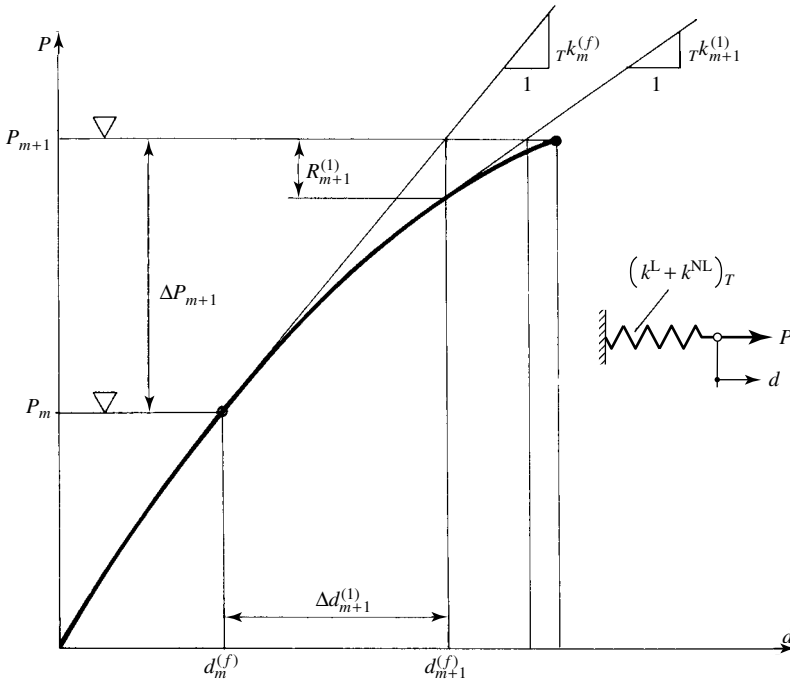


Figure 11.2.7 Schematic illustration of computations corresponding to higher load level.

is already determined. In this equation the superscripts (f) and (1) refer, again, to the final iterative cycle corresponding to the previous load level and the initial iterative cycle of the new load increment, respectively. The first approximation of the displacement vector (Fig. 11.2.6) is obtained from

$$\Delta \bar{\mathbf{d}}_{m+1}^{(1)} = (\bar{\mathbf{K}}_{T,m}^{(f)})^{-1} \Delta \bar{\mathbf{p}}_{m+1}. \quad (11.2.27)$$

Now, the algorithm to reach the final equilibrium state becomes

$$\begin{aligned} \bar{\mathbf{r}}^{(j)} &= \bar{\mathbf{K}}_{T,m+1}^{(j)} \Delta \bar{\mathbf{d}}_{m+1}^{(j)} - \Delta \bar{\mathbf{p}}_{m+1}, \\ \Delta \bar{\mathbf{d}}_{m+1}^{(j+1)} &= (\bar{\mathbf{K}}_{T,m+1}^{(j)})^{-1} \bar{\mathbf{r}}^{(j)}. \end{aligned} \quad (11.2.28)$$

The final displacements pertinent to load level $\bar{\mathbf{p}}_{m+1}$ are computed from

$$\bar{\mathbf{d}}_{m+1}^{(f)} = \bar{\mathbf{d}}_m^{(f)} + \sum_{j=1}^n \Delta \bar{\mathbf{d}}_{m+1}^{(j)} \quad \text{for } j = 1, 2, 3, \dots, n. \quad (11.2.29)$$

This procedure is schematically illustrated in Fig. 11.2.7.

Needless to say, programming the complete procedure requires a certain amount of expertise in this field. Instead of applying the tangent stiffness matrices, however,

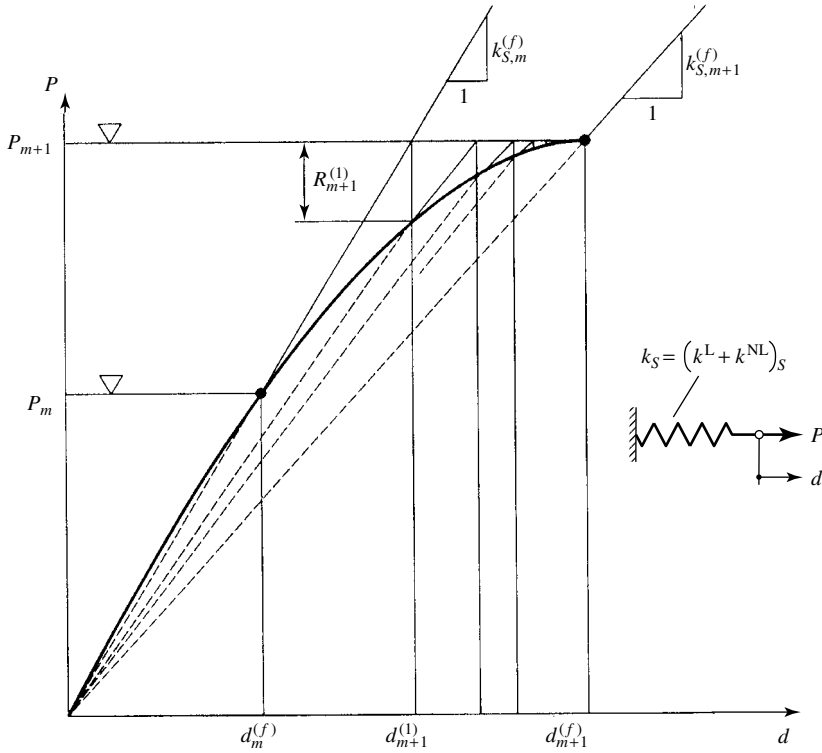


Figure 11.2.8 Incremental procedure using secant stiffness matrix.

one can select the *secant* matrix $\bar{\mathbf{K}}_S$, approach (Fig. 11.2.8) or even a combination of tangent-secant matrix procedures, as shown in Fig 11.2.9, by using a simple 1-DOF system.

b. Iterative (or Newton-Raphson) procedure. This alternative solution technique for nonlinear plate analysis uses the well-known Newton-Raphson method. Mathematically, this procedure is based on a truncated Taylor's series expansion. For this purpose, we write the equation of the nonlinear load-displacement curve in the form

$$p = f(d). \quad (11.2.30)$$

The Taylor's series expansion of this function at position d_m is

$$p = f(d_m) + \frac{d - d_m}{1!} f'(d_m) + \frac{(d - d_m)^2}{2!} f''(d_m) + \frac{(d - d_m)^3}{3!} f'''(d_m) + \dots \quad (11.2.31)$$

After neglecting the higher-order terms, we obtain the curtailed expression

$$p = f(d_m) + (d - d_m) f'(d_m), \quad (11.2.32)$$

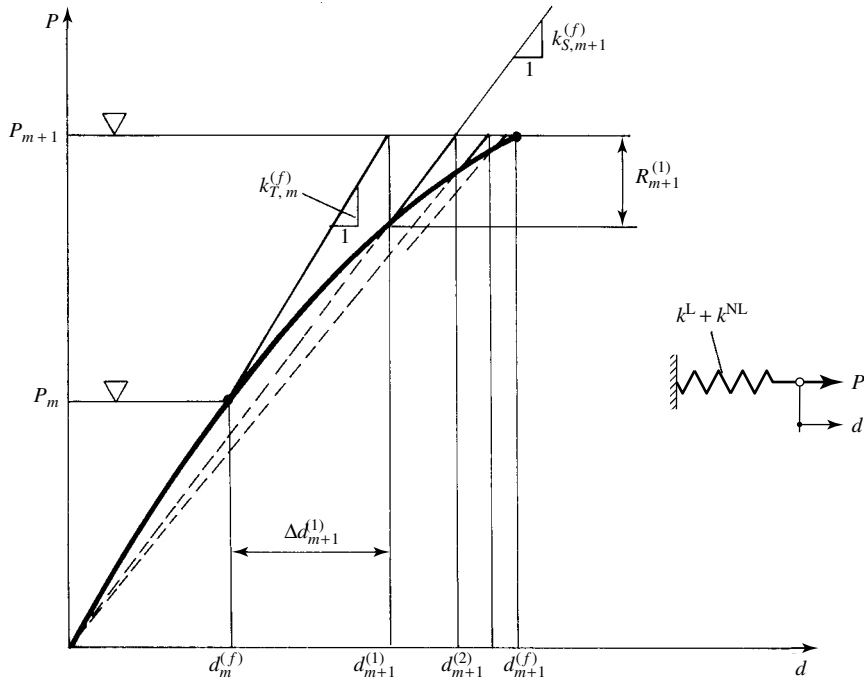


Figure 11.2.9 Combination of tangent and secant matrix approaches.

and from this the incremental displacement

$$\Delta d_m = [f'(d_m)]^{-1} [p - f(d_m)] = k_{T,m} \Delta q_m \quad (11.2.33)$$

can be obtained, where $k_{T,m}$ is the tangential stiffness and Δq_m represents the difference between the total external load and the load sustained by the structure at position d_m . The pertinent finite element computational algorithm describing this iterative process is

$$\begin{aligned} \bar{\mathbf{d}}_0 &= (\bar{\mathbf{K}}^L)^{-1}_T, \\ \Delta \bar{\mathbf{d}}_1 &= [\bar{\mathbf{K}}^L + \bar{\mathbf{K}}^{NL}(\bar{\mathbf{d}}_0)]^{-1}_T \Delta \bar{\mathbf{q}}_1, \\ \Delta \bar{\mathbf{d}}_2 &= [\bar{\mathbf{K}}^L + \bar{\mathbf{K}}^{NL}(\bar{\mathbf{d}}_1)]^{-1}_T \Delta \bar{\mathbf{q}}_2, \\ \Delta \bar{\mathbf{d}}_3 &= [\bar{\mathbf{K}}^L + \bar{\mathbf{K}}^{NL}(\bar{\mathbf{d}}_2)]^{-1}_T \Delta \bar{\mathbf{q}}_3, \\ &\vdots \end{aligned} \quad (11.2.34)$$

Here, as mentioned before, $\Delta \bar{\mathbf{q}}_n$ represents the difference between the total load applied $\bar{\mathbf{p}}$ and the load equilibrated by the nodal forces after the previous step, which is computed from $\bar{\mathbf{K}}_{T,n-1} \bar{\mathbf{d}}_{n-1}$. This iterative process is continued until $\Delta \bar{\mathbf{q}} \approx 0$. The

resulting displacements are

$$\mathbf{d}^{(f)} = \mathbf{d}_0 + \sum_{n=1}^N \Delta \mathbf{d}_n. \quad (11.2.35)$$

This iterative algorithm is schematically illustrated in Fig. 11.2.10.

To eliminate problems associated with repeated solutions of completely new equations at each iterative cycle, one may keep the stiffness matrix of the system constant throughout the whole iterative process by using $\bar{\mathbf{K}}_T = \bar{\mathbf{K}}_T^L$. This simplified iterative technique is termed a *modified* Newton-Raphson method (Fig. 11.2.11). Although its convergence is slower than that of the conventional Newton-Raphson procedure, however, not only is its use more economical but also writing a corresponding computer program is a relatively easy task. A possible improvement of convergence can be achieved by updating $\bar{\mathbf{K}}_T$ after some iteration. Unfortunately, both methods display some *drifting* tendency from the actual load-displacement curve.

c. Combined Incremental-Iterative Solutions. Occasionally, it may be useful to combine the incremental solution technique with an iterative solution of nonlinear problems. Using again a simple one-dimensional problem, Fig. 11.2.12 schematically illustrates the combination of the previously introduced incremental process with the *modified* Newton-Raphson iteration. Such a mixed method tends to combine the advantages of both the incremental and iterative procedures while somewhat mitigating their disadvantages.

Summary. In this section analytical and numerical procedures dealing with geometrical nonlinearity of plates are introduced. In general, solutions of these problems are quite involved. Therefore, application of the proposed analytical

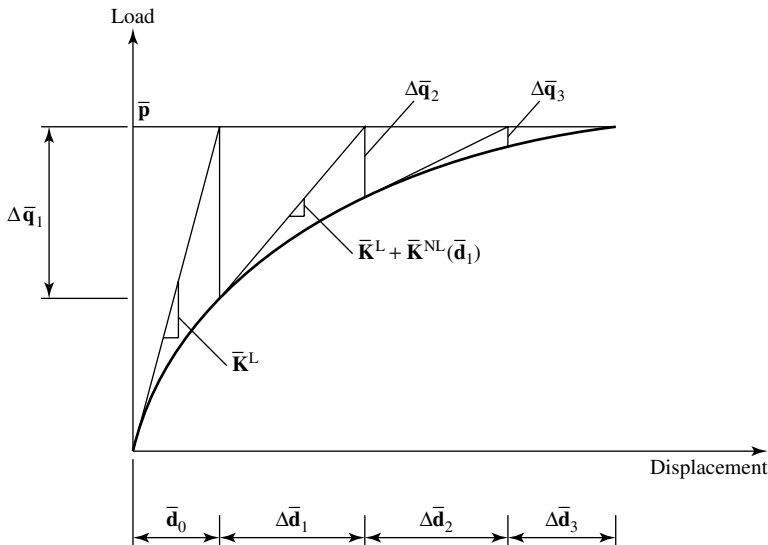


Figure 11.2.10 Iterative Newton/Raphson procedure.

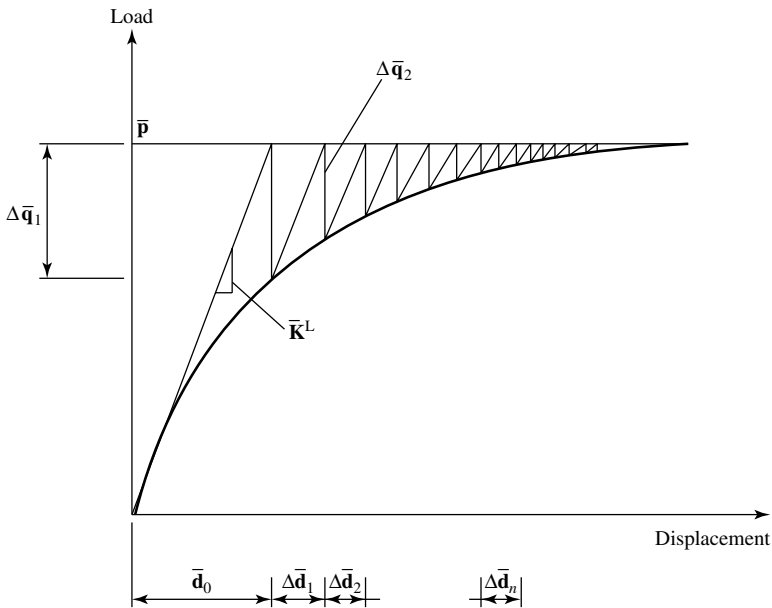


Figure 11.2.11 Modified Newton/Raphson procedure.

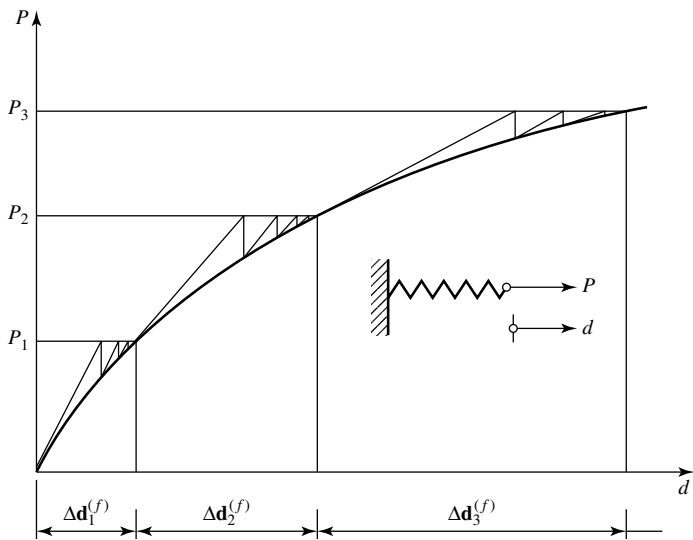


Figure 11.2.12 Mixed procedure.

methods are restricted to relatively simple one-bay plate geometry. Almost the same can be stated with respect to the finite difference approach, which, however, appears to be somewhat more flexible and therefore more applicable, provided the plate structure is not large. In everyday engineering practice, however, one of the various finite element procedures is generally applied to solve “real-life” nonlinear

plate problems. A survey of the numerous finite element procedures presently available [11.2.7–11.2.12] reveals that none of the nonlinear solution techniques can be considered a universal method. The modified Newton-Raphson iteration technique appears to be the simplest procedure for computer coding. However, the principal disadvantage of all iterative methods is that there is no assurance that the solution will converge to the exact value of the problem. The incremental methods are better in this respect but require considerably more programming effort, and executing such programs is time consuming. A combination of incremental and iterative approaches may offer some advantages over using either one individually. A significant improvement in accuracy and stability of the incremental procedure can be achieved by one-step energy- balancing at each load increment [11.2.5].

References and Bibliography

- [11.2.1] ODEN, J. T., *Finite Elements of Nonlinear Continua*, McGraw-Hill Book Co., New York, 1972.
- [11.2.2] TSCAN, S. S., "Nonlinear Analysis of Thin Plates by Framework Method," *AIAA J.*, 5 (1967), 1890–1892.
- [11.2.3] WANG, T. Y., *Finite Element Structural Analysis*, Prentice-Hall, Englewood Cliffs, New Jersey, 1986.
- [11.2.4] SZILARD, R., and POWELL, R., "Dynamic Stability Analysis of Prismatic Shells by Framework Method," in R. Krapfenbauer (Ed.) *Proceedings of the IASS Symposium on Folded Plate Structures*, held in Vienna, Krapfenbauer, Vienna, Austria, 1970.
- [11.2.5] SZILARD, R., "An Energy Balancing Method for Large Displacement Analysis of Structures," *Comp. Meth. Appl. Mech. Eng.*, 34 (1982), 801–818.
- [11.2.6] SZILARD, R., "A Hybrid, Finite Element Finite Difference Approach to Large Deflection Analysis of Structures," *Comp. Struct.*, 9 (1978), 341–350.
- [11.2.7] BERGAN, P. G., et al., *Finite Elements in Nonlinear Mechanics*, TAPIR, Norwegian Institute of Technology, Trondheim, Norway, 1978.
- [11.2.8] LIU, W. K., et al. (Eds.), *Innovative Methods for Nonlinear Problems*, Penridge, Swansea, United Kingdom, 1984.
- [11.2.9] CRISFIELD, M. A., *Nonlinear Finite Element Analysis*, Vol. 1, John Wiley & Sons, New York, 1988.
- [11.2.10] BATHE, K.-J., *Finite Element Procedures*, Prentice-Hall, Upper Saddle River, New Jersey, 1996.
- [11.2.11] KLEIBER, M., *Incremental Finite Element Modelling in Non-Linear Solid Mechanics*, Ellis Horwood, Chichester, United Kingdom, 1989.
- [11.2.12] STEIN, E. (Ed.), *Nichtlineare Berechnungen im konstruktiven Ingenieurbau*, Springer-Verlag, Berlin, 1989.

11.3 Material Nonlinearity

11.3.1 Nonlinear Stress-Strain Relationships

In the previous sections of this chapter we have assumed that structural material behaves linear-elastically. There are, however, plate problems in which linear-elastic behavior is not preserved. Consequently, we should also treat problems where the nonlinearity of the structural response stems from the nonlinear stress-strain relationship of the material. Here we will consider only *nonlinear-elastic* and *elastic-plastic* material behaviors. The much more difficult treatment of time-dependent nonlinear

material response is considered to be beyond the scope of this book. Although there are a few analytical solutions concerning material nonlinearities in plates, their scope is very limited. In addition, their application is quite cumbersome. Consequently, we are treating here, as in the previous section, only the more practical finite element approach to this nonlinear problem.

Since in plates the state of stress is essentially two dimensional, strictly speaking, a pertinent but more difficult stress-strain relationship should also be used in the computations. However, considerable simplification of such inherently complex handling of the two-dimensional state of stress and strain may be obtained by introducing the concept of *equivalent uniaxial stress* [11.3.1–11.3.4],

$$\sigma_e = \sqrt{\sigma_x^2 + \sigma_y^2 - \sigma_x \sigma_y + 2\tau^2}, \quad (11.3.1)$$

and that of the corresponding *equivalent uniaxial strain*,

$$\varepsilon_e = \frac{2}{\sqrt{3}} \sqrt{\frac{\varepsilon_x^2 + \varepsilon_y^2 + \varepsilon_{xy} + \gamma^4}{4}}. \quad (11.3.2)$$

In the following discussion, we will tacitly assume that such an equivalent stress-strain relationship is used in all computations.

Figure 11.3.1a shows a nonlinear-elastic stress-strain curve. In this case, loading and unloading follow the same path. However, this curve can be simplified, without losing significant accuracy, by substituting it with an equivalent bilinear stress-strain relationship, as shown in Fig. 11.3.1b. Such material follows only two Hooke's laws in loading and unloading.

The basic assumptions for an ideal elastic-plastic material are as follows:

- The stress-strain relationship obeys a law similar to that shown in Fig. 11.3.2a.
- Prior to yield, the material behaves elastically and follows Hooke's law in loading and unloading.

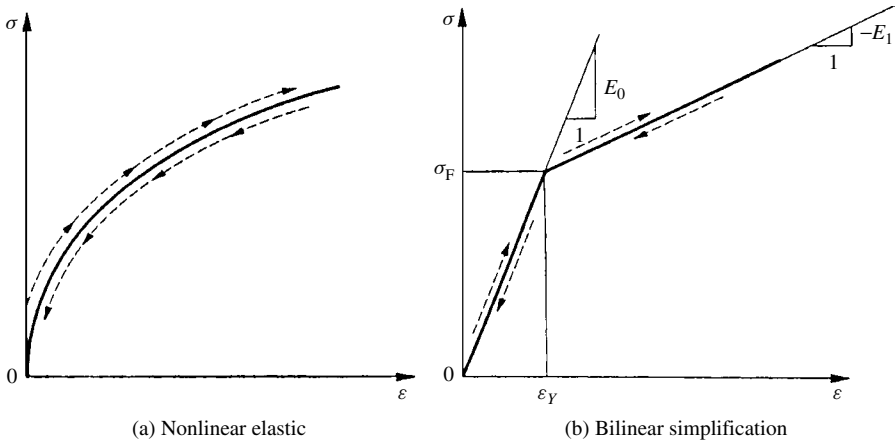


Figure 11.3.1 Nonlinear stress-strain curves.

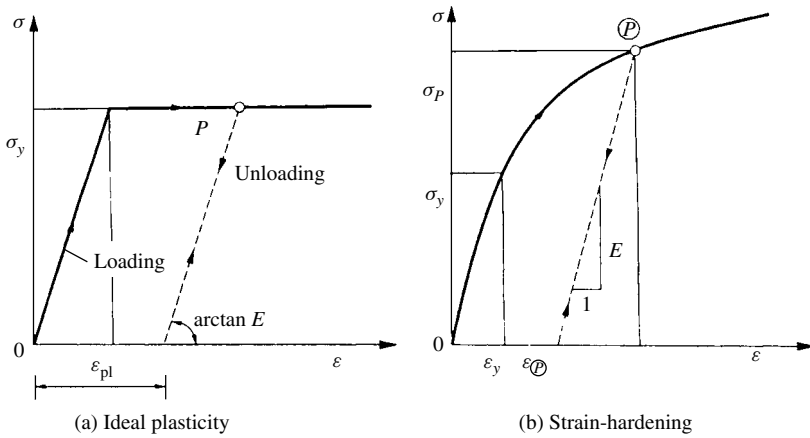


Figure 11.3.2 Stress-strain relationships of plastic materials.

- In the plastic range, however, the unloading produces permanent strain ε_{pl} .
- Under a two-dimensional state of stress, it is useful to engage the above-introduced equivalent uniaxial stress σ_e , the yield point of which is the yield stress in simple tension ($\sigma_{e,y} = \sigma_y$).

While the stress-strain relationship of structural steel can be well approximated by using such ideal elastic-plastic stress-strain relationship, there are, also more complicated strain-hardening cases, as shown in Fig. 11.3.2b, that must also be considered.

The commonly used solution procedures usually apply the *tangent* stiffness concept. But unlike the linear tangent modulus of elasticity E_t , its nonlinear counterparts, $E_t(\varepsilon)$, are not constant anymore since they depend on the current values of strain (Fig. 11.3.3a). Thus, they should be defined by

$$E_{t,i} = \left(\frac{d\sigma}{d\varepsilon} \right)_i \approx \left(\frac{\Delta\sigma}{\Delta\varepsilon} \right)_i. \quad (11.3.3)$$

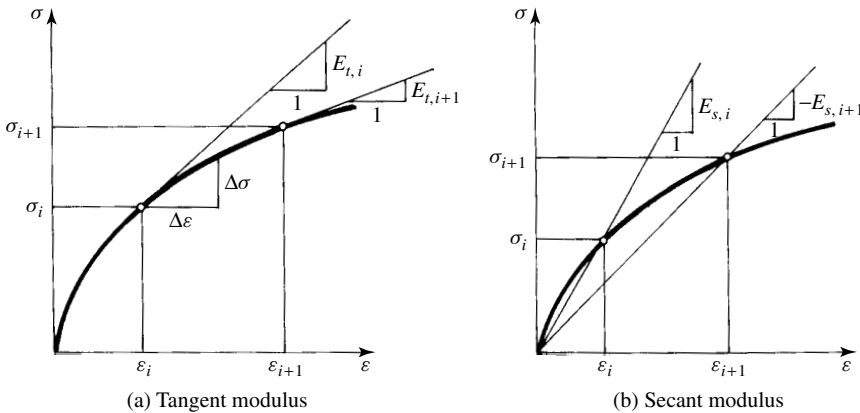


Figure 11.3.3 Two types of elastic modulus.

However, when the $\sigma - \varepsilon$ curve becomes quite flat, the tangent modulus of elasticity will approach zero. In this case, the *secant* modulus of elasticity (Fig. 11.3.3b)

$$E_{si} = \frac{\sigma_i}{\varepsilon_i} \quad (11.3.4)$$

must be employed.

11.3.2 Computational Procedures

Both *incremental* and *iterative* methods are used for nonlinear elasticity and elasto-plasticity. In addition, two modified methods are also often employed for elastic-plastic analysis: the *initial-strain method* and the *initial-stress method*. By the very nature of these numerical techniques, the reader will find some overlap with the procedures discussed in the previous section. Although here we will apply these procedures exclusively in connection with the FEM, their use can also be logically extended to other numerical approaches.

One of the simplest numerical techniques to deal with nonlinear plate problems is the *incremental* or Euler method, which utilizes the tangent stiffness matrix concept. If no unloading occurs, the solution procedure is straightforward. If it occurs, special modification to the procedure may become necessary.

The element stiffness matrix for this nonlinear analysis is computed by following the standard finite element procedures,[†]

$$\mathbf{K}_e(\sigma_i) = \int_V \mathbf{D}^T \mathbf{E}(\sigma_i) \mathbf{D} dV, \quad (11.3.5)$$

where $\mathbf{E}(\sigma_i)$ is now variable and represents the matrix of tangent moduli corresponding to the obtained stress level σ_i . In other words, the matrix \mathbf{K}_e is updated for each load increment. Consequently, the tangent stiffness is computed at the end of each increment and used for the succeeding increment. For elastic-plastic material, it is more useful to compute the element stiffness matrix from

$$\mathbf{K}_e(\varepsilon_i) = \int_V \mathbf{D}^T \mathbf{E}(\varepsilon_i) \mathbf{D} dV. \quad (11.3.6)$$

To schematically illustrate this and all finite element procedures discussed in this section, we use simple 1-DOF systems. The corresponding algorithms, however, should be interpreted for the total structure represented in a $\bar{X}, \bar{Y}, \bar{Z}$ global coordinate system.

The relatively simple algorithm for the incremental procedure can be written as

$$\Delta \bar{\mathbf{d}}_{i+1} = [\bar{\mathbf{K}}(E_i)]^{-1} \Delta \bar{\mathbf{p}}_i \quad (11.3.7)$$

and

$$\bar{\mathbf{d}} = \sum_{i=1}^m \Delta \bar{\mathbf{d}}_i, \quad (11.3.8)$$

which is schematically illustrated in Fig. 11.3.4.

[†] See Sec. 7.3.2.

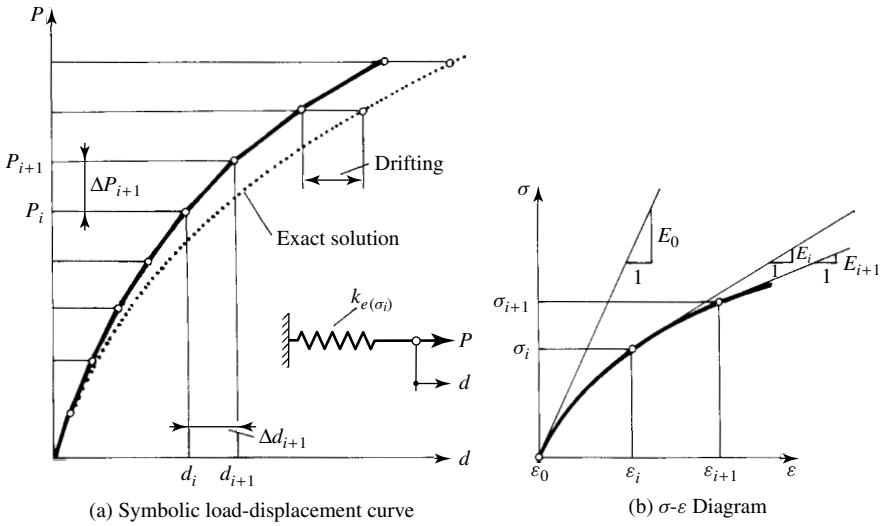


Figure 11.3.4 Basic incremental procedure.

The principal drawbacks of the incremental approach are as follows:

- It is necessary to compute new elasticity matrices and to assemble and invert the overall stiffness matrix $\bar{\mathbf{K}}(E_i)$ for each incremental step.
- Unless very small load increments are used, this procedure has an undesirable *drifting* tendency, as shown in Fig. 11.3.4.
- If tangent stiffness is used, the incremental method fails completely in the plastic region of an ideal elastic-plastic material for the reasons already discussed.

Instead of using very small load increments, the undesirable drifting tendency of the incremental method can also be eliminated by applying the *mixed step iteration* procedure, which is a combination of incremental and iterative schemes. This method, often referred to as the Newton-Raphson procedure, is schematically shown in Fig. 11.3.5. Here, we also apply the load by increments, but after each increment, successive iterations are performed to satisfy the condition of equilibrium. While the accuracy of the results are considerably improved by applying the Newton-Raphson procedure, the higher accuracy is obtained at the price of more computer effort.

The corresponding algorithm for the nonincremental version of the Newton-Raphson method (Fig. 11.3.6) is as follows:

1. In the first step, the structure is subjected to the total load $\bar{\mathbf{p}}$, and the first approximation of the displacements are computed from

$$\bar{\mathbf{d}}_0 = [\bar{\mathbf{K}}_0(E_0)]^{-1} \bar{\mathbf{p}}, \quad (11.3.9)$$

where the stiffness matrix of the total system is determined by using the starting value E_0 for the modulus of elasticity.

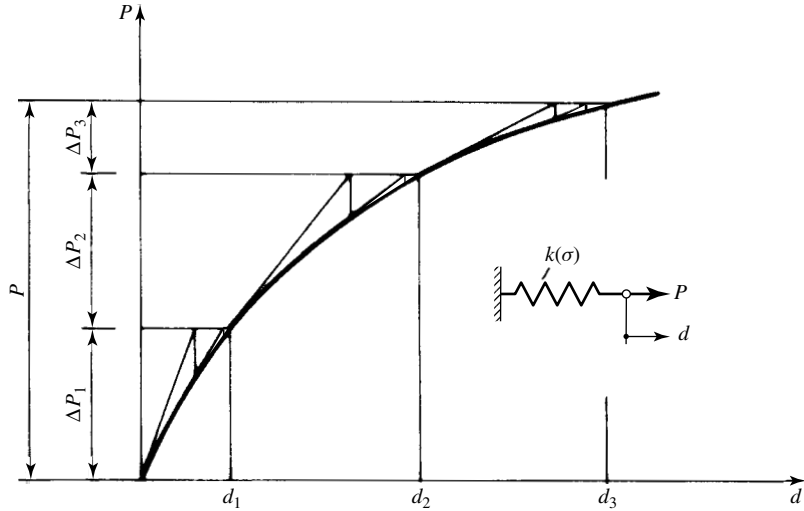


Figure 11.3.5 Step iteration or mixed procedure.

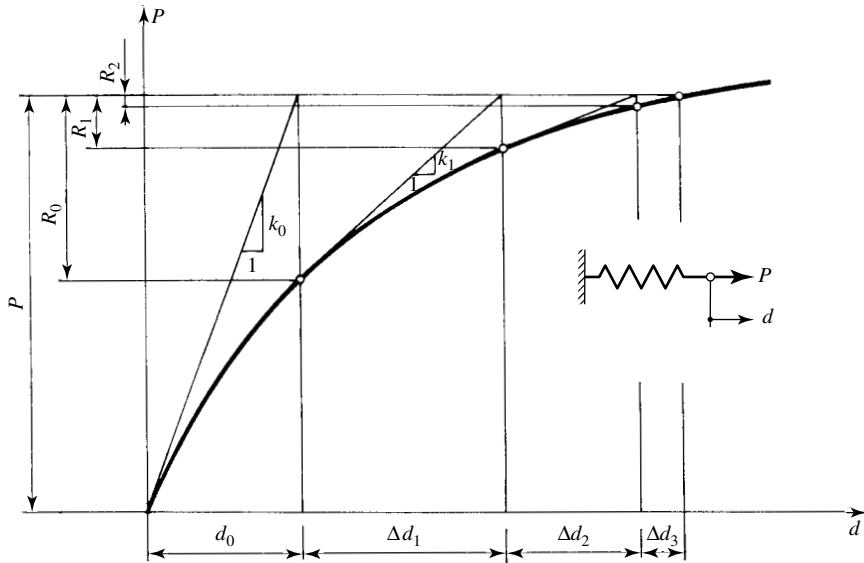


Figure 11.3.6 Iterative tangent stiffness procedure.

2. Based on the results obtained for displacements, the stress σ (or strain ϵ) and the corresponding modulus of elasticity $E_i^{(N)}$, are determined in each element. A check of the state of equilibrium with the updated stiffness matrix reveals an unbalanced residual force vector

$$\bar{\mathbf{r}}_0 = \bar{\mathbf{K}}_1(E_1)\bar{\mathbf{d}}_0 - \bar{\mathbf{p}}. \tag{11.3.10}$$

3. These unbalanced forces produce additional displacements

$$\Delta \bar{\mathbf{d}}_1 = [\bar{\mathbf{K}}_1(E_1)]^{-1} \bar{\mathbf{r}}_0. \quad (11.3.11)$$

4. These new deflections of the plate, $\bar{\mathbf{d}}_1 = \bar{\mathbf{d}}_0 + \Delta \bar{\mathbf{d}}_1$, create new residual forces $\bar{\mathbf{r}}_2$ and corresponding incremental displacements $\Delta \bar{\mathbf{d}}_2$, and so on.

Consequently, the general form of this algorithm can be written as

$$\boxed{\begin{aligned} \bar{\mathbf{r}}_j &= \bar{\mathbf{K}}_{j+1}(E_{j+1})\bar{\mathbf{d}}_j - \bar{\mathbf{p}}, \\ \Delta \bar{\mathbf{d}}_{j+1} &= [\bar{\mathbf{K}}_{j+1}(E_{j+1})]^{-1} \bar{\mathbf{r}}_j, \\ \text{for } j &= 1, 2, 3, \dots \end{aligned}} \quad (11.3.12)$$

When the magnitudes of the residual forces become negligibly small, the iteration is terminated. The final deflections are the sum of the incremental displacements; thus

$$\bar{\mathbf{d}} = \bar{\mathbf{d}}_0 + \sum_{j=0}^m \Delta \bar{\mathbf{d}}_{j+1}. \quad (11.3.13)$$

This iterative procedure can also be combined with the incremental scheme (Fig. 11.3.5). In this case, however, the above given algorithm is valid only for a load increment $\Delta \bar{\mathbf{p}}_i$.

For elastic-plastic materials, the *secant stiffness* approach must be applied in an iterative procedure. A schematic representation of this numerical technique is shown in Fig. 11.3.7. In this case, the secant modulus of elasticity $E_{s,i}$ is used (Fig. 11.3.3b) to compute the element stiffness matrices. The corresponding computational scheme is

$$\bar{\mathbf{K}}_i(E_{s,i})\bar{\mathbf{d}}_i = \bar{\mathbf{p}}. \quad (11.3.14)$$

The initial-strain method can also be employed to determine the structural response in the plastic region. While the incremental and iterative procedures introduced above always require the recomputation of element stiffness matrices and the solution of the governing matrix equation at every stage of computation, the initial-strain method uses the same stiffness matrix, $\bar{\mathbf{K}}(E_0)$, throughout the whole computational sequence. The basic idea of this procedure is schematically illustrated in Fig. 11.3.8.

Using the stiffness matrix $\bar{\mathbf{K}}(E_0)$ of the total structure based on the elastic modulus of elasticity E_0 , the first estimate of displacements is computed from

$$\bar{\mathbf{d}}_A = [\bar{\mathbf{K}}(E_0)]^{-1} \bar{\mathbf{p}} \quad (11.3.15)$$

The correct state of equilibrium, however, is at point (B) on the nonlinear load-deflection curve (Fig. 11.3.8). The difference between the correct displacements $\bar{\mathbf{d}}_B$ and their previously obtained first estimate $\bar{\mathbf{d}}_A$, is

$$\bar{\mathbf{d}}_0 = \bar{\mathbf{d}}_B - \bar{\mathbf{d}}_A \quad (11.3.16)$$

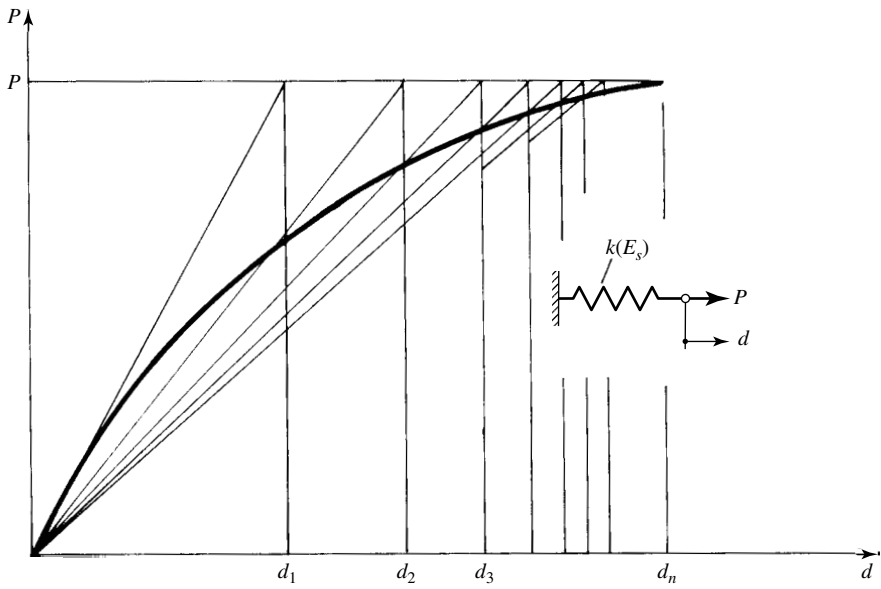


Figure 11.3.7 Symbolic presentation of secant stiffness procedure.

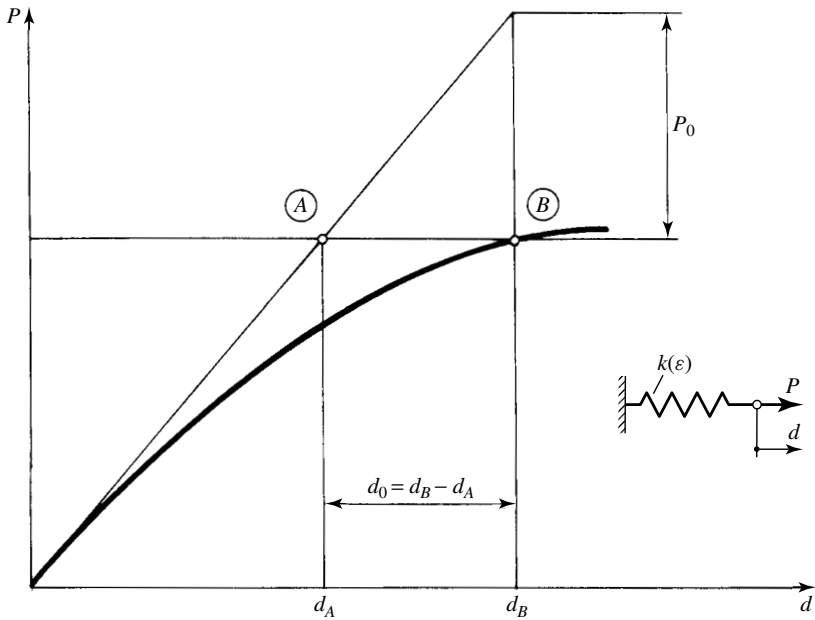


Figure 11.3.8 Basis of initial-strain method.

The initial-strain vector $\bar{\epsilon}_0$ corresponding to the load \bar{p}_0 is obtained from

$$\bar{\epsilon}_0 = \bar{D} \bar{d}_0. \quad (11.3.17)$$

A load vector to improve the first estimate of displacements, \bar{d}_A , is found from

$$\bar{p}_0 = \int_V \bar{D}^T \bar{E} \bar{\epsilon}_0 dV. \quad (11.3.18)$$

This computation is repeated with

$$\bar{p} = \bar{p} \pm \bar{p}_0 \quad (11.3.19)$$

until convergence ($\bar{p}_0 \approx 0$) is achieved. Using this procedure for the elastic-plastic material, we can write

$$\epsilon_0 = \epsilon_{pl} \quad (11.3.20)$$

Since the initial-strain method fails in the *ideal* plastic region of the material, Zienkiewicz and his co-workers introduced the initial-stress method as an alternative procedure [11.3.10]. This mixed approach also uses the linear stiffness matrix $\bar{K}_1(E_0)$ for the first estimate of the displacements. The required corrections of the displacement vector is obtained, as in the initial-strain method, with the help of a load vector. In the region of plasticity, however, numerous iterative steps are required until the state of equilibrium is reached.

The following steps are used for the initial-strain method: The incremental displacements due to the i th load increment are computed from

$$\bar{K}(E_0) \Delta \bar{d}_i^{(0)} = \Delta \bar{p}_i \quad (11.3.21)$$

by using the linear stiffness matrix $\bar{K}(E_0)$ of the total system. The pertinent vector of strains is

$$\Delta \bar{\epsilon}_i^{(0)} = \bar{D}^T \Delta \bar{d}_i^{(0)}. \quad (11.3.22)$$

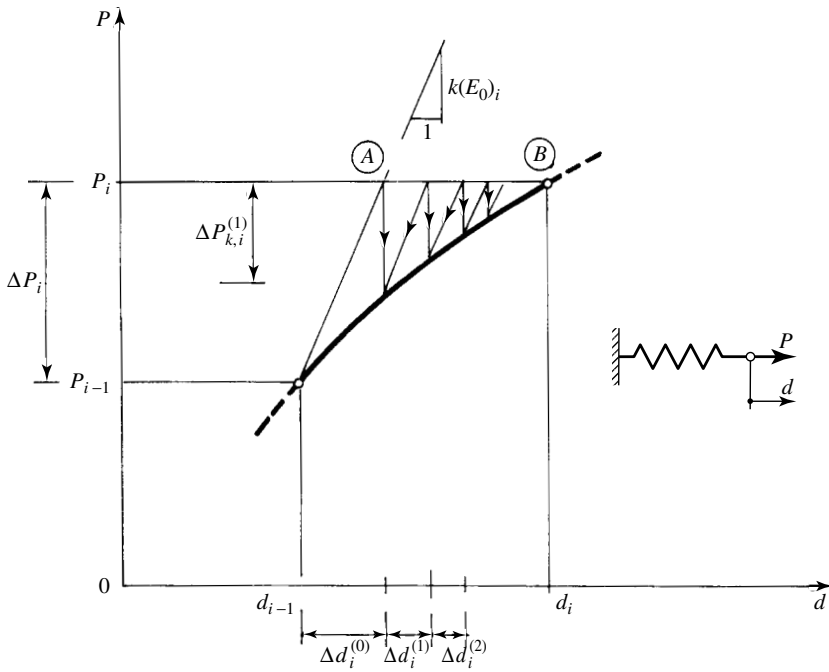
The corresponding increment in stress, $\Delta \bar{\sigma}_i^{(0)}$, as shown in Fig. 11.3.9b, is obtained from

$$\Delta \bar{\sigma}_i^{(0)} = \bar{E}_0 \Delta \bar{\epsilon}_i^{(0)}. \quad (11.3.23)$$

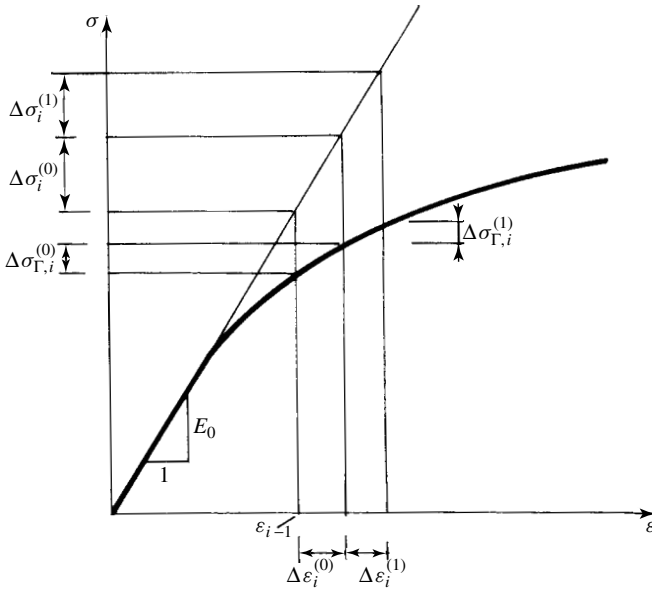
But, due to the nonlinearity of the stress-strain relationship, the stress vector[†] should have been $\Delta \bar{\sigma}_{r,i}^{(0)}$. The force required for this corrections is

$$\Delta \bar{p}_{k,i}^{(1)} = \int_V \bar{D}^T (\Delta \bar{\sigma}_i^{(0)} - \Delta \bar{\sigma}_{r,i}^{(0)}) dV. \quad (11.3.24)$$

[†] The superscript refers to the number of the iterative cycle, and the subscript represents the number of load increments.



(a) Load-deflection curve



(b) Stress-strain curve

Figure 11.3.9 Iterative initial-stress method.

For the further iterative steps, the following algorithm should be used:

$$\begin{aligned} \overline{\mathbf{K}}(E_0) \Delta \overline{\mathbf{d}}_i^{(j)} &= \Delta \overline{\mathbf{p}}_i + \Delta \overline{\mathbf{p}}_{k,i}^{(j)}, \\ \Delta \overline{\mathbf{p}}_{k,i}^{(j)} &= \int_V \overline{\mathbf{D}}^T \left(\Delta \overline{\boldsymbol{\sigma}}_i^{(j)} - \Delta \overline{\boldsymbol{\sigma}}_{r,i}^{(j)} \right) dV. \end{aligned} \quad (11.3.25)$$

This computation is repeated with $\Delta \overline{\mathbf{p}}_i + \Delta \overline{\mathbf{p}}_{r,i}$ until

$$\Delta \overline{\boldsymbol{\sigma}}_i^{(j)} - \Delta \overline{\boldsymbol{\sigma}}_{r,i}^{(j)} \approx 0. \quad (11.3.26)$$

If the nonlinear stress-strain relationship is represented by an equivalent bilinear curve (Fig. 11.3.1b), this procedure can be especially effective. In this case, a simplified form of corrections can be used:

$$\Delta \overline{\mathbf{p}}_{k,i}^{(j)} = \int_V \overline{\mathbf{D}}^T (E_0 - E_1) \Delta \overline{\boldsymbol{\varepsilon}}_i^{(j)} dV \quad \text{for } j = 1, 2, 3, \dots \quad (11.3.27)$$

A combination of the initial-stress approach and the tangent stiffness procedure offers the following additional advantages:

- smaller number of iterations and
- a more realistic representation of the stiffness matrix $\overline{\mathbf{K}}$.

Finally, it should be mentioned that the initial-strain method can also handle the quite difficult loading and unloading situations in plastic regions [11.3.9, 11, 3.10].

Summary. In this section we have treated various finite element procedures for the analysis of material nonlinearities of plates by assuming small displacements and small strains. Incremental, iterative and mixed solution techniques were briefly introduced. A comparison of these numerical methods indicates that probably the incremental method is the most general. Another advantage of this procedure is that it gives a complete description of the load-deformation curve of the structure. Furthermore, it is relatively easy to program. Unfortunately, the solution has a tendency to drift from exact values. Application of iterative methods is generally not as time consuming as that of incremental ones. The iterative procedure combined with the secant stiffness approach is capable of handling even elastic-plastic material behaviors, where incremental methods fail. Iterative methods, however, do not give information concerning the load-deformation curve of the structure, since only the final displacements are determined for the total load. It appears that mixed methods can combine the advantages of the two numerical techniques while their disadvantages are minimized to a certain degree.

References and Bibliography

- [11.3.1] HENCKY, H., "Zur Theorie plastischer Deformationen und der hierdurch im Material hervorgerufenen Nachspannungen," *Z. Angew. Math. Mech.*, 4 (1924), 323–334.

- [11.3.2] ILYUSIN, A. A., "Stability of Plates and Shells beyond the Proportional Limit," NACA TN-1116, National Advisory Committee for Aeronautics, Washington, D.C., 1947.
- [11.3.3] STOWELL E. Z., "A Unified Theory of Plastic Buckling of Columns and Plates," NACA Rep. 898, National Advisory Committee for Aeronautics, Washington, D.C., 1958.
- [11.3.4] RAMBERG, W., and OSGOOD, W. R., "Description of Stress-Strain-Curve by Three Parameters," NACA TN 902, National Advisory Committee for Aeronautics, Washington, D.C., 1943.
- [11.3.5] YAMADA, Y., et al., "Plastic Stress-Strain Matrix and Its Application for Solution of Elastic-Plastic Problems by the Finite Element Method," *Int. J. Mech. Sci.*, 10 (1968), 343–354.
- [11.3.6] BERGAN, P., et al. (Eds.), *Finite Elements in Nonlinear Mechanics*, Vol. 1, Tapir, Trondheim, Norway, 1978.
- [11.3.7] HILTON, E., et al. (Eds.), *Recent Advances in Nonlinear Computational Mechanics*, Pineridge Press, Swansea, United Kingdom, 1982.
- [11.3.8] LIU, W. K., et al., *Innovative Methods for Nonlinear Problems*, Pineridge Press, Swansea, United Kingdom, 1984.
- [11.3.9] OWEN, D. R. J., and HINTON, E., *Finite Elements in Plasticity*, Pineridge Press, Swansea, United Kingdom, 1980.
- [11.3.10] ZIENKIEWICZ, O. C., et al., "Elasto-Plastic Solutions of Engineering Problems: Initial Stress Finite Element Approach," *Int. J. Mech. Sci.*, 1 (1969), 75–100.

11.4 Combined Geometrical and Material Nonlinearities

Under high load levels, geometrical and material nonlinearities often occur jointly. However, due to the high complexity of such problems, realistic treatments of the structural response to such high loads are usually too sophisticated for any practical use. Thus, in spite of past achievements in this field, a more practical procedure is required that efficiently integrates the most relevant aspects of nonlinear material and nonlinear structural behavior.

In this section, we present a simplified numerical procedures for the analysis of plates subjected to such combined nonlinearities. Our approach is based on the FEM, which includes nonlinear effects due to the actual behavior of structural material under high load and the geometrical nonlinear effects due to large deflections. In addition, we intend to achieve computational simplicity and economy by means of some approximations.

As mentioned above, the present model of analysis is based on the displacement formulation of the FEM or GWM. The *incremental-iterative* approach used here employs the total Lagrangian formulation, which is by far the most widely used frame of reference in nonlinear structural analysis. Furthermore, the associated computational strategies may utilize both the tangential stiffness and secant stiffness approaches introduced in the previous section. The nonlinear geometric effects caused by large displacements of the plate must be considered since they are not negligible compared to the plate thickness. They are included in the stiffness matrices of the plate elements. Strains are assumed to be small compared to unity.

To simplify the treatment of material nonlinearity, we use again a bilinear stress-strain relationship, shown in Fig. 11.4.1. In addition, in all further computations we assume that the stresses σ and strains ε represent their two-dimensional counterparts, given in Eqs. (11.3.1) and (11.3.2), respectively; thus $\sigma = \sigma_e$ and $\varepsilon = \varepsilon_e$. That is, experience shows that such bilinear representation of the stress-strain diagram results in considerable simplification in treating material nonlinearities without noticeably affecting the achievable accuracy [11.4.1, 11.4.2].

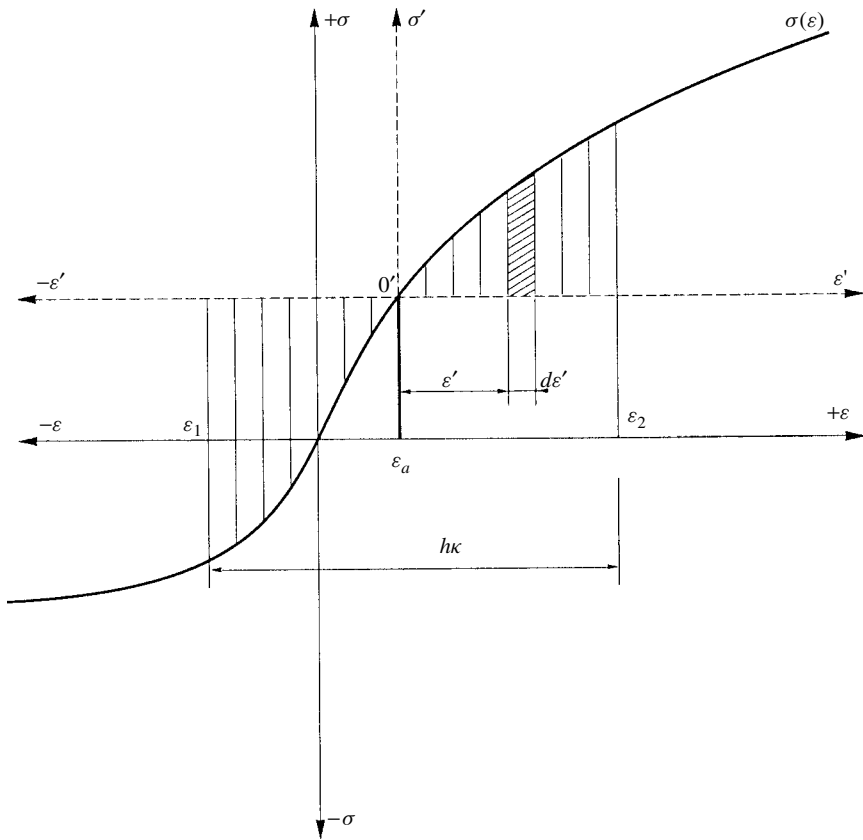


Figure 11.4.2 Equivalent stress distribution.

direction can be approximated by

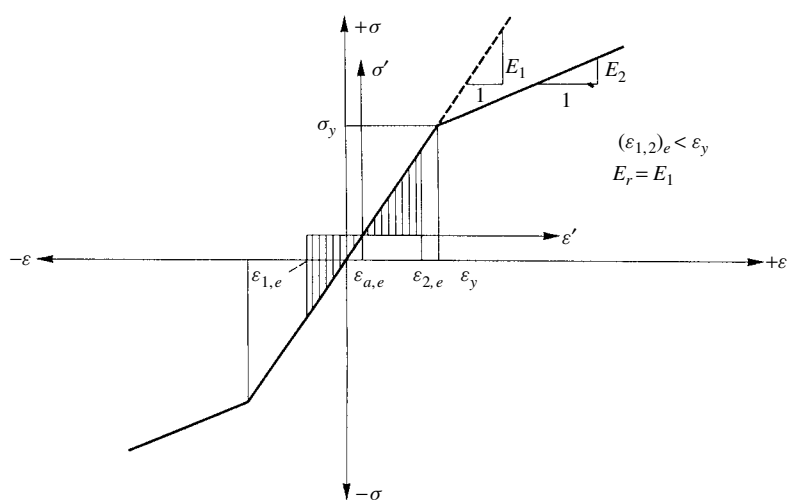
$$(\kappa_x)_{m+1,e}^{(j)} = \left(\frac{w_{,xx}}{1 + w_{,x}^2} \right)_{m+1,e}^{(j)} \quad \text{for } j = 0, 1, 2, 3, \dots \quad (11.4.2)$$

A similar expression can be written in the Y direction by simply replacing the subscripts x by y . Consequently, in the case of bending coupled with membrane forces, the reduced modulus of elasticity in the X direction can be defined by

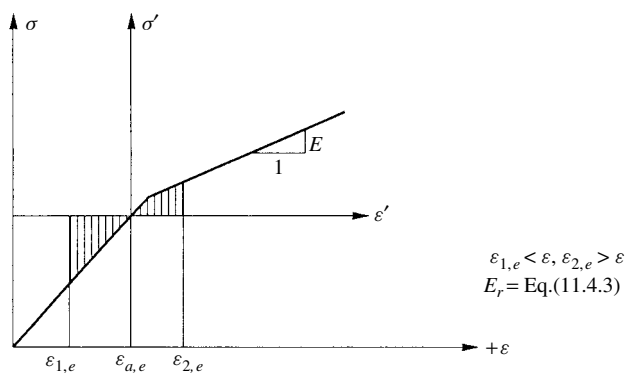
$$(E_{xr})_{m+1,e}^{(j)} = \left[\frac{12}{(h\kappa_x)^3} \int_{\varepsilon_1}^{\varepsilon_2} (\sigma' \varepsilon') d\varepsilon' \right]_{m+1,e}^{(j)}. \quad (11.4.3)$$

In these equations the subscript m represents the load level and the superscript (j) refers to the number of iterative cycles required to obtain equilibrium.

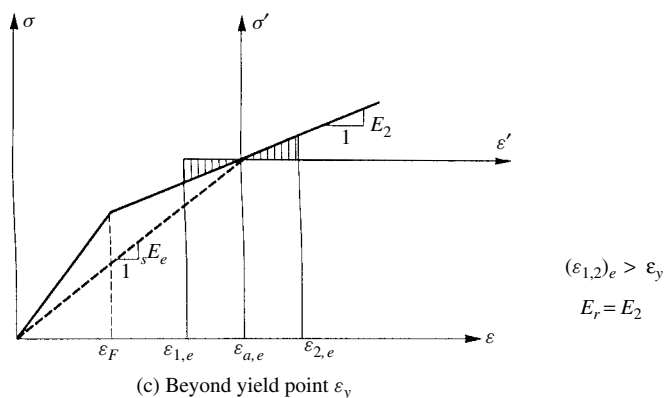
Figure 11.4.3 illustrates the determination of the moduli of elasticity in the assumed bilinear stress-strain relationship. Consequently, the corresponding *reduced flexural*



(a) Linear elastic region



(b) General case



(c) Beyond yield point ε_y

Figure 11.4.3 Determination of reduced moduli of elasticity.

rigidity of the plate in the X direction can be expressed by

$$(D_{xr})_{m+1,e}^{(j)} \approx \left[\frac{E_{xr} h^3}{12(1-\nu^2)} \cdot \frac{1}{(1+w_{,x}^2)^{3/2}} \right]_{m+1,e}^{(j)}. \quad (11.4.4)$$

Again, a similar expression can be written for D_{yr} by replacing the subscript x by y . Since the reduced moduli of elasticity and the corresponding reduced flexural rigidities are different in the X and Y directions, respectively, *orthotropic* finite elements must be employed in the computational procedures. However, if the GWM is used instead of the FEM, the corresponding reduced moments of inertia are

$$I_{rx} = \frac{I_x}{(1+w_{,x}^2)^{3/2}} \quad \text{and} \quad I_{ry} = \frac{I_y}{(1+w_{,y}^2)^{3/2}}. \quad (11.4.4a)$$

b. Outline of Computational Strategy. Logically, all previously introduced incremental-iterative procedures for nonlinear plate analysis can be applied in combination with the above-introduced simplifications. In any case, such a procedure tends to be quite involved. However, if we merely want to obtain a reasonable *estimate* of the plate response to high loads considering combined nonlinearities, the simplest approach appears to be Euler's incremental method without equilibrium iteration. A further aid can be the use of the GWM.

Again, the external load is divided into m increments. Euler's forward strategy gives the starting vector of the displacements

$$\Delta \bar{\mathbf{d}}_0 = (\bar{\mathbf{K}}_{T,b}^L)^{-1} \Delta \bar{\mathbf{p}}_1, \quad (11.4.5)$$

where $\bar{\mathbf{K}}_{T,b}^L$ represents the linear tangent stiffness matrix of the system considering only the bending part. At the end of the first load increment and that of all other m th increments, the element stiffness matrices must be updated by using the current displacement vector $\bar{\mathbf{d}}_m$ and the corresponding reduced tangent modulus of elasticity $E_{T,r}$ and the pertinent reduced moment of inertias I_{rx} and I_{ry} , respectively. For this purpose, the simplified expression or Green's strain can be used. Thus, for an equivalent beam oriented in the X direction, we can write

$$\varepsilon_x \approx u_{,x} + \frac{1}{2}w_{,x}^2 \pm z\kappa_x = u_{,x} + \frac{1}{2}w_{,x}^2 \pm z \frac{w_{,xx}}{(1+w_{,x}^2)^{3/2}}. \quad (11.4.6)$$

Similarly, the strain for a beam oriented in the Y direction is

$$\varepsilon_y \approx v_{,y} + \frac{1}{2}w_{,y}^2 \pm z \frac{w_{,yy}}{(1+w_{,y}^2)^{3/2}}. \quad (11.4.7)$$

Consequently, for any higher load level

$$\bar{\mathbf{p}}_{m+1} = \bar{\mathbf{p}}_m + \Delta \bar{\mathbf{p}}_{m+1}, \quad (11.4.8)$$

the tangent stiffness matrix of the plate becomes

$$\bar{\mathbf{K}}_{T,m} = [\bar{\mathbf{K}}_a^L(E_r) + \bar{\mathbf{K}}_b^L(I_r) + \bar{\mathbf{K}}^{\text{NL}}(\bar{\mathbf{d}})]_{T,m}, \quad (11.4.9)$$

where \mathbf{K}_a^L is the axial (i.e., membrane) stiffness matrix. Assuming that the plastic region is not yet reached in the elements, the incremental displacement vector is computed from

$$\Delta \bar{\mathbf{d}}_{m+1} = (\bar{\mathbf{K}}_{T,m})^{-1} \Delta \bar{\mathbf{p}}_{m+1}. \quad (11.4.10)$$

As the load intensity is increased, the strain in some beams will be larger than the yield point ε_y of the material. In such a case, provided that E_2 is not too small, we can continue the procedure outlined above by using E_2 in calculating the reduced moduli of elasticity along with the reduced moment of inertias for such beam elements. As before, the displacement vector is the sum of the incremental displacements

$$\bar{\mathbf{d}} = \sum_{m=0}^M \Delta \bar{\mathbf{d}}_m. \quad (11.4.11)$$

However, if E_2 becomes small or even approaches zero, the tangent stiffness approach fails and must be replaced by a combination of tangent and secant stiffness approaches [11.4.2].

Summary. Plate problems involving both geometrical and material nonlinearities can be considered one of the most difficult tasks to solve. Research in this category of nonlinear problems is still in progress. Most solution procedures apply the versatile FEM or GWM. A common numerical technique for solution of the resulting matrix equations is Euler's incremental procedure. Since this procedure tends to drift away from the true solution, the use of relatively small increment loads is recommended. Although equilibrium iterations can eliminate this drifting tendency, they considerably complicate the computational strategy. The same can be said of the energy-balancing approach developed for planar beam-type structures [11.4.2] if it will be extended to the solution of such nonlinear plate problems. To simplify the analysis of plates subjected to these combined nonlinearities, an approximate solution procedure has been introduced in this section.

References and Bibliography

- [11.4.1] CAJES, A., "Inelastic Deflections of Beams," *J. Struct. Div., ASCE*, 94 (1968), 1549–1565.
- [11.4.2] SZILARD, R., "An Energy Balancing Strategy for Solution of Combined Geometrical and Material Nonlinear Problems," *Comp. and Struct.*, 23 (1986), 147–162.
- [11.4.3] TIMOSHENKO, S., *Strength of Materials, Part II: Advanced Theory and Problems*, Van Nostrand, Princeton New Jersey, 1956.
- [11.4.4] POWELL, G. H., "Theory of Nonlinear Elastic Structures," *J. Struct. Div., ASCE*, 95 (1969), 2687–2701.
- [11.4.5] YAGMAI, S., "Incremental Analysis of Large Deformations in Mechanics of Solids," Ph.D. Dissertation, University of California, Berkeley, 1966.
- [11.4.6] GADALA, M. S., and ORAVAS, A. E., "Numerical Solutions of Nonlinear Problems of Continua," *Comp. and Struct.*, 19 (1984), 865–877.
- [11.4.7] ROCA, P., et al., "Geometric and Material Nonlinearities in Steel Plates," *J. Struct. Div., ASCE*, 122 (1996), 1427–1438.

11.5 Reinforced-Concrete Slabs

a. Introduction. The nonlinear analysis of reinforced-concrete (RC) slabs represents an inherently complex problem caused by the following factors:

- (a) nonlinear relationships of concrete and steel,
- (b) cracking of concrete,
- (c) imperfect bond between reinforcement and concrete and
- (d) other effects such as creep and shrinkage.

In the last decades numerous sophisticated mathematical models have been developed for the nonlinear analysis of RC slabs [11.5.1–11.5.4]. In general, the behavior of RC slabs can be classified into two distinctively different stages: linear-elastic behavior of the uncracked concrete and elastoplastic behavior of the cracked RC slab. Its nonlinear elastoplastic behavior is mainly governed by the following factors: (1) compressive response of the concrete between cracks, (2) bond between concrete and reinforcing bars and (3) shear transfer effect due to aggregate interlock between cracked concrete surface and dowel action of the reinforcing bars crossing the cracks.

Of these, the forming of cracks under short time loading is generally recognized to be the most important factor governing the nonlinear behavior of RC slabs. Mathematical models for handling this phenomenon can be divided into two main categories: *smear crack concept and discrete models*. Discrete models can be either *bond slip* or *layered*. Although nowadays the FEM is used almost exclusively for nonlinear analysis of RC slabs, a solution technique based on the FDM [11.5.5] may offer a more usable approach, provided its present limitation concerning simply supported boundary conditions can be eliminated.

b. Smear Crack Concept. This FEM deals with distributed cracks that are “smeared” over either the element or its integration points. It is assumed that the cracks are uniformly distributed at small distances normal to the maximum principal stress and the reinforcing steel is also evenly distributed throughout the finite element. In addition, this concept uses two material laws, one for the equivalent medium cracks and the other for the concrete between the cracks. However, fixed values for these constitutive laws are hard to determine. A usual practice is to adjust the parameters of these laws independently for each sampling point in the finite element mesh according to the element size and try to match them with some experimental values. When the crack width is less than 0.05 mm, shear transfer takes place. With larger than 1.2 mm crack width, however, no such load transfer is possible. Adoption of fixed values for these constitutive laws can lead to unobjectional results. For this reason, it is not as widely used as the layered model subsequently discussed. Readers who want to obtain specifics on the use of shear crack models should consult Refs. [11.5.12] and [11.5.13].

c. Bond-Slip Model. In the behavior of RC slabs under short-term load, the interface between concrete and reinforcing bars plays an important role. The most common approach in modeling this phenomenon is the introduction of so-called *interface elements* [11.5.6, 11.5.7], as shown in Fig. 11.5.1. These elements connect a node of the concrete element with a node of the steel element (Fig. 11.5.2). Although this concept was originally developed for modeling plane stress problems of RC, its application

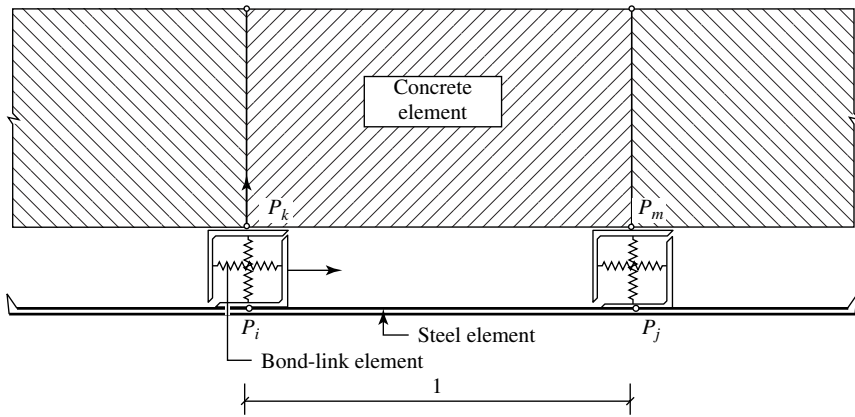


Figure 11.5.1 Bond-slip model for plane stress.

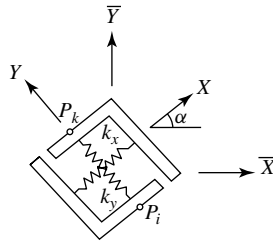


Figure 11.5.2 Bond-link interface element (two dimensions).

can be extended to cover nonlinear bending analysis of RC slabs by using appropriate three-dimensional elements for concrete and steel. The stiffness of such linkage is usually determined on the basis of experimental tests. Consequently, a wide variation in this value can be expected. As in all three-dimensional finite element analysis, the computer requirements for this concept are considerable.

d. Layered RC Elements. For the bending analysis of RC slabs, probably the use of layered finite elements appears to be the most promising. The plate elements are divided into layers of concrete and steel (Fig. 11.5.3). Thus the stress distribution in

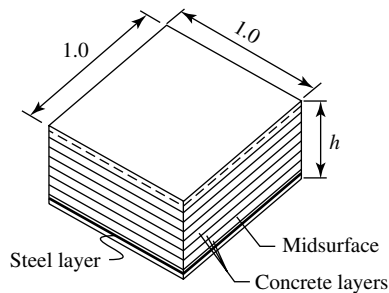


Figure 11.5.3 Layered element.

the RC slab is approximated with layers of *plane stress* elements. The plane stress properties are assigned to each of these layers. Consequently, the state of plane stress varies from layer to layer. It should be noted, however, that this layered-element concept is not capable of including nonlinear responses to transverse shear effects, which occur in the case of punching shear, for instance. By including *nonlinear* properties of concrete and steel, however, this method can predict failure that involves flexural or even membrane force systems. It is of importance to note that the material models used in these analyses can be rather crude. The application of such a two-dimensional model for RC is justified on the grounds that by making the concrete layers thin enough, the variation of stresses and strains across the thickness of the slab can be well accounted for.

A variety of *material models* have been proposed for the use of layered nonlinear analysis of RC slabs. The model of reinforcing steel is usually represented by a uniaxial stress-strain curve, in which the steel is considered an elastic-plastic material. Its stress-strain curve is taken to be identical in tension and compression (Fig. 11.5.4a). The material properties of the concrete can also effectively be approximated by a bilinear stress-strain curve with tensile strength (Fig. 11.5.4b). A common practice is to assume $0.1\sigma_{c,u}$ for its maximum tensile strength. Because of the two-dimensional nature of plate problems, the assumed uniaxial concrete stress-strain curve must be modified to cover the biaxial stress states. For this purpose, one may use the approaches presented in Refs. [11.5.17] and [11.5.18]. An assumed yield surface for biaxial stresses in plain concrete is shown in Fig. 11.5.5.

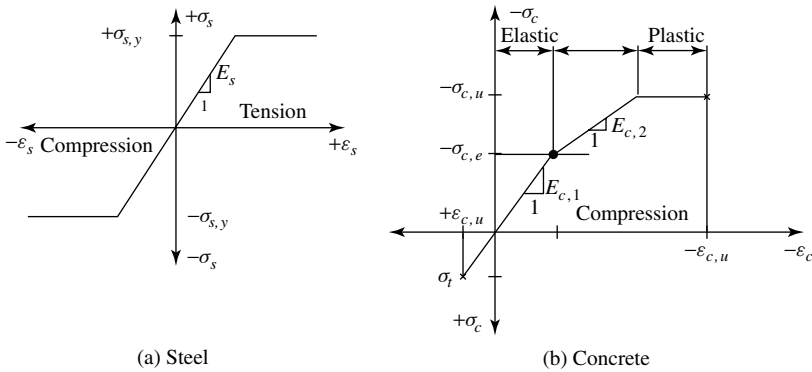


Figure 11.5.4 Assumed stress-strain curves for steel and concrete.

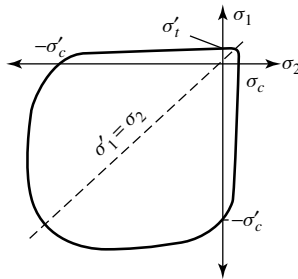


Figure 11.5.5 Yield surface for biaxial stress in concrete.

Considering all the various numerical methods for nonlinear analysis of RC slabs [11.5.1–11.5.4], only the layered plate approach is discussed here briefly, since it offers, if combined with the versatile FEM, the most flexibility in RC slab analysis. For finite elements, one uses mostly relatively simple rectangular, four-node membrane and bending elements.

Under lateral loads, the layers of the RC elements are subjected mainly to membrane stresses. However, due to the eccentric locations of most of these layers, additional bending moments are also activated. Consequently, coupling exists between the in-plane extension and transverse bending. Thus, by developing the membrane stiffness of the elements, these coupling effects must also be considered. By their very nature, the steel layers possess only membrane stiffness. Furthermore, we can assume that the transverse displacements $w(x, y)$ are the same for each layer. To satisfy this requirement, the in-plane displacements are augmented by terms that represent interlayer compatibility. Consequently, for the i th layer we can write [11.5.15]

$$u_i(x, y) = u_{mc}(x, y) \pm \frac{h_c \theta_{xc}(x, y)}{2} \pm \sum_{p=l_1}^{l_2} h_p \theta_{xp}(x, y) \pm \frac{h_i \theta_{xi}(x, y)}{2},$$

$$v_i(x, y) = v_{mc}(x, y) \pm \frac{h_c \theta_{yc}(x, y)}{2} \pm \sum_{p=l_1}^{l_2} h_p \theta_{yp}(x, y) \pm \frac{h_i \theta_{yi}(x, y)}{2},$$
(11.5.1)

where c represents a sequential number of the *central layer* and θ_x and θ_y are rotations of a general point within the i th layer. The thickness of the layers is h_i . The layers should be numbered sequentially starting from the top. With nine layers as shown in Fig. 11.5.6, for instance, where $c = 5$,

$$l_1 = i + 1 \quad \text{and} \quad l_2 = c - 1 \quad \text{for } i = 1, 2, 3, \quad (11.5.2)$$

$$l_1 = c + 1 \quad \text{and} \quad l_2 = i - 1 \quad \text{for } i = 7, 8, 9. \quad (11.5.3)$$

Using a simple rectangular four-node element (Fig. 11.5.7) for the membrane part, we can utilize, for instance, the quadratic displacement functions

$$u_{mc}(x, y) = \alpha_1 + \alpha_2 x + \alpha_3 y + \alpha_4 xy + \alpha_5 y^2,$$

$$v_{mc}(x, y) = \alpha_6 + \alpha_7 x + \alpha_8 y + \alpha_9 xy + \alpha_{10} x^2,$$
(11.5.4)

which yield good convergence characteristics (Fig. 11.5.8).

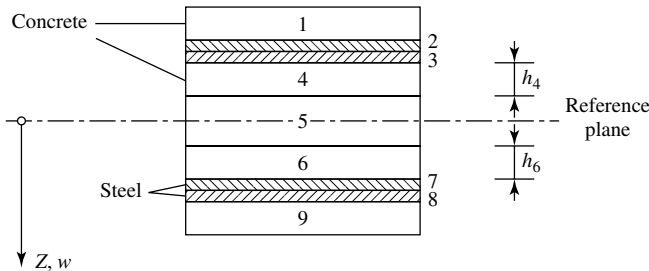


Figure 11.5.6 Laminated section.

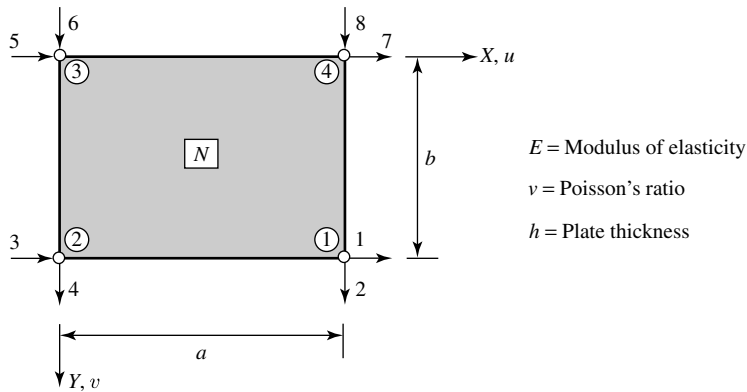


Figure 11.5.7 Finite element for plane stress in concrete.

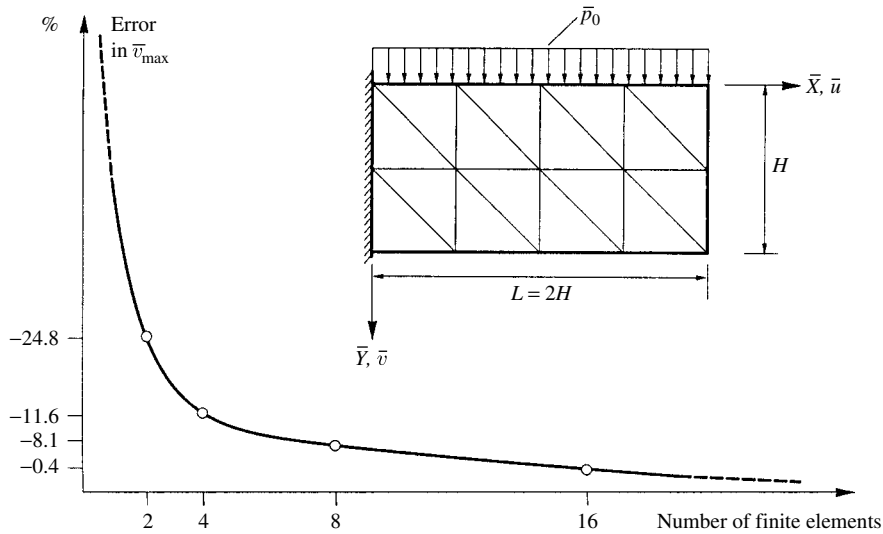


Figure 11.5.8 Convergence characteristics of element shown in Fig. 11.5.7.

Computation of the layer stiffness follows the already introduced standard procedures[†] for finite elements. Consequently, the strain vector for the membrane part considering the i th element becomes

$$\varepsilon_m = \left\{ \begin{array}{c} \frac{\partial u_{mi}}{\partial x} \\ \frac{\partial v_{mi}}{\partial y} \\ \frac{\partial u_{mi}}{\partial y} + \frac{\partial v_{mi}}{\partial x} \end{array} \right\} = \sum_{j=1}^4 \mathbf{D}_{ji}^{(m)} \mathbf{d}_{ej}, \tag{11.5.5}$$

[†] See Secs. 7.1 and 7.2.

where \mathbf{d}_{ej} is the vector of the displacements of the four nodes ($j = 4$) and $\mathbf{D}_{ji}^{(m)}$ represents the strain-displacement matrix obtained from differentiations of the shape functions.

Similarly, we can also select again a simple four-node element for the bending part. Such an element is shown in Fig. 7.6.1. Its convergence characteristics are illustrated in Fig. 7.6.2. The pertinent shape function is given in Eq. (7.6.2). The bending part of the strain vector for the i th layer is

$$\varepsilon_b = \begin{Bmatrix} -\frac{\partial \theta_{xi}}{\partial x} \\ -\frac{\partial \theta_{yi}}{\partial y} \\ -\frac{\partial \theta_{xi}}{\partial y} - \frac{\partial \theta_{yi}}{\partial x} \end{Bmatrix} = \sum_{j=1}^4 \mathbf{D}_{ji}^{(b)} \mathbf{d}_{ej}. \quad (11.5.6)$$

The subscripts and superscripts m and b in Eqs. (11.5.5) and (11.5.6) refer to membrane and bending components, respectively. The stiffness matrix of the elements can be written as

$$\mathbf{K}_{e,i} = \mathbf{K}_{e,i}^{(m)} + \mathbf{K}_{e,i}^{(b)} = \sum_{i=1}^L \iint \mathbf{D}_i^{(m)T} \mathbf{E}_i^{(m)} \mathbf{D}_i^{(m)} dA + \iint \mathbf{D}_i^{(b)T} \mathbf{E}_i^{(b)} \mathbf{D}_i^{(b)} dA, \quad (11.5.7)$$

where L represents the total number of layers per element. The elasticity matrix for the concrete layers is

$$\mathbf{E}_i^{(m)} = \begin{bmatrix} \frac{E_x}{1 - nv_1^2} & \frac{v_1 E_y}{1 - nv_1^2} & 0 \\ \frac{v_1 E_y}{1 - nv_1^2} & \frac{E_y}{n(1 - nv_1^2)} & 0 \\ 0 & 0 & G_{xy} \end{bmatrix}$$

for $n = \frac{E_x}{E_y}$, $v_1 = \sqrt{v_x v_y}$, $G_{xy} = \frac{\sqrt{E_x E_y}}{2(1 + v_1)}$, (11.5.8)

and for the steel layer we can use

$$\mathbf{E}_{s,i}^{(m)} = h_i \begin{bmatrix} E_{st} & 0 & 0 \\ 0 & 0 & 0 \\ 0 & 0 & 0 \end{bmatrix}. \quad (11.5.9)$$

The elasticity matrix for the bending part can be given as

$$\mathbf{E}_i^{(b)} = \begin{bmatrix} D_x & D_1 & 0 \\ D_1 & D_y & 0 \\ 0 & 0 & \sqrt{D_x D_y} \end{bmatrix}, \quad (11.5.10)$$

where the sectional properties D_x and D_1 are already defined in Sec. 10.1.

The reader can find other approaches for the nonlinear analysis of RC slabs using layered finite elements in Refs. [11.5.9] and [11.5.12], respectively.

Using the incremental procedure described in Sec. 11.3, we start with the uncracked sections of the RC slab. By applying an initially small load level $\Delta \mathbf{p}_1$, we compute the corresponding vectors of the displacements $\Delta \mathbf{d}_1$ and stresses $\Delta \boldsymbol{\sigma}_1$. Next, we use, again, a small load increment $\Delta \mathbf{p}_2$. Now the $\mathbf{p}_2 = \Delta \mathbf{p}_1 + \Delta \mathbf{p}_2$ load gives $\mathbf{d}_2 = \Delta \mathbf{d}_1 + \Delta \mathbf{d}_2$ displacements and yields $\boldsymbol{\sigma}_2 = \Delta \boldsymbol{\sigma}_1 + \Delta \boldsymbol{\sigma}_2$ stresses, and so on. If the tensile stress of the concrete exceeds $0.1\sigma_u$, cracks will develop and the stiffness matrix of the elements must be computed using the methods for layered sections described above. As we continue with the incremental loading, the depth of the cracks will increase. Thus, more and more concrete layers will not be able to sustain tensile forces. This situation requires a constant recomputation of the element stiffness matrices corresponding to the actual stress levels in concrete and steel. Needless to say, coding such an incremental procedure is highly complex and consequently time consuming. The same can be said for the computer time required to execute such a nonlinear analysis.

We can considerably simplify the layered-element method described above and still obtain usable *estimates* of the nonlinear behavior of RC slabs. To keep this approach as simple as possible, the lamination of the concrete should be relatively crude and only a limited number of equilibrium iterations between the individual load increments should be carried out. The steps of this simplified approach are as follows:

1. For the small initial load increment, the uncracked concrete section is used. The transverse displacements $w(x, y)$ are computed with the help of the bending stiffness matrix given in Eq. (7.6.12).
2. Step 1 is repeated for the next load increments until the tensile strength of the concrete is reached in one of the outer fibers of the sections. Next, the lateral displacements must be recomputed based on the equivalent transformed sections (Fig. 10.2.3) using the reinforcing steel and the uncracked portion of the concrete. The in-plane displacements u, v of the nodal points corresponding to the individual layers are estimated from their rotations.
3. The corresponding steel and concrete stresses are computed with the help of the matrices given in Fig. 11.5.9.
4. This procedure is repeated, always using the obtained stress levels in concrete and steel in computing the element stiffness and stress matrices.

e. Composite Finite Elements. These finite elements are assemblies of a single concrete plate element and n steel beam elements representing the reinforcing bars [11.5.19]. The rectangular concrete element combines the 8-DOF plane stress element (Fig. 11.5.9) with the 12-DOF nonconforming plate bending element introduced in Sec. 7.6. The steel elements are the commonly used beam column elements with 6 DOF. It is assumed that a perfect bond between concrete and steel exists. This assumption results in the following compatibility equations for a beam element oriented in the X direction:

$$u_s = u_c = e \frac{\partial w_c}{\partial x} \quad \text{and} \quad w_s = w_c, \quad (11.5.11)$$

where e is the distance between the centroidal axis of the beam element and the mid surface of the concrete plate element.

$$Ik_e]^{(N)} = \frac{Eh}{180(1-\nu^2)} \times \begin{bmatrix} 1 & 2 & 3 & 4 & 5 & 6 & 7 & 8 \\ A\beta^{-1} + B\beta & A\beta + B\beta^{-1} & \text{Symmetric} & \beta = \bar{a}/\bar{b} & C = 30 - \frac{30\nu^2}{1-\nu} \\ D & & & A = 60 + \frac{30\nu^2}{1-\nu} & 1 \\ -A\beta^{-1} + B\beta & \bar{E} & A\beta^{-1} + B\beta & & D = 22.5(1+\nu) \\ -\bar{E} & C\beta - B\beta^{-1} & -D & A\beta + B\beta^{-1} & \bar{E} = 22.5(1-3\nu) \\ -C\beta^{-1} - B\beta & -D & C\beta^{-1} - B\beta & \bar{E} & 3 \\ -D & -C\beta - B\beta^{-1} & -\bar{E} & A\beta + B\beta^{-1} & 4 \\ C\beta^{-1} - B\beta & -\bar{E} & -C\beta^{-1} - B\beta & \bar{D} & 5 \\ \bar{E} & -A\beta + B\beta^{-1} & D & -C\beta - B\beta^{-1} & 6 \\ & & & & A\beta^{-1} + B\beta \\ & & & & -D \\ & & & & A\beta + B\beta^{-1} \end{bmatrix}$$

$$\mathbf{S}_e^{(N)} = \frac{E}{1-\nu^2} \begin{bmatrix} 1 & 2 & 3 & 4 & 5 & 6 & 7 & 8 \\ 1/a & \nu/b & -1/a & 0 & 0 & 0 & 0 & -\nu/b \\ \nu/a & 1/b & -\nu/a & 0 & 0 & 0 & 0 & -1/b \\ 0 & \frac{1-\nu}{2a} & \frac{1-\nu}{2b} & -\frac{1-\nu}{2a} & -\frac{1-\nu}{2b} & 0 & 0 & 0 \\ \hline 1/a & 0 & -1/a & \nu/b & 0 & -\nu/b & 0 & 0 \\ \nu/a & 0 & -\nu/a & 1/b & 0 & -1/b & 0 & 0 \\ 0 & \frac{1-\nu}{2a} & \frac{1-\nu}{2b} & -\frac{1-\nu}{2a} & -\frac{1-\nu}{2b} & 0 & 0 & 0 \\ \hline 0 & 0 & 0 & \nu/b & -1/a & -\nu/b & 1/a & 0 \\ 0 & 0 & 0 & 1/b & -\nu/a & 1/b & \nu/a & 0 \\ 0 & 0 & \frac{1-\nu}{2b} & -\frac{1-\nu}{2a} & -\frac{1-\nu}{2b} & -\frac{1-\nu}{2a} & 0 & \frac{1-\nu}{2a} \\ \hline 0 & \nu/b & 0 & 0 & -1/a & 0 & 1/a & -\nu/b \\ 0 & 1/b & 0 & 0 & -\nu/a & 0 & \nu/a & -1/b \\ \frac{1-\nu}{2b} & 0 & 0 & 0 & 0 & -\frac{1-\nu}{2a} & -\frac{1-\nu}{2b} & \frac{1-\nu}{2a} \end{bmatrix} \begin{matrix} \textcircled{1} \\ \textcircled{2} \\ \textcircled{3} \\ \textcircled{4} \end{matrix}$$

Figure 11.5.9 Stiffness and stress matrix of membrane finite element shown in Fig. 11.5.7.

Using this compatibility condition, the stiffness matrix of the steel beam element is transformed from its local coordinate system into the coordinate system X, Y, Z of the plate element by

$$\mathbf{K}'_{e,s} = \mathbf{T}^T \mathbf{K}_{e,s} \mathbf{T}. \quad (11.5.12)$$

In this way, the stiffness matrix of the *composite* finite element becomes simply the assembly of the individual elements. Consequently, we can write

$$\mathbf{K}_{e,\text{comp}} = \mathbf{K}_{e,c} + \sum_{i=1}^n (\mathbf{K}_{e,s})_i, \quad (11.5.13)$$

where n is the total number of reinforcing steel bars.

Based on the composite nature of this element, the corresponding constitutive modeling consists of two parts. For the steel reinforcement, a uniaxial elastic-plastic stress-strain relationship can be used. But modeling the concrete behavior is much more complex, details of which are available in Ref. [11.5.20]. However, a considerable simplification can be achieved by using the previously introduced equivalent bilinear stress-strain relationship for the concrete. In this case, the solution procedure should use an appropriate incremental-iterative approach, discussed in the foregoing section. When the maximum tensile stress of the concrete is reached in the lower fibers, the thickness of the concrete element must be reduced to take care of the already cracked condition of the concrete.

Summary. Reinforced-concrete slabs are, by their very nature, difficult to analyze since they combine two different materials each with nonlinear properties. In addition, the concrete cracks in tension and can crush in compression. Furthermore, the bond between reinforcing steel and concrete can also slip and even fail.

Because of these difficulties, the present design practice is based on the assumptions that the RC slab is uncracked, homogeneous, isotropic and linear-elastic. Using these assumptions, the internal forces are computed either analytically or, nowadays, mostly numerically. The required slab thickness and the amount of reinforcing steel are determined by applying the ultimate strength approach. While such a simple design philosophy may be admissible for small slabs in buildings, larger plate structures such as bridges require more exact considerations of the nonlinear behavior of slabs under static and dynamic loadings.

In recent years, there has been considerable research of the nonlinear analysis of RC slabs. These mostly academic research efforts, however, led to increase in complexity and sophistication of various material models proposed to represent the actual nonlinear behavior of RC slabs. Unfortunately, the results of these researches have little or no impact on current engineering practice. This may be partially due to the directions taken by academic researchers. A simplified *composite* element approach might indicate a direction that can result in development of a numerical method that may be accepted by practicing engineers in their everyday work.

The layered plate element approach combined with the FEM has been discussed here in somewhat more detail, since it offers good accuracy combined with flexibility. For this reason, even some commercially available program systems have already incorporated this solution technique into their finite element program libraries. It is evident that future research is required to simplify the nonlinear analysis of RC slabs.

In the meantime, the yield-line method[†] in combination with the ultimate load design technique—for determining the required slab thickness and the amount of reinforcing steel—is recommended for the design of smaller RC slabs. Researchers who intend to write their own computer code covering a layered slab analysis, should consult Ref. [11.5.13].

References and Bibliography

- [11.5.1] MEYER, C. (Ed.), *Finite Element Analysis of Reinforced Concrete Structures*, American Society of Civil Engineers, New York, 1985.
- [11.5.2] ASCE TASK COMMITTEE, *Finite Element Analysis of Reinforced Concrete*, American Society of Civil Engineers, New York, 1982.
- [11.5.3] DAMJANIC, F., et al. (Eds.), *Computer-Aided Analysis and Design of Concrete Structures*, (Proc. Int. Conf. held in Split, Croatia, Sept. 11–21, 1984), Pineridge Press, Swansea, United Kingdom, 1984.
- [11.5.4] BICANIC, N., et al. (Eds.), *Computer-Aided Analysis and Design of Concrete Structures*, Pineridge Press, Swansea, United Kingdom, 1990.
- [11.5.5] GOSZCZYNSKI, S., and MUCHA, J., “Computer Nonlinear Analysis of Reinforced Concrete Beams and Slabs,” in J. Damjanic et al. (Eds.), *Computer-Aided Analysis and Design of Concrete Structures*, Pineridge Press, Swansea, United Kingdom, 1984, pp. 1355–1368.
- [11.5.6] NGO, D., and SCORDELIS, A. C., “Finite Element Analysis of Reinforced Concrete Beams,” *ACI J.*, **64** (1967), 152–163.
- [11.5.7] SCORDELIS, A. C., “Finite Element Analysis of Reinforced Concrete Structures,” in *Proceedings of the Speciality Conference on Finite Element Methods in Civil Engineering*, J. O. McCutcheon et al. (Eds.), Engineering Institute of Canada, Montreal, Quebec, Canada, 1972, pp. 711–714.
- [11.5.8] SCHNOBRICH, W. C., and SUIDAN, M. “Finite Element Analysis of Reinforced Concrete,” *Struct. Div., ASCE*, **99**(1973), 2109–2121.
- [11.5.9] MELHORN, G., and KOLLEGER, J., “Anwendung der finite Elemente Methode im Stahlbetonbau,” in G. Melhorn (Ed.), *Ingenieurbau: Rechenorientierte Baumechanik*, Ernst & Sohn, Berlin, 1995.
- [11.5.10] LIN, C. S., *Nonlinear Analysis of Reinforced Concrete Slabs*, University of California, Berkeley, 1973.
- [11.5.11] AVRAN, C., et al., *Numerical Analysis of Reinforced Concrete Structures*, Elsevier, Amsterdam, 1993.
- [11.5.12] DEBORST, R., and NAUTA, P., “Non-orthogonal Cracks in a Smeared Finite Element Model,” *Eng. Comp.*, **2** (1985), 35–46.
- [11.5.13] PASTOR, B., “Computer Code Implementation of a Linear Triangular Plate Bending Element,” M.Sc. Thesis, University College of Swansea, United Kingdom, Oct. 1989.
- [11.5.14] HAND F. R., et al., “Nonlinear Layered Analysis of Reinforced Concrete Plates and Shells,” *J. Struct. Div., ASCE*, **99** (1973), 1491–1505.
- [11.5.15] KANKAM, J. A., and DAGHER, H. J., “Nonlinear Finite Element Analysis of RC Skew Bridges,” *J. Struct. Div., ASCE*, **121** (1995), 1338–1345.
- [11.5.16] COPE, R. J., et al., “Modelling of RC Behavior for Finite Element Analysis of Bridge Slabs,” in *Numerical Methods for Nonlinear Problems*, Vol. 1, Pineridge Press, Swansea, United Kingdom, C. Taylor et al. (Eds.), 1980, pp. 457–470.
- [11.5.17] KUPFER, H., et al., “Behavior of Concrete under Biaxial Stress,” *ACI J.*, **66** (1969), 656–666.
- [11.5.18] VECCHIO, F. J., and COLLINS, M. P., *The Response of Reinforced Concrete to In-plane Shear and Normal Stresses*, Publ. No. 82–03, University of Toronto, Toronto, Canada, 1982.

[†] See Chapter 13.

- [11.5.19] JIANG, J., and MIRZA, F. A., "Nonlinear Analysis of Reinforced Concrete Slabs by Discrete Finite Element Approach," *Comp. Struct.*, 65 (1997), 585–592.
- [11.5.20] JIANG, J., "Modelling the Mechanical Behavior of Concrete Structures," Ph.D. Dissertation, McMaster University, Hamilton, Canada, 1988.

11.6 Summary and Conclusions

This chapter has presented a compilation of analysis procedures related to the solution of nonlinear plate problems the reader may encounter in engineering practice. Because of the inherently complex nature of such problems, we concentrated almost exclusively on numerical methods in general and the corresponding application of the FEM in particular. Despite the significant progress already made in the development of suitable analysis procedures, accurate prediction of the overall deformation characteristics of plates subjected to geometrical and material nonlinearities still remains a difficult task. This is due mainly to the fact that to accurately model the mathematical behavior of such plates is extremely difficult or even impossible. Of the many possible nonlinear effects, the two most important nonlinearities represented by large deflections and nonlinear material behaviors have been presented here. To limit the size of the book, however, only the algorithmic paths of recommended solution procedures were given, without going into such details as actual computer programming. That is, in many cases this material is provided in commercially available larger program systems. Therefore, the presentation has consisted primarily of discussing the fundamentals to furnish readers with sufficient background either to use such computer programs intelligently or to be able to develop their own program system. In the latter case, however, one must consider that the required coding efforts can be quite excessive and time consuming.

Problems[†]

- 11.1.1 Redo the Illustrative Example of Sec. 11.1 by using Ritz's energy method.
- 11.2.1 Develop a correction factor C to improve the results of finite difference solutions of large-deflection analysis of plates.
- 11.2.2 Solve the Illustrative Example in Sec. 11.1 using the ordinary FDM.
- 11.3.1 Develop a computer program for large-deflection analysis of plates using the ordinary FDM and the incremental procedure. Assume a simply supported square plate. Use your favorite programming language.

[†] The first two numbers refer to the corresponding section.

Part IV

Engineering Solution Procedures

12

Practical Design Methods

12.1 Need for Engineering Solution Procedures

The solution of plate problems via the classical route, as shown in Part I, is limited to simple geometry, load and boundary conditions. If these conditions are not satisfied, the classical analysis becomes increasingly complex or even impossible. In such cases numerical methods, introduced in Parts II and III, must be used to obtain reliable results concerning the behavior of plates subjected to various types of static loads.

By employing numerical methods in plate analysis, however, the analyst must have *ab ovo* the plate thickness as an input. This can be satisfactorily *estimated* by using simple engineering solution techniques. Furthermore, after a solution is obtained, utilizing either classical or numerical procedures, the analyst must *validate* the results by means of an *independent check*. Usually, numerical solutions are either acceptable or entirely “out-of-bounds.” To detect the latter case, again, simple engineering methods can be employed. In addition, in many cases *alternative* design schemes must be evaluated before a final selection of the type of structural system to be used in the actual design can be made. Engineering solution methods permit such comparative preliminary design evaluations economically.

In engineering applications of the theory of plates, we are usually dealing with *inaccurate input data*. In the first place, the external loads are known only with a certain degree of accuracy. Next, the material properties, such as the modulus of elasticity E and Poisson’s ratio ν , contain considerable inaccuracies. Furthermore, the actual boundary conditions of plate structures are merely an approximation of the theoretical ones. Additional sources of errors in numerical computations are roundoff and truncation errors, to name a few. Finally, in all types of computations *human errors* may also be present. Consequently, even “exact” analytical solutions are merely approximations of the actual plate behavior under static loading.

Last, but not least, the *economy* of computational procedures must always be considered. That is, for reasons of various error sources inherent in all computations, as discussed above, a method that yields the required results in an economical way but has $\pm 10\%$ error of calculation is almost invariably selected over a more exact approach. Plate analysis using engineering methods can always be accomplished by “long-hand” computations in a relatively short time. Thus, these practical design methods do not require either computers or pertinent software. Furthermore, there

are some simple plate structures, such as two-way floor slabs in buildings, that can be analyzed quite effectively by employing one of the methods introduced in this chapter. In addition, when a *lower-bound* engineering solution is checked by an *upper-bound* practical solution technique, such as the work method of yield-line analysis,[†] the average of the results obtained yields quite acceptable solutions for all engineering purposes.

12.2 Elastic Web Analogy for Continuous Plate Systems

The oldest engineering approach for analyzing continuous plate systems was introduced by Marcus [12.2.1]. The plate system was considered by him as an *elastic web* (*elastische Gewebe*) consisting of *plate strips* located at midspans of the individual plates. Application of this approach is limited to uniformly (per-panel) distributed lateral loads and to aspect ratios l_x/l_y given in the tables. Furthermore, sizes of the neighboring panels should not vary more than approximately 50%.

Let us consider, first, two simply supported plate strips, as shown in Fig. 12.2.1. It is evident that the center deflection of these two connected strips must be equal; thus

$$(w_x)_{l_x/2} = (w_y)_{l_y/2} = \frac{5}{384} \frac{p_1 l_x^4}{D_x} = \frac{5}{384} \frac{p_2 l_y^4}{D_y}. \quad (12.2.1)$$

Furthermore,

$$p_0 = p_1 + p_2 \quad \text{and} \quad D_x = D_y = D; \quad (12.2.2)$$

hence, from the total lateral load p_0 , we can assign

$$p_1 = \frac{l_y^4}{l_x^4 + l_y^4} p_0 \quad \text{and} \quad p_2 = \frac{l_x^4}{l_x^4 + l_y^4} p_0 \quad (12.2.3)$$

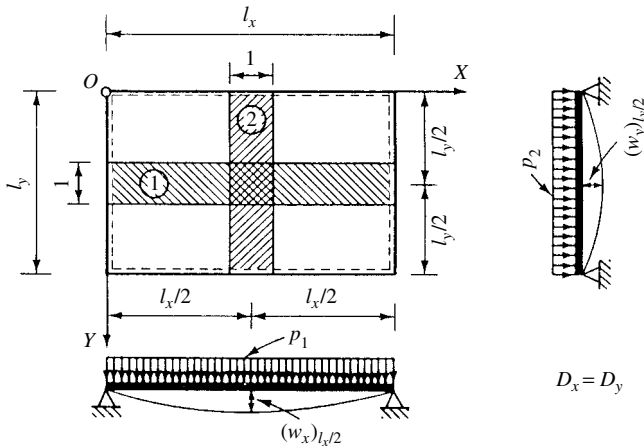


Figure 12.2.1 Equivalent plate strips.

[†] See Sec. 13.2.

to the plate strips in the X and Y directions, respectively. Equation (12.2.3), written in more general form, becomes

$$p_1 = \kappa p_0, \quad p_2 = \rho p_0, \quad (12.2.4)$$

where

$$\kappa = \frac{c_y l_y^4}{c_x l_x^4 + c_y l_y^4} \quad \text{and} \quad \rho = 1 - \kappa. \quad (12.2.5)$$

In Eq. (12.2.5) c_x and c_y represent correction factors, the values of which depend on the boundary conditions. These coefficients are easily obtained from the deflection ordinates of beams at $l_x/2$ and $l_y/2$ and are shown in Fig. 12.2.2.

As mentioned earlier, the fundamental difference between the structural behavior of an open gridwork and that of a plate is the presence of transverse shear forces along the edges of the plate strips. These shear forces, caused by the continuity between individual plate strips, produce torsional resistance, which in turn reduces the deflections of the substitute gridwork. By considering the effect of the torsional resistance of the plate, Marcus [12.2.1] obtained the following approximate expressions[†] for the maximum positive moments:

$$m_x = m'_x \left[1 - \frac{5}{6} (\varepsilon^*)^2 \frac{m'_x}{M_x} \right] = \alpha p_0 l_x^2 \quad (12.2.6)$$

and

$$m_y = m'_y \left[1 - \frac{5}{6} \varepsilon^2 \frac{m'_y}{M_y} \right] = \beta p_0 l_y^2, \quad (12.2.7)$$

where $\varepsilon^* = l_x/l_y$ and $\varepsilon = l_y/l_x$. Furthermore, m'_x and m'_y denote the positive moments of the plate strips at the center ($l_x/2, l_y/2$), while

$$M_x = \frac{1}{8} p_0 l_x^2 \quad \text{and} \quad M_y = \frac{1}{8} p_0 l_y^2 \quad (12.2.8)$$

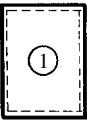

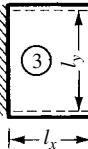
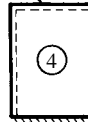
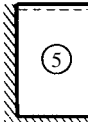
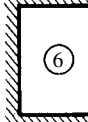
Case						
κ	$\frac{l_y^4}{l_x^4 + l_y^4}$	$\frac{5l_y^4}{2l_x^4 + 5l_y^4}$	$\frac{5l_y^4}{l_x^4 + 5l_y^4}$	$\frac{l_y^4}{l_x^4 + l_y^4}$	$\frac{2l_y^4}{l_x^4 + 2l_y^4}$	$\frac{l_y^4}{l_x^4 + l_y^4}$
ρ	$1 - \kappa$	$1 - \kappa$	$1 - \kappa$	$1 - \kappa$	$1 - \kappa$	$1 - \kappa$

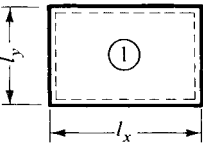
Figure 12.2.2 Typical cases.

[†] For $\nu = \frac{1}{6}$.

represent the maximum moments of simply supported beams subjected to the total load p_0 .

The coefficients α , β , κ and ρ for various span ratios and boundary conditions have been calculated by Löser [12.2.2] and are given in Table 12.2.1a–f.† Figure 12.2.2 illustrates the six possible combinations of fixed and simply supported boundary conditions. Stencils for compilation of these exterior and interior panels into various

Table 12.2.1 Bending Moments

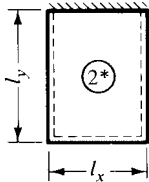
a. Case ①					Moments at center of plate:				
					$m_{x,\max} = +\alpha_1 p_0 l_x^2$ $m_{y,\max} = +\beta_1 p_0 l_y^2$ $p_0 = \text{const}$				
$\varepsilon = l_y : l_x$	α_1	β_1	κ_1	ρ_1	$\varepsilon = l_y : l_x$	α_1	β_1	κ_1	ρ_1
1	2	3	4	5	6	7	8	9	10
0.60	0.01053	0.08127	0.1147	0.8853	1.00	0.03646	0.03646	0.5000	0.5000
0.62	0.01160	0.07851	0.1287	0.8713	1.02	0.03792	0.03503	0.5198	0.4802
0.64	0.01271	0.07575	0.1437	0.8563	1.04	0.03940	0.03368	0.5391	0.4609
0.66	0.01385	0.07301	0.1595	0.8405	1.06	0.04088	0.03238	0.5580	0.4420
0.68	0.01503	0.07029	0.1761	0.8239	1.08	0.04238	0.03115	0.5764	0.4236
0.70	0.01623	0.06761	0.1936	0.8064	1.10	0.04388	0.02997	0.5942	0.4058
0.72	0.01746	0.06497	0.2118	0.7882	1.12	0.04538	0.02884	0.6114	0.3886
0.74	0.01871	0.06240	0.2307	0.7693	1.14	0.04689	0.02776	0.6281	0.3719
0.76	0.01998	0.05990	0.2502	0.7498	1.16	0.04840	0.02673	0.6442	0.3558
0.78	0.02127	0.05747	0.2702	0.7298	1.18	0.04990	0.02574	0.6597	0.3403
0.80	0.02258	0.05512	0.2906	0.7094	1.20	0.05141	0.02479	0.6746	0.3254
0.82	0.02390	0.05286	0.3113	0.6887	1.24	0.05439	0.02300	0.7028	0.2972
0.84	0.02524	0.05069	0.3324	0.6676	1.28	0.05732	0.02135	0.7286	0.2714
0.86	0.02659	0.04861	0.3536	0.6464	1.32	0.06020	0.01983	0.7522	0.2478
0.88	0.02796	0.04662	0.3749	0.6251	1.36	0.06300	0.01842	0.7738	0.2262
0.90	0.02934	0.04471	0.3962	0.6038	1.40	0.06572	0.01711	0.7935	0.2065
0.92	0.03073	0.04290	0.4174	0.5826	1.44	0.06835	0.01589	0.8113	0.1887
0.94	0.03214	0.04117	0.4384	0.5616	1.48	0.07087	0.01477	0.8275	0.1725
0.96	0.03357	0.03952	0.4593	0.5407	1.54	0.07447	0.01324	0.8490	0.1510
0.98	0.03501	0.03795	0.4798	0.5202	1.62	0.07889	0.01145	0.8732	0.1268

b. Case ②					Moments at center of plate:				
					$$m_{x,\max} = +\alpha_2 p_0 l_x^2$$ $$m_{y,\max} = +\beta_2 p_0 l_y^2$$				
					Edge moment:				
					$$M_x = -\frac{1}{8}\kappa_2 p_0 l_x^2$$ $$p_0 = \text{const}$$				
$\varepsilon = l_y : l_x$	α_2	β_2	κ_2	ρ_2	$\varepsilon = l_y : l_x$	α_2	β_2	κ_2	ρ_2
1	2	3	4	5	6	7	8	9	10
0.60	0.01172	0.07302	0.2447	0.7553	1.00	0.03341	0.02721	0.7143	0.2857
0.62	0.01273	0.06993	0.2698	0.7302	1.02	0.03445	0.02584	0.7302	0.2698
0.64	0.01375	0.06689	0.2955	0.7045	1.04	0.03547	0.02453	0.7452	0.2548
0.66	0.01479	0.06391	0.3217	0.6783	1.06	0.03648	0.02330	0.7594	0.2406

† For span ratios between the values given, the coefficients can be obtained by linear interpolation.

Table 12.2.1 (continued)

$\varepsilon = l_y : l_x$	α_2	β_2	κ_2	ρ_2	$\varepsilon = l_y : l_x$	α_2	β_2	κ_2	ρ_2
0.68	0.01584	0.06100	0.3483	0.6517	1.08	0.03746	0.02213	0.7728	0.2272
0.70	0.01691	0.05818	0.3751	0.6249	1.10	0.03842	0.02102	0.7854	0.2146
0.72	0.01799	0.05545	0.4019	0.5981	1.12	0.03936	0.01997	0.7973	0.2027
0.74	0.01908	0.05281	0.4285	0.5715	1.14	0.04027	0.01897	0.8085	0.1915
0.76	0.02017	0.05027	0.4548	0.5452	1.16	0.04116	0.01803	0.8191	0.1809
0.78	0.02128	0.04783	0.4806	0.5194	1.18	0.04202	0.01714	0.8290	0.1710
0.80	0.02239	0.04548	0.5059	0.4941	1.20	0.04286	0.01629	0.8383	0.1617
0.82	0.02351	0.04324	0.5306	0.4694	1.24	0.04446	0.01473	0.8553	0.1447
0.84	0.02463	0.04110	0.5545	0.4455	1.28	0.04595	0.01334	0.8703	0.1297
0.86	0.02574	0.03905	0.5776	0.4224	1.32	0.04736	0.01209	0.8836	0.1164
0.88	0.02686	0.03710	0.5999	0.4001	1.36	0.04867	0.01097	0.8953	0.1047
0.90	0.02798	0.03524	0.6212	0.3788	1.40	0.04989	0.00997	0.9057	0.0943
0.92	0.02908	0.03347	0.6417	0.3583	1.44	0.05102	0.00907	0.9149	0.0851
0.94	0.03018	0.03178	0.6612	0.3388	1.48	0.05208	0.00827	0.9230	0.0770
0.96	0.03127	0.03018	0.6798	0.3202	1.54	0.05353	0.00721	0.9336	0.0664
0.98	0.03235	0.02866	0.6975	0.3025	1.62	0.05526	0.00604	0.9451	0.0549
$\varepsilon^* = l_x : l_y$	β_2^*	α_2^*	ρ_2^*	κ_2^*	$\varepsilon^* = l_x : l_y$	β_2^*	α_2^*	ρ_2^*	κ_2^*



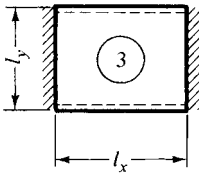
Notes:

For case (2)* use values marked with asterisk:

$$m_{x,\max}^* = +\alpha_2^* p_0 l_x^2 \quad M_y^* = -\frac{1}{8} \rho_2^* p_0 l_y^2$$

$$m_{y,\max}^* = +\beta_2^* p_0 l_y^2$$

c. Case (3)



Moments at center of plate:

$$m_{x,\max} = +\alpha_3 p_0 l_x^2$$

$$m_{y,\max} = +\beta_3 p_0 l_y^2$$

Edge moments:

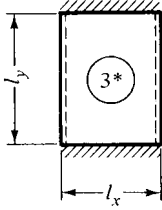
$$M_x = -\frac{1}{12} \kappa_3 p_0 l_x^2$$

$$p_0 = \text{const}$$

$\varepsilon = l_y : l_x$	α_3	β_3	κ_3	ρ_3	$\varepsilon = l_y : l_x$	α_3	β_3	κ_3	ρ_3
1	2	3	4	5	6	7	8	9	10
0.60	0.01141	0.06204	0.3932	0.6068	1.00	0.02668	0.01794	0.8333	0.1667
0.62	0.01227	0.05864	0.4249	0.5751	1.02	0.02734	0.01686	0.8440	0.1560
0.64	0.01313	0.05536	0.4562	0.5438	1.04	0.02778	0.01585	0.8540	0.1460
0.66	0.01399	0.05219	0.4868	0.5132	1.06	0.02829	0.01490	0.8632	0.1368
0.68	0.01485	0.04916	0.5167	0.4833	1.08	0.02878	0.01402	0.8718	0.1282
0.70	0.01570	0.04626	0.5456	0.4544	1.10	0.02925	0.01320	0.8798	0.1202
0.72	0.01655	0.04350	0.5733	0.4267	1.12	0.02970	0.01243	0.8872	0.1128
0.74	0.01739	0.04088	0.5999	0.4001	1.14	0.03013	0.01172	0.8941	0.1059
0.76	0.01822	0.03840	0.6252	0.3748	1.16	0.03035	0.01105	0.9005	0.0995
0.78	0.01903	0.03605	0.6492	0.3508	1.18	0.03094	0.01042	0.9065	0.0935
0.80	0.01983	0.03383	0.6719	0.3281	1.20	0.03131	0.00983	0.9120	0.0880
0.82	0.02061	0.03175	0.6933	0.3067	1.24	0.03202	0.00877	0.9220	0.0780
0.84	0.02138	0.02979	0.7134	0.2866	1.28	0.03266	0.00785	0.9307	0.0693
0.86	0.02212	0.02794	0.7323	0.2677	1.32	0.03324	0.00703	0.9382	0.0618
0.88	0.02284	0.02621	0.7499	0.2501	1.36	0.03378	0.00632	0.9448	0.0552
0.90	0.02354	0.02460	0.7664	0.2336	1.40	0.03427	0.00569	0.9505	0.0495
0.92	0.02422	0.02308	0.7817	0.2183	1.44	0.03472	0.00513	0.9556	0.0444

Table 12.2.1 (continued)

$\varepsilon = l_y : l_x$	α_3	β_3	κ_3	ρ_3	$\varepsilon = l_y : l_x$	α_3	β_3	κ_3	ρ_3
0.94	0.02487	0.02166	0.7971	0.2039	1.48	0.03513	0.00464	0.9600	0.0400
0.96	0.02550	0.02034	0.8094	0.1906	1.54	0.03568	0.00400	0.9657	0.0343
0.98	0.02610	0.01910	0.8218	0.1782	1.62	0.03633	0.00331	0.9718	0.0282
$\varepsilon^* = l_x : l_y$	β_3^*	α_3^*	ρ_3^*	κ_3^*	$\varepsilon^* = l_x : l_y$	β_3^*	α_3^*	ρ_3^*	κ_3^*



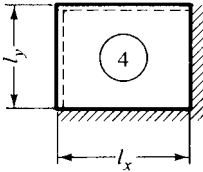
Notes:

For Case (3)* use values marked with asterisk:

$$m_{x,\max} = +\alpha_3^* p_0 l_x^2 \quad M_y = -\frac{1}{12} \rho_3^* p_0 l_y^2$$

$$m_{y,\max} = +\beta_3^* p_0 l_y^2$$

d. Case (4)



Moments at center of plate:

$$m_{x,\max} = +\alpha_4 p_0 l_x^2$$

$$m_{y,\max} = +\beta_4 p_0 l_y^2$$

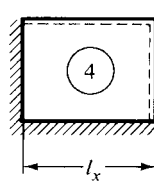
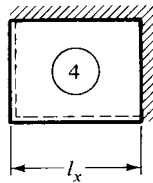
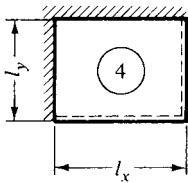
Edge moments:

$$M_x = -\frac{1}{8} \kappa_4 p_0 l_x^2$$

$$M_y = -\frac{1}{8} \rho_4 p_0 l_y^2$$

$$p_0 = \text{const}$$

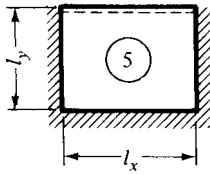
$\varepsilon = l_y : l_x$	α_4	β_4	κ_4	ρ_4	$\varepsilon = l_y : l_x$	α_4	β_4	κ_4	ρ_4
1	2	3	4	5	6	7	8	9	10
0.60	0.00686	0.05295	0.1147	0.8853	1.00	0.02692	0.02692	0.5000	0.5000
0.62	0.00763	0.05164	0.1287	0.8713	1.02	0.02799	0.02586	0.5198	0.4802
0.64	0.00844	0.05031	0.1437	0.8563	1.04	0.02905	0.02483	0.5391	0.4609
0.66	0.00929	0.04895	0.1595	0.8405	1.06	0.03010	0.02384	0.5580	0.4420
0.68	0.01017	0.04758	0.1761	0.8239	1.08	0.03114	0.02289	0.5764	0.4236
0.70	0.01109	0.04620	0.1936	0.8064	1.10	0.03216	0.02197	0.5942	0.4058
0.72	0.01204	0.04480	0.2118	0.7882	1.12	0.03317	0.02108	0.6114	0.3886
0.74	0.01302	0.04341	0.2307	0.7693	1.14	0.03416	0.02022	0.6281	0.3719
0.76	0.01402	0.04202	0.2502	0.7498	1.16	0.03513	0.01940	0.6442	0.3558
0.78	0.01504	0.04063	0.2702	0.7298	1.18	0.03608	0.01861	0.6597	0.3403
0.80	0.01608	0.03926	0.2906	0.7094	1.20	0.03702	0.01785	0.6746	0.3254
0.82	0.01714	0.03791	0.3113	0.6887	1.24	0.03883	0.01642	0.7028	0.2972
0.84	0.01821	0.03658	0.3324	0.6676	1.28	0.04055	0.01511	0.7286	0.2714
0.86	0.01929	0.03526	0.3536	0.6464	1.32	0.04219	0.01390	0.7522	0.2478
0.88	0.02038	0.03398	0.3749	0.6251	1.36	0.04374	0.01278	0.7738	0.2262
0.90	0.02147	0.03272	0.3962	0.6038	1.40	0.04520	0.01177	0.7935	0.2065
0.92	0.02256	0.03150	0.4174	0.5826	1.44	0.04658	0.01083	0.8113	0.1887
0.94	0.02366	0.03030	0.4384	0.5616	1.48	0.04788	0.00998	0.8275	0.1725
0.96	0.02475	0.02914	0.4593	0.5407	1.54	0.04968	0.00883	0.8490	0.1510
0.98	0.02584	0.02801	0.4798	0.5202	1.62	0.05182	0.00752	0.8732	0.1268



Note: The cases at the bottom are identical to the one shown at the top.

Table 12.2.1 (continued)

e. Case ⑤



Moments at center of plate:

$$m_{x,\max} = +\alpha_5 p_0 l_x^2$$

$$m_{y,\max} = +\beta_5 p_0 l_y^2$$

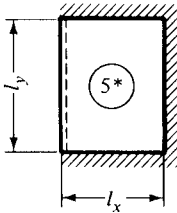
Edge moments:

$$M_x = -\frac{1}{12} \kappa_5 p_0 l_x^2$$

$$M_y = -\frac{1}{8} \rho_5 p_0 l_y^2$$

$$p_0 = \text{const}$$

$\varepsilon = l_y : l_x$	α_5	β_5	κ_5	ρ_5	$\varepsilon = l_y : l_x$	α_5	β_5	κ_5	ρ_5
1	2	3	4	5	6	7	8	9	10
0.60	0.00722	0.04835	0.2059	0.7941	1.00	0.02263	0.01977	0.6667	0.3333
0.62	0.00794	0.04672	0.2282	0.7718	1.02	0.02329	0.01879	0.6840	0.3160
0.64	0.00869	0.04507	0.2513	0.7487	1.04	0.02394	0.01786	0.7006	0.2994
0.66	0.00945	0.04342	0.2751	0.7249	1.06	0.02456	0.01696	0.7164	0.2836
0.68	0.01023	0.04177	0.2995	0.7005	1.08	0.02516	0.01612	0.7313	0.2687
0.70	0.01103	0.04013	0.3244	0.6756	1.10	0.02574	0.01532	0.7454	0.2546
0.72	0.01184	0.03850	0.3496	0.6504	1.12	0.02631	0.01455	0.7589	0.2411
0.74	0.01265	0.03690	0.3749	0.6251	1.14	0.02685	0.01382	0.7716	0.2284
0.76	0.01347	0.03532	0.4002	0.5998	1.16	0.02737	0.01314	0.7836	0.2164
0.78	0.01428	0.03378	0.4254	0.5746	1.18	0.02788	0.01248	0.7950	0.2050
0.80	0.01509	0.03228	0.4503	0.5497	1.20	0.02835	0.01187	0.8057	0.1943
0.82	0.01590	0.03081	0.4749	0.5251	1.24	0.02926	0.01073	0.8254	0.1746
0.84	0.01670	0.02939	0.4989	0.5011	1.28	0.03010	0.00971	0.8430	0.1570
0.86	0.01750	0.02802	0.5225	0.4775	1.32	0.03088	0.00879	0.8586	0.1414
0.88	0.01828	0.02669	0.5453	0.4547	1.36	0.03159	0.00797	0.8725	0.1275
0.90	0.01905	0.02541	0.5675	0.4325	1.40	0.03224	0.00724	0.8848	0.1152
0.92	0.01980	0.02419	0.5890	0.4110	1.44	0.03285	0.00658	0.8958	0.1042
0.94	0.02053	0.02301	0.6096	0.3904	1.48	0.03340	0.00599	0.9056	0.0944
0.96	0.02125	0.02188	0.6295	0.3705	1.54	0.03415	0.00522	0.9184	0.0816
0.98	0.02195	0.02080	0.6485	0.3515	1.62	0.03501	0.00436	0.9323	0.0677
$\varepsilon^* = l_x : l_y$	β_5^*	α_5^*	ρ_5^*	κ_5^*	$\varepsilon^* = l_x : l_y$	β_5^*	α_5^*	ρ_5^*	κ_5^*



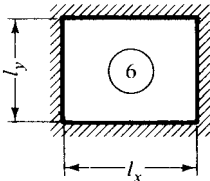
Notes:

For Case ⑤* use values marked with asterisk:

$$m_{x,\max}^* = +\alpha_5^* p_0 l_x^2 \quad M_x^* = -\frac{1}{8} \kappa_5^* p_0 l_x^2$$

$$m_{y,\max}^* = +\beta_5^* p_0 l_y^2 \quad M_y^* = -\frac{1}{12} \rho_5^* p_0 l_y^2$$

f. Case ⑥



Moments at center of plate:

$$m_{x,\max} = +\alpha_6 p_0 l_x^2$$

$$m_{y,\max} = +\beta_6 p_0 l_y^2$$

Edge moments:

$$M_x = -\frac{1}{12} \kappa_6 p_0 l_x^2$$

$$M_y = -\frac{1}{12} \rho_6 p_0 l_y^2$$

$$p_0 = \text{const}$$

$\varepsilon = l_y : l_x$	α_6	β_6	κ_6	ρ_6	$\varepsilon = l_y : l_x$	α_6	β_6	κ_6	ρ_6
1	2	3	4	5	6	7	8	9	10
0.60	0.00436	0.03362	0.1147	0.8853	1.00	0.01794	0.01794	0.5000	0.5000

Table 12.2.1 (continued)

$\varepsilon = l_y : l_x$	α_6	β_6	κ_6	ρ_6	$\varepsilon = l_y : l_x$	α_6	β_6	κ_6	ρ_6
0.62	0.00486	0.03295	0.1287	0.8713	1.02	0.01865	0.01723	0.5198	0.4802
0.64	0.00540	0.03220	0.1437	0.8563	1.04	0.01935	0.01654	0.5391	0.4609
0.66	0.00597	0.03146	0.1595	0.8405	1.06	0.02004	0.01588	0.5580	0.4420
0.68	0.00656	0.03069	0.1761	0.8239	1.08	0.02072	0.01523	0.5764	0.4236
0.70	0.00718	0.02991	0.1936	0.8064	1.10	0.02138	0.01460	0.5942	0.4058
0.72	0.00782	0.02911	0.2118	0.7882	1.12	0.02203	0.01400	0.6114	0.3886
0.74	0.00849	0.02830	0.2307	0.7693	1.14	0.02266	0.01341	0.6281	0.3719
0.76	0.00917	0.02748	0.2502	0.7498	1.16	0.02327	0.01285	0.6442	0.3558
0.78	0.00987	0.02666	0.2702	0.7298	1.18	0.02387	0.01231	0.6597	0.3403
0.80	0.01058	0.02583	0.2906	0.7094	1.20	0.02445	0.01179	0.6746	0.3254
0.82	0.01130	0.02500	0.3113	0.6887	1.24	0.02556	0.01081	0.7028	0.2972
0.84	0.01204	0.02418	0.3324	0.6676	1.28	0.02661	0.00991	0.7286	0.2714
0.86	0.01278	0.02336	0.3536	0.6464	1.32	0.02758	0.00909	0.7522	0.2478
0.88	0.01352	0.02254	0.3749	0.6251	1.36	0.02849	0.00833	0.7738	0.2262
0.90	0.01426	0.02174	0.3962	0.6038	1.40	0.02934	0.00764	0.7935	0.2065
0.92	0.01501	0.02095	0.4174	0.5826	1.44	0.03013	0.00701	0.8113	0.1887
0.94	0.01575	0.02017	0.4384	0.5616	1.48	0.03086	0.00643	0.8275	0.1725
0.96	0.01649	0.01941	0.4593	0.5407	1.54	0.03186	0.00566	0.8490	0.1510
0.98	0.01722	0.01867	0.4798	0.5202	1.62	0.03302	0.00479	0.8732	0.1268

arrangements of continuous plates are shown in Fig. 12.2.3. If one or more exterior boundaries are clamped, the pertinent stencils should be changed logically by applying suitable exterior panels with fixed boundaries. For the cases marked by an asterisk, the X and Y directions should be interchanged.

The negative moments above the intermediate supports are calculated from

$$M_x = -\frac{1}{k}\kappa p_0 l_x^2 \quad \text{and} \quad M_y = -\frac{1}{k}\rho p_0 l_y^2, \quad (12.2.9)$$

where $k = 8$, provided the slab is continuous only over two spans in the direction under consideration. The use of $k = 10$ and $k = 12$ is recommended for other interior supports, depending on their location (Fig. 12.2.3). The maximum negative moment is obtained by loading the adjoining panels simultaneously with the total dead and live loads: $p_0 = p_{DL} + p_{LL}$. If the negative moment on one side of the support is less than 80% of the moment calculated for the other side, a one-step moment distribution can be applied to distribute this unbalanced moment. In calculating the stiffness coefficients of the individual panels, Table 12.2.1 can be used. In the case of RC slabs, built monolithically with the supporting beams, girders or walls, the reduction of the maximum negative moments by rounding off the peaks (Fig. 12.2.4) may be permitted.

To calculate the maximum positive moments, first, the total load $p_0 = p_{DL} + p_{LL}$ is resolved into two parts:

$$p'_0 = p_{DL} + \frac{1}{2}p_{LL} \quad \text{and} \quad p''_0 = \frac{1}{2}p_{LL}. \quad (12.2.10)$$

Next, all panels are loaded with p'_0 and each alternative panel in a checkerboard fashion with $\pm p''_0$, as shown in Fig. 12.2.5. This checkerboard-type loading pattern should be moved so that the panel under investigation receives $+p''_0$ load (shaded area). For an interior panel the p'_0 loading creates boundary conditions equivalent to those of complete fixity at the support above which the plate is continuous; consequently, the pertinent cases with fixed boundaries should be used in the calculation.

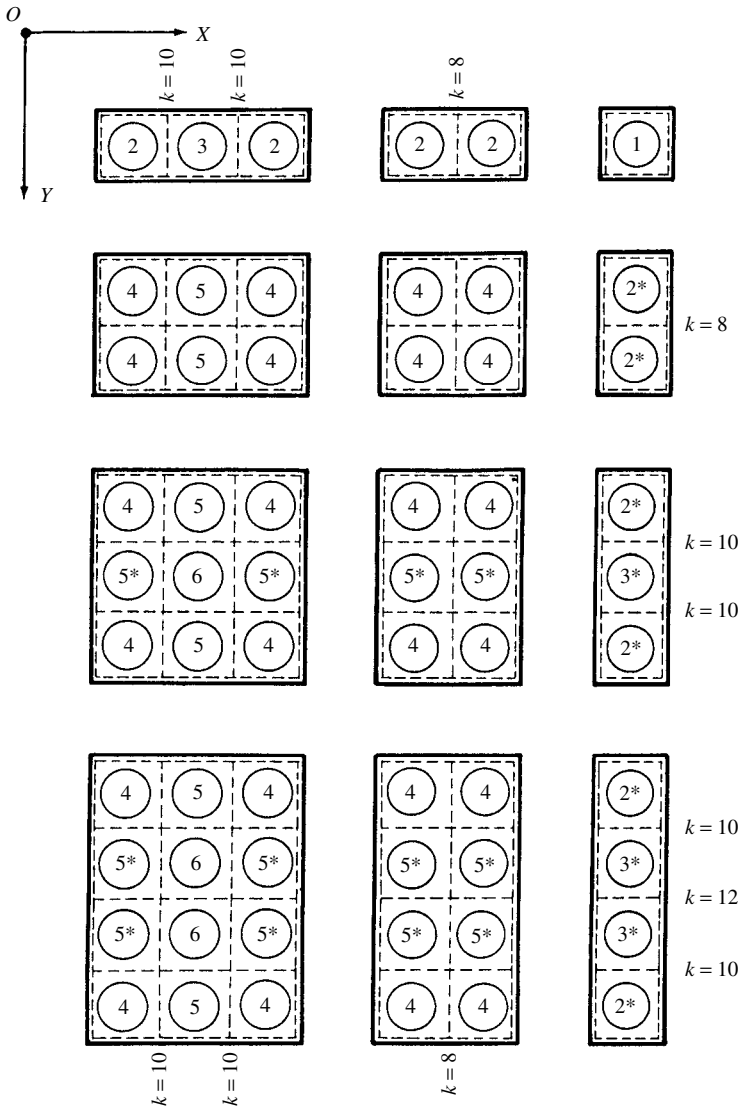


Figure 12.2.3 Stencils for continuous slabs.

On the other hand, the antisymmetric part of the loading ($\pm p'_0$) produces hinged boundary conditions; thus case ① should be applied. The maximum and minimum field moments for the individual panels are

$$m_{x,\max} = p'_0 \alpha_{\ominus} l_x^2 + p''_0 \alpha_1 l_x^2, \quad m_{x,\min} = p'_0 \alpha_{\ominus} l_x^2 - p''_0 \alpha_1 l_x^2$$

and

$$m_{y,\max} = p'_0 \beta_{\ominus} l_y^2 + p''_0 \beta_1 l_y^2, \quad m_{y,\min} = p'_0 \beta_{\ominus} l_y^2 - p''_0 \beta_1 l_y^2,$$

(12.2.11)

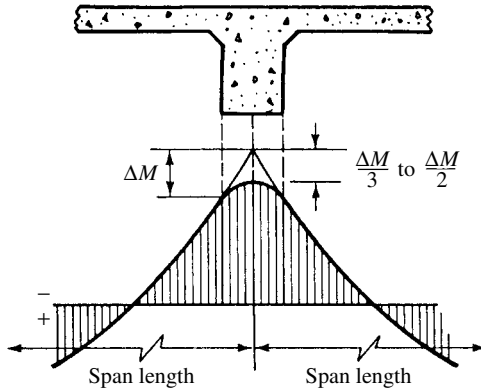


Figure 12.2.4 Reduction of negative moment above wide girder.

where (n) represents the case number (Fig. 12.2.2), assuming complete fixity at the adjoining edges. The results of these two computations are superimposed. By logical application of the technique, shown in Fig. 12.2.6, an approximate moment diagram can be drawn. This moment diagram eliminates one of the inherent weaknesses of the method presented; that is, the locations of the actual maximum positive moments are not always at midspans. In case of doubt, for short spans, the course of the moment diagram between the calculated maximum and minimum points could follow that of an equivalent continuous beam. In addition, Fig. 12.5.3 gives useful approximations for the loads acting on the supporting beams.

Maximum deflections, which sometimes might govern the plate design, can also be *estimated* by Marcus's method. Using Eq. (12.2.4) and the pertinent κ and ρ factors, given in Fig. 12.2.2, usable estimates are obtained from the corresponding beam formulas.

For deflection control of two-way RC slabs, the following formula can be used [12.2.4]:

$$h_{\min} = l_{n1} K_1 K_2 K_3 \left(\frac{l_{n1} P_{DL} + \gamma P_{LL}}{E_c} \right)^{1/3}, \quad (12.2.12)$$

where l_{n1} is the length of the clear spans in the direction of the longer span, d_{\lim} is the limiting deflection and

$$\begin{aligned} K_1 &= 0.535 - [0.093 - 0.015(\beta - 1)^2] \sqrt{\alpha} - 0.086\beta \geq 0.15 + \frac{0.16}{\beta}, \\ K_2 &= 1.18 + 0.042\beta - 0.025 \frac{\alpha}{\beta} \geq 1.0, \\ K_3 &= 1.02 + 0.16\beta - 0.022 \frac{\alpha}{\beta} \geq 1.0, \end{aligned} \quad (12.2.13)$$

where α is the ratio of the flexural stiffness of the beam to the flexural stiffness of the slab ($E_c I_b / D$) in the direction of the longer span. Furthermore, in this formula β denotes the ratio of spans in the long direction to spans in the short

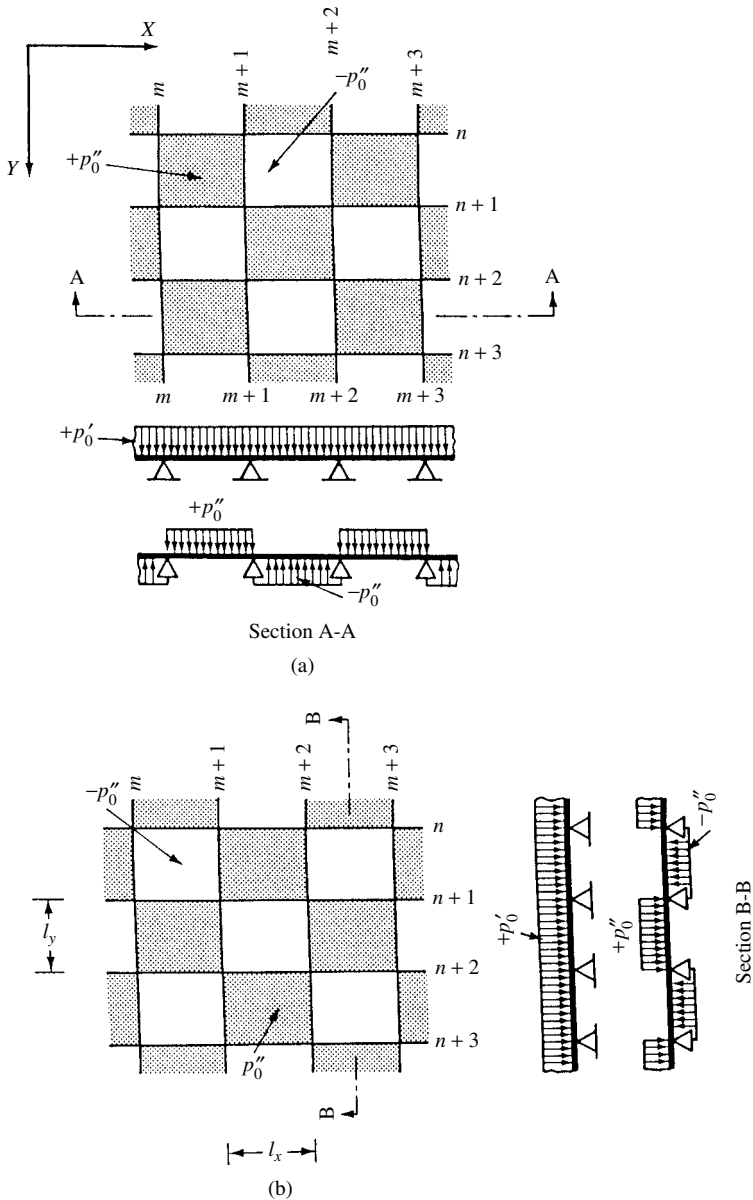


Figure 12.2.5 Critical loading patterns for maximum positive moments.

direction, and $\gamma = 1 + \lambda$ represents a multiplier with λ for additional long-term deflection.

For uncracked slab K_2 becomes 1.0. For interior panels K_3 equals unity. It should be noted that Eq. (12.2.12) can also be utilized for determining the deflections of RC slabs by using the prescribed plate thickness as h_{\min} .

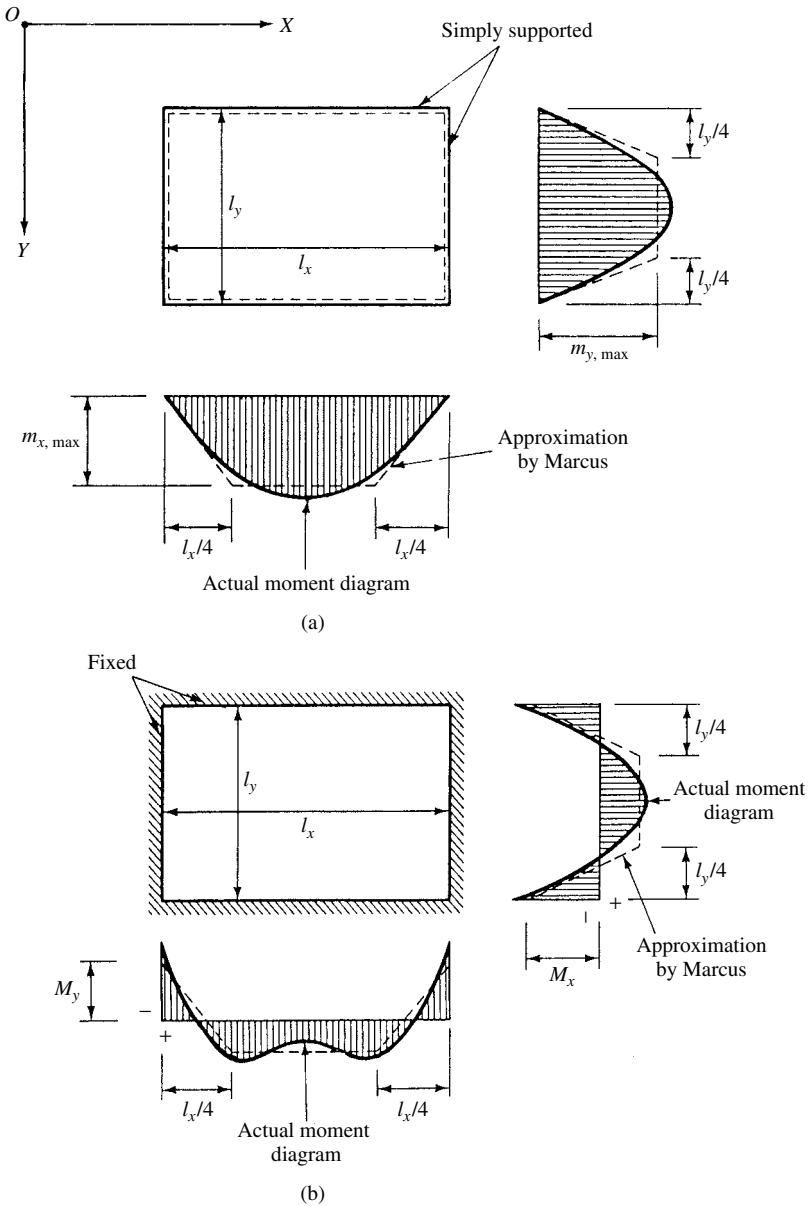


Figure 12.2.6 Approximate moment diagrams.

ILLUSTRATIVE EXAMPLE

The framing plan of a RC floor slab is shown in Fig. 12.2.7. The dead load of this floor system is 2.394 kN/m^2 . In addition to the dead load, the slab supports a live load of 4.788 kN/m^2 . Determine the approximate moments in the X and Y directions by using Marcus's approach.

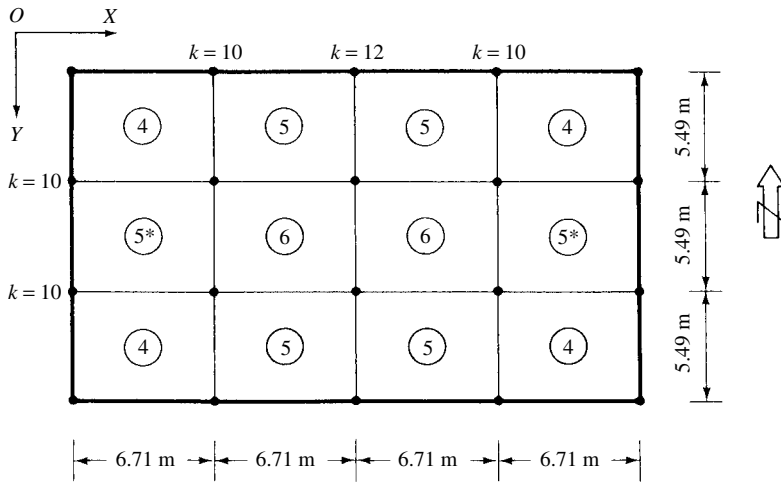


Figure 12.2.7 Framing plan.

First, based on Fig. 12.2.3, we determine the pertinent case numbers ($n = 4, 5, 5^*, 6$). These data are also indicated on the framing plan (Fig. 12.2.7). Next, the design loads are grouped into

$$\begin{aligned} p_0 &= p_{DL} + p_{LL} = 2.394 + 4.788 = 7.182 \text{ kN/m}^2, \\ p'_0 &= p_{DL} + \frac{1}{2}p_{LL} = 2.394 + 2.394 = 4.788 \text{ kN/m}^2, \\ p''_0 &= \pm p_{LL} = \pm 2.394 \text{ kN/m}^2. \end{aligned}$$

The span ratios are

$$\varepsilon = \frac{l_y}{l_x} = \frac{5.49}{6.71} = 0.82 \quad \text{and} \quad \varepsilon^* = \frac{l_x}{l_y} = 1.22.$$

Corner Panel (4). From Table 12.2.1d the pertinent coefficients for $\varepsilon = 0.82$ are

$$\alpha_4 = 0.017, \quad \beta_4 = 0.038, \quad \kappa_4 = 0.311, \quad \rho_4 = 0.689.$$

The coefficients for simply supported boundary conditions are taken from Table 12.2.1a. This gives

$$\alpha_1 = 0.024 \quad \text{and} \quad \beta_1 = 0.053.$$

The maximum positive moments are calculated from Eq. (12.2.11); thus

$$\begin{aligned} m_{x,\max} &= p'_0 \alpha_4 l_x^2 + p''_0 \alpha_1 l_x^2 \\ &= 4.788 \times 0.017 \times 6.71^2 + 2.394 \times 0.024 \times 6.71^2 = 6.251 \text{ kN-m/m}, \end{aligned}$$

$$\begin{aligned}
 m_{y,\max} &= p'_0 \beta_4 l_y^2 + p''_0 \beta_1 l_y^2 \\
 &= 4.788 \times 0.038 \times 5.49^2 + 2.394 \times 0.053 \times 5.49^2 = 9.308 \text{ kN-m/m.}
 \end{aligned}$$

The maximum negative moments are determined from Eq. (12.2.9):

$$\begin{aligned}
 M_x &= -\frac{1}{10} \kappa_4 p_0 l_x^2 = -\frac{1}{10} (0.311 \times 7.182 \times 6.71^2) = -10.056 \text{ kN-m/m,} \\
 M_y &= -\frac{1}{10} \rho_4 p_0 l_y^2 = -\frac{1}{10} (0.689 \times 7.182 \times 5.49^2) = -14.914 \text{ kN-m/m.}
 \end{aligned}$$

A similar approach is used for the other panels.

Exterior Panel (5). From Table 12.2.1e, the corresponding coefficients for $\varepsilon = 0.82$ are

$$\alpha_5 = 0.016, \quad \beta_5 = 0.031, \quad \kappa_5 = 0.475, \quad \rho_5 = 0.525.$$

The maximum positive moments are

$$\begin{aligned}
 m_{x,\max} &= p'_0 \alpha_5 l_x^2 + p''_0 \alpha_1 l_x^2 \\
 &= 4.788 \times 0.016 \times 6.71^2 + 2.587 = 6.035.56 \text{ kN-m/m,} \\
 m_{y,\max} &= p'_0 \beta_5 l_y^2 + p''_0 \beta_1 l_y^2 \\
 &= 4.788 \times 0.031 \times 5.49^2 + 3.824 = 8.298 \text{ kN-m/m.}
 \end{aligned}$$

The maximum negative moments are

$$\begin{aligned}
 M_x^I &= -\left(\frac{1}{k^I}\right) \kappa_5 p_0 l_x^2 = -\frac{1}{10} (0.475 \times 7.182 \times 6.71^2) = -15.358 \text{ kN-m/m,} \\
 M_x^{II} &= -\left(\frac{1}{k^{II}}\right) \kappa^5 p_0 l_x^2 = -\frac{1}{12} (0.475 \times 7.182 \times 6.71^2) = -12.799 \text{ kN-m/m,} \\
 M_y &= -\left(\frac{1}{k}\right) \rho_5 p_0 l_y^2 = -\frac{1}{10} (0.525 \times 7.182 \times 5.49^2) = -11.364 \text{ kN-m/m.}
 \end{aligned}$$

Exterior Panel (5).* With $\varepsilon^* = 1.22$, the corresponding coefficients are

$$\alpha_5^* = 0.011, \quad \beta_5^* = 0.029, \quad \rho_5^* = 0.816, \quad \kappa_5^* = 0.185.$$

The maximum positive moments are

$$\begin{aligned}
 m_{x,\max} &= p'_0 \alpha_5^* l_x^2 + p''_0 \alpha_1 l_x^2 \\
 &= 4.788 \times 0.011 \times 6.71^2 + 2.587 = 4.958 \text{ kN-m/m,} \\
 m_{y,\max} &= p'_0 \beta_5^* l_y^2 + p''_0 \beta_1 l_y^2 \\
 &= 4.788 \times 0.029 \times 5.49^2 + 3.824 = 8.009 \text{ kN-m/m.}
 \end{aligned}$$

The maximum negative moments are

$$M_x^* = -\frac{1}{10}\kappa_5^* p_0 l_x^2 = -\frac{1}{10}(0.185 \times 7.182 \times 6.71^2) = -5.982 \text{ kN-m/m},$$

$$M_y^* = -\frac{1}{10}\rho_5^* p_0 l_y^2 = -\frac{1}{10}(0.816 \times 7.182 \times 5.49^2) = -17.664 \text{ kN-m/m}.$$

Interior Panel (6). With $\varepsilon = 0.82$, the corresponding coefficients are

$$\alpha_6 = 0.011, \quad \beta_6 = 0.025, \quad \kappa_6 = 0.311, \quad \rho_6 = 0.689.$$

The maximum positive moments are

$$\begin{aligned} m_{x,\max} &= p_0' \alpha_6 l_x^2 + p_0'' \alpha_1 l_x^2 \\ &= 4.788 \times 0.011 \times 6.71^2 + 2.587 = 4.958 \text{ kN-m/m}, \end{aligned}$$

$$\begin{aligned} m_{y,\max} &= p_0' \beta_6 l_y^2 + p_0'' \beta_1 l_y^2 \\ &= 4.788 \times 0.025 \times 5.49^2 + 3.824 = 7.432 \text{ kN-m/m}. \end{aligned}$$

The maximum negative moments are

$$M_x^I = -\frac{1}{k^I} \kappa_6 p_0 l_x^2 = -\frac{1}{10}(0.311 \times 7.182 \times 6.71^2) = -10.056 \text{ kN-m/m},$$

$$M_x^{II} = -\frac{1}{k^{II}} \kappa_6 p_0 l_x^2 = -\frac{1}{12}(0.311 \times 7.182 \times 6.71^2) = -8.380 \text{ kN-m/m},$$

$$M_y = -\frac{1}{k} \rho_6 p_0 l_y^2 = -\frac{1}{10}(0.689 \times 7.182 \times 5.49^2) = -14.915 \text{ kN-m/m}.$$

An independent check of these results is performed in Sec. 13.4 by the yield-line approach.

References and Bibliography

- [12.2.1] MARCUS, H., *Die Theorie elastischer Gewebe und ihre Anwendung auf biegsame Platten*, Springer-Verlag, Berlin, 1924.
- [12.2.2] LÖSER, B., *Bemessungsverfahren: Zahlentafeln und Zahlenbeispiele*, 12th ed., W. Ernst & Sohn, Berlin, 1950.
- [12.2.3] EISENBIEGLER, G., "Die Berücksichtigung von Momentenumlagerung von vierseitig gestützten Durchlaufplatten," *Beton- und Stahlbetonbau*, 9 (1983), 251–255.
- [12.2.4] HWANG, S.-J., "Deflection Control of Two-Way Reinforced Concrete Slabs," *J. Struct. Div., ASCE*, 122 (1996), 160–168.

12.3 Simplified Slope-Deflection Method

As mentioned earlier, application of the classical approach for the solution of continuous two-way floor slabs represents an extremely tedious task, as demonstrated in Ref. [12.3.1]. That is, the classical approach results in a number of coupled

seven-moment equations, one for each supporting edge. However, we can quite effectively use a considerably simplified procedure introduced by Maugh and Pan [12.3.2]. This simplified version of the slope-deflection method is based partially on the classical approach[†] and on a slightly modified version of the slope-deflection technique used for the analysis of continuous beams and frames.

If the external lateral loads are fairly *symmetric* about the center of the individual panels, then the distribution of the moments along the edges can be represented by the simple sinusoidal functions

$$M_r = A_r \sin \frac{\pi x}{a} \quad \text{and} \quad M_s = B_s \sin \frac{\pi y}{b}. \quad (12.3.1)$$

Furthermore, it is sufficient to express the continuity between the individual panels only at the middle of each edge, since the resulting slopes are also sinusoidal. Therefore, the resulting slope at the i th edge created by all loads acting on panel (K) (Fig. 12.3.1) can be expressed by

$$\theta_{i=1}^{(K)} = \alpha \frac{M_1^{(K)}}{D_K} a + \beta \frac{M_2^{(K)}}{D_K} a + \gamma \frac{M_3^{(K)} + M_4^{(K)}}{D_K} b + \varphi_{is}^{(K)}, \quad (12.3.2)$$

where φ_{is} is the edge slope at point (i) due to the lateral loading acting on the *simply supported* panel (K). All terms should carry their proper sign. The corresponding sign convention is shown in Fig. 12.3.2.

Values for the constants α , β and γ in the above equation can be taken from Fig. 12.3.3, while the edge slopes φ_{is} produced by the lateral loads acting on the corresponding simply supported panels can be easily computed by applying Navier's method and differentiating the obtained equation of the deflected plate surface with respect to x and y , respectively. The values of φ_{is} for the most commonly used loads are given in diagrams (Fig. 12.3.4). Accuracy of this simplified approach is satisfactory for all practical purposes, provided the loading is fairly *symmetric* with respect

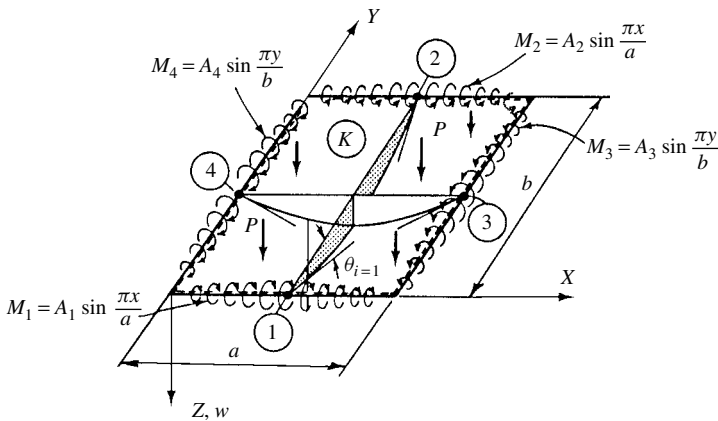


Figure 12.3.1 Typical interior panel.

[†] See Sec. 3.9.

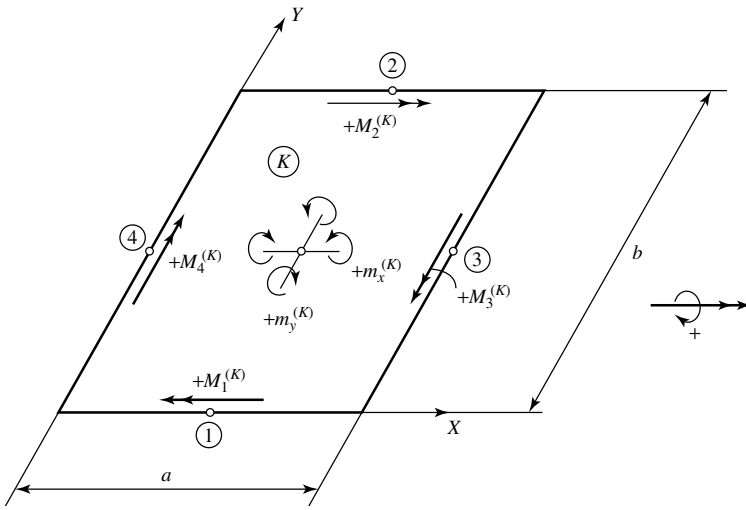


Figure 12.3.2 Sign convention for edge and field moments.

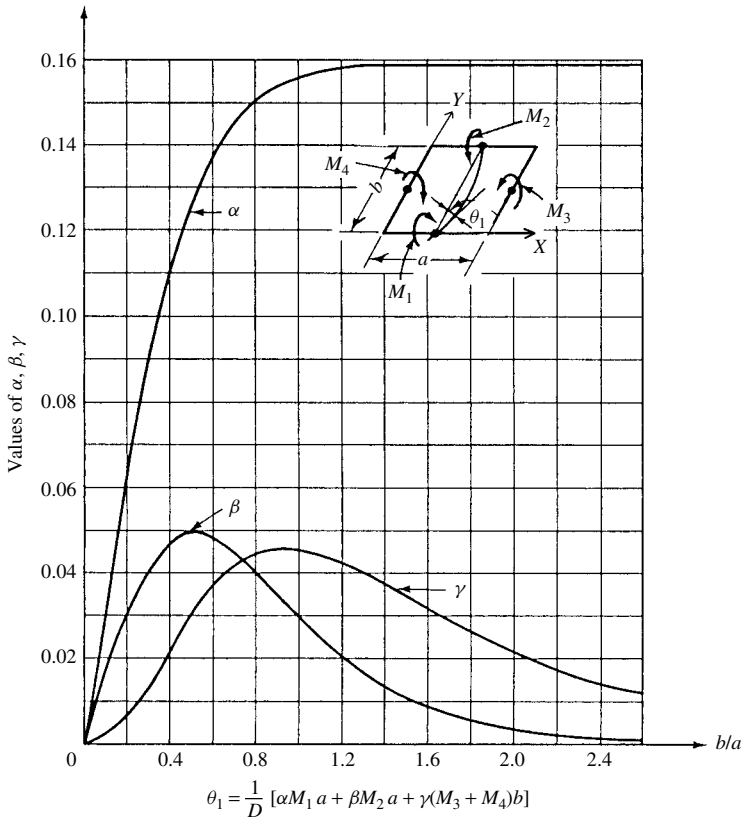


Figure 12.3.3 Coefficients of slope due to edge moments.

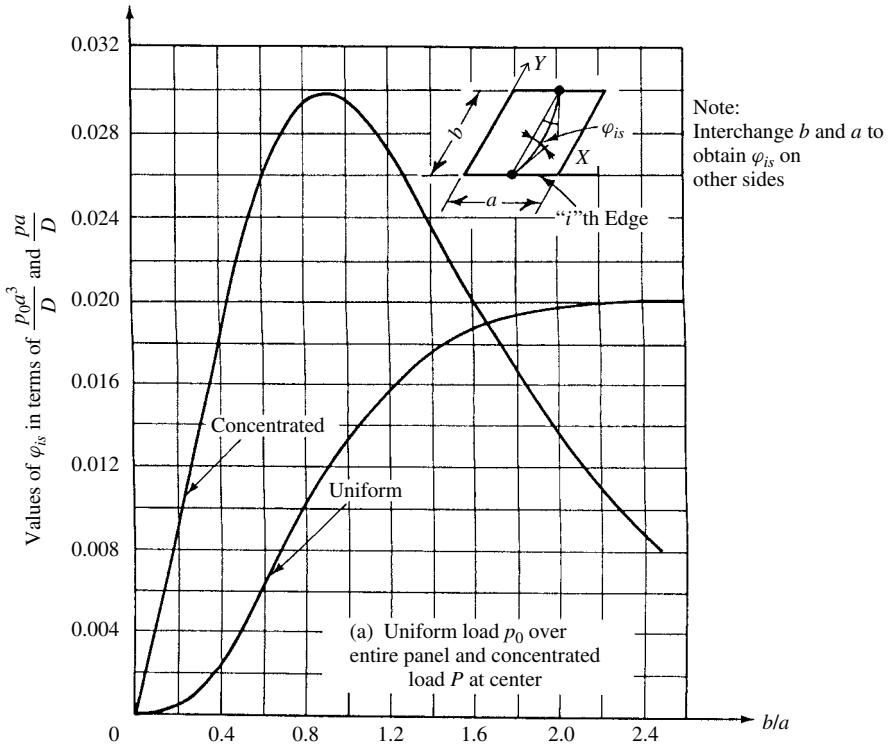


Figure 12.3.4 Edge slopes due to lateral loading.

to the center of each panel. Continuity between the various panels is maintained only at the middle of each edge by equating the slopes of the adjoining panels, that is, $\theta_i^{(K)} = \theta_i^{(M)}$.

By knowing the edge moments M_i at the center of the supporting beams, the continuous plate problems can be considered as solved. That is, the field moments at the center of various panels can be determined by taking the algebraic sum of the edge moments upon which the maximum positive moment of the corresponding simply supported plate is superimposed. These maximum positive moments of simply supported plates due to lateral loads can be calculated by using readily available tables[†] or even any of the classical methods treated in Part I. For the sake of convenience, however, one may utilize the graphs shown in Figs. 12.3.5 and 12.3.6, respectively. That is, by considering the approximate nature of this procedure, the center moments for uniformly distributed load p_0 and the concentrated load P acting at the center of the plates, the center moments can be evaluated from these graphs with acceptable accuracy. The center moments caused by the sinusoidal distribution of the edge moments can be calculated from Eqs. (3.15) and (3.17), respectively. Again, we may considerably simplify this procedure by using Fig. 12.3.7. For effects of moments along the adjacent sides, the values of a/b and the direction of X and Y can be interchanged. Care must be taken, however, in determining these values

[†] Listed on the accompanying CD.

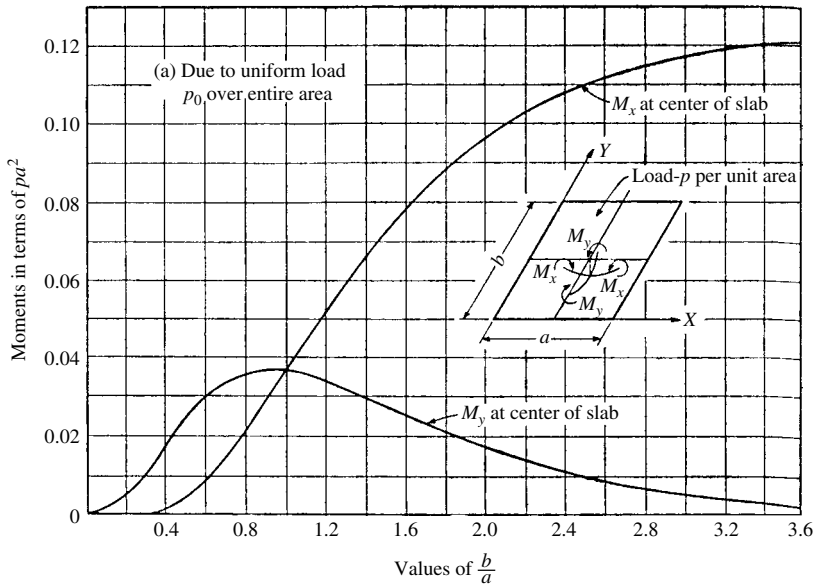


Figure 12.3.5 Moments at center due to uniformly distributed load.

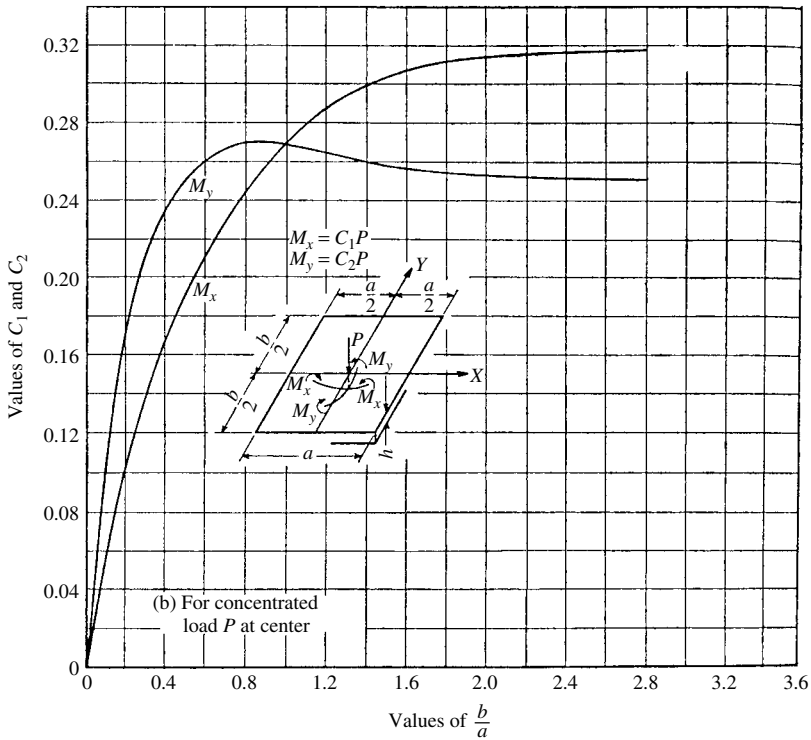


Figure 12.3.6 Moments at center due to concentrated force acting at center.

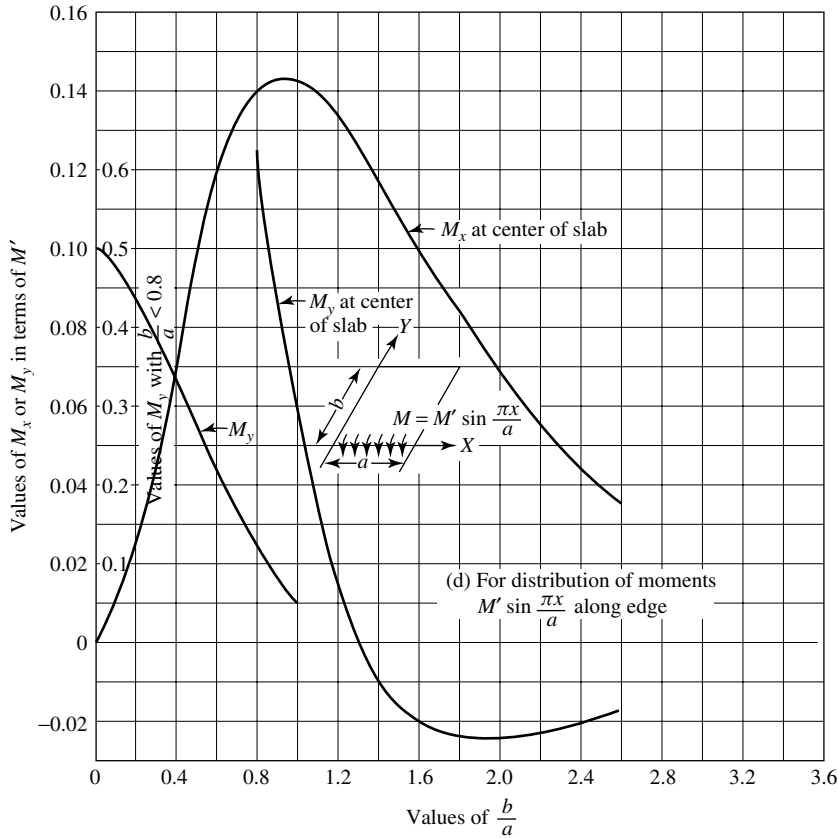


Figure 12.3.7 Center moments due to sinusoidal edge moments.

since the moments M_x and M_y are dependent on the edge direction. For approximate moment diagrams and loads acting on the supporting beams, see Figs. 12.5.2 and 12.5.3, respectively.

ILLUSTRATIVE EXAMPLE I

Figure 12.3.8 shows a continuous plate system, the shaded areas of which are loaded with $p_0 = 3.0 \text{ kN/m}^2$ uniformly distributed lateral load. The thicknesses of the individual panels are $h_A = h_C = 0.18 \text{ m}$ and $h_B = 0.24 \text{ m}$. The modulus of elasticity of this plate system is $E = 15,000 \text{ N/mm}^2$, and Poisson's ratio ν is 0.3. Determine the edge and field moments by using the simplified slope-deflection method described above.

Applying logically the sign convention shown in Fig. 12.3.2 and using Eq. (12.3.2), we can establish the equality of slopes at point ①. This gives

$$\alpha_A \frac{M_1^A}{D_A} 10 + \varphi_{1s} = -\alpha_B \frac{M_1^B}{D_B} 10 - \gamma_B \frac{M_2^B}{D_B} - \beta_B \frac{M_3^B}{D_B} 10 \tag{12.3.3a}$$

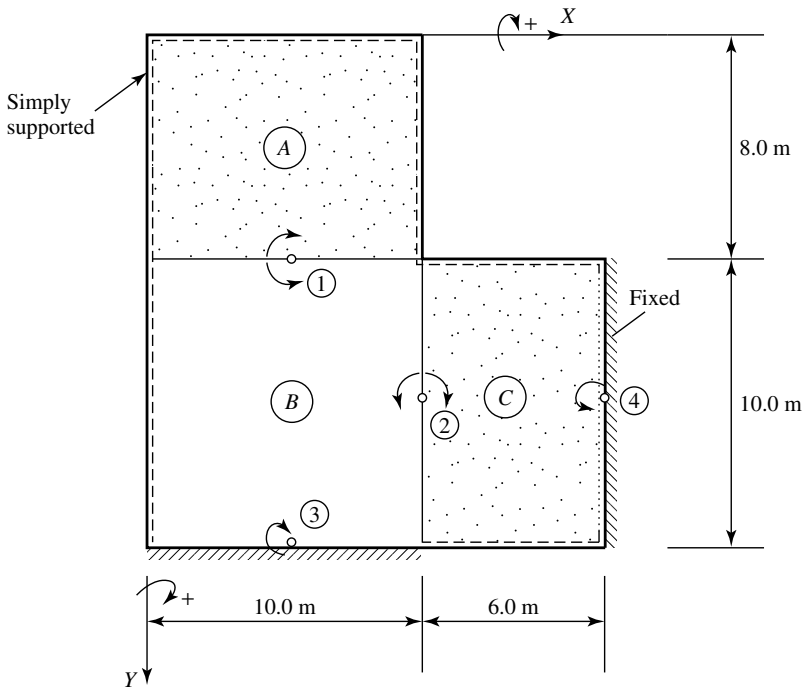


Figure 12.3.8 Continuous plate system.

or

$$\frac{\alpha_A}{D_A} M_1 + \frac{\varphi_{1s}}{10} + \frac{\alpha_B}{D_B} M_1 + \frac{\gamma_B}{D_B} M_2 + \frac{\beta_B}{D_B} M_3 = 0. \quad (12.3.3b)$$

At point ② we obtain the slope equality equation

$$\alpha_C \frac{M_2^C}{D_C} 10 + \beta_C \frac{M_4^C}{D_C} 10 + \varphi_{2s} = -\alpha_B \frac{M_2^B}{D_B} 10 - \gamma_B \frac{M_1^B + M_3^B}{D_B} 10 \quad (12.3.4a)$$

or

$$\frac{\gamma_B}{D_B} M_1 + \left(\frac{\alpha_C}{D_C} + \frac{\alpha_B}{D_B} \right) M_2 + \frac{\gamma_B}{D_B} M_3 + \frac{\beta_C}{D_C} M_4 + \frac{\varphi_{2s}}{10} = 0. \quad (12.3.4b)$$

Similarly, the equality of slopes at point ③ gives

$$\alpha_B \frac{M_3^B}{D_B} 10 + \beta_B \frac{M_1^B}{D_B} + \gamma_B \frac{M_2^B}{D_B} 10 = 0 \quad (12.3.5a)$$

or

$$\frac{\alpha_B}{D_B} M_3 + \frac{\beta_B}{D_B} M_1 + \frac{\gamma_B}{D_B} M_2 = 0. \quad (12.3.5b)$$

Finally, the equality of slopes at point ④ yields

$$\alpha_C \frac{M_4^C}{D_C} 10 + \beta_C \frac{M_2^C}{D_C} 10 + \varphi_{2s} = 0 \quad (12.3.6a)$$

or

$$\frac{\beta_C}{D_C} M_2 + \frac{\alpha_C}{D_C} + \frac{\varphi_{2s}}{10} = 0. \quad (12.3.6b)$$

Using Figs. 12.3.3 and 12.3.4, we determine the corresponding coefficients for these equations. For panel ① these are

$$\frac{b}{a} = 0.8, \quad \alpha_A = 0.151, \quad \varphi_{1s} = \frac{0.0102 p_0 a^3}{D_A} = 0.0038, \quad (12.3.7)$$

$$D_A = 8.01 \times 10^3 \text{ kN-m.}$$

For panel ② we obtain

$$\frac{b}{a} = 1.0, \quad \alpha_B = 0.155, \quad \beta_B = 0.03, \quad \gamma_B = 0.045, \quad (12.3.8)$$

$$D_B = 18.99 \cdot 10^3 \text{ kN-m.}$$

The coefficients for panel ③ are

$$\begin{aligned} \frac{b}{a} &= 0.6, & \alpha_C &= 0.1362, & \beta_C &= 0.0475, \\ \varphi_{2s} &= \frac{0.0062 p_0 a^3}{D_C} = 0.0023, & D_C &= D_A. \end{aligned} \quad (12.3.9)$$

By substituting these values into Eqs. (12.3.3b), (12.3.4b), (12.3.5b) and (12.3.6b), we obtain the following set of simultaneous equations:

$$\begin{bmatrix} 2.7013 & 0.237 & 0.158 & 0.000 \\ 0.237 & 2.5166 & 0.237 & 0.593 \\ 0.158 & 0.237 & 0.8162 & 0.000 \\ 0.000 & 0.593 & 0.00 & 1.7004 \end{bmatrix} \begin{Bmatrix} M_1 \\ M_2 \\ M_3 \\ M_4 \end{Bmatrix} = \begin{Bmatrix} -38.00 \\ -23.00 \\ 0.00 \\ -23.00 \end{Bmatrix}, \quad (12.3.10)$$

from which

$$\mathbf{m} = \begin{Bmatrix} M_1 \\ M_2 \\ M_3 \\ M_4 \end{Bmatrix} = \begin{Bmatrix} -13.8345 \\ -5.5042 \\ 4.2763 \\ -11.6067 \end{Bmatrix} \text{ kN-m/m.} \quad (12.3.11)$$

These results are checked in Sec. 12.4 by applying the moment distribution procedure. By knowing the edge moments M_i at the center of each supporting beam, the field moment at the center of each plate is determined by utilizing the graphs given in Figs. 12.3.5 and 12.3.7, respectively.

Consequently, by using these graphs we calculate the following moments for panel (A):

$$\begin{aligned}
 \text{With } \frac{b}{a} &= 0.8, & M_{x0} &= 0.0323 p_0 a^2 = 9.69 \text{ kN-m/m}, \\
 M_{y0} &= 0.066 p_0 b^2 = 12.672 \text{ kNm/m:} \\
 m_x &= 0.112 M_1 + M_{x0} = 8.1405 \text{ kN-m/m}, \\
 m_y &= 0.145 M_1 + M_{y0} = 10.666 \text{ kN-m/m}.
 \end{aligned} \tag{12.3.12}$$

For panel (B) a similar procedure gives

$$\begin{aligned}
 \text{With } \frac{b}{a} &= 1.0, & M_{x0} &= M_{y0} = 0.00: \\
 m_x &= 0.147(M_1 + M_3) + 0.056 M_2 = 2.9705 \text{ kN-m/m}, \\
 m_y &= 0.056(M_1 + M_3) + 0.147 M_2 = 1.8233 \text{ kN-m/m}.
 \end{aligned} \tag{12.3.13}$$

Finally, for panel (C) we obtain

$$\begin{aligned}
 \text{With } \frac{a}{b} &= 0.6, & M_{x0} &= 0.0176 p_0 a^2 = 5.28 \text{ kN-m/m}, \\
 M_{y0} &= 0.0844 p_0 b^2 = 9.6552 \text{ kN-m/m:} \\
 m_x &= 0.117(M_2 + M_4) + M_{x0} = 5.994 \text{ kN-m/m}, \\
 m_y &= 0.045(M_2 + M_4) = 9.9298 \text{ kN-m/m}.
 \end{aligned} \tag{12.3.14}$$

ILLUSTRATIVE EXAMPLE II

Figure 12.3.9 shows a larger RC floor slab consisting of seven panels. The shaded panels carry $p_0 = 4.0 \text{ kN/m}^2$ lateral load. Utilizing the apparent symmetry of the structure and loading, let us determine the joint-point moments M_1, M_2, \dots, M_6 by using the simplified slope-deflection method. The flexural rigidity of all panels is D .

For each joint point we write the slope equations (12.3.2) $\theta_i^{(K)}$. The subscript i in these equations refers to the joint point, and the superscript (K) represents the number of individual panels. Thus we can write:

$$\begin{aligned}
 \text{At point } \textcircled{1} \\
 \theta_1^{(5)} &= \alpha_5 \frac{M_1}{D} 5.0 + \beta_5 \frac{M_2}{D} 5.0 + \gamma_5 \frac{M_3}{D} 5.0 = 0.
 \end{aligned} \tag{12.3.15}$$

$$\begin{aligned}
 \text{At point } \textcircled{2} \\
 \theta_2^{(5)} &= \alpha_5 \frac{M_2}{D} 5.0 + \beta_5 \frac{M_1}{D} 5.0 + \gamma_5 \frac{M_3}{D} 5.0, \\
 \theta_2^{(4)} &= \alpha_4 \frac{M_2}{D} 5.0 + \beta_4 \frac{M_4}{D} 5.0 + \gamma_4 \frac{M_4 + M_2}{D} 5.0 + \varphi_{4s}.
 \end{aligned} \tag{12.3.16}$$

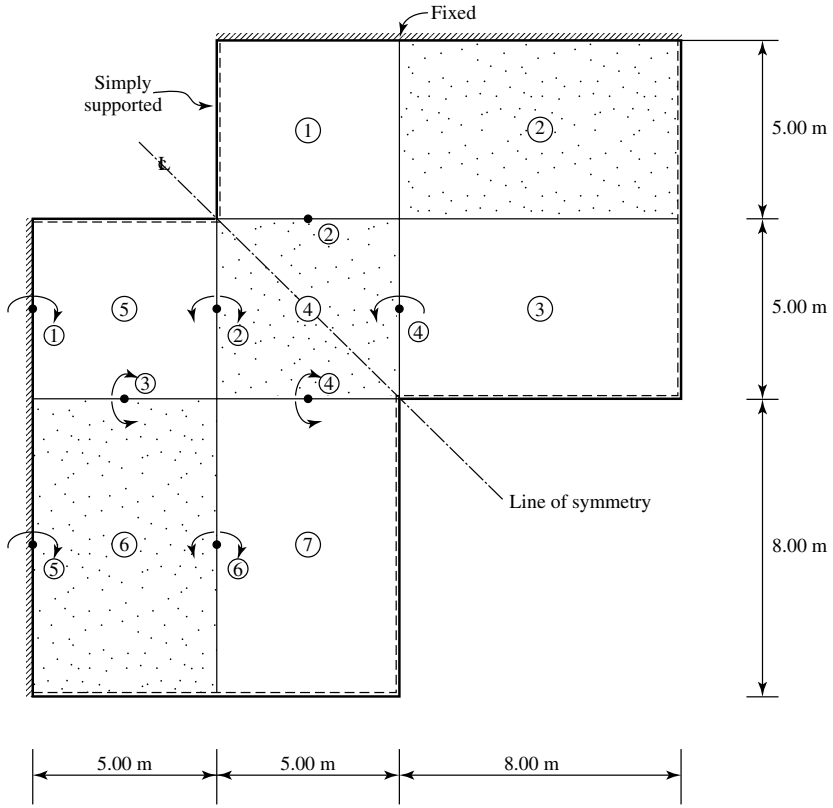


Figure 12.3.9 Reinforced-concrete floor slab.

At point ③

$$\begin{aligned}\theta_3^{(5)} &= \alpha_5 \frac{M_3}{D} 5.0 + \gamma_5 \frac{M_1 + M_2}{D} 0.5, \\ \theta_3^{(6)} &= \alpha_6 \frac{M_3}{D} 5.0 + \gamma_6 \frac{M_5 + M_6}{D} 8.0 + \varphi_{6s}.\end{aligned}\quad (12.3.17)$$

At point ④

$$\begin{aligned}\theta_4^{(4)} &= \alpha_4 \frac{M_4}{D} 5.0 + \beta_4 \frac{M_2}{D} 5.0 + \gamma_4 \frac{M_2 + M_4}{D} 5.0 + \varphi_{4s}, \\ \theta_4^{(7)} &= \alpha_7 \frac{M_4}{D} 5.0 + \gamma_7 \frac{M_6}{D} 8.0.\end{aligned}\quad (12.3.18)$$

At point ⑤

$$\theta_5^{(6)} = \alpha_5 \frac{M_5}{D} 8.0 + \beta_6 \frac{M_6}{D} 8.0 + \gamma_6 \frac{M_3}{D} 5.0 + \varphi_{6s} = 0. \quad (12.3.19)$$

At point ⑥

$$\begin{aligned}\theta_6^{(6)} &= \alpha_6 \frac{M_6}{D} 8.0 + \beta_6 \frac{M_5}{D} 8.0 + \gamma_6 \frac{M_3}{D} 5.0 + \varphi_{6s}, \\ \theta_6^{(7)} &= \alpha_7 \frac{M_6}{D} 8.0 + \gamma_7 \frac{M_4}{D} 5.0.\end{aligned}\quad (12.3.20)$$

Using Figs. 12.3.3 and 12.3.4, we determine the following coefficients:

	Point 4	Point 5	Point 6	Point 7
b/a	1.0	1.0	1.6	1.6
α	0.157	0.157	0.159	0.159
β	0.03	0.03	0.009	0.009
γ	0.045	0.045	0.032	0.032
φ_{is}	0.0125C	—	0.0185C	—

$$\left(C = \frac{P_0 a^3}{D} \right).$$

Next, we substitute these values into the slope equations and state the equality of slopes $\theta_i^{(K)} = \theta_i^{(M)}$ at each joint point,

$$\begin{aligned}\theta_1^{(5)} &= 0.0, & \theta_2^{(5)} &= -\theta_2^{(4)}, & \theta_3^{(5)} &= -\theta_3^{(6)}, & \theta_4^{(4)} &= -\theta_4^{(7)}, \\ \theta_5^{(6)} &= 0.0, & \theta_6^{(6)} &= -\theta_6^{(7)}.\end{aligned}\quad (12.3.21)$$

We obtain the simultaneous equations

$$\begin{bmatrix} 0.785 & 0.150 & 0.225 & 0.00 & 0.00 & 0.00 \\ 0.150 & 1.795 & 0.225 & 0.375 & 0.00 & 0.00 \\ 0.225 & 0.225 & 1.580 & 0.00 & 0.256 & 0.256 \\ 0.00 & 0.375 & 0.00 & 1.805 & 0.00 & 0.256 \\ 0.00 & 0.00 & 0.160 & 0.00 & 1.272 & 0.072 \\ 0.00 & 0.00 & 0.160 & 0.160 & 0.072 & 2.544 \end{bmatrix} \begin{Bmatrix} M_1 \\ M_2 \\ M_3 \\ M_4 \\ M_5 \\ M_6 \end{Bmatrix} = \begin{Bmatrix} 0.00 \\ -6.25 \\ -9.25 \\ -6.25 \\ -9.25 \\ -9.25 \end{Bmatrix}, \quad (12.3.22)$$

the solution of which gives

$$\mathbf{m} = \begin{Bmatrix} M_1 \\ M_2 \\ M_3 \\ M_4 \\ M_5 \\ M_6 \end{Bmatrix} = \begin{Bmatrix} 1.688 \\ -2.578 \\ -4.171 \\ -2.497 \\ -6.576 \\ -3.031 \end{Bmatrix} \quad \text{kN-m/m.} \quad (12.3.23)$$

References and Bibliography

- [12.3.1] POMAROV, V. V., et al., *Szilárdságtani Számítások a Gépészetben (Strength of Material Computations in Mechanical Engineering)*, Vol. 3 (Hungarian translation of the Russian original), Műszaki Könyvkiadó, Budapest, 1965, pp. 143–159.

- [12.3.2] MAUGH, L. C., and PAN, C. W., "Moments of Continuous Rectangular Slabs on Rigid Supports," *Trans. ASCE*, 107 (1942), 1118–1142.
- [12.3.3] SIESS, C. P., and NEWMARK, N. M., "Moments in Two-Way Concrete Floor Slabs," *Bull. Univ. Ill. Eng. Exp. Sta.*, No. 385 (Feb. 1950).

12.4 Moment Distribution Applied to Continuous Plates

Moment distribution, introduced by Cross in 1932 [12.4.1], can be mathematically classified as a special relaxation procedure applied to slope-deflection equations of structural mechanics. Since this relaxation technique in the solution of continuous beams and frames [12.4.2] offers numerous advantages, the idea of extending the method to continuous plates is obvious. Based on the initial work by Fischer [12.4.3] and Newmark [12.4.4], Brunner [12.4.5] has introduced the moment distribution method to continuous plates, subjected to uniformly distributed lateral loads.

In the following discussion the reader's familiarity with moment distribution as applied to continuous beams is assumed. To be able to extend the general procedure of this simple, yet highly successful, method to continuous plates, the *stiffness* and *carry-over factors* of the individual plates must first be determined. Limiting ourselves to uniformly distributed lateral loads, we may assume that all edge moments vary as the half waves of the sine curve, which is in close agreement with the real conditions. This simplifying assumption permits locating the joint points (where continuity is expressed) at the center of the plate edges.

Brunner [12.4.5] uses nine typical cases for individual panels, which are shown in Fig. 12.4.1. The shorter span is always described by $l_x = a$, while the longer one is $l_y = b$. All quantities, depending on span lengths, are expressed as functions of the shorter span ($l_x = a$).

Applying a sinusoidal edge moment of unit amplitude at the shorter span of a simply supported, rectangular plate (Fig. 12.4.2a), the following slopes are produced at the center of the edges:

$$\alpha'_1 = \frac{1}{2\pi} \frac{\sinh 2\beta - 2\beta}{\cosh 2\beta - 1} \frac{a}{D}, \quad (12.4.1)$$

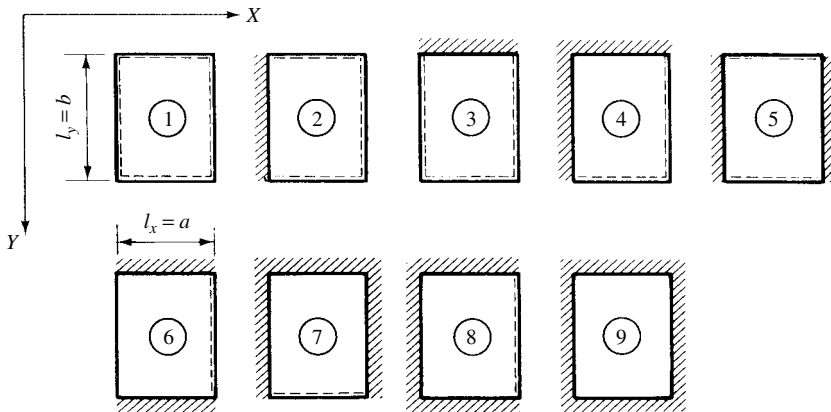


Figure 12.4.1 Typical cases. (Note: Always use l_x for shorter span!).

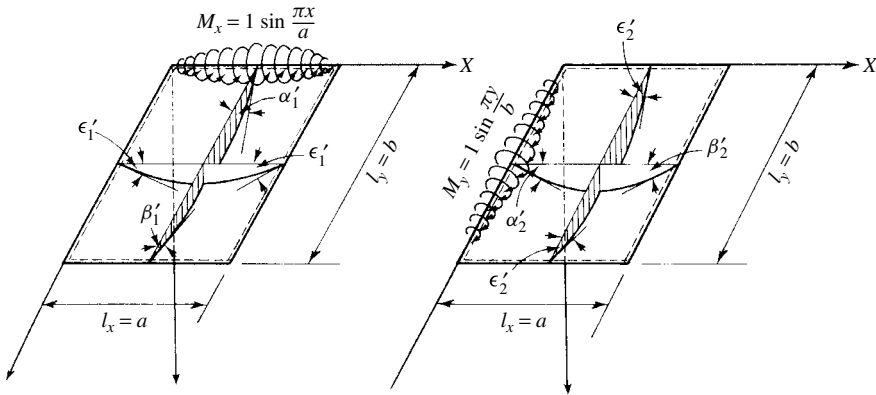


Figure 12.4.2 Sinusoidal edge moments.

$$\beta'_1 = \frac{1}{\pi} \frac{\beta \cosh \beta - \sinh \beta}{\cosh 2\beta - 1} \frac{a}{D}, \quad (12.4.2)$$

$$\varepsilon'_1 = \frac{1}{8} \frac{\sinh(\beta/2)}{\cosh^2(\beta/2)} \frac{b}{D}, \quad (12.4.3)$$

where $\beta = \pi b/a$ and D represents the flexural rigidity of the plate [Eq. (1.2.28)].

Analogous expressions can be obtained when the sinusoidal edge moment is applied to one of the longer edges ($\alpha'_2, \beta'_2, \varepsilon'_2$) by replacing a with b and b with a in the above-given simple formulas (Fig. 12.4.2b).

In determining the stiffness factors of individual plates, it is assumed that the continuous edges are fixed and that the distribution of the reactive fixed-end moments is also sinusoidal. Edge moments producing unit rotation at the joint points are defined as stiffness factors and are designated by K for the short edges and by \bar{K} for the long edges. To illustrate how plate stiffness factors are determined, let us investigate Case 9 (Fig. 12.4.1). Applying the classical method, a simply supported plate is used upon which the effects of edge moments M_n are superimposed. The slopes at the joint points (Fig. 12.4.3), due to a sinusoidal edge moment, producing unit rotation at joint point ①, are the following:

$$\begin{aligned} \text{At point ① :} & \quad M_1 \alpha'_1 - M_2 \beta'_1 - 2M_4 \varepsilon'_2 = 1. \\ \text{At point ② :} & \quad M_1 \beta'_1 - M_2 \alpha'_1 - 2M_4 \varepsilon'_2 = 0. \\ \text{At point ④ :} & \quad M_1 \varepsilon'_1 - M_2 \varepsilon'_1 - M_4 (\alpha'_2 + \beta'_2) = 0. \end{aligned} \quad (12.4.4)$$

From symmetry

$$M_3 = M_4.$$

Solving (12.4.4) for M_1 , we obtain

$$M_1 = K_9 = \frac{\alpha'_1 (\alpha'_2 + \beta'_2) - 2\varepsilon'_1 \varepsilon'_2}{(\alpha'_1 - \beta'_1) [(\alpha'_1 + \beta'_1)(\alpha'_2 + \beta'_2) - 4\varepsilon'_1 \varepsilon'_2]}. \quad (12.4.5)$$

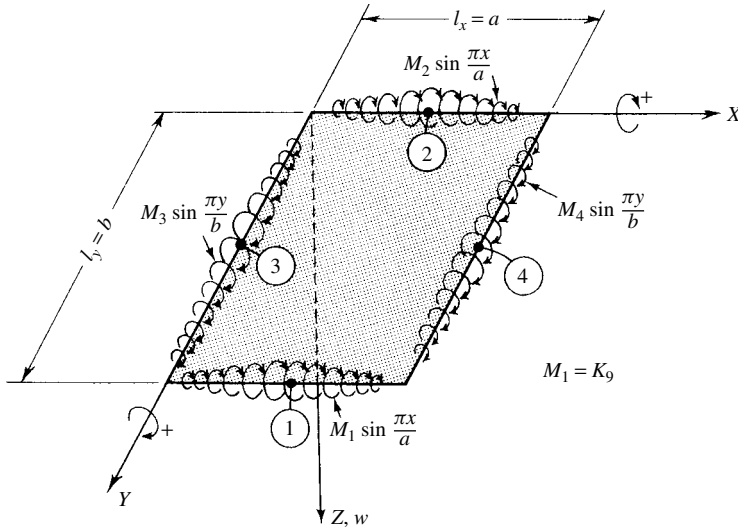


Figure 12.4.3 Edge moments on clamped plate (Case 9).

The ratio of the far-end moment to the joint moment is defined as the carry-over factor to opposite edges. Thus

$$\mu = \frac{M_2}{M_1} = \frac{\beta'_1(\alpha'_2 + \beta'_2) - 2\varepsilon'_1\varepsilon'_2}{\alpha'_1(\alpha'_2 + \beta'_2) - 2\varepsilon'_1\varepsilon'_2}. \quad (12.4.6)$$

Similarly, the carry-over factor to the adjoining edges (Fig. 12.4.3) is determined from

$$\mu' = \frac{M_4}{M_1} = \frac{M_3}{M_1} = \frac{\varepsilon'_1(\alpha'_1 - \beta'_1)}{\alpha'_1(\alpha'_2 + \beta'_2) - 2\varepsilon'_1\varepsilon'_2}. \quad (12.4.7)$$

The stiffness and carry-over factors for the other typical cases can be calculated following the same approach. The results of this computation are given in Table 12.4.1.

The sign convention, used for continuous beams [12.4.1], can be applied to continuous plates (Fig. 12.4.4a). It should be noted, however, that while the carry-over factors for beams are always positive, carry-over factors assigned to adjoining edges, μ' , can be either positive or negative, as illustrated in Fig. 12.4.4b.

The distribution factor DF is defined as the ratio of the stiffness factors. Thus

$$(DF)_R = \frac{K_R}{K_R + K_L} \quad \text{and} \quad (DF)_L = \frac{K_L}{K_R + K_L}, \quad (12.4.8)$$

where the subscripts R and L denote right and left, respectively.

Fixed-end moments of uniformly loaded rectangular plates are given in the technical literature listed on the accompanying CD. Since the computational procedure of moment distribution for plates is identical to that of beams and frames, a detailed treatment of this part can be eliminated.

For calculating moments at the center of individual plates, we can follow a procedure similar to that already introduced in Sec. 12.3. That is, at the center of the

Table 12.4.1 Stiffness and Carry-over Factors

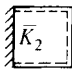
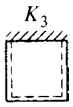
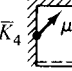
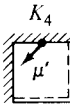
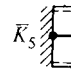

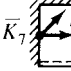

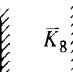


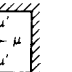

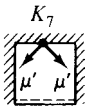
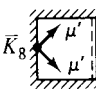
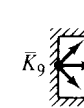
	Case 2	Case 3	Case 4				Case 5		Case 6		Case 7			
														
l_y/l_x	\bar{K}_2	K_3	\bar{K}_4	μ'	K_4	μ'	\bar{K}_5	μ	K_6	μ	\bar{K}_7	μ	μ'	l_y/l_x
1.00	6.41	6.41	7.01	0.293	7.01	0.293	6.65	0.190	6.65	0.190	7.10	0.114	0.259	1.00
1.05	6.13	6.37	6.72	0.309	6.98	0.277	6.42	0.208	6.58	0.173	6.83	0.134	0.267	1.05
1.10	5.90	6.35	6.44	0.322	6.94	0.262	6.21	0.224	6.52	0.158	6.60	0.153	0.273	1.10
1.15	5.68	6.33	6.20	0.334	6.91	0.247	6.03	0.239	6.47	0.142	6.38	0.172	0.277	1.15
1.20	5.49	6.32	5.97	0.345	6.88	0.233	5.87	0.255	6.43	0.128	6.19	0.189	0.279	1.20
1.25	5.31	6.31	5.77	0.353	6.85	0.220	5.72	0.267	6.40	0.115	6.02	0.205	0.281	1.25
1.30	5.16	6.31	5.58	0.361	6.82	0.207	5.59	0.279	6.38	0.104	5.86	0.220	0.282	1.30
1.35	5.01	6.30	5.41	0.368	6.79	0.195	5.48	0.285	6.36	0.094	5.73	0.237	0.282	1.35
1.40	4.89	6.30	5.25	0.374	6.76	0.183	5.37	0.301	6.34	0.084	5.59	0.249	0.281	1.40
1.45	4.76	6.30	5.10	0.378	6.73	0.172	5.28	0.311	6.33	0.075	5.48	0.264	0.279	1.45
1.50	4.66	6.29	4.97	0.382	6.70	0.161	5.20	0.321	6.32	0.067	5.38	0.276	0.277	1.50
1.55	4.56	6.29	4.84	0.385	6.68	0.151	5.12	0.330	6.32	0.059	5.28	0.289	0.275	1.55
1.60	4.47	6.29	4.73	0.389	6.66	0.142	5.05	0.339	6.31	0.053	5.20	0.301	0.272	1.60
1.65	4.38	6.29	4.62	0.391	6.64	0.133	4.99	0.347	6.31	0.047	5.12	0.312	0.269	1.65
1.70	4.31	6.29	4.53	0.392	6.61	0.125	4.93	0.355	6.30	0.041	5.05	0.322	0.266	1.70
1.75	4.23	6.28	4.44	0.393	6.59	0.117	4.88	0.362	6.30	0.037	4.99	0.331	0.262	1.75
1.80	4.17	6.28	4.36	0.393	6.57	0.110	4.83	0.368	6.29	0.033	4.93	0.340	0.259	1.80
1.85	4.11	6.28	4.29	0.393	6.55	0.103	4.78	0.374	6.29	0.028	4.88	0.348	0.256	1.85
1.90	4.06	6.28	4.22	0.392	6.53	0.097	4.74	0.380	6.29	0.025	4.83	0.355	0.252	1.90
1.95	4.00	6.28	4.15	0.390	6.51	0.090	4.71	0.385	6.29	0.021	4.78	0.362	0.248	1.95
2.00	3.96	6.28	4.09	0.389	6.50	0.085	4.67	0.390	6.29	0.019	4.74	0.369	0.245	2.00
∞	3.00	6.28	3.00	~ 0.38	~ 6.5	0	4.00	0.500	6.28	0	4.00	0.500	~ 0.24	∞
MF	D/l_x	D/l_x	D/l_x		D/l_x		D/l_x		D/l_x		D/l_x		MF	
	Case 7		Case 8				Case 9							
														
l_y/l_x	K_7	μ'	\bar{K}_8	μ'	K_8	μ	μ'	\bar{K}_9	μ	μ'	\bar{K}_9	μ	μ'	l_y/l_x
1.00	7.49	0.246	7.49	0.246	7.10	0.114	0.259	7.51	0.054	0.233	7.51	0.054	0.233	1.00
1.05	7.43	0.230	7.20	0.263	7.04	0.095	0.250	7.23	0.073	0.243	7.45	0.037	0.222	1.05
1.10	7.37	0.214	6.91	0.278	6.99	0.080	0.241	6.97	0.092	0.252	7.38	0.023	0.209	1.10
1.15	7.31	0.199	6.65	0.292	6.95	0.065	0.231	6.73	0.111	0.259	7.32	0.010	0.197	1.15
1.20	7.25	0.186	6.40	0.305	6.90	0.052	0.221	6.51	0.131	0.265	7.25	0.000	0.186	1.20
1.25	7.19	0.173	6.17	0.317	6.86	0.042	0.211	6.32	0.148	0.270	7.20	-0.009	0.175	1.25
1.30	7.14	0.162	5.97	0.327	6.83	0.032	0.200	6.14	0.166	0.273	7.15	-0.015	0.164	1.30
1.35	7.08	0.150	5.76	0.336	6.79	0.023	0.189	5.98	0.183	0.275	7.09	-0.020	0.154	1.35
1.40	7.04	0.140	5.59	0.345	6.76	0.016	0.180	5.82	0.200	0.276	7.04	-0.024	0.144	1.40
1.45	6.98	0.130	5.42	0.352	6.73	0.010	0.169	5.69	0.216	0.276	6.99	-0.027	0.135	1.45
1.50	6.94	0.122	5.27	0.358	6.70	0.005	0.160	5.57	0.232	0.275	6.94	-0.029	0.126	1.50
1.55	6.89	0.113	5.12	0.364	6.68	0.001	0.151	5.46	0.247	0.274	6.90	-0.031	0.117	1.55
1.60	6.85	0.106	4.99	0.369	6.66	-0.002	0.142	5.36	0.262	0.272	6.86	-0.032	0.109	1.60
1.65	6.81	0.099	4.86	0.373	6.64	-0.005	0.134	5.27	0.275	0.270	6.82	-0.032	0.102	1.65
1.70	6.77	0.092	4.75	0.376	6.61	-0.008	0.126	5.18	0.288	0.268	6.78	-0.033	0.095	1.70
1.75	6.74	0.086	4.65	0.379	6.59	-0.010	0.118	5.11	0.299	0.265	6.75	-0.033	0.089	1.75
1.80	6.71	0.080	4.55	0.380	6.57	-0.011	0.111	5.04	0.310	0.262	6.71	-0.032	0.083	1.80
1.85	6.67	0.075	4.46	0.381	6.55	-0.012	0.104	4.98	0.320	0.259	6.68	-0.031	0.078	1.85
1.90	6.65	0.070	4.38	0.382	6.53	-0.013	0.098	4.92	0.330	0.256	6.66	-0.031	0.072	1.90

Table 12.4.1 (continued)

Case 7			Case 8					Case 9						
														
l_y/l_x	K_7	μ'	\bar{K}_8	μ'	K_8	μ	μ'	\bar{K}_9	μ	μ'	\bar{K}_9	μ	μ'	l_y/l_x
1.95	6.62	0.066	4.30	0.383	6.51	-0.014	0.091	4.87	0.339	0.252	6.63	-0.030	0.067	1.95
2.00	6.60	0.061	4.23	0.382	6.50	-0.014	0.086	4.82	0.348	0.249	6.60	-0.030	0.062	2.00
∞	~ 6.6	0	3.00	~ 0.38	~ 6.5	0	0	4.00	0.500	~ 0.24	~ 6.6	0	0	∞
MF	D/l_x		D/l_x		D/l_x			D/l_x			D/l_x			MF

Notes: l_x is always the shorter span! D = flexural rigidity (1.2.28); MF = multiplication factor. From Ref. [12.4.5].

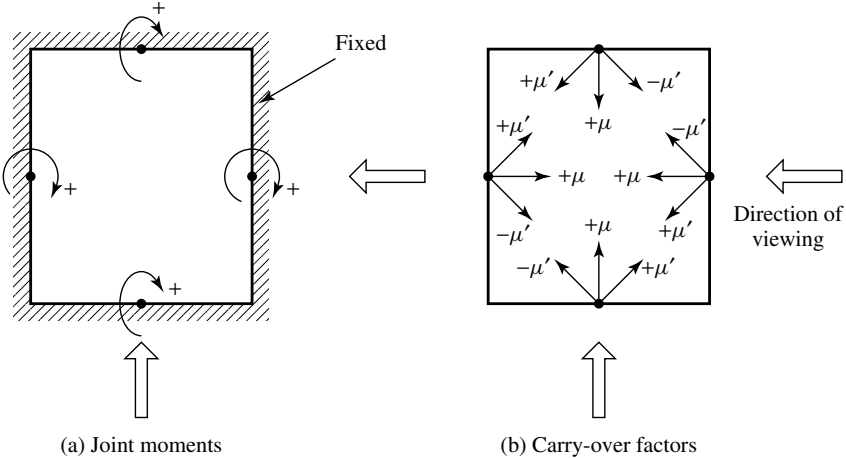


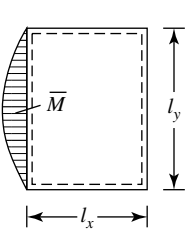
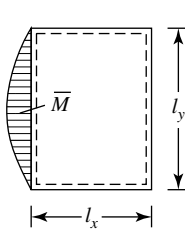
Figure 12.4.4 Sign conventions.

plate, we take the algebraic sum of moments caused by sinusoidal edge moments upon which the moments of the simply supported plate subjected to lateral loads are superimposed. Again, to determine these center moments of simply supported plates, we may either use the readily available formulas published in the pertinent technical literature[†] or calculate these moments by using Navier’s method. Calculating the corresponding effects caused by the restraining edge moments, however, is much more complex. Although theoretically we may use Eqs. (3.15) and (3.17) for this purpose, this approach is quite tedious. Instead, we can utilize the following formulas developed by Brunner [12.4.5]:

$$\begin{aligned} m_x &= (M_1 + M_3)\bar{c}_x + (M_2 + M_4)c_x, \\ m_y &= (M_1 + M_3)\bar{c}_y + (M_2 + M_4)c_y. \end{aligned} \tag{12.4.9}$$

[†] See also the “Plate Formulas” on the accompanying CD.

Table 12.4.2 Coefficients for Field Moments

$\nu = 0$					$\nu = 0.3$				
									
l_y/l_x	\bar{c}_x	\bar{c}_y	c_x	c_y	\bar{c}_x	\bar{c}_y	c_x	c_y	l_y/l_x
1.00	0.056	0.144	0.144	0.056	0.099	0.160	0.160	0.099	1.00
1.05	0.070	0.144	0.142	0.042	0.112	0.165	0.155	0.086	1.05
1.10	0.083	0.144	0.140	0.032	0.126	0.169	0.150	0.074	1.10
1.15	0.098	0.143	0.136	0.023	0.139	0.172	0.144	0.064	1.15
1.20	0.109	0.142	0.133	0.015	0.152	0.175	0.138	0.055	1.20
1.25	0.123	0.141	0.129	0.000	0.165	0.177	0.133	0.047	1.25
1.30	0.136	0.139	0.126	-0.002	0.177	0.179	0.127	0.039	1.30
1.35	0.148	0.137	0.122	-0.004	0.188	0.181	0.122	0.033	1.35
1.40	0.161	0.135	0.118	-0.008	0.201	0.182	0.115	0.027	1.40
1.45	0.172	0.131	0.113	-0.012	0.212	0.183	0.110	0.023	1.45
1.50	0.185	0.128	0.109	-0.015	0.223	0.183	0.104	0.018	1.50
1.55	0.196	0.125	0.104	-0.017	0.233	0.184	0.099	0.014	1.55
1.60	0.207	0.122	0.100	-0.019	0.243	0.184	0.094	0.011	1.60
1.65	0.218	0.118	0.095	-0.021	0.252	0.184	0.085	0.008	1.65
1.70	0.228	0.116	0.091	-0.022	0.262	0.184	0.084	0.005	1.70
1.75	0.238	0.112	0.087	-0.024	0.270	0.183	0.080	0.003	1.75
1.80	0.247	0.108	0.084	-0.025	0.279	0.183	0.076	0.000	1.80
1.85	0.256	0.106	0.079	-0.025	0.287	0.182	0.071	-0.001	1.85
1.90	0.264	0.103	0.075	-0.025	0.295	0.182	0.067	-0.002	1.90
1.95	0.272	0.100	0.071	-0.024	0.302	0.181	0.064	-0.003	1.95
2.00	0.280	0.097	0.068	-0.024	0.310	0.181	0.060	-0.004	2.00
∞	0.500	0.000	0.000	0.000	5.000	0.150	0.000	0.000	∞

The coefficients c_x , \bar{c}_x , c_y and \bar{c}_y for RC ($\nu = 0$) and for steel ($\nu = 0.3$) are listed in Table 12.4.2. The above-given equations consider that all four edge moments M_1 , M_2 , M_3 and M_4 are acting simultaneously on all edges (Fig. 12.4.4).

Although Brunner developed this moment distribution technique for uniformly distributed lateral loads, the procedure can also be used for other types of lateral loads, provided the edge moments are fairly symmetrical with respect to the joint points. For entirely arbitrary loading conditions, the application of a similar *slope distribution* procedure is recommended [12.4.7, 12.4.8]. This approach is, however, somewhat more complicated since more than one term in the sine series expressions of the edge moments must be considered.

ILLUSTRATIVE EXAMPLE I

Let us check the joint-point moments of the plate problem shown in Fig. 12.3.8 by applying the moment distribution method.

To obtain the required fixed-end moment at the joint point ①, we use the “Plate Formulas” listed on the accompanying CD. This gives

$$\frac{l_y}{l_x} = \frac{10}{8} = 1.25, \quad M_1^* = -0.1006 p_0 l_x^2 = -19.32 \text{ kN-m/m.} \quad (12.4.10)$$

Similarly, for joint point ② we obtain

$$\begin{aligned} \frac{l_y}{l_x} &= \frac{10}{6} = 1.666, & M_2^* &= -0.0828 p_0 l_x^2 = -8.94 \text{ kN-m/m,} \\ M_4^* &= -M_2^* = -8.94 \text{ kN-m/m.} \end{aligned} \quad (12.4.11)$$

The flexural rigidities of the individual panels are

$$D_A = D_C = 8.01 \times 10^3 \text{ kN-m} \quad \text{and} \quad D_B = 18.99 \times 10^3 \text{ kN-m.} \quad (12.4.12)$$

The stiffness and carry-over factors for each panel are determined from Table 12.4.1:

Panel ①, type 2, $l_y/l_x = 1.25$:

$$\begin{aligned} \text{At point ①:} \quad \bar{K}_A &= 5.31 \left(\frac{8.019 \times 10^3}{8} \right) = 5.32 \times 10^3, \\ \mu &= 0.0. \end{aligned}$$

Panel ②, type 8, $l_y/l_x = 1.0$:

$$\begin{aligned} \text{At point ①:} \quad \bar{K}_B &= 7.1 \left(\frac{18.99 \times 10^3}{10} \right) = 13.48 \times 10^3, \\ \mu &= 0.114, \\ \mu' &= 0.259. \\ \text{At point ②:} \quad \bar{K}_B &= 7.49 \left(\frac{18.99 \times 10^3}{10} \right) = 14.22 \times 10^3, \\ \mu' &= 0.246. \end{aligned}$$

Panel ③, type 5, $l_y/l_x = 1.667$:

$$\begin{aligned} \text{At point ②:} \quad \bar{K}_C &= 4.98 \left(\frac{8.01 \times 10^3}{6} \right) = 6.65 \times 10^3, \\ \mu &= 0.349. \end{aligned}$$

The moment distribution factors are

$$\begin{aligned} (\text{DF})_A &= \frac{\bar{K}_A}{\bar{K}_A + \bar{K}_B} = \frac{5.32}{5.32 + 13.48} = 0.283, \\ (\text{DF})_B &= \frac{\bar{K}_B}{\bar{K}_A + \bar{K}_B} = \frac{13.48}{5.32 + 13.48} = 0.717 \end{aligned} \quad (12.4.13a)$$

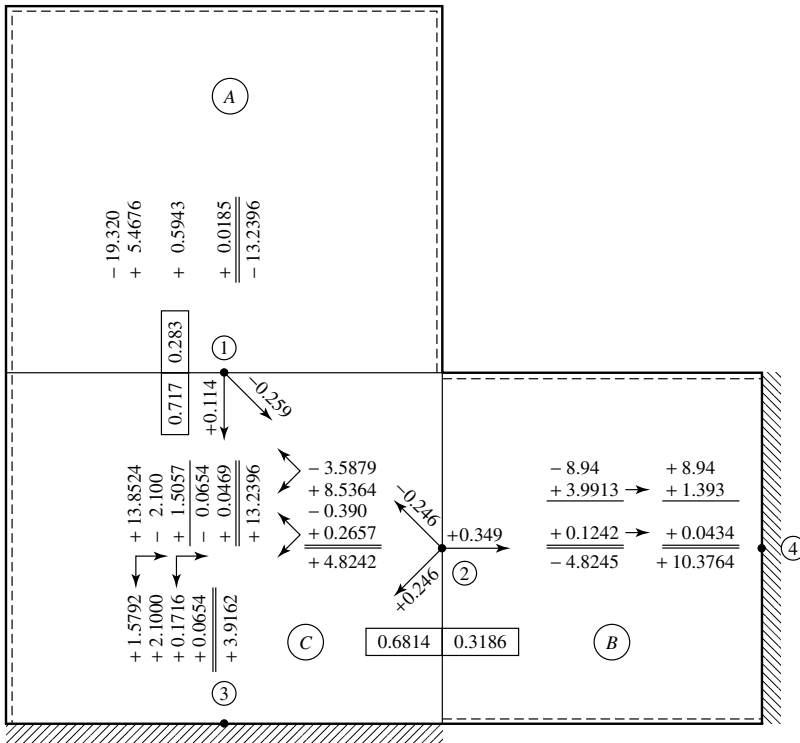


Figure 12.4.5 Moment distribution applied to plate shown in Fig. 12.3.8.

and

$$(DF)_B = \frac{14.22}{14.22 + 6.65} = 0.6814, \quad (DF)_C = \frac{6.65}{14.22 + 6.65} = 0.3186. \quad (12.4.13b)$$

The corresponding moment distribution process is illustrated in Fig. 12.4.5. Consequently, the final joint-point moments are

$$\mathbf{m} = \begin{Bmatrix} M_1 \\ M_2 \\ M_3 \\ M_4 \end{Bmatrix} = \begin{Bmatrix} -13.2396 \\ -4.8242 \\ +3.9162 \\ -10.3764 \end{Bmatrix} \quad \text{kN-m/m} \quad \begin{pmatrix} -4.30\% \\ -12.35\% \\ -8.42\% \\ -10.6\% \end{pmatrix}. \quad (12.4.14)$$

The percentile deviations from the previously obtained results are listed in parentheses. By taking the average of this and in Sec. 12.3 the calculated results

$$\mathbf{m}_{av} = \begin{Bmatrix} -13.54 \\ -5.16 \\ +4.10 \\ -10.99 \end{Bmatrix} \quad \text{kN-m/m}, \quad (12.4.15)$$

a good approximation of the joint-point moments can be achieved.

ILLUSTRATIVE EXAMPLE II

Panel (A) of the continuous RC square plate shown in Fig. 12.4.6 is subjected to a uniformly distributed lateral load $p_0 = 4.788 \text{ kN/m}^2$. Assume that the thickness $h = 1.0 \text{ m}$ of all panels is the same. Determine the edge moments at points (1), (2), (3) and (4) by applying the moment distribution method.

Again, we use the “Plate Formulas” listed on the accompanying CD to calculate the fixed-end moments at joint points (1) and (4). These are

$$M_1^* = M_4^* = -0.0677 p_0 l_x^2 = -32.4 \text{ kN-m/m}.$$

Since the flexural rigidity is the same for each panel, we can write

$$D_A = D_B = D_C = D_D = \frac{Eh^3}{12(1-\nu^2)} = \frac{20.68 \times 10^3}{12} = 1723 \text{ kN-m}. \quad (12.4.16)$$

The stiffness and carry-over factors are obtained from Table 12.4.1:

Panel (A), type 4, $l_y/l_x = 1.0$:

$$\text{At point (1): } K_A = \frac{7.01 \times 1723}{10} = 1207.8,$$

$$\mu' = 0.293,$$

$$\mu = 0.0.$$

The same values are valid also for panels (B), (C) and (D).

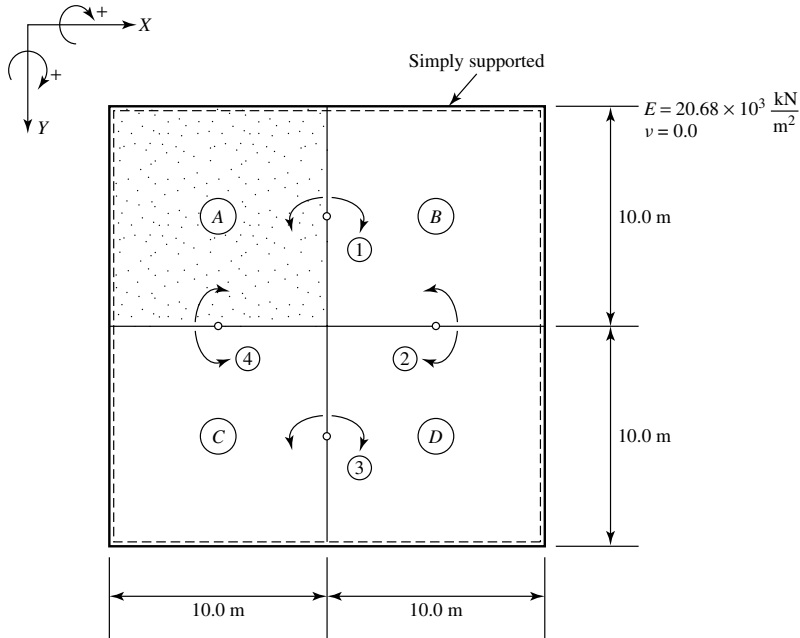


Figure 12.4.6 Continuous RC slab.

The moment distribution factor at point ① is

$$(DF)_A = \frac{1207.8}{1207.8 + 1207.8} = 0.5. \quad (12.4.17)$$

In this case, we can use the same factors for points ②, ③ and ④. The moment distribution process is shown in Fig. 12.4.7. This yielded the following joint-point moments:

$$\mathbf{m} = \begin{Bmatrix} M_1 \\ M_2 \\ M_3 \\ M_4 \end{Bmatrix} = \begin{Bmatrix} -18.57 \\ +2.37 \\ +2.37 \\ -18.57 \end{Bmatrix} \text{ kN-m/m.} \quad (12.4.18)$$

Checking the results with the simplified slope deflection method, practically no deviations could be found in the joint-point moments.

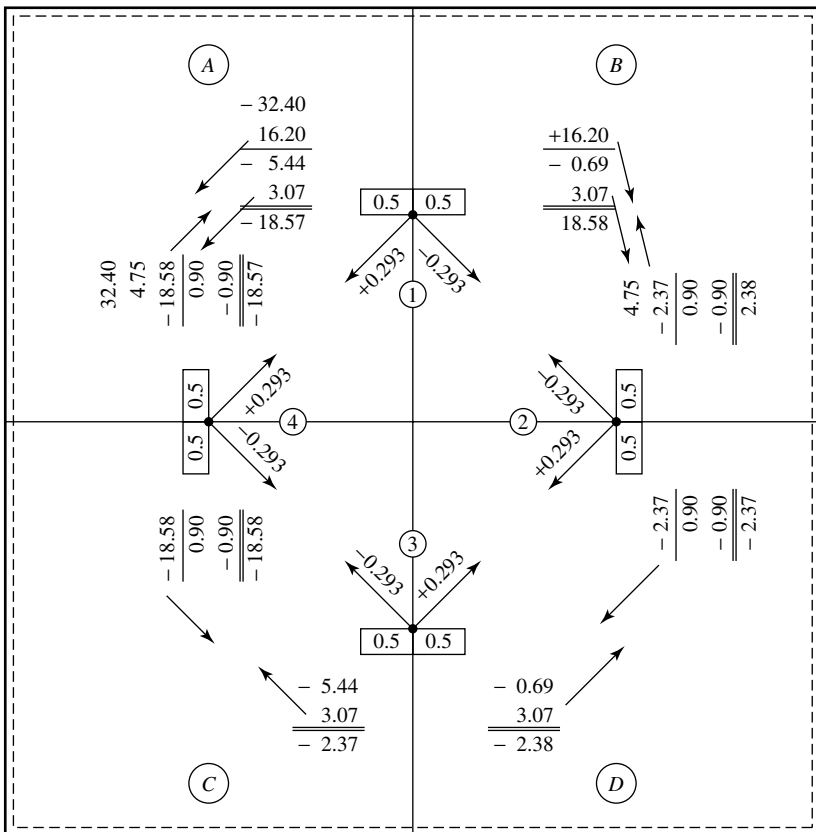


Figure 12.4.7 Moment distribution for plate shown in Fig. 12.4.6.

References and Bibliography

- [12.4.1] CROSS, H., "Analysis of Continuous Beams and Frames by Distributing the Fixed-End Moments," *Trans. ASCE*, 96 (1932), 1–10.
- [12.4.2] BORG, S. F., and GENARO, J. F., *Advanced Structural Analysis*, D. Van Nostrand, New York, 1960.
- [12.4.3] FISCHER, G., *Beitrag zur Berechnung kreuzweise gespannter Fahrbahnplatten im Stahlbrückenbau*, W. Ernst & Sohn, Berlin, 1952.
- [12.4.4] NEWMARK, N. M., "A Distribution Procedure for the Analysis of Continuous Rectangular Plates," *Bull. Eng. Exp. Sta.*, No. 304, University of Illinois, Urbana, 1938, p. 20.
- [12.4.5] BRUNNER, W., "Momentenausgleichsverfahren zur Berechnung durchlaufender Platten für gleichmässig verteilte Belastung," *Schweizerische Bauzeitung*, 75 (March 1957), 187–191.
- [12.4.6] ANG, A., "The Development of a Distribution Procedure for the Analysis of Continuous Rectangular Plates," *Civil Eng. Studies, Struct. Res. Series*, No. 176, University of Illinois, Urbana, 1959.
- [12.4.7] BRUNNER, W., "Drehwinkel-Ausgleichsverfahren zur Berechnung beliebig belasteter durchlaufenden Platten," *Beton- und Stahlbetonbau*, 56 (June 1961), 140–148.
- [12.4.8] SZILARD, R., *Theory and Analysis of Plates: Classical and Numerical Methods*, Prentice-Hall, Englewood Cliffs, New Jersey, 1974.

12.5 Practical Analysis of RC Floor Slabs

A simple, yet effective engineering procedure was developed by Pieper and Martens [12.5.1] for the analysis of RC floor slabs used in building construction. Applying this approach, the field moments at the center of individual panels can be calculated by taking the average of the corresponding field moments of plates with simply supported boundary conditions and those with completely fixed edges. To further simplify the application of this procedure, the pertinent constants are given in table or graphical forms.

Thus, the *field moments* at the center of plates with various types of boundary conditions can be obtained from

$$m_{fx} = \frac{ql_x^2}{f_x} \quad \text{and} \quad m_{fy} = \frac{ql_y^2}{f_y}, \quad (12.5.1)$$

where q is the sum of dead and live loads ($q = p_{DL} + p_{LL}$) and the constants f_x and f_y are listed in Table 12.5.1. In Eq. (12.5.1), l_x always represents the shorter span in the local coordinate system X, Y, Z of individual panels. One can even interpolate within this table between the given values.

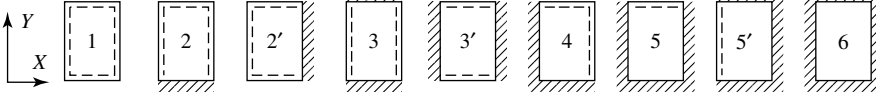
However, if the corners of simply supported plates are not properly anchored, one should use

$$m_{fx} = \frac{ql_x^2}{f_x^0} \quad \text{and} \quad m_{fy} = \frac{ql_y^2}{f_y^0}. \quad (12.5.2)$$

Again, the corresponding factors are listed in Table 12.5.1.

Similarly, negative moments at the supports are obtained by averaging the negative moments of plates with completely fixed boundaries, provided this average value is not smaller than 75% of the largest negative moment. This procedure is valid only if the span ratios of the neighboring panels are smaller than 5:1. If it is not the case, one should use the edge moment of the larger panel.

Table 12.5.1 Coefficients for Field and Support Moments

Types														
														
Type	Span Ratio l_y/l_x Coefficient	1.0	1.1	1.2	1.3	1.4	1.5	1.6	1.7	1.8	1.9	2.0	$> \infty$	
1	f_x	27.2	22.4	19.1	16.8	15.0	13.7	12.7	11.9	11.3	10.8	10.4	8.0	
	f_y	27.2	27.9	29.1	30.9	32.8	34.7	36.1	37.3	38.5	39.4	40.3	*	
	f_x^0	20.0	16.6	14.5	13.0	11.9	11.1	10.6	10.2	9.8	9.5	9.3	8.0	
	f_y^0	20.0	20.7	22.1	24.0	26.2	28.3	30.2	31.9	33.4	34.7	35.9	*	
2	f_x	32.8	26.3	22.0	18.9	16.7	15.0	13.7	12.8	12.0	11.4	10.9	8.0	
	f_y	29.1	29.2	29.8	30.6	31.8	33.5	34.8	36.1	37.3	38.4	39.5	*	
	s_y	11.9	10.9	10.1	9.6	9.2	8.9	8.7	8.5	8.4	8.3	8.2	8.0	
	f_x^0	26.4	21.4	18.2	15.9	14.3	13.0	12.1	11.5	10.9	10.4	10.1	8.0	
	f_y^0	22.4	22.8	23.9	25.1	26.7	28.6	30.4	32.0	33.4	34.8	36.2	*	
2'	f_x	29.1	24.6	21.5	19.2	17.5	16.2	15.2	14.4	13.8	13.3	12.9	10.2	
	f_y	32.8	34.5	36.8	38.8	40.9	42.7	44.1	45.3	46.5	47.2	47.9	*	
	s_x	11.9	10.9	10.2	9.7	9.3	9.0	8.8	8.6	8.4	8.3	8.3	8.0	
	f_x^0	22.4	19.2	17.2	15.7	14.7	13.9	13.2	12.7	12.3	12.0	11.8	10.2	
	f_y^0	26.4	28.1	30.3	32.7	35.1	37.3	39.1	40.7	42.2	43.3	44.8	*	
3	f_x	38.0	30.2	24.8	21.1	18.4	16.4	14.8	13.6	12.7	12.0	11.4	8.0	
	f_y	30.6	30.2	30.3	31.0	32.2	33.8	35.9	38.3	41.1	44.9	46.3	*	
	s_y	14.3	12.7	11.5	10.7	10.0	9.5	9.2	8.9	8.7	8.5	8.4	8.0	
3'	f_x	30.6	26.3	23.2	20.9	19.2	17.9	16.9	16.1	15.4	14.9	14.5	12.0	
	f_y	38.0	39.5	41.4	43.5	45.6	47.6	49.1	50.3	51.3	52.1	52.9	*	
	s_x	14.3	13.5	13.0	12.6	12.3	12.2	12.0	12.0	12.0	12.0	12.0	12.0	
4	f_x	33.2	27.3	23.3	20.6	18.5	16.9	15.8	14.9	14.2	13.6	13.1	10.2	
	f_y	33.2	34.1	35.5	37.7	39.9	41.9	43.5	44.9	46.2	47.2	48.3	*	
	s_x	14.3	12.7	11.5	10.7	10.0	9.6	9.2	8.9	8.7	8.5	8.4	8.0	
	s_y	14.3	13.6	13.1	12.8	12.6	12.4	12.3	12.2	12.2	12.2	12.2	11.2	
	f_x^0	26.7	22.1	19.2	17.2	15.7	14.6	13.8	13.2	12.7	12.3	12.0	10.2	
	f_y^0	26.7	27.6	29.2	31.4	33.8	36.2	38.1	39.8	41.4	42.8	44.2	*	
5	f_x	33.6	28.2	24.4	21.8	19.8	18.3	17.2	16.3	15.6	15.0	14.6	12.0	
	f_y	37.3	38.7	40.4	42.7	45.1	47.5	49.5	51.4	53.3	55.1	58.9	*	
	s_x	16.2	14.8	13.9	13.2	12.7	12.5	12.3	12.2	12.1	12.0	12.0	12.0	
	s_y	18.3	17.7	17.5	17.5	17.5	17.5	17.5	17.5	17.5	17.5	17.5	17.5	
5'	f_x	37.3	30.3	25.3	22.0	19.5	17.7	16.4	15.4	14.6	13.9	13.4	10.2	
	f_y	33.6	34.1	35.1	37.3	39.8	43.1	46.6	52.3	55.5	60.5	66.1	*	
	s_x	18.3	15.4	13.5	12.2	11.2	10.6	10.1	9.7	9.4	9.0	8.9	8.0	
	s_y	16.2	14.8	13.9	13.3	13.0	12.7	12.6	12.5	12.4	12.3	12.3	11.2	
6	f_x	36.8	30.2	25.7	22.7	20.4	18.7	17.5	16.5	15.7	15.1	14.7	12.0	
	f_y	36.8	38.1	40.4	43.5	47.1	50.6	52.8	54.5	56.1	57.3	58.3	*	
	s_x	19.4	17.1	15.5	14.5	13.7	13.2	12.8	12.5	12.3	12.1	12.0	12.0	
	s_y	19.4	18.4	17.9	17.6	17.5	17.5	17.5	17.5	17.5	17.5	17.5	17.5	

Notes: If $h < 10$ cm, multiply the moment with $15(h + 5)$. The smaller span is l_x .

The negative moments at the supports can be calculated from

$$m_s = \begin{cases} \frac{m_{s01} + m_{s02}}{2} \geq 0.75 \min m_{s0} & \text{for } l_1 : l_2 < 5 : 1, \\ \min m_{s0} & \text{for } l_1 : l_2 > 5 : 1, \end{cases} \quad (12.5.3)$$

where

$$m_{s0} = -\frac{ql_x^2}{s_x} \quad \text{or} \quad m_{s0} = -\frac{ql_y^2}{s_y}. \quad (12.5.4)$$

Again, the corresponding coefficients s_x and s_y are listed in Table 12.5.1 for various panel types. The whole procedure is valid for[†]

$$p_{LL} \leq \frac{1}{3}q, \quad p_{LL} \leq 2p_{DL}, \quad p_{DL} \geq 0.5p_{LL}. \quad (12.5.5)$$

So far, we have assumed that the variation of spans between adjacent panels is relatively normal. There are, however, floor configurations where two small panels

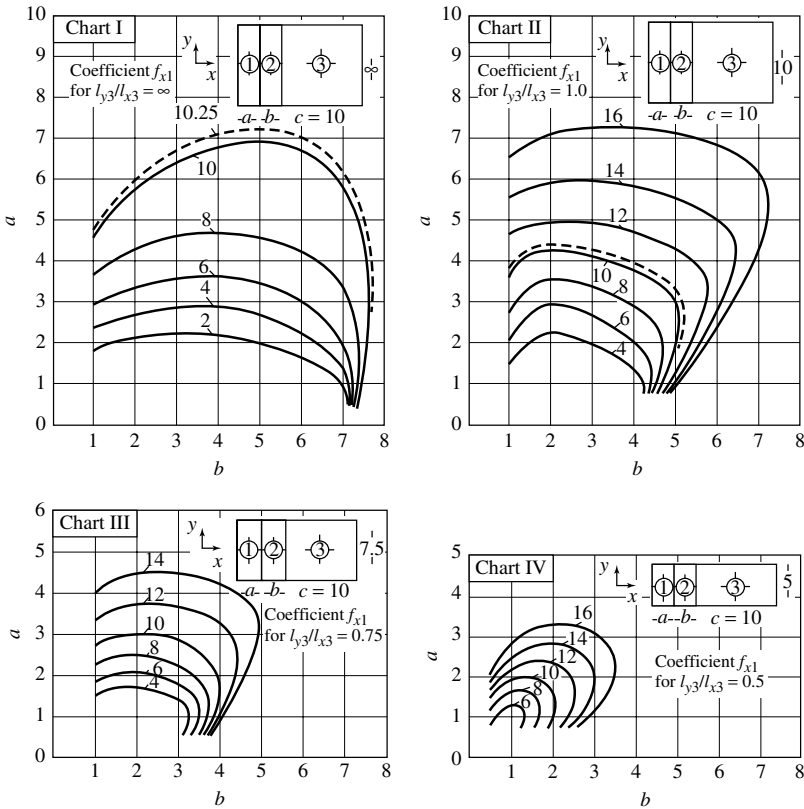


Figure 12.5.1 Design charts for uncommon span ratios.

[†] However, according to Ref. [12.5.2] the method can also be used for $p_{LL}/q \leq \frac{2}{3}$.

are attached to a large one. In such cases, the positive field moments of the **first** panel should be calculated from

$$m_{fx1} = \frac{ql_{x1}^2}{f_{x1}}. \quad (12.5.6)$$

The pertinent coefficients, f_{x1} , can be determined from the charts given in Fig. 12.5.1 for span ratios $l_{y3}/l_{x3} = \infty, 1.0, 0.75, 0.5$ and for $a = 10l_{x1}/l_{x3}$, $b = 10l_{x2}/l_{x3}$. In

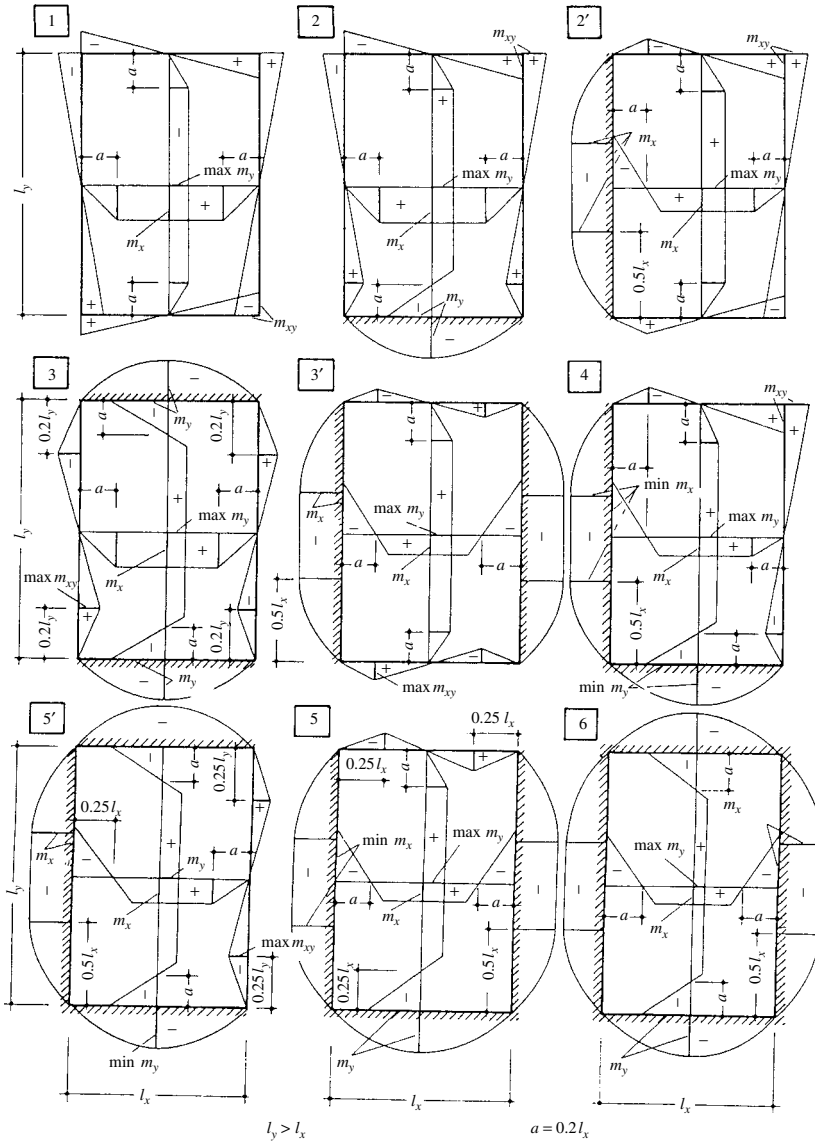


Figure 12.5.2 Approximate moment diagrams.

general, however, it is sufficient to use the chart that has a span ratio in the third panel nearest to the span ratio of the problem at hand. In that case, when the chart with lower values of l_{y3}/l_{x3} is selected, it is recommended that the number of reinforcing bars should be somewhat increased. If $f_{x1} > 10.25$, one should work with the coefficients given in Table 12.5.1.

The field moment at the center of the *second* panel is

$$m_{fx2} = \frac{1}{12}ql_{x2}^2. \tag{12.5.7}$$

However, if $f_{x1} < 10.25$, this indicates completely clamped edges on both sides. Thus, one should refer to the corresponding type in Table 12.5.1.

After the field moment m_{fx1} is determined, the edge moment at the first interior support can be calculated from

$$m_b = (\sqrt{2qm_{fxi}})l_{x1} - \frac{1}{2}ql_{x1}^2. \tag{12.5.8}$$

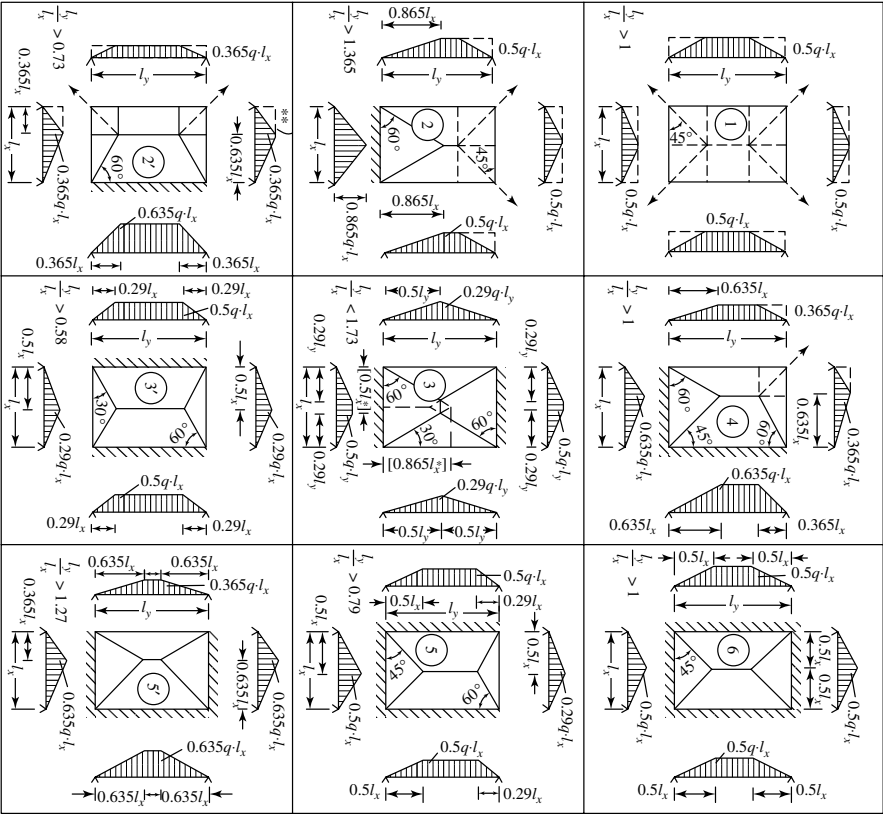


Figure 12.5.3 Approximate loads on supporting beams.

Again, if $f_{x1} < 10.25$, this indicates completely fixed boundaries on both sides, and one should proceed accordingly.

Approximate moment diagrams are shown in Fig. 12.5.2. Furthermore, the lateral load can be assigned to the corresponding supports according to Fig. 12.5.3. *Both figures can also be used for the other engineering methods treated earlier.* In addition, it is noteworthy to mention that the method of Pieper and Martens can also handle cases where only three edges meet at a corner point, as shown below in Illustrative Example II.

ILLUSTRATIVE EXAMPLE I

Let us determine the positive field and negative support moments of the RC slab configuration shown in Fig. 12.5.4. All panels carry uniformly distributed loads $p_{DL} = 0.3q$ and $p_{LL} = 0.7q$, where $q = p_{LL} + p_{DL}$; thus $p_{DL}/q = 0.3$.

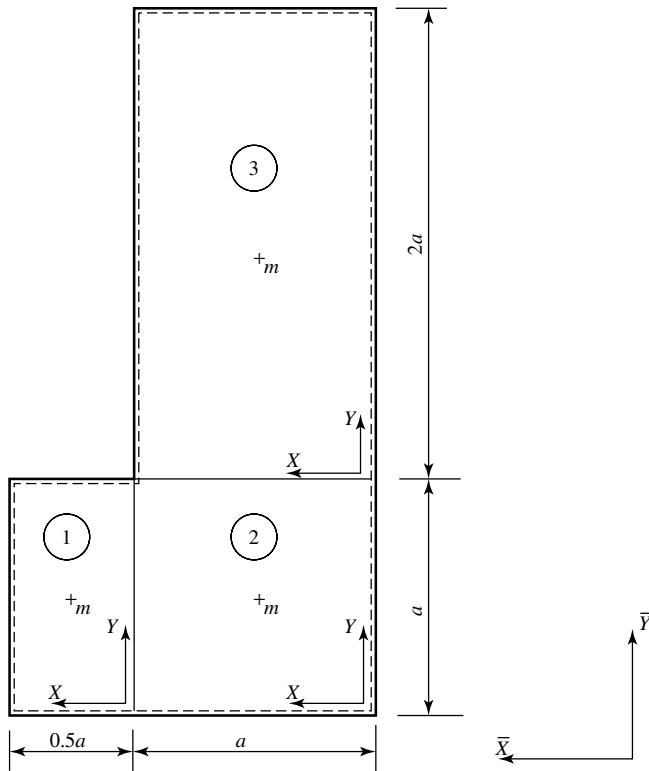


Figure 12.5.4 Floor slab with various aspect ratios.

Table 12.5.2 summarizes the calculation of the field moments at the center of each panel, and Table 12.5.3 summarizes the calculation of the negative edge moments at the partially clamped boundaries.

Table 12.5.2 Moments at Center of Panels (Fig. 12.5.4)

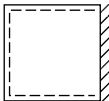
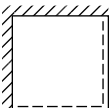
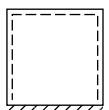
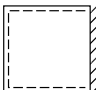
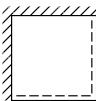
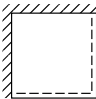
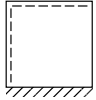
Panel Number	Type	l_y	l_x	$\varepsilon = l_y/l_x$	Coefficients		Moments		
					f_x	f_y	m_{x_m}	m_{y_m}	
1		2'	a	$0.5a$	2.0	12.9	47.9	$0.0194qa^2$	$0.0052qa^2$
2		4	a	a	1.0	33.2	33.2	$0.0301qa^2$	$0.0301qa^2$
3		2	$2a$	a	2.0	10.9	39.5	$0.0917qa^2$	$0.0253qa^2$

Table 12.5.3 Moments at Middle of Supports (Fig. 12.5.4)

Panel i , Panel k	Type	l_y	l_x	$\varepsilon = l_y/l_x$	Coefficients		Moments			
					s_x	s_y	m_{s_0}	$m_{s_{i-k}} \geq$	$0.75m_{s_{0,min}}$	
1		2'	a	$0.5a$	2.0	-8.3	—	$-0.0301qa^2$	$-0.0500qa^2$	$-0.0525qa^2$
2		4	a	a	1.0	-14.3	—	$-0.0699qa^2$	$-0.0500qa^2$	$-0.0525qa^2$
2		4	a	a	1.0	—	-14.3	$-0.0699qa^2$	$-0.0960qa^2$	—
3		2	$2a$	a	2.0	—	-8.2	$-0.1220qa^2$	$-0.0960qa^2$	—

ILLUSTRATIVE EXAMPLE II

Figure 12.5.5 shows an unconventional floor-slab configuration where at corner point k only three plate edges meet. Let us determine the positive field moments at the center of each panel and the negative edge moments at the partially clamped plate boundaries. The floor-slab configuration carries a uniformly distributed load $q = \text{const}$. Poisson's ratio is $\nu = 0$.

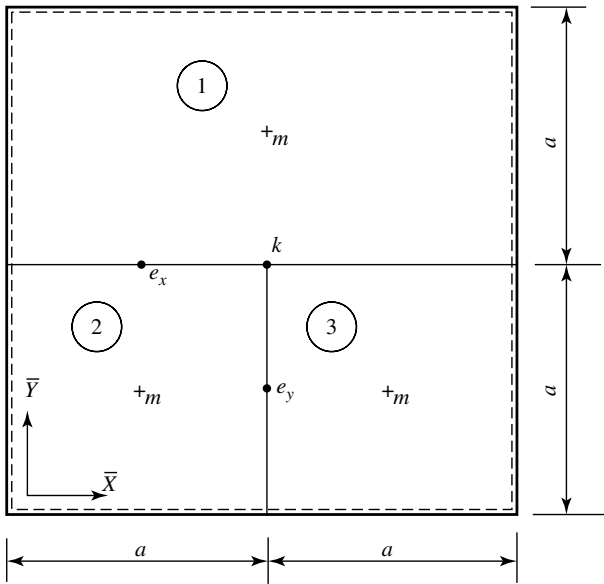


Figure 12.5.5 Uncommon slab configuration.

Calculation of the positive moments at the center of each panel is summarized in Table 12.5.4. Similarly, calculation of the negative moments at the panel supports is given in Table 12.5.5.

Table 12.5.4 Field Moments of Slab Shown in Fig. 12.5.5

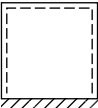
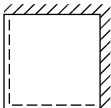
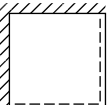
Panel Number	Type	l_x	l_y	$\varepsilon = l_y/l_x$	Coefficients		Moments		
					f_x	f_y	m_{x_m}	m_{y_m}	
①		2'	a	$2a$	2	12.9	47.9	$0.0775qa^2$	$0.0209qa^2$
②		4	a	a	1	33.2	33.2	$0.0301qa^2$	$0.0301qa^2$
③		4	a	a	1	33.2	33.2	$0.0301qa^2$	$0.0301qa^2$

Table 12.5.5 Moments at Supports (Fig. 12.5.5)

Panel <i>i</i> , Panel <i>k</i>		Type	l_x	l_y	$\varepsilon = l_y / l_x$	Coefficients		Moments				
						s_x	s_y	m_{s_0}	$m_{s_{i-k}}$	$\geq 0.75m_{s_{0,min}}$		
①	①		2'	a	$2a$	2	-8.3	—	$-0.1204qa^2$	$-0.0952qa^2$	—	$\hat{=} m_{x_{ex}}$
②	③		4	a	a	1	-14.3	—	$-0.0699qa^2$	$-0.0952qa^2$	—	$\hat{=} m_{x_{ex}}$
②			4	a	a	1	—	-14.3	$-0.0699qa^2$	$-0.0699qa^2$	—	$\hat{=} m_{y_{ey}}$
③			4	a	a	1	—	-14.3	$-0.0699qa^2$	$-0.0699qa^2$	—	$\hat{=} m_{y_{ey}}$

References and Bibliography

[12.5.1] PIEPER, K., and MARTENS, P., “Durchlaufende vierseitig gestützte Platten im Hochbau,” *Beton- und Stahlbetonbau*, 6 (1966), 158–162.

[12.5.2] UTESCHER, G., “Zuschrift zu K. Pieper und P. Martens: Durchlaufende vierseitig gestützte Platten im Hochbau,” *Beton- und Stahlbetonbau*, 7 (1967), 150–151.

12.6 Equivalent Frame Method Applied to Flat Slabs

The analytical solution of flat-slab problems is inherently complex, as described in Sec. 10.6 and demonstrated in Refs. [12.6.1] and [12.6.2]. To simplify this analytical procedure, we have even neglected the flexural stiffness of the supporting columns. This simplification gives usable results as long as the columns are quite slender or carry only vertical reactions. In the case of realistic column dimensions and uneven column spacing or alternative loading of panels, however, the interaction between columns and slabs can no longer be neglected.

Since all analytical procedures that consider the monolithic connection between columns and slab are highly complex and therefore time consuming, it is more advantageous to use simplified engineering methods for routine design of flat slabs. A suitable practical approach, which is in good agreement with pertinent test results, replaces the flat-slab–column structure by an *equivalent* rigid frame. Such a frame consists of a row of upper and lower columns at each floor, as shown in Fig. 12.6.1.

Codes of practice for RC structures [12.6.3, 12.6.4] permit the use of such *equivalent frames* for the analysis of flat slabs and flat plates. However, the usefulness of such simplification in predicting the actual structural response of these structures

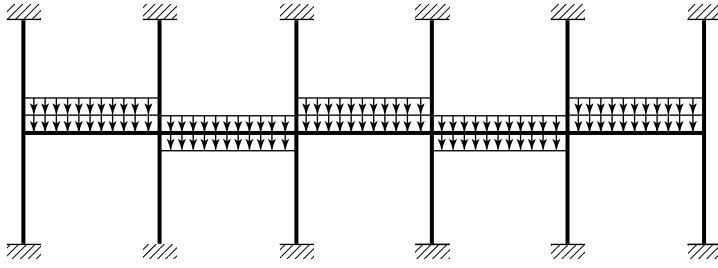


Figure 12.6.1 Equivalent rigid frame.

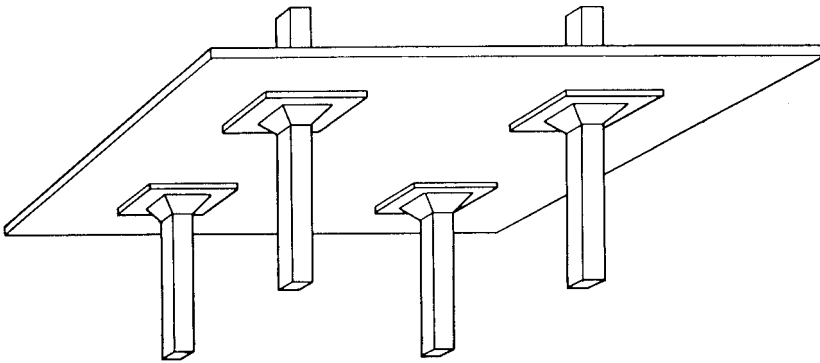


Figure 12.6.2 Flat slab with drop panels and column capitals.

depends to a large extent on realistic evaluation of the flexural stiffness of the equivalent beam and on the fraction of the total frame moments distributed across the panels. This procedure becomes somewhat more complicated for flat slabs with drop panels and/or with column capitals (Fig. 12.6.2), which cause a variation in the flexural stiffness of the slab. For this reason, here we use recommendations for the stiffness of flat slabs with drop panels given in Ref. [12.6.5]. Furthermore, we distribute the total frame moments across the panels according to Fig. 12.6.3. All designs of flat slabs without column capitals also apply to flat plates.

For the equivalent beams, we take the continuous floor slab of a bay width; thus, its moments of inertia in the X and Y directions are

$$I_x = I_y \frac{h^3}{12} \quad \text{and} \quad I_y = I_x \frac{h^3}{12}. \quad (12.6.1)$$

We usually analyze these equivalent rigid frames by applying the familiar moment distribution technique [12.4.2] in the longitudinal and transverse directions at each floor level. However, the obtained positive and negative moments ($\pm M$) must be distributed across the panels, according to Fig. 12.6.3, or be modified as follows:

$$m_x = \begin{cases} \frac{M_x}{l_y} \left(1 - \frac{1}{5} \cos \frac{\pi y}{b} \right) & \text{at } x = 0, \\ \frac{M_x}{l_y} \left(1 - \frac{3}{5} \cos \frac{\pi y}{b} \right) & \text{at } x = \pm a. \end{cases} \quad (12.6.2)$$

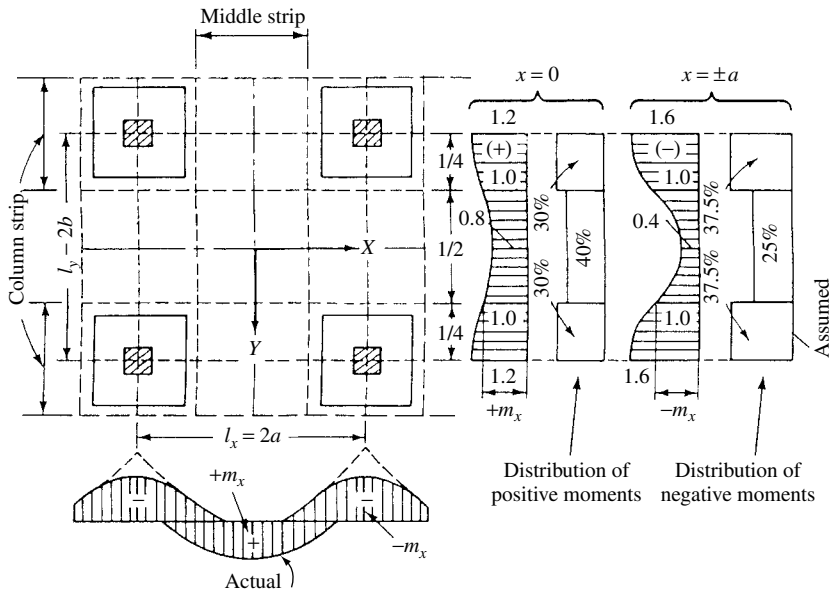


Figure 12.6.3 Assumed distribution of frame moments across panel.

A similar expression gives the distribution of frame moments in the Y direction. The shear forces are also determined from the analysis of the equivalent frame.

If required, further refinement in the equivalent frame analysis can be obtained by considering the variable moment of inertia of the slab. That is, if dropped panels are used, the cross section of the slab near the columns becomes T shaped. At the edge of the column, the moment of inertia of the equivalent horizontal beam must be further increased, because it includes a portion of the drop panel or column capital. Since calculation of the required coefficients for the moment distribution method is quite tedious, design charts are presented in Fig. 12.6.4 to simplify this part of the analysis. For example, for coefficients k_{ij} of the chart, the flexural stiffness of the slab with drop panel is

$$K_{ij} = \frac{k_{ij} E I_{ij}}{l_{ij}}, \quad (12.6.3)$$

where I_{ij} is the moment of inertia of the slab as defined by Eq. (12.6.1). Similarly the fixed-end moment of the l_{ij} span is calculated from

$$M_{ij}^* = f_{ij} P_0 l_{ij}^2, \quad (12.6.4)$$

while c_{ij} gives the carry-over factor of the equivalent frame. In this notation the first subscript represents the joints in question and P_0 denotes the uniformly distributed resultant line load (per unit length of the bay span).

For the following reasons, the equivalent frame method presented here is more general than the so-called direct design method described in various codes:

- There are no limitations on dimensions or loading.

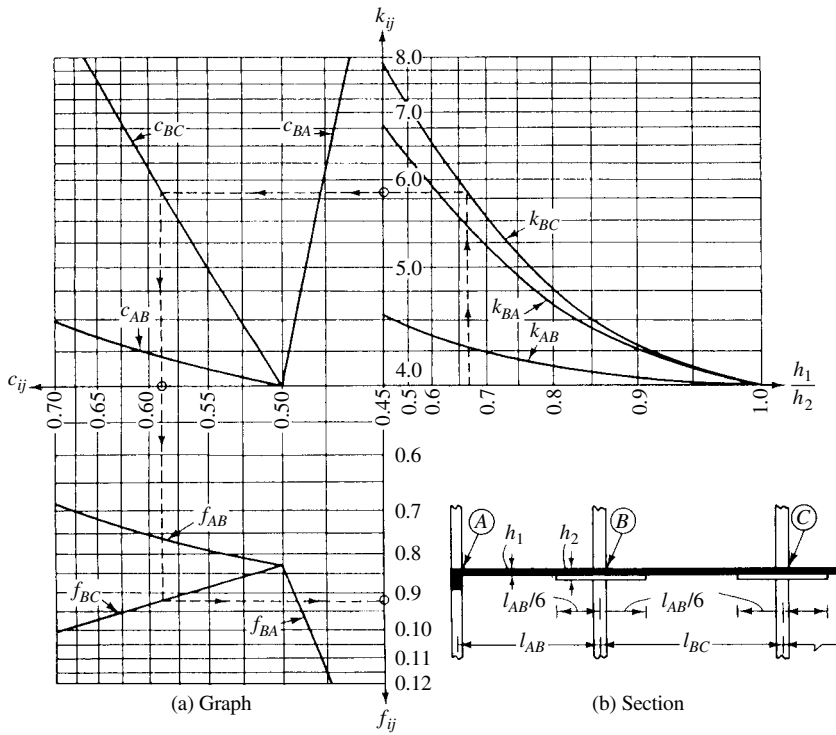


Figure 12.6.4 Charts for coefficients of equivalent frame.

- The moments of the equivalent rigid frame are determined by classical elastic analysis.
- It can also be used for lateral load condition.

As the Illustrative Example demonstrates, the results are in good agreement with those calculated by the yield-line method (Sec. 13.6).

One can extend this approach even to flat slabs with flared column capitals by introducing

$$l'_x = l_x - 2c_x \quad \text{and} \quad l'_y = l_y - 2c_y \quad (12.6.5)$$

equivalent interior span lengths. Similarly, for exterior panels the equivalent span lengths are

$$l'_x = l_x - c_x \quad \text{and} \quad l'_y = l_y - c_y. \quad (12.6.6)$$

In these expressions the value of c , the *effective support size*, depends on the type of *column flare*, as illustrated in Fig. 12.6.5.

Deflections of the flat slab can also be estimated by using the equivalent frame method [12.6.10]. It is convenient to find the midspan deflection of each panel as a sum of three parts: (a) deflection of the panel assumed to be fixed at both ends and (b) deflections caused by the additional rotations of the left and right supports.

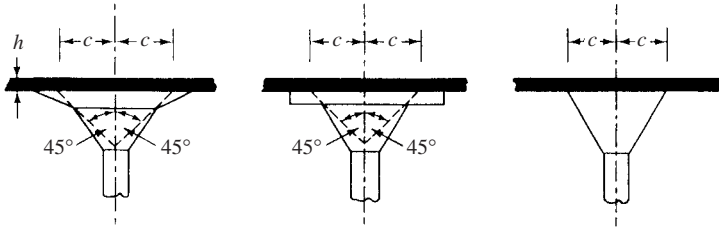


Figure 12.6.5 Effective support size for flared columns.

To obtain the fixed-end deflection of the column strip, we first calculate the midspan deflection of a uniformly loaded beam with fixed ends. This gives

$$d_{\text{beam}} = \frac{pl^4}{384EI_{\text{frame}}}, \quad (12.6.7)$$

where p is the load per unit length acting on the full width of the equivalent frame and I_{frame} represents the moment of inertia of the equivalent frame by considering, again, its full width, as given in Eq. (12.6.1).

Equation (12.6.7) provides a basis for further determination of the fixed-end deflection of the column strip or middle strip using the M/EI ratio of the strip in question to that of the full panel. Thus, we write

$$d_{\text{strip}} = d_{\text{beam}} \frac{M_{\text{strip}}}{M_{\text{frame}}} \frac{EI_{\text{frame}}}{EI_{\text{strip}}}, \quad (12.6.8)$$

where I_{strip} is the moment of inertia of the column strip or the middle strip.

The joint-point rotation can be expressed by

$$\theta = \frac{M_{\text{net}}}{K_c}, \quad (12.6.9)$$

where M_{net} is the net applied moment of the equivalent frame at the column and K_c denotes the column stiffness. Thus, the center deflection of the equivalent frame subjected to θ rotation (expressed in radians) at one of its fixed ends is

$$d\theta = \frac{1}{8}\theta l. \quad (12.6.10)$$

Consequently, the total deflection at the midspan of the panel becomes

$$d = d_{\text{strip}} + d_{0,\text{left}} + d_{0,\text{right}}. \quad (12.6.11)$$

ILLUSTRATIVE EXAMPLE

A RC flat slab with drop panels has 5×5.00 m column spacings in the X direction and 4×4.00 m in the Y direction. This floor carries the weight of the slab and toppings ($p_{\text{DL}} = 5.1$ kN/m²) and a live-load $p_{\text{LL}} = 2.55$ kN/m². The slab thickness is $h = 0.13$ m, and the thickness of the drop panels is

0.10 m. The other properties of the RC slab are $E = 2.25 \times 10^3 \text{ kN/cm}^2$ and $\nu = \frac{1}{6}$. The slab is supported by $0.40 \times 0.40\text{-m}$ square RC columns in monolithic construction. To be able to design this floor system, we have to determine all positive and negative moments to which the individual panels are subjected.

Since the structure and lateral loads have double symmetry, it is sufficient to consider only one analysis quadrant of this plate system, as shown in Fig. 12.6.6. A typical section of the slab at a column is illustrated in Fig. 12.6.7. Furthermore, to analyze this flat slab, we utilize the *equivalent frame method*. Strictly speaking, to obtain the maximum field moments, we should use the loading patterns given in Fig. 10.6.6. Similarly, the critical loading for the negative moments at the columns requires that dead and live loads act on all panels around the columns. Although we can use these loading patterns without any complications to rationalize our calculations, we apply the *load factor* approach here, which, according to American Concrete Institute (ACI) building codes [12.6.3], specifies that

$$p_0 = 1.4p_{DL} + 1.7p_{LL} = 15.85 \text{ kN/m}^2, \quad (12.6.12)$$

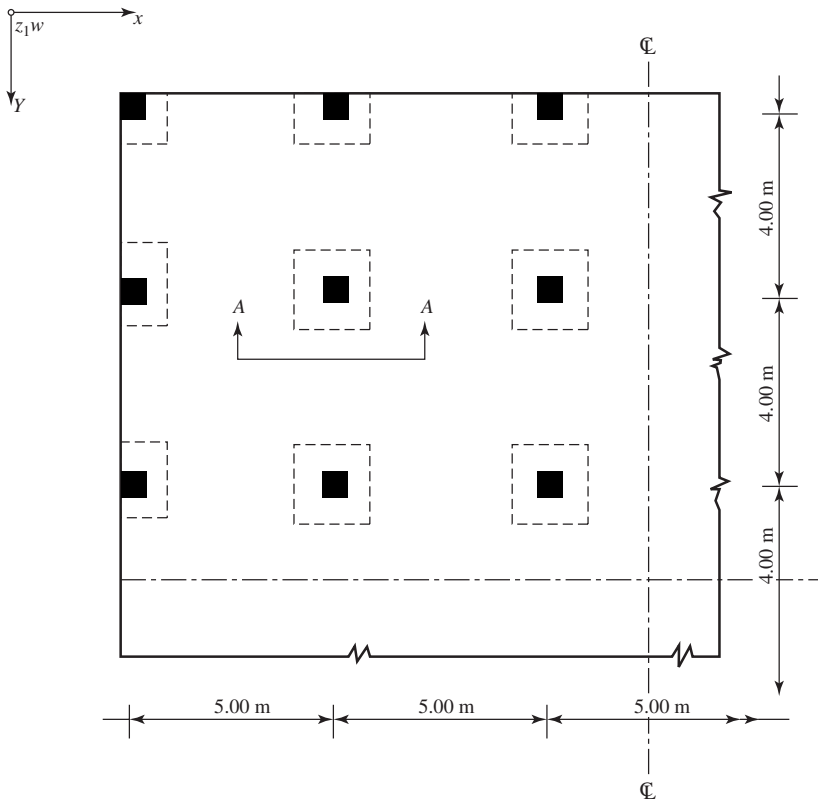


Figure 12.6.6 Analysis quadrant of flat-slab floor.

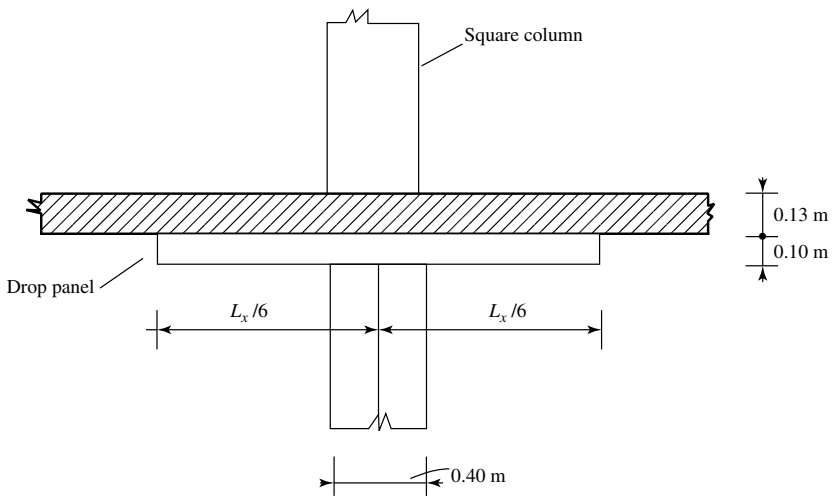


Figure 12.6.7 Typical section A-A.

a uniformly distributed *factored* load to be resisted by the related internal forces of the slab. In addition, we make use of the design charts given in Fig. 12.6.4 to determine the stiffness factors, carry-over factors and fixed-end moments of the equivalent frame required for the conventional moment distribution procedure of rigid frames.

Let us assume that the uniformly distributed *factored* load is 15.85 kN/m^2 and the length of the columns is 3.0 m . The equivalent frame for the *interior* slab column configuration in the X direction is shown in Fig. 12.6.8. The line load carried by this frame amounts to $p_0 = 15.85 \times 4 = 63.4 \text{ kN/m}$. Using the previously introduced design charts,[†] we obtain the following coefficients[‡] for

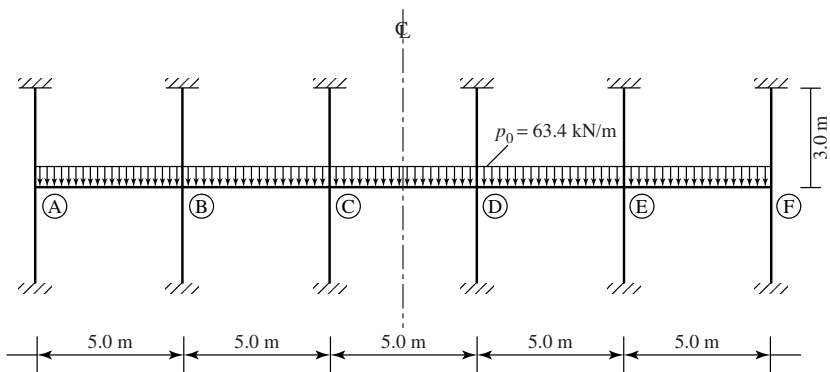


Figure 12.6.8 Equivalent frame for interior panels in X direction.

[†] See Fig. 12.6.4.

[‡] Because of symmetry, coefficients for the other members, CD , DC and DE , ED , are the same.

the ratio of the slab to the slab and drop panel ($13/23 \approx 0.565$):

$ij; ji$	k_{ij}	c_{ij}	f_{ij}
$AB; EF$	4.40	0.651	0.071
$BA; FE$	6.08	4.54	0.114
$BC; CB$	7.00	0.624	0.096

(12.6.13)

With

$$I_{AB} = \frac{bh^3}{12} \approx 91.54 \times 10^3 \text{ cm}^4, \quad (12.6.14)$$

Eq. (12.6.3) gives the flexural stiffness of the equivalent beam members. For member AB , for instance, we obtain

$$K_{AB} = \frac{k_{AB}EI_{AB}}{l_{AB}} = 18.12 \times 10^3 \text{ kN-m}. \quad (12.6.15)$$

The corresponding fixed-end moment is calculated from Eq. (12.6.4). This gives

$$M_{AB} = f_{AB}p_0l_{AB}^2 = 0.071 \times 63.4 \times 25 = 112.5 \text{ kN-m}. \quad (12.6.16)$$

A similar approach for the other beam members gives

ij	K_{ij} (kN-m)	M_{ij} (kN-m)
AB	18.12×10^3	112.54
BA	25.03×10^3	178.19
BC	28.83×10^3	152.17

(12.6.17)

The stiffness of the columns is

$$I_{\text{col}} = \frac{d^4}{12} = \frac{40^4}{12} = 21.333 \times 10^4 \text{ cm}^4, \quad (12.6.18)$$

$$K_{\text{col}} = \frac{EI_{\text{col}}}{l_{\text{col}}} = \frac{(2.25 \times 10^6)(21.333 \times 10^4)}{300} = 16 \times 10^8 \text{ N-cm}.$$

The distribution factors required for the moment distribution are defined by

$$r_{ij} = \frac{K_{ij}}{\sum (K_{ij} + K_{\text{col}})}. \quad (12.6.19)$$

Thus, at joint B , for instance, the distribution factor for the beam member BA is

$$r_{BA} = \frac{K_{BA}}{K_{BA} + K_{BC} + 2K_{\text{col}}} = \frac{25.03}{25.03 + 28.83 + 2 \times 16} = 0.292. \quad (12.6.20)$$

In a similar way we obtain the other distribution factors:

$$r_{AB} = 0.452 \quad \text{and} \quad r_{BC} = r_{CB} = r_{CD} = r_{DC} = 0.336. \quad (12.6.21)$$

The carry-over factors c_{ij} and the fixed-end moments are already given in Eqs. (12.6.13) and (12.6.17), respectively.

Now, we are able to carry out the moment distribution on the equivalent frame. This procedure gives the following results for the joint moments[†]:

$$\begin{Bmatrix} M_{AB} \\ M_{BA} \\ M_{BC} \\ M_{CB} \\ M_{CD} \\ M_{DC} \end{Bmatrix} = \begin{Bmatrix} -66.77 \\ -194.83 \\ -171.56 \\ -142.75 \\ -156.38 \\ -156.38 \end{Bmatrix} \quad \text{kN-m.} \quad (12.6.22)$$

The corresponding positive field moments can be approximated by

$$m_{ij} \approx \frac{1}{8} p_0 l_{ij}^2 + \frac{1}{2} (M_{ij} + M_{ji}), \quad (12.6.23)$$

which gives

$$m_{AB} = 67.32 \text{ kN-m}, \quad m_{BC} = 40.97 \text{ kN-m}, \quad m_{CD} = 41.74 \text{ kN-m}. \quad (12.6.24)$$

In the next step, the obtained positive and negative moments of the equivalent frame should be distributed according to Fig. 12.6.3 between the column and middle strip. This distribution is summarized in Table 12.6.1.

Table 12.6.1 Distribution of Moments Across Panel

Span ($ij; ji$)	$M_{ij}; m_{ij}$ (kN-m)	Column (%)	Strip ($M_s; m_s$)	Middle (%)	Strip ($M_s; m_s$)
AB	-66.77	75	-50.08	25	-16.69
AB	+67.32	60	+40.39	40	+26.93
BA	-194.83	75	-146.12	25	-48.71
BC	-171.56	75	-128.67	25	-42.89
BC	+40.97	60	+24.58	40	+16.39
CB	-142.75	75	-107.06	25	-35.69
CD	-156.38	75	-117.28	25	-39.10
CD	+41.74	60	+25.01	40	+16.70
DC	-156.38	75	-117.28	25	-39.10

A similar procedure is used for the *exterior* column-slab configuration. These calculations should also be repeated for the *Y* direction to obtain a complete picture of the structural response of this flat slab. Needless to say, the analysis of a multistory flat-slab construction, even utilizing an engineering approach, is a difficult task.

[†] For the other members, again, symmetry should be applied.

References and Bibliography

- [12.6.1] LEWE, V., *Pilzdecken*, W. Ernst & Sohn, Berlin, 1926.
- [12.6.2] GREIN, K., *Pilzdecken: Theorie und Berechnung*, 3rd ed., W. Ernst & Sohn, Berlin, 1948.
- [12.6.3] ACI COMMITTEE 318, Building Code Requirements for Reinforced Concrete, American Concrete Institute, Detroit, Michigan, 1995.
- [12.6.4] COMITÉ EURO-INTERNATIONAL DU BETON (CEB), CEB-FIP Model Code, Bull. d'Information, Swiss Federal Institute at Technology, Lausanne, Switzerland, 1990.
- [12.6.5] MORRIS, D., "Design Coefficients for Flat Slab Structures with Drop Panels," *ACI J.*, 66 (Oct. 1967), 276–282.
- [12.6.6] DUDDECK, H., "Praktische Berechnung der Pilzdecken ohne Stützenkopfverstärkung," *Beton- und Stahlbetonbau*, 58 (Mar. 1963), 56–63.
- [15.6.7] FRASER, D. F., "Simplified Frame Analysis for Flat Plate Construction," *Concrete Int.* (Sept. 1984), 32–41.
- [12.6.8] PECKNOLD, D. F., "Slab Effective Width for Equivalent Frame Analysis," *ACI J.*, 72 (1975), 135–137.
- [12.6.9] FRASER, D. J., "Equivalent Frame Method for Beam Slab Structures," *ACI J.*, 74 (1977), 223–228.
- [12.6.10] NILSON, A. H., and WALTERS, D. B., "Deflection of Two-Way Floor Systems by Equivalent Frame Method," *ACI J.*, 72 (May 1975), 210–212.

12.7 Other Practical Design Methods

12.7.1 Approximate Analysis of Bridge Decks

Approximate values of moments in bridge-deck slabs produced by wheel loads of trucks can be calculated applying the simplified approach developed Rüschi [12.7.1], which gives

$$+m_{\max} \approx \mathbf{k}(+m_0) \quad \text{and} \quad -m_{\max} \approx \mathbf{k}(-m_0), \quad (12.7.1)$$

where m_0 is the pertinent maximum positive or negative moment due to the wheel load in the individual slabs with various boundary conditions and

$$\mathbf{k} = \frac{1.2}{1 + [l_x(\text{m})/100]} k_0 \quad \text{for } l_x \leq 20 \text{ m.} \quad (12.7.2)$$

Coefficient k_0 is given in Table 12.7.1. The last column in this table contains approximate values for moments at the first support, assuming that the slab is built monolithically with its supporting beam. It should be noted that l_x (in meters) is always the respective direction under consideration, as shown in Fig. 12.7.1.

Since beams usually provide elastic supports, the maximum moments given in Eq. (12.7.1) should be further corrected to take into account this effect. Thus, we can write

$$+m_{\max} \approx \mathbf{k}(+m_0)(1 + \alpha) \quad \text{and} \quad -m_{\max} \approx \mathbf{k}(-m_0)(1 - \alpha), \quad (12.7.3)$$

where

$$\alpha = \frac{lh^3 E_p}{12I_g E_g}. \quad (12.7.4)$$

In this expression, l is the span between the supporting beams or girders, h the thickness of the slabs, I_g the moment of inertia of the beam, E_p the modulus of elasticity of the slab and E_g the modulus of elasticity of the beam.

Table 12.7.1 Correction Factors for Moments of Continuous Bridge Slabs

		<i>k₀ at Points Shown in Fig. 12.7.1</i>				
	<i>l_y/l_x</i>	①	Ⓑ	②	Ⓒ	Ⓐ
Slab Supported at All Four Boundaries	≤0.8	1.00	1.00	1.05	1.00	$\frac{1}{2}M_B$
	1.0	1.05	0.96	1.13	1.00	$\frac{1}{2}M_B$
	1.2	1.07	0.94	1.18	1.00	$\frac{1}{2}M_B$
	∞	1.10	0.92	1.23	1.00	$\frac{1}{3}M_B$
Slab Supported at Two Opposite Boundaries Only	∞	1.10	0.92	1.23	1.00	$\frac{1}{3}M_B$
	1.0	1.14	0.89	1.30	1.00	$\frac{1}{3}M_B$
	0.50	1.22	0.82	1.45	1.00	$\frac{1}{3}M_B$
	0.25	Slab behaves as a continuous beam.				

Note: From Ref. [12.7.1].

Kupfer and Maier [12.7.2] have improved Rüsçh’s method by introducing equivalent plates, shown in Fig. 12.7.2. First, the maximum positive moment $+m_0$ and the maximum negative moment $-m_0$ of these individual roadway slabs are computed, preferably using the corresponding influence surfaces [10.5.1] or Lévy’s method. The effect of continuity and of loading on adjacent slabs can be approximated by the use of proper coefficients; thus

$$+m_{\max} \approx c_1(+m_0) \quad \text{and} \quad -m_{\max} \approx c_2(-m_0). \tag{12.7.5}$$

The coefficients to be used for *all* panels are given in Tables 12.7.2 and 12.7.3. The minimum moments for exterior slabs can be computed from

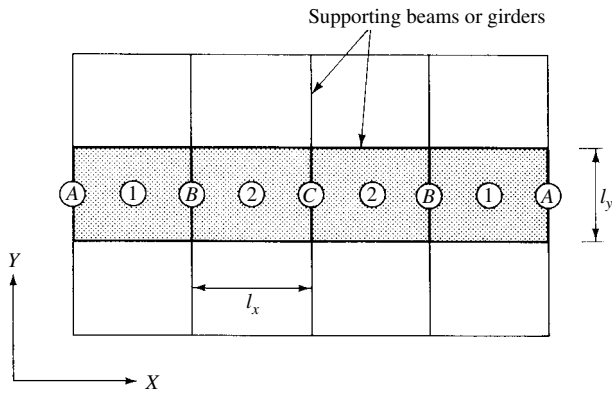
$$m_{\min} = (1 - c_1)(+m_0). \tag{12.7.6}$$

For the interior panels, Eq. (12.7.6) should be multiplied by 2.

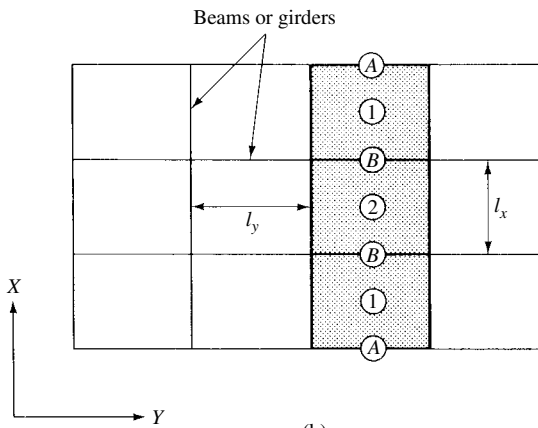
Table 12.7.2 Coefficient c_1

		<i>l_y/l_x</i>	≤0.8	1.0	1.2	1.4	1.6	1.8	2.0	3.0	3.5	∞
Edges simply supported (Fig. 12.7.2)	≤2.0 m		1.03	1.03	1.07	1.09	1.09	1.10	1.10	1.10	1.10	1.10
	6.0 m		1.03	1.06	1.12	1.16	1.18	1.20	1.22	1.22	1.22	1.22
	≥20.0 m		1.03	1.06	1.12	1.17	1.21	1.23	1.26	1.29	1.30	1.35
Free longitudinal edges (not shown)	≤2.0 m		1.40	1.40	1.40	1.29	1.21	1.15	1.10	1.10	1.10	1.10
	6.0 m		1.40	1.40	1.40	1.33	1.28	1.25	1.22	1.22	1.22	1.22
	≥20.0 m		1.40	1.40	1.40	1.38	1.37	1.36	1.35	1.35	1.35	1.35

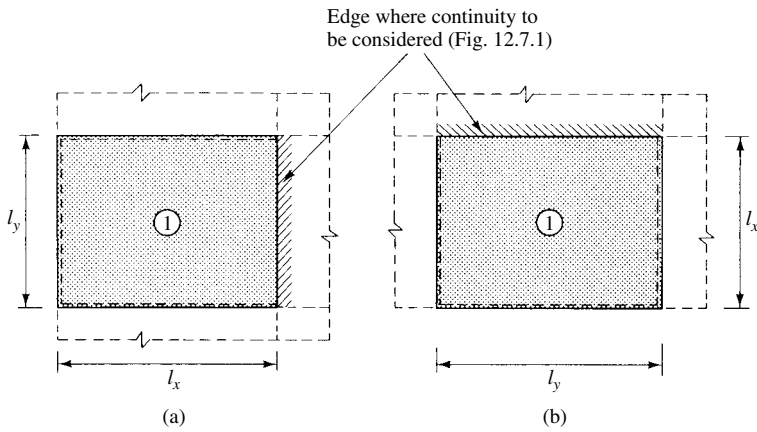
Note: Use $c_1 = 1.0$ along free-edges. After Ref. [12.7.2].



(a)



(b)

Figure 12.7.1 Continuous bridge slab.

(a)

(b)

Figure 12.7.2 Equivalent plates.

Table 12.7.3 Coefficient c_2

Span Length (m)	Bridge Type DIN 1075		
	60	30	12
$l_x \leq 2.0$	0.90	0.90	0.90
$l_x \approx 6.0$	0.62	0.71	0.82
$l_x \geq 20.0$	0.75	0.85	0.92

Notes: DIN = Deutsche Industrie Normen. For fixed end supports use $c_2 = 1.0$. After Ref. [12.7.2].

The method can also be used when the spans of the individual panels vary, provided the ratio of the smaller span to the larger is less than 0.8. In such a case the use of the larger span length is recommended for the equivalent plate.

Approximate moment diagrams of bridge slabs due to moving wheel loads are shown in Fig. 12.7.3.

Other satisfactory methods for the approximate analysis of continuous rectangular slabs are listed in the bibliography at the end of the section. Based on the ultimate load-carrying capacity of plates, the recently introduced yield-line analysis treated in Chapter 13 offers another powerful tool for the economical solution of continuous rectangular plates. An additional advantage of the latter approach is that it is not limited to uniformly distributed loads or to simply supported or fixed boundary conditions.

12.7.2 Simplified Treatments of Skew Plates

As discussed earlier, analytical methods, with the exception of the simplest cases, are too cumbersome for practical analysis of skew plates. In Sec. 10.3 numerical methods were introduced for handling such plate problems. The GWM and FEM appear to be the most effective numerical techniques, but under certain circumstances even the FDM can yield usable results. In all cases, however, care should be exercised when assessing stresses in acute or obtuse corners and near column heads, where stress concentration is known to occur.

Engineering design procedures for analysis of skew plates rely heavily upon extensive tables and design charts in order to simplify the inherently complex manual calculations. In Ref. [12.7.3], for instance, readily usable tables are given for bending and twisting moments of uniformly loaded skew plates simply supported at two opposite edges and free at the other two edges (Fig. 12.7.4). These tables cover aspect ratios $\kappa = b/a$ of $\frac{1}{3}$, $\frac{1}{2}$, $\frac{2}{3}$, $\frac{1}{1}$ and $\frac{3}{2}$ aspect ratios and skew angles φ of 0° , 15° , 30° , 45° , $52^\circ 30'$, and 60° . However, to simplify our discussion, we are dealing here only with $\kappa = \frac{1}{3}$, $\frac{1}{2}$, $\frac{1}{1}$ and $\varphi = 30^\circ$, 45° , 60° .

The plate deflections $w(x, y)$ can be expressed by

$$w(x, y) = k_w \frac{p_0 \lambda^4}{D} \quad \text{for } \lambda = \frac{b}{a}, \tag{12.7.7}$$

where k_w is a coefficient value (see Tables 12.7.4–12.7.6) and λ represents the mesh width.

Similarly, using the coefficients, k_x , k_y and k_{xy} bending and twisting moments at given points can be calculated from

$$m_x = k_x p_0 \lambda^2 \qquad m_y = k_y p_0 \lambda^2, \qquad m_{xy} = k_{xy} p_0 \lambda^2 \tag{12.7.8}$$

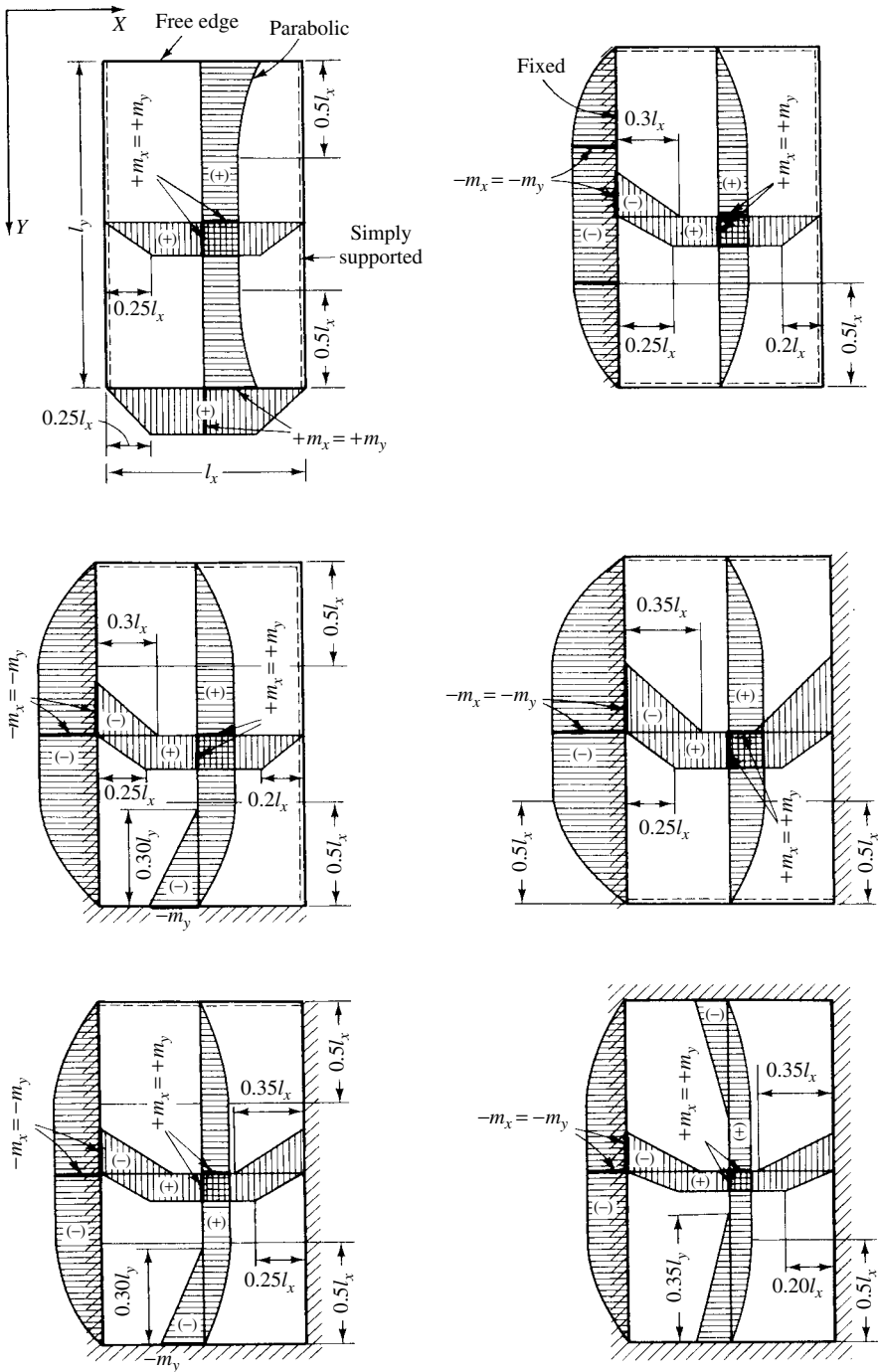


Figure 12.7.3 Approximate moment diagrams due to wheel loads after Ref. [12.7.1].

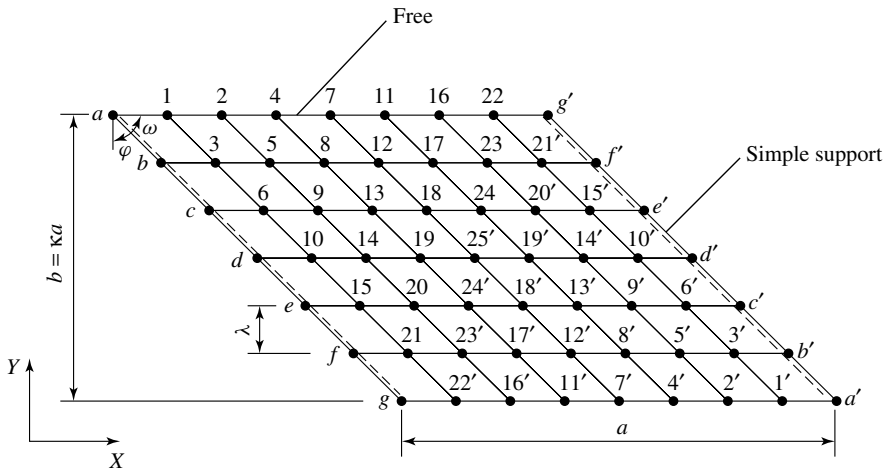


Figure 12.7.4 Reference points of parallelogram plate.

Table 12.7.4 Coefficients for $\kappa = 1/3$

$Point$	$\varphi = 30^\circ$				$\varphi = 45^\circ$				$\varphi = 60^\circ$			
	k_w	k_x	k_y	k_{xy}	k_w	k_x	k_y	k_{xy}	k_w	k_x	k_y	k_{xy}
b	0	-0.64	0.64	0.37	0	-0.01	0.01	0	0	0.40	-0.40	0.23
c	0	-1.31	1.31	0.75	0	-0.30	0.30	0	0	0.94	-0.94	0.54
d	0	-2.15	2.15	1.24	0	-0.96	0.96	0	0	1.32	-1.32	0.76
e	0	-3.47	3.47	2.00	0	-2.44	2.44	0	0	1.11	-1.11	0.64
f	0	-5.69	5.69	3.28	0	-5.82	5.82	0	0	-0.88	0.88	-0.51
1	330.16	5.58	0	2.59	181.20	2.01	0	1.21	76.75	0.77	0	0.28
2	631.26	14.60	0	5.01	351.94	6.42	0	3.29	149.46	2.65	0	1.14
3	332.16	6.63	1.74	3.53	181.23	2.82	1.33	1.82	75.51	1.70	0.35	0.83
4	856.35	22.92	0	7.22	489.24	11.78	0	5.96	208.39	4.92	0	2.59
5	631.31	15.95	1.73	6.46	348.90	7.60	2.02	4.69	142.46	3.72	0.95	2.11
6	336.23	7.49	2.82	4.81	182.04	3.33	2.51	2.83	72.59	2.46	0.59	1.51
7	962.11	28.25	0	8.94	565.18	16.61	0	8.55	241.68	7.03	0	4.65
8	848.91	23.97	1.35	8.52	478.76	13.03	2.00	7.74	190.85	5.69	1.54	4.05
9	635.89	17.29	2.65	7.90	348.89	8.59	3.41	6.49	132.89	4.25	1.93	3.30
10	342.94	8.26	3.47	6.41	184.63	3.50	3.60	4.20	68.48	2.73	1.07	2.20
11	920.76	29.28	0	10.35	554.66	19.08	0	10.70	238.34	8.45	0	7.13
12	942.86	28.48	1.07	9.83	542.48	17.32	1.62	10.09	210.95	7.21	1.94	6.55
13	847.84	25.01	2.02	9.50	473.95	14.19	3.04	9.52	172.76	5.72	3.01	5.90
14	645.89	18.75	2.86	9.43	354.15	9.60	4.08	8.75	123.67	3.96	3.15	4.88
15	353.75	9.16	3.64	8.68	191.23	3.41	4.57	6.65	65.00	1.99	2.23	3.16
16	726.94	25.27	0	11.69	444.78	17.39	0	12.53	190.97	7.18	0	9.67
17	889.46	28.34	1.00	10.81	517.45	18.36	1.36	11.66	195.20	8.60	1.98	9.03
18	931.32	28.60	1.67	10.25	527.75	17.73	2.41	11.18	185.46	6.66	3.37	8.65
19	853.70	26.09	2.11	10.30	477.23	15.45	3.16	11.15	160.97	5.20	4.11	8.30
20	662.97	20.54	2.39	10.92	368.68	11.15	3.70	11.46	121.58	2.98	4.35	7.94
21	371.48	10.79	2.92	12.26	206.94	3.83	4.64	12.06	67.73	0.42	4.54	7.62
22	401.51	14.61	0	13.18	244.33	8.43	0	14.07	101.03	2.13	0	10.59
23	689.34	22.82	1.25	11.81	397.98	14.04	1.77	12.94	141.59	4.29	2.42	10.38
24	867.30	27.23	1.72	10.75	491.30	16.96	2.44	11.95	166.43	5.56	3.60	9.95
25	927.47	28.64	1.86	10.41	522.57	17.85	2.63	11.63	174.78	5.96	3.96	9.81

Table 12.7.5 Coefficients for $\kappa = 1/2$

Point	$\varphi = 30^\circ$				$\varphi = 45^\circ$				$\varphi = 60^\circ$			
	k_w	k_x	k_y	k_{xy}	k_w	k_x	k_y	k_{xy}	k_w	k_x	k_y	k_{xy}
<i>b</i>	0	0.035	-0.035	-0.020	0	0.239	-0.239	0	0	0.266	-0.286	0.165
<i>c</i>	0	-0.109	0.109	0.063	0	0.391	-0.391	0	0	0.756	-0.756	0.436
<i>d</i>	0	-0.352	0.352	0.203	0	0.364	-0.364	0	0	1.071	-1.071	0.618
<i>e</i>	0	-0.844	0.844	0.487	0	-0.035	0.035	0	0	0.957	-0.957	0.552
<i>f</i>	0	-1.879	1.879	1.085	0	-1.331	1.331	0	0	0.230	-0.230	0.133
1	64.555	2.562	0	0.696	35.593	1.042	0	0.293	15.758	0.381	0	0.106
2	123.179	6.342	0	1.705	68.775	3.055	0	1.032	30.634	1.301	0	0.449
3	64.482	3.305	0.852	1.222	35.163	1.783	0.546	0.717	15.163	1.095	0.121	0.548
4	167.125	9.824	0	2.819	94.888	5.235	0	2.092	42.501	2.423	0	1.006
5	121.644	7.074	1.146	2.466	66.411	3.824	1.045	1.764	27.838	2.122	0.460	1.148
6	64.708	3.774	1.344	1.774	34.459	2.236	0.942	1.156	13.592	1.654	0.101	1.014
7	188.337	12.243	0	3.876	108.885	7.079	0	3.337	48.760	3.405	0	1.774
8	162.876	10.308	1.157	3.583	89.212	5.772	1.335	3.017	35.781	2.962	0.799	1.912
9	121.200	7.639	1.779	3.222	64.108	4.222	1.816	2.539	23.395	2.408	0.883	1.754
10	65.440	4.038	1.682	2.417	33.805	2.341	1.371	1.625	11.366	1.756	0.271	1.322
11	181.216	13.011	0	4.814	106.500	8.080	0	4.612	47.141	3.866	0	2.740
12	180.698	12.267	1.060	4.474	99.169	7.159	1.420	4.282	37.177	3.253	1.151	2.780
13	160.700	10.698	1.772	4.255	84.685	5.941	2.243	3.967	27.967	2.638	1.673	2.543
14	122.183	8.143	2.030	4.040	62.721	4.281	2.420	3.447	18.772	1.990	1.560	2.081
15	67.195	4.205	1.913	3.413	33.868	2.006	1.992	2.400	9.377	1.249	0.860	1.345
16	143.982	11.587	0	5.633	85.417	7.539	0	5.783	36.574	3.245	0	3.868
17	170.540	12.357	0.994	5.150	93.106	7.363	1.403	5.337	31.490	2.567	1.570	3.544
18	176.125	12.212	1.659	4.869	92.377	6.896	2.328	5.082	27.078	2.101	2.484	3.224
19	160.864	11.105	1.935	4.824	82.664	5.954	2.718	4.916	22.174	1.589	2.810	2.882
20	125.395	8.808	1.859	4.960	63.862	4.275	2.706	4.802	16.195	0.775	2.765	2.533
21	71.099	4.636	1.804	5.395	36.264	1.314	2.742	4.876	8.899	-0.698	2.734	2.272
22	79.933	6.864	0	6.176	46.885	3.610	0	6.310	18.496	0.181	0	4.056
23	132.164	9.984	1.082	5.637	70.544	5.341	1.665	5.915	20.469	0.595	2.148	3.529
24	163.928	11.656	1.652	5.162	85.006	6.358	2.436	5.540	22.286	1.067	3.031	3.310
25	174.593	12.174	1.858	5.020	89.875	6.680	2.687	5.430	22.982	1.245	3.281	3.250

For small skew bridges (span < 10 m) with edge beams, which do not warrant extensive computations, we may also use an approximate method based on use of design charts [12.7.4]. For this purpose, the skew plate under consideration is replaced by an equivalent orthogonal plate, as shown in Fig. 12.7.5. By multiplying the maximum moments $m_{x,\max}$ and $m_{y,\max}$ of this substitute structure by appropriate correction factors, good estimates of the corresponding maximum moments in the skew plate can be obtained; thus

$$\bar{m}_{x,\max} \approx c_x m_{x,\max}, \quad \bar{m}_y \approx c_y m_{y,\max}, \quad -\bar{m}_{y,\max} \approx c'_y (-m_{y,\max}). \quad (12.7.9)$$

The factors c_x , c_y and c'_y , in the above equation are listed in Table 12.7.7. (Note: For the coefficients k_1 , k_2 , and k_3 , given in Table 12.7.7 see Fig. 12.7.6.)

In addition, the reader is referred to Refs. [12.7.5] and [12.7.6] for extensive tables used in the analysis of skew plates.

12.7.3 Degree-of-Fixity Procedure

This simplified method for continuous plates estimates the degree of fixity at the corresponding supports of each individual panel [12.7.7]. The degree of fixity is defined by

$$\eta = \frac{m_{\text{support corresponding to } m_{\text{field,max}}}}{m_{\text{support with complete fixity}}}. \quad (12.7.10)$$

Table 12.7.6 Coefficients for $\kappa = 1/1$

Point	$\varphi = 30^\circ$				$\varphi = 45^\circ$				$\varphi = 60^\circ$			
	k_w	k_x	k_y	k_{xy}	k_w	k_x	k_y	k_{xy}	k_w	k_x	k_y	k_{xy}
<i>b</i>	0	0.0730	-0.0730	-0.0422	0	0.1433	-0.1433	0	0	0.2006	-0.2006	0.1158
<i>c</i>	0	0.0801	-0.0801	-0.0463	0	0.2161	-0.2161	0	0	0.2444	-0.2444	0.1411
<i>d</i>	0	0.0520	-0.0520	0.0300	0	0.1745	-0.1745	0	0	0.1327	-0.1327	0.0766
<i>e</i>	0	-0.0171	0.0171	0.0098	0	0.0722	-0.0722	0	0	0.0387	-0.0387	0.0223
<i>f</i>	0	-0.1852	0.1852	0.1068	0	-0.0779	0.0779	0	0	0.0213	-0.0213	0.0123
1	4.0590	0.6986	0	0.0688	2.2756	0.3303	0	0.0261	1.0425	0.1979	0	0.0492
2	7.7138	1.6178	0	0.3255	4.3602	0.8364	0	0.1952	1.9705	0.4139	0	0.0528
3	3.9830	1.0294	0.2638	0.3070	2.1467	0.6545	0.1583	0.2630	0.8340	0.4088	0.0207	0.2782
4	10.4326	2.4534	0	0.6216	5.9608	1.3684	0	0.4502	2.6590	0.6401	0	0.1849
5	7.3959	1.9136	0.4595	0.6242	3.9300	1.1421	0.3910	0.5475	1.4335	0.5611	0.2339	0.4389
6	3.8997	1.1533	0.3789	0.4295	1.9522	0.7455	0.2780	0.3812	0.5801	0.3648	0.1678	0.3044
7	11.7319	3.0349	0	0.9307	6.7696	1.7892	0	0.7555	2.9771	0.8099	0	0.3900
8	9.7460	2.5909	0.5633	0.9164	5.0903	1.5082	0.5618	0.8322	1.7308	0.6339	0.4180	0.5777
9	7.1686	2.0136	0.6775	0.8099	3.4999	1.1549	0.6554	0.7150	0.9652	0.4420	0.4909	0.4366
10	3.8456	1.1677	0.4610	0.5195	1.7952	0.6850	0.4152	0.4313	0.4422	0.2483	0.3166	0.2367
11	11.2752	3.2294	0	1.2288	6.5433	1.9665	0	1.0850	2.8266	0.8514	0	0.6568
12	10.6513	2.9400	0.6061	1.1661	5.4321	1.6485	0.6891	1.0777	1.7018	0.5927	0.5705	0.6551
13	9.3378	2.5844	0.8517	1.1012	4.4426	1.3796	0.9348	0.9743	1.1420	0.4505	0.7333	0.5056
14	7.0601	2.0157	0.7954	0.9382	3.2341	1.0469	0.8537	0.7690	0.7712	0.3400	0.6355	0.3518
15	3.8634	1.1161	0.5436	0.6452	1.7302	0.5683	0.5510	0.4560	0.4020	0.2037	0.3716	0.1931
16	8.9502	2.8787	0	1.4800	5.1793	1.7296	0	1.4037	2.1836	0.6801	0	0.9749
17	9.9141	2.8455	0.6158	1.3382	4.8865	1.4682	0.7912	1.2191	1.3848	0.4218	0.6848	0.6280
18	10.0939	2.7971	0.9301	1.2803	4.6772	1.3839	1.1176	1.1182	1.1289	0.3957	0.8825	0.4999
19	9.1851	2.5526	0.9779	1.2099	4.1496	1.2341	1.1505	1.0026	0.9648	0.3694	0.8583	0.4095
20	7.1335	2.0088	0.8305	1.1073	3.1847	0.8955	1.0149	0.8625	0.7219	0.2449	0.7451	0.3161
21	4.0557	1.0099	0.6512	1.0950	1.8003	0.2055	0.8934	0.7859	0.3799	-0.1099	0.6890	0.1980
22	4.9596	1.6749	0	1.5513	2.8145	0.7773	0	1.4579	1.1470	0.1909	0	0.9340
23	7.5900	2.1963	0.6282	1.3642	3.5678	0.9220	0.8781	1.1547	0.8898	0.1491	0.7400	0.4670
24	9.3214	2.6013	0.9297	1.3030	4.2190	1.1906	1.1702	1.0924	0.9720	0.3115	0.9022	0.4276
25	9.9275	2.7387	1.0335	1.3035	4.4620	1.2892	1.2545	1.0878	1.0275	0.3731	0.9382	0.4264

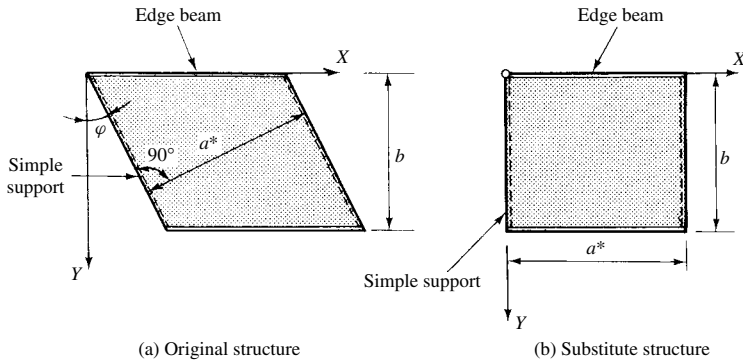


Figure 12.7.5 Substitute orthogonal structure.

Table 12.7.7 Correction Factors for Skew Plates

Type of Loading	For m_x	For m_y	For $(-)m_y$
Plate			
Uniformly distributed	$c_x = 1 + k_1$	$c_y = 1 + k_x$	—
Concentrated	$c_x = 1 + \frac{k_1}{2}$	$c_y = 1 + \frac{k_2}{2}$	$c'_y = 1 + \frac{k_2}{4}$
Edge beam			
Uniformly distributed	$c_b = 1 + k_3$		
Concentrated	$c_b = 1 + \frac{k_3}{2}$		

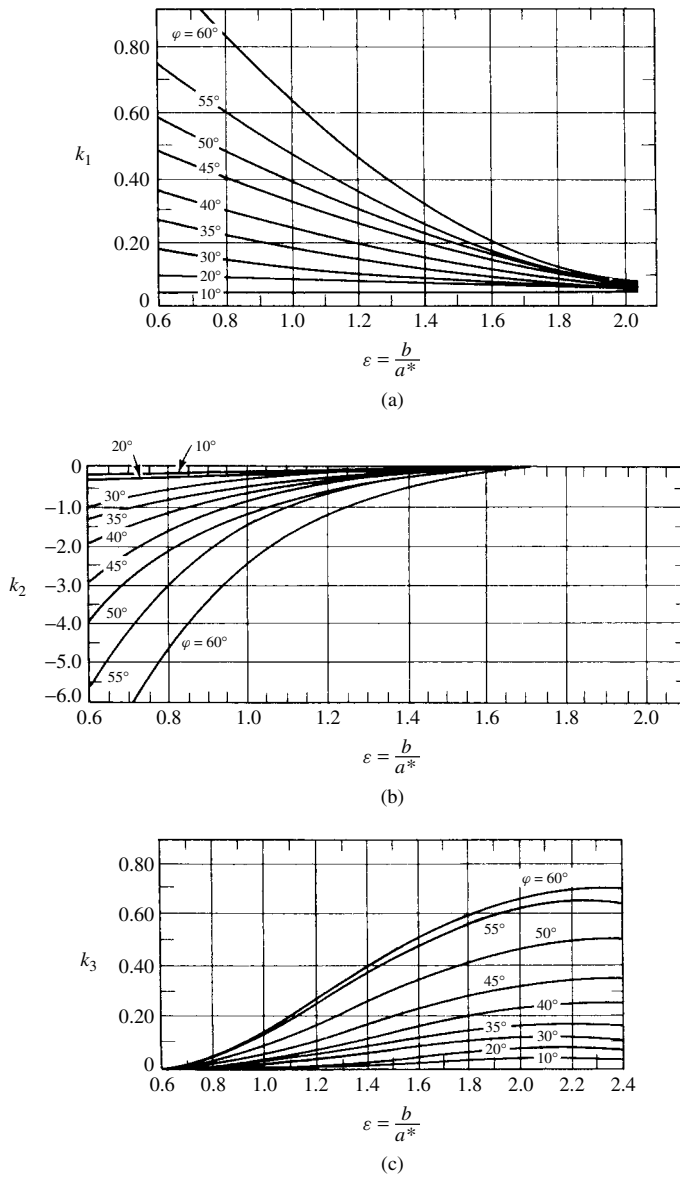


Figure 12.7.6 Coefficients for approximate analysis of skew bridges [12.7.6].

One can calculate η from the following *empirical* formula:

$$\eta = \frac{\varphi + n^3}{n^2 + n^3} - \frac{11(n-1) - 2.5(7-2n)(n-1)\varphi}{100}, \quad (12.7.11)$$

where $\varphi = p_{DL}/(p_{DL} + p_{LL})$ and $n = l_2/l_1$ represents the ratio of the shorter span of a panel to the shorter span of the neighboring panels (l_2), (l_1).

Bending moments can be calculated from

$$m = \eta m_i + (1 - \eta) m_0, \quad (12.7.12)$$

where m_i is the moment of the individual panels assuming complete fixity at the interior supports and m_0 denotes the moment of the corresponding simply supported plate.

Evaluation of Eqs. (12.7.11) and (12.7.12) is greatly facilitated by extensive tables given in Ref. [12.7.7]. Using the values from these tables, we can write

$$m = (p_{DL} + p_{LL}) l_x l_y m_i, \quad (12.7.13)$$

where m_i is obtained from [12.7.7].

ILLUSTRATIVE EXAMPLE

Let us check the results obtained in Illustrative Example I of Sec. 12.5 by estimating the degree of support fixities. The global and local coordinate systems are shown in Fig. 12.7.7.

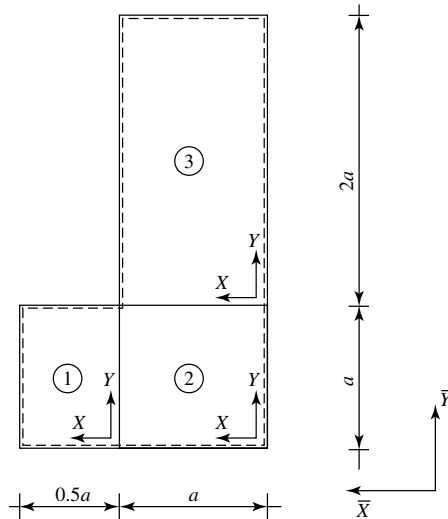
The field moments $m_f = m_{xm}$ and m_{ym} are calculated from

$$m_f = q l_x l_y m_i \quad \text{for } q = p_{DL} + p_{LL}, \quad (12.7.14)$$

In addition, the moment above the support is obtained from

$$m_{s_{i-k}} = q l_x l_y [(-0.5m_e)_i + (-0.5m_e)_k] \geq 0.75m_{e,\min}. \quad (12.7.15)$$

For calculation of these moments required values of m_i , m_e and η are taken from tables in Ref. [12.7.7]. The analysis procedure and results are listed in Tables 12.7.8 and 12.7.9. Comparing these values with those given in Tables 12.5.4 and 12.5.5s, respectively, we see relatively good agreement if we consider the approximate nature of both engineering methods.



l_x is always the smaller span:

Figure 12.7.7 Continuous RC floor slab.

Table 12.7.8 Field Moments of Slab Shown in Fig. 12.7.7

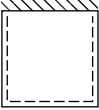
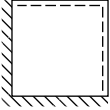
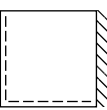
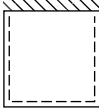
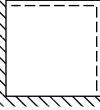
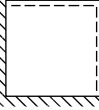
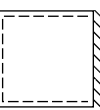
Panel Number	Type	Data				m_i		Field Moments	
		l_y, l_x	$n = \frac{l_2}{l_1}, l_2 > l_1$	$\varepsilon = l_y/l_x$	$K = gl_x l_y$	η	\bar{X} direction	\bar{Y} direction	m_{x_m} m_{y_m}
1		a	2.0	2.0	$0.5qa^2$	0.604	0.0369	0.0101	$0.0185qa^2$ $0.0051qa^2$
		$0.5a$							
2		a	2.0	1.0	qa^2	0.604	0.0296	0.0296	$0.0296qa^2$ $0.0296qa^2$
		a	1.0	1.0	qa^2	0.650	0.0296	0.0296	$0.0296qa^2$ $0.0296qa^2$
3		$2a$	1.0	2.0	$2qa^2$	0.650	0.0454	0.0128	$0.0908qa^2$ $0.0256qa^2$
		a	1.0	2.0	$2qa^2$	0.650	0.0454	0.0128	$0.0908qa^2$ $0.0256qa^2$

Table 12.7.9 Moments at Supports (Fig. 12.7.7)

Panel Number	Type	Data				Moments		
		l_y	l_x	$\varepsilon = l_y/l_x$	$K = q l_x l_y$	η	$-0.5m_{x_e}$	$0.75m_{e_{min}}$
1		a	$0.5a$	2.0	$0.5qa^2$	0.604	—	—
							-0.0301	$-0.0501qa^2$
2		a	a	1.0	qa^2	0.604	—	—
							-0.0350	$-0.0501qa^2$
2		a	a	1.0	qa^2	0.65	—	—
							-0.0350	$-0.0960qa^2$
3		$2a$	a	2.0	$2qa^2$	0.65	—	—
							-0.0305	$-0.0960qa^2$

References and Bibliography

- [12.7.1] RÜSCH, H., *Berechnungstabeln für rechtwinklige Fahrbahnplatten*, 6th ed., W. Ernst & Sohn, Berlin, 1965.
- [12.7.2] KUPFER, H., and MAIER, A., "Beiwerte zur Berechnung der Momentengrenzwerte für durchlaufende rechtwinklige Fahrbahnplatten von Strassenbrücken," *Beton und Stahlbetonbau*, 64 (Oct. 1969), 233–240.
- [12.7.3] HANUSKA, A., and BALAS, J., "Hauptbiegungsmomentenlinien schiefer Platten, Der Bauingenieur, 40 (Heft 7, 1965), 265–267.
- [12.7.4] BÖLCSKEI, E., *Beton- Vasbeton és Feszített Hidak* (Concrete, Reinforced Concrete and Prestressed Bridges), Tankönyvkiadó, Budapest, 1968.
- [12.7.5] SCHLEICHER, C., and WEGENER, B., *Durchlaufende schiefe Platten: Continuous Skew Slabs*, VEB Verlag für Bauwesen, Berlin, 1968.
- [12.7.6] JÁVOR, T., *Tables of Influence Surfaces* (in Slovak, English, German and Russian), Slovenské Vydavateľstvo Tech. Lit., Bratislava, 1967.
- [12.7.7] SCHRIEVER, H., *Einspanngradverfahren*, Werner-Verlag, Düsseldorf, 1970.
- [12.7.8] HAHN, J., *Durchlaufträger, Rahmen, Platten und Balken auf elastischer Bettung*, 11th ed., Werner-Verlag, Düsseldorf, 1971.

12.8 Summary and Conclusions

Classical methods for solution of continuous RC floor slabs lead to extensive computations. Such efforts, however, are not warranted in the routine design of floors. An engineering method originally developed by Marcus and later improved by Löser yields usable results for uniformly loaded floor slabs.

A simplified slope-deflection method offers an economical way to solution of continuous plate systems subjected to either uniformly distributed loads or concentrated forces acting at the center of the panels. Corresponding design charts developed by Maugh and Pan greatly facilitate the practical application of this engineering approach, which gives good results in a relatively easy way.

Similar is the case with the moment distribution technique. The computational procedure is analogous to that used for continuous beams and rigid frames. Consequently, it is familiar to structural engineers. However, instead of design charts, Brunner gives extensive tables for stiffness and carry-over factors. Although this method has been primarily developed for uniformly distributed lateral loads, its applicability can be extended to other types of loading, provided the deviation of the produced edge moments from the assumed sinusoidal shape is not too pronounced. Comparing all engineering approaches discussed in this chapter, the moment distribution method gives the best results, followed closely by the slope-deflection technique.

The simplified design method for RC floor slabs developed by Pieper and Martens relies heavily on the use of tables and charts. This is the simplest and fastest method. The method based on estimated fixity of individual slabs has some serious limitation. That is, it is not easy to use without the corresponding tables, which are not always readily available.

All the engineering procedures for the routine design of floor slabs introduced in this chapter do not give a complete elastic analysis of such plate systems but only yield reliable estimates for the maximum positive field moments and the negative moments at supports. Their deviation from the more exact solutions obtained by numerical methods can be estimated as 10–15%, which lies within the error range of corresponding input data.

Because of the inherent complexity of the classical analysis of RC flat slabs, it is necessary to make various simplifying approximations. An engineering approach based on an equivalent rigid-frame analogy gives acceptable results for most practical purposes. Again, tables and design charts facilitate the approximate analysis of skew plates.

It is of great practical importance that all results obtained from these engineering approximations can be easily checked by means of the yield-line method, discussed in Chapter 13 in general and demonstrated in Sec. 13.4 and 13.5 in particular. That is, if one uses the energy-based work method of this ultimate design approach and calculates the average of the results obtained by the elastic analysis and those of the yield-line analysis, then quite reliable values for the design moments can be acquired; that is, the elastic methods give lower-bound solutions, while the results of the energy-based yield-line analysis are upper bound. Consequently, their average lies quite close to the more exact results.

Problems[†]

- 12.2.1. Assume a typical RC floor slab with 4×3 panels with spans $l_x = 5.5$ m and $l_y = 4.3$ m in the X and Y directions, respectively. The dead load of each panel is $p_{DL} = 2.0$ kN/m², and the live load carried by the floor amounts to $p_{LL} = 4.0$ kN/m². All exterior boundaries of this continuous plate system are simply supported. Determine the design moments by using the Marcus-Löser approximate analysis technique.
- 12.2.2. Check the results obtained in Illustrative Example I of Sec. 12.5 by the Marcus-Löser engineering solution technique.
- 12.3.1. Redo problem 12.2.2 this using time the simplified slope-deflection method.
- 12.3.2. A simply supported floor slab consists of four square panels. Assume that the span of these panels is a . Only one of the panels carries a live-load $p_{LL} = p_0$. By neglecting the dead load, determine the maximum positive and negative moments using the simplified slope-deflection method.
- 12.4.1. A simply supported continuous plate consists of three subsequent equal panels. Assume that the middle panel is subjected to p_0 uniformly distributed live load. Calculate the maximum moments of this continuous plate by applying the moment distribution method. The dead load of the plates can be neglected.
- 12.4.2. Redo problem 12.4.1, but this time assume that all panels carry a p_{DL} . The ratio of dead load to live load is $\frac{1}{2}$.
- 12.4.3. Check the results obtained in Illustrative Example I of Sec. 12.5 by moment distribution.
- 12.5.1. Apply the design approach of Piper and Martens to the floor system shown in Fig. 12.4.6.
- 12.5.2. Apply the Piper-Martens method to the floor system shown in Fig. 12.3.9.
- 12.5.3. Check the results obtained problem 12.4.2 by using the Piper-Martens approximation.

[†] The first two numbers refer to the corresponding section.

- 12.6.1.** Assume that the RC floor system shown in Fig. 12.2.7 represents flat slabs with drop panels. Use the same loadings and concrete dimensions used in the Illustrative Example of Sec. 12.6. Determine the design moments for the interior panels in the X direction by utilizing the equivalent frame approximation.
- 12.7.1.** Check the results obtained in Illustrative Example II of Sec. 10.3 using one of the simplified methods for analysis of skew plates and draw your own conclusions.

13

Yield-Line Method

13.1 Introduction to Yield-Line Method

Although a structural analysis based on *elastic theory* yields good results for deformations and stresses produced by working (service) loads, it fails to assess the real load-carrying capacity of the structure. At failure, the fundamental assumptions of the theory of elasticity (Hooke's law and small deformations) are no longer valid; consequently, information obtained on the factor of safety against collapse is not accurate. In most cases, an elastic design is overly conservative. There are conditions, however, when elastic theory might even give unsafe results. Furthermore, for the aerospace industry, for instance, the reduction of weight is of prime importance; thus, a knowledge of the *real* factor of safety is mandatory for all flight structures. Another serious limitation of elastic analysis, with the exception of the simplest cases, is its mathematical complexity. Although contemporary numerical methods, based on extensive use of computers, are potentially capable of solving the most difficult plate problems, there is a pronounced need for a simple analytical method against which computerized solutions can be checked. Yield-line analysis is such an alternative computational technique. This method is especially useful for RC slabs.[†] *Yield-line analysis* eliminates (at least partially) these limitations of elastic design, since it deals with the ultimate load-carrying capacity of plates, assuming impending collapse.

The objective of this chapter is to introduce the reader to the fundamental concepts of yield-line analysis and to its practical application for most support and loading conditions. The few problematics of the method will also be mentioned, but their extensive discussion is avoided. The mathematical *theory of plasticity* of plates is often more complex than its elastic counterpart; consequently, its treatment is considered to be beyond the scope of this book. For a more complete study of the yield-line method, the reader is referred to the pertinent literature.

a. Basic Concepts and Assumptions. In 1914 Kazinczy [13.1.1] observed that the ultimate load-carrying capacity of clamped steel beams was considerably higher than predicted by the theory of elasticity. This increased load-carrying capacity is due to the ductility (plasticity) of most structural materials such as steel, aluminum, and

[†] The method also can logically be extended to metallic plates.

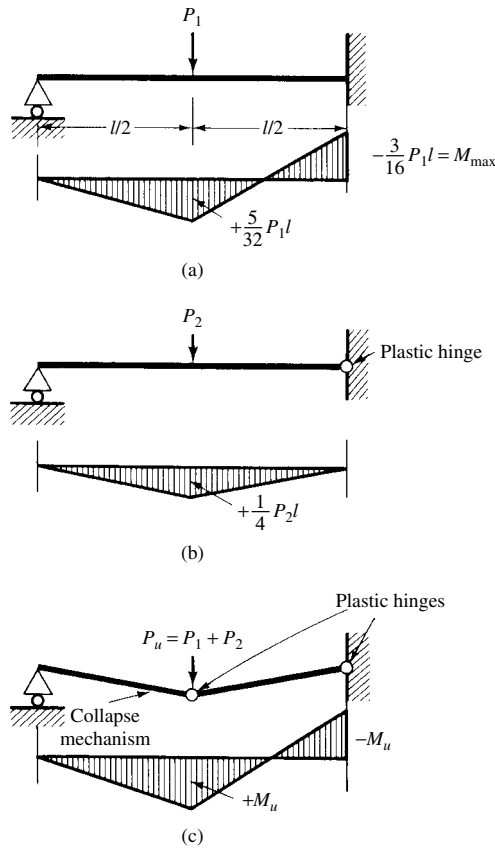


Figure 13.1.1 Bending moments before and after development of plastic hinges.

RC [13.1.2]. When a beam, as shown in Fig. 13.1.1, is loaded so that at the location of the maximum moment the maximum stresses are below the proportional limit, the stress distribution follows the familiar triangular pattern assumed by elastic theory. By gradually increasing the lateral load, however, the outer fibers of the beam in the vicinity of the maximum moments reach the yield stress σ_Y . As the load is further increased, the yield stresses will penetrate toward the neutral axis of the section until the stress distribution is nearly rectangular (Fig. 13.1.2).

By introducing an idealized stress-strain relationship and a rectangular stress pattern (Fig. 13.1.3), we can estimate the true moment-carrying capacity of the beam. The *fully plastic* or *ultimate moment* of a rectangular beam, for instance, is

$$M_u = \int_{(A)} z \sigma_Y dA = \sigma_Y \int_{(A_1)} z dA - \sigma_Y \int_{(A_2)} z dA = \sigma_Y \frac{bh^2}{4}, \quad (13.1.1)$$

or, per unit length,

$$m_u = \sigma_Y \frac{h^2}{4}. \quad (13.1.1a)$$

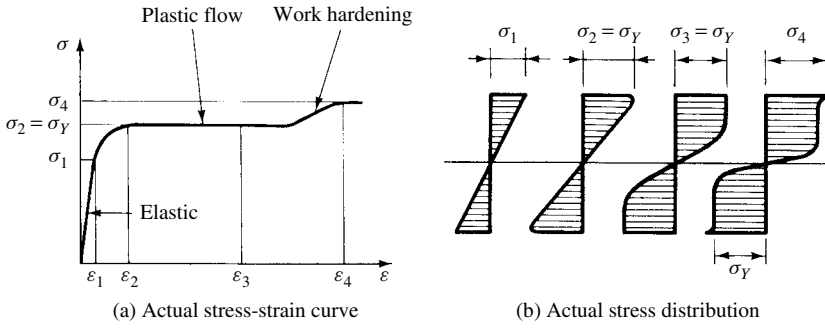


Figure 13.1.2 Stress distribution during plastic bending.

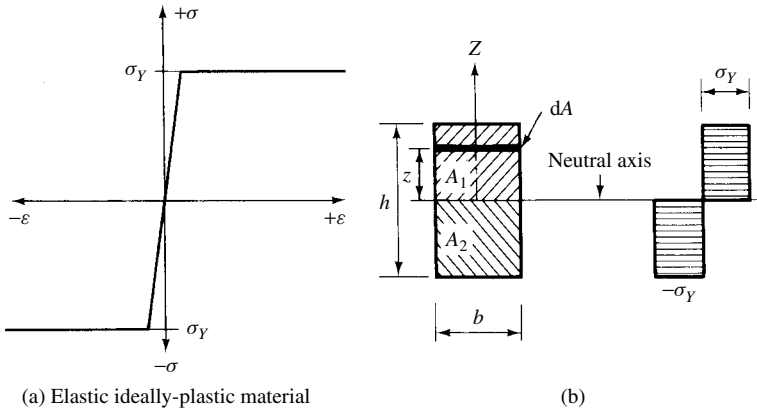


Figure 13.1.3 Idealized plastic bending.

A comparison of this ultimate moment with the moment capacity of the section, obtained from elastic theory,

$$\frac{m_u}{m_{el}} = \frac{\sigma_Y h^2 / 4}{\sigma_Y h^2 / 6} = 1.5, \quad (13.1.2)$$

indicates a 50% increase.

At the fully plasticized section a *plastic hinge* is formed (Fig. 13.1.1). This boundary condition is analogous to the *elastic restraint* in the theory of elasticity; that is, the plastic hinge rotates under the effect of a constant moment, but its deformation is permanent. The constant moment in this case is the ultimate moment capacity of the section under consideration. An additional load, P_2 , can be carried without further increasing the moment at the clamped boundary (Fig. 13.1.1b). Failure is reached when a second plastic hinge is developed at the location of the maximum positive moment (Fig. 13.1.1c). The deformation pattern, called the *collapse* or *failure mechanism*, consists basically of rigid-body motions. Even in the case of distributed loads the elastic deformations between the plastic hinges are of a negligible order of magnitude in comparison with rigid-body motions.

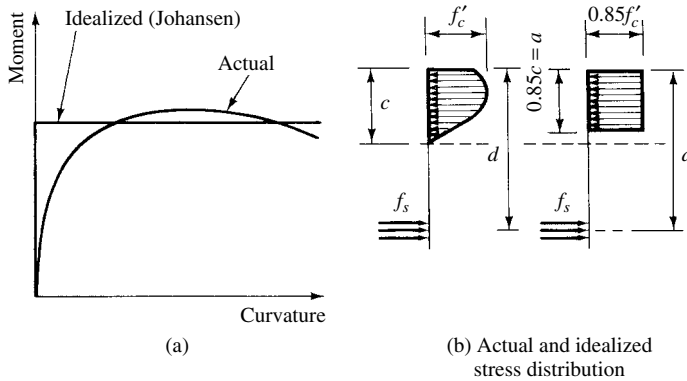


Figure 13.1.4 Plastic bending of properly reinforced-concrete beam or slab.

The behavior of underreinforced-concrete[†] beams is similar.[‡] Near the ultimate load, the distribution of compressive stresses in the concrete is parabolic, which can be approximated by an *equivalent* rectangular stress block, as shown in Fig. 13.1.4b. Consequently, the ultimate moment capacity of a rectangular RC section, which fails by reaching the yield point of the steel, is [13.1.4]

$$M_u = \phi [bd^2 f'_c q (1 - 0.59q)], \quad (13.1.3)$$

where $\phi = 0.90$ = factor for flexural members

$$q = pf_Y / f'_c$$

$$p = A_s / bd = \text{reinforcement ratio} (p \leq 0.75)$$

A_s = area of reinforcing steel (tension)

$f_Y = \sigma_Y$ = yield stress of steel

f'_c = compressive strength of concrete

Using the extensive test results obtained by Mörsch, Bach, and Graf at the Technical University of Stuttgart, first Ingerslev [13.1.5] derived an analytical approach to ultimate load design of plates. Johansen [13.1.3] extended the ultimate load analysis of beam and frame structures to RC slabs by introducing the concept of *yield lines*, which are the two-dimensional counterparts of plastic hinges. Instead of calculating the shape of the elastically deformed slab, yield-line analysis seeks of all possible failure patterns the one that corresponds to the smallest failure load, called the *critical* or *ultimate load*. When a laterally loaded slab is on the verge of collapse (collapse is impending), yield lines are formed at the locations of the maximum positive and negative moments. These yield lines, as shown in Fig. 13.1.5, subdivide the slab into plane segments. Since the lateral deflections along the yield lines are large, the slab segments rotate as rigid bodies in a manner similar to beam parts between plastic hinges. Provided that the correct failure pattern is known, the critical load can be obtained either from virtual work or from equilibrium considerations, as discussed in the subsequent sections. Both approaches use the following basic assumptions:

[†] Most concrete slabs are underreinforced. This condition can be assured by setting the upper limit ratio of reinforcement [13.1.3].

[‡] For ultimate moments of prestressed concrete, see Ref. [13.1.4].

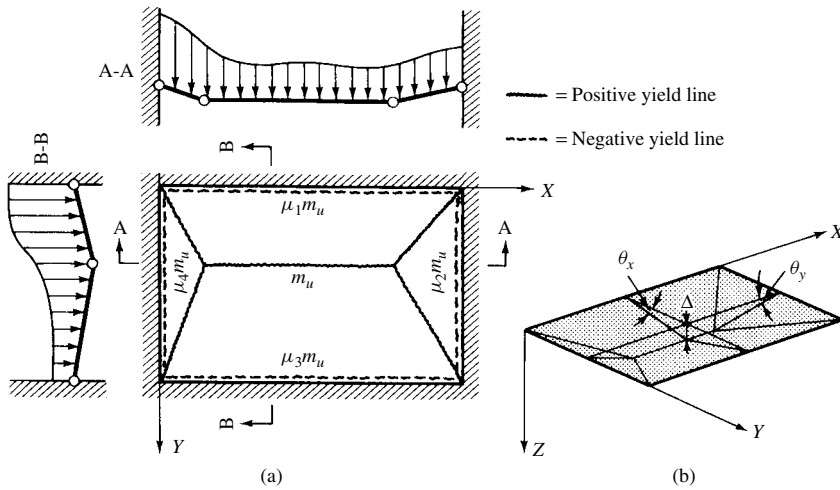


Figure 13.1.5 Failure mechanism of rectangular slab.

1. At impending collapse, yield lines are developed at the location of the maximum moments.
2. The yield lines are straight lines.[†]
3. Along the yield lines, *constant* ultimate moments (m_u) are developed.
4. The elastic deformations within the slab segments are negligible in comparison with the rigid-body motions created by the large deformations along the yield lines.
5. Of the many possible collapse mechanisms, only one, pertinent to the lowest failure load, is important. In this case the yield-line pattern is *optimum*.
6. When yield lines are in the optimum position only ultimate bending moments, but no twisting moments or transverse shear forces, are present along the yield lines.

For our discussion, we further assume that the slabs are of uniform thickness and that the reinforcing is the same in both directions (isotropy). The treatment of orthotropic reinforcements, variable thicknesses, and so on, is basically the same. The reader is referred to Refs. [13.1.6], [13.1.7], [13.1.9] and [13.1.10] for further study of these subjects. In the same works, experimental verifications of the above-mentioned assumptions can also be found. In addition, Olszak and Sawczuk [13.1.18] have demonstrated the good agreement obtained between experiments and analytic calculations. Although the primary application of the yield-line method is in connection with the ultimate load analysis of under reinforced-concrete or prestressed-concrete slabs, the method gives usable estimates for the ultimate load-carrying capacity of overreinforced-concrete slabs and for ductile metallic plates [13.1.6], provided that the pertinent ultimate moments are used. The resulting discrepancy between experimental and analytical approaches originates from the fact that Johansen's *square* yield criterion (Fig. 13.1.4) approximates better the actual failure

[†] Strictly speaking, this statement is valid only for distributed loads; point loads do have curved yield lines, as discussed in Sec. 13.5.

conditions of underreinforced-concrete slabs than those of metallic plates [13.1.15, 13.1.16]. Hopkins [13.1.17] has shown that in most cases the yield-line analysis may be used for *estimating* ultimate loads of metallic plates. Caution should be exercised, however, when concentrated loads act on metallic plates with fixed boundaries.

When the slab is subjected to concentrated loads or is supported by columns, the yield-line analysis, which gives the bending strength of the slab, *must always be supplemented by checking the punching shear*.

b. Guidelines for Estimating Failure Patterns. The location and orientation of yield lines determine the collapse mechanism of the slab. Assuming an optimum yield-line pattern, the *work method* gives an upper-bound solution to the *critical load*. Using a *true* equilibrium approach, in connection with the same collapse mechanism, a lower-bound solution can be obtained in a different manner. Thus, in both cases, the crux of the analysis is to estimate the most probable optimum yield-line pattern, which can be improved by an iterative technique. The following guidelines are helpful to establish the required collapse mechanism:

1. Yield lines developed under distributed critical loads are usually straight.
2. For one-way slabs and for the smaller span lengths of two-way slabs, the location of the maximum positive plate-strip moment obtained from elastic theory gives a good starting point.
3. Along fixed boundaries, *negative* yield lines develop (Fig. 13.1.5).
4. Yield lines pass through the intersection of the axis of rotation of adjacent slab segments (Figs. 13.1.5 and 13.1.6).
5. Lines of support generally serve as axes of rotation, as shown in Fig. 13.1.6.
6. Increased stiffness in the plate invites development of yield lines, while flexibility counteracts their formation.

Yield lines usually obey these general rules. There are cases, however, when the optimum collapse mechanism follows different yield-line patterns than those discussed and illustrated. With some experience, the designer can find with relative ease the optimum failure mechanism using a trial-and-error procedure coupled with an iterative technique discussed in the subsequent section. A study of Refs. [13.1.7], [13.1.9], [13.1.10] and [13.1.13] for the selection of suitable yield-line patterns is strongly recommended. For plate problems of high complexity, the optimum yield-line pattern can quickly be established by model tests using plaster of Paris, for instance, reinforced by mild steel wires. Complex yield-line patterns can be calculated by computers [13.1.12].

The determination of the optimum yield-line pattern becomes quite involved when different types of loads, such as distributed and concentrated, act simultaneously on a given slab. Johansen's *superposition* theorem [13.1.11], however, offers a simple method of calculation. This theorem states: The sum of the ultimate moments for series of loads is greater than or equal to the ultimate moment for the sum of the loads. Thus, we can write

$$m_{u1} + m_{u2} + m_{u3} + \cdots + m_{uk} + \cdots + m_{un} \geq m_{\Sigma P}, \quad (13.1.4)$$

where m_{uk} is the ultimate moment corresponding to the p_{uk} ultimate load and yield-line pattern and $m_{\Sigma P}$ is the ultimate moment pertinent to the yield-line pattern

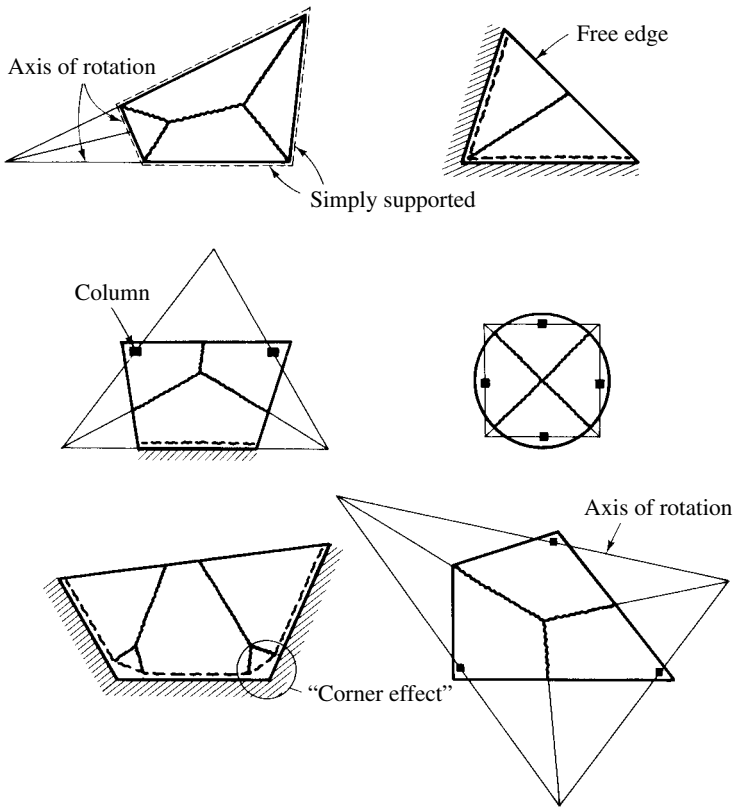


Figure 13.1.6 Possible yield-line patterns.

produced by the total loads: $p_{u1} + p_{u2} + p_{u3} + \cdots + p_{un} = \sum_n P$. The designer's equation is Eq. (13.1.4), but with an equality sign.

c. Estimating Deflections. Since a plate design might be governed by allowable deflections rather than by allowable stresses, a reasonable attempt should be made to find some approximate values for the maximum deflections produced by *working* loads.

The approximate method of Marcus [12.2.1], discussed in Sec. 12.2, can be extended to obtain estimates of the maximum deflections produced by service loads. This approximation is based on the general expression of maximum beam deflection expressed in terms of the governing moment. Thus,

$$w_{\max} = c \frac{m_{\max} l^2}{EI}, \quad (13.1.5)$$

where the constant c depends on the shape of the moment diagram, as shown in Fig. 13.1.7, and $m_{\max} = m_u$; the boundaries are simply supported. While yield-line analysis assumes constant ultimate moments along the yield lines, elastic theory generally yields a parabolic moment distribution. This discrepancy can be compensated

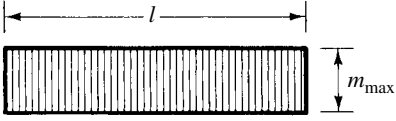

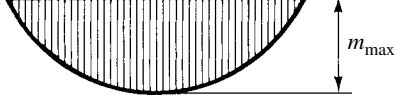

Moment diagram	c
	$\frac{1}{8}$
	$\frac{1}{8} \rightarrow \frac{1}{10}$
	$\frac{1}{9.6}$
	$\frac{1}{12}$

Figure 13.1.7 Factor c in Eq. (13.1.5) pertinent to various moment diagrams.

for by introduction of a correction factor obtained from equating the areas of the rectangular and parabolic moment diagrams. Thus, using an average value $\frac{1}{9}$ for c , Eq. (13.1.5) becomes

$$w_{\max} = \frac{3}{2} c \frac{m_u l^2}{EI} = \frac{1}{6} \frac{m_u l^2}{EI}. \quad (13.1.6)$$

The same expression as (13.1.6) can be used for other boundary conditions provided that for l the distance between the points of zero moment is substituted.

The accuracy of two methods discussed for estimating maximum deflections is approximately the same. The actual deflections in both cases are smaller than the computed ones; consequently, the results are on the safe side. In Table 13.1.1 the obtainable accuracy of these methods for various span ratios is illustrated, assuming uniformly loaded, simply supported, rectangular plates whose maximum deflection can be written as

$$w_{\max} = C \frac{5}{384} p_0 l_x^4. \quad (13.1.7)$$

Table 13.1.1 Variation of Coefficient *C* in Eq. (13.1.7)

Method	$l_x/l_y = 0.4$	$l_x/l_y = 0.6$	$l_x/l_y = 0.8$	$l_x/l_y = 1.00$
“Exact”	0.887	0.67	0.47	0.315
Marcus	0.97	0.88	0.71	0.500
Eq. (13.1.7)	0.99	0.768	0.65	0.533

From Ref. [13.1.8].

References and Bibliography

[13.1.1] V. KAZINCZY, G., “Experiments with Clamped Beams” (in Hungarian), *Betonszemle*, 1, Nos. 4, 5, and 6 (1914).

[13.1.2] V. KAZINCZY, G., “Die Plastizität des Eisenbetons,” *Beton und Eisen*, 32, No. 5 (May 1933), 74–80.

[13.1.3] JOHANSEN, K. W., *Brudlinieteorier*, J. Gjellerup, Copenhagen, 1943.

[13.1.4] *Building Code Requirements for Reinforced Concrete*, ACI 318-95, American Concrete Institute, Detroit, Michigan, 1995.

[13.1.5] INGERSLEV, A., “Om en elementaer Beregningsmetode of krydsarmerede Plader,” *Ingeniøren*, 30, No. 69 (1921), 507.

[13.1.6] WOOD, R. H., *Plastic and Elastic Design of Slabs and Plates*, Thames and Hudson, London, 1961.

[13.1.7] JONES, L. L., and WOOD, R. H., *Yield-Line Analysis of Slabs*, American Elsevier Publishing Company, New York, 1967.

[13.1.8] HAASE, H., *Bruchlinientheorie von Platten: Grundlagen und Anwendungen*, Werner-Verlag, Düsseldorf, 1962.

[13.1.9] SAWCZUK, A., and JAEGER, T., *Grenztragfähigkeitstheorie der Platten*, Springer-Verlag, Berlin, 1963.

[13.1.10] KALISZKY, S., *Analysis of Reinforced Concrete Slabs by Plastic Theory* (in Hungarian), Műszaki Könyvkiadó, Budapest, 1967.

[13.1.11] JOHANSEN, K. W., *Yield-Line Theory*, Cement and Concrete Association, London, 1962.

[13.1.12] NIELSEN, M. P., “On the Calculation of Yield-Line Patterns with Curved Yield Lines,” in *Proceedings of the Symposium on the Use of Computers in Civil Engineering*, Vol. 1, Laboratório Nacional de Engenharia Civil, Lisbon, 1962, paper No. 22.

[13.1.13] COMITÉ EUROPÉEN DU BÉTON, “The Application of the Yield-Line Theory to Calculations of the Flexural Strength of Slabs and Flat-slab Floors,” *Information Bulletin No. 35*, Cement and Concrete Association, London, 1962.

[13.1.14] JONES, L. L., *Ultimate Load Analysis of Reinforced and Prestressed Concrete Structures*, John Wiley & Sons, New York, 1962.

[13.1.15] HODGE, PH. G., *Limit Analysis of Rotationally Symmetric Plates and Shells*, Prentice-Hall, Englewood Cliffs, New Jersey, 1963.

[13.1.16] HOPKINS, H. G., and PRAYER, W., “The Load Carrying Capacity of Circular Plates,” *J. Mech. Phys. Solids*, 2 (1953), 1–13.

[13.1.17] HOPKINS, H. G., “Some Remarks Concerning the Dependence of The Solution of Plastic Plate Problems upon the Yield-Line Criterion,” in *Proceedings of the 9th International Congress on Applied Mechanics* held in Brussels 1956, Vol. 6, University of Brussels 1957, p. 448.

[13.1.18] OLSZAK, W., and SAWCZUK, A., “Experimental Verification of the Limit Analysis of Plates,” *Bull. Acad. Polonaise Sci.*, 3, No. 4 (1955), 195–200.

[13.1.19] ARMER, G. S. T., “The Strip Method; A New Approach to Design of Slabs,” *Concrete (London)*, 2, No. 9 (Sept. 1968), 358–363.

[13.1.20] NEALE, K. W., and LIND, N. C., “Limit Analysis of Plates under Combined Loads,” *Proc. ASCE, J. EM Div.*, 96 (Oct. 1970), 711–728.

- [13.1.21] SAVE, M. A., and MASSONNET, C. E., *Plastic Analysis and Design of Plates, Shells and Disks*, North-Holland Publishing Co. Amsterdam, 1972.
- [13.1.22] ACI COMMITTEE 224, *Cracking, Deflection and Ultimate Load of Concrete Slab Systems*, ACI SP-30, American Concrete Institute, Detroit, Michigan, 1972.
- [13.1.23] WOLFENSBERGER, R., *Traglast und optimale Bemessung von Platten*, 2nd ed., Beton Verlag, Düsseldorf, 1967.

13.2 Work Method

The work (or energy) method gives an *upper-bound* solution to the critical load at which the slab, with a certain ultimate resisting moment, will fail. Of a family of possible yield-line patterns, we seek a particular configuration that gives the lowest value of the ultimate load p_u . The solution is based on the principle of virtual work.

Using the general guidelines established in Sec. 13.1, a probable yield-line pattern is assumed. We assume that the yield lines have already been formed but the complete collapse is merely impending. Consequently, the external forces and the internal ultimate moments are still in equilibrium. For an infinitesimally small disturbance of this equilibrium condition, we can state that the work done by the external forces equals the work done by the internal forces; thus,

$$\boxed{W_e = W_i.} \quad (13.2.1)$$

The work of the external forces due to a virtual displacement $w(x, y)$ is

$$W_e = \sum_n \left(\iint_{(A_u)} p_u w(x, y) dA_n + \oint_l \bar{P}_u w(s) ds + \sum_i P_{ui} w_i \right), \quad (13.2.2)$$

where $n = 1, 2, 3, \dots$ indicates the number of plate segments formed after the yield-line pattern has been established. The second and third terms in Eq. (13.2.2) represent the work done by line and concentrated loads, respectively. During an assumed small virtual displacement the individual rigid plate segments rotate. The virtual work of the internal forces (moment times corresponding angle of rotation) can be calculated from

$$W_i = \sum_n \left[\int_l \theta m_u ds \right], \quad (13.2.3)$$

where the integration is carried out along each yield line. The summation in (13.2.3) indicates, again, that the internal work must be calculated for each plate segment and the values, so obtained, added together. Instead of using Eq. (13.2.3), it is more convenient to use the components of the moment vectors projected to the axes of rotation multiplied by the corresponding slab rotations $\bar{\theta}$ (Fig. 13.2.1). Thus, an alternative form of the work done by the internal forces is

$$W_i = \sum_n [\bar{\theta}_j \bar{m}_{uj} \ell_j], \quad (13.2.3a)$$

where $\bar{\theta}_j$ is the “normal” rotation of the plate segments j , \bar{m}_{uj} represents the ultimate moments (per unit length) projected to the axis of rotation of each rigid portion and

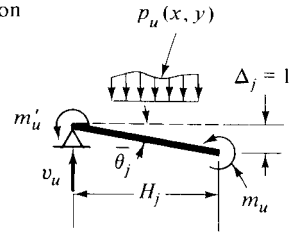
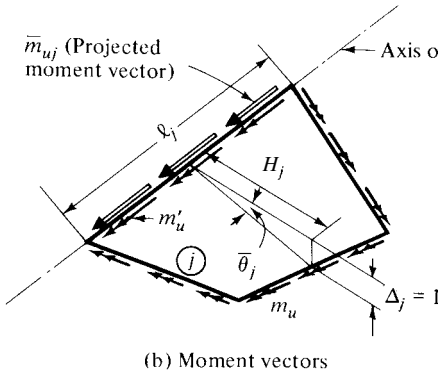
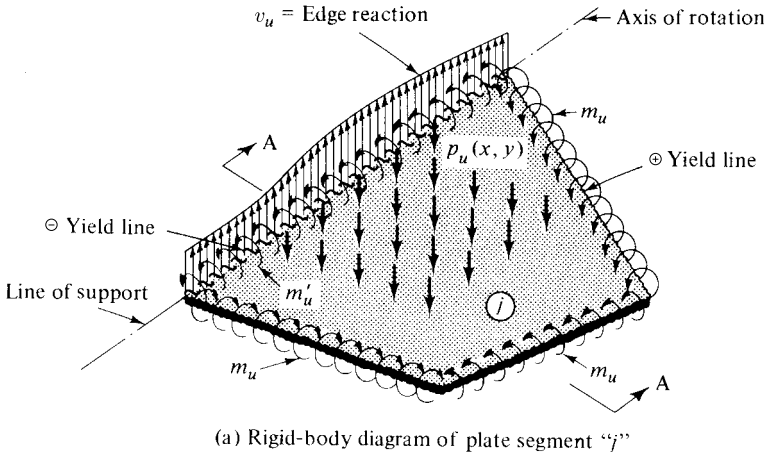


Figure 13.2.1 Plate segment.

ℓ is the total projected length. Figure 13.2.1 illustrates this simple procedure. Since along the yield lines the moment and rotation vectors have the same direction, the work of the internal forces, including that of the negative ultimate moments, always have the same signs in these computations.

To identify the optimum collapse mechanism, that is the yield-line pattern corresponding to the smallest ultimate load p_u , we introduce $x_1, x_2, x_3, \dots, x_r$ variables that define the geometry of an assumed yield-line pattern. Thus, for a given slab, the general expression of the ultimate load becomes

$$p_u = m_u f(x_1, x_2, x_3, \dots, x_r). \quad (13.2.4)$$

Therefore, the optimum configuration of yield lines can be obtained from the minimization procedure of differential calculus, which can be written as

$$\frac{\partial p_u}{\partial x_1} = 0, \quad \frac{\partial p_u}{\partial x_2} = 0, \quad \frac{\partial p_u}{\partial x_3} = 0, \quad \dots, \quad \frac{\partial p_u}{\partial x_r} = 0. \quad (13.2.5)$$

This analytical procedure results in coupled (*usually nonlinear*) equations from which the unknown parameters can be calculated.

With the exception of simple cases, however, such an analytical process tends to be cumbersome; thus, its use would defeat the main virtue of yield-line analysis, that is, *simplicity*. Fortunately, an iterative technique based on the familiar trial-and-error approach, often applied in engineering practice, gives very satisfactory results economically.

Before proceeding further, let us express the negative ultimate moment capacity of isotropic slabs, m'_u , as some multiple of the positive ultimate moment:

$$m'_u = -\mu m_u, \quad (13.2.6)$$

which simplifies the arithmetic of the work equations.

Next, based on the guidelines for estimating the location and orientation of yield lines, a probable failure mechanism is assumed. The yield-line pattern so imposed subdivides the slab into a series of inclined plane elements. Equating the maximum deflection ordinate to unity, the *normal* rotations $\bar{\theta}_1, \bar{\theta}_2, \dots, \bar{\theta}_j, \dots, \bar{\theta}_n$ for each rigid region are calculated from the geometrical relationship

$$\bar{\theta}_j = \frac{\Delta_j}{H_j} = \frac{1}{H_j}. \quad (13.2.7)$$

Then, virtual work expressions (13.2.3a) are formed keeping all variables constant, with the exception of one that most likely will dominate. After solving the equations thus obtained for the ultimate load p_u and plotting the results in function of the selected parameter, the minimum value of the ultimate load can easily be determined from the diagram (Fig. 13.2.2a) with satisfactory accuracy. By adopting another variable, one repeats the procedure. Since the work method is generally not sensitive to the exactness of the yield-line pattern, the variation of two or three parameters is usually sufficient. To be certain that the optimum yield-line pattern has been attained, one should check the critical load by the equilibrium method, discussed in the subsequent section.

Since the functions of the unknown variables are generally nonlinear, mathematically more than one solution for the parameter x_i is possible (Fig. 13.2.2b). Of the multiple solutions, the one that gives the lowest ultimate load should be selected. The

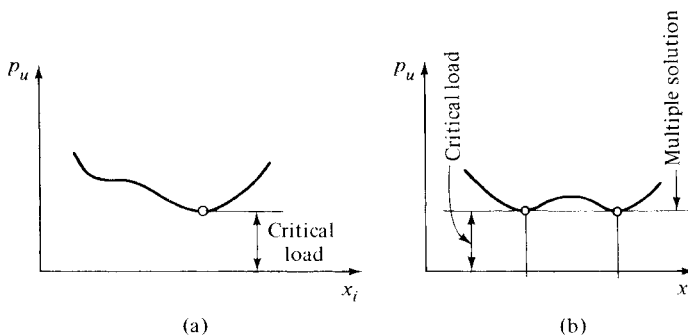


Figure 13.2.2 Diagram of ultimate load vs. governing parameter.

nonlinear interaction among various parameters usually does not affect the accuracy of the described iterative procedure, except in the rare case when the collapse load is overly sensitive to changes in the yield-line pattern. Such a case, which can easily be detected from the diagram of the ultimate load, might call for a more accurate analytic procedure.

Summary. Based on simple guidelines, a probable yield-line pattern is assumed. Using a trial-and-error procedure, the *optimum* configuration of yield lines can rapidly be established with satisfactory accuracy, even for complex boundary-load combinations. The ultimate load of a given slab is obtained from *simple* work equations. Since the energy method yields upper-bound solutions, the minimum ultimate load, selected semigraphically, should be used in the design of slabs. The work method is not overly sensitive to the assumed optimum failure mechanism; thus, it can offer distinct advantages in the case of difficult plate problems. The critical load so obtained should be checked by the equilibrium method, or in the absence of such a check, the selected ultimate load should be further reduced by 5% to cover possible errors made in selection of the optimum yield-line pattern. Yield-line analysis is highly recommended for checking the actual strength of plates analyzed by elastic theory. The limitations of the method are listed in Sec. 13.6.

ILLUSTRATIVE EXAMPLE I

A rectangular slab, shown in Fig. 13.2.3, is subjected to a uniform lateral load. Find the *critical* load by the work method, assuming that the positive ultimate moment of the slab is $m_u = 0.8M$ and the negative ultimate moment $m'_u = -1.6M$ is adopted.

For this problem the coordinate axes X and Y coincide with the axes of rotation of the individual plate segments. According to the guidelines established in Sec. 13.1, the positive yield line must pass through the intersection of these axes[†]. As shown in Fig. 13.2.3, the only variable for the failure mechanism is the distance x at $y = b$.

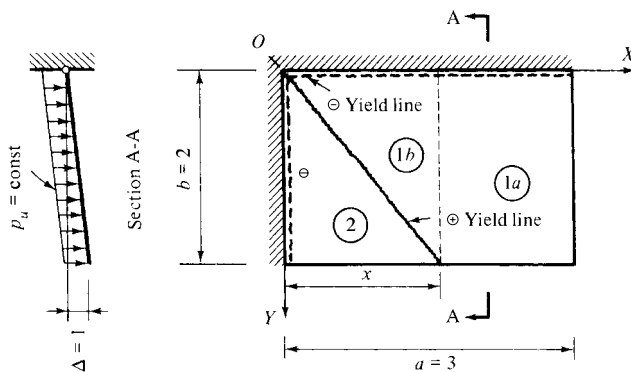


Figure 13.2.3 Uniformly loaded rectangular plate with free and clamped boundary conditions.

[†] An alternative failure mechanism is a single straight line running from the top right to the bottom left corner.

Assuming that the maximum virtual displacement is unity ($\Delta = 1$), the work of the external forces can be calculated from

$$W_e = p_u \sum_n V_{in} = p_u (V_{1a} + V_{1b} + V_2), \quad (13.2.8)$$

where V_{in} represents the volumes of wedges and pyramids produced by the virtual displacements of the individual slab segments. Thus, we can write

$$W_e = p_u \Delta \left[(a-x) \frac{b}{2} + \frac{bx}{3} \right] = \left(3 - \frac{x}{3} \right) p_u. \quad (13.2.9)$$

The normal angles pertinent to slab segments ① and ② are

$$\bar{\theta}_1 = \frac{\Delta}{b} = \frac{1}{2} \quad \text{and} \quad \bar{\theta}_2 = \frac{\Delta}{x} = \frac{1}{x}. \quad (13.2.10)$$

Consequently, using Eq. (13.2.3a), the work done by the internal forces is

$$\begin{aligned} W_i &= \left(0.8M \frac{1}{2}x + 1.6M \frac{1}{2}a \right) + \left(0.8M \frac{1}{x}b + 1.6M \frac{1}{x}b \right) \\ &= \left(2.4 + 0.4x + \frac{4.8}{x} \right) M. \end{aligned} \quad (13.2.11)$$

Equating the work of the exterior and interior forces,

$$W_e = W_i, \quad (13.2.12)$$

gives

$$p_u = M \frac{2.4 + 0.4x + (4.8/x)}{3 - (x/3)}. \quad (13.2.13)$$

Assigning various values to parameter x , a diagram representing the variation of the ultimate load in terms of the governing parameter is drawn (Fig. 13.2.4). The critical load for the slab is at $x = \frac{2}{3}a$. As Fig. 13.2.4 illustrates, the ultimate load is not sensitive to variation of the governing parameter.

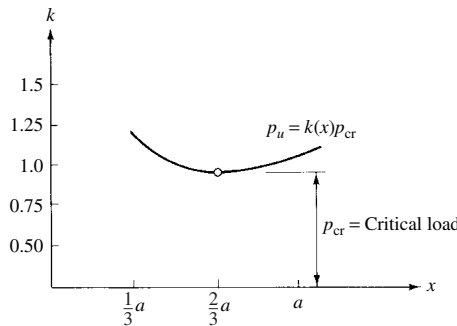


Figure 13.2.4 Graphical determination of minimum ultimate load.

Equating the work of the external and internal forces, we obtain

$$p_u = \frac{2m_u}{b[b - (x_1/3)]} \left[8 + b \left(\frac{x_1 + x_2}{x_1 x_2} \right) \right]. \quad (13.2.17)$$

Next, we seek the minimum value of this expression. We assume for one variable the value $x_1 = 0.3b$ and let $x_2 = k_2 b$; then we have

$$p_u = \frac{2m_u}{0.9b^2} \left[8 + \left(\frac{1}{k_2} + 3.33 \right) \right]. \quad (13.2.18)$$

This expression will be minimum when $k_2 = 1$ or $x_2 = b$. Using this result and introducing the notation $x_1 = k_1 b$, Eq. (13.2.17) can be written as

$$p_u = \frac{6m_u}{b^2} \left[\frac{9k_1 + 1}{k_1(3 - k_1)} \right]. \quad (13.2.19)$$

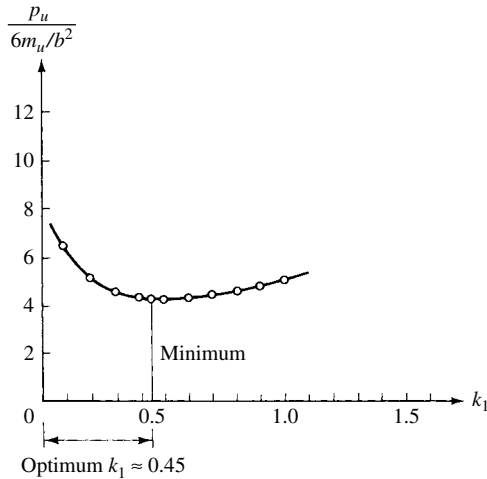


Figure 13.2.6 Graphical method for selection of optimum failure pattern.

As Fig. 13.2.6 shows, the minimum value for p_u occurs at $k_1 = 0.45$. Consequently, with $x_1 = 0.45b$ and $x_2 = b$, the ultimate lateral load is

$$p_u = \frac{26.3m_u}{b^2}. \quad (13.2.20)$$

References and Bibliography

- [13.2.1] NIELSEN, M. P., "Limit Analysis of Reinforced Concrete Slab," *Acta Polytechnica Scandinavica*, Civil Eng. Build. Constr. Series No. 26, 1964, p. 167.

- [13.2.2] HOGNESTADT, E., "Yield-Line Theory for the Ultimate Flexural Strength of Reinforced Concrete Slabs, *ACI J.*, 24, No. 7 (Mar. 1953), 637–656.
- [13.2.3] MANSFIELD, E. H., "Studies in Collapse Analysis of Rigid-Plastic Plates with a Square Yield Diagram," *Proc. Roy. Soc., Series A*, 241 (1957), 311–338.
- [13.2.4] SAWZUK, A., "Grenztragfähigkeit der Platten," *Bauplanung—Bautechnik*, 11, Nos. 7 and 8 (1957), pp. 315–320 and 359–364.
- [13.2.5] OLSZAK, W., and PERZYNA, P., "Variational Theorems in the Theory of Nonhomogeneous Orthotropic Circular Plates," *Arch. Mech. Stosowanej*, 9, No. 9 (1957).
- [13.2.6] PEREDY, J., "Über eine Minimumaufgabe der technischen Festigkeitslehre," *Acta Technica Sci., Hung.*, XXIV, Nos. 3/4 (1959), 329–346.
- [13.2.7] SCHELLENBERGER, R., "Beitrag zur Bemessung von Platten nach der Bruchtheorie," Ph.D. Dissertation, Technische Hochschule, Karlsruhe, 1958.
- [13.2.8] NIELSEN, M. P., *Limit Analysis on Concrete Plasticity*, 2nd ed., CRC Press, Boca Raton, Florida, 1998.

13.3 Equilibrium Method

The *true* equilibrium method [13.3.1, 13.3.2] provides lower-bound solutions for the failure load. Such lower-bound solutions are only attained if the equilibrium requirements are satisfied at *all* points of the plate. Mathematically, bracketing of an approximate solution by lower and upper bounds is highly desirable since such a bracketing yields usable estimates concerning the accuracy of the results. Furthermore, by averaging the lowest upper-bound and the highest lower-bound solutions,

$$p_{u,av} = \frac{\min p_{u,1} + \max p_{u,2}}{2}, \quad (13.3.1)$$

usually an improved, *most probable* failure load is obtained (Fig. 13.3.1). It should be noted that all elastic solutions are acceptable, unique, lower-bound solutions; consequently, by combining the elastic solution with that of yield-line analysis, the actual failure load can be bracketed. Since the elastic moments vary along the spans and clamped edges, respectively, the constant ultimate moments can be considered as the *average* value of the elastic moments. Consequently, for a valid comparison, the pertinent moment areas should be used.

The equilibrium method presented in this chapter is an upper-bound solution of the *critical* load. It is based on the equilibrium of each slab segment (vs. that of

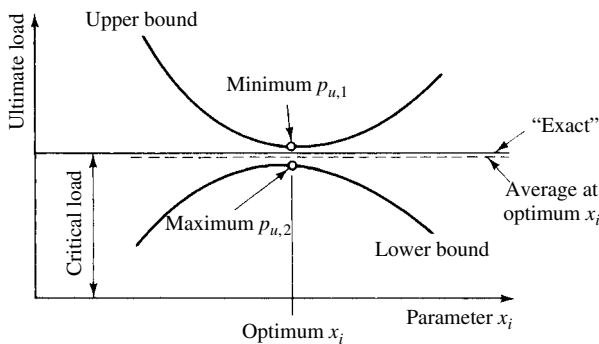


Figure 13.3.1 Bracketing critical load.

each point) created by the optimum yield-line pattern of an impending complete collapse. Although the mathematical manipulations involved in the work and equilibrium methods are quite different, they yield the same results [13.1.7], provided that the *optimum* yield-line pattern has been used in both methods. Thus, the work method provides a valuable check concerning the accuracy of the graphical minimization process, especially when the previously described iterative technique is used. When the discrepancy in the results obtained by these two methods is larger than 5%, the minimization of the upper-bound solution should be repeated. Unfortunately, agreement between the two solutions merely indicates that for the assumed yield-line pattern the minimum collapse load has been found, but it does not exclude the possibility of other, probably more critical, yield-line patterns.[†] Identical upper- and lower-bound solutions, on the other hand, are proof that the collapse mechanism indeed corresponds to the critical load.

The equilibrium of each slab segment studied as a “free body” yields, in a general case, one force and two moment equilibrium equations,

$$\sum P_z = 0, \quad \sum M_x = 0, \quad \sum M_y = 0, \quad (13.3.2)$$

assuming that the external loads are lateral loads. This general equation is used only when the slab segment under consideration has no exterior supports. For column-(point-) supported segments, two moment equations are required, while for segments supported along a line, one moment equation is sufficient, provided that one of the axes of the selected Cartesian coordinate system coincides with the line on the support.

If we assume an optimum yield-line pattern, a given segment is under the action of the external loads, that is, the reactions produced at the support, the moments along the yield lines and certain concentrated forces called *nodal forces*. These nodal forces, introduced by Johansen [13.1.11], appear at the intersections of positive and negative yield lines and where they meet free-edges (Fig. 13.3.2) or along curved yield-lines.[‡] Nodal forces are required to maintain the equilibrium of individual segments and are analogous to the anchorage forces,[§] discussed in Sec. 1.3. It should be noted that,

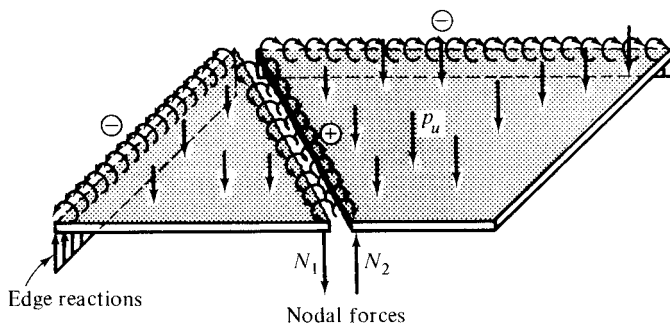


Figure 13.3.2 Nodal forces.

[†] In some cases, when the assumed yield-line pattern has less than a sufficient number of parameters, the discrepancy in the two solutions can also indicate that the assumed and actual failure mechanisms are different [13.1.6].

[‡] See Sec. 13.5.

[§] As a result of “Kirchhoff’s supplementary forces.”

theoretically, the introduction of nodal forces is also required at the intersection of yield lines with simply supported and clamped edges, but since moments are usually taken about these lines, they are eliminated in the actual computation.

Let us investigate the case when a yield line intersects a free-edge that is parallel to the X axis. The boundary conditions [Eq. (1.3.2)]

$$m_y = 0 \quad \text{and} \quad v_y = q_y + \frac{\partial m_{yx}}{\partial x} = q_y + q_y^* = 0 \quad (13.3.3)$$

state only that the sum of the transverse shear forces and the reactions produced by the torsional moment m_{yx} must be zero; consequently, q_y and $\partial m_{yx}/\partial x$ are not necessarily zero. Considering the moment equilibrium of a small element at the intersection of a free-edge and a positive yield line (Fig. 13.3.3), the projection of moment vectors on axis ① gives

$$m_u \cos \beta - q_y^* \sin \beta = 0, \quad (13.3.4)$$

or

$$q_y^* = m_u \cot \beta = N_1(\downarrow). \quad (13.3.5)$$

The same force with opposite sign ($N_2 = -N_1$) is attached to the adjoining element to maintain the equilibrium of the total slab (Fig. 13.3.2). In a similar way, nodal forces acting at the intersections of positive and negative yield lines can be derived. The results of these simple derivations are given in Fig. 13.3.4.

Considering the equilibrium of each slab segment, a sufficient number of equilibrium equations can be obtained to determine the unknown parameters, x_1, x_2, \dots, x_n , defining the optimum yield-line pattern. Although in some cases the equilibrium method has distinct advantages over the work method (requiring less algebraic manipulations), the fundamental concepts of calculating the critical load by the energy method is considered simpler, since it does not require the use of *nodal forces*. Furthermore, applying the work method, we calculate the virtual work of the total slab, while the equilibrium method considers the equilibrium of each segment separately;

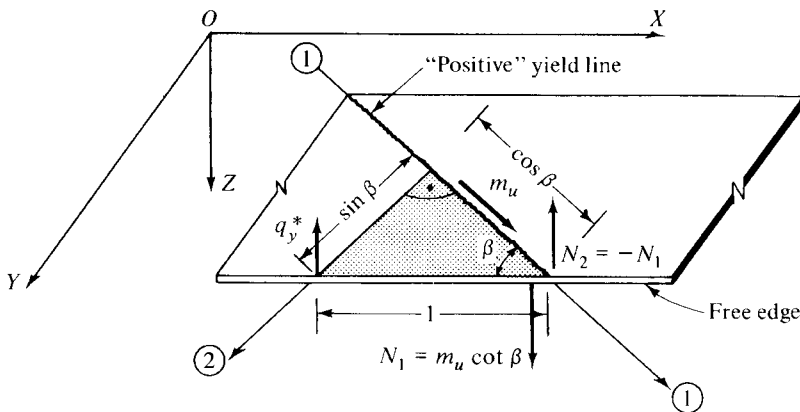


Figure 13.3.3 Intersection of yield line and free-edge. Note: Change signs for negative yield line.

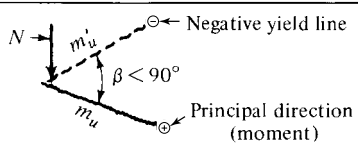
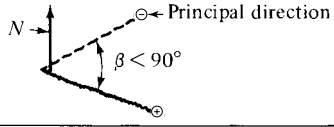
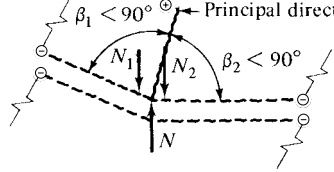
Configuration	Nodal Force
	$N = (m_u + m'_u) \cot \beta$
	$N = -(m_u + m'_u) \cot \beta$
	$\begin{aligned} N_1 &= (m_u + m'_u) \cot \beta_1 \\ N_2 &= (m_u + m'_u) \cot \beta_2 \\ N &= -(N_1 + N_2) \end{aligned}$

Figure 13.3.4 Nodal forces corresponding to various yield-line configurations.

thus, the latter method is more sensitive to errors in assuming an optimum yield-line pattern. In this book, the equilibrium method is used mostly to check the results obtained by the work method.

Summary. The equilibrium method involving the use of nodal forces is an alternative technique for obtaining upper-bound solutions to the critical load. The use of the equilibrium method for checking the results obtained from the energy principle is strongly recommended. Provided that the optimum yield-line pattern already has been established by the work method, the required computations are remarkably simple. It should be noted, however, that the equilibrium method is more sensitive to errors made in assuming the optimum failure mechanisms than the work method. For some plate problems, the use of the equilibrium method can offer distinct advantages.

ILLUSTRATIVE EXAMPLE I

Let us check the critical load obtained in Illustrative Example I of Sec. 13.2 by the equilibrium method.

Using the energy principle we have previously established (13.2.13),

$$p_{cr} = \left[M \frac{2.4 + 0.4x + (4.8/x)}{3 - (x/3)} \right]_{x=2} = 2.4M. \quad (13.3.6)$$

Taking moments about the X axis for part ①, it is found that

$$-2p_u - \frac{4}{3}p_u + (1.6 + 4.8)M + 0.8M(\cot \beta)2 = 0, \quad (13.3.7)$$

where, for $x = 2$, $\cot \beta = x/2 = 1$. The last term in Eq. (13.3.7) represents the moment of nodal forces, N_2 (Fig. 13.3.2); hence

$$p_u = \frac{8.0M}{3.333} = 2.4M. \quad (13.3.8)$$

Since the minimization process has yielded an “exact” solution, the same result is obtained by taking the moments of part ② about the Y axis. Thus,

$$-\frac{4}{3}p_u + (3.2 + 1.6)M - 0.8M(\cot \beta)2 = 0; \quad (13.3.9)$$

hence

$$p_u = \frac{3.2M}{1.333} = 2.4M. \quad (13.3.10)$$

Both solutions agree with the results of the energy method.

ILLUSTRATIVE EXAMPLE II

Let us check the results of the second example presented in the previous section using the equilibrium method.

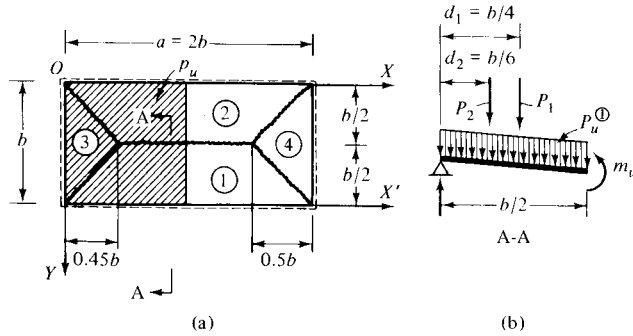


Figure 13.3.5 Assumed failure mechanism.

We assume that the yield-line pattern (Fig. 13.3.5a) determined by the energy method is the optimum. Since only positive yield lines intersect, the moment equations, taken about the supports of the individual segments, do not contain nodal forces. From the moment equilibrium ($\sum M_{x'} = 0$) of panel ① we obtain

$$2bm_u = p_u^{(1)}(b - x_1)\frac{b}{2}\frac{b}{4} + p_u^{(1)}\left(\frac{1}{2}x_1\frac{b}{2}\right)\frac{b}{6}. \quad (13.3.11)$$

Substituting $x_1 = 0.45b$, the ultimate load from Eq. (7.3.11) becomes

$$p_u^{(1)} = \frac{23m_u}{b^2}. \quad (13.3.12)$$

This expression is also valid for panel ②.

In a similar manner, taking moments for panel ③ about axis Y gives

$$m_u = \frac{1}{2}(2p_u^{③} 0.45 \times 0.15b^2); \quad (13.3.13)$$

hence

$$p_u^{③} = \frac{29.5m_u}{b^2}. \quad (13.3.14)$$

The results of these computations indicate that the assumed yield-line pattern is not quite optimum. Taking the average of these solutions, however, gives

$$p_u \approx \frac{26.25m_u}{b^2}, \quad (13.3.15)$$

which compares favorably with the result [Eq. (13.2.20)] obtained by the work method.

This example illustrates the sensitivity of the equilibrium method to the exactness of the optimum yield-line pattern.

References and Bibliography

- [13.3.1] HOPKINS, H. G., and PRAGER W., "The Load Carrying Capacities of Circular Plates," *J. Mech. Phys. Solids*, 2 (1953), 1–13.
- [13.3.2] SCHUMANN, W., "On Limit Analysis of Plates," *Quart. Appl. Math.*, 16 (1958), 61–71.
- [13.3.3] INGERSLEV, A., "The Strength of Rectangular Slabs," *J. Inst. Struct. Eng.*, 1, No. 1 (Jan. 1923), 3–14.
- [13.3.4] HALÁSZ, O., "On the Limit Equilibrium of Reinforced Concrete Slabs" (in Russian), *Izv. Akad. Nauk USSR Otd. Tech. Nauk*, No. 8 (1956), 42–54.
- [13.3.5] OLSZAK, W., "Probleme der Grenzlasttheorie der orthotropen Platten," *Acta Techn. Acad. Sci. Hungaricae*, XIV, Nos. 1 and 2 (1956), 3–37.
- [13.3.6] GVASDEV, A. A., *Limit Analysis of Structures by Equilibrium Method* (in Russian), Stroiizdat, Moscow, 1949.
- [13.3.7] NIELSEN, M. P., "A New Nodal Force Theory," in *Recent Developments in Yield-Line Theory*, Magazine of Concrete Research, Cement and Concrete Association, London, 1965 (special publication), pp. 25–30.
- [13.3.8] JONES, L. L., "The Use of Nodal Forces in Yield-Line Analysis," in *Recent Development in Yield-Line Theory*, Magazine of Concrete Research, Cement and Concrete Association, London 1965 (special publication), pp. 63–74.

13.4 Further Applications of Yield-Line Analysis

a. Approximate Solution for Combined Loadings. Let us assume that the slab is subjected to $p_1(x, y)$, $p_2(x, y)$, \dots , $p_n(x, y)$ lateral loads of various intensities acting at various locations. Determination of the optimum yield-line pattern due to such combined loading is usually a difficult task, even by the simplified trial-and-error procedure. Fortunately, a simple superposition principle in the form

$$m_u \leq m_{u1} + m_{u2} + \dots + m_{un} \quad (13.4.1)$$

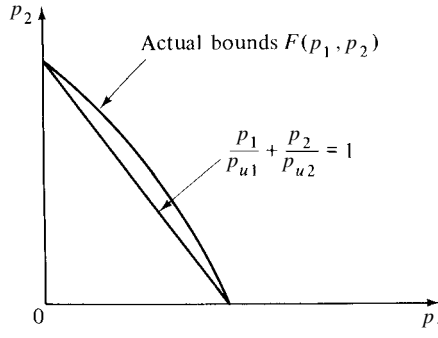


Figure 13.4.1 Bounds of multiple loadings.

yields safe results. Equation (13.4.1) states that the moment resistance of the slab required to carry the combined load is equal to or less than the sum of the ultimate moments corresponding to p_1, p_2, \dots, p_n loads.

To determine limiting bounds for the *critical multiple* load, we consider first a slab subjected to two independent distributed loads, $p_1(x, y), p_2(x, y)$. Intersections of the enveloping curve of the critical loads with the coordinate axes are p_{u1} and p_{u2} , as shown in Fig. 13.4.1. Hodge [13.1.15] has shown that the bounding curve for critical loads is always convex. Consequently, using a

$$\frac{p_1}{p_{u1}} + \frac{p_2}{p_{u2}} = 1 \quad (13.4.2)$$

enveloping straight-line (Fig. 13.4.1), safe values for the critical combined loads can be obtained.

In an analogous manner, the enveloping surface for the critical combined load when three independent surface loads act simultaneously can be approximated by

$$\frac{p_1}{p_{u1}} + \frac{p_2}{p_{u2}} + \frac{p_3}{p_{u3}} = 1. \quad (13.4.3)$$

b. Continuous Slabs. Yield-line analysis of slabs continuous over beam supports is of considerable practical interest. Let us assume, first, that the supporting beams are sufficiently strong to carry the critical slab loads without developing plastic hinges. This case involves merely the study of independent slab failures. When on each panel dead and live loads are acting simultaneously, the collapse mechanism of the individual slabs is similar to the one shown in Fig. 13.1.5. However, by superimposing on the dead load a checkerboard-type live loading, a different yield-line pattern, as shown in Fig. 13.4.2, can be obtained. This failure mechanism should be used to determine the cutoff points (ξa and ξb) for top bars of RC two-way slabs. Craemer [13.4.4] has derived the following equation for the parameter ξ :

$$4\xi^3 - 6\xi^2 + (1 + 2\delta)\xi - 3\delta = 0, \quad (13.4.4)$$

where

$$\delta = \frac{\mu_1 m_u + \mu_3 m_u}{p_{DL} b^2} + \frac{\mu_2 m_u + \mu_4 m_u}{p_{DL} a^2}. \quad (13.4.5)$$

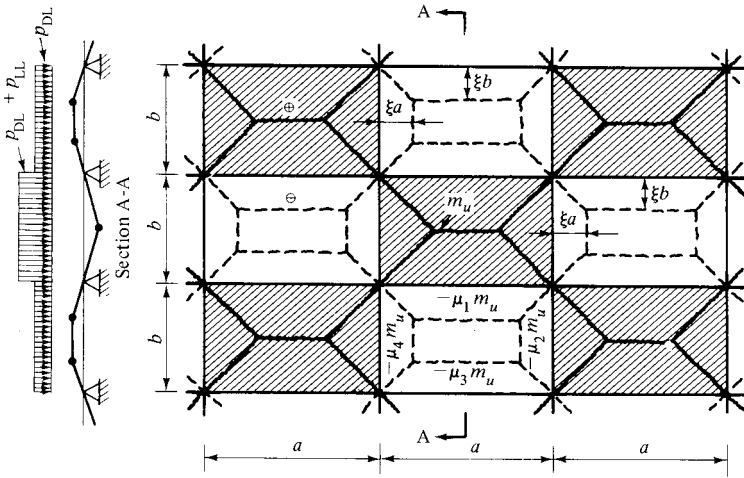


Figure 13.4.2 Yield-line pattern of continuous two-way slab (live load on alternative panels).

A usable approximate value for ξ is

$$\xi \approx \frac{1}{2 + (1/\delta)}. \quad (13.4.6)$$

A considerable simplification in the yield-line analysis of continuous two-way slabs is due to Ingerslev and Johansen [13.1.1], who developed simple formulas based on *reduced spans* a_r and b_r , respectively. The critical load of an interior panel is computed from an *equivalent* simply supported slab having reduced span lengths. Johansen's simplified formula gives

$$p_u \approx \frac{8m_u[1 + (a_r/b_r) + (b_r/a_r)]}{a_r b_r}, \quad (13.4.7)$$

where

$$a_r = \frac{2a}{\sqrt{1 + \mu_2} + \sqrt{1 + \mu_4}} \quad \text{and} \quad b_r = \frac{2b}{\sqrt{1 + \mu_1} + \sqrt{1 + \mu_3}}. \quad (13.4.8)$$

In these expressions, μ_i is, again, defined as the ratio of the negative moment capacity of the slab to the positive moment resistance ($m'_{ui} = -\mu_i m_u$), as shown in Fig. 13.1.5a. By assigning zero degree of restraint ($\mu_i = 0$) to any support, the validity of this simplified equation (13.4.7) can be extended to cover other boundary conditions.

The required negative moments of resistance computed from the adjoining panels (using the method described above) may differ at the mutual edges. When the discrepancy is small, averaging yields satisfactory results. In the case of significant differences, however, one-step moment distribution should be applied to distribute the unbalanced moments above the supports. To calculate the pertinent distribution factors, the reader is referred to the tables given in Sec. 12.4. Since the total moment resistance of the panel must remain the same, the positive moments should be adjusted

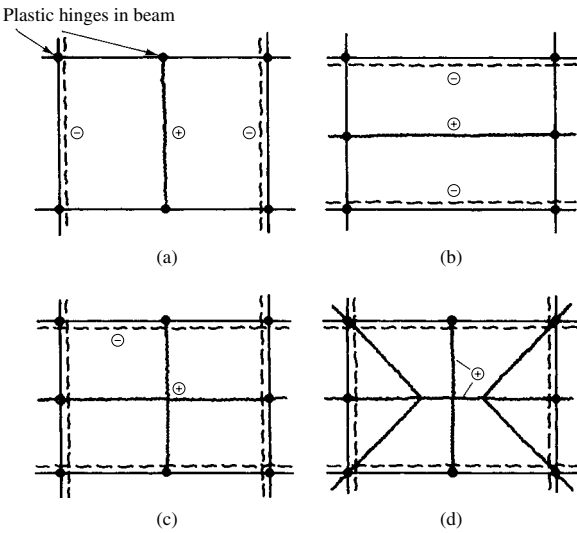


Figure 13.4.3 Combined beam and slab failures.

by moving the baseline of the moment diagrams for each span. Such a correction is required only when the spans of the adjacent panels differ significantly.

The study of the combined collapse of beams and slabs is more complex, since in this case the location of plastic hinges of the edge beams considerably influences the location of yield lines in the slab. Some possible yield-line patterns for combined slab and beam failures are shown in Fig. 13.4.3. For further study of this subject, the reader is referred to the pertinent literature [13.1.7, 13.1.9].

c. Affine Transformation of Certain Orthotropic Slabs. In RC slabs, the reinforcement is usually different in the X and Y directions. If the ratio of the negative moment resistance of the slab to the positive moment resistance is the same in both directions, then the orthotropic slab can be substituted by an equivalent isotropic slab by a simple transformation. This transformation is based on the factor of orthotropy λ , which is defined by

$$\lambda = \frac{m_{ux}}{m_{uy}}. \tag{13.4.9}$$

The following transformation rules can easily be verified by the energy principle of the work method [13.1.10]:

<i>Orthotropic slab</i>	<i>Equivalent isotropic slab</i>	
x	$= \xi$	
y	$= \eta = y/\sqrt{\lambda}$	
a	$= a'$	
b	$= b' = b/\sqrt{\lambda}$	
$p_u(x, y)$ (distributed)	$= p_u(\xi, \eta)$	
P_u (concentrated)	$= P_u/\sqrt{\lambda}$	
\overline{p}_u (line)	$= \overline{p}_u/\sqrt{\lambda \cos^2 \omega + \sin^2 \omega}$	(13.4.10)

Here ω is the angle between the line along which the load acts and the X axis, measured in the clockwise direction.

ILLUSTRATIVE EXAMPLE

Let us check the elastic design of the two-way slab floor system used as the Illustrative Example in Sec. 12.2 by the yield-line method. Again, we assume that the supports are unyielding and the slab is isotropic.

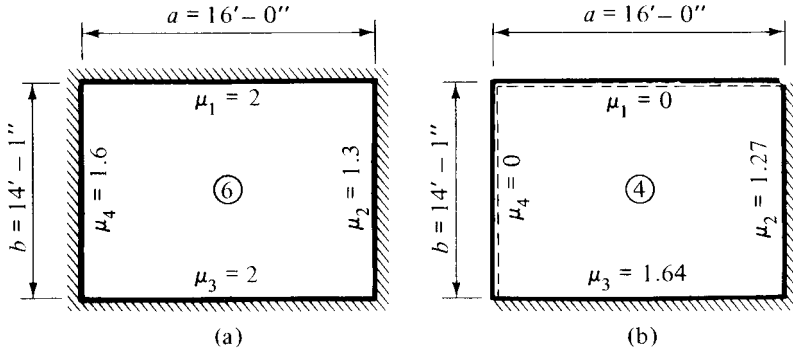


Figure 13.4.4 Interior and corner panels of RC floor slab.

Interior Panel ⑥ (Fig. 13.4.4a). To determine the degrees of restraint μ_i , we use the pertinent ratios of elastic moments. Thus, the following degrees of restraint are obtained:

$$\begin{aligned}\mu_1 &= \frac{|M_y|}{m_y} = \frac{14.915}{7.432} \approx 2.00, & \mu_2 &= \frac{|M_x^{\text{II}}|}{m_y} = \frac{8.380}{7.432} \approx 1.13, \\ \mu_3 &= \frac{|M_y|}{m_y} = \frac{14.915}{7.432} \approx 2.00, & \mu_4 &= \frac{|M_y^{\text{II}}|}{m_y} = \frac{10.056}{7.432} \approx 1.35.\end{aligned}\quad (13.4.11)$$

Using Eq. (13.4.8), the reduced spans are

$$\begin{aligned}a_r &= \frac{2a}{\sqrt{1+\mu_2} + \sqrt{1+\mu_4}} = \frac{2 \times 6.71}{\sqrt{1+1.3} + \sqrt{1+1.35}} = 4.49 \text{ m}, \\ b_r &= \frac{2b}{\sqrt{1+\mu_1} + \sqrt{1+\mu_3}} = \frac{2 \times 5.49}{\sqrt{1+2.0} + \sqrt{1+2.0}} = 3.17 \text{ m}.\end{aligned}\quad (13.4.12)$$

From Eq. (13.4.7) we obtain the required moment capacity of the slab:

$$\begin{aligned}m_u &= \frac{p_0 a_r b_r}{8[1 + (a_r/b_r) + (b_r/a_r)]} \\ &= \frac{7.182 \times 4.49 \times 3.17}{8[1 + (4.49/3.17) + (3.17/4.49)]} = 4.082 \text{ kN-m/m},\end{aligned}\quad (13.4.13)$$

By equating the areas of the rectangular and parabolic moment diagrams, we obtain

$$+m_{u,\max} = \frac{3}{2}m_u \frac{1}{0.8} = 7.654 \text{ kN-m/m.} \quad (13.4.14)$$

The required negative moments of resistance are calculated from $m'_{ui} = -\mu_i m_u$. The comparable maximum values are $1.5\mu'_{ui}$. This multiplication factor is obtained by assuming that the elastic moment diagram is parabolic. Thus, the negative moments above the supports are

$$\begin{aligned} m'_{u1} &= -\mu_1 m_u = -2.0 \times 4.082 = -8.165 \text{ kN-m/m,} & m_{1,\max} &= -1.5 \times 8.165 = -12.247, \\ m'_{u2} &= -\mu_2 m_u = -1.13 \times 4.082 = -4.613 \text{ kN-m/m,} & m_{2,\max} &= -1.5 \times 4.613 = -6.92, \\ m'_{u3} &= -\mu_3 m_u = -2.0 \times 4.082 = -8.165 \text{ kN-m/m,} & m_{3,\max} &= -1.5 \times 8.165 = -12.247, \\ m'_{u4} &= -\mu_4 m_u = -1.35 \times 4.082 = -5.511 \text{ kN-m/m,} & m_{4,\max} &= -1.5 \times 5.511 = -8.267. \end{aligned} \quad (13.4.15)$$

Corner Panel (4) (Fig 13.4.4b). Based on the elastic analysis, the assumed degrees of restraint are

$$\mu_1 = \mu_4 = 0, \quad \mu_2 = \frac{|M_x|}{m_y} = \frac{10.06}{9.308} \approx 1.08, \quad \mu_3 = \frac{|M_y|}{m_y} \approx 1.6. \quad (13.4.16)$$

Thus, for the reduced spans we obtain

$$\begin{aligned} a_r &= \frac{2a}{\sqrt{1+\mu_2} + \sqrt{1+\mu_4}} = \frac{2 \times 6.71}{\sqrt{1+1.08} + 1.0} = 5.49 \text{ m,} \\ b_r &= \frac{2b}{\sqrt{1+\mu_1} + \sqrt{1+\mu_3}} = \frac{2 \times 5.49}{1 + \sqrt{1+1.6}} = 4.20 \text{ m.} \end{aligned} \quad (13.4.17)$$

The required positive moment of resistance of the exterior panel is

$$\begin{aligned} m_u &= \frac{p_0 a_r b_r}{8[1 + (a_r/b_r) + (b_r/a_r)]} \\ &= \frac{7.182 \times 5.49 \times 4.20}{8[1 + (5.49/4.2) + (4.2/5.49)]} = 6.732 \text{ kN-m/m,} \end{aligned} \quad (13.4.18)$$

By equating the corresponding moment areas, the maximum positive moment becomes

$$+m_{\max} = \frac{3}{2}m_u \frac{1}{0.95} = 10.629 \text{ kN-m/m.} \quad (13.4.19)$$

For the negative moments we obtain

$$\begin{aligned} m'_{u2} &= -\mu_2 m_u = -1.08 \times 6.732 = -7.27 \text{ kN-m/m,} & m_{2,\max} &= -1.5 \times 7.27 = -10.905, \\ m'_{u3} &= -\mu_3 m_u = -10.771 \text{ kN-m/m,} & m_{3,\max} &= -1.5 \times 10.771 = -16.156. \end{aligned} \quad (13.4.20)$$

In Table 13.4.1 we compare the results obtained with those of the elastic analysis based on the Marcus-Löser approximation (Sec. 12.2). Although these two engineering methods for designing continuous floor slabs are *fundamentally* different, relatively good agreement was achieved. However, by averaging the resulting values, even more reliable design moments can be obtained.

Table 13.4.1 Comparison of Results

Panel	Moment	Marcus	Yield Line	Discrepancy (%)	Average
⑥	$+m_{y,\max}$	7.432	7.654	3.0	7.543
	$-M_{x,\max}^I$	-10.056	-8.267	17.8	-9.162
	$-M_{x,\max}^{II}$	-8.380	-6.920	17.4	-7.65
	$-M_{y,\max}$	-14.914	-12.247	17.9	-13.580
④	$+m_{y,\max}$	9.308	10.629	14.2	9.968
	$-M_{x,\max}$	-10.056	-10.905	8.5	-10.480
	$-M_{y,\max}$	-14.914	-16.156	8.3	-15.535

References and Bibliography

- [13.4.1] MROZ, Z., "On Design of Nonhomogeneous Technically Orthotropic Plates," in *Proceedings of the I.U.T.A.M. Symposium on Nonhomogeneity and Plasticity*, held in Warsaw, Sept. 1958, Pergamon Press, New York, 1959.
- [13.4.2] WOOD, R. H., "Studies in Composite Construction," Pt. II, *Research Reports No. 13 and 22*, National Building Research Studies, Building Research Board, Her Majesty's Stationery Office, London, 1952, 1955.
- [13.4.3] PALOTÁS, L., "Stahlbetonplatten-Versuche und die Bruchtheorie," *Zement*, No. 22 (1961), 1-16.
- [13.4.4] CRAEMER, H., "Berechnung kreuzweise-bewehrter Rechteckplatten nach der Plastizitätstheorie," *Nachr. Oest. Betonvereins, XIV*, No. 4 (1954), 17-21. [Supplement to *Österreichische Bauzeitung*, 9, No. 4 (1954).]
- [13.4.5] PARK, R., "Ultimate Strength of Rectangular Concrete Slabs Under Short-Time Uniform Loading with Edges Restrained Against Lateral Movement," *Proc. Inst. Civil Eng.*, 28 (June 1964), 125-150.
- [13.4.6] DUBINSKY, A. M., *Analysis of Two-Way Reinforced Concrete Slabs by Collapse Condition* (in Russian), Sbornik trudov Ukrainskovo Naut. Inst., Kiev, 1948.
- [13.4.7] DUBINSKY, A. M., *Limit-Analysis of Reinforced Concrete Slabs* (in Russian), Gosstrojizdat USSR, Kiev, 1961.
- [13.4.8] GAMBLE, W. L., SOZEN, M. A., and SIESS, C. P., "An Experimental Study of Reinforced Concrete Two-Way Floor Slabs," *Civil Eng. Studies, Struct. Res. Series No. 211*. University of Illinois, Urbana, June 1961.
- [13.4.9] VANDERBILT, M. D., SOZEN, M. A., and SIESS, C. P., "An Experimental Study of Reinforced Concrete Two-Way Floor Slabs with Shallow Beams," *Civil Eng. Stud. Struct. Res. Series No. 228*, University of Illinois, Urbana, Oct. 1961.
- [13.4.10] GAMBLE, W. L., SOZEN, M. A., and SIESS, C. P., "Tests of a Two-Way Reinforced Concrete Floor Slab," *Proc. ASCE J., Struct. Div.*, 95, ST6 (June 1969), 1073-1096.
- [13.4.11] NAGARAJA, R., and LASH, S. D., "Ultimate Load Capacity of Reinforced Concrete Beam-and-Slab Highway Bridges," *ACI J.*, 67, No. 12 (Dec. 1970), 1003-1006.

[13.4.12] GESUND, H., and KAUSHIK, Y. P., "Yield Line Analysis of Punching Failures in Slabs," *Publ. IABSE 30-I* (1970), 41–60.

13.5 Yield Lines due to Concentrated Loads

a. Point Load. Before we discuss the yield-line analysis of slabs subjected to concentrated loads, the reader's attention is called to the problem of *punching* shear. Quite often the punching shear strength, rather than the moment resistance, limits the load-carrying capacity of point-supported slabs. Although the theoretical solution of the problem is quite complex, the following simple formula gives satisfactory results for *interior* point loads or column supports.

For concentrated loads distributed on a *small* circular area, the punching shear can be estimated from

$$\tau \approx \frac{P}{\pi(d+h)h}, \quad (13.5.1a)$$

which should be less than the allowable value of shear, $\tau_{\text{allowable}}$, given in the pertinent specifications. In this expression, d is the diameter of the small circular area upon which the load is distributed and h represents the thickness of the slab. Similarly, when the concentrated load is distributed over a small square area, we require that

$$\frac{P}{4(d+h)h} \leq \tau_{\text{allowable}}. \quad (13.5.1b)$$

The use of these expressions can be logically extended to point loads acting at the edge of the slab. Codes and specifications for reinforced- and prestressed-concrete slabs contain safe recommendations to prevent failures due to punching shear; thus, they should always be consulted in actual design work.

Failure under a concentrated load is a localized slab collapse [13.5.1]. Positive yield lines radiate straight from the point of application of the concentrated load until they intersect with a curved, negative yield line (Fig. 13.5.1a), which bounds

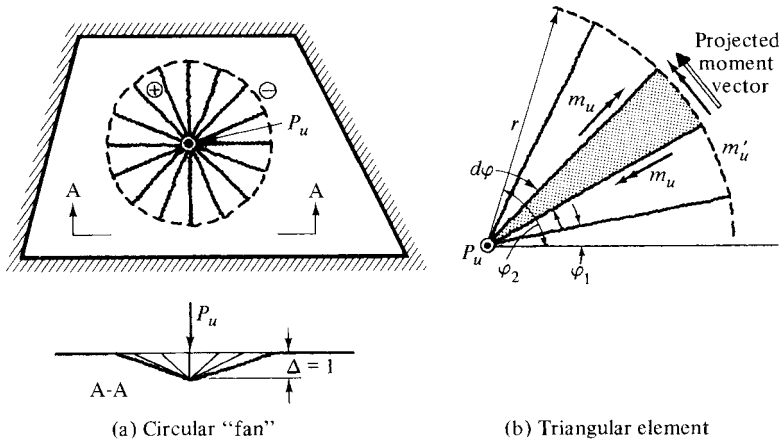


Figure 13.5.1 Localized failure under concentrated load.

the conical failure mechanism [13.5.2]. Such a collapse mode is called a *fan* in the pertinent literature [13.1.7].

Using a convenient polar coordinate system, as shown in Fig. 13.5.1b, the work of the internal forces is obtained from

$$W_i = \int_{\varphi_2}^{\varphi_1} (m_u + m'_u) \frac{\Delta}{r} r d\varphi, \quad (13.5.2)$$

which, using $\Delta = 1$ and a complete circle,[†] becomes

$$W_i = 2\pi(1 + \mu)m_u. \quad (13.5.3)$$

Since the work of the concentrated force is

$$W_e = P_u \Delta = P_u, \quad (13.5.4)$$

the critical concentrated load for an isotropic slab can be expressed by

$$P_u = 2\pi(1 + \mu)m_u. \quad (13.5.5)$$

This result is independent of the radius of a circle, provided that the load is a real point load. The only requirement is that the failure mechanism should be within the boundary of the slab, as shown in Fig. 13.5.1a.

The yield-line pattern is somewhat more complicated when the concentrated load is applied near a simply supported edge, as shown in Fig. 13.5.2. In this case, the work equation becomes

$$P_u = (m_u + m'_u) \int_{\alpha}^{2\pi-\alpha} d\varphi + m_u 2d \tan \alpha \frac{1}{d} = 0, \quad (13.5.6)$$

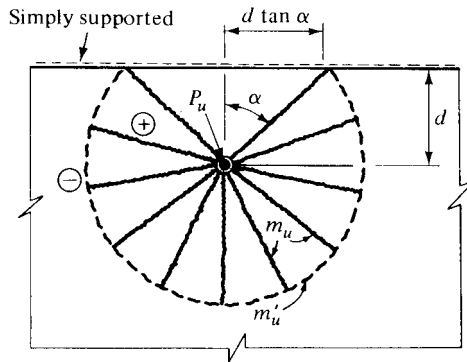


Figure 13.5.2 Failure pattern due to concentrated load near simply supported edge.

[†] Although other noncircular fans such as logarithmic spirals are possible, the assumption of circular fans yields safe results [13.1.7].

or

$$P_u = (m_u + m'_u)(2\pi - 2\alpha) + 2m_u \tan \alpha. \quad (13.5.7)$$

Differentiating this expression with respect to the parameter α , we obtain

$$\frac{dP_u}{d\alpha} = -2(m_u + m'_u) + 2m_u \sec^2 \alpha = 0; \quad (13.5.8)$$

hence

$$\tan \alpha = \sqrt{\frac{m'_u}{m_u}}. \quad (13.5.9)$$

Yield-line patterns of narrow bridge deck slabs are characterized by the appearance of two separate fans (Fig. 13.5.3a). The work equation in this case becomes

$$P_u = 2m_u(1 + \mu)(\pi - \alpha_1 - \alpha_2) + 2m_u \tan \alpha_1 + 2m_u \tan \alpha_2, \quad (13.5.10)$$

which can best be minimized by the trial-and-error procedure described in Sec. 3.2. A straight-line approximation of the two-fan collapse pattern, as shown in Fig. 13.5.3b, gives a somewhat lower, thus safer, ultimate load. Similar straight-line failure patterns (Fig. 13.5.4) can yield very good approximations, provided that they are used to *substitute* more complex fan-type failure mechanisms. Various yield-line patterns due to point loads acting on slabs of different shape and boundary conditions are described in Refs. [13.1.7], [13.1.9] and [13.1.10].

When the equilibrium method is used, the *nodal forces* per unit length along the circular bounding yield line can be calculated from

$$n = \frac{m_u + m'_u}{r}. \quad (13.5.11)$$

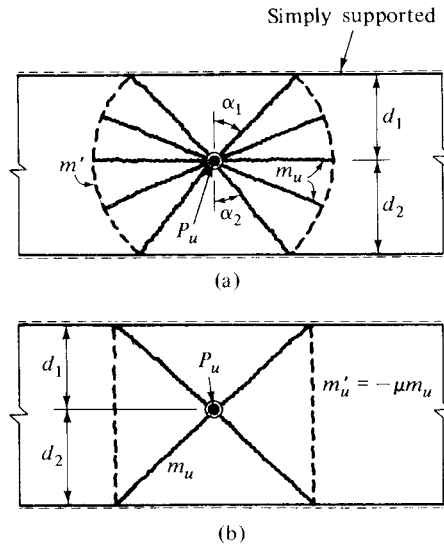


Figure 13.5.3 Actual and simplified yield-line patterns due to concentrated load.

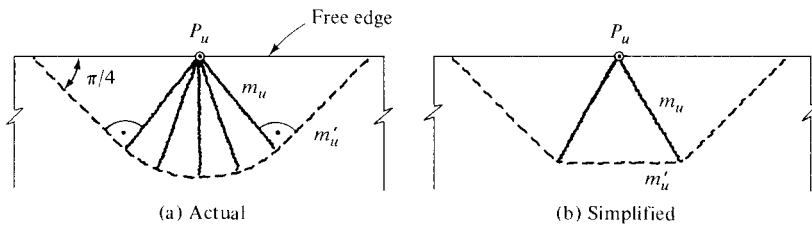


Figure 13.5.4 Yield lines due to concentrated load on free-edge.

For multiple loadings consisting of distributed and concentrated forces, Johansen's principle of superposition [Eq. 13.4.1] is still applicable. In practice, however, distributed loads are usually large in relation to the concentrated forces; thus, most of the foregoing discussion is of rather academic interest. An exception in this respect is the wheel load acting on bridge deck slabs.

b. Point (Column) Support. Point supports can be considered as special cases of point loadings. When the slab is supported only by columns without beams in the regions of the concentrated reactions, an *inverted fan-type* failure mechanism can form. The first trial for the *optimum* collapse mode should follow the yield lines shown in Fig. 13.5.5a. To guard against local failures, however, an alternative collapse mode consisting of fan-type yield-line patterns (Fig. 13.5.5b) must also be considered. This alternative failure mode may govern in certain cases.

The most often encountered point support conditions in civil and architectural engineering are the *flat-plate* and *flat-slab* floors introduced in Sec. 10.6. In the ultimate load analysis of flat plates, three yield-line patterns should be considered. The simplest consists of *one-way* collapse modes (Fig. 13.5.6a), either in the *X* or *Y* direction. Investigating the one-way collapse of a continuous slab subjected to uniformly distributed lateral load (Fig. 13.5.7), the equilibrium equations for the two plate segments can be written as

$$m_u + m'_{u1} = \frac{1}{2} p_u x^2 \quad \text{and} \quad m_u + m'_{u2} = \frac{1}{2} p_u (1 - x)^2. \quad (13.5.12)$$

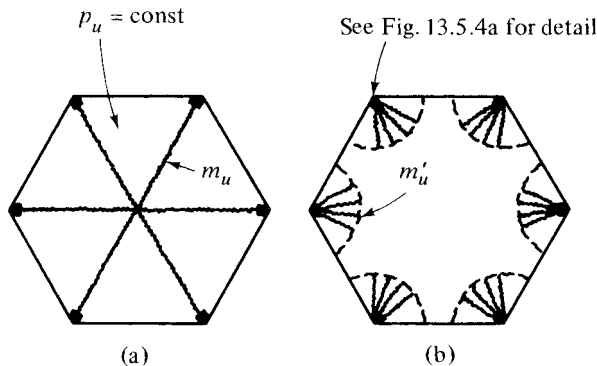


Figure 13.5.5 Straight-line and conical collapse modes.

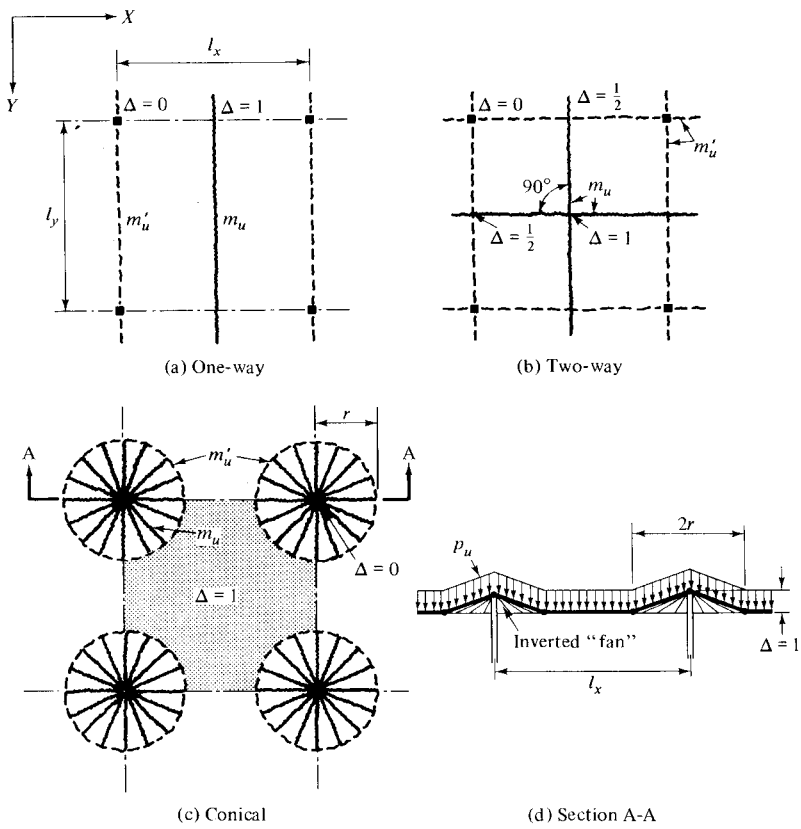


Figure 13.5.6 Collapse modes of flat plates.

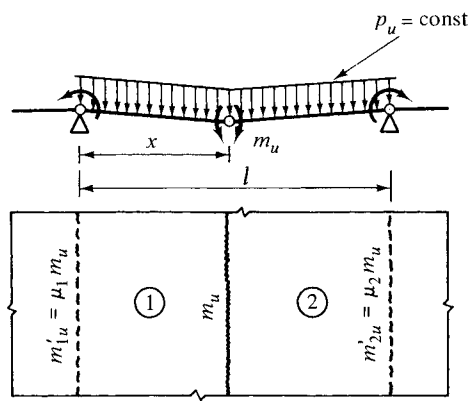


Figure 13.5.7 One-way collapse mode of continuous slab.

Introducing the following factors of restraint,[†]

$$\mu_1 = \frac{m'_{u1}}{m_u} \quad \text{and} \quad \mu_2 = \frac{m'_{u2}}{m_u}, \quad (13.5.13)$$

we solve the two equations (13.5.12) for x ; then the critical load is obtained from either of these equations. Thus

$$p_u = \frac{2m_u}{l^2} \left(\sqrt{1 + \mu_1} + \sqrt{1 + \mu_2} \right)^2, \quad (13.5.14)$$

which for $\mu_1 = \mu_2 = \mu$ becomes

$$p_u = \frac{8m_u(1 + \mu)}{l^2}; \quad (13.5.15)$$

hence

$$m_u = \frac{p_u l^2}{8(1 + \mu)}. \quad (13.5.16)$$

For simultaneous *two-way collapse*, the same yield-line pattern turned 90° is superimposed on the yield lines of the one-way failure, as shown in Fig. 13.5.6b. The critical load, however, remains unchanged (13.5.14) because of the right angle between these yield lines.

Considering the alternative yield-line pattern, consisting of inverted fans (Fig. 13.5.6c), we assume that the shaded part of one panel ($l_x \times \varepsilon l_y$) is dropped with $\Delta = 1$ displacement (Fig. 13.5.6d); consequently, the work of the external forces for one panel is

$$W_e = p_u(l_x^2 \varepsilon - \pi r^2 + \frac{1}{3} 2\pi r^2) = p_u(l_x^2 \varepsilon - \frac{1}{3} \pi r^2), \quad (13.5.17)$$

while the work of the internal forces within the fans can be computed from

$$W_i = 2\pi m_u(1 + \mu). \quad (13.5.18)$$

Thus, the energy equation ($W_e = W_i$) gives

$$p_u = \frac{2\pi m_u(1 + \mu)}{l_x^2 \varepsilon - (\pi r^2/3)} = \frac{2\pi m_u(1 + \mu)}{l_x^2 [\varepsilon - (\pi/3)(r^2/l_x^2)]}. \quad (13.5.19)$$

To find the critical radius of fans at which two-way and conical collapse modes appear simultaneously, we equate Eqs. (13.5.15) and (13.5.19), so that

$$\frac{8m_u(1 + \mu)}{l_x^2} = \frac{2\pi m_u(1 + \mu)}{l_x^2 [\varepsilon - (\pi/3)(r^2/l_x^2)]}, \quad (13.5.20)$$

[†] Recommended μ values are 1.0–1.5.

or

$$8 = \frac{2\pi}{\varepsilon - (\pi/3)(r^2/l_x^2)}; \quad (13.5.21)$$

hence

$$\frac{r}{l_x} = \sqrt{\frac{3\varepsilon}{\pi} - \frac{3}{4}}. \quad (13.5.22)$$

This result indicates that in the case of square panels ($\varepsilon = 1$) the critical radius is $r \approx 0.45l_x$. On the other hand, if $\varepsilon < 0.785$, no conical collapse mode is possible [13.1.7].

The results obtained for flat plates can be used for flat slabs by introducing

$$l'_x = l_x - 2c_x \quad \text{and} \quad l'_y = l_y - 2c_y \quad (13.5.23)$$

equivalent interior span lengths. Similarly, for exterior panels the equivalent spans are

$$l'_x = l_x - c_x \quad \text{and} \quad l'_y = l_y - c_y. \quad (13.5.24)$$

In these expressions the value of c , called *effective support size*, depends on the type of *column flare*, as illustrated in Fig. 12.6.5. The yield-line pattern of a correctly designed flat slab is shown in Fig. 13.5.8.

Sawczuk [13.1.9] has derived expressions for moment resistance of flat slabs considering various ratios of restraint.

Equation (13.5.15) states only that the external load is counteracted by the internal moments of resistance developed at the yield lines but does not give information on the variation of moments under the service load. Based on analytical and experimental investigations [13.5.3–13.5.10], the positive and negative panel moments

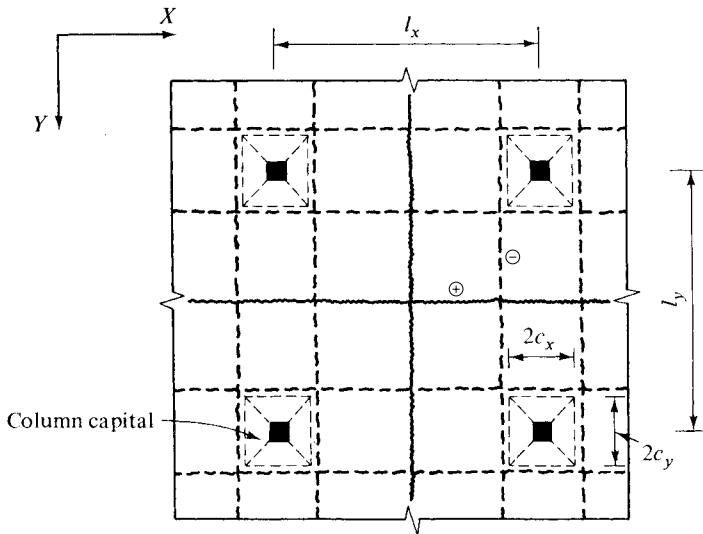


Figure 13.5.8 Yield-line pattern of typical interior panels of flat slabs.

($M = m_u l$, $M' = m'_u l$) can be distributed as shown in Fig. 12.6.3. This distribution approximately follows the variation of moments under service loads and thus reduces the permanent deflection of the flat slab. The panels are divided into *middle* and *column strips*, and constant moments throughout each strip are assumed. When checking elastic design by yield-line analysis, the calculated moment areas should approximately add up to the total panel moments ($M + M'$). The method given here is generally valid and can be used for checking most plate designs based on elastic theory. When yield-line analysis is used for flat slabs, the reader is urged to consult the pertinent specifications. Finally, it should be mentioned that the desirable ratio of positive to negative moments of resistance is $\mu = 1-1.5$.

Summary. Collapse mechanisms due to heavily concentrated loads (or reactions) are more complicated than those formed under distributed loads. The assumption that the collapse mode of isotropic slabs subjected to point load is conical (circular fan) yields safe results. The recommended analytical procedure is the work method coupled with a trial-and-error procedure. The computation can be simplified by using polygonal yield lines instead of curved ones. For multiple loadings, Johansen's superposition principle is applicable. Fan-type collapse modes are likely to occur under the following conditions [13.1.7]:

1. under large point loads,
2. under heavily concentrated reactions (point supports),
3. with slabs subjected to distributed loads having acute angled corners[†] and
4. with free-edges.

ILLUSTRATIVE EXAMPLE I

A point load is applied at the corner of a cantilever slab, shown in Fig. 13.5.9. Determine its ultimate load-carrying capacity, assuming a localized failure.

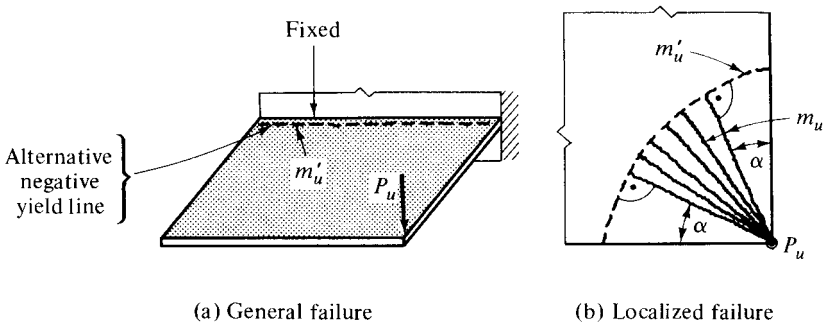


Figure 13.5.9 Concentrated load at corner of cantilever plate.

[†] Although the assumption of corner fans gives better results, the use of straight-line collapse modes is acceptable.

Since in the vicinity of the load the edges are free, limited fans similar to those shown in Fig. 13.5.4, are postulated. The energy equation gives

$$P_u = m_u(1 + \mu) \left(\frac{\pi}{2} - 2\alpha \right) + 2\mu m_u \tan \alpha. \quad (13.5.25)$$

The only variable in this expression is the angle α . By minimizing Eq. 13.5.25, we obtain

$$\frac{dP_u}{d\alpha} = 0 = -2m_u(1 + \mu) + 2\mu m_u \sec^2 \alpha; \quad (13.5.26)$$

hence $\tan \alpha = \sqrt{\mu}$; thus the critical load is

$$P_u = 2m_u\sqrt{\mu} + m_u(1 + \mu) \left(\frac{\pi}{2} - 2 \tan^{-1} \sqrt{\frac{1}{\mu}} \right). \quad (13.5.27)$$

Investigating the results, we can conclude that the load-carrying capacity of the slab depends on the ratio of its positive and negative moments of resistance. It should be noted that the use of Eq. (13.5.27) can be extended to the case of free-edges supported by columns (Fig. 13.5.5b).

ILLUSTRATIVE EXAMPLE II

A flat-slab floor system with drop panels consists of 5×5 bays. Spans between the supporting columns are $l_x = l_y = 5.00$ m. The thickness of the slab and drop panel is $h = 0.13$ m. Dimensions of the square columns are given in Fig. 13.5.10. The floor carries a total load $p = 10.12$ kN/m². An equivalent frame analysis gives the following moments for an interior column row:

$$\begin{aligned} M_{AB} &= -80.33 \text{ kN-m}, & M_{CD} &= -104.85 \text{ kN-m}, \\ m_{AB} &= +60.25 \text{ kN-m}, & m_{CD} &= +53.27 \text{ kN-m}, \\ M_{BA} &= -115.40 \text{ kN-m} & M_{DC} &= -104.85 \text{ kN-m}. \end{aligned} \quad (13.5.28)$$

Let us check these moments by the yield-line method. For the ratios of negative moments to positive moments, μ , we may use the moments given above.

a. Interior Panel. For a typical interior panel a simple one-way collapse mechanism (Fig. 13.5.11a) is assumed. Using the equilibrium approach, with $\mu_1 = \mu_2 = 10.48/53.27 \approx 1.97$ we obtain the following positive ultimate moment per unit length:

$$m_u = \frac{pl^2}{2(\sqrt{1 + \mu_1} + \sqrt{1 + \mu_2})^2} = \frac{10.12 \times 5.00^2}{2(2\sqrt{2.97})^2} = 10.65 \text{ kN-m/m}. \quad (13.5.29)$$

The corresponding negative moments are calculated from

$$m'_{u1} = m'_{u2} = -\mu_1 m_u = -\mu_2 m_u = -1.97 \times 10.65 = -20.98 \text{ kN-m/m}. \quad (13.5.30)$$

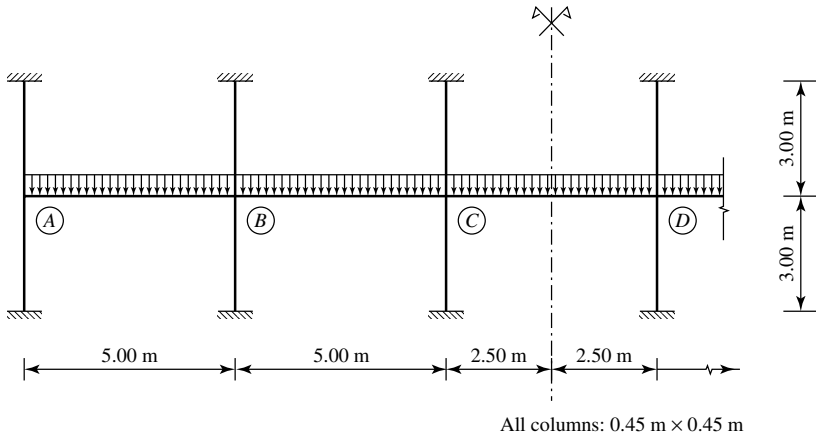


Figure 13.5.10 Equivalent frame representation of flat-slab floor system.

However, to be able to compare these values with those given in Eq. (13.5.28), we must multiply them by the span length $l_y = 1$. This gives

$$\begin{aligned} M_{CD} = M_{DC} = m'_{u1}l &= -20.98 \times 5.00 = -104.9 \text{ kN-m}, \\ m_{CD} = m_ul &= 10.65 \times 5.00 = +53.25 \text{ kN-m}. \end{aligned} \quad (13.5.31)$$

A comparison of Eq. (13.5.31) with Eq. (13.5.28) indicates only insignificant discrepancies.

b. Edge Panel. We select again a typical one-way collapse mechanism, as shown in Fig. 13.5.11b. The required degrees of restraint are calculated from the corresponding moments given in Eq. (13.5.28). Thus

$$\mu_1 = \frac{80.33}{60.25} \approx 1.33 \quad \text{and} \quad \mu_2 = \frac{115.40}{60.25} \approx 1.92. \quad (13.5.32)$$

The equilibrium approach yields the following positive ultimate moment:

$$m_{ui} = \frac{pl^2}{2(\sqrt{1+\mu_1} + \sqrt{1+\mu_2})^2} = \frac{10.12 \times 5.00^2}{2(\sqrt{2.33} + \sqrt{2.92})^2} = 12.09 \text{ kN-m/m}. \quad (13.5.33)$$

The corresponding negative moments per unit length are

$$\begin{aligned} m'_{u1} &= -\mu_1 m_{ui} = -16.08 \text{ kN-m/m} \quad \text{and} \\ m'_{u2} &= -\mu_2 m_{ui} = -23.21 \text{ kN-m/m}. \end{aligned} \quad (13.5.34)$$

Again, we must multiply these results by the span length to obtain

$$\begin{aligned} M_{AB} = m_{u1}l &= -16.08 \times 5.00 = -80.4 \text{ kN-m}, \\ M_{BA} = -m_{u2}l &= -23.21 \times 5.00 = -116.05 \text{ kN-m}, \\ m_{AB} = m_ul &= 12.09 \times 5.00 = +60.05 \text{ kN-m}. \end{aligned} \quad (13.5.35)$$

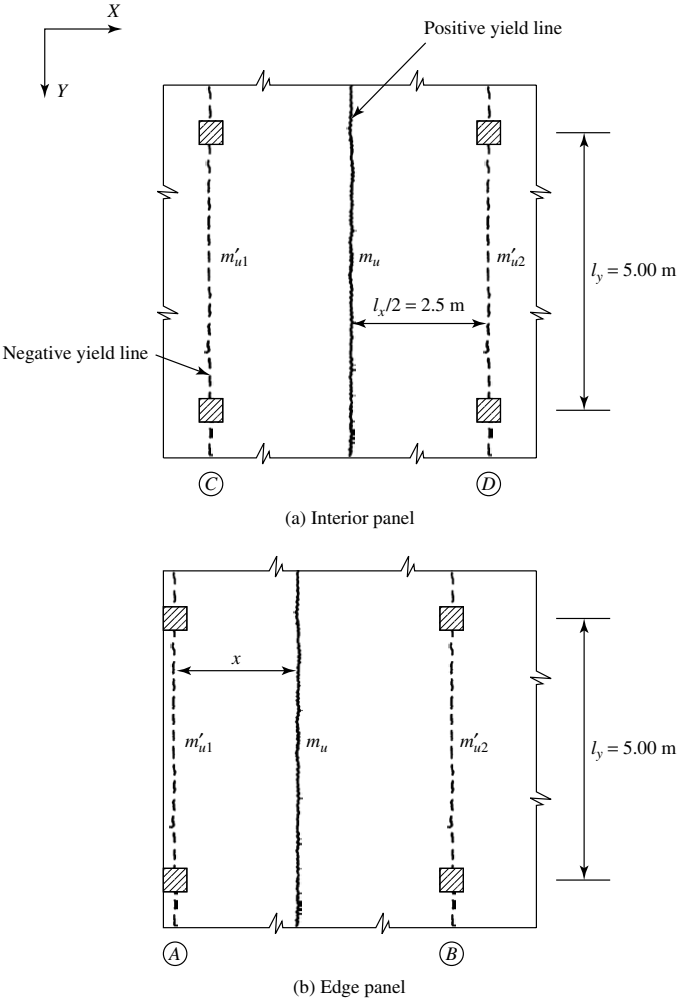


Figure 13.5.11 Assumed collapse patterns.

Again, by comparing these values with those given in the first column of Eq. (13.5.28), we can state that remarkable good agreement has been achieved between the results of the equivalent frame analysis and those of the yield-line method. Yield-line analysis of the corner panel, however, requires more effort, since its collapse pattern is more complex.

References and Bibliography

[13.5.1] RZHANITSYN, A. R., *Analysis of Structures by Considering Plastic Material Properties* (in Russian), Stroivoenmorizdat, Moscow, 1949.

- [13.5.2] RZHANITSYN, A. R., "The Shape at Collapse of Elastic-Plastic Plates Simply Supported Along the Edges," Office of Naval Res., Technical Report No. 19, Division of Applied Mathematics, Brown University, Providence, Rhode Island, Jan. 1957.
- [13.5.3] OLSZAK, W., and SAWCZUK, A., "Experimental Verification of the Limit Analysis of Plates," Pt. I, *Bull. Acad. Pol. Sci., Cl. IV, III*, No. 4 (1955), 195–200.
- [13.5.4] PALOTÁS, L., "Versuche mit Stahlbetonplatten und Pilzdecken und ihre Auswertung auf Grund der Bruchtheorie, *Wissen. Zeitschrift Hochschule für Bauwesen, Cottbus*, 5, No. 9. 3/4 (1962), 235–253.
- [13.5.5] MORICE, P. B., *Local Effects of Concentrated Loads on Bridge Deck Slab Panels*, Concrete and Cement Association, London, 1955.
- [13.5.6] SELF, M. W., "Ultimate Strength of Reinforced Concrete Flat Slabs," *Proc. ASCE, 90, Struct. Div. J.* (1964), 205–233.
- [13.5.7] PALOTÁS, L., "Design of Continuous Concrete Slabs by Fracture Theory" (in Hungarian), *Mélyépítéstudományi Szemle, XI*, No. 8 (1961), 350–355.
- [13.5.8] HATCHER, D. S., SOZEN, M. A., and SIESS, C. P., "An Experimental Study of a Quarter-Scale Reinforced Concrete Flat-Slab Floor," *Civil Eng. Stud. Struct. Res. Series No. 200*, University of Illinois, Urbana, June 1960.
- [13.5.9] HATCHER, D. S., SOZEN, M. A., and SIESS, C. P., "A Study of Tests on a Flat Plate and Flat Slab," *Civil Eng. Stud. Struct. Res. Series No. 217*, University of Illinois, Urbana, July 1961.
- [13.5.10] HATCHER, D. S., SOZEN, N. A., and SIESS, C. P., "Test of a Reinforced Concrete Flat Slab," *Proc. ASCE, J. Struct. Div. 95, ST6* (June 1969), 1051–1072.

13.6 Summary and Conclusions

Since stress analysis based on classical elastic theory fails to assess the *real* load-carrying capacity of structures, there is an increasing tendency to design structures by the limit analysis procedure. Yield-line analysis provides such an alternative design method for plates.

This remarkably simple method, which uses concepts and techniques familiar to structural engineers, furnishes realistic *upper bounds* of collapse loads even for arbitrary shape, boundary and loading conditions. Although the yield-line method was primarily developed for the design of RC slabs, its basic principles are generally applicable for the analysis of plates, provided that the plate material has the ability to deform plastically and that its stress-strain behavior can be reasonably well approximated by Johansen's *rigid ideally plastic* yield criterion. With the exception of certain troublesome boundary conditions and load combinations, such as concentrated loads and fixed boundaries, the yield-line analysis also furnishes usable estimates of the failure loads for bending of metal plates.

The accuracy of this simplified limit design method, when applied to RC slabs, as demonstrated by numerous independent tests, is good, provided that the proper failure mechanism has been assumed. With some experience, the assumption of the critical failure pattern is relatively simple. The same can be stated for the required computational work, especially if an iterative technique rather than an analytical minimization process is used to obtain the *lowest mode of collapse*. Using a trial-and-error procedure, the optimum failure pattern and the critical load can easily be determined. This procedure in combination with the energy method yields acceptable estimates in *all circumstances*. While the energy method is not sensitive to the assumed yield-line pattern, the work method really shows how well the optimum yield-line pattern has been determined. Since the equilibrium equations of the individual parts should

give the same critical load, the results are acceptable only if these values are sufficiently close. It is recommended that the results obtained from the energy equation be checked by the equilibrium method.

The advantages of the yield-line method are as follows:

1. The method is simple and economical.
2. Information is provided on the *real load-carrying capacity* of the slab.
3. For RC slabs close agreement is obtained between experimental and analytical results.
4. The basic principles used are familiar to structural engineers; furthermore, it applies procedures that can be easily visualized. Consequently, in the hands of an experienced structural engineer, the yield-line method always yields usable results irrespective of the complexity of the problem.
5. The method also gives acceptable estimates for the ultimate load-carrying capacity of structural steel plates.
6. Resulting designs are often more economical.

The present limitations of the method are as follows:

1. Since the total ultimate load-carrying capacity of the plate is obtained, the results cannot be applied *directly* to design.
2. Maximum deflections, which might control the design, can be estimated only via crude approximations.
3. The method fails in vibration analysis and cannot be used in the case of repeated static or dynamic loads (but can be applied effectively for suddenly applied one-time loads).
4. Theoretically, the law of superposition is not valid.

Although the yield-line method is not yet fully developed, it offers, especially for the practicing engineer, certain advantages over the elastic stress analysis approaches. Recently, one of the most important applications of this simple technique concerns the computerized solutions of complex plate problems; that is, it offers *quick independent* checks for computer results.

Problems[†]

- 13.2.1.** Using the work approach of the yield-line method, determine the ultimate load capacity of a simply supported square plate subjected to hydrostatic pressure.
- 13.2.2.** Solve problem 13.2.1 but this time assume clamped boundary conditions.
- 13.2.3.** An L-shaped RC slab carries a uniformly distributed load p . Determine the lowest upper-bound solution of the critical load by the work method. The outside dimensions of the L shape is $3a \times 3a$, where a represents

[†] The first two numbers refer to the corresponding section.

dimensions of the square panels. Assume that the outside boundaries are simply supported.

- 13.3.1–13.3.3.** Check the results obtained for problems 13.2.1–13.2.3 by the equilibrium approach of the yield-line method.
- 13.4.1.** Check the moments listed in Tables 12.5.2 and 12.5.3 by using the equilibrium approach of the yield-line method.
- 13.4.2.** Assume that all panels of the RC continuous slab shown in Fig. 12.3.8 carry uniformly distributed loads. Determine the critical loads for each panel by the yield-line method. Elastic properties of the slab are given in Illustrative Example I in Sec. 12.3.
- 13.4.3.** Assume that the RC floor system treated in Illustrative Example II of Sec. 13.5 has nonyielding continuous supports instead of supporting columns. Design this floor system using the yield-line method. To estimate the corresponding degrees of restraint μ_i , use the engineering method discussed in Sec. 12.5.
- 13.4.4.** Check the results obtained in Illustrative Example II in Sec. 12.3 by the yield-line method.
- 13.5.1.** Using the work approach of the yield-line method, verify the results of Illustrative Example II in Sec. 13.5.
- 13.5.2.** Prove that all yield-line patterns shown in Fig. 13.5.6 give identical results for the interior panel in Illustrative Example II in Sec. 13.5. Use the equilibrium approach.
- 13.5.3.** Redo problem 13.5.2 using the work method.
- 13.5.4.** A hexagonal RC slab with fixed boundaries is subjected to a uniformly distributed load plus a point load acting at its center. Determine the required moment resistance.
- 13.5.5.** Check the results obtained for problem 12.6.1 using the yield-line method.

Part V

Dynamic Analysis of Elastic Plates

14

Classical and Energy Methods in Dynamic Analysis

14.1 Introduction to Structural Dynamics

a. General Concepts. All loads considered in the preceding chapters have been static. In engineering practice, however, plate problems often involve consideration of dynamic disturbances produced by time-dependent external forces or displacements. Dynamic loads may be created by, for example, moving vehicles, wind gusts, seismic disturbances, unbalanced machines, wave impacts, flight loads, shock or blast and sound. Structural dynamics deals with time-dependent motions of structures and analyzes the internal forces associated with them. Thus, its *objective is to determine the effect of vibrations on the performance of the structure*. Vibrations of a plate bridge, for instance, may be objectionable or even critical, while vibrations of a membrane may be necessary to the performance of its task.

Since the reader is not assumed to have any prior knowledge of structural dynamics, we shall treat here, in a condensed form, the fundamental concepts of dynamic analysis. For this purpose, let us introduce a single-DOF system, shown in Fig. 4.1.1. Understanding the dynamic behavior of this simple system is essential for later treatment of more advanced topics. Furthermore, simple structures, such as beams and plates can be idealized by introducing equivalent single-DOF systems [4.1.2]. Components of such dynamic systems are a mass \bar{m} , a spring with spring constant k and a time-dependent excitation $P(t)$. This system has one degree of freedom, since only one coordinate, x , is required to define the position of the mass at a given time t .

Let us first define the two parameters \bar{m} and k , which are invariant with time and represent the given dynamic characteristics of the vibrating system. The mass \bar{m} is defined by Newton's law, which states that the product of mass and its acceleration equals the force applied to the mass. Consequently, we can write

$$P = \bar{m} \frac{d^2 x}{dt^2} \quad \text{and} \quad \bar{m} = \frac{P}{\ddot{x}}. \quad (14.1.1)$$

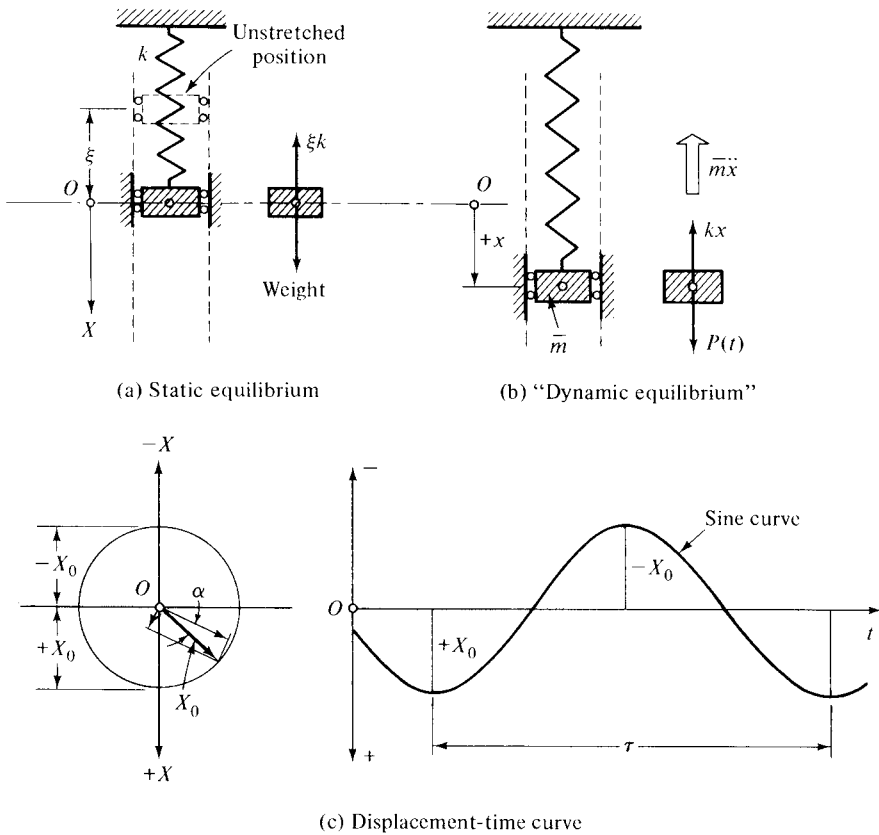


Figure 14.1.1 Free vibration of spring-mass system.

The *weightless* spring produces spring forces only when it is deformed. In the vibration of elastic systems we deal with linear springs, and their spring constant k represents the force required to produce unit deformation. Such a system is called a linear system for which the important *principle of superposition* is valid.

The time-dependent force $P(t)$ acting on the mass can be *harmonic*, such as $P(t) = P_0 \sin pt$, producing *steady-state* vibration. Suddenly applied loads, or forces acting on the system for short duration, are called *transient* forces. Vibrations in a system may also be produced by harmonic or transient motion of the support. For simplicity, we assume that there is no damping; its effect on the vibration will be considered later.[†]

In a vibrating system a new form of energy, corresponding to the velocity[‡] ($v = \dot{x}$) of the mass, is also present. This so-called *kinetic energy* (T) is computed from the work done by the inertia force. The product of the force ($P = \bar{m}\ddot{x}$) and the

[†] See Sec. 15.3.

[‡] Dots indicate differentiation with respect to time.

corresponding displacement component ($dx = v dt$) yields the kinetic energy density:

$$dT = P dx = \bar{m} \left(\frac{dv}{dt} \right) (v dt) = \bar{m} v dv. \quad (14.1.2)$$

By integrating this expression, we obtain the kinetic energy:

$$T = \bar{m} \int_{v=0}^v v dv = \frac{1}{2} \bar{m} v^2 = \frac{1}{2} \bar{m} (\dot{x})^2. \quad (14.1.3)$$

Hence, the total potential of the undamped vibrating system is

$$\boxed{\Pi = U + V + T.} \quad (14.1.4)$$

Since Π remains constant with time, the undamped vibrating system is said to be *conservative*. The energy enters into the system through external excitation. The energy approach is of great value in the dynamic analysis of more complicated systems and will be discussed in greater detail in Sec. 14.5.

b. Equation of Motion. The general equation of motion is derived by applying d'Alembert's dynamic equilibrium principle. Since we measure the displacement x from the static equilibrium position of the system, the effect of gravity (weight) need not be included, because it is counteracted by the spring force (Fig. 14.1.1a). If we displace the mass from its equilibrium position by applying a force $P(t)$, then the spring force $-kx$ tends to return it to its equilibrium position. The inertia force $\bar{m}\ddot{x}$ also acts against the dynamic force. Thus, the summation of all forces yields

$$P(t) - kx - \bar{m}\ddot{x} = 0, \quad (14.1.5)$$

or

$$\boxed{\bar{m}\ddot{x} + kx = P(t),} \quad (14.1.5a)$$

which represents the general equation of forced motion. If the disturbing force $P(t)$ is zero, we obtain the equation of *free vibration* of the single-DOF system; therefore

$$\bar{m}\ddot{x} + kx = 0. \quad (14.1.6)$$

Free vibration of a dynamic system is produced by introducing an initial velocity or displacement into the system; thereafter, however, no disturbance is applied to it.

In Eq. (14.1.6) we have a linear homogeneous differential equation of second order that can be solved by the usual mathematical procedures. In this particular case, however, Eq. (14.1.6) can be solved easily, since certain trigonometric functions, such as sine and cosine, satisfy the differential equation. Thus, let us assume a simple harmonic motion in the form

$$x = X_0 \sin \omega t. \quad (14.1.7)$$

Substitution of this expression into Eq. (14.1.6) yields

$$-\bar{m}X_0\omega^2 \sin \omega t + kX_0 \sin \omega t = 0; \quad (14.1.8)$$

hence

$$\omega^2 = \frac{k}{\bar{m}} \quad \text{or} \quad \omega = \sqrt{\frac{k}{\bar{m}}}. \quad (14.1.9)$$

The term ω is called the *natural circular frequency* of the vibration and is customarily measured in radians per second (rad/s). The resulting vibration is represented graphically in Fig. 14.1.1c.

Equation (14.1.7) represents a simple harmonic vibration, where one cycle has been completed when the amplitude vector X_0 has made one complete revolution. Thus, the angle of the function ω has varied through 2π radians. Hence, we can write

$$\tau = \text{period of vibration} = \frac{2\pi}{\omega} \quad (\text{s}). \quad (14.1.10)$$

The *natural frequency*, which is the reciprocal of the period, is defined as[†]

$$f = \frac{1}{\tau} = \frac{\omega}{2\pi} \quad (\text{Hz}). \quad (14.1.10a)$$

The natural frequency is often used for appraisal of the dynamic characteristics of structural elements and complete systems.

A more general form for solution of Eq. (14.1.6) is

$$x = C_1 \sin \omega t + C_2 \cos \omega t, \quad (14.1.11)$$

where C_1 and C_2 are arbitrary constants. These constants can be determined by specifying the initial conditions.[‡] For example, let the mass be pulled down to $x = X_0$ and then released. If the time is measured from the moment of release, then

$$(x)_{t=0} = X_0 \quad \text{and} \quad (\dot{x})_{t=0} = 0. \quad (14.1.12)$$

Substituting the first condition into (14.1.11), we have

$$X_0 = C_1 \cdot 0 + C_2 \cdot 1 \quad \text{or} \quad C_2 = X_0. \quad (14.1.13)$$

Differentiating Eq. (14.1.11) and substituting the second initial condition ($\dot{x} = 0$) into the result, we obtain $C_1 = 0$; therefore,

$$x = X_0 \cos \omega t. \quad (14.1.14)$$

The vibration so obtained is represented graphically in Fig. 14.1.2.

[†] The SI unit of natural frequency is the hertz (Hz), which equals one cycle per second.

[‡] The initial conditions can also be described by a phase angle α ; thus Eq. (14.1.11) becomes $x = X_0 \sin(\omega t \pm \alpha)$. The phase angle α indicates the initial position of the amplitude vector X_0 .

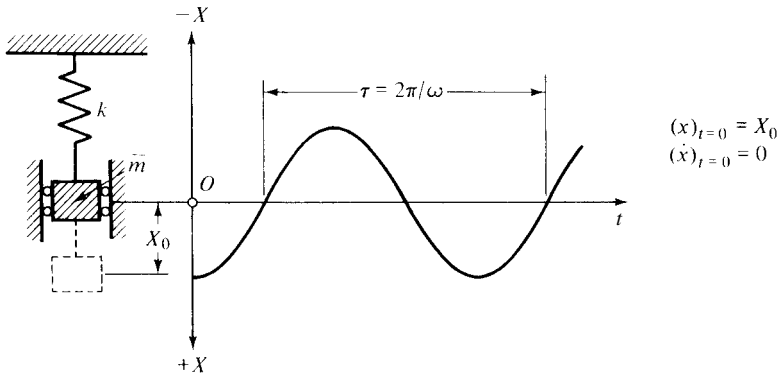


Figure 14.1.2 Free vibration with initial condition.

Let us consider, again, the same single-DOF system, as shown in Fig. 14.1.1, assuming that a harmonic force $P(t)$ is acting upon the mass; consequently, energy is being added to the system at all times, producing a *forced vibration*. We can write the differential equation of forced vibration as

$$\bar{m}\ddot{x} + kx = P_0 \sin pt, \quad (14.1.15)$$

where p is the frequency (in radians per second) of the simple harmonic disturbance.

The theory of differential equations states that the general solution of this type of equation is the sum of the homogeneous solution and a particular solution. Consequently, the general solution is

$$x = x_H + x_P. \quad (14.1.16)$$

We already have the first part of the solution, x_H , since the homogeneous form of Eq. (14.1.15) represents the differential equation of the free vibration (14.1.6). The particular solution, x_P , is obtained by applying Navier's method to this problem; thus, we express the particular solution in a form similar to the disturbing force:

$$x_P = \bar{X}_0 \sin pt. \quad (14.1.17)$$

Substitution of this assumed solution into the differential equation of motion (14.1.15) yields

$$-mp^2\bar{X}_0 + k\bar{X}_0 = P_0; \quad (14.1.18)$$

hence

$$\bar{X}_0 = \frac{P_0}{k - \bar{m}p^2} = \frac{P_0/k}{1 - (\bar{m}/k)p^2} = \frac{P_0/k}{1 - (p/\omega)^2}. \quad (14.1.19)$$

Therefore, the complete general solution of the equation of undamped forced motions is

$$x = C_1 \sin \omega t + C_2 \cos \omega t + \frac{P_0/k}{1 - (p/\omega)^2} \sin pt. \quad (14.1.20)$$

This general solution is the sum of harmonic functions having different frequencies and hence no harmonic function itself. The physical meaning of Eq. (14.1.20) is the following: The system will tend to vibrate at its natural frequency ω as well as to follow the frequency of the excitation, p . Since all real structures have some damping, the free-vibration part slowly dies out, and the system will eventually vibrate with the frequency of the excitation. This condition is called *steady-state* vibration.

If the support of the system vibrates up and down, with a motion of $x_s = S \sin \omega t$, then another class of forced-vibration problems is created. Examples of these types of dynamic excitations are earthquake loads, ground motions due to blast and vibrations induced by pile driving. The mathematical formulation of the problem is similar to that discussed for external load. Let us assume that the support is accelerated by \ddot{x}_s ; then, the governing differential equation of motion becomes

$$\bar{m}\ddot{x} + kx = -\bar{m}\ddot{x}_s(t) = \bar{m}S\omega^2 \sin \omega t, \quad (14.1.21)$$

which is of the same form as Eq. (14.1.15).

Navier's solution, used for simple harmonic excitation, can easily be extended to arbitrary periodic forces by expanding the time-dependent function into Fourier sine or cosine series, as discussed in Appendix A.1. The dynamic response of the system is then obtained by simple superposition of the results, calculated from the individual terms of the Fourier expansion.

c. Resonance. Let us consider, again, the forced-vibration part (14.1.17) of the general solution [Eq. (14.1.20)]. Since the static deflection of the spring under the constant load P_0 is

$$X_{st} = \frac{P_0}{k}, \quad (14.1.22)$$

we can write Eq. (14.1.19) as

$$\boxed{\frac{X_0}{X_{st}} = \frac{1}{1 - (p/\omega)^2} = \text{DLF}}, \quad (14.1.23)$$

which is called the *dynamic load factor* (DLF) and represents the ratio between the maximum dynamic and static displacements. A static load equivalent to a dynamic load can be obtained by multiplying the maximum dynamic load intensity by the dynamic load factor. If the p/ω ratio approaches unity, the amplitude of the forced motion becomes infinitely large. This condition, which is most feared by structural engineers, is called *resonance*.

The resonance diagram of a vibrating system is shown in Fig. 14.1.3. For certain values of p/ω the amplitude of the forced vibration is negative; however,

$$-X_p \sin \alpha = X_p \sin(\alpha + 180^\circ); \quad (14.1.24)$$

therefore, the negative amplitude is equivalent to the positive amplitude of a sine wave 180° out of phase; hence the negative sign is often disregarded and the resonance curve is drawn in the dotted position in Fig. 14.1.3. Three points on the

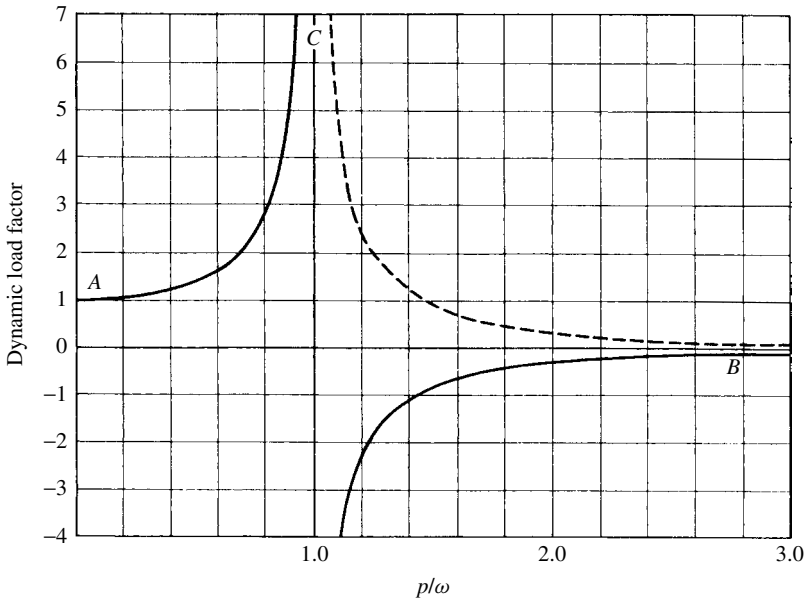


Figure 14.1.3 Resonance diagram.

diagram are of particular interest. At point *A*, the frequency of the excitation is very low; hence the mass is deflected to its static deflection and the ordinate of the curve approximates unity. At point *B*, the force varies so fast that the system does not have time to respond; hence the ordinate approaches zero. At point *C*, the frequency of the excitation coincides with the natural circular frequency of the vibrating system and the amplitude becomes infinite. This is the case of resonance, mentioned above.

d. Transient Response. The most convenient treatment of dynamic response of structural systems to arbitrary excitation is the representation of the forcing function by a Fourier series, containing only sine or cosine terms.

In the case of suddenly applied loads, however, care should be taken that the fictitious load (resulting from arbitrary continuation of the forcing function) is applied to the system with a sufficient time delay so that it will not interfere with its vibration during the time of interest (Fig. 14.1.4). By expanding the transient disturbance into sine series, for instance, we have

$$p_x(t) = \sum_{n=1}^n P_n \sin p_n t, \quad (14.1.25)$$

where

$$p_n = \frac{2n\pi}{T} \quad (14.1.26)$$

and $T = 2L$ represents the period of the half-range expansion, discussed in Appendix A.1.

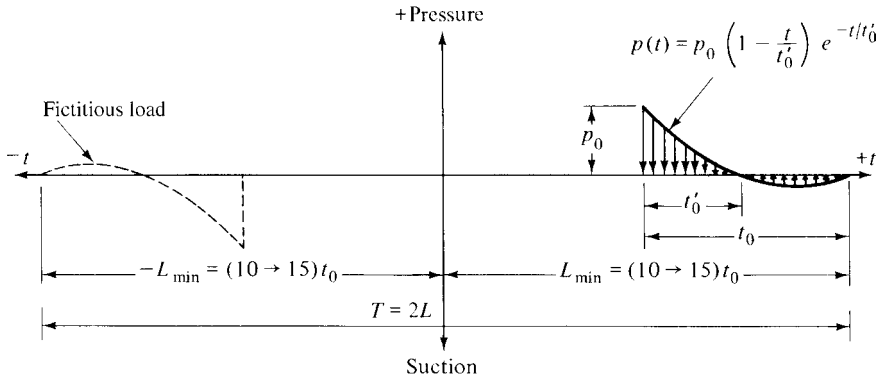


Figure 14.1.4 Approximation of transient load by periodic function.

The particular solution in this case is

$$x_P(t) = \sum_1^n X_n \sin p_n t. \quad (14.1.27)$$

In this way, again, the differential equation of the problem has been transformed into an algebraic equation. Additional advantages of the Fourier series representation of transient load are connected with computerized solutions of forced-vibration problems.

Another method for evaluating the dynamic response of a single-DOF system is based on a *definite integral*. Let us assume that at time $t = 0$ the mass is not displaced ($x = 0$). After applying an impulse $\mathbf{I} = \overline{m}v = P\Delta t$, the system vibrates freely. At $t = 0$, $x = 0$ and $v = \mathbf{I}/\overline{m}$, the constants in Eq. (14.1.11) become $C_1 = v/\omega$ and $C_2 = 0$, respectively; hence

$$x = \frac{\mathbf{I}}{\overline{m}\omega} \sin \omega t. \quad (14.1.28)$$

If the impulse \mathbf{I}_1 is applied at $t = t^*$ (Fig. 14.1.5), assuming that until $t = t^*$ the mass has been at rest, then

$$x = \frac{\mathbf{I}_1}{\overline{m}\omega} \sin \omega(t - t^*) \quad \text{for } t > t^*. \quad (14.1.29)$$

The increment in displacement due to this impulse can be written as

$$\Delta x = \frac{P(t^*)\Delta t^*}{\overline{m}\omega} \sin \omega(t - t^*). \quad (14.1.30)$$

If we consider that the exciting force $P(t)$ is composed of a large number of impulses, then by summing up the impulses, the final displacement is obtained:

$$x = \frac{1}{\overline{m}\omega} \int_0^t P(t^*) \sin \omega(t - t^*) dt^*. \quad (14.1.31)$$

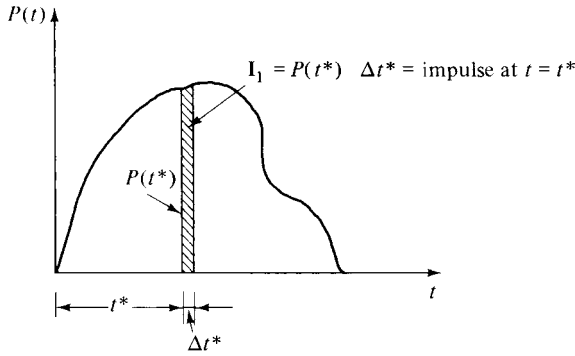


Figure 14.1.5 Arbitrary transient load.

Let us multiply and divide the right-hand side of this equation by ω and recall that $P(t^*) = P_0 f(t^*)$; then the substitution of Eqs. (14.1.9) and (14.1.22) results in

$$x = X_{st} \left[\omega \int_0^t f(t^*) \sin \omega(t - t^*) dt^* \right] = X_{st}(\text{DLF}). \quad (14.1.32)$$

The integral in this equation is known as Duhamel's integral or convolution integral.

Even if the forcing function can be integrated, evaluation of Duhamel's integral is usually a tedious process. One can, of course, use a computer program with symbolic mathematical capabilities to simplify this problem. In many practical vibration problems, however, the loading functions are given numerically. Consequently, the integral in Eq. (14.1.32) must also be evaluated numerically. For this purpose, we apply the trigonometric identity $\sin(\omega t - \omega t^*) = \sin \omega t \cos \omega t^* - \cos \omega t \sin \omega t^*$ and write Eq. (14.1.31) in the form

$$x(t) = \sin \omega t \frac{1}{m\omega} \int_0^t P(t^*) \cos \omega t^* dt^* - \cos \omega t \frac{1}{m\omega} \int_0^t P(t^*) \sin \omega t^* dt^*, \quad (14.1.31a)$$

or

$$x(t) = A(t) \sin \omega t - B(t) \cos \omega t, \quad (14.1.31b)$$

where

$$A(t) = \frac{1}{m\omega} \int_0^t P(t^*) \cos \omega t^* dt^* \quad \text{and} \quad B(t) = \frac{1}{m\omega} \int_0^t P(t) \sin \omega t^* dt^*. \quad (14.1.31c)$$

Since a plate under impact behaves approximately as a single-DOF system, the above-derived dynamic load factor may be used for simplified dynamic plate analysis, provided that the plate has neither displacement nor velocity, when the excitation is applied.

Other methods, such as Laplace transforms and numerical integration[†] of the equation of motion, can also be used to calculate the transient responses of structures.

[†] See Sec. 15.2.3.c.

These methods, however, are beyond the scope of this introductory treatise; therefore, they are not discussed here. For further study on the subject the reader is referred to the pertinent references [14.1.2, 14.1.8].

e. Continuous and Discrete Systems. A structural system is defined as an assemblage of components acting together. To describe the static or dynamic response of structures, we introduce mathematical models. These models, as already introduced in the static analysis, can be either continuous or discrete. In any case the mathematical model must be chosen so that its behavior closely resembles that of the real structure. Plates are continua, since their mass and elastic properties are distributed continuously over their middle surface. Some plate problems can be analyzed as distributed systems, but in the majority of the cases it is necessary to represent the plate by an *equivalent* discrete system, having lumped parameters.

Discrete systems that will satisfactorily represent the dynamic behavior of plates are finite difference, gridwork, finite strip and finite element representations of the elastic continua. All these discrete methods have already been introduced for the static analysis of plates. If we lump the inertia forces at discrete points, these methods can easily be extended to analysis of complex dynamic plate problems. Since the classical single-DOF system is basically a discrete system, matrix equations of motion can be obtained directly from the above-derived equations by introducing matrix notations. The matrix equation governing free vibrations of a *lumped-parameter* system, for instance, can be obtained from Eq. (14.1.6) by applying suitable matrix notation; thus

$$[\overline{m}]\{\ddot{x}\} + [k]\{x\} = 0. \quad (14.1.33)$$

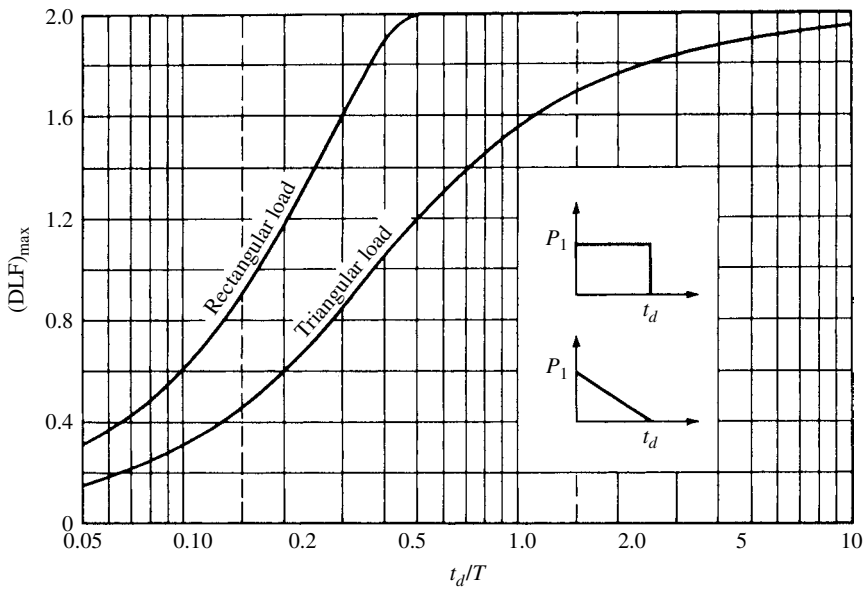
In this approach, each lumped mass is assumed to be a rigid body. The discrete masses are connected by springs that are assumed to have no masses. In this way, the inertia and stiffness properties are separated.

The behavior of continuous vibratory systems such as plates is described by partial differential equations. In setting up the governing differential equations of motion, d'Alembert's principle is of considerable help, since it states that any dynamic problem may be treated as a static problem by addition of the appropriate inertia forces. Consequently, dynamic problems of the plate theory can be reduced to the corresponding static problems; therefore, in the solutions, all previously introduced analytical and numerical methods can be applied.

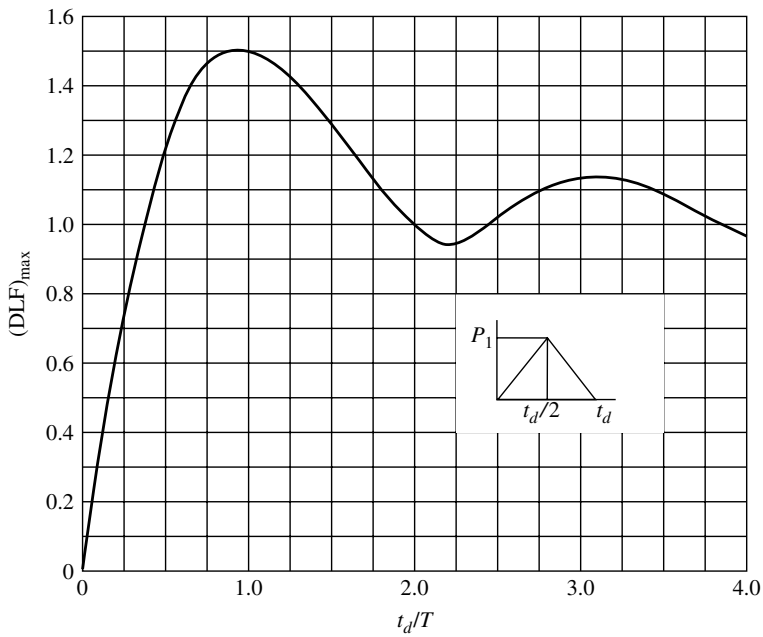
The integrals in these equations can be evaluated numerically either by the trapezoidal rule or by Simpson's rule or even using a simple summation technique.

The ratio of duration of time, t_d , to the natural period of the vibrating system, T , is a deciding factor for the maximum DLF. Figure 14.1.6 shows the maximum dynamic response of an undamped single-DOF system to various types of suddenly applied forces.

f. Equivalent One-DOF System. In a *simplified* approach to the dynamic analysis of plates, we may even use equivalent single-DOF systems for response calculation. This can be accomplished by introducing appropriate *transformation factors* that define the equivalent loads, masses and spring factors in terms of those of the actual system. In determining the dynamic parameters of the equivalent system (Fig. 14.1.7b), we equate the kinetic and strain energies and the works of the external



(a) Rectangular and triangular loading functions



(b) Loading function in isosceles triangular form

Figure 14.1.6 Maximum dynamic load factors for single-DOF systems.

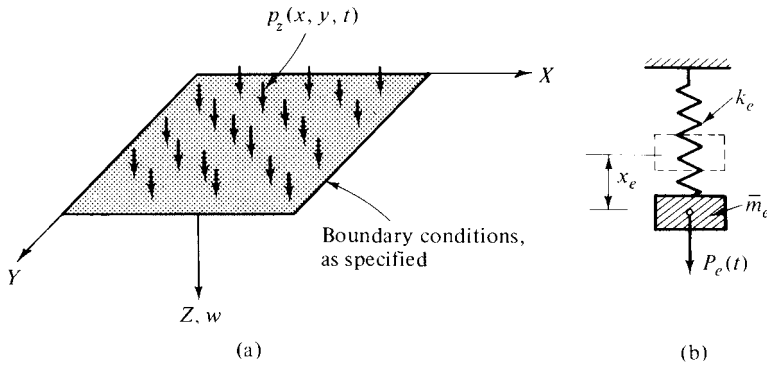


Figure 14.1.7 Actual and substitute vibrating systems.

forces in the real and substitute systems. In these work and energy expressions we use the static deflections

$$W(x, y)_{\text{static}} = W_{\text{max}} \phi(x, y) \quad (14.1.34)$$

due to the dynamic peak load applied statically and make the maximum deflections of the two systems equal:

$$x_{\text{max}} = W_{\text{max}}. \quad (14.1.35)$$

Furthermore, we assume that the load-time variations in both systems are the same.

From the work of the external forces we obtain

$$\frac{1}{2} P_e x_{\text{max}} = \frac{1}{2} W_{\text{max}} \iint_{(A)} \phi(x, y) p_z(x, y) dA; \quad (14.1.36)$$

hence

$$P_e = \iint_{(A)} \phi(x, y) p_z(x, y) dA. \quad (14.1.37)$$

Multiplying the total load P_T acting on the plate by the load factor c_L , the equivalent load is obtained. Therefore, the load factor can be determined from

$$c_L = \frac{P_e(t)}{P_T(t)} = \frac{\iint_{(A)} \phi(x, y) p_z(x, y) dA}{\iint_{(A)} p_z(x, y) dA}. \quad (14.1.38)$$

Similarly, by equating the kinetic energies

$$T_e = T_{\text{real}}, \quad (14.1.39)$$

or

$$\frac{1}{2}\bar{m}_e(\dot{x})^2 = \frac{1}{2} \iint_{(A)} \bar{m}(x, y)(\dot{w})^2 dA, \quad (14.1.40)$$

the equivalent mass \bar{m}_e is obtained:

$$\bar{m}_e = \iint_{(A)} \bar{m}(x, y)\phi^2(x, y) dA. \quad (14.1.41)$$

Hence, the mass factor c_m is

$$c_m = \frac{\bar{m}_e}{\bar{m}_T}, \quad (14.1.42)$$

where \bar{m}_T represents the total mass of the plate.

The definition of the equivalent spring factor c_k is

$$k_e = c_k K, \quad (14.1.43)$$

where K is the spring constant of the plate, obtained from

$$K = \frac{P_T}{W_{\max}} = \frac{\iint_{(A)} p_z(x, y) dA}{W_{\max}}. \quad (14.1.44)$$

Equations (14.1.35), (14.1.43) and (14.1.44) yield

$$c_k = \frac{k_e}{K} = \frac{P_e/x_{\max}}{P_T/W_{\max}} = \frac{P_e}{P_T} = c_L. \quad (14.1.45)$$

Consequently, we can state that the load and spring factors are the same.

Dynamic reactions of the plate can be approximated by determining the maximum dynamic displacements using a quasi-static analysis:

$$(\text{DLF})W_{\text{static}} = (\text{DLF})x_{\max}\phi(x, y). \quad (14.1.46)$$

By substitution of this expression into Eq. (1.3.3), approximate values for the reactions can be obtained.

Summary. By studying vibrations of one-DOF systems, the reader is introduced to the fundamentals of structural dynamics. Results of the response analysis of one-DOF systems can be used for the simplified dynamic analysis of plates. This is accomplished by employing an idealized vibrating system. The required parameters of such an equivalent system are obtained from work and energy principles. Fortunately, the analysis is quite simple and its accuracy is acceptable. The method can be extended to cover the failure behavior of plates [14.1.14].

ILLUSTRATIVE EXAMPLE

Determine the required transformation factors for a simply supported square plate to obtain an equivalent single-DOF system. Assume that the plate is subjected to a uniformly distributed dynamic load $p_z = p_0\theta(t)$.

Deflections of the plate under the peak load p_0 acting statically can be written in the simplified form

$$W(x, y)_{\text{static}} = W_{\max} \sin \frac{\pi x}{a} \sin \frac{\pi y}{a}, \quad (14.1.47)$$

where $W_{\max} = 0.00406 p_0 a^4 / D$, determined by Navier's method.

Equation (14.1.38) yields the load and spring factors:

$$c_L = c_k = \frac{\int_0^a \int_0^a \sin(\pi x/a) \sin(\pi y/a) dx dy}{a^2} = \frac{4}{\pi^2} \approx 0.406. \quad (14.1.48)$$

By considering more terms in the expression for deflections, we obtain an improved value, $c_L = 0.45$, for these factors.

Similarly, the mass factor is calculated from Eq. (14.1.42):

$$c_{\bar{m}} = \frac{\bar{m}_e}{\bar{m}_T} = \frac{\int_0^a \int_0^a \sin^2(\pi x/a) \sin^2(\pi y/a) dx dy}{a^2} \approx 0.25. \quad (14.1.49)$$

Again, using Eq. (2.2.11) instead of Eq. (14.1.47), we obtain $c_{\bar{m}} = 0.31$.

Hence, the dynamic parameters of the equivalent single-DOF systems are

$$\begin{aligned} P_e(t) &= c_L P_T(t) = 0.45 p_0 a^2 \theta(t), \\ \bar{m}_e &= c_{\bar{m}} \bar{m}_T = 0.31 \bar{m} a^2, \\ k_e &= c_k K = 0.45 \frac{D}{0.00406 a^2}. \end{aligned} \quad (14.1.50)$$

All further response analysis can be carried out on this equivalent single-DOF system, as previously described. Let us now check these results by computing the lowest natural frequency of the plate from the equivalent single-DOF system. Thus, Eq. (14.1.9) gives

$$\omega_1 = \sqrt{\frac{k_e}{\bar{m}_e}} \approx \frac{18.9}{a^2} \sqrt{\frac{D}{\bar{m}}}, \quad (14.1.51)$$

whereas the "exact" value, calculated from Eq. (14.3.8), is

$$\omega_{11} = \frac{19.73}{a^2} \sqrt{\frac{D}{\bar{m}}}. \quad (14.1.52)$$

This shows an acceptable accuracy for most design purposes.

References and Bibliography

- [14.1.1] ROGERS, G. L., *Dynamics of Framed Structures*, John Wiley & Sons, New York, 1959.
- [14.1.2] NORRIS, N. C. H., et al., *Structural Design for Dynamic Loads*, McGraw-Hill Book Co., New York, 1959.
- [14.1.3] BIGGS, T. M., *Introduction to Structural Dynamics*, McGraw-Hill Book Co., New York, 1964.
- [14.1.4] KLOTTER, K., *Technische Schwingungslehre*, 2nd ed., Vols. I and II, Springer-Verlag, Berlin, 1951 and 1960.
- [14.1.5] WARBURTON, G. B., *The Dynamical Behavior of Structures*, Pergamon Press, Elmsford, New York, 1964.
- [14.1.6] DEN HARTOG, J. P., *Mechanical Vibrations*, 4th ed., McGraw-Hill Book Co., New York, 1956.
- [14.1.7] JACOBSEN, L. S., and AYRE, R. S., *Engineering Vibrations*, McGraw-Hill Book Co., New York, 1958.
- [14.1.8] TIMOSHENKO, S., and YOUNG, D. H., *Vibration Problems in Engineering*, 3rd ed., Van Nostrand Reinhold Co., New York, 1955.
- [14.1.9] GRÜNING, G., "Baudynamik," in *Ingenieur Taschenbuch Bauwesen*, Vol. I, Pfalz-Verlag, Basel, 1964, pp. 736–859.
- [14.1.10] TSE, F. S., et al., *Mechanical Vibrations*, Allyn and Bacon, Boston, 1963.
- [14.1.11] VERNON, J. B., *Linear Vibration Theory: Generalized Properties and Numerical Methods*, John Wiley & Sons, New York, 1967.
- [14.1.12] BARTON, M. V. (Ed.), *Shock and Structural Response*, papers presented at colloquium on shock and structural response at the Annual Meeting of the ASME, Nov. 30, 1960, American Society of Mechanical Engineers, New York, 1960.
- [14.1.13] MORROW, CH. T., *Shock and Vibration Engineering*, John Wiley & Sons, New York, 1963.
- [14.1.14] U.S. ARMY, CORPS OF ENGINEERS, *Engineering Manual for Protective Construction*, Pt. 3, MIT-DA-49-129-Eng. 178, Washington, D. C.
- [14.1.15] THOMPSON, W. T., *Theory of Vibration with Applications*, Prentice-Hall, Englewood Cliffs, New Jersey, 1973.
- [14.1.16] BURTON, R., *Vibration and Impact*, Dover Publications, New York, 1968.
- [14.1.17] BREBBIA, C. A., et al., *Vibration of Engineering Structures*, Computational Mechanics, Southampton, 1976.
- [14.1.18] MAJOR, A., *Dynamics in Civil Engineering*, Vol. 1, Akadémiai Kiadó, Budapest, 1980.
- [14.1.19] MEIROVITCH, L., *Computational Methods in Structural Dynamics*, Sijthoff & Noordhoff, Rockville, Maryland, 1980.
- [14.1.20] CHOPRA, A. K., *Dynamics of Structures: A Primer*, Earthquake Engineering Research Institute, Berkeley, California, 1980.
- [14.1.21] GASCH, R., and KNOTHE, K., *Strukturmechanik*, Springer-Verlag, Berlin, 1989.
- [14.1.22] PAZ, M., *Structural Dynamics: Theory and Computation*, Van Nostrand Reinhold, New York, 1991.
- [14.1.23] CRAIG, R. R., *Structural Dynamics: An Introduction to Computer Methods*, John Wiley & Sons, New York, 1982.
- [14.1.24] IRVINE, M., *Structural Dynamics for Practicing Engineers*, E & F Spon, London, 1986.
- [14.1.25] SMITH, J. W., *Vibration of Structures*, E & F Spon, London, 1988.
- [14.1.26] MEIROVITCH, L., *Dynamics and Control of Structures*, Wiley Interscience, New York, 1990.
- [14.1.27] AL-KHAFAJI, A., *Dynamics for Engineers*, Springer, New York, 1997.
- [14.1.28] ARGYRIS, J., and MLEJNEK, H. P., *Dynamics of Structures*, North-Holland, Amsterdam, 1991.
- [14.1.29] HART, G. C., and WONG, K., *Structural Dynamics for Structural Engineers*, John Wiley & Sons, New York, 2000.
- [14.1.30] BRAUM, S. G., EWINS, D. J., and RAO, S. S., *Encyclopedia of Vibration*, Academic Press, New York, 2001.

14.2 Differential Equations of Lateral Motion

In the previous section, we briefly considered the vibration of the classic single-DOF system and that of systems consisting of discrete masses connected by springs. The mass was assumed to be a rigid body and the spring was assumed to have no mass; in other words the inertia and stiffness properties were separated. Now our task is to describe in mathematical form the governing equations of motion of plates that are continuous elastic systems. Since usually only the lateral vibration is of interest, we can reduce the number of degrees of freedom by neglecting the effects of rotational inertia; therefore, merely the inertia forces, associated with the lateral translation of the plate, will be considered. Although we can, for all practical purposes, describe the lateral vibrations of plates even by imposing such hypothetical restraint,[†] it should be remembered that certain physical phenomena observed in tests might not be explained by such a simplified theory. The case with damping is similar. Damping effects are caused either by internal friction or by the surrounding media. Although structural damping is theoretically present in all plate vibrations, it has usually little or no effect on (1) the natural frequencies and (2) the steady-state amplitudes; consequently, it can be safely ignored in the initial treatment of the problem.

In writing the governing differential equations of motion, basically two approaches are possible. We may either apply d'Alembert's dynamic equilibrium principle or use a work formulation based on the conservation of energy. In the following, the dynamic equilibrium of a plate element will be used exclusively for writing the governing differential equations of motions, since it appears to be simpler. The inertia force associated with the lateral translation of a plate element (Fig. 1.1.2) can be expressed by

$$p_z^* = -\bar{m} \frac{\partial^2 w}{\partial t^2} = -\bar{m} \ddot{w}, \quad (14.2.1)$$

where \bar{m} represents the mass[‡] of the plate per unit area.

In the dynamic analysis of plates, the lateral loads, and therefore the resulting deflections, are time dependent. A convenient way for expressing such time dependency is by means of the Fourier series, as discussed in Sec. 14.1. Thus, the forcing function, for example, can be written as

$$p_z(x, y, t) = p_z(x, y)(\theta t) = p_z(x, y) \sum_n P_n \sin p_n t. \quad (14.2.2)$$

Extending the differential equation of static equilibrium (1.2.30) by adding the inertia force [Eq. (14.1.1)], the differential equation of forced, undamped motion of plates is obtained:

$$D \nabla^2 \nabla^2 w(x, y, t) = p_z(x, y, t) - \bar{m} \frac{\partial^2 w(x, y, t)}{\partial t^2}, \quad (14.2.3)$$

where x and y are Cartesian coordinates in the plane of the middle surface, as described in Sec. 1.2.

[†] An additional restriction is the neglect of the effect of shearing forces.

[‡] $\bar{m} = \gamma h / g = \rho h$, where γ = specific weight of the material and g = gravitational acceleration.

For the case of a freely vibrating plate, the external force p_z is zero, and the differential equation of the undamped motion becomes

$$D\nabla^2\nabla^2w + \bar{m}\frac{\partial^2w}{\partial t^2} = 0. \quad (14.2.4)$$

Assuming a harmonic vibration, we may write

$$w(x, y, t) = W(x, y) \sin \omega t, \quad (14.2.5)$$

where $W(x, y)$ is the *shape function* describing the modes of the vibration and ω is the natural circular frequency of the plate. Substitution of Eq. (14.2.5) into Eq. (14.2.4) gives

$$\nabla^2\nabla^2W(x, y) - \frac{\bar{m}\omega^2}{D}W(x, y) = 0, \quad (14.2.6)$$

or

$$\nabla^2\nabla^2W - \lambda^*W = 0. \quad (14.2.7)$$

Similarly, the extension of the governing plate equation expressed in polar coordinates (1.4.11) yields

$$D\nabla_r^2\nabla_r^2w(r, \varphi, t) = p_z(r, \varphi, t) - \bar{m}\frac{\partial^2w(r, \varphi, t)}{\partial t^2}, \quad (14.2.8)$$

from which the differential equation of free undamped vibration is

$$D\nabla_r^2\nabla_r^2w(r, \varphi, t) + \bar{m}\frac{\partial^2w(r, \varphi, t)}{\partial t^2} = 0, \quad (14.2.9)$$

or

$$\nabla_r^2\nabla_r^2W(r, \varphi) - \lambda^*W(r, \varphi) = 0, \quad (14.2.10)$$

where

$$\lambda^* = \frac{\bar{m}\omega^2}{D}. \quad (14.2.11)$$

If the plate is subjected to simultaneous, static, in-plane loadings (3.3.7), the differential equation of lateral motion becomes

$$D\nabla^2\nabla^2w(x, y, t) = p_z(x, y, t) + n_x\frac{\partial^2w}{\partial x^2} + n_y\frac{\partial^2w}{\partial y^2} + 2n_{xy}\frac{\partial^2w}{\partial x\partial y} - \bar{m}\frac{\partial^2w(x, y, t)}{\partial t^2}. \quad (14.2.12)$$

In an analogous way, differential equations of motion can be derived for triangular, oblique and trapezoidal plates [14.2.1]. In all these equations, uniform plate thickness was assumed. As in the case of static problems, for most boundary conditions and shapes, “exact” solutions of dynamic plate problems are not available.

Summary. As in the case of the classic single-DOF system, the differential equations of motion for plates can be conveniently derived by applying the dynamic equilibrium principle. The effects of rotatory inertia, shear forces and damping have been neglected.

References and Bibliography

- [14.2.1] GONTKEWITSCH, W. S., “*Eigenschwingungen von Platten und Schalen*” (German translation of the original Russian text), VEB Fachbuchverlag, Leipzig, 1967.
- [14.2.2] MINDLIN, R. D., “Influence of Rotatory Inertia and Shear on Flexural Motion of Isotropic Elastic Plates,” *J. Appl. Mech., Trans. ASME*, 18, No. 1 (1951), 31–38.
- [14.2.3] NAGARAJA, J. V., “A Note on Vibration of Cantilever Trapezoidal Plates,” *J. Inst. Eng. (India)*, 37, Pt I., No. 3 (1956), 213–215.
- [14.2.4] LAKSHMANA-RAO, S., “An Exposition of the Classical Problem of Vibration of Membranes and Plates,” *J. Inst. Telecomm. Eng.*, 4, No. 2 (1958), 96.
- [14.2.5] KLEIN, B., “Fundamental Frequencies of Arbitrarily Shaped Simply-Supported Triangular Plates,” *J. Roy. Aeron. Soc.*, 60, No. 541 (1956), 63–64.
- [14.2.6] KLEIN, B., “Vibration of Simply-Supported Isosceles Trapezoidal Flat Plates,” *J. Acoust. Soc. Am.*, 27 (1955), 1059–1060.
- [14.2.7] EPSTEIN, P. S., “On the Theory of Elastic Vibrations of Plates and Shells,” *J. Math. Phys.*, 21 (1942), 198–209.
- [14.2.8] LEISSA, A. W., *Vibration of Plates*, NASA SP-160, Scientific and Technical Information Division of the National Aeronautics and Space Administration, Washington, D.C., 1969.

14.3 Free Flexural Vibration of Plates

a. Rectangular Plates. The undamped free flexural vibrations of rectangular plates are basically boundary value problems of the mathematical physics. Since the solution in the case of freely vibrating plates reduces to that of homogeneous differential equations (14.2.4), the methods described in Secs. 2.2 and 2.3 for the solution of the homogeneous biharmonic equations ($\nabla^4 w = 0$) can logically be extended. As mentioned earlier, in Eq. (14.2.4) the effects of the rotational inertia forces are neglected

We investigate the solution of Eq. (14.2.4) in the form

$$w(x, y, t) = W(x, y) \cdot \theta(t), \quad (14.3.1)$$

where

$$W(x, y) = X(x) \cdot Y(y) \quad (14.3.2)$$

represents the *shape function* of the vibration, while the time dependency of the displacements, $\theta(t)$, are assumed to be harmonic.[†]

$$\theta(t) = \sin \omega t \quad \text{or} \quad \theta(t) = \cos \omega t. \quad (14.3.3)$$

The solution $w(x, y, t)$ must satisfy the boundary conditions of the plate and the initial conditions of the motion at $t = 0$; these conditions are $(w)_{t=0}$ and $(\dot{w})_{t=0}$. Let us

[†] A more general form of the solution can be written as $w = (A \sin \omega t + B \cos \omega t)W(x, y)$. The arbitrary constants A and B are determined from specifying the initial conditions, as described in Sec. 14.1.

substitute Eq. (14.3.1) into Eq. (14.2.4), and use primes to denote differentiation with respect to the independent variables x and y , while dots indicate differentiation with respect to time; thus, the governing differential equation of free vibration becomes

$$X''''(x) \cdot Y(y) \cdot \theta(t) + 2X''(x) \cdot Y''(y) \cdot \theta(t) + X(x) \cdot Y''''(y) \cdot \theta(t) + \frac{\bar{m}}{D} X(x) \cdot Y(y) \cdot \bar{\theta}(t) = 0, \quad (14.3.4)$$

or

$$X''''Y + 2X''Y'' + XY'''' - \frac{\bar{m}\omega^2}{D}XY = 0. \quad (14.3.5)$$

For simply supported boundary conditions, the shape function can be given by double Fourier series,

$$W(x, y) = X(x) \cdot Y(y) = \sum_{m=1}^{\infty} \sum_{n=1}^{\infty} W_{mn} \sin \frac{m\pi x}{a} \sin \frac{n\pi y}{b} \quad \text{for } m, n = 1, 2, 3, \dots, \quad (14.3.6)$$

which corresponds to Navier's solution, discussed in Sec. 2.2. Substitution of Eq. (14.3.6) into Eq. (14.3.5) gives

$$\frac{m^4\pi^4}{a^4} + 2\frac{m^2\pi^2}{a^2} \cdot \frac{n^2\pi^2}{b^2} + \frac{n^4\pi^4}{b^4} - \frac{\bar{m}\omega^2}{D} = 0; \quad (14.3.7)$$

hence

$$\omega_{mn} = \pi^2 \left[\frac{m^2}{a^2} + \frac{n^2}{b^2} \right] \sqrt{\frac{D}{\bar{m}}}, \quad (14.3.8)$$

where $m, n = 1, 2, 3, \dots$. The fundamental mode of flexural vibration is a single sine wave in the X and Y directions, respectively, and the pertinent natural frequency is associated with $m = 1$ and $n = 1$ values. Taking either m or n equal to 2 and the other equal to 1, the next two higher modes are obtained. Although these two modes have the same frequencies, the associated mode shapes are different; in such a case the two vibration modes can be superimposed in any ratio of their maximum deflections, provided that the a/b ratio is rational. For a simply supported square plate, for instance, such a combination is

$$W(x, y) = C_1 \sin \frac{2\pi x}{a} \sin \frac{\pi y}{b} + C_2 \sin \frac{\pi x}{a} \sin \frac{2\pi y}{b}, \quad (14.3.9)$$

where C_1 and C_2 are arbitrary constants. In Fig. 14.3.1 such combined modes are shown.

Lévy's type of solution can be applied to plates that are simply supported at two opposite edges. Assuming that the simple supports are at $x = 0$ and $x = a$, the shape

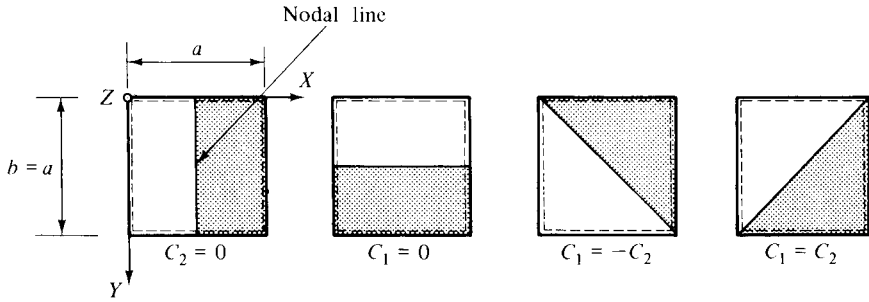


Figure 14.3.1 Combination of modes.

function takes the form of Eq. (2.3.9):

$$W(x, y) = \sum_{m=1}^{\infty} Y(y) \sin \frac{m\pi x}{a}. \quad (14.3.10)$$

Substituting this expression into Eq. (14.3.5) and using a specific value of m yield

$$\frac{m^4 \pi^4}{a^4} Y - 2 \frac{m^2 \pi^2}{a^2} Y'' + Y^{IV} - \frac{\bar{m} \omega^2}{D} Y = 0. \quad (14.3.11)$$

The general solution for Y is found to be

$$Y(y) = C_1 \cosh \alpha y + C_2 \sinh \alpha y + C_3 \cos \beta y + C_4 \sin \beta y, \quad (14.3.12)$$

where

$$\alpha = \sqrt{\omega \sqrt{\frac{\bar{m}}{D}} + \frac{m^2 \pi^2}{a^2}} \quad \text{and} \quad \beta = \sqrt{\omega \sqrt{\frac{\bar{m}}{D}} - \frac{m^2 \pi^2}{a^2}}. \quad (14.3.13)$$

The constants (C_1, C_2, C_3 and C_4) are determined from the boundary conditions at $y = 0$ and $y = b$, as described in Sec. 2.3. The boundary conditions yield the frequency equation from which ω is determined. The boundary conditions for fixed edges, for instance, are

$$\begin{aligned} (Y)_{y=0} &= C_1 + C_3 = 0, \\ \left(\frac{\partial Y}{\partial y} \right)_{y=0} &= \alpha C_2 + \beta C_4 = 0, \\ (Y)_{y=b} &= C_1 \cosh \alpha b + C_2 \sinh \alpha b + C_3 \cos \beta b + C_4 \sin \beta b = 0, \\ \left(\frac{\partial Y}{\partial y} \right)_{y=b} &= \alpha C_1 \sinh \alpha b + \alpha C_2 \cosh \alpha b - \beta C_3 \sin \beta b + \beta C_4 \cos \beta b = 0. \end{aligned} \quad (14.3.14)$$

The nodal patterns corresponding to free vibrations of a square plate with fixed boundaries are shown in Fig. 14.3.2.

Like its static counterpart treated in Sec. 2.3, the free-vibration analysis of rectangular plates by Lévy's method creates some mathematical difficulties to the analyst in

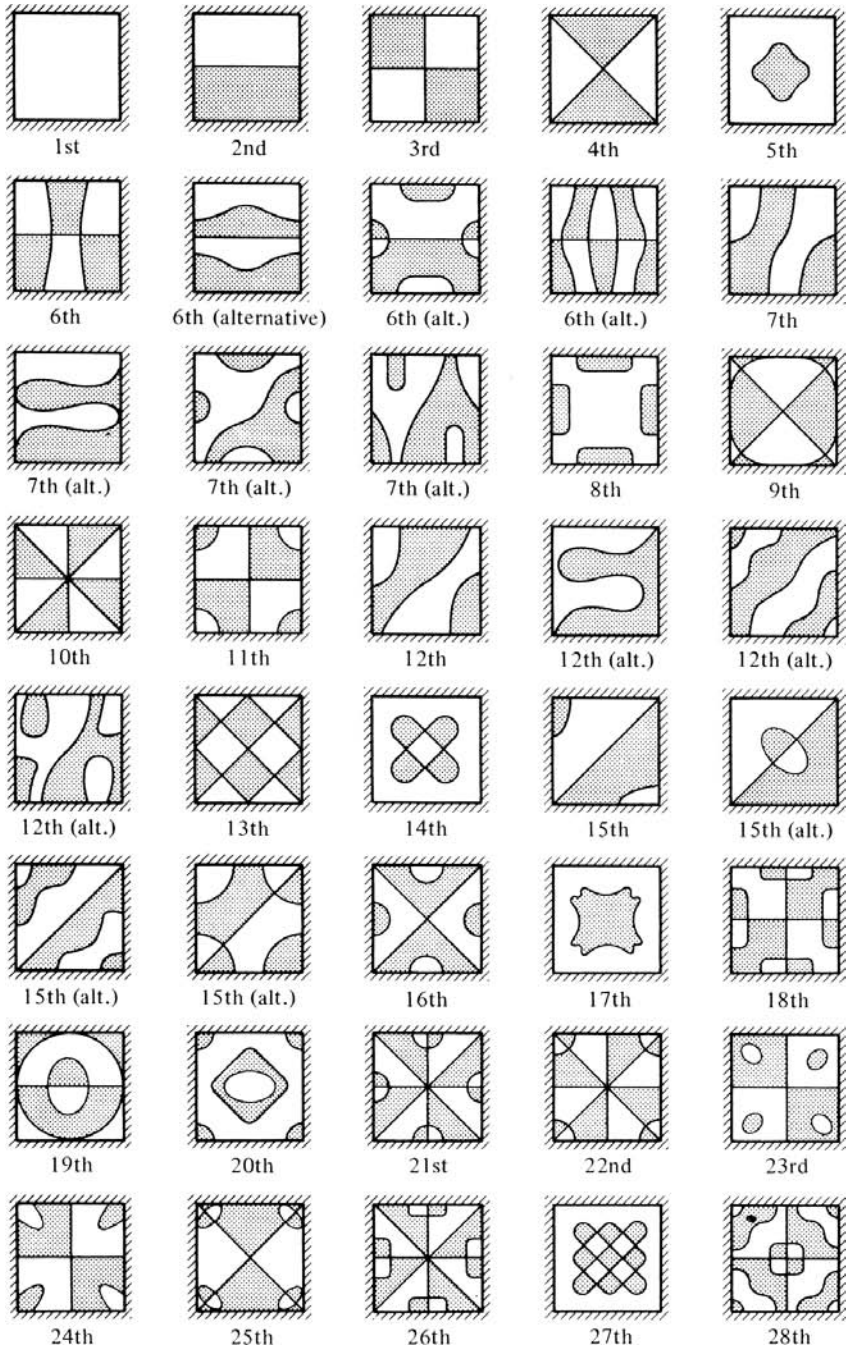


Figure 14.3.2 Some nodal patterns of clamped square plates.

selecting suitable shape functions that simultaneously satisfy the differential equation of motion and the prescribed boundary conditions. For this reason, the location of the coordinate system can be important. The reader will note that in the foregoing discussion we located the origin of our coordinate system, as usual, at the upper left corner of the plate to determine the fundamental modes of plate vibrations. However, locating the Y axis along the center of the plate, as shown in Fig. 2.3.1, may offer certain advantages in dealing with higher mode shapes. That is, by using such a coordinate system, the symmetric and antisymmetric modes of vibration can be uniformly treated. Gorman [14.3.12] presents a comprehensive study of free-vibration analysis of rectangular plates by Lévy's method.

For other than the above-discussed Navier-and Lévy-type boundary conditions, the exact solution of free vibration creates considerable mathematical difficulties.

b. Circular Plates. The governing differential equation of the undamped, free vibration of circular plates is Eq. (14.2.9). The solution to this differential equation is assumed in the form

$$w(r, \varphi, t) = R(r) \cdot \Phi(\varphi) \cdot \theta(t) = R(r) \cdot \Phi(\varphi) \cdot \sin \omega t, \quad (14.3.15)$$

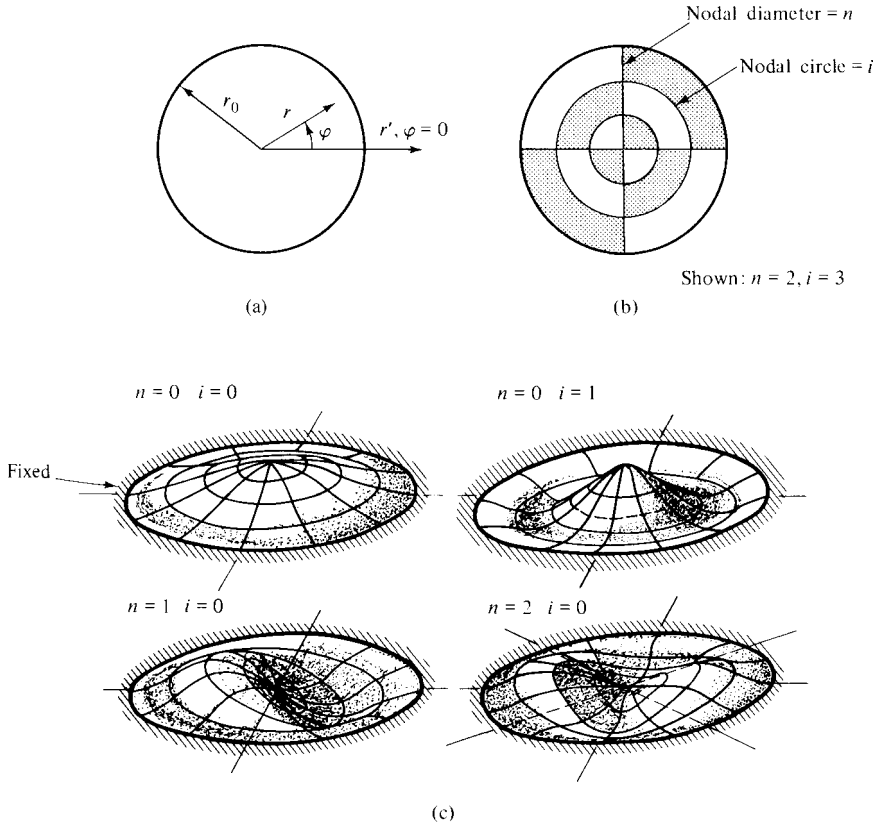


Figure 14.3.3 Typical nodal patterns for circular plate.

where $\Phi(\varphi)$ can be represented by $\cos m\varphi$, for instance, where m denotes the number of nodal diameters. Functions $R(r)$ must satisfy the governing differential equation (14.2.9) and the boundary conditions.

In the case of the lowest mode, the shape function is symmetric; thus the method described in Sec. 2.8 can be applied. *Modified or hyperbolic Bessel functions* [14.3.1, 14.3.2] can also be used to obtain higher modes and pertinent frequencies. The nodal lines for plates are either concentric circles or diameters, as shown in Fig. 14.3.3. In the general case, however, the classical approach to the free-vibration problems of plates leads to such mathematical complexities that solutions cannot be obtained.

Summary. Provided that the boundary conditions permit, we can use either Navier's or Lévy's method for the determination of circular frequencies and modal shapes of freely vibrating plates. For the other, more general, cases, the classical methods for determination of plate frequencies and associated vibration modes involve considerable mathematical difficulties; thus, from the point of view of practical application, these methods should be abandoned in favor of numerical or approximate approaches, treated in Chapters 14 and 15, respectively.

Finally, the reader's attention should be called to the monograph *Vibration of Plates* by Leissa [28, 14.2.8], which contains a wealth of information in readily usable form.

ILLUSTRATIVE EXAMPLE

Determine the natural frequencies and associated modal shapes of a simply supported rectangular, orthotropic plate of size $a \times b$. Assume that the principal directions of orthotropy coincide with X and Y coordinate axes, respectively.

The differential equation of motion is obtained by adding the inertia term of the lateral translation to Eq. (10.1.6) and setting $p_z = 0$. Thus, we can write

$$D_x \frac{\partial^4 w}{\partial x^4} + 2B \frac{\partial^4 w}{\partial x^2 \partial y^2} + D_y \frac{\partial^4 w}{\partial y^4} = -\bar{m} \frac{\partial^2 w}{\partial t^2}. \quad (14.3.16)$$

For a plate that is simply supported at all four edges, the differential equation (14.3.16) and the boundary conditions are satisfied by taking the solution in the form

$$w(x, y, t) = W(x, y)\theta(t) = W_{mn} \sin \frac{m\pi x}{a} \sin \frac{n\pi y}{b} \sin \omega t \quad (14.3.17)$$

for $m, n = 1, 2, 3, \dots$

Substituting this expression into Eq. (14.3.16), we obtain

$$D_x \left(\frac{m\pi}{a} \right)^4 + 2B \left(\frac{mn\pi^2}{ab} \right)^2 + D_y \left(\frac{n\pi}{b} \right)^4 - \omega^2 \bar{m} = 0; \quad (14.3.18)$$

hence

$$\omega_{mn} = \frac{\pi^2}{b^2} \sqrt{\frac{1}{\bar{m}}} \sqrt{D_x \left(\frac{mb}{a} \right)^4 + 2Bn^2 \left(\frac{mb}{a} \right)^2 + D_y n^4}, \quad (14.3.19)$$

and the corresponding modal shapes are

$$w(x, y) = W_{mn} \sin \frac{m\pi x}{a} \sin \frac{n\pi y}{b} \sin \omega_{mn} t. \quad (14.3.20)$$

The lowest circular frequency is obtained by taking $m = n = 1$:

$$\omega_{11} = \frac{\pi^2}{a^2} \sqrt{\frac{1}{\bar{m}}} \sqrt{D_x \left(\frac{b}{a}\right)^4 + 2B \left(\frac{b}{a}\right)^2 + D_y}. \quad (14.3.21)$$

References and Bibliography

- [14.3.1] MEIROVITCH, L., *Analytical Methods in Vibrations*, Macmillan Company, New York, 1967.
- [14.3.2] AIREY, J., "The Vibration of Circular Plates and Their Relation to Bessel Functions," *Proc. Phys. Soc. London*, 23 (1910–1911), 27.
- [14.3.3] DUFFIN, K. J., "Nodal Lines of a Vibrating Plate," *J. Math. Phys.*, 31, No. 4 (1953), 294–299.
- [14.3.4] WARBURTON, G. B., "The Vibration of Rectangular Plates," *Proc. Inst. Mech. Eng. London*, 168 (1954), 371–381.
- [14.3.5] SÖCHTING, F., *Berechnung mechanischer Schwingungen*, Springer-Verlag, Vienna, 1951.
- [14.3.6] EPSTEIN, P. S., "On the Theory of Elastic Vibrations of Plates and Shells," *J. Math. Phys.*, 21 (1942), 198–207.
- [14.3.7] IGUCHI, S., "Biegeschwingungen der vierseitig eingespannten rechteckigen Platte," *Ing.-Arch.*, 8, No. 1 (1937), 11–25.
- [14.3.8] HABATA, U., "On the Lateral Vibration of a Rectangular Plate Clamped at Four Edges," *Trans. Japan Soc. Mech. Eng.*, 23, No. 131 (1957).
- [14.3.9] IGUCHI, S., "Die Eigenschwingungen und Klangfiguren der vierseitig freien rechteckigen Platte," *Ing.-Arch.*, 21 (1954), 303–322.
- [14.3.10] SHUL'MAN S. G., *Sobstvennye kolebaniia priamougol'nykh platinok v zhidkosti (Free Vibration of Rectangular Plates in Liquid)*, Energiia, Leningrad, 1968.
- [14.3.11] NOWACKI, W., *Dynamics of Elastic Systems*, John Wiley & Sons, New York, 1963.
- [14.3.12] GORMAN, D. J., "A Comprehensive Free Vibration Analysis of Rectangular Plates with Two Opposite Edges Simply Supported," Paper No. 76-WA/DE, American Society of Mechanical Engineers, New York, 1976.
- [14.3.13] GORMAN, D. J., "Solution of Lévy Type for the Free Vibration Analysis of Diagonally Supported Rectangular Plates," *J. Sound Vibr.*, 66 (1979), 239–246.

14.4 Free Transverse Vibration of Membranes

a. Rectangular Membranes. The differential equation of motion is obtained from Eq. (1.7.2) by adding the inertia force pertinent to lateral translation of the membrane. Thus, we can write

$$\frac{\partial^2 w}{\partial x^2} + \frac{\partial^2 w}{\partial y^2} = \frac{\bar{m}}{\sigma h} \frac{\partial^2 w}{\partial t^2} - \frac{p_z}{\sigma h}, \quad (14.4.1)$$

where \bar{m} is the mass of the membrane per unit area and σh is the uniform tensile force, the change of which is assumed to be negligible during the vibration. Furthermore, as in Sec. 1.7, we assume that the lateral deflections are small.

When the external excitation p_z is zero, Eq. (14.4.1) becomes

$$\boxed{\nabla^2 w - \frac{\bar{m}}{\sigma h} \frac{\partial^2 w}{\partial t^2} = 0}, \quad (14.4.2)$$

which represents the differential equation of the free vibration of rectangular membranes.

We seek the solution of Eq. (14.4.2) in the form

$$w = w(x, y, t) = W(x, y) \cdot \theta(t), \quad (14.4.3)$$

where $W(x, y)$ is the shape function and $\theta(t)$ represents the time dependency of the free vibration. Assuming, again, a harmonic type of oscillation,

$$\theta(t) = \sin \omega t, \quad (14.4.4)$$

and representing the shape function by a double sine series,[†]

$$W(x, y) = \sum_{m=1}^{\infty} \sum_{n=1}^{\infty} W_{mn} \sin \frac{m\pi x}{a} \sin \frac{n\pi y}{b}, \quad (14.4.5)$$

the substitution of Eqs. (14.4.3) and (14.4.5) into (14.4.2) yields (for specific m and n values)

$$\frac{\pi^2 m^2}{a^2} + \frac{\pi^2 n^2}{b^2} = \omega^2 \frac{\bar{m}}{\sigma h}; \quad (14.4.6)$$

hence

$$\omega_{mn} = \pi \sqrt{\frac{\sigma h}{\bar{m}} \left(\frac{m^2}{a^2} + \frac{n^2}{b^2} \right)}. \quad (14.4.7)$$

Using $m, n = 1, 2, 3, \dots$, which represents the number of half-waves in the X and Y directions, respectively, the circular frequencies pertinent to various modes of free vibration can easily be calculated.

If the a/b ratio is rational, there is more than one combination of m, n values for which the circular frequency is the same. In the case of square membranes, for instance, there is more than one mode of vibration (Fig. 14.4.1) that yields the same circular frequency. The modes pertinent to the same frequencies can be superimposed in any ratio of their maximum deflections and are called *combined* or *resultant* modes of free vibration.

In the case of forced vibration, a particular solution of the differential equation of motion (14.4.1) is obtained by extending Navier's method.[‡] That is, we express the forcing function $p_z(x, y, t)$ and the deflected membrane surface $w(x, y, t)$ in a trigonometric series of the same type. Since this approach is fundamentally the same as the one discussed in Sec. 1.5, further treatment of this problem is unnecessary.

[†] See Sec. 1.7 for a discussion of the boundary conditions.

[‡] See Sec. 2.2.

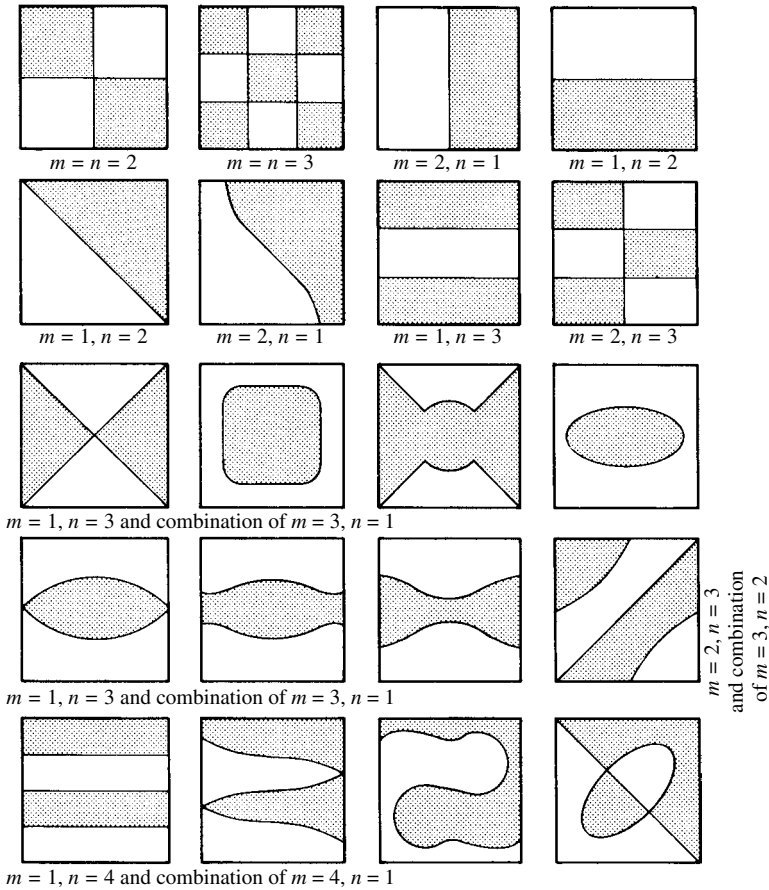


Figure 14.4.1 Nodal patterns of square membranes pertinent to higher modes.

b. Circular Membranes. By augmenting Eq. (1.7.4) with the inertia term, the governing differential equation of the forced vibration of circular membranes can be written as

$$\frac{\partial^2 w}{\partial r^2} + \frac{1}{r^2} \frac{\partial^2 w}{\partial \varphi^2} + \frac{1}{r} \frac{\partial w}{\partial r} = \frac{\bar{m}}{\sigma h} \frac{\partial^2 w}{\partial t^2} - \frac{p_z}{\sigma h}. \quad (14.4.8)$$

If $p_z = 0$, the differential equation of the free vibration of membranes, expressed in polar coordinates, is obtained:

$$\frac{\partial^2 w}{\partial r^2} + \frac{1}{r^2} \frac{\partial^2 w}{\partial \varphi^2} + \frac{1}{r} \frac{\partial w}{\partial r} = \frac{\bar{m}}{\sigma h} \frac{\partial^2 w}{\partial t^2}. \quad (14.4.9)$$

Again, we seek the solution of Eq. (14.4.9) in the form of a product of three functions:

$$w = w(r, \varphi, t) = R(r) \cdot \phi(\varphi) \cdot \theta(t). \quad (14.4.10)$$

Assuming a harmonic vibration,

$$w = R(r) \cdot \phi(\varphi) \sin \omega t, \quad (14.4.11)$$

the substitution of Eq. (14.4.11) into (14.4.9) gives

$$\frac{R''(r)}{R(r)} + \frac{1}{r^2} \frac{\phi''(\varphi)}{\phi(\varphi)} + \frac{1}{r} \frac{R'(r)}{R(r)} + \omega^2 \frac{\bar{m}}{\sigma h} = 0, \quad (14.4.12)$$

where primes indicate differentiation with respect to the pertinent arguments.

By introducing

$$\lambda^2 = \omega^2 \frac{\bar{m}}{\sigma h}, \quad (14.4.13)$$

we reduce Eq. (14.4.12) to

$$\left[R''(r) + \frac{1}{r} R'(r) \right] \phi(\varphi) + \frac{R(r)}{r^2} \phi''(\varphi) + \lambda^2 R(r) \phi(\varphi) = 0. \quad (14.4.14)$$

This equation can be separated into two ordinary differential equations:

$$\frac{d^2 \phi(\varphi)}{d\varphi^2} + n^2 \phi(\varphi) = 0 \quad (14.4.15)$$

and

$$\frac{d^2 R(r)}{dr^2} + \frac{1}{r} \frac{dR(r)}{dr} + \left(\lambda^2 - \frac{n^2}{r^2} \right) R(r) = 0, \quad (14.4.16)$$

where the constant n^2 must be so selected that we obtain a harmonic equation in φ . Consequently, the solution of Eq. (14.4.15) is a trigonometric function:

$$\phi_n(\varphi) = C_{1n} \sin n\varphi + C_{2n} \cos n\varphi \quad \text{for } n = 0, 1, 2, 3. \quad (14.4.17)$$

Since Eq. (14.4.16) is a Bessel-type differential equation [14.4.2], its solution for a fixed boundary condition becomes

$$R(r) = J_n(\lambda, r_0) = 0, \quad (14.4.18)$$

where $J_n(\lambda, r_0)$ is a Bessel function of the first kind and of n th order.

The roots of Eq. (14.4.18) take the form [14.3.1]

$$\omega_{ni} = \frac{\alpha_{ni}}{r_0} \sqrt{\frac{\sigma h}{\bar{m}}}. \quad (14.4.19)$$

The constants α_{ni} for various n and i values are given in Table 14.4.1. The physical meaning of n and i are the following: n is the number of nodal diameters and i

Table 14.4.1 Parameter α_{ni}

i	$n = 0$	$n = 1$	$n = 2$	$n = 3$	$n = 4$	$n = 5$
1	2.404	3.832	5.135	6.379	7.586	8.708
2	5.520	7.016	8.417	9.760	11.064	12.339
3	8.654	10.173	11.620	13.017	14.373	15.700
4	11.792	13.323	14.796	16.224	17.616	18.982
5	14.931	16.470	17.960	19.410	20.827	22.220
6	18.071	19.616	21.117	22.583	24.018	25.431
7	21.212	22.760	24.270	25.749	27.200	28.628
8	24.353	25.903	27.421	28.909	30.371	31.813
9	27.494	29.047	30.571	32.050	33.512	34.983

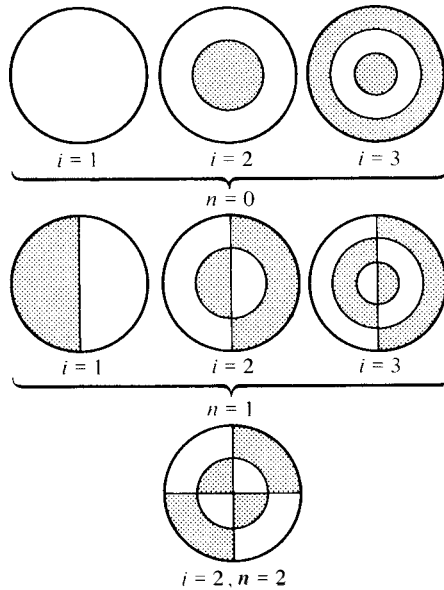


Figure 14.4.2 Nodal patterns of clamped circular membrane.

represents the number of nodal circles. Several modes of free vibration of a clamped circular membrane are shown in Fig. 14.4.2.

Summary. For other boundary conditions than those discussed above, application of classical methods becomes quite tedious; consequently, the use of approximate or numerical methods is recommended.

References and Bibliography

- [14.4.1] LAMÉ, G., *Leçons sur la théorie mathématique de l'élasticité des corps solides*, Bachelier, Paris, 1852.
- [14.4.2] AUERBACH, F., and HART, W., *Handbuch der physikalischen und technischen Mechanik, Vol. 3: Statik u. Dynamik elast. Körper*, J. A. Barth, Leipzig, 1927.
- [14.4.3] PATTANTYUS, A. G., *Gépészeti Lengésstan (Mechanical Vibrations)*, Akadémiai Könyvkiadó, Budapest, 1952.

- [14.4.4] COURANT, R., and HILBERT, D., *Methods of Mathematical Physics*, Vol. 1, John Wiley & Sons (Interscience Division), New York, 1961.
- [14.4.5] BERGMANN, L., "Experiments with Vibrating Soap Membranes," *J. Acoust. Soc. Am.*, 28, No. 6 (1956), 1043–1047.
- [14.4.6] BISHOP, R. E. D., and JOHNSON, D., *Vibration Analysis Tables*, Cambridge University Press, New York, 1956.
- [14.4.7] COHEN, H., and HANDLEMAN, G., "On the Vibration of Circular Membranes with Added Mass," *J. Acoust. Soc. Am.*, 27, No. 2 (1957), 229–233.
- [14.4.8] DUNWOODY, N. T., "The Free Vibration of Membranes with Elliptical Boundaries," *Quart. J. Mech. Appl. Math.*, 13, No. 3 (1960), 359–368.
- [14.4.9] KARAS, K., "Die Schirmschwingungen der Kreismembrane unter allgemeinen Bedingungen," *Österr. Ing.-Arch.*, 10, Nos. 2–3 (1956), 200–220.
- [14.4.10] MATHIEU, E., "Mémoire sur le mouvement vibratoire d'une membrane de forme elliptique," *J. Math. Pures Appliquées*, 13 (1868), 137–203.
- [14.4.11] PAYNE, L., and WEINBERGER, H., "Lower Bounds for Vibrational Frequency of Elastically Supported Membranes and Plates," *J. Soc. Ind. Appl. Math.*, 5 (1957), 171–182.
- [14.4.12] POISSON, S. D., "Mémoire sur l'équilibre et le mouvement des corps élastiques," *Mém. de L'Acad. Sci.*, 8 (1829), 357–570.
- [14.4.13] REINSTEIN, E., "Untersuchungen über die Transversalschwingungen der gleichförmig gespannten elliptisch oder kreisförmig begrenzten Vollmembranen und Kreisringmembranen mit nach speziellen Gesetzen variierter ungleichförmiger Spannung," Dissertation, University of Göttingen, J. A. Brath, Leipzig, 1911.

14.5 Energy Methods for Determination of Natural Frequencies

a. Kinetic Energy of Plates. The energy methods for solution of boundary value problems of plates subjected to static loading have already been studied in Secs. 4.2 and 4.3. Now the use of these methods will be extended to find approximate solutions to dynamic plate problems when exact solutions are unavailable or too cumbersome for practical application.

Considering a vibrating plate, the total potential energy, given in Eq. (4.2.11) for the static case, must be augmented by an additional term, representing the kinetic energy (14.1.3), which can be written as

$$T = \frac{1}{2} \iint_{(A)} \bar{m}(x, y) \left[\frac{\partial w(x, y, t)}{\partial t} \right]^2 dx dy, \quad (14.5.1)$$

or, in terms of polar coordinates,

$$T = \frac{1}{2} \iint_{(A)} \bar{m}(r, \phi) \left[\frac{\partial w(r, \phi, t)}{\partial t} \right]^2 r dr d\phi, \quad (14.5.2)$$

where \bar{m} is the mass of the plate per unit area and the integration extends over the entire surface of the plate. Thus, the total energy of a vibrating plate becomes

$$\Pi = U + V + T, \quad (14.5.3)$$

where U represents the strain energy of the plate and V is the potential energy of the external forces. Both types of energy are described in detail in Sec. 4.1.

b. Rayleigh's Method. An approximate method for determining the lowest natural frequency of a vibrating system was developed by Lord Rayleigh [14.5.1]. This method involves determination of the kinetic and potential energies of the structural system, using assumed shape functions, which satisfy the geometrical boundary conditions and approximate the actual modes of vibrations. If the vibrating system is conservative (no energy is added or lost), the maximum kinetic energy must equal the maximum potential energy. Thus, in the case of free flexural vibration, we can write

$$U_{b,\max} = T_{\max}. \quad (14.5.4)$$

Assuming that the plate is undergoing harmonic oscillations, the lateral deflection can be written as

$$w(x, y, t) = W(x, y) \sin \omega t, \quad (14.5.5)$$

where $W(x, y)$ is the shape function and ω represents the unknown natural circular frequency of the plate pertinent to the assumed shape function. Substituting Eq (14.5.5) into the expression of the kinetic energy of the oscillating plate (14.5.1), we obtain

$$T = \frac{\omega^2}{2} \cos^2 \omega t \iint_{(A)} \bar{m}(x, y) W^2(x, y) dx dy. \quad (14.5.6)$$

The kinetic energy is at a maximum when the velocity of the plate is maximum, which occurs when $w(x, y, t)$ is zero. This will be true if $\sin \omega t$ is zero; thus

$$\omega t = n\pi \quad \text{for } n = 0, 1, 2, 3, \dots \quad (14.5.7)$$

Substituting these values into (14.5.6), we find the expression for the maximum kinetic energy:

$$T_{\max} = \frac{\omega^2}{2} \iint_{(A)} \bar{m}(x, y) W^2(x, y) dx dy = \frac{\omega^2}{2} \mathcal{J}. \quad (14.5.8)$$

The bending part of the strain energy [Eq. (4.1.8a)] is at a maximum when the deflection of the plate is maximum. From Eq. (14.5.5), it is obvious that this occurs when $\sin \omega t$ equals unity. This is true when

$$\omega t = (n + \frac{1}{2})\pi \quad \text{for } n = 0, 1, 2, 3, \dots \quad (14.5.9)$$

Using these values of ωt , the maximum strain energy of the plate is identical to Eq. (4.2.5).

In applying Rayleigh's method, we first select an appropriate deflection shape, $W(x, y)$; then we equate the maximum kinetic and strain energies. From this,

$$\omega^2 = \frac{2U_{b,\max}}{\iint_{(A)} \bar{m}(x, y) W^2(x, y) dx dy}, \quad (14.5.10)$$

where

$$U_{b,\max} = U_b = \frac{1}{2} \iint_{(A)} D \left\{ \left(\frac{\partial^2 w}{\partial x^2} + \frac{\partial^2 w}{\partial y^2} \right)^2 + 2(1 - \nu) \left[\left(\frac{\partial^2 W}{\partial x \partial y} \right)^2 - \frac{\partial^2 W}{\partial x^2} \frac{\partial^2 W}{\partial y^2} \right] \right\} dx dy. \quad (14.5.11)$$

For plates with fixed boundary conditions, Eq. (14.5.11) can be simplified, as discussed in Sec. 4.2. If polar coordinates are used, the expression of strain energy given in polar coordinates (4.2.9) should be combined with Eq. (14.5.2) to obtain an approximate value for the lowest natural frequency of the vibrating circular plate.

The approximate natural frequencies calculated from Rayleigh's method are always higher than the "exact values," since we have arbitrarily *stiffened* the plate by assuming a modal shape, thus increasing its frequencies. This method can also be used to obtain approximate values pertinent to the second and third modes of free vibration. A modification of Rayleigh's method is described in Sec. 14.6.

c. Ritz Method. Ritz [14.5.2] has extended Rayleigh's method by including more than one parameter in the expression of shape functions. In this way, not only can a more accurate value for the lowest natural frequency be obtained, but also additional information concerning the higher frequencies and pertinent mode shapes is gained.

Assuming the shape function $W(x, y)$ in the form of a series, we can write

$$W(x, y) = C_1 \varphi_1(x, y) + C_2 \varphi_2(x, y) + \cdots + C_n \varphi_n(x, y), \quad (14.5.12)$$

where $\varphi_1(x, y), \varphi_2(x, y), \dots, \varphi_n(x, y)$ are appropriate displacement functions, which individually satisfy at least the geometrical boundary conditions. Again, satisfaction of the differential equation of motion (14.2.4) is not required. The unknown coefficients (C_1, C_2, \dots, C_n) in Eq. (14.5.12) are obtained from the minimum total energy principle, discussed in Sec. 4.2. Thus, based on Eq. (4.2.2), we may write

$$\frac{\partial \Pi}{\partial C_i} = 0 \quad \text{for } i = 1, 2, 3, \dots, n, \quad (14.5.13)$$

where

$$\Pi = U_{b,\max} - T_{\max}. \quad (14.5.14)$$

From Eqs. (14.5.8) and (14.5.13) we obtain the following set of equations:

$$\begin{aligned}\frac{\partial U_b}{\partial C_1} - \frac{1}{2}\omega^2 \frac{\partial \mathfrak{J}}{\partial C_1} &= 0, \\ \frac{\partial U_b}{\partial C_2} - \frac{1}{2}\omega^2 \frac{\partial \mathfrak{J}}{\partial C_2} &= 0, \\ &\vdots \\ \frac{\partial U_b}{\partial C_n} - \frac{1}{2}\omega^2 \frac{\partial \mathfrak{J}}{\partial C_n} &= 0.\end{aligned}\tag{14.5.15}$$

Next, we substitute Eq. (14.5.12) into Eq. (14.5.15) and evaluate the definite integrals indicated in Eqs. (14.5.8) and (14.5.11). This procedure yields a set of homogeneous linear equations in $C_{\textcircled{1}}$. In this way, the problem is reduced to an *eigenvalue* and *eigenvector* problem.

If the relationship between $W(x, y)$ and C_1, C_2, \dots, C_n parameters is nonlinear,

$$W(x, y) = \varphi(C_1, C_2, C_3, \dots, C_n, x, y),\tag{14.5.16}$$

the simultaneous equations obtained from (14.5.15) are also nonlinear. By plotting, however, the family of curves pertinent to

$$(\omega^*)^2(C_1, C_2, C_3, \dots, C_n),\tag{14.5.17}$$

where

$$(\omega^*)^2 = \frac{2U_b}{\mathfrak{J}},\tag{14.5.18}$$

an extremum of the function (14.5.17) can be determined graphically.

d. Galerkin-Vlasov Method. We can also extend the Galerkin-Vlasov method to solution of free-vibration problems of plates by applying the variational principle to Eq. (14.2.6), which expresses the dynamic equilibrium of the plate. Thus, assuming again a shape function in the form of a series (14.5.12), which satisfies, term by term, all boundary conditions,[†] we obtain

$$\begin{aligned}\iint_{(A)} [D\nabla^2\nabla^2 W(x, y) - \omega^2 \overline{m}(x, y) W(x, y)] \varphi_1(x, y) dx dy &= 0, \\ \iint_{(A)} [D\nabla^2\nabla^2 W(x, y) - \omega^2 \overline{m}(x, y) W(x, y)] \varphi_2(x, y) dx dy &= 0, \\ &\vdots \\ \iint_{(A)} [D\nabla^2\nabla^2 W(x, y) - \omega^2 \overline{m}(x, y) W(x, y)] \varphi_n(x, y) dx dy &= 0.\end{aligned}\tag{14.5.19}$$

[†] An additional requirement in the case of plate problems is that the fourth derivative of (14.5.12) does not vanish.

After substitution of a suitable series expression for $W(x, y)$, we evaluate the definite integrals over the whole surface of the plate. This procedure leads, again, to a set of homogeneous algebraic equations and to an *eigenvalue-eigenvector* problem, described in the subsequent sections. In selecting appropriate shape functions, the same techniques recommended in Secs. 4.2 and 4.3 for the static analysis of plates can be applied. Concerning shape functions obtained from static deflection analysis, the reader is referred to Sec. 14.6.

Since the use of the eigenfunctions of vibrating beams,[†] as introduced by Vlasov and extended by Oniashvili [14.5.3], offers special advantages in the vibration analysis of plates, this method will be discussed now in more detail.

Let us represent the shape function $W(x, y)$ in Eq. (14.5.5) as an infinite series,

$$W(x, y) = \sum_n \sum_m W_{mn} \phi_{mn}(x, y), \quad (14.5.20)$$

where $W_{mn} = 1$ represents the normalized amplitudes of the free-vibration modes and $\phi_{mn}(x, y)$ is the product of the pertinent eigenfunctions of lateral beam vibrations,

$$\phi_{mn}(x, y) = X_m(x) \cdot Y_n(y), \quad (14.5.21)$$

which satisfy the prescribed boundary conditions. Consequently, in Eq. (14.5.21), $X_m(x)$ represents the m th mode of a freely vibrating uniform beam with span a , given in Table 4.3.1. Similarly, $Y_n(y)$ is the n th mode of a beam of length b .

By applying the variational method discussed above, the problem of free flexural vibration of plates can be reduced to the solution of the following variational equations:

$$\iint_{(A)} [D \nabla^2 \nabla^2 \phi_{mn}(x, y) - \bar{m} \omega^2 \phi_{mn}(x, y)] \phi_{mn}(x, y) dx dy = 0, \quad (14.5.22)$$

where $m, n = 1, 2, 3, \dots$ By introducing the notation

$$I_1 = \iint_{(A)} [\phi_{mn}(x, y) \nabla^2 \nabla^2 \phi_{mn}(x, y)] dx dy \quad (14.5.23)$$

and

$$I_2 = \iint_{(A)} \phi_{mn}^2(x, y) dx dy, \quad (14.5.24)$$

an approximate analytical expression for the frequencies of the free flexural vibration of plates of uniform thickness is obtained:

$$\omega_{mn}^2 = \frac{I_1}{I_2} \cdot \frac{D}{\bar{m}}. \quad (14.5.25)$$

[†] The idea of using eigenfunctions of beams for solving plate vibration problems was originally proposed by Ritz [14.5.2]; Vlasov, however, combined the use of eigenfunctions and Galerkin's method.

The definite integrals given in Eqs. (14.5.23) and (14.5.24) can be further expanded on the basis of Eq. (14.5.21). Thus, if a rectangular plate is considered, we can write

$$\begin{aligned} I_1 &= \int_0^a \int_0^b \{X_m(x)Y_n(y)\nabla^2\nabla^2[X_m(x)Y_n(y)]\} dx dy \\ &= \int_0^a \int_0^b [X_m''''(x)Y_n(y) + 2X_m''(x)Y_n''(y) + X_m(x)Y_n''''(y)]X_m(x)Y_n(y) dx dy, \end{aligned} \quad (14.5.26)$$

where the primes and dots indicate differentiations with respect to x and y , respectively.

Similarly,

$$I_2 = \int_0^a \int_0^b X_m^2(x) \cdot Y_n^2(y) dx dy. \quad (14.5.27)$$

The quasi-orthogonality of the eigenfunctions of beams permits the introduction of the following definite integrals:

$$\begin{aligned} I_3 &= \int_0^a X_m^2(x) dx, \\ I_4 &= \int_0^a Y_n^2(y) dy, \\ I_5 &= \int_0^a X_m''''(x)X_m(x) dx, \\ I_6 &= \int_0^a X_m''(x)X_m(x) dx, \\ I_7 &= \int_0^a Y_n''(y)Y_n(y) dy, \\ I_8 &= \int_0^a Y_n''''(y)Y_n(y) dy. \end{aligned} \quad (14.5.28)$$

Using these expressions, the circular frequencies of free vibrations of plates become

$$\omega_{mn} = \sqrt{\frac{I_4 I_5 + 2I_6 I_7 + I_3 I_8}{I_3 I_4}} \cdot \sqrt{\frac{D}{\bar{m}}}. \quad (14.5.29)$$

Since the definite integrals indicated in Eq. (5.1.28) can be evaluated numerically, Eq. (14.5.29) can also be used for plates of arbitrary contour.

Summary. As in the case of static analysis of plates, the energy methods occupy an important position among the approximate methods for solving free-vibration problems. When only the lowest frequency is of interest, Rayleigh's method gives remarkably accurate results that are slightly higher than the actual frequencies. Although the Ritz method is capable of yielding information on the higher frequencies, the accuracy of these frequencies usually deteriorates progressively for the higher modes.

The other variational methods are more general. Especially noteworthy is the extension of Galerkin's method by Vlasov, which affords the possibility of an approximate solution of dynamic problems of plates having arbitrary contours and, to some extent, arbitrary boundary conditions. Solution of such problems by the classical methods is very difficult or often impossible. Vlasov's method uses linear combinations of the eigenfunctions of lateral beam vibrations, which are able to satisfy most boundary conditions. In this way, the determination of natural circular frequencies is reduced to evaluation of definite integrals of simple functions. Tables given in Refs. [11], [4.3.21], and [4.3.22] can facilitate the computational work. The required mathematical operations are simple, but occasionally the computation tends to be quite lengthy. Although the accuracy of all the energy methods depends on the selection of appropriate shape functions, the free-vibration analysis of plates by energy methods is not as sensitive to the proper choice of these functions as its static counterpart.

The energy methods presented in this section can logically be extended to cover forced vibrations of plates by adding the potential energy of the dynamic forces to the total energy of the vibrating system. With the exception of the simplest case, however, the required computational work is tedious. In the author's opinion, computerized solutions based either on finite element or finite difference methods are more economical for forced-vibration analyses. Estimates of the dynamic response, however, can be obtained with relative ease by energy methods via the dynamic load factor, which requires the knowledge of the lowest frequency of the structure. Further details of the application of energy methods to the solution of dynamic plate problems, including the obtainable accuracy, can be found in the bibliography at the end of this section.

ILLUSTRATIVE EXAMPLE

Find the lowest circular frequency of a rectangular plate clamped on all edges (Fig. 14.5.1) using the Ritz method and check the result by the Galerkin method.

To be able to utilize the computational advantages offered by the double symmetry of the problem, we transfer the origin of the coordinate system to the center of the plate.

a. Ritz Method. In selecting a suitable infinite series expression of the deflection that satisfies the geometrical boundary conditions and closely approximates the shape of the first mode of vibration, we use

$$W(x, y) = C_1 \varphi_1(x, y) = C_1 (x^2 - a^2)^2 (y^2 - b^2)^2, \quad (14.5.30)$$

which represents the first term of Eq. (14.5.12). This expression is obtained from the static deflection formulas of uniformly loaded beams clamped at both ends.

Since the plate is clamped all along the edges, the simplified form of the strain energy expression (4.2.6) is applicable; thus,

$$\begin{aligned} U_b &= \frac{D}{2} \int_{-a}^{+a} \int_{-b}^{+b} \left(\frac{\partial^2 W}{\partial x^2} + \frac{\partial^2 W}{\partial y^2} \right)^2 dx dy \\ &= C_1^2 D \frac{2^8}{5^2} a^9 b^9 \left(\frac{1}{a^4} + \frac{2^8}{3^2 \times 7^2} \frac{1}{a^2 b^2} + \frac{1}{b^4} \right). \end{aligned} \quad (14.5.31)$$

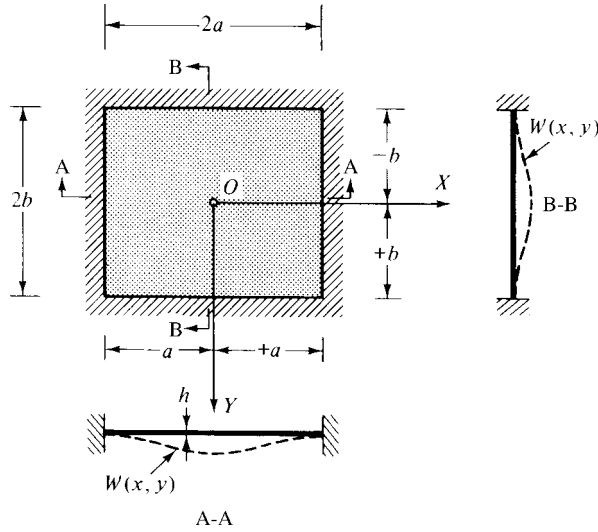


Figure 14.5.1 First mode of vibration of clamped plate.

The maximum kinetic energy of the plate, calculated from Eq. (14.5.8), is

$$T_{\max} = \frac{1}{2} \omega_1^2 \mathcal{J} = \frac{1}{2} \omega_1^2 \bar{m} \int_{-a}^{+a} \int_{-b}^{+b} W^2(x, y) dx dy = \frac{1}{2} \omega_1^2 \bar{m} C_1^2 \frac{2^4}{5^2} a^9 b^9. \quad (14.5.32)$$

From minimization of the total energy (14.5.15),

$$\frac{\partial U_b}{\partial C_1} - \frac{1}{2} \omega_1^2 \frac{\partial \mathcal{J}}{\partial C_1} = 0,$$

we obtain

$$\omega_1 = 4 \sqrt{2 \left(\frac{1}{a^4} + \frac{2^8}{3^2 \times 7^2} \cdot \frac{1}{a^2 b^2} + \frac{1}{b^4} \right) \cdot \sqrt{\frac{D}{\bar{m}}}}, \quad (14.5.33)$$

or, for a square plate ($a = b$),

$$\omega_1 = \frac{9.09}{a^2} \sqrt{\frac{D}{\bar{m}}}. \quad (14.5.33a)$$

This result agrees within 1.04% with the value obtained from more exact computation. Using two additional terms in Eq. (14.5.12), the “exact” value of the lowest circular frequency is obtained.

b. Galerkin's Method. The first modal shape is approximated, again, by Eq. (14.5.30). Thus, the variational equation (14.5.19) becomes

$$\int_{-a}^{+a} \int_{-b}^{+b} [D \nabla^2 \nabla^2 W(x, y) - \omega^2 \bar{m} W(x, y)] W(x, y) dx dy = 0. \quad (14.5.34)$$

Substitution of Eq. (14.5.30) into (14.5.34) gives

$$\begin{aligned} \int_{-a}^{+a} \int_{-b}^{+b} C_1 \{ & D[24(y^2 - b^2)^2 + 32(3x^2 - a^2)(3y^2 - b^2) + 24(x^2 - a^2)^2] \\ & - \omega^2 \bar{m}(x^2 - a^2)^2(y^2 - b^2)^2 \} (x^2 - a^2)^2 \\ & \times (y^2 - b^2)^2 dx dy = 0, \end{aligned} \quad (14.5.35)$$

which, after evaluation of the definite integrals, becomes

$$C_1 \left\{ \frac{D \cdot 2^{15}}{3^2 \times 5^2 \times 7} \left[a^9 b^5 + \frac{4}{7} a^7 b^7 + a^5 b^9 \right] - \omega^2 \frac{2^{16} \bar{m}}{3^4 \times 5^2 \times 7^2} a^9 b^9 \right\} = 0; \quad (14.5.36)$$

hence

$$\omega = 3 \sqrt{\frac{7}{2} \left(\frac{1}{a^4} + \frac{4}{7} \frac{1}{a^2 b^2} + \frac{1}{b^4} \right) \sqrt{\frac{D}{\bar{m}}}}. \quad (14.5.37)$$

Therefore, the lowest circular frequency for square plates is

$$\omega = \frac{9}{a^2} \sqrt{\frac{D}{\bar{m}}}. \quad (14.5.38)$$

The obtained result agrees almost completely with the exact solution of the problem:

$$\omega_{\text{exact}} = \frac{8.9965}{a^2} \sqrt{\frac{D}{\bar{m}}}.$$

References and Bibliography

- [14.5.1] RAYLEIGH, J. W., *The Theory of Sound*, 2nd ed., Dover Publications, New York, 1945.
- [14.5.2] RITZ, W., "Theorie der Transversalschwingungen einer quadratischen Platte mit freien Rändern," *Ann. Phys.*, 28 (1909), 737–786.
- [14.5.3] ONIASHVILI, O. D., *Nektorye dinamicheskie zadachi teorii oblocheck (Certain Dynamic Problems of the Theory of Shells)*[†], Press of the Academy of Sciences of the USSR, Moscow, 1957.
- [14.5.4] SZILARD, R., "Estimating Natural Frequencies and Modes of Arch Dams with the Theory of Plates on Elastic Foundation," in *Proceedings of the 4th World Conference on Earthquake Engineering, Santiago, Chile, Jan. 13–18, 1969*, Vol. 2, Chilean Association on Seismology and Earthquake Engineering, Santiago de Chile, 1970, pp. 141–154.
- [14.5.5] TEMPLE, G., "The Accuracy of Rayleigh's Method of Calculating the Natural Frequencies of Vibrating Systems," *Proc. Roy. Soc. London*, 211 (1952), 204–224.
- [14.5.6] WARBURTON, G. B., "The Vibration of Rectangular Plates," *Proc. Inst. Mech. Eng. London*, 168 (1954), 371–381.
- [14.5.7] ANDERSON, B. W., "Vibration of Triangular Cantilever Plates," *J. Appl. Mech., Trans. Am. Soc. Mech. Eng.*, 18, No. 4 (1954), 129–134.

[†] Available also in English translation, Morris D. Friedman, West Newton, Massachusetts

- [14.5.8] YOUNG, D., "Vibration of Rectangular Plates by the Ritz Method," *J. Appl. Mech., Trans. Am. Soc. Mech. Eng.*, 17 (1950), 448–453.
- [14.5.9] PÖSCHL, TH., "Über eine mögliche Verbesserung der Ritzschen Methode," *Ing.-Arch.*, 23, No. 5 (1955), 365–372.
- [14.5.10] SOUTHWELL, R. V., "Some Extensions of Rayleigh Principle," *Quart. J. Mech. Appl. Math.*, 6, Pt. 3 (1953), 257–272.
- [14.5.11] GOLDMAN, E., "Anwendung der Ritzschen Methode auf die Theorie der Transversalschwingungen freischwingender Platten von rechteckiger, rhombischer, dreieckiger und elliptischer Begrenzung," Ph.D. Dissertation, Technische Hochschule Breslau, Breslau, 1918.
- [14.5.12] FORSYTH, E. M., and Warburton, G. B., "Transient Vibration of Rectangular Plates," *J. Mech. Eng. Sci.*, 2, No. 4 (Dec. 1960), 325–330.
- [14.5.13] KAUL, R. K., and CADAMBE, V., "The Natural Frequencies of Thin Skew Plates," *Aeron. Quart.*, 7 (1956), 337–352.

14.6 Natural Frequencies Obtained from Static Deflections

The Rayleigh method, described in Sec. 14.5, depends upon equating the maximum potential and kinetic energies. The same principle can be used to determine circular frequencies by utilizing the static deflection curves due to symmetric or antisymmetric inertia forces. These forces, which correspond to the lateral translations, can be the dead loads.

Let us divide the plate into many small sections. Using a suitable network, we lump the mass of each section at discrete points. When the plate is in the position of maximum deflection, all the energy of the system is stored as potential energy.

Assuming, again, that the free vibration is harmonic,

$$w(x, y, t) = W(x, y) \sin \omega t, \quad (14.6.1)$$

the potential energy can be written as the sum of the products of the average forces and deflections; thus

$$U_{\max} \approx \frac{1}{2} k_1 w_1^2 + \frac{1}{2} k_2 w_2^2 + \frac{1}{2} k_3 w_3^2 + \cdots + \frac{1}{2} k_n w_n^2 = \frac{1}{2} \sum_{i=1}^n k_i w_i^2, \quad (14.6.2)$$

where k_i is the effective spring constant and w_i is the lateral displacement for the i th mass. Similarly, the maximum kinetic energy T_{\max} can be written as

$$T_{\max} \approx \frac{1}{2} \sum_{i=1}^n \bar{m}_i w_i^2 \omega_r^2, \quad (14.6.3)$$

where \bar{m}_i is the mass of the i th section and ω_r is the natural circular frequency pertinent to the r th vibration mode under investigation. Equating Eqs. (14.6.2) and (14.6.3),

we have

$$\omega_r^2 = g \frac{\sum_{i=1}^n k_i w_i^2}{\sum_{i=1}^n q_i w_i^2}, \quad (14.6.4)$$

where g is the gravitational acceleration and q_i is the weight of the i th section. Since the dynamic response in the first mode has approximately the same shape as the static deflection, we can assume, based on Eq. (14.1.23), that the dynamic deflection ordinates are proportional to the static deflections W_i ; therefore

$$w_i = c W_i, \quad (14.6.5)$$

where c represents the constant of proportionality. Next, we substitute Eq. (14.6.5) into Eq. (14.6.4) and express the natural frequency, corresponding to the desired mode of vibration, in terms of the pertinent static deflections of the plate; thus

$$\omega_r^2 = g \frac{\sum_{i=1}^n k_i W_i^2}{\sum_{i=1}^n q_i W_i^2}. \quad (14.6.6)$$

Since the spring constant for each mass is

$$k_i = \frac{q_i}{W_i}, \quad (14.6.7)$$

for discrete systems, Eq. (14.6.6) becomes

$$\boxed{\omega_r^2 = g \frac{\sum_{i=1}^n q_i W_i}{\sum_{i=1}^n q_i W_i^2}}. \quad (14.6.8)$$

This expression is called the modified Rayleigh quotient or Morley's formula. [14.6.1].

For continuous systems the summation in Eq. (14.6.8) is replaced by integrals; thus,

$$\omega_r^2 = g \frac{\iint_{(A)} q(x, y) \cdot W(x, y) \, dx \, dy}{\iint_{(A)} q(x, y) \cdot W^2(x, y) \, dx \, dy}. \quad (14.6.9)$$

The use of these formulas is very convenient, since it involves merely the determination of static deflections of a plate, which may be obtained using the analytical or numerical methods. Furthermore, deflections for the most common types of plates are readily available. Knowing the circular frequencies, we can easily obtain the dynamic load factors [Eq. (14.1.23) or (14.1.32)] for a quasi-static structural analysis,

Equations (14.6.8) and (14.6.9) can also be used for calculating the natural frequencies corresponding to the second and higher modes. When the second mode is sought, for instance, the plate is loaded antisymmetrically with q , representing the inertia forces (Fig. 14.6.1b). Unfortunately, these modal shapes, except for the lowest modes, are not always known, a fact that limits the application of this simple technique. Modal shapes, however, can be obtained with relative ease using ordinary finite difference techniques. Consequently, the combination of these two methods

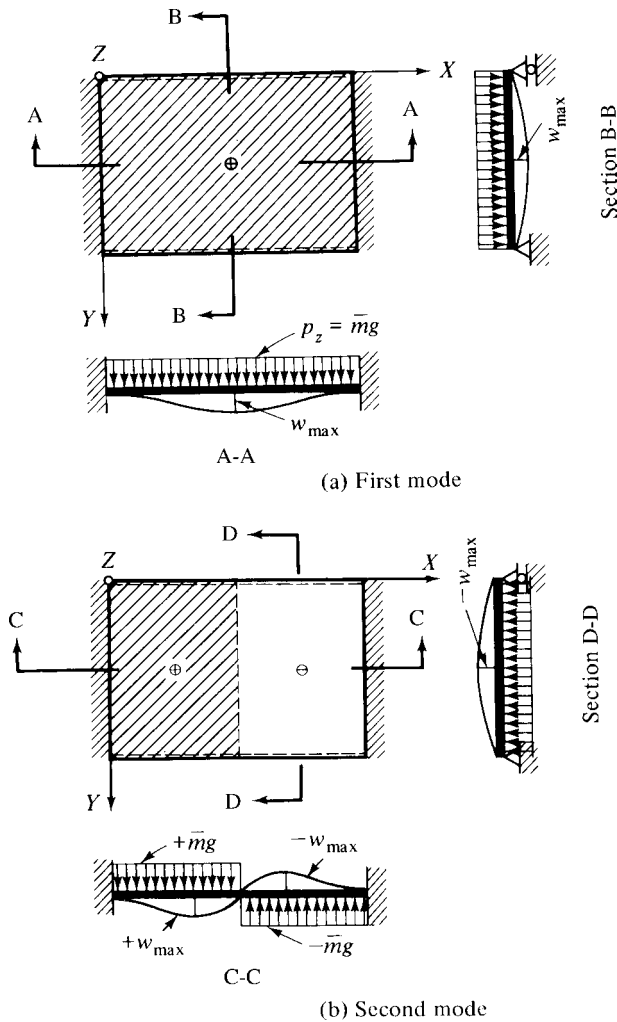


Figure 14.6.1 Loading and deflection patterns for simplified free-vibration analysis.

may offer distinct advantages, especially in the case of small computers with limited storage capacity.

The accuracy of this method is generally good, since the results are seldom more than 5% in error. The obtainable accuracy depends largely on how closely the static deflection shape $W(x, y)$ approximates the fundamental mode. It should be noted that the circular frequencies obtained from Eq. (14.6.8) are somewhat higher than the actual ones.

The Stodola-Vianello [14.6.7] iterative technique described in Sec. 15.1 can be used to improve the obtained results. For continuous systems, improved frequencies are obtained from

$$\omega^{(1)} = \sqrt{\frac{\iint_{(A)} p^{(0)}(x, y) W^{(1)}(x, y) dA}{\iint_{(A)} \bar{m}(x, y) [W^{(1)}(x, y)]^2 dA}}, \quad (14.6.10)$$

where $p^{(0)}$ is a fictitious load (5.2.14) containing the first estimate of the natural frequency $\omega^{(0)}$ and $W^{(1)}$ represents the static deflections due to such a load.

For estimating natural frequencies of continuous plates, the following simple procedure may be used, provided the spans of the individual panels are approximately the same in both directions. First, we determine the lowest frequencies of the individual panels, assuming that the plate is (1) simply supported and (2) clamped at all boundaries; this yields f_{li} and f_{li}^* , respectively. Then, the *average values*

$$f_1 \approx \sqrt[4]{\frac{n}{\sum_{i=1}^n \frac{1}{f_{li}^4}}} \quad \text{and} \quad f_1^* \approx \sqrt[4]{\frac{\sum_{i=1}^n (f_{li}^*)^4}{n}} \quad (14.6.11)$$

provide estimates of the natural frequencies.[†] In these expressions n represents the number of individual panels. A similar approach can be taken for the frequencies corresponding to second modes of free vibration. These approximate formulas are based on Dunkerley's derivation and yield lower-bound solutions.

Summary. This simplified energy approach to free-vibration problems yields sufficiently accurate results in a convenient way. By applying an iterative technique, the accuracy can be further increased to any desired degree. In the case of unknown modal shapes, this approach can be combined with finite difference or finite element methods. If evaluation of eigenvalues and eigenvectors of large matrices create special problems, this method can be used to eliminate the determination of eigenvalues. Consequently, Morley's formula is well suited for hand computation or for use on programmable desk calculators.

[†] The relation between circular and natural frequencies is $f = \omega/2\pi$; see Sec. 14.1.

ILLUSTRATIVE EXAMPLE

Find the circular frequencies pertinent to the first and second modes of free vibration of a simply supported square plate.

Since the plate thickness is constant, Eq. (14.6.9) can be written as

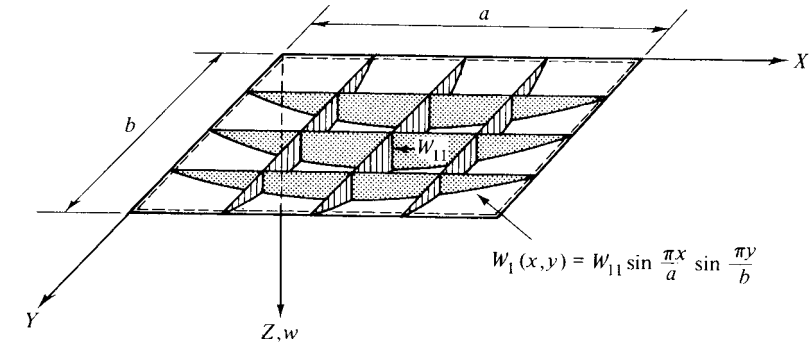
$$\omega_n^2 = g \frac{\int_0^a \int_0^a W_n(x, y) dx dy}{\int_0^a \int_0^a W_n^2(x, y) dx dy}. \quad (14.6.12)$$

For simplicity, a one-term sinusoidal deflected shape is assumed (Fig. 14.6.2a); thus

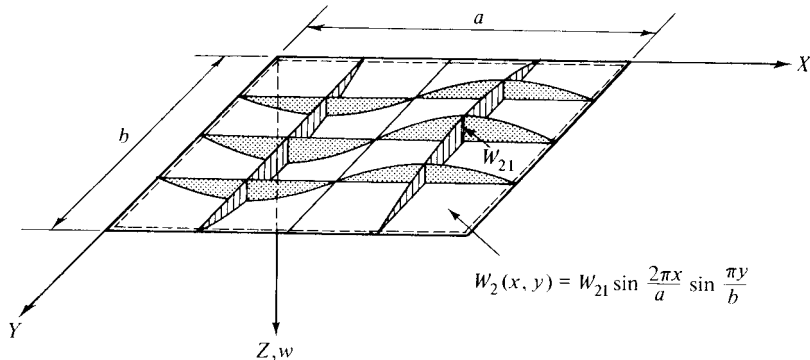
$$W_1(x, y) = W_{11} \sin \frac{\pi x}{a} \sin \frac{\pi y}{a}, \quad (14.6.13)$$

where

$$W_{11} = 0.00416 \frac{p_z a^4}{D} = 0.00416 \frac{\bar{m} g a^4}{D}, \quad (14.6.14)$$



(a) First mode



(b) Second mode

Figure 14.6.2 First and second modes of simply supported plate.

which represents the maximum deflection ordinate. By substituting Eq. (14.6.13) into Eq. (14.6.12), we obtain

$$\begin{aligned}\omega_1^2 &= \frac{g}{W_{11}} \frac{\int_0^a \int_0^a \sin(\pi x/a) \sin(\pi y/a) dx dy}{\int_0^a \int_0^a \sin^2(\pi x/a) \sin^2(\pi y/a) dx dy} \\ &= \frac{g}{W_{11}} \frac{[(a/\pi) \cos(\pi x/a)]_0^a \times [(a/\pi) \cos(\pi y/a)]_0^a}{[\frac{1}{2}x - (a/4\pi) \sin(2\pi x/a)]_0^a \times [\frac{1}{2}y - (a/4\pi) \sin(2\pi y/a)]_0^a} \\ &= \frac{g}{W_{11}} \frac{16}{\pi^2}.\end{aligned}\quad (14.6.15)$$

Hence, the circular frequency pertinent to the first mode of vibration is

$$\omega_1 = \frac{4}{\pi a^2} \sqrt{\frac{D}{0.00416\bar{m}}} = \frac{19.722}{a^2} \sqrt{\frac{D}{\bar{m}}}.\quad (14.6.16)$$

A comparison with the exact solution of the problem [14.1.8],

$$\omega_1 = \frac{2\pi^2}{a^2} \sqrt{\frac{D}{\bar{m}}} = \frac{19.74}{a^2} \sqrt{\frac{D}{\bar{m}}},\quad (14.6.17)$$

indicates a discrepancy of a negligible order of magnitude.

Similarly, for the second mode, we assume the following sinusoidal deflection shape (Fig. 14.6.2b):

$$W_2(x, y) = W_{21} \sin \frac{2\pi x}{a} \sin \frac{\pi y}{a}.\quad (14.6.18)$$

Substitution of this expression in Eq. (14.6.12) yields

$$\begin{aligned}\omega_2^2 &= \frac{g}{W_{21}} \frac{\int_0^{a/2} \int_0^a \sin(2\pi x/a) \sin(\pi y/a) dx dy}{\int_0^{a/2} \int_0^a \sin^2(2\pi x/a) \sin^2(\pi y/a) dx dy} \\ &= \frac{g}{W_{21}} \frac{[(a/2\pi) \cos(2\pi x/a)]_0^{a/2} \times [(a/\pi) \cos(\pi y/a)]_0^a}{[\frac{1}{2}x - (a/8\pi) \sin(2\pi x/a)]_0^{a/2} \times [\frac{1}{2}y - (a/4\pi) \sin(2\pi y/a)]_0^a} \\ &= \frac{g}{W_{21}} \frac{16}{\pi^2}.\end{aligned}\quad (14.6.19)$$

The corresponding maximum deflection ordinate at $x = a/4$ is

$$W_{21} = 0.01013 \frac{\bar{m}g}{D} \left(\frac{a}{2}\right)^4 = 0.000634 \frac{\bar{m}g}{D} a^4;\quad (14.6.20)$$

hence

$$\omega_2 = \frac{4}{\pi a^2} \sqrt{\frac{D}{0.000634\bar{m}}} = \frac{50.6}{a^2} \sqrt{\frac{D}{\bar{m}}}, \quad (14.6.21)$$

while the exact solution (14.3.8.) is

$$\omega_2 = \pi^2 \left(\frac{4}{a^2} + \frac{1}{a^2} \right) \sqrt{\frac{D}{\bar{m}}} = \frac{5\pi^2}{a^2} \sqrt{\frac{D}{\bar{m}}}. \quad (14.6.22)$$

The error of this approximate solution for the frequency pertinent to the second mode is less than 2.5%.

In both cases the good accuracy obtained is due to the fact that the assumed deflection shapes and the actual modes are identical.

References and Bibliography

- [14.6.1] MORLEY, A., "The Calculation of Vibration and Whirling Speeds," *Engineering*, 88 (1909), 135.
- [14.6.2] MYKLESTAD, N. O., *Fundamentals of Vibration Analysis*, McGraw-Hill Book Co., New York, 1956.
- [14.6.3] BARTON, M. V., "Vibration of Rectangular and Skew Cantilever Plates," *J. Appl. Mech.*, 18 (1951), 129–134.
- [14.6.4] MAJOR, A., *Berechnung und Planung von Maschinen- und Turbinenfundamenten*, Verlag der Ungarischen Akademie der Wissenschaften, Budapest, 1961.[†]
- [14.6.5] KORENEW, B. G., *Dynamik von Baukonstruktionen*, VEB-Verlag Technik, Berlin, 1953.
- [14.6.6] RAUSCH, E., *Maschinenfundamente und andere dynamisch beanspruchte Baukonstruktionen*, 3rd ed., VDI-Verlag, Düsseldorf, 1959.
- [14.6.7] STODOLA, A., *Steam and Gas Turbines*, 6th ed., Peter Smith, Gloucester, Massachusetts, 1957.

14.7 Forced Transverse Vibration of Rectangular Plates

In the previous sections classical methods for the free-vibration analysis of plates and membranes have been discussed. Let us now consider the dynamic response of plates to time-dependent disturbing forces $P(t)$ that produce so-called *forced vibration* in the structure. In determining the dynamic response of a plate to external exciting forces $p_z(x, y, t)$, we seek an expression for the deflections $w(x, y, t)$ from which other quantities, such as velocities, accelerations and stresses, can be derived.

Forced-vibration analysis of plates by classical methods involves solution of boundary value problems in a manner similar to those discussed in Chapter 1. Let us consider a simply supported plate acted upon by an arbitrary (in-space) lateral load that varies harmonically over the time:

$$p_z(x, y, t) = P^*(x, y)\theta(t) = P^*(x, y) \sin pt. \quad (14.7.1)$$

[†] Available also in English translation under the title *Vibration Analysis and Design of Foundations for Machines and Turbines*, Collet's Holdings, London, 1962.

In the presence of this simple harmonic excitation the governing differential equation of motion is Eq. (14.2.3). Again, we seek the solution in two parts,

$$w(x, y, t) = w_H(x, y, t) + w_P(x, y, t), \quad (14.7.2)$$

where w_H represents the solution of the homogeneous form of the equation of motion (14.2.4) and w_P is a particular solution of Eq. (14.2.3). Since the homogeneous solution is associated with the free vibration of the plate at its natural frequency (treated in Sec. 14.3), it is sufficient to discuss here merely the particular solution, corresponding to the steady-state oscillation at the frequency (p) of the exciting force.

In the first part of our discussion, we assume that the free vibration is successfully damped; consequently, we consider only the action of the harmonic excitation. The time-invariant part of the forcing function can be represented by a double trigonometric series:

$$P^*(x, y) = \sum_{m=1}^{\infty} \sum_{n=1}^{\infty} P_{mn} \sin \frac{m\pi x}{a} \sin \frac{n\pi y}{b}. \quad (14.7.3)$$

Thus, Eq. (14.7.1) can be written as

$$p_z(x, y, t) = \sin pt \sum_{m=1}^{\infty} \sum_{n=1}^{\infty} P_{mn} \sin \frac{m\pi x}{a} \sin \frac{n\pi y}{b}. \quad (14.7.1a)$$

In accordance with Navier's method,[†] we shall look for the particular solution in the form

$$w_P(x, y, t) = \sin pt \sum_{m=1}^{\infty} \sum_{n=1}^{\infty} W_{mn} \sin \frac{m\pi x}{a} \sin \frac{n\pi y}{b}. \quad (14.7.4)$$

The substitution of Eqs. (14.7.4) and (14.7.1a) into the governing differential equation of motion (14.2.3) using a specific set of m, n values yields

$$W_{mn} \left[D\pi^4 \left(\frac{m^2}{a^2} + \frac{n^2}{b^2} \right)^2 - \bar{m}p^2 \right] = P_{mn}. \quad (14.7.5)$$

Let us express the first term on the left-hand side of Eq. (14.7.5) in terms of free vibration (14.3.8); then

$$W_{mn} = \frac{P_{mn}}{\bar{m}(\omega_{mn}^2 - p^2)}. \quad (14.7.6)$$

If the time-dependent changes of the excitation are very slow, p will be small in comparison with ω_{mn} and the displacements will correspond to those obtained from the static loading; thus, for the static case, Eq. (14.7.6) becomes

$$W_{mn}^* = \frac{P_{mn}}{\bar{m}\omega_{mn}^2}. \quad (14.7.7)$$

[†] See Sec. 2.2.

Therefore, the dynamic load factor for simply supported plates can be expressed as the ratio of W_{mn}/W_{mn}^* . This gives

$$\text{DLF} = \frac{1}{1 - (p/\omega_{mn})^2}, \quad (14.7.8)$$

which is the same expression as Eq. (14.1.23), obtained for a single-DOF system.

Next, let us assume the simultaneous action of free and forced vibrations. It is evident that the superposition of Eqs. (14.3.1) and (14.7.4) will correspond to this condition. The lateral deflections of a freely vibrating simply supported plate can be expressed by

$$w = \sum_{m=1}^{\infty} \sum_{n=1}^{\infty} \bar{W}_{mn} \sin \frac{m\pi x}{a} \sin \frac{n\pi y}{b} \sin(\omega_{mn}t - \alpha), \quad (14.7.9)$$

where α represents the phase angle[†] and can be determined from the initial conditions. If the initial conditions, for instance, are

$$w = 0 \quad \text{and} \quad \frac{\partial w}{\partial t} = 0 \quad \text{at } t = 0, \quad (14.7.10)$$

then α is zero. The combined solution of simultaneous free and forced vibrations can be written as

$$\begin{aligned} w(x, y, t) = & \sum_{m=1}^{\infty} \sum_{n=1}^{\infty} \bar{W}_{mn} \sin \frac{m\pi x}{a} \sin \frac{n\pi y}{b} \sin(\omega_{mn}t - \alpha) \\ & + \sin pt \sum_{m=1}^{\infty} \sum_{n=1}^{\infty} W_{mn} \sin \frac{m\pi x}{a} \sin \frac{n\pi y}{b}. \end{aligned} \quad (14.7.11)$$

From the second initial condition ($\dot{w} = 0$ at $t = 0$), we obtain

$$\bar{W}_{mn} = -\frac{p}{\omega_{mn}} W_{mn}. \quad (14.7.12)$$

Consequently, Eq. (14.7.11) becomes

$$w(x, y, t) = \sum_{m=1}^{\infty} \sum_{n=1}^{\infty} \left(\sin pt - \frac{p}{\omega_{mn}} \sin \omega_{mn}t \right) W_{mn} \sin \frac{m\pi x}{a} \sin \frac{n\pi y}{b}, \quad (14.7.13)$$

where W_{mn} is calculated from Eq. (14.7.6).

[†] Known also as angle of lag of response.

A similar approach can be taken when the excitation is not simple harmonic but arbitrary periodic or even transient. For such conditions, we separate the variables in the forcing function, as well as in the expression for displacements:

$$\begin{aligned} p_z(x, y, t) &= \sum_m \sum_n \sum_r P_{mnr} X_m(x) \cdot Y_n(y) \cdot \theta_r(t), \\ w(x, y, t) &= \sum_m \sum_n \sum_r W_{mnr} X_m(x) \cdot Y_n(y) \cdot \theta_r(t). \end{aligned} \quad (14.7.14)$$

In these series expressions the time-dependent parts are also expressed in Fourier series. The dynamic response of the system is obtained by superimposing the results of the individual terms $\theta_r(t)$.

Let us now investigate the case when the frequency of the forcing function, p , has approximately the same magnitude as one of the free-vibration frequencies ω_{ik} . We consider only one term in Eq. (14.7.13), which corresponds to this special case; thus, $m = i$ and $n = k$. We denote the difference in frequencies by

$$\omega_{ik} - p = 2\Delta_{ik}. \quad (14.7.15)$$

Since the two frequencies are nearly equal, Δ_{ik} represents a small quantity. By neglecting small quantities with the coefficients of $2\Delta_{ik}/p$, Eq. (14.7.13), corresponding to the selected set of values for m and n , can be written as

$$w_{ik} = -2(\sin \Delta_{ik}t) \cos \frac{(p + \omega_{ik})t}{2} W_{ik} \sin \frac{i\pi x}{a} \sin \frac{k\pi y}{b}. \quad (14.7.16)$$

Since Δ_{ik} is a small quantity, the function of $\Delta_{ik}t$ varies slowly, with the large period $2\pi/\Delta_{ik}$. Equation (14.7.16) can be considered as an imaginary vibration with the period of $4\pi/(p + \omega_{ik})$ and with the amplitude

$$2(\sin \Delta_{ik}t) W_{ik} \sin \frac{i\pi x}{a} \sin \frac{k\pi y}{b}. \quad (14.7.17)$$

This phenomenon, which occurs whenever the frequency of the excitation is close to the natural frequency of the system, is called *beat*. Figure 14.7.1 illustrates the general nature of this type of vibration. The dashed lines are the envelopes of the amplitudes. The period of the beat increases as the vibration approaches the resonance condition. When $p = \omega_{ik}$, Eq. (14.7.16) becomes

$$w_{ik} = -2\Delta_{ik}t \cos \frac{(p + \omega_{ik})t}{2} W_{ik} \sin \frac{i\pi x}{a} \sin \frac{k\pi y}{b} \quad (14.7.18)$$

and the amplitude will increase without bounds, as shown in Fig. 14.7.2. Oniashvili has treated the forced vibrations of double-curved shallow and nonshallow shells in a similar manner [14.5.3].

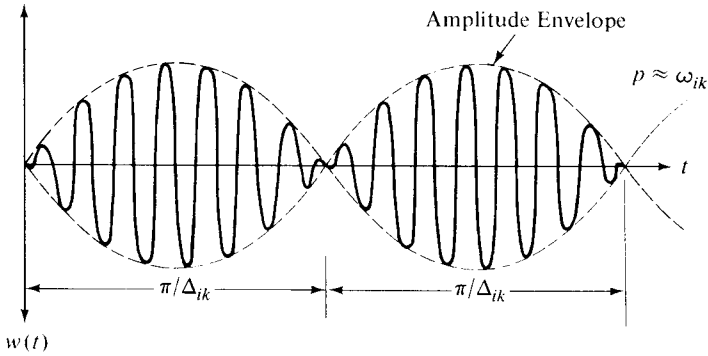


Figure 14.7.1 Oscillations called "beat."

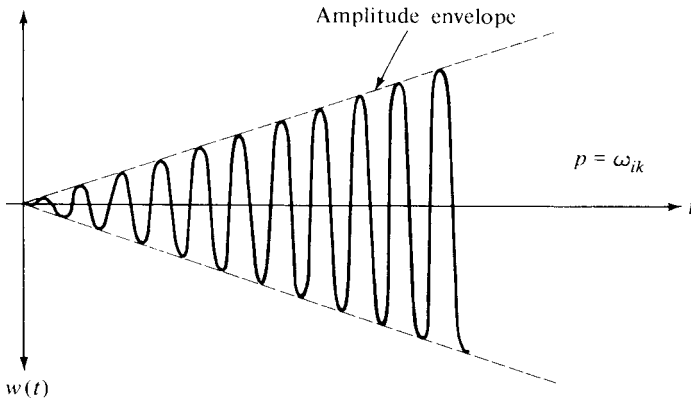


Figure 14.7.2 Resonance.

It is also possible to extend Lévy's method, described in Secs. 2.3 and 14.3, to obtain a particular solution to Eq. (14.2.3), provided that the boundary conditions satisfy the requirements of this method. The mathematical operations, however, become increasingly involved.

Dynamic responses of plate bridges, produced by *smooth-running* wheel loads, seldom create more than a 10% stress increase. Consequently, the dynamic behavior of the bridge can be approximated by applying a dynamic load factor [14.1.8],

$$\text{DLF} = 1 + \frac{v^2 Pl}{3gEI_e}(\text{RF}), \quad (14.7.19)$$

where P is the rolling load and v represents its velocity. In calculating the moment of inertia I_e , the *effective width* in bending should be used. Furthermore, since the other girders also participate in the load-carrying action, a reduction factor (RF) should be applied to the wheel load [10.1.10, 10.1.17]. More exact analysis of a similar problem can be found in Ref. [1.1.8], pp. 234–237.

Irregularities on the surface of the bridge deck, however, may produce much higher impact than that given in Eq. (14.7.19). In this case, the load-time relationship of the

excitation can be expressed [14.1.8] by

$$P(t) = -\frac{P}{g} \frac{\partial^2(w + \eta)}{\partial t^2}, \quad (14.7.20)$$

where η represents the shape of the low spot (Fig. 14.7.3), given by

$$\eta = \frac{\Delta}{2} \left(1 - \cos \frac{2\pi vt}{l^*} \right). \quad (14.7.21)$$

In both cases of excitations, computerized solutions, based on either finite difference or finite element methods,[†] can yield more accurate results.

The static behavior of highway bridges can be approximated with good accuracy by the orthotropic plate theory, as discussed in Sec. 10.1. In a similar manner, the orthotropic plate theory can offer considerable improvement over the quasi-static approach in formulating the dynamic response of beam-slab bridges. A satisfactory representation for the wheel loads of the moving vehicle is obtained by means of simple spring-mass systems, as shown in Fig. 14.7.4. The equations of motion, neglecting damping, can be written as

$$D_x \frac{\partial^4 w}{\partial x^4} + 2B \frac{\partial^4 w}{\partial x^2 \partial y^2} + D_y \frac{\partial^4 w}{\partial y^4} + \bar{m} \frac{\partial^2 w}{\partial t^2} = \bar{M} \left(g - \frac{\partial^2 \bar{w}}{\partial t^2} \right) f(x - vt, y) \quad (14.7.22)$$

and

$$\bar{M} \frac{\partial^2 \bar{w}}{\partial t^2} + k(\bar{w} - w|_{x=vt}) = 0, \quad (14.7.23)$$

where \bar{M} represents the mass of the wheel load, k is its spring constant and \bar{w} denotes the absolute deflection of the spring-mass system. For the time-dependent function f , which distributes the load over the surface of the small bridge, we may assume uniform values over the $c \times d$ area and zero elsewhere.

While a relatively tedious analytical solution of this problem is possible [14.7.9], the numerical treatment of Eqs. (14.7.22) and (14.7.23), based on finite difference methods, is straightforward.[‡] In addition, the use of an iterative approach similar to the one described in Sec. 11.1 is recommended. In the first cycle we assume that $\bar{w} = w$

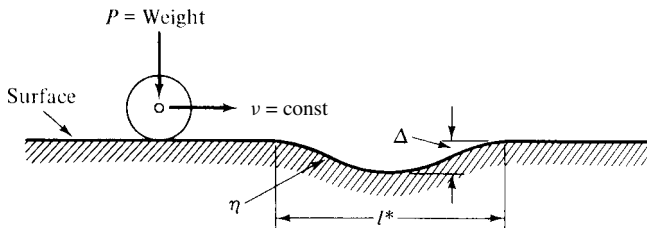


Figure 14.7.3 Irregular plate surface.

[†] See Secs. 15.1 and 15.2.

[‡] See Sec. 15.1.

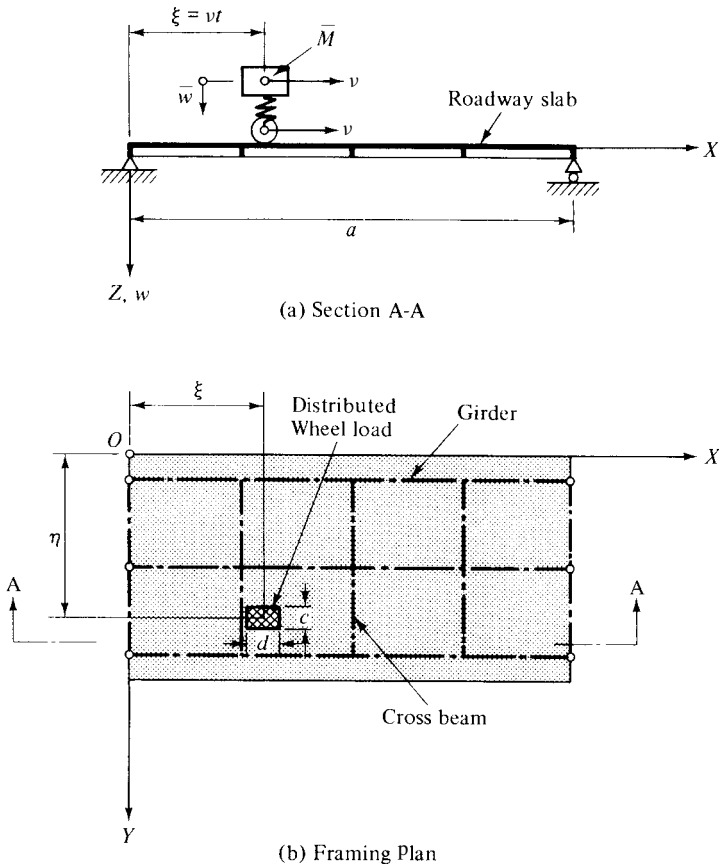


Figure 14.7.4 Highway bridge under moving load.

in Eq. (14.7.22). More sophisticated vehicle representations may involve three-DOF systems having some damping mechanism [14.7.10]. The essential features of the dynamic behavior of the bridge, however, can also be obtained by employing the aforementioned, simple spring-mass systems, either for the individual wheel loads or for the whole moving vehicle [14.7.9]; see Sec. 15.4 for more details.

Summary. Transverse forced vibration of simply supported plates can be solved with relative ease by applying Navier's method to the governing equation of motion. Because of damping (which exists in every real structure), the free-vibration part of the motion will eventually disappear, and the plate will oscillate with the frequency of the exciting force. Consequently, in most cases only the steady-state vibration, corresponding to the particular solution of the differential equation of motion, is of interest. With the exception of simply supported boundary conditions, classical solutions of forced-vibration problems are extremely tedious, in many instances even impossible. The use of dynamic load factors, however, offers a simple technique for estimating the maximum stresses.

ILLUSTRATIVE EXAMPLE

Determine the steady-state response of a simply supported rectangular plate to a uniformly distributed, pulsating load, shown in Fig. 14.7.5.

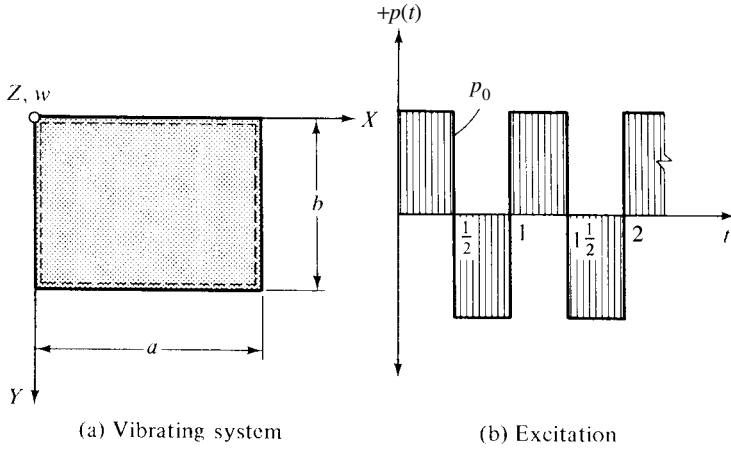


Figure 14.7.5 Plate subjected to pulsating load.

In the first step, we expand the time-dependent part of the excitation into a sine series:

$$\theta(t) = \sum_r P_r \sin p_r t. \quad (14.7.24)$$

Since $\theta(t)$ is an odd function, the coefficients of expansions can be computed from Eq. (A.1.20):

$$P_r = \frac{2}{0.5} \int_0^{0.5} p_0 \sin \frac{r\pi t}{0.5} dt = \begin{cases} 0 & \text{if } r \text{ even,} \\ \frac{4p_0}{r\pi} & \text{if } r \text{ odd;} \end{cases} \quad (14.7.25)$$

therefore

$$\theta(t) = \frac{4p_0}{\pi} \left[\sin 2\pi t + \frac{\sin 6\pi t}{3} + \frac{\sin 10\pi t}{5} + \dots \right]. \quad (14.7.26)$$

Since we are concerned only with the particular solution of the differential equation of motion, it is sufficient to apply Eq. (14.7.6). Preparatory to this, we must calculate the Fourier coefficients of the time-invariant part of the load. These are obtained from Eq. (A.1.37); thus, combining with Eq. (14.7.25), we have

$$P_{mnr} = P_{mn} \cdot P_r = \left(\frac{16}{\pi^2 mn} \right) \left(\frac{4p_0}{r\pi} \right) = \frac{64p_0}{\pi^3 mnr}. \quad (m, n = 1, 2, 3, \dots \text{ and } r = 1, 3, 5, \dots). \quad (14.7.27)$$

Next, the undamped circular frequencies ω_{mn} of the plate are determined. Equation (14.3.8) gives

$$\omega_{mn}^2 = \frac{\pi^4 D}{m} \left(\frac{m^2}{a^2} + \frac{n^2}{b^2} \right)^2 \quad \text{for } m, n = 1, 2, 3, \dots \quad (14.7.28)$$

For simplicity, let us limit ourselves to $r = m = n = 1$ and $a = b$; hence,

$$\omega_{11} = \frac{19.73}{a^2} \sqrt{\frac{D}{m}} \quad \text{and} \quad p_1 = 2\pi. \quad (14.7.29)$$

Substitution of these values into Eq. (14.7.6) gives

$$W_{11,1} = \frac{P_{mnr}}{m(\omega_{11}^2 - p_1^2)} = \frac{64p_0}{\pi^3[(389.27D/a^4) - (2\pi)^2 m]}. \quad (14.7.30)$$

This is the amplitude of the dynamic response of the plate corresponding to the $m = n = r = 1$ values (14.7.14). The rest of the computation is a simple repetition of the above-illustrated technique using different sets of m , n and r . It should be noted, however, that if the frequency of one of the terms in the expansion of the forcing function happens to be close to one of the natural frequencies ($\omega_{ik} \approx p_r$), the result will be unrealistic. In such a case, the approach based on a definite integral [Eq. (14.1.32)] should be used.

References and Bibliography

- [14.7.1] WARREN, A. G., "Free and Forced Oscillations of Thin Bars, Flexible Discs and Annuli," *Phil. Mag.*, 9 (1930), 881–901.
- [14.7.2] RAYLEIGH, J. W., *Theory of Sound*, Dover Publications, New York, 1945.
- [14.7.3] TIMOSHENKO, S., and YOUNG, D. H., *Advanced Dynamics*, McGraw-Hill Book Co., New York 1948.
- [14.7.4] GOLDENBLAT, I. I., and SISOW, A. M., *Die Berechnung von Baukonstruktionen und Schwingungen* (German translation of the Russian work), Verlag Technik, Berlin, 1955.
- [14.7.5] WINAND, A., "Effets dynamiques sur les tabliers des ponts," *Publ. IABSE, Zurich*, 29-I (1969), 149–166.
- [14.7.6] MACKEY, S., and YING, K. T., "Dynamic Analysis of Floor Systems," *Publ. IABSE, Zurich*, 20-I (1969), 33–47.
- [14.7.7] SONNTAG, S., and SONNTAG G., "Symmetrischer Biegestoss gegen eine Kreisplatte," *Forschung auf d. Gebiete d. Ingenieurwesens, Ausgabe B*, 14, No. 6 (Nov.–Dec. 1943), 137–148.
- [14.7.8] BISHOP, R. E. D., and JOHNSON, D. C., *The Mechanics of Vibrations*, Cambridge University Press, New York, 1960.
- [14.7.9] SUNDARA RAJA IYENGAR, K. T., and JAGADISH, K. S., "Dynamic Response of Highway Bridges to Moving Loads," *Publ. IABSE, Zurich*, 30-II (1970), 57–76.
- [14.7.10] REILLY, R. J., and LOONEY, C. T. G., "Dynamic Behavior of Highway Bridges," Final Report for Maryland State Road Commission and U. S. Bureau of Public Roads, Civil Engineering Department, Univ. of Maryland, College Park, Maryland, 1966.

14.8 Free Vibration of Moderately Thick Plates

As discussed in Sec. 1.5, the moderately thick plate theory includes the effects of transverse shear deformations. Neglecting transverse shear effects and to a lesser extent that of rotary inertia leads to significant errors when calculating natural frequencies of such plates. Consequently, the previously introduced vibration theory based on Kirchhoff's classical assumptions cannot be directly applied to moderately thick plates.

Here we consider a simply supported moderately thick plate, as shown in Fig. 14.8.1. Applying Mindlin's plate theory introduced in Sec. 1.5, the corresponding displacement components are w , ψ_x and ψ_y . The quantity ψ_x represents the total rotation in the XZ plane during the deformation process of a straight line that initially lies along the Z axis, as shown in Fig. 1.5.2. The quantity ψ_y is defined in a similar manner.

By normalizing the rectangular coordinates and the transverse displacement w^* , we introduce

$$\xi = \frac{x}{a}, \quad \eta = \frac{y}{b}, \quad w = \frac{w^*}{b}. \quad (14.8.1)$$

According to Ref. [14.8.1], the strain energy of an isotropic moderately thick plate can be expressed by

$$\begin{aligned} U = & \frac{D}{2} \int_0^1 \int_0^1 \left\{ \left(\frac{1}{a} \frac{\partial \psi_x}{\partial \xi} + \frac{1}{b} \frac{\partial \psi_y}{\partial \eta} \right)^2 - 2(1 - \nu) \right. \\ & \times \left[\frac{1}{ab} \frac{\partial \psi_x}{\partial \xi} \frac{\partial \psi_y}{\partial \eta} - \frac{1}{4} \left(\frac{1}{b} \frac{\partial \psi_x}{\partial \eta} + \frac{1}{a} \frac{\partial \psi_y}{\partial \xi} \right)^2 \right] + \frac{\kappa^2 Gh}{D} \\ & \times \left[\left(\psi_x + \frac{b}{a} \frac{\partial w}{\partial \xi} \right)^2 + \left(\psi_y + \frac{\partial w}{\partial \eta} \right)^2 \right] \Big\} ab \, d\xi \, d\eta. \end{aligned} \quad (14.8.2)$$

During vibration the maximum kinetic energy of the plate becomes

$$T = \frac{1}{2} \omega^2 \rho h \int_0^1 \int_0^1 \left[w^2 + \frac{1}{12} h^2 (\psi_x^2 + \psi_y^2) \right] ab \, d\xi \, d\eta. \quad (14.8.3)$$

Here ω represents the angular frequency of the vibration and ρ symbolizes the material density per unit volume.

To simplify our further discussion, we introduce the following dimensionless terms:

$$\beta = \frac{h}{b}, \quad \chi = \frac{a}{b}, \quad \lambda = \frac{\omega^2 b^4 \rho h}{D}, \quad (14.8.4)$$

where β is the thickness-to-width ratio of the plate, χ represents its aspect ratio and λ denotes a frequency ratio. Thus, the energy functional pertinent to this problem

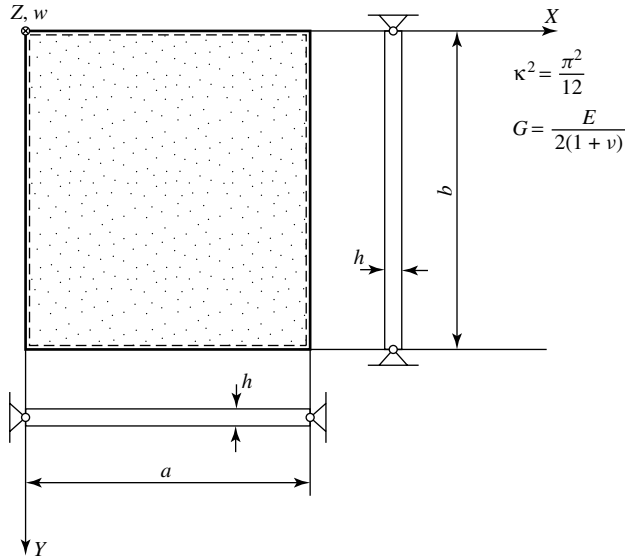


Figure 14.8.1 Simply supported Mindlin plate.

can be given [14.8.3] by

$$\begin{aligned}
 \Pi = \frac{2(U - T)b}{aD} = \int_0^1 \int_0^1 & \left\{ \left(\frac{1}{\chi} \frac{\partial \psi_x}{\partial \xi} + \frac{\partial \psi_y}{\partial \eta} \right)^2 - 2(1 - \nu) \right. \\
 & \times \left[\frac{1}{\chi} \frac{\partial \psi_x}{\partial \xi} \frac{\partial \psi_y}{\partial \eta} - \frac{1}{4} \left(\frac{\partial \psi_x}{\partial \eta} + \frac{1}{\chi} \frac{\partial \psi_y}{\partial \xi} \right)^2 \right] \\
 & + \frac{6(1 - \nu)\kappa^2}{\beta^2} \left[\left(\psi_x + \frac{1}{\chi} \frac{\partial w}{\partial \xi} \right)^2 + \left(\psi_y + \frac{\partial w}{\partial \eta} \right)^2 \right] \\
 & \left. - \lambda \left[w^2 + \frac{1}{12} \beta^2 (\psi_x^2 + \psi_y^2) \right] \right\} d\xi d\eta. \quad (14.8.5)
 \end{aligned}$$

Considering the boundary conditions, we recall that in Mindlin plate theory three conditions must be specified compared with two in classical plate theory. Consequently, solutions of the present vibration problem are sought in the forms

$$\begin{aligned}
 \psi_x &= A_{mn} \cos(m\pi\xi) \sin(n\pi\eta), \\
 \psi_y &= B_{mn} \sin(m\pi\xi) \cos(n\pi\eta), \\
 w &= C_{mn} \sin(m\pi\xi) \sin(n\pi\eta),
 \end{aligned} \quad (14.8.6)$$

where A_{mn} , B_{mn} and C_{mn} are coefficients, the values of which are determined by applying Ritz's energy method. Accordingly, we are setting to zero each partial

derivative of the total potential, Π , with respect to these coefficients. Thus, we can write

$$\frac{\partial \Pi}{\partial A_{mn}} = 0, \quad \frac{\partial \Pi}{\partial B_{mn}} = 0, \quad \frac{\partial \Pi}{\partial C_{mn}} = 0. \quad (14.8.7)$$

Next, the substitution of Eq. (14.8.6) into Eq. (14.8.5) and the above-described minimization process yield a set of equations that can be solved [14.8.3] for the vibration frequencies.

To eliminate this relatively tedious procedure, Wang derived the following *closed-form solution* [14.8.3] for the free vibration of simply supported Mindlin plates:

$$\omega_i^2 = \frac{3\kappa^2 E}{\rho h^2(1+\nu)} \left\{ \left[1 + \omega_i^* h \sqrt{\frac{\rho(1-\nu^2)}{12E}} \left(1 + \frac{2}{(1-\nu)\kappa^2} \right) \right] - \sqrt{\left[1 + \omega_i^* h \sqrt{\frac{\rho(1-\nu^2)}{12E}} \left(1 + \frac{2}{(1-\nu)\kappa^2} \right) \right]^2 - \frac{2(\omega_i^*)^2 \rho h^2(1+\nu)}{3\kappa^2 E}} \right\}, \quad (14.8.8)$$

where ω_i is the angular frequency corresponding to the i th mode of free vibration and ω_i^* represents the pertinent quantity of the Kirchhoff plate. Since the effect of rotary inertia on the free vibration of moderately thick plates is relatively small, it can be neglected without losing significant accuracy. Thus, Eq. (14.8.8) can be simplified to

$$\omega_i^2 \approx \frac{(\omega_i^*)^2}{1 + [(\omega_i^*)^2 h^2 / 6(1-\nu)\kappa^2] \sqrt{\rho h / D}}, \quad (14.8.8a)$$

where $\kappa^2 \approx \frac{5}{6}$ represents, again, the shear correction factor introduced in Sec. 1.5.

It is of considerable interest to note that Eq. (14.8.8) be used also for other types of simply supported plates having skew, circular and annular sectorial surface geometry, and it delivers almost exact solutions to such free-vibration problems. Although Wang's formula is exact only for simply supported Mindlin plates, it appears that Eq. [14.8.8] can predict angular frequencies with reasonably good accuracy for any simply supported moderately thick plates.

Furthermore, a similar energy-based approach can also be taken for other than simply supported plates, provided that the assumed displacement fields can represent the expected free-vibration patterns and satisfy the prescribed boundary conditions.

References and Bibliography

- [14.8.1] DAWE, G. J., and ROUFAIEL, O. L., "Rayleigh-Ritz Vibration Analysis of Mindlin Plates," *J. Sound Vibr.*, 69 (1980), 345–359.

- [14.8.2] HINTON, E., and VUKSANOVIC, D., "Closed Form Solutions for Dynamic Analysis of Mindlin Plates," in E. HINTON (Ed.), *Numerical Methods and Software for Dynamic Analysis of Plates and Shells*, Pineridge Press, Swansea, United Kingdom, 1987.
- [14.8.3] WANG, C. M., "Natural Frequencies Formula for Simply Supported Mindlin Plates," *Trans. ASME*, 116 (1994), 536–540.
- [14.8.4] SRINIVAS, S., and RAO, A. K., "Bending, Vibration and Buckling of Simply Supported Thick Orthotropic Rectangular Plates and Laminates," *Int. J. Solids Struct.*, 6 (1970), 1463–1481.
- [14.8.5] BRUNELLE, E. J., and ROBERTSON, S. R., "Vibration of an Initially Stressed Thick Plate," *J. Sound Vibr.*, 45 (1976), 405–416.
- [14.8.6] BAZZILY, S. F., and DICKSON, S. M., "Buckling and Lateral Vibration of Rectangular Plates Subject to In-Plane Loads: A Ritz Approach," *J. Sound Vibr.*, 24 (1972), 219–238.
- [14.8.7] ROUFAIEL, O. L., and DAWE, D. J., "Rayleigh-Ritz Vibration Analysis of Rectangular Mindlin Plates Subjected to Membrane Stresses," *J. Sound Vibr.*, 82 (1982), 263–275.

14.9 Summary and Conclusions

This chapter was devoted to the dynamic analysis of plates based on classical methods. As in static analysis, exact solutions of the differential equation of motion are limited to the simplest geometry, loading and boundary conditions. The various energy-based solution techniques offer somewhat more flexibility. However, practical dynamic problems of "real life" can be solved only by numerical methods, as shown in Chapter 15.

Since the effect of structural damping is, in most cases, of negligible order of magnitude, solutions of undamped free and forced vibrations have been emphasized. However, to provide a generally usable tool for the rare cases when damping must be considered, numerical solution of damped vibrations is briefly treated in Sec. 15.3.

Since the natural frequencies of free vibration can serve as an important index capable of describing the dynamic characteristics of plate structures, considerable attention is paid to their free-vibration analysis. For simply supported, isotropic, rectangular plates of uniform thickness, the extension of Navier's method yields the natural frequencies in a relatively simple manner. Also, the forced vibration of such plates can be solved without too much difficulty by expressing the time dependency of the forcing function in trigonometric series. Similarly, the extension of Lévy's method can yield, in a somewhat more complex way, solutions to free vibrations of rectangular plates having two opposite edges simply supported while the other two edges are free or fixed. Solution of forced vibrations of such plates, however, tends to be extremely tedious. Similar is the case of the free-vibration analysis of rectangular and circular plates having all edges free or clamped.

As mentioned previously, energy methods are somewhat more general than the above-discussed classical methods and yield remarkably accurate results even if the boundary conditions are more difficult. Application of these methods can also be extended to plates of various shapes and of variable thickness. Their accuracy, however, depends to a large extent on a suitable selection of eigenfunctions. This need to select appropriate shape functions that satisfy the geometric boundary conditions and approximate the modes of vibrations is the main disadvantage of energy methods, since it requires experience and certain skill on the part of the investigator. Methods have been introduced to facilitate the selection of suitable shape functions.

When the only information sought is the lowest natural frequency of the plate, the use of Rayleigh's method, which often yields good accuracy, is highly recommended.

A modification of Rayleigh's method by Morley uses merely the dead-load deflections of plates. In certain cases this approach can be extended to obtain natural frequencies pertinent to second and even to third modes as well. The resulting solutions, as all energy solutions, are upper bound.

The Ritz method is based on the principle of minimum potential. This approach is more general than Rayleigh's solution techniques, since it can give information on frequencies and mode shapes of higher modes. The accuracy of the first and second modes is usually good. However, the accuracy for higher than second mode, in general, deteriorates progressively. It is important to note that Ritz's method can also be applied to moderately thick plates, as demonstrated in Sec. 14.8.

Russian scientists working on the theory of elasticity have significantly contributed to the development of energy methods. Like the method of Ritz, the energy-based method developed by Galerkin assumes the solution of modal shapes in the form of series, terms of which individually satisfy all boundary conditions and have fourth derivatives.

Galerkin's approach applies the lateral displacements directly to the differential equation of motion, which leads to a simpler way of obtaining eigenvalues and eigenfunctions. In the first step, the vibration problem of plates is reduced to the evaluation of definite integrals of simple functions selected in advance. Next, this integral transformation results in a system of homogeneous linear equations that has a nontrivial solution only when the system determinant vanishes. Thus, the final solution of a plate vibration problem is further reduced to the determination of eigenvalues and eigenvectors.

Vlasov's method eliminates (1) the problem of selecting shape functions and (2) the solution of the above-mentioned eigenvalue problem. This simplification is achieved by separating the variables and by introducing linear combinations of eigenfunctions of transverse vibrations of beams as shape functions. An additional advantage of this approach is that its accuracy does not deteriorate with higher modes, as is the case for Ritz's method and to a lesser extent for Galerkin's. Although the required mathematical operations are relatively simple, they tend to be lengthy. Vlasov's method can be extended to cover forced vibrations of plates, but numerical methods are better suited to handle arbitrary plate geometry, boundary conditions and loadings. Simple estimates for forced vibrations can be obtained by applying the dynamic load factor, based on circular frequencies of the plate.

As is the case with the classical solutions of static plate problems, classical methods in plate dynamics serve one important purpose: that the results obtained can be used as benchmarks for all numerical methods.

Problems[†]

- 14.1.1.** Determine an approximate value for the lowest circular frequency of a rectangular plate ($a/b = 2$) with fixed boundary conditions by using an *equivalent single-DOF* system.
- 14.1.2.** Redo problem 14.1.1 but assume that two opposite edges are simply supported while the others are clamped.

[†] The first two numbers refer to the corresponding section.

- 14.1.3.** The plate described in problem 14.1.1 is subjected to a uniformly distributed transient load $p(t)$. Determine the dynamic response of this plate assuming that the time-dependent part of the forcing function has a triangular shape. The plate is initially at rest.
- 14.1.4.** Obtain an approximate value for the lowest natural frequency of a circular plate by using the equivalent single-DOF system. First, assume simply supported boundary conditions; next, repeat your calculation with fixed boundary.
- 14.1.5.** Find the dynamic response of the plate described in problem 14.4.1 assuming that the time-dependent part of the uniformly distributed dynamic load has a triangular shape. Find a solution to the simultaneous free and forced vibrations by using an equivalent single-DOF system.
- 14.3.1.** A simply supported rectangular plate vibrates freely. Find the mode shapes and corresponding frequencies for the second and third modes. Use the classical approach described in Sec. 14.3.
- 14.5.1.** Solve problem 14.1.1 by Rayleigh's method. Compare the result with that obtained in solving problem 14.1.1.
- 14.5.2.** Redo problem 14.5.1 by using Galerkin's approach.
- 14.5.3.** Find the lowest natural frequency of the plate shown Fig. 14.6.1 by using Vlasov's solution technique.
- 14.5.4.** Redo problem 14.5.1 using Ritz's energy-based solution method.
- 14.6.1.** Determine the lowest circular frequency of an isotropic rectangular plate ($a/b = 1.4$) by applying Morley's formula. Assume that all boundaries of the plate are fixed.
- 14.6.2.** Check the results obtained in the Illustrative Example of Sec. 14.3 using Morley's formula.
- 14.6.3.** Redo problem 14.6.1 assuming that the plate is orthotropic.
- 14.7.1.** An isotropic square plate with simple supported boundary conditions is subjected to a harmonic excitation. Consider simultaneous free and forced vibrations.
- 14.8.1.** Find the lowest circular frequency of the moderately thick RC plate shown in Fig. 14.8.1 by applying Eq. (14.8.8). Use the following dimensions for this plate: $a = 5.00$ m, $b = 7.00$ m, $h = 1.50$ m, $E = 30 \times 10^3$ MN/m² and $\nu = \frac{1}{6}$.

15

Numerical Methods in Plate Dynamics

15.1 Solution of Differential Equation of Motion by Finite Differences

a. Free Undamped Vibration. Let us assume that the plate performs harmonic oscillations about its equilibrium position; then the lateral deflections can be expressed as

$$w(x, y, t) = W(x, y) \sin \omega t, \quad (15.1.1)$$

where $W(x, y)$ is the *shape function* that satisfies the boundary conditions and represents the shape of the deflected middle surface of the vibrating plate. The time-dependent part of the harmonic oscillations is represented by $\sin \omega t$, where ω is the natural circular frequency of the plate.

The substitution of Eq. (15.1.1) into the governing differential equation of motion (14.2.4) yields

$$\nabla^2 \nabla^2 W(x, y) - \omega^2 \frac{\bar{m}}{D} W(x, y) = 0. \quad (15.1.2)$$

Replacing the derivatives by ordinary finite difference expressions as described in Sec. 5.1 (for quadratic mesh), Eq. (15.1.2) becomes

$$\begin{aligned} \frac{1}{(\Delta x)^4} [20W_{m,n} - 8(W_{m+1,n} + W_{m-1,n} + W_{m,n+1} + W_{m,n-1}) \\ + 2(W_{m+1,n+1} + W_{m-1,n+1} + W_{m+1,n-1} + W_{m-1,n-1}) \\ + W_{m+2,n} + W_{m-2,n} + W_{m,n+2} + W_{m,n-2}] = \omega^2 \frac{\bar{m}}{D} W_{m,n} \end{aligned} \quad (15.1.3)$$

The boundary value problems are also treated in the same manner as that described in Sec. 5.1.

For each finite difference mesh point, an equation similar to Eq. (15.1.3) is obtained. These algebraic equations can be written in more general terms as

$$\begin{aligned}
 a_{11}x_1 + a_{12}x_2 + a_{13}x_3 + \cdots + a_{1n}x_n &= \lambda x_1 b_1, \\
 a_{21}x_1 + a_{22}x_2 + a_{23}x_3 + \cdots + a_{2n}x_n &= \lambda x_2 b_2, \\
 a_{31}x_1 + a_{32}x_2 + a_{33}x_3 + \cdots + a_{3n}x_n &= \lambda x_3 b_3, \\
 &\vdots \\
 a_{n1}x_1 + a_{n2}x_2 + a_{n3}x_3 + \cdots + a_{nn}x_n &= \lambda x_n b_n
 \end{aligned} \tag{15.1.4}$$

or, using matrix notation,

$$\mathbf{A}\mathbf{x} = \lambda\mathbf{B}\mathbf{x}; \tag{15.1.5}$$

therefore

$$(\mathbf{A} - \lambda\mathbf{B})\mathbf{x} = 0, \tag{15.1.6}$$

where $\mathbf{x} = \{x_i\}$ is a column matrix whose elements x_i represent the amplitudes of the free vibration, $\mathbf{A} = [a_{ij}]$ is a square matrix obtained from the finite difference expression of the biharmonic operator $\nabla^2 \nabla^2(\cdot)$ and $\mathbf{B} = [b_{ii}]$ is a diagonal matrix representing the constants in the right-hand term of Eq. (15.1.3) and $\lambda = \omega^2$.

Premultiplying Eq. (15.1.6) by \mathbf{B}^{-1} , we obtain

$$(\mathbf{C} - \lambda\mathbf{I})\mathbf{x} = 0, \tag{15.1.7}$$

where $\mathbf{C} = \mathbf{B}^{-1}\mathbf{A}$ and \mathbf{I} is the identity matrix.

To have a solution of Eq. (15.1.7) other than the trivial one ($x_1, x_2, x_3, \dots, x_n = 0$), the determinant of the coefficients must equal zero; thus we can write

$$|\mathbf{C} - \lambda\mathbf{I}| = \begin{vmatrix} c_{11} - \lambda & c_{12} & c_{13} & \cdots & c_{1n} \\ c_{21} & c_{22} - \lambda & c_{23} & \cdots & c_{2n} \\ c_{31} & c_{32} & c_{33} - \lambda & \cdots & c_{3n} \\ \vdots & \vdots & \vdots & \ddots & \vdots \\ c_{n1} & c_{n2} & c_{n3} & \cdots & c_{nn} - \lambda \end{vmatrix} = 0. \tag{15.1.8}$$

The expansion of this determinant yields an n th-order equation in λ , which is called the *characteristic polynomial* or *characteristic equation*. The roots ($\lambda_1, \lambda_2, \dots, \lambda_n$) are the *characteristic numbers* or *eigenvalues* of the vibrating system, from which the natural circular frequencies

$$\omega_r = \sqrt{\lambda_r}, \quad \text{for } r = 1, 2, 3, \dots, n \tag{15.1.9}$$

can be calculated. If matrix $[c_{ij}]$ is symmetric and its diagonal elements are all positive, all eigenvalues are real. It should be noted that the characteristic polynomial may yield multiple roots. The eigenvalue problem represented by Eq. (15.1.7) is a *special* or *classical* eigenvalue problem.

The conventional Laplace expansion of the determinant (15.1.8) is generally not well suited for computer use. For digital computer expansion of large matrices, Householder's technique [7.3.11] is recommended. Householder expressed the *characteristic equation* as

$$\lambda^n + K_1\lambda^{n-1} + K_2\lambda^{n-2} + \cdots + K_{n-1}\lambda + K_n = 0, \quad (15.1.10)$$

where the coefficients K_1, K_2, \dots, K_n are defined by

$$\begin{aligned} K_1 &= -T_1, \\ K_2 &= -\frac{1}{2}(K_1T_1 + T_2), \\ K_3 &= -\frac{1}{3}(K_2T_1 + K_1T_2 + T_3), \\ &\vdots \\ K_n &= -\frac{1}{n}(K_{n-1}T_1 + K_{n-2}T_2 + \cdots + K_1T_{n-1} + T_n). \end{aligned} \quad (15.1.11)$$

In Eq. (15.1.11), $T_1, T_2, T_3, \dots, T_n$ represent the *traces* of the matrices \mathbf{A}^n , which are defined as the sum of the diagonal elements of the corresponding matrix [4.3.14]. Thus, we can write

$$\begin{aligned} T_1 &= \text{trace } \mathbf{A}, \\ T_2 &= \text{trace } \mathbf{A}^2, \\ &\vdots \\ T_n &= \text{trace } \mathbf{A}^n. \end{aligned} \quad (15.1.12)$$

Each eigenvalue gives a solution in the form

$$\mathbf{w}_{ir} = \begin{Bmatrix} W_{1r} \\ W_{2r} \\ \vdots \\ W_{nr} \end{Bmatrix} \times \sin \omega_r t = \{W_{ir}\} \sin \omega_r t. \quad (15.1.13)$$

The amplitude matrix $\{W_{ir}\}$ is the *eigenvector* pertinent to the r th eigenvalue. Since the matrix equation (15.1.6) is homogeneous, the eigenvectors cannot be uniquely defined; only the ratios of the deflection ordinates can be obtained. Normally, the largest deflection ordinate is chosen as unity and the remaining ordinates are shown as fractions of that value.

To obtain the desired information, which consists of the natural circular frequencies (eigenvalues) and the principal modes of oscillation (eigenvectors), computer programs are readily available. To be able to use these computer programs, however it is required that the problem be formulated in a matrix form similar to Eq. (15.1.7).

Improved finite difference methods, as described in Sec. 5.2, can be used to advantage to obtain high accuracy with a relatively coarse finite difference mesh. The

procedure is identical to the one described above. Thus, after introducing the inertia forces due to lateral displacements, the pertinent stencils of either the funicular polygon or the multilocal methods can be applied.

Approximate results, obtained for frequencies and mode shapes using finite difference methods, *can be improved to any desired degree of accuracy* by means of the *Stodola-Vianello* iterative procedure [14.6.7]. This simple technique is especially useful for improving frequencies and eigenfunctions associated with the first mode of free vibration.[†] The required iterative steps are as follows:

1. Obtain an approximate shape function $W^{(0)}(x, y)$ and the corresponding natural circular frequency $\omega^{(0)}$ using the ordinary finite difference method, for instance.
2. Based on the first estimate of frequency, $\omega^{(0)}$, introduce a fictitious inertia force $p_z^{(0)}$ acting in the direction of displacements. The intensity of this lateral force at the i th mesh point is given by

$$p_i^{(0)} = (\omega^{(0)})^2 \bar{m}_i W_i^{(0)}. \quad (15.1.14)$$

3. The plate is subjected to this static loading, and improved deflection ordinates $W_i^{(1)}$ of the shape function are determined, again, by the finite difference method.
4. An improved value for frequency associated with the specific mode shape can be calculated from

$$\omega^{(1)} = \sqrt{\frac{\sum_i^n p_i^{(0)} W_i^{(1)}}{\sum_i^n \bar{m}_i (W_i^{(1)})^2}} = \omega^{(0)} \sqrt{\frac{\sum_i^n W_i^{(0)} W_i^{(1)}}{\sum_i^n (W_i^{(1)})^2}}. \quad (15.1.15)$$

The iterative cycle is now repeated using $\omega^{(1)}, \omega^{(2)}, \dots$ until the last cycle shows no marked improvement in comparison with results of the previous cycle. This *self-correcting* iterative technique converges to the exact solution. Consequently, its use is highly recommended, especially in connection with the lower modes.

b. Forced Vibration. Let us now investigate the effect of time-dependent lateral forces $p_z(x, y, t)$ that act on the vibrating system. As in the previous sections, sinusoidal forcing functions, which produce steady-state vibrations, are our major interest.

Suppose that the plate is acted upon by a simple harmonic excitation,

$$p_z = P(x, y) \sin pt; \quad (15.1.16)$$

then the steady-state response, assuming that the free-vibration part is already damped, is easily obtained by using the dynamic load factor (14.1.23). Consequently,

$$w_{i,\max} = \frac{1}{1 - (p/\omega)^2} W_i, \quad (15.1.17)$$

where W_i represents the deflection ordinate at mesh point i under the peak load, taken statically.

[†] Although improvement of eigenvalues obtained by finite difference techniques are discussed here, the method is applicable to any approximate analytic or numerical method.

If the frequency of the forcing functions varies at certain mesh points, the steady-state response can be evaluated separately and the results superimposed. Similarly, the superposition technique can be applied in determining the response of the plate to arbitrary periodic excitations, as described in Secs. 14.1 and 14.5. Considerably more effort is required, however, for evaluation of the transient response unless a dynamic load factor based on a definite integral [Eq. (14.1.32)] is again introduced and the computation is carried out for a quasi-static load. Since in the finite difference approach to response analysis of plates we have idealized the vibrating system by using a network of lumped masses, the method described in the subsequent section can logically be extended to cover also finite element techniques.

Summary. The ordinary finite difference method, especially in connection with the Stodola-Vianello iterative procedure, represents a generally applicable mathematical tool for dynamic analysis of plates. This method is recommended, for example, when arbitrary geometry, variable thickness or nonuniform distribution of the dynamic load makes the use of analytical techniques too cumbersome or even impossible. Improved finite difference methods are capable of yielding high accuracy, even with relatively coarse mesh. Concerning the relative advantages and disadvantages of the various finite difference techniques, the reader is referred to Secs. 5.1 and 5.2.

ILLUSTRATIVE EXAMPLE I

Using the funicular polygon method, determine the natural circular frequencies associated with the first and second modes of a square plate with clamped boundaries.

The differential equation of free, undamped vibration is

$$\nabla^2 \nabla^2 W - \frac{\omega^2}{D} \bar{m} W = 0.$$

The mesh points are numbered as indicated in Fig. 15.1.1a. Applying Eq. (5.2.19), the following expressions for the inertia forces are obtained:

$$P_1 = \frac{(\Delta x)^2}{144} \bar{m} (100W_1 + 10W_2 + 10W_4 + W_5),$$

$$P_2 = \frac{(\Delta x)^2}{144} \bar{m} (10W_1 + 100W_2 + 10W_3 + W_4 + 10W_5 + W_6),$$

$$P_3 = \frac{(\Delta x)^2}{144} \bar{m} (10W_2 + 100W_3 + W_5 + 10W_6),$$

$$P_4 = \frac{(\Delta x)^2}{144} \bar{m} (10W_1 + W_2 + 100W_4 + 10W_5 + 10W_7 + W_8),$$

$$P_5 = \frac{(\Delta x)^2}{144} \bar{m} (W_1 + 10W_2 + W_3 + 10W_4 + 100W_5 + 10W_6 \\ + W_7 + 10W_8 + W_9),$$

$$P_6 = \frac{(\Delta x)^2}{144} \bar{m} (W_2 + 10W_3 + 10W_5 + 100W_6 + W_8 + 10W_9),$$

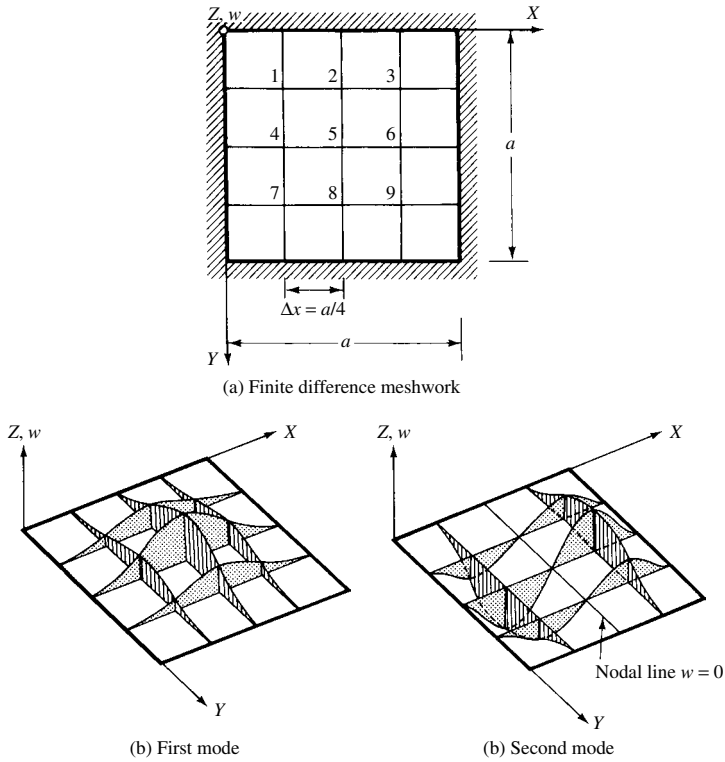


Figure 15.1.1 Free vibration of clamped square plate.

$$P_7 = \frac{(\Delta x)^2}{144} \bar{m} (10W_4 + W_5 + 100W_7 + 10W_8),$$

$$P_8 = \frac{(\Delta x)^2}{144} \bar{m} (W_4 + 10W_5 + W_6 + 10W_7 + 100W_8 + 10W_9),$$

$$P_9 = \frac{(\Delta x)^2}{144} \bar{m} (W_5 + 10W_6 + 10W_8 + 100W_9).$$

By introducing the notation $\lambda^* = \bar{m}\omega^2(\Delta x)^4/144D = \omega^2\bar{m}a^4/144 \times 256D$, the finite difference equations at the various mesh points (Figs. 5.2.10 and 5.2.14) can be written as

At point 1:

$$\begin{aligned} & 3816W_1 - 765W_2 + 120W_3 - 765W_4 \\ & - 180W_5 + 51W_6 + 120W_7 + 51W_8 + 8W_9 \\ & = \lambda^* (13,122W_1 + 2916W_2 + 162W_3 + 2916W_4 \\ & + 648W_5 + 36W_6 + 162W_7 + 36W_8 + 2W_9). \end{aligned}$$

At point 2:

$$\begin{aligned}
 & -768W_1 + 3888W_2 - 768W_3 - 132W_4 \\
 & -1134W_5 - 132W_6 + 64W_7 + 144W_8 + 64W_9 \\
 & = \lambda^*(3240W_1 + 16,524W_2 + 3240W_3 + 720W_4 \\
 & \quad + 3672W_5 + 720W_6 + 40W_7 + 204W_8 + 40W_9).
 \end{aligned}$$

At point 3:

$$\begin{aligned}
 & 120W_1 - 765W_2 + 3816W_3 + 51W_4 \\
 & -180W_5 - 765W_6 + 8W_7 + 51W_8 + 120W_9 \\
 & = \lambda^*(162W_1 + 2916W_2 + 13,122W_3 + 36W_4 \\
 & \quad + 648W_5 + 2916W_6 + 2W_7 + 36W_8 + 162W_9).
 \end{aligned}$$

At point 4:

$$\begin{aligned}
 & -768W_1 + 132W_2 + 64W_3 + 3888W_4 \\
 & -1134W_5 + 144W_6 - 768W_7 - 132W_8 + 64W_9 \\
 & = \lambda^*(3240W_1 + 720W_2 + 40W_3 + 16,524W_4 \\
 & \quad + 3672W_5 + 204W_6 + 3240W_7 + 720W_8 + 40W_9).
 \end{aligned}$$

At point 5:

$$\begin{aligned}
 & -32W_1 - 576W_2 - 32W_3 - 576W_4 \\
 & +1872W_5 - 576W_6 - 32W_7 - 576W_8 - 32W_9 \\
 & = \lambda^*(400W_1 + 2040W_2 + 400W_3 + 2040W_4 \\
 & \quad -10,404W_5 + 2040W_6 + 400W_7 + 2040W_8 + 400W_9).
 \end{aligned}$$

At point 6:

$$\begin{aligned}
 & 64W_1 - 132W_2 - 768W_3 + 144W_4 \\
 & -1134W_5 + 3888W_6 + 64W_7 - 132W_8 - 768W_9 \\
 & = \lambda^*(40W_1 + 720W_2 + 3240W_3 + 204W_4 \\
 & \quad + 3672W_5 + 16,524W_6 + 40W_7 + 720W_8 + 3240W_9).
 \end{aligned}$$

At point 7:

$$\begin{aligned}
 & 120W_1 + 51W_2 + 8W_3 - 765W_4 \\
 & -180W_5 + 51W_6 + 3816W_7 - 765W_8 + 120W_9 \\
 & = \lambda^*(162W_1 + 36W_2 + 2W_3 + 2916W_4 \\
 & \quad + 648W_5 + 36W_6 + 13,122W_7 + 2916W_8 + 162W_9).
 \end{aligned}$$

At point 8:

$$\begin{aligned} &64W_1 + 144W_2 + 64W_3 - 132W_4 \\ &- 1134W_5 - 132W_6 - 768W_7 + 3888W_8 - 768W_9 \\ &= \lambda^*(40W_1 + 204W_2 + 40W_3 + 720W_4 \\ &\quad + 3672W_5 + 720W_6 + 3240W_7 + 16,524W_8 + 3240W_9). \end{aligned}$$

At point 9:

$$\begin{aligned} &8W_1 + 51W_2 + 120W_3 + 51W_4 \\ &- 180W_5 - 765W_6 + 120W_7 - 765W_8 + 3816W_9 \\ &= \lambda^*(2W_1 + 36W_2 + 162W_3 + 36W_4 \\ &\quad + 648W_5 + 2916W_6 + 162W_7 + 2916W_8 + 13,122W_9). \end{aligned}$$

These equations are of the form

$$[A]\{W\} = \lambda^*[B]\{W\}$$

or

$$([A] - \lambda^*[B])\{W\} = 0,$$

which, premultiplied by $[B]^{-1}$, gives

$$[C] - \lambda^*[I] = 0,$$

where $[C] = [B]^{-1}[A]$. Consequently, the problem is reduced to an *eigenvalue-eigenvector problem* for which computer programs are readily available.

The results of the computer solution are as follows:

	First Mode	Second Mode
Eigenvalues	$\frac{1}{\lambda_1^*} = 28.99915$	$\frac{1}{\lambda_2^*} = 7.33362$
Eigenvectors	$W_1 = 0.27550$	$W_1 = -0.5236$
	$W_2 = 0.53268$	$W_2 = 0.0000$
	$W_3 = 0.27550$	$W_3 = 0.5236$
	$W_4 = 0.53268$	$W_4 = -1.0000$
	$W_5 = 1.00000$	$W_5 = 0.0000$
	$W_6 = 0.53268$	$W_6 = 1.0000$
	$W_7 = 0.27549$	$W_7 = -0.5236$
	$W_8 = 0.53268$	$W_8 = 0.0000$
	$W_9 = 0.27549$	$W_9 = 0.5236$

These two fundamental modes are plotted in Figs. 15.1.1b and c. Thus, the lowest natural *circular* frequency of the plate is

$$\omega_1 = \frac{12 \times 16}{5.3851} \frac{1}{a^2} \sqrt{\frac{D}{m}} = 35.65 \frac{1}{a^2} \sqrt{\frac{D}{m}} \quad \text{rad/s,}$$

which, in comparison with the “exact” solution [14.1.8], shows an error of less than 2%.

Similarly,

$$\omega_2 = \frac{12 \times 16}{2.708} \frac{1}{a^2} = 70.90 \frac{1}{a^2} \sqrt{\frac{D}{m}} \quad \text{rad/s.}$$

The error is, again, less than 2.5%. It should be noted, however, that if frequencies pertinent to higher modes are also required, the introduction of more nodal points is necessary, since limited nodal points are not able to describe the true shapes of these modes effectively.

ILLUSTRATIVE EXAMPLE II

Solve the problem given in the first example by Collatz’s multilocal method.

By introducing the notation $\lambda^* = (\Delta x)^4 \omega^2 (\bar{m}/D)$, the stencils (given in Figs. 5.2.3 and 5.2.6) yield the following finite difference equations:

At point 1:

$$448W_1 - 124W_2 + 16W_3 - 124W_4 + 8W_6 + 16W_7 + 8W_8 = \lambda^*(12W_1).$$

At point 2:

$$\begin{aligned} & -80W_1 + 336W_2 - 80W_3 + 16W_4 - 144W_5 + 16W_6 + 32W_8 \\ & = \lambda^*(2W_1 + 8W_2 + 2W_3). \end{aligned}$$

At point 3:

$$16W_1 - 124W_2 + 448W_3 + 8W_4 - 124W_6 + 8W_8 + 16W_9 = \lambda^*(12W_3).$$

At point 4:

$$\begin{aligned} & -80W_1 + 16W_2 + 336W_4 - 144W_5 + 32W_6 - 80W_7 + 16W_8 \\ & = \lambda^*(2W_1 + 8W_4 + 2W_7). \end{aligned}$$

At point 5:

$$\begin{aligned} & -2W_1 - 10W_2 - 2W_3 - 10W_4 + 36W_5 - 10W_6 - 2W_7 - 10W_8 - 2W_9 \\ & = \frac{\lambda^*}{2}(W_2 + W_4 + 2W_5 + W_6 + W_8). \end{aligned}$$

At point 6:

$$16W_2 - 80W_3 + 32W_4 - 144W_5 + 336W_6 + 16W_8 - 80W_9 \\ = \lambda^*(2W_3 + 8W_6 + 2W_9).$$

At point 7:

$$16W_1 + 8W_2 - 124W_4 + 8W_6 + 448W_7 - 124W_8 + 16W_9 \\ = \lambda^*(12W_7).$$

At point 8:

$$32W_2 + 16W_4 - 144W_5 + 16W_6 - 80W_7 + 336W_8 - 80W_9 \\ = \lambda^*(2W_7 + 8W_8 + 2W_9).$$

At point 9:

$$8W_2 + 16W_3 + 8W_4 - 124W_6 + 16W_7 - 124W_8 + 448W_9 \\ = \lambda^*(12W_9).$$

The computer solution of these homogeneous, linear, algebraic equations has yielded

$$\lambda_1^* = 5.2496 \quad \text{and} \quad \lambda_2^* = 19.5542.$$

Thus,

$$\omega_1 = 36.659 \frac{1}{a^2} \sqrt{\frac{D}{m}} \quad (\text{error} \approx 1.8\%)$$

and

$$\omega_2 = 70.75 \frac{1}{a^2} \sqrt{\frac{D}{m}} \quad (\text{error} \approx 2.5\%).$$

Comparing these results with those obtained from the funicular polygon method, it can be stated that the accuracy of the two methods in the free-vibration analysis of plates is approximately the same.

ILLUSTRATIVE EXAMPLE III

Find the lowest natural circular frequency of the plate shown in Fig. 15.1.1a by the ordinary finite difference method and improve the results by the Stodola-Vianello iterative technique.

Since we are interested merely in the circular frequency associated with the first mode, we may utilize the apparent double symmetry of the problem to reduce the number of unknowns; thus, we can write

$$W_1 = W_3 = W_7 = W_9$$

and

$$W_2 = W_4 = W_6 = W_8.$$

Let us introduce the notation $\lambda^* = (\Delta x)^4 \omega_1^2 (\bar{m}/D)$ and represent the fixed boundary conditions in accordance with Fig. 5.1.5a. The difference equations (15.1.3) can be written in matrix form as

$$\begin{bmatrix} 24 - \lambda^* & -16 & +2 \\ -16 & 26 - \lambda^* & -8 \\ +8 & -32 & 20 - \lambda^* \end{bmatrix} \begin{Bmatrix} W_1 \\ W_2 \\ W_5 \end{Bmatrix} = 0.$$

The vanishing determinant of these equations gives the *characteristic* equation

$$(\lambda^*)^3 - 70(\lambda^*)^2 + 1096(\lambda^*) - 2848 = 0.$$

The lowest root of this equation is $\lambda^* = 3.25$, obtained by Newton's method. Thus, the first estimate of the fundamental frequency is

$$\omega_1^{(0)} = \sqrt{\frac{\lambda^* D}{\bar{m}(\Delta x)^4}} = \frac{28.95}{a^2} \sqrt{\frac{D}{\bar{m}}} \quad \text{rad/s.}$$

This result, in comparison with the exact solution [14.2.1], has an error of approximately 15%. The ordinates W_i of the shape function are obtained by substituting $\lambda^* = 3.25$ into the homogeneous algebraic equations and taking the largest ordinate as unity. Thus, we have

$$\begin{bmatrix} +20.75 & -16 & +2 \\ -16 & +22.75 & -8 \\ +8 & -32 & +16.75 \end{bmatrix} \begin{Bmatrix} W_1^{(0)} \\ W_2^{(0)} \\ W_5^{(0)} = 1 \end{Bmatrix} = 0;$$

hence

$$W_1^{(0)} = 0.384 \quad \text{and} \quad W_2^{(0)} = 0.622.$$

To improve this first approximation of frequency and, that of the pertinent mode shape by the Stodola-Vianello iterative technique, we first compute the fictitious loads $p_i^{(0)}$ from Eq. (15.1.14). Next, the static deflections due to $p_i^{(0)}$ are determined from the following finite difference equations:

$$\begin{bmatrix} +24 & -16 & +2 \\ -16 & +26 & -8 \\ +8 & -32 & +20 \end{bmatrix} \begin{Bmatrix} W_1^{(1)} \\ W_2^{(1)} \\ W_5^{(1)} \end{Bmatrix} = \begin{Bmatrix} 0.384 \\ 0.622 \\ 1.00 \end{Bmatrix} (\omega_1^{(0)})^2 \bar{m} \frac{(\Delta x)^4}{D};$$

hence

$$W_1^{(1)} = 0.119(\omega_1^{(0)})^2 \bar{m} \frac{(\Delta x)^4}{D}, \quad W_2^{(1)} = 0.193(\omega_1^{(0)})^2 \bar{m} \frac{(\Delta x)^4}{D}$$

and

$$W_5^{(1)} = 0.316(\omega_1^{(0)})^2 \bar{m} \frac{(\Delta x)^4}{D}.$$

Substituting these deflection ordinates into Eq. (15.1.15), an improved value for the lowest circular frequency is obtained:

$$\omega_1^{(1)} = \sqrt{\frac{0.4897D}{0.12869\bar{m}(\Delta x)^4}} = \frac{31}{a^2} \sqrt{\frac{D}{\bar{m}}}.$$

This result has an error of approximately 9%. By repeating this iterative cycle, the accuracy of the solution can be improved further. Using static deflections for determining the first estimates $\omega_1^{(0)}$, $W^{(0)}$, as described in Sec. 14.6, even the calculation of eigenvalues and eigenvectors can be eliminated. Such an approach is of importance only if computers are not readily available and hand computation must be used, since the solution of high-order polynomials can be cumbersome. On the other hand, with advanced scientific calculators a reasonable number of algebraic equations can be solved with ease.

References and Bibliography

- [15.1.1] NISHIMURA, T., "Studies on Vibration Problems of Flat Plates by Means of Difference Calculus," in *Proc. 3rd Japan Nat. Congr. Appl. Mech.* (1953), Japan National Committee for Theoretical and Applied Mechanics, Tokyo, 1954, pp. 417–420.
- [15.1.2] IGUCHI, S., "Die Eigenwertprobleme für die elastische rechteckige Platte," in *Memoirs of the Faculty of Engineering*, Vol. 4, Hokkaido University, Sapporo, 1938, p. 305.
- [15.1.3] COLLATZ, L., *The Numerical Treatment of Differential Equations*, 3rd ed., Springer-Verlag, Berlin, 1968.
- [15.1.4] GREENWOOD, D., *Some Difference Methods of Plate Vibration Analysis*, NASA Grant NSG-63-60 CFSTI No. N62-14018, National Aeronautics and Space Administration, Washington, D.C., 1960.
- [15.1.5] WALTON, W. C., JR., *Applications of a General Finite Difference Method for Calculating Bending Deformations of Solid Plates*, NASA TN D-536, National Aeronautics and Space Administration, Washington, D.C., 1960.

15.2 Application of Finite Element Method to Plate Dynamics

15.2.1 Matrix Equations of Free Vibrations

The problem most frequently encountered in the vibration analysis of plates is to find the natural frequencies and modes of the oscillations corresponding to free vibrations. Lagrange's equations of motion written for such a system with n degrees of

freedom are

$$\begin{aligned} m_{11}\ddot{d}_1 + \cdots + m_{1n}\ddot{d}_n + k_{11}d_1 + \cdots + k_{1n}d_n &= 0, \\ m_{21}\ddot{d}_1 + \cdots + m_{2n}\ddot{d}_n + k_{21}d_1 + \cdots + k_{2n}d_n &= 0, \\ &\vdots \\ m_{n1}\ddot{d}_1 + \cdots + m_{nn}\ddot{d}_n + k_{n1}d_1 + \cdots + k_{nn}d_n &= 0, \end{aligned} \quad (15.2.1)$$

where d represents individual displacement components and k and m are the corresponding stiffness and mass components, respectively. The two dots refer to differentiation with respect to time. This set of homogeneous equations can be conveniently written in matrix form in the global reference system $\bar{X}, \bar{Y}, \bar{Z}$ of the plate:

$$\bar{\mathbf{M}} \ddot{\bar{\mathbf{d}}} + \bar{\mathbf{K}} = \{0\}, \quad (15.2.2)$$

where $\bar{\mathbf{d}}$ is the vector of displacement components and $\bar{\mathbf{M}}$ and $\bar{\mathbf{K}}$ are the mass and stiffness matrices of the vibrating system, respectively. It has already been shown that $\bar{\mathbf{K}}$ is a symmetric matrix. The same can be said for $\bar{\mathbf{M}}$, as discussed later in the subsequent section. Consequently, we can write

$$\bar{m}_{ij} = \bar{m}_{ji} \quad \text{and} \quad \bar{k}_{ij} = \bar{k}_{ji}. \quad (15.2.3)$$

Incidentally, the kinetic and potential energies may also be expressed in easily usable matrix form as

$$T = \frac{1}{2} \dot{\bar{\mathbf{d}}}^T \bar{\mathbf{M}} \dot{\bar{\mathbf{d}}} \quad \text{and} \quad U = \frac{1}{2} \bar{\mathbf{d}}^T \bar{\mathbf{K}} \bar{\mathbf{d}}. \quad (15.2.4)$$

Let us now consider a solution of Eq. (15.2.2) in the form

$$\bar{\mathbf{d}} = \{A\} \sin(\omega t + \alpha), \quad (15.2.5)$$

where $\{A\}$ is the column matrix of the amplitudes, ω represents the angular frequency and α denotes an arbitrary phase angle. Substituting this solution (15.2.5) into Eq. (15.2.2), we have

$$(\bar{\mathbf{K}} - \omega^2 \bar{\mathbf{M}}) \{A\} = \{0\}. \quad (15.2.6)$$

Let us multiply both sides of Eq. (15.2.6) by $\bar{\mathbf{K}}^{-1}$. Then,

$$(\mathbf{I} - \omega^2 \bar{\mathbf{K}}^{-1} \bar{\mathbf{M}}) \{A\} = \{0\}, \quad (15.2.7)$$

where \mathbf{I} is the unit matrix of order n . Next, let

$$\bar{\mathbf{D}} = \bar{\mathbf{K}}^{-1} \bar{\mathbf{M}}. \quad (15.2.8)$$

This matrix is called the *dynamic matrix*. Then Eq. (15.2.7) becomes

$$(\mathbf{I} - \omega^2 \bar{\mathbf{D}}) \{A\} = \{0\}, \quad (15.2.9)$$

or

$$\boxed{\mathbf{I} - \omega^2 \bar{\mathbf{D}} = \{0\}}. \quad (15.2.9a)$$

Next, let

$$\lambda = \frac{1}{\omega^2}; \quad (15.2.10)$$

then, Eq. (15.2.9) becomes

$$(\lambda \mathbf{I} - \bar{\mathbf{D}}) \{A\} = \{0\}. \quad (15.2.11)$$

This matrix equation represents a system of linear homogeneous equations in the amplitude constants $\{A\}$. For other than its trivial solution, the determinant of the coefficients must equal zero. Thus, we can write

$$\det |\lambda \mathbf{I} - \bar{\mathbf{D}}| = 0. \quad (15.2.12)$$

The expansion of this determinant yields an n th-order equation in λ for which it can be proved that all roots are real and positive. For each of the roots λ_r , we find the value of ω_r from

$$\omega_r = \sqrt{\frac{1}{\lambda_r}} \quad \text{for } r = 1, 2, 3, \dots, n. \quad (15.2.13)$$

These values of ω_r are called *natural circular frequencies* of the vibrating system. Each value of ω_r yields a solution in the form

$$\bar{\mathbf{d}}_r = \left\{ \begin{array}{c} A_{1r} \\ A_{2r} \\ \vdots \\ A_{nr} \end{array} \right\} \sin(\omega_r t + \alpha_r). \quad (15.2.14)$$

Therefore, a *general solution* of Eq. (15.2.2) is the sum of all solutions of form (15.2.14):

$$\bar{\mathbf{d}} = \sum_{r=1}^n \{A\} \sin(\omega_r t + \alpha_r). \quad (15.2.15)$$

Any particular column of amplitude constants $\{A\}$ will satisfy Eq. (15.2.6), where ω_r is used; hence

$$\omega_r^2 \bar{\mathbf{M}} \{A_r\} = \bar{\mathbf{K}} \{A_r\}. \quad (15.2.16)$$

This equation establishes the ratio of the amplitude constants. We may choose an arbitrary value—usually the expected maximum amplitude value—for any element

of $\{A\}$, and by Eq. (15.2.14) the other elements are known in terms of the chosen element. Hence, we see that the general solution (15.2.15) has $2n$ arbitrary constants, one for each column matrix of amplitudes and n values of the phase angle α . These constants may be determined for the particular vibrating plate if all amplitudes and velocities are known at a particular time. Usually, the *general solution is not of particular interest*. That is, the desired information of a freely vibrating plate consists only of the natural frequencies and corresponding mode shapes. Each solution of Eq. (15.2.14) represents a pure harmonic motion without damping and is called the *principal oscillation* of the plate. Furthermore, the amplitudes represented by the column matrix $\{A\}$ are called *natural modes* of the free oscillation. As mentioned above, normally the assumed largest amplitude is selected and the remaining amplitudes are expressed as a fraction of this value.

Equations (15.2.9) and (15.2.9a) represent a classical eigenvalue-eigenvector problem of mathematical physics. As already stated in the previous section, solution of eigenvalue problems by using the characteristic equation resulting from the expansion of Eq. (12.2.12) is a very difficult task. Thus, it can be used only in the case of small vibrating systems with a limited number of degrees of freedom. Fortunately, numerous very usable eigenvalue-eigenvector subroutines readily available in the pertinent literature [15.2.1–15.2.6] are usually based on vector iteration such as Houshoder's or Jacobi's transformation procedures. In general, in using such computer programs one can choose to determine one of the following options:

- all eigenvalues and eigenvectors,
- all eigenvalues and some eigenvectors and
- some eigenvalues and the corresponding eigenvectors.

The reader will find readily usable computer programs for dynamic analysis of plates in the WinPlatePrimer 2001 program system (see Appendix A.4.2). Furthermore, nowadays most of the commercially available larger program systems have provisions for vibration analysis of large structural systems, including those for plates and shells.

An important property of the eigenfunctions is known as the *orthogonality relationship*, which has already been briefly mentioned in Sec. 4.3 in connection with vibrating beams. The orthogonality conditions of natural modes state that

$$\begin{aligned}\bar{\mathbf{d}}_r^T \bar{\mathbf{M}} \bar{\mathbf{d}}_s &= 0 \quad \text{for } r \neq s, \\ \bar{\mathbf{d}}_r^T \bar{\mathbf{K}} \bar{\mathbf{d}}_s &= 0 \quad \text{for } r \neq s,\end{aligned}\tag{15.2.17}$$

where $\bar{\mathbf{d}}_r$ and $\bar{\mathbf{d}}_s$ are any two column matrices of amplitude constants associated with ω_r and ω_s circular frequencies, respectively. These relationships can also be used to check the accuracy of the computed eigenvectors. In addition, one may also utilize the matrix form of Rayleigh's quotient

$$\lambda_r = \frac{\bar{\mathbf{d}}_r^T \bar{\mathbf{K}} \bar{\mathbf{d}}_r}{\bar{\mathbf{d}}_r^T \bar{\mathbf{M}} \bar{\mathbf{d}}_r}\tag{15.2.18}$$

to checking the obtained natural frequencies and even to *improve* them.

15.2.2 Mass Matrix

a. Lumped Masses. In the finite element approach to plate dynamics, the mass matrix $\bar{\mathbf{M}}$, represents the inertia properties of the plate structure. In plate structures the mass is always a continuously distributed property. Consequently, if we use a discrete solution technique such as the FEM, we must also discretize the continuous mass of the plates, as we did with its load-carrying stiffness properties. The most common and easiest approach is lumping the masses at the nodal points according to their corresponding tributary areas. In the case of a rectangular element, for instance, we simply divide the total mass of the element by 4 and put the results along the diagonal of the mass matrix of the element, \mathbf{M}_e , with sequence w_1, w_2, w_3, w_4 . To combine the element mass matrices \mathbf{M}_e into the mass matrix $\bar{\mathbf{M}}$ of the total structure, we follow the procedures introduced in Sec. 7.2 for stiffness matrices. However, to avoid the undesirable zeros in the principal diagonal of the dynamic matrix $\bar{\mathbf{D}}$, the lumped rotary inertias can also be approximated by taking the mass moment of inertia of thin-plate elements. Thus, if we employ rectangular finite elements, for instance, for an internal nodal point of the discretized plate, we may use

$$\bar{m}_{ii} \approx \mu ab, \quad \bar{m}_{jj} \approx \frac{1}{12} \mu ba^3 \quad \text{or} \quad \bar{m}_{jj} \approx \frac{1}{12} \mu ab^3 \quad (15.2.19)$$

in the principal diagonal of the mass matrix of the system. In this expressions μ represents the mass of the plate per unit area. Thus, the lumped mass matrix of the plate has the following diagonal form:

$$\bar{\mathbf{M}} = \begin{bmatrix} \bar{m}_{11} & & & & & \\ & \bar{m}_{22} & & & & \\ & & \bar{m}_{33} & & & \\ & & & \ddots & & \\ & & & & \bar{m}_{ii} & \\ & & & & & \bar{m}_{jj} \\ & & & & & & \ddots \\ & & & & & & & \bar{m}_{nn} \end{bmatrix}. \quad (15.2.19a)$$

An important advantage of this simple lumping process is that it contributes only diagonal terms in the mass matrix; that is, an acceleration of the i th degree of freedom is affected only by the inertia of that degree of freedom and is independent of the others. Such diagonal mass matrices offer considerable computational advantage because they are easy to store and invert; in addition, they preserve the all-important symmetry of the dynamic matrix $\bar{\mathbf{D}}$. Consequently, the use of lumped mass matrices considerably simplifies the solution of the resulting matrix equations of motion.

In many plate problems, it may be sufficient to use lumped masses in their dynamic analysis, provided that a sufficiently large number of elements is used. However, the error created by lumping the masses increases with higher modes and with the complexity of the finite elements employed in the dynamic analysis [15.2.7].

b. Kinematically Consistent Mass Matrices. In the finite element formulation of the free vibration of plates, the accuracy of the eigenvalues, especially those pertinent to higher modes, can be improved by using the so called *kinematically-consistent mass matrices*. Such mass matrices can be derived by comparing the kinetic energy of the original structure with that of the discretized finite element system.

The most important convergence criterion of the FEM requires that the energy of the substitute discretized system approaches that of the original continuum when the number of elements is increased. In the dynamic analysis, the total energy of the vibrating system also includes the kinetic energy. Considering, for instance, only the kinetic energy associated with the lateral translation of a rectangular plate, the convergence criterion involving the kinetic energy of the plate element can be written as

$$\frac{1}{2} \int_0^a \int_0^b \mu(x, y) \left(\frac{\partial w}{\partial t} \right)^2 dx dy \approx \bar{\mathbf{d}}_e^T \mathbf{M}_e \mathbf{d}_e, \quad (15.2.20)$$

where \mathbf{M}_e is the mass matrix of the element and \mathbf{d}_e represents the corresponding vector of displacements.

Let us express the lateral deflection $w(x, y)$ of the plate as the sum of the products of the shape functions N_i associated with the unit displacement of the nodes and that of the pertinent displacement d_i ; thus we can write

$$w(x, y, t) = \sum_{i=1}^r N_i(x, y) d_i(t). \quad (15.2.21)$$

Substitution of Eq. (15.2.21) into Eq. (15.2.20) yields the coefficients of the kinematically consistent mass matrix for a rectangular plate element in the form

$$m_{ij} = \mu \int_0^a \int_0^b N_i(x, y) \times N_j(x, y) dx dy. \quad (15.2.22)$$

The same result is obtained by determining the concentrated dynamic nodal forces corresponding to the distributed inertia force system (e.g., $\mu \ddot{w}$) by applying the concept of virtual work. Following this second approach, we state that the work done by the concentrated dynamic forces assigned to the nodes equals the work done by the distributed dynamic forces acting on the element. Assuming the same time dependency $\theta(t)$ for the element displacements as for the displacements of the nodes, we obtain

$$\ddot{\theta}(t) m_{ij} \times 1 = \ddot{\theta}(t) \int_0^a \int_0^b \mu N_i(x, y) \times N_j(x, y) dx dy, \quad (15.2.23)$$

which reduces to Eq. (15.2.22).

The shape functions N_i and N_j are identical to those used in derivations of stiffness coefficients. Consequently, the stiffness and inertia properties of the finite elements are intimately related.

The mass matrix for a rectangular plate element in matrix form becomes

$$\mathbf{M}_e = \mu \int_0^a \int_0^b \mathbf{N}_i^T \mathbf{N}_j \, dx \, dy, \quad (15.2.24)$$

where \mathbf{N}_i and \mathbf{N}_j represent the corresponding matrices of the shape functions. We can also use the *generalized coordinates*, as described in Sec. 7.3. In this case, the shape functions can also be expressed as $\mathbf{N} = \mathbf{\Phi} \mathbf{A}^{-1}$. Thus, the mass matrix of the plate element becomes

$$\mathbf{M}_e = \mu [\mathbf{A}^T]^{-1} \left(\int_0^a \int_0^b \mathbf{\Phi}^T \mathbf{\Phi} \, dx \, dy \right) \mathbf{A}^{-1}. \quad (15.2.25)$$

Similar procedures can be used for triangular elements. However, usually numerical integrations must be employed to evaluate Eq. (15.2.22). Consequently, explicit formulations for mass matrices of triangular elements are rare.

For the simple rectangular plate-element (Fig. 7.6.1) Dawe [15.2.8] obtained the consistent mass matrix in the following explicit form:

$$\mathbf{M}_e = \mathbf{Q} \hat{\mathbf{M}} \mathbf{Q}, \quad (15.2.26)$$

where

$$\mathbf{Q} = \begin{bmatrix} \mathbf{q} & 0 & 0 & 0 \\ 0 & \mathbf{q} & 0 & 0 \\ 0 & 0 & \mathbf{q} & 0 \\ 0 & 0 & 0 & \mathbf{q} \end{bmatrix} \quad \text{with} \quad \mathbf{q} = \begin{bmatrix} 1 & 0 & 0 \\ 0 & a & 0 \\ 0 & 0 & b \end{bmatrix} \quad (15.2.27)$$

and

$$\mathbf{M} = \frac{\mu ab}{25,200} \times \begin{bmatrix} 3454 & & & & & & & & & & & \\ 461 & 80 & & & & & & & & & & \\ -461 & -63 & 80 & & & & & & & & & \\ 1226 & 199 & -274 & 3454 & & & & & & & & \\ 199 & 40 & -42 & 461 & 80 & & & & & & & \\ 274 & 42 & -60 & 461 & 63 & 80 & & & & & & \\ 394 & 116 & -116 & 1226 & 274 & 199 & 3454 & & & & & \\ -116 & -30 & 28 & -274 & -60 & -42 & -461 & 80 & & & & \\ 116 & 28 & -30 & 199 & 42 & 40 & 461 & -63 & 80 & & & \\ 1226 & 274 & -199 & 394 & 116 & 116 & 1226 & -199 & 274 & 3454 & & \\ -274 & -60 & 42 & -116 & -30 & -28 & -199 & 40 & -42 & -461 & 80 & \\ -199 & -42 & 40 & -116 & -28 & -30 & -274 & 42 & -60 & -461 & 63 & 80 \end{bmatrix} \begin{matrix} 1 \\ 2 \\ 3 \\ 4 \\ 5 \\ 6 \\ 7 \\ 8 \\ 9 \\ 10 \\ 11 \\ 12 \end{matrix} \quad (15.2.28)$$

Since the coefficients m_{ij} of the element mass matrix are not overly sensitive to the correctness of the shape functions used in their evaluation, we can considerably simplify the required procedures by employing the products of beam shape functions[†] in Eq. (15.2.24). The obtained simplified element mass matrix, which yields quite acceptable results in the dynamic analysis of plates, is given in Table 15.2.1.

For the higher-order rectangular plate element shown in Fig. 7.7.1, we use the shape functions given in Eq. (7.7.5) to generate coefficients of the corresponding mass matrix. These can be expressed by

$$m_{ij} = \frac{\mu ab}{1225} \beta_7 a^{\beta_5} b^{\beta_6}, \quad (15.2.29)$$

where the required parameters β_5 , β_6 and β_7 are listed in Table 7.7.1. Furthermore, the *index scheme* given in Table 7.7.2 is also valid for Eq. (15.2.29).

We can also formulate a usable *quasi-consistent* mass matrix for a rectangular gridwork cell by proportionally assigning the mass of the plate (corresponding to the cell area) only to the beams located at its boundaries and by utilizing the following mass matrix of a typical beam (Fig. 15.2.1):

$$(\mathbf{M}_{e,b})^{(N)} = \frac{(\mu^* l)^{(N)}}{420} \begin{bmatrix} 1 & 2 & 3 & 4 \\ 156 & 22l & 54 & -13l \\ 22l & 4l^2 & 13l & -3l^2 \\ 54 & 13l & 156 & -22l \\ -13l & -3l^2 & -22l & 4l^2 \end{bmatrix} \begin{matrix} 1 \\ 2 \\ 3 \\ 4 \end{matrix}, \quad (15.2.30)$$

where μ^* represents the allocated mass of the beam per unit length. As usual, by changing the local numbering in Eq. (15.2.30) to the global one and summing the mass coefficients of identical indices, as we always do by developing the pertinent stiffness matrices for a cell, we obtain the mass matrix given in Table 15.2.2. Equation (12.2.30) can also be successfully applied to Salonen's triangular gridwork[‡] by using, again, a procedure similar to that employed in formulating the stiffness matrix of the system. Furthermore, an analogous procedure is also required when the local coordinate axes of the element are not parallel to those of the global ones. In such a case, the usual coordinate transformation

$$(\mathbf{M}_e')^{(N)} = (\mathbf{T}\mathbf{M}_e\mathbf{T}^T)^{(N)} \quad (15.2.31)$$

is also necessary before compiling the mass matrix of the total system from the mass matrices of the individual elements.

It is of interest to know that, in general, the use of kinematically consistent mass matrices results in upper-bound solutions for natural frequencies, while the lumped mass matrix approach gives lower-bound results, as illustrated in Fig. 15.2.1. Consequently, one can calculate the average of these results to improve the required frequencies without resorting to fine subdivisions.

Although the inverted stiffness matrix $\bar{\mathbf{K}}^{-1}$ of the system and the consistent mass matrix $\bar{\mathbf{M}}$ of the plate are symmetric matrices, their product, the dynamic matrix $\bar{\mathbf{D}}$, is unsymmetric. It is usually very difficult to obtain eigenvalues of an unsymmetric matrix that is larger than 150×150 . If only the first three lowest eigenvalues

[†] See Illustrative Example III.

^{*} See Sec. 6.2.

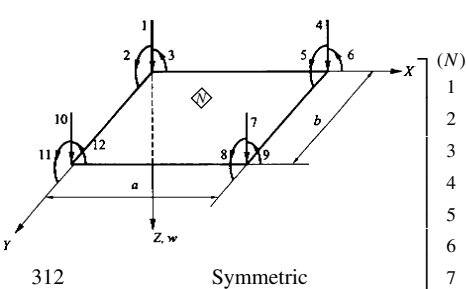
Table 15.2.1 Simplified Consistent Mass Matrix for Rectangular Plate Elements

$\mathbf{MM}_e^{(N)} = (\mu a^2 b^2)^{(N)} \times$	1	2	3	4	5	6	7	8	9	10	11	12
1	$\frac{169}{1225} \cdot \frac{1}{ab}$											
2	$\frac{858}{44,100} \cdot \frac{1}{a}$	$\frac{13}{3675} \cdot \frac{b}{a}$										
3	$-\frac{858}{44,100} \cdot \frac{1}{b}$	$-\frac{121}{44,100}$	$\frac{13}{3675} \cdot \frac{a}{b}$									
4	$\frac{117}{2450} \cdot \frac{1}{ab}$	$\frac{297}{44,100} \cdot \frac{1}{a}$	$\frac{-2028}{176,400} \cdot \frac{1}{b}$	$\frac{169}{1225} \cdot \frac{1}{ab}$								
5	$\frac{297}{44,100} \cdot \frac{1}{a}$	$\frac{9}{7350} \cdot \frac{b}{a}$	$\frac{-143}{88,200}$	$\frac{858}{44,100} \cdot \frac{1}{a}$	$\frac{13}{3675} \cdot \frac{b}{a}$							
6	$\frac{2028}{176,400} \cdot \frac{1}{b}$	$\frac{143}{88,200}$	$\frac{-13}{4900} \cdot \frac{a}{b}$	$\frac{858}{44,100} \cdot \frac{1}{b}$	$\frac{121}{44,100}$	$\frac{13}{3675} \cdot \frac{a}{b}$						
7	$\frac{81}{4900} \cdot \frac{1}{ab}$	$\frac{117}{29,400} \cdot \frac{1}{a}$	$\frac{-117}{29,400} \cdot \frac{1}{b}$	$\frac{117}{2450} \cdot \frac{1}{ab}$	$\frac{2028}{176,400} \cdot \frac{1}{a}$	$\frac{297}{44,100} \cdot \frac{1}{b}$	$\frac{169}{1225} \cdot \frac{1}{ab}$					
8	$-\frac{117}{29,400} \cdot \frac{1}{a}$	$-\frac{9}{9800} \cdot \frac{b}{a}$	$\frac{169}{176,400}$	$\frac{-2028}{176,400} \cdot \frac{1}{a}$	$\frac{-13}{4800} \cdot \frac{b}{a}$	$\frac{-143}{88,200}$	$\frac{-858}{44,100} \cdot \frac{1}{a}$	$\frac{13}{3675} \cdot \frac{b}{a}$				
9	$\frac{117}{29,400} \cdot \frac{1}{b}$	$\frac{169}{176,400}$	$\frac{-9}{9800} \cdot \frac{a}{b}$	$\frac{297}{44,100} \cdot \frac{1}{b}$	$\frac{143}{88,200}$	$\frac{9}{7350} \cdot \frac{a}{b}$	$\frac{858}{44,100} \cdot \frac{1}{b}$	$\frac{-121}{44,100}$	$\frac{13}{3675} \cdot \frac{a}{b}$			
10	$\frac{117}{2450} \cdot \frac{1}{ab}$	$\frac{2028}{176,400} \cdot \frac{1}{a}$	$\frac{-297}{44,100} \cdot \frac{1}{b}$	$\frac{81}{4900} \cdot \frac{1}{ab}$	$\frac{117}{29,400} \cdot \frac{1}{a}$	$\frac{117}{29,400} \cdot \frac{1}{b}$	$\frac{117}{2450} \cdot \frac{1}{ab}$	$\frac{-297}{44,100} \cdot \frac{1}{a}$	$\frac{2028}{176,400} \cdot \frac{1}{b}$	$\frac{169}{1225} \cdot \frac{1}{ab}$		
11	$-\frac{2028}{176,400} \cdot \frac{1}{a}$	$\frac{-13}{4900} \cdot \frac{b}{a}$	$\frac{143}{88,200}$	$\frac{-117}{29,400} \cdot \frac{1}{a}$	$\frac{-9}{9800} \cdot \frac{b}{a}$	$\frac{-169}{176,400}$	$\frac{-297}{44,100} \cdot \frac{1}{a}$	$\frac{9}{7350} \cdot \frac{b}{a}$	$\frac{-143}{88,200}$	$\frac{-858}{44,100} \cdot \frac{1}{a}$	$\frac{13}{3675} \cdot \frac{b}{a}$	
12	$-\frac{297}{44,100} \cdot \frac{1}{b}$	$\frac{-143}{88,200}$	$\frac{9}{7350} \cdot \frac{a}{b}$	$\frac{-117}{29,400} \cdot \frac{1}{b}$	$\frac{-169}{176,400}$	$\frac{9800}{176,400} \cdot \frac{a}{b}$	$\frac{-2028}{176,400} \cdot \frac{1}{b}$	$\frac{143}{88,200}$	$\frac{-13}{4900} \cdot \frac{a}{b}$	$\frac{-858}{44,100} \cdot \frac{1}{b}$	$\frac{121}{44,100}$	$\frac{13}{3675} \cdot \frac{a}{b}$

Table 15.2.2 Quasi-Consistent Mass Matrix for Quadratic Gridwork Cells

$$\mathbf{M}_e^{(N)} = \frac{(\mu a^2)^{(N)}}{1680} \times$$

312											
22a	4a ²										
-22a	0	4a ²									
54	0	-13a	312								
0	0	0	22a	4a ²							
13a	0	-3a ²	22a	0	4a ²						
0	0	0	54	13a	0	312					
0	0	0	-13a	-3a ²	0	-22a	4a ²				
0	0	0	0	0	0	22a	0	4a ²			
54	13a	0	0	0	0	54	0	13a	312		
-13a	-3a ²	0	0	0	0	0	0	0	-22a	4a ²	
0	0	0	0	0	0	-13a	0	-3a ²	-22a	0	4a ²
1	2	3	4	5	6	7	8	9	10	11	12



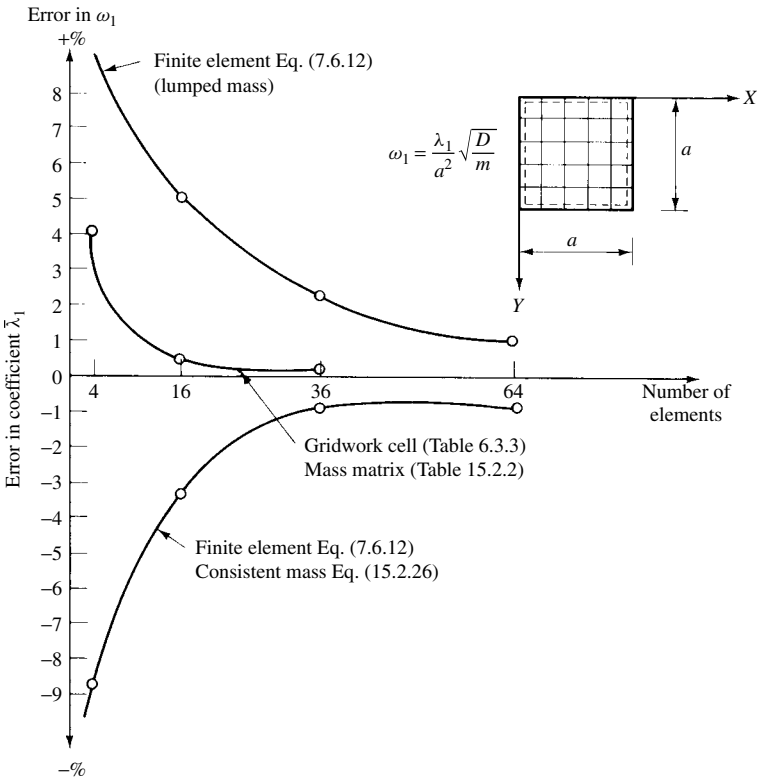


Figure 15.2.1 Convergence characteristics of various mass representations.

are of interest, the iterative method and Rayleigh's quotient can be applied. However, the obtainable accuracy of these procedures is not always satisfactory. A better approach, especially if all eigenvalues should be determined, is to apply simple matrix manipulations to obtain an equivalent symmetric dynamic matrix.

For this purpose, we write the mass matrix in triangular form,

$$\bar{\mathbf{M}} = \bar{\mathbf{L}} \bar{\mathbf{L}}^T, \quad (15.2.32)$$

in which $\bar{\mathbf{L}}$ is the lower triangular matrix having only zero coefficients above the principal diagonal. Furthermore, multiplying Eq. (12.2.9a) by $\bar{\mathbf{D}}^{-1}$, the eigenvalue problem of the free vibration of plates becomes

$$\boxed{\bar{\mathbf{D}}^{-1} - \lambda \mathbf{I} = \{0\}}. \quad (15.2.33)$$

Substituting Eq. (15.2.32), we obtain

$$\bar{\mathbf{L}}^{T-1} \bar{\mathbf{L}}^{-1} \bar{\mathbf{K}} - \lambda \mathbf{I} = \{0\}, \quad (15.2.34)$$

which premultiplied by $\bar{\mathbf{L}}^T$ gives

$$\bar{\mathbf{L}}^{-1} \bar{\mathbf{K}} - \lambda \bar{\mathbf{L}}^T \mathbf{I} = \{0\}. \quad (15.2.35)$$

Postmultiplying this equation by $[\bar{\mathbf{L}}^T]^{-1}$ yields

$$\bar{\mathbf{L}}^{-1} \bar{\mathbf{K}} [\bar{\mathbf{L}}^T]^{-1} - \lambda \mathbf{I} = \{0\}, \quad (15.2.36)$$

or

$$\mathbf{C} - \lambda \mathbf{I} = \{0\}. \quad (15.3.37)$$

Since Eqs. (15.2.34) and (15.2.36) are the same, matrix \mathbf{C} has to be symmetric.

ILLUSTRATIVE EXAMPLE I

Determine the coefficients m_{27} and m_{89} of a kinematically consistent mass matrix corresponding to the rectangular finite element shown in Fig. 7.6.1 using the product of beam functions (Fig. 7.5.7) as simplified shape functions.

Introducing the notations $\xi = x/a$ and $\eta = y/b$, respectively, the simplified shape functions can be written as

$$\begin{aligned} N_2(\xi, \eta) &= b[(1 - \eta)^2 \eta] \times [3(1 - \xi)^2 - (1 - \xi)^3] \\ &= b(\eta - 2\eta^2 + \eta^3) \times (1 - 3\xi^2 + 2\xi^3), \\ N_7(\xi, \eta) &= (3\xi^2 - 2\xi^3) \times (3\eta^2 - 2\eta^3), \\ N_8(\xi, \eta) &= -b[\eta^2(1 - \eta) \times (3\xi^2 - 2\xi^3)], \\ N_9(\xi, \eta) &= a(\xi^2 - \xi^3) \times (3\eta^2 - 2\eta^3). \end{aligned} \quad (15.2.38)$$

These expressions substituted in Eq. (15.2.22) give

$$\begin{aligned}
 m_{27} &= \mu ab \int_0^1 \int_0^1 N_2(\xi, \eta) \times N_7(\xi, \eta) d\xi d\eta \\
 &= \mu ab^2 \left[\int_0^1 (3\xi^2 - 2\xi^3)(1 - 3\xi^2 + 2\xi^3) d\xi \right] \\
 &\quad \times \left[\int_0^1 (\eta - 2\eta^2 - \eta^3)(3\eta^2 - 2\eta^3) d\eta \right] = \frac{117}{29,400} \mu ab^2
 \end{aligned} \tag{15.2.39}$$

and

$$\begin{aligned}
 m_{89} &= -\mu a^2 b^2 \left[\int_0^1 (\xi^2 - \xi^3)(3\xi^2 - 2\xi^3) d\xi \right] \\
 &\quad \times \left[\int_0^1 (\eta^2 - \eta^3)(3\eta^2 - 2\eta^3) d\eta \right] = -\frac{121}{44,100} \mu a^2 b^3.
 \end{aligned} \tag{15.2.40}$$

These results agree with the corresponding coefficients of the mass matrix given in Table 15.2.1

ILLUSTRATIVE EXAMPLE II

Let us determine the lowest circular frequency ω_1 of the clamped square plate shown in Fig. 15.2.2a, by applying the FEM.

We discretize the plate by only four finite elements (Fig. 15.2.2b). Utilizing the apparent double symmetry of the plate, we can deal with one element. By changing the local number 9 to global number $\bar{1}$, Eq. (7.7.7) gives, in connection with the corresponding Table 7.7.1, the stiffness coefficient

$$\bar{k}_{11} = \bar{\mathbf{K}} = \frac{D}{(a/2)^2} \left(\frac{156}{35} + \frac{156}{35} + \frac{72}{25} \right) = 11.7943 \frac{D}{(a/2)^2}. \tag{15.2.41}$$

Similarly, we calculate the corresponding coefficient of the mass matrix from Eq. (15.2.29). This gives

$$\bar{m}_{11} = \bar{\mathbf{M}} = \frac{\mu (a/2)^2}{1225} 169 = 0.138 \mu \left(\frac{a}{2} \right)^2. \tag{15.2.42}$$

From the eigenvalue problem

$$[\bar{\mathbf{K}} - \omega_1^2 \bar{\mathbf{M}}] \bar{\mathbf{d}}_1 = \{0\}, \tag{15.2.43}$$

we obtain

$$\omega_1^2 = \frac{\bar{\mathbf{K}}}{\bar{\mathbf{M}}} \approx \frac{\bar{k}_{11}}{\bar{m}_{11}} = \frac{11.7943}{0.138(a/2)^4} \frac{D}{\mu} = \frac{85.46}{(a/2)^4} \frac{D}{\mu}, \tag{15.2.44}$$

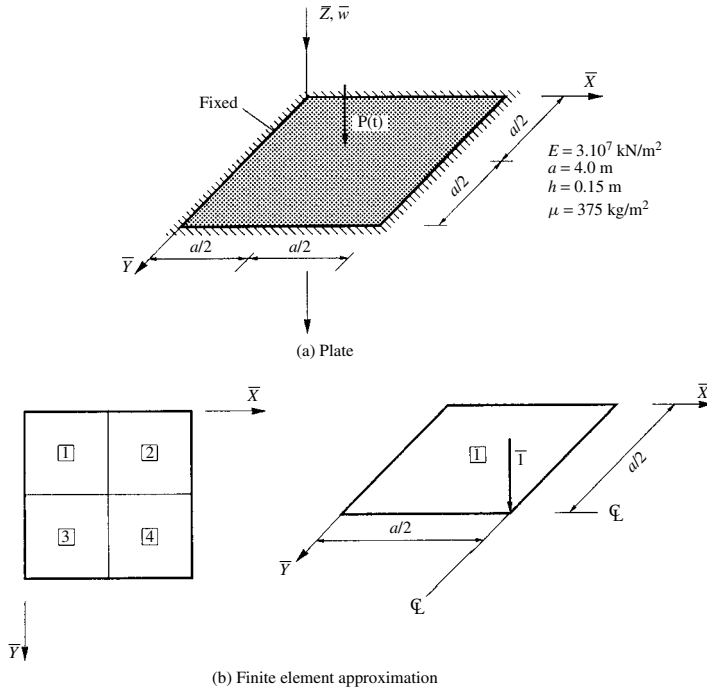


Figure 15.2.2 Dynamic analysis of clamped plate.

from which

$$\omega_1 = \frac{36.98}{a^2} \sqrt{\frac{D}{\mu}} \quad (\text{rad/s}) \quad (\text{error: } +2.7\%). \quad (15.2.45)$$

ILLUSTRATIVE EXAMPLE III

The static response of the simply supported plate shown in Fig. 6.4.9a was already determined by using the gridwork method. Now, we are interested in its free-vibration behavior. Thus, let us compute the lowest circular frequency ω_1 and the corresponding mode of vibration of this plate using the same gridwork approach.

For the free-vibration analysis the required stiffness matrix $\bar{\mathbf{K}}$ of the analysis quadrant (Fig. 6.4.9b) is already established during the static analysis of the plate and is listed on the left-hand side of Eq. (6.4.22). Next, we calculate the diagonal elements of the lumped mass matrix using the approximations given in Eq. (15.2.19). These calculations result in

$$\begin{aligned} \bar{m}_{11} &= \frac{1}{4} \mu a^2 = 0.14063 \mu, & \bar{m}_{22} &= \bar{m}_{99} = \frac{1}{2} \mu a^2 = 0.28125 \mu, \\ \bar{m}_{33} &= \bar{m}_{10,10} = \frac{1}{24} \mu a^4 = 0.01318 \mu, & \bar{m}_{44} &= \bar{m}_{11,11} = \frac{1}{48} \mu a^4 = 0.00659 \mu, \\ \bar{m}_{55} &= \bar{m}_{12,12} = \frac{1}{24} \mu a^4 = 0.01318 \mu, & \bar{m}_{66} &= \mu a^2 = 0.56250 \mu, \\ \bar{m}_{77} &= \bar{m}_{88} = \frac{1}{12} \mu a^4 = 0.02637 \mu. \end{aligned} \quad (15.2.46)$$

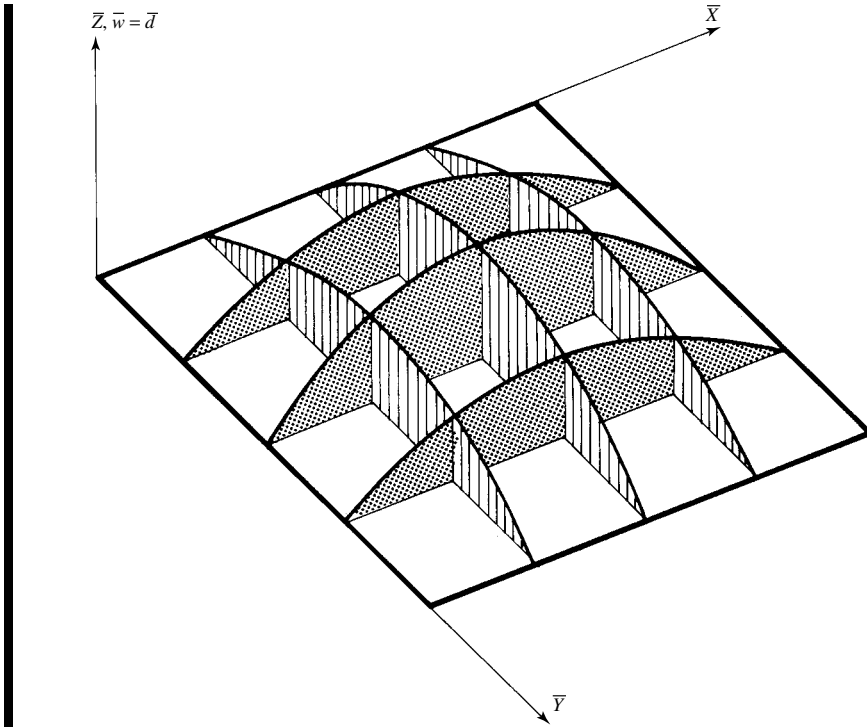


Figure 15.2.3 First mode shape of simply supported plate.

- a finer subdivision,
- a gridwork cell with better convergence characteristics such as the one given in Table 6.3.3 and
- the quasi-consistent mass matrix (Table 15.2.2).

15.2.3 Forced Vibrations

a. Estimating Dynamic Response Using DLF. Strictly speaking, the dynamic load factor (DLF) introduced in Sec. 14.1 is valid only for undamped single-DOF systems. However, its use can be extended for *estimating* the dynamic response of plates. That is, the maximum dynamic deflections produced by the dynamic load $P(t)$ applied to a plate with neither initial displacements nor initial velocity can be approximated by

$$\bar{\mathbf{d}}_{\text{dynamic}} \approx \bar{\mathbf{d}}_{\text{static}} \times (\text{DLF}). \quad (15.2.52)$$

This equation states that the structural response produced by a given dynamic load is independent of motion of the structure when the load is applied. In this case, the static displacements $\bar{\mathbf{d}}_{\text{static}}$ are determined by the FEM. The DLF is usually computed using Eq. (14.1.32).

The dynamic response determined with the help of the DLF can also be superimposed on the free vibration caused by initial displacements or initial velocity.

Consequently, we can also estimate the *total* dynamic behavior of a plate that already has displacements and velocity when subjected to the dynamic load $P(t)$.

b. Harmonic Analysis. The first stage of the dynamic response of a structural system before the free part is damped out is called the *transient state* and will be discussed subsequently. The stage after the free part of vibration has been damped out, the *steady state*, will be discussed first.

We assume that the plate is subjected to a harmonic forcing function with Ω exiting frequency. Such harmonic force, for instance, may be exerted by reciprocating electric motors supported by the plate. In this case, dynamic response of the plate can be classified as *steady-state* vibration, and the pertinent equation of undamped motion can be written as

$$\bar{\mathbf{M}}\ddot{\bar{\mathbf{d}}} + \bar{\mathbf{K}}\bar{\mathbf{d}} = \bar{\mathbf{p}}_0 \sin \Omega t, \quad (15.2.53)$$

where $\bar{\mathbf{p}}_0$ represents the time-independent vector of amplitudes. Alternate forms for the forcing function are

$$\bar{\mathbf{p}}(t) = \bar{\mathbf{p}}_0 \sin (\Omega t \pm \alpha) \quad (15.2.53a)$$

and

$$\bar{\mathbf{p}}(t) = \bar{\mathbf{p}}_0 e^{i\Omega t}. \quad (15.2.53b)$$

In Eq. (15.2.53a) α is the phase-lag angle, as shown in Fig. 11.1.1c.

After the free-vibration phase dies out, the plate moves with the frequency of the exiting function. Consequently, the solution of Eq. (15.2.53) can be written as

$$\bar{\mathbf{d}}_P(t) = \bar{\mathbf{d}}_P \sin \Omega t, \quad (15.2.54a)$$

$$\bar{\mathbf{d}}_P(t) = \bar{\mathbf{d}}_P \sin (\Omega t + \alpha), \quad (15.2.54b)$$

$$\bar{\mathbf{d}}_P(t) = \bar{\mathbf{d}}_P e^{i\Omega t}. \quad (15.2.54c)$$

Substituting, for instance, Eq. (15.2.54a) in the equation of motion (15.2.53), we obtain a set of simultaneous algebraic equations in the form

$$[\bar{\mathbf{K}} - \Omega^2 \bar{\mathbf{M}}] \bar{\mathbf{d}}_P = \bar{\mathbf{p}}_0, \quad (15.2.55)$$

the solution of which is

$$\bar{\mathbf{d}}_P = [\bar{\mathbf{K}} - \Omega^2 \bar{\mathbf{M}}]^{-1} \bar{\mathbf{p}}_0 \quad (15.2.56)$$

and represents the amplitude vector of the forced part of the harmonic vibration. A similar procedure can be applied when using Eqs. (15.2.53a) and (15.2.53b), respectively. In many cases, it can be advantageous to divide the forcing function in two parts,

$$\bar{\mathbf{p}}(t) = \bar{\mathbf{p}}_1 \sin \Omega t + \bar{\mathbf{p}}_2 \cos \Omega t, \quad (15.2.57)$$

and use similar expressions for the displacements,

$$\bar{\mathbf{d}}_r(t) = \bar{\mathbf{d}}_{r,1} \sin \Omega t + \bar{\mathbf{d}}_{r,2} \cos \Omega t \quad (15.2.58)$$

It should be noted, however, that using the FEM steady-state vibration analysis results are accurate only for forcing frequencies ranging from zero to an upper bound that depends on the mesh size of the FEM.

In engineering practice, dynamic forces acting on plates are typically *transient*, that is, of limited duration. Even if the time dependency of a transient force is of a *general* nature, we can still represent such force by piecewise periodic functions using Fourier series expansion, as discussed in Appendix A.1 and demonstrated in Illustrative Example II of this section. With arbitrary transient forces, usually the *half-range* expansions (sine or cosine) are preferred. We assume that the nonperiodic excitation is a periodic one having a relatively long period T compared to the actual duration of the disturbance and expand the nonperiodic function into sine series, for instance. Because of the assumed linearity of the vibrating system, we analyze the structure for each individual term in the series expansion in the manner discussed above. The final dynamic response of the system will consist of the sum of the responses of these harmonic components. The result will improve by increasing the period of expansion. The “exact” solution is obtained when T approaches infinity. But usually, the use of long enough T and consideration of a sufficient number of terms in the half-range expansion yield sufficient accuracy for all practical purposes. Standard computer programs are available for harmonic analysis of structures. This procedure can be considered one of the most useful because the dynamic response of the plates to arbitrary (in space and time) exiting forces can be evaluated using the principle of superposition, even when the time dependency of the dynamic force varies from nodal point to nodal point.

The procedure for such harmonic analysis is, assuming that all nodal forces have the same time dependency, the following.

Harmonic Analysis Procedure

- The governing differential equation of motion in matrix form is

$$\overline{\mathbf{M}}\ddot{\overline{\mathbf{d}}}(t) + \overline{\mathbf{K}}\overline{\mathbf{d}}(t) = \overline{\mathbf{p}}(t)$$

- The time-dependent forcing function is expressed by Fourier sine series

$$\overline{\mathbf{p}}(t) = \sum_{m=1}^N \overline{\mathbf{p}}_m \sin \Omega_m t$$

- A similar expression is used for the time-dependent displacement vector

$$\overline{\mathbf{d}}(t) = \sum_{m=1}^N \overline{\mathbf{d}}_m \sin \Omega_m t$$

- Substitution of force and displacement vectors into the differential equation of motion gives for each term m of the series expression:

$$[\overline{\mathbf{K}} - \Omega_m^2 \overline{\mathbf{M}}]\overline{\mathbf{d}}_m = \overline{\mathbf{p}}_m$$

- The corresponding displacement vector is computed from

$$[\bar{\mathbf{K}} - \Omega_m^2 \bar{\mathbf{M}}]^{-1} \bar{\mathbf{p}}_m = \bar{\mathbf{d}}_m$$

- The sum of these solutions gives the deflections in function of time, thus

$$\bar{\mathbf{d}}(t) = \sum_{m=1}^N \bar{\mathbf{d}}_m \sin \Omega_m t$$

c. Numerical Integration Methods.[†] Numerical integration of the equation of motion consists in obtaining numerical values of displacements and velocities at discrete times Δt . This can be achieved by *step-by-step* integration procedures, starting with necessary initial conditions and evaluating the equation of motion at the end of discrete time increments $t + \Delta t$. The better-known numerical integration procedures are

- the constant-acceleration method,
- the linear acceleration procedure and
- the constant-velocity approach.

In this section we will only consider two variants of the constant-acceleration method that are currently the most applied numerical integration techniques.

Newmark's method. In his paper [15.2.9], Newmark extended the linear acceleration method that had been commonly used up to the year 1959. He approximated the velocities and displacements of a multi-DOF system at the incremental time $t + \Delta t$ with the following assumptions:

$$\begin{aligned} \dot{\mathbf{d}}_{t+\Delta t} &= \dot{\mathbf{d}}_t + [(1 - \delta)\ddot{\mathbf{d}}_t + \delta\ddot{\mathbf{d}}_{t+\Delta t}]\Delta t, \\ \mathbf{d}_{t+\Delta t} &= \mathbf{d}_t + \dot{\mathbf{d}}_t \Delta t + \left[\left(\frac{1}{2} - \alpha\right)\ddot{\mathbf{d}}_t + \alpha\ddot{\mathbf{d}}_{t+\Delta t}\right]\Delta t^2, \end{aligned} \quad (15.2.59)$$

where α and δ are parameters that govern the accuracy and stability of the procedure and the dots indicate differentiation with respect to time t . The parameter α produces an algorithmic damping within the time step Δt .

In addition, the equilibrium of the vibrating system at time $t + \Delta t$ is also used by considering the corresponding matrix equation

$$\mathbf{M}_{t+\Delta t} \ddot{\mathbf{d}} + \mathbf{C} \dot{\mathbf{d}}_{t+\Delta t} + \mathbf{K} \mathbf{d}_{t+\Delta t} = \mathbf{p}_{t+\Delta t}, \quad (15.2.60)$$

where \mathbf{C} represents the damping matrix of the system to be discussed in the next section. For undamped systems $\mathbf{C} = 0$. When $\delta = \frac{1}{2}$ and $\alpha = \frac{1}{4}$, this numerical procedure is unconditionally stable. Newmark's constant-acceleration scheme is illustrated in Fig. 15.2.4.

[†] To simplify the presentation of matrix equations, in this section we omit the overbars since it would interfere with other notation.

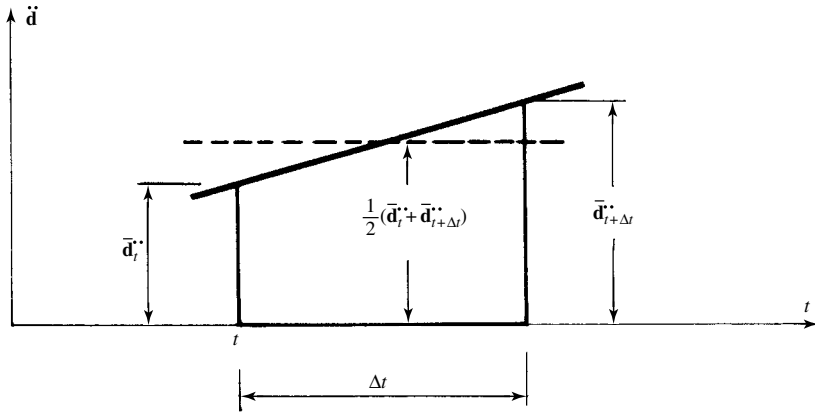


Figure 15.2.4 Average acceleration.

Rather than going into a detailed discussion of the underlying derivations,[†] we restrict ourself here only to a description of the step-by-step procedure. The solution algorithm starts with computation of the initial conditions of \mathbf{d}_t , $\dot{\mathbf{d}}_t$ and $\ddot{\mathbf{d}}_t$ and selection of time step Δt . Next, the parameters

$$\delta \geq 0.5 \quad \text{and} \quad \alpha \geq 0.25 (0.5 + \delta)^2 \quad (15.2.61)$$

are calculated along with the integrations constants

$$\begin{aligned} a_0 &= \frac{1}{\alpha \Delta t^2}, & a_1 &= \frac{\delta}{\alpha \Delta t}, & a_2 &= \frac{1}{\alpha \Delta t}, & a_3 &= \frac{1}{2\alpha} - 1, \\ a_4 &= \frac{\delta}{\alpha} - 1, & a_5 &= \frac{\Delta t}{2} \left(\frac{\delta}{\alpha} - 2 \right), & a_6 &= \Delta t (1 - \delta), & a_7 &= \delta \Delta t \end{aligned} \quad (15.2.62)$$

required for the subsequent step. This involves the use of an *effective* stiffness matrix

$$\hat{\mathbf{K}} = \mathbf{K} + a_0 \mathbf{M} + a_1 \mathbf{C} \quad (15.2.63)$$

and that of the corresponding *effective* load vector computed from

$$\hat{\mathbf{p}}_{t+\Delta t} = \mathbf{p}_{t+\Delta t} + \mathbf{M}(a_0 \mathbf{d}_t + a_2 \dot{\mathbf{d}}_t + a_3 \ddot{\mathbf{d}}_t) + \mathbf{C}(a_1 \mathbf{d}_t + a_4 \dot{\mathbf{d}}_t + a_5 \ddot{\mathbf{d}}_t). \quad (15.2.64)$$

In the next step, we solve the matrix equation

$$\mathbf{d}_{t+\Delta t} = \hat{\mathbf{K}}^{-1} \hat{\mathbf{p}}_{t+\Delta t} \quad (15.2.65)$$

to obtain the displacement vector at time $t + \Delta t$. Consequently, the corresponding accelerations are

$$\ddot{\mathbf{d}}_{t+\Delta t} = a_0 (\mathbf{d}_{t+\Delta t} - \mathbf{d}_t) - a_2 \dot{\mathbf{d}}_t - a_3 \ddot{\mathbf{d}}_t. \quad (15.2.66)$$

Similarly, the velocities at time $t + \Delta t$ become

$$\dot{\mathbf{d}}_{t+\Delta t} = \dot{\mathbf{d}}_t + a_6 \ddot{\mathbf{d}}_t + a_7 \ddot{\mathbf{d}}_{t+\Delta t}. \quad (15.2.67)$$

[†] For details see Ref. [15.2.9].

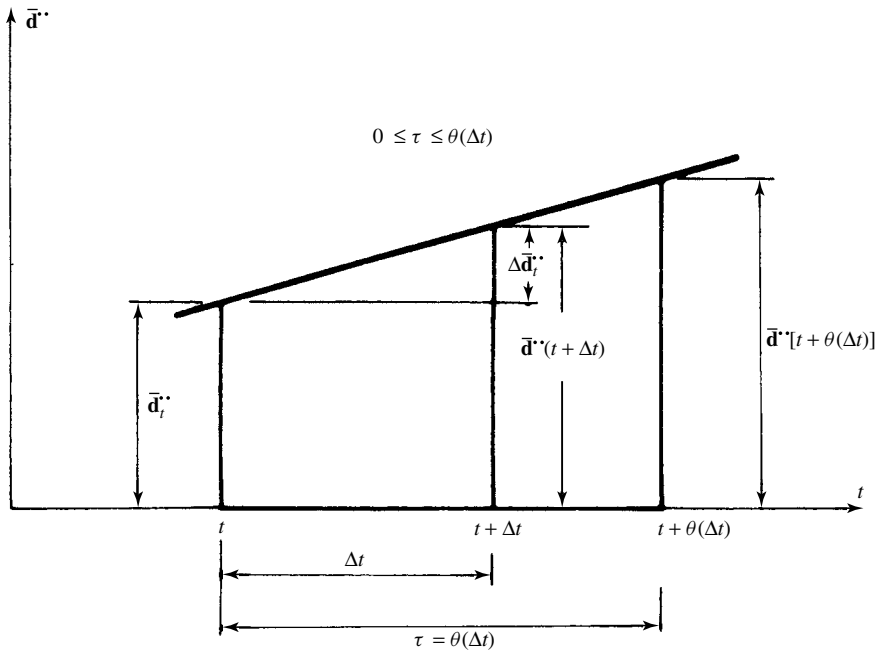


Figure 15.2.5 Linear acceleration with extended time step.

From these results, the initial conditions for the next time step are given. The whole process can then be repeated for as many steps as desired.

Wilson's θ -method. This numerical step-by-step integration procedure is, again, an extension of the linear acceleration method in which a linear variation of accelerations from time t to time $t + \Delta t$ is used. The basic assumption of Wilson's θ -approach [15.2.10] is that the acceleration \ddot{d} varies linearly even over an extended time step $\tau = \theta(\Delta t)$, as illustrated in Fig. 15.2.5. During this time step the incremental acceleration is $\Delta \ddot{d}_\tau = \theta(\Delta \ddot{d}_t)$. It can be shown that for the value $\theta = 1.4$ the method has an unconditional numerical stability.

Based on the linear acceleration assumption, the acceleration at the end of the extended time can be expressed by

$$\ddot{d}_{t+\tau} = \ddot{d}_t + \frac{\tau}{\theta(\Delta t)}(\ddot{d}_{t+\tau} - \ddot{d}_t). \quad (15.2.68)$$

By integrating this equation with respect to time, we obtain the matrix equation for the velocities at time $t + \tau$ as

$$\dot{d}_{t+\tau} = \dot{d}_t + \ddot{d}_t \tau + \frac{\tau^2}{2\theta(\Delta t)}(\ddot{d}_{t+\tau} - \ddot{d}_t) \quad (15.2.69)$$

and the corresponding vector of displacements in the form

$$d_{t+\tau} = d_t + \dot{d}_t \tau + \frac{1}{2} \ddot{d}_t \tau^2 + \frac{1}{6\theta(\Delta t)} \tau^3 (\ddot{d}_{t+\tau} - \ddot{d}_t). \quad (15.2.70)$$

From Eq. (15.2.69) and (15.2.70) we have

$$\dot{\mathbf{d}}_{t+\tau} = \frac{3}{\theta(\Delta t)}(\mathbf{d}_{t+\tau} - \mathbf{d}_t) - 2\dot{\mathbf{d}}_t - \frac{\theta(\Delta t)}{2}\ddot{\mathbf{d}}_t \quad (15.2.71)$$

and

$$\ddot{\mathbf{d}}_{t+\tau} = \frac{6}{\theta^2(\Delta t)^2}(\mathbf{d}_{t+\tau} - \mathbf{d}_t) - \frac{6}{\theta(\Delta t)}\dot{\mathbf{d}}_t - 2\ddot{\mathbf{d}}_t. \quad (15.2.72)$$

In addition, a linearly *extrapolated* load vector is employed in the matrix equation of equilibrium,

$$\mathbf{M}\ddot{\mathbf{d}}_{t+\tau} + \mathbf{C}\dot{\mathbf{d}}_{t+\tau} + \mathbf{K}\mathbf{d}_{t+\tau} = \mathbf{p}_t + \theta(\mathbf{p}_{t+\Delta t} - \mathbf{p}_t), \quad (15.2.73)$$

to obtain the solutions for the displacements, velocities and accelerations at time $t + \Delta t$.

The corresponding algorithm for this integration process, based on Refs. [15.2.11] and [15.2.13], is given here in detail.

After computing \mathbf{K} , \mathbf{M} and \mathbf{C} ,[†] the initial conditions for \mathbf{d}_0 , $\dot{\mathbf{d}}_0$ and $\ddot{\mathbf{d}}_0$ are determined and the time step Δt is selected. In addition, the integration constants

$$\begin{aligned} a_0 &= \frac{6}{\theta(\Delta t)^2}, & a_1 &= \frac{3}{\theta(\Delta t)}, & a_2 &= 2a_1, \\ a_3 &= \frac{\theta(\Delta t)}{2}, & a_4 &= \frac{a_0}{\theta}, & a_5 &= -\frac{a_2}{\theta}, \\ a_6 &= 1 - \frac{3}{\theta}, & a_7 &= \frac{\Delta t}{2}, & a_8 &= \frac{(\Delta t)^2}{6} \end{aligned} \quad (15.2.74)$$

are calculated. Next, the *effective* stiffness matrix

$$\hat{\mathbf{K}} = \mathbf{K} + a_0\mathbf{M} + a_1\mathbf{C} \quad (15.2.75)$$

along with the *effective* load vector

$$\hat{\mathbf{p}}_{t+\tau} = \mathbf{p}_t + \theta(\mathbf{p}_{t+\Delta t} - \mathbf{p}_t) + \mathbf{M}(a_0\mathbf{d}_t + a_2\dot{\mathbf{d}}_t + 2\ddot{\mathbf{d}}_t) + \mathbf{C}(a_1\mathbf{d}_t + 2\dot{\mathbf{d}}_t + a_3\ddot{\mathbf{d}}_t) \quad (15.2.76)$$

are computed.

Solution of the pseudostatic matrix equation

$$\mathbf{d}_{t+\tau} = (\hat{\mathbf{K}})^{-1}\hat{\mathbf{p}}_{t+\tau} \quad (15.2.77)$$

[†] For undamped systems $\mathbf{C} = 0$.

yields the displacement vector at the end of the extended time $t + \tau$. Hence, the vectors of displacements, velocities and accelerations at time $t + \Delta t$ can be determined from

$$\begin{aligned}\ddot{\mathbf{d}}_{t+\Delta t} &= a_4(\mathbf{d}_{t+\tau} - \mathbf{d}_t) + a_5\dot{\mathbf{d}}_t + a_6\ddot{\mathbf{d}}_t, \\ \dot{\mathbf{d}}_{t+\Delta t} &= \dot{\mathbf{d}}_t + a_7(\ddot{\mathbf{d}}_{t+\Delta t} + \ddot{\mathbf{d}}_t), \\ \mathbf{d}_{t+\Delta t} &= \mathbf{d}_t + (\Delta t)\dot{\mathbf{d}}_t + a_8(\ddot{\mathbf{d}}_{t+\Delta t} + 2\ddot{\mathbf{d}}_t).\end{aligned}\tag{15.2.78}$$

In general, the dynamic analysis of a plate structure by this method gives good accuracy for motions of structures associated with periods of vibration at least 5–10 times greater than the selected time steps Δt . In Refs. [15.2.11], [15.2.13] and [15.2.14], the will reader find readily usable computer programs for Wilson's θ -method.

Summary. In the preceding discussions of the dynamic response of plates, it has been assumed that the structure is linear elastic. In this section, we introduced three numerical methods for dealing with *forced* vibrations:

- dynamic load factors (DLFs),
- harmonic analysis based on Fourier series representation of the forcing function and
- direct integration of the matrix equation of motion.

At first glance, use of the DLF appears to be the most attractive choice, provided the engineer is interested only in obtaining the maximum dynamic effects, that is, displacements and/or stresses. For instance, with the help of Duhamel *integral* provided in Eq. (14.1.32), the maximum transient response of the structure is obtained by multiplying its static response by the DLF. If the applied forcing function is given in analytical form, the definite integral can be evaluated by formal integration. But even in such a case, the integration process may be too tedious. Thus, to make practical use of the DLF approach, it is advisable to use numerical integration procedures.

On the other hand, if the dynamic response analysis must cover the entire time domain, one can apply one of two fundamentally different numerical approaches: (a) harmonic analysis or (b) step-by-step integration of the matrix equation of motion.

Harmonic analysis is employed to study the steady-state vibration of plates for a specific frequency range. That is, if the exciting frequency is approximately equal to one of the natural frequencies of the plate, a near resonance occurs; that is, the response amplitude can increase substantially. An extension of harmonic analysis involves determination of the dynamic response in the time domain due to transient forces. In this case, the time-dependent load is expressed usually by half-range Fourier expansions, and the superposition of the resulting terms of sine- or cosine-type excitations yields the dynamic response of the structure in the time domain, as demonstrated in Illustrative Example II of this section. This method is easy and economical; in addition, it is unconditionally stable even when one of the terms of the Fourier series is an "illusory" resonance with the plate. The relatively new concept of *fast Fourier transform* [15.2.15] has made harmonic analysis even more appealing to engineers working with real-life dynamic problems.

Numerical integration methods integrate the matrix equation of motion step by step. Instead of trying to always satisfy this differential equation, the aim is to satisfy it only at discrete time intervals Δt apart. The basic assumption of these procedures is that acceleration varies linearly during the load time increments while the properties of the structure remain constant during these time steps. Although such an approach is simple in concept, it may require *extremely small* time steps to achieve numerical stability. This aspect makes the method impractical or even impossible to use. In contrast, the two variants of the linear acceleration methods discussed in this section offer unconditional numerical stability. Newmark's method uses a constant-acceleration formula. Thus, the acceleration of the vibrating system at the beginning of time step Δt is taken to be constant within the step. Another widely used modification of the linear acceleration method due to Wilson [15.2.10] and co-workers applies a θ -factor to expand the linearity of accelerations beyond the Δt interval. For $\theta = 1.4$ this approach is also unconditionally stable.

ILLUSTRATIVE EXAMPLE I

A rectangular plate with fixed boundaries (Fig. 15.2.6a) is subjected to a uniformly distributed transient load in the form

$$p(t^*) = p_0 \left(1 - \frac{t^*}{t_d} \right), \quad (15.2.79)$$

where $p_0 = 10.0 \text{ kN/m}^2$ and the duration of the suddenly applied triangular load is $t_d = 0.1 \text{ s}$ (Fig. 15.2.6b). Assuming that the plate is initially at rest, let us determine the maximum dynamic response of this plate by applying a corresponding DLF.

Since we can utilize the double symmetry of the structure and the load, it is sufficient to analyze only one quadrant of the vibrating system. This analysis quadrant is discretized by nine finite elements, as shown in Fig. 15.2.6c. Using the conforming plate element with 16 DOFs, introduced in Sec. 7.7.1, our computation yielded the following lateral displacements[†] under load p_0 that was assumed to act statically:

$$\bar{\mathbf{w}}_{\text{stc}} = \left\{ \begin{array}{l} W_1 = 0.705 \\ W_2 = 0.643 \\ W_3 = 0.459 \\ W_4 = 0.184 \\ W_6 = 0.563 \\ W_7 = 0.515 \\ W_8 = 0.369 \\ W_9 = 0.149 \\ W_{11} = 0.227 \\ W_{12} = 0.209 \\ W_{13} = 0.152 \\ W_{14} = 0.052 \end{array} \right\} 10^{-2} \text{ m}. \quad (15.2.80)$$

[†] Zero displacements are not given.

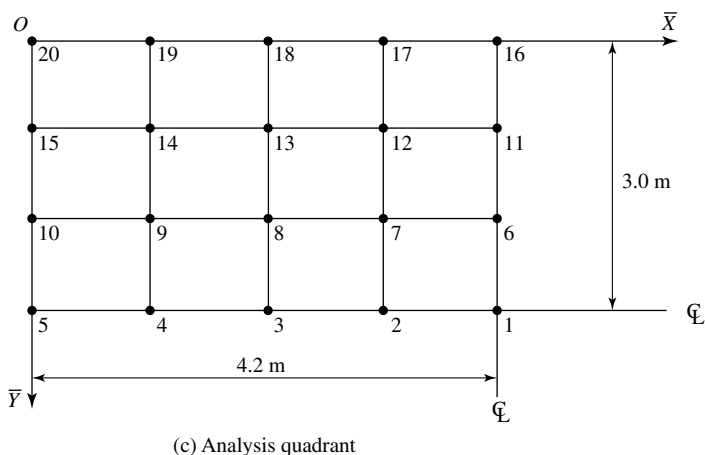
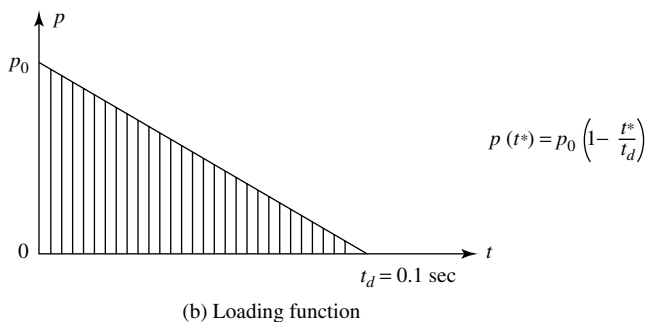
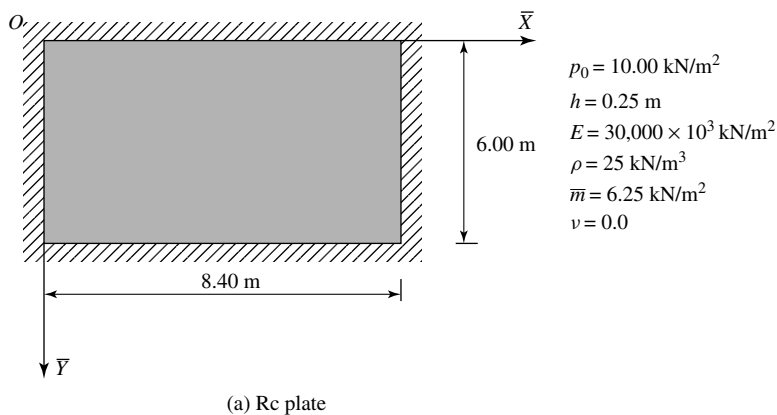


Figure 15.2.6 Dynamically loaded RC plate.

The corresponding maximum moments are

$$\begin{aligned}
 m_{x, \textcircled{1}} &= 12.202 \text{ kN-m/m}, & m_{y, \textcircled{1}} &= 4.333 \text{ kN-m/m}, \\
 m_{x, \textcircled{16}} &= -25.55 \text{ kN-m/m}.
 \end{aligned}
 \tag{15.2.81}$$

Next, using Morley's formula, given in Eq. (14.6.8), we calculate the circular frequency of the plate by utilizing only the static deflection ordinates. Thus, we obtain

$$\omega_1 \approx \sqrt{8 \frac{\sum_{i=1}^4 W_i + 4 \sum_{i=6}^{14} W_i}{\sum_{i=1}^4 W_i^2 + 4 \sum_{i=6}^{14} W_i^2}} = \sqrt{8.91 \frac{10.935 \times 10^{-2}}{4.603 \times 10^{-4}}} = 46 \text{ rad/s.} \quad (15.2.82)$$

With a finer subdivision, we improve the value of the circular frequency to $\omega_2 = 54 \text{ rad/s}$. Hence the period of free vibration becomes $T = 2\pi/\omega_2 = 0.116 \text{ s}$. For the triangular forcing function given in Fig. 15.2.6b, Duhamel's integral and hence the DLF is

$$\text{DLF} = \frac{1}{2\pi(t_d/T)} \left[\sin 2\pi \frac{t}{T} - \sin 2\pi \left(\frac{t}{T} - \frac{t_d}{T} \right) \right] - \cos 2\pi \frac{t}{T}. \quad (15.2.83)$$

The plot of the maximum DLF as a function of the ratio t_d/T , shown in Fig. 14.1.6, gives $\text{DLF}_{\max} \approx 1.6$. Consequently, the maximum dynamic response of the plate can be *estimated* as

$$\begin{aligned} w_{\max} &= 1.6 \times 0.705 \times 10^{-2} = 1.12 \times 10^{-2} \text{ m,} \\ +m_{x,\max} &= 1.6 \times 12.202 = 19.52 \text{ kN-m/m,} \\ +m_{y,\max} &= 1.6 \times 4.333 = 6.93 \text{ kN-m/m,} \\ -m_{x,\max} &= -1.6 \times 25.55 = -40.88 \text{ kN-m/m.} \end{aligned} \quad (15.2.84)$$

It is evident that the dynamic nature of the load significantly increases the response of the plate.

ILLUSTRATIVE EXAMPLE II

The plate shown in Fig. 15.2.2 is now subjected to a concentrated dynamic load acting at its center. The time dependency of this suddenly applied load has the shape of an isosceles triangle (Fig. 15.2.7) with duration $t_d = 0.5 \text{ s}$. Let us determine the maximum deflection of the plate, $w_{\max}(t)$, in the time domain.

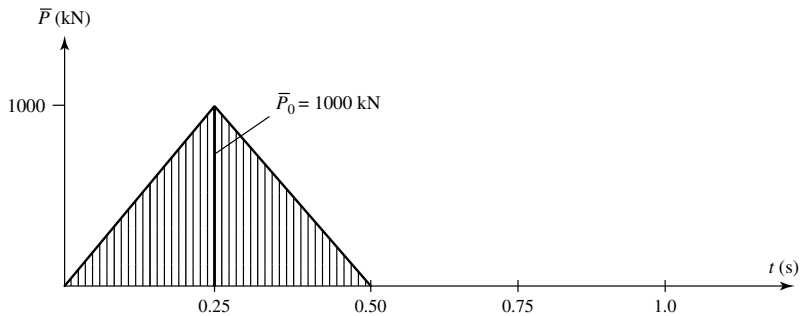


Figure 15.2.7 Loading function.

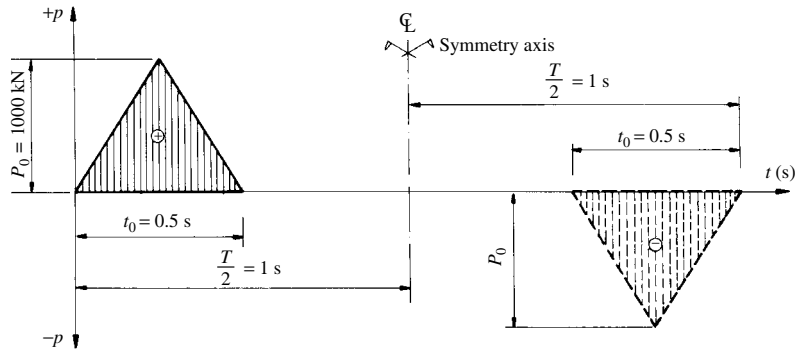
The plate is discretized by using four conforming finite elements introduced in Sec. 7.7.1. Since the structure and load have double symmetry, it is sufficient to consider only one quarter plate. In our case, this substitute structure consists of only one element (Fig. 15.2.2b). Its characteristic structural properties are already determined in the Illustrative Example II of Sec. 15.2.2 and are given in Eqs. (15.2.41) and (15.2.42). Since the substitute structure has only one degree of freedom, these coefficients simultaneously represent the corresponding stiffness matrix $\bar{\mathbf{K}}$ and mass matrix $\bar{\mathbf{M}}$ respectively.

Applying the *harmonic analysis* technique, we express one-fourth of the loading function by sine series. For this purpose, we arbitrarily continue the actual load, as shown in Fig. 15.2.8, and employ the half-range Fourier expansion, as described in Appendix A.1. This gives

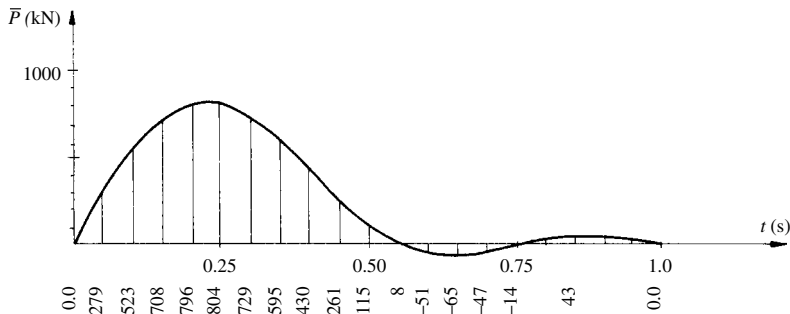
$$\bar{P}_1(t) \approx \sum_{m=1}^3 \bar{P}^* \sin \Omega_m t = \frac{1}{4} (336.4 \sin \Omega t + 408.6 \sin 2\Omega t + 221.5 \sin 3\Omega t), \quad (15.2.85)$$

where

$$\Omega_m = m\Omega = \frac{m2\pi}{T} = m\pi \quad \text{for } m = 1, 2, 3. \quad (15.2.86)$$



(a) Arbitrary continuation of loading function



(b) Three terms in sine series

Figure 15.2.8 Fourier series representation of transient load.

Repeated solution of the equation of motion,

$$(\bar{\mathbf{K}} - \Omega_m^2 \bar{\mathbf{M}}) \bar{\mathbf{d}}_m = \bar{\mathbf{p}}_m \quad \text{or} \quad (k_{11} - \Omega_m^2 \bar{m}_{11}) = P_m^* \quad \text{for } m = 1, 2, 3, \quad (15.2.87)$$

gives

$$\bar{d}_m = \frac{\bar{P}_m^*}{\bar{k}_{11} - \Omega_m^2 \bar{m}_{11}}, \quad (15.2.88)$$

or with $\bar{k}_{11} = 25,915$ and $\bar{m}_{11} = 207$,

$$\bar{d}_1 = 3.52 \times 10^{-3}, \quad \bar{d}_2 = 5.75 \times 10^{-3}, \quad \bar{d}_3 = 7.36 \times 10^{-3}. \quad (15.2.89)$$

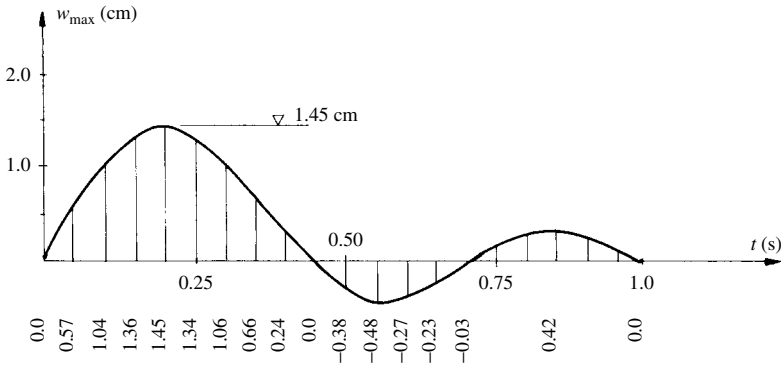


Figure 15.2.9 Dynamic response in function of time.

Consequently, the maximum deflection of the plate in the time domain (Fig. 15.2.9) becomes

$$w_{\max}(t) = (3.52 \sin \Omega t + 5.75 \sin 2\Omega t + 7.36 \sin 3\Omega t) \times 10^{-3}. \quad (15.2.90)$$

In comparison with the maximum deflection caused by the statically applied load P_0 , we can state, again, that the dynamic response of the plate is considerably greater.

References and Bibliography

- [15.2.1] GRIFFITHS, D. V., and SMITHS, I. M., *Numerical Methods for Engineers*, CRC Press, Boca Raton, Florida, 1991.
- [15.2.2] PRESS, H. W., et al., *Numerical Recipes in FORTRAN 90: The Art of Parallel Scientific Computing*, Cambridge University Press, Cambridge, Massachusetts, 2000.
- [15.2.3] ACTON, F. S., *Numerical Methods That Works*, Mathematical Association of America, Washington, D.C., 1990.
- [15.2.4] WILKINSON, J. H., and REINSCH, C., *Handbook of Automatic Computation*, Vol. 2: *Linear Algebra*, Springer-Verlag, New York, 1971.

- [15.2.5] SMITH, B. T., *Lecture Notes in Computer Science*, Vol. 6: *Matrix Eigensystem Routines, EISPACK Guide*, 2nd ed., Springer-Verlag, New York, 1976.
- [15.2.6] STOER, J., and BULIRSCH, R., *Introduction to Numerical Analysis*, Springer-Verlag, New York, 1980.
- [15.2.7] CLOUGH, R. W., "Analysis of Structural Vibrations and Dynamic Response," in Y. Gallagher et al. (Eds.), *Recent Advances in Matrix Structural Analysis and Design*, University of Alabama Press, Huntsville, Alabama, 1971.
- [15.2.8] DAWE, D. J., "A Finite Element Approach to Plate Vibration Problems," *J. Mech. Eng. Sci.*, 7 (1965), 28.
- [15.2.9] NEWMARK, N. M., "A Method of Computation in Structural Dynamics," *J. Struct. Div., ASCE*, 85 (Mar. 1959), 67–94.
- [15.2.10] WILSON, E. L., et al., "Nonlinear Dynamic Analysis of Complex Structures," *Earthquake Eng., Struct. Dynam.*, 1 (1973), 241–252.
- [15.2.11] BATHE, K. J., *Finite Element Procedures*, Prentice-Hall, Upper Saddle River, New Jersey, 1996.
- [15.2.12] PAZ, M., *Microcomputer Aided Engineering: Structural Dynamics*, Van Nostrand Reinhold Co., New York, 1986.
- [15.2.13] PAZ, M., *Structural Dynamics: Theory and Computation*, 4th ed., Kluwer Academic Publishers, Norwell, Massachusetts, 1997.
- [15.2.14] WEAVER, W., and JOHNSTON, P. R., *Structural Dynamics by Finite Elements*, Prentice-Hall, Englewood Cliffs, New Jersey, 1987.
- [15.2.15] COOLEY, J. W., and TUKEY, J. W., "An Algorithm for Machine Calculation of Complex Fourier Series," *Math. Comput.*, 19 (1965), 297.
- [15.2.16] DOKAINISCH, M. A., and SUBBARAJ, K., "A Survey of Direct Time-Integration Methods in Computational Structural Dynamics I, Explicit Methods," *Comp. Struct.*, 32 (1989), 1371–1386.
- [15.2.17] BATHE, K.-J., and WILSON, E. L., *Numerical Methods in Finite Element Analysis*, Prentice-Hall, Englewood Cliffs, New Jersey, 1976.
- [15.2.18] IRONS, B., "Eigenvalue Economisers in Vibration Problems I," *Roy. Aeronaut. Soc.*, 67 (1963), 526–528.
- [15.2.19] ZURMÜHL, R., and FALK, S., *Matrices und Ihre Anwendungen*, 5th ed., Springer-Verlag, Berlin, 1986.
- [15.2.20] MEIROVITCH, L., *Computational Methods in Structural Dynamics*, Sijthoff & Noordhoff, Alphen aan Rijn, The Netherlands, 1980.

15.3 Damping of Discrete Systems

a. General Concepts. In the preceding treatment of free and forced vibrations of plates it was assumed that the vibrating system possesses no damping. While this mathematically convenient assumption closely approximates, in most cases, the actual dynamic behavior of the structure, there is always some damping effect in any real system. As a result of damping, the free vibration dies out when, after initial excitation, the structure is left alone. The rates of decay at which the amplitudes decrease are measured by the ratio of two successive amplitudes (Fig. 15.3.1). The effect of the damping is usually given as the logarithm of this ratio and is called the *logarithmic decrement*. The force that produces the dissipation of free vibration is called the *damping force*. All damping forces oppose the motion of the vibrating system.

Damping forces acting on a structural system usually fall into two categories: external and internal forces. *External damping* forces can be produced by the surrounding media, such as water, air and soil, or by the friction in the structural connections. *Internal damping* forces are attributed to the hysteresis of elastic materials; that is, the work required to produce certain deformations is larger than the energy regained

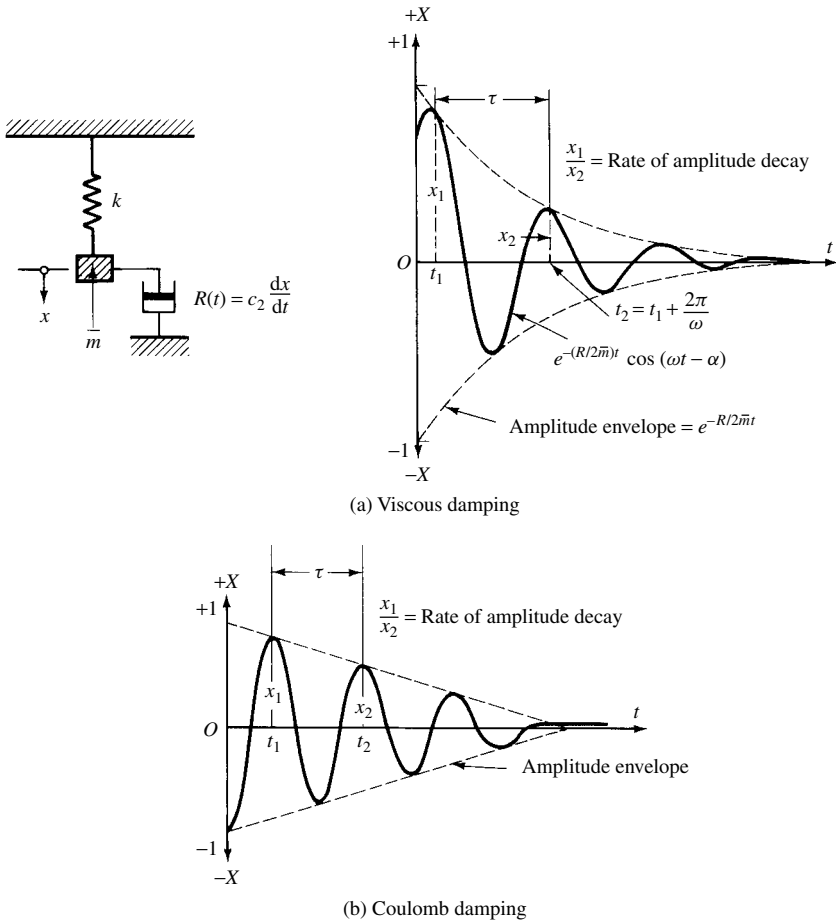


Figure 15.3.1 Amplitude vs. time in free vibration with damping.

in the reloading process. Consequently, there is a loss of energy, which can have a pronounced effect on the vibration only when the deformations are in the plastic range. Since, strictly speaking, these internal damping forces are stress dependent, their exact consideration in the analysis is cumbersome. Fortunately, the influence of the internal damping forces on the free and steady-state vibrations is small. In the case of a single-DOF system, for instance, a relatively strong damping force capable of reducing the amplitudes of free vibration to half within a period will have only a negligible effect ($\pm 0.6\%$) on the lowest circular frequency.

Occasionally, damping effects of the surrounding media should be considered [15.3.1, 15.3.2, 15.3.11], especially in connection with transient excitations. Damping can also be intentionally introduced to the system to provide shock isolation [15.3.3]. While the stiffness matrix represents the structural characteristics of the system, the damping force is an inherent physical property of the material and that of the environment.

The effect of the damping force $R(t)$ is customarily described by one of the following *damping laws*:

Coulomb damping [15.3.4]. In this formulation, the damping force is expressed by

$$R(t) = c_1 P, \quad (15.3.1)$$

where c_1 is the coefficient of kinetic or dry friction and P is the normal pressure between the two surfaces in contact. The use of Eq. (15.3.1) is limited to specific cases.

Viscous damping. This damping law associates the velocity \dot{x} and the damping force and is usually represented by a *dashpot*. Thus, the viscous damping force is

$$R(t) = c_2 \dot{x}. \quad (15.3.2)$$

The modification of Eq. (15.3.2) is called *the velocity-squared* damping and is represented by

$$R(t) = c_3 (\dot{x})^2. \quad (15.3.3)$$

The formulation of damping forces, as given by Eq. (15.3.2), can be handled mathematically in the matrix equation of motion with relative ease. The determination of the coefficient c_2 , however, may create some problems. Since Eq. 15.3.2 is able to represent not only hydraulic or soil resistance but structural damping as well, it is one of the most widely used damping laws [15.3.5].

Structural damping. A recently introduced formulation of damping employed extensively in the dynamic analysis of aerospace structures [15.3.6], expresses damping as a function of the imaginary number ($i = \sqrt{-1}$) and that of the displacement; thus

$$R(t) = c_4 i x, \quad (15.3.4)$$

or, in another form,

$$R(t) = i c_5 k x, \quad (15.3.5)$$

where the damping factor c_5 is approximately 0.03–0.05 for most structural materials and k is the stiffness of the spring (or vibrating system). In Eq. (15.3.5) the damping coefficient is attached to the stiffness coefficient.[†]

b. Free Vibration with Viscous Damping. The differential equation of motion of damped free vibration is obtained from Eq. (15.3.6) by adding the matrix of the damping force. Thus, assuming the viscous damping law (15.3.2), the matrix equation of the free vibration of a discrete system representing the plate becomes

$$\mathbf{M}\ddot{\mathbf{d}} + \mathbf{C}\dot{\mathbf{d}} + \mathbf{K}\mathbf{d} = \{0\}, \quad (15.3.6)$$

[†] The damping coefficient can also be attached to the mass [15.3.7].

where \mathbf{C} is the damping matrix, which is given customarily in diagonal form, provided that the fictitious dampers are attached to the nodal points. From the theory of differential equations we know that the motion of the j th mass can be expressed in the form

$$d_j = A_j e^{\lambda t}. \quad (15.3.7)$$

Hence, for the solution of the matrix equation of motion we can assume that

$$\mathbf{d} = \{A\} e^{\lambda t}. \quad (15.3.8)$$

Substitution of Eq. (15.3.8) into the differential equation of motion (15.3.6) yields

$$(\mathbf{M}\lambda^2 + \mathbf{C}\lambda + \mathbf{K})\{A\}e^{\lambda t} = \{0\}, \quad (15.3.9)$$

or

$$\mathbf{M}\lambda^2 + \mathbf{C}\lambda + \mathbf{K} = \{0\}, \quad (15.3.10)$$

where \mathbf{M} , \mathbf{C} and \mathbf{K} are symmetric square matrices of order n . Since Eq. (15.3.10) represents a set of coupled, linear, homogeneous equations for the nontrivial solution, the system determinant must vanish; consequently,

$$\det |\mathbf{M}\lambda^2 + \mathbf{C}\lambda + \mathbf{K}| = \{0\}. \quad (15.3.11)$$

By expanding Eq. (15.3.11), an equation of degree $2n$ in λ is obtained. In this way, the problem is reduced to a *general eigenvalue problem*. Equation (15.3.11) is called Lagrange's determinantal equation. It can be shown that the roots of Eq. (15.3.11) have the following properties:

1. None of the roots are real positive.
2. If the damping matrix \mathbf{C} is zero, the roots are all pure imaginary.
3. If the damping matrix \mathbf{C} is zero or the stiffness matrix \mathbf{K} is zero but the damping matrix \mathbf{C} is not equal to zero, the roots are real and negative so the motion dies out exponentially. This case corresponds to the *overdamped* system.
4. If the elements of the damping matrix \mathbf{C} are not too large, all roots are conjugate complex numbers with a negative real part. This condition permits damped vibrations and is the most frequently encountered in practice.

We solve Eq. (15.3.11) for the $2n$ roots of λ . Then, substituting the results into Eq. (15.3.9), we obtain $2n$ equations of the form

$$(\mathbf{M}\lambda_r^2 + \mathbf{C}\lambda_r + \mathbf{K})\{A_r\} = \{0\}, \quad (15.3.12)$$

where λ_r is a particular root of Eq. (15.3.11) and $\{A_r\}$ represents a column matrix of coefficients associated with the root λ_r ; thus

$$\{A_r\} = \begin{Bmatrix} A_{1r} \\ A_{2r} \\ A_{3r} \\ \vdots \\ A_{nr} \end{Bmatrix}. \quad (15.3.13)$$

Then, the general solution of the matrix differential equation of motion can be written as

$$\mathbf{d} = \sum_{r=1}^{2n} \{A_r\} e^{\lambda_r t}. \quad (15.3.14)$$

The ratio of A 's for any particular value of r is fixed by Eq. (15.3.9). Thus, there is one arbitrary factor for each column of A 's, making a total of $2n$ arbitrary constants in the general solution. These constants can be determined from the initial conditions of vibration.

In the usual case, the values of λ_r appear in complex conjugate pairs. For this case, the general solution may be written as

$$\begin{aligned} \mathbf{d} &= \sum_{r=1}^{2n} \{A_r\} e^{\lambda_r t} = \sum_{r=1}^n (\{A_r\} e^{\lambda_r t} + \{\bar{A}_r\} e^{\bar{\lambda}_r t}) \\ &= \sum_{r=1}^n \{B_r\} e^{\beta_r t} \cos(\omega_r t + \alpha_r). \end{aligned} \quad (15.3.15)$$

Again, we have $2n$ arbitrary constants, the ratio of B 's and the phase angle α for n values of r . The motion described by the general solution (15.3.15) may be analyzed as follows: Each coordinate performs the resultant of n damped harmonic oscillations of different period. The phase and the damping factors of any single oscillation of a particular period are the same for all coordinates. The absolute value of the amplitudes for any particular coordinate is arbitrary, but ratios of the amplitudes for a particular circular frequency ω_r can be determined. When the system has large number of degrees of freedom, the computation will be quite cumbersome.

c. Damped Forced Vibrations. Let us assume that an external harmonic force is acting upon each discrete mass of the vibrating system. Then, the differential equation of motion becomes

$$\mathbf{M}\ddot{\mathbf{d}} + \mathbf{C}\dot{\mathbf{d}} + \mathbf{K}\mathbf{d} = \mathbf{p}_0 e^{ipt}, \quad (15.3.16)$$

where p represents the frequency of the harmonic excitation. To obtain the particular solution of this differential equation, we assume the solution in the form

$$\mathbf{d} = \mathbf{d}_0 e^{ipt}, \quad (15.3.17)$$

where \mathbf{d}_0 is the column matrix of amplitudes. Substituting this assumed solution into Eq. (15.3.16), we obtain

$$(-p^2 \mathbf{M} + ip \mathbf{C} + \mathbf{K}) \mathbf{d}_0 = \mathbf{p}_0. \quad (15.3.18)$$

This matrix equation represents a set of linear, nonhomogeneous equations in the desired amplitudes.

Let us introduce

$$\mathbf{N} = (-p^2 \mathbf{M} + ip \mathbf{C} + \mathbf{K}); \quad (15.3.19)$$

then

$$\mathbf{N}\mathbf{d}_0 = \mathbf{p}_0; \quad (15.3.20)$$

hence

$$\mathbf{d}_0 = \mathbf{N}^{-1}\mathbf{p}_0 e^{ipt}. \quad (15.3.21)$$

Consequently, the steady-state part of the vibration is represented by

$$\mathbf{d} = \mathbf{N}^{-1}\mathbf{p}_0 e^{ipt}. \quad (15.3.22)$$

The response of discrete vibrating systems to transient excitations can be calculated in a similar manner; that is, we expand the time-dependent part of the forcing function into Fourier series using its *complex form*. Thus

$$\mathbf{p}(t) = \sum_m \mathbf{p}_{0m} e^{ipt}. \quad (15.3.23)$$

Then, we repeat the above-described procedure for each individual term m of the Fourier expansion.

An alternative approach uses the DLF obtained from Duhamel's integral, provided that the required circular frequencies of the corresponding free vibration have already been determined. The response of a damped system expressed by Duhamel's integral is obtained in a similar manner as discussed in Sec. 14.1c for undamped structures, with the exception that now the impulse $P(t^*) \Delta t^*$ producing the initial velocity is substituted into the corresponding equations of damped free vibrations. In this way, one obtains the following, somewhat more complex, expression instead of the simpler Eq.(14.1.31):

$$x = \frac{1}{m\omega_D} \int_0^t f(t^*) e^{-\xi\omega(t-t^*)} \sin \omega_D(t-t^*) dt^*, \quad (15.3.24)$$

where ω_D is the circular frequency of the damped system, ω is the circular frequency of the undamped one and ξ represents the damping ratio. The integral in this equation can be conveniently evaluated by using one of the symbolic mathematics program. Furthermore, if the damping of the system is relatively moderate, one can even circumvent the rather tedious classical process introduced above for determining the circular frequencies of a damped system by using the following *approximate* procedure:

- Circular frequencies of the undamped system are determined by the methods described in Sec. 15.2.1.
- Applying the corresponding mode shapes, the *static* matrix equation for the damped system is solved for lateral deflections by using the uniformly distributed weight as the load.
- The required circular frequencies of the damped system are calculated from Morley's formula (14.6.8) using the obtained static deflections.

In the case of short-pulse, transient loading, the maximum response usually occurs before damping has had much effect; thus, damping may be completely neglected. For

long-pulse, transient excitations, however, the effect of damping must be significant and, therefore, must be considered.

Summary. If the vibrating system has many degrees of freedom, the procedures described in this section will become quite cumbersome. Fortunately, in most cases of vibration analysis, the damping of the system is so small that its effect can be neglected. To simplify the solutions for damped systems, one can use Morley's formula to obtain approximate values for the circular frequencies of free vibrations, as described above. To compute the maximum response to forced vibrations, the modified Duhamel integral for damped systems (15.3.24) is the recommended approach.

References and Bibliography

- [15.3.1] ZIENKIEWICZ, O. C., IRONS, B., and NATH, B., "Natural Frequencies of Complex, Free or Submerged, Structures by the Finite Element Methods," in *Symposium on Vibrations in Civil Engineering*, held in London, April 1965, Butterworth & Co., London, 1966.
- [15.3.2] *Proceedings of the Symposium on Soil-Structure Interaction*, Engineering Research Laboratory, University of Arizona, Tucson, 1964.
- [15.3.3] CREDE, C. E., *Vibration and Shock Isolation*, John Wiley & Sons, New York, 1951.
- [15.3.4] COULOMB, C. A., "Théorie des machines simples, on ayant égard au frottement de leurs parties et de la roideur de leurs cordages," *Memoirs de Mathématique et de Physique Présentés à L'Academie Royale des Sciences par Divers Savants* Paris, 1785, pp. 161–332.
- [15.3.5] KOELLE, H. H., *Handbook of Astronautical Engineering*, McGraw-Hill Book Co., New York, 1961.
- [15.3.6] SCANLAN, R. H., and ROSENBAUM, R., *Aircraft Vibration and Flutter*, Macmillan Company, New York, 1951.
- [15.3.7] HURTY, W. C., and RUBINSTEIN, M. F., *Dynamics of Structures*, Prentice-Hall, Englewood Cliffs, New Jersey, 1964.
- [15.3.8] ROSEAU, M., *Vibrations non linéaires et théorie de stabilité*, Springer-Verlag, Berlin, 1966.
- [15.3.9] LANZAN, B. J., *Damping of Materials and Members in Structural Mechanics*, Pergamon Press, Elmsford, New York, 1968.
- [15.3.10] DUNCAN, W. J., and COLLAR, A. R., "A Method for the Solution of Oscillation Problems by Matrices," *Phil. Mag.*, 17, Ser. 7 (1934), 865–909.
- [15.3.11] SZILARD, R. (Ed.), *Hydromechanically Loaded Shells*, Proceedings of IAAS Pacific Symposium, Part I, held in Honolulu, Oct. 10–15, 1971, Univ. of Hawaii Press, Honolulu, 1973.
- [15.3.12] INSTITUTE OF CIVIL ENGINEERS, *Symposium on Vibrations in Civil Engineering*, held in London, April 1965, Butterworth & Co., London, 1966.
- [15.3.13] LINK, M., *Finite Elemente in der Statik und Dynamik*, B. G. Teubner, Stuttgart, 1984.
- [15.3.14] GASCH, R., and KNOTHE, K., *Strukturdynamik: Kontinua und ihre Diskretisierung*, Springer-Verlag, Berlin, 1989.
- [15.3.15] RAGGETT, J. D., "Estimating Damping of Real Structures," *J. Struct. Div., ASCE*, 101 (1975), 1823–1835.
- [15.3.16] HARRIS, C. M., *Shock and Vibration Handbook*, McGraw-Hill Book Co., New York, 1987.
- [15.3.17] KRÄTZIG, W. B., and LINK, M., "Baudynamik und Systemidentifikation," in G. Mehlhorn (Ed.), *Der Ingenieurbau; Baustatik und Baudynamik*, Ernst & Sohn, Berlin, 1995.

15.4 Slab Bridges under Moving Loads

a. Human-Induced Rhythmic Loads. When a group of soldiers march in rhythmic steps over a slab bridge, these rhythmic movements create a special art of

dynamic load. In general, such periodic loading can be expressed by using Fourier series[†] as

$$p_m(t) = A_0 + \sum_{n=1}^N \left[A_n \cos\left(\frac{2n\pi t}{T}\right) + B_n \sin\left(\frac{2n\pi t}{T}\right) \right] \\ \text{for } n = 1, 2, 3, \dots, \quad (15.4.1)$$

where $p_m(t)$ is the time-dependent dynamic load, $m = 1, 2, 3, \dots, M$ is the index number for an individual soldier representing the number of people in the group, A_0 is the weight of the average soldier, A_n and B_n are Fourier series coefficients and T is the period of expansion. If we also consider the phase lag among the soldiers, an approximation for such human-induced load may be expressed according to Ref. [15.4.1] as

$$q(t, M) = \frac{1}{A} \sum_{m=1}^M \sum_{n=1}^N \left[A_{mn} \cos\left(\frac{2n\pi t}{T} - \alpha_m\right) + B_{mn} \sin\left(\frac{2n\pi t}{T} - \alpha_m\right) \right], \quad (15.4.2)$$

where $q(t, M)$ is the intensity of the dynamic load, A represents the area occupied by the military group and α_m is the phase lag for the m th individual in the group.

In general, this phase lag is a function of the frequency of motion; its minimum value can be taken to be 2 Hz. However, the probability distribution of the phase angle α_m can be expressed by an exponential function given in Ref. [15.4.1].

b. Vehicle-Bridge Interaction. The analysis of the dynamic response of a slab bridge to moving heavy vehicles is of considerable interest to bridge designers. Modeling the moving vehicle, which represents a highly complex dynamic system, is a difficult task. Consequently, some simplification is required for the everyday analysis. In our first simplification, we assume that the plate bridge is subjected to a concentrated load of magnitude P that has a mass \bar{m} (Fig. 15.4.1). Furthermore, we assume that this load, representing the heavy vehicle, moves with a constant velocity v . If the bridge can be modeled as an orthotropic plate, then the corresponding differential equation of motion without considering the damping in structure and vehicle is

$$D_x \frac{\partial^4 w}{\partial x^4} + 2B \frac{\partial^4 w}{\partial x^2 \partial y^2} + D_y \frac{\partial^4 w}{\partial y^4} + \mu \frac{\partial^2 w}{\partial t^2} \\ = \delta(x - x_0) \delta(y - vt) \left[P - \bar{m} \frac{\partial^2 w}{\partial t^2} \right], \quad (15.4.3)$$

where μ is the mass of the plate per unit area. If the plate is isotropic, then this equation reduces to

$$D \nabla^4 w(x, y, t) + \mu \frac{\partial^2 w}{\partial t^2} = \delta(x - x_0) \delta(y - vt) \left[P - \bar{m} \frac{\partial^2 w(x, y, t)}{\partial t^2} \right]. \quad (15.4.4)$$

[†] See Appendix A.1.

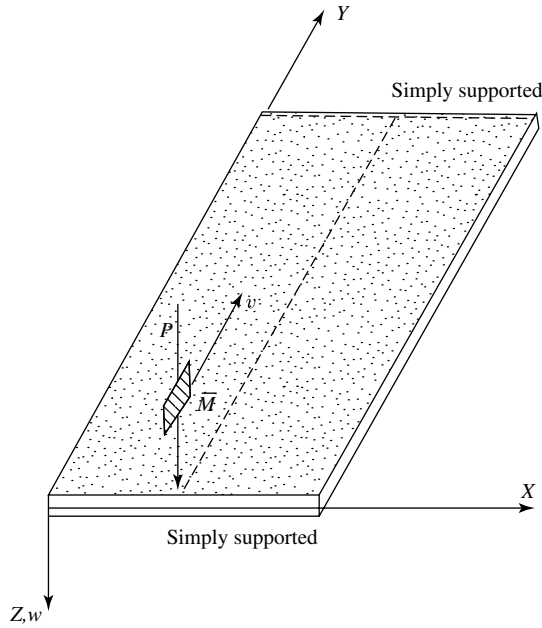


Figure 15.4.1 Slab bridge under moving load.

Both these differential equations of motions can be solved by applying the ordinary FDM introduced in Sec. 5.1.

If we model the structure using the FEM, then the equation of dynamic equilibrium in the global reference system without considering damping becomes[†]

$$\mathbf{M}\ddot{\mathbf{d}} + \mathbf{K}\mathbf{d} = \mathbf{p}. \quad (15.4.5)$$

The nodal forces for the elements are

$$\mathbf{p}_e = \mathbf{N}^T \mathbf{P}, \quad (15.4.6)$$

where \mathbf{N} is the matrix of the shape functions[‡] used in generating the element stiffness matrices. The load vector \mathbf{p} is obtained by proper summation of the element nodal forces \mathbf{p}_e in the manner discussed in Chapter 7. Equation (15.4.5) can be solved by applying the step-by-step direct iteration technique treated in Sec. 15.2.3.c.

In the above-given matrix equation the stiffness coefficient k_v of the vehicle was neglected. Although vehicle models with varying degrees of refinements have been used in the past, experience shows that for vehicle representation a single mass supported by a spring (Fig. 15.4.2) can give acceptable results. Thus, this vehicle model represents our second simplified approach. Again, damping in the structure and vehicle is considered to be of a negligible order of magnitude.

[†] Again, to simplify our notation in plate dynamics the overbars that refer to the global reference system are omitted in this section.

[‡] See Sec. 7.5.

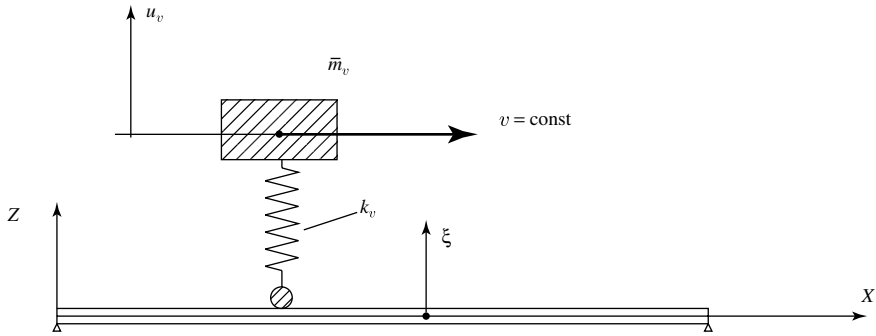


Figure 15.4.2 Single-DOF vehicle model on slab bridge.

If the bridge is an isotropic plate, the governing differential equation of motion can be written as

$$\nabla^4 w + \frac{\mu}{D} \frac{\partial^2 w}{\partial t^2} = -\frac{\bar{m}_v}{D} \left(g + \frac{\partial^2 u_v}{\partial t^2} \right) \times f(x - vt, y), \quad (15.4.7)$$

where g is the gravitational acceleration, $f(\cdot)$ represents a time-dependent function describing the position of the load over the plate surface and u is the absolute displacement of the spring-mass system (Fig. 15.4.2). Again, this differential equation can be solved by using the ordinary FDM.

Neglecting the damping in the structure and vehicle, the matrix equation of motion for finite element representation of the plate is given by

$$\mathbf{M}\ddot{\mathbf{d}} + \mathbf{K}\mathbf{d} = \hat{\mathbf{p}}, \quad (15.4.8)$$

where the *effective* force vector $\hat{\mathbf{p}}$ derived from the equation of motion of the spring-mass system (Fig. 15.4.3) is expressed by

$$\hat{\mathbf{p}} = \mathbf{N}^T [-m_v \ddot{\xi} + k_v (u_v - \xi) - \bar{m}_v g]. \quad (15.4.9)$$

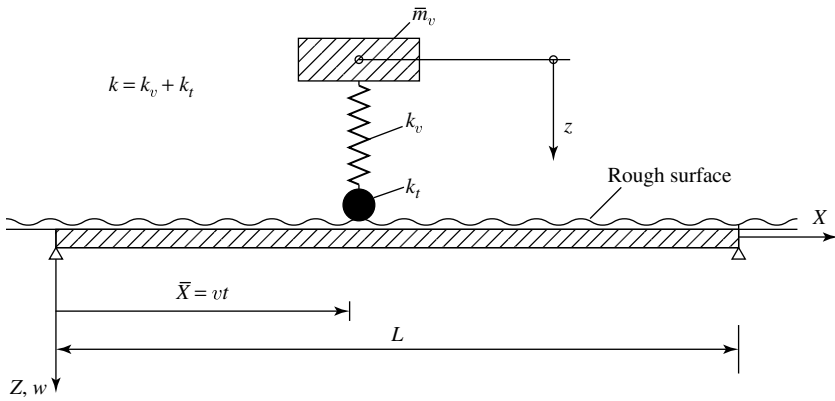
In this equation \mathbf{N} represents the matrix of shape functions that relates ξ to the displacements \mathbf{d} . That is, as the vehicle moves along a straight line parallel to the bridge span, the vertical displacement ξ of the vehicle contact point is expressed as a product, $\xi = \mathbf{N}\mathbf{d}$.

A more explicit expression for Eq. (15.4.8) according to Ref. [15.4.3] is

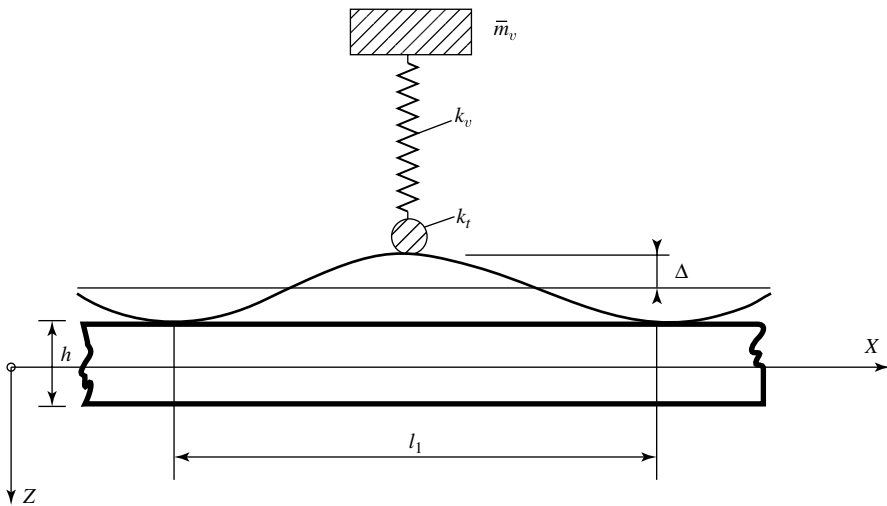
$$\begin{bmatrix} m_v & \mathbf{0} \\ \mathbf{0} & \mathbf{M} \end{bmatrix} \begin{Bmatrix} \ddot{u}_v \\ \ddot{\mathbf{d}} \end{Bmatrix} + \begin{bmatrix} k_v & -k_v \mathbf{N} \\ -k_v \mathbf{N}^T & \mathbf{K} + k_v \mathbf{N}^T \mathbf{N} \end{bmatrix} \begin{Bmatrix} u_v \\ \mathbf{d} \end{Bmatrix} = -mg \begin{Bmatrix} u_v \\ \mathbf{0} \end{Bmatrix}. \quad (15.4.10)$$

Since the matrix \mathbf{N} is a function of time, these equations are nonlinear and can be solved using the step-by-step numerical integration techniques introduced in Sec. 15.2.3.3.

c. Unevenness in the Bridge Deck. Rough pavement surfaces exist in most slab bridges due to poor construction or maintenance. In addition, some ice build-ups



(a) Vehicle-bridge interaction



(b) Model of unevenness in bridge deck

Figure 15.4.3 Model of vehicle on rough pavement.

during winter can also contribute to unevenness of the bridge deck. Let us consider a one-span plate bridge with constant flexural rigidity D and a span length L under the load

$$p(t) = k[z - w(\bar{x}, t) - f(\bar{x})] + \bar{m}_v g, \quad (15.4.11)$$

where k is the combined stiffness of the tire and spring, \bar{m}_v is the mass of the vehicle, the expression $x = vt$ gives the position of the vehicle and z is the vertical displacement of the vehicle with respect to its static equilibrium.

The expression $f(x)$ approximates the unevenness of the deck by

$$f(\bar{x}) \approx \Delta \left(1 - \cos \frac{2\pi \bar{x}}{l_1} \right), \quad (15.4.12)$$

in which Δ is the amplitude of the unevenness and its wavelength is l_1 (Fig. 15.4.3). Thus, the equation of motion of an orthotropic plate bridge and moving vehicle upon it becomes

$$D_x \frac{\partial^4 w}{\partial x^4} + 2B \frac{\partial^4 w}{\partial x^2 \partial y^2} + D_y \frac{\partial^4 w}{\partial y^4} + \frac{\mu}{D} \frac{\partial^2 w}{\partial t^2} = p(t), \quad (15.4.13)$$

or in the case of an isotropic plate

$$D \nabla^4 w + \frac{\partial^2 w}{\partial t^2} = p(t). \quad (15.4.14)$$

These differential equations can be repeatedly solved for every position of the vehicle by using the ordinary FDM. The corresponding matrix equation of motion is

$$\mathbf{M}\ddot{\mathbf{d}} + \mathbf{K}\mathbf{d} = \mathbf{p}(t), \quad (15.4.15)$$

where the load vector $\mathbf{p}(t)$ always has one nonzero value corresponding to the instantaneous location of the moving vehicle. Thus, repeated solution of Eq. (15.4.15) will give a complete dynamic response to the unevenness of the bridge deck.

Summary. Dynamic responses of slab bridges to a group of people performing rhythmic movements and to heavy vehicle motion were treated in this section. The bridge was idealized either as an orthotropic slab or an isotropic plate. In addition, the idealization of the vehicle consisted of using a simple, single spring-mass configuration. Damping both in the bridge and vehicle was ignored, since in most cases it is of a negligible order of magnitude. Experience indicates that such a simplified approach can still deliver quite usable estimates to the dynamic behavior of slab bridges. In addition to the bridge-vehicle interaction, poor road surface may also produce undesirable dynamic effects in the bridge. Both the profile length of the unevenness and its depth may be significant factors in creating excessive dynamic responses. Although the ordinary FDM can be used for numerical solution of the various differential equations of motion, the versatile FEM appears to be more readily adaptable to the solution of such dynamic problems as slab bridges that may be of arbitrary shape and boundary condition. Step-by-step direct numerical integration techniques are recommended for solution of the resulting matrix equations of motion. One should, however, not overlook the fact that radical changes in the dynamic behavior of the structure can occur when near resonance is apparent. Consequently, the designer must always consider this dangerous scenario by computing first the free vibration of the structure using the numerical methods treated in previous sections and only then deal with the forced-vibration problems.

References and Bibliography

- [15.4.1] EBRAHIMPOUR, A., and FITTS, L. L., "Measuring Coherency of Human-Induced Rhythmic Loads Using Force Plate," *J. Struct. Div., ASCE*, 122 (1996), 829–831.

- [15.4.2] GREEN, M. F., and CEBON, D., "Dynamic Interaction between Heavy Vehicles and Highway Bridges," *Comp. Struct.*, 62 (1997), 253–264.
- [15.4.3] HUMAR, J. L., and KASHIF, A., "Dynamic Response of Slab-Type Bridges," *J. Struct. Div., ASCE*, 121 (1995), 48–61.
- [15.4.4] FLEMING, J. F., and ROMVALDI, J. P., "Dynamic Response of Highway Bridges," *J. Struct. Div., ASCE*, 87 (1961), 31–61.
- [15.4.5] SUNDARA, R. I., and JAGADISH, K. S., "The Response of Beam and Slab Bridges to Moving Forces," *Publ. Int. Assoc. Bridge Struct. Eng.*, 28 (1968, II), 69–86.
- [15.4.6] SUNDARA, R. I., and JAGADISH, K. S., "Dynamic Response of Highway Bridges to Moving Loads," *Publ. Int. Assoc. Bridge Struct. Eng.*, 30 (1970, II), 57–76.
- [15.4.7] VELETOS, A. S., and HUANG, T., "Analysis of Dynamic Response of Highway Bridges," *J. Eng. Mech. Div., ASCE*, 96 (1970), 593–620.
- [15.4.8] YOSHIDA, D. M., and WEAVER, W., "Finite Element Analysis of Beams and Plates with Moving Loads," *Publ. Int. Assoc. Bridge Struct. Eng.*, 31 (1971, I), 179–195.
- [15.4.9] WU, J.-S., et al., "The Dynamic Analysis of a Flat Plate under a Moving Load by the Finite Element Method," *Int. J. Num. Meth. Eng.*, 24 (1987), 743–762.
- [15.4.10] INBANATHAN, M. J., and WIELAND, M., "Bridge Vibration due to the Vehicle Moving over Rough Surface," *J. Struct. Div., ASCE*, 113 (1987), 1994–2008.
- [15.4.11] BIGGS, J. M., et al., "Vibration of Simple Span Highway Bridges," *J. Struct. Div., ASCE*, 83 (1957), 1186–1–1186–32.
- [15.4.12] ABDEL-ROHMAN, M., and AL-DUAII, J., "Dynamic Response of Hinged Single Span Bidges with Uneven Deck," *Comp. Struct.*, 59 (1996), 291–299.
- [15.4.13] NEWLAND, D. E., *Mechanical Vibration Analysis and Computation*, Longman, London, 1989.
- [15.4.14] O'BRIEN, E. J., and KEOGH, D. L., *Bridge Deck Analysis*, E & F Spon, London, United Kingdom, 1999.

15.5 Large-Amplitude Free-Vibration Analysis

During large-amplitude flexural oscillations membrane forces n_x , n_y and n_{xy} are created in the plate. These amplitude-dependent in-plate forces are the primary cause of nonlinearity. Other not so dominant sources of nonlinearity are

- large curvatures developed during vibrations,
- longitudinal inertia forces, and
- rotary inertia forces.

Here, only the effects of the rotary inertia forces and those of the in-plane forces will be considered, since the others, including damping, are usually of negligible order of magnitude.

Because exact solutions of the governing differential equation are not available, approximate and numerical methods offer the only practical approach to solution of such difficult nonlinear vibration problems. Direct variational methods such as the ones by Rayleigh-Ritz and Galerkin can only be applied to simple geometrical configurations coupled with relatively easy to handle boundary conditions [15.5.1, 15.5.2]. However, the inherent complexity of "real-life" plate problems requires more generally applicable computer-based solution techniques. Consequently, here we will use the gridwork and the versatile finite element methods.

The governing differential equations of motion for plates undergoing moderately large deflections are obtained by simply adding the inertia terms $\mu(\partial w^2/\partial t^2)$ to the large-deflection differential equations introduced in Sec. 11.1. Thus, we can write

$$D \nabla^4 w = p_z(x, y, t) + h \left(\frac{\partial^2 \Phi}{\partial y^2} \frac{\partial^2 w}{\partial x^2} + \frac{\partial^2 \Phi}{\partial x^2} \frac{\partial^2 w}{\partial y^2} - 2 \frac{\partial^2 \Phi}{\partial x \partial y} \frac{\partial^2 w}{\partial x \partial y} \right) - \mu \frac{\partial^2 w}{\partial t^2},$$

$$\nabla^4 \Phi = E \left[\left(\frac{\partial^2 w}{\partial x \partial y} \right)^2 - \frac{\partial^2 w}{\partial x^2} \frac{\partial^2 w}{\partial y^2} \right], \quad (15.5.1)$$

where Φ represents a *time-dependent* Airy-type stress function and μ is the mass of the plate per unit area.

Expressions for the membrane forces n_x, n_y and n_{xy} created by large transverse displacements are given in Eq. (11.1.2). If there are no external loads (i.e., $p_z = 0$), Eq. (15.5.1) becomes

$$D \nabla^4 w + \mu \frac{\partial^2 w}{\partial t^2} = n_x(t) \frac{\partial^2 w}{\partial x^2} + 2n_{xy}(t) \frac{\partial^2 w}{\partial x \partial y} + n_y(t) \frac{\partial^2 w}{\partial y^2}, \quad (15.5.2)$$

where

$$w(x, y, t) = w(x, y)\theta(t). \quad (15.5.3)$$

The time dependency $\theta(t)$ of the free vibration is a cyclical function having the following properties:

$$\theta(t + 2\pi) = \theta(t), \quad \frac{d^2 \theta(t)}{dt^2} = -\omega_i^2 \theta(t)$$

$$\text{for } -1 \leq \theta(t) \leq +1, \quad (15.5.4)$$

where ω_i represents the circular frequency corresponding to the i th mode of vibration.

It can be shown [15.5.3] that by applying Galerkin's variational method to Eq. (15.5.1) the *time-dependent* membrane forces can be expressed in the form

$$n_x(t) = n_x \widehat{w}_n^2(t), \quad n_y(t) = n_y \widehat{w}_n^2(t), \quad n_{xy}(t) = n_{xy} \widehat{w}_n^2(t), \quad (15.5.5)$$

where

$$\widehat{w}_n(t) = \frac{w(x, y) \times \theta(t)}{h} \quad (15.5.6)$$

represents the *normalized* (with respect to the plate thickness) lateral displacements.

Equation (15.5.5) is now used to develop the corresponding matrix equation of motion by adding to the small-amplitude matrix equation of motion (15.2.2) the nonlinear term containing the time-dependent membrane forces. Thus, we obtain

$$\ddot{\mathbf{M}} \mathbf{\ddot{d}} + \mathbf{\bar{K}}^L \mathbf{\ddot{d}} + \widehat{w}_n^2(t) \mathbf{\bar{K}}^{NL} \mathbf{\ddot{d}} = \{0\}, \quad (15.5.7)$$

where the nonlinear stiffness matrix $\mathbf{K}^{\text{NL}}(d, t)$ is now not only the function of displacements but also that of time. Furthermore

$$\widehat{w}_n(t) = \widehat{W}_n \times \theta(t), \quad (15.5.8)$$

where \widehat{W}_n represents the normalized (with respect to the plate thickness) amplitude of vibration.

Let us now express the vector of displacements in the form

$$\bar{\mathbf{d}} = \{\bar{X}\}\theta(t). \quad (15.5.9)$$

Substituting this equation into Eq. (15.5.7) and using Eq. (15.5.5), we obtain

$$-\omega_i^2 \bar{\mathbf{M}}\{\bar{X}\}_i + \bar{\mathbf{K}}^{\text{L}}\{\bar{X}\}_i + \widehat{W}_n^2 \theta^2(t) \mathbf{K}^{\text{NL}}\{\bar{X}\}_i = \{0\}. \quad (15.5.10)$$

A closer look at this matrix equation reveals several important properties. First, the nonlinear term contains \widehat{W}_n^2 , indicating the pronounced effect of the normalized amplitudes on the free vibration of the plate. Second, the nonlinear term has the coefficients $\theta^2(t)$. Thus, ω_i is not a constant value, as is the case in linear vibrations, but the circular frequency varies with time. When $\theta(t)$ is small, $\theta^2(t)$ approaches zero. Thus, the lower-bound value of ω_i approaches that of the small-amplitude vibration. The upper-bound value of ω_i is pertinent to $\theta^2(t) = 1$. This occurs when the plate deflections are maximum. For a comparison of the result obtained by using the above described approach, we introduce the average value ω_{av} at $t = \pi/4$, which gives, for $\theta(t) = \sin \omega t$, the value $\theta^2(t) = 0.5$. Consequently, Eq (15.5.10) becomes

$$\left(-\omega_{\text{av}}^2 \bar{\mathbf{M}} + \bar{\mathbf{K}}^{\text{L}} + 0.5 \widehat{W}_n^2 \bar{\mathbf{K}}^{\text{NL}}\right) \{\bar{X}\} = \{0\}; \quad (15.5.11)$$

hence

$$\boxed{\omega_{\text{av}}^2 = \bar{\mathbf{M}}^{-1} \bar{\mathbf{K}}^{\text{L}} + 0.5 \widehat{W}_n^2 \bar{\mathbf{M}}^{-1} \bar{\mathbf{K}}^{\text{NL}}}. \quad (15.5.12)$$

Provided that matrices $\bar{\mathbf{K}}^{\text{L}}$, $\bar{\mathbf{K}}^{\text{NL}}$ and $\bar{\mathbf{M}}$ are known, this equation can be solved, for instance, by applying Stodola's iterative solution technique[†] for various values of amplitudes. As already mentioned in Sec. 15.1, this method represents a self-correcting, numerically stable solution procedure.

The nonlinear element stiffness properties are dependent on the membrane forces developed during the large-deflection vibrations. According to our assumption that the amplitudes are only moderately large, the modes of nonlinear vibrations can be assumed to be affine to those of the linear system. Consequently, in the first step we solve the corresponding linear eigenvalue problem represented by Eq. (15.2.2). Next, the selected linear mode shapes at the time of investigation will be amplified by a multiplication factor

$$\text{MF} \approx c \times h \quad \text{for } c \approx 1.0-2.5 \quad (15.5.13)$$

to obtain the corresponding large-deflection, free-vibration mode.

[†] See Eq. (15.1.15).

Having introduced above the nonlinear finite element formulation of circular frequencies covering large-amplitude oscillations, the next step involves determining the properties of the finite element or gridwork cells to be employed in the analysis. Linear stiffness matrices for the most commonly used finite elements are already given explicitly in Secs. 7.6 and 7.7. The stiffness matrices for gridwork cells are treated in Sec. 6.3. The corresponding consistent mass matrices can be found in Sec. 15.2.2. Determining only the nonlinear element stiffness matrices appears to be somewhat problematic, since they depend on the in-plane forces developed during the large-amplitude oscillations. A “hybrid” finite element–finite difference approach has been successfully employed for large-deflection analysis of structures [15.5.4]. Following a similar solution technique, we can also use improved finite difference expressions[†] to evaluate the instantaneous membrane forces at each nodal points.

In an effort to assess the obtainable accuracy of the above-described procedure for large-amplitude free-vibration analysis, a simply supported square plate was selected (Fig. 15.5.1). The corresponding discrete model having 3×3 gridwork cells per quarter plate has been used for the first mode of large deflection vibrations with various amplitudes. A graphical comparison of the results with those determined analytically shows good agreement (Fig. 15.5.2).

Summary. A new approach to the inherently difficult large-amplitude free-vibration analysis of plates is introduced. It is based on a hybrid finite element–finite difference solution technique combined with Stodola’s iterative procedure that yields the

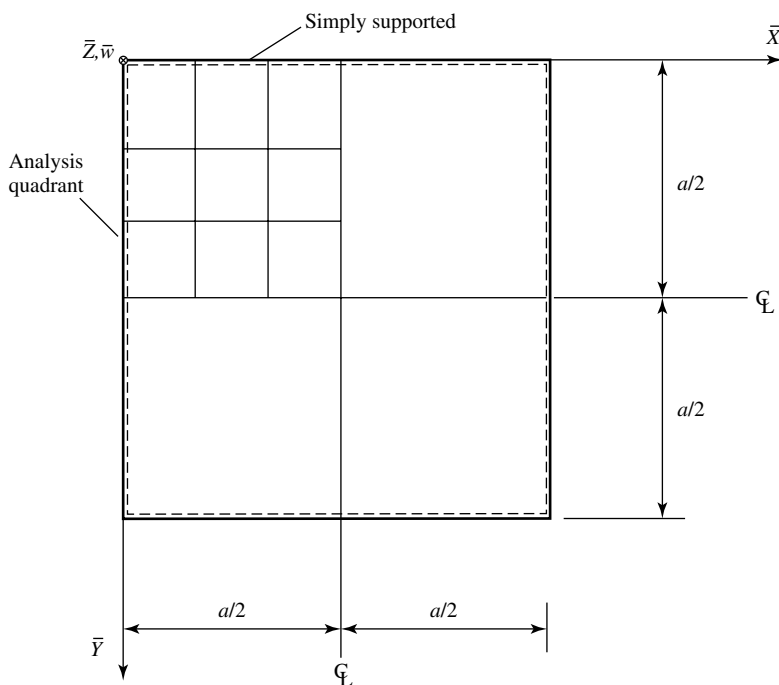


Figure 15.5.1 Test problem for large-amplitude free vibration.

[†] See Sec. 5.2.

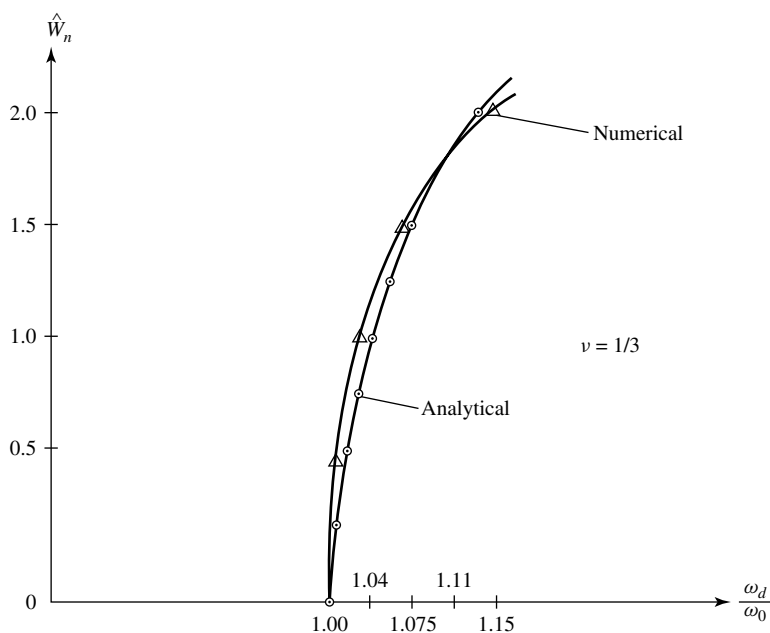


Figure 15.5.2 Comparison of results.

required circular frequencies. The results compare favorably with those calculated analytically [15.5.2].

References and Bibliography

- [15.5.1] SRINIVASAN, A. V., "Non-Linear Vibrations of Beams and Plates," *J. Non-Linear Mech.*, 1 (1966), 179–191.
- [15.5.2] CHU, A., and HERRMANN, G., "Influence of Large Amplitudes on Flexural Vibration of Rectangular Elastic Plates," *J. Appl. Mech.*, 23 (1956), 532–540.
- [15.5.3] POWELL, R. O., "Nonlinear Dynamic Stability Analysis of Plates by Finite Element Method," *Ph.D. Dissertation*, University of Hawaii, Honolulu, 1971.
- [15.5.4] SZILARD, R., "A Hybrid Finite Element-Finite Difference Approach to Simplified Large Deflection Analysis of Structures," *Comp. Struct.*, 9 (1978), 341–350.
- [15.5.5] CHIA, C.-J., *Nonlinear Analysis of Plates*, McGraw-Hill Book Co., New York, 1980.

15.6 Summary and Conclusions

Chapters 14 and 15 of this book are devoted to the dynamic analysis of plates. As in the static analysis, the classical solution of the differential equation of motion is limited to the simplest geometry, loading and boundary conditions. Consequently, numerical and approximate methods are treated more extensively, since they permit the solution of dynamic plate problems, where the classical approaches fail.

The effect of structural damping is, in most cases, of a negligible order of magnitude; thus, solutions of undamped free and forced vibrations have been emphasized.

To provide, however, a generally usable tool for the rare cases when damping must be considered, the matrix solution of damped vibrations of discrete systems is briefly discussed.

Since the natural frequencies of free vibration can serve as an important index capable of describing by one quantity the dynamic characteristics of a complex structure, considerable attention is paid to the free-vibration analysis of plates. For simply supported rectangular plates of uniform thickness, the extension of Navier's method yields the natural frequencies in a relatively simple manner. Also, forced vibrations of such plates can be solved without too much difficulty by expressing the time dependency of the dynamic forces in Fourier (sine or cosine) series. Similarly, the extension of Lévy's method yields solutions to the free vibrations of rectangular plates having two opposite edges simply supported while the other two edges are free or fixed. The solution of forced-vibration problems by Lévy's method, however, tends to be tedious. Similar is the case of the free-vibration analysis of rectangular and circular plates having all the edges free or clamped.

Energy methods are more general than the so-called classical approaches and yield remarkably accurate results even if the boundary conditions are more difficult. These methods can also be extended to plates of various shapes and of variable thickness. The accuracy of the solution, however, depends to a large extent on the choice of the eigenfunctions. This need to select appropriate shape functions that satisfy the geometric boundary conditions and approximate the modes of vibrations is the main disadvantage of the energy methods, since it requires experience and skill on the part of the investigator. Methods have been introduced to facilitate the selection of suitable shape functions.

When the only information sought is the lowest natural frequency, the use of Rayleigh's method, which often yields very good accuracy, is highly recommended. A modification of Rayleigh's method by Morley uses dead-load deflections of plates. In certain cases this method can be extended to obtain natural frequencies pertinent to the second and third modes as well. The resulting solutions, as all energy solutions, are upper bound.

The Ritz method is based on the principle of minimum potential. This approach is more general than Rayleigh's solution, since it can give information on frequencies and modal shapes of higher modes. While the accuracy of the first and second modes is good, it deteriorates progressively; thus, the highest frequencies and modes are, in general, quite inaccurate, because of the nature of the assumptions involved.

Russian scientists working in the field of theory of elasticity have significantly contributed to the development of energy methods. Like the method of Ritz, Galerkin's method assumes the solution of the modal shapes in the form of a series, terms of which individually satisfy all boundary conditions and have fourth derivatives. The reasoning of Galerkin, that the variation of the lateral displacements should be applied directly to the differential equation of motion, leads to a simpler way of obtaining eigenvalues and eigenfunctions. The problem is reduced to evaluation of definite integrals of simple functions selected in advance. This integral transformation results in a system of homogeneous linear equations that has a nontrivial solution only when the determinant of this system equals zero. In this way, the original problem is further reduced to an eigenvalue-eigenvector problem.

Vlasov's method eliminates (1) the problem of selecting eigenfunctions and (2) the solution of the above-mentioned eigenvalue problem. These simplifications are achieved by separating the variables and by introducing linear combinations of

eigenfunctions of transverse vibrations of beams for shape functions. An additional advantage of this technique is that its accuracy does not deteriorate significantly with higher modes, as is the case for the methods of Ritz and Galerkin. Although the required mathematical operations are simple, they tend to be quite lengthy. The method can be extended to cover forced vibration, but in the author's opinion, numerical methods using digital computers are better suited to handle arbitrary loading and boundary conditions. Simple estimates of the dynamic response can be obtained via the DLF, based on the circular frequencies of the plate.

While ordinary FDMs yield acceptable results, for the solution of free or forced vibrations of plates, the application of improved finite difference techniques is recommended whenever high accuracy is required. It is of interest to note that the Stodola-Vianello iterative approach can improve approximate results of free-vibration analysis to any desired degree of accuracy. The economy of numerical analysis of plate vibration problems is enhanced by the general availability of computer programs for eigenvalue-eigenvector problems. Furthermore, reliable programs for solution of a large number of simultaneous algebraic equations are also readily available. To obtain high accuracy for higher modes, however, a relatively fine network is required to permit all deformation shapes to take place. A further advantage of the improved FDMs is their generality. The most common boundary conditions, arbitrary loads, variable plate thickness, and so on, can be handled with relative ease. Disadvantages of this technique are (1) the method requires a mathematically trained investigator; (2) certain boundary conditions such as elastic support and restraints, for instance, are difficult to handle and (3) the complete automation of the procedure to cover all possible cases is complex, if not impossible.

The versatile FEM based on matrix displacement analysis is extremely well suited to the computerized solution of free- and forced-vibration problems, associated with complex plate or shell structures. Computer solutions based on FEMs are more general and flexible than those of other numerical techniques. For example, arbitrary geometry, loads and boundary conditions can be handled with ease. Computer programs, involving complete automation of dynamic analysis of plate and shells, are readily available. A further advantage of the method is that it uses concepts familiar to structural engineers. Although the derivation of suitable stiffness coefficients, assuring monotonic convergence of the solution to the exact number, is a difficult task, it needs only be done once; that is, the results are reusable. All stiffness coefficients given in this book have been tested extensively and yield from acceptable to excellent accuracy. The use of kinematically consistent mass matrices, when high accuracy must be achieved in the vibration analysis, is considered to be mandatory. Disadvantages of finite element techniques in dynamic analysis of plates are (1) without a computer of fairly good capacity, the method is useless; (2) the accuracy of the solution of dynamic problems depends to a certain extent on the boundary conditions; (3) problems with convergence of the solution may occur and (4) operations with large matrices may create special problems. The use of FEMs is encouraged, provided that well-tested stiffness and consistent mass matrices for discrete elements are readily available. Finite-element-based forced-vibration analysis of plates can be effectively handled by either using the Fourier series approach or applying one of the direct numerical integration techniques.

Finally, it should be mentioned that free vibrations of moderately thick plate can be treated by Ritz's energy method. If the plate is simply supported, even a closed-form solution is available.

Problems[†]

- 15.1.1.** Find the lowest circular frequency of a simply supported square plate by using the ordinary FDM. Improve the result by Stodola's iterative technique.
- 15.1.2.** Redo problem 15.1.1 using the improved FDM.
- 15.1.3.** Find the two lowest circular frequencies of the plate shown in Fig. 5.2.17 using the ordinary FDM. Check your results by calculating these frequencies from corresponding static deflections.
- 15.2.1.** Redo problem 15.1.3 using gridwork cells and their corresponding consistent mass matrices.
- 15.2.2.** Using the enclosed computer program system, determine the lowest circular frequency of a simply supported rectangular plate ($a/b = 2$).
- 15.2.3.** Determine the dynamic response of the plate shown in Fig. 15.2.6 using harmonic analysis.
- 15.2.4.** Redo problem 15.2.3 this time using one of the direct numerical integration techniques.

[†] The first two numbers refer to the corresponding section.

Part VI

Buckling of Plates

16

Fundamentals of Stability Analysis

16.1 Basic Concepts

Thin-plate elements used in naval and aeronautical structures are often subjected to normal (Fig. 16.1.1) and shearing forces acting in the plane of the plate. If these in-plane forces are sufficiently small, the equilibrium is stable and the resulting deformations are characterized by the absence of lateral displacements ($w = 0$, $u \neq 0$, $v \neq 0$). As the magnitude of these in-plane forces increases, at a certain load intensity, a marked change in the character of the deformation pattern takes place. That is, simultaneously with the in-plane deformations, lateral displacements are introduced. In this condition, the originally *stable* equilibrium becomes *unstable* and the plate is said to have buckled. The load producing this condition is called the *critical load*. The importance of the critical load is the initiation of a deflection pattern that, if the load is further increased, rapidly leads to very large lateral deflections and eventually to complete failure of the plate. This is a dangerous condition that must be avoided.

The fundamental concepts of buckling of plates can be illustrated by a simple analogy involving the various states of equilibrium of a rigid sphere, shown in Fig. 16.1.2. If the sphere is resting in a large concave bowl (case I), its equilibrium is said to be *stable*. If we disturb this equilibrium condition by introducing a small displacement δx , the sphere, after some oscillations, returns to its original position. If the sphere rests on a plane surface (case II), the pertinent equilibrium condition is said to be *neutral*; that is, a small displacement δx does not change either the forces maintaining equilibrium or the potential of the sphere. If the sphere rests on another sphere (case III), the state of equilibrium is *unstable*. That is, the smallest disturbance (δx) will create a complete loss of equilibrium and therefore a failure. It is important to note that in the *classical buckling theory* the *path leading from a stable to an unstable equilibrium always passes through a neutral state of equilibrium*. All mathematical formulations of the linear-elastic stability analysis of plates are based on this important statement. Although a plate has infinite degrees of freedom, several features of this analogy can be used directly in connection with its stability analysis.

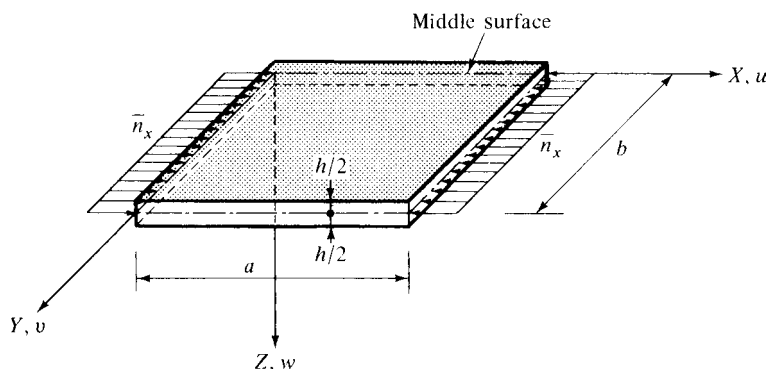


Figure 16.1.1 Rectangular plate subjected to in-plane edge loading.

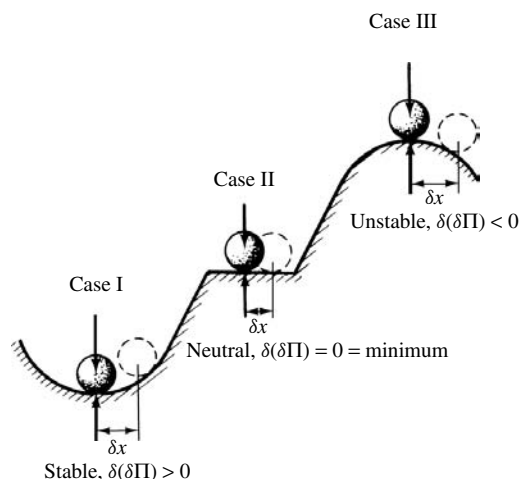


Figure 16.1.2 Analogy of various states of equilibrium.

In the mathematical formulation of elastic stability problems of plates, we use the neutral equilibrium assuming a *bifurcation* of the deformations. That is, at the critical load, of the possible two paths of deformations (one associated with the stable equilibrium and the other one pertinent to the unstable equilibrium condition, as shown in Fig. 16.1.3), the plate always takes the buckled form. In addition to the existence of this bifurcation of equilibrium paths, the elastic stability analysis of plates assumes the validity of Hooke's law.

Besides this *classical buckling theory*, the behavior of flat plates after buckling is of considerable practical interest. The *postbuckling* analysis of plates is usually difficult, since it is basically a nonlinear problem. Slightly curved plates subjected to simultaneous action of in-plane compressive forces and lateral loads exhibit a third kind of instability behavior called *snap-through* buckling, which is characterized by reversal deflections produced by the nonlinear relationship between the buckling load and the deflections. During continuous loading the plate may begin to deflect in one direction, but at a certain load, it buckles in the reverse direction, assuming again a stable shape.

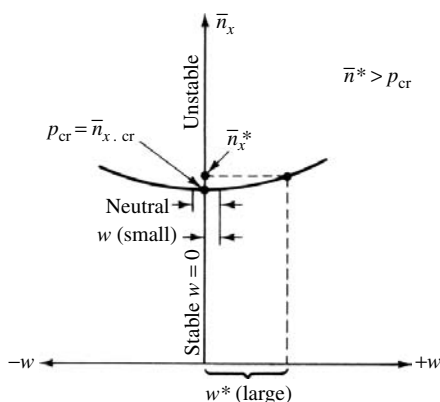


Figure 16.1.3 Bifurcation diagram.

Classical buckling problems of plates can be formulated using (1) the differential equation of static equilibrium, (2) various energy methods and (3) dynamic approaches.

a. Equilibrium Method. In the equilibrium method, we assume that the plate has buckled slightly. It is of basic importance that the differential equation of equilibrium be written for this deformed shape. Thus, the equilibrium equation is obtained by considering the simultaneous bending and stretching of the plate. When the in-plane edge loads are slightly above the critical load, the lateral deflections w are approaching very large values, regardless of how small the increase in the edge loads becomes (Fig. 16.1.3). The *smallest* load corresponding to this condition is the critical load.

An alternative and more general formulation of the equilibrium method transforms the stability problem into an eigenvalue problem. For this purpose, we multiply a reference value of the external forces (\bar{n}_0) by a *load parameter* λ . Hence, certain terms of the differential equation of equilibrium will contain the multiplier λ . The solution of the so-obtained homogeneous differential equation, $w(x, y)$, will have arbitrary constants ($C_1, C_2, C_3, \dots, C_n$) to be determined from the boundary conditions. Equating the determinant of these equations to zero, a polynomial (characteristic) equation in λ is obtained. The lowest eigenvalue gives λ_{cr} , and the *critical load* is calculated from

$$\bar{n}_{cr} = \lambda_{cr} \bar{n}_0. \quad (16.1.1)$$

The trivial solution ($\lambda = 0$) of the characteristic equation corresponds to the unbuckled (flat) state of equilibrium.

b. Energy Methods. Stability problems of plates can also be formulated by extending the various energy theorems, discussed in Secs. 4.2 and 4.3.

Applying the law of *conservation of energy* [Eq. (4.1.1)], for instance, we state that as the plate passes from a stable to an unstable equilibrium, it goes through the neutral state of equilibrium, which is characterized by conservation of energy. The physical interpretation of this statement is the following: In the state of neutral

equilibrium, the plate changes its original flat shape to a curved shape without gaining or losing energy. The corresponding energy equation is

$$\Delta W_i + \Delta W_e = W_i^* + W_e^*(\lambda) = 0. \quad (16.1.2)$$

Since the small bending is caused without stretching the middle surface, the work done by the external compressive forces, W_e^* , is due to the in-plane displacements produced by bending. Similarly, the work of the internal forces, W_i^* , is in the form of potential energy due to bending (U_b^*). Furthermore, we assume that, during buckling, the intensity of the external forces remains the same. The work of the external forces is usually given as a function of the load parameter λ , as discussed above. It is evident that Eq. (16.1.2) can only be used when the expression for the deflection surface contains merely one undetermined coefficient.

More often, however, we formulate the buckling problem using the *variational principle*. That is, the plate is considered to be in a state of equilibrium to which an infinitesimally small disturbance is applied. Since the work of the external and internal forces must vanish, Eq. (16.1.2) can be written in terms of potentials,

$$\Pi_0 + \Delta\Pi = 0, \quad (16.1.3)$$

where Π_0 denotes the total potential of the plate load system pertinent to the stable state of equilibrium and $\Delta\Pi$ is the *increment* in the total potential, representing the *neighboring state of equilibrium*, in which the middle surface is slightly curved due to the small increase in the load. It is evident that for the stable equilibrium condition the total potential must vanish ($\Pi_0 = 0$).

Let us now express the increment of the total potential, $\Delta\Pi$, by the Taylor series[†]:

$$\Delta\Pi = \delta\Pi + \frac{1}{2!}\delta^2\Pi + \dots \quad (16.1.4)$$

From Eq. (16.1.3) $\Delta\Pi$ must be zero, but for an equilibrium system the first variation of potential [Eq. (4.1.11)] is zero ($\delta\Pi = 0$); consequently, the second variation of the total potential must also vanish. Thus, we can write

$$\delta^2\Pi = \delta(\delta\Pi) = \delta[\delta\Pi(c_1, c_2, c_3, \dots, c_n)] = 0. \quad (16.1.5)$$

This more rigorous requirement for the neutral equilibrium condition is based on the *minimum potential energy* principle [Eq. (4.1.11)] and involves the usual minimization process [Eq. (4.2.2)]:

$$\frac{\partial(\Delta\Pi)}{\partial c_i} = \frac{\partial\Pi^*}{\partial c_i} = 0 \quad \text{for } i = 1, 2, 3, \dots, n, \quad (16.1.6)$$

where $\Pi^* = \Delta\Pi$ represents the total potential in the neighboring state of equilibrium. Therefore, this approach can also be used when the expression of the deflected surface contains more than one undetermined coefficient ($c_1, c_2, c_3, \dots, c_n$).

[†] The third- and higher-order terms in this expression are of negligible order of magnitude.

To be able to reduce Eq. (16.1.6) to an *eigenvalue-eigenvector* problem, we again introduce a load factor λ . First, the plate is considered to be in a state of equilibrium under the given loads and its middle surface is assumed to be flat. Next we disturb this equilibrium condition by increasing the load, using a load factor λ , until the slightly curved neighboring state of equilibrium is reached (bifurcation). In this neutral state of equilibrium the sum of the strain energy of the plate (due to the resulting *lateral* displacements) and the potential of the edge forces should be a minimum. The smallest nonzero solution for λ is the critical load factor λ_{cr} .

Furthermore, the type of equilibrium condition can also be determined from the second variation of the total potential:

$$\begin{aligned} \text{For stable equilibrium:} \quad & \delta^2 \Pi > 0, & \delta \Pi &= 0. \\ \text{For neutral equilibrium:} \quad & \delta^2 \Pi = 0 = \min, & \delta \Pi &= 0. \\ \text{For unstable equilibrium:} \quad & \delta^2 \Pi < 0, & \delta \Pi &= 0. \end{aligned} \quad (16.1.7)$$

c. Dynamic Approach. The fact that stability problems can be formulated by dynamic methods is frequently overlooked. Again, the analogy shown in Fig. 16.1.2 can be used to explain the fundamental concepts of such an approach. It is characteristic to a stable state of equilibrium that after the introduction of small *oscillations* the system will return to its original position. If the state of equilibrium is unstable, the system will not return to its initial position, since the small disturbance will be followed by increasingly large deflections.

In setting up the differential equation of transverse vibration, the effect of the in-plane forces must be considered; thus, the equation of motion will contain the load factor λ . The smallest value of λ producing lateral deflections that increase without limit is the critical load factor.

An alternative approach to the dynamic solution of stability problems of plates can be derived by comparing the differential equations of buckling and vibration [16.1.12]. If the buckling shapes and the free-vibration modes are the same,[†] the critical load and the lowest natural frequency occur under the same conditions. They differ only by a constant, which can be obtained by comparing the two differential equations.

The investigation of the dynamic stability of plates can be reduced to the analysis of its free vibrations and its static stability, as shown in Sec. 16.6. For nonlinear stability problems Lyapunov's method [16.1.19] may offer distinct advantages.

d. Buckling under Combined Loads. When plates are subjected to the simultaneous actions of in-plane compressive and shear forces, combined with lateral bending, buckling occurs at lower load intensities than when these forces act individually. The effect of the combined loading can be approximated by the so-called *interaction equation*, which has the form

$$R_1^n + R_2^m + R_3^k + \cdots \leq 1, \quad (16.1.8)$$

where R_i is the load ratio defined by

$$R_i = \frac{\text{\textit{i}th edge load acting alone}}{\text{corresponding \textit{i}th critical load}} = \frac{\bar{n}_i}{\bar{n}_{cr,i}}. \quad (16.1.9)$$

[†] The extension of this concept to cases when the buckling and vibration modes are merely similar yields usable approximations.

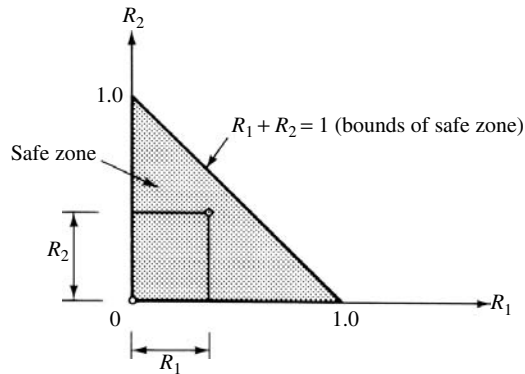


Figure 16.1.4 Interaction curve.

Equation (16.1.8) represented graphically gives the *interaction curves* (Fig. 16.1.4) or *interaction surfaces*. Buckling takes place when the plot of the forces is on or above these limiting bounds.

Gerard [16.1.4] has derived the following interaction equations for rectangular plates:

- Simply supported plate
subjected to biaxial compression: $\dots R_x + R_y \leq 1$.
 - Simply supported plate with
 $a/b \geq 1$ and long plates with
elastically restrained edges
subjected to longitudinal compression
and shear: $\dots R_{\text{comp}} + R_{\text{shear}}^2 \leq 1$.
 - Bending and shear: $\dots R_{\text{bend}}^2 + R_{\text{shear}}^2 \leq 1$.
- (16.1.10)

Summary. The objectives of this chapter on stability of plates are to formulate the problem and to sketch the contemporary trends in solving buckling problems. Again, generally applicable methods will be developed rather than giving solutions for specific problems. The application of these various methods used in the stability analysis of plates is shown on simple problems. Since the literature on the subject is quite extensive [6.1.13], the reader is urged to consult the pertinent references given after each section in this chapter.

References and Bibliography

- [16.1.1] TIMOSHENKO, S. P., and GERE, J. M., *Theory of Elastic Stability*, 2nd ed., McGraw-Hill Book Co., New York, 1961.
- [16.1.2] BLEICH, F., *Buckling Strength of Metal Structures*, McGraw-Hill Book Co., New York, 1952.
- [16.1.3] PFLÜGER, A., *Stabilitätsprobleme der Elastostatik*, 3rd ed., Springer-Verlag, Berlin, 1974.
- [16.1.4] GERARD, G., and BECKER, H., "Buckling of Flat Plates," in *Handbook of Structural Stability*, NACA Tech. Note 3781, Pt. I, National Advisory Committee on Aeronautics, Washington, D.C., July 1957.

- [16.1.5] PONOMAREV, S. D., et al., *Raschety na prochost'v machinostroenil (Stress Analysis in Mechanical Engineering)*, Mashgiz, Moscow, 1958.
- [16.1.6] LEIPHOLZ, H., *Stabilitätstheorie*, B. G. Teubner, Stuttgart, 1968.
- [16.1.7] ARGYRIS, J. H., and DUNNE, P. C., *Structural Principles and Data*, Pt. 2, *Structural Analysis*, 4th ed., Sir Issac Pitman & Sons, London, 1952.
- [16.1.8] COX, H. L., *The Buckling of Plates and Shells*, Macmillan Co., New York, 1963.
- [16.1.9] TIMOSHENKO, S. F., in *Strength of Materials*, 2nd ed., Pt. II, Secs. 41 and 42, Van Nostrand Reinhold Co., New York, 1940.
- [16.1.10] SCHLEICHER, F., "Stabilitätsfälle," in *Taschenbuch für Bauingenieure*, Vol. 1, Springer-Verlag, Berlin, 1955, pp. 965–1047.
- [16.1.11] BÜRGERMEISTER, G., and STEUP, H., "Stabilitätsfälle im Bauwesen," in *Ingenieurtaschenbuch Bauwesen*, Vol. II, B. G. Teubner Verlagsgesellschaft, Leipzig, 1968, pp. 140–238.
- [16.1.12] DULÁCSKA, E., "Experimental Determination of the Critical Load of Shell Structures," in *Proc. Intern. Symp. on Shell Struct. in Engng. Practice (IASS)*, Vol. 2., Kultura, Budapest, 1965, pp. 249–257.
- [16.1.13] COLUMN RESEARCH COMMITTEE OF JAPAN, *Handbook of Structural Stability*, Pt. II, *Plates*, Corona Publishing Co., Tokyo, 1971.
- [16.1.14] KOLLBRUNNER, C. F., and MEISTER, M., *Ausbeulen*, Springer-Verlag, Berlin, 1958.
- [16.1.15] KRETZSCHMAR, H., "Zur Spannungstheorie II Ordnung prismatischer Faltwerke," Dissertation, Technical University, Dresden, 1965.
- [16.1.16] BULSON, P. S., *The Stability of Plates*, American Elsevier Publishing Co., New York, 1969.
- [16.1.17] SULLINS, R. T., *Manual for Structural Stability Analysis of Sandwich Plates and Shells*, NASA CR-1457, National Aeronautics and Space Administration, Washington, D.C., 1969.
- [16.1.18] SOLOMENKO, N. S., *Strength and Stability of Plates and Shells in Ship-Hull* (in Russian), Sudostroenie, Leningrad, 1967.
- [16.1.19] HAHN, W., "Probleme und Methoden der modernen Stabilitätstheorie," *MTW-Mitt.* (Technische Hochschule, Vienna), No. IV/5 (1957), 119–134.
- [16.1.20] IYENGAR, N. G., *Structural Stability of Columns and Plates*, Halsted Press, New York, 1988.
- [16.1.21] STEUP, H., *Stabilitätsprobleme im Bauwesen*, Ernst & Sohn, Berlin, 1990.
- [16.1.22] BAŽANT, Z., and CEDOLIN, L., *Stability of Structures*, Oxford University Press, New York, 1991.
- [16.1.23] BLOOM, F., and COFFIN, D., *Handbook of Thin Plate Buckling*, Chapman & Hall/CRC Press, Boca Raton, Florida, 2001.
- [16.1.24] ALLEN, H. G., and BULSON, P. S., *Background to Buckling*, McGraw-Hill Book Co., New York, 1980.
- [16.1.25] KOLLÁR, L., *Structural Stability Practice*, Routledge, London, United Kingdom, 1999.

16.2 Equilibrium Method

a. Rectangular Plates. Let us investigate a flat rectangular plate subjected to the action of in-plane forces \bar{n}_x, \bar{n}_y and \bar{n}_{xy} applied at the boundaries of the middle surface, as shown in Fig. 16.2.1. Specifying these edge forces by their relative magnitude, rather than by their absolute value, we can write[†]

$$\bar{n}_x = -\lambda \bar{n}_{x0}, \quad \bar{n}_y = -\lambda \bar{n}_{y0}, \quad \bar{n}_{xy} = -\lambda \bar{n}_{xy0}, \quad (16.2.1)$$

[†] Sign convention: (+), tensile force; (–), compressive forces.

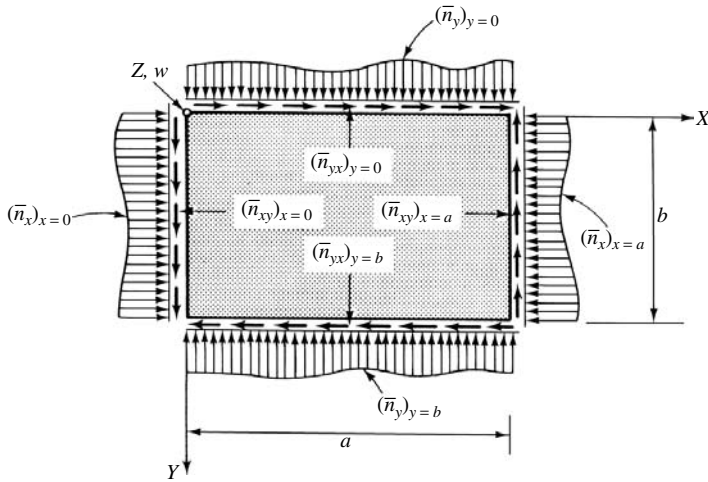


Figure 16.2.1 Rectangular plate subjected to edge forces.

where the common factor λ is the load factor. A gradual increase of this factor results in an increase of in-plane edge loads. At a certain value of λ , the deformed configuration of the plate is no longer unique; that is, regardless of the absence of transverse loading ($p_z = 0$) the plate deflects laterally; thus, the originally in-plane deformations bifurcate (Fig. 16.1.3). In the absence of lateral loads, the differential equation pertinent to this neutral state of equilibrium is the homogeneous form of Eq. (3.3.7) ($p_z = 0$). Consequently, the governing differential equation of plate buckling becomes

$$\frac{\partial^4 w}{\partial x^4} + 2 \frac{\partial^4 w}{\partial x^2 \partial y^2} + \frac{\partial^4 w}{\partial y^4} = \frac{1}{D} \left(\bar{n}_x \frac{\partial^2 w}{\partial x^2} + 2 \bar{n}_{xy} \frac{\partial^2 w}{\partial x \partial y} + \bar{n}_y \frac{\partial^2 w}{\partial y^2} \right). \quad (16.2.2)$$

Substituting Eq. (16.2.1), we obtain an alternative form of the governing differential equation of elastic instability of plates:

$$\nabla^4 w + \frac{\lambda}{D} \left(\bar{n}_{x0} \frac{\partial^2 w}{\partial x^2} + 2 \bar{n}_{xy0} \frac{\partial^2 w}{\partial x \partial y} + \bar{n}_{y0} \frac{\partial^2 w}{\partial y^2} \right) = 0. \quad (16.2.3)$$

We seek the lowest value of λ at which bifurcation of the deflections occurs (Fig. 16.1.3); that is, the plate can be in neutral equilibrium in a slightly bent position.

The differential equation (16.2.3) is homogeneous and linear. The load factor appears in the coefficients of the lower-order terms. Solutions of such equations are classified as eigenvalue problems of mathematics. The rigorous solutions w must satisfy Eq. (16.2.3) and the given boundary conditions. Because of the homogeneous form of Eq. (16.2.3), the order of magnitude of the deflections is undetermined; that is, if w represents a solution, then a multiple of w is also a solution. Consequently, the additional equations obtained from the boundary conditions are also homogeneous.

To simplify the analysis, when the plate is under the combined action of edge forces, we usually specify the relation between them by constant ratios. If, for

instance, the compressive edge forces in the X direction are governing, we can define the other edge forces by

$$\bar{n}_{y0} = \alpha \bar{n}_{x0} \quad \text{and} \quad \bar{n}_{xy0} = \beta \bar{n}_{x0}, \quad (16.2.4)$$

where α and β are constants defining the ratios between the edge forces.

A further simplification is obtained by using Euler's buckling formulas of an isolated plate strip (assuming that it acts as a column) for reference values. Thus, for the problem illustrated in Fig. 16.2.2, we can write

$$\bar{n}_{x0} = \frac{\pi^2 D}{a^2} = \frac{\pi^2 E h^3}{12(1 - \nu^2) a^2}. \quad (16.2.5)$$

There are cases, however, when the use of

$$\bar{n}_{x0} = \frac{\pi^2 D}{b^2} \quad (16.2.5a)$$

as a reference value is more advantageous.

We usually seek the solution of plate buckling in the form

$$w(x, y) = \sum_m \sum_n W_{mn} X_m(x) \cdot Y_n(y), \quad (16.2.6)$$

which is the sum of the products of two functions each of which depends on a single argument.

The substitution of these expressions into the governing differential equation (16.2.3) yields the *characteristic equation* of the problem. A nontrivial solution exists only if we satisfy the characteristic equation. By calculating the minimum value of the load factor ($\lambda_{\min} = \lambda_{\text{cr}}$), the critical load is obtained from[†]

$$p_{\text{cr}} = (\bar{n}_x)_{\text{cr}} = \lambda_{\text{cr}} \bar{n}_{x0}. \quad (16.2.7)$$

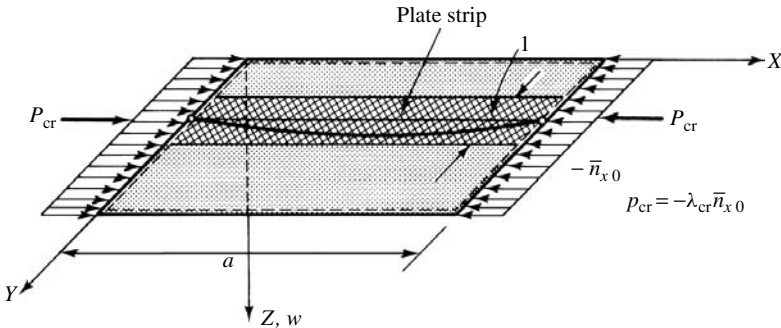


Figure 16.2.2 Buckling of plate strip.

[†] Assumed that \bar{n}_x is the governing edge load.

If the edges of the plate are simply supported and free from shearing forces ($\bar{n}_{xy} = 0$), Eq. (16.2.6) becomes

$$w(x, y) = \sum_m \sum_n W_{mn} \sin \frac{m\pi x}{a} \sin \frac{n\pi y}{b} \quad \text{for } m, n = 1, 2, 3, \dots \quad (16.2.8)$$

Minimization of the characteristic equation directly yields λ_{cr} .

The solution for other types of boundary conditions is more complex. Provided that at least two opposite boundaries are simply supported and the plate is not subjected to shearing forces along the edges ($\bar{n}_{xy} = 0$), Lévy's method can be used. Assuming that the simply supported edges are at $x = 0$ and $x = a$, the mode shape of the buckling can be represented by

$$w(x, y) = \sum_m Y_m(y) \sin \frac{m\pi x}{a}. \quad (16.2.9)$$

The solution follows the general pattern described in Sec. 2.3, with the notable exception that the linear algebraic equations derived from the boundary conditions are also homogeneous. Thus, the nontrivial solution for the integration constants A_m , B_m , C_m and D_m is obtained by equating the determinant of these algebraic equations to zero. The required mathematical operations, however, are quite tedious [16.2.1, 16.2.2]. For other boundary conditions, it is usually impossible to obtain a rigorous solution to buckling.

When body forces (per unit area) and lateral loads are also present, Eq. (16.2.2) becomes

$$D \nabla^4 w = p_z + \bar{n}_x \frac{\partial^2 w}{\partial x^2} + 2\bar{n}_{xy} \frac{\partial^2 w}{\partial x \partial y} + \bar{n}_y \frac{\partial^2 w}{\partial y^2} - p_x \frac{\partial w}{\partial x} - p_y \frac{\partial w}{\partial y}, \quad (16.2.10)$$

where the last two terms represent the transverse components of these in-plane forces, acting on the deflected plate. Since the solution of plate buckling under combined load, even by approximate or numerical methods, can be tedious, the use of interaction equations (16.1.10) is strongly recommended.

The effect of a small initial curvature on the buckling load and the use of large-deflection theory in postbuckling analysis are treated in Sec. 16.10.

b. Circular Plates. The governing differential equation of a rectangular plate (16.2.2) subjected to the same uniformly distributed loads acting in two perpendicular directions ($\bar{n}_x = \bar{n}_y = -\bar{n}$; $\bar{n}_{xy} = 0$) has the form

$$\nabla^2 \nabla^2 w = -\frac{1}{D} \bar{n} \nabla^2 w, \quad (16.2.11)$$

which can be used to obtain the differential equation of buckling of a circular plate under uniform radial loading. Replacing in Eq. (16.2.11) the Laplacian operator ∇^2 ,

expressed in a Cartesian coordinate system [Eq. (1.2.31)], by ∇_r^2 , which is given in terms of polar coordinates [Eq. (1.4.10)], we can write

$$D \nabla_r^2 \nabla_r^2 w(r, \varphi) = -\bar{n} \nabla_r^2 w(r, \varphi). \quad (16.2.12)$$

Considerable simplification, however, can be obtained when the buckling shape is rotationally symmetric. In this case, the buckling mode is independent of φ , and the Laplacian operator given in Eq. (2.8.1) is applicable.

Consequently, Eq. (16.2.12) becomes

$$D \left(\frac{d^4 w}{dr^4} + \frac{2}{r} \frac{d^3 w}{dr^3} - \frac{1}{r^2} \frac{d^2 w}{dr^2} + \frac{1}{r^3} \frac{dw}{dr} \right) + \bar{n} \left(\frac{d^2 w}{dr^2} + \frac{1}{r} \frac{dw}{dr} \right) = 0. \quad (16.2.13)$$

By introducing

$$\lambda^2 = \frac{\bar{n}}{D} \quad \text{and} \quad \rho = \lambda r, \quad (16.2.14)$$

we obtain a relatively simple form for the governing differential equation of buckling of uniform circular plates under radial thrusts:

$$\frac{d^4 w}{d\rho^4} + \frac{2}{\rho} \frac{d^3 w}{d\rho^3} + \left(1 - \frac{1}{\rho^2} \right) \frac{d^2 w}{d\rho^2} + \frac{1}{\rho} \left(1 + \frac{1}{\rho^2} \right) \frac{dw}{d\rho} = 0. \quad (16.2.15)$$

The rigorous solution of Eq. (16.2.15) for full circular plates simply supported or fixed at the edge has the form

$$w(\rho) = C_1 + C_2 J_0(\rho), \quad (16.2.16)$$

where C_1 and C_2 are integration constants and $J_0(\rho)$ is the zeroth-order Bessel function of the first kind

Summary. The rigorous solution of a limited number of plate buckling problems can be obtained from the equilibrium method. Following this approach, the execution of the following computational steps is required:

1. The differential equation of the problem is set up based on the neutral state of equilibrium, which describes the slightly bent equilibrium configuration of an initially flat plate. In the mathematical formulation, we state that in a plate subjected to compressive in-plane forces, lateral displacements w occur without the presence of lateral loads ($p_z = 0$). The differential equations so obtained are homogeneous.
2. We seek a solution, $w(x, y)$, that satisfies the governing differential equation of plate buckling and the given boundary conditions. For rectangular plates, Navier's and Lévy's methods yield exact solutions, provided the plate is subjected only to compressive edge forces ($\bar{n}_{xy} = 0$) and the boundary conditions permit the use of these approaches. For circular plates with rotationally symmetric deflections, a rigorous solution can be obtained in the form of Bessel functions.

3. Since we seek the smallest load that maintains the slightly buckled shape in equilibrium, the critical load is usually calculated from the lowest eigenvalue (load factor) obtained through a minimization process.

Although rigorous solutions are rare, the mathematical formulation of the elastic instability problems of plates based on the differential equations of the neutral state of equilibrium is of fundamental importance, since these equations can be solved by various approximate methods of higher analysis, as shown in the subsequent sections. In all these equilibrium equations, small-deflection theory has been used.

ILLUSTRATIVE EXAMPLE I

Let us determine the critical load of a simply supported rectangular plate subjected to a uniformly distributed compressive edge load acting in the X direction ($\bar{n}_x = -\lambda \bar{n}_{x0}$), as shown in Fig. 16.2.3.

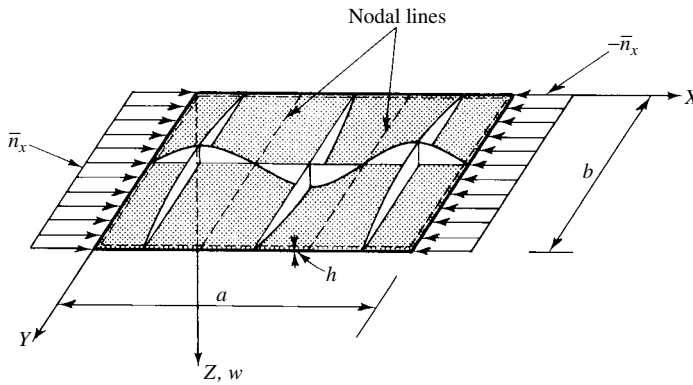


Figure 16.2.3 Buckling of simply supported plate under compressive axial forces.

The governing differential equation is obtained from Eq. (16.2.3) by using $\bar{n}_{y0} = \bar{n}_{xy0} = 0$. Thus, we can write

$$D \nabla^4 w + \lambda \bar{n}_{x0} \frac{\partial^2 w}{\partial x^2} = 0, \quad (16.2.17)$$

where

$$\bar{n}_x = \lambda \bar{n}_{x0} = \lambda \frac{\pi^2 D}{a^2}, \quad (16.2.18)$$

defined by Eqs. (16.2.1) and (16.2.5), respectively.

Since the plate is simply supported, the deflected surface of the buckled plate can be expressed [Eq. (16.2.8)] by

$$w = \sum_m \sum_n W_{mn} \sin \frac{m\pi x}{a} \sin \frac{n\pi y}{b}$$

for $m, n = 1, 2, 3, \dots$, (16.2.19)

which satisfies the boundary conditions ($w = 0, m_x = 0, m_y = 0$) along all the edges. By substituting Eq. (16.2.19) into Eq. (16.2.17), we obtain

$$D \left[\left(\frac{m\pi}{a} \right)^4 + 2 \left(\frac{m\pi}{a} \right)^2 \left(\frac{n\pi}{b} \right)^2 + \left(\frac{n\pi}{b} \right)^4 \right] - \left(\frac{m\pi}{a} \right)^2 \bar{n}_x = 0; \quad (16.2.20)$$

hence

$$\bar{n}_x = D\pi^2 \frac{[(m/a)^2 + (n/b)^2]^2}{(m/a)^2} = \left(m + \frac{n^2}{m} + \frac{a^2}{b^2} \right)^2 \frac{D\pi^2}{a^2} = \lambda \bar{n}_{x0}. \quad (16.2.21)$$

It is evident that the smallest value of λ can be determined by taking $n = 1$; this corresponds to a buckling shape of one half-wave in the Y direction; thus

$$\lambda = \left(m + \frac{1}{m} \frac{a^2}{b^2} \right)^2. \quad (16.2.22)$$

For a given aspect ratio a/b , the critical load is obtained by selecting m so that it makes Eq. (16.2.22) a minimum. For square plates, $m = 1$ satisfies this requirement; thus

$$(\bar{n}_x)_{cr} = \lambda_{\min} \bar{n}_{x0} = \frac{4\pi^2 D}{a^2}. \quad (16.2.23)$$

ILLUSTRATIVE EXAMPLE II

Determine the critical load of a rectangular plate simply supported at the $x = 0$, $x = a$ and $y = 0$ edges and free at $y = b$. The plate is subjected to uniformly distributed edge loading $\bar{n}_x = -\lambda \bar{n}_{x0}$, as shown in Fig. 16.2.4.

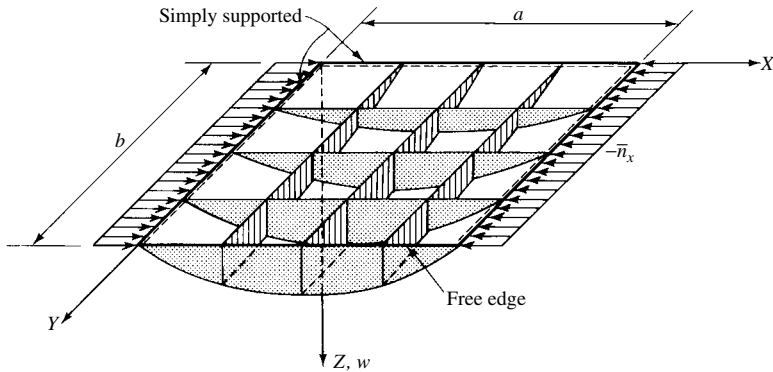


Figure 16.2.4 Buckling of rectangular plate.

Because of the boundary conditions, Lévy's method can be used; thus we seek the solution in the form

$$w = \sum_m Y_m(y) \sin \frac{m\pi x}{a}, \quad (16.2.24)$$

which, substituted into (16.2.17), for a specific m value gives

$$\frac{d^4 Y_m}{dy^4} - 2 \left(\frac{m\pi}{a} \right)^2 \frac{d^2 Y_m}{dy^2} + \left[\left(\frac{m\pi}{a} \right)^4 - \frac{\lambda \bar{n}_{x0}}{D} \left(\frac{m\pi}{a} \right)^2 \right] Y_m = 0. \quad (16.2.25)$$

The pertinent characteristic equation

$$f^4 - 2 \left(\frac{m\pi}{a} \right)^2 f^2 + \left[\left(\frac{m\pi}{a} \right)^4 - \frac{\lambda \bar{n}_{x0}}{D} \left(\frac{m\pi}{a} \right)^2 \right] = 0 \quad (16.2.26)$$

has the following real roots, provided that $\lambda \bar{n}_{x0}/D > m^2 \pi^2/a^2$:

$$f_1 = \sqrt{\left(\frac{m\pi}{a} \right)^2 + \frac{m\pi}{a} \sqrt{\kappa}} \quad \text{and} \quad f_2 = \sqrt{-\left(\frac{m\pi}{a} \right)^2 + \frac{m\pi}{a} \sqrt{\kappa}}, \quad (16.2.27)$$

where $\kappa = \lambda \bar{n}_{x0}/D$.

We assume the general solution of Eq. (16.2.25) in the form

$$Y_m = A \sinh \alpha y + B \cosh \alpha y + C \sin \beta y + \bar{D} \cos \beta y, \quad (16.2.28)$$

where $\alpha = f_1$ and $\beta = f_2$.

The boundary conditions in the Y direction are, at $y = 0$,

$$w = Y_m = 0, \quad \frac{\partial^2 w}{\partial y^2} = \frac{\partial^2 Y_m}{\partial y^2} = 0 \quad (16.2.29)$$

and, at $y = b$,

$$\frac{\partial^2 w}{\partial y^2} + \nu \frac{\partial^2 w}{\partial x^2} = 0, \quad \frac{\partial^3 w}{\partial y^3} + (2 - \nu) \frac{\partial^3 w}{\partial y \partial x^2} = 0. \quad (16.2.30)$$

The boundary conditions at $y = 0$ [Eq. (16.2.29)] yield $B = \bar{D} = 0$. Thus, the mode shape of buckling can be written in the form

$$w = (A \sinh \alpha y + C \sin \beta y) \sin \frac{m\pi x}{a}. \quad (16.2.31)$$

The boundary conditions at $y = b$ [Eq. 6.2.30)] yield

$$\begin{aligned} A(\sqrt{\kappa} + 1 - \nu) \sinh \alpha b - C(\sqrt{\kappa} - 1 + \nu) \sin \beta b &= 0, \\ A\sqrt{\sqrt{\kappa} + 1}(\sqrt{\kappa} - 1 + \nu) \cosh \alpha b - C\sqrt{\sqrt{\kappa} - 1}(\sqrt{\kappa} + 1 - \nu) \cos \beta b &= 0. \end{aligned} \quad (16.2.32)$$

[†] This is always the case, since there is a restraint along one edge of the plate strip.

A nontrivial solution is obtained by equating the determinant of Eq. (16.2.32) to zero; this gives

$$\begin{aligned} & \sqrt{\sqrt{\kappa} - 1}(\sqrt{\kappa} + 1 - \nu)^2 \tanh m\pi\sqrt{\sqrt{\kappa} + 1} \left(\frac{b}{a}\right) \\ &= \sqrt{\sqrt{\kappa} + 1}(\sqrt{\kappa} - 1 + \nu)^2 \tan m\pi\sqrt{\sqrt{\kappa} - 1} \left(\frac{b}{a}\right) = 0. \end{aligned} \quad (16.2.33)$$

For a specific aspect ratio b/a and Poisson ratio ν , the lowest value for $\sqrt{\kappa}$ can be determined by either a trial-and-error procedure or graphically. We assign $m = 1, 2, 3, \dots$ in succession and solve Eq. (16.2.23) for $\sqrt{\kappa}$. The lowest value for $\sqrt{\kappa}$ is with $m = 1$. The critical load for long plates ($a/b \geq 10$), for instance, assuming $\nu = 0.25$, becomes [16.1.1]

$$(\bar{n}_x)_{cr} \approx \left(0.456 + \frac{b^2}{a^2}\right) \frac{\pi^2 D}{b^2}. \quad (16.2.34)$$

References and Bibliography

- [16.2.1] BRYAN, G. H., "On the Stability of a Plane Plate Under Thrusts in Its Own Plane with Application to the Buckling of the Sides of a Ship," *Proc. Lond. Math. Soc.*, 22 (1891), 54–67.
- [16.2.2] HARTMANN, F., *Knickung, Kippung, Beulung*, Deuticke, Vienna, 1937.
- [16.2.3] MEISSNER, E., "Über das Knicken kreisringförmiger Scheiben," *Schweiz. Bauzeitung*, 101 (1933), 87–89.
- [16.2.4] NÁDAI, Á., "Über das Ausbeulen von kreisförmigen Platten," *Z. Verein deutscher Ing.*, 59, Nos. 9 and 11 (1915), 169–174, 221–224.
- [16.2.5] REISSNER, H., "Über die Knicksicherheit ebener Bleche," *Zentralbl. Bauverw.*, 29 (1909), 93.
- [16.2.6] SCHLEICHER, F., "Knickspannungen von eingespannten Rechteckplatten," *Mitt. Forsch.-Anst. Gutehoffnungshütte Konzern*, 1 (1931), 186–193.
- [16.2.7] WOINOWSKY-KRIEGER, S., "Über die Beulsicherheit von Rechteckplatten mit querverschieblichen Rändern," *Ing.-Arch.*, 19 (1951), 200–207.
- [16.2.8] TIMOSHENKO, S., "Stabilitätsprobleme der Elastizität," in *Handbuch der physikalischen und technischen Mechanik*, Vol. 4, Pt. 1, J. A. Barth, Leipzig, 1931, pp. 146–198.

16.3 Energy Methods in Stability Analysis

From the preceding section it is evident that with increasing complexity in the geometrical configuration, boundary conditions and loadings, the rigorous mathematical determination of the buckling load of the plate becomes progressively more difficult and finally impossible. To obtain approximate analytic expressions for the critical load, various energy methods, discussed in Secs. 4.1–4.3, can be used advantageously. In the stability analysis of plates, usually the *critical load* is of practical importance, that is, the minimum buckling load that corresponds to the *first mode* of the buckled plate shape.

In the mathematical formulation of classical plate buckling by the energy methods, we again use the *neutral state of equilibrium* at which bifurcation of displacements occurs, as discussed in Sec. 16.1. Furthermore, it is assumed that the in-plane displacements of the plate are due to the small bending (created by the buckling) and not due to the in-plane shortening. The reason for this assumption is clear if one considers that our datum configuration is the stable equilibrium condition of the plate immediately prior to buckling. Thus, up to this point, the strain energy due to compression of the middle surface equals the work done by the external in-plane forces and therefore cancels out ($\Pi_0 = 0$) in the energy equations.

a. Rayleigh's Method. Rayleigh's powerful method [16.3.1] is based on the principle of *conservation of energy* [16.1.1].

In formulating the buckling problem of a flat plate by energy methods, we first assume that the plate, subjected to

$$\bar{n}_x = -\lambda \bar{n}_{x0}, \quad \bar{n}_y = -\lambda \bar{n}_{y0}, \quad \bar{n}_{xy} = -\lambda \bar{n}_{xy0} \quad (16.3.1)$$

in-plane edge forces,[†] is in a stable equilibrium. Next, the load is gradually increased. As we increase the load factor λ at a certain value, the plate will pass from its flat shape to its curved shape without changing its total potential; thus

$$W_l^* + \lambda W_e^* = U_b^*(w) + \lambda V^*(w) = 0. \quad (16.3.2)$$

Based on our previous discussion,[‡] this expression is only a function of the lateral deflections. As already mentioned, the total potential, corresponding to the stable state of equilibrium, Π_0 , has been eliminated from Eq. (16.3.2). Consequently, here we are only concerned with the total potential pertinent to the *neutral* state of equilibrium.

Since expansion of Eq. (16.3.2) yields only one algebraic equation, its use is limited to one undetermined coefficient, c , in the expression of the deflections,

$$w(x, y) = cf(x, y) = cX(x)Y(y). \quad (16.3.3)$$

Furthermore, it is required that Eq. (16.3.3) satisfy at least the geometrical boundary conditions.

In Eq. (16.3.2) U_b^* represents the bending part of the strain energy, introduced in Sec. 4.1. The potential of the external forces is the negative work done by the external forces ($V^* = -W_e^*$), which remain constant during buckling, as previously defined. We have assumed that as the middle surface bends no membrane stresses are produced, but the edges draw together, creating in-plane displacements; thus, we can neglect the membrane part of the strain energy ($U_m^* = 0$). From Fig. 11.1.2 the in-plane displacement in the X directions is

$$u^* = ds - dx \approx \frac{1}{2} \left(\frac{\partial w}{\partial x} \right)^2 dx. \quad (16.3.4)$$

[†] See preceding sections for the definition of \bar{n}_{x0} , \bar{n}_{y0} and \bar{n}_{xy0} .

[‡] See also Sec. 16.1.

Consequently, the work of the \bar{n}_x force (acting on the dy length of the plate element) is

$$dW_{e,x}^* = (\bar{n}_x dy) u^* = \frac{1}{2} \lambda \bar{n}_{x0} \left(\frac{\partial w}{\partial x} \right)^2 dx dy. \quad (16.3.5)$$

An identical expression is obtained from the membrane part of the strain energy [Eq. (4.2.14)]. Using this alternative approach, we assume that (1) the edge force \bar{n}_x remains constant and (2) the corresponding strain is exclusively due to bending. This leads to

$$dU_m^* = \bar{n}_x \varepsilon_x^{\text{NL}} dx dy = \frac{1}{2} \lambda \bar{n}_{x0} \left(\frac{\partial w}{\partial x} \right)^2 dx dy, \quad (16.3.6)$$

and

$$-W_e^* = V^* = -U_m^*. \quad (16.3.7)$$

Consequently, the potential of the external forces can be written in terms of the in-plane strains $\varepsilon_x^{\text{NL}}$, $\varepsilon_y^{\text{NL}}$ and γ^{NL} produced by the lateral deflections:

$$V^* = -\lambda \iint_{(A)} (\bar{n}_{x0} \varepsilon_x^{\text{NL}} + \bar{n}_{y0} \varepsilon_y^{\text{NL}} + \bar{n}_{xy0} \gamma^{\text{NL}}) dx dy, \quad (16.3.8)$$

where

$$\varepsilon_x^{\text{NL}} = \frac{1}{2} \left(\frac{\partial w}{\partial x} \right)^2, \quad \varepsilon_y^{\text{NL}} = \frac{1}{2} \left(\frac{\partial w}{\partial y} \right)^2, \quad \gamma^{\text{NL}} = \frac{\partial w}{\partial x} \frac{\partial w}{\partial y}, \quad (16.3.9)$$

as introduced in Sec. 11.1.

The substitution of these expressions into Eq. (16.3.8) gives

$$V^* = -\frac{\lambda}{2} \iint_{(A)} \left[\bar{n}_{x0} \left(\frac{\partial w}{\partial x} \right)^2 + \bar{n}_{y0} \left(\frac{\partial w}{\partial y} \right)^2 + 2\bar{n}_{xy0} \left(\frac{\partial w}{\partial x} \frac{\partial w}{\partial y} \right) \right] dx dy. \quad (16.3.10)$$

Using, for instance, Eq. (4.2.5) for the strain energy U_b^* , the load factor can be expressed as a quotient [Eq. (16.3.2)]:

$$\lambda = \frac{\iint_{(A)} \left\{ D \left(\frac{\partial^2 w}{\partial x^2} + \frac{\partial^2 w}{\partial y^2} \right)^2 - 2(1-\nu) \left[\frac{\partial^2 w}{\partial x^2} \frac{\partial^2 w}{\partial y^2} - \left(\frac{\partial^2 w}{\partial x \partial y} \right)^2 \right] \right\} dx dy}{\iint_{(A)} \left[\bar{n}_{x0} \left(\frac{\partial w}{\partial x} \right)^2 + \bar{n}_{y0} \left(\frac{\partial w}{\partial y} \right)^2 + 2\bar{n}_{xy0} \frac{\partial w}{\partial x} \frac{\partial w}{\partial y} \right] dx dy}. \quad (16.3.11)$$

This expression, often called *Rayleigh's quotient*, directly gives the critical load factor ($\lambda = \lambda_{\text{cr}}$); therefore, its use is very convenient.

b. Ritz Method. Ritz [16.3.2] has eliminated the restriction of Rayleigh's method by applying the *minimum potential energy principle* [Eq. (16.1.6)], which permits the expression of the deflected plate surface as a sum of functions,

$$w(x, y) = \sum_{i=1}^n c_i f_i(x, y) \quad \text{for } i = 1, 2, 3, \dots, \quad (16.3.12)$$

containing undetermined coefficients c_1, c_2, \dots, c_n . The continuous functions $f_i(x, y)$ should satisfy at least the geometrical boundary conditions but not necessarily the governing differential equation (16.2.3). By virtue of the minimum potential energy theorem, discussed in Secs. 4.1 and 16.1, we may state that of the several functions satisfying the geometrical boundary conditions, the function that makes the total potential of the plate-load system a minimum represents the best approximation to the buckling mode and to the solution of the governing differential equation (16.2.3).

The variation of the total potential $\delta\Pi^* = 0$ can be written in terms of arbitrary variation of the undetermined expansion coefficients c_1 :

$$\delta(\delta\Pi) = \delta\Pi^* = \frac{\partial\Pi^*}{\partial c_1}\delta c_1 + \frac{\partial\Pi^*}{\partial c_2}\delta c_2 + \dots + \frac{\partial\Pi^*}{\partial c_n}\delta c_n = 0. \quad (16.3.13)$$

Thus, the necessary and sufficient conditions for $\partial\Pi^* = 0$ are

$$\frac{\partial\Pi^*}{\partial c_1} = 0, \quad \frac{\partial\Pi^*}{\partial c_2} = 0, \quad \dots, \quad \frac{\partial\Pi^*}{\partial c_n} = 0. \quad (16.3.14)$$

This leads to a set of linear homogeneous algebraic equations in the undetermined coefficients c_i . Other than the trivial solution ($c_1, c_2, \dots, c_n = 0$), representing the unbuckled plate, these equations have solutions only if the coefficient-determinant of the unknowns (c_i) vanishes. In this way, again, the buckling problem of plates has been transformed to an eigenvalue-eigenvector problem of the mathematical physics:

$$[A] - \lambda[I] = \{0\}. \quad (16.3.15)$$

The smallest eigenvalue, λ_{cr} , is required in Eq. (16.1.1) to obtain the minimum buckling load.

The expression of the total potential of the buckled plate, called *Bryan's equation*, has the following form in the Cartesian coordinate system,

$$\begin{aligned} \Pi^* = U_b^* + V^* = \frac{1}{2} \iint_{(A)} D \left\{ \left(\frac{\partial^2 w}{\partial x^2} + \frac{\partial^2 w}{\partial y^2} \right)^2 - 2(1 - \nu) \right. \\ \left. \times \left[\frac{\partial^2 w}{\partial x^2} \frac{\partial^2 w}{\partial y^2} - \left(\frac{\partial^2 w}{\partial x \partial y} \right)^2 \right] \right\} dx dy \end{aligned}$$

$$\begin{aligned}
& -\frac{\lambda}{2} \iint_{(A)} \left[\bar{n}_{x0} \left(\frac{\partial w}{\partial x} \right)^2 + \bar{n}_{y0} \left(\frac{\partial w}{\partial y} \right)^2 \right. \\
& \quad \left. + 2\bar{n}_{xy0} \frac{\partial w}{\partial x} \frac{\partial w}{\partial y} \right] dx dy, \quad (16.3.16)
\end{aligned}$$

which represents the sum of Eqs. (4.2.5) and (16.3.10). If the boundary conditions permit the use of Eq. (4.2.6), Bryan's equation can be considerably simplified.

For selection of the proper shape functions, which satisfy at least the geometrical boundary conditions and are capable of approximating the true buckled shapes of the plate, the reader is referred to Sec. 4.2. The required calculations can be further simplified by choosing functions that form an orthogonal set:

$$w(x, y) = \sum_m \sum_n W_{mn} X_m(x) \cdot Y_n(y). \quad (16.3.17)$$

While the numerical solution of the eigenvalue problem [Eq. (16.3.15)] is readily obtainable by means of high-speed digital computers, evaluation of the integrals in Eq. (16.3.16) can be tedious. Fortunately, suitable one-term expressions for the buckling modes usually yield sufficient accuracy ($\pm 5\%$ discrepancy) for most practical purposes, since the errors introduced by, for example, idealized material properties and boundary conditions are, in general, greater than those resulting from such analytical approximations. It is of interest to note that, in this case, the expressions for Rayleigh's and Ritz's methods become identical; consequently, the two methods are often called the *Rayleigh-Ritz* method in the pertinent literature.

The restrictive boundary condition requirement of the Ritz method, that the geometrical boundary conditions be satisfied by every term of the series expression of the lateral deflections [Eq. (16.3.12)], can be further eased. The *Lagrangian multiplier method*[†] [16.3.3, 16.3.4] requires merely that the total expression of the deflections satisfies the geometrical boundary conditions. Since in this case the choice of series expressions for w is less restricted, the Lagrangian multiplier method can offer some computational advantages.

c. Galerkin's Method. An alternative formulation of plate buckling in terms of energy integrals can be obtained by Galerkin's method [16.3.5]. The method consists of using the governing differential equation of plate buckling (16.2.3) to express the total potential of the system.

We assume, again, that the buckling modes are in the form of series expressions, as in Eq. (16.3.12) or (16.3.17). The requirement in the usual application of Galerkin's method is that the functions $f_i(x, y)$ satisfy all boundary conditions, not merely those imposed by the geometry of the supports. For elastic buckling of rectangular plates, the basic variational equation (4.3.3) becomes

$$\iint_{(A)} \left[D \nabla^4 w + \lambda \left(\bar{n}_{x0} \frac{\partial^2 w}{\partial x^2} + 2\bar{n}_{xy0} \frac{\partial^2 w}{\partial x \partial y} + \bar{n}_{y0} \frac{\partial^2 w}{\partial y^2} \right) \right] \delta w dx dy = 0, \quad (16.3.18)$$

[†] See Sec. 4.4.

the expansion of which gives

$$\begin{aligned}
 \iint_{(A)} [\text{Diff. Eq.}] f_1(x, y) \, dx \, dy &= 0, \\
 \iint_{(A)} [\text{Diff. Eq.}] f_2(x, y) \, dx \, dy &= 0, \\
 &\vdots \\
 \iint_{(A)} [\text{Diff. Eq.}] f_n(x, y) \, dx \, dy &= 0.
 \end{aligned}
 \tag{16.3.19}$$

If we substitute *all terms* of the deflection function [Eq. (16.3.12)] into the bracketed parts of Eqs. (16.3.19), then, after evaluation of the indicated definite integrals, a system of homogeneous algebraic equations in terms of the undetermined coefficients (c_1, c_2, \dots, c_n) is obtained. Equating the system determinant to zero, the characteristic equation for λ can be calculated. The lowest eigenvalue ($\lambda_{\min} = \lambda_{\text{cr}}$) determines the critical load, as per Eq. (16.1.1).

The mathematical operations required using Galerkin's method in the stability analysis of plates are basically identical to those discussed in Secs. 4.3 and 14.5. The variational principle has merely been applied to a different differential equation of equilibrium. The variational solution of the buckling problem (16.3.19) requires the evaluation of certain simple definite integrals. The required computational work can be further reduced by selecting orthogonal shape functions. Galerkin's method can be used in solving more complex stability problems of plates, when geometrical and material nonlinearities are also to be considered. Since the differential equations of linear and nonlinear plate buckling are readily available in the pertinent literature and the fundamental functions of the lateral beam vibrations are known to satisfy most boundary conditions of practical importance, the Galerkin-Vlasov method can be considered as one of the most general approximate methods that uses analytical techniques.

Summary. The advantages of the energy methods in determining the critical buckling load are obvious since the problem is reduced to (1) the determination of certain simple definite integrals and (2) the solution of eigenvalue problems. The energy methods require the execution of the following steps:

1. Suitable shape functions (in series form) that satisfy the boundary conditions need to be determined, as discussed in Secs. 4.2 and 4.3.
2. The potential energy of the system is expressed either directly (Rayleigh-Ritz method) or indirectly, by applying the variational principle to the governing differential equation of plate buckling (Galerkin's method).
3. In the first approach a minimization procedure leads to a set of homogeneous algebraic equations, and in the second method these algebraic equations are obtained by integrating the variational equations of the problem.

4. The vanishing system determinant defines the characteristic equation. The lowest eigenvalue is λ_{cr} .

The critical loads obtained by these energy methods are always slightly higher than their exact values; consequently, the results are somewhat on the unsafe side. The accuracy of the energy methods is usually high, provided that the shape function used is capable of approximating the exact buckling modes. The orthogonal properties of certain shape functions lead to further simplification of the required analytical operations. Strictly speaking, the accuracy of these energy methods diminishes as the order of the characteristic number increases. This problem, however, is rather academic, since in stability analysis only the lowest eigenvalue is of practical interest.

ILLUSTRATIVE EXAMPLE I

Using Rayleigh's method, let us determine the lowest buckling load of a rectangular plate subjected to uniformly distributed compressive edge loads $\bar{n}_x = -\lambda \bar{n}_{x0}$. The edges of the plate are simply supported at $x = 0$ and $x = a$, while the other boundaries are fixed, as shown in Fig. 16.3.1.

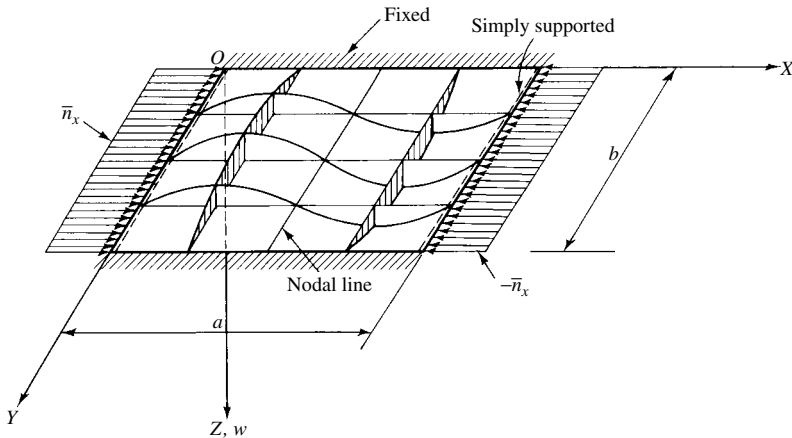


Figure 16.3.1 Buckling mode of rectangular plate simply supported and fixed boundary conditions at opposite edges.

The buckling mode of the plate is approximate in the form

$$w(x, y) = c \sin \frac{m\pi x}{a} \left(1 - \cos \frac{2\pi y}{b} \right), \quad (16.3.20)$$

which satisfies the given static and geometric boundary conditions:

$$(w = 0)_{x=0, x=a}, \quad (\nabla^2 w = 0)_{x=0, x=a}, \quad (16.3.21)$$

and

$$(w = 0)_{y=0, y=b}, \quad \left(\frac{\partial w}{\partial y} = 0 \right)_{y=0, y=b}.$$

Observing that $\bar{n}_{y0} = \bar{n}_{xy0} = 0$, the substitution of Eq. (16.3.20) into (16.3.11) yields

$$\lambda = \frac{(\pi^4/8)[(3m^4b/a^3) + (8m^2/ab) + (16a/b^3)]Dc^2}{(3\pi^2/8)(m^2b/a)\bar{n}_{x0}c^2}. \quad (16.3.22)$$

Using Eq. (16.2.5a),

$$\bar{n}_{x0} = \frac{\pi^2 D}{b^2}; \quad (16.3.23)$$

for reference value, the critical load becomes

$$\bar{n}_{cr} = \lambda_{cr} \frac{\pi^2 D}{b^2}, \quad (16.3.24)$$

where

$$\lambda_{cr} = \frac{1}{3} \left[\frac{16}{m^2} \left(\frac{a}{b} \right)^2 + 3m^2 \left(\frac{b}{a} \right)^2 + 8 \right]. \quad (16.3.25)$$

A comparison of this result with the exact solution of the problem [16.1.1] indicates that the error of the derived approximate solution is always less than 5% for the aspect ratios $0.4 \leq a/b \leq 1$. Therefore, this approximate solution is acceptable for most design purposes.

ILLUSTRATIVE EXAMPLE II

Let us check the exact solution of Illustrative Example II in the preceding section by the energy method.

We approximate the buckling mode by a simple, one-term expression

$$w(x, y) = cy \sin \frac{m\pi x}{a} \quad (16.3.26)$$

that satisfies only the geometrical boundary conditions of the given problem; consequently, Rayleigh's method should be applied. By substituting Eq. (16.3.26) into (16.3.11), we obtain

$$\lambda = \frac{(\pi^4/12)m^2(b/a)\{[m(b/a)]^2 + [6(1-\nu)/2\pi^2]\}Dc^2}{(\pi/12)m^2(b^3/a)\bar{n}_{x0}c^2}; \quad (16.3.27)$$

hence

$$(\bar{n}_x)_{cr} = \left[\left(m \frac{b}{a} \right)^2 + \frac{6(1-\nu)}{\pi^2} \right] \frac{\pi^2 D}{b^2} = \lambda_{cr} \frac{\pi^2 D}{b^2}. \quad (16.3.28)$$

If we assume that $\nu = 0.25$ and $m = 1$, the critical load becomes

$$(\bar{n}_x)_{cr} = \left(0.456 + \frac{b^2}{a^2}\right) \frac{\pi^2 D}{b^2}, \quad (16.3.29)$$

which is the same as the solution given in Eq. (16.2.34).

This example illustrates both the simplicity and the obtainable accuracy of the energy methods.

ILLUSTRATIVE EXAMPLE III

Let us solve the first illustrative problem (Fig. 16.3.1) by Galerkin's method assuming that the buckling mode has the form

$$w(x, y) = \sin \frac{\pi y}{b} \sum_m \sum_n W_{mn} \sin \frac{m\pi x}{a} \sin \frac{n\pi y}{b}, \quad (16.3.30)$$

which satisfies the given boundary conditions [Eq. (16.3.21)].

To illustrate the mathematical operations involved, we limit ourselves to one term ($m = 1, n = 1$); thus Eq. (16.3.30) becomes

$$w(x, y) = W_{11} \sin \frac{\pi x}{a} \sin^2 \frac{\pi y}{b}. \quad (16.3.31)$$

Consequently, the variational equation (16.3.19) can be written as

$$\int_0^a \int_0^b \left(D \nabla^4 w + \lambda \bar{n}_{x0} \frac{\partial^2 w}{\partial x^2} \right) \sin \frac{\pi x}{a} \sin^2 \frac{\pi y}{b} dx dy = 0. \quad (16.3.32)$$

The substitution of Eq. (16.3.31) into this expression leads to

$$\begin{aligned} W_{11} \int_0^a \int_0^b D \left\{ \left[\frac{\pi^4}{a^4} \sin \frac{\pi x}{a} \sin^2 \frac{\pi y}{b} + \frac{4\pi^4}{a^2 b^2} \left(\sin^2 \frac{\pi y}{b} - \cos^2 \frac{\pi y}{b} \right) \sin \frac{\pi x}{a} \right. \right. \\ \left. \left. + \frac{8\pi^4}{b^4} \left(\sin^2 \frac{\pi y}{b} - \cos^2 \frac{\pi y}{b} \right) \sin \frac{\pi x}{a} \right] \right. \\ \left. - \lambda \bar{n}_{x0} \frac{\pi^2}{a^2} \sin \frac{\pi x}{a} \sin^2 \frac{\pi y}{b} \right\} \sin \frac{\pi x}{a} \\ \times \sin^2 \frac{\pi y}{b} dx dy = 0. \end{aligned} \quad (16.3.33)$$

Carrying out the indicated multiplication and integrating term by term, Eq. (16.3.33) becomes

$$\frac{3\pi^4 b}{16a^3} + \frac{\pi^4 a}{b^3} + \frac{\pi^4}{2ab} - \lambda \frac{\bar{n}_{x0}}{D} \frac{3\pi^2 b}{16a} = 0. \quad (16.3.34)$$

Let us introduce

$$\bar{n}_{x0} = \frac{\pi^2 D}{b^2}; \quad (16.3.35)$$

then the load factor becomes

$$\lambda = \lambda_{cr} = \frac{1}{3} \left[16 \left(\frac{a}{b} \right)^2 + 3 \left(\frac{b}{a} \right)^2 + 8 \right], \quad (16.3.36)$$

which is identical to Eq. (16.3.25) for $m = 1$.

Using the series expression (16.3.30) for w , the variational equation (16.3.19) yields a system of homogeneous algebraic equations in terms of the undetermined expansion coefficients W_{mn} , and the problem becomes an eigenvalue problem. By considering more terms, the accuracy of the solution can be considerably improved.

References and Bibliography

- [16.3.1] TEMPLE, G., and BICKLEY, W. G., *Rayleigh's Principle and Its Application to Engineering*, Dover Publications, New York, 1965.
- [16.3.2] RITZ, W., "Über eine neue Methode zur Lösung gewisser Randwertaufgaben," *Göttingen, Ges. d. Wiss. Nachr.* (1908), 236.
- [16.3.3] TREFFTZ, E., "Die Bestimmung der Knicklast gedrückter, rechteckiger Platten," *Z. Angew. Math. Mech.*, 15 (1935), 339–344.
- [16.3.4] BUDIANSKY, B., and HU, P. C., "The Lagrangian Multiplier Method in Finding Upper and Lower Limits to Critical Stresses of Clamped Plates," Report No. 848, National Advisory Committee for Aeronautics, Washington, D. C., 1946.
- [16.3.5] DUNCAN, W. J., "The Principles of Galerkin's Method," Rep. Memo., No. 1848, Aeron. Research Council (Gt. Brit.), London, 1938.
- [16.3.6] SOUTHWELL, R. V., "Some Extensions of Rayleigh's Principle," *Quart. J. Mech. Appl. Math.*, 6 (1953), 257–272.
- [16.3.7] TAYLOR, G. I., "The Buckling Load for a Rectangular Plate with Clamped Edges," *Z. Angew. Math. Mech.*, 13 (1933), 147–152.
- [16.3.8] IGUCHI, S., "Allgemeine Lösung der Knickungsaufgabe für rechteckige Platten," *Ing.-Arch.*, 7 (1936), 207–215.
- [16.3.9] IGUCHI, S., "Die Knickung der rechteckigen Platten durch Schubkräfte," *Ing.-Arch.*, 9, No. 1 (1938), 1–12.
- [16.3.10] WANG, C. T., "Principle and Application of Complimentary Energy Method for Thin Homogeneous and Sandwich Plates and Shells with Finite Deflections," NACA TN2620, National Advisory Committee for Aeronautics, Washington, D. C., Feb. 1952.
- [16.3.11] IYENGAR, N. G. R., *Structural Stability of Columns and Plates*, Halsted Press, New York, 1988.
- [16.3.12] REDDY, J. N., *Theory and Analysis of Elastic Plates*, Taylor & Francis, Philadelphia, Pennsylvania, 1999.
- [16.3.13] BLOOM, F., and COFFIN, D., *Handbook of Thin Plate Buckling*, Chapman & Hall/CRC Press, Boca Raton, Florida, 2001.

16.4 Finite Differences Solution of Plate Buckling

The critical load can be determined numerically by applying the FDMs introduced in Secs. 5.1 and 5.2. Replacing the partial derivatives in the governing differential

equations of plate buckling by finite differential expressions and treating the specific boundary value problems in accordance with Sec. 5.1d, difficult plate buckling problems can be handled with relative ease.

Let us consider, for instance, the buckling of rectangular plates subjected to in-plane compressive edge forces \bar{n}_x, \bar{n}_y . The distribution of these forces (including the boundary conditions) can be quite arbitrary, as shown in Fig. 16.4.1. The governing differential equation (16.2.3) of the problem

$$D \nabla^4 w + \lambda \left(\bar{n}_{x0} \frac{\partial^2 w}{\partial x^2} + \bar{n}_{y0} \frac{\partial^2 w}{\partial y^2} \right) = 0, \quad (16.4.1)$$

written in ordinary finite difference form ($\Delta x = \Delta y = \Delta$) becomes

$$\begin{aligned} \frac{D}{\Delta^4} [20w_{m,n} - 8(w_{m+1,n} + w_{m-1,n} + w_{m,n+1} + w_{m,n-1}) \\ + 2(w_{m+1,n+1} + w_{m-1,n+1} + w_{m+1,n-1} + w_{m-1,n-1}) \\ + w_{m+2,n} + w_{m-2,n} + w_{m,n+2} + w_{m,n-2}] \\ + \frac{\lambda}{\Delta^2} [\bar{n}_{x0}(w_{m+1,n} - 2w_{m,n} + w_{m-1,n}) \\ + \bar{n}_{y0}(w_{m,n+1} - 2w_{m,n} + w_{m,n-1})] = 0. \end{aligned} \quad (16.4.2)$$

Applying Eq. (16.4.2) to all the mesh points and observing the given boundary conditions, we obtain a matrix equation in the form

$$[A]\{w\} - \lambda^*[B]\{w\} = \{0\}, \quad (16.4.3)$$

where $[A]$ and $[B]$ are matrices of the coefficients of the deflection ordinates and λ^* is an expression containing $D, \lambda, \bar{n}_{x0}, \bar{n}_{y0} = \alpha \bar{n}_{x0}$ and Δ .

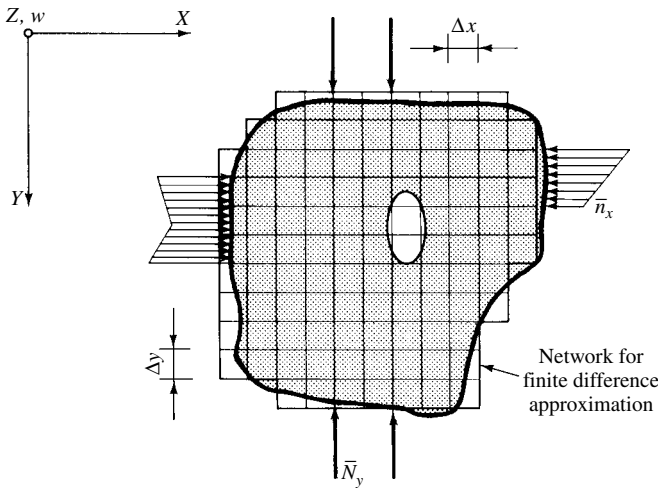


Figure 16.4.1 Plate of arbitrary shape under arbitrary in-plane forces.

It is evident from Eq. (16.4.3) that the problem has been reduced to a classical eigenvalue-eigenvector problem:

$$[C] - \lambda^*[I] = \{0\}. \quad (16.4.4)$$

Of all the eigenvalues obtained from a computerized solution of Eq. (16.4.4), we seek the lowest one, $\lambda_{\min} = \lambda_{\text{cr}}$, which, substituted into Eq. (16.1.1), gives the lowest buckling load.

The obtainable accuracy of the ordinary FDM can usually be increased by using the two-stage solution described in Sec. 5.1f, provided that the plate is simply supported and loaded by uniformly distributed compressive forces $\bar{n}_x = \bar{n}_y = -\lambda\bar{n}_{x0}$. In this case, the governing differential equation (16.4.1) becomes

$$\nabla^2 \mathfrak{M} + \lambda^* \mathfrak{M} = 0, \quad (16.4.1a)$$

where \mathfrak{M} is the moment-sum defined by Eq. (1.2.42) and $\lambda^* = \lambda\bar{n}_{x0}/D$.

Furthermore, FDMs can be used to obtain approximate solutions of more difficult plate buckling problems that involve the consideration of variable plate thickness, large deflections and even postbuckling behavior. Such problems, although of great practical importance, very seldom can be solved analytically.

The critical loads so obtained can be considerably improved by means of a simple extrapolation technique. Let us assume that the error of the computed critical load is inversely proportional to the squares of the subdivisions (N), used in two subsequent finite difference solutions (1 and 2 in Illustrative Example I below). Then, we can write

$$\bar{n}_{\text{cr,exact}} - \bar{n}_{\text{cr}}^{(1)} = \frac{C}{N_{(1)}^2} \quad \text{and} \quad \bar{n}_{\text{cr,exact}} - \bar{n}_{\text{cr}}^{(2)} = \frac{C}{N_{(2)}^2}, \quad (16.4.5)$$

where C is an unknown constant that is eliminated when solving for $\bar{n}_{\text{cr,exact}} \approx \bar{n}_{\text{cr, improved}}$.

Stodola-Vianello's iterative technique [16.4.5], described in Sec. 15.1, can also be successfully applied to improve the results of any approximate solution of plate stability problems. Suppose that the first ordinary finite difference solution has resulted in an approximate value for the critical load $\bar{n}_{\text{cr}}^{(0)} = \lambda_{\text{cr}}^{(0)}\bar{n}_{x0}$, which corresponds to the mode shape $w^{(0)}$; then, an improved value of the critical load can be computed from

$$\lambda_{\text{cr}}^{(1)} = \frac{\iint_{(A)} w^{(0)} dA}{\iint_{(A)} w^{(1)} dA} \approx \frac{\sum_{i=1}^r w_i^{(0)}}{\sum_{i=1}^r w_i^{(1)}}. \quad (16.4.6)$$

To obtain the required improved buckling shape $w^{(1)}$, however, we must solve the differential equation

$$D \nabla^4 w^{(1)} = -\lambda_{\text{cr}}^{(0)} \mathcal{L}(w^{(0)}) = p_z^{(0)} \quad (16.4.7)$$

assuming that $p_z^{(0)}$ is a fictitious load. The deflections ($w^{(0)}, w^{(1)}$) in Eq. (16.4.7) are normalized. For a finite difference solution, the use of an improved load representation in combination with a higher-order finite difference expression in the differential operator $\mathcal{L}(\cdot)$ is recommended. If required, the iterative cycle can be repeated.

Summary. By replacing the derivatives in the governing differential equations of plate buckling by ordinary finite differences, difficult stability problems involving arbitrary configurations, boundary conditions and loadings can be solved numerically. With sufficient fine subdivision, the method yields acceptable accuracy (less than 5% discrepancy). The obtained results can be improved by Stodola-Vianello's iterative technique. When high accuracy is required, improved FDMs [16.4.1] should be used; their application, however, may require the development of new stencils, which is by no means an easy task.

Finally, it should be noted that in some cases the finite difference approach to the critical load yields nonmonotonic convergence; that is, the results may oscillate about the true value [16.4.4].

ILLUSTRATIVE EXAMPLE I

Find the critical load of a simply supported square plate subjected to $\bar{n}_x = \bar{n}_y = -\lambda \bar{n}_{x0}$ edge forces by the ordinary FDM using a 3×3 grid (Fig. 16.4.2).

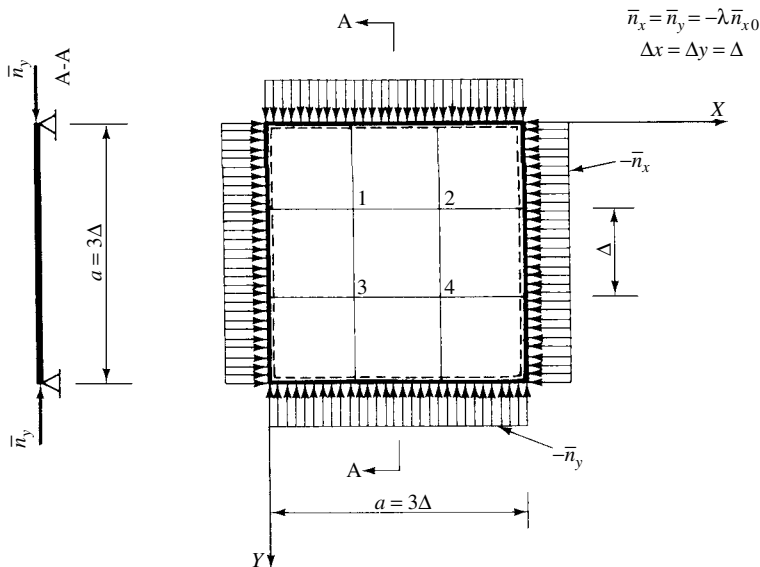


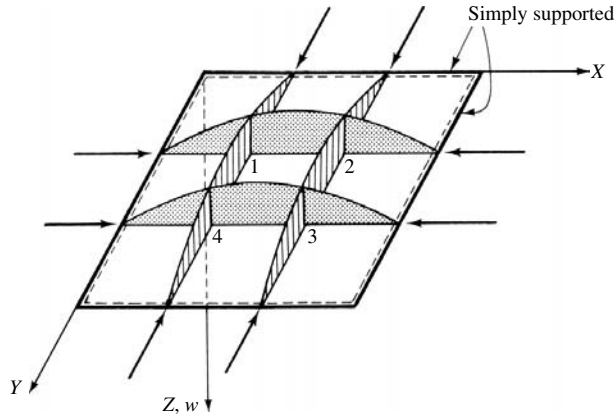
Figure 16.4.2 Simply supported plate under uniform thrust.

1. The governing differential equation of the problem (16.4.1) is

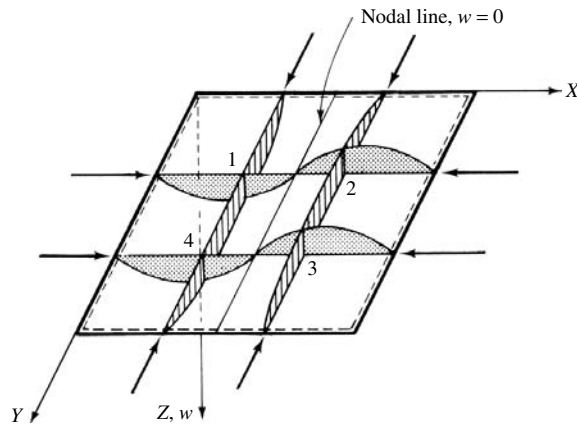
$$D \nabla^4 w + \lambda \bar{n}_{x0} \nabla^2 w = 0. \quad (16.4.8)$$

Since the lowest buckling load is pertinent to a symmetrical buckling shape and therefore $w_1 = w_2 = w_3 = w_4 = w$ (Fig. 16.4.3), the finite difference form of Eq. (16.4.8) has the following simplified form:

$$\frac{D}{\Delta^4}(20 - 8 - 1 - 8 + 2 - 1)4w + \frac{\lambda \bar{n}_{x0}}{\Delta^2}(-4 + 1 + 1)4w = 0. \quad (16.4.9)$$



(a) First mode



(b) Second mode

Figure 16.4.3 Buckling modes of square plate.

By introducing

$$\bar{n}_{x0} = \frac{\pi^2 D}{a^2} = \frac{\pi^2 D}{(3\Delta)^2}, \quad (16.4.10)$$

we obtain

$$\lambda_{cr} = \frac{18}{\pi^2} \approx 1.83; \quad (16.4.11)$$

hence

$$\bar{n}_{cr} = \lambda_{cr} \bar{n}_{x0} \approx \frac{1.83\pi^2 D}{a^2}, \quad (16.4.12)$$

versus the theoretical solution [16.1.1] $\bar{n}_{cr} = 2\pi^2 D/a^2$, which represents an error less than 9%. The accuracy of the solution can be improved by using a finer net combined with the extrapolation technique given in Eq. (16.4.5).

2. Since the boundary condition and in-plane loads permit the use of Eq. (16.4.1a), let us repeat the previous calculation, but let us also determine the buckling forces pertinent to the higher modes.

Since the moment-sum at the edges is zero, we shall deal only with $\mathfrak{M}_1, \mathfrak{M}_2, \mathfrak{M}_3$ and \mathfrak{M}_4 unknown moments (Fig. 16.4.2). Using ordinary finite differences and $\Delta x = \Delta y = \Delta = a/3$, Eq. (16.4.1a) becomes

$$\begin{aligned} \text{At point 1:} \quad & \frac{1}{\Delta^2}(-4\mathfrak{M}_1 + \mathfrak{M}_2 + \mathfrak{M}_4) + \lambda^* \mathfrak{M}_1 = 0. \\ \text{At point 2:} \quad & \frac{1}{\Delta^2}(\mathfrak{M}_1 - 4\mathfrak{M}_2 + \mathfrak{M}_3) + \lambda^* \mathfrak{M}_2 = 0. \\ \text{At point 3:} \quad & \frac{1}{\Delta^2}(\mathfrak{M}_2 - 4\mathfrak{M}_3 + \mathfrak{M}_4) + \lambda^* \mathfrak{M}_3 = 0. \\ \text{At point 4:} \quad & \frac{1}{\Delta^2}(\mathfrak{M}_1 + \mathfrak{M}_3 - 4\mathfrak{M}_4) + \lambda^* \mathfrak{M}_4 = 0. \end{aligned} \quad (16.4.13)$$

The system determinant of these homogeneous equations is

$$\begin{vmatrix} \lambda^* - \frac{4}{\Delta^2} & \frac{1}{\Delta^2} & 0 & \frac{1}{\Delta^2} \\ \frac{1}{\Delta^2} & \lambda^* - \frac{4}{\Delta^2} & \frac{1}{\Delta^2} & 0 \\ 0 & \frac{1}{\Delta^2} & \lambda^* - \frac{4}{\Delta^2} & \frac{1}{\Delta^2} \\ \frac{1}{\Delta^2} & 0 & \frac{1}{\Delta^2} & \lambda^* - \frac{4}{\Delta^2} \end{vmatrix}. \quad (16.4.14)$$

The vanishing determinant yields the characteristic equation

$$\left(\lambda^* - \frac{4}{\Delta^2}\right)^4 - \frac{4}{\Delta^4} \left(\lambda^* - \frac{4}{\Delta^2}\right)^2 = 0, \quad (16.4.15)$$

the roots of which are

$$\lambda_1^* = \frac{2}{\Delta^2}, \quad \lambda_2^* = \lambda_3^* = \frac{4}{\Delta^2}, \quad \lambda_4^* = \frac{6}{\Delta^2}. \quad (16.4.16)$$

Introducing, again, the datum value

$$\bar{n}_{x0} = \frac{\pi^2 D}{a^2} = \frac{\pi^2 D}{9\Delta^2} \quad (16.4.17)$$

and using the smallest root $\lambda_1^* = 2/\Delta^2$, the critical load factor λ_{cr} becomes

$$\lambda_{cr} = \frac{\lambda_1^* D}{\bar{n}_{x0}} = \frac{18}{\pi^2}, \quad (16.4.18)$$

which is identical with the result obtained previously. Had we not used symmetry in part 1 of the solution, part 2 would have shown some improvement in accuracy.

The first and second buckling modes are shown in Fig. 16.4.3.

ILLUSTRATIVE EXAMPLE II

The orthotropic plate shown in Fig. 16.4.4a is subjected to $\bar{n}_x = \bar{n}_y$ compressive, in-plane forces. Let us determine the critical buckling load \bar{n}_{cr} of the plate by applying the ordinary FDM. The flexural rigidity of the plate in the Y direction and its torsional stiffness (represented by $2B$) are related to the flexural rigidity D_x in the X direction as follows: $D_y = 0.5D_x$ and $2B = 2.496D_x$.

In this case, the governing differential equation of this stability problem is represented by Eq. (16.4.1). The corresponding finite difference representation of this equation is given in Eq. (16.4.2). The finite difference mesh along with the numbering of mesh points are shown in Fig. 16.4.3b. Applying Eq. (16.4.2) at each mesh point, we obtain the matrix equation

$$\left(\frac{D_x}{\Delta^4} \mathbf{A} + \frac{\lambda \bar{n}_{x0}}{\Delta^2} \mathbf{B} \right) \mathbf{w} = \{0\} \quad \text{or} \quad \left(\mathbf{A} + \frac{\lambda \bar{n}_{x0}}{D_x} \Delta^2 \mathbf{B} \right) \mathbf{w} = \{0\}, \quad (16.4.19)$$

The corresponding matrices \mathbf{A} and \mathbf{B} are

$\mathbf{A} =$

$$\begin{bmatrix} 1 & 2 & 3 & 4 & 5 & 6 & 7 & 8 & 9 & 10 & 11 & 12 \\ 20.2184 & & & & & & & & & & & \\ -6.8592 & 19.7184 & & & & & & & & & & \\ 0.5 & -6.8592 & 20.2184 & & & & & & & & & \\ -8.8592 & & & 19.2184 & & & & & & & & \\ & -8.8592 & & -6.8592 & 18.7184 & & & & & & & \\ & & -8.8592 & 0.5 & -6.8592 & 19.2184 & & & & & & \\ 1 & & & -8.8592 & & & 19.2184 & & & & & \\ & 1 & & & -8.8592 & & -6.8592 & 18.7184 & & & & \\ & & 1 & & & -8.8592 & 0.5 & -6.8592 & 19.2184 & & & \\ & & & 1 & & & -8.8592 & & & 20.2184 & & \\ & & & & 1 & & & -8.8592 & & -6.8592 & 19.7184 & \\ & & & & & 1 & & & -8.8592 & 0.5 & -6.8592 & 20.2184 \end{bmatrix} \begin{matrix} 1 \\ 2 \\ 3 \\ 4 \\ 5 \\ 6 \\ 7 \\ 8 \\ 9 \\ 10 \\ 11 \\ 12 \end{matrix}, \quad (16.4.20)$$

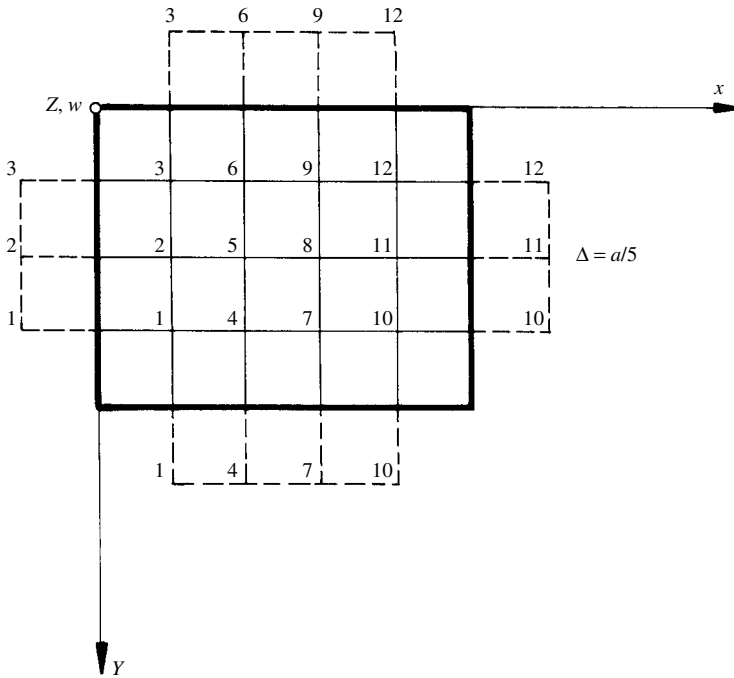
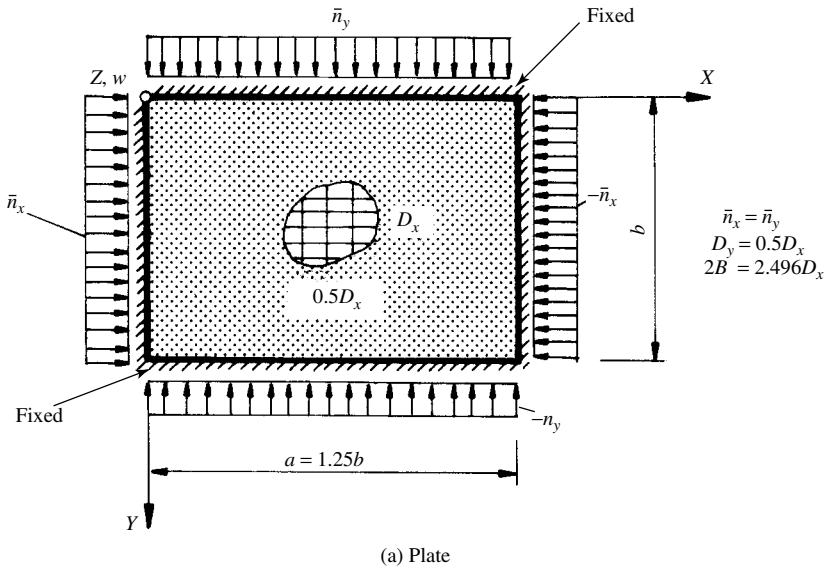


Figure 16.4.4 Orthotropic plate subjected to in-plane forces.

B =

$$\begin{bmatrix}
 1 & 2 & 3 & 4 & 5 & 6 & 7 & 8 & 9 & 10 & 11 & 12 \\
 -4.5 & & & & & & & & & & & \\
 1.25 & -4.5 & & & & & & & & & & \\
 & 1.25 & -4.5 & & & & & & & & & \\
 1 & & & -4.5 & & & & & & & & \\
 & 1 & & 1.25 & -4.5 & & & & & & & \\
 & & 1 & & 1.25 & -4.5 & & & & & & \\
 & & & 1 & & & -4.5 & & & & & \\
 & & & & 1 & & 1.25 & -4.5 & & & & \\
 & & & & & 1 & & 1.25 & -4.5 & & & \\
 & & & & & & 1 & & & -4.5 & & \\
 & & & & & & & 1 & & 1.25 & -4.5 & \\
 & & & & & & & & 1 & & 1.25 & -4.5 \\
 & & & & & & & & & 1 & & 1.25 & -4.5
 \end{bmatrix}
 \begin{matrix}
 1 \\ 2 \\ 3 \\ 4 \\ 5 \\ 6 \\ 7 \\ 8 \\ 9 \\ 10 \\ 11 \\ 12
 \end{matrix}
 \quad (16.4.21)$$

Multiplying the second equation in Eq. (16.4.19) by **B**⁻¹ yields

$$(\mathbf{B}^{-1}\mathbf{A} - \lambda\mathbf{I})\mathbf{w} = \{0\} \quad \text{or} \quad (\mathbf{C} - \lambda\mathbf{I})\mathbf{w} = \{0\}, \quad (16.4.22)$$

and a typical eigenvalue-eigenvector problem is created, where **I** represents the identity matrix.

Since we are only interested in the lowest eigenvalue, $\lambda_1 = \lambda_{\min}$, the Mises inverse matrix iterative technique can be used. For this purpose, we write Eq. (16.4.22) in the form

$$\left(\mathbf{C}^{-1} - \frac{1}{\lambda} \mathbf{I} \right) \mathbf{w} = \{0\}. \quad (16.4.23)$$

This procedure yields $\lambda_1 = \lambda_{\min} = 1.8003$. The corresponding eigenvector

$$\mathbf{w} = \begin{Bmatrix}
 -0.2793 \\
 -0.4265 \\
 -0.2793 \\
 -0.1934 \\
 -0.2953 \\
 -0.1934 \\
 0.1934 \\
 0.2953 \\
 0.1934 \\
 0.2713 \\
 0.4265 \\
 0.2793
 \end{Bmatrix} \quad (16.4.24)$$

represents the buckling mode of the plate, shown in Fig. 16.4.5.

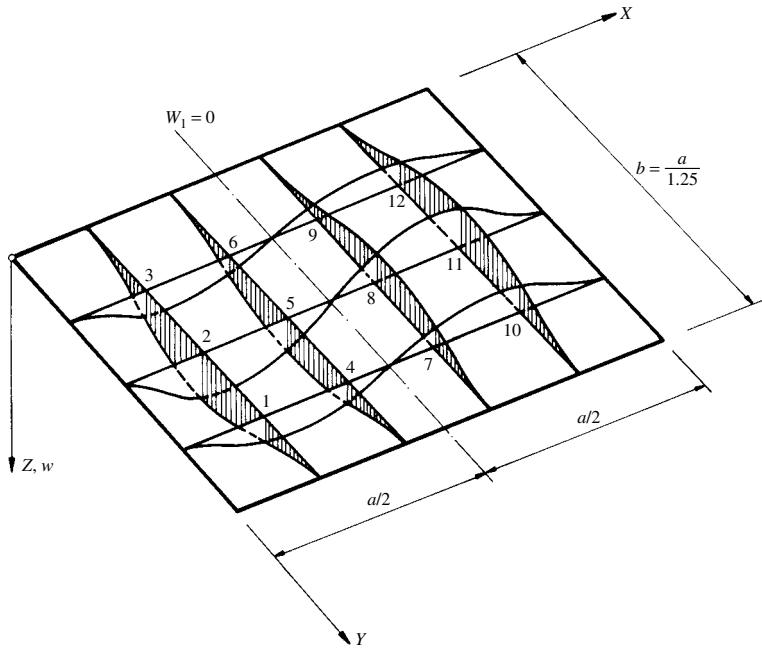


Figure 16.4.5 Buckling mode.

Using the relationships

$$\bar{n}_{x0} = \frac{\pi^2 D_x}{a^2} \quad \text{and} \quad \lambda_1 = \lambda_{cr} \bar{n}_{x0} \frac{\Delta^2}{D_x}, \quad (16.4.25)$$

we can write

$$\lambda_{cr} = \frac{\lambda_1 D_x}{\bar{n}_{x0} \Delta^2} = \frac{1.8003 D_x}{(\pi^2 D_x / a^2)(a/5)^2} = 4.5602. \quad (16.4.26)$$

Hence, the critical load of the plate becomes

$$\bar{n}_{cr} = \lambda_{cr} \bar{n}_{x0} = 4.5602 \frac{\pi^2 D_x}{a^2} = 45.01 \frac{D_x}{a^2}. \quad (16.4.27)$$

An independent check using an energy approach gives

$$\bar{n}_{cr} = \frac{47.46 D_x}{a^2}. \quad (16.4.28)$$

Since our finite difference approach yields a lower-bound solution while the energy approach is inherently upper bound, their average value

$$\bar{n}_{cr} = \frac{46.23 D_x}{a^2} \quad (16.4.29)$$

results in a quite reliable solution of this stability problem.

References and Bibliography

- [16.4.1] STÜSSI, F., "Berechnung der Beulspannungen gedrückter Rechteckplatten," *Publ. IABSE*, 17 (1947), 236–248.
- [16.4.2] BÜRGERMEISTER, G., and STEUP, H., *Stabilitätstheorie*, Vol. I, Akademie-Verlag, Berlin, 1957.
- [16.4.3] HEESCH, O., "Die Berechnung der Beulspannungen ebener Platten mit Hilfe von Differenzgleichungen unter besonderer Berücksichtigung von Dreiecksplatten," Ph.D. Dissertation, Technical University of Hanover, Hanover, Germany 1936.
- [16.4.4] SALVADORI, M. G., "Numerical Computation of Buckling Loads by Finite Differences," *Proc. ASCE*, 75 (Dec. 1949), 1441–1475.
- [16.4.5] VIANELLO, L., "Graphische Untersuchung der Knickfestigkeit gerader Stäbe," *VDI Zeitschrift*, 42 (1898), 1436–1443.
- [16.4.6] BUBLIK, B. N., *Chislennoe reshenie zadach dinamiki plastin i obolochek (Numerical Solution of Dynamic Plate and Shell Problems)*, Izd. Kievskogo Universiteta, Kiev, 1969.
- [16.4.7] IYENGAR, N. G. R., *Structural Stability of Columns and Plates*, Halsted Press, New York, 1988.

16.5 Finite Element and Gridwork Approach to Stability Analysis

a. Elastic Buckling. This section extends the FEM and GWM to deal with problems of linear, elastic instability of plates. In the case of plate-type structures—often encountered in ships and in aeroplanes—the linear instability analysis can quite accurately define the critical buckling loads of plates under which failure occur. In comparison with the finite difference solution of plate buckling treated in the foregoing section, the FEM and GWM are more versatile, since they can cope with variable loads and boundary conditions along with irregular plate geometries. The general principles of stability analysis, as presented in Sec. 16.1, can be easily applied to finite element and gridwork approaches, since stability analysis is a *geometrically nonlinear problem* already treated in Sec. 11.2. We assume a single smooth equilibrium path that emerges from the undeformed state of the plate as the in-plane loads are gradually increased from zero to the bifurcation point.

Thus, let us assume that we gradually increase the in-plane loads $\bar{\mathbf{p}}_0$ by a load factor λ . At a certain point, the originally flat plate defects laterally. In passing from the flat state of equilibrium, the deformation bifurcates, as shown in Fig. 16.1.3. In this situation, the lateral displacements will also create membrane-type of forces. Consequently, the developments of in-plane and lateral deformations at the same time are not separate but coupled. Assuming further that throughout the loading range beyond the bifurcation point the loads and the displacement-dependent part of the stiffness matrix, $\bar{\mathbf{K}}^{\text{NL}}(d)$ varies with the load factor, Eq. (11.2.5) becomes

$$[\bar{\mathbf{K}}^{\text{L}} + \lambda \bar{\mathbf{K}}^{\text{NL}}] \bar{\mathbf{d}} = \lambda \bar{\mathbf{p}}_0. \quad (16.5.1)$$

The linear part of the stiffness matrix $\bar{\mathbf{K}}^{\text{L}}$ consists of two uncoupled parts, $\bar{\mathbf{K}}^{\text{L}} = \bar{\mathbf{K}}_m + \bar{\mathbf{K}}_b$, representing the corresponding membrane and bending effects, respectively. In the *neutral* state of equilibrium, which is infinitesimally close to the *stable* equilibrium, the in-plane forces $\bar{\mathbf{p}}_0$ are equilibrated by the membrane stresses.

Consequently, in the absence of lateral forces, we obtain the homogeneous form of Eq. (16.5.1). Therefore, we can write

$$(\bar{\mathbf{K}}_b^L + \lambda \bar{\mathbf{K}}^{\text{NL}}) \bar{\mathbf{d}} = \{0\}, \quad (16.5.2)$$

which is, in fact, the matrix version of the equilibrium statement expressed by Eq. (16.2.3), provided that this equation is integrated over the total area of the middle surface of the plate.

Since in this case $\bar{\mathbf{K}}^{\text{NL}}$ has a reducing effect on the bending stiffness of the plate, Eq. (16.5.2) can be written as

$$\bar{\mathbf{K}}_b^L - \lambda \bar{\mathbf{K}}^{\text{NL}} = \{0\} \quad (16.5.3)$$

or, in another form,

$$\mathbf{C} - \lambda \mathbf{I} = \{0\} \quad \text{with} \quad \mathbf{C} = (\bar{\mathbf{K}}^{\text{NL}})^{-1} \bar{\mathbf{K}}_b, \quad (16.5.4)$$

where \mathbf{I} represents the identity matrix. Solving this typical eigenvalue problem, λ can be obtained. Again, we seek the lowest eigenvalue, $\lambda_{\min} = \lambda_{\text{cr}}$, at which bifurcation occurs. For this purpose, we put Eq. (16.5.4) in the following form so that Mises's inverse matrix iteration technique can be applied:

$$\mathbf{C}^{-1} - \lambda^* \mathbf{I} = \{0\} \quad \text{for } \lambda^* = \frac{1}{\lambda}. \quad (16.5.5)$$

The critical load is obtained from

$$\bar{\mathbf{p}}_{\text{cr}} = \lambda_{\text{cr}} \bar{\mathbf{p}}_0, \quad (16.5.6)$$

where $\bar{\mathbf{p}}_0$ represents some trial load, usually associated with buckling of plate strips, as introduced in Illustrative Example II of Sec. 16.4. For the linear-elastic instability analysis of plates, the eigenvalue formulation discussed above is more advantageous than the incremental procedures treated in Sec. 11.2.1.

By generating the nonlinear parts of the element stiffness matrices

$$(\mathbf{K}_e^{\text{NL}})^{(N)} = (\mathbf{K}_{e,x}^{\text{NL}} + \mathbf{K}_{e,y}^{\text{NL}} + \mathbf{K}_{e,xy}^{\text{NL}})^{(N)}, \quad (16.5.7)$$

we follow the same procedures described in Sec. 11.2. Consequently, the nonlinear stiffness matrices for finite elements and gridwork cells, respectively, which are given in explicit forms in the Sec. 16.4, can also be directly applied in the present stability analysis. Furthermore, it is interesting to note that these nonlinear element stiffness matrices representing the instability effects are independent from the material properties of the plate. Hence, they can be equally applied in the stability analysis of isotropic as well as orthotropic plates.

As Fig. 16.5.1 shows, the conforming gridwork cell has far better convergence characteristics in stability analysis than those obtained for a nonconforming finite element with 12 DOF. Similarly, the gridwork cell also exhibits good convergence properties in the case of rather difficult shear loading (Fig. 16.5.2); results are also

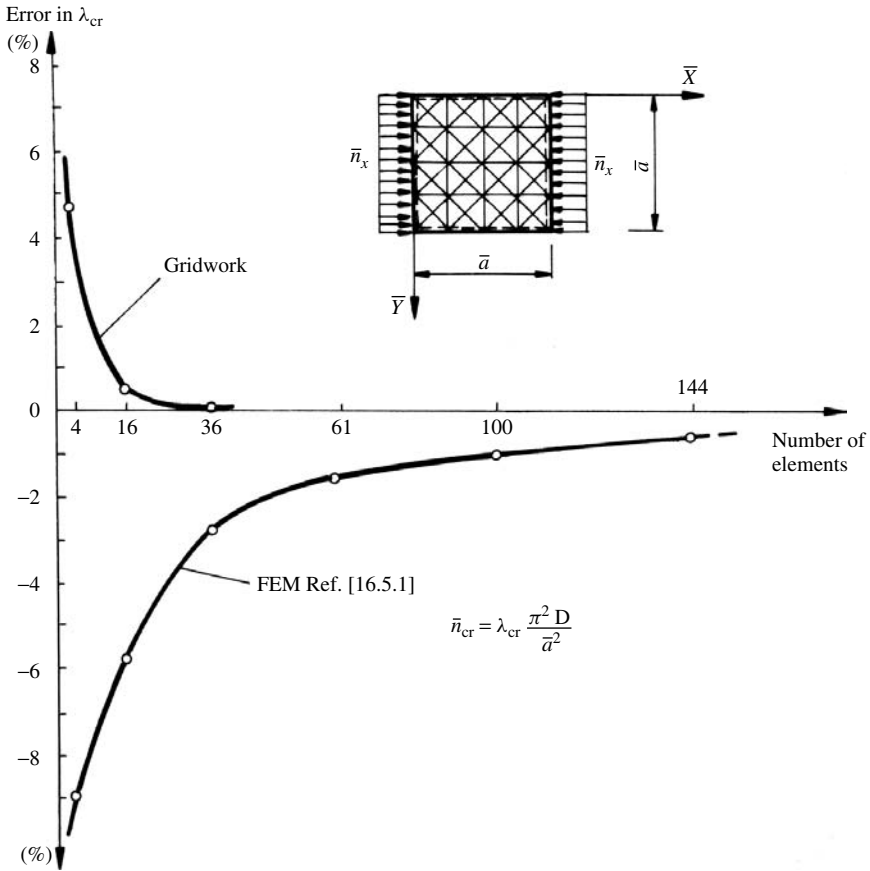


Figure 16.5.1 Comparison of convergence properties in stability analysis.

quite good when the plate is subjected to combined in-plane compressive and shearing forces (Fig. 16.5.3).

If required, the Stodola-Vianello iterative technique, as described in previous sections, can be applied to improve the obtained eigenvalues. However, considering the rapid convergence properties of conforming finite elements and gridwork cells, such improvement should be limited to cases when (1) only computers of limited capacity are available or (2) large plate structures are analyzed for their instability behavior and high accuracy is required.

b. Inelastic Buckling. The inelastic stability analysis of plates represents a relatively complex computational problem, since one must consider combined geometrical and material nonlinearities when the critical loads are to be determined. We can *indirectly* extend the finite element approach to include inelastic buckling. However, it is important to note that such buckling analysis is sensitive to small imperfections in the plates. Therefore, the treatment of such instability cases as pure bifurcation problems may lead to some errors. Consequently, it is recommended that the analyst

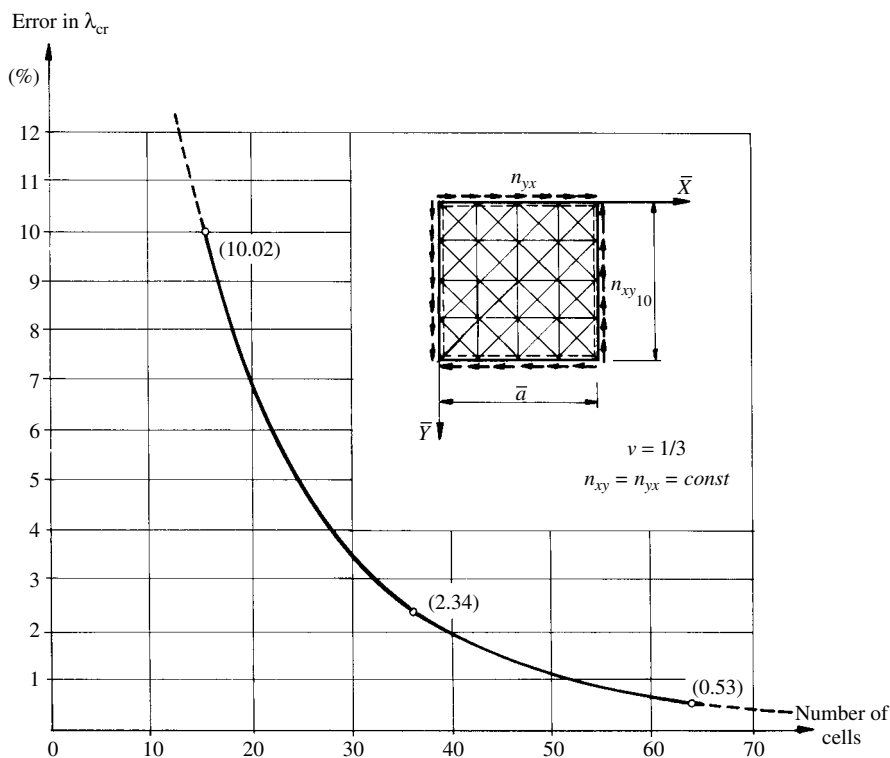


Figure 16.5.2 Convergence characteristics of gridwork cells subjected to shearing forces.

combine one of the incremental methods introduced in Sec. 11.4 with eigenvalue problems to detect the critical loads.

The following *simplified* method may be used in inelastic stability analysis of plates. At some trial load level, the corresponding displacements and stresses are evaluated and the matrices $\mathbf{K}_b(I_r)$ and $\mathbf{K}^{\text{NL}}(\mathbf{d})$ are computed.[†] Introducing again a load parameter λ , we formulate the instability of plates as eigenvalue problems corresponding to the trial load level and write

$$(\bar{\mathbf{K}}_b(I_r) + \lambda \bar{\mathbf{K}}^{\text{NL}}(\bar{\mathbf{d}})) = \{0\}. \quad (16.5.8)$$

Next, this eigenvalue problem is solved and the lowest eigenvalue λ_{\min} is examined. If $\lambda = 1.0$, the buckling criterion is satisfied. However, if λ_{\min} is greater or less than 1, the trial load is less or greater than the critical load. In this case, the trial load is either incremented or reduced, respectively. As mentioned, this is a simplified procedure. For more elaborate solution procedures the reader is referred to Refs. [16.5.4] and [16.6.8].

Summary. In the stability analysis of plates the FEM and GWM have the following advantages:

[†] See Sec. 11.4.

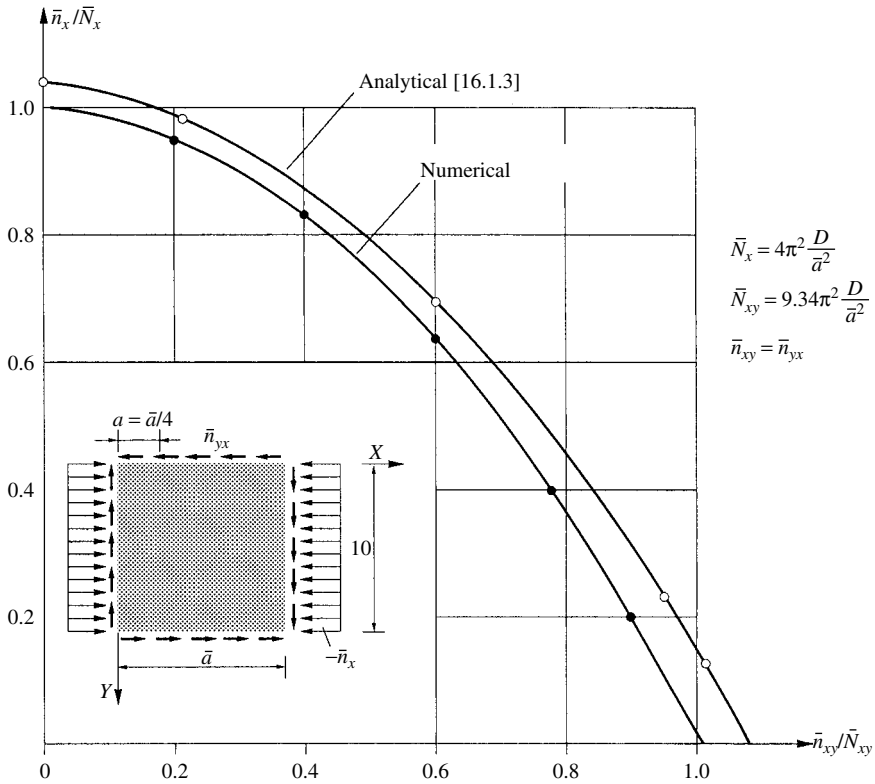


Figure 16.5.3 Approximation of interaction curve.

- The mathematical formulation is straightforward.
- Since the instability problem of plates is usually reduced to solution of classic eigenvalue-eigenvector problems, the lowest mode of buckling cannot be missed, provided that the buckling occurs in the elastic range.
- Because we usually seek only the lowest eigenvalue, the inverse matrix iteration technique from Mises can be advantageously applied.
- The FEM and GWM are able to solve a wide variety of difficult instability problems involving arbitrary boundaries, boundary conditions and irregular plate geometry and even anisotropic plates.
- The results compare favorably with experimental and analytical solutions.
- Basically, these methods can also be extended to inelastic buckling problems. In such a case, however, an incremental solution technique should be combined with the eigenvalue analysis.

In addition to some disadvantages of the FEM and GWM discussed earlier, another one must be considered when these methods are used for instability analysis; that is, the geometrically nonlinear element matrices must be computed for a variety of loading conditions, as shown in Sec. 11.2. But these matrices are reusable; thus, strictly speaking, this aspect constitutes only an inconvenience.

Finally, it should be noted that the use of nonconforming shape functions in generating linear and nonlinear element matrices results in a lower-bound approach to the theoretical value of the critical load, whereas conforming shape functions yield upper-bound solutions, as shown in Fig. 16.5.1.

ILLUSTRATIVE EXAMPLE

Let us determine the critical buckling load of a simply supported square plate subjected to uniformly distributed edge forces $-n_x$, as shown in Fig. 16.5.4a. We use the GWM in the computation.

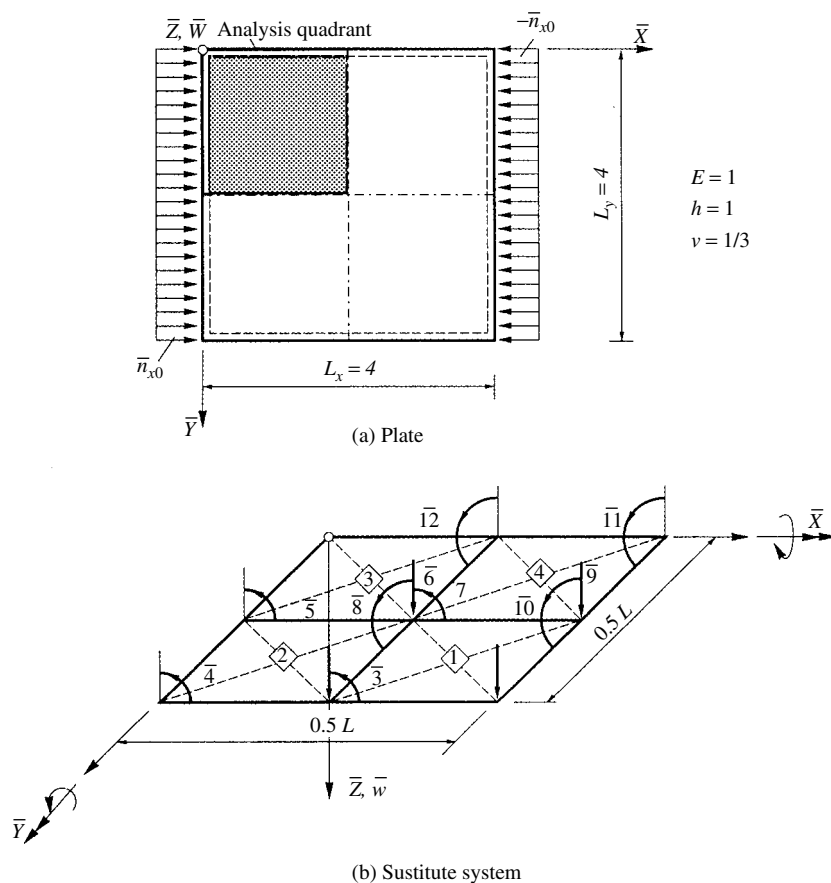


Figure 16.5.4 Stability analysis of square plate by GWM.

The bending part of the linear stiffness matrix of the gridwork cell (Fig. 16.5.5) is given in Table 6.3.3, and its nonlinear counterpart is listed in Table 11.2.4. Since we are dealing with compressive in-plane forces, n_x must be negative in this expression. Determining the first buckling mode, the double symmetry of the structure can be utilized. Consequently, we can subdivide the analysis quadrant of the plate into four gridwork cells (Fig. 16.5.4b).

DOFs, The nonlinear stiffness matrix of the plate is obtained in the following from:

$$\bar{\mathbf{K}}^{\text{NL}} = -\bar{n}_{x0} \times \begin{bmatrix} 0.400 & & & & & & & & & & \\ -0.400 & 0.800 & & & & & & & & & \\ 0.033 & 0.000 & 0.133 & & & & & & & & \\ 0.000 & 0.033 & -0.011 & 0.067 & & & & & & & \\ 0.000 & 0.017 & -0.006 & 0.000 & 0.133 & & & & & & \\ -0.200 & 0.400 & 0.000 & 0.017 & 0.067 & 1.600 & & & & & \\ 0.017 & 0.000 & 0.000 & -0.006 & -0.022 & 0.000 & 0.267 & & & & \\ -0.017 & 0.033 & 0.000 & -0.006 & 0.000 & 0.000 & 0.000 & 0.000 & & & \\ 0.200 & -0.200 & 0.017 & 0.000 & 0.000 & -0.800 & 0.067 & 0.000 & 0.800 & & \\ 0.017 & -0.017 & -0.006 & 0.000 & 0.000 & 0.000 & 0.000 & 0.000 & 0.000 & 0.000 & \\ 0.000 & 0.000 & 0.000 & 0.000 & 0.000 & -0.017 & -0.006 & -0.006 & 0.017 & 0.006 & 0.000 \\ 0.000 & 0.000 & 0.000 & 0.000 & -0.006 & 0.033 & 0.000 & 0.011 & -0.017 & -0.006 & 0.000 & 0.000 \end{bmatrix} \quad \text{Symmetric} \quad (16.5.11)$$

The iterative solution of the pertinent *inverse* eigenvalue problem

$$(\bar{\mathbf{K}}_b^{\text{L}})^{-1} \bar{\mathbf{K}}^{\text{NL}} - \frac{1}{\lambda} \mathbf{I} = \{0\} \quad (16.5.12)$$

written in another form

$$\mathbf{C} - \lambda^* \mathbf{I} = \{0\} \quad (16.5.13)$$

yields the lowest eigenvalue, $\lambda_{\min} = 3.719D^*$, and the corresponding eigenvector

$$\bar{\mathbf{d}} = \begin{Bmatrix} 1.00000 \\ 0.70756 \\ -0.55728 \\ -0.78954 \\ -0.55829 \\ 0.50032 \\ -0.39406 \\ 0.39102 \\ 0.70711 \\ 0.55269 \\ 0.78162 \\ 0.55299 \end{Bmatrix} \quad (16.5.14)$$

Therefore, the critical load of the plate is

$$\bar{n}_{\text{cr}} = 3.719D^* = 2.476D. \quad (16.5.15)$$

A comparison with the analytical solution [16.1.1] of this problem,

$$\bar{n}_{\text{cr}} = 4.0 \frac{\pi^2 D}{L^2} = 2.467D, \quad (16.5.16)$$

shows an error of only 0.4%.

References and Bibliography

- [16.5.1] KAPUR, K. K., and HARTZ, B. J., "Stability of Thin Plates Using Finite Element Method," *Proc. ASCE*, 92, *J. Eng. Mech. Div. EM*, 2 (Apr. 1966), 177–195.
- [16.5.2] MARTIN, H. C., "On the Derivation of Stiffness Matrices for the Analysis of Large Deflection and Stability Problems," in *Proceedings of the First Conference on Matrix Method in Structural Mechanics*, AF Publ. AFFDL TR-68-150, Wrights Patterson AFB, Dayton, Ohio, 1969, pp. 697–716.
- [16.5.3] ARGYRIS, J. H., KELSEY, S., and KAMEL, H., "Matrix Methods in Structural Analysis—A Précis of Recent Developments," in *Proceedings of the First Conference on Matrix Method in Structural Mechanics*, AF Publ. AFFDL TR-68-150, Wrights Patterson AFB, Dayton, Ohio, 1969, pp. 1–164.
- [16.5.4] PIFKO, A., and ISAKSON, G., "A Finite Element Method for the Plastic Buckling Analysis of Plates," *AIAA J.*, 7, No. 10 (Oct. 1969), 1950–1959.
- [16.5.5] HARTZ, B. J., "Matrix Formulation of Structural Stability Problems," *Proc. ASCE*, 91, *J. Struct. Div.*, ST, 6 (Dec. 1965), 141–157.
- [16.5.6] CARSON, W. G., and NEWTON, R. E., "Plate Buckling Analysis Using a Fully Compatible Finite Element," *AIAA J.*, 7, No. 3 (Mar. 1969), 527–529.
- [16.5.7] HOLAND, I., and MOAN, T., "The Finite Element Method in Plate Buckling," in Ref. [16.5.14], pp. 475–500.
- [16.5.8] HARRIS, H. G., and PIFKO, A. B., "Elastic-Plastic Buckling of Stiffened Rectangular Plates," in Ref. [16.5.14], pp. 207–253.
- [16.5.9] RICHARD, R. M., and BLACKLOCK, J. R., "Finite Element Analysis of Inelastic Structures," *AIAA J.*, 7, No. 3 (Mar. 1969), 433–438.
- [16.5.10] GALLAGHER, R. H., and PADLOG, J., "Discrete Element Approach to Structural Instability Analysis," *AIAA J.*, 1, No. 6 (June 1963), 1437–1439.
- [16.5.11] GALLAGHER, R. H., et al., "A Discrete Element Procedure for Thin Shell Instability Analysis," *AIAA J.*, 5, No. 1 (Jan. 1967), 138–145.
- [16.5.12] RAMBERG, W., and OSGOOD, W. R., "Description of Stress-Strain Curves by Three Parameters," NACA TN 902, National Advisory Committee for Aeronautics, Washington, D.C., 1943.
- [16.5.13] HRENNIKOFF, A., MATHEW, C. I., and SEN, R., "Stability of Plates Using Rectangular Bar Cells," *Publ. IABSE*, 32-1 (1972), 109–126.
- [16.5.14] ROWAN, W. R., and HACKETT, M. (Eds.), *Proceedings of the Symposium on Application of Finite Element Method in Civil Engineering*, held at Nashville, Tennessee, Nov. 13–14, 1969, School of Engineering, Vanderbilt University, Nashville, Tennessee, 1969.
- [16.5.15] IYENGAR, N. G. R., *Structural Stability of Columns and Plates*, Halsted Press, New York, 1988.
- [16.5.16] STEUP, H., *Stabilitätstheorie im Bauwesen*, Ernst & Sohn, Berlin, 1990.

16.6 Dynamic Buckling

a. Introduction. Plates used in naval and aerospace structures are often subjected to dynamic in-plane forces. In many cases, for instance, damage to ship structures results from buckling of the main deck during storms [16.6.1]. Dynamic buckling of folded plate roofs under the influence of horizontal earthquake forces is another example that illustrates the practical importance of dynamic stability analysis of plates. These inherently difficult problems can be solved conveniently by extending the resonance concept of forced vibration of elastic systems. By introducing the concept of *parametric resonance*, a definite relation between the natural frequency of the lateral vibration of the plate and the frequency of the external pulses can be established [16.6.2].

A flat plate upon which periodic in-plane forces act will usually undergo axial vibrations, provided that the maximum intensity of the in-plane forces is less than that of the critical load of static buckling. If this is not the case, the in-plane forces can excite intense lateral vibrations. Such an in-plane loading is said to be *parametric* with respect to transverse deformations. *When the amplitudes of the lateral vibration become infinitely large, parametric resonance occurs.* Although the mathematical relationship of the frequencies is different from that which is conventionally used in calculating resonance of forced vibration, the concept of parametric resonance is very useful. In this way, the problem of dynamic stability of plates can be reduced to (1) solution of free lateral vibration and (2) static stability analysis. Since several analytical and numerical methods for solution of these plate problems have already been introduced, it is sufficient here to limit our discussion to this generalization of the resonance concept.

b. Parametric Resonance. Let us consider a flat plate, as shown in Fig. 16.2.1, subjected to periodic edge forces $-\bar{n}_x(t)$, $-\bar{n}_y(t)$ and $-\bar{n}_{xy}(t)$. The governing differential equation of motion can be obtained by adding the inertia term to von Kármán's large-deflection equations of plates (11.1.4). Thus, we can write

$$\begin{aligned} D \nabla^2 \nabla^2 w &= h \left(\frac{\partial^2 \Phi}{\partial y^2} \frac{\partial^2 w}{\partial x^2} + \frac{\partial^2 \Phi}{\partial x^2} \frac{\partial^2 w}{\partial y^2} - 2 \frac{\partial^2 \Phi}{\partial x \partial y} \frac{\partial^2 w}{\partial x \partial y} \right) - \bar{m} \frac{\partial^2 w}{\partial t^2}, \\ \nabla^2 \nabla^2 \Phi &= E \left[\left(\frac{\partial^2 w}{\partial x \partial y} \right)^2 - \frac{\partial^2 w}{\partial x^2} \frac{\partial^2 w}{\partial y^2} \right], \end{aligned} \quad (16.6.1)$$

where $\Phi(x, y, t)$ is the time-dependent Airy stress function and \bar{m} represents the mass of the plate per unit area. The inertia forces associated with rotation and the effect of structural damping have been neglected, as customary in the vibration analysis of plates.

Since the compressive external forces are independent of lateral deflection w , Eq. (16.6.1) can be linearized, yielding

$$D \nabla^4 w + \bar{n}_x \frac{\partial^2 w}{\partial x^2} + 2\bar{n}_{xy} \frac{\partial^2 w}{\partial x \partial y} + \bar{n}_y \frac{\partial^2 w}{\partial y^2} + \bar{m} \frac{\partial^2 w}{\partial t^2} = 0, \quad (16.6.2a)$$

$$\nabla^2 \nabla^2 \Phi = 0. \quad (16.6.2b)$$

We seek the solution of Eq. (16.6.2a) in the form

$$w(x, y, t) = W(x, y) \cdot \theta(t), \quad (16.6.3)$$

where $\theta(t)$ represents the time dependency. Substituting Eq. (16.6.3) into (16.6.2), the governing differential equation of the dynamic stability analysis of plates becomes

$$\frac{\nabla^4 W}{W} + \frac{1}{WD} \left(\bar{n}_x \frac{\partial^2 W}{\partial x^2} + 2\bar{n}_{xy} \frac{\partial^2 W}{\partial x \partial y} + \bar{n}_y \frac{\partial^2 W}{\partial y^2} \right) + \frac{\bar{m}}{D\theta(t)} \frac{\partial^2 \theta(t)}{\partial t^2} = 0. \quad (16.6.4)$$

To simplify the problem, let us assume, first, that the static components of the edge forces are zero and that the time dependency of the pulsating in-plane forces can be expressed by

$$\bar{n}_x = \bar{n}_t \cos pt, \quad \bar{n}_y = \alpha \bar{n}_t \cos pt, \quad \bar{n}_{xy} = \beta \bar{n}_t \cos pt, \quad (16.6.5)$$

where \bar{n}_t represents the amplitude of the pulsating force. The constants α and β define the ratios between the edge forces, as discussed in Sec. 16.2. It is required that the frequency of the forcing function p be smaller than the fundamental frequency of the axial vibration of the plate ($p < \omega_{\text{membr.}}$).

Equation (16.6.4) contains the governing differential equation of the static buckling (16.2.3) and that of the free lateral vibration (14.2.4), provided that the mode shape functions for buckling, W_λ , and for free lateral vibration, W_ω , are approximately the same[†]:

$$[W_\lambda(x, y) \approx W_\omega(x, y)] = W(x, y). \quad (16.6.6)$$

Substitution of Eq. (16.6.3) into the differential equation of the free lateral vibration of plates (14.2.4) yields

$$\frac{\nabla^4 W}{W} + \frac{\bar{m}}{D\theta(t)} \frac{\partial^2 \theta(t)}{\partial t^2} = 0. \quad (16.6.7)$$

If we assume that $\theta(t) = \sin \omega t$, the natural circular frequencies can be determined from

$$\omega_i = c_i \sqrt{\frac{D}{\bar{m}}} \quad \text{for } i = 1, 2, 3, \dots, \quad (16.6.8)$$

where c_i is a constant containing the effect of the boundary conditions and spans. From (16.6.8) we obtain

$$\frac{\bar{m}}{D} = \frac{c_i^2}{\omega_i^2}. \quad (16.6.9)$$

The critical in-plane load \bar{n}_{cr} is determined from Eq. (16.6.4) under the assumption that $\theta(t) = \text{const}$, that is, the in-plane forces act statically. Thus, using Eq. (16.6.5), we can write

$$D \nabla^4 W + \lambda \bar{n}_{x0} \left(\frac{\partial^2 W}{\partial x^2} + \alpha \frac{\partial^2 W}{\partial y^2} + 2\beta \frac{\partial^2 W}{\partial x \partial y} \right) = 0, \quad (16.6.10)$$

which represents the governing differential equation of the static buckling of plates (16.2.3). In Eq. (16.6.10) λ is the load factor and \bar{n}_{x0} defines a reference value, as described in Sec. 16.2. The lowest value of the load factor yields the critical load for static buckling ($\bar{n}_{\text{cr}} = \lambda_{\text{cr}} \bar{n}_{x0}$), the solution of which has the general form

$$\bar{n}_{\text{cr},i} = \lambda_i \frac{\pi^2 D}{b^2} \quad \text{for } i = 1, 2, 3, \dots, \quad (16.6.11)$$

where i represents the modes.

[†] If Eq. (16.6.6) is not satisfied, an incremental approach should be used for numerical solution of Eq. (16.6.4).

In the case of a specific problem, we select a shape function $W(x, y)$ that satisfies the boundary conditions and the governing differential equation of the problem. The substitution of $W(x, y)$ into Eq. (16.6.4) yields a differential equation for $\partial^2\theta/\partial t^2$. Using Eqs. (16.6.8) and (16.6.11), the differential equation so obtained can be reduced to the *Mathieu equation*,

$$\frac{\partial^2\theta(t)}{\partial t^2} + \omega_i^2 \left(1 - \frac{\bar{n}_t}{\bar{n}_{cr,i}} \cos pt\right) \theta(t) = 0, \quad (16.6.12)$$

which is generally given in the form

$$\frac{\partial^2\theta(t)}{\partial t^2} + \frac{4\omega_i^2}{p^2} (1 - \eta_i \cos 2\vartheta) \theta(t) = 0 \quad \text{for } i = 1, 2, 3, \dots, \quad (16.6.13)$$

where

$$\vartheta = \frac{pt}{2} \quad \text{and} \quad \eta_i = \frac{\bar{n}_t}{\bar{n}_{cr,i}}. \quad (16.6.14)$$

In these expressions ω_i and $n_{cr,i}$ represent the circular frequencies of the free lateral vibrations and the critical loads, respectively. Both are pertinent to the modes $i = 1, 2, 3, \dots$

Similar results are obtained when the static component \bar{n}_s of the in-plane load is present. In this case

$$\bar{n}_x = \bar{n}_s + \bar{n}_t \cos pt \quad (16.6.15)$$

and

$$\eta_i = \frac{\bar{n}_t}{\bar{n}_{cr,i} - \bar{n}_s}. \quad (16.6.16)$$

Furthermore, in determining the circular frequencies Ω_i , the effect of the static in-plane loads on the free vibration of the plates must be considered.

In a more general case, when

$$\bar{n}_x = \bar{n}_s + \bar{n}_t \Phi(t), \quad (16.6.17)$$

the problem can be reduced to the Hill equation, which has the general form

$$\frac{\partial^2\theta(t)}{\partial t^2} + \Omega_i^2 [1 - \eta_i \Phi(t)] \theta(t) = 0. \quad (16.6.18)$$

The interesting characteristic of the Mathieu equation is that for given η_i , $2\omega_i/p$ and $\vartheta \rightarrow \infty$ the solution will increase without limit in the zones of instability. Without discussing the mathematical theory of the Mathieu differential equation and its solution [16.6.8], the important results will be set forth briefly. The zones of dynamic instability are bounded by the following values [16.6.3]:

$$p_{cr} = \frac{2\omega_1}{\sqrt{1 \pm (\eta/2) + (7\eta^2/32) \pm (55\eta^3/512)}} \quad (16.6.19)$$

for the first mode,

$$p_{cr} = \frac{2\omega_2}{\sqrt{4 - (\eta^2/3)}} \quad \text{and} \quad p_{cr} = \frac{2\omega_2}{\sqrt{4 + (5\eta^2/3)}} \tag{16.6.20}$$

for the second mode and

$$p_{cr} = \frac{3\omega_3}{\sqrt{9 + (81\eta^2/64) \pm (9\eta^3/8)}} \tag{16.6.21}$$

for the third mode. These expressions are quite general; thus they can also be used for the dynamic stability analysis of shells [16.6.4] and folded plates [16.6.5]. The values of $2\omega_i/p_{cr}$ for $\eta = 0.2-1.8$ are given in Table 16.6.1. These results can best be illustrated by the Strutt diagram (Fig. 16.6.1), in which the regions where dynamic instability occurs are shaded.

Summary. The investigation of the dynamic stability of plates can be reduced to the solution of appropriate free lateral vibration and static stability problems. In the case

Table 16.6.1 Boundaries of Instability Zones

η	$2\omega_i/p_{cr}$					
	First Mode		Second Mode		Third Mode	
0.2	1.054	0.9487	1.995	2.015	3.010	3.007
0.3	1.082	0.9306	1.992	2.037	3.025	3.013
0.5	1.149	0.8837	1.977	2.102	3.082	3.027
0.7	1.225	0.8491	1.957	2.195	3.162	3.040
0.8	1.265	0.8276	1.944	2.249	3.225	3.040
1.0	1.353	0.7823	1.916	2.381	3.376	3.023
1.2	1.418	0.7266	1.876	2.53	3.578	2.980
1.4	1.556	0.588	1.828	2.694	3.821	2.898
1.6	1.673	0.5657	1.775	2.874	4.099	2.762
1.8	1.797	0.4243	1.709	3.066	4.427	2.557

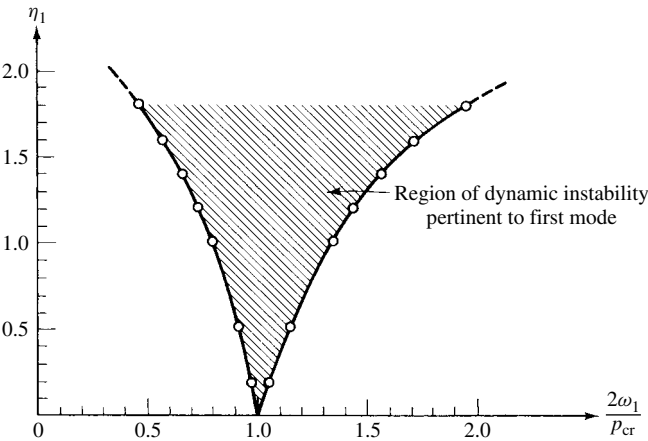


Figure 16.6.1 Strutt diagram.

of arbitrary geometry, loading and boundary conditions, the finite difference or framework methods [16.6.5] can be used advantageously for determination of the required circular frequencies and critical buckling loads. The field of dynamic buckling is still in the stage of development. Further research is needed to economically treat suddenly applied loads and nonlinear problems, to name a few areas of considerable practical interest.

ILLUSTRATIVE EXAMPLE

A square plate, shown in Fig. 16.6.2, is subjected to a $\bar{n}_x = -\bar{n}_t \cos pt$ pulsating edge force.

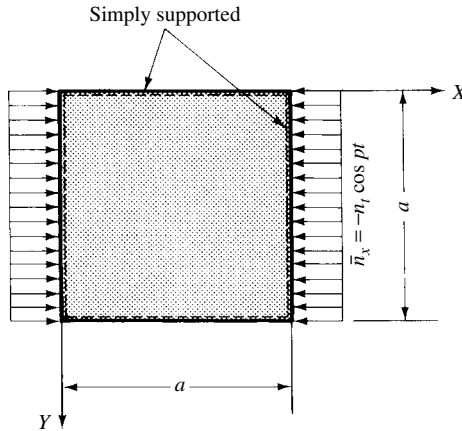


Figure 16.6.2 Plate subjected to dynamic in-plane forces.

1. Show that the governing differential equation can be reduced to the Mathieu equation.
2. Determine the paired critical frequencies pertinent to the first mode by assuming that $n_t/n_{cr} = 0.8$.

Since the boundaries are simply supported, the shape of the first mode of vibration and buckling can be expressed by

$$W(x, y) = W_\lambda(x, y) = W_\omega(x, y) = \sin \frac{\pi x}{a} \sin \frac{\pi y}{a}. \quad (16.6.22)$$

Substituting this expression into Eq. (16.6.4) and observing that $\bar{n}_y = \bar{n}_{xy} = 0$, we obtain

$$\frac{\bar{m}}{D\theta(t)} \frac{\partial^2 \theta(t)}{\partial t^2} + \frac{4\pi^4}{a^4} + \frac{\bar{n}_x}{D} \frac{\pi^2}{a^2} = 0. \quad (16.6.23)$$

The critical value of \bar{n}_x , when it acts statically, is

$$\bar{n}_{cr} = \lambda_{cr} \bar{n}_{x0} = 4 \frac{\pi^2 D}{a^2}; \quad (16.6.24)$$

hence

$$\frac{\bar{n}_{cr}}{D} = \frac{4\pi^2}{a^2}. \quad (16.6.25)$$

The circular frequency of the free lateral vibration pertinent to the first mode is determined from

$$\omega_1 = \frac{2\pi^2}{a^2} \sqrt{\frac{D}{\bar{m}}}, \quad (16.6.26)$$

from which

$$\frac{\bar{m}}{D} = \frac{4\pi^4}{a^4 \omega_1^2}. \quad (16.6.27)$$

Using Eqs. (16.6.25) and (16.6.27), Eq. (16.6.23) is easily reduced to

$$\frac{\partial^2 \theta(t)}{\partial t^2} + \omega_1 \left(1 - \frac{\bar{n}_t \cos pt}{\bar{n}_{cr}} \right) \theta(t) = 0, \quad (16.6.28)$$

which is the Mathieu equation sought.

For $\eta = \bar{n}_t / \bar{n}_{cr} = 0.8$, the paired critical frequencies of the forcing function are

$$p_{cr}^I = \frac{2\omega_1}{1.265} \quad \text{and} \quad p_{cr}^{II} = \frac{2\omega_1}{0.8276}. \quad (16.6.29)$$

If the frequency p is between these limits, dynamic instability occurs.

References and Bibliography

- [16.6.1] HERRMANN, G. (Ed.), "Dynamic Stability of Structures," in *Proceedings of an International Conference held at Northwestern University, Evanston, Ill.*, Oct. 18–20, 1965, Pergamon Press, Elmsford, New York 1967.
- [16.6.2] BOLOTIN, V. V., *The Dynamic Stability of Elastic Systems* (translation of the Russian original), Holden-Day, San Francisco, 1964.
- [16.6.3] BONDER, B. A., "Stability of Plates under the Effect of Longitudinal Periodic Forces" (in Russian), *Prikl. Mat. i. Mekh.*, 2, No. 1 (1938), 87–104.
- [16.6.4] ONIASHVILI, O. D., *Certain Dynamic Problems of the Theory of Shells* (translation of the Russian original), Morris D. Friedman, Tech. Translations, West Newton, Massachusetts 1959.
- [16.6.5] SZILARD, R., and POWELL, R. O., "Dynamic Analysis of Prismatic Shells by Framework Method," in *IASS Symposium on Folded Plates and Prismatic Structures, Vienna*, Sept. 28–30, 1970, Vol. I, published by the editor. Session II/B, Prof. R. Krapfenbauer, Vienna, 1973.
- [16.6.6] HUTT, J. M., "Dynamic Stability of Plates by Finite Elements," Ph.D. Thesis, Oklahoma State University, Stillwater, 1968.
- [16.6.7] BOLOTIN, V. V., *Nonconservative Problems of the Theory of Elastic Stability* (translation of the Russian original), Pergamon Press, Elmsford, New York 1963.
- [16.6.8] STRUTT, M. J. O., *Lamésche, Mathieusche und verwandte Funktionen in der Physik und Technik*, Springer-Verlag, Berlin, 1932.

16.7 Buckling of Stiffened Plates

a. Basic Concepts. The relatively low in-plane load that a plate can carry without buckling can considerably be increased by addition of stiffeners. But by increasing the critical load, the difficulties encountered in the analysis are also increased. That is, the number of variables to be considered becomes greater; in addition, the buckling modes are usually more complex. Consequently, in engineering practice mostly simplified formulas [16.1.16, 16.7.1] or charts [16.7.2] [16.7.3] are used for the design of such plates.

While longitudinal stiffeners placed parallel to the in-plane load carry a portion of the applied force, transverse stiffeners are used merely to subdivide the plate into smaller units, since the portion of the load carried by them is relatively small. Combination of longitudinal and transverse stiffeners results in grid-stiffened plates. Conventional structural shapes used for stiffeners are angle, channel, T- and inverted T-sections. In aerospace structures Z-, U- and Y-type stiffeners are also common (Fig. 16.7.1a).

In the stability analysis of stiffened plates, usually two forms of buckling are considered. One possible mode is the *local* buckling of the plate between the stiffeners, provided that the plate is reinforced with sturdy ribs. In the second case, an overall buckling of the plate-stiffener combination occurs. The latter is called *primary* buckling in the pertinent literature.

In some structures we may require that local buckling of the plate takes place first, without substantial distortion of the ribs themselves. In this case, there is little structural interaction between the plate and stiffeners, and the ribs merely enforce the nodal lines of the buckling modes of the plates. Consequently, the problem is reduced to (1) finding the critical loads of the unstiffened panels and (2) determination of the minimum flexural rigidity of the ribs that guarantees early plate buckling.

The customary assumption of simply supported boundary conditions for the individual panels yields a safe, but conservative, design. Any of the previously discussed

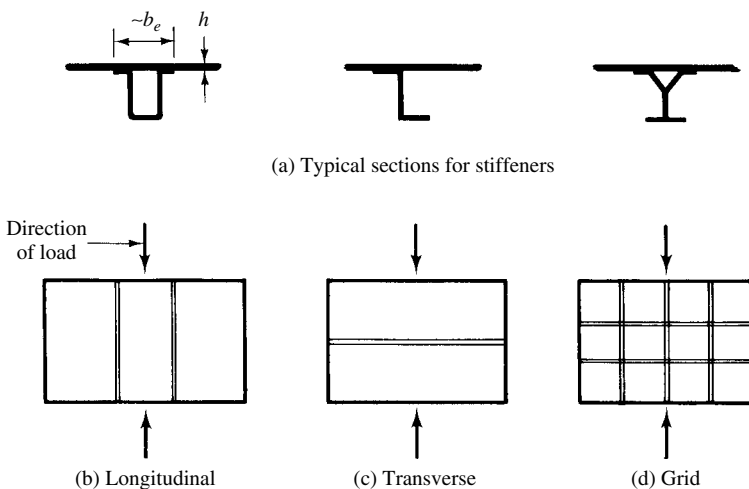


Figure 16.7.1 Various stiffener types.

analytical or numerical methods, however, can be used for consideration of more realistic boundary conditions. Especially, the finite element technique, as described in the Illustrative Example of Sec. 16.5, is recommended in dealing with elastically restrained and/or supported boundary conditions. The critical load in the stiffeners can be determined from the appropriate column buckling formula

$$(P_{cr})_s = \frac{\pi^2 EI_s}{l_{cr}^2}, \quad (16.7.1)$$

which, for simply supported ends, becomes

$$(\sigma_{cr})_s \approx \frac{\pi^2 EI_s}{a^2 A_s}, \quad (16.7.2)$$

where $(\sigma_{cr})_s$ is the critical stress in the stiffener. In the structural properties of the stiffeners, A_s , I_s , strictly speaking, the effective plate width for bending should also be considered. In practical computation, however, it is sufficient to include only that part of the plate that is attached to the flange of the stiffener.

A considerably more economical design can be obtained if we permit simultaneous local and primary buckling at about the same stress level. Consequently, in the elastic stability analysis of stiffened plates, the structural interaction of plate and stiffeners should be taken into account. If the plate is reinforced with many equally spaced, parallel stiffeners of the same size, such an assembly can effectively be approximated by the orthotropic plate theory. In addition to this general case, more specific problems, such as stiffened plates reinforced with three or less ribs, must be treated. That is, there is no marked difference in the critical load if the number of stiffeners is infinite or more than 3 [16.7.4] [16.7.5].

b. Buckling of Orthotropic Plates. When the number of parallel stiffeners in one or both principal directions is large, the critical load of stiffened plates can be approximated by assuming that the stiffened plate acts as a homogeneous orthotropic plate (Fig. 16.7.2).

For this case, the governing differential equation of elastic stability (16.2.3) becomes

$$D_x \frac{\partial^4 w}{\partial x^4} + 2B \frac{\partial^2 w}{\partial x^2 \partial y^2} + D_y \frac{\partial^4 w}{\partial y^4} + \lambda \left(\bar{n}_{x0} \frac{\partial^2 w}{\partial x^2} + 2\bar{n}_{xy0} \frac{\partial^2 w}{\partial x \partial y} + \bar{n}_{y0} \frac{\partial^2 w}{\partial y^2} \right) = 0. \quad (16.7.3)$$

If possible, the flexural and torsional rigidities D_x , D_y and B defined in Sec. 10.1 should be determined by tests. Approximate values for these sectional properties for

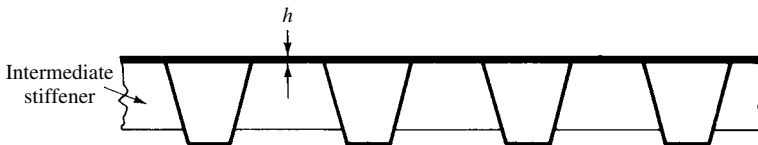


Figure 16.7.2 Closely placed ribs.

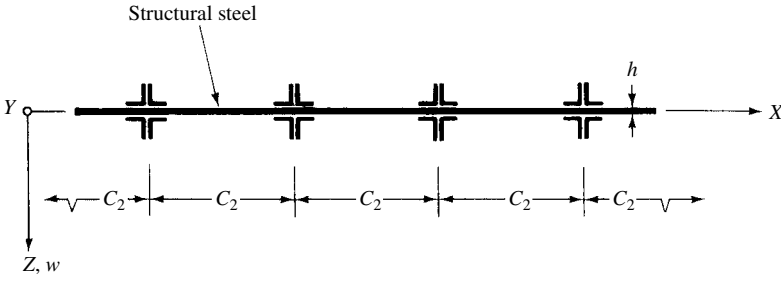


Figure 16.7.3 Section of plate reinforced with multiple stiffeners in Y direction.

an isotropic plate reinforced with parallel stiffeners symmetrically distributed on both sides of the middle surface (Fig. 16.7.3) are

$$B \approx D_x = \frac{Eh^3}{12(1-\nu^2)}, \quad D_y = \frac{Eh^3}{12(1-\nu^2)} + \frac{EI_y}{c_2}, \quad (16.7.4)$$

or, in the case of grid-type stiffeners that are symmetrical about the middle surface,

$$D_x = \frac{Eh^3}{12(1-\nu^2)} + \frac{EI_x}{c_1}, \quad B = \frac{Eh^3}{12(1-\nu^2)}, \quad D_y = \frac{Eh^3}{12(1-\nu^2)} + \frac{EI_y}{c_2}. \quad (16.7.5)$$

In these expressions I_x and I_y are the moments of inertia of the ribs about the middle surface and c_1 and c_2 denote the spacings of the ribs in the X and Y directions, respectively. Additional approximations for flexural rigidities, if the ribs are only on one side of the plate, are given in Sec. 10.1.

Using Eq. (16.7.3), the required lowest load factor ($\lambda_{\min} = \lambda_{cr}$) can easily be determined either by Galerkin's variational method or by ordinary finite difference techniques, in the same way as described in Secs. 16.3 and 16.4.

Wittrick [16.7.6] has derived critical loads for stiffened rectangular plates with various boundary conditions using the orthotropic plate idealization of the problem.

If the longitudinal stiffeners are flexible enough to permit the overall buckling of the plate, then the critical stress can be estimated [16.7.4] by

$$\sigma_{cr} = \frac{4\pi^2 E}{12(1-\nu^2)} \left(\frac{h}{b} \right)^2 \left\{ 1 + \left[1 + 12(1-\nu^2) \frac{I_x}{c_1 h^3} \right]^{1/2} \right\}. \quad (16.7.6)$$

It is assumed that the longitudinal stiffeners run in the X direction.

c. Plates Reinforced with Three or Less Stiffeners. If the plate is reinforced with few ribs, the convenient orthotropic plate idealization cannot be used to obtain reliable values for the critical load. Since the stiffeners are rigidly fastened to the plate, we should treat the plate and stiffeners as a structural unit; consequently, at mutual points, the rib deflects and twists in the same way as the plate. The critical load is usually determined by the Rayleigh-Ritz method [16.7.7], as discussed in Sec. 16.3. To the already introduced strain energy of the plate (4.2.5), however, the strain energy of the individual stiffeners must be added.

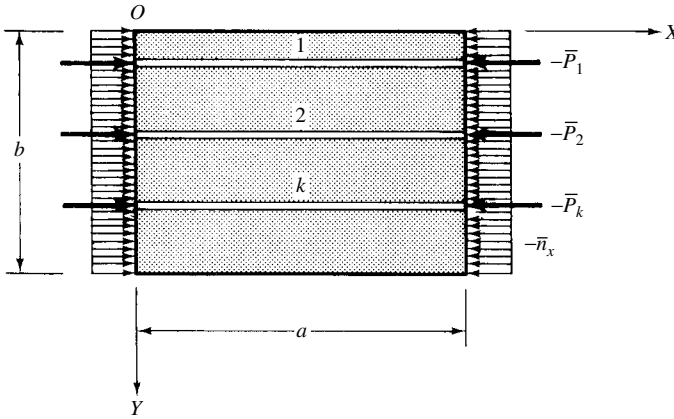


Figure 16.7.4 Plate reinforced with few ribs.

Contribution of the longitudinal ribs to the strain energy of the plate, compressed by a uniformly distributed edged load (Fig. 16.7.4), is

$$U_s^* = \frac{1}{2} \sum_k \left[E I_k \int_0^a \left(\frac{\partial^2 w}{\partial x^2} \right)_{y_k}^2 dx + G I_0 \int_0^a \left(\frac{\partial^2 w}{\partial x \partial y} \right)_{y_k}^2 dx \right], \quad (16.7.7)$$

where I_k represents the moment of inertia of the individual rib and $G I_0$ is its torsional rigidity, assuming that the centroid of each stiffener cross section lies in the middle surface of the plate.

The additional work done by the external load \bar{P}_k acting on the k th stiffener is

$$W_s^* = \frac{1}{2} \sum_{k=1}^n \bar{P}_k \int_0^a \left(\frac{\partial w}{\partial x} \right)_{y_k}^2 dx. \quad (16.7.8)$$

Thus, the total work done by the external forces becomes

$$W_e^* = \frac{\bar{n}_x}{2} \int_0^a \int_0^b \left(\frac{\partial w}{\partial x} \right)^2 dx dy + \frac{\bar{P}_k}{2} \sum_{k=1}^n \int_0^a \left(\frac{\partial w}{\partial x} \right)_{y_k}^2 dx. \quad (16.7.9)$$

When the stiffeners are attached to one side of the plate, the moment of inertia of the stiffeners should be computed with respect to the neutral axis of the cross section (Fig. 10.1.4), as described in Sec. 10.1.

This approach is straightforward, but it becomes tedious when the stiffeners are not symmetrically placed in relation to the symmetry axes of the plate. If this is the case, the FDMs may offer considerable advantages. In setting up the differential equation of the problem, however, the above-discussed interaction of plate and stiffeners should be considered. Further simplifications are obtained by neglecting the torsional stiffness of *open-section* ribs, such as angles and channels made up of bent plates, and by assuming that the plate is reinforced with sturdy ribs.

Summary. Since elastic stability analysis of stiffened plates is usually complex, for routine design work the use of available extensive design tables [16.3.16, 16.7.7] or design charts [16.7.2, 16.7.3] is recommended. The most economical structure results when local and primary buckling occur simultaneously under the critical load. If the number of stiffeners in one or the other principal direction is large, the assumption that the stiffened plate acts as an orthotropic plate yields good approximation for a wide variety of stiffened plates. Based on this idealization, stiffened plates can conveniently be analyzed either by the variational method or by finite difference techniques. When plates are stiffened by less than four ribs, the extension of the Rayleigh-Ritz method, which considers the interaction of plate and stiffeners, is the analytical tool generally used. The FEM appears to be a flexible and powerful technique that can be extended even into the plastic range [16.5.8].

ILLUSTRATIVE EXAMPLE I

Determine the critical buckling load of a simply supported rectangular plate reinforced by a longitudinal stiffener at $y = b/2$ (Fig. 16.7.5). Assume that the stiffened plate is subjected to a uniformly distributed edge load \bar{n}_x and that the torsional rigidity of the rib is negligible. The plate and the rib buckle together.

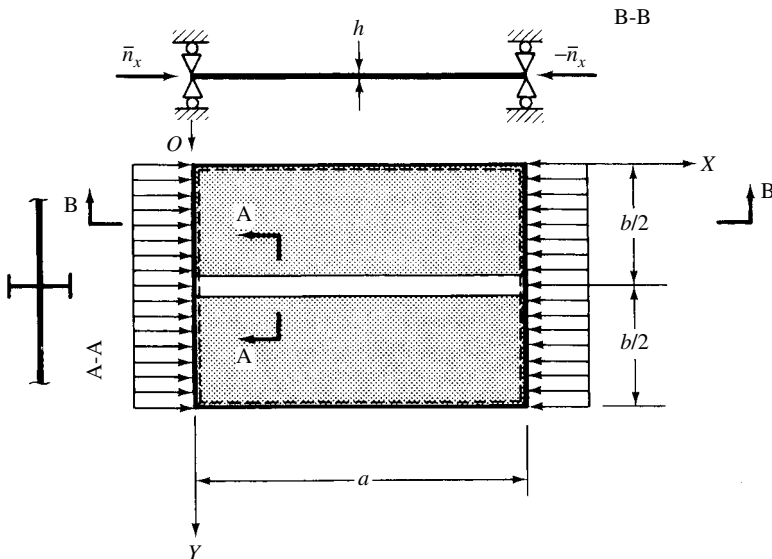


Figure 16.7.5 Rectangular plate with one longitudinal stiffener.

We express the deflection surface of the buckled plate in the form

$$w(x, y) = W \sin \frac{\pi x}{a} \sin \frac{\pi y}{b}. \quad (16.7.10)$$

The total potential of the stiffened plate can be written as

$$\begin{aligned} \Pi = \frac{D}{2} \int_0^a \int_0^b \left\{ \left(\frac{\partial^2 w}{\partial x^2} + \frac{\partial^2 w}{\partial y^2} \right)^2 \right. \\ \left. - 2(1-\nu) \left[\frac{\partial^2 w}{\partial x^2} \frac{\partial^2 w}{\partial y^2} - \left(\frac{\partial^2 w}{\partial x \partial y} \right)^2 \right] \right\} dx dy \\ + \frac{EI_1}{2} \int_0^a \left(\frac{\partial^2 w}{\partial x^2} \right)_{y=b/2}^2 dx - \frac{\bar{n}_x}{2} \int_0^a \int_0^b \left(\frac{\partial w}{\partial x} \right)^2 dx dy \\ - \frac{\bar{P}_1}{2} \int_0^a \left(\frac{\partial w}{\partial x} \right)_{y=b/2}^2 dx, \end{aligned} \quad (16.7.11)$$

where $\bar{P}_1/\bar{n}_x = A_1/h$. Equation (16.7.11), after substitution of Eq. (16.7.10) and $\bar{n}_x = \lambda \bar{n}_{x0}$, becomes

$$\begin{aligned} \Pi = \frac{\pi^4 b D}{8a^3} \left[W^2 \left(\frac{1}{a^2} + \frac{1}{b^2} \right)^2 + \frac{2EI_1}{bD} \left(W \sin \frac{\pi}{2} \right)^2 \right] \\ - \frac{\pi^2 b}{8a} \lambda \bar{n}_{x0} \left[W^2 + 2 \frac{A_1}{bh} \left(W \sin \frac{\pi}{2} \right)^2 \right], \end{aligned} \quad (16.7.12)$$

where $\bar{n}_{x0} = \pi^2 D/b^2$ represents the reference value of the critical load; furthermore, A_1 and I_1 denote the cross-sectional area and the moment of inertia of the rib, respectively. Hence, the critical load factor becomes

$$\lambda = \lambda_{cr} = \frac{(1 + \beta^2)^2 + 2\gamma}{\beta^2(1 + 2\delta)}, \quad (16.7.13)$$

where

$$\beta = \frac{a}{b}, \quad \gamma = \frac{EI_1}{bD}, \quad \delta = \frac{A_1}{bh}.$$

Therefore,

$$(\bar{n}_x)_{cr} = \lambda_{cr} \bar{n}_{x0}, \quad (16.7.14)$$

which gives usable results for square or nearly square plates and very accurate solutions [16.1.1] for longer plates ($\beta > 2$). It is, of course, always possible to carry more than one term in the double trigonometric series expression of the deflection surface.

ILLUSTRATIVE EXAMPLE II

A simply supported rectangular plate, shown in Fig. 16.7.6, is reinforced with a flexible grid-stiffening arrangement that is symmetrical about the middle surface. The plate is subjected to combined bending and compression. Determine the critical load by Rayleigh's method.

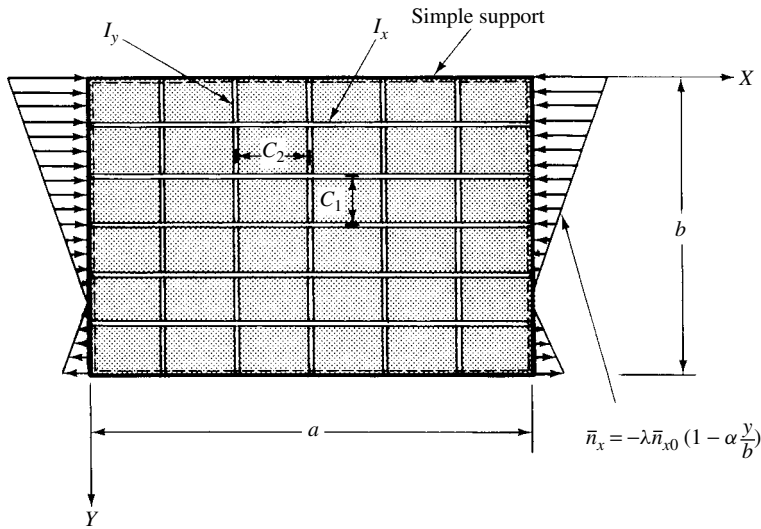


Figure 16.7.6 Grid-stiffened plate subjected to combined bending and compression.

Since we have assumed that the grid-stiffening system is flexible, the problem can conveniently be treated by the orthotropic plate theory. Approximate values for the sectional properties are given in Eq. (16.7.5).

The intensity of the edge force can be expressed as

$$\bar{n}_x = -\lambda \bar{n}_{x0} \left(1 - \alpha \frac{y}{b}\right). \quad (16.7.15)$$

The first mode of buckling can be approximated by a one-term double trigonometric expression

$$w = W_{11} \sin \frac{m\pi x}{a} \sin \frac{n\pi y}{b}, \quad (16.7.16)$$

which satisfies the simply supported boundary conditions. From our previous discussion[†] we know that the smallest value of λ can be obtained when the buckled shape has one half-sine-wave in the Y direction, which corresponds to $n = 1$.

The work done by the external forces during buckling is calculated from Eq. (16.3.10):

$$W_e^* = \frac{\lambda \bar{n}_{x0}}{2} \int_0^a \int_0^b \left(1 - \alpha \frac{y}{b}\right) \left(\frac{\partial w}{\partial x}\right)^2 dx dy. \quad (16.7.17)$$

The strain energy expression of the orthotropic plate follows from Eqs. (4.1.8a), (4.2.4) and (10.1.3); thus, we can write

[†] See Illustrative Example I in Sec. 16.2.

$$\begin{aligned}
 U_b^* &= \frac{1}{2} \int_0^a \int_0^b (m_x \kappa_x + m_y \kappa_y + 2m_{xy} \chi) \, dx \, dy \\
 &= \frac{1}{2} \int_0^a \int_0^b \left[D_x \left(\frac{\partial^2 w}{\partial x^2} \right)^2 + 2\nu_y D_x \frac{\partial^2 w}{\partial x^2} \frac{\partial^2 w}{\partial y^2} \right. \\
 &\quad \left. + D_y \left(\frac{\partial^2 w}{\partial y^2} \right)^2 + 4D_t \left(\frac{\partial^2 w}{\partial x \partial y} \right)^2 \right] dx \, dy, \quad (16.7.18)
 \end{aligned}$$

where D_t represents the torsional rigidity of the stiffened plate, as defined by Eq. (10.1.4b)

Substituting Eq. (16.7.16) with $n = 1$ into Rayleigh's quotient ($\lambda = U_b^* / W_e^*$), we obtain

$$\lambda = \frac{\pi^2 D_{xy}}{b^2(1 - 0.5\alpha)\bar{n}_{x0}} \left[\left(\frac{mb}{a} \right)^2 \sqrt{\frac{D_x}{D_y}} + \frac{2B}{D_{xy}} + \sqrt{\frac{D_y}{D_x}} \left(\frac{a}{bm} \right)^2 \right], \quad (16.7.19)$$

where $D_{xy} = \sqrt{D_x D_y}$ and B are defined by Eq. (10.1.4b). For the reference value \bar{n}_{x0} , Eq. (16.2.5a) can be used with $D = D_{xy}$. Assuming a specific aspect ratio a/b , the smallest value of $\lambda(\lambda_{\min} = \lambda_{cr})$ can be determined by trial and error.

It should be noted that Eq. (16.7.19) is valid only for small α , that is, when the bending stresses are small in comparison with uniform compressive stresses. If $\alpha = 0$, Eq. (16.7.19) can be used for determination of the critical load factor of uniformly compressed orthotropic plates. For pure bending ($\alpha = 2$), Eq. (16.7.19) becomes meaningless. In such a case, two or more terms should be considered in the double trigonometric series expression for the buckling modes:

$$w = \sum_{m=1}^{\infty} \sum_{n=1}^{\infty} W_{mn} \sin \frac{m\pi x}{a} \sin \frac{n\pi y}{b}. \quad (16.7.20)$$

The use of this expression, however, calls for the Ritz (instead of the Rayleigh) method, as described in Secs. 16.1 and 16.3.

References and Bibliography

- [16.7.1] BLEICH, F., *Buckling Strength of Metal Structures*, McGraw-Hill Book Co., New York, 1952.
- [16.7.2] BLEICH, F., and RAMSEY, L. B., *Design Manual on the Buckling Strength of Metal Structures*, Tech. Res. Bulletin No. 2-3, Society of Naval Architects and Marine Engineers, New York, 1951.
- [16.7.3] "Metallic Materials and Elements for Flight Vehicle Structures," *Military Handbook MIL-HDBK-5A*, Feb. 8, 1966.
- [16.7.4] SEIDE, P., and STEIN, M., "Compressive Buckling of Simply Supported Plate with Longitudinal Stiffeners," NACATN 1825, National Advisory Committee for Aeronautics, Washington, D. C., 1949.

- [16.7.5] RATZERSDOFER, J., "Rectangular Plates with Stiffeners," *Aircraft Eng.* 14 (Sept. 1942), 260–263.
- [16.7.6] WITTRICK, W. H., "Correlation Between Some Stability Problems for Orthotropic and Isotropic Plates Under Biaxial and Uniaxial Stress," *Aeron. Quart.*, 4 (Aug. 1952), 83–92.
- [16.7.7] KÖPPEL, K., and SCHEER, J., *Beulwerte ausgesteifter Platten*, W. Ernst und Sohn, Berlin, 1960.
- [16.7.8] WANG, T. K., "Buckling of Transverse Stiffened Plates in Shear," *J. Appl. Mech.*, 14 (Dec. 1947), A269–A274.
- [16.7.9] HELLER, C. O., *Behavior of Stiffened Plates*, Eng. Dept. Rept. 67-1, Vol. 1: *Analysis*, U.S. Naval Academy, Annapolis, Indiana, 1967.
- [16.7.10] BORNSCHEUER, F. W., "Beitrag zur Berechnung ebener gleichmässig gedrückten Rechteckplatten, versteift durch eine Langssteife," Ph.D. Thesis, Technische Hochschule, Darmstadt, 1946.
- [16.7.11] GERARD, G., *Handbook of Structural Stability*, Pt. II: *Buckling of Composite Elements*, NACA TN 3785, National Advisory Committee for Aeronautics, Washington, D.C., 1957.
- [16.7.12] TROITSKY, M. S., *Stiffened Plates: Bending, Stability and Vibration*, Elsevier, New York, 1959.
- [16.7.13] STEUP, H., *Stabilitätstheorie im Bauwesen*, Ernst & Sohn, Berlin, 1990.
- [16.7.14] KURETI, A. R., and CHERAGHI, E., "Analysis Procedure for Stiffened Plate System Using an Energy Approach," *Comp. Struct.*, 46 (1993), 649–657.
- [16.7.15] HUGHES, O. F., and MA, M., "Inelastic Analysis of Panel Collapse by Stiffener Buckling," *Comp. Struct.*, 61 (1996), 107–117.
- [16.7.16] MIKAMI, I., and NIWA, K., "Ultimate Compressive Strength of Orthogonally Stiffened Steel Plates," *J. Struct. Eng. Div., ASCE*, 122 (1996), 674–682.
- [16.7.17] BEDAIR, O. K., and SHERBOURNE, A. N., "Plate/Stiffener Assemblies under Edge Compression," *J. Struct. Eng. Div., ASCE*, 121 (1995), 1603–1612.
- [16.7.18] JIANG, W., et al., "Finite Element Modeling of Stiffened and Unstiffened Orthotropic Plates," *Comp. Struct.*, 63 (1997), 105–117.

16.8 Thermal Buckling

Plate components used extensively in naval and aerospace structures or in box and plate girders are susceptible to buckling when subjected to thermal loads. Temperature variation in such structures may represent a predominant load that sometimes can lead to failures. Considering an isotropic plate of uniform thickness having zero thermal moment ($m_T = 0$) but nonzero in-plane thermal forces, the governing differential equation of thermal buckling is

$$D \nabla^4 w = \lambda \left(n_x \frac{\partial^2 w}{\partial x^2} + 2n_{xy} \frac{\partial^2 w}{\partial x \partial y} + n_y \frac{\partial^2 w}{\partial y^2} \right), \quad (16.8.1)$$

where λ represents the load factor and

$$n_x = \frac{\partial^2 \Phi}{\partial y^2}, \quad n_y = \frac{\partial^2 \Phi}{\partial x^2}, \quad n_{xy} = -\frac{\partial^2 w}{\partial x \partial y}, \quad (16.8.2)$$

In Eq. (16.8.2) $\Phi(x, y)$ is the Airy stress function. First we must determine $\Phi(x, y)$, which must satisfy the differential equation

$$\nabla^4 \Phi(x, y) = -(1 - \nu) \nabla^2 n_T, \quad (16.8.3)$$

and the appropriate boundary conditions. Then, the critical load factor λ_{cr} can be computed by solving the corresponding eigenvalue problem represented by Eq. (16.8.1). Finding an exact solution to this complex problem is extremely difficult [16.8.4] or even impossible. One can, however, obtain usable numerical solutions to such general, thermally induced buckling problems by utilizing a two-stage finite difference approach. That is, first Eq. (16.8.3) is solved for Φ by using the FDM, then the so-obtained values are substituted into Eq. (16.8.1), and the pertinent eigenvalue problem is evaluated. Even such a numerical approach is quite time consuming and tedious. Therefore, for practical applications we are forced to *simplify* this general thermal buckling problem by assuming that the lateral deflections $w(x, y)$ are small and the in-plane stress resultants are independent of w . In addition, we solve first a corresponding eigenvalue problem treated in the previous sections by applying any of the already introduced analytical or numerical methods. Next, using appropriate relationships provided by the theory of elasticity, we *convert* the so-obtained critical loads to thermal loads. This simplified solution technique is illustrated in the Illustrative Example given below.

Summary. Exact solution of thermally induced general buckling problems of plates is very difficult and in many cases even impossible. A two-stage finite difference approach, however, can yield usable results. Even such a numerical solution appears to be tedious and time consuming. Therefore, the use of a simplified method is recommended.

ILLUSTRATIVE EXAMPLE

As an example for our simplified approach, let us consider a clamped rectangular plate of $a \times b$ dimensions. This plate is subjected to a uniformly distributed temperature load. The ambient temperature of the plate is T_0 , which is slowly increased to $T = T_0 + T_{in}$. Let us determine the temperature at which the plate will buckle.

Using the above-mentioned simplified approach, first we determine the critical loads $n_{x,cr}$ and $n_{y,cr}$. Let us assume that an energy method has yielded the following expression for these values:

$$\left[n_x + \left(\frac{a^2}{b^2} \right) n_y \right]_{cr} = - \frac{4\pi^2 D a^2}{3} \left(\frac{3}{a^4} + \frac{2}{a^2 b^2} + \frac{3}{b^4} \right). \quad (16.8.4)$$

Next, we convert these critical loads to pertinent thermal loads. For this purpose, we apply the two-dimensional Hook law and calculate the expansions caused by the temperature increase. However, since all four boundaries of the plate are fixed, no expansion can take place in the X and Y directions. Consequently, we can write

$$\frac{1}{E}(\sigma_x - \nu \sigma_y) + \alpha_T T_{in} a = 0, \quad \frac{1}{E}(\sigma_y - \nu \sigma_x) + \alpha_T T_{in} b = 0, \quad (16.8.5)$$

from which

$$\sigma_x = - \frac{\alpha_T T_{in} E (\nu b + a)}{1 - \nu^2} \quad (16.8.6)$$

and

$$\sigma_y = -\frac{\alpha_T T_{in} E (va + b)}{1 - \nu^2}. \quad (16.8.7)$$

Since $n_x = h\sigma_x$ and $n_y = h\sigma_y$, substitution of Eqs. (16.8.6) and (16.8.7) into Eq. (16.8.4) gives

$$\begin{aligned} & -\frac{\alpha_T T_{in} E (vb + a)}{1 - \nu^2} + \frac{a^2}{b^2} \left[-\frac{\alpha_T T_{in} E (va + b)}{1 - \nu^2} \right] \\ & = -\frac{4\pi^2 Da^2}{3h} \left(\frac{3}{a^4} + \frac{2}{a^2 b^2} + \frac{3}{b^4} \right). \end{aligned} \quad (16.8.8)$$

Hence

$$T_{in} = \frac{4\pi^2 Da^2 (1 - \nu^2) (3/a^4 + 2/a^2 b^2 + 3/b^4)}{\alpha_T E [(vb + a) + (a^2/b^2)(va + b)]}. \quad (16.8.9)$$

Consequently, we can state that the plate will buckle approximately at temperature $T = T_0 + T_{in}$.

References and Bibliography

- [16.8.1] BOLEY, B. A., and WEINER, J. H., *Theory of Thermal Stresses*, John Wiley & Sons, New York, 1960.
- [16.8.2] TAUCHERT, T. R., "Thermally Induced Flexure, Buckling and Vibration," *Appl. Mech. Rev.*, **44** (1991), 347–360.
- [16.8.3] MANSFIELD, E. H., "Bending, Buckling and Curling of Heated Thin Plates," *Proc. Roy. Soc., A268* (1962), 316–327.
- [16.8.4] BLOOM, F., and COFFIN, D., *Handbook of Thin Plate Buckling and Postbuckling*, Chapman & Hall/CRC Press, Boca Raton, Florida, 2001.

16.9 Buckling of Moderately Thick Plates

As already mentioned in Sec. 1.5, Kirchhoff's classical plate theory, which neglects transverse shear deformation, can lead to significant errors when applied to moderately thick plates. In contrast to classical plate theory, the Reissner/Mindlin theory of moderately thick plates removes the basic assumption that normals to the undeformed middle surface remain normal to the deformed ones due to effects of transverse shear deformations. Consideration of the additional transverse shear effects results in added flexibility of the plate, causing *lower buckling loads*.

Using, for instance, Reissner's theory, the governing equation for buckling can be written [16.9.2] as

$$\nabla^4 w = \left[1 - \frac{h^2}{5(1 - \nu)} \nabla^2 \right] \left(n_x \frac{\partial^2 w}{\partial x^2} - 2n_{xy} \frac{\partial^2 w}{\partial x \partial y} + n_y \frac{\partial^2 w}{\partial y^2} \right) \quad (16.9.1)$$

and

$$\nabla^4 \Phi = Eh \left[\left(\frac{\partial^2 w}{\partial x \partial y} \right)^2 - \frac{\partial^2 w}{\partial x^2} \frac{\partial^2 w}{\partial y^2} \right], \quad (16.9.2)$$

where $\Phi(x, y)$ denotes the stress function for the in-plane resultants

$$n_x = \frac{\partial^2 \Phi}{\partial y^2}, \quad n_y = \frac{\partial^2 \Phi}{\partial x^2}, \quad n_{xy} = -\frac{\partial^2 \Phi}{\partial x \partial y}. \quad (16.9.3)$$

Equations (16.9.1) and (16.9.2) represent *nonlinear large deflections* of the plate, including transverse shear effects. Needless to say, obtaining exact solutions of these differential equations is quite difficult.

To simplify such complex buckling problems, Wang established an exact relationship between the buckling loads of Mindlin and Kirchhoff plates [16.9.3]. For simply supported isotropic polygonal plates subjected to uniformly distributed edge loads, this relationship has the form

$$n^M = \frac{n^K}{1 + n^K / \kappa^2 Gh}, \quad (16.9.4)$$

where the superscripts M and K refer to the pertinent Mindlin and Kirchhoff plate theories, respectively. In addition, κ^2 is the shear correction factor introduced in Sec. 1.5 and G denotes the shear modulus of the plate. This simple relationship has also been extended to plates of various shapes, including plates of elastic foundations [16.9.4–16.9.7].

In the case of Winkler foundation, for instance, the Mindlin-Kirchhoff buckling load relationship becomes

$$n^M = \frac{n^K}{1 + \frac{n^K}{\kappa^2 Gh}} + \frac{kD}{n^K} + G_b, \quad (16.9.5)$$

where k represents the modulus of subgrade reaction for the foundation and G_b denotes the shear modulus of the subgrade (Fig. 16.9.1).

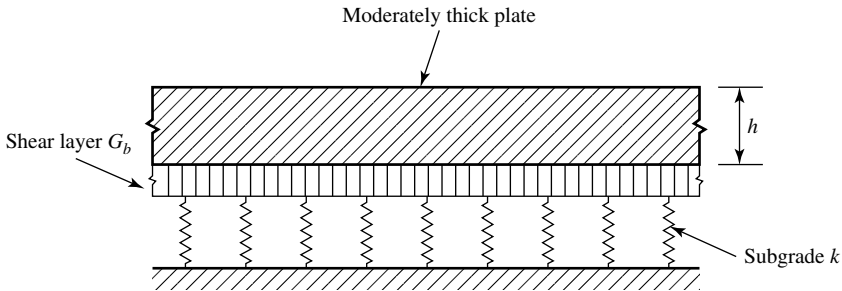


Figure 16.9.1 Moderately thick plate on elastic foundation.

Summary. While the exact solution of moderately thick plate buckling problems is difficult, Eqs. (16.9.4) and (16.9.5) establish simple relationships between the buckling loads of Kirchhoff and Mindlin plates, including those supported by elastic foundations. Consequently, using already available buckling solutions of simply supported Kirchhoff plates, critical buckling loads of moderately thick plates can be readily calculated.

ILLUSTRATIVE EXAMPLE

A moderately thick, simply supported square plate shown in Fig. 16.9.2 is uniformly compressed in the X direction. Determine the critical buckling load of this plate.

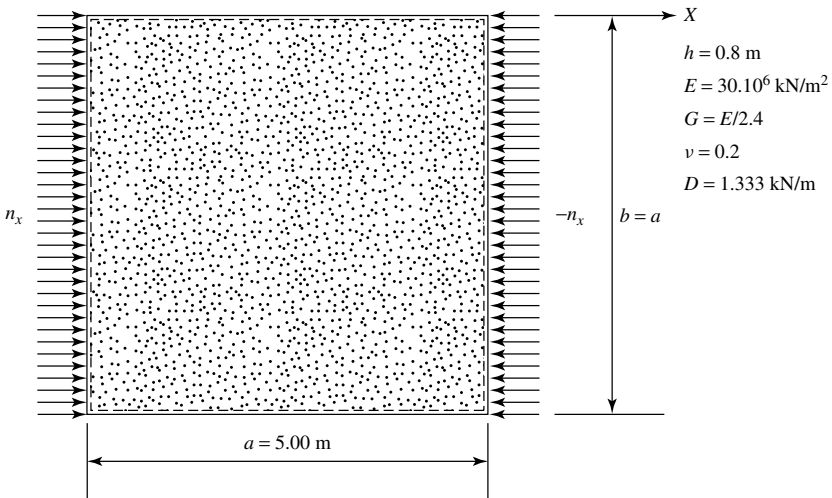


Figure 16.9.2 Moderately thick square plate subjected to in-plane compressive forces.

Since the plate is simply supported, we can apply the Mindlin-Kirchhoff buckling load relationship given in Eq. (16.9.4). For this purpose, we must determine first the critical load of the corresponding Kirchhoff plate, which, according to Ref. [16.1.1], is

$$n_{x,\text{cr}}^K = \frac{4\pi^2 D}{b^2} = 2.106 \times 10^6 \text{ kN/m.} \quad (16.9.6)$$

Consequently, using Eq. (16.9.4), we obtain

$$n_{x,\text{cr}}^M = \frac{2.106 \times 10^6}{1 + (2.106 \times 10^6)/(0.8333 \times 12.5 \times 10^6 \times 0.8)} = 1.6811 \text{ kN/m.} \quad (16.9.7)$$

It is apparent that the critical buckling load of the moderately thick plate is considerably less than that of the corresponding Kirchhoff plate.

References and Bibliography

- [16.9.1] SRINIVAS, M., and RAO, A. K., "Buckling of Thick Rectangular Plates," *AIAA J.*, 7 (1969), 1645–1646.
- [16.9.2] HUI-SHEN, S., "Buckling and Postbuckling of Moderately Thick Plates," *Appl. Math. Mech.*, 11 (1990), 367–376.
- [16.9.3] WANG, C. M., et al., "Buckling Solutions for Mindlin Plates of Various Shapes," *Eng. Struct.*, 16(2) (1994), 119–127.
- [16.9.4] WANG, C. M., "Buckling of Polygonal and Circular Sandwich Plates," *AIAA J.*, 33 (1995), 962–964.
- [16.9.5] WANG, C. M., and XIANG, Y., "Deducing Buckling Loads of Sectorial Mindlin Plates from Kirchhoff Plates," *J. Eng. Mech. Div., ASCE*, 125 (1999), 596–598.
- [16.9.6] WANG, C. M., et al., "Axisymmetric Buckling of Reddy Circular Plates on Pasternak Foundation," *Eng. Mech. Div., ASCE*, 127 (2001), 255–259.
- [16.9.7] WANG, C. M., et al., "Relationship Between Buckling Loads of Kirchhoff, Mindlin and Reddy Polygonal Plates on Pasternak Foundation," *J. Eng. Mech. Div., ASCE*, 123 (1997), 1134–1137.
- [16.9.8] REDDY, J. N., and PHAN, N. D., "Stability and Vibration of Isotropic and Laminated Plates According to a High Order Shear Deformation Theory," *J. Sound Vibr.*, 98 (1985), 157–170.
- [16.9.9] WANG, C. M., et al., *Shear Deformable Beams and Plates*, Elsevier, Oxford, United Kingdom, 2000.

16.10 Postbuckling Behavior

a. Effects of Large Deflections. The *critical loads* found in the previous sections represent merely the loads at which buckling begins. Experiments [16.10.1] indicate that the *postbuckling behavior* of plates is markedly different from that of thin rods. While a small increase in the critical load for struts will produce a complete collapse, the critical load may be but a small fraction of the buckling load that causes failure in plates (Fig. 16.10.1). This increased load-carrying capacity, beyond the critical load, originates from the effect of large deflections and from the fact that the longitudinal edges of plates are usually constrained to remain straight.

The use of this additional strength is of great practical importance in the design of ship and aerospace structures, since by considering the postbuckling behavior of

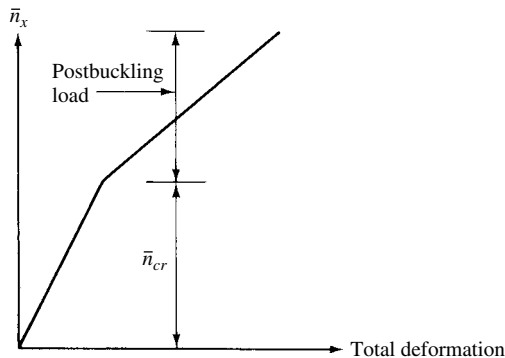


Figure 16.10.1 Increased load-carrying capacity of plates beyond critical load.

plates, considerable weight savings can be achieved. In these structures, the edges of the plates are usually supported by stringers in such a way that they remain straight. This construction practice permits the use of higher than critical loads as allowable edge forces, even under service conditions. Although the postbuckling loads are markedly different from the critical loads, the results of small-deflection theory are not without value, since they provide a lower bound for the buckling loads and may limit deformations provided that such a limitation is required. Furthermore, the critical stresses produced by the critical loads give a convenient datum value in the approximate analysis of this complex problem.

In the previous sections the determination of the critical load was based on small-deflection theory; consequently, the membrane forces produced by large deflections have been neglected. Increasing the edge loading beyond its critical value, however, will result in lateral deflections eventually reaching or surpassing the order of the plate thickness. Since, in such a condition, the strain energy due to stretching of the middle surface can be of the same order as the strain energy due to bending, the resulting membrane forces cannot be neglected. Furthermore, if the longitudinal edges are constrained to remain straight, the occurrence of local bulging (Fig. 16.10.2) produces additional membrane forces, which further increase the load-carrying capacity of the plate.

Since in the analysis of the postbuckling behavior of plates the nonlinear, large-deflection theory must be used, the resulting mathematical difficulties are considerable. Additional difficulties are encountered in assuming suitable deflection shapes.

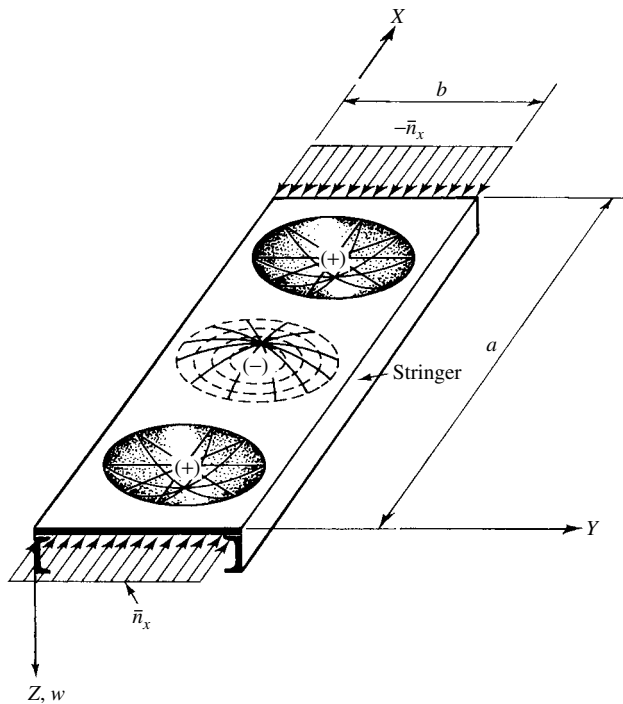


Figure 16.10.2 Local bulging in plate with constrained edges.

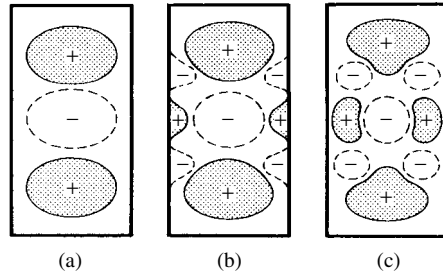


Figure 16.10.3 Progressive changes in buckling modes.

After reaching the first stage of buckling form, for instance, the shape of the buckled plate may change as the load is increased beyond its critical value (Fig. 16.10.3). These changes, however, are always progressive. That is, the first form of buckling keeps developing until the energy stored is sufficient to carry the plate into a second buckling form and so on.

The governing differential equation for the investigation of postbuckling behavior of plates of constant thickness is von Kármán's large-deflection equation (11.1.4) derived in Sec. 11.1. Assuming that the lateral force p_z is zero, we can write

$$\frac{D}{h} \nabla^4 w = \frac{\partial^2 \Phi}{\partial y^2} \frac{\partial^2 w}{\partial x^2} + \frac{\partial^2 \Phi}{\partial x^2} \frac{\partial^2 w}{\partial y^2} - 2 \frac{\partial^2 \Phi}{\partial w \partial y} \frac{\partial^2 w}{\partial x \partial y} = \mathfrak{L}_1(\Phi, w) \quad (16.10.1)$$

and

$$\frac{1}{E} \nabla^4 \Phi = \left[\left(\frac{\partial^2 w}{\partial x \partial y} \right)^2 - \frac{\partial^2 w}{\partial x^2} \frac{\partial^2 w}{\partial y^2} \right] = \mathfrak{L}_2(w, w), \quad (16.10.2)$$

where $\Phi(x, y)$ is a stress function of the middle surface, as defined in Sec. 11.1. Since these differential equations are nonlinear, exact solutions very seldom can be obtained [16.10.2]. The most generally used techniques for the analytical treatment of postbuckling of plates are based on energy methods.

For simple cases, such as the one shown in Fig. 16.10.2, we can combine the variational method with the direct solution of one of the governing differential equations. Let us assume, for instance, that the plate compressed in the X direction (Fig. 16.10.2) is simply supported along its four boundaries. Thus, an approximate expression for the buckled middle surface is

$$w(x, y) = W_{11} \sin \frac{\pi x}{a} \sin \frac{\pi y}{b}, \quad (16.10.3)$$

which substituted into Eq. (16.10.2) gives

$$\frac{1}{E} \nabla^2 \nabla^2 \Phi = \frac{1}{2} W_{11}^2 \frac{\pi^4}{a^2 b^2} \left(\cos \frac{2\pi x}{a} + \cos \frac{2\pi y}{b} \right). \quad (16.10.4)$$

If we further assume that the edge beams do not prevent the in-plane motions of the plate in the Y direction, then the solution of Eq. (16.10.2) can be written as

$$\Phi = \Phi_P + \Phi_H = \frac{EW_{11}^2}{32} \left[\left(\frac{a}{b} \right)^2 \cos \frac{2\pi x}{a} + \left(\frac{b}{a} \right)^2 \cos \frac{2\pi y}{b} \right] - \frac{\bar{n}_x y^2}{2h}. \quad (16.10.5)$$

The substitution of this expression into the differential equation of equilibrium (16.10.1), to which Galerkin's variational technique is applied, yields

$$\int_0^a \int_0^b [\text{Diff. Eq. (16.10.1)}] \delta w = 0; \quad (16.10.6a)$$

hence,

$$D \frac{\pi^4 ab}{4} W_{11} \left(\frac{1}{a^2} + \frac{1}{b^2} \right)^2 - \bar{n}_x W_{11} \frac{\pi^2 ab}{a^2} \frac{1}{4} + E \frac{\pi^4 W_{11}^3 h}{64} \left(\frac{1}{a^4} + \frac{1}{b^4} \right) ab = 0, \quad (16.10.6b)$$

and finally

$$\bar{n}_x = \sigma_{cr} h = D \frac{\pi^2}{b^2} \left(\frac{b}{a} + \frac{a}{b} \right)^2 + E \frac{h\pi^2}{16b^2} W_{11}^2 \left(\frac{b^2}{a^2} + \frac{a^2}{b^2} \right). \quad (16.10.6c)$$

Since the first term on the right-hand side of Eq. (16.10.6c) represents the linear case of buckling (16.2.21), it is evident that the plate can sustain greater than the linear buckling load, and its load-carrying capacity is more pronounced when the unloaded edges are constrained to remain straight ($\bar{n}_y \neq 0$).

In a more general case, we apply Galerkin's method for the solution of Eqs. (16.10.1) and (16.10.2) and express the lateral deflections and stress function as an infinite series:

$$w(x, y) = \sum_m \sum_n W_{mn} w_{mn}(x, y), \quad \Phi = \sum_m \sum_n F_{mn} \varphi_{mn}(x, y). \quad (16.10.7)$$

The functions $\varphi_{mn}(x, y)$ and $w_{mn}(x, y)$ must satisfy the static and geometrical boundary conditions, but not necessarily the governing differential equations. Depending on the given boundary conditions, trigonometric functions or linear combinations of the fundamental functions of beam vibration are the prime choices for $\varphi_{mn}(x, y)$ and $w_{mn}(x, y)$, since these functions are orthogonal and quasi-orthogonal, respectively. Namely, the orthogonality can lead to considerable simplification in expansion of the variational equations, as discussed in Sec. 4.3. The basic variational equations for solution of postbuckling problems of plates can be written in the general form

$$\begin{aligned} \iint_{(A)} \left[\frac{D}{h} \nabla^4 w - \mathfrak{L}_1(\Phi, w) \right] w_{ij}(x, y) dx dy &= 0, \\ \iint_{(A)} \left[\frac{1}{E} \nabla^4 \Phi - \mathfrak{L}_2(w, w) \right] \varphi_{ij}(x, y) dx dy &= 0. \end{aligned} \quad (16.10.8)$$

It should be noted that the variations of these differential equations are not interrelated. The general pattern for expansion of Eq. (16.10.8) and for evaluation of the definite integrals is analogous to the procedure used in Sec. 11.1 for large-deflection analysis of plates. Since the resulting simultaneous equations are nonlinear, usually not more than three terms are taken in the series expressions of the stress function and lateral displacements to avoid additional mathematical difficulties.

An alternative method for the solution of postbuckling problems is based on the principle of minimum potential energy (Ritz method). Applying the Ritz method to postbuckling problems, however, the nonlinear expressions of the strain components must also be substituted into the membrane part of the strain energy expression, U_m^* . Furthermore, in considering the potentials of the in-plane forces, the method described in Sec. 16.3 is applicable. Since, in the general expression of the strain energy, all three displacement components (u, v, w) appear, the solution may be simplified by expressing the strain energy of the plate in terms of the lateral displacement w and that of the stress function Φ :

$$U_b^* + U_m^* = \iint_{(A)} \left\{ \frac{D}{2} \left[(\nabla^2 w)^2 - (1 - \nu) \mathcal{L}(w, w) \right] - \frac{h}{2E} [(\nabla^2 \Phi)^2 - (1 + \nu) \mathcal{L}(\Phi, \Phi)] - \frac{h}{2} \Phi \mathcal{L}(w, w) \right\} dx dy, \quad (16.10.9)$$

where the operator $\mathcal{L}(\cdot)$ is defined by

$$\mathcal{L}(\cdot) = \frac{\partial^2(\cdot)}{\partial x^2} \frac{\partial^2(\cdot)}{\partial y^2} + \frac{\partial^2(\cdot)}{\partial y^2} \frac{\partial^2(\cdot)}{\partial x^2} - 2 \frac{\partial^2(\cdot)}{\partial x \partial y} \frac{\partial^2(\cdot)}{\partial x \partial y}. \quad (16.10.10)$$

This expression is valid only for plates with no lateral deflection at the edges. The stress function $\Phi(x, y)$ in Eq. (16.10.9) is Airy's stress function.

b. Effective Width Method. As the buckling load is increased beyond the critical load, the distribution of the stresses along the loaded edges becomes progressively nonlinear. Tests have shown [16.10.1] that the loaded edges are more heavily stressed in the vicinity of the unloaded edges and that stresses remain virtually unchanged at the center of the loaded edges, where the stresses are equal to (or less than) the critical stress $\sigma_{cr} = \bar{\pi}_{cr}/h$ (Fig. 16.10.4a). The actual distribution of these compressive stresses depends on the boundary conditions and on the length-to-width ratio a/b , provided that this ratio is less than 3. When failure of the plate is impending, almost the total compressive force is carried by two strips located along the unloaded edges. Based on this observation, von Kármán et al. [16.10.3] have proposed a simplified approach to obtain an estimate for the ultimate load carried by the plate. This simplified method is based on the following assumptions:

1. The unloaded plate is perfectly flat.
2. The ultimate buckling load of the plate is carried exclusively by two strips of equal width located along the unloaded edges.
3. The maximum stress at the loaded edge, σ_e , is uniformly distributed over the two plate strips.
4. The stringers, jointly with the effective width portion of the plate, act as columns.

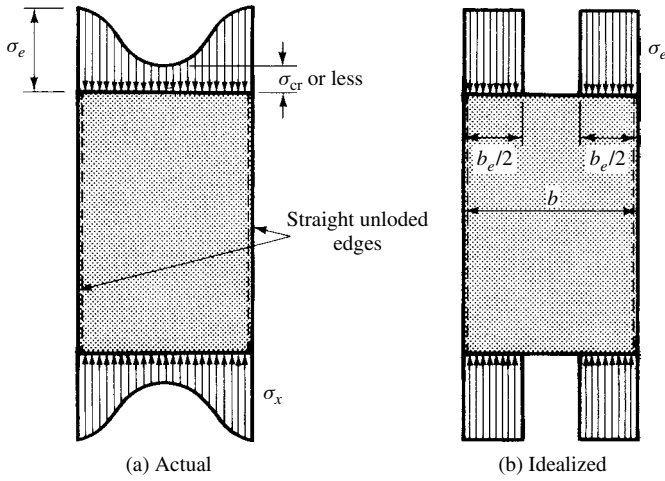


Figure 16.10.4 Stress distribution at loaded edges.

From these assumptions, the *effective width* (Fig. 16.10.4b) is

$$b_e = \frac{1}{\sigma_e} \int_0^b \sigma_x dy, \quad (16.10.11)$$

assuming that the buckling load acts in the X direction. If the stiffeners are relatively strong, the yield criterion can conveniently be used in connection with the effective width concept to obtain the ultimate edge load the plate is able to carry; thus

$$\bar{P} = \sigma_e b_e h = \sigma_y^* b_e h, \quad (16.10.12)$$

provided that the stringers and the adjacent plate strips reach the yield stresses σ_y^* simultaneously without buckling. If the stringers are relatively weak, they may fail by instability before yield stresses are developed. In such a case, the maximum stress developed in the stringer must be substituted for σ_e in Eq. (16.10.12).

Let us now determine the effective width b_e using the critical stress σ_{cr} produced by the critical loads as a reference value. The critical stress can be given in the form

$$\sigma_{cr} = \frac{\bar{n}_{cr}}{h} = \lambda_{cr} \frac{D}{h} \left(\frac{\pi}{b} \right)^2 = kE \left(\frac{h}{b} \right)^2, \quad (16.10.13)$$

where $k = \pi^2 \lambda_{cr} / [12(1 - \nu^2)]$ is the *buckling coefficient* and λ_{cr} is the critical load factor introduced in Secs. 16.1 and 16.2. An expression similar to Eq. (16.10.13) can be written for the equivalent plate of width b_e :

$$\sigma_e = kE \left(\frac{h}{b_e} \right)^2. \quad (16.10.14)$$

A simple comparison of Eqs. (16.10.13) and (16.10.14) gives

$$\frac{\sigma_e}{\sigma_{cr}} = \frac{b^2}{b_e^2}; \quad (16.10.15)$$

hence

$$b_e = b \sqrt{\frac{\sigma_{cr}}{\sigma_e}} \quad (16.10.16)$$

In addition to von Kármán's original formula (16.10.16), the following general expressions are most commonly used for the effective width:

Marguerre's formula[†] [16.10.4, 16.10.9]:

$$\boxed{b_e = b \sqrt[3]{\frac{\sigma_{cr}}{\sigma_e}}}. \quad (16.10.17)$$

Sechler's formula [16.10.5]:

$$b_e = 0.5b \left(1 + \frac{\sigma_{cr}}{\sigma_e}\right) \left(\frac{\sigma_{cr}}{\sigma_e}\right)^{0.37\sigma_e/\sigma_y^*}. \quad (16.10.18)$$

Marguerre's formula for square plates and large postbuckling loads [16.10.9]:

$$b_e = b \left(0.19 + 0.81 \sqrt{\frac{\sigma_{cr}}{\sigma_e}}\right). \quad (16.10.19)$$

Koiter's formula [16.10.7]:

$$b_e = b \left[1.2 \left(\frac{\sigma_{cr}}{\sigma_e}\right)^{0.4} - 0.65 \left(\frac{\sigma_{cr}}{\sigma_e}\right)^{0.8} + 0.45 \left(\frac{\sigma_{cr}}{\sigma_e}\right)^{1.2} \right]. \quad (16.10.20)$$

Equation (16.10.20) is applicable for long plates only. It gives satisfactory results for simply supported, fixed and elastically supported longitudinal (unloaded) edges.

For small postbuckling loads having $\sigma_e/\sigma_{cr} \leq 5$ ratios, Marguerre [16.10.9] recommends the use of the following approximate expressions:

- rectangular plates with longitudinal (unloaded) edges free to move transversely,

$$b_e = b \left[\frac{1 + \beta^4}{1 + 3\beta^4} + \frac{2\beta^4}{1 + 3\beta^4} \left(\frac{\sigma_{cr}}{\sigma_e}\right) \right], \quad (16.10.21)$$

where $\beta = b/a$;

[†] Agrees well with test results, especially for clamped unloaded edges. The recommended range of the formula is $2 \leq \sigma_e/\sigma_{cr} \leq 20$.

- square plates with unloaded edges free to move transversely,

$$b_e = b \left(0.5 + 0.5 \frac{\sigma_{cr}}{\sigma_e} \right) \quad (16.10.22)$$

- and square plates with constrained unloaded edges,

$$b_e = \frac{b}{3 + \nu} \left(2 + \frac{\sigma_{cr}}{\sigma_e} \right). \quad (16.10.23)$$

Additional formulas for the effective widths of plates in compression can be obtained from Refs. [16.10.8, 16.10.10] and from most of the pertinent works listed in the bibliography at the end of this section. In Lévy's report [16.10.2], the reader will find a valuable comparison of the various most commonly used formulas.

The above-given formulas assume, a priori, the existence of very heavy stiffeners, customary in aerospace structures. In shipbuilding practice, however, where the width-to-thickness ratios of plates are considerably smaller, better results can be obtained by considering the neglected stresses in the center portion of the plate. Thus, for this condition Eq. (16.10.12) becomes

$$P_u = P_u^I + P_u^{II} = \sigma_e b_e h + \sigma_{cr} (b - b_e) h. \quad (16.10.12a)$$

Montgomerie's semiempirical formula [16.10.11] for ultimate stress,

$$\sigma_u = \frac{18}{2240 + 2.36(a/h)^{1.75}} \quad (\text{psi}), \quad (16.10.24)$$

yields acceptable results for crippling loads of plates considering stringer spacings (a) and plate thicknesses (h) generally used in ship structures. These dimensions should be substituted into (Eq. 16.10.24) in inches.

When the edge-supporting stringers fail in instability before the yield stress is reached, a trial-and-error procedure should be used to obtain an estimate for the maximum edge stresses. First, we assume an effective width $b_e^{(1)}$ ($b_e = 0.3b - 0.8b$), from which $\sigma_e^{(1)}$ is determined, considering that the stringer and the effective width portion of the plate act as a column. Using the so-obtained $\sigma_e^{(1)}$ value, a new estimate for $b_e^{(2)}$ can be obtained. The procedure is repeated until the interrelationship between these two variables is satisfied.

c. Effects of Initial Imperfections. Plates used in practice are seldom perfectly flat, as assumed in our previous investigations. Small initial imperfections have been found to have only minor effect on the effective width [16.10.12], provided that maximum edge stresses σ_e are well above (or below) the value of the critical stress σ_{cr} . Small initial imperfections reduce somewhat the effective width in the region of $\sigma_{cr}/\sigma_e = 0.5 - 1$.

The behavior of plates with initial curvature, however, can be markedly different (Fig. 16.10.5). If the curvature parameter

$$Z_c = \frac{b^2}{Rh} \sqrt{1 - \nu^2} \quad (16.10.25)$$

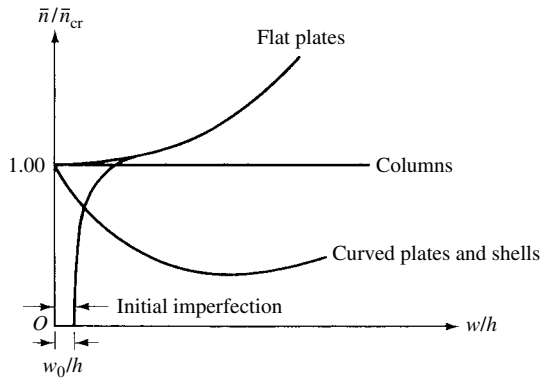


Figure 16.10.5 Postbuckling behavior of flat and curved plates.

is between 10 and 1000, the postbuckling behavior of curved plates represents a transition between flat plate and cylindrical shell [16.10.13]. If the curvature parameter is less than 10, the postbuckling behavior of the curved plate is similar to that of the perfectly flat plate, while beyond $Z_c > 1000$ the plate buckles like a cylindrical shell; that is, the boundary conditions do not exert significant influence on the ultimate load.

A semiempirical formula [16.10.6, 16.10.13] for the *effective width* of axially compressed, long curved plates with clamped boundary conditions along the unloaded edges is

$$b_e = h \sqrt{k_c} \sqrt{\frac{E}{\sigma_e}}, \quad (16.10.26)$$

where k_c is the buckling coefficient of curved plate,

$$k_c = \frac{\pi^2 \lambda_{cr}^*}{12(1 - \nu^2)}, \quad (16.10.27)$$

and λ_{cr}^* can be taken from Fig. 16.10.6. The usable range of Eq. (16.10.26) is $0 \leq Z_c \leq 31$ and $b_e/b \geq 0.45$. For effective widths $b_e/b \leq 0.45$ and for curvature parameters $0 \leq Z_c \leq 125$, an approximate formula,

$$b_e \approx b \lambda_{cr}^{0.43} \left(\frac{h}{b} \sqrt{\frac{E}{\sigma_e}} \right)^{0.85}, \quad (16.10.28)$$

can be applied. In this expression λ_{cr} is the critical load factor for flat plates. For long clamped flat plates the use of $\lambda_{cr} \approx 6.3$ is recommended. Since Eqs. (16.10.26) and (16.10.27) are derived from test results, some caution should be exercised in their use beyond $Z_c > 28$.

Laterally loaded curved plates may exhibit snap-through buckling if they are subjected to external pressure. The discussion of snap-through buckling, however, is considered to be beyond the scope of this book.

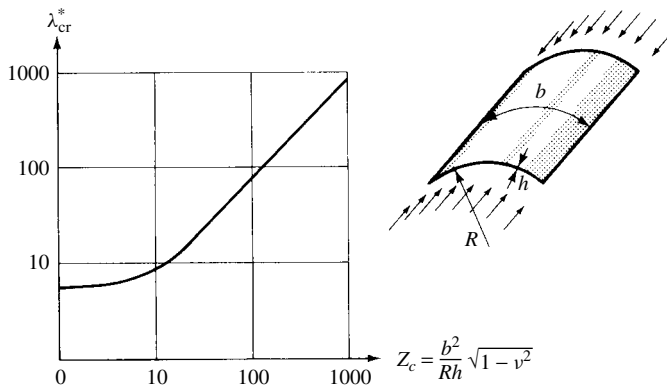


Figure 16.10.6 Critical load factors for axially compressed curved plates.

Summary. Considering the significant membrane stresses developed in the plate after buckling, flat plates can support much larger in-plane loads than indicated by the classical buckling analysis.[†] Because of the resulting savings in weight, the behavior of plates beyond the critical buckling load is of great practical interest to aerospace and shipbuilding industries. The analysis of postbuckling of plates requires the use of large-deflection theory; consequently, the analytical solution of the problem is inherently complex. Although the required computation is tedious, Galerkin's method, based on the variational principle, yields acceptable results, provided that proper deflection shapes are assumed. The greatest difficulties, however, are encountered in assuming these deflection shapes, since the buckling mode progressively changes as the plate approaches failure.

For routine design purposes, simplified methods based on the concept of *effective width in compression* have been introduced by numerous investigators. The most commonly used effective width formulas are given in this section. Slight deviations from flatness have little influence on the effective width at large postbuckling load ($\sigma_e/\sigma_{cr} \geq 5$). Some reduction occurs in the vicinity of the critical stresses ($\sigma_e/\sigma_{cr} = 1$).

ILLUSTRATIVE EXAMPLE

Assess the ultimate edge load of a rectangular plate stiffened along both longitudinal edges and uniformly compressed in the X direction (Fig. 16.10.7). Use the effective width method. Assume that the stringer and the adjacent plate strip simultaneously approach the compressive yield strength of the structural steel ($\sigma_Y^* = 33,000$ psi); the stringer, however, will not fail due to instability before the plate buckles.

Since we have assumed that failure occurs shortly after the stresses become equal to the yield strength of the material near the edges, we substitute $\sigma_e = \sigma_Y^*$ in the pertinent formula for the effective width.

Next, we determine the critical stress in the plate using the conservative assumption of simply supported boundary conditions. From Eq. (16.2.22) the

[†] Provided that the plate edges are rigidly supported.

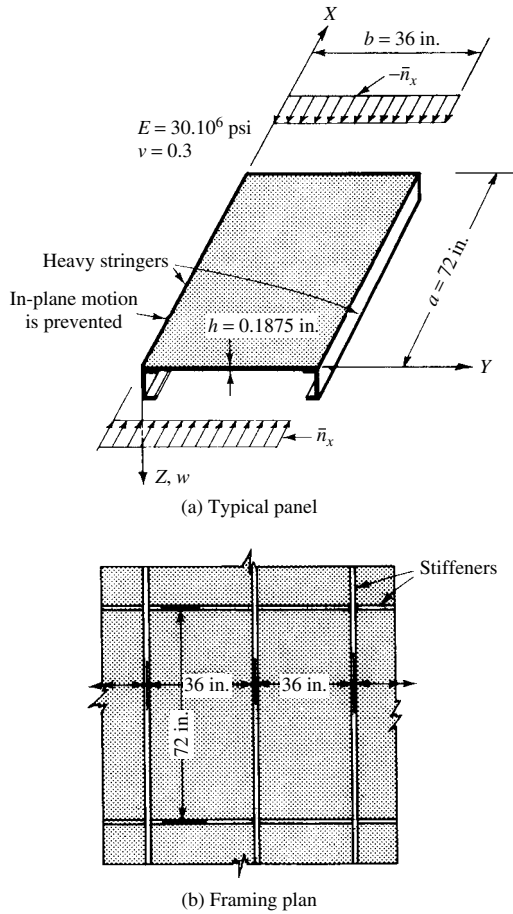


Figure 16.10.7 Axially loaded steel plate with sturdy stiffeners.

critical load factor is the minimum value of

$$\lambda = \left(m + \frac{1}{m} \frac{a^2}{b^2} \right)^2.$$

Since the aspect ratio $a/b = 2$, two half-waves ($m = 2$) in the X direction give

$$\lambda_{cr} = \lambda_{min} = 16.$$

Therefore, the critical stress for the plate becomes

$$\begin{aligned} \sigma_{cr} &= \frac{\bar{n}_{cr}}{h} = \frac{\lambda_{cr} \bar{n}_{x0}}{h} = 16 \frac{\pi^2 E}{12(1 - \nu^2)} \frac{h^2}{a^2} \\ &= 16 \frac{\pi^2 (30 \times 10^6) (0.1875)^2}{12(1 - 0.3^2) 72^2} = 2942 \text{ psi.} \end{aligned}$$

Since the ratio

$$\frac{\sigma_e}{\sigma_{cr}} = \frac{33,000}{2942} \approx 11.2$$

indicates a large postbuckling load, Marguerre's formula (16.10.17) for the effective width is applicable; therefore,

$$b_e = b \sqrt[3]{\frac{\sigma_{cr}}{\sigma_e}} = 36 \sqrt[3]{\frac{2942}{33,000}} = 16.08 \text{ in.}$$

The approximate value of the *collapse load* carried by the two plate strips is

$$\bar{P}_{ult} \cong \sigma_y^* h b_e = 33,000 \times 1875 \times 16.08 = 99,500 \text{ lb.}$$

The use of other empirical formulas gives somewhat different results.

References and Bibliography

- [16.10.1] KOLLBRUNNER, C. F., "Das Ausbeulen der auf einseitigen, gleichmassig verteilten Druck beanspruchten Platten im elastischen und plastischen Bereich," *Mitteilungen No. 17*, Institut für Baustatik, Eidgenössische Technische Hochschule, Zurich, 1946.
- [16.10.2] LÉVY, S., "Bending of Rectangular Plates with Large Deflections," Tech. Rept. No. 737, National Advisory Committee for Aeronautics, Washington, D. C., 1942.
- [16.10.3] VON KÁRMÁN, T. H., SECHLER, E. E., and DONNELL, L. H., "The Strength of Thin Plates in Compression," *Trans. ASME*, 54 (1932), 53–57.
- [16.10.4] MARGUERRE, K., "Die mittragende Breite der gedrückten Platte," *Luftfahrtforschung*, 14, No 3 (1937), 121–128.
- [16.10.5] SECHLER, E. E., "The Ultimate Strength of Thin Flat Sheets in Compression," Publ. No. 27, Guggenheim Aeronautical Laboratory, California Institute of Technology, Pasadena, 1933.
- [16.10.6] GERARD, G., "Handbook of Structural Stability, Part IV—Failure of Plates and Composite Elements," NACA TN 3784, National Advisory Committee for Aeronautics, Washington, D.C., 1957.
- [16.10.7] KOITER, W. T., "The Effective Width of Flat Plates for Various Longitudinal Edge Conditions at Loads Far Beyond the Buckling Load," Rep. No. 5287, National Luchtvaart Laboratorium, The Netherlands, 1943.
- [16.10.8] ARGYRIS, J. H., and DUNNE, P. C., *Handbook of Aeronautics*, Vol. 1, Pt. 2, 4th ed., Pitman Publishing, New York, 1952.
- [16.10.9] MARGUERRE, K., "The Apparent Width of the Plate in Compression," Tech. Memo. No. 833, National Advisory Committee for Aeronautics, Washington, D.C., 1937.
- [16.10.10] MAYERS, J., and BUDIANSKY, B., "Analysis of Behavior of Simply Supported Flat Plates Compressed Beyond the Buckling Load into the Plastic Range," NACA TN 3368, National Advisory Committee for Aeronautics, Washington, D.C., 1955.
- [16.10.11] MONTGOMERIE, J., "Experiments on Compression of Samples of Deck Plating and Application of Results to Determine Safe Limiting Thickness for Weather Decks in Certain Conditions of Loading," *Zosenkiokai* (J. Soc. Naval Architects of Japan), 54 (Oct. 1934), 121–163.
- [16.10.12] HU, P. C., LUNDQUIST, E. E., and BATDORF, S. B., "Effect of Small Deviations from Flatness on Effective Width and Buckling of Plates in Compression," NACA TN 1124, National Advisory Committee for Aeronautics, Washington, D.C., 1946.

- [16.10.13] GERARD, G., and BECKER, H., "Handbook of Structural Stability, Part III—Buckling of Curved Plates and Shells," NACA TN 3783, National Advisory Committee for Aeronautics, Washington, D.C., 1957.
- [16.10.14] VAN DER NEUT, A., "Postbuckling Behavior of Structures," AGARD Rept. No. 60, Advisory Group for Aeronautical Research and Development, NATO, Paris, 1956.
- [16.10.15] STOWELL, E. Z., "A Unified Theory of Plastic Buckling of Columns and Plates," Tech. Rept. 898, National Advisory Committee for Aeronautics, Washington, D.C., 1948.
- [16.10.16] ASHWELL, D. G., "The Equilibrium Equations of the Inextensional Theory for Thin Flat Plates," *Quart. J. Mech. Appl. Math.*, 10 (1957), 169–182.
- [16.10.17] ASHWELL, D. G., "A Characteristic Type of Instability in the Large Deflections of Elastic Plates (I), Curved Rectangular Plates Bent About One Axis," *Proc. Roy. Soc. (London)*, A-214 (1952), 98–118.
- [16.10.18] MARGUERRE, K., "Zur Theorie der gekrümmten Platte grosser Formänderung," in *Proceedings of the 5th International Congress of Applied Mechanics, Cambridge, Mass.*, John Wiley & Sons, New York, 1939, pp. 93–101.
- [16.10.19] COX, H. L., "The Distortion of a Flat Rectangular Plate in Its Own Plane," Rep. Memo. No. 2200, Aeronautical Research Council, London, 1949.
- [16.10.20] GERARD, G., "Effective Width of Elastically Supported Flat Plates," *J. Aeron. Sci.*, 10 (1946), 518–523.
- [16.10.21] MARGUERRE, K., and TREFFTZ, E., "Über die Tragfähigkeit eines Plattenstreifens nach Überschreiten der Beullast," *Z. f. Angew. Math. u. Mech.*, 17 (1937), 85–100.
- [16.10.22] ABDEL-SAYED, G., "Effective Width of Thin Plates in Compression," *Proc. ASCE*, 95, *J. Struct. Div.*, ST 10 (Oct. 1969), 2183–2203.
- [16.10.23] WINTER, G., "Performance of Compression Plates as Parts of Structural Member," Research: Engineering, Structures Supplement, *Colston Papers*, Vol. 2, Colston Res. Soc. London, 1949, p. 179.
- [16.10.24] STEUP, H., "Vorbeulungs- und Eigenspannungs-Einflüsse bei der überkritischen Beulung von Platten," *Publ. IABSE*, 29-1 (1969), 73–93.
- [16.10.25] KLÖPPEL, K., SCHMIED, R., and SCHUBERT, J., "Die Traglast mittig und aussermittig gedrückter dünnwandiger Kastenträger unter Verwendung der nichtlinearen Beultheorie," *Der Stahlbau*, 35 (1966), 321–337.
- [16.10.26] OWEN, D. R., ROCKEY, K. C., and SKALLOUD, M., "Ultimate Load Behavior of Longitudinally Reinforced Webplates Subjected to Pure Bending," *Publ. IABSE*, 30, Pt. I (1970), 113–148.
- [16.10.27] YANG, T. Y., "Elastic Postbuckling Prediction of Plates Using Discrete Elements," *AIAA J.*, 9, No. 9 (Sept. 1971), 1665–1666.
- [16.10.28] IYENGAR, N. G. R., *Structural Stability of Columns and Plates*, Halsted Press, New York, 1988.
- [16.10.29] BLOOM, F., and COFFIN, D., *Handbook of Thin Plate Buckling and Postbuckling*, Chapman & Hall/CRC Press, Boca Raton, Florida, 2001.

16.11 Inelastic Buckling and Failure of Plates

a. Buckling in Plastic Range. Determination of the plastic buckling load of a plate is considerably more difficult than that of its elastic counterpart, since the stress-strain relationship beyond the proportional limit is more complex. Additional mathematical difficulties in the analysis originate from the stress dependence of Poisson's ratio, $\nu(\sigma)$, and that of the critical load factor, $\lambda(\sigma)$. Consequently, numerical methods are strongly recommended for stability analysis of plates in the plastic region.

Although the theory of plastic buckling of columns is well developed, several aspects in the theory of plastic buckling of plates are still controversial. The primary difficulty lies in the proper representation of the stress-strain relationship. That is, in

the case of plastic buckling of columns the stresses are uniaxial, whereas in plate buckling the state of stress is two or three dimensional. Furthermore, plastic buckling can be analyzed using either flow [16.11.1] or deformation theories [16.11.2] of plasticity. Since analytical investigations based on deformation theories show good correlation with experimental results [16.11.4], the use of this approach is recommended. It is evident, from what has been said above, that in the solution of plastic buckling of plates, the formulation of suitable stress-strain laws beyond the proportional limit is of basic importance. A convenient analytic expression is due to Ramberg-Osgood [16.5.12].

Because of the inherent complexity of the plastic buckling analysis of plates, usually a simplified method based on a *rational* approach to the problem is used in engineering practice.

When the buckling stress exceeds the proportional limit of the material, the modulus of elasticity is reduced, which in turn alters the load-carrying capacity of the plate in the plastic region. Consequently, if in a plate subjected to in-plane forces plastic yielding occurs prior to reaching the critical load, its load-carrying capacity is reduced. This phenomenon can be approximated by multiplying the critical load \bar{n}_{cr} obtained from linear-elastic theory by an appropriate *plasticity reduction* factor η . In this single coefficient all the effects created by exceeding the proportional limit are incorporated. Thus, we can write

$$(\bar{n}_{cr})_{\text{plastic}} = \eta \lambda_{cr} \bar{n}_0 = \eta \lambda_{cr} \frac{\pi^2 D}{b^2}. \quad (16.11.1)$$

Hence, the critical stress in the plastic region is

$$(\sigma_{cr})_{\text{plastic}} = \eta \lambda_{cr} \frac{\pi^2 E}{12(1 - \nu^2)} \left(\frac{h}{b} \right)^2. \quad (16.11.2)$$

Since in the elastic range $\eta = 1$, Eq. (16.11.1) covers the elastic as well as the inelastic buckling of plates. Recommended values for the plasticity reduction coefficients are given in Table 16.11.1. The plastic Poisson ratio ν^* appearing in these expressions can be calculated [16.11.5] from

$$\nu^* = 0.5 - (0.5 - \nu) \frac{E_s}{E}, \quad (16.11.3)$$

where E is Young's modulus of elasticity and E_s represents the secant modulus. For a three-dimensional state of stress, E_s and the tangent modulus E_t are defined in Sec. 11.2. While the fully plastic Poisson ratio for incompressible isotropic materials approaches the value of $\nu^* = 0.5$, this, however, is generally not the case for orthotropic materials.

The inelastic interaction equation for simultaneous action of longitudinal compression and edge shear is

$$R_{\text{comp.}}^2 + R_{\text{shear}}^2 \leq 1, \quad (16.11.4)$$

where R represents the load ratio, as defined in Sec. 16.1.

A similar approach can be taken in the case of plastic buckling of stiffened plates, considering that η depends on factors pertinent to the plate and stiffeners, respectively.

Table 16.11.1 Plasticity Reduction Factor η

Loading	Structure	η/j
Compression	Long flange, one unloaded edge simply supported	1
	Long flange, one unloaded edge clamped	$0.330 + 0.335[1 + (3E_t/E_s)]^{1/2}$
	Long plate, both unloaded edges simply supported	$0.500 + 0.250[1 + (3E_t/E_s)]^{1/2}$
	Long plate, both unloaded edges clamped	$0.352 + 0.324[1 + (3E_t/E_s)]^{1/2}$
	Short plate loaded as a column ($a/b < 1$)	$0.250[1 + (3E_t/E_s)]$
	Square plate loaded as a column ($a/b = 1$)	$0.114 + 0.886(E_t/E_s)$
	Long column ($a/b > 1$)	E_t/E_s
Shear	Rectangular plate, all edges elastically restrained	$0.83 + 0.17(E_t/E_s)$

Source: After Ref. [16.11.5].

Note: $j = (E_s/E)(1 - \nu^2)[1 - (\nu^*)^2]$; a = length of plate.

The recommended plasticity reduction factor for stiffened plates subjected either to longitudinal compression or to shear [16.11.5] is

$$\eta = \frac{(1 - \nu^2)E_s}{[1 - (\nu^*)^2]E}, \quad (16.11.5)$$

provided that the ribs enforce the buckling modes. Equation (16.11.5) can also be used for Z- and channel-shaped ribs subjected to compression. In both cases, the torsional resistance of the stiffeners have been neglected.

The moment distribution technique, introduced in Sec. 12.4 for the analysis of laterally loaded continuous plates, can also be extended to determine the inelastic buckling loads of plates reinforced with stiffeners [16.11.8].

b. Failure of Plates. Discussing the postbuckling behavior of plates in Sec. 16.10, we already have shown that plates can carry considerably larger in-plane loads than the critical load, provided that the unloaded edges are constrained to remain straight. Failure of plates is usually caused by a combination of large deflections and plasticity effects. Consequently, in the analysis, both the geometrical and material nonlinearities must simultaneously be included, which makes analytical solutions, in most cases, very difficult. The variational method appears to be a usable analytical approach [16.11.9] to obtain solutions to this complex problem. Since the calculations are performed by high-speed electronic computers, the finite element technique can economically combine geometrical and material nonlinearities by the incremental approach. Other nonlinear formulations generally use the *Newton-Raphson* method to obtain nonlinear stiffness relations [16.11.10].

The ultimate in-plane load at which the load-carrying capacity of the flat plate terminates depends considerably on the boundary conditions of the unloaded edges. Gerard [16.10.6] recommends the following simple formulas for determination of the stress level σ_f at which flat plates under compressive edge loads fail:

$$\begin{aligned} \sigma_f &= \alpha \sigma_{cr} \left(\frac{\sigma_{cY}}{\sigma_{cr}} \right)^n & \text{for } \sigma_{cr} \leq (\alpha)^{1/n} \sigma_{cY}, \\ \sigma_f &= \sigma_{cr} & \text{for } \sigma_{cr} > (\alpha)^{1/n} \sigma_{cY}, \end{aligned} \quad (16.11.6)$$

Table 16.11.2 Coefficients α and n in Eq. (16.11.6)

<i>Element</i>	α	n
Simply supported plate with straight unloaded edges	0.78	0.80
Simply supported and clamped plate edges, free to warp (test)	0.80	0.58
Three-bay plate (test)	0.80	0.65

where σ_{CY} represents the compressive yield stress of the structural material. Recommended values for α and n are given in Table 16.11.2.

Determination of failure stresses of unstiffened and stiffened plates subjected to edge shear is more complicated. For further study of this subject, the reader is referred to Ref. [16.11.11].

Summary. In this section, mainly the problematics involved in calculation of inelastic buckling loads and failure stresses have been treated. Because of the inherent complexity of the problem, no attempt was made to discuss in detail any analytical or numerical technique that can be applied to obtain solutions. For the practicing engineer, however, simplified design formulas are presented. Interested readers are referred to the rather extensive literature covering the subject matter.

References and Bibliography

- [16.11.1] HANDELMAN, G. H., and PRAGER, W., "Plastic Buckling of a Rectangular Plate Under Edge Thrusts," NACA Report 946, National Advisory Committee for Aeronautics, Washington, D.C., 1949.
- [16.11.2] BILLAARD, P. P., "Theory and Tests of Plastic Stability of Plates and Shells," *J. Aeron. Sci.*, 16 (Sept. 1949), 529–541.
- [16.11.3] ILYUSHIN, A. A., "The Elasto-Plastic Stability of Plates," NACA TN 1188, National Advisory Committee for Aeronautics, Washington, D.C., Dec. 1947.
- [16.11.4] PRIDE, R. A., and HEIMERL, G. J., "Plastic Buckling of Simply Supported Compressed Plates," NACA TN 1817, National Advisory Committee for Aeronautics, Washington, D.C., Apr. 1949.
- [16.11.5] GERARD, G., and BECKER, H., "Handbook of Structural Stability," Pts. I and II, NACA TN 3781 and 3782, National Advisory Committee for Aeronautics, Washington, D.C., 1957.
- [16.11.6] STOWELL, E. Z., HEIMERL, G. J., LIBOVE, C., and LUNDQUIST, E. E., "Buckling Stresses for Flat Plates and Sections," *Proc. ASCE*, 77, Separate No. 7 (July 1951), 31.
- [16.11.7] GERARD, G., "Critical Shear Stress of Plates above the Proportional Limit," *J. Appl. Mech. Trans. ASME*, 15 (March 1948) 7–12.
- [16.11.8] LUNDQUIST, E. E., STOWELL, E. Z., and SCHUETTE, E. H., "Principles of Moment Distribution Applied to Stability of Structures Composed of Bars or Plates," NACA WRL-326, National Advisory Committee for Aeronautics, Washington, D.C., 1943.
- [16.11.9] MAYERS, J., and BUDIANSKY, B., "Analysis of Behavior of Simply Supported Flat Plates Compressed Beyond the Buckling Load into the Plastic Range," NACA TN 3368, National Advisory Committee for Aeronautics, Washington, D.C., 1955.
- [16.11.10] ODEN, J. T., "Finite Element Application in Nonlinear Structural Analysis," in *Proceedings of the Symposium on Application of Finite Element Method in Civil Engineering* held at Nashville, Tenn., Nov. 13–14, 1969, W. H. Rowan and R. M. Hackett (Eds.), School of Engineering, Vanderbilt University, Nashville, 1969.

- [16.11.11] KUHN, P., PETERSON, J. P., and LEVIN, L. R., "A Summary of Diagonal Tension," Part I, Methods of Analysis, NACA TN 3781, National Advisory Committee for Aeronautics, Washington, D.C., 1957.
- [16.11.12] TEZCAN, S. S., MAHAPATRA, B. C., and MATHEWS, C. I., "Tangent Stiffness Matrices for Finite Elements," *Publ. IABSE* 30, Pt. I (1970), 217–246.

16.12 Summary and Conclusions

Plates used in ship and aerospace structures are often subjected to in-plane forces. As these forces are gradually increased, at certain values, the plate loses its stability and deflects laterally (buckles), even in the absence of transverse loading. In the classical stability theory the *critical load* is defined as the load at which *bifurcation* of the deformations occurs. In the analysis, we generally use the *neutral state of equilibrium* for formulating instability problems, assuming that the neighboring state of equilibrium, corresponding to the bent form, is infinitely near the unbuckled state. Since we deal with infinitely small deformations, most of the higher-order terms in the expression of strains can be neglected.

In this chapter, in addition to formulating the buckling problem mathematically, various analytical and numerical methods for analysis of instability problems of plates have been introduced. Numerical examples illustrate the applicability and the limitations of these computational techniques. Since "exact" solutions can be found only for a limited number of buckling problems of practical interest, the use of various approximate solutions is emphasized.

The minimum buckling load, called the *critical load*, is usually the value sought. By introducing a load factor λ and a reference value of the in-plane load, \bar{n}_0 , the solutions of plate instability problems are reduced to determination of λ_{\min} , which corresponds to the lowest eigenvalue of the resulting homogeneous algebraic equations.

Rayleigh's method, based on the energy principle, expresses the equality of the work done by the external and internal forces at the instant of transition from the stable state of equilibrium (corresponding to the straight form) into an unstable one (bent form). Although easy to use, the method is confined to the cases in which merely one undetermined coefficient in the expression of the lateral deflections can represent a sufficiently close approximation of the bent shape of the plate. This limitation of the otherwise very effective technique can be overcome by the Ritz method, based on the minimum potential of the elastic system, which permits the use of more than one term in the series expression of the lateral deflections. The required minimum value of the load, factor λ is determined by equating to zero the determinant of the resulting homogeneous set of algebraic equations. All previously discussed requirements concerning selections of proper shape functions are also valid for stability analysis. Although the Ritz method appears to be one of the most generally applicable analytical tools in the solution of instability problems of plane and stiffened plates, its practical application might become quite tedious.

Galerkin's variational method, which operates on the governing differential equation of stability, can also be extended to solution of instability problems of plates, even when nonlinear large-deflection theory must be applied, as in the case of post-buckling. The somewhat more limited (in comparison with the Ritz method) selection of admissible shape functions can easily be overcome by using the fundamental functions of lateral beam vibrations, which are known to satisfy most prescribed boundary conditions. The method is well suited for elastic stability analysis of rectangular,

isotropic or orthotropic plates. The latter can also approximate plates stiffened by many ribs. The procedure of finding the lowest load factor is basically similar to that described in calculating the fundamental circular frequency of free vibration. Although the application of Galerkin's method is straightforward, the evaluation of the required definite integrals can be laborious.

Other energy methods, such as the Lagrangian multiplier and the complimentary energy techniques, which are not treated in this book, might offer some advantages in special cases.

All energy methods are recommended for hand computation. Since in the majority of practical cases it is possible to obtain good accuracy the first term of the series expression for $w(x, y)$, preference should be given to Rayleigh's method. The results, if required, can be further improved by Stodola-Vianello's iterative technique. It should be noted that the critical loads obtained by energy methods are always somewhat higher than the exact solutions.

Although for elastic stability analysis of rectangular plates (plane or stiffened) extensive tables and charts are available for the designer, consideration of, for example, arbitrary contours, variable thicknesses and openings in the plate calls for more generally applicable numerical techniques. The ordinary FDMs, in combination with Stodola-Vianello's iteration, offer usable approaches to most of the elastic stability problems that cannot be solved analytically.

The finite element technique appears to be a flexible and powerful tool in the stability analysis of plates of arbitrary shape and boundary condition. An excellent convergence coupled with simple formulation can be achieved by gridwork cell representation of the elements. Since the problem is reduced to solution of classical eigenvalue-eigenvector problems, the lowest mode of buckling cannot be missed. Various investigators have extended the FEM for predicting the buckling behavior of plane and stiffened plates in the plastic range. This technique, like most of the numerical methods, requires, however, high-speed electronic computers of considerable storage capacity.

The investigation of postbuckling behavior of plates is inherently complex, since large deflections occur after buckling. Fortunately, a simplified method based on the effective width in buckling yields usable estimates.

Similarly, a semiempirical approach that modifies the results of the elastic buckling analyses by a *plasticity correction* factor gives information concerning the buckling loads of plates in the plastic region.

With suitable boundary conditions, flat plates can support in-plane loads that are considerably in excess of the critical loads predicted by classical buckling theory.

Problems[†]

- 16.2.1.** A simply supported square plate is subjected to uniformly distributed compressive in-plane loads $n_x = n_y = -\lambda n_{x0}$. Determine the critical load using the equilibrium method.
- 16.2.2.** Solve the above-given problem assuming that $n_x = -\lambda n_{x0}$, $n_y = -0.5n_{x0}$ and $n_{xy} = -0.2n_{x0}$ compressive in-plane forces are acting on the plate.

[†] The first two numbers refer to the corresponding section.

- 16.2.3.** A rectangular plate is simply supported at $x = 0$ and $x = a$ boundaries; the other two boundaries are fixed. Determine the lowest value of the elastic buckling load by applying the equilibrium method. Assume that the plate is subjected to uniformly distributed compressive in-plane forces at the simply supported edges.
- 16.3.1.** Solve problem 16.2.1 by Galerkin's energy method using a suitable shape function taken from Table 4.3.1.
- 16.3.2.** Solve problem 16.2.1 by Ritz's method.
- 16.3.3.** Investigate buckling of a clamped circular plate subjected to uniform radial trust using Rayleigh's method. Assume a $w = c(r_0^2 - r^2)^2$ function for the fundamental buckling mode.
- 16.3.4.** Determine the critical load of a simply supported rectangular plate subjected to uniform shear forces ($n_{xy} = n_{yx}$) by Galerkin's method. Use the following shape function:

$$w(x, y) = \sum_{m=1}^3 \sum_{n=1}^3 W_{mn} \sin \frac{m\pi x}{a} \sin \frac{n\pi y}{b}.$$

- 16.4.1.** Solve problem 16.2.3 using the ordinary FDM. Find also the buckling modes and corresponding critical loads pertinent to the second and third modes.
- 16.4.2.** Check the results of Illustrative Example I in Sec. 16.2. by the ordinary FDM.
- 16.4.3.** Determine the convergence characteristics of the finite difference solution in problem 16.4.2 by systematically reducing the mesh size.
- 16.4.4.** Find the critical load of a simply supported square plate subjected to concentrated compressive forces P acting at $y = b/2$. Use the ordinary FDM.
- 16.4.5.** Improve your solution of problem 16.4.4 by extrapolation and by the Stodola-Vianello technique.
- 16.5.1.** Find the critical load in problem 16.2.1 using the finite element approach based on gridwork cells.
- 16.5.2.** Check the solution of problem 16.4.4 by the FEM using gridwork cells.
- 16.7.1.** Design a stiffened rectangular steel plate subjected to buckling by permitting simultaneous loss of local and primary elastic stability at the same stress level.
- 16.8.1.** A square plate has three clamped edges while its fourth edge is free. This plate is subjected to uniformly distributed temperature load. The ambient temperature of the plate is T_0 , which is slowly increased to $T = T_0 + T_{in}$. Determine the temperature T_{cr} at which the plate will buckle.
- 16.9.1.** A moderately thick, simply supported rectangular plate is made of reinforced concrete. Its dimensions are $a = 6.5$ m, $b = 4.0$ m and $h = 0.7$ m. This plate is subjected to uniformly distributed, compressive, in-plane forces in its longitudinal direction. Determine the critical buckling load of the plate.
- 16.10.1.** Compare the various empirical formulas for "effective width" given in Sec. 16.10. Use a rectangular steel plate and draw your own conclusion.

Appendix A.1

Fourier Series

Perhaps the most influential of the French mathematicians in the 1820s was J. Fourier (Fig. A.1.1). His chief contribution to applied mathematics was the idea that any function $y = f(x)$ can be represented by a series in the form

$$y = \frac{1}{2}a_0 + a_1 \cos x + a_2 \cos 2x + \cdots + a_n \cos nx + \cdots \\ + b_1 \sin x + b_2 \sin 2x + \cdots + b_n \sin nx + \cdots, \quad (\text{A.1.1})$$

where

$$a_0 = \frac{1}{\pi} \int_{-\pi}^{\pi} f(x) dx, \quad a_n = \frac{1}{\pi} \int_{-\pi}^{\pi} f(x) \cos nx dx, \\ b_n = \frac{1}{\pi} \int_{-\pi}^{\pi} f(x) \sin nx dx. \quad (\text{A.1.2})$$

Such a series representation[†] of functions affords considerable generality. That is, even if there are many points at which the function is not continuous or at which the derivative of the function does not exist, the function can be expanded into a Fourier series. Consequently, the power of series expansion is greatly increased, since the terms of such a series can individually be handled without much difficulty. Thus, the Fourier series became an indispensable instrument in the analytical treatment of many problems of mathematical physics, such as the solution of partial differential equations in the theory of elasticity, vibrations, flow of heat, transmission of electricity and electromagnetic waves. The extension of the Fourier series leads to Fourier integrals and transforms. Although these methods are very powerful tools of higher analysis, they are not utilized here for the solution of plate problems in order to maintain the introductory level of this book. Many excellent texts, however, have been published on these subjects. Some of them are listed in Refs. [A.1.1–A.1.12], consultation of which is highly recommended for more advanced studies.

[†] The first use of such a series to solve certain problems connected with vibrating strings must, however, be attributed to D. Bernoulli.



Figure A.1.1 Joseph Fourier (1768–1830).

a. Single Fourier Series. As already mentioned, Fourier's theorem states that any arbitrary function $y = f(x)$ can be expressed by an infinite series consisting of sine and cosine terms. Thus the original function is replaced by the superposition of numerous sine and cosine waves.[†] If $f(x)$ is a *periodic function*,[‡] Fourier's theorem states that

$$f(x) = \frac{1}{2}A_0 + A_1 \cos \frac{2\pi x}{T} + A_2 \cos \frac{4\pi x}{T} + \cdots + A_n \cos \frac{2n\pi x}{T} + \cdots \\ + B_1 \sin \frac{2\pi x}{T} + B_2 \sin \frac{4\pi x}{T} + \cdots + B_n \sin \frac{2n\pi x}{T} + \cdots \quad (\text{A.1.3})$$

or, in more concise form,

$$f(x) = \frac{1}{2}A_0 + \sum_1^{\infty} A_n \cos n\omega x + \sum_1^{\infty} B_n \sin n\omega x, \quad (\text{A.1.4})$$

[†] Note that certain mathematical restrictions imposed upon the use of the Fourier series are of no consequence in this engineering application.

[‡] A function $f(x)$ is said to be periodic of period T if $f(x + T) = f(x)$, as shown in Fig. A.1.2.

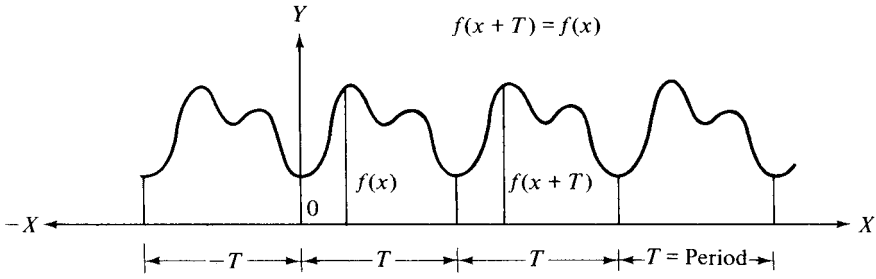


Figure A.1.2 Arbitrary periodic function.

where A_0 , A_n and B_n ($n = 1, 2, 3, \dots$) are the coefficients of the Fourier expansion, ω represents

$$\omega = \frac{2\pi}{T} \quad (\text{A.1.5})$$

and T is the period of the function (Fig. A.1.2).

Equation (A.1.4) is valid for any piecewise regular periodic function, which might also have discontinuities, and represents the arbitrary periodic function $f(x)$ in the full range from $x = -\infty$ to $x = +\infty$; thus it is called *full-range expansion*.

The coefficients A_0 , A_n and B_n are obtained from [A.1.1–A.1.3]

$$A_0 = \frac{2}{T} \int_0^T f(x) dx, \quad (\text{A.1.6})$$

$$A_n = \frac{2}{T} \int_0^T f(x) \cos n\omega x dx \quad (\text{A.1.7})$$

and

$$B_n = \frac{2}{T} \int_0^T f(x) \sin n\omega x dx \quad \text{for } n = 1, 2, 3, \dots \quad (\text{A.1.8})$$

When the function $f(x)$ is not given in analytical form or it is too complicated to perform the integrations prescribed, then the so-called harmonic analysis, which replaces the integrals by summations, can be advantageously utilized. Dividing the period T into $2m$ equal intervals (Fig. A.1.3), the Fourier coefficients are determined from

$$A_0 = \frac{1}{m} \sum_{k=0}^{2m-1} y_k, \quad (\text{A.1.9})$$

$$A_n = \frac{1}{m} \sum_{k=0}^{2m-1} y_k \cos \frac{kn\pi}{m} \quad (\text{A.1.10})$$

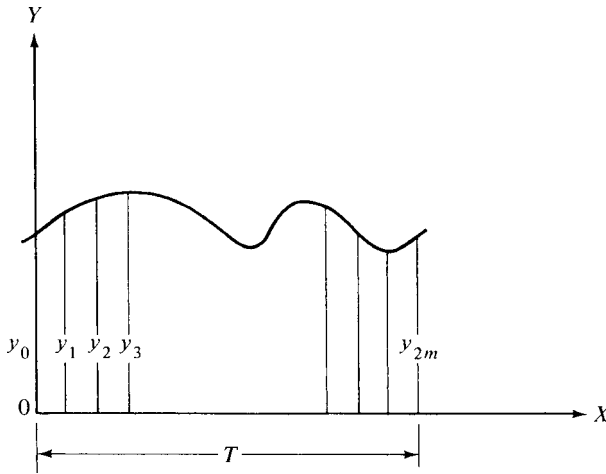


Figure A.1.3 Harmonic analysis.

and

$$B_n = \frac{1}{m} \sum_{k=0}^{2m-1} y_k \sin \frac{kn\pi}{m}$$

for $k = 0, 1, 2, \dots, 2m, n = 1, 2, 3, \dots, m$. (A.1.11)

Another approximate method for evaluating the constant of the Fourier expansion consists of plotting $f(x)$, $f(x) \cos(2n\pi x/T)$ and $f(x) \sin(2n\pi x/T)$ curves and determining the area of the respective curves by planimeter.

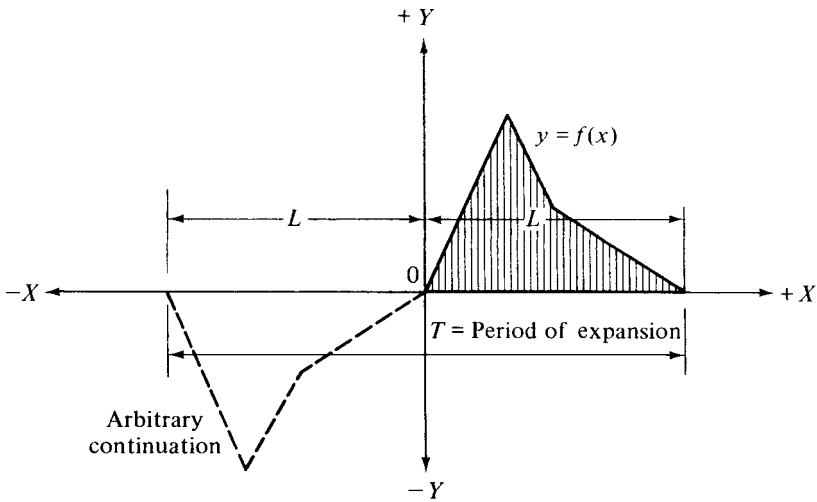
If the function is nonperiodic, it can be made periodic by arbitrary continuation of the function outside of its interval. This arbitrary continuation can be even harmonic, odd harmonic (Fig. A.1.4) or even and odd (Fig. A.1.5). Since in most cases we would like to represent the function $f(x)$ only over a certain length L , it is convenient to use *half-range expansion*, in which case the repetition interval $T = 2L$ with the center at the origin, as is shown in Fig. A.1.5.

Suppose that it is required to express the function $f(x)$ by cosine terms only. Let us make, by our arbitrary continuation, an even function in x of our originally nonperiodic function (Fig. A.1.5a), for which the

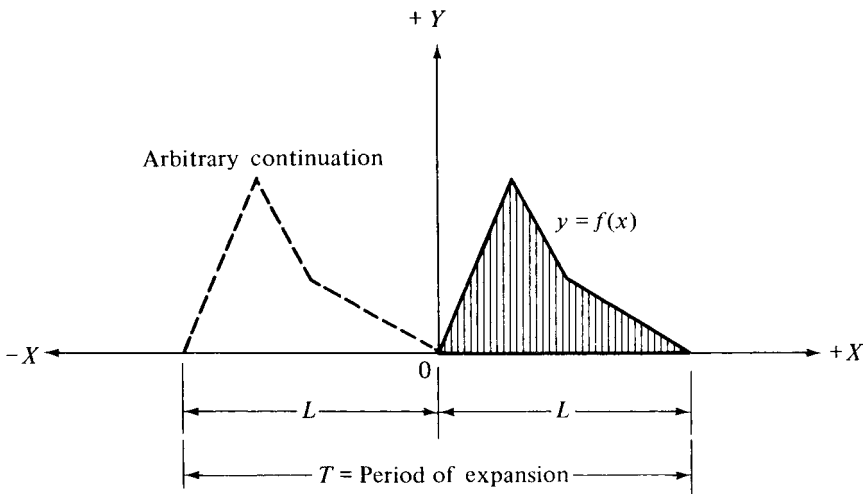
$$f(x) = f(-x) \tag{A.1.12}$$

relationship is valid; then the sine terms in Eq. (A.1.4) disappear during the integration. Similarly, making an odd function (Fig. A.1.5b) for which the

$$f(x) = -f(-x) \tag{A.1.13}$$



(a) Odd harmonic



(b) Even harmonic

Figure A.1.4 Even and odd harmonic functions.

relationship holds, the cosine terms disappear during the integration and we obtain a trigonometric series of sines by means of half-range Fourier series expansion. The latter, since it does not contain a constant A_0 [which is actually a cosine term according to Eqs. (A.1.6) and (A.1.7)] and can describe the geometrical boundary conditions of the simple support, can be used effectively in the solution of pertinent boundary value problems.

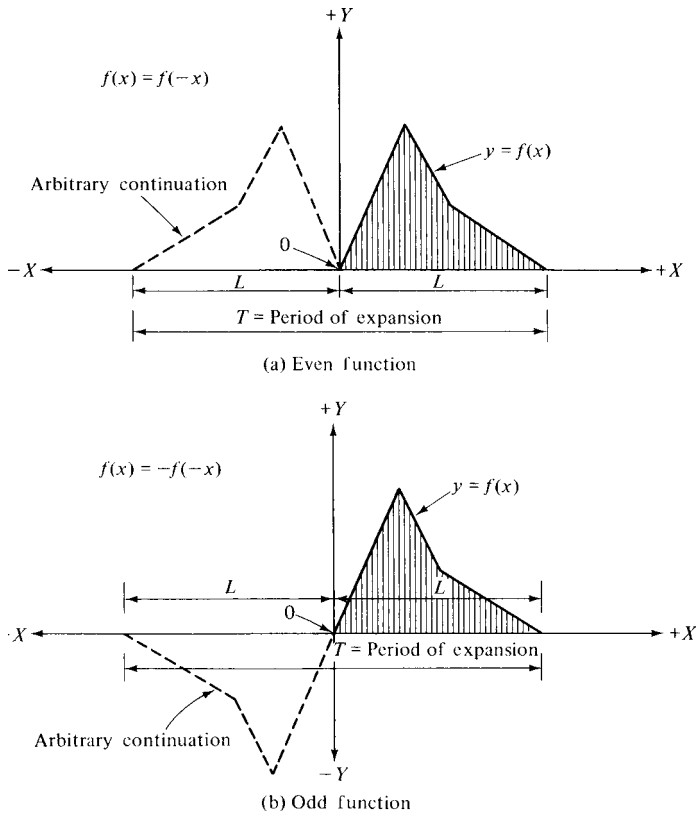


Figure A.1.5 Even and odd functions.

ILLUSTRATIVE EXAMPLE (Single Series Expansion)

Expand the function shown in Fig. A.1.6 into a Fourier series in three ways:

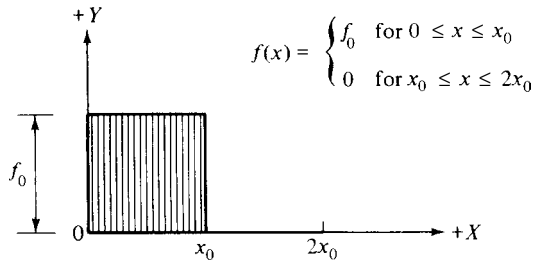


Figure A.1.6 Function to be expanded into Fourier series.

1. full-range expansion containing a constant and sine and cosine terms,
2. half-range expansion containing sine terms only and
3. half-range expansion containing cosine terms only.

(a) For a full-range expansion, the period of expansion is $T = 2x_0$. The constant term is obtained from Eq. (A.1.6):

$$A_0 = \frac{1}{x_0} \int_0^{2x_0} f(x) dx = f_0. \quad (\text{A.1.14})$$

Equation (A.1.7) yields

$$A_n = \frac{1}{x_0} \int_0^{2x_0} f(x) \cos \frac{n\pi x}{x_0} dx = 0 \quad \text{for } n = 1, 2, 3, \dots \quad (\text{A.1.15})$$

The coefficients of the sine terms are obtained from Eq. (A.1.8):

$$\begin{aligned} B_n &= \frac{1}{x_0} \int_0^{2x_0} f(x) \sin \frac{n\pi x}{x_0} dx \\ &= \frac{f_0}{x_0} \int_0^{x_0} \sin \frac{n\pi x}{x_0} dx + 0 = -\frac{f_0}{n\pi} (\cos n\pi - 1), \end{aligned} \quad (\text{A.1.16})$$

which gives

$$B_n = \begin{cases} \frac{2f_0}{n\pi} & \text{for } n = 1, 3, 5, \dots, \\ 0 & \text{for } n = 2, 4, 6, \dots \end{cases} \quad (\text{A.1.17})$$

Substituting these values into Eq. (A.1.4), the full-range Fourier series expansion of the function can be written as

$$f(x) = \frac{1}{2}f_0 + \frac{2f_0}{\pi} \left(\sin \frac{\pi x}{x_0} + \frac{1}{3} \sin \frac{3\pi x}{x_0} + \frac{1}{5} \sin \frac{5\pi x}{x_0} + \dots \right). \quad (\text{A.1.18})$$

The plot of the first three terms of Eq. (A.1.18) is shown in Fig. A.1.7a.

(b) Let us develop the same function (Fig. A.1.6) into a trigonometric series containing sine terms only. For this expansion the half-range expansion with period $T = 4x_0$ will be used. The function is arbitrarily continued beyond the origin so that an odd function is obtained (Fig. A.1.5b). Since the integrands $f(x)$ and $f(x) \cos n\omega x$ are each odd, Eqs. (A.1.6) and (A.1.7) yield $A_0 = A_n = 0$. But $f(x) \sin n\omega x = F(x)$ is even, and for even functions

$$\int_0^T F(x) dx = 2 \int_0^L F(x) dx, \quad (\text{A.1.19})$$

where $T = 2L$. Thus Eq. (A.1.8) becomes[†]

$$B_n = \frac{2}{L} \int_0^L f(x) \sin \frac{n\pi x}{L} dx. \quad (\text{A.1.20})$$

[†] See the footnote on p. 993.

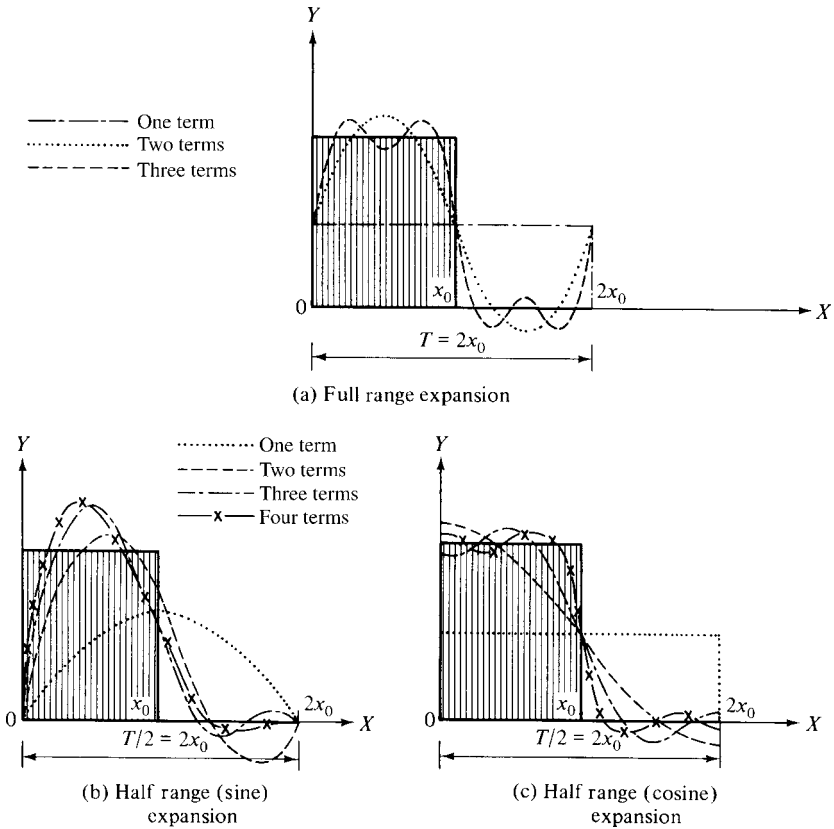


Figure A.1.7 Graphical representation of Fourier series expansions.

Substituting the specific values of our example into Eq. (A.1.20), we obtain

$$\begin{aligned}
 B_n &= \frac{2}{2x_0} \int_0^{2x_0} f(x) \sin \frac{n\pi x}{2x_0} dx = \frac{1}{x_0} \int_0^{x_0} f_0 \sin \frac{n\pi x}{2x_0} dx + 0 \\
 &= -\frac{f_0}{x_0} \left[\frac{2x_0}{n\pi} \cos \frac{n\pi x}{2x_0} \right]_0^{x_0} = -\frac{2f_0}{n\pi} \left(\cos \frac{n\pi}{2} - 1 \right), \quad (\text{A.1.21})
 \end{aligned}$$

which, for various value of n , yields

$$B_n = \begin{cases} \frac{2f_0}{n\pi} & \text{for } n = 1, 3, 5, \dots, \\ \frac{4f_0}{n\pi} & \text{for } n = 2, 6, 10, \dots, \\ 0 & \text{for } n = 4, 8, 12, \dots \end{cases} \quad (\text{A.1.22})$$

It follows from these values and from Eq. (A.1.4) that

$$\begin{aligned} f(x) &= \sum_1^{\infty} B_n \sin n\omega x \\ &= \frac{2f_0}{\pi} \left(\sin \frac{\pi x}{2x_0} + \sin \frac{\pi x}{x_0} + \frac{1}{3} \sin \frac{3\pi x}{2x_0} + \frac{1}{5} \sin \frac{5\pi x}{2x_0} + \dots \right). \end{aligned} \quad (\text{A.1.23})$$

The graphical representation of the summation of these various terms is shown in Fig. A.1.6b.

(c) Next, we expand the same function (Fig. A.1.6) into a trigonometric series containing cosine terms only. Again, a half-range expansion will be used with a period of $T = 2L = 4x_0$. In this case, however, we obtain an even function by arbitrary continuation beyond the origins, as shown in Fig. A.1.5a.

Now the integrands $f(x)$ and $f(x) \cos n\omega x$ in Eqs. (A.1.6) and (A.1.7) are even, while $f(x) \cdot \sin n\omega x$ in Eq. (A.1.8) is odd. Thus, we may conclude that $B_n = 0$, and from Eqs. (A.1.6) and (A.1.7), we obtain

$$A_0 = \frac{2}{L} \int_0^L f(x) dx \quad \text{and} \quad A_n = \frac{2}{L} \int_0^L f(x) \cos \frac{n\pi x}{L} dx.^\dagger \quad (\text{A.1.24})$$

Hence the Fourier expansion for any even function $f(x)$ of period $2L$ takes the form

$$f(x) = \frac{1}{2} A_0 + \sum_1^{\infty} A_n \cos \frac{n\pi x}{L}. \quad (\text{A.1.25})$$

Solving for the coefficients, we obtain

$$A_0 = \frac{f_0}{x_0} \int_0^{x_0} dx = \frac{f_0}{x_0} [x]_0^{x_0} = f_0 \quad (\text{A.1.26})$$

and

$$\begin{aligned} A_n &= \frac{1}{x_0} \int_0^{x_0} f_0 \cos \frac{n\pi x}{2x_0} dx + 0 = \frac{f_0}{x_0} \left[\frac{2x_0}{n\pi} \sin \frac{n\pi x}{2x_0} \right]_0^{x_0} \\ &= \frac{2f_0}{n\pi} \left(\sin \frac{n\pi}{2} - 0 \right), \end{aligned} \quad (\text{A.1.27})$$

which, for various values of n , becomes

$$A_n = \begin{cases} \frac{2f_0}{n\pi}, & \text{for } n = 1, 5, 9, \dots, \\ 0 & \text{for } n = 2, 4, 6, \dots, \\ -\frac{2f_0}{n\pi} & \text{for } n = 3, 7, 11, \dots \end{cases} \quad (\text{A.1.28})$$

[†] This equation can be expressed in terms of polar coordinates by substituting $x = \varphi$ and $L = \pi$.

The substitution of these values into Eq. (A.1.25) gives

$$f(x) = \frac{f_0}{2} + \frac{2f_0}{\pi} \left(\cos \frac{\pi x}{2x_0} - \frac{1}{3} \cos \frac{3\pi x}{2x_0} + \frac{1}{5} \cos \frac{5\pi x}{2x_0} + \dots \right). \quad (\text{A.1.29})$$

The summations of these various terms are plotted in Fig. A.1.7c.

b. Double Fourier Series. In the static and dynamic analysis of plates, a given function $f(x, y)$ is often expanded into the sine series of two variables x and y using the expression

$$f(x, y) = \sum_{m=1}^{\infty} \sum_{n=1}^{\infty} F_{mn} \sin \frac{m\pi x}{a} \sin \frac{n\pi y}{b}. \quad (\text{A.1.30})$$

Equation (A.1.30) represents a half-range sine expansion in x multiplied by a half-range sine expansion in y using for the period of expansion $T = 2a$ and $T = 2b$, respectively. To obtain the coefficient F_{mn} , we first multiply Eq. (A.1.30) by $\sin(k\pi y/b) dy$ and then integrate between the limits zero and b . Thus, we can write

$$\int_0^b f(x, y) \sin \frac{k\pi y}{b} dy = \sum_{m=1}^{\infty} \sum_{n=1}^{\infty} F_{mn} \sin \frac{m\pi x}{a} \int_0^b \sin \frac{n\pi y}{b} \sin \frac{k\pi y}{b} dy. \quad (\text{A.1.31})$$

If $n \neq k$, then

$$\int_0^b \sin \frac{n\pi y}{b} \sin \frac{k\pi y}{b} dy = 0. \quad (\text{A.1.32})$$

If $n = k$, then

$$\int_0^b \sin^2 \frac{n\pi y}{b} dy = \frac{b}{2}. \quad (\text{A.1.33})$$

Utilizing a similar approach for the variable x , we obtain

$$\int_0^a \sin^2 \frac{m\pi x}{a} dx = \frac{a}{2}. \quad (\text{A.1.34})$$

Thus Eq. (A.1.30) becomes

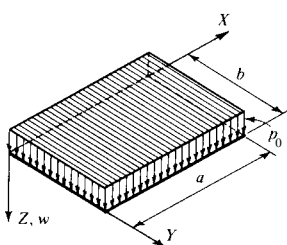
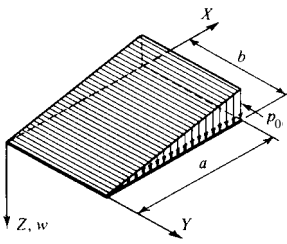
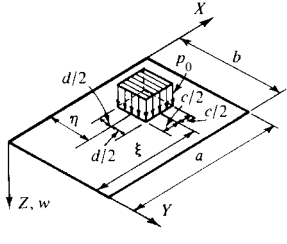
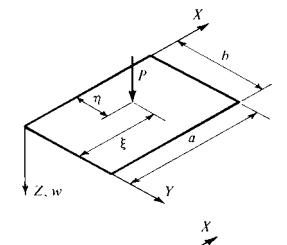
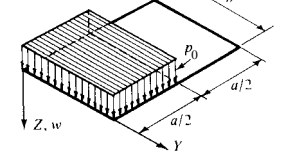
$$F_{mn} \frac{a}{2} \frac{b}{2} = \int_0^a \int_0^b f(x, y) \sin \frac{m\pi x}{a} \sin \frac{n\pi y}{b} dx dy. \quad (\text{A.1.35})$$

Hence the coefficient of the double Fourier expansion is

$$F_{mn} = \frac{4}{ab} \int_0^a \int_0^b f(x, y) \sin \frac{m\pi x}{a} \sin \frac{n\pi y}{b} dx dy. \quad (\text{A.1.36})$$

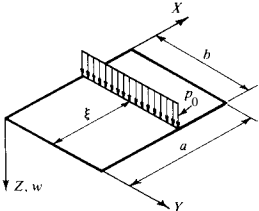
In Table A.1.1 the reader will find double Fourier expansions of the most important loads, which can be directly used in Navier-type solutions of the pertinent plate problems.

Table A.1.1 Double Trigonometric Series Expansion of Loads

Load Number	Load $p_z(x, y) = \sum_m \sum_n P_{mn} \sin \frac{m\pi x}{a} \sin \frac{n\pi y}{b}$	Expansion Coefficients P_{mn} [Determined from (Eq. A.1.36)]	Notes
1		$P_{mn} = \frac{16p_0}{\pi^2 mn}$ for $m, n = 1, 3, 5, \dots$	Eq. (A.1.37)
2		$P_{mn} = -\frac{8p_0 \cos m\pi}{\pi^2 mn}$ for $m, n = 1, 2, 3, \dots$	Eq. (2.2.19)
3		$P_{mn} = \frac{16p_0}{\pi^2 mn} \sin \frac{m\pi \xi}{a} \sin \frac{n\pi \eta}{b}$ $\times \sin \frac{m\pi c}{2a} \sin \frac{n\pi d}{2b}$ for $m, n = 1, 2, 3, \dots$	Eq. (2.4.30)
4		$P_{mn} = \frac{4P}{ab} \sin \frac{m\pi \xi}{a} \sin \frac{n\pi \eta}{b}$ for $m, n = 1, 2, 3, \dots$	Eq. (2.4.37)
5		$P_{mn} = \begin{cases} \frac{8p_0}{\pi^2 mn} & \text{for } m, n = 1, 3, 5, \dots \\ \frac{16p_0}{\pi^2 mn} & \text{for } \begin{cases} m = 2, 6, 10, \dots \\ n = 1, 3, 5, \dots \end{cases} \end{cases}$	

(continued overleaf)

Table A.1.1 (continued)

Load Number	Load	Expansion Coefficients P_{mn} [Determined from (Eq. A.1.36)]	Notes
	$p_z(x, y) = \sum_m \sum_n \frac{m\pi x}{a} \sin \frac{n\pi y}{b}$		
6		$P_{mn} = \frac{8p_0}{\pi an} \sin \frac{m\pi \xi}{a}$ for $\begin{cases} m = 1, 2, 3, \dots \\ n = 1, 3, 5, \dots \end{cases}$	

The latest development concerning the Fourier series is the introduction of the so-called *fast Fourier transforms* (FFT) by Cooley and Tukey [A.1.15]. This new numerical algorithm, based on the *complex* form of the Fourier series, is especially efficient for determination of the dynamic response of structures in the frequency domain. A considerable reduction in computer time (Fig. A.1.8.) is achieved by breaking down the computation of discrete Fourier transform coefficients into two parts and introducing a new way of evaluating the equations obtained. By realizing that a sequence of n elements may be divided into two shorter sequences of $n/2$ elements each by placing the even-numbered elements into the first sequence and the odd-numbered ones into the second [A.1.16], the required computer time is drastically reduced.

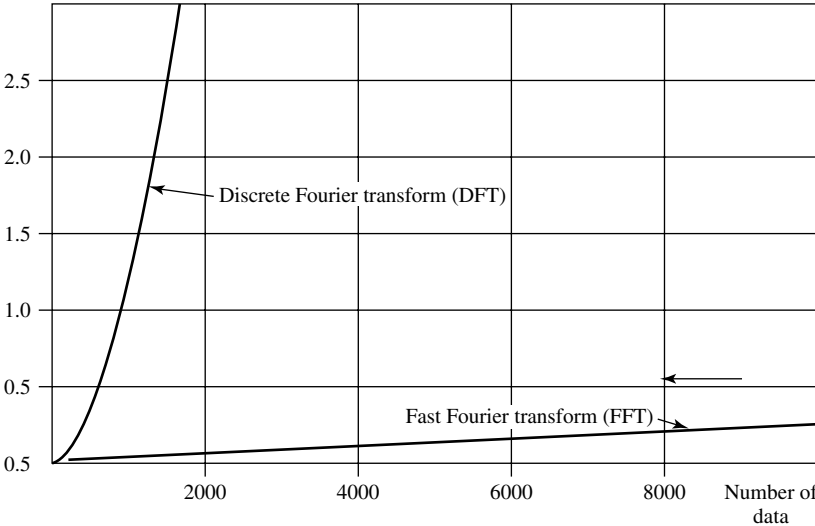


Figure A.1.8 Approximate time requirements for DFT and FFT procedures.

Readily usable computer programs for FFT are available in Refs. [A.1.17–A.1.21]. The user of these programs, however, must consider that the definition for the FFT is in many instances different from the one used in this section. In such a case, the factors and the signs of the exponents must be changed accordingly.

Summary. Expansion of a function into single or double Fourier series is an important mathematical tool. Calculation of the required coefficients, however, can be quite laborious. To facilitate the analytical evaluation of the required definite integrals, one may use integral formulas given in Refs. [A.1.13] and [A.1.14]. Nowadays, computer programs using “symbolic mathematics” can perform this tedious task quite easily [A.1.17–A.1.21]. Some programs even offer complete Fourier sine or cosine transformations of analytically given functions. If the function is not given in analytical form, discrete Fourier transform (DFT) can be performed [A.1.18].

ILLUSTRATIVE EXAMPLE [†] (Double Trigonometric Series Expansion)

Let us expand into a function that is constant over the whole area double Fourier series, bounded by $x = 0$, $x = a$ and $y = 0$, $y = b$ in a rectangular Cartesian coordinate system.

Thus the expression of the function is $f(x, y) = f_0$; then from Eq. (A.1.36) the coefficients of expansion can be calculated:

$$\begin{aligned} F_{mn} &= \frac{4f_0}{ab} \int_0^a \sin \frac{m\pi x}{a} dx \int_0^b \sin \frac{n\pi y}{b} dy \\ &= \frac{4f_0}{ab} \frac{a}{m\pi} \left[-\cos \frac{m\pi x}{a} \right]_0^a \cdot \frac{b}{n\pi} \left[-\cos \frac{n\pi y}{b} \right]_0^b \\ &= \begin{cases} \frac{16f_0}{\pi^2 mn} & \text{for odd } m, n, \\ 0 & \text{otherwise.} \end{cases} \end{aligned} \quad (\text{A.1.37})$$

Substituting Eq. (A.1.37) into Eq. (A.1.30), we obtain

$$\begin{aligned} f(x, y) &= \frac{16f_0}{\pi^2} \sum_m \sum_n \frac{1}{mn} \sin \frac{m\pi x}{a} \sin \frac{n\pi y}{b} \\ &\quad \text{for } m, n = 1, 3, 5, \dots \end{aligned} \quad (\text{A.1.37})$$

References and Bibliography

- [A.1.1] FRANKLIN, P., *An Introduction to Fourier Methods and Laplace Transformation*, Dover Publications, New York, 1958.
- [A.1.2] CHURCHILL, R. V., *Fourier Series and Boundary Value Problems*, McGraw-Hill Book Co., New York, 1941.

[†] For further examples, see Secs. 2.2 and 2.4.

- [A.1.3] WOLFF, J., *Fourier'sche Reihen mit Aufgaben*, P. Noordhoff N. V., Groningen, Netherlands, 1931.
- [A.1.4] CHISHOLM, J. S. R., and MORRIS, R. M., *Mathematical Methods in Physics*, North-Holland Publishing Co., Amsterdam, 1964.
- [A.1.5] WYLIE, C. R., *Advanced Engineering Mathematics*, McGraw-Hill Book Co., New York, 1960.
- [A.1.6] MILLER, F. H., and REDDICK, H. W., *Advanced Mathematics for Engineers*, John Wiley & Sons, New York, 1960.
- [A.1.7] JOOS, G., and KALUZA, TH., *Höhere Mathematik für den Praktiker*, 8th ed. Johann Ambrosius Barth, Leipzig, 1956.
- [A.1.8] ZURMÜHL, R., *Praktische Mathematik für Ingenieure und Physiker*, 5th ed., Springer-Verlag, Berlin, 1965.
- [A.1.9] KANTOROVICH, L. V., and KRYLOV, V. I., *Approximate Methods of Higher Analysis*, John Wiley & Sons (Interscience Division), New York, 1958.
- [A.1.10] DEBNATH, L., *Integral Transforms and Their Applications*, CRC Press, Boca Raton, Florida, 1995.
- [A.1.11] BRACEWELL, R., *The Fourier Transform and Its Applications*, McGraw-Hill Book Co, New York, 1986.
- [A.1.12] GARCIA-GUERVA, J., et al. (Eds.), *Fourier Analysis and Partial Differential Equations*, CRC Press, Boca Raton, Florida, 1995.
- [A.1.13] BRONSTEIN, I., and SEMENDJAJEW, K., *Taschenbuch der Mathematik*, 7th ed., Teubner Verlagsgesellschaft, Leipzig, 1960.
- [A.1.14] GRÖBNER, W., and HOFREITER, N., *Integral Tafel*, 3rd ed., Springer-Verlag, Vienna, 1961.
- [A.1.15] COOLY, P. M., and TUKEY, J. W., "An Algorithm for the Machine Computation of Complex Fourier Series", *Math. Comput.*, 19 (1965), 297–301.
- [A.1.16] RAMIREZ, R. W., *The FFT: Fundamentals and Concepts*, Prentice-Hall, Englewood Cliffs, New Jersey, 1985.
- [A.1.17] PRESS, W. H., et al., *Numerical Recipes in FORTRAN: The Art of Scientific Computing*, 2nd ed., Cambridge University Press, Cambridge, Massachusetts, 1992.
- [A.1.18] SOFTWAREHOUSE, *DERIVE a Mathematical Assistant for Your Personal Computer*, Version 3, Honolulu, Hawaii, 1995.
- [A.1.19] MATHSOFT, *Mathcad, vs. 6*, Cambridge, Massachusetts, 1995.
- [A.1.20] MAPLESOFTWARE, Release 4, Waterloo, Ontario, Canada, 1996.
- [A.1.21] WOLFRAM RESEARCH, *Mathematica*, Version 2.0, Champaign, Illinois, 1992.
- [A.1.22] THE MATHWORKS, INC., *Mathlab*, Natick, Massachusetts, 1998.
- [A.1.23] HOWELL, K., *Principles of Fourier Analysis*, CRC Press, Boca Raton, Florida, 2001.
- [A.1.24] WALKER, J. S., *Fast Fourier Transforms*, 2nd ed., CRC Press, Boca Raton, Florida, 1996.

Appendix A.2

Conversion from One Poisson Ratio to Another

If the deflections or the internal forces of a plate are known for a Poisson ratio ν_1 , then these values can easily be calculated for ν_2 .

The conversion formula for deflections is

$$w_2 = w_1 \frac{D_1}{D_2} = w_1 \frac{1 - \nu_2^2}{1 - \nu_1^2}, \quad (\text{A.2.1})$$

provided that the Poisson ratio does not appear in the boundary conditions.

Similarly, if the bending and torsional moments are known for ν_1 , then these internal forces can also be calculated for ν_2 by using the following expressions:

$$\begin{aligned} m_{x2} &= \frac{1}{1 - \nu_1^2} [(1 - \nu_1 \nu_2) m_{x1} + (\nu_2 - \nu_1) m_{y1}], \\ m_{y2} &= \frac{1}{1 - \nu_1^2} [(1 - \nu_1 \nu_2) m_{y1} + (\nu_2 - \nu_1) m_{x1}], \\ m_{xy2} &= \frac{1 - \nu_2}{1 - \nu_1} m_{xy1}. \end{aligned} \quad (\text{A.2.2})$$

The shear forces are independent from ν ; consequently,

$$q_{x2} = q_{x1} \quad \text{and} \quad q_{y2} = q_{y1}. \quad (\text{A.2.3})$$

If $\nu_1 = 0$, we can write Eq. (A.2.2) in a simplified form:

$$\begin{aligned} m_{x2} &= m_{x1} + \nu_2 m_{y1}, \\ m_{y2} &= m_{y1} + \nu_2 m_{x1}, \\ m_{xy2} &= (1 - \nu_2) m_{xy1}. \end{aligned} \quad (\text{A.2.4})$$

Formulas for the conversion of the edge forces are

$$\begin{aligned} v_x &= q_{x2} + \frac{1 - \nu_2}{1 - \nu_1} \cdot \frac{\partial}{\partial y} m_{xy1}, \\ v_y &= q_{y2} + \frac{1 - \nu_2}{1 - \nu_1} \cdot \frac{\partial}{\partial x} m_{xy1}. \end{aligned} \tag{A.2.5}$$

Again, for the special case of $\nu_1 = 0$, we can write

$$\begin{aligned} v_{x2} &= q_{x2} + (1 - \nu_2) \cdot \frac{\partial}{\partial y} m_{xy1}, \\ v_{y2} &= q_{y2} + (1 - \nu_2) \cdot \frac{\partial}{\partial x} m_{xy1}. \end{aligned} \tag{A.2.6}$$

These expressions can also be used to estimate the error caused by neglecting Poisson's ratio. Since the deflections are inversely proportional to the plate stiffness D , consequently, the error created by using $\nu = 0$ is approximately 2% for reinforced-concrete slabs with ν values of 0.15–0.2. This can of course be neglected. Considerably larger discrepancies (10–15%), however, are created by assuming $\nu = 0$ for the bending and torsional moments. As Eq. (A.2.3) shows, the shear forces are independent from Poisson's ratio.

Appendix A.3

Units

In the numerical examples, the new SI[†] metric units and symbols have been used. Accordingly, the basic units of length and mass are the meter (m) and kilogram (kg), respectively. The basic unit for time is the second (s) and that for temperature is the kelvin(K). Wide use is also made of degrees celsius (°C). Derived units are formed by combining basic units. Consequently, the unit of force is Newton ($N = \text{kg} \cdot \text{m}/\text{s}^2$), representing the force required to accelerate a 1-kg mass over one meter per second squared. Other derived units in structural engineering are the hertz ($\text{Hz} = \text{cycles}/\text{s}$) for frequency and the pascal ($\text{Pa} = \text{N}/\text{m}^2$) for pressure and stress, respectively. Energy and work are measured in joules ($\text{J} = \text{N} \cdot \text{m}$). The SI unit for velocity is meters per second (m/s), and that for angular velocity is radians per second (rad/s). In order to avoid very large or very small numbers in the computations, multiples and submultiples of the base units are often employed. The most used multiple of the SI units in structural engineering is kilo ($k = 10^3$), while centi ($c = 10^{-2}$) and milli ($m = 10^{-3}$) represent frequently utilized submultiples. Table A.3.1 lists the pertinent prefixes.

Useful conversion factors from U.S. Customary System (USCS) to SI units are provided in Table A.3.2. Conversions for the SI units are given in Table A.3.3.

Table A.3.1 SI Unit Prefixes

<i>Prefix</i>	<i>Symbol</i>	<i>Factor</i>
tera	T	10^{12}
giga	G	10^9
mega	M	10^6
kilo	k	10^3
hecto	h	10^2
deka	da	10^1
deci	d	10^{-1}
centi	c	10^{-2}
milli	m	10^{-3}
micro	μ	10^{-6}
nano	n	10^{-9}

[†] International System of Units (the modernized metric system), *Système International d'Unités*.

Table A.3.2 Conversion Factors from USCS to SI Units

<i>To Obtain</i>	<i>Multiply</i>	<i>By the Factor</i>
Millimeters	Inches	25.4
Millimeters	Feet	304.8
Centimeters	Inches	2.54
Centimeters	Feet	30.48
Centimeters	Yards	91.44
Meters	Inches	0.0254
Meters	Feet	0.3048
Meters	Yards	0.9144
Square millimeters	Square inches	645.16
Square millimeters	Square feet	92903.04
Square centimeters	Square inches	6.4516
Square centimeters	Square feet	929.0304
Square meters	Square feet	0.092903
Square meters	Square yards	0.836127
Kilograms	Pounds	0.453592
Kilograms	Short tons	907.1847
Kilograms	Long tons	1016.047
kg/cm ²	lb/in. ²	0.070307
kg/cm ²	lb/ft ²	4.8824 × 10 ⁻⁴
N/m ²	lb/in. ²	6894.757
N/m ²	lb/ft ²	47.88026
m kg	Foot pounds	0.138255
m/s	ft/s	0.3048
m/s	ft/min	0.00508

Table A.3.3 Conversion Factors in SI System

A. Forces

	N	kN	MN
1 N	= 1	10 ⁻³	10 ⁻⁶
1 kN	= 10 ³	1	10 ⁻³
1 MN	= 10 ⁶	10 ³	1
1 kp	= 10	10 ⁻²	10 ⁻⁵
1 Mp	= 10 ⁴	10	10 ⁻²
N	newton		
kN	kilonewton		
MN	meganeutron		
kp	kilopond		
Mp	megapond		

B. Pressure or Surface Loads

	N/mm ²	N/cm ²	kN/mm ²	kN/cm ²	kN/m ²	MN/cm ²	MN/m ²
1 N/mm ²	= 1	10 ²	10 ⁻³	10 ⁻¹	10 ³	10 ⁻⁴	1
1 N/cm ²	= 10 ⁻²	1	10 ⁻⁵	10 ⁻³	10	10 ⁻⁶	10 ⁻²
1 kN/mm ²	= 10 ³	10 ⁵	1	10 ²	10 ⁶	10 ⁻¹	10 ³
1 kN/cm ²	= 10	10 ³	10 ⁻²	1	10 ⁴	10 ⁻³	10
1 kN/m ²	= 10 ⁻³	10 ⁻¹	10 ⁻⁶	10 ⁻⁴	1	10 ⁻⁷	10 ⁻³
1 MN/cm ²	= 10 ⁴	10 ⁶	10	10 ³	10 ⁷	1	10 ⁴
1 MN/m ²	= 1	10 ²	10 ⁻³	10 ⁻¹	10 ³	10 ⁻⁴	1

Appendix A.4

About the CD

A.4.1 Plate Formulas

Although the present trend in engineering is to use computers and pertinent software to obtain numerical solutions of various plate problems, readily usable plate formulas still do have their place in modern-day engineering practice. That is, there are some instances when the engineer may need them. These are, for example, (a) to obtain quick results of a specific problem that cannot be handled by the engineer's software; (b) when neither a computer nor software is readily available; (c) when the reader of this book wants to test the accuracy and convergence characteristics of his or her commercially available program system by using more exact analytical solutions and (d) when formulas can provide quicker solutions than computers. A carefully selected collection of plate formulas can therefore be an asset to engineers who frequently deal with various plate problems in everyday practice.

For this reason, 170 plate formulas are included on the accompanying CD-ROM in PDF format. These include static and dynamic solutions of circular, rectangular, triangular, trapezoidal and continuous plates with various boundary conditions subjected to diverse lateral loads in the elastic range. To cover also the plastic region, yield lines and ultimate moments of such plates are also listed. In addition, circular frequencies of numerous rectangular and circular plates are given in explicit forms. Finally, elastic stability of rectangular and stiffened plates are also briefly treated.

The PDF is organized into 15 tables describing the various formulas. A sample of such a table is shown in Fig. A.4.1. Using these tables, the reader can quickly select the plate problem of special interest. Then, clicking on the selected file number, one readily obtains the desired plate formula. Selecting files numbers 163–164 from Table 15 shown in Fig. A.4.1, for instance results in Fig. A.4.2. If for some computers this convenient *hyperlink* does not work, one can also scroll directly to the desired formula. Although the so-obtained screen pictures fill the full screen, the possibility also exists to further enlarge a specified part of them.

<i>File Number</i>	<i>Case Number</i>	<i>Geometrical Shape</i>	<i>In-Plane Loading</i>	<i>Boundary Conditions</i>
158	158	Rectangular	Uniformly distributed compressive forces in X direction	Simply supported or free
159–160	159	Do	Uniformly distributed compressive forces in X and Y directions	Simply supported
Do	160	Rectangular and orthotropic	Triangular compressive and tensile forces in X direction; maximum at $b = 0$, b , zero at $b/2$	Do
161	161	Rectangular	Concentrated force acting at $a/2$ center of edges $b = 0$, b	All edges simply supported or clamped; two opposite edges simply supported or clamped
162	162	Do	In-plane shear forces acting along edges	Simply supported or clamped; two opposite edges simply supported others clamped
163–164	163	Rectangular with stiffener at $b/2$	Linearly varying compressive forces in X direction	All edges simply supported
Do	164	Do	Triangular compressive and tensile forces in X direction; maximum at $b/2$, zero at center	Do
165–166	165	Rectangular with stiffener at arbitrary distance y	Do	Do
Do	166	Rectangular with stiffener at $b/2$	In-plane shear forces acting along edges	Do
167–168	167	Rectangular with stiffener at $a/2$	Linearly varying compression forces in X direction	Do
Do	168	Do	Triangular compressive and tensile forces in X direction, maximum at $b = 0$, b zero at $b/2$	Do
169–170	169	Do	In-plane shear forces acting along edges	Do
Do	170	Multiple panels with vertical stiffeners	Do	Do

Figure A.4.1 Table 15 in file *Plate Formulas*.

A.4.2 WinPlatePrimer Program System

a. General Description. Along with the Plate Formulas, the CD-ROM accompanying this book also contains the WinPlatePrimer (WPP) program system for static and dynamic analysis of plates. Since this system is considerably interactive, all its programs are very user friendly. The WPP is based on the widely used *finite element* analysis technique and is capable of handling even moderately sized plate problems encountered in everyday engineering practice. Because the versatile FEM was employed, this program system can treat a wide variety of boundary and loading

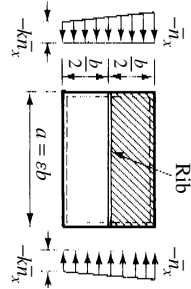
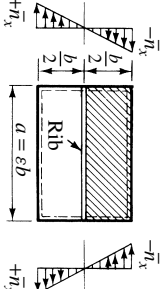
Case Number	Structural System and In-Plane Loading	Required Minimum Stiffness Ratios for Sturdy Ribs	Notation	Source	Notes
163		<p>If $\epsilon < \sqrt{8(1 + 2\delta) - 1}$:</p> $\gamma_{\min} = (0.53 + 0.47k) \left\{ \frac{\epsilon^2}{2} [16(1 + 2\delta) - 2] - \frac{\epsilon^4}{2} + \frac{1 + 2\delta}{2} \right\}$ <p>If $\epsilon > \sqrt{8(1 + 2\delta) - 1}$:</p> $\gamma_{\min} = (0.53 + 0.47k) \left\{ \frac{1}{2} [8(1 + 2\delta) - 1]^2 + \frac{1 + 2\delta}{2} \right\}$ $\gamma^* = 3\gamma_{\min}$	$\epsilon = \frac{a}{b}$ $\delta = \frac{A}{bh}$ and $\gamma = \frac{EI}{bD}$ where A = cross-sectional area of ribs, I = moment of inertia of ribs with respect to middle surface of plate. γ^* = stiffness ratio for very sturdy ribs, see notes.	[A3], [A19], and [A32]	If $\gamma > \gamma_{\min}$, calculate critical load of shaded panel, assuming simple supports. If $\gamma < \gamma_{\min}$, use corresponding orthotropic plate cases. Ribs are symmetrical with respect to middle surface of plate. To prevent deformation of ribs even during failure, use $\gamma^* = C\gamma_{\min}$.
164		$\gamma_{\min} = 1.3$ $\gamma^* = 3.9$			

Figure A.4.2 Formulas 163–164.

conditions, as described in Chapters 6 and 7. To be consistent with these chapters, the same notation and sign conventions employed there have also been used in these programs. For rectangular plate elements the higher-order element with 16 DOF, as described in Sec. 7.7.1, was selected, whereas for triangular finite elements the DKT element, as described in Sec. 7.7.2, was used. Both these elements have from very good to excellent convergence characteristics, as documented in Chapters 6 and 7. Thus, even with a relatively crude subdivision of the plate continuum, good results can be obtained. Although use of the modernized metric system (SI) is recommended, the customary U.S. units can also be employed. However, care must be taken that all inputs use *consistent* units. For example, if the centimeter (cm) and newton (N) are selected as primary units, the corresponding input for the modulus of elasticity E must be in newtons per centimeter squared. Accordingly, the lateral dimensions will be computed in centimeters and the nodal forces and internal stress components will also carry the pertinent units.

In addition to the readily applicable EXE files, which can be run by simply clicking on the WPP icons located on the corresponding WPP folders, FORTRAN source codes are also listed on the CD-ROM. These codes serve a dual purpose. First, they can teach the reader how to write a finite element program system. The large number of “comment lines” makes these FORTRAN codes very readable for the user. Second, they can serve as a *basis* if the engineer must develop programs to suit some specific need, and such programs are not covered in the commercially available program systems. Both the static and dynamic parts have a detailed and illustrated User’s Guide leading the engineer step by step in the application of these programs.

Although nowadays the finite element meshes are usually generated by computer, with the exception of simple routines, such mesh generators, according to the author’s opinion, cannot successfully take over this complex task. As discussed in detail in Sec. 7.12, modeling of a fine element plate analysis cannot be effectively automated in the foreseeable future. Consequently, in this case, the manual design of suitable finite element meshes represents an important part of the FEM of plates, which will affect the accuracy of the results. That is, a badly designed mesh may lead to inaccurate results. The mesh design will be influenced by the following factors:

- shape of the boundary,
- prescribed boundary conditions,
- zones of rapid variation of external forces,
- locations of expected stress concentrations, and
- locations of openings in the plate continuum.

Thus, it is recommended that the engineer first prepare a drawing (preferably to scale) using pencil and paper. Then, he or she should follow the rules discussed in Sec. 6.4.2 to create a suitable finite element mesh and to number the created finite elements accordingly. It should be noted, however, that a combination of triangular elements with rectangular ones is not permitted in this program system. In numbering the nodal points, one should go clockwise in the pertinent finite elements starting at the left-hand side of the horizontal X or Y axis of the global reference system XYZ , where Z is always pointing downward. One common mistake made by novices to the

FEM is to design meshes that are not properly connected. Fortunately, the interactive nature of the WPP program system will notice such mistakes and ask for correction. That is, during the *preprocessing* phase, after “new” is selected from the file menu, the mesh and the nodal and element numberings subsequently appear at the right-hand side of the computer screen and grow along with the input of the geometry as the input table on the left-hand side is filled in. However, it should be noted that *all* small rectangular cells in the input table must be filled in; otherwise the user cannot continue with the input procedures. Consequently, when no data are present, a zero (0) should be used as a substitute input. When the input procedure is completed, the geometrical configuration of the plate along with the given loadings and prescribed boundary condition are graphically presented on the right-hand side of the screen.

After completion of the input, the *analysis* part can be activated by clicking on the SAVE AND COMPUTE command located in the menu bar at the top of the screen. Depending on the size of the problem and the random-access memory (RAM) and clock speed of the computer, it takes usually only a few seconds to complete the entire plate analysis. Of course, in the case of larger plate problems, this process may take minutes.

The *postprocessing* part of the analysis can be started by subsequently clicking on the DEFLECTION, NODAL INTERNAL FORCES and STRESS AT THE CENTER OF ELEMENT commands located under the menu bar. In this way, the user obtains not only the computed numerical data but also the pertinent two-dimensional presentations of these results with contour lines (regions) in color, as subsequently discussed and illustrated in more detail. The input and output data are saved as text files with the extensions .dat and .out after the corresponding filenames. These input and output files can be printed with any text program such as MS Word or WordPad, for instance.

b. Static Module. Since the static module of the WPP program system cannot be run directly from the CD-ROM, it is required that the user create a folder (say WPP-S) on the hard disk of the computer and subsequently copy the files Solved Problems, Source Codes, User's Guide and WPP into this folder. Before trying to run the WPP programs, it is strongly recommended that the *User's Guide* be printed. This file contains information on the hardware and software requirements for the static module of WPP, along with detailed and well-illustrated step-by-step instructions concerning application of this program. Similarly, it is also useful to print out the table of Solved Problems given in the corresponding file. That is, the learning process of how to use the static part of WPP can be significantly shortened by starting with the application of one of these solved problems. This table contains 16 solved plate problems. The pertinent plate geometries are represented graphically along with the loading and boundary conditions of the plates. Furthermore, the obtained maximum lateral deflections are compared with their analytically calculated counterparts. When such analytical results do not exist, numerical values of w_{\max} are checked against computer results obtained from one of the commercially available program systems, such as ANSYS. In all cases good agreements were achieved.

The static module of the WPP program system can be activated by clicking on the WinPlatePrimer icon in the WPP folder. As already mentioned above, when using the program for the first time, it is recommended to start by practicing with one of the test problems listed in the Solved Problems file. Although the User's Guide gives step-by-step information on how to deal with such solved problems, we intend to summarize

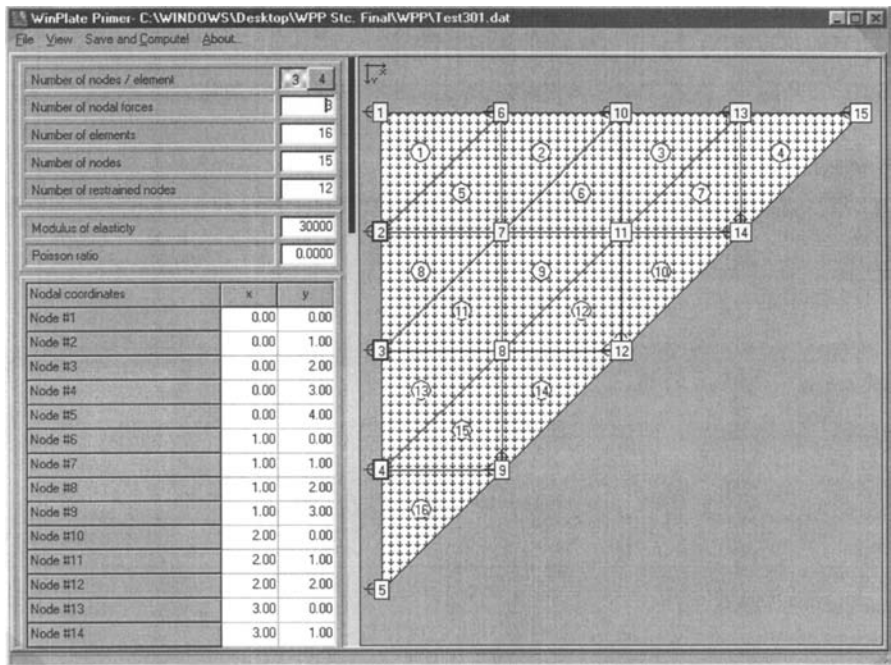


Figure A.4.3 Input and finite element discretization of triangular plate.

here only the highlights of the required procedure. In the File menu we select the OPEN command and click on one of the test problems appearing on the right-hand side of the screen. Let us assume that we selected Test301; then Fig. A.4.3 appears. The left-hand side of this picture contains the already filled-in input table, while the right-hand side shows in two-dimensional form the geometrical configuration of the plate in question along with its boundary and loading conditions. Next, SAVE AND COMPUTE in the menu bar is activated. In this case, the analysis of this plate problem takes only a few seconds. To obtain the computed results, we click first on the DIS-PLACEMENT button. Then, the numerical values of all nodal displacements appear in table form on the left-hand side of the screen. Simultaneously, a two-dimensional color presentation of the lateral nodal deflections is shown by means of corresponding contour lines and regions (Fig. A.4.4). A similar approach is taken for the internal nodal forces (Fig. A.4.5) and for stresses at the center of the finite elements.

After the engineer has already become familiar with the introductory procedure, he or she is ready to solve a new plate problem. In this respect, we refer again to the User's Guide for detailed step-by-step instructions. It is recommended that, at the first trial, the user selects a plate problem with known analytic solution for checking purposes. The folder PLATE FORMULAS contains a large number of such analytical solutions covering various plate problems for easy selection. However, before the program can be applied, manual creation of a suitable finite element mesh is required, as described in the first part of this section. After starting the program, in the File menu the word "new" should be highlighted and confirmed with the Enter button. Subsequently, the input table appears at the left-hand side of the screen. Based on the already prepared finite element mesh, either triangular or rectangular elements

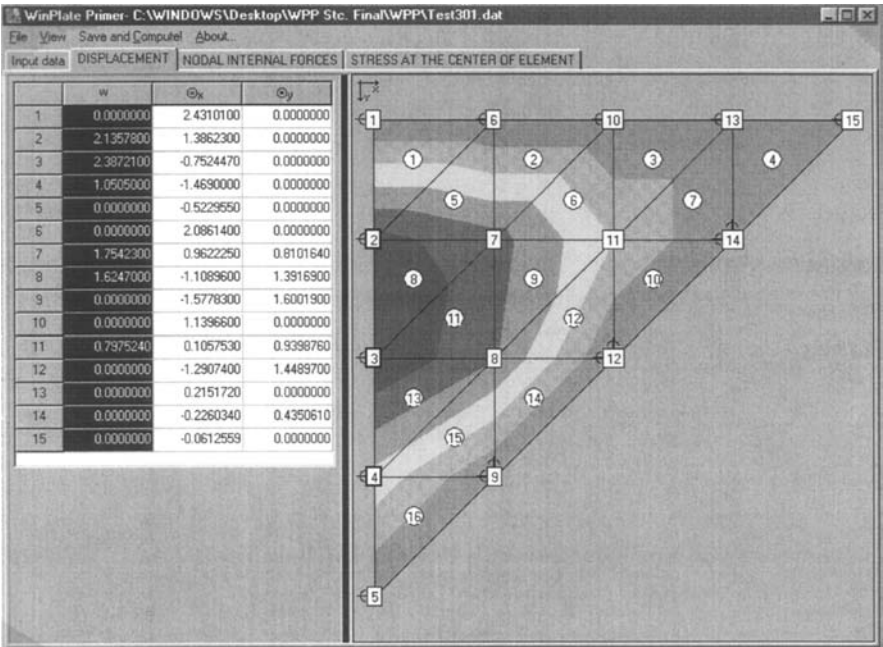


Figure A.4.4 Resulting nodal deflections.

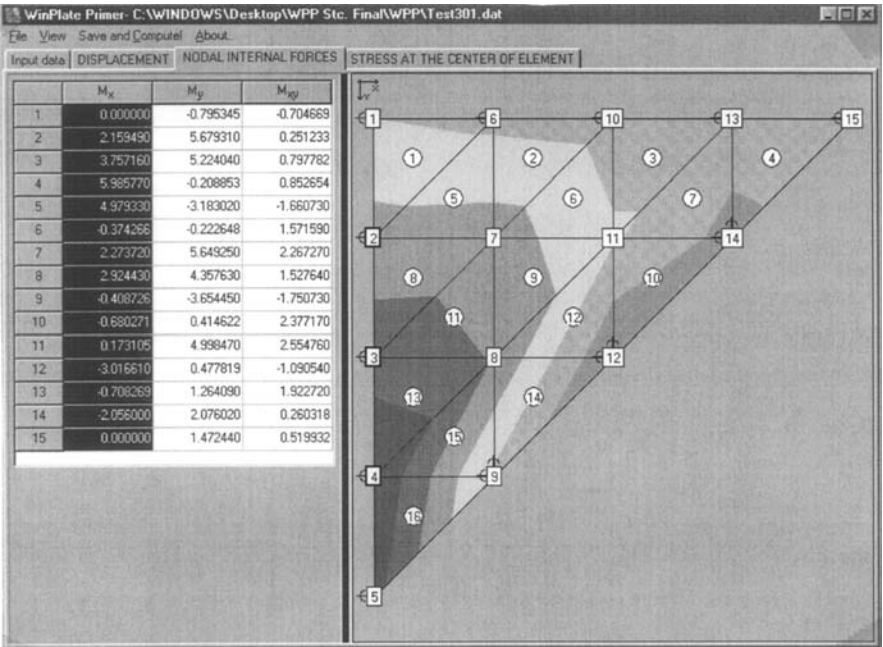


Figure A.4.5 Corresponding nodal forces.

must be chosen. This selection is carried out by using the *number of nodes/element* input. It should be noted, however, that the global coordinate system is different for rectangular and triangular finite element subdivisions. In filling out the input table, the user is interactively guided step by step. It is important that all rectangular boxes be filled in; otherwise the input cannot proceed, as already mentioned. When there is no input, zero must be used. As the engineer begins to fill out the input table, a two-dimensional graphical representation of the finite element mesh will appear on the right-hand side of the screen. This picture grows as the input proceeds. The final graphical representation of the finite element mesh will be similar to that shown in Fig. A.4.3. This also includes loading and boundary conditions of the plate in question. Beyond that, all the following steps are identical to those already discussed in connection with the use of solved problems.

Finally, it should be mentioned that the practical capacity of the static part of the WPP program system is approximately 1000 elements. Although, theoretically, 11,000 elements can be used, the required manual input procedure puts the above given limit on the element numbers.

All the solved test problems deal with single panel plates, but continuous plates can also be easily solved by applying the familiar procedures used in the FEM or, in the case of continuous beams, when the matrix displacement method is applied.

c. Dynamic Module1 (Free Vibration). This part of the WPP system deals with the free-vibration problems of *rectangular* plates neglecting damping. This programs determines the first mode shape of the freely vibrating system along with the pertinent lowest circular frequency ω_1 (in radians per second). Again, it is required that the folder of the Dynamic Module be copied from the CD-ROM into a corresponding folder (say WPP-D1) created for this purpose on the hard disk of the computer. The folder in the CD-ROM contains the following files: Solved Problems, Source Code, WPP_free_vibration, and User's Guide. The latter contains, again, detailed step-by-step instructions for the application of the corresponding programs amply illustrated with numerous screen shots. We assume that the user is already familiar with the use of the static part of WPP. Since the general procedure of the free-vibration analysis of plates is quite similar to that treated above in connection with the static part of this program system, we will concentrate here mostly on the small differences unique to free-vibration analysis. Our previous recommendation concerning printing the User's Guide and the table of Solved Problems remains the same. Similarly, we recommend, again, that the first-time user of the Dynamic Module1 start with the implementation of one of the solved problems. In the corresponding Table 12 the user will find cases of plate vibrations. The geometrical configurations of these plates including their boundary conditions are graphically presented along with the computed lowest circular frequencies. Comparison of these results with their analytically calculated counterparts shows very good agreement. Again, when analytical solutions were not available, this comparison was based on results obtained by using the independent ANSYS computer program system.

Activation of the winplateprimerD.exe program is carried out by clicking on the winplateprimerD icon in the above-mentioned WPP_free. . . file. To open and recompute an already solved test problem, we activate the File menu and select the OPEN option. Next, the list of the already solved problems appears on the right-hand side of the screen. Clicking, for instance, on Dtest41, the computer shows the already filled in input table on the left-hand side of the screen, while on the right appears the geometrical configuration of the selected plate along with its finite element subdivision

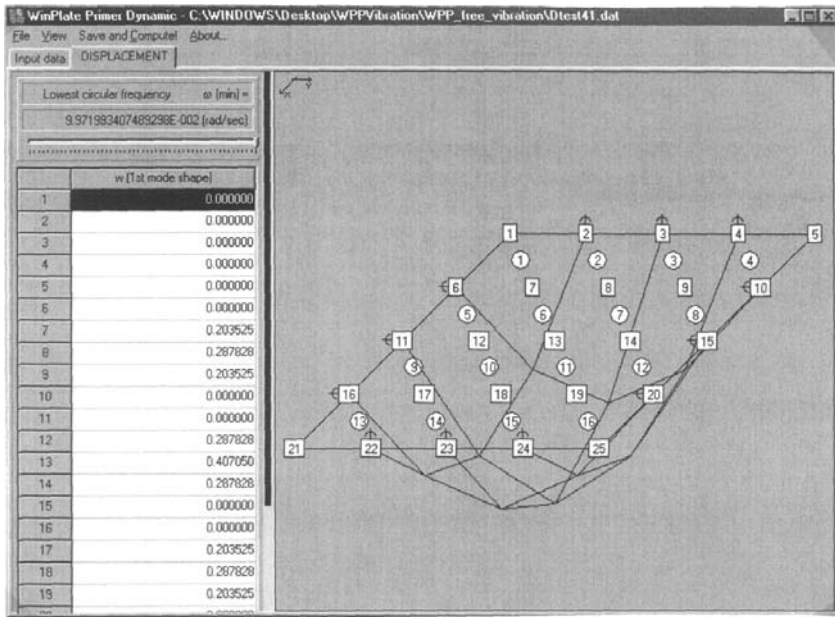


Figure A.4.6 First mode shape of freely vibrating plate.

and boundary conditions. Before we proceed any further, it is wise to opt in the View menu for “axonometric” and “wire frame” presentation of the resulting deflections to obtain a more appealing picture of the resulting nodal deflections. By activating the SAVE AND COMPUTE and subsequently the DEFLECTION commands, we obtain Fig. A.4.6, which shows the lowest natural frequency ω_1 of the plate and the corresponding first mode shape in three-dimensional form. A similar approach should be taken when a new plate will be analyzed for free vibration. Logically, in this case the user must opt for New in the File menu and subsequently the empty input table must be filled in. This process is similar to that already treated in connection with the static part of the WPP program system. Again, for detailed information we refer readers to the User’s Guide.

Finally, it should be mentioned that the lowest circular frequency, ω_1 , of the freely vibrating plate serves as a quasi finger print or DNA for the system. Consequently, all dynamic load factors (DLF)[†] are based on this vital characteristic which describes, to a certain extent, the dynamic behavior of plates. In engineering practice, the forced vibration of plates is usually treated by simply multiplying the maximum static deflections and internal forces by the so-calculated DLF.

d. Dynamic Module2 (Forced Vibration). As mentioned above, applying the dynamic load factor (DLF) yields valuable *estimates* for determining the maximum dynamic response of plates subjected to transient loads. However, for a more exact computation one should utilize a more direct approach. For this purpose, the *Harmonic Analysis* procedure (page 871–873) was selected for the WPP program system.

[†] See Sec. 14.1.

The conforming 16-DOF rectangular finite element[†] was employed in the pertinent FORTRAN programs. It was also assumed that all nodal forces have the same time dependency. The forcing function is expanded by using half-range Fourier series expansion containing only sine terms (see Sec. A.1), as required in the harmonic analysis procedure.

Again, it is recommended that the user of WPP forced vibration programs first prints the corresponding User's Guide, which gives detailed well-illustrated step-by-step instructions for their application. As is the case with the static and free vibration parts of WPP, the forced vibration cannot be run directly from the CD-ROM. Thus, it must first be installed on one of the hard disks of the user's computer by creating a special folder for this purpose. Like the other parts of WPP, the Dynamic Module2 (folder WPP_df) contains the following files: User's Guide, FORTRAN source codes, solved test problems, and WinPlatePrimer DF file. To *activate* the harmonic analysis procedure, the user should click on the pertinent WPP_df icon.

A first-time user of WPP DF should start with one of the solved test problems to get familiarized with the application of programs. For this purpose, one should select the OPEN command from the File menu and click on a solved program. Following this action, on the left-hand side of the screen appears the input table filled with corresponding node numbers, nodal coordinates, loading and boundary conditions, etc. Simultaneously, the graphical representation of the plate problem in question is shown on the right-hand side of the screen. The input data for the time dependency of the forcing function includes the number of Fourier terms and the time steps used in the corresponding expansion. Scrolling down to the end in the Time Dependency column the user finds a command for PREVIEW FOURIER TRANSFORMATION AND TERMS. By activating this command the result of this procedure is graphically illustrated at the bottom of the screen.

Next, the SAVE AND COMPUTE command in the menu bar should be activated. By clicking on DISPLACEMENTS in the menu bar, we obtain at the left-hand side the results of the corresponding computation. However, to obtain the pertinent graphical illustrations of the lateral displacements of the plate, one must click on the *dotted* line at the left-hand side of the screen located right below the menu bar. This dotted line graphically represents the time interval of the forcing function. As a default, the results of the last time step are presented graphically on the right-hand side of the screen, as shown in Fig. A.4.7. By clicking at some other location on this dotted line, however, the results pertinent to the corresponding time step are presented. The very same procedure should be used for obtaining the NODAL FORCES and STRESS AT THE CENTER OF ELEMENTS. Figure A.4.7 illustrates the resulting screen picture of such a computation. As in the case of static computation, one can select in the View file the desired way for a graphic presentation. To obtain a hard copy of the numerical results, the user should consult the User's Guide.

In general, the procedure for solution of the dynamic response of a new problem follows the above-described steps. Consequently, it is sufficient to deal here only with the apparent differences. Again, the user should click on the NEW in the File menu. The fundamental deviation in the input procedure involves the consideration of the time dependency of the forcing functions. For this purpose, the user should fill in the table of Time Dependency, the activation command of which is under the menu bar at the left-hand side of the screen. The required inputs are the number of time steps

[†] See Sec. 7.7.1.

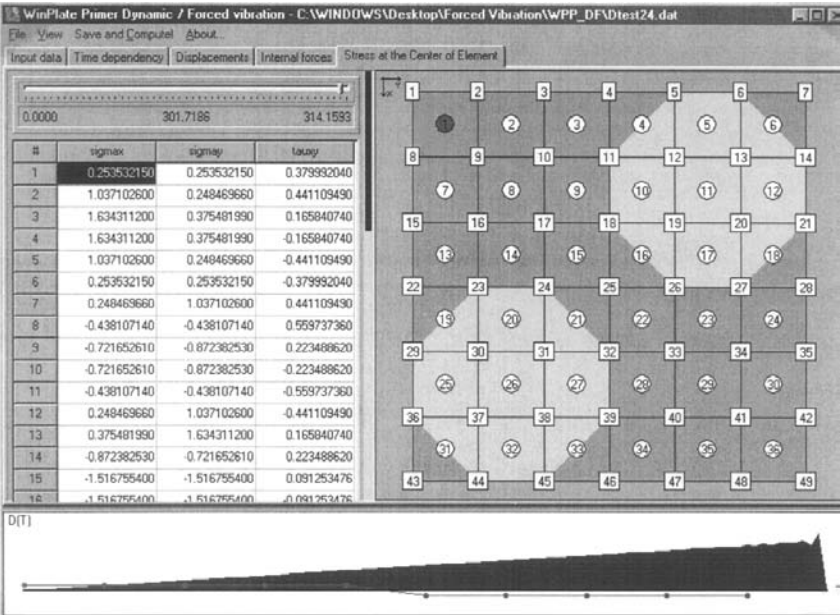


Figure A.4.7 Screen picture of the results.

and the pertinent ordinates of the time-dependent forcing function and the number of Fourier terms to be used in the Fourier expansion. Please note that the first time step must be zero. Again, it must be remembered that *all cells* in the input tables must be filled in; otherwise the user cannot continue with the program. If there is no input data, zero must be used. After completion of the inputs, [enter] should be pressed to transfer these data to the computer. Click also on PREVIEW OF FOURIER TRANSFORMATION to see the result of the already executed Fourier expansion of the forcing function in graphical form. Then, activate SAVE AND COMPUTE to solve the dynamic response of the plate in question. All other steps are identical to those already described above.

Index

A

- Airy's stress function, 65, 190, 616, 947, 964, 968, 970
- Argyris, J. H., 366

B

- Beam functions, 374, 378, 401, 480, 600, 866
- Bending and stretching, 147–149, 511
 - solution of, 149–150
- Bogner, F. K., 399
- Boundary conditions of
 - curved boundaries, 40
 - finite difference methods, 253–260, 517
 - large deflections, 618
 - moderately thick plates, 46, 49
 - straight boundaries, 35–40
 - thermal bending, 564
 - thick plates, 56
- Boundary element method,
 - 496–504
 - discretization of boundary, in, 497, 501

- fundamental solution for, 496–497

- Buckling of rectangular plates. *See also* Cases 158–162 of Plate formulas on accompanying CD
 - FS, inplane load, 917, 926
 - S, inplane load, 916, 931
 - SF, inplane load, 925, 927
- Buckling, general. *See also* Stability analysis
 - analytical methods, in, 911–919
 - concepts of, 905–910
 - energy methods in, 919–928
 - numerical methods, in, 928–946
 - finite difference approach, with, 928–937
 - finite element approach, with, 938–947

C

- Categories of plates, 5–7
- CD-ROM accompanying the book
 - Plate formulas, 1003–1005
 - WPP program system, 1004–1012
- Cheung, Y. K., 17, 18, 366, 518
- Chladni, E. F. F., 10, 17

Note: The following letters refer to the boundary conditions of the plates: C = clamped, F = free edge, S = simple supported edge.

- Circular plates, dynamic analysis
 - of, 808. *See also* Cases 138–144 of Plate formulas on accompanying CD
 - Circular plates, static solution of. *See also* Cases 1–64 of Plate formulas on accompanying CD
 - C, concentrated force, 159
 - C, uniform load, 66, 113
 - S, eccentric force, 161
 - S, hydrostatic load, 157
 - S, linearly increasing load, 114
 - Code number technique, 347, 355, 416, 444
 - Colatz, L., 16, 282
 - Conjugate plate analogy, 121, 124, 303, 308–310, 450–452
 - Continuous plates, 173–179
 - engineering solutions for, 676–718
 - finite difference method for, 270
 - finite element method for, 558–559
 - flat slabs, 583–587, 718–727
 - influence surface of, 576
 - loading patterns for, 685
 - point supported, 578–583
 - stencils for, 683
 - yield-line analysis of, 764–769
 - Convergence in buckling analysis, 940
 - Convergence in dynamic analysis
 - effect of mass representation, 865
 - Convergence, static
 - finite elements
 - membrane element, 666
 - orthotropic, 522
 - rectangular conforming, 423
 - rectangular nonconforming, 410, 433
 - requirements for, 590
 - tests for, 591, 593
 - triangular DKT, 428–429
 - funicular polygon method of, 295
 - gridwork method of, 335
 - ordinary finite difference method of, 262, 518
 - Corner forces, 36, 551, 760–761
 - Conservation of energy, 215, 221–223
 - Courant, R., 17, 18, 365
 - Curvatures
 - constants, 391, 591
 - vector of, 373
- D**
- Damping of motion
 - concept of, 883–885
 - viscous damping with, 885
 - Differential equations of plates
 - in buckling, 912, 915
 - in Cartesian coordinate system, 31
 - in motion, 802
 - in oblique coordinate system, 548
 - in polar coordinate system, 42
 - in thermal bending, 564
 - laminated and sandwich, 533–535
 - moderately thick, 45, 47–49
 - orthotropic, 510–511
 - thick of, 53–57
 - with bending and stretching, 148
 - with large deflections, 616
 - with variable thickness, 139, 143
 - Discrete Kirchhoff Triangular (DKT) element, 423–426
 - Donnell's approximation, 303
 - Duhamel's integral, 795, 888
 - Dynamic analysis using classical methods
 - circular frequency in, 790

Note: The following letters refer to the boundary conditions of the plates: C = clamped, F = free edge, S = simple supported edge.

- differential equation for, 802–803
- equation of dynamic equilibrium in, 789, 802
- equation of motion in, 789
- equivalent one DOF system with, 796–800
- general concepts of, 787–789
- initial condition of, 791
- impulse in, 794
- membranes for, 810–814
- natural frequency in, 790
- Navier method, 791, 805
- transient response, 793–796
- vibration of spring-mass in, 788
- Dynamic analysis using finite differences, 845–856
- Dynamic analysis using finite elements
 - forced vibration, 870–882
 - free vibration, 856–859
 - mass matrix, 860–866
 - Rayleigh quotient with, 859
- Dynamic load factors, 792, 795, 797, 832, 834, 848, 870, 878, 888
- Dynamic matrix, 860, 866
- E**
- Edge moments, 165–168
- Effective width
 - bending, in, 104–106
 - postbuckling, in, 970–973
- Eigenfunctions
 - column buckling of, 205–206, 479–480
 - vibrations of beam of, 202–203, 478–479
- Eigenvalue problems, 846, 852, 886, 907, 922, 924, 930, 936, 939
- Elastic modulus
 - secant, 647
 - tangent, 647
- Elasticity matrix, 372, 386, 388, 437, 483, 602
- Energy methods for moderately thick plates, 231–233
- Energy methods in bending
 - basic concepts of, 181–186
 - Galerkin method, 196–200, 206–208
 - minimum of potential, 187, 384
 - Ritz method, 187–196, 381
 - shape functions for, 191, 202, 205
 - virtual work, with, 182, 383
 - Vlasov approach, 200–206
- Energy. *See also* Strain energy
 - total potential, 189, 381
- Engineering methods. *See also* Yield-line analysis
 - bridge decks, for, 727–730
 - degree of fixity, 733–739
 - elastic web analogy, 676–689.
 - flat slabs for, 718–727
 - moment distribution, 700–709.
 - Pieper and Martins approach, 710–718
 - simplified slope deflection, 689–699.
 - skew plates for, 730–733
- Equations. *See also* Differential equations
 - equilibrium, 26, 335, 346, 377, 383
 - variational, 199
- Equivalent stress, strain, 646
 - stress distribution of, 658
- Error distribution technique, 226–231

Note: The following letters refer to the boundary conditions of the plates: C = clamped, F = free edge, S = simple supported edge.

F

Finite difference method, ordinary
 boundary conditions for,
 253–260, 517
 convergence of, 264, 518
 large deflections for, 624–626
 load representation, in, 258–262
 orthotropic plates for, 516,
 526–528
 plate equation, in, 251–252
 sandwich plates for, 542–545
 skew plates for, 549–554
 static analysis with, 238,
 247–276

Finite difference methods,
 improved
 funicular polygon method,
 285–292, 296–297
 boundary conditions of,
 293–294,
 convergence of, 295
 higher approximations, with,
 277, 300–302
 multilocal method, 278–285, 297
 boundary conditions of,
 284–289
 successive approximation,
 292–295, 298–300

Finite element method
 element stiffness matrices, 409,
 420–423
 assembly of, 377
 formulation of, 372–377
 orthotropic, 519–523, 528
 large deflections for, 626–629
 engineering approach for,
 370–380
 history of, 366
 introduction to, 364
 mathematical formulation of,
 380–383
 alternative, 385

 minimum of potential, 384
 virtual work, 383
 nonlinear procedures, 626–661

Finite strip method, classical
 computational procedures for,
 488–493
 concepts of, 475–477
 formulation of, 481–488
 stiffness matrices for, 485–486

Flat slabs, plates, 583–587
 analytical solution of, 579–589
 approximate analysis of,
 718–728, 778–780

Flexural rigidity, 31
 orthotropic, 511–515
 reduced, 657, 660
 transformed, 533

Fourier, J., 986

Fourier series, 985–997
 coefficients for, 987–988, 991,
 994–996
 double, 994–997
 fast, 996
 single, 986–994

Frequency
 circular, 790
 natural, 790

G

Galerkin's method in
 buckling of plates, 923, 927
 large-deflection analysis,
 617–619, 622–623
 static analysis, 196–200,
 206–208
 vibration of plates, 818–823

Generalized coordinates, 385

Geometrical forms, various
 elliptical, C, uniform load, 151
 sector-shape, FS, uniform load,
 153
 triangular, S, uniform load, 152

Note: The following letters refer to the boundary conditions of the plates: C = clamped, F = free edge, S = simple supported edge.

Geometric nonlinearity, procedures
of,
combined , 643–645
incremental (Euler), 638–641
iterative (Newton-Raphson),
641–643
Germain, Sophie, 12
Gridwork method in dynamic
analysis
convergence of, 865
mass matrices, 864–865
Gridwork method in static analysis
concepts of, 317–320
cross-sectional properties for
Hrennikoff's model, 321
other models, 329
Salonen's model, 321–323
load representation in, 340
programming, 343–348
sandwich plates for, 537
skew plates for, 555–558
solutions with, 348–360
stiffness matrices for,
Hrennikoff's cell, 333
nonlinear, 634–637
Salonen's cell, 334
H
Harmonic
analysis procedure, 871–873,
881
even, odd functions, 988–990
motion, 804,
Hermitian
elements, 399, 404
methods, 278, 285
polynomials, 201–402
shape functions, 401–402
Hill equation, 949
Homogeneous equation, 63, 71, 77,
82, 86, 90
Hrennikoff, A., 16, 18, 320, 366

I

Influence surfaces, 571–578
continuous plate of, 576–577
loads for generation of, 573–574
singularity method in, 572
Initial imperfection in buckling,
973–975
Interaction curve in buckling, 910,
942
Internal forces and stresses, 30–34
acting on arbitrary planes, 33
Iterative approach
large deflection for, 621
Richardson's extrapolation for,
265
Runge's principle in, 292
Stodolla-Vianello technique, 848,
855–856

J

Johansen, W. K., 16, 765, 750

K

Kantorovich's method, 214–215,
223–225
von Kármán, von, Th., 617, 947,
968, 970
Kirchhoff, G. R., 14
publications of, 18, 35
supplementary forces of, 14, 37

L

Laplacian operator in
Cartesian coordinate system, 31
oblique coordinate system, 547
polar coordinate system, 44
Large-deflection analysis, 614–623
analytical solutions of, 617–623
differential equations of,
616–617
numerical buckling in, 947

Note: The following letters refer to the boundary conditions of the plates: C = clamped, F = free edge, S = simple supported edge.

Large-deflection analysis
 (*continued*)
 numerical postbuckling in, 968
 numerical solutions of, 624–644
 Loads on supporting beams, 714

M

Mapping, 412–414, 462
 isoparemetric, 594–596
 skew plates of, 549
 Marcus, H., 676, 689
 Mass matrix, explicit expressions
 for, 862, 864–865
 convergence characteristics of,
 865
 Material nonlinearity procedures
 incremental (Euler), 648–649
 initial strain approach, 651–653
 initial stress approach, 653
 iterative (Newton-Raphson),
 649–651
 Mathieu equation, 949, 952
 Membrane forces
 due to large deflection, 616
 Membranes, solution of, 116–117
 circular, 118–119
 dynamic analysis, in, 810–814
 rectangular, 117–118
 Method of images, 97–99
 Mindlin, R. D., 15, 18
 Moderately thick plate, theories of
 circular plates for, 51
 higher order, 49–51
 Mindlin, 47–49
 Reissner, 49–51
 Speare and Kemp simplification,
 47
 Moderately thick plates, solutions
 of
 buckling of, 963–965
 conjugate plate analogy with,
 124–125, 308–310,
 450–452

Donnell's approximation for,
 310–312
 energy methods with, 231–233
 finite difference method with,
 308–310
 finite strip method for, 606–609
 free vibration for, 839–831
 Lévy's approach with, 121–124
 Navier method with, 120–121
 Wang's formula for, 841
 Moment diagrams
 approximate, 686, 713, 720, 731
 reduction of, 582, 586, 684
 Moments, internal
 Kirchhoff plates in, 31, 44
 moderately thick plates in,
 46–48
 orthotropic plates in, 509
 sandwich plates of, 536
 thermal bending in, 567,
 Moment-sum, 34, 550, 930
 Morley's formula, 825, 880

N

Nádai, Á., 15, 16
 Navier, L., 13
 lecture notes of, 18
 Newmark method, 873
 Nonlinearity
 combined, 656–661
 geometric, 614–644
 material, 645–655
 Nonlinear solutions,
 incremental-iterative
 techniques, 657–661
 Numbering of joint-points, 339
 Numerical integration, 456–462

O

Orthogonality of functions, 201,
 480
 Orthotropic plates, 507–529

Note: The following letters refer to the boundary conditions of the plates: C = clamped, F = free edge, S = simple supported edge.

- analysis procedures with
 - affine transformation, 766
 - buckling, 954–955
 - finite element method, 519–523, 528
 - finite difference method, 515–517, 526–528
 - gridwork method, 516
 - Lévy's method, 524
 - Navier's method, 523
 - differential equation of, 510
 - flexural rigidities of, 511–515
 - theory of, 508
- P**
- Patch test, 591
 - Periodic functions, 987
 - even or odd harmonic, 989
 - Plate strips, 99–109
 - CS, uniform load, 106
 - S, concentrated force, 109
 - S, uniform load, 63, 107
 - Plate theories, static
 - elastic, 26–26
 - moderately thick, 45–51
 - thick, 53–57
 - Plates on elastic foundation, 129
 - Lévy solution, 132–135
 - S, concentrated force, 136–137
 - Navier solution, 130–132, 136
 - Poisson ratio, conversion of, 999
 - Polynomials for
 - rectangular finite elements, 396–406
 - triangular finite elements, 394–396
 - Postbuckling, 966–977
 - Potential energy. *See also* Energy
 - minimum of, 187, 384, 908
 - nonlinear, 627
 - postbuckling, in, 970
 - stiffened plates of, 958
 - Principal stresses, 34
 - Program system on CD-ROM
 - forced vibration, 1011–1013
 - free vibration, 1010–1011
 - static analysis, 1007–1010
 - Punching shear, 583, 747
- R**
- Rayleigh's method
 - quotient, with, 817, 825, 859, 921, 960
 - stability analysis, in, 920, 926, 958
 - vibration analysis, in, 816
 - Rectangular plates, free vibrations
 - of. *See also* Cases 146–154 of
 - Plate formulas on
 - accompanying CD
 - C, 821–823, 867
 - S, 805–807, 809, 828–830, 868–870
 - Rectangular plates, static solutions
 - of. *See also* Cases 74–105 of
 - Plate formulas on
 - accompanying CD
 - C, concentrated force, 229, 415, 430, 442
 - C, thermal load, 569
 - C, uniformly loaded, 194, 206, 223
 - S, concentrated force, 89, 348, 430
 - S, hydrostatic load, 74
 - S, parabolic load, 84
 - S, partially loaded, 90, 756
 - S, prismatic load, 269, 296
 - S, small area loaded, 88
 - S, triangular load, 192
 - S, uniformly loaded, 72, 79, 355
 - SC, sinusoidal load, 81
 - SC, uniformly loaded, 208, 218, 221, 271, 298
 - SF, concentrated force, 491

Note: The following letters refer to the boundary conditions of the plates: C = clamped, F = free edge, S = simple supported edge.

Rectangular plates, static solutions
 of (*continued*)
 SF, line load, 310
 thermal load, 569
 Reinforced concrete
 models of, 662–667
 orthotropy of, 508
 rigidity of, 511
 Reissner, E., 15, 18
 Resonance, 792, 834
 Richardson's extrapolation formula,
 265
 Rigid body motions, 390
 Ritz method in
 dynamic analysis, 817–818, 821
 large-deflection analysis, 620
 postbuckling, 970
 stability analysis, 922
 static analysis, 187–195, 381
 Robinson's test, 593
 Rotation of coordinate systems, 32,
 330, 345, 382

S

Shape functions for finite elements
 computed, 605
 conforming, 390, 399, 403
 finite plate strips, for, 478–481
 moderately thick plates, for,
 446–450, 456, 607
 nonconforming, 390, 396, 407
 polynomials, 392–405
 requirements of, 389–392
 triangular elements, for,
 394–396, 424, 443
 Shear correction factor, 48
 Shear modulus, orthotropic, 509
 Shear stresses, forces
 inplane, 27–28
 moderately thick plates of,
 46–47, 49–50
 orthotropic plates of, 510
 sandwich plates of, 536

 thermal, 564
 transverse, 46–47, 49
 Sign conventions, 7, 347, 387
 Singularity, 65, 572
 Skew plates, 546–559
 analytical solution of, 547–548
 numerical solution, approximate
 methods for, 730–736
 numerical solutions of, 549–559
 Solution methods, classical
 exact, 63, 66–67
 generalization of Navier's
 approach, 92
 homogeneous part of, 63
 Lévy's approach, 75–83, 85–87,
 89–92
 Navier's approach, 69–75,
 83–85, 87–89
 particular part of, 65, 76
 Spline finite strip method, 598–605
 element stiffness matrix of, 603
 formulation of, 600–604
 load vector, for, 604
 spline function, for, 598–600
 Stress-strain curve, bilinear, 657
 Stability analysis, analytical
 approaches
 basic concepts of, 905–910
 bifurcation, in, 906
 circular plates of, 914
 dynamic approach, for, 909
 energy methods for, 907–909,
 919–928
 equilibrium method for, 907,
 911–919
 snap-through in, 906
 thermal buckling in, 961
 under combined loads, 909–910
 Stability analysis, numerical
 methods
 dynamic buckling in, 946–952
 finite difference method with,
 928–938

Note: The following letters refer to the boundary conditions of the plates: C = clamped, F = free edge, S = simple supported edge.

- finite element method with, 938–943
 - gridwork method with, 943–946
 - Stiffened plates, buckling. *See also*
 - Cases 163–170 of Plate
 - formulas on accompanying CD
 - orthotropic plates of, 954, 959–960
 - three or less stiffeners with, 955, 957
 - Stiffness matrices, explicit
 - finite strips of, 485–486
 - gridwork of, 333–334
 - membrane finite element of, 669
 - nonlinear for, 628–630
 - orthotropic finite element of, 520
 - rectangular finite elements of, 409, 420–422
 - spline strip of, 603
 - triangular finite element, 427
 - Stodola-Vianello iteration, 827, 848, 855, 897, 930, 940
 - Strain energy, 182
 - bending, in, 184, 187, 188
 - equivalence of, 324–328
 - membranes for, 184, 189–190, 620
 - sandwich plates of, 535
 - Strains, 29–30, 187, 373, 508
 - large deflections of, 616
 - spline strip method, in, 602
 - thermal, 563
 - vector for, 382, 388, 454, 482, 666
 - Stress
 - matrices, 436, 438, 439, 483, 521, 669
 - orthotropic, 509
 - resultants, 372, 378, 436–445, 509
 - sandwich plates, of, 536
 - spline strips of, 603
 - thermal, 563
 - vector, 384, 364
 - Strutt diagram, 950
 - Stüssi, F., 16, 285
 - Szillard, R., 65, 214, 226, 657
- T**
- Taylor series, 263, 277
 - Thermal bending, 561–570
 - governing equations of, 562–566
 - methods of solution of, 566–570
 - thermal loads, for, 564
 - thermal stretching, 566
 - Thermal buckling, 961–963
 - Thermal expansion coefficient, 562
 - Thick plate elements, 453–457
 - Timoshenko, S. P., 15, 18, 19, 570, 657
 - Transformation matrices. *See also*
 - Rotation of coordinate systems
 - matrices, 330–345, 376, 382
 - rotation matrices, 32, 376
 - Triangular plates, analysis of. *See also*
 - Cases 108–110 of Plate
 - formulas on accompanying CD
 - exact, 63
 - finite difference method with, 274–275
 - gridwork method with, 351–355
- U**
- Ultimate load technique. *See also*
 - Yield-line method
 - Unit motions of nodal points, 374–375, 403.
 - Units, SI
 - conversion factors, for, 1002
 - prefixes of, 1001
 - Use of plates in engineering
 - 3–6

Note: The following letters refer to the boundary conditions of the plates: C = clamped, F = free edge, S = simple supported edge.

V

- Variable thickness
 - circular plates of, 140–146
 - rectangular plates of, 139–140
- Variational methods, 185–186
 - equation of plate bending in, 199
 - stability analysis in, 908.
- Vehicle-bridge interaction, 890–892
- Vibration, forced, analytical
 - solutions for, 830–834
 - irregular surface, due to, 835, 892–894
 - moving loads, due to, 835–836
 - Navier method 831–833
 - pulsating loads, due to, 837
- Vibration, forced, numerical
 - methods. *See also* Dynamic Module2, 1011–1013
 - finite element method, with, 870–878
 - harmonic analysis, 871–873, 880–882
 - Newmark's method, 873–875
 - numerical integration, 873–882
 - Wilson's method, 875–877
- Vibration, free, numerical methods. *See also* Dynamic Module1, 845–848, 1010–1011
 - finite difference, 845–856
 - finite element, 856–882
 - large amplitude, 895–899
- Vibrations of plates, analytical
 - procedures
 - energy methods, 815–823
 - forced, 830–838
 - free, 789, 815–823
 - moderately thick plates of, 839–841
 - Morley's formula, with, 825

- Stodola-Vianello iteration, 827
- using static deflections, 824–830

- Vibrations of membranes
 - circular, 812–814
 - rectangular, 810–811
- Vlasov's method in
 - dynamic analysis, 818–821
 - large-deflection analysis, 619–621
 - static analysis, 200–206, 208–211

W

- Wang, C. M., 126, 312, 841, 964
- Wilson's method, 875–877
- Work
 - external forces of, 182, 215
 - internal forces of, 182, 215
 - virtual, 182, 383

Y

- Yield-line analysis. *See also* Cases 120–136 of Plate formulas on accompanying CD
 - assumptions, 742–747
 - concentrated forces, in, 770–780
 - continuous slabs, for, 764–769
 - combined loadings, for, 763
 - deflections, estimating, in, 748–750
 - equilibrium method, in, 758–763
 - nodal forces in, 760–761
 - superposition theorem in, 747, 763
 - work methods in, 751–757

Z

- Zienkiewicz, O. C., 17, 366, 414, 518, 653

Note: The following letters refer to the boundary conditions of the plates: C = clamped, F = free edge, S = simple supported edge.

John Wiley & Sons, Inc.

End-User License Agreement

READ THIS. You should carefully read these terms and conditions before opening the software packet(s) included with this book “Book”. This is a license agreement “Agreement” between you and John Wiley & Sons, Inc. “JWS”. By opening the accompanying software packet(s), you acknowledge that you have read and accept the following terms and conditions. If you do not agree and do not want to be bound by such terms and conditions, promptly return the Book and the unopened software packet(s) to the place you obtained them for a full refund.

1. **License Grant.** JWS grants to you (either an individual or entity) a nonexclusive license to use one copy of the enclosed software program(s) (collectively, the “Software”) solely for your own personal or business purposes on a single computer (whether a standard computer or a workstation component of a multi-user network). The Software is in use on a computer when it is loaded into temporary memory (RAM) or installed into permanent memory (hard disk, CD-ROM, or other storage device). JWS reserves all rights not expressly granted herein.
2. **Ownership.** JWS is the owner of all right, title, and interest, including copyright, in and to the compilation of the Software recorded on the disk(s) or CD-ROM “Software Media”. Copyright to the individual programs recorded on the Software Media is owned by the author or other authorized copyright owner of each program. Ownership of the Software and all proprietary rights relating thereto remain with JWS and its licensors.
3. **Restrictions on Use and Transfer.**
 - (a) You may only (i) make one copy of the Software for backup or archival purposes, or (ii) transfer the Software to a single hard disk, provided that you keep the original for backup or archival purposes. You may not (i) rent or lease the Software, (ii) copy or reproduce the Software through a LAN or other network system or through any computer subscriber system or bulletin-board system, or (iii) modify, adapt, or create derivative works based on the Software.
 - (b) You may not reverse engineer, decompile, or disassemble the Software. You may transfer the Software and user documentation on a permanent basis, provided that the transferee agrees to accept the terms and conditions of this Agreement and you retain no copies. If the Software is an update or has been updated, any transfer must include the most recent update and all prior versions.
4. **Restrictions on Use of Individual Programs.** You must follow the individual requirements and restrictions detailed for each individual program in the About the CD-ROM appendix of this Book. These limitations are also contained in the individual license agreements recorded on the Software Media. These limitations may include a requirement that after using the program for a specified period of time, the user must pay a registration fee or discontinue use. By opening the Software packet(s), you will be agreeing to abide by the licenses and restrictions for these individual programs that are detailed in the

About the CD-ROM appendix and on the Software Media. None of the material on this Software Media or listed in this Book may ever be redistributed, in original or modified form, for commercial purposes.

5. Limited Warranty.

- (a) JWS warrants that the Software and Software Media are free from defects in materials and workmanship under normal use for a period of sixty (60) days from the date of purchase of this Book. If JWS receives notification within the warranty period of defects in materials or workmanship, JWS will replace the defective Software Media.
- (b) JWS AND THE AUTHOR(S) OF THE BOOK DISCLAIM ALL OTHER WARRANTIES, EXPRESS OR IMPLIED, INCLUDING WITHOUT LIMITATION IMPLIED WARRANTIES OF MERCHANTABILITY AND FITNESS FOR A PARTICULAR PURPOSE, WITH RESPECT TO THE SOFTWARE, THE PROGRAMS, THE SOURCE CODE CONTAINED THEREIN, AND/OR THE TECHNIQUES DESCRIBED IN THIS BOOK. JWS DOES NOT WARRANT THAT THE FUNCTIONS CONTAINED IN THE SOFTWARE WILL MEET YOUR REQUIREMENTS OR THAT THE OPERATION OF THE SOFTWARE WILL BE ERROR FREE.
- (c) This limited warranty gives you specific legal rights, and you may have other rights that vary from jurisdiction to jurisdiction.

6. Remedies.

- (a) JWS' entire liability and your exclusive remedy for defects in materials and workmanship shall be limited to replacement of the Software Media, which may be returned to JWS with a copy of your receipt at the following address: Software Media Fulfillment Department, Attn.: Theories and Applications of Plate Analysis: Classical, Numerical and Engineering Methods, Wiley, 10475 Crosspoint Blvd., Indianapolis, IN 46256, or call 1-800-762-2974. Please allow four to six weeks for delivery. This Limited Warranty is void if failure of the Software Media has resulted from accident, abuse, or misapplication. Any replacement Software Media will be warranted for the remainder of the original warranty period or thirty (30) days, whichever is longer.
- (b) In no event shall JWS or the author be liable for any damages whatsoever (including without limitation damages for loss of business profits, business interruption, loss of business information, or any other pecuniary loss) arising from the use of or inability to use the Book or the Software, even if JWS has been advised of the possibility of such damages.
- (c) Because some jurisdictions do not allow the exclusion or limitation of liability for consequential or incidental damages, the above limitation or exclusion may not apply to you.

- 7. U.S. Government Restricted Rights.** Use, duplication, or disclosure of the Software for or on behalf of the United States of America, its agencies and/or instrumentalities "U.S. Government" is subject to restrictions as stated in paragraph (c)(1)(ii) of the Rights in Technical Data and Computer Software clause

of DFARS 252.227-7013, or subparagraphs (c) (1) and (2) of the Commercial Computer Software - Restricted Rights clause at FAR 52.227-19, and in similar clauses in the NASA FAR supplement, as applicable.

- 8. General.** This Agreement constitutes the entire understanding of the parties and revokes and supersedes all prior agreements, oral or written, between them and may not be modified or amended except in a writing signed by both parties hereto that specifically refers to this Agreement. This Agreement shall take precedence over any other documents that may be in conflict herewith. If any one or more provisions contained in this Agreement are held by any court or tribunal to be invalid, illegal, or otherwise unenforceable, each and every other provision shall remain in full force and effect.